Virchows Arch (2007) 450:1–13
DOI 10.1007/s00428-006-0302-6

RECOMMENDATION

Recommendations for the reporting of surgically resected specimens of colorectal carcinoma

Jeremy R. Jass · Michael J. O'Brien · Robert H. Riddell · Dale C. Snover

Received: 21 August 2006 / Accepted: 23 August 2006 / Published online: 25 November 2006
© Springer-Verlag 2006

Scope of guidelines

The reporting of colorectal cancer is facilitated by the provision of a checklist giving the features required for good patient care. However, the practicalities of applying such a checklist may not be straightforward. Familiar examples include finding the prescribed number of lymph nodes, distinguishing mesenteric tumor deposits from replaced lymph nodes, and deciding if a cluster of malignant cells in a lymph node sinus counts as a metastasis. Checklists have traditionally focused on prognostic factors and particularly tumor stage. It is becoming increasingly clear that additional factors, whether morphological or molecular, will be needed for future clinical management. It is also evident that prognosis is strongly influenced by surgical technique, most notably by the introduction of total mesorectal excision in the case of rectal cancer.

This paper was the product of a team of experts on behalf of the Association of Directors of Anatomic and Surgical Pathology (ADASP).

J. R. Jass (✉)
Department of Pathology, McGill University,
Duff Medical Building, 3775 University Street,
Montreal, Quebec H3A 2B4, Canada
e-mail: jeremy.jass@mcgill.ca

M. J. O'Brien
Department of Pathology, Mallory Institute of Pathology,
Boston University School of Medicine,
Boston, MA, USA

R. H. Riddell
Department of Pathology, Mount Sinai Hospital,
Toronto, ON, Canada

D. C. Snover
Department of Pathology, Fairview Southdale Hospital,
Edina, MN, USA

Adjuvant therapy is playing an increasingly important role in the management of colorectal cancer, and it is inevitable that both morphological and molecular markers will be used to predict responses to the expanding range of therapeutic modalities. Neo-adjuvant or pre-operative radiotherapy is being offered to patients with advanced rectal cancer and can greatly modify the pathological findings in the operative specimen. For all the preceding reasons, the work of the diagnostic pathologist has become increasingly complex and demanding. The sixth edition of the tumor, node, and distant metastasis (TNM) classification fails to meet many of the challenges posed by the realities of modern cancer management. In fact, by changing the rules for staging without strong justification and introducing diagnostic criteria that are unhelpful and lacking a good evidence base, there is a real danger that the community of pathologists will fail to engage with reporting recommendations in a standardized manner and that the quality of reporting will fall.

Quality reporting is facilitated by the development of checklists that are simple to use and encompass the most important pathological features. The checklist represents "what", but will not be applied in a consistent and reproducible manner unless it is supported by "why" and also by "how". At the same time, the following guideline is not intended as a detailed treatise on dissection and histological examination. It merely serves to identify the more controversial and difficult components of reporting and to offer practical advice that will directly meet the needs of pathologists as well as benefiting other clinicians and ultimately the patient. In general, we have followed and built upon the recommendations of the AJCC sixth edition Cancer Staging Manual, the guidelines of the College of American Pathologists (CAP), and the TNM classification of intestinal tumors.

We have varied from these recommendations only where we have identified elements that are clearly ambiguous and we have then reached consensus on alternatives that are more evidence-based and/or that conform to a more practically based approach. We cannot eliminate subjectivity and arbitrariness altogether (there are clear elements of both in ostensibly objective TNM staging) but trust that in difficult cases pathologists will be able to use their training, experience, and common sense to reach an informed decision.

Features the Association recommends for inclusion in the final report are selected on the basis that they are generally accepted as being of prognostic importance, required for therapy, and/or traditionally expected.

A. Gross description

1. How the specimen was received: fresh, in formalin, opened, unopened, etc.
2. How the specimen was identified: labeled (with name, number) and designated as, e.g., right hemicolectomy
3. Parts of intestine included: length of each segment, other structures included (e.g., terminal ileum, appendix, anal canal, attached/adherent organs, identified vessels)
4. Tumor description
   a. Site within colorectum. In the case of rectal cancer state the distance of the most distal point of the anterior peritoneal reflection from the distal margin and the length of the tumor above and below the reflection. State, if possible, the quadrant showing the site of deepest tumor invasion (anterior, right lateral, posterior, and left lateral) and estimate the proportion of the circumference that is involved (multiples of 10%).
   b. Distance (centimeter) to nearest margin (given as distal or proximal, if known). Distance from circumferential or radial margin is based on microscopic evaluation (see B.9 below).
   c. Gross subtype (e.g., polypoid, ulcerating, stricturing, annular, infiltrative, linitis plastica).
   d. Dimensions (state longitudinal and transverse dimensions, unless tumor is circumferential)
   e. Macroscopic depth of invasion (the final T stage requires histological confirmation)
   f. Appearance of serosa deep to tumor (e.g., retracted)
   g. Appearance of mesorectal excision in the case of rectal cancer (complete when invested by shiny fascia and with only minor breaches <5 mm across, nearly complete but with breaches in fascia greater than 5 mm, incomplete with breaches extending to the muscularis propria) [30].

Note: Consideration should be given to transverse slicing of well-fixed but unopened rectal specimens for the assessment of mesorectal spread and clearance at the circumferential resection margin (painted with ink before fixation) [36]. This procedure avoids distortion of the mesorectum that occurs when opening the specimen anteriorly (where the mesorectum is thinnest). Digital photographs of the bowel rings also provide a direct comparison with slices obtained by imaging modalities and are useful for surgical correlation. The various measurements of the tumor can be reconstructed from the rings. Routine blocks for histology can be taken from the rings after photography.

5. Presence of features of obstruction (proximal dilatation)
6. Presence of perforation
7. Additional pathology (e.g., polyps, inflammatory bowel disease, diverticular disease)
8. Lymph nodes identified
9. Tissue submitted for special investigation

B. Diagnostic information

1. Site of tumor and part of bowel resected
2. Histological type: the WHO/UICC classification of colorectal adenocarcinoma is recommended [14]
   a. Adenocarcinoma, NOS
   b. Mucinous carcinoma (>50% mucinous)
   c. Signet ring cell carcinoma (>50% signet ring cells)
   d. Squamous cell carcinoma
   e. Adenosquamous carcinoma
   f. Small-cell undifferentiated carcinoma
   g. Medullary carcinoma
   h. Undifferentiated carcinoma
   i. Carcinoid, NOS
   j. Other(specify)

Note: In mucinous carcinoma, 50% of the area of the tumor should comprise epithelium that is differentiated towards mucin production as evidenced by the presence of mucin [identified haematoxylin and eosin (H&E) sections] that is intracellular and/or luminal and/or interstitial. This recommendation differs slightly from the WHO classification of mucinous carcinoma that stipulates that >50% of the tumor should be composed of mucin. It is more meaningful biologically to focus on differentiation by epithelium towards mucin production rather than the amount of mucin that happens to accumulate in distended glands or extracellular pools.

Medullary carcinoma has a solid pattern overall, but cribriforming and/or areas of glandular differentiation may identify it as a variant of adenocarcinoma. These tumors show relatively little nuclear pleomorphism. Nuclei are often vesicular with a prominent nucleolus, while cytoplasm is abundant and eosinophilic. The tumors are very well circumscribed and are associated with marked lymphocytic infiltration. Many show DNA microsatellite instability and the prognosis is relatively good despite the lack of glandular differentiation. We recommend that medullary carcinoma should not be graded (grade not applicable). While tumor typing does not have major prognostic significance, the fact that certain types (mucinous and signet ring as well as medullary) are associated with DNA microsatellite instability and Lynch syndrome (hereditary nonpolyposis colorectal cancer) provides a justification for reporting these variants [51].

3. Histological grade: A modification of the WHO/UICC classification is recommended [14].
    a. Well differentiated: Simple or complex tubules, easily discerned nuclear polarity, uniformity of nuclear size, close resemblance to benign precursor lesion.
    b. Moderately differentiated: Less regular glandular differentiation, nuclear polarity poorly discerned or lost.
    c. Poorly differentiated: Highly irregular glands or loss of glandular differentiation and loss of nuclear polarity.

Note: The terms well, moderate and poor differentiation are equivalent to Grades 1-3 in the UICC/TNM/AJCC systems. Grading is subjective, particularly for mucinous carcinoma, but the distinction between low-grade (well and moderate) vs high grade (poor) has been shown to be prognostically useful [33]. Signet ring cell carcinoma should be Grade III or poorly differentiated. Grade IV applies to undifferentiated carcinoma and is grouped with high-grade. The use of a four grade (I–IV) or a two grade system (low vs high grade) is equally acceptable but we recommend that grading be based on the worst area even if this does not predominate [20]. However, the worst area should be distinguished from the finding at the invasive margin of focal de-differentiation or tumor budding (see B.4 below). Undifferentiated carcinoma should be distinguished from the relatively undifferentiated medullary carcinoma that is not associated with a particularly adverse prognosis. We recommend that medullary carcinoma should not be graded.

4. Tumor budding.

Note: Tumor budding refers to the de-differentiation or loss of cell cohesion at the invasive margin that gives rise to single tumor cells or small clusters of up to four cells. Tumor budding is associated with poor prognosis, an infiltrative invasive margin, vascular invasion, lymph node metastasis and distant metastasis [15, 16, 25, 27, 44, 50]. Because of the adverse prognostic effect, the possibility of quantifying tumor budding [44], and the possible confusion of tumor budding with poor differentiation we recommend that this feature be distinguished from tumor grade and scored separately as present or absent.

5. Depth of invasion: This is based on the T component of the TNM classification [1].
    a. Invasion of submucosa but not muscularis propria (T1).
    b. Invasion into but not through the muscularis propria (T2).
    c. Invasion through the muscularis propria into subserosal adipose tissue and/or mesenteric fat (T3).
    d. Invasion into adjacent organs (state which) (T4a).
    e. Invasion through serosa with tumor on free peritoneal surface (T4b). State if accompanied by perforation.

Note on spread beyond muscularis propria (T3): The outer edge of the muscularis propria was used initially in the Dukes classification as the line of demarcation for determining whether a tumor was within or beyond the bowel wall. This practice was followed by the TNM system. T3 indicates spread in continuity beyond the bowel wall and does not apply to either lymphatic or venous invasion within the mesenteric layer. It should be noted that this long established TNM rule does not appear to apply to nodules of tumor in the mesenteric fat that lack the ‘form and smooth contour’ of a replaced lymph node. These are classified in the T category (i.e. T3) in the 6th editions of the TNM staging system and AJCC staging manual and the CAP guidelines and despite the fact that these examples of discontinuous extramural extension are considered as the likely sequelae of venous invasion [1, 47]. As such metastatic deposits are usually associated with advanced disease (at least T3 on the basis of direct spread in continuity), most cases will not present a diagnostic dilemma. Occasionally, cancer may spread as far as the outer edge of the muscularis propria but not beyond. If no muscle separates the cancer from mesenteric tissue then the muscle coat should be interpreted as breached (T3). Studies have shown that the extent of spread beyond the bowel wall has prognostic significance in the case of rectal cancer [26]. However, a large study of colorectal cancer showed that the extent of spread beyond the muscle coat had no impact upon prognosis provided that there was no transperitoneal

spread (T4b) or involvement of the circumferential resection margin [32]. We recommend giving a measurement of the extent of spread beyond the muscularis propria in mm but not the use of T3 substages. This measurement will necessarily be an approximation only when the muscularis propria has been destroyed by tumor.

Note on invasion through serosa: Although invasion into adjacent organs (T4a) and transperitoneal spread (T4b) are grouped together as pT4 for the purposes of deriving a final stage, there is evidence that invasion through the serosa predisposes to tumor spread within the peritoneal cavity and a particularly poor prognosis [42, 43]. Therefore the peritoneal surface deep to the tumor should be carefully sampled, especially in areas of retraction, and positive findings should be reported separately from invasion of adjacent organs. See also comments on staging below (C.1). The determination of transperitoneal spread is not straightforward. T4b should apply when tumor cells are observed on the free peritoneal surface even if admixed with fibrin. When tumor is within 1 mm of the free peritoneal surface this should be recorded as an indication of possible transperitoneal spread but staged as T3 on the basis that the peritoneum serves as an effective barrier to malignant spread. According to the TNM system, stage T4a applies to the finding of macroscopic adherence of the tumor to adjacent organs. If there is no microscopic evidence of invasion of adjacent organs then the pathological stage becomes pT3. We recommend that the pathological report should refer only to a single T stage that is based on microscopic findings.

Note on Tis: Although the TNM/AJCC classification includes a level Tis to represent either in-situ carcinoma or carcinoma showing invasion of lamina propria (intramucosal carcinoma), we note that this practice is based primarily on the aim of achieving a uniform staging system across all organ systems. Because colorectal neoplasia has not be shown to have metastasizing potential until it has invaded the submucosa we prefer to avoid the term Tis and instead use the term high grade dysplasia (equivalent to high grade intra-epithelial neoplasia). We also note that it is frequently impossible to determine whether or not there is microscopic invasion of the lamina propria except in the rarely encountered situations of poorly differentiated or signet ring cell carcinoma. Adenomas with Tis should be regarded as adenomas and not as carcinomas for the purposes of diagnosis and cancer registration.

6. Lymph node metastases - stated as number of involved nodes and total number of nodes. Using the TNM system, N0 indicates no nodes with metastases, N1 indicates 1–3 nodes with metastases and N2 indicates four or more nodes with metastases. This applies only to the regional lymph nodes that directly drain the tumor. Involvement of the nodes obtained from the lateral pelvic wall (e.g. common or external iliac lymph nodes) indicates distant disease and is staged as M1 in the TNM system [1]. Direct invasion of a regional lymph node should be regarded as a metastasis.

Note on lymph node numbers: All macroscopically evident (palpable and/or visible) lymph nodes in a well-fixed specimen should be dissected and examined histologically [5, 9, 24]. Many factors influence lymph node numbers apart from the care taken in the dissection [2, 56] and the range for node numbers can be from 0 to 100 or more. There is ***no unacceptably low number of lymph nodes*** for an individual dissection but the ***mean number of nodes*** in a series of dissections gives an indication of good practice and should be approximately 12–15. In the case of rectal cancer and the increasing use of neo-adjuvant (pre-operative) radiotherapy, the mean number may fall below 12 despite an intense search. The decision to return to the specimen when low numbers of lymph nodes are found will depend on whether the person who performed the initial dissection has a proven track-record for finding lymph nodes. The surgeon-pleasing practice of boosting lymph node numbers by submitting extra blocks of mesenteric fat (after an adequate initial dissection) that may contain minute lymphoid aggregates has not been shown to increase the proportion of lymph node metastasis-positive cases or to improve the survival of lymph node negative cases. The reduced survival in stage II cases with few lymph nodes may be due to factors other than under-staging such as depressed tumor immunity [4, 5, 41]. In lymph node positive cases it is usual to find one or more of the positive nodes in the mesenteric tissues deep to the tumor (the likely location for sentinel nodes). Therefore it is prudent to be particularly careful in examining extramural tissues deep to the tumor. These sub-tumoral nodes may be included within tumor slices if encased by tumor or dissected out if free.

Note on lymph node sampling for metastases: Multiple slicing of lymph nodes, step-sectioning, immunostaining, and molecular technology will increase the metastasis-positive rate and lead to ‘upstaging’ [13, 52, 53]. However, such occult metastatic disease will usually take the form of minute tumor deposits down to cell clusters or even single cells floating in a sinus. The effort of detecting such occult disease is considerable but could be lessened by being combined with ex vivo sentinel lymph node mapping [3, 6, 40]. Nevertheless, sentinel node sampling has a false negative rate for lymph node positivity of around 5–10% [5]. Additionally, there is no consensus that occult metastatic disease detected by immuno-histochemistry or other methods discriminates between high- and low-risk groups of patients [8]. The 6th edition of the TNM classification has finessed the situation by stating that

intra-nodal tumor cell clusters measuring less than 0.2 mm do not constitute metastases and do not affect the N stage [47]. This advice is arbitrary though does make biologic sense and fits with the lack of clinical significance of occult nodal metastases according to the majority of observational data [8]. However, we would prefer to base the diagnostic decision not on an imposed size rule but on evidence of establishment of the metastasis. Single cells or small clusters in a sinus should not be equated with lymph node metastasis but should be recorded if seen. Tumor foci that show evidence of growth (e.g. glandular differentiation, distension of sinus, or stromal reaction) should be diagnosed as a lymph node metastasis irrespective of size.

7. Presence of mesenteric tumor deposits.

Note: Histological examination of dissected nodal structures may disclose the presence of nodules of tumor that are not contained within recognizable lymph nodes. These may be either small lymph nodes or lymphoid aggregates that have been totally replaced by tumor or discontinuous foci of tumor within a perineural, perivascular or intravascular location [10]. The 5th edition of the TNM classification states that such nodules should be counted as lymph nodes if they are greater than 3 mm in diameter [46]. The 6th edition of the TNM classification recognizes the heterogeneity of these lesions and suggests that they be classified as positive lymph nodes if they occur in the connective tissue of a lymph drainage area and have the 'form and smooth contour of a lymph node' (size not stipulated) [1, 47]. If they have an irregular contour then they should be classified under T as discontinuous extramural extension (i.e. T3) (see note on T3 stage under B.5 above). The 6th editions of both TNM and AJCC indicate that nodules with an irregular contour may also be coded as venous invasion. As careful histologic examination of the non-lymph node-like group of metastatic nodules indicates that some cancer foci occur in perineural or perivascular spaces [10], it is unclear why they should all be classed as intra-vascular invasion. It is probable that many represent metastasis within a minute lymphoid aggregate. The preceding points appear to relate to nodules that were identified macroscopically during dissection and are therefore likely to be larger than 3 mm. Metastatic or discontinuous tumor foci that are identified only ***microscopically*** pose further difficulty. The 6th edition of AJCC cancer staging manual indicates that the presence of multiple ***microscopic*** metastatic foci in pericolic fat (it is unclear if this is meant to exclude perirectal fat) should be equated with lymph node involvement for the purposes of nodal staging [1]. The 6th edition of TNM classification of malignant tumors does not discuss the significance of multiple microscopic metastatic foci in pericolic fat [47]. Taken to its logical conclusion, the preceding advice can result in lesions with identical microscopic appearances being diagnosed as either lymph nodes or vascular invasion merely on the basis of size, number, and anatomical location. It is necessary to disentangle the preceding incompatible suggestions in a way that recognizes the adverse significance of mesenteric tumor nodules but avoids subjective assessments and the use of arbitrary advice relating to either the size or number of lesions. The use of the subjective descriptor 'form and smooth contour of a lymph node' may lead to inappropriate upstaging [17]. In the light of this finding, the Royal College of Pathologists (United Kingdom) (http://www.rcpath.org/resources/pdf/UpdatedStatementonTNM61edited.pdf) has elected to recommend that its members follow the guidelines of the 5th and not the 6th TNM classification. The current dilemma can be traced to two facts: (1) the historical precedent of placing too much reliance on an unnecessarily limited set of prognostic variables (such as lymph node status) for the purposes of stratifying patients and making therapeutic decisions, and (2) the impossibility of determining the actual nature of a high proportion of mesenteric deposits. It is recommended that in the situation where small mesenteric tumor deposits cannot be diagnosed as replaced lymph nodes, the total number and the size of the largest deposit should be recorded and the clinician should be made aware that these lesions are likely to be associated with an adverse prognosis [10]. Fortunately, small metastatic deposits in the mesentery tend to be associated with unequivocal nodal involvement so that final N stage is not often determined on the basis of an isolated mesenteric deposit.

8. Other sites biopsied for metastatic disease (e.g. peritoneum, adjacent organs, liver, ovary). Discontinuous peritoneal deposits that are not included in sections of the tumor bed should be counted as distant disease or M1 in the TNM system.
9. Adequacy of local excision: circumferential (deep, lateral or radial), proximal and distal. Assessment of the proximal and distal resection margins is performed routinely in surgical specimens of colorectal cancer, as it is in other organs, but these margins are rarely involved unless close (less than 2 cm) or the tumor is poorly differentiated. In the case of the rectum, the mesorectum below the peritoneal reflection should be inked and after adequate fixation the tumor should be sliced transversely at 2–3 mm intervals [37]. Alternatively the unopened rectal resection can be sliced into 2–3 mm rings (see A.4 above). Tumor slices should be selected for histology on the basis of close proximity of the advancing tumor edge to the inked circumferential margin and the presence in the mesorectum of lymph nodes or veins containing suspected tumor. In the TNM system R0 indicates no margin involvement

(or residual disease), R1 indicates microscopic involvement (excision complete grossly), and R2 indicates gross residual disease that was not resected. We do not use R for coding purposes and regard its use as optional. The distance from the advancing edge of the tumor to the closest resection margin should be given in mm. A tumor margin should be regarded as involved microscopically if there is tumor within 1 mm from a resection margin [36]. This advice is based on a majority of studies though an increased incidence of local recurrence was described in one study when tumor was within 2 mm of the circumferential resection margin [29]. Similar consideration should be given to the deep or non-peritonealized resection margin in other parts of the colon (e.g. cecum, ascending colon, and descending colon) and when tumor is growing beyond a section of bowel wall that is retroperitoneal.

10. Pre-operative radiotherapy and tumor regression. Changes secondary to pre-operative radiotherapy include ulceration, fibrosis of submucosa, tumor regression, mucin lakes, calcification, shrinkage of lymph nodes, and down-staging [28, 39, 54]. Pathological staging after therapy (designated ypTNM) is based on the finding of viable tumor cells and not on the inferred site of involvement. Therefore mucin pools with no viable tumor should not be used to infer a stage with the ypTNM system. However, it is reasonable to suggest a pre-treatment stage on the basis of the presence of mucin lakes in the bowel wall or lymph nodes. Tumor regression should be scored as: (1) complete or marked, (2) moderate, (3) little or none [39]. It may be necessary to sample tissues widely to demonstrate complete regression, though the prognosis is unlikely to be affected by the persistence of small tumor foci [39]. At least five blocks should be taken from the center of the lesion. If no tumor is found then the entire area should be blocked and consideration given to step-sectioning to deem that a tumor has regressed completely. The pathologist should be told the location of the tumor before radiotherapy so that sampling of tissues can be targeted efficiently. Given the tendency of radiotherapy to cause lymph node atrophy all deposits of tumor in the mesentery should be equated with lymph node metastasis.
11. Inflammatory infiltrate. A peritumoral inflammatory reaction that includes lymphocytes has been associated with a favorable prognosis but the assessment of this feature is subjective [20]. Tumor infiltrating (intra-epithelial) lymphocytes and a Crohn-like reaction are also associated with a favorable prognosis and with the presence of DNA microsatellite instability (occurring in both Lynch syndrome and sporadically) [7, 11, 12, 21, 38, 45]. Relatively low numbers of tumor infiltrating lymphocytes have been shown to be both sensitive and specific for the presence of DNA microsatellite instability [12, 45]. We recommend that ten X40 high-power fields be assessed and that tumor infiltrating lymphocytes are scored as present if at least one field shows five intra-epithelial lymphocytes. A Crohn-like reaction may be scored as present if at least four transmural lymphoid aggregates are counted in an X4 field.
12. Venous invasion. We advocate the recording of invasion of extramural veins [48, 49] but regard the use of a V code as optional.
13. Other significant disease (e.g. polyps, inflammatory bowel disease, diverticular disease).
14. If it is not possible to provide prognostically important information then this should be stated in the report.

C. Features considered optional in the final report

The following features are considered optional because they represent specific institutional preferences (e.g. the use of staging that requires the specific marking of lymph nodes), there is no widespread consensus with respect to their prognostic significance, or their assessment is subjective and has been associated with inter-observer variation.

1. Stage: The repeated modifications of the TNM system are not only difficult to keep up with by all those involved with patient care but continue to have shortcomings with respect to the prognostic grouping that are generated. The over-dependence on a static staging system and failure to heed the independent effects of other adverse prognostic features (e.g. incomplete resection, transperitoneal spread, perforation, venous invasion, absence of lymphocytic infiltration, tumor grade and budding, and mesenteric deposits) cannot lead to the best possible prognostic grouping. We regard the conversion of T and N findings into a final stage (I to IV) as optional as critically important information regarding distant disease (M) is rarely known to the pathologist. The TNM Supplement states that the final TNM classification rests with a designated individual who has access to the most complete data [55]. We also find the proliferation of letters for coding purposes, the

changing rules with each TNM edition, and the inevitable differences from organ to organ a source of confusion and irritation. The use of 'p' for pathological staging is very useful in clinicopathological correlation but is redundant in pathology reports. The pathologist is encouraged to place greater emphasis on the accurate identification of prognostic information and including this in the report by means of simple and unambiguous language.

a. Tis and T0: We advocate the term high grade dysplasia instead of Tis (see B.5 above). When no tumor is found in a surgical resection specimen after excision of a malignant adenoma, we advocate giving a 'global' T1 stage rather than a T0 stage in the situation where both polyp and surgical specimen are available and the findings can be integrated. Stage T0 may be used when it is not possible to review the initial lesion. The prefix yp serves as a useful indication that pathological staging has followed neo-adjuvant therapy. For example, ypT0 serves to indicate histologically proven complete tumor regression after neo-adjuvant radiotherapy.

b. **New staging in 6th edition of TNM and AJCC** [1, 47]:

Stage II has been stratified as IIA (T3 N0 M0) and IIB (T4 N0 M0).

Stage III has been stratified as IIIA (T1-T2 N1 M0), IIIB (T3-T4 N1 M0), and IIIC (any T N2 M0). The good prognosis of lymph node positive cancers that are limited to the bowel wall has been known for some time [22]. This IIIA category was included previously as Astler-Coller stage C1. An evaluation of this re-invented stage has shown that the prognosis is better than for stage IIB disease [34]. Whether this is due to the fact that stage III patients are more likely to receive adjuvant chemotherapy or because stage IIB disease includes patients with transperitoneal spread who at high risk of intra-abdominal recurrence is unknown [42, 43]. This illustrates the importance of recording all the discrete elements that are collapsed and lost within the final TNM stage.

c. Perforation and transperitoneal spread: The 6th edition of the TNM system still fails to incorporate the adverse feature of perforation [35] in TNM staging. Additionally, by failing to separate transperitoneal spread (T4b) and involvement of adjacent organs (T4a) (both grouped as T4) it will be difficult to determine the basis for the poor outcome of stage IIB disease [34].

2. Results of ancillary tests and special investigations (e.g. (1) diagnostic markers such as differentiation antigens and loss of expression of DNA mismatch repair proteins, (2) prognostic markers such as alterations of TP53 and KRAS, loss of heterozygosity at 18q, DNA microsatellite status, gene expression profiling, (3) adjuncts to staging such as sentinel node sampling, and (4) predictive markers such as thymidylate synthase and EGFR).
3. Specific named lymph nodes. This has disappeared from the 6th edition of the TNM system as has N3 stage. Surgeons may now identify one or more sentinel nodes as part of lymphatic mapping or may sample the apical node. Prognosis worsens progressively with increasing numbers of involved nodes and additional N categories have been suggested on the basis of node numbers [34].
4. Nature of invasive tumor margin as expanding or infiltrating. All cancers infiltrate normal tissues. The term 'infiltrating' applies to the subset with extensive and diffuse dissection of normal tissues by tumor regardless of the grade of differentiation and has been linked with a poor prognosis [19, 23].
5. Peritumoral inflammatory reaction. An inflammatory reaction at the invasive margin that includes a population of lymphocytes has been associated with a good prognosis. As the assessment is subjective and more objective aspects of lymphocytic infiltration have been recommended for inclusion in the report, this feature is left as optional (see B.11).
6. Lymph vessel invasion. Invasion of small vessels is particularly important in locally excised colorectal cancer where it serves as an indication for additional possible lymph node involvement and hence for radical surgery [31]. While identified as a prognostic factor, small vessel involvement is a somewhat subjective feature. The use of an L code is optional.
7. Residual adenoma at the edge of the carcinoma. While unlikely to be of prognostic importance it is logical to note this observation along with the presence of discrete polyps. In addition, serrated polyps have been linked with subtypes of colorectal cancer showing DNA microsatellite instability and/or DNA methylation [18].
8. Presence of one or more histological features linked with DNA microsatellite instability (mucinous, signet ring cell or medullary type, tumor infiltrating lymphocytes, Crohn-like reaction). The revised Bethesda guidelines recommend testing for DNA microsatellite status if one or more of these features is present and the patient is <60 years of age [51].

ASSOCIATION OF DIRECTORS OF ANATOMIC AND SURGICAL PATHOLOGY
Final Anatomic Diagnosis Checklist

COLORECTAL CARCINOMA

Accession No.: **Part No.** **Date:**
Patient Name:

ORGAN:	SITE:	OPERATION:
Small bowel	Cecum	Total colectomy
Appendix	Ascending colon	Hemicolectomy (R)
Colon	Hepatic flexure	Hemicolectomy (L)
Rectum	Transverse colon	Segmental resection
Anus	Splenic flexure	Anterior resection
	Descending colon	Abdominoperineal
	Sigmoid colon	resection
	Rectosigmoid	
	Rectum	
	Right colon, NOS	
	Left colon, NOS	
Other_____	Other_____	Other_____

Tumor Size: *Required* _____ cm. (long) x _____ cm. (trans) (unless circumferential)

Other gross features: *Required*

Describe appearance of tumor, state of mesorectum, presence of obstruction, presence of perforation, distance (cm) from closest margin (proximal, distal, unknown)

Tumor type: *Required*

Adenocarcinoma, NOS
Mucinous
(>50% of tumor demonstrates mucinous differentiation)
Signet Ring Cell Type
(>50% of tumor demonstrates signet ring cell differentiation)
Squamous cell carcinoma
Adenosquamous carcinoma
Small cell undifferentiated carcinoma
Medullary carcinoma
Undifferentiated carcinoma
Carcinoid, NOS
Other:_____

ASSOCIATION OF DIRECTORS OF ANATOMIC AND SURGICAL PATHOLOGY
Final Anatomic Diagnosis Checklist

COLORECTAL CARCINOMA

Histologic Grade: *Required*

I	(= well differentiated)
II	(= moderately differentiated)
III	(= poorly differentiated)
IV	(= undifferentiated)
Not applicable	(applies to medullary carcinoma)

Note: *I, II and III, IV may be combined as low and high grade respectively*

Tumor budding: *Required*

Present or absent

Depth of Tumor Invasion: *Required*

No evidence of primary tumor (T0)
High grade dysplasia (no invasion beyond muscularis mucosae (Tis)
Tumor invades submucosa but does not invade into muscularis propria (T1)
Tumor invades muscularis propria (T2)
Tumor invades through the muscularis propria into mesentery or subserosa (T3)*
Tumor invades adjacent organs (T4a)*
Tumor shows transperitoneal spread (T4b)* ϕ

*State extent of spread beyond muscularis propria (mm): _____
ϕState if spread is within 1mm of peritoneal membrane but stage as T3: Yes/No

Margins of Resection: *Required*

No tumor identified at margins (R0)
Tumor present at proximal/distal/radial margin, microscopically (R1)
Tumor present at proximal/distal/radial margin, grossly (R2)

State clearance at deep or radial resection margin (mm): _____

Note: radial margin involved if tumor is within 1mm

Lymph nodes (regional): ***Required***

Number examined:_____
Number positive:_____
Comments:_____
Nodes marked by surgeon (e,g. apical or sentinel) : _____

ASSOCIATION OF DIRECTORS OF ANATOMIC AND SURGICAL PATHOLOGY
Final Anatomic Diagnosis Checklist

COLORECTAL CARCINOMA

Mesenteric tumor nodules: *Required*

Present (number and size of largest) or absent

Extramural venous invasion: *Required*

Identified
Not Identified

Lymphatic invasion: *Optional*

Identified
Not Identified

Lymphocytic infiltration:

Tumor infiltrating lymphocytes: *Required*	Present or absent
Crohn-like reaction: *Required*	Present or absent
Peritumoral: *Optional*	Present or absent

Features of microsatellite instability present: *Optional*

Present if one or more of following features is present: mucinous, signet ring cell, or medullary type, tumor infiltrating lymphocytes or Crohn-like reaction

Pattern of invasion: *Optional*

Tumor invades with broad front
Tumor invades diffusely with dissecting glands

Tumor regression grade: *Required*

Not applicable
Complete, incomplete, or little/none

Residual adenoma in carcinoma: *Optional*

If yes, specify type: _____

Additional findings: *Required*

Diverticular disease, Ulcerative colitis, Crohn disease, Familial Adenomatous Polyposis, other forms of polyposis, etc.

Specify: _____

ASSOCIATION OF DIRECTORS OF ANATOMIC AND SURGICAL PATHOLOGY
Final Anatomic Diagnosis Checklist

COLORECTAL CARCINOMA

Polyps present (specify type, number, size): _____

Ancillary studies: *Optional*

Special stains are performed, the results are as follows:
A. _____
B. _____
C. _____
D. _____
Interpretation_____
_____

Immunohistochemical studies are performed, the results are as follows:
A. _____
B. _____
C. _____
D. _____
Interpretation_____
_____

pTN Stage: *Required*

A. Primary Tumor

pTX Primary tumor cannot be assessed
pT0 No evidence of primary tumor
pTis Carcinoma in situ and intramucosal carcinoma (high grade dysplasia)
pT1 Tumor invades submucosa
pT2 Tumor invades muscularis propria
pT3 Tumor invades through the muscularis propria into subserosa or into nonperitonealized pericolic or perirectal tissue
pT4a Tumor invades other organs or structures
pT4b Tumor perforates the visceral peritoneum

B. Regional Lymph Nodes

pNX Regional lymph nodes cannot be assessed
pN0 No regional lymph node metastasis
pN1 Metastasis in 1 to 3 regional lymph nodes
pN2 Metastasis in 4 or more regional lymph nodes

ASSOCIATION OF DIRECTORS OF ANATOMIC AND SURGICAL PATHOLOGY
Final Anatomic Diagnosis Checklist

COLORECTAL CARCINOMA

C. Distant Metastasis

pMX Cannot be assessed
pM0 No distant metastasis
pM1 Distant metastasis

Reference:

AJCC Cancer Staging Manual. Lippincott-Raven Press, 6th edition, 2002 (pg. 113-119).

References

1. AJCC cancer staging manual (2002). Lipincott-Raven, Philadelphia
2. Baxter NN, Virnig DJ, Rothenberger DA, Morris AM, Jessurun J, Virnig BA (2005) Lymph node evaluation in colorectal cancer patients: a population-based study. J Natl Cancer Inst 97:219–225
3. Bell SW, Mourra N, Flejou JF, Parc R, Tiret E (2005) Ex vivo sentinel lymph node mapping in colorectal cancer. Dis Colon Rectum 48:74–79
4. Berger AC, Sigurdson ER, LeVoyer T, Hanlon A, Mayer RJ, Macdonald JS, Catalano PJ, Haller DG (2005) Colon cancer survival is associated with decreasing ratio of metastatic to examined lymph nodes. J Clin Oncol 23:8706–8712
5. Cserni G (2002) Nodal staging of colorectal carcinomas and sentinel nodes. J Clin Pathol 56:327–335
6. Doekhie FS, Peeters KCMJ, Kuppen PJK, Mesker WE, Tanke HJ, Morreau H, van de Velde CJH, Tollenaar RA (2005) The feasibility and reliability of sentinel node mapping in colorectal cancer. Eur J Surg Oncol 31:854–862
7. Dolcetti R, Viel A, Doglioni C, Russo A, Guidoboni M, Capozzi E, Vecchiato NEM, Fornasarig M, Boiocchi M (1999) High prevalence of activated intraepithelial cytotoxic T lymphocytes and increased neoplastic cell apoptosis in colorectal carcinomas with microsatellite instability. Am J Pathol 154:1805–1813
8. Fisher ER, Colangelo L, Wieand S, Fisher B, Wolmark N (2003) Lack of influence of cytokeratin-positive mini micrometastases in "negative node" patients with colorectal cancer: Findings from the National Surgical Adjuvant Breast and Bowel Projects protocols R-01 and C-01. Dis Colon Rectum 46:1021–1026
9. Goldstein NS (2002) Lymph node recoveries from 2427 pT3 colorectal resection specimens spanning 45 years: recommendations for a minimum number of recovered lymph nodes based on predictive probabilities. Am J Surg Pathol 26:179–189
10. Goldstein NS, Turner JR (2000) Pericolonic tumor deposits in patients with T3N+MO colon adenocarcinomas. Markers of reduced disease free survival and intra-abdominal metastases and their implications for TNM classification. Cancer 88:2228–2238
11. Gologan A, Krasinskas A, Hunt J, Thull DL, Farkas L, Sepulveda AR (2005) Performance of the revised Bethesda guidelines for identification of colorectal carcinomas with high level microsatellite instability. Arch Pathol Lab Med 129:1390–1397
12. Greenson JK, Bonner JD, Ben-Yzhak O, Cohen HI, Miselvich I, Resnick MB, Trougouboff P, Tomsho LD, Kim E, low M et al (2003) Phenotype of microsatellite unstable colorectal carcinomas. Am J Surg Pathol 27:563–570
13. Greenson JK, Isenhart CE, Rice R, Mojzisik C, Houchens D, Martin EWJ (1994) Identification of occult micrometastases in pericolic lymph nodes of Dukes' B colorectal cancer patients using monoclonal antibodies against cytokeratin and CC49. Correlation with long-term survival. Cancer 73:563–569
14. Hamilton SR, Aaltonen LA (2000) World Health Organization classification of tumours. Pathology and genetics. IARC, Lyon
15. Hase K, Shatney C, Johnson D, Trollope M, Vierra M (1993) Prognostic value of tumor "budding" in patients with colorectal cancer. Dis Colon Rectum 36:627–635
16. Hori H, Fujimori T, Fujii S, Ichikawa K, Ohkura Y, Tomita S, Ono Y, Imura J, Kuroda Y (2005) Evaluation of tumor cell dissociation as a predictive marker of lymph node metastasis in submucosal invasive colorectal carcinoma. Dis Colon Rectum 48:938–945
17. Howarth SM, Morgan JM, Williams GT (2004) The new (6th edition) TNM classification of colorectal cancer—a stage too far. Gut 53:A81
18. Jass JR (2005) Serrated adenoma of the colorectum and the DNA-methylator phenotype. Nat Clin Pract Oncol 2:398–405
19. Jass JR, Ajioka Y, Allen JP, Chan YF, Cohen RJ, Nixon JM, Radojkovic M, Restall AP, Stables SR, Zwi LJ (1996) Assessment of invasive growth pattern and lymphocytic infiltration in colorectal cancer. Histopathology 28:543–548
20. Jass JR, Atkin WS, Cuzick J, Bussey HJR, Morson BC, Northover JMN, Todd IP (1986) The grading of rectal cancer: historical perspectives and a multivariate analysis of 447 cases. Histopathology 10:437–459
21. Jass JR, Do K-A, Simms LA, Iino H, Wynter C, Pillay SP, Searle J, Radford-Smith G, Young J, Leggett B (1998) Morphology of sporadic colorectal cancer with DNA replication errors. Gut 42:673–679
22. Jass JR, Love SB (1989) Prognostic value of direct spread in Dukes' C cases of rectal cancer. Dis Colon Rectum 32:477–480
23. Jass JR, Love SB, Northover JMA (1987) A new prognostic classification of rectal cancer. Lancet 1:1303–1306
24. Jass JR, Morson BC (1987) Reporting colorectal cancer. J Clin Pathol 40:1016–1023
25. Kazama S, Watanabe T, Ajioka Y, Kanazawa H, Nagawa H (2006) Tumour budding at the deepest invasive margin correlates with

lymph node metastasis in submucosal cancer detected by anti-cytokeratin antibody CAM5.2. Br J Cancer 94:293–298
26. Merkel S, Mansmann U, Siassi M, Papadopoulos T, Hohenberger W, Hermanek P (2001) The prognostic inhomogeneity in pT3 rectal carcinomas. Int J Colorect Dis 16:298–304
27. Morodomi T, Isomoto H, Shirouzu K, Kakegawa K, Irie K, Morimatsu M (1989) An index for estimating the probability of lymph node metastasis in rectal cancers. Lymph node metastasis and the histopathology of actively invasive regions of cancer. Cancer 63:539–543
28. Nagtegaal ID, Marijnen CAM, Kranenbarg EK, Mulder-Stapel A, Hermans J, van de Velde CJH, van Krieken JHJM (2002) Short-term preoperative radiotherapy interferes with the determination of pathological parameters in rectal cancer. J Pathol 197:20–27
29. Nagtegaal ID, Marijnen CAM, Kranenbarg EK, van de Velde CJH, van Krieken JHJM (2002) Circumferential margin involvement is still important predictor of local recurrence in rectal carcinoma. Not one millimeter but two millimeters is the limit. Am J Surg Pathol 26:350–357
30. Nagtegaal ID, van de Velde CJH, van der Worp E, Kapiteijn E, Quirke P, van Krieken JH (2002) Macroscopic evaluation of rectal cancer resection specimen: clinical significance of the pathologist in quality control. J Clin Oncol 20:1729–1734
31. Nascimbeni R, Burgart LJ, Nivatvongs S, Larson DR (2002) Risk of lymph node metastasis in T1 carcinoma of the colon and rectum. Dis Colon Rectum 45:200–206
32. Newland RC, Chapuis PH, Smyth EJ (1987) The prognostic value of substaging colorectal carcinoma. A prospective study of 1,117 cases with standardized pathology. Cancer 60:852–857
33. Newland RC, Dent OF, Chapuis PH, Bokey L (1995) Survival after curative resection of lymph node negative colorectal carcinoma: a prospective study of 910 patients. Cancer 76:564–571
34. O'Connell JB, Maggard MA, Ko CY (2004) Colon cancer survival rates with the new American Joint Committee on Cancer sixth edition staging. J Natl Cancer Inst 96:1420–1425
35. Petersen VC, Baxter KJ, Love SB, Shepherd NA (2002) Identification of objective pathological prognostic determinants and models of prognosis in Dukes' B colon cancer. Gut 51: 65–69
36. Quirke P (2003) Training and quality assurance for rectal cancer: 20 years of data is enough. Lancet Oncol 4:695–702
37. Quirke P, Durdey P, Dixon MF, Williams NS (1986) Local recurrence of rectal adenocarcinoma due to inadequate surgical resection. Histopathological study of lateral tumour spread and surgical excision. Lancet 2:996–999
38. Ropponen KM, Eskelinen MJ, Lipponen PK, Alhava E, Kosma V-M (1997) Prognostic value of tumour-infiltrating lymphocytes (TILs) in colorectal cancer. J Pathol 182:318–324
39. Ryan R, Gibbons D, Hyland JMP, Treanor D, White A, Mulcahy HE, O'Donoghue DP, Moriarty M, Fennely D, Sheahan K (2005) Pathological response following long-course neoadjuvant chemo-radiotherapy for locally advanced rectal cancer. Histopathology 47:141–146
40. Saha S, Dan AG, Viehl CT, Zuber M, Wiese D (2005) Sentinel lymph node mapping in colon and rectal cancer: its impact on staging, limitations, and pitfalls. Cancer Treat Res 127:105–122
41. Sarli L, Bader G, Iusco D, Salvemini C, Mauro DD, Mazzeo A, Regina G, Roncoroni L (2005) Number of lymph nodes examined and prognosis of TNM stage II colorectal cancer. Eur J Cancer 41: 272–279
42. Shepherd NA, Baxter KJ, Love SB (1995) Influence of local peritoneal involvement on pelvic recurrence and prognosis in rectal cancer. J Clin Pathol 48:849–855
43. Shepherd NA, Baxter KR, Love SB (1997) The prognostic importance of peritoneal involvement in colonic cancer: a prospective evaluation. Gastroenterology 112:1096–1102
44. Shinto E, Mochizuki H, Ueno H, Matsubara O, Jass JR (2005) A novel classification of tumour budding in colorectal cancer based on the presence of cytoplasmic pseudo-fragments around budding foci. Histopathology 47:25–31
45. Smyrk TC, Watson P, Kaul K, Lynch HT (2001) Tumor-infiltrating lymphocytes are a marker for microsatellite instability in colorectal cancer. Cancer 91:2417–2422
46. Sobin LH, Wittekind C (1997) TNM Classification of malignant tumours. Wiley-Liss, New York
47. Sobin LH, Wittekind C (2002) TNM Classification of malignant tumours. Wiley-Liss, New York
48. Talbot IC, Ritchie S, Leighton M, Hughes AO, Bussey HJ, Morson BC (1981) Invasion of veins by carcinoma of rectum: method of detection, histological features and significance. Histopathology 5:141–163
49. Talbot IC, Ritchie S, Leighton MH, Hughes AO, Busey HJ, Morson BC (1981) Spread of rectal cancer within veins. Histologic features and clinical significance. Histopathology 5: 141–163
50. Ueno H, Murphy J, Jass JR, Mochizuki H, Talbot IC (2002) Tumour 'budding' as an index to estimate the potential of aggressiveness in rectal cancer. Histopathology 40:127–132
51. Umar A, Boland CR, Terdiman JP, Syngal S, de la Chapelle A, Ruschoff J, Fishel R, Lindor NM, Burgart LJ, Hamelin R et al (2004) Revised Bethesda guidelines for hereditary nonpolyposis colorectal cancer (Lynch syndrome) and microsatellite instability. J Natl Cancer Inst 96:261–268
52. van Wyk Q, Hosie KB, Balsitis M (2000) Histopathological detection of lymph node metastases from colorectal carcinoma. J Clin Pathol 53:685–687
53. Verrill C, Carr NJ, Wilkinson-Smith E, Seel EH (2004) Histopathological assessment of lymph nodes in colorectal carcinoma: does triple levelling detect significantly more metastases? J Clin Pathol 57:1165–1167
54. Wheeler JMD, Warren BF, Jones AC, Mortensen NJM (1999) Preoperative radiotherapy for rectal cancer: implications for surgeons, pathologists and radiologists. Br J Surg 86:1108–1120
55. Wittekind C, Greene FL, Henson DE, Hutter RVP, Sobin LH (2003) TNM Supplement. A commentary on uniform use. Wiley-Liss, New York
56. Wright FC, Law CHL, Last L, Khalifa M, Arnaout A, Naseer Z, Klar N, Gallinger S, Smith AJ (2003) Lymph node retrieval and assessment in stage II colorectal cancer: a population-based study. Ann Surg Oncol 10:903–909

Virchows Arch (2007) 450:15–23
DOI 10.1007/s00428-006-0301-7

RECOMMENDATION

Recommendations for the reporting of pleural mesothelioma

Kelly J. Butnor · Thomas A. Sporn · Nelson G. Ordonez

Received: 22 August 2006 / Accepted: 23 August 2006 / Published online: 25 November 2006
© Springer-Verlag 2006

Introduction for ADASP reporting guidelines

It has been evident for decades that pathology reports are very variable even within a single institution. Standardization of reporting is the optimal way to insure that information necessary for patient management, prognostic and predictive factor assessment, grading, staging, analysis of outcomes, and tumor registries are included in pathology reports. In recent years, two societies [first, the Association of Directors of Anatomic and Surgical Pathology (ADASP) and then the College of American Pathologists (CAP)] have undertaken to publish guidelines for the reporting of common cancers. The CAP assigned multidisciplinary groups of pathologists, surgeons, and radiation and medical oncologists to develop the protocols. Other pathologists and clinicians then reviewed them. After those reviews, the protocols were reviewed by multiple CAP committees and finally approved by the Board of Governors.

The ADASP, in contrast, chose a pathologist expert in each field to assemble a group from within the pathology community (with clinician input if desired) to write specific cancer protocols. These were then approved by the ADASP Council and subsequently by the membership. Even though both societies began the process at approximately the same time, the streamlined approach adopted by the ADASP enabled them to publish years earlier in pathology journals frequented by anatomic pathologists. While the formats are somewhat different, the contents are essentially the same.

The American College of Surgery Commission on Cancer (ACSCoC) accredits cancer centers in the USA. Recently, the CoC decided to require elements deemed as essential by the CAP to be described in all pathology reports in their accredited cancer centers as of January 2004. Importantly, they do not require that the specific CAP protocols or synoptic reports be utilized. ADASP has updated all of its protocols to comply with the CoC requirements in the form of 37 uniform checklists. The checklists use the staging criteria cited in the American Joint Committee on Cancer 2002 Staging Manual (sixth edition) but include a variety of other references listed in each of the checklists. Moreover, the checklists are formatted for ease of use. They may be used as templates for uniform reporting and are designed to be compatible with voice-activated transcription.

The different elements in these revised ADASP Diagnostic Checklists have been divided into *required* and *optional*. The term *required* in this context only signifies compliance with the CoC guidelines. ADASP realizes that specimens and practices vary and it will not be possible to report these elements in every case. However, ADASP hopes that pathologists will find these checklists to be useful in daily clinical practice while facilitating compliance with the new CoC requirements.

The checklists are in standard PDF file format and may be easily downloaded from the ADASP website. They are not to be reproduced, altered, or used for commercial purposes without consent from ADASP.

Features required to be included in the final report

The following features are recommended by the association to be included in the final report because they are generally

K. J. Butnor · T. A. Sporn · N. G. Ordonez
Department of Pathology, University of Vermont,
Burlington, VT, USA

K. J. Butnor · T. A. Sporn · N. G. Ordonez
Duke University,
Durham, NC, USA

K. J. Butnor · T. A. Sporn · N. G. Ordonez
M.D. Anderson Cancer Center,
Houston, TX, USA

K. J. Butnor (✉)
Department of Pathology, Fletcher Allen Health Care,
111 Colchester Ave., ACC Building, EP2-120,
Burlington, VT 05401, USA
e-mail: kelly.butnor@vtmednet.org

accepted as being of prognostic importance, required for therapy and/or traditionally expected [1–4].

Gross description

1. How the specimen was received: unfixed or in formalin, intact or disrupted, oriented or not
2. How the specimen was identified and its procedure: labeled (with the patient's name, medical record number, surgical pathology accession number, etc.), designated as pleura (and other organs where applicable), laterality and procedure (core needle biopsy, thoracoscopic biopsy, thoracotomy, and incisional biopsy, pleurectomy, or extrapleural pneumonectomy)
3. Size and tissue(s) included: The overall size of the specimen should be measured in three dimensions, and the tissues included in the specimen (pleura, chest wall adipose tissue and/or skeletal muscle, rib(s), diaphragm, lymph nodes, mediastinal structures, etc.) should be documented.
4. Tumor description:
   (a) Distribution: diffuse, nodular, localized/solitary
   (b) Extent of pleura involved (circumferential, subtotal) and presence or absence of involvement of fissures and interlobular septa
   (c) Document dominant tumor mass(es) and size
   (d) Appearance: color(s), texture (e.g., firm, soft, gritty), infiltrative
   (e) Distance to the closest resection margins [lateral soft tissue (chest wall) margin, bronchus, pulmonary vessels, mediastinal structures (if included), diaphragm]
   (f) Document appearance of excised thoracoscopic sites, if applicable (usually submitted separately)

Note: Closest resection margins should be inked and sampled using perpendicular sections for areas where there is gross suspicion of involvement of adjacent tissues (e.g., diaphragm, pericardium, lung, ribs, chest wall adipose tissue, or skeletal muscle)

   (g) Lymph nodes: number received (if any), site of origin, size, and description of cut surface
   (h) Specify location or orientation of each tissue block taken for routine processing
   (i) Description of the non-neoplastic pleura, lung, and other tissues
   (j) Whether a diagnostic frozen section was performed and the intraoperative diagnosis

Diagnostic information

1. Site, laterality, and procedure
2. Histologic type [5]:
   – Epithelioid
   – Sarcomatoid
   – Biphasic
   – Desmoplastic
   – Other (specify)
3. Extent of invasion: document involvement of parietal and visceral pleura, diaphragm, lung, endothoracic fascia, mediastinal adipose tissue and/or organs, chest wall soft tissue (solitary or diffuse involvement), and rib(s)
4. Resection margin status: positive (state which margin) or negative
5. Lymph node status (if present): specific site(s) and number involved out of total for each site

Features optional for the final report

Features listed below may impact on either the likelihood of recurrence or overall prognosis. They represent specific institutional preferences or they are considered inconclusive vis-à-vis prognostic significance.

– Lymphovascular invasion
– Blood vessel invasion
– Findings in the non-neoplastic pleura/lung (e.g., changes consistent with prior talc pleurodesis, plaques, fibrosis, asbestos bodies, and asbestosis)

Note: Due to the etiologic association between asbestos exposure and malignant mesothelioma, quantitative fiber burden analysis may be requested in cases that include lung tissue as part of the specimen. Formalin-fixed non-neoplastic lung tissue (at least 5 g), preferably from the lower lobe, may be stored for this purpose.

– Results of any ancillary studies (e.g., histochemical stains, immunohistochemistry, and electron microscopy)

Note: Given the cytomorphologic overlap between malignant epithelioid mesothelioma and metastatic adenocarcinoma or malignant sarcomatoid mesothelioma and primary or metastatic sarcomas, ancillary techniques (e.g., immunohistochemistry and/or electron microscopy) are routinely utilized to facilitate diagnosis. As no single immunohistochemical marker is entirely sensitive or specific for malignant mesothelioma, a panel of stains should be employed. The association does not prescribe a particular panel of markers but recommends that at least two mesothelial-associated marker (e.g., calretinin, cytokeratins 5/6, D2-40, WT1) be used in conjunction with two or more markers that are usually negative in malignant mesothelioma (e.g., CEA, TTF-1, Ber-EP4, MOC-31) [6–10]. The results of ancillary techniques should be carefully correlated with the radiographic and gross distribution of tumor.

References

1. Rusch VW (1995) A proposed new international TNM staging system for malignant pleural mesothelioma. From the International Mesothelioma Interest Group. Chest 108: 1122–1128
2. Rusch VW, Venkatraman ES (1999) Important prognostic factors in patients with malignant pleural mesothelioma, managed surgically. Ann Thorac Surg 68:1799–1804
3. Sugarbaker DJ, Flores RM, Jaklitsch MT et al (1999) Resection margins, extrapleural nodal status, and cell type determine postoperative long-term survival in trimodality therapy of malignant pleural mesothelioma: results in 183 patients. J Thorac Cardiovasc Surg 117:54–63
4. Sugarbaker DJ, Garcia JP, Richards WG et al (1996) Extrapleural pneumonectomy in the multimodality therapy of malignant pleural mesothelioma. Results in 120 consecutive patients. Ann Surg 224:288–294
5. Churg A, Roggli VL, Galateau-Salle F et al (2004) Mesothelioma. In: Travis WD, Brambilla E, Muller-Hermelink HK, Harris CC (eds) World health organization classification of tumours Pathology and genetics of tumours of the lung, pleura, thymus, and heart. IARC, Lyon pp 128–136
6. Chu AY, Litzky LA, Pasha TL et al (2005) Utility of D2-40, a novel mesothelial marker, in the diagnosis of malignant mesothelioma. Mod Path 18:105–110
7. Cury PM, Butcher DN, Fisher C et al (2000) Value of the mesothelium-associated antibodies thrombomodulin, cytokeratin 5/6, calretinin, and CD44H in distinguishing epithelioid pleural mesothelioma from adenocarcinoma metastatic to the pleura. Mod Path 13:107–112
8. Di Loreto C, Puglisi F, Di Lauro V et al (1998) TTF-1 protein expression in pleural malignant mesotheliomas and adenocarcinomas of the lung. Cancer Lett 124:73–78
9. Ordonez NG (1998) Value of cytokeratin 5/6 immunostaining in distinguishing epithelial mesothelioma of the pleura from lung adenocarcinoma. Am J Surg Pathol 22: 1215–1221
10. Ordonez NG (1998) Value of the Ber-EP4 antibody in differentiating epithelial pleural mesothelioma from adenocarcinoma. The M.D. Anderson experience and a critical review of the literature. Am J Clin Pathol 109:85–89

ASSOCIATION OF DIRECTORS OF ANATOMIC AND SURGICAL PATHOLOGY
Final Anatomic Diagnosis Checklist

PLEURAL MESOTHELIOMA

(Ver 1.2 2-06)

Accession No.: **Part No.** **Date:**

Patient Name:

Organ	Site	Operation
Parietal pleura	Right	Core needle biopsy*
	Left	Thoracoscopic biopsy*
Visceral pleura	Diaphragmatic	Thoracotomy and incisional biopsy*
		Pleurectomy*
		Extrapleural pneumonectomy

Other: _____

_____

* This checklist is primarily for extrapleural pneumonectomy specimens. For less extensive resection/biopsy specimens not all of the checklist elements will apply.

-Primary tumor diagnosis:*Required*

Epithelioid (epithelial) mesothelioma

Sarcomatoid mesothelioma

Biphasic mesothelioma

Desmoplastic mesothelioma

Other: _____

_____

ASSOCIATION OF DIRECTORS OF ANATOMIC AND SURGICAL PATHOLOGY
Final Anatomic Diagnosis Checklist

PLEURAL MESOTHELIOMA

A. Extent of tumor: *Required*

Tumor involves parietal pleura with/without involvement of the ipsilateral visceral pleura

Tumor involves ipsilateral parietal/visceral/parietal and visceral pleura with:
- confluence of tumor involving the visceral pleura (including the fissure)
- invasion into but not through the diaphragm
- invasion of lung parenchyma
- invasion of the endothoracic fascia
- invasion into mediastinal adipose tissue
- solitary focus of tumor invading the soft tissue of the chest wall
- invasion into but not through the pericardium
- diffuse or multiple foci of tumor invading the soft tissue of the chest wall
- invasion of rib
- invasion through the diaphragm into the peritoneum
- invasion into great vessels/esophagus/trachea/other_____*(mediastinal organ)*
- direct extension into contralateral pleura
- invasion of the _____ vertebra
- involvement of the inner surface of the pericardium
- invasion of the myocardium
- invasion of the brachial plexus

-Margins of excision: *Required*

Surgical margins are free of malignant mesothelioma

Malignant mesothelioma is present at _____margin(s) of excision

ASSOCIATION OF DIRECTORS OF ANATOMIC AND SURGICAL PATHOLOGY
Final Anatomic Diagnosis Checklist

PLEURAL MESOTHELIOMA

Note: *All of the following lymph node groups will not be identified in most cases. However, appropriate designations are provided below.*

-Lymph nodes (peribronchial, *specify laterality*):

A. Number examined:_____
B. Number positive:_____
C. Comment:_____

-Lymph nodes (hilar, *specify laterality*):

A. Number examined:_____
B. Number positive:_____
C. Comment:_____

-Lymph nodes (_____):

A. Number examined:_____
B. Number positive:_____
C. Comment:_____

-Lymph nodes (_____):

A. Number examined:_____
B. Number positive:_____
C. Comment:_____

-Lymph nodes (_____):

A. Number examined:_____
B. Number positive:_____
C. Comment:_____

-Lymph nodes (_____):

A. Number examined:_____
B. Number positive:_____
C. Comment:_____

-Lymph nodes (_____):

A. Number examined:_____
B. Number positive:_____
C. Comment:_____

Note: *Regional lymph nodes include internal mammary, intrathoracic, scalene, and supraclavicular lymph nodes. The regional lymph node mapping and staging are the same as for pulmonary carcinoma.*

ASSOCIATION OF DIRECTORS OF ANATOMIC AND SURGICAL PATHOLOGY
Final Anatomic Diagnosis Checklist

PLEURAL MESOTHELIOMA

-Additional tumor features: *Optional*

A. Lymphatic vessel invasion: Identified Not Identified

B. Blood vessel invasion: Identified Not Identified

-Non-neoplastic lung/pleura: *Optional*

Asbestos bodies identified
Pleural plaques identified
Interstitial fibrosis present
Changes consistent with prior talc pleurodesis identified
Comment: _____
_____
_____

-Ancillary studies: *Optional*

Special stains are performed, and the results are as follows:
A. _____
B. _____
C. _____
D. _____
Interpretation: _____
_____

Immunohistochemical studies are performed, and the results are as follows:
A. _____
B. _____
C. _____
D. _____
E. _____
F. _____
G. _____
H. _____
Interpretation: _____
_____

ASSOCIATION OF DIRECTORS OF ANATOMIC AND SURGICAL PATHOLOGY
Final Anatomic Diagnosis Checklist

PLEURAL MESOTHELIOMA

-pTN stage[1]: *Required*

A. Primary tumor:

pTX Primary tumor cannot be assessed
pT0 No evidence of primary tumor
pT1a Tumor involves ipsilateral parietal (mediastinal, diaphragmatic) pleura, without involvement of the visceral pleura
pT1b Tumor involves ipsilateral parietal (mediastinal, diaphragmatic) pleura, with focal involvement of the visceral pleura
pT2 Tumor involves any of the ipsilateral pleural surfaces with at least one of the following:
- confluent visceral pleural tumor (including fissure)
- invasion of diaphragmatic muscle
- solitary focus of tumor invading the soft tissues of the chest wall
- invasion of lung parenchyma

pT3 Tumor involves any of the ipsilateral pleural surfaces with at least one of the following:
- invasion of the endothoracic fascia
- invasion intro mediastinal fat
- solitary focus of tumor invading the soft tissues of the chest wall
- non-transmural involvement of the pericardium

pT4 Tumor involves any of the ipsilateral pleural surfaces with at least one of the following:
- diffuse or multifocal invasion of the soft tissues of the chest wall
- any involvement of rib
- invasion through the diaphragm into the peritoneum
- invasion of any mediastinal organs
- direct extension to the contralateral pleura
- invasion into the spine
- extension to the internal surface of the pericardium
- pericardial effusion with positive cytology
- invasion of the myocardium
- invasion of the brachial plexus

B. Regional Lymph Nodes:

pNX Regional lymph nodes cannot be assessed
pN0 No regional lymph node metastasis
pN1 Metastasis in ipsilateral bronchopulmonary and/or hilar lymph node(s)
pN2 Metastasis in the subcarinal lymph node(s) and/or ipsilateral internal mammary or mediastinal lymph node(s)
pN3 Metastasis in contralateral mediastinal, internal mammary, or hilar lymph node(s) and/or the ipsilateral or contralateral supraclavicular or scalene lymph node(s)

ASSOCIATION OF DIRECTORS OF ANATOMIC AND SURGICAL PATHOLOGY
Final Anatomic Diagnosis Checklist

PLEURAL MESOTHELIOMA

C. Distant Metastasis

pMX Cannot be assessed
pM0 No distant metastasis
pM1 Distant metastasis

Reference:
1. AJCC Cancer Staging Manual, 6th edn. (2002) Lippincott-Raven, Hagerstown, Maryland pp 179-184.

Virchows Arch (2007) 450:25–29
DOI 10.1007/s00428-006-0303-5

RECOMMENDATION

Recommendations for the reporting of fallopian tube neoplasms

Teri A. Longacre · Esther Oliva · Robert A. Soslow · The Association of Directors of Anatomic and Surgical Pathology

Received: 22 August 2006 / Accepted: 23 August 2006 / Published online: 25 November 2006
© Springer-Verlag 2006

Features to be included in the final pathology report

Primary malignancies of the fallopian tube are extremely uncommon, in part, due to (admittedly arbitrary) definitional criteria. By convention, epithelial tumors that involve the ovary or peritoneal surfaces are considered to have arisen either in the ovary or endometrium or, in absence of significant ovarian or endometrial involvement, in the peritoneum, irrespective of whether the fallopian tube mucosa is also involved. Evidence from the World Health Organization and recently from case-control studies of BRCA mutation carriers suggests that the fallopian tube may have a more direct role in the development of at least some of these carcinomas [5–9]. An alternative hypothesis for the origin of ovarian and peritoneal carcinoma has even been proposed, based on the concept of transport and implantation of malignant cells from the tube to the ovary and peritoneum. Malignancies in the fallopian tube can therefore be classified as (1) arising primarily in the fallopian tube, either from preexisting endometriosis (or more rarely, a mature teratoma) or directly from tubal mucosa with metastasis to adjacent tissues; (2) arising in the ovary, endometrium, or peritoneum with metastasis to the tubal serosa or mucosa; or (3) arising primarily in the fallopian tube, ovary, endometrium or peritoneum (simultaneous primary tumors). Because there are currently no evidence-based criteria for distinguishing primary tubal carcinoma from primary ovarian or primary endometrial carcinoma in patients with high stage disease, the Association of Directors of Anatomic and Surgical Pathology (ADASP) recommended strategies for assignment of site of origin are based on current standard practices.

T. A. Longacre (✉)
Department of Pathology, Stanford University,
300 Pasteur Drive,
Stanford, CA 94305, USA
e-mail: longacre@stanford.edu

E. Oliva
Massachusetts General Hospital,
Boston, MA, USA

R. A. Soslow
Memorial Sloan-Kettering Cancer Center,
New York, NY, USA

General description

A. How the specimen is identified: name, medical record, and laterality
B. How the specimen is received: intraoperative, fresh, or formalin
C. Procedure: salpingectomy, partial salpingectomy, salpingo-oophorectomy, or staging procedure (specify)
D. Relevant clinical history

Note: Although these guidelines and the accompanying checklist are chiefly designed for fallopian tube malignancies, the processing of fallopian tubes from patients with known gene mutations that are associated with a predisposition to tubal carcinoma (e.g., BRCA1 and BRCA2) requires special handling (see "Recommended sections" for prophylactic salpingectomy).

Gross description

A. Specimen received: intact, fragmented, with (or without) attached ovary, etc.
B. Size in three dimensions
C. Tumor mass: location (e.g., isthmus, ampulla, infundibulum, and fimbria), size (in three dimensions),

appearance, necrosis, depth of invasion (mucosal, intramural, penetrates serosal surface, etc.), relationship to contiguous structures (e.g., adhesed to ovary, or pelvic peritoneum)

D. Presence of cysts, adhesions, nodules: size and region of involvement (e.g., ampulla, isthmus, and fimbria)
E. Lumen: normal, dilated, or occluded
F. Fimbria: normal or fused

Recommended sections

A. Fallopian tube
   a. Fallopian tube primary tumor mass: at least three sections. Sections should be taken to demonstrate relation to uninvolved tubal mucosa, depth of invasion, and involvement of contiguous structures if present.
   b. Prophylactic: Section fallopian tube(s) at 2- to 3-mm intervals and submit entirely for microscopic examination. Tubal fimbriae should be extensively sectioned, either by serial cross-sections or preferably by serial sagittal (lengthwise) sections, to maximize examination of the tubal plicae [6].
   c. Routine: Section fallopian tube(s) at 2- to 3-mm intervals and submit three sections to represent isthmus, ampulla, and infundibulum/fimbria (one block).
B. Ovaries
   a. Ovaries should be serially sectioned and carefully examined with all suspicious areas submitted to exclude stromal or surface involvement by carcinoma (possible primary site).
C. Uterus
   a. Cervix should be serially sectioned and carefully examined with sufficient sections submitted to exclude cervical involvement by carcinoma.
   b. Endometrium should be serially sectioned and carefully examined with sufficient sections submitted to exclude endometrial involvement by carcinoma (possible primary site).
   c. Routine sections of myometrium and serosa.
D. Omentum
   a. Sections of gross tumor if present. Note size of largest gross tumor deposit.
   b. Multiple sections are optimal when no tumor is present on gross evaluation because studies in ovarian cancer have demonstrated improved tumor detection in this setting. However, there are no established guidelines regarding number of sections.
E. Lymph nodes
   a. Sample each grossly positive lymph node.
   b. Submit entire grossly negative lymph node(s). Bivalve through hilum if large.
F. Other staging biopsies
   a. Submit entirely if small.
   b. Representative sections if grossly positive or if grossly negative and large.
G. All sections should be specified by a unique letter or number.

Diagnostic information

A. Type of procedure
B. Histologic type of tumor (modified WHO) [1]

Benign epithelial
Papilloma
Metaplastic papilloma (metaplastic papillary tumor)
Cystadenoma (serous, mucinous, etc)
Borderline epithelial
Serous tumor of low malignant potential
Endometrioid tumor of low malignant potential
Mucinous tumor of low malignant potential
Malignant epithelial
Carcinoma in situ
Serous carcinoma
Endometrioid carcinoma
Mucinous carcinoma
Clear cell carcinoma
Transitional cell carcinoma
Squamous cell carcinoma
Mixed carcinoma
Undifferentiated carcinoma
Metastatic carcinoma
Mixed epithelial–mesenchymal
Adenofibroma
Adenosarcoma
Carcinosarcoma
Germ cell tumors
Teratoma
Mesothelial
Adenomatoid tumor
Mesothelioma
Gestational trophoblastic disease
Hydatidiform mole
Choriocarcinoma
Placental site trophoblastic tumor
Others, specify

C. Histologic grade of fallopian tube carcinoma: Report tumor grade and specify grading system. There is no standard grading system for tubal carcinoma. Although

completely arbitrary, the Gynecologic Oncology Group (GOG) studies use a single grading system for ovary, endometrium, and fallopian tube. The chief advantage of this system is that it serves to maintain consistency in diagnosis and classification. Other grading schemes have been proposed for gynecological cancer, including two-tiered systems, which also have merit, particularly with respect to ovarian and extraovarian serous carcinoma. We do not recommend any one system over another; however, the ADASP does recommend the use of a single grading system for all müllerian epithelial malignancies whenever possible. The association acknowledges that there is a need for future refinement and standardization in histologic grading of these malignancies. The ADASP Fallopian Tube Neoplasms checklist uses a modification of the GOG system.

D. Maximum dimension
E. Depth of invasion

Note: It is recommended that the presence of invasion into lamina propria be distinguished from invasion into muscularis mucosa, whenever possible, even though current American Joint Committee on Cancer/International Federation of Gynecology and Obstetrics (AJCC/FIGO) staging systems do not distinguish between the two.

F. Presence of in situ carcinoma in adjacent uninvolved tubal mucosa

Note: The fallopian tube may exhibit a variety of epithelial proliferative changes, which do not necessarily reflect a neoplastic or malignant process [4]. Strict histologic criteria should be utilized before rendering a diagnosis of in situ carcinoma because this may lead to a staging procedure and prophylactic chemotherapy.

G. Involvement of ovary or endometrium: The presence of significant ovarian parenchymal or endometrial involvement by tumor of similar histologic type excludes primary fallopian tube carcinoma. Parenchymal involvement of the ovaries, if present, should be minimal (e.g., ≤0.5 cm), predominantly confined to the surface, and of significantly smaller magnitude than the tubal tumor for the carcinoma to be considered a primary tubal neoplasm. There are no established or recommended size criteria with respect to the presence of endometrial involvement, but myometrial invasion, cervical stromal involvement, and/or lymphovascular space invasion are more likely to be associated with a primary endometrial tumor with metastasis to the tube than a tubal primary or simultaneous tubal and endometrial primary. The above criteria are admittedly arbitrary, but serve to maintain consistency in diagnosis and classification.
H. Involvement of other pelvic or intraabdominal structures, omentum, and lymph nodes
I. Other findings: salpingitis (acute, chronic, or granulomatous), salpingitis isthmica nodosa, hydrosalpinx, hematosalpinx, Walthard cell rests, paratubal müllerian cysts, tubo-ovarian adhesions, endosalpingiosis, endometriosis, etc.
J. Additional studies (report as appropriate)
    a. Cytology: Correlate with surgical findings (e.g., positive ascitic fluid or peritoneal washings should reflect the diagnosis of the primary fallopian tube tumor).
    b. Immunoperoxidase studies (p53). The distinction between atypical proliferative tubal epithelial lesions and in situ carcinoma can be difficult. The presence of inflammation and admixed ciliated cells favors a benign process, but some cancers may also be associated with an inflammatory cell infiltrate. In general, carcinoma in situ is strongly immunoreactive for p53, whereas reactive processes are not.
    c. Receptor status (ER/PR).
    d. Growth factors (HER2neu).

Optional features in diagnostic report

In some cases, one or more of the following features may impact on the diagnosis or prognosis:

A. The presence of endometriosis, although not a feature of the current staging system, may help to establish a primary site in some instances.
B. The presence of an associated mature teratoma. This may be especially useful in establishing the primary site for squamous or mucinous carcinoma.
C. Presence of absence of vascular invasion, irrespective of vessel type

Appendix

Association of Directors of Anatomic and Surgical Pathology Final Anatomic Diagnosis Checklist

Fallopian tube neoplasms
Version 1.0 (3-06)

Accession no.: Patient name:	Part no(s).:	Date:
Organ:	Procedure:	
Fallopian tube (*specify laterality*)	Salpingectomy	
Fallopian tube and ovary (*specify laterality*)	Salpingo-oophorectomy	

Accession no.: Patient name:	Part no(s).:	Date:
Uterus, cervix, bilateral ovaries, and fallopian tubes	Hysterectomy and bilateral salpingo-oophorectomy	
Uterus, cervix, bilateral ovaries, bilateral fallopian tubes, and lymph nodes (*specify site*)	Hysterectomy, bilateral salpingo-oophorectomy, and lymphadenectomy	
Uterus, cervix, bilateral ovaries, bilateral fallopian tubes, omentum, and lymph nodes (*specify site*)	Hysterectomy, bilateral salpingo-oophorectomy, omentectomy, and lymphadenectomy	
Uterus, cervix, bilateral ovaries, bilateral tubes, omentum, peritoneal biopsies, and lymph nodes (*specify sites*)	Hysterectomy, bilateral salpingo-oophorectomy, omentectomy, peritoneal biopsies, and lymphadenectomy	
Others		

Primary tumor diagnosis [10]: *Required*
- Serous tumor of low malignant potential
- Endometrioid tumor of low malignant potential
- Serous adenocarcinoma
- Endometrioid adenocarcinoma
- Mucinous adenocarcinoma
- Clear cell adenocarcinoma
- Transitional cell carcinoma
- Squamous cell carcinoma
- Mixed (each component should comprise 10% or more of the tumor)
- Undifferentiated carcinoma
- Metastatic carcinoma
- Others (specify)

Tumor site: *Required*
- Isthmus
- Ampulla
- Infundibulum (fimbria)

Note: Fimbrial carcinomas may have a poorer prognosis due to tumor cell shedding directly to the peritoneum even in the absence of invasion [2].

Tumor grade: *Required*

Note: Because a universal or standard grading scheme for fallopian tube carcinoma has not been established, the grading scheme must be specified. The GOG arbitrarily uses a single grading system for endometrium, ovary, and fallopian tube, which serves to maintain consistency in diagnosis and classification. Other grading schemes have also been proposed and we do not endorse one system over another. However, regardless of the grading system used, the ADASP strongly endorses a single uniform grading scheme for ovarian, fallopian tube, and extraovarian carcinoma whenever possible. The GOG system is provided below [3]. Other systems may also be used so long as this is clearly stated in the report.

Grade cannot be assessed: specify reason

Low malignant potential (borderline)

G1 (well-differentiated): 5% or less of a nonsquamous or nonmorular solid growth pattern

G2 (moderately differentiated): 6–50% of a nonsquamous or nonmorular solid growth pattern

G3 (poorly differentiated): >50% of a nonsquamous or nonmorular solid growth pattern

G4 (undifferentiated)

Notable nuclear atypia, inappropriate for the architectural grade, raises the grade of a grade 1 or grade 2 tumor by one level. Clear cell carcinomas are generally not graded.

Extent of tumor [1]: *Required*

Tumor is
- Limited to tubal mucosa *or*
- Confined to one fallopian tube with invasion of the lamina propria only, no positive pelvic washings *or*
- Confined to one fallopian tube with invasion of the muscularis propria only, no positive pelvic washings *or*
- Confined to both fallopian tubes with invasion of the lamina propria only, no positive pelvic washings *or*
- Confined to both fallopian tubes with invasion of the muscularis propria only, no positive pelvic washings *or*
- Confined to one or both tubes with peritoneal surface involvement and/or positive pelvic washings
- Present in one or both tubes with pelvic extension (specify whether extension involves uterus[a] and/or ovaries[a] or other pelvic structures) *or*
- Present in one or both tubes with peritoneal implants outside the pelvis and/or regional lymph node metastasis (specify microscopic, macroscopic but less than 2.0 cm, greater than 2.0 cm, and/or regional lymph node metastasis) *or*
- Present in distant metastasis including malignant cells in pleural fluid or parenchymal liver metastasis

[a]Involvement of ovaries and/or endometrium

Note: Current AJCC and FIGO staging do not distinguish between invasion into lamina propria only and invasion into muscularis propria. However, because substaging is based on depth of invasion in other hollow organs with muscle walls, such as gastrointestinal tract and urinary bladder, the ADASP recommends a similar staging standard for fallopian tube carcinoma. Different survival rates depending upon the depth of invasion have been reported [2].

Lymphovascular space invasion: *Optional*
- Absent
- Present

Associated features: *Optional*
- Endosalpingiosis
- Endometriosis
- Others

Other findings: *Optional*

Ancillary studies: *Required (if performed)*

pTNM/FIGO stage [1]: *Required*

Primary tumor: [b]

TNM	FIGO	
pTX		Primary tumor cannot be assessed
pT0		No evidence of primary tumor
pTis	0	Carcinoma in situ (tumor limited to tubal mucosa)

Accession no.: Patient name:	Part no(s).:	Date:
pT1	I	Tumor limited to the fallopian tube(s)
pT1a	IA	Tumor limited to one fallopian tube, without penetration of serosal surface, no malignant ascites or peritoneal washings
pT1b	IB	Tumor limited to both fallopian tubes, without penetration of serosal surface, no malignant ascites or peritoneal washings
pT1c	IC	Tumor limited to one or both fallopian tubes with extension onto or through the serosal surface, or with malignant cells in ascites or peritoneal washings
pT2	II	Tumor involves one or both fallopian tubes with pelvic extension
pT2a	IIA	Extension and/or metastasis to the uterus and/or ovaries
pT2b	IIB	Extension to other pelvic structures
pT2c	IIC	Pelvic extension with malignant cells in ascites or peritoneal washings
pT3	III	Tumor involves one or both fallopian tubes with peritoneal implants outside the pelvis[c]
pT3a	IIIA	Microscopic peritoneal metastasis outside the pelvis
pT3b	IIIB	Macroscopic peritoneal metastasis outside the pelvis 2.0 cm or less in greatest dimension
pT3c	IIIC	Peritoneal metastasis greater than 2.0 cm in greatest dimension
Regional lymph nodes:		
pNX		Regional lymph nodes cannot be assessed
pN0		No regional lymph node metastases
pN1	IIIC	Regional lymph node metastases
Distant metastases:		
pMX		Presence of distant metastases cannot be assessed
pM0		No distant metastases
pM1	IV	Distant metastases

[b]In the absence of other specific staging instructions, it is recommended that all other primary malignancies of the fallopian tube be staged accordingly (e.g., carcinosarcoma)

[c]Liver capsule metastasis is T3; liver parenchymal metastasis is M1.

References

1. AJCC (2002) AJCC cancer staging manual, 6th edn. Lippincott-Raven, pp 285–290
2. Alvarado-Cabrero I, Young RH, Vamvakas EC, Scully RE (1999) Carcinoma of the fallopian tube: a clinicopathological study of 105 cases with observations on staging and prognostic factors. Gynecol Oncol 72:367–379
3. Benda JA, Zaino R (1994) GOG pathology manual. Gynecologic Oncology Group, Buffalo, NY
4. Cheung AN, Young RH, Scully RE (1994) Pseudocarcinomatous hyperplasia of the fallopian tube associated with salpingitis. A report of 14 cases. Am J Surg Pathol 18:1125–1130
5. Colgan TJ, Murphy J, Cole DE et al (2001) Occult carcinoma in prophylactic oophorectomy specimens: prevalence and association with BRCA germline mutation status. Am J Surg Pathol 25:1283–1289
6. Medeiros F, Muto MG, Lee Y et al (2006) The tubal fimbria is a preferred site for early adenocarcinoma in women with familial ovarian cancer syndrome. Am J Surg Pathol 30:230–231
7. Narod SA, Sun P, Ghadirian P et al (2001) Tubal ligation and risk of ovarian cancer in carriers of BRCA1 or BRCA2 mutations: a case-control study. Lancet 357:1467–1470
8. Powell CB Kenley E, Chen LM et al (2005) Risk-reducing salpingo-oophorectomy in BRCA mutation carriers: role of serial sectioning in the detection of occult malignancy. J Clin Oncol 23:127–132
9. Rosenblatt KA, Thomas DB (1996) Reduced risk of ovarian cancer in women with a tubal ligation or hysterectomy. The World Health Organization collaborative study of neoplasia and steroid contraceptives. Cancer Epidemiol Biomark Prev 5:933–935
10. World Health Organization Classification of Tumours (2003) Pathology & genetics. Tumours of the breast and female genital organs. IARC Press, Lyon

Virchows Arch (2007) 450:31–40
DOI 10.1007/s00428-006-0311-5

ORIGINAL ARTICLE

Ontogenesis of human cerebellar cortex and biopathological characterization in sudden unexplained fetal and infant death

Anna Maria Lavezzi · Giulia Ottaviani · Luigi Matturri

Received: 26 May 2006 / Accepted: 6 September 2006 / Published online: 25 November 2006
© Springer-Verlag 2006

Abstract The aims of this study were to investigate in the human cerebellar cortex the structural and biological ontogenetic features, the possible presence of alterations in cases of sudden unexplained fetal and infant death, and the involvement of the maternal cigarette smoking in developmental abnormalities. We analyzed 52 brains of fetal and infant death victims, aged from the second gestational trimester to 12th postnatal month. In the cerebellar cortex we evaluated, besides the morphological aspects, the expression of several biomarkers implicated in proliferative processes (c-*fos*, proliferating cell nuclear antigen, and apoptosis) as well as the presence of the neurotransmitter somatostatin, which is strongly implicated in central nervous system differentiation, and of EN2 gene. The observed features of the cerebellar cortex, mainly confined to the transient external granular layer, were high proliferative activity and high expression of both somatostatin and EN2 gene in prenatal life and high apoptotic index after birth. In 41% of the sudden unexplained death victims, in the greater part with smoking mothers, we observed different biopathological alterations of the cerebellar cortex. Maternal smoking is increasingly being demonstrated to be one of the main contributors to developmental neurological alterations in the offspring.

Keywords Human cerebellar cortex · Sudden unexplained perinatal death · Sudden infant death syndrome · SIDS · Maternal cigarette smoking

Abbreviations

ED	explained death
gw	gestational week
PCNA	proliferating cell nuclear antigen
SIDS	sudden infant death syndrome
SIUD	sudden intrauterine unexplained death
SNUD	sudden neonatal unexplained death
SUD	sudden unexplained death

Introduction

The cerebellar cortex is one of the most studied areas of the brain. Its laminar pattern and rectilinear geometry have long been exploited to provide an important model for understanding the development and fiber connections of the central nervous system [2, 3, 30, 37, 53, 54].

Specific features of development are observed in the cerebellar cortex regarding the origin sites, the routes and patterns of migration, and the time frames of the two major neural cell population (granule cells and Purkinje cells).

In mammalians, the ventricular zone of the fourth ventricle produces in an early embryonic stage a small number of precursors of the Purkinje cells [4, 37]. They undergo terminal mitoses in this location and only in the postmitotic phase they migrate from the germinal zone into the cerebellar wall, probably following radial glial guides [17], where they

A. M. Lavezzi (✉) · G. Ottaviani · L. Matturri
Institute of Pathology, "Lino Rossi" Research Center,
University of Milan,
Via della Commenda, 19,
Milan 20122, Italy
e-mail: anna.lavezzi@unimi.it

G. Ottaviani
e-mail: giulia.ottaviani@unimi.it

L. Matturri
e-mail: luigi.matturri@unimi.it

aggregate to form an immature layer of 10–15 cells thick. During birth, the Purkinje cells form a row of large somata and start to extend elaborate dendritic arbor synapses.

The granule cells precursors arise later, toward the end of the embryonic period, from the dorsal portion of the metencephalon within a structure called the rhombic lip, from where the arcuate nucleus of the medulla oblongata also arises [37, 48, 56]. These cells reach the superficial zone of the cerebellum and organize themselves into a pluristratified layer, the external granular layer, which persists for different periods of time according to species but eventually becomes thinner and ultimately disappears.

Extensive proliferation of these cells during the first postnatal weeks gives rise to more than 100 million granule cells that migrate across the molecular layer and Purkinje cell layer to reach the internal granular layer, under the guidance of the radial glia [17].

To date, only few authors have studied the morphological and functional development of the cerebellar cortex in man [10, 47]. The results of such studies are prevalently based on the developmental patterns from experimental research in different animal species [10, 47]. The first aim of the present study was to investigate the structural and biological patterns of human cerebellar cortex development in a large group of fetal and infant death victims, aged from the 17th gestational week (gw) to 1 year of life. In particular, in the cerebellar cortex, besides the morphological aspects, we evaluated the expression of several biomarkers implicated in proliferative processes [c-*fos*, proliferating cell nuclear antigen (PCNA), and apoptosis], of somatostatin, a neurotransmitter strongly implicated in central nervous system differentiation [7, 44], and of EN2, a homeobox-engrailed gene that seems to be involved in the anatomic organization of structures derived from the rhombic lip, particularly the external granular layer of the cerebellar cortex [38, 39, 52].

Our second purpose was to evaluate whether morpho-functional disorders of the cerebellar cortex are present in cases of sudden and unexplained fetal and infant death, which we have previously demonstrated to be associated to specific alterations of the brainstem [6, 21, 22, 24, 31, 32].

Finally, the suggestion by some authors that the protracted development of the cerebellar cortex should make this structure particularly vulnerable to a broad spectrum of extrinsic environmental injuries [5, 14, 16] and the observation in our previous studies of a significantly increased incidence of structural and/or functional alterations of different brainstem nuclei in stillborns and sudden infant death syndrome (SIDS) victims with smoker mothers [23, 25, 27, 46], prompted us to determine whether maternal cigarette smoking could also be related to morphological and/or physiological developmental abnormalities of the cerebellar cortex.

Materials and methods

A total of 52 brains were collected from 21 fetuses (17–39 gw), 8 newborns who had died within the first month of life, and 23 infants aged 1–12 months.

Classification of cases

In 32 cases, after the in-depth necropsy examination, the result of death is totally unexplained (sudden unexplained death, SUD).

A case was classified as SIDS when an infant death, between 1 and 12 months, was sudden, completely unexpected, and unexplained after a thorough case investigation, including performance of a complete autopsy, examination of the death scene, and a review of the clinical history [34, 55].

A case was classified as sudden intrauterine unexplained death (SIUD) when a fetus died suddenly with no explained cause after the 25th gw, before complete expulsion or extraction of the fetus from the mother, resulting in a stillbirth for which there was no explanation despite postmortem examinations [20, 34].

Similarly, a case was classified as sudden neonatal unexplained death (SNUD) when a newborn suddenly died with no explained cause, from birth to the end of the first postnatal month of life [21].

A case was classified as explained death (ED) when a precise cause of death was documented by autopsy.

Accordingly, in this study, a diagnosis of SIUD was established for 12 fetuses, of SNUD for 5 newborns, and of SIDS for 15 infants. In the remaining 20 cases a precise cause of death was formulated at autopsy.

While taking the medical history, the mother was asked for information about any smoking habit before, during, and after pregnancy. Smoking habit was assigned to two categories (smokers vs nonsmokers). Overall, 21 out of the 52 mothers (40%) were smokers already before the onset of the pregnancy, and 31 were nonsmokers (60%).

The cases were examined in blinded fashion, without initial knowledge of the cause of death, age, or other clinicopathologic information. Only after the histologic and immunohistochemistry assessment of the cerebellum had been completed the pathologic findings were matched with the corresponding records.

Table 1 summarizes the case profiles in this study, with their relative diagnosis and the mother's smoking habit.

Autopsy and pathological techniques

The victims were subjected to a complete autopsy, including examination of the placental disk, umbilical cord, and membranes in fetuses. Every case was submitted to

Table 1 Case profiles of the study

Victims (*n*)	Age	Death diagnosis (*n*)	Maternal smoking habit	
			Smokers	Nonsmokers
Fetuses (21)	17–39 gw	Voluntary abortion (3)	1	2
		Necrotizing chorioamnionitis (2)	1	1
		Congenital heart diseases (3)	1	2
		Potter's syndrome (1)	–	1
		SIUD (12)	6	6
Newborns (8)	1–4 pd	Congenital heart diseases (3)	–	3
		SNUD (5)	2	3
Infants (23)	1–12 m	Pneumonia (3)	1	2
		Congenital heart diseases (4)	2	2
		Pericarditis (1)	–	1
		SIDS (15)	7	8

gw Gestational week, *pd* postnatal day, *m* month, *SIUD* sudden intrauterine unexplained death, *SNUD* sudden neonatal unexplained death, *SIDS* sudden infant death syndrome

accurate and specialized investigations including the study of the brainstem and the cardiac conduction system on serial sections, according to the protocol routinely followed by the Institute of Pathology, University of Milan [34, 36].

All infants, neonates, and fetuses selected for this study were submitted to a complete necropsy examination about 24 h after death. Multiple samples from all organs were immediately fixed in 10% phosphate-buffered formalin. After an average period of 2 weeks, the samples were processed and embedded in paraffin; 5-μm sections were stained with hematoxylin–eosin. After fixation, the brain was cut in coronal sections. On multiple samples of the various lobes, after fixation and processing, 5-μm sections were obtained and stained with hematoxylin–eosin and Klüver–Barrera. For the heart samples, 5-μm sections were stained with hematoxylin–eosin and trichromic Heidenhain (Azan). To examine the cardiac conduction system, two blocks of heart tissue were obtained for paraffin embedding and serial cutting. The first block contains the junction of superior vena cava and right atrium encompassing the entire area of the sinoatrial node. The second block contains the atrioventricular node, His bundle down to bifurcation, and bundle branches. All sections were cut serially at intervals of 40 μm (levels), as described previously [45].

In particular, the cerebellum, the target of this study, was firstly excised from the brainstem by cutting through the cerebellar peduncles. Then coronal sections of either cerebellar hemispheres were obtained through both the anterior (frontal) and the posterior (parietooccipital) cortices. Each sample included the full thickness of the ventricular wall. Care was taken to examine corresponding folia from different subjects whenever possible. For each case, two 5-μm sections were stained with hematoxylin–eosin and Klüver–Barrera. Additional sections were subjected to immunohistochemistry for the study of (1) the PCNA, (2) the c-*fos* gene, (3) the apoptosis, (4) the neurotransmitter somatostatin, (5) and the EN2 gene expression. The remaining sections were saved and stained as deemed necessary for further investigations.

Immunohistochemical methods

Apoptosis was detected by terminal deoxynucleotidyl transferase biotin-dUTP nick end labeling (TUNEL) method, using deoxynucleotidyl transferase (0.3 U/ml) to incorporate digoxigenin-conjugated deoxyuridine (dUTP) into the ends of DNA fragments.

To analyze the immunoexpression of *PCNA*, c-*fos*, *EN2*, and *somatostatin*, we used specific primary antibodies after the application of the avidin-biotin-peroxidase method, in conformity with the conventional immunohistochemical procedures.

A detailed description of the immunohistochemical techniques applied in this study is available in our previous works [21, 22, 26, 27].

Immunohistochemistry evaluation All the immunostained sections were examined at light microscope separately in each layer (external granular layer, molecular layer, Purkinje cell layer, and internal granular layer), using a ×40 lens (high magnification). We quantified the scoring for each case on at least 15 random fields. Only the cells with intense brown immunostaining were considered to be positive.

We quantified the scoring for each case, as follows:

–	=	no positive cell
+	=	a number of positive cells ≤30% per unit area (moderate positivity)
++	=	a number of positive neurons >30% per unit area (strong positivity)

Statistical analysis

Statistical methods were employed to evaluate the association between maternal cigarette smoking habit and cerebellar cortex alterations in the two groups (SUD and sudden ED groups), using Fisher's exact test. The level of significance was set at $p<0.05$.

Results

Analysis of the morphological and immunohistochemical data obtained in this study demonstrated homogeneous, progressive developmental steps of cerebellar cortex maturation in most cases.

Morphological features

At the earliest observation (17–18 gw) the cerebellar cortex shows high, diffuse cellularity. Only the external granular layer is outlined, whereas the molecular layer, Purkinje cell layer, and internal granular layer are not identifiable or scarcely delineated (Fig. 1a).

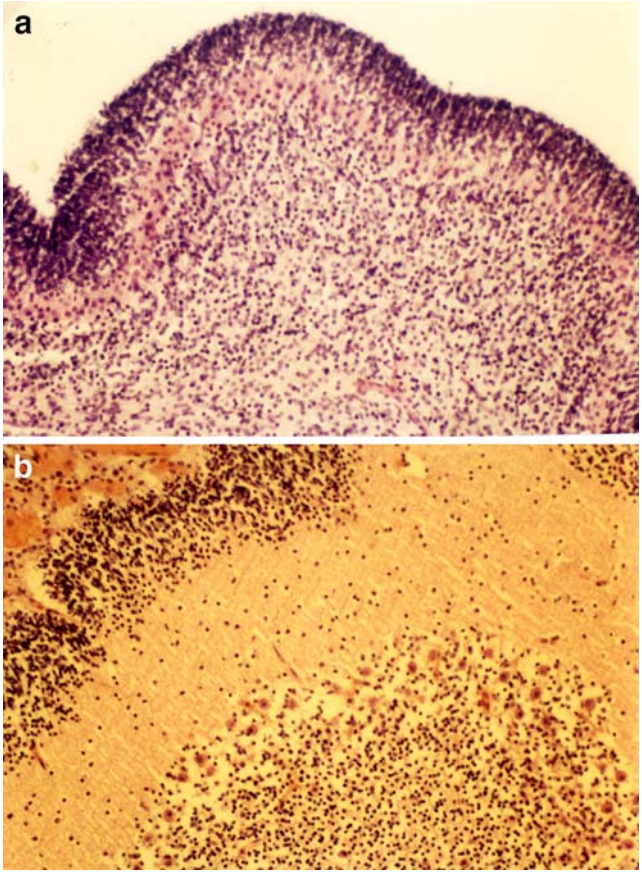

Fig. 1 Morphological aspects of the normal cerebellar cortex development. **a** Diffuse cellularity in the cerebellar cortex in a fetus aged 17 gw (hematoxylin–eosin, magnification ×20). **b** Four-layered structure of the cerebellar cortex in a 35 gw fetus. Note the dense layer of the Purkinje cells (hematoxylin–eosin, magnification ×20)

From the 20th to the 22nd week, besides a well-defined 10–12 cells thick pluristratified external granular layer, a dense row of small cells appears in correspondence of the Purkinje cell layer.

After 30 weeks, a four-layered structure is recognizable (Fig. 1b). The external granular layer is formed by six to eight rows of densely packed small round cells. Several mitoses can be detected in this layer. The molecular layer contains numerous cells resembling cells of the external granular layer, clearly in the migratory phase. The Purkinje cells form an ordered five to six cells thick layer of round immature larger neurons located between the molecular layer and the internal granular layer. This morphological pattern remains stable until the first days of life.

At 1 month after birth the external granular layer presents a superficial zone of small round cells and a substrate of horizontal bipolar neurons that are sometimes oriented centripetally toward the molecular layer.

From the second month of life the external granular layer preserves this cellular morphology but becomes progressively thinner. The molecular layer increases in thickness and shows lower cell density. The Purkinje cell layer is formed by numerous large cells with immature dendritic trees aligned in a single layer. Only in a few tracts are clusters of Purkinje cells still present. The internal granular layer is increased in thickness and neuronal density.

Between 5 and 7 months the external granular layer is constituted by three to four rows of prevalently elongated bipolar neurons and Purkinje cells show large mature somata, frequently polygonal in shape, with an evident axon and dendrites. They are now much more widely spaced and reduced in number.

At 10 months the external granular layer is a discontinuous single layer. In many areas the molecular layer represents the external surface.

Finally, by 12 months the external granular layer is totally absent. The cerebellar cortex shows the three-layered definitive structure (molecular layer, Purkinje cell layer, and internal granular layer).

Biological functional features

PCNA immunohistochemistry In fetuses, PCNA immunoreactivity is observed throughout the cerebellar cortex thickness from the 20th gw. Successively, positive cells are mainly localized in the external granular layer (++), being far less represented in the molecular layer and internal granular layer (+) and totally absent in the Purkinje cell layer. Within the internal granular layer, positive nuclei are concentrated at the boundaries of the Purkinje cell layer. This pattern of immunopositivity is still observed at birth,

but declines thereafter. At 2 months of life, rare PCNA-immunoreactive cells are detectable only in the upper part of the external granular layer.

c-fos immunohistochemistry From 17 to 25 gw, the vast majority of cells in the cerebellar cortex is c-*fos*-labeled (++). Then the positivity decreases and at 35 gw only rare c-*fos*-positive cells are visible, which are scattered in the external granular layer. By the last fetal period and in postnatal life c-*fos* expression is fully negative.

Apoptosis immunohistochemistry Immunostaining for apoptotic cells reveals only sporadic positive nuclei in the external granular layer in prenatal life after the 30th gw and in the first postnatal month. Between 2 and 4 months, the number of dying cells increases, confined to the outer part of the external granular layer (Fig. 2). This process becomes more marked during regression of the external granular layer, affecting the vast majority of its cells (++). Apoptotic neurons display intense staining by highly condensed chromatin and various nuclear fragmentation stages.

Somatostatin immunohistochemistry The somatostatin expression presents high levels in the Purkinje cell layer uring the prenatal period, reaching a maximum around the 28–30 gw (++), and starting to decline after birth at 1–2 months of life (+).

EN2 immunohistochemistry High expression of the EN2 gene is demonstrable in all the external granular layer cells from the 17th to 22nd gw (++). Successively, EN2 expression decreases up to the first days after birth (+), and is constantly negative in infants aged 1–12 months.

We found the above described cytoarchitectural and biological features in the vast majority of cases. Nevertheless, the cerebellar cortex of 16 cases (13 sudden unexpected deaths and 3 ED) showed different aspects (Table 2). In four cases diagnosed as SIDS, aged 4–6 months, and in two subjects who died at 3 months of hypertrophic cardiomyopathy, at histological examination, the external granular layer was exclusively constituted by small round cells, without any bipolar neurons in the inner rows. In two further SIDS cases, aged 3 and 4 months, respectively, the search for apoptotic cells was negative, particularly in the external granular layer. In another case of SIDS, aged 1 month, almost all the cells of the internal granular layer were immunostained for apoptosis (Fig. 3a).

An unexpected finding was the observation of programmed cell death of all the Purkinje cells in an infant who died of SIDS at 7 months (Fig. 3b,c).

In two fetuses who died suddenly and unexpectedly at 34 and 36 gw, respectively, EN2 gene expression was negative in the external granular layer. Somatostatin was also negative in the Purkinje cell layer of three stillborns, aged 32–36 gw (two dead of unknown cause and one dead of known causes). Finally, in a 2-day-old SNUD case, intense c-*fos* positivity was appreciable in all the layers, particularly in the Purkinje cell layer.

Overall, structural and biological alterations of the cerebellar cortex were present in 13 of the 32 SUD victims (41%) and in 3 of the 20 ED victims (15%) (Table 2).

Finally, we correlated the findings with the mother's smoking habit. A significant correlation was evident between maternal smoking, SUD, and anomalous features of the cerebellar cortex (Fig. 4). In fact, 12 among the 13 SUD and 2 of the 3 ED victims with cerebellar cortex alterations had smoker mothers (Table 3).

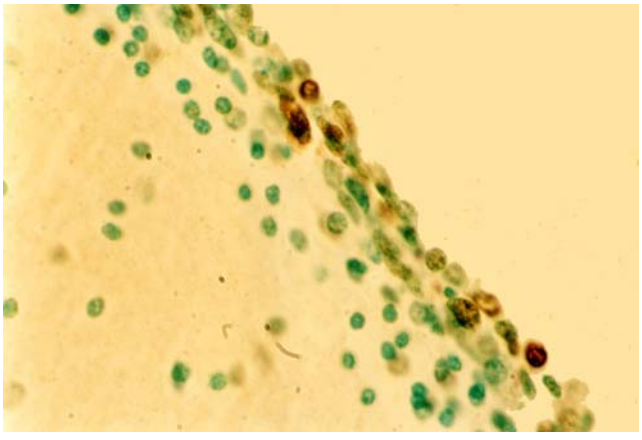

Fig. 2 Normal apoptotic aspects in the regressive process of the external granular layer in an infant deceased at 4 months (TUNEL method, magnification ×20)

Discussion

In this study, we have delineated the dynamic sequence of morphological and biological steps that occur in human cerebellar cortex development, from the second trimester of gestation to the first postnatal year.

Around the 17th–18th weeks of fetal life, the external granular layer is the only recognizable layer, with a thickness of 10–15 small cells. Successively, a pluristratified Purkinje cell layer is also identifiable and, after 30 weeks, a four-layered structure is evident (external granular layer, molecular layer, Purkinje cell layer, and internal granular layer).

In prenatal life proliferation is the predominant phase, testified by c-*fos* and PCNA positivity, which is at first widespread throughout the thickness of the cortex, and subsequently restricted to the external granular layer. Therefore, this layer contains at this stage undifferentiated small neurons, which progressively undergo proliferation and differentiation. In fact, c-*fos* and PCNA are known to

Table 2 Distribution of the cerebellar cortex alterations

Cerebellar cortex alterations	Fetuses		Cerebellar cortex alterations	Newborns		Cerebellar Cortex alterations	Infants	
	SIUD	ED		SNUD	ED		SIDS	ED
Negative EN2 in the external granular layer	2	–[a]	Positive c-*fos* in all layers	1	–[b]	Immaturity of the external granular layer	4	2
Negative somatostatin in the Purkinje cell layer	2	1				Negative apoptosis in the external granular layer	2	–[c]
						Positive apoptosis in the Purkinje cell layer	1	–[d]
						Positive apoptosis in the internal granular layer	1	–[e]

SIUD Sudden intrauterine unexplained death, *SNUD* sudden neonatal unexplained death, *SIDS* sudden infant death syndrome, *ED* explained death
[a] Presence of EN2-positive cells in the external granular layer (normal pattern)
[b] Absence of c-*fos*-positive cells in all cerebellar layers (normal pattern)
[c] Presence of apoptotic positive cells in the external granular layer (normal pattern)
[d] Absence of apoptotic positive cells in the Purkinje cell layer (normal pattern)
[e] Absence of apoptotic positive cells in the internal granular layer (normal pattern)

be markers of cell replication that regulate growth and maturation in a variety of tissues. First, the protooncogene c-*fos* synthesizes the corresponding DNA-binding protein as a signal for cell activation with mitogenic effect [11, 19]. Thus, it precedes the PCNA manifestation indicative of DNA duplication [40].

The biological features of cerebellar cortex development include positivity to the neurotransmitter somatostatin and the EN2 gene, observed to be more intensely expressed in the second and third gestational trimesters, respectively.

The somatostatin is a neuropeptide with a wide distribution in the central nervous system that controls various physiological processes [7, 44]. We have previously documented intense positivity of the somatostatin in brainstem nuclei involved in cardiorespiratory activity in stillbirths and its abrupt reduction in postnatal deaths [21, 22]. In the present study, we also observed high levels of somatostatin expression confined to the Purkinje cell layer during prenatal life and declining after birth. This finding diverges from the report by Laquerriere et al. [28]. These authors, with the use of different methods (precisely, by binding and autoradiographic studies on frozen human cerebellar samples), found from midgestation to the 15th postnatal month a high concentration of somatostatin receptors mainly in the granule cells of both the external and internal layers.

However, we believe that, independent of a specific localization, the somatostatin plays an important role, rather than in neurotransmitter activity, in the development and maturation of the cerebellar cortex, as of other structures of the central nervous system.

Moreover, the EN are homeobox-engrailed genes that were implicated in the development of the central nervous system. In particular, the EN2 gene seems to have an essential role in the anatomic organization of structures derived from the rhombic lip, in particular, of the arcuate nucleus in the ventral surface of the brainstem and of the external granular layer in the cerebellar cortex [10, 56].

We recently observed that the expression of the EN2 gene is very high in human arcuate nucleus neurons from the 17th to 22nd gw, which decreases thereafter up to the first day after birth and then disappears [26]. The same temporal pattern of EN2 manifestation was found in this study in the external granular layer neurons of the cerebellar cortex, confirming the same embryologic origin as that of the arcuate nucleus.

During the postnatal period, the external granular layer involutes leading to the definitive three-layered organization of the cerebellar cortex observed at 12 months of life. Many of the small undifferentiated neurons of the external granular layer migrate across the molecular and Purkinje cell layers, under the guidance of the radial glia, giving rise to the mature neurons of the internal granular layer. In addition, at this stage of development, a high number of pre- and postmitotic neurons of the external granular layer die upon activation of an apoptotic program [41, 57]. Therefore, the main biological observations in the cerebellar cortex after birth are (1) an abrupt decline of c-*fos*, PCNA, EN2, and somatostatin expression and (2) an increasing number of dying cells in the external granular layer, responsible for its progressive reduction in thickness.

In this study we observed several variations from the above delineated cytoarchitectural and biological steps of cerebellar cortex development, prevalently in cases of sudden death. Unexpected findings in SIDS victims were (1) immaturity of the external granular layer neurons observed in four cases and (2) anomalous apoptotic models in four cases. The anomalous apoptosis consisted of programmed death of all the Purkinje cells in an infant who died at 7 months and of the internal granular layer cells in an infant aged 1 month; lack of apoptotic expression in

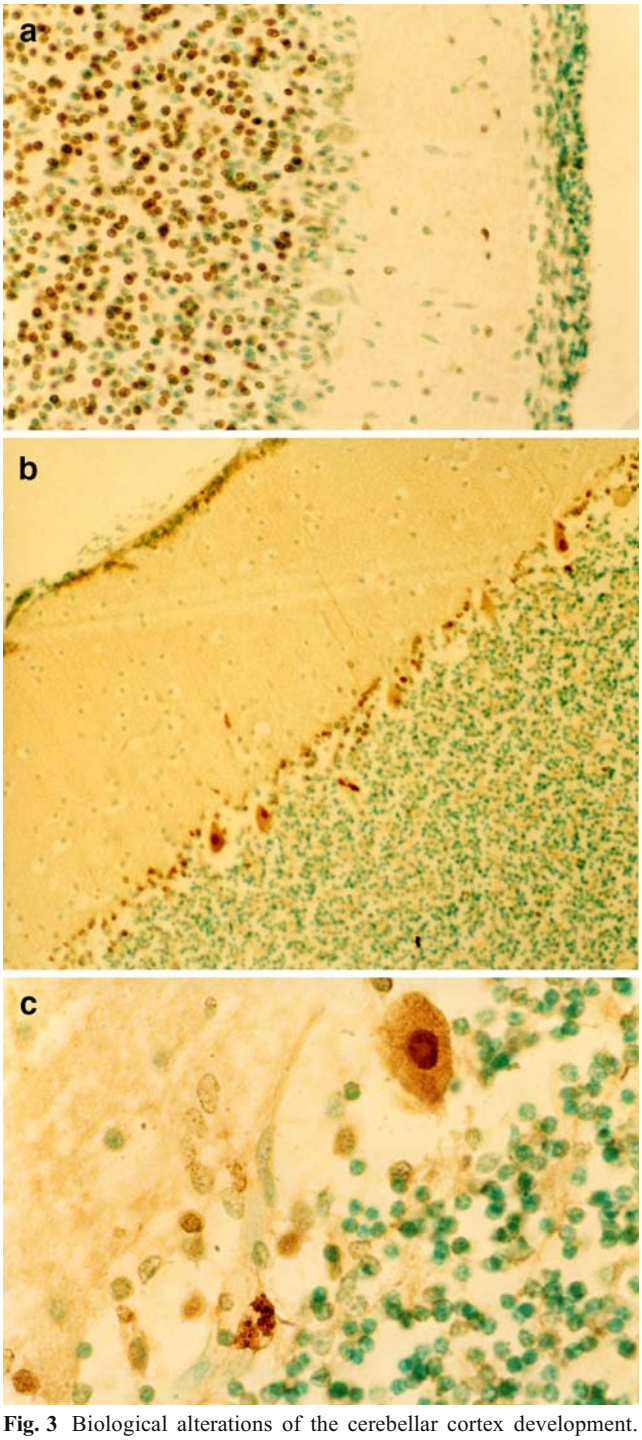

Fig. 3 Biological alterations of the cerebellar cortex development. **a** High apoptotic index of the internal granular layer in a SIDS victim aged 1 month (TUNEL method, magnification ×20). **b** High apoptotic index of the Purkinje cell layer in a SIDS victim aged 7 month (TUNEL method, magnification ×20). **c** Magnified detail (×100) of subpanel **b**: programmed cell death of a Purkinje cell and a Purkinje fragmented nucleus (TUNEL method)

the external granular layer could be the cause of death in two cases aged 2 and 4 months, respectively. In addition, we observed negative expression of somatostatin in three cases and of the EN2 gene in two cases of fetal death, and

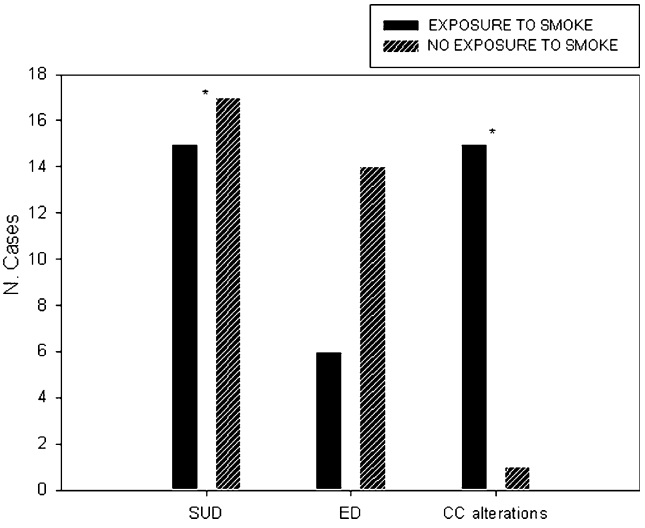

Fig. 4 Significant correlation between maternal smoking, *SUD* compared to *ED*, and anomalous features of the cerebellar cortex (*CC*) ($p<0.05$). *SUD*=Sudden Unexplained death; *ED*=Explained Death

intense c-*fos* positivity in a newborn who died 2 days after birth.

Dissimilar alterations were reported in literature in the cerebellar cortex of SIDS victims. One of the earliest papers showed a decreased number of the internal granular layer cells [15]. Further investigation indicated increased density of Purkinje cells among the youngest SIDS infants [42]. Instead, other authors observed a greater thickness and cell density of the external granular layer in SIDS cases than in age-related controls [9, 49].

We suggest that all these findings, including our own observations, are different manifestations of delayed or faulty maturation of the cerebellar cortex in sudden unexpected death victims. In stillbirths and infants, for which there was no explanation of death despite postmortem examination, we previously found morpho-functional developmental alterations of specific nuclei of the brainstem that are classically implicated in respiratory control (the parabrachial/Kölliker–Fuse complex and locus coeruleus in the pons, the dorsal motor vagal nerve, the tractus solitarius, the ambiguus, the hypoglossus,

Table 3 Distribution of neurodevelopmental defects of the cerebellar cortex in unexplained and ED in relation to maternal smoking habit

	Smoking mothers (n=21)		Non smoking mothers (n=31)	
	SUD	ED	SUD	ED
Cerebellar cortex alterations (n=16)	12	2	1	1
Normal cerebellar cortex structure (n=36)	3	4	16	13

SUD Sudden unexplained death, *ED* explained death

and the arcuate nuclei in the medulla oblongata) [6, 21, 22, 31, 32].

Thus, we believed that neuronal mechanisms responsible for compensatory responses to hypercapnia and/or hypoxia were associated to substantial functional changes of these nuclei.

Because the axons of the granule cells and Purkinje cells seem to have connections with dorsal and ventral medulla and with specific areas in the pons, as reported in experimental studies [18], we suggest that even the cerebellar cortex could be a putative neuronal region subserving ventilatory control.

In particular, the cerebellar cortex contributes to the control of muscle activity, working as a clock determining the time intervals between two successive contractions [12]. This activity should also extend to respiratory muscles that are implicated in the restoration of blood pressure and breathing rhythm in cases of hypoxia [58].

Moreover, severe hypoxic injuries may determine more harmful effects on the cerebellar cortex than on other central nervous system structures because the long duration of its development may increase its vulnerability to DNA-damaging conditions, including nicotine absorption.

In particular, smoke exposure reduces tissue oxygenation due to increased blood levels of carboxyhemoglobin. In fact, carbon monoxide, a gaseous combustion product of nicotine, is easily absorbed into the systemic circulation, crossing the placenta by passive diffusion in cases of maternal smoking in pregnancy [29]. It inhibits the release of oxygen, causing hypoxia especially in the most susceptible organs, namely, the brain and, to an even greater extent, the cerebellar cortex [43, 50, 51].

Animal studies have confirmed the presence of neurobehavioral deficits in the cerebellar cortex (a reduction in number of the Purkinje cells, high expression of glial fibrillary acidic protein, and changes in nicotinic receptors) associated to nicotine exposure [1, 8, 13].

We have previously studied the consequences of chronic exposure to tobacco smoke in utero on the morphological and functional development of different brainstem nuclei in perinatal and infant SUD [23, 25, 27, 46]. In particular, we have observed a significant correlation between maternal smoking during pregnancy and hypoplasia and negative expression of EN2 gene of the arcuate nucleus, hypoplasia and altered expression of the somatostatin in the hypoglossus nucleus, and decreased synthesis of catecholamines in the locus coeruleus.

We postulate that smoke can also exert adverse influences on the successful deployment of the genetic programs committed to the protracted process of pre- and postnatal cerebellar cortex development. The morphobiological defects of the cerebellar cortex layers observed in this study could have contributed to the failure of regulatory reactions to breathing challenges, leading to sudden death in vulnerable periods. Further studies on triggering factors and related functional mechanisms are needed to gain a better understanding of the complex pathophysiology of SUD. The results presented in this study may contribute to orient researches in this field.

In conclusion, this study provides suggestion that nicotine toxicity from maternal smoking is increasingly being demonstrated to be one of the main contributors to developmental neurological alterations in the offspring [23, 25, 27]. Therefore, all women should be warned that smoking places their children at serious risk of a variety of morphological, genetic, and functional abnormalities of the brain that can even lead to sudden, apparently unexplained death.

Acknowledgements This study was supported by the Lombardy Region target project for the Reduction of the Risk of Sudden Infant Death and Unexpected Perinatal Death, converging to the Institute of Pathology, University of Milan, all SIDS and unexpected perinatal death cases (decree no. 11693, 20/06/02) and by Ministry of Foreign Affairs (joint project of particular relevance no. 269/P/0085087 "Anatomopathologic and genetic study of the unexplained perinatal death and SIDS"), Milan, Italy.

References

1. Abdel-Rahman A, Dechkovskaia AM, Sutton JM, Chen WC, Guan X, Khan WA, Abou-Donia MB (2005) Maternal exposure of rats to nicotine via infusion during gestation produces neurobehavioral deficits and elevated expression of glial fibrillary acidic protein in the cerebellum and CA1 subfield in the offspring at puberty. Toxicology 209:245–261
2. Altman J (1972) Postnatal development of the cerebellar cortex in the rat. I. The external granular layer and the transitional molecular layer. J Comp Neurol 145:353–398
3. Armstrong CL, Hawkes R (2000) Pattern formation in the cerebellar cortex. Biochem Cell Biol 78:551–562
4. Baader SL, Schilling ML, Rosengarten B, Pretsch W, Teutsch HF, Oberdick J, Schilling K (1996) Purkinje cell lineage and the topographic organization of the cerebellar cortex. Dev Biol 174:393–406
5. Bautista JR, Rubin SA, Moran TH, Schwartz GJ, Carbone KM (1995) Developmental injury to the cerebellum following perinatal Borna disease virus infection. Brain Res Dev Brain Res 90:45–53
6. Biondo B, Lavezzi AM, Tosi D, Turconi P, Matturri L (2003) Delayed neuronal maturation of medullary arcuate nucleus in SIDS (sudden infant death syndrome). Acta Neuropathol (Berl) 106:545–551
7. Carpentier V, Vaudry H, Laquerriere A, Tayot J, Leroux P (1996) Anatomical distribution of somatostatin receptors in the brainstem of the human fetus. Neuroscience 73:865–879
8. Chen WJA, Edwards RB, Romero RD, Parnell SE, Monk RJ (2003) Long-term nicotine exposure reduces Purkinje cell number in the adult rat cerebellar vermis. Neurotoxicol Teratol 25:329–334
9. Cruz-Sanchez FF, Lucena J, Ascaso C (1997) Cerebellar cortex delayed maturation in sudden infant death syndrome. J Neuropathol Exp Neurol 56:340–346
10. ten Donkelaar HJ, Lammens M, Wesseling P, Thijssen HO, Renier WO (2003) Development and developmental disorders of the human cerebellum. J Neurol 250:1025–1036

11. Dony C, Gruss P (1987) Proto-oncogene c-fos in growth regions of fetal bone and mesodermal tissue. Nature 299:711–714
12. Freeman JA (1982) The cerebellum as a timing device: an experimental study in the frog. In: Llinàs R (ed) Neurobiology of cerebellar evolution and development. American Medical Association, Chicago, pp 397–420
13. Fucile S, Renzi M, Lauro C, Limatola C, Ciotti T, Eusebi F (2004) Nicotinic cholinergic stimulation promotes survival and reduces motility of cultured rat cerebellar granule cells. Neuroscience 127:53–61
14. Fukuda K, Aihara N, Sagar SM, Sharp FR, Pitts LH, Honkaniemi J, Noble LJ (1996) Purkinje cell vulnerability to mild traumatic brain injury. J Neurotrauma 13:255–266
15. Gadson DR, Emery JL (1976) Quantitative morphological studies of developing human cerebellar cortex in various disease states. Arch Dis Child 51:964–967
16. Hamre KM, West JR (1993) The effects of the timing of ethanol exposure during the brain growth spurt on the number of cerebellar Purkinje and granule cells nuclear profiles. Alcohol Clin Exp Res 17:610–622
17. Hatten ME (1990) Riding the glial monorail: a common mechanism for glial-guided neuronal migration in different regions of the developing mammalian brain. Trends Neurosci 13:179–184
18. Heck D, Sultan F (2002) Cerebellar structure and function: making sense of parallel fibers. Hum Mov Sci 21:411–421
19. Herrera DG, Robertson HA (1996) Activation of c-fos in the brain. Prog Neurobiol 50:83–107
20. Lavezzi AM, Ottaviani G, Ballabio G, Rossi L, Matturri L (2004) Preliminary study on the cytoarchitecture of the human parabrachial/Kölliker–Fuse complex, with reference to sudden infant death syndrome and sudden intrauterine unexplained death. Pediatr Dev Pathol 7:171–179
21. Lavezzi AM, Ottaviani G, Matturri L (2004) Involvement of somatostatin in breathing control before and after birth, and in perinatal and infant sudden unexplained death. Folia Neuropathol 42:59–65
22. Lavezzi AM, Ottaviani G, Matturri L (2004) Role of Somatostatin and apoptosis in breathing control in sudden perinatal and infant unexplained death. Clin Neuropathol 23:304–310
23. Lavezzi AM, Ottaviani G, Mauri M, Matturri L (2004) Hypoplasia of the arcuate nucleus and maternal smoking during pregnancy in sudden unexplained perinatal and infant death. Neuropathology 24:284–289
24. Lavezzi AM, Ottaviani G, Rossi L, Matturri L (2004) Hypoplasia of the parabrachial/Kölliker–Fuse complex in perinatal death. Biol Neonate 86:92–97
25. Lavezzi AM, Ottaviani G, Matturri L (2005) Adverse effects of prenatal tobacco smoke exposure on biological parameters of the developing brainstem. Neurobiol Dis 20:601–607
26. Lavezzi AM, Ottaviani G, Mauri M, Terni L, Matturri L (2005) Involvement of the EN-2 gene in normal and abnormal development of the human arcuate nucleus. Int J Exp Pathol 86:25–31
27. Lavezzi AM, Ottaviani G, Mingrone R, Matturri L (2005) Analysis of the human locus coeruleus in perinatal and infant sudden unexplained deaths. Possible role of the cigarette smoking in the development of this nucleus. Dev Brain Res 154:71–80
28. Laquerriere A, Leroux P, Gonzales B, Bodenant C, Tayot J, Vaudry H (1992) Somatostatin receptors in the human cerebellum during development. Brain Res 573:251–259
29. Longo LD (1982) Some health consequences of maternal smoking: issues without answers. Birth Defects Orig Artic Ser 18:13–31
30. Lossi L, Ghidella S, Marroni P, Merighi A (1995) The neurochemical maturation of the rabbit cerebellum. J Anat 187:709–722
31. Matturri L, Biondo B, Mercurio P, Rossi L (2000) Severe hypoplasia of medullary arcuate nucleus: quantitative analysis in sudden infant death syndrome. Acta Neuropathol 99:371–375
32. Matturri L, Minoli I, Lavezzi AM, Cappellini A, Ramos S, Rossi L (2002) Hypoplasia of medullary arcuate nucleus in unexpected late fetal death (stillborn infants): a pathologic study. Pediatrics 109:E43
33. Matturri L, Lavezzi AM, Cappellini A, Ottaviani G, Minoli I, Rubino B, Rossi L (2003) Association between pulmonary hypoplasia and hypoplasia of arcuate nucleus in stillbirth. J Perinatol 23:328–332
34. Matturri L, Ottaviani G, Alfonsi G, Crippa M, Rossi L, Lavezzi AM (2004) Study of the brainstem, particularly the arcuate nucleus, in sudden infant death syndrome (SIDS) and sudden intrauterine unexplained death (SIUD). Am J Forensic Med Pathol 25:44–48
35. Matturri L, Ottaviani G, Alfonsi G, Rossi L, Lavezzi AM (2005) Guidelines in pathological and forensic-medical diagnostics of sudden unexpected infant (SIDS) and fetal death. Lombardy Region Project for reduction of the risk for SIDS and/or sudden fetal death. Available at http://users.unimi.it/~pathol/sids/linee_guida_e.html. Accessed 1 Jun 2005
36. Matturri L, Ottaviani G, Lavezzi AM (2005) Techniques and criteria in pathologic and forensic-medical diagnostics of sudden unexpected infant and perinatal death. Am J Clin Pathol 124:259–268
37. Miale I, Sidman RL (1961) An autoradiographic analysis of histogenesis in the mouse cerebellum. Exp Neurol 4:277–296
38. Millen KJ, Hui CC, Joyner AL (1995) A role for En-2 and other murine homologues of Drosophila segment polarity genes in regulating positional information in the developing cerebellum. Development 121:3935–3945
39. Millet S, Alvarado-Maliart RM (1995) Expression of the homeobox gene En-2 during the development of the chick central nervous system. Eur J Neurosci 7:777–791
40. Morris GF, Mattheuws MB (1989) Regulation of proliferating cell nuclear antigen during the cell cycle. Cell Biol 64:13856–13864
41. Nat R, Voiculescu B, Stanciu C, Vidulescu C, Cergan R, Badiu C, Popescu LM (2001) Apoptosis in human embryo development: 2. Cerebellum. J Cell Mol Med 5:179–187
42. Oehmichen M, Wullen B, Zilles K, Saternus KS (1989) Cytological investigations on the cerebellar cortex of sudden infant death victims. Acta Neuropathol (Berl) 78:404–409
43. Okeda R, Matsuo T, Kuroiwa T, Tajima T, Takahashi H (1986) Experimental study on pathogenesis of the fetal brain damage by acute carbon monoxide intoxication of the pregnant mother. Acta Neuropathol (Berl) 69:244–252
44. Olpe HR, Balcar VJ, Bittiger H, Rink H, Sicher P (1981) Central actions of somatostatin. Eur J Pharmacol 63:127–133
45. Ottaviani G, Matturri L, Rossi L, James TN (2003) Crib death: further support for the concept of fatal electrical instability as the final common pathway. Int J Cardiol 92:17–26
46. Ottaviani G, Matturri L, Rossi L, James TN (2003) Crib death: further support for the concept of fatal electrical instability as the final common pathway. Int J Cardiol 59:497–500
47. Rakic P, Sidman RL (1970) Histogenesis of cortical layers in human cerebellum, particularly the lamina dissecans. J Comp Neurol 139:473–500
48. Rivas RJ, Hatten ME (1995) Motility and cytoskeletal organization of migrating cerebellar granule neurons. J Neurosci 15:981–999
49. Srch M (1992) The cerebellar cortex in sudden infant death. Soud Lek 37:33–36
50. Storm JE, Fechter LD (1985) Prenatal carbon monoxide exposure differentially affects postnatal weight and monoaminic concentration of rat brain regions. Toxicol Appl Pharmacol 81:139–146
51. Storm JE, Valdes JJ, Fechter LD (1986) Postnatal alterations in cerebellar GABA content, GABA uptake and morphology following exposure to carbon monoxide early in development. Dev Neurosci 8:251–261
52. Vollmer JY, Clerc RG (1998) Homeobox genes in the developing mouse brain. J Neurochem 71:1–19

53. Wang VY, Zoghbi HY (2001) Genetic regulation of cerebellar development. Nat Rev Neurosci 2:484–491
54. Wassef M, Joyner AL (1997) Early mesencephalon/metencephalon patterning and development of the cerebellum. Perspect Dev Neurobiol 5:3–16
55. Willinger M, James LS, Catz C (1991) Defining the sudden infant syndrome (SIDS): deliberations of an expert panel convened by the National Institute of Child Health and Human Development. Pediatr Pathol 11:677–684
56. Wingate RJT (2001) The rhombic lip and early cerebellar development. Curr Opin Neurobiol 11:82–88
57. Wood KA, Dipasquale B, Youle RJ (1993) In situ labelling of granule cells for apoptosis-associated DNA fragmentation reveals different mechanisms of cell loss in developing cerebellum. Neuron 11:621–632
58. Xu F, Owen J, Frazier DT (1994) Cerebellar modulation of ventilatory response to progressive hypercapnia. J Appl Physiol 77:1073–1080

Virchows Arch (2007) 450:41–50
DOI 10.1007/s00428-006-0335-x

ORIGINAL ARTICLE

A comparison of pathomolecular markers of fibrosis and morphology in kidney from autopsies of African Americans and whites

Betty Pat · Michael D. Hughson · Jennifer L. Nicol · Wendy E. Hoy · Glenda C. Gobe

Received: 20 October 2005 / Accepted: 20 October 2006 / Published online: 23 November 2006
© Springer-Verlag 2006

Abstract African Americans have an increased incidence of chronic kidney disease (CKD) due to hypertension and arteriosclerosis and increased death due to coronary artery disease, compared with whites. The pathogenesis of CKD involves the increased presence and activation of myofibroblasts and macrophages, promotion of tubulointerstitial fibrosis, and effects of tubulointerstitial cell mitosis and apoptosis. We hypothesized that increased risk of hypertensive vascular disease may be identified by renal pathomolecular markers that are associated with progressive CKD. Renal sections were available from 50 autopsies of 33 African Americans (55% males) and 17 whites (76% males) undergoing forensic autopsy for unexpected death. Sclerotic glomeruli, severity of cortical fibrosis, and renal arteriolosclerosis, total glomerular number (N_{glom}), average glomerular volume (V_{glom}), birth weights, and blood pressure were known. Presence and locality of markers for myofibroblasts (alpha-SMA), macrophages (CD68), collagen, pro-fibrotic transforming growth factor-beta1 were scored in renal autopsies, and tubulointerstitial apoptosis was recorded. The results demonstrated a strong positive correlation between age, cortical fibrosis and alpha-SMA ($p<0.05$), and between CD68 and hypertension and coronary artery disease ($p<0.05$). The findings confirm the role of myofibroblasts and macrophages in pathogenesis of human CKD. However, the markers showed no significant relationships to V_{glom}, N_{glom}, birth weight, or race.

Keywords Chronic renal failure · Fibrosis · Molecular markers · Apoptosis · Growth factor · Myofibroblast · Macrophage

B. Pat · G. C. Gobe (✉)
Molecular and Cellular Pathology, School of Medicine,
University of Queensland,
Herston Road, Herston,
4006 Brisbane, Australia
e-mail: g.gobe@uq.edu.au

M. D. Hughson
University of Mississippi Medical Center,
Jackson, MS, USA

J. L. Nicol · W. E. Hoy
Centre for Chronic Disease, School of Medicine,
University of Queensland,
Brisbane, Australia

Introduction

Chronic kidney disease (CKD), coronary artery disease (CAD), and cerebrovascular disease (CVD) have an increased incidence in African Americans and many other black indigenous populations compared with whites [2, 16, 31, 34, 37]. CKD has an established relationship with CAD and CVD because hypertension is one of the most common causes of CKD and is a major risk factor for CAD and CVD [12]. Recent clinical investigations have also shown that CAD strongly predicts current and future CKD, establishing a bidirectional link between chronic diseases of both organs [27].

Genetic differences may play a role in development of causative diseases such as hypertension, but environmental factors that include socioeconomic status, diet, and tobacco use also contribute. In 1988, Brenner et al. [5] proposed that essential hypertension may be the result of a congenital nephron deficit or low glomerular number. A congenital nephron deficit has been linked to low birth weight (LBW)

in experimental studies and in human autopsy studies [18–20]. African Americans have rates of LBW that are three to six times greater than whites, and LBW has been shown to predict the development of hypertension in adulthood and a greater risk of CAD death [4, 19, 25, 26].

Several studies have found that glomeruli in kidneys of African Americans and other racial groups at high risk for CKD, such as native Americans and Australian aborigines, are larger than those of whites [1, 2, 16, 17, 31, 34, 37]. The cause of this racial difference in glomerular size has not been clearly established, but there is increasing evidence that it is due to LBW and low glomerular number [18, 20].

Renal fibrosis is a correlate of CKD. In this paper, we explore the hypothesis that pathomolecular markers of renal fibrosis may be useful predictors of progressive CKD in at-risk populations. The development of renal fibrosis is a dynamic, multifactorial process that occurs as part of renal healing but is also a progressive pathological process in which the normal balance of genesis and breakdown of extracellular matrix (ECM) is deranged [8]. It involves the participation of various acute and chronic inflammatory cells that synthesize and secrete fibrogenic growth factors. Myofibroblasts and macrophages are two key chronic inflammatory cell types [8, 9, 24, 36]. Both of these cell types produce peptide growth factors such as transforming growth factor-β1 (TGF-β1), basic fibroblast growth factor, platelet-derived growth factor and tumor necrosis factor-α [3, 24, 30]. Of these, TGF-β1 appears to have the closest temporal and spatial links with both the development of fibrosis and with the pro-fibrotic cell populations [24, 32]. Expansion of the ECM is usually accompanied by focal atrophy of the tubular epithelium and with compensatory focal hypertrophy in other areas [6, 9, 13]. Apoptosis of myofibroblasts, identified by electron microscopy, and double immunohistochemical staining for α-smooth muscle actin (αSMA) and terminal dideoxyuridine transferase-mediated nick end labeling (TUNEL), has also been recorded. They were found in proportionally higher numbers in smaller fibrotic lesions early in the experimental process, suggesting a role for myofibroblast apoptosis in limiting the early development of fibrosis [24].

The identification of markers of risk for CKD is important. They may provide additional information for identifying individuals and populations in whom treatment to prevent or ameliorate CKD and CAD/CVD may be helpful. We investigated correlations between selected pathomolecular markers (TGF-β1, collagen V, α-SMA and CD68) and structural characteristics of CKD such as glomerulosclerosis, renal fibrosis, renal arteriolosclerosis, glomerular number (N_{glom}), and glomerular volume (V_{glom}) in renal sections from autopsies of African Americans and whites from one geographic locality in the South-Eastern United States known to have high rates and racial differences in CKD and CAD/CVD [19].

Materials and methods

Autopsy specimens

Analyses were performed using 50 autopsies of 33 African Americans (55% males) and 17 whites (76% males) undergoing forensic autopsy for unexpected death. The research protocol was approved by the Institutional Review Board of the University of Mississippi Medical Center (Jackson, MS, USA). All autopsies were performed at this Center. The autopsies and kidney tissues were used with the permission and informed consent of County Coroners and First-of-Kin.

Specimens were collected from subjects, 50 years of age or less, who had no gross or microscopic evidence of kidney disease other than arteriolar nephrosclerosis. Kidneys with more than a mild degree of renal scarring, as determined macroscopically, were not collected, and cases of diabetic nephropathy were excluded. Right kidneys were collected, bisected, and immersed in 10% buffered formalin. After 10 days, both halves of the kidney were cut into 4 mm slices and sampled according to a previously described protocol for stereological analysis to estimate the total number of glomeruli (N_{glom}) and the average volume of glomeruli (V_{glom}) [18].

Renal tissue not sampled for stereology that contained cortex and medulla was embedded in paraffin and prepared routinely for histological and immunohistochemical techniques. The percentage of globally sclerotic glomeruli and the severity of renal arteriolosclerosis were determined on periodic acid-Schiff reagent (PAS)-stained sections. The severity of arteriolosclerosis was measured, using Image-Pro Plus (Silver Spring, MD) morphometric software, as the intimal thickness to the outer diameter of interlobular arteries 80 to 250 μm in diameter. Cortical fibrosis was calculated using Masson's trichrome stained sections with a 64-point counting grid as the proportion of points overlying blue-stained tissue divided by the total number of points overlying non-glomerular and nonvascular cortex.

Clinical data

Information was available from autopsy records for race, age, gender, height, and body weight, heart weight, left ventricular thickness, and cause of death. On the basis of clinical history, recorded blood pressures, heart weight, left ventricular thickness, and renal arteriolosclerosis, subjects were categorized as hypertensive or non-hypertensive. Birth

weights were obtained on all subjects from the Division of Vital Statistics of the Mississippi State Department of Health. Body surface area (bSA) was calculated from height and weight using an internet program (http://www.ultradrive.com/bsac.htm).

Immunohistochemistry and histochemistry

Microscopic analysis of renal autopsy sections for the molecular markers of fibrosis was carried out blinded to clinical, histological, and stereological data. Numbered paraffin sections from the autopsy specimens (4 μm thick) were dewaxed and rehydrated to buffer. For routine light microscopy, sections were stained with hematoxylin and eosin (HE) and PAS for morphological assessment and also for quantification of apoptosis (see the following section for these details). Sections were also stained using the Gomori trichrome method for extent of collagen. Specific structures assessed for the pathomolecular markers were glomeruli, tubular epithelium on the proximal and distal nephron, interstitium, and vessels. Primary antibodies (Sigma Immunochemicals, Castle Hill, Australia) were all antihuman and were α-SMA for myofibroblasts (1:400 dilution); CD68 for macrophages (1:50 dilution); TGF-β1 as a pro-fibrotic growth factor (1:50 dilution), and Type V collagen for matrix assembly [29] (1:50 dilution). Antibodies were diluted in 1% bovine serum albumin in Tris-buffered saline (BSA/TBS) and applied at room temperature for 1 h, followed by 3×TBS washes. Sections were blocked for nonspecific peroxidase activity with 0.1% sodium azide plus 2% hydrogen peroxide (H_2O_2) in TBS and for nonspecific antibody binding with 4% non-fat powdered milk (blotto) in TBS followed by a 1:100 dilution of horse serum in 1% BSA/TBS, all before primary antibody application. The secondary antibody (Zymed, Invitrogen, Mt Waverley, Australia) was a universal antibody, horseradish peroxidase conjugated (1:200 dilution) in 1% BSA/TBS, applied for 1 h at room temperature, followed by 3× TBS washes, and then, development with the chromogen 3,3-diaminobenzidine tetrahydrochloride (DAB). Sections were washed then lightly counterstained with hematoxylin, dehydrated in alcohols, cleared in xylene, and mounted in Depex. Negative controls had nonimmune serum and no primary antibody applied and positive controls were human tissue with a known positivity for the antibodies, as advised on the suppliers' notes. Each antibody procedure was carried out with the 50 sections as a "batch" to minimize incidental variability in staining intensity.

General quantification methods

For each of the markers, one section per kidney from each autopsy specimen was assessed. All sections were scanned under light microscopy using ×20 and ×40 microscope objectives (×200 and ×400 magnification, respectively) to record the intensity and extent of staining in the various renal structures (glomeruli, tubular epithelium, vessels). Intensity of stain was scored at 0, 1, 2, or 3 indicating no stain, visible but weak, moderate, or very strong staining, respectively. Frequency at which the stain was observed was assessed in each structure from cortex through to medulla and was graded: 0=no staining; 1=detectable rarely, <10% of structures; 2=detectable occasionally, >10% but <25% of structures, 3=detectable moderately, >25% but <50% of structures; 4=detectable frequently >50% but <75%; and 5=detectable in most to all structures, >75%. Similar scoring systems have been used by us previously [24]. A score for each stain, which combined the measures for intensity and frequency, was also generated and was graded: 0=no stain; 1=weak to moderate intensity detectable rarely or often; 2=moderate to very strong intensity detectable in <50% of structures; 3=moderate to very strong intensity detectable frequently or in most to all structures.

Identification and biochemical verification of apoptosis

Apoptotic cells in the renal structures were sought on the basis of morphology [21] in HE-stained sections. Apoptosis was verified biochemically in paired sections using TUNEL. Morphological features included condensed nucleus and eosinophilic cytoplasm and an associated clear ring around these cells, condensed nuclear chromatin typically in crescents against the nuclear envelope, and blebbing into defined, membrane-bound, apoptotic bodies. For TUNEL, the ApopTag® Peroxidase In Situ Apoptosis Detection Kit was used according to the manufacturer's protocol for paraffin embedded sections (Serologicals Corporation, Chemicon, Boronia, Australia). This assay identifies strand breaks in DNA that are typical of apoptosis. Positive cells were visualized with DAB. Sections were lightly counterstained with Mayer's hematoxylin before dehydration in ethanols, clearing in xylene, and mounting with glass coverslips in Depex. Positive and negative controls were performed for TUNEL.

Statistical analyses

N_{glom}, V_{glom}, and birth weight were normally distributed. The percentage of glomerulosclerosis, cortical fibrosis, and renal arteriosclerosis were not normally distributed, and no transformations were appropriate; therefore, categorical variables were generated for analysis. The relationships between age, bSA, N_{glom}, V_{glom}, birth weight, percent glomerulosclerosis, cortical fibrosis, and renal arteriolar sclerosis were analyzed using Spearman's product moment correlation. Fisher's exact test was used to investigate the

Table 1 Summary statistics of the general autopsy data categorized by race

n=50	White n=17	African American n=33	p
Age (years)	28.17±18.43	28.18±14.55	1.00[b]
Male	13 (76.47%)	18 (54.55%)	0.13[c]
bSA (all)	1.62±0.82	1.81±0.63	0.35[b]
bSA (adults)	2.08±0.07	2.02±0.05	0.50
N_{glom}[a]	907,550±254,383	952,163±336,025	0.63[b]
V_{glom} (all)[a]	5.10±2.83	6.81±3.22	0.07[b]
V_{glom} (adults)	6.54±1.90	7.55±2.52	0.23
Birthweight (g)	3,364.71±313.51	3,192.33±590.83	0.27[b]
Percent glomerulosclerosis (%)	2.03 (0.75–3.31)	1.46 (0.78–2.14)	0.18[d]
Renal fibrosis[a]	0.058 (0.026–0.115)	0.063 (0.038–0.123)	0.75[e]
Arteriolosclerosis	0.04 (0.02–0.07)	0.05 (0.03–0.06)	0.06[d]

N_{glom}*and* V_{glom}Number and volume of glomeruli, respectively, *bSA* body surface area
*p<0.05
[a] Geometric mean and interquartile range
[b] Student's t test
[c] Pearson chi-squared test
[d] Fisher's Exact test after variable categorized into 4 groups
[e] Mann–Whitney test

association between intensity or frequency of stain and the categorical levels of glomerulosclerosis, fibrosis, and arteriolosclerosis. Multivariate analyses were used to further analyze the data generated, according to advice from the statistician (JLN). Ordinal logistic regression and the likelihood ratio test were used when adjustment for other predictor variables was included. Analysis of variance and analysis of covariance were used when the associations between pathologic variables and intensity or frequency of staining was investigated. Hypertension was scored as 1 and non-hypertension 0, CAD or CVD deaths were scored 1 and non-CAD/CVD deaths 0, male gender 1 and female 0, African American race 1 and white race 0. Stepwise regression was used to evaluate the relationship of the dependent variable CAD/CVD to the independent variables of race, gender, bSA, N_{glom}, V_{glom}, birth weight, percent glomerulosclerosis, cortical fibrosis, renal arteriolosclerosis, and hypertension. Stepwise regression was also used to evaluate the relationships of the dependent variables CAD/CVD and hypertension to the pathomolecular marker scores. For all statistical procedures, significance was assessed at p<0.05.

Results

Relationships within clinical data

A summary of the autopsy data by race is provided in Table 1. When all cases were considered, V_{glom} had a strong direct correlation with age (adults or subjects≥18 years of age vs children; r=0.504, p<0.0001) and bSA (r=0.530, p<0.0001), reflecting glomerular growth from infancy to adulthood. N_{glom} was directly correlated with birth weight (r=0.417, p=0.0027) but there was no statistically significant relationship between N_{glom} and V_{glom} (r=−0.171, p=0.233). When only adults were considered, N_{glom} was directly correlated with birth weight (r=0.360, p=0.025),

Table 2 Correlation between clinical variables

	bSA	N_{glom}	V_{glom}	BW	Percent GS (%GS)	CF	It
Age	0.189; 0.248	0.0186; 0.909	0.143; 0.383	0.194; 0.236	0.672; >0.0001	0.464; >0.0001	0.722; >0.0001
BSA		0.191; 0.242	0.0212; 0.897	0.347; 0.0306	−0.149; 0.362	−0.0796; 0.628	0.0293; 0.859
Nglom			−0.616; 0.0001	0.360; 0.0245	−0.00102; 0.995	−0.149; 0.364	−0.00935; 0.954
Vglom				−0.209; 0.200	0.0700; 0.670	0.0150; 0.927	0.0517; 0.753
BW					0.0746; 0.649	−0.139; 0.396	−0.0860; 0.600
Percent GS (%GS)						0.601; >0.0001	0.645; >0.0001
CF							0.450; 0.0042

Correlations are made between continuous variables of age, body surface area (bSA), number and volume of glomeruli (N_{glom} and V_{glom}), birth weight (BW), % glomerulosclerosis (%GS), cortical fibrosis (CF) and intimal arterial thickening (It).

and V_{glom} also showed a strong inverse correlation with N_{glom} ($r=-0.616$, $p<0.0001$) in which low N_{glom} predicted large V_{glom}. In the age range of 18 to 50 years, there was no appreciable loss of glomeruli due to glomerulosclerosis. While glomerulosclerosis, cortical fibrosis, and renal arteriolosclerosis increased significantly with age, V_{glom} showed no tendency to change with any of these variables. A summary of the correlations between continuous clinical variables of age, bSA, N_{glom}, and V_{glom}, birth weight, percent (%) glomerulosclerosis, cortical fibrosis, and intimal arterial thickening is demonstrated in Table 2.

Immunohistochemistry

Examples of immunohistochemistry for TGF-β1, α-SMA, CD68, and collagen V are given in Fig. 1. Summary data for the intensity or frequency of the α-SMA, CD68, TGF-β1, and collagen V are represented in bar graphs in Figs. 2 and 3. Assessment of Gomori histochemical stain was similar to the immunohistochemistry for collagen, and only immunohistochemical results are detailed. Cross-tabulations of general autopsy data variables for intensity and frequency of stains were carried out, and p values are presented in Tables 3 and 4. For the purposes of using analysis of variance and analysis of covariance, an assumption was made that V_{glom} and N_{glom} were normally distributed in these data sets. Only α-SMA had a significant correlation with renal fibrosis (Table 3) which was lost after adjustment for bSA and age (Table 4). α-SMA, TGF-β1, and collagen V significantly correlated with V_{glom} (Table 3), and this significance was maintained only in TGF-β1 after adjustment for bSA and age (Table 4).

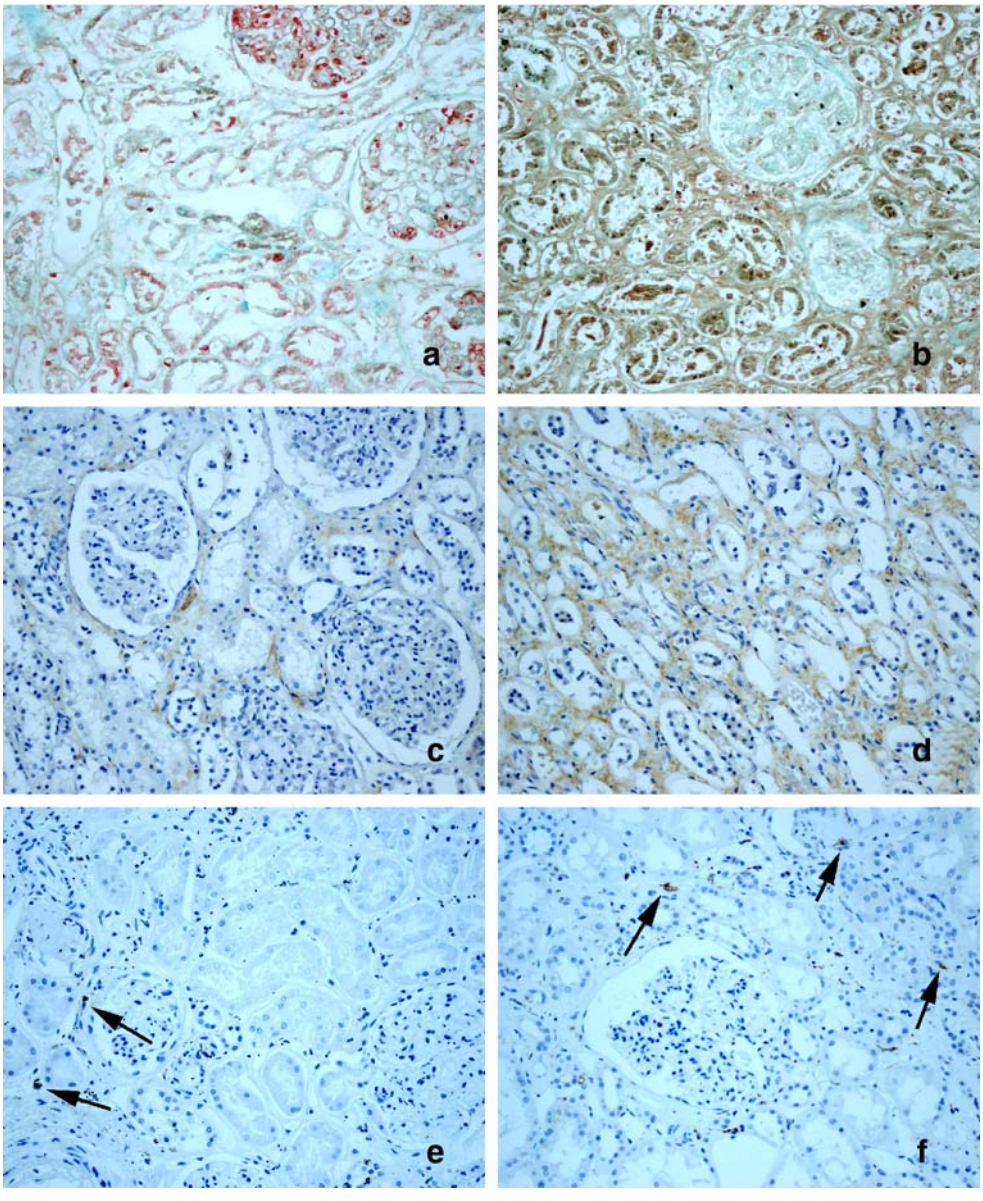

Fig. 1 Immunohistochemistry of molecular markers. Representative immunohistochemistry of molecular markers is demonstrated from selected non-matching sections. **a** demonstrates low intensity and frequency of TGF-β1 in comparison with high intensity and frequency in **b**. TGF-β1 protein is identified by brown DAB stain. These sections were double-stained with Gomori for collagen (*blue-green*), with the *red stain* being background stain from the Gomori process. This was not scored. **c** and **d** represent immunohistochemistry for α-SMA. **c** is an example of low frequency but high intensity and **d** is an example of high frequency and intensity. α-SMA was seen mainly in the interstitial spaces (DAB, *brown*). **e** and **f** represent CD68, with DAB-positive macrophages *arrowed* in the interstitium. Although these sections were not used to score glomerulomegaly, some large glomeruli can be seen in these examples which are all photographed at the same magnification, each ×480

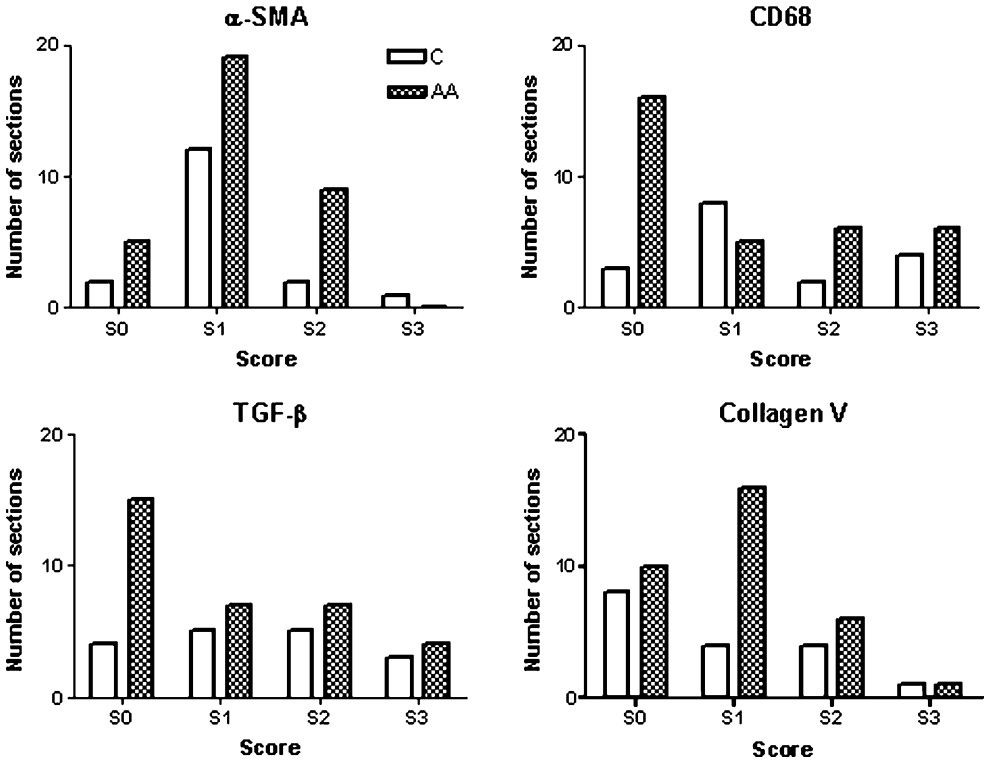

Fig. 2 Immunohistochemistry intensity scores. Summary graphs demonstrate numbers of sections showing different immunohistochemistry intensity scores for α-smooth muscle actin (*α-SMA*), transforming growth factor-β1 (*TGF-β1*), CD68 and collagen V, separated into race. *S0* No stain, *S1* visible but weak, *S2* moderate, *S3* very strong staining, *C* whites, AA African Americans

Apoptosis

Examples of apoptosis and TUNEL (ApopTag) are given in Fig. 4. Paired sections for HE and TUNEL from the one autopsy are demonstrated in Fig. 4a and b. In the HE section, shrunken cells with a distinct plasma membrane, uniformly dense nuclear chromatin and eosinophilic cytoplasm are arrowed (Fig. 4a). These might represent

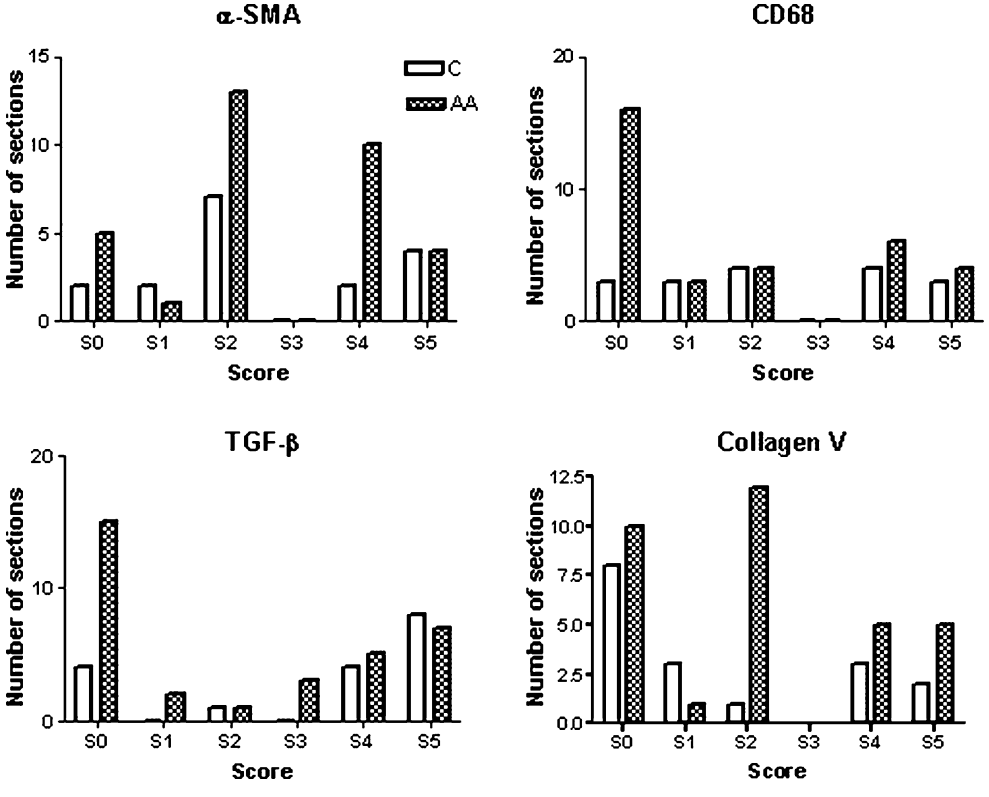

Fig. 3 Immunohistochemistry frequency scores. Summary graphs demonstrate numbers of sections showing different immunohistochemistry frequency scores for α-smooth muscle actin (*α-SMA*), transforming growth factor-β1 (*TGF-β1*), CD68, and collagen V, separated into race. *S0* No staining, *S1* detectable rarely, <10% of structures, *S2* detectable occasionally, >10% but <25% of structures, *S3* detectable often, >25% but <50% of structures, *S4* detectable frequently >50% but <75%, and *S5* detectable in most to all structures, >75%, *C* whites, *AA* African Americans

Table 3 *P* values for cross-tabulations of general autopsy data variables for intensity and frequency of stains, individually and as a combined measure

	Glomerular sclerosis[a]	Closed arteries[a]	Renal fibrosis[a]	$V_{glom}{}^2$	Race[a]
α-SMA intensity	0.49	0.09	0.09	0.01*	0.36
α-SMA frequency	0.78	0.15	0.006*	0.03*	0.40
α-SMA	0.88	0.13	0.07	0.02*	0.65
CD68 intensity	0.10	0.17	0.16	0.30	0.06
CD68 frequency	0.72	0.64	0.65	1.00	0.26
CD68	0.25	0.82	0.47	0.98	0.10
TGF-β1 stain	0.46	0.60	0.54	0.88	0.48
TGF-β1 frequency	0.37	0.80	0.99	0.03*	0.22
TGF-β1	0.46	0.28	0.83	0.77	0.25
Collagen V intensity	0.39	0.38	0.39	0.04*	0.35
Collagen V frequency	0.33	0.44	0.49	0.06	0.07
Collagen V	0.56	0.75	0.83	0.03*	0.51

Note that an assumption has been made that V_{glom} is normally distributed in the data set for the purposes of using analysis of variance.

*$p<0.05$

[a] Cross-tabulations using Fisher's exact test

[b] Analysis of variance

Table 4 *P* values for cross-tabulations of general autopsy data variables for intensity and frequency of stains, individually and as a combined measure from Table 2, after adjusting for age and body surface area

	Glomerular sclerosis[a]	Closed arteries[a]	Renal fibrosis[a]	V_{glom}[b]	Race[a]
αSMA stain	0.93	0.88	0.83	0.58	0.94
αSMA frequency	0.85	0.55	0.98	0.98	0.57
αSMA	0.79	0.24	0.87	0.90	0.63
CD68 stain	0.40	0.40	0.52	0.68	0.27
CD68 frequency	0.73	0.84	0.31	0.86	0.17
CD68	0.83	0.55	0.66	0.71	0.24
TGFβ stain	0.40	0.05	0.07	0.71	0.26
TGFβ frequency	0.23	0.11	0.95	0.01	0.08
TGFβ	0.49	0.05	0.51	0.43	0.13
Collagen stain	0.25	0.77	0.96	0.22	0.75
Collagen frequency	0.06	0.37	0.19	0.48	0.25
Collagen	0.05	0.90	0.98	0.21	0.54

Note that an assumption has been made that V_{glom} is normally distributed in the data set for the purposes of using analysis of covariance.

[a] Ordinal logistic regression LR test

[b] Analysis of covariance

apoptosis in the tubular epithelium, although some tubules had many such cells (demonstrated with asterisks in 4a), perhaps indicative of autolytic pyknosis commonly seen in autopsy specimens. However, no cells with such pyknotic morphology were found in the interstitial spaces, where apoptosis of chronic inflammatory cells may have played a role in minimizing the deposition of ECM. Because of the concern for identification of apoptosis using morphology, TUNEL-positive nuclei were also sought in the sections, as a biochemical marker of apoptosis. Examples are demonstrated in Fig. 4b and c, in both the interstitium and the tubular epithelium. As depicted in 4d, however, there were occasional apoptotic bodies in the interstitial spaces that did not stain positive for TUNEL. This may be a result of delayed tissue preservation in the autopsies although, morphologically, the preservation was impressive. Using TUNEL positivity alone, apoptosis was identified very infrequently, with 80% of Caucasian and 92% of African American renal autopsy sections having zero counts. This may relate to the general lack of pathology, in these cases, undergoing autopsy for unexpected deaths. Because of the general infrequency of the observations of apoptosis, using morphology or TUNEL, no statistical analyses were performed on the observations.

Associations and disease analysis

Rank order correlation between age, cortical fibrosis, N_{glom}, pathomolecular marker expression and hypertension showed strong direct relationships between age and α-SMA frequency ($p<0.0001$) and strength ($p=0.0025$). Cortical fibrosis directly correlated with α-SMA frequency ($p=0.014$) and strength ($p=0.040$) and with hypertension ($p=0.012$). Hypertension had a strong direct association with age ($p=0.0083$), with the youngest hypertensive subject being 35 years old. No relationship was found between N_{glom} and hypertension ($p=0.839$). Stepwise regression using race, gender, age, bSA, N_{glom}, V_{glom}, birth weight, percent (%) glomerulosclerosis, cortical fibrosis, arteriosclerosis, and hypertension as independent variables showed that cardiovascular disease (CAD and CVD) could be predicted by race ($p=0.043$), cortical fibrosis (0.013), age ($p<0.0001$), and hypertension ($p=0.001$). When CD68, α-SMA, TGF-β1, and collagen V strength and frequency were used as independent variables, CD68 strength ($p=0.042$) and frequency ($p=0.037$) predicted cardiovascular disease death. When hypertension was used as the dependent variable, CD68 strength was the significant independent variable ($p=0.022$) with CD68 frequency ($p=0.085$), α-SMA strength (0.068), and α-SMA frequency (0.087) approaching significance.

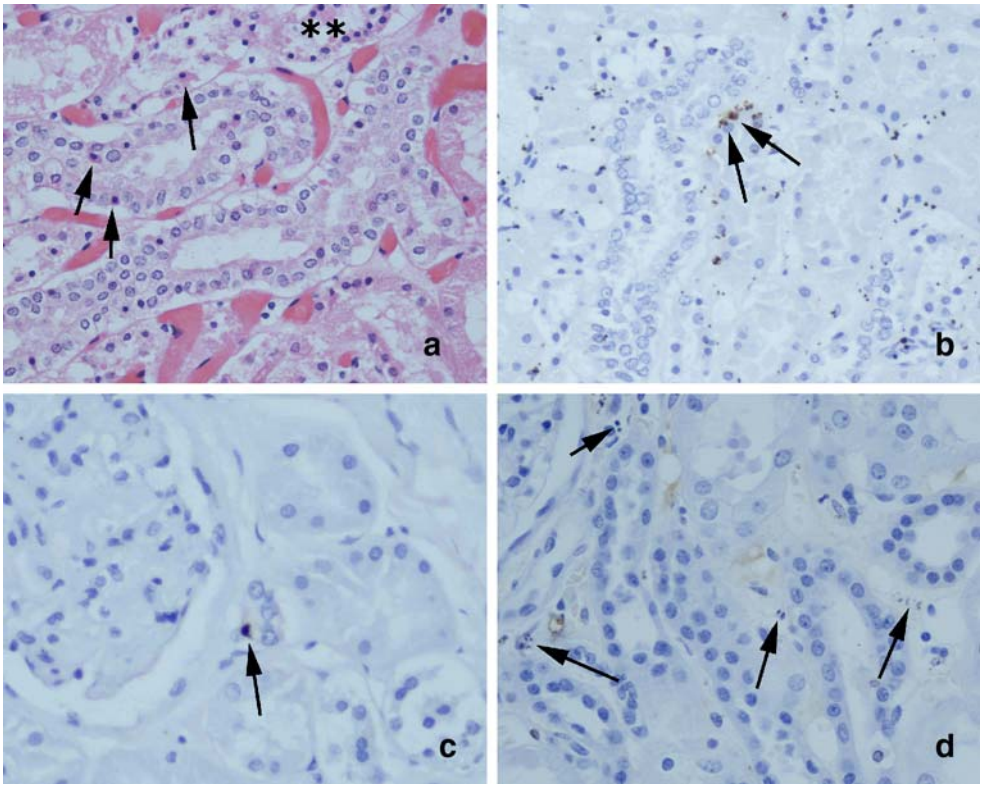

Fig. 4 Apoptosis morphology and TUNEL. Paired sections for HE and TUNEL are given in **a** and **b**. In the HE section, shrunken cells with a distinct plasma membrane, uniformly dense nuclear chromatin and eosinophilic cytoplasm are arrowed in **a**. Many such cells are indicated in the tubule marked with *asterisks*, perhaps, indicative of autolytic pyknosis commonly seen in autopsy specimens. Examples of TUNEL-positive nuclei, as biochemical verification of the presence of apoptosis, are *arrowed* in **b** and **c** (haematoxylin counterstain). TUNEL staining was also used in **d**; however, in this instance, occasional apoptotic bodies identified using morphology in the interstitial spaces did not stain positive for TUNEL. **a**–**d** ×720

Discussion

The progression of CKD involves several interlinked processes, including arteriolosclerosis, glomerulosclerosis, and tubulointerstitial fibrosis with tubular atrophy and loss. The fibrotic process itself involves the infiltration of tissue by inflammatory cells and activation of the cells with the generation of free radicals and the release of pro-fibrotic chemokines, cytokines, and growth factors.

The relative importance of myofibroblasts vs other chronic inflammatory cells such as macrophages and T-lymphocytes in the development and progression of renal fibrosis is still under debate. Goumenos and colleagues [14] described the presence of the myofibroblast as a strong predictor of progressive renal insufficiency. Typically, the differentiating feature between myofibroblasts and their cells of origin is the induction of smooth muscle characteristics and the expression of α-SMA by the myofibroblasts [11]. Although the most likely pre-myofibroblast candidate is the fibroblast, the proposal that tubular epithelial cells may be pro-fibrogenic, with the capacity to transdifferentiate to myofibroblasts, remains an important consideration. In the present study, interstitial cells were often positive, and cells within the tubular epithelium were occasionally found to express α-SMA, supporting the idea of tubular epithelial transdifferentiation to a myofibroblast phenotype in the progression of renal fibrosis [28].

Although we found no relationship to race, the expression of α-SMA for myofibroblasts was positively correlated with renal cortical fibrosis and age, and CD68 expression was associated with hypertension and death due to cardiovascular disease. In human and in experimental studies, TGF-β1 expression often shows a strong temporal and spatial association with fibrosis [6, 24]. Its expression is found in renal tubular epithelial cells and myofibroblasts and is located in the ECM. Myofibroblasts produce TGF-β1, possess active TGF-β1 receptors, and synthesize connective tissue under the influence of TGF-β1 [15]. In the present study, while myofibroblasts increased with age and fibrosis, TGF-β1 did not. This apparent discrepancy may be due to the relatively mild degree of renal pathology that was present in our case material.

Finding macrophage infiltrates associated with CVD and hypertension corresponds well to current concepts that regard arteriosclerosis and hypertension as inflammatory states. This is the basis for evaluating clinical CVD risk with serum C-reactive protein levels [22]. Salt-sensitive hypertension in the rat is an established model in which renal macrophage infiltrates are associated with the elevation of blood pressure [33]. Other experimental models of hypertension in which renal macrophage infiltrates have been shown to play a role include Goldblatt hypertension and the ageing rat [33, 35].

The kidneys in these autopsy subjects were essentially normal for age, and the collection was limited to subjects, 50 years old or less. This was done to prevent the advanced glomerulosclerosis of the more elderly [7] from producing an acquired nephron deficit in our studies on the relationship between nephron number and hypertension. Our study was also restricted for age because the State Department of

Health did not archive birth weights on persons older than 50 years of age at the time the collection began. In this sense, these kidneys represent a baseline for these pathomolecular markers because they show only the glomerulosclerosis, arteriolosclerosis, and the attendant cortical fibrosis expected with the early years of aging and the development of hypertension. Hypertension is strongly age related. It is uncommon in younger individuals, affecting just 6% of the US population between 18 to 34 years of age but rising to 48% of the population, 55 to 64 years old, and to 65% of the population, 65 to 74 years of age [10]. It is possible that subtle age related inflammatory kidney damage may precede the development of hypertension.

The role of apoptosis in the development of renal fibrosis may be either detrimental or beneficial. For example, apoptosis of the tubular epithelium may lead to atrophy and loss of renal function, but it may help resolve otherwise progressive glomerular or tubulointerstitial fibrosis by the deletion of inflammatory cells [23, 24]. In attempting to formulate a reason for the higher incidence of CKD and hypertension in African Americans compared with whites, we hypothesized that apoptosis would be found to a greater extent in the interstitium of the whites, leading to fewer activated interstitial chronic inflammatory calls and a better control of synthesis of pro-fibrotic cytokines. An alternate hypothesis was that increased apoptosis would be associated with more severe cortical fibrosis and tubulointerstitial damage [33]. In the present analysis, there were very few apoptotic cells identified. Those found were located both in the interstitium and the tubular epithelium for both races. The general infrequency of apoptosis may, again, reflect the relatively mild renal changes found in these subjects.

In conclusion, the development of renal fibrosis has a strong positive correlation with age, hypertension, and with renal myofibroblasts and their pathomolecular marker, α-SMA. We could see no relationship between hypertension and N_{glom}, but we did find that renal macrophage infiltrates were associated with hypertension and cardiovascular disease death. The findings resemble those seen in several experimental models of hypertension and indicate that experimental modeling, relating renal inflammatory damage to hypertension, may apply to humans.

Acknowledgements This work was supported by grants from the Colonial Foundation Trust and from the National Institutes of Health NIH1 RO1 DK065970-01.

References

1. Abdi R, Slakey D, Kittur D, Burdick J, Racusen L (1998) Baseline glomerular size as a predictor of function in human renal transplantation. Transplantation 15:329–333
2. Abdi R, Slakey D, Kittur D, Racusen LC (1998) Heterogeneity of glomerular size in normal donor kidneys: impact of race. Am J Kidney Dis 32:43–46
3. August P, Suthanthiran M (2003) Transforming growth factor beta and progression of renal disease. Kidney Int Suppl 87:S99–S104
4. Barker DJP, Gluckman PD, Godfrey KM et al (1993) Fetal nutrition and cardiovascular disease in adult life. Lancet 341:938–941
5. Brenner BM, Garcia DL, Anderson S (1988) Glomeruli and blood pressure: less of one, more the other? Am J Hypertens 1:333–347
6. Chatziantoniou C, Dussaule JC (2005) Insights into the mechanisms of renal fibrosis: is it possible to achieve regression? Am J Physiol Renal Physiol 289:F227–F234
7. Delahunt B, Stehbens WE, Gilbert-Barness E, Shozawa T, Ruger BM (2000) Progeria kidney has abnormal mesangial collagen distribution. Pediatr Nephrol 15:279–285
8. Eddy A (2000) Molecular basis of renal interstitial fibrosis. Pediatr Nephrol 15:290–301
9. El Nahas A, Muchaneta-Kubara E, Essawy M, Soylemezoglu O (1997) Renal fibrosis: insights into pathogenesis and treatment. Int J Biochem Cell Biol 29:55–62
10. Fields LE, Burt VL, Cutler JA, Hughes J, Roccella EJ, Sorlie P (2004) The burden of adult hypertension in the United States 1999–2000. Hypertension 44:398–404
11. Gabbiani G (1996) The cellular derivation and life span of the myofibroblast. Pathol Res Pract 192:708–711
12. Go AS, Chertow GM, Fan D et al (2004) Chronic kidney disease and the risk of death, cardiovascular events, and hospitalization. N Engl J Med 351:1296–1305
13. Gobe G, Axelsen R (1991) The role of apoptosis in the development of renal cortical tubular atrophy associated with healed experimental renal papillary necrosis. Pathology 23:213–223
14. Goumenos D, Brown C, Shortland J, El Nahas A (1994) Myofibroblasts, predictors of progression of mesangial IgA nephropathy Nephrol Dial Transplant 9:1418–1425
15. Goumenos D, Tsamandas A, Oldroyd S, Sotsiou F, Tsakas S, Petropoulou C, Bonikos D, El Nahas A, Vlachojannis J (2001) Transforming growth factor-β1 and myofibroblasts: a potential pathway towards renal scarring in human glomerular disease. Nephron 87:240–248
16. Hoy WE, Hughson MD, Smith SM, Megill DM (1993) Mesangial proliferative glomerulonephritis in southwestern American Indians. Am J Kidney Dis 21:486–496
17. Hughson MD, Johnson K, Young RJ, Hoy WE, Bertram JF (2002) Glomerular size and glomerulosclerosis: relationships to disease categories, glomerular solidification, and ischemic obsolescence. Am J Kidney Dis 39:679–688
18. Hughson M, Farris AB 3rd, Douglas-Denton R, Hoy WE, Bertram JF (2003) Glomerular number and size in autopsy kidneys: the relationship to birth weight. Kidney Int 63:2113–2122
19. Hughson MD, Douglass-Denton R, Bertram JF, Hoy WE (2006) Hypertension, glomerular number, and birth weight in African American and white subjects in the Southeastern United States. Kidney Int 69:671–678
20. Keller G, Zimmer G, Mall G et al (2003) Nephron number in patients with primary hypertension. N Engl J Med 348:101–108
21. Kerr JFR, Gobe G, Winterford C, Harmon BV (1995) Anatomical methods in cell death. In: Schwartz LM, Osborne BA (eds) Methods in cell biology. Academic, San Diego, CA, pp 1–27
22. Labarrere CA, Zolaga GP (2004) C-reactive protein: from innocent bystander to pivotal mediator of atherosclerosis. Am J Med 117:499–507
23. Lan H, Mitsuhashi H, Ng Y, Nikolic-Paterson D, Yang N, Mu W, Atkins R (1997) Macrophage apoptosis in rat crescentic glomerulonephritis. Am J Pathol 151:531–538
24. Lane A, Johnson DW, Pat B, Winterford C, Endre Z, Wei M, Gobe GC (2002) Interacting roles of myofibroblasts, apoptosis

and fibrogenic growth factors in the pathogenesis of renal tubulointerstitial fibrosis. Growth Factors 20:109–119
25. Law CM, deSwiet M, Osmond C et al (1993) Initiation of hypertension in utero and its amplification throughout life. BMJ 306:24–27
26. Lopes AA, Port FK (1995) The low birth weight hypothesis as a plausible explanation for the back/white differences in hypertension, non-insulin dependent diabetes, and end-stage renal disease. Am J Kidney Disease 25:350–356
27. McClellan WM, Langston RD, Presley (2004) Medicare patients with cardiovascular disease have a high frequency of chronic kidney disease and a high rate of progression to end-stage renal disease. J Am Soc Nephrol 15:1912–1919
28. Ng Y-Y, Huang T-P, Yang W-C, Chen Z-P, Yang A-H, Mu W, Nicolic-Paterson D, Atkins R, Lan H (1998) Tubular epithelial-myofibroblast transdifferentiation in progressive tubulointerstitial fibrosis in 5/6 nephrectomized rats. Kidney Int 54:864–876
29. Morita H, Hasegawa T, Minamoto T, Oda Y, Inui K, Tayama H, Nakao N, Nakamoto Y, Ideura T, Yoshimura A (2003) Collagenofibrotic glomerulopathy with a widespread expression of type-V collagen. Virchows Arch 442:163–168
30. Ong A, Fine L (1993) Tubular-derived growth factors and cytokines in the pathogenesis of tubulointerstitial fibrosis: implications for human renal disease progression. Am J Kidney Dis 23:205–209
31. Pesce CM, Schmidt K, Fogo A et al (1994) Glomerular size and the incidence of renal disease in African Americans and Caucasians. J Nephrol 7:355–358
32. Peters H, Border WA, Noble NA (1998) Targeting TGF-β overexpression in renal disease: maximising the anti-fibrotic action of angiotensin II blockade. Kidney Int 54:1570–1580
33. Rodriguez-Iturbe B, Pons H, Quiroz Y, Gordon K, Rincon J, Chaves M, Parra G, Herrera-Acosta J, Gomez-Garre D, Largo R, Egido J, Johnson RJ (2001) Mycophenolate mofetil prevents salt-sensitive hypertension resulting from angiotensin II exposure. Kidney Int 59:2222–2232
34. Schmidt K, Pesce C, Liu QL et al (1992) Large glomerular size in Pima Indians: lack of change with diabetic nephropathy. J Am Soc Nephrol 3:229–235
35. Thomas SE, Anderson S, Gordon KL, Oyama TT, Shankland SJ, Johnson RJ (1998) Tubulointerstitial damage in ageing: evidence for underlying peritubular capillary damage, a potential role for ischemia. J Am Soc Nephrol 9:231–242
36. Young B, Burdmann E, Johnson R, Alpers C, Giachelli C, Eng E, Andoh T, Bennett W, Couser W (1995) Cellular proliferation and macrophage influx precede interstitial fibrosis in cyclosporine nephrotoxicity. Kidney Int 48:439–448
37. Young RJ, Hoy WE, Kincaid-Smith P, Seymour AE, Bertram JF (2000) Glomerular size and glomerulosclerosis in Australian aborigines. Am J Kidney Dis 36:481–489

Virchows Arch (2007) 450:51–58
DOI 10.1007/s00428-006-0330-2

ORIGINAL ARTICLE

Differing distributions of CXCR3- and CCR4-positive cells among types of interstitial pneumonia associated with collagen vascular diseases

Shigeki Shimizu · Takeo Yoshinouchi · Takashi Niimi · Yuji Ohtsuki · Jiro Fujita · Hiroyoshi Maeda · Shigeki Sato · Ichiro Yamadori · Tadaaki Eimoto · Ryuzo Ueda

Received: 11 May 2006 / Accepted: 17 October 2006 / Published online: 24 November 2006
© Springer-Verlag 2006

Abstract Interstitial pneumonia (IP) is an important complication in collagen vascular diseases (CVDs). We examined the distribution of helper T cell subsets in lung biopsies of cases of IP associated with CVD (CVD-IP). The tissues from 27 CVD-IP patients with rheumatoid arthritis (RA), 8 with polymyositis or dermatomyositis (PM/DM), and 8 with systemic sclerosis (SSc) were compared with those from 10 patients with idiopathic pulmonary fibrosis (IPF) in our previous study. The expressions of CXCR3 and CCR4 (chemokine receptors associated in vitro with Th1 and Th2 cells, respectively) in the mononuclear infiltrate were analyzed immunohistochemically. The positive cells were semiquantified in fibrosing areas of the CVD-IP and IPF cases. The number of CXCR3-positive cells was significantly greater in RA-IP than in PM/DM-IP, SSc-IP, or IPF, whereas there were fewer CCR4-positive cells in RA-IP, PM/DM-IP, and SSc-IP than in IPF. The CXCR3-/CCR4-positive cells ratio was significantly higher in RA-IP and PM/DM-IP (but not in SSc-IP) than in IPF. These results support previous reports of the dominance of Th2 cells in some SSc-IP and IPF cases. However, Th1-type immune responses may predominate in RA-IP and PM/DM-IP. Our findings suggest that the pathogenesis of CVD-IPs differs with the helper T cell subset.

Keywords Helper T cells · Chemokines · Receptors · Th1 cells · Th2 cells

S. Shimizu · T. Niimi · H. Maeda · S. Sato (✉) · R. Ueda
Department of Internal Medicine and Molecular Science,
Nagoya City University Medical School,
Kawasumi 1, Mizyho-ku,
Nagoya, Aichi 467-8601, Japan
e-mail: ssato@med.nagoya-cu.ac.jp

S. Shimizu · T. Eimoto
Department of Pathology,
Nagoya City University Medical School,
Nagoya, Aichi, Japan

T. Yoshinouchi
Department of Internal Medicine, Toyokawa City Hospital,
Toyokawa, Aichi, Japan

T. Niimi
Department of Respiratory Medicine, Nagoya Central Hospital,
Nagoya, Aichi, Japan

Y. Ohtsuki
Division of Pathology, Matsuyama-shimin Hospital,
Matsuyama, Japan

J. Fujita
Department of Medicine and Therapeutics, Faculty of Medicine,
University of the Ryukyus,
Okinawa 903-0215, Japan

I. Yamadori
Department of Pathology, National Okayama Medical Center,
Okayama, Japan

Introduction

Pulmonary complications are common in patients with collagen vascular diseases (CVDs) [23, 28, 39], which may be the main cause of mortality in these patients. However,

the prognosis of interstitial pneumonia (IP) associated with CVD (CVD-IP) is variable. Patients with rheumatoid arthritis (RA)-IP generally respond to withdrawal of methotrexate or gold, and the prognosis is usually good [33]. In polymyositis/dermatomyositis (PM/DM)-IP (especially DM-IP), the pathological pattern of diffuse alveolar damage is sometimes evident, which has the worst prognosis [7, 17, 23, 36]. Corticosteroids may produce subjective and objective improvements in patients with RA-IP and PM/DM-IP [22, 33, 39]. Nevertheless, the prognosis is better in systemic sclerosis (SSc)-IP than in idiopathic pulmonary fibrosis (IPF) [39]. While the pulmonary manifestations of each CVD have their own characteristic histologic patterns, there is a considerable overlap between the various types [9, 18], which makes it impossible for pathologists to determine the underlying condition by reviewing a lung biopsy. While detailed communication between clinicians and pathologists regarding the patient's clinical history and radiological findings is essential, reliable markers in each type of CVD-IP may also supply information that is vital to both diagnosis and treatment.

Balbi et al. [3] demonstrated in RA-IP a preferential increase in Tec T-5, 9-positive T cells, a subset of CD4-positive lymphocytes responsible for many helper T cell (Th cell) functions. Such expansion might reflect the T-cell-dependent stimulation of B cells that produces immunoglobulins in the lungs of RA patients. Examining subsets of CD4-positive lymphocytes may be very important in CVD-IP. It is reported that Th1 and Th2 cells express the chemokine receptors CXCR3 and CCR4, respectively [6, 25]. These studies have primarily employed in vitro regimens to induce T cell polarization, and the significance of Th1- and Th2-cell differentiation in physiologic and pathologic settings remains controversial [29]. However, each of the many chemoattractant receptors expressed on leukocyte surfaces may contribute to the versatility and efficiency of leukocyte targeting in vivo [15]. It is possible that variations in the distributions of CXCR3- or CCR4-positive cells are associated with the infiltration of Th1 and Th2 cells, as shown in studies involving bronchoalveolar lavage in patients with sarcoidosis and IPF [24, 31]. Thus, it is worthwhile to assess the pathogenesis of CVD-IP from the viewpoint of chemokine receptor expression in infiltrating lymphocytes.

We have previously confirmed that CXCR3- or CCR4-positive cells are associated with different subtypes of Th cells, and demonstrated that CXCR3- and CD4-positive T cells infiltrate more in IP associated with primary Sjögren syndrome than in IPF [38]. Our results suggested that the distributions of CXCR3-positive cells and CCR4-positive cells vary with the type of CVD-IP. In the present study, we investigated the distributions and subpopulations of T cell subsets in the lung specimens from patients with RA-IP, PM/DM-IP, and SSc-IP, and compared them with those in IPF lungs in our previous study [38].

Materials and methods

Lung biopsy materials

We studied lung biopsy specimens from 27 patients with a diagnosis of CVD-IP (11 RA-IP, 8 PM/DM-IP, and 8 SSc-IP cases). Those from ten patients with IPF in our previous study [38] were also included for comparison. All cases of CVDs were diagnosed according to the criteria of American College of Rheumatology [1]. RA-IP patients comprised six men and five women aged 66.8±2.8 (mean±standard error) years; PM/DM-IP patients comprised one man and seven women aged 56.7±3.1 years; SSc-IP patients comprised two men and six women aged 52.5±3.4 years; and IPF patients comprised ten men aged 62±2.6 years. The pathological patterns of IP in each case are listed in Table 1. In RA-IP, five cases showed the pattern of usual interstitial pneumonia (UIP), four showed that of nonspecific interstitial pneumonia (NSIP), one (case 3) showed foci of UIP and NSIP patterns, and one (case 9) showed a UIP pattern that superposed the diffuse alveolar damage pattern. In PM/DM-IP, two cases showed the UIP pattern and six cases showed the NSIP pattern. In SSc-IP, three cases showed the UIP pattern and five cases showed the NSIP pattern. All IPF cases showed the UIP pattern.

Immunohistochemical staining

The antibodies used were for CD20 (L20, DAKO), CD4 (clone IF6, Novocastra, Newcastle upon Tyne, UK), CD8 (clone 4B11, Novocastra), CXCR3 (BD Bioscience, Franklin Lakes, NJ, USA), and CCR4 (Kyowa Hakko, Tokyo, Japan). In our preliminary study, both anti-CXCR3 and anti-CCR4 antibodies resulted in positive staining in lymphocytes of synovial tissues from patients with RA and skin biopsy specimens from patients with atopic dermatitis. The reactivity of these antibodies was similar in formalin-fixed, paraffin-embedded cell blocks, and flow cytometry specimens of peripheral blood mononuclear cells [19]. For the anti-CCR4 antibody, immunoabsorption using the CCR4 antigen resulted in negative staining of these specimens [19].

Immunohistological staining was performed using the SS MultiLink Detection Kit HRP/DAB (BioGenex Laboratories, San Ramon, CA, USA) for formalin-fixed, paraffin-embedded sections, as described previously [37, 38]. Sections of malignant lymphomas known to be positive for each antigen were used as positive controls, and each primary antibody was substituted with normal serum as a negative control.

Table 1 Lymphocyte subsets in fibrosing areas of IP associated with CVDs and IPF

Patient no.	Diagnosis	Age (years)	Sex	Pathology	CXCR3-positive cells per 20 HPFs	CCR4-positive cells per 20 HPFs	CXCR3-/CCR4-positive cells (ratio)
1	RA	64	M	UIP	10	4	2.5
2	RA	68	F	NSIP	110	10	11.0
3	RA	89	M	UIP, NSIP	92	6	15.3
4	RA	59	F	NSIP	60	5	12
5	RA	71	M	UIP	208	60	77.6
6	RA	73	F	UIP	309	15	20.6
7	RA	57	M	NSIP	48	8	6
8	RA	56	F	UIP	159	41	3.9
9	RA	64	M	UIP, DAD	140	25	5.6
10	RA	62	F	UIP	280	10	28
11	RA	72	M	NSIP	298	2	149
12	PM/DM	44	F	NSIP	80	1	80
13	PM/DM	69	F	NSIP	30	3	10
14	PM/DM	45	F	NSIP	38	6	6.3
15	PM/DM	56	F	NSIP	30	10	3
16	PM/DM	61	F	UIP	51	20	2.6
17	PM/DM	65	F	NSIP	41	25	1.6
18	PM/DM	58	F	UIP	138	58	2.4
19	PM/DM	57	M	NSIP	19	9	2.1
20	SSc	50	F	NSIP	21	1	21.0
21	SSc	58	F	NSIP	20	72	0.28
22	SSc	56	F	NSIP	17	44	0.39
23	SSc	38	M	UIP	231	46	5.0
24	SSc	50	M	NSIP	23	34	0.68
25	SSc	41	F	UIP	41	4	10.0
26	SSc	67	F	UIP	20	20	1
27	SSc	60	F	NSIP	96	43	2.2
28	IPF	73	M	UIP	34	30	1.13
29	IPF	61	M	UIP	63	82	0.77
30	IPF	58	M	UIP	29	51	0.57
31	IPF	67	M	UIP	48	26	1.85
32	IPF	67	M	UIP	47	41	1.15
33	IPF	50	M	UIP	64	87	0.73
34	IPF	62	M	UIP	71	74	0.96
35	IPF	74	M	UIP	97	74	1.31
36	IPF	67	M	UIP	122	115	1.06
37	IPF	52	M	UIP	74	46	1.61

RA Rheumatoid arthritis, *PM/DM* polymyositis or dermatomyositis, *SSc* systemic sclerosis, *UIP* usual interstitial pneumonia, *NSIP* nonspecific interstitial pneumonia, *DAD* diffuse alveolar damage, *HPFs* high-power fields

Semiquantitative assessments of CXCR3- or CCR4-positive cells

The infiltrating mononuclear cells that stained positively for each of CXCR3 and CCR4 were separately evaluated in fibrosing areas of CVD-IP. The positive cells were counted in 20 randomly selected high-power fields (HPFs) (×400) of fibrosing areas [38], and the ratio of CXCR3-positive cells to CCR4-positive cells (CXCR3/CCR4) was calculated.

Statistical analysis

The Mann–Whitney *U* test was used to compare the numbers of CXCR3- or CCR4-positive cells and the CXCR3/CCR4 ratios among the CVD-IP and IPF cases. Differences were considered significant when the probability value was less than 0.05.

Results

Distributions of CD20-, CD4-, or CD8-positive cells in lymphoid clusters and fibrosing areas

CVD-IP cases showed lymphoid clusters, including lymphoid follicles in fibrosing areas, peribronchiolar areas, and pleura. There was marked hyperplasia of the lymphoid tissue surrounding bronchioles in some cases, particularly those of RA-IP (Fig. 1). In contrast, IPF showed only small

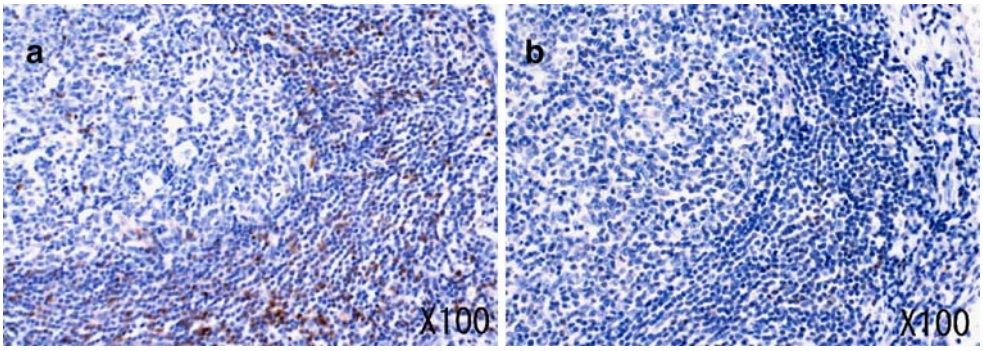

Fig. 1 Immunohistochemical staining with anti-CXCR3 and anti-CCR4 antibodies in lymphoid follicles of IP associated with RA (**a**, **b**). In serial sections the CXCR3-positive cells (**a**) were more numerous than CCR4-positive cells (**b**). (Original magnification, ×100)

lymphocyte aggregates, predominantly in fibrosing areas. CD20-positive cells were seen mainly in lymphoid clusters, with few in fibrosing areas of all CVD-IP and IPF cases. CD4- or CD8-positive cells infiltrated in fibrosing areas and lymphoid clusters of all CVD-IP cases, being more prominent in the latter areas.

Distributions of CXCR3- or CCR4-positive cells in lymphoid clusters

The distributions of CXCR3- or CCR4-positive cells were similar to that of CD4-positive cells in lymphoid clusters of CVD-IP cases. The findings were consistent with our previous study showing that most CXCR3-positive cells and CCR4-positive cells were also positive for CD4, according to a mirror section method [38]. In lymphoid clusters of all CVD-IP and IPF cases, infiltration by CXCR3-positive cells dominated over that of CCR4-positive cells in all cases, and the number of these cells and the CXCR3/CCR4 ratios did not differ significantly among the CVD-IP and IPF cases.

Semiquantitative assessments of CXCR3- or CCR4-positive cells in fibrosing areas

The distributions of CXCR3- or CCR4-positive cells were also similar to those of CD4-positive cells in fibrosing areas of CVD-IP and IPF cases. The proportion of CXCR3-positive cells was lower in fibrosing areas than in lymphoid clusters in CVD-IP. The infiltrations of CXCR3- or CCR4-positive cells differed between cases, in contrast to lymphoid clusters (Figs. 2 and 3). The infiltration varied a little in fibrosing areas of each case, but counting the positive cells in 20 random HPFs yielded fairly consistent values. In all cases of CVD-IP, the numbers of CXCR3-positive cells or CCR4-positive cells and the CXCR3/CCR4 ratios did not differ significantly between the UIP and NSIP patterns (p=0.08, 0.22, and 0.35, respectively). The infiltration of these cells varied among SSc-IP cases, with CXCR3-positive cells and CCR4-positive cells predominating in four cases, respectively.

The number of CXCR3-positive cells was significantly greater in RA-IP (mean 155.8, standard error 31.7) than in PM/DM-IP (53.4, 13.7), SSc-IP (58.6, 26.3), and IPF (64.9, 9.0) (p=0.0017, 0.0032, and 0.038, respectively) (Fig. 4). The numbers of CXCR3-positive cells did not differ significantly among PM/DM-IP, SSc-IP, and IPF cases. On the other hand, only a small number of CCR4-positive cells were detected in most CVD-IP cases, except for four cases of SSc-IP. The numbers of these cells did not differ significantly with the type of CVD-IP. However, the number of CCR4-positive cells was significantly greater in IPF (62.6, 9.0) than in each type of CVD-IP: RA-IP (6.9, 5.5), PM/DM-IP (16.5, 6.6), and SSc-IP (33.0, 8.4) (p= 0.0008, 0.002, and 0.037, respectively) (Fig. 4).

The CXCR3/CCR4 ratios were significantly higher in RA-IP (30.1, 13.5) and PM/DM-IP (13.5, 9.6) than in IPF (1.1, 0.1) (p=0.0001 and 0.00073, respectively) (Fig. 5). The ratio was higher in RA-IP than in PM/DM-IP and SSc-IP (5.1, 2.6) (p=0.048 and 0.013, respectively). However, the CXCR3/CCR4 ratio did not differ between PM/DM-IP and SSc-IP (p=0.23) or between SSc-IP and IPF (p=0.93).

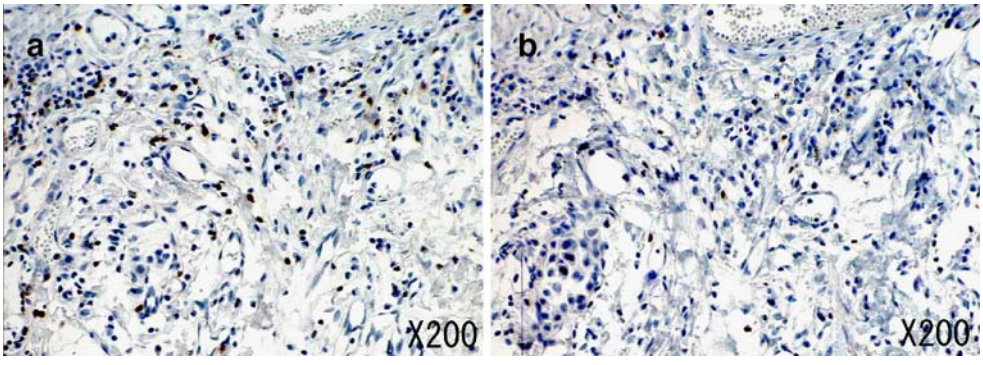

Fig. 2 Immunohistochemical staining with anti-CXCR3 and anti-CCR4 antibodies in fibrosing areas of IP associated with RA (**a**, **b**). In serial sections the CXCR3-positive cells (**a**) were more numerous than CCR4-positive cells (**b**). (Original magnification, ×200)

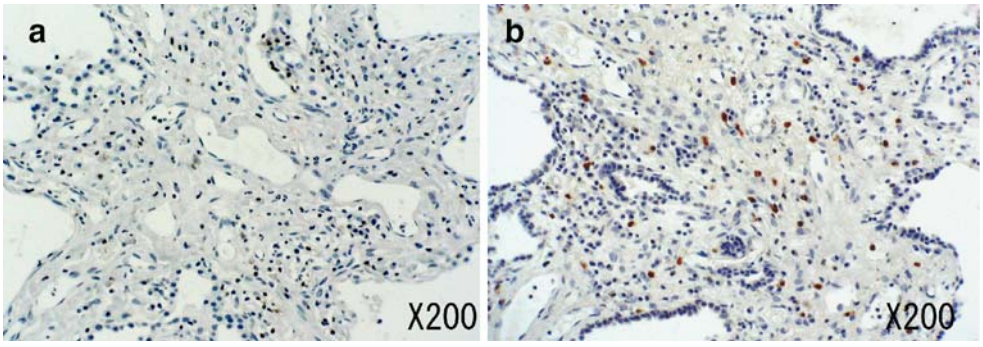

Fig. 3 Immunohistochemical staining with anti-CXCR3 and anti-CCR4 antibodies in fibrosing areas of IP associated with SSc (**a**, **b**). CCR4-positive cells (**b**) were more numerous than CXCR3-positive cells (**a**). (Original magnification ×200)

Discussion

We have previously demonstrated that CXCR3- and CD4-positive T cells infiltrate more in IP associated with primary Sjögren syndrome than in IPF [38]. Recently, Pignatti et al. [31] also reported an imbalance in CXCR3/CCR4 expression on CD4 lymphocytes in bronchoalveolar lavage from patients with IPF. In the present study, we extended the analysis to various types of CVD-IP other than Sjögren-syndrome-IP and found that CXCR3-positive T cells dominantly infiltrate in RA-IP and PM/DM-IP as well. Clones of CD4-positive cells diverge into Th1- and Th2-cell subpopulations. Recent in vitro studies indicate that Th1 and Th2 cells express the chemokine receptors CXCR3 and CCR4, respectively [6, 25]. Previous studies have suggested that the Th2-cell pattern predominates in the most patients with IPF and SSc-IP [2, 5, 28], but there is no such information for RA-IP and PM/DM-IP. Our results suggest that chemokines and their receptors in inflammatory infiltrates differ among these IP cases, and that Th1 cells may predominate over Th2 cells in fibrotic areas of RA-IP and PM/DM-IP, but not in those of IPF and SSc-IP cases.

In our study, CXCR3-positive cells infiltrated significantly more than CCR4-positive cells in the fibrotic areas of RA-IP, most prominently among CVD-IP cases. The Th1-cell dominance in the Th1/Th2-cell balance in RA-IP is compatible with recent findings that the number of Th1-cytokine-producing CD4 T cells increases in RA synovial fluid [4], and that immunostaining shows an increase in the number of CXCR3- and CCR5-positive T cells in RA synovial fluid [32]. The mechanism of inflammation may be similar in the lung and joints of patients with RA. In a murine model of Th1-cell-induced lung injury, the adoptive transfer of alloreactive Th1 cells produced pulmonary inflammation characterized by mononuclear cell vasculitis, alveolitis, and IP [13]. Our results are compatible with the

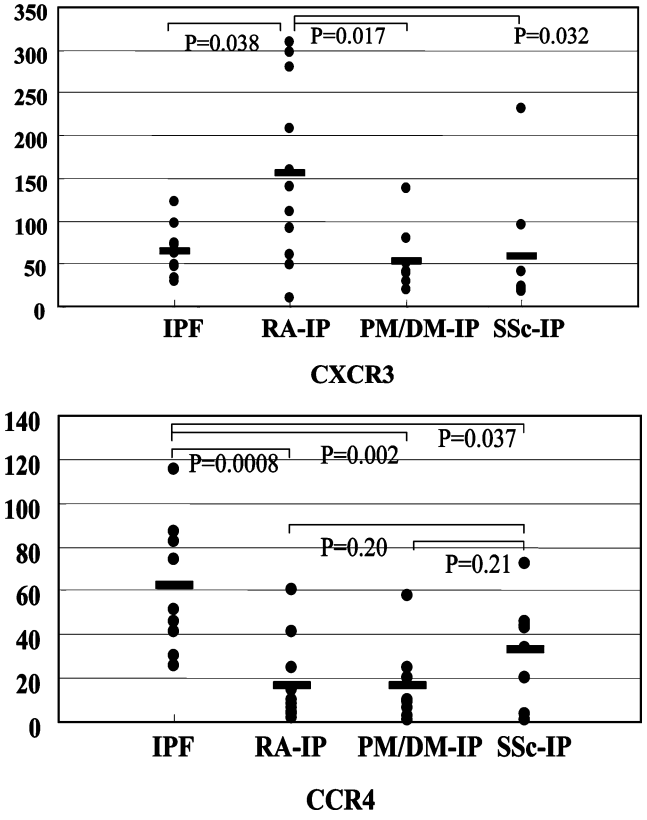

Fig. 4 Comparison of CXCR3- and CCR4-positive cells between IP associated with CVDs and IPF in fibrosing areas. *PM/DM* Polymyositis or dermatomyositis

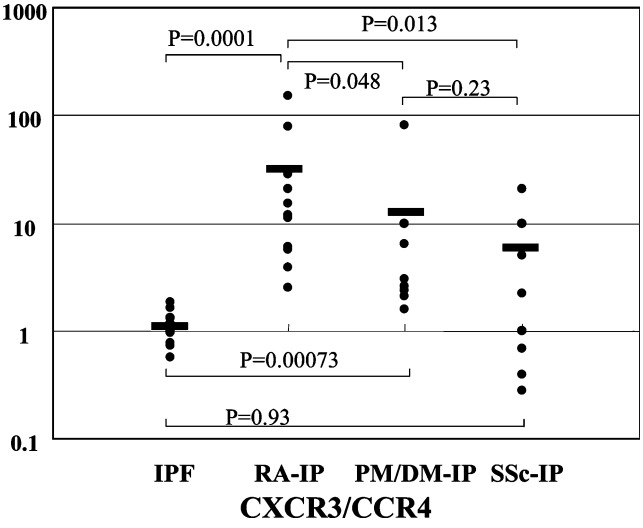

Fig. 5 Comparison of the ratio of CXCR3-positive cells to CCR4-positive cells between IP associated with CVDs and IPF in fibrosing areas

theory that Th1-cell-induced inflammation is important to the pathogenesis of RA-IP.

Lepidi et al. [26] reported that proinflammatory and Th1 cytokines are mainly detected in the muscular tissues of patients with idiopathic inflammatory myopathy, including PM/DM. On the other hand, Aleksza et al. [1] found that the frequency of IL-4-/interferon-gamma-positive Th cells in peripheral blood samples was significantly increased in active DM, but not in PM or in inactive DM. These studies indicate that in patients with PM/DM, Th1-cell inflammation may predominate in muscular tissues, though not throughout the body. Our study suggests that the inflammation in PM/DM-IP involves Th1 cells, and is similar in muscular tissues. The lower numbers of CXCR3-positive cells and lower CXCR3/CCR4 ratio in PM/DM-IP compared with RA-IP suggest that Th1-cell inflammation is milder in the former condition. So far, the total number of cases in all studies is small and hence no definitive conclusions can be drawn. However, in the light of the present and former results, the differences in the expression of Th1 and Th2 cells could be related to disease activity, disease aggressiveness, differences in the pathogenesis, or whether the disease is local or systemic.

CXCR3 is a G-protein-coupled receptor that exhibits selectivity for three chemokines (termed IP10, Mig, and I-TAC) that are commonly produced by local cells in inflammatory lesions [8, 27]. This receptor not only promotes the adhesion of effector T cells to endothelium in the blood flow, but also drives transendothelial migration, and the presence of its ligands is correlated with the outcome of inflammatory liver diseases [10]. CXCR3 may promote the recruitment of regulatory T cells to inflamed tissues, also in inflammatory liver diseases [14]. Similar roles may be ascribed to CXCR3 and its ligands in inflammatory lung disease, and our results suggest that they may participate in the recruitment of inflammatory cells in the RA-IP and PM/DM-IP lungs.

The CXCR3/CCR4 ratio did not differ significantly between SSc-IP and IPF in the present study, and Th2 cells were shown to dominate in both SSc-IP and IPF in previous studies [2, 5, 35]. Rottoli et al. [35] reported that flow cytometry analysis of intracellular cytokines in bronchoalveolar lavage revealed theTh2 profiles predominant in IPF and SSc-IP, and that proteomic analysis showed quantitative differences between IPF and SSc-IP. The results of these studies are compatible with those in at least half of our SSc-IP cases. However, the infiltrations of CXCR3- and CCR4-positive cells varied in SSc-IP cases in the present study, which may be due to the stages of SSc-IP progression. Another possibility is that some cases of SSc-IP are mediated by Th1 cells because some studies have found that either pulse or oral cyclophosphamide therapy is effective in suppressing active alveolitis in SSc-IP [34, 39]. Cyclophosphamide has selective effects on immune responses, such as suppression of Th1-cell activity and enhancement of Th2-cell responses, and was used in the treatment of multiple sclerosis, a Th1-cell-mediated autoimmune disease of the central nervous system [40]. Therapies for SSc-IP might be more effective in cases with a higher prevalence of CXCR3-positive cells.

Clinical and pathologic findings of vascular damage and endothelial cell activation strongly support the hypothesis that a unique vascular disease is an important and primary process in SSc [11, 16]. The SSc fibroblasts may promote leukocyte migration across endothelial cell monolayers in tissue culture via an MCP-1-dependent mechanism [12]. CCR4 is a receptor for MCP-1, MIP-1, RANTES, and TARC, which are the cytokines related to endothelial cells and/or platelets [21, 30]. The infiltration of CCR4-positive cells in SSc-IP in the present study might be associated with vascular damage or endothelial cell activation in the pulmonary interstitium.

The present results for CXCR3- or CCR4-positive cells suggest that the distributions of Th-cell subsets differ among IP cases. In particular, the balance of Th1/Th2-cells in inflammation might differ between the different types of CVD-IP. Furthermore, CXCR3 is a target for the development of small molecular weight antagonists [41], and the defucosylated chimeric anti-CCR4 monoclonal antibody was tested in the development of a novel immunotherapy for malignant lymphomas [20]. More studies on this topic are needed, but it seems likely that an improved understanding of the cells bearing CXCR3 or CCR4 will provide new insight into the pathogenesis of connective tissue diseases and IP and lead to the development of effective new treatments.

Acknowledgements We thank Kyowa Hakko, Tokyo, Japan, and Dr. Masamichi Koike for supplying the CCR4 antibody. We also thank Mr. Seino Nagaya, Department of Pathology, Nagoya City University Medical School, for his excellent technical assistance.

References

1. Aleksza M, Szegedi A, Antal-Szalmas P, Irinyi B, Gergely L, Ponyi A, Hunyadi J, Sipka S, Zeher M, Szegedi G, Danko K (2005) Altered cytokine expression of peripheral blood lymphocytes in polymyositis and dermatomyositis. Ann Rheum Dis 64:1485–1489
2. Atamas SP, Yurovsky VV, Wise R, Wigley FM, Goter Robinson CJ, Henry P, Alms WJ, White B (1999) Production of type 2 cytokines by CD8+ lung cells is associated with greater decline in pulmonary function in patients with systemic sclerosis. Arthritis Rheum 42:1168–1178
3. Balbi B, Cosulich E, Risso A, Sacco O, Balzano E, Rossi GA (1987) The interstitial lung disease associated with rheumatoid arthritis: evidence for imbalance of helper T-lymphocyte subpopulations at sites of disease activity. Bull Eur Physiopathol Respir 23:241–247

4. Berner B, Akca D, Jung T, Muller GA, Reuss-Borst MA (2000) Analysis of Th1 and Th2 cytokines expressing CD4+ and CD8+ T cells in rheumatoid arthritis by flow cytometry. J Rheumatol 27:1128–1135
5. Bolster MB, Ludwicka A, Sutherland SE, Strange C, Silver RM (1997) Cytokine concentrations in bronchoalveolar lavage fluid of patients with systemic sclerosis. Arthritis Rheum 40:743–751
6. Bonecchi R, Bianchi G, Bordignon PP, D'Ambrosio D, Lang R, Borsatti A, Sozzani S, Allavena P, Gray PA, Mantovani A, Sinigaglia F (1998) Differential expression of chemokine receptors and chemotactic responsiveness of type 1 T helper cells (Th1s) and Th2s. J Exp Med 187:129–134
7. Bonnefoy O, Ferretti G, Calaque O, Coulomb M, Begueret H, Beylot-Barry M, Laurent F (2004) Serial chest CT findings in interstitial lung disease associated with polymyositis-dermatomyositis. Eur J Radiol 49:235–244
8. Clark-Lewis I, Mattioli I, Gong JH, Loetscher P (2003) Structure–function relationship between the human chemokine receptor CXCR3 and its ligands. J Biol Chem 278:289–295
9. Colby TV (1998) Pulmonary pathology in patients with systemic autoimmune diseases. Clin Chest Med 19:587–612, vii
10. Curbishley SM, Eksteen B, Gladue RP, Lalor P, Adams DH (2005) CXCR 3 activation promotes lymphocyte transendothelial migration across human hepatic endothelium under fluid flow. Am J Pathol 167:887–899
11. Del Papa N, Colombo G, Fracchiolla N, Moronetti LM, Ingegnoli F, Maglione W, Comina DP, Vitali C, Fantini F, Cortelezzi A (2004) Circulating endothelial cells as a marker of ongoing vascular disease in systemic sclerosis. Arthritis Rheum 50:1296–1304
12. Denton CP, Shi-Wen X, Sutton A, Abraham DJ, Black CM, Pearson JD (1998) Scleroderma fibroblasts promote migration of mononuclear leucocytes across endothelial cell monolayers. Clin Exp Immunol 114:293–300
13. Dixon AE, Mandac JB, Madtes DK, Martin PJ, Clark JG (2000) Chemokine expression in Th1 cell-induced lung injury: prominence of IFN-gamma-inducible chemokines. Am J Physiol Lung Cell Mol Physiol 279:L592–L599
14. Eksteen B, Miles A, Curbishley SM, Tselepis C, Grant AJ, Walker LS, Adams DH (2006) Epithelial inflammation is associated with CCL28 production and the recruitment of regulatory T Cells expressing CCR10. J Immunol 177:593–603
15. Foxman EF, Campbell JJ, Butcher EC (1997) Multistep navigation and the combinatorial control of leukocyte chemotaxis. J Cell Biol 139:1349–1360
16. Freemont AJ, Hoyland J, Fielding P, Hodson N, Jayson MI (1992) Studies of the microvascular endothelium in uninvolved skin of patients with systemic sclerosis: direct evidence for a generalized microangiopathy. Br J Dermatol 126:561–568
17. Fujisawa T, Suda T, Nakamura Y, Enomoto N, Ide K, Toyoshima M, Uchiyama H, Tamura R, Ida M, Yagi T, Yasuda K, Genma H, Hayakawa H, Chida K, Nakamura H (2005) Differences in clinical features and prognosis of interstitial lung diseases between polymyositis and dermatomyositis. J Rheumatol 32:58–64
18. Hunninghake GW, Fauci AS (1979) Pulmonary involvement in the collagen vascular diseases. Am Rev Respir Dis 119:471–503
19. Ishida T, Utsunomiya A, Iida S, Inagaki H, Takatsuka Y, Kusumoto S, Takeuchi G, Shimizu S, Ito M, Komatsu H, Wakita A, Eimoto T, Matsushima K, Ueda R (2003) Clinical significance of CCR4 expression in adult T-cell leukemia/lymphoma: its close association with skin involvement and unfavorable outcome. Clin Cancer Res 9:3625–3634
20. Ishida T, Iida S, Akatsuka Y, Ishii T, Miyazaki M, Komatsu H, Inagaki H, Okada N, Fujita T, Shitara K, Akinaga S, Takahashi T, Utsunomiya A, Ueda R (2004) The CC chemokine receptor 4 as a novel specific molecular target for immunotherapy in adult T-cell leukemia/lymphoma. Clin Cancer Res 10:7529–7539
21. Ito WD, Arras M, Winkler B, Scholz D, Schaper J, Schaper W (1997) Monocyte chemotactic protein-1 increases collateral and peripheral conductance after femoral artery occlusion. Circ Res 80:829–837
22. Jinnin M, Ihn H, Asano Y, Yamane K, Yazawa N, Tamaki K (2003) Effect of D-penicillamine on pulmonary fibrosis in patients with systemic sclerosis. Ann Rheum Dis 62:1019–1020
23. Kang EH, Lee EB, Shin KC, Im CH, Chung DH, Han SK, Song YW (2005) Interstitial lung disease in patients with polymyositis, dermatomyositis and amyopathic dermatomyositis. Rheumatology 44:1282–1286
24. Katchar K, Eklund A, Grunewald J (2003) Expression of Th1 markers by lung accumulated T cells in pulmonary sarcoidosis. J Intern Med 254:564–571
25. Kim CH, Rott L, Kunkel EJ, Genovese MC, Andrew DP, Wu L, Butcher EC (2001) Rules of chemokine receptor association with T cell polarization in vivo. J Clin Invest 108:1331–1339
26. Lepidi H, Frances V, Figarella-Branger D, Bartoli C, Machado-Baeta A, Pellissier JF (1998) Local expression of cytokines in idiopathic inflammatory myopathies. Neuropathol Appl Neurobiol 24:73–79
27. Loetscher P, Pellegrino A, Gong JH, Mattioli I, Loetscher M, Bardi G, Baggiolini M, Clark-Lewis I (2001) The ligands of CXC chemokine receptor 3, I-TAC, Mig, and IP10, are natural antagonists for CCR3. J Biol Chem 276:2986–2991
28. Majumdar S, Li D, Ansari T, Pantelidis P, Black CM, Gizycki M, du Bois RM, Jeffery PK (1999) Different cytokine profiles in cryptogenic fibrosing alveolitis and fibrosing alveolitis associated with systemic sclerosis: a quantitative study of open lung biopsies. Eur Respir J 14:251–257
29. Nanki T, Lipsky PE (2000) Lack of correlation between chemokine receptor and T(h)1/T(h)2 cytokine expression by individual memory T cells. Int Immunol 12:1659–1667
30. Nomura S, Ishii K, Kanazawa S, Inami N, Kamitsuji Y, Uoshima N, Ishida H, Yoshihara T, Kitayama H, Hayashi K (2006) Role of platelet-derived chemokines (RANTES and ENA-78) after stem cell transplantation. Transpl Immunol 15:247–253
31. Pignatti P, Brunetti G, Moretto D, Yacoub MR, Fiori M, Balbi B, Balestrino A, Cervio G, Nava S, Moscato G (2006) Role of the chemokine receptors CXCR3 and CCR4 in human pulmonary fibrosis. Am J Respir Crit Care Med 173:310–317
32. Qin S, Rottman JB, Myers P, Kassam N, Weinblatt M, Loetscher M, Koch AE, Moser B, Mackay CR (1998) The chemokine receptors CXCR3 and CCR5 mark subsets of T cells associated with certain inflammatory reactions. J Clin Invest 101:746–754
33. Roschmann RA, Rothenberg RJ (1987) Pulmonary fibrosis in rheumatoid arthritis: a review of clinical features and therapy. Semin Arthritis Rheum 16:174–185
34. Rossi GA, Bitterman PB, Rennard SI, Ferrans VJ, Crystal RG (1985) Evidence for chronic inflammation as a component of the interstitial lung disease associated with progressive systemic sclerosis. Am Rev Respir Dis 131:612–617
35. Rottoli P, Magi B, Perari MG, Liberatori S, Nikiforakis N, Bargagli E, Cianti R, Bini L, Pallini V (2005) Cytokine profile and proteome analysis in bronchoalveolar lavage of patients with sarcoidosis, pulmonary fibrosis associated with systemic sclerosis and idiopathic pulmonary fibrosis. Proteomics 5:1423–1430
36. Selva-O'Callaghan A, Labrador-Horrillo M, Munoz-Gall X, Martinez-Gomez X, Majo-Masferrer J, Solans-Laque R, Simeon-Aznar CP, Morell-Brotard F, Vilardell-Tarres M (2005) Polymyositis/dermatomyositis-associated lung disease: analysis of a series of 81 patients. Lupus 14:534–542
37. Shimizu S, Yoshinouchi T, Ohtsuki Y, Fujita J, Sugiura Y, Banno S, Yamadori I, Eimoto T, Ueda R (2002) The appearance of S-100 protein-positive dendritic cells and the distribution of lymphocyte subsets in idiopathic nonspecific interstitial pneumonia. Respir Med 96:770–776

38. Shimizu S, Yoshinouchi T, Naniwa T, Nakamura M, Sato S, Ohtsuki Y, Fujita J, Yamadori I, Eimoto T, Ueda R (2004) Distribution of CXCR3- or CCR4-positive cells in interstitial pneumonia associated with primary Sjögren's syndrome. Virchows Arch 445:477–484
39. Steen VD (2005) The lung in systemic sclerosis. J Clin Rheumatol 11:40–46
40. Takashima H, Smith DR, Fukaura H, Khoury SJ, Hafler DA, Weiner HL (1998) Pulse cyclophosphamide plus methylprednisolone induces myelin-antigen-specific IL-4-secreting T cells in multiple sclerosis patients. Clin Immunol Immunopathol 88:28–34
41. Tokuyama H, Ueha S, Kurachi M, Matsushima K, Moriyasu F, Blumberg RS, Kakimi K (2005) The simultaneous blockade of chemokine receptors CCR2, CCR5 and CXCR3 by a non-peptide chemokine receptor antagonist protects mice from dextran sodium sulfate-mediated colitis. Int Immunol 17:1023–1034

Virchows Arch (2007) 450:59–64
DOI 10.1007/s00428-006-0316-0

ORIGINAL ARTICLE

CD24 expression in urothelial carcinoma of the upper urinary tract correlates with tumour progression

Alexandra Winkler · Richard Zigeuner · Peter Rehak · Georg Hutterer · Thomas Chromecki · Cord Langner

Received: 11 August 2006 / Accepted: 12 September 2006 / Published online: 17 November 2006
© Springer-Verlag 2006

Abstract Expression of the mucin-like adhesion molecule CD24 has been implicated in the progression of several types of cancer and has been identified as new prognostic factor. We evaluated CD24 expression in 268 consecutive cases of upper urinary tract urothelial carcinoma with respect to associations with tumour stage, grade, angioinvasion and infiltrative growth pattern using a tissue microarray technique and correlated data with patient outcome. CD24 expression was demonstrated in 161/259 (62%) evaluable tumours and was associated with high tumour stage [77/139 (55%) pTa/pT1 vs 84/120 (70%) pT2–pT4; P=0.02] and high tumour grade [68/139 (49%) low vs 93/120 (78%) high grade; P<0.001] as well as presence of angioinvasion (P=0.002) and infiltrative pattern of invasion (P=0.007). Patients with CD24-positive tumours tended to have a higher risk of disease progression (P=0.065). Multivariate analysis, however, proved pT stage >1 [P<0.001, risk ratio (RR)=5.87, 95% confidence interval (CI)=2.88–11.95] and high tumour grade (P<0.001, RR=3.30, 95% CI 1.75–6.22) as only independent predictors of metastatic disease. In conclusion, CD24 expression in upper urinary tract urothelial cancer is associated with advanced tumour stage and high tumour grade as well as histopathological features indicative of aggressive tumour behaviour, but it lacks independent impact on patient outcome.

Keywords Urothelial carcinoma · Transitional cell carcinoma · Upper urinary tract · CD24 · Prognosis

A. Winkler · C. Langner (✉)
Institute of Pathology, Medical University of Graz,
Auenbruggerplatz 25,
A-8036 Graz, Austria
e-mail: cord.langner@meduni-graz.at

R. Zigeuner · G. Hutterer · T. Chromecki
Department of Urology, Medical University of Graz,
Auenbruggerplatz 7, A-8036 Graz, Austria

P. Rehak
Research Unit for Biomedical Engineering and Computing,
Department of Surgery, Medical University of Graz,
Auenbruggerplatz 29,
A-8036 Graz, Austria

Introduction

Upper urinary tract urothelial carcinoma (UC) accounts for approximately 5% of all urothelial and for 10% of all renal cancers. Smoking, occupational carcinogens and analgesic abuse are accepted as main risk factors [3, 6]. The most common initial presenting symptom is gross haematuria. Tumour stage and grade are valuable prognostic factors and have the most significant impact on patient survival.

In addition, a substantial number of molecular markers have been investigated in recent studies to improve accuracy of outcome prediction and facilitate identification of patients at high risk for failure who might benefit from adjuvant therapy. Overall, these markers can be subdivided into two groups depending on whether their expression is reduced or increased during tumour progression. Biomarkers that are overexpressed during cancer progression are of special interest because they may not only be used to predict patient outcome, but may also serve as potential targets in cancer therapy.

CD24 is a small, heavily glycosilated cell surface protein that is attached to the cell membrane by a glycosylphosphatidylinositol (GPI) anchor. CD24 serves as a specific ligand for P-selectin, an adhesion molecule which is expressed by activated endothelial cells and platelets. Physiologically, the binding of CD24 with P-selectin plays an important role in

marginal adhesion and migration of cells, e.g. leucocytes [10, 16]. Initially CD24 was identified as a B cell marker; later it was found to be expressed in various haematologic malignancies. In the last few years, a large body of literature has also implicated CD24 expression in tumourigenesis and in progression of several types of cancer [10, 17]. Hence, CD24 has been identified as a new prognostic variable in ovarian cancer [8, 25], breast [12, 24], prostate [9] and colorectal adenocarcinoma [26], intrahepatic cholangiocarcinoma [23] as well as non-small cell lung cancer [11]. However, no significant impact on patient outcome was identified in pancreatic adenocarcinomas [4].

A recent study by Smith et al. [21] reported CD24 overexpression in bladder cancer compared to normal urothelium; however, no correlation with tumour stage and grade was noted. Although only 23 cancer samples had been included in the investigation, patients with tumours with strong CD24 immunoreactivity tended to have a shorter disease-free survival ($p=0.07$).

The aim of the present study was to validate the observations by Smith et al. [21] using tissue microarrays (TMAs) of a large sample of upper urinary tract UCs recently constructed by our group [15]. In addition, we focused our attention on possible associations between CD24 expression and histopathological features indicative of aggressive tumour behaviour, such as angioinvasion and infiltrative pattern of invasion because literature data are currently unavailable in this respect.

Materials and methods

Case selection

Two hundred sixty-eight consecutive upper urinary tract UCs (169 pelvic and 99 ureteral tumours) from 239 consecutive patients (108 females, 131 males; ratio 1:1.2) operated between January 1984 and December 2004 were chosen and analysed. Mean and median ages of patients were 69.8 and 70.8 (range 39–89) years, respectively. pT stages were assessed according to the UICC 2002 issue of the tumour node metastasis (TNM) classification [22]. Grading was performed according to the recently published two-tiered WHO grading system, corresponding to the WHO/ISUP consensus classification [18].

For the correlation of pathological findings with metastasis-free survival, all non-invasive cancers (41 tumours) and all tumours from patients with multiple invasive cancers (37 tumours) were excluded resulting in a final sample of 190 UCs (134 pelvic and 56 ureteral tumours) from 190 patients (77 females, 113 males; ratio 1:1.5). Patients either underwent nephroureterectomy with bladder-cuff resection ($n=130$), nephrectomy alone ($n=40$), or distal ureteral resection with reimplant ($n=20$). No adjuvant therapy was given.

Follow-up regimen included abdominal ultrasound and cystoscopy at 3-month intervals for the first 3 years, 6-month intervals for the next 2 years and yearly thereafter as well as chest X-ray and computerised tomography at 6-month intervals for the first 3 years and yearly thereafter. All procedures were in accordance with the ethical standards established by our institution. Informed consent is not required for retrospective analyses dealing with archive material obtained during routine medical treatment.

Immunohistochemistry

For immunohistochemical evaluation a tissue microarray technique was used. The details of this technique have been described previously [7]. Briefly, tissue microarrays (TMAs) were constructed using a manual tissue-arraying instrument (Beecher, Silver Spring, MD, USA). To account for tumour heterogeneity, at least three cylindrical core biopsies, 0.6 mm in diameter, were taken from different sites of each tumour and arrayed in a recipient paraffin TMA block. Four micrometer TMA sections were incubated with the mouse monoclonal antibody CD24 (GPI-linked surface mucin) Ab-2 (clone SN3b; Lab Vision, Fremont, CA, USA) using the BenchMark® XT automated immunostaining system (Ventana Medical Systems, Illkirch, France). Binding of the primary antibody was assessed by the iView™ DAB Detection KIT (Ventana).

Immunohistochemical evaluation and controls

Immunoreactivity was assessed by two investigators (A.W. and C.L.) who were blinded to clinicopathologic data. Discrepancies were resolved by simultaneous reexamination of the slides by both investigators using a double-headed microscope. A distinct cytoplasmic and/or membranous staining was considered positive, and each tumour was scored assessing the average positivity of the core biopsies. A case of breast cancer, known to express CD24, served as positive control. Negative controls included omission of the primary antibody and incubation with Ventana Antibody Diluent (Cat # 251-018).

Statistical analysis

Subgroups according to pT stage and tumour grade were compared with respect to possible differences in immunoreactivity using the Fisher's exact test. Disease-free survival was assessed using the Kaplan–Meier method and compared by the log-rank test. For multivariate testing, a Cox's proportional hazards regression model was performed. All reported P values were two-sided with significance at $P<0.05$.

Table 1 Upper urinary tract urothelial carcinomas related to tumour stage (pTa–pT4) and tumour grade

	All tumours		Pelvic tumours		Ureteral tumours	
	n	%	*n*	%	*n*	%
pTa	41	15	19	11	22	22
pT1	102	38	60	36	42	42
pT2	37	14	20	12	17	17
pT3	80	30	62	37	18	18
pT4	8	3	8	5	–	–
LG	141	53	84	50	57	58
HG	127	47	85	50	42	42
Total	268	100	169	100	99	100

LG Low grade, *HG* high grade

Results

Histopathology

Stage pTa was present in 41 (15%), pT1 in 102 (38%), pT2 in 37 (14%), pT3 in 80 (30%) and pT4 in eight (3%) cases, respectively. There were 141 (53%) low and 127 (47%) high-grade cases. Pelvic and ureteral UCs showed a comparable distribution regarding the different categories (Table 1).

Regarding invasive tumours only, 82/227 (36%) UCs showed lymph vessel (L1) and/or blood vessel (V1) invasion. In a recent study, we were able to show that the presence of angioinvasion in upper tract UCs is associated with high tumour stage and high tumour grade and proves to be a useful independent prognosticator [14]. According to the criteria by Jiminez et al. [5], the pattern of tumour invasion was nodular in 49/227 (22%), trabecular in 95/227 (42%) and infiltrative in 83/227 (37%) cases, respectively.

Immunohistochemistry

Cancer tissue allowing a reliable evaluation of CD24 immunoreactivity was present in 259/268 (97%) cases. Distinct cytoplasmic and/or membranous CD24 expression was observed in 161/259 (62%) tumours and was associated with high tumour stage [77/139 (55%) pTa/pT1 vs 84/120 (70%) pT2–pT4; $P=0.02$] and high tumour grade [68/139 (49%) low vs 93/120 (78%) high grade; $P<0.001$]. The vast majority of tumours showed strong cytoplasmic CD24 expression with only occasional membranous staining. Some cases, however, revealed predominantly membranous staining (Fig. 1a–d). No association between the preferential location of CD24 expression (cytoplasmic vs membranous) and tumour stage and grade was found (data not shown). Pelvic and ureteral UCs showed comparable staining results regarding the different tumour categories (Table 2).

In invasive cancers (219 evaluable cases), expression of CD24 was associated with presence of lymph and/or blood vessel invasion. Thus, 62/78 (79%) UCs with angioinva-

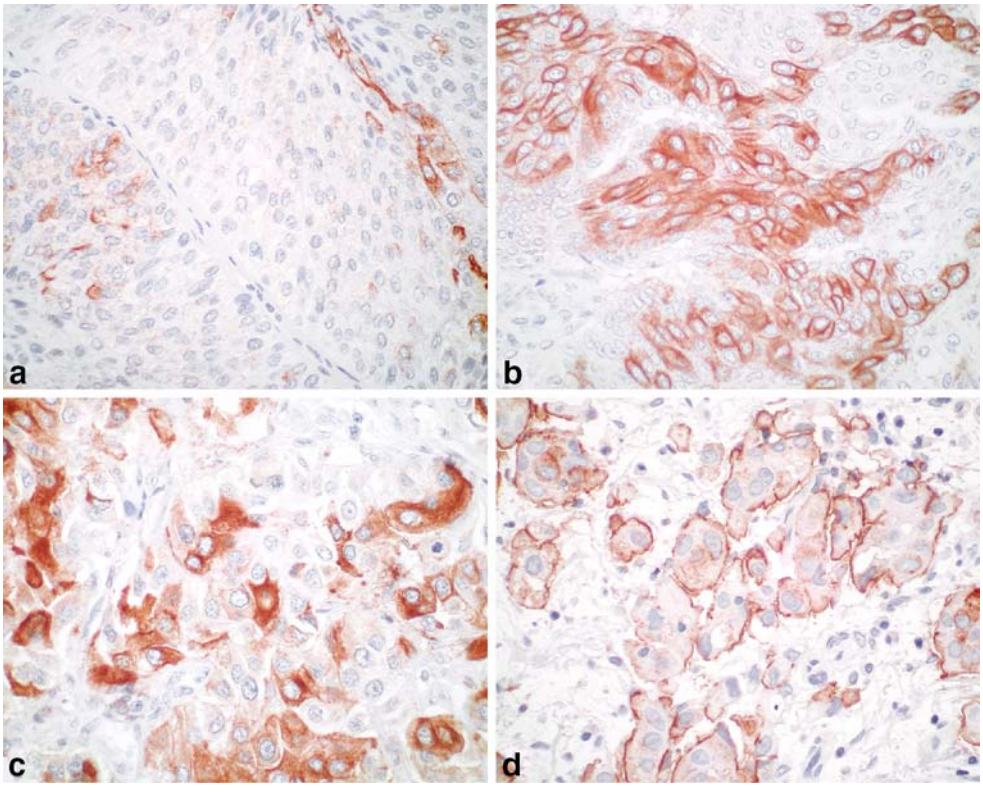

Fig. 1 Examples of CD24 immunoreactivity in urothelial carcinoma of the upper urinary tract: focal expression in non-invasive (pTa) cancer (**a**, original ×100), heterogeneous expression in low-grade invasive cancer (**b**, original ×100), as well as predominantly cytoplasmic (**c**, original ×100) and predominantly membranous (**d**, original ×100) immunolabelling in high grade cancer

Table 2 CD24 expression in upper urinary tract urothelial carcinomas related to tumour stages (pTa–pT4) and tumour grades

	All tumours		Pelvic tumours		Ureteral tumours	
	n	%	*n*	%	*n*	%
pTa	17/40	43	11/18	61	6/22	27
pT1	60/99	61	34/57	60	26/42	62
pT2	23/36	64	12/20	60	11/16	69
pT3	56/76	74	44/60	73	12/16	75
pT4	5/8	63	5/8	63	–	–
LG	68/139	49	47/82	57	21/57	37
HG	93/120	78	59/81	73	34/39	87
Total	161/259	62	106/163	65	55/96	57

LG Low grade, *HG* high grade

sion demonstrated CD24 immunoreactivity, compared to 82/141 (58%) UCs lacking angioinvasion (P=0.002). In addition, CD24 immunoreactivity was associated with infiltrative pattern of invasion. Thus, 60/77 (78%) tumours with this pattern showed CD24 expression, compared to 84/142 (59%) tumours showing either nodular or trabecular pattern of invasion (P=0.007).

Survival analysis

Follow-up data were available for 184/190 (97%) patients with solitary invasive UCs. After a mean and median follow-up of 53 and 36 months, respectively, progressive disease was observed in 74/184 (40%) patients including 54 patients who died from cancer and 20 patients who currently are alive with metastatic disease. The lung was the most common site of metastasis. Mean time to progression was 22 months (median 9, range 0–127). 31 patients died from causes not related to upper urinary tract cancer.

The development of distant metastases was not significantly associated with the presence of CD24 immunoreactivity. Thus, 52/123 (42%) patients with UCs with CD24 expression developed disease progression, compared with 22/61 (36%) patients with UCs without CD24 expression (P=0.065, log-rank test; Fig. 2).

Consequently, in a Cox's proportional hazards regression model (including patient age, gender, tumour stage, tumour grade and CD24 expression), pT stage >1 [P<0.001, risk ratio (RR)=5.87, 95% confidence interval (CI)=2.88–11.95] and high tumour grade (P<0.001, RR=3.30, 95% CI 1.75–6.22) proved to be the only independent predictors of metastatic disease.

Discussion

The small mucin-like adhesion molecule CD24 has recently attracted considerable attention in cancer biology because the acquisition of properties that allow the interaction with platelets and endothelial cells is of advantage for tumour cells. Thus, binding to platelets protects intravasal tumour

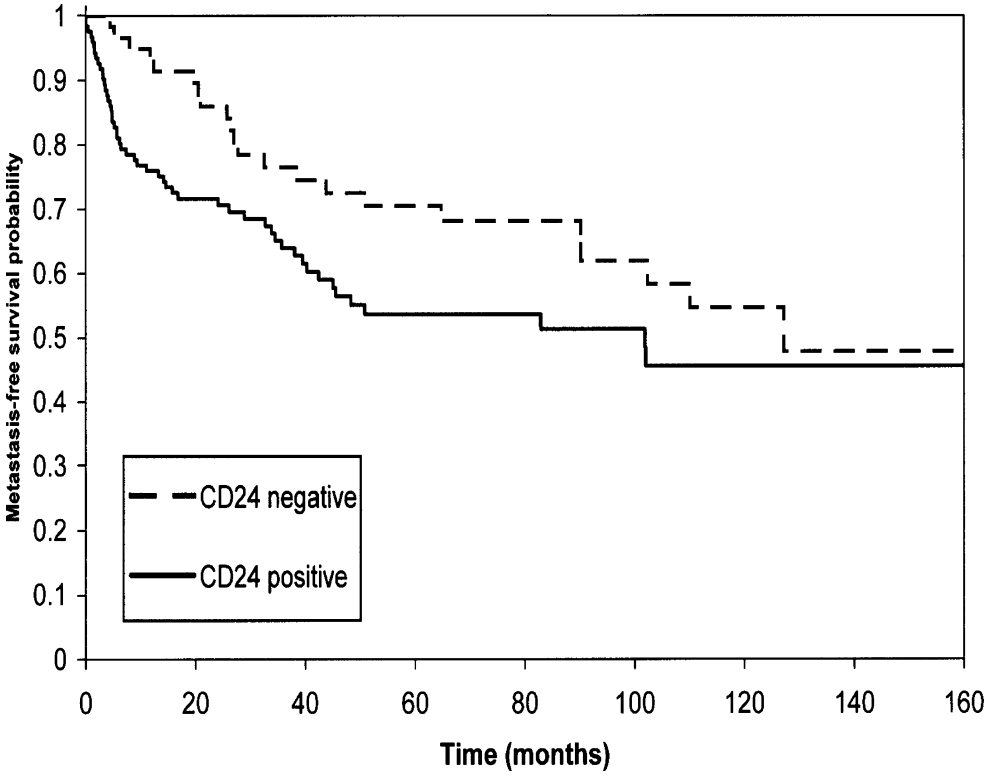

Fig. 2 Metastasis-free survival (months) in patients with upper tract urothelial carcinomas related to the presence of CD24 immunoreactivity (P=0.065, log-rank test)

cell aggregates from destruction and facilitates their transport through the blood stream to new destinations. In addition, the interaction with endothelial cells and extracellular matrix proteins facilitates uncontrolled intra- and extravasation as well as tissue penetration [10, 16], marking the most important steps of the metastatic process.

In vitro data demonstrate that CD24 increases tumour cell proliferation and supports cell motility as well as tumour cell spreading, thus promoting tumour invasion and metastasis in experimental animals [1]. On the contrary, loss of CD24 function in cell lines derived from common tumour types is associated with significant change in cell morphology and the actin cytoskeleton, decreased rates of cell proliferation and induction of apoptosis [21].

Recently, Smith et al. [21] reported a 4.4-fold overexpression of CD24 in bladder cancer compared with normal mucosa. By immunohistochemistry, no association with either tumour stage or grade was found; the investigation, however, was restricted to only 23 cases. According to our results, the expression of CD24 in UCs is significantly associated with both high tumour stage and high tumour grade; thus, confirming previous data obtained from colorectal adenocarcinoma [26], whereas in ovarian [8], breast [12, 24] and non-small cell lung cancer [11], no association was noted. At least focal CD24 immunostaining, however, was observed already in almost every second non-invasive urothelial tumour.

In addition, our study aimed to investigate the relation between CD24 expression and histopathological features suggestive of aggressive tumour growth. In two previous studies, we were able to demonstrate that both angioinvasion as well as the infiltrative pattern of tumour invasion which is characterised by a high degree of tumour cell dissociation at the invasion front are significantly associated with high tumour stage and grade and may additionally be applied as independent predictors of poor prognosis in patients with upper urinary tract UC [13, 14].

The significant association between CD24 expression and presence of angioinvasion observed in the present investigation may reflect the CD24-mediated interaction between tumour cells and endothelial cells, thus facilitating intravasation. Similarly, the strong CD24 immunoreactivity of tumours showing a high degree of tumour cell dissociation at the invasion front may be related to interactions of CD24 with extracellular matrix proteins, such as collagen, laminin and fibronectin that enable tumour cells to migrate in an unfamiliar surrounding.

In the last few years, a large body of literature has correlated CD24 expression with shortened disease-free and overall survival in cancer patients [8, 9, 11, 12, 23–26]. Regarding bladder cancer, Smith et al. [21] reported that increased CD24 expression correlated with shorter patient disease-free survival. Their results obtained from only 23 patients, however, were not significant ($p=0.07$). Despite largely expanding the sample size, we came to almost identical data ($p=0.065$). It is interesting to note that the Kaplan–Meier curves in our investigation considerably diverged during the first years of follow-up. The difference between CD24-positive and CD24-negative tumours is significant at 60 months ($p=0.029$). During the following years, however, the curves almost coalesce and the difference disappears. Thus, CD24 may promote metastatic cancer cell spread especially during the early phases of tumour progression, whereas later in the disease course, additional factors seem to be more important in determining patient outcome.

Post-transplant lymphomas have successfully been treated with intravenous administration of CD21/CD24-specifc antibodies [2]. Whether CD24-targeted therapy may be similarly effective in solid tumours, is currently under investigation. First promising in vitro data have just very recently been obtained from human pancreatic and colorectal adenocarcinoma cell lines that express CD24. Administration of anti-CD24 monoclonal antibodies resulted in growth inhibition of cancer cells in a dose and time dependent manner [19, 20].

In conclusion, CD24 expression in upper urinary tract UCs correlates with high tumour stage and grade as well as histopathological features associated with aggressive tumour behaviour, such as angioinvasion and infiltrative pattern of invasion. However, no significant impact on prognosis was noted. CD24 may be a promising target in future cancer therapy.

Acknowledgements The authors are grateful to Mrs. M. Gogg-Kamerer, Mrs. M. Lindbauer, Mr. M. Al-Effah and Ms. A. Kaps for excellent technical assistance.

References

1. Baumann P, Cremers N, Kroese F, Orend G, Chiquet-Ehrismann R, Uede T, Yagita H, Sleeman JP (2005) CD24 causes the acquisition of multiple cellular properties associated with tumor growth and metastasis. Cancer Res 65:10783–10793
2. Garnier JL, Stevenson G, Blanc-Brunat N, Touraine JL, Milpied N, Leblond V, Blay JY (2002) Treatment of post-transplant lymphomas with anti-B-cell monoclonal antibodies. Recent Results Cancer Res 159:113–122
3. Genega EM, Porter CR (2002) Urothelial neoplasms of the kidney and ureter. An epidemiologic, pathologic, and clinical review. Am J Clin Pathol 117(Suppl):S36–S48
4. Jakob J, Bellach J, Grutzmann R, Alldinger I, Pilarsky C, Dietel M, Kristiansen G (2004) Expression of CD24 in adenocarcinomas of the pancreas correlates with higher tumor grades. Pancreatology 4:454–460
5. Jimenez RE, Gheiler E, Oskanian P, Tiguert R, Sakr W, Wood DP Jr, Pontes JE, Grignon DJ (2000) Grading the invasive component of urothelial carcinoma of the bladder and its relationship with progression-free survival. Am J Surg Pathol 24:980–987

6. Kirkali Z, Tuzel E (2003) Transitional cell carcinoma of the ureter and the renal pelvis. Crit Rev Oncol Hematol 47:116–155
7. Kononen J, Bubendorf L, Kallioniemi A, Barlund M, Schraml P, Leighton S, Torhorst J, Mihatsch MJ, Sauter G, Kallioniemi OP (1998) Tissue microarrays for high-throughput molecular profiling of tumor specimens. Nat Med 4:844–847
8. Kristiansen G, Denkert C, Schlüns K, Dahl E, Pilarsky C, Hauptmann S (2002) CD24 is expressed in ovarian cancer and is a new independent prognostic marker of patient survival. Am J Pathol 161:1251–1221
9. Kristiansen G, Pilarsky C, Pervan J, Sturzebecher B, Stephan C, Jung K, Loening S, Rosenthal A, Dietel M (2004) CD24 expression is a significant predictor of PSA relapse and poor prognosis in low grade or organ confined prostate cancer. J Hered 58:183–192
10. Kristiansen G, Sammar M, Altevogt P (2004) Tumour biological aspects of CD24, a mucin-like adhesion molecule. J Mol Histol 35:255–262
11. Kristiansen G, Schlüns K, Yongwei Y, Denkert C, Dietel M, Petersen I (2003) CD24 is an independent prognostic marker of survival in nonsmall cell lung cancer patients. Br J Cancer 88:231–236
12. Kristiansen G, Winzer KJ, Mayordomo E, Bellach J, Schlüns K, Denkert C, Dahl E, Pilarsky C, Altevogt P, Guski H, Dietel M (2003) CD24 expression is a new prognostic marker in breast cancer. Clin Cancer Res 9:4906–4913
13. Langner C, Hutterer G, Chromecki T, Rehak P, Zigeuner R (2006) Patterns of invasion and histological growth as prognostic indicators in urothelial carcinoma of the upper urinary tract. Virchows Arch 448:604–611
14. Langner C, Hutterer G, Chromecki T, Winkelmayer I, Rehak P, Zigeuner R (2006) pT classification, grade, and vascular invasion as prognostic indicators in urothelial carcinoma of the upper urinary tract. Mod Pathol 19:272–279
15. Langner C, Rupar G, Leibl S, Hutterer G, Chromecki T, Hoefler G, Rehak P, Zigeuner R (2006) Alpha-methylacyl-CoA racemase (AMACR/P504S) protein expression in urothelial carcinoma of the upper urinary tract correlates with tumour progression. Virchows Arch 448:325–330
16. Lim SC (2005) CD24 in human carcinomas: tumor biological aspects. Biomed Pharmacother 59(Suppl 2):S351–S354
17. Lim SC, Oh SH (2005) The role of CD24 in various human epithelial neoplasias. Pathol Res Pract 201:479–486
18. Lopez-Beltran A, Sauter G, Gasser T, Hartmann A, Schmitz-Dräger BJ, Helpap B, Ayala AG, Tamboli P, Knowles MA, Sidransky D, Cordon-Cardo C, Jones PA, Cairns P, Simon R, Amin MB, Tyczynski JE (2004) Tumours of the urinary system. Infiltrating urothelial carcinoma. In: Eble JN, Sauter G, Epstein JI, Sesterhenn IA (eds) World Health Organization classification of tumours. Pathology and genetics. Tumours of the urinary system and male genital organs. IARC, Lyon, pp 93–109
19. Sagiv E, Kazanov D, Arber N (2006) CD24 plays an important role in the carcinogenesis process of the pancreas. Biomed Pharmacother 60:280–284
20. Sagiv E, Memeo L, Karin A, Kazanov D, Jacob-Hirsch J, Mansukhani M, Rechavi G, Hibshoosh H, Arber N (2006) CD24 Is a new oncogene, early at the multistep process of colorectal cancer carcinogenesis. Gastroenterology 131:630–639
21. Smith SC, Oxford G, Wu Z (2006) The metastasis-associated gene CD24 is regulated by Ral GTPase and is a mediator of cell proliferation and survival in human cancer. Cancer Res 66:1917–1922
22. Sobin LH, Wittekind C (eds) (2002) TNM classification of malignant tumors, 6th edn. Wiley, New York
23. Su MC, Hsu C, Kao HL, Jeng YM (2006) CD24 expression is a prognostic factor in intrahepatic cholangiocarcinoma. Cancer Lett 235:34–39
24. Surowiak P, Materna V, Gyorffy B, Matkowski R, Wojnar A, Maciejczyk A, Paluchowski P, Dziegiel P (2006) Multivariate analysis of oestrogen receptor alpha, pS2, metallothionein and CD24 expression in invasive breast cancers. Br J Cancer 95:339–346
25. Surowiak P, Materna V, Kaplenko I, Spaczynski M, Dietel M, Kristiansen G, Lage H, Zabel M (2006) Unfavorable prognostic value of CD24 expression in sections from primary and relapsed ovarian cancer tissue. Int J Gynecol Cancer 16:515–521
26. Weichert W, Denkert C, Burkhardt M, Gansukh T, Bellach J, Altevogt P, Dietel M, Kristiansen G (2005) Cytoplasmic CD24 expression in colorectal cancer independently correlates with shortened patient survival. Clin Cancer Res 11:6574–6581

Virchows Arch (2007) 450:65–71
DOI 10.1007/s00428-006-0327-x

ORIGINAL ARTICLE

High-risk human papillomavirus type 16 E7 oncogene associates with Cdc25A over-expression in oral squamous cell carcinoma

Ujjal Kumar Bhawal · Masaru Sugiyama · Yuji Nomura · Masahiko Sawajiri · Keiichi Tsukinoki · Masa-Aki Ikeda · Hiroki Kuniyasu

Received: 27 March 2006 / Accepted: 11 October 2006 / Published online: 17 November 2006
© Springer-Verlag 2006

Abstract Cells expressing high-risk human papillomavirus (HPV) E7 protein display impaired checkpoint control after DNA damage and exhibit elevated rates of mutagenesis. Repression of HPV E7 expression results in the subsequent accumulation of hypophosphorylated retinoblastoma protein and repression of the Cdc25A genes. No study has been conducted to elucidate the role of Cdc25A in the development and progression of human oral carcinomas. To confirm Cdc25A protein expression together with HPV, immunohistochemistry, Western blotting, polymerase chain reaction (PCR), and reverse transcriptase (RT)-PCR were performed using various histological subtypes of oral carcinomas. Cdc25A protein was localized predominantly in the cell nuclei in carcinomas, and high expression was found in 54% of primary tumors. HPV-16 E7 was not found in non-neoplastic oral tissues, whereas it was observed in eight (36%) of 22 oral carcinomas. We found a significant correlation between Cdc25A over-expression and HPV-16 E7 positive carcinomas. There was a strong positive correlation between Cdc25A over-expression and tumor size and TNM stage. This study suggests that Cdc25A is likely to be an important mediator in the progression of oral tumors, and HPV-16 E7 may be a sensitive indicator of the involvement of viral oncogenes in oral carcinogenesis.

Keywords Human papillomavirus-16 E7 · Cdc25A · Oral · Squamous cell carcinoma

Bhawal and Sugiyama contributed equally to this work.

U. K. Bhawal
Department of Dental and Medical Biochemistry,
Graduate School of Biomedical Sciences, Hiroshima University,
Kasumi 1-2-3, Minami-ku,
Hiroshima 734-8553, Japan

M. Sugiyama
Department of Oral Health Research,
School for Oral Health Science, Faculty of Dentistry,
Hiroshima University,
Hiroshima, Japan

Y. Nomura
Department of Biomaterials Science,
Graduate School of Biomedical Sciences, Hiroshima University,
Hiroshima, Japan

M. Sawajiri
Department of Oral and Maxillofacial Radiology,
Graduate School of Biomedical Sciences, Hiroshima University,
Hiroshima, Japan

U. K. Bhawal · K. Tsukinoki
Department of Diagnostic Science, Division of Pathology,
Kanagawa Dental College,
Kanagawa, Japan

M.-A. Ikeda
Section of Molecular Embryology,
Tokyo Medical and Dental University,
Tokyo, Japan

U. K. Bhawal (✉) · H. Kuniyasu
Department of Molecular Pathology, Nara Medical University,
Kashihara, Japan
e-mail: bhawal2002@yahoo.co.in

Introduction

Subcategorization of human papillomavirus (HPV) can be made based on disease association with low-risk HPVs (HPV-6 and HPV-11) causing benign lesions and high-risk HPVs (HPV-16 and HPV-18) contributing to more aggressive forms of malignancies. In the case of HPV, a direct etiological link can be established between viral infection

and the onset of carcinogenesis. We focused on HPV 16 that is by far the most frequently detected HPV type in oral squamous cell carcinoma (SCC) [22]. Studies on high-risk HPV-16 have demonstrated that the product of the early gene E7 plays a key role in the immortalization and malignant transformation of the host cell.

Cells expressing high-risk E7 protein display impaired checkpoint control after DNA damage and exhibit elevated rates of mutagenesis. Repression of HPV E7 expression results in the subsequent accumulation of hypophosphorylated retinoblastoma protein and repression of the E2F1 and Cdc25A genes [5]. Cdc25A appears to regulate earlier cell cycle transitions. E2F transcription factor stimulates Cdc25A expression in mid to late G1 [7, 24]. Over-expressed Cdc25A shortens G1 and prematurely activates Cdk2 [2, 19]. The role of Cdc25A in initiation of DNA replication is also consistent with the ubiquitin–proteasome-mediated destruction of Cdc25A in G1- and intra-S-phase checkpoint responses to DNA damage and replicational stress [6, 14, 15]. The potentiality of being an oncogene has been experimentally demonstrated with Cdc25A, which is shown to transform murine fibroblasts in cooperation with mutated Ha-ras or loss of Rb [8]. The most dramatic effect of Cdc25A expression was observed in fibroblasts lacking the tumor suppressor RB1, in which introduction of the Cdc25A gene alone causes oncogenic transformation.

During carcinogenesis, Cdc25A is over-expressed in various human malignancies, including non-Hodgkin's lymphoma, breast cancer, non-small-cell lung cancer, and head and neck cancer [8, 9, 11, 26]. However, no study has been conducted to elucidate the role of Cdc25A in the development and progression of human oral carcinomas. In this paper, we attempted to determine the role of Cdc25A in a database of human oral cancers. We found that Cdc25A levels are highly increased in HPV-16 E7-expressing tissues, and Cdc25A over-expression is more strongly associated with advanced clinical stage.

Materials and methods

Sample collection and study population

Fresh frozen tumor specimens were obtained from 22 patients diagnosed with oral SCC from the Department of Clinical Laboratory, Hiroshima University Dental Hospital. Cancers with patient-matched non-neoplastic tissues where available were obtained at operation. Moreover, ten normal gingival from healthy donors were included as control. The patients provided written informed consent under a protocol approved by the appropriate institutional review boards. Tumor specimens were divided into two parts. One part was snap-frozen in liquid nitrogen immediately after surgery and stored at −80°C. The second part was formalin fixed and paraffin-embedded. Histopathological assessment was performed on paraffin sections. The median age of the 22 oral SCC patients was 66.6 years. Three patients were in stage I, four in stage II, six in stage III, and nine in stage IV, according to the TNM classification [21]. The grade of tumor differentiation was determined according to the criteria proposed by the World Health Organization [25].

DNA extraction and PCR

DNA was extracted from fresh-frozen tissue using the genomic DNA purification kit (Promega, Madison, WI) according to the manufacture's protocol. PCR for HPV-16 E7 was performed as described previously [20].

RNA extraction and RT-PCR

Total cellular RNA was isolated using the RNeasy total RNA purification kit (Qiagen K.K., Tokyo). RT was performed using an oligo-dT-primer pd6 coupled with an adaptor sequence following the manufacturer's instructions (Amersham Biosciences, Buckinghamshire, UK). For quality control, all cDNAs were probed with primers for the human β-actin gene. cDNA was amplified using primers specific for Cdc25A [9], HPV-16 E7 [16], and β-actin [10] The PCR reactions were carried out for 25–30 cycles. The amplified products were separated by electrophoresis in a 2% agarose gel, and the bands were visualized by ethidium bromide staining and quantified by densitometric scanning.

Protein extraction and immunoblot analysis

Preparation of whole-cell lysates from tumor tissues was made, and Western blotting was performed as described previously [27]. Protein concentrations were determined by Bradford protein assay (Bio-Rad, Hercules, CA, USA) with bovine serum albumin used as the standard. Lysates (40 μg) were solubilized in Laemmli's sample buffer by boiling and then subjected to 10% sodium dodecyl sulfate–polyacrylamide gel electrophoresis followed by electrotransfer onto a nitrocellulose filter. The filters were incubated with rabbit polyclonal antibody to Cdc25A (144, Santa Cruz Biotechnology, Santa Cruz, CA). For internal control for the amount of loaded protein, tubulin was detected by the specific antibody (Zymed Laboratories, south San Francisco, CA) at 1:1,000. The immune complex was visualized using the enhanced chemiluminescent western blot detection system (Amersham, Aylesbury, UK). For semi-quantification, the specific signals on immunoblotted membrane detected by the antibody were computer-captured and quantified with the National Institutes of Health (NIH)

image computer software (Bethesda, MD). The signal intensities were compensated for by tubulin intensities as internal controls. Cases were considered over-expressing when the ratio between expression in the tumor and expression in normal tissue was ≥3 [9].

Immunohistochemistry

Serial paraffin sections of 4 μm thick were deparaffinized in xylene, rehydrated, and immunostained according to the Dako envision kit/horse radish peroxide (HRP; DAB; Dako Cytomation, Kyoto, Japan). In brief, microwave pretreatment in citrate buffer was performed for 10 min to retrieve antigenicity. Endogenous peroxidase was blocked by applying 0.03% hydrogen peroxidase containing sodium azide from the envision kit (Dako) for 10 min. These sections were also incubated with protein block (Dako Cytomation) for 10 min to eliminate non-specific binding. This was followed by incubation overnight at 4°C with the rabbit polyclonal anti-human Cdc25A antibody (1:200) diluted in antibody diluent. The sections were then sequentially incubated with the labelled polymer, HRP for 30 min and with ready-to-use DAB+substrate–chromogen solution (1–3 min). Then, the sections were counterstained with Mayer's hematoxylin. Specificity was confirmed by applying phosphate-buffered saline instead of the primary antibody or by replacing the primary antibody with non-immune serum. We regarded the cells as positive for Cdc25A when their immunoreactivity was clearly observed in their nuclei. For evaluation of Cdc25A expression levels, Cdc25A-positive cell number was counted from 1,000 cells observed microscopically. The frequency distribution of the percentage of Cdc25A positive tumor cells vs non-metastatic cells in each tumor was evaluated. Normal rabbit IgG at the same concentration as the primary antibodies served as negative controls. Immunostaining was interpreted independently by two different observers who were blind to genetic abnormalities.

Statistical analysis

Significant differences were analyzed by Fischer's exact test. *P* values less than 0.05 were regarded as statistically significant.

Results

Immunohistochemical expression of Cdc25A

To determine whether Cdc25A was over-expressed in oral carcinoma tissues, we used a series of 22 oral carcinomas including available corresponding non-neoplastic tissues. Ten normal gingival tissues that were obtained from non-cancer patients during third-molar tooth extraction were also subjected to the study. In the non-neoplastic tissues, Cdc25A staining was occasionally observed in the nuclei of basal and parabasal layer cells, but it was rarely seen in stromal cells. In carcinomas, Cdc25A protein was observed mainly in tumor epithelial cells and occasionally in stromal cells. The Cdc25A positive ratio in stromal cells tended to correlate with the positive ratio in tumor epithelial cells.

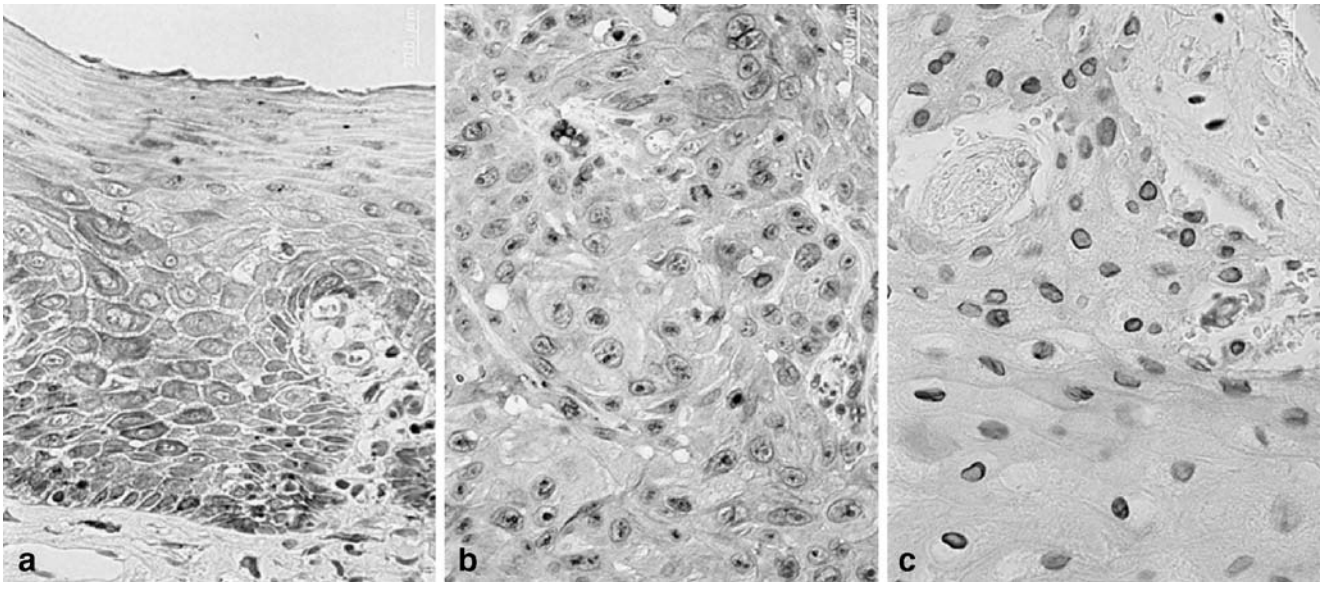

Fig. 1 Immunohistochemical analysis of Cdc25A protein. Representative expression in non-neoplastic tissue (**a**), negative (**b**), and positive (**c**) expression in oral cancer tissues. The sections were counterstained with Mayer's hematoxylin. CDC25A staining was occasionally observed in the nuclei of basal and parabasal layer cells in non-neoplastic tissue, whereas it was localized predominantly in the cell nuclei in carcinomas. Original magnification ×40 (**a**, **b**, **c**)

Representative positive and negative expression of Cdc25A protein was shown in Fig. 1.

Cdc25A protein is over-expressed in oral cancer

Over-expression of Cdc25A was found in 12 of 22 (54%) primary tumors when compared with the adjacent non-neoplastic tissues (Fig. 2a, Table 1). Cases were considered over-expressing when the ratio between expression in the tumor and expression in non-neoplastic oral tissues was ≥3.

RT-PCR of Cdc25A

To determine whether Cdc25 protein over-expression was also associated with mRNA upregulation, we examined all tumor samples by RT-PCR. In agreement with the data obtained by Western blot, Cdc25A mRNA expression levels were very low or undetectable in non-neoplastic oral tissues. Cdc25A mRNA in tumors was variable ranging from low to high levels (Fig. 2b). Twelve of 22 oral carcinoma samples (54%) were found to express higher levels of Cdc25A, and five samples showed (22%) lower Cdc25A expression when compared with the adjacent non-neoplastic tissue.

Expression of HPV E7 DNA and mRNA in oral cancer tissues

Very low or undetectable HPV-16 E7 DNA was found in non-neoplastic oral tissues, whereas it was observed in 8 of 22 (36%) oral carcinomas. We examined whether E7 mRNA expression could be detected in all HPV-16 E7 DNA-positive cases. After a reverse transcription of total RNA extracted from tumors, E7 mRNA expression was found in all HPV-16 E7 DNA-positive carcinomas. The level of HPV-16 E7 mRNA varied in cancer tissues (Fig. 2c).

Relationship of CDC25A expression with clinico-pathological factors and HPV-16 E7

Table 2 summarizes the relationship between Cdc25A over-expression and clinico-pathological factors. Cdc25A over-expression was more frequent in T3, T4 cases (10/13) than in T1, T2 cases (2/9) and stage III, stage IV cases (11/15) than in stage I, stage II cases (1/7; TNM classification, 1997). Thus, there was a strong positive correlation between Cdc25A over-expression and tumor size and TNM stage (Table 2).

We investigated the association of Cdc25A with viral oncogene HPV 16 E7. Over-expression of Cdc25A was found in seven of eight (87%) HPV-16 E7-positive cancers and 5 of 14 (35%) HPV-16 E7 negative. We found a significant correlation between Cdc25A over-expression and HPV-16 E7 positive carcinomas (p=0.0310) (Table 3).

Discussion

The cell-cycle gene, Cdc25A, activates Cdk2, promoting entry into S-phase of the cell cycle. Over-expression of Cdc25A, which has been shown previously to have oncogenic potential, eliminates this checkpoint. According to our findings, Cdc25A was frequently over-expressed in oral carcinomas. Dixon et al. [4] showed an elevated expression of Cdc25A in nuclear fractions of colon carcinoma, which was confirmed by an immunohistochemical study [23] similar to our results. However, in esophageal carcinoma, Cdc25A was accumulated both in

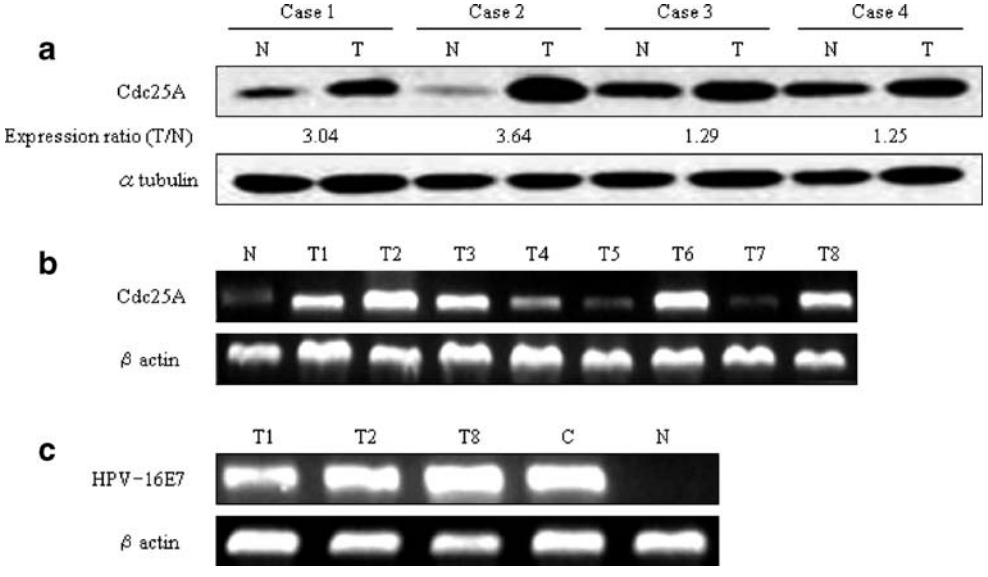

Fig. 2 **a** Immunoblot analysis of Cdc25A protein in oral cancer tissues (*T*) and non-neoplastic oral tissues (*N*). Over-expression of Cdc25A was found in 12 of 22 (54%) primary tumors when compared with the adjacent non-neoplastic tissues, according to densitometry measurements. **b** RT-PCR analysis of Cdc25A mRNA in oral cancer tissues. **c** HPV-16E7 in oral cancer tissues. *C* Control, *N* non-neoplastic oral tissue

Table 1 Immunohistochemical expression of Cdc25A in oral cancer tissues

Case	Age (year)/sex	Tumor site	Tumor grade			Tumor differentiation	Disease stage	Frequency of Cdc25A positively stained cells (tumor/normal)	Cdc25A protein Western blotting (tumor/normal)	HPV-16E7 DNA and mRNA
			T	N	M					
1	59/M	Oral floor	3	0	0	WD	IV	6.5	3.04	+
2	62/F	Tongue	3	0	0	WD	III	6.8	3.64	+
3	79/F	Tongue	1	0	0	MD	I	2.5	1.29	−
4	67/M	Tongue	2	0	0	MD	II	2.6	1.25	−
5	42/M	Tongue	3	1	0	MD	IV	2.3	1.06	−
6	70/F	Gingiva	4	0	0	WD	IV	4.8	3.10	−
7	72/F	Gingiva	3	0	0	MD	III	2.5	1.12	−
8	58/F	Tongue	1	0	0	WD	I	8.0	3.45	+
9	48/M	Tongue	3	0	0	WD	III	5.5	3.21	−
10	80/F	Gingiva	2	0	0	MD	II	0.7	<0.1	−
11	58/F	Tongue	2	2b	0	MD	IV	1.1	<0.1	−
12	65/F	Palate	4	0	0	WD	IV	6.0	3.27	−
13	82/M	Gingiva	4	2b	0	MD	IV	8.9	3.76	−
14	61/M	Gingiva	2	0	0	WD	II	0.9	<0.1	+
15	72/M	Tongue	2	0	0	WD	II	0.6	<0.1	−
16	82/M	Gingiva	4	3	0	WD	IV	7.2	3.50	+
17	57/M	Buccal mucosa	1	0	0	MD	I	2.8	1.89	−
18	57/M	Gingiva	3	0	0	MD	III	5.5	3.14	+
19	73/F	Tongue	3	1	0	MD	IV	6.0	3.61	+
20	73/M	Buccal mucosa	3	0	0	WD	III	6.4	3.63	+
21	59/M	Gingiva	4	0	0	WD	IV	7.5	3.71	−
22	89/M	Gingiva	3	0	0	WD	III	0.4	<0.1	−
									Total 12/22 over-expressing[a]	

[a] Cases were considered over-expressing when the ratio between expression in the tumor and expression in normal tissue was ≥3.

cytoplasms and nuclei [18]; in ovarian carcinoma, its immunoreactivity was seen mainly in cytoplasms [3], indicating that the localization of this phosphatase depends on the origin of the carcinoma.

Over-expression of Cdc25A was also significantly associated with the more proliferative and clinically aggressive variants of oral cancers (Table 2). These findings suggest that Cdc25A deregulation may participate in the development of aggressive oral cancers. In primary head and neck cancer, Cdc25A was over-expressed in 80% of tumors. Over-expression has been considered when the ratio between expression in the tumor and expression in normal tissue was ≥3 [9]. In our immunohistochemical study, 12 of 22 tumors analyzed (54%) exhibited more frequent Cdc25A protein when compared with the adjacent non-neoplastic tissues. In these tumors, the level of Cdc25A was 0.4- to 8.9-fold the expression of corresponding non-neoplastic tissues (Table 1), with about 50% of the cases showing over-expression levels above fivefold. Our findings are concordant with the study in which Cdc25A over-expression was also detected by RT-PCR in head and neck carcinomas [9]. Although evidence from previous studies support the concept that over-expression of Cdc25A may

Table 2 Relationship between Cdc25A expression and clinico-pathological parameters in oral cancer tissues

	Total	Cdc25A		
		Over-expression	Lower expression	*P* value
Age (years)		65.6±10.4	67.7±13.6	0.6971
Gender				
Male	12	7	5	1.0000
Female	10	5	5	
Tumor size				
pT1, pT2	9	2	7	0.0274
pT3, pT4	13	10	3	
TNM stage				
I, II	7	1	6	0.0201
III, IV	15	11	4	

Table 3 Relationship between Cdc25A expression and HPV-16 E7 in oral cancer tissues

HPV	Total	Cdc25A		
		Over-expression	Low expression	*P* value
positive	8	7	1	0.0310
negative	14	5	9	

play an important role in certain human cancers, the mechanisms causing such over-expression are not known.

In the present study, we have shown that Cdc25A was highly expressed in 54% of oral tumors. Furthermore, we have demonstrated that Cdc25A is also upregulated at the protein level concordantly with mRNA expression. The differential expression of this gene among non-neoplastic samples and oral tumors suggests that its over-expression may, indeed, participate in the development and/or progression of these tumors.

Analysis of the interaction of viral proteins such as papillomavirus E7 protein and the cell cycle machinery can be expected to provide new insights into virus–cell interactions and cell growth regulation. It has been suggested that the expression level of HPV E7 is closely correlated with transforming potential [13] and that detection of HPV E6/E7 mRNA may be more significant than that of viral sequences alone [1]. Using RT-PCR analysis, we found that 36% of oral cancer patients were infected by high-risk HPV-16. The detection of specific HPV oncogene transcripts may be a sensitive indicator of the involvement of viral oncogenes in carcinogenesis.

To further evaluate the role of the HPV-16 E7 oncoprotein in the modulation of Cdc25A gene expression, we prepared total cell extracts from oral tissues and available corresponding non-neoplastic tissues. Cdc25A was highly expressed in E7-positive tissues and weak or absent in non-neoplastic tissues, suggesting that its expression may be modulated by the viral oncoprotein. These results are consistent with experiments done with NIH 3T3 cells in which HPV-16 E7 can also maintain elevated Cdc25A gene expression [12, 17]. Taken together, these results suggest that Cdc25A may be a crucial target of HPV-16 E7 in virus-mediated transactivation of cells.

However, markedly varied estimates of HPV prevalence have made it difficult to clarify the timing and nature of the contribution of HPV to oral carcinogenesis. We have shown that Cdc25A is likely to be an important mediator in the progression of oral tumors. To more specifically assess the consequences of HPV-16 E7-mediated Cdc25A activation in relation to viral oncogenesis, additional experiments will be needed. It may be that the simultaneous determination of Cdc25A phosphatase and of other viral and cellular proteins involved in the cell cycle regulation will allow for better definition of clusters of oral cancer patients. In conclusion, our findings indicate that Cdc25A is over-expressed in human oral cancers, and it may participate in the progression of these tumors where HPV-16 E7 expression plays a key role.

Acknowledgement This work was supported by a grant (No. 16390590) from the Ministry of Education, Sports, and Science to Professor Masaru Sugiyama.

References

1. Biswas C, Kell B, Mant C, Jewers RJ, Cason J, Muir P, Raju KS, Best JM (1997) Detection of human papillomavirus type 16 early-gene transcription by reverse transcription-PCR is associated with abnormal cervical cytology. J Clin Microbiol 35:1560–1564
2. Blomberg I, Hoffmann I (1999) Ectopic expression of Cdc25A accelerates the G(1)/S transition and leads to premature activation of cyclin E- and cyclin A-dependent kinases. Mol Cell Biol 19:6183–6194
3. Broggini M, Buraggi G, Brenna A, Riva L, Codegoni AM, Torri V, Lissoni AA, Mangioni C, D'Incalci M (2000) Cell cycle-related phosphatases CDC25A and B expression correlates with survival in ovarian cancer patients. Anticancer Res 20:4835–4840
4. Dixon D, Moyana T, King MJ (1998) Elevated expression of the cdc25A protein phosphatase in colon cancer. Exp Cell Res 240:236–243
5. Goodwin Edward C, DiMaio D (2001) Induced senescence in HeLa cervical carcinoma cells containing elevated telomerase activity and extended telomeres. Cell Growth Differ 12:525–534
6. Falck J, Mailand N, Syljuasen RG, Bartek J, Lukas J (2001) The ATM-Chk2–Cdc25A checkpoint pathway guards against radio-resistant DNA synthesis. Nature 410:842–847
7. Galaktionov K, Chen X, Beach D (1996) Cdc25 cell-cycle phosphatase as a target of c-myc. Nature 382:511–517
8. Galaktionov K, Lee AK, Eckstein J, Draetta G, Meckler J, Loda M, Beach D (1995) CDC25 phosphatases as potential human oncogenes. Science 269:1575–1577
9. Gasparotto D, Maestro R, Piccinin S, Vukosavljevic T, Barzan L, Sulfaro S, Boiocchi M (1997) Overexpression of CDC25A and CDC25B in head and neck cancers. Cancer Res 57:2366–2368
10. Gonzalgo ML, Hayashida T, Bender CM, Pao MM, Tsai YC, Gonzales FA, Nguyen HD, Nguyen TT, Jones PA (1998) The role of DNA methylation in expression of the p19/p16 locus in human bladder cancer cell lines. Cancer Res 58:1245–1252
11. Hernandez S, Hernandez L, Bea S, Cazorla M, Fernandez PL, Nadal A, Muntane J, Mallofre C, Montserrat E, Cardesa A, Campo E (1998) cdc25 cell cycle-activating phosphatases and c-myc expression in human non-Hodgkin's lymphomas. Cancer Res 58:1762–1767
12. Katich SC, Zerfass-Thome K, Hoffmann I (2001) Regulation of the Cdc25A gene by the human papillomavirus type 16 E7 oncogene. Oncogene 20:543–550
13. Liu Z, Ghai J, Ostrow RS, Faras AJ (1995) The expression levels of the human papillomavirus type 16 E7 correlate with its transforming potential. Virology 207:260–270
14. Mailand N, Falck J, Lukas C, Syljuasen RG, Welcker M, Bartek J, Lukas J (2000) Rapid destruction of human Cdc25A in response to DNA damage. Science 288:1425–1429
15. Molinari M, Mercurio C, Dominguez J, Goubin F, Draetta GF (2000) Human Cdc25 A inactivation in response to S phase inhibition and its role in preventing premature mitosis. EMBO Rep 1:71–79
16. Nees M, Geoghegan JM, Munson P, Prabhu V, Liu Y, Androphy E, Woodworth CD (2000) Human papillomavirus type 16 E6 and E7 proteins inhibit differentiation-dependent expression of transforming growth factor-beta2 in cervical keratinocytes. Cancer Res 60:4289–4298
17. Nguyen DX, Westbrook TF, McCance DJ (2002) Human papillomavirus type 16 E7 maintains elevated levels of the cdc25A tyrosine phosphatase during deregulation of cell cycle arrest. J Virol 76:619–632
18. Nishioka K, Doki Y, Shiozaki H, Yamamoto H, Tamura S, Yasuda T, Fujiwara Y, Yano M, Miyata H, Kishi K, Nakagawa H, Shamma A, Monden M (2001) Clinical significance of CDC25A

and CDC25B expression in squamous cell carcinomas of the oesophagus. Br J Cancer 85:412–421
19. Sexl V, Diehl JA, Sherr CJ, Ashmun R, Beach D, Roussel MF (1999) A rate limiting function of cdc25A for S phase entry inversely correlates with tyrosine dephosphorylation of Cdk2. Oncogene 18:573–582
20. Shen J, Tate JE, Crum CP, Goodman ML (1996) Prevalence of human papillomaviruses (HPV) in benign and malignant tumors of the upper respiratory tract. Mod Path 9:15–20
21. Sobin LH, Fleming ID (1997) TNM classification of malignant tumors, 5th edn. Union Internationale Contre le Cancer and the American Joint Committee on Cancer. Cancer 80:1803–1804
22. Sugiyama M, Bhawal UK, Dohmen T, Ono S, Miyauchi M, Ishikawa T (2003) Detection of human papillomavirus-16 and HPV-18 DNA in normal, dysplastic, and malignant oral epithelium. Oral Surg Oral Med Oral Pathol Oral Radiol Endo 95:594–600
23. Takemasa I, Yamamoto H, Sekimoto M, Ohue M, Noura S, Miyake Y, Matsumoto T, Aihara T, Tomita N, Tamaki Y, Sakita I, Kikkawa N, Matsuura N, Shiozaki H, Monden M (2000) Overexpression of CDC25B phosphatase as a novel marker of poor prognosis of human colorectal carcinoma. Cancer Res 60:3043–3050
24. Vigo E, Muller H, Prosperini E, Hateboer G, Cartwright P, Moroni MC, Helin K (1999) CDC25A phosphatase is a target of E2F and is required for efficient E2F-induced S phase. Mol Cell Biol 19:6379–6395
25. Wasi PN, Cohen B, Luthra UK, Torloni H (1971) Histological typing of oral and oropharyngeal tumors. Int Histol Classif Tumours, Geneva, World Health Organization: 17–18
26. Wu W, Fan YH, Kemp BL, Walsh G, Mao L (1998) Overexpression of cdc25A and cdc25B is frequent in primary non-small cell lung cancer but is not associated with overexpression of c-myc. Cancer Res 58:4082–4085
27. Yasui W, Ayhan A, Kitadai Y, Yokozaki H, Ito H, Tahara E (1993) Increased expression of p34cdc2 and its kinase activity in human gastric and colonic carcinomas. Int J Cancer 53:36–41

Virchows Arch (2007) 450:73–80
DOI 10.1007/s00428-006-0334-y

ORIGINAL ARTICLE

P-cadherin and cytokeratin 5: useful adjunct markers to distinguish basal-like ductal carcinomas in situ

Joana Paredes · Nair Lopes · Fernanda Milanezi · Fernando C. Schmitt

Received: 7 June 2006 / Accepted: 19 October 2006 / Published online: 23 November 2006
© Springer-Verlag 2006

Abstract Gene expression profiles of invasive breast carcinomas have identified a subgroup of tumours with worse prognosis, which have been called "basal-like". These are characterized by a specific pattern of expression, being estrogen receptor (ER) and HER2 negative, and frequently expressing at least one basal marker such as basal cytokeratins or epidermal growth factor receptor (EGFR). Previously, our group characterized basal-like tumours in a series of invasive breast carcinomas using P-cadherin (P-CD), p63 and cytokeratin 5 (CK5). Based on that study, we hypothesized that those high-grade basal-like invasive carcinomas might have a pre-invasive counterpart, which could be identified using the same approach. A series of 79 ductal carcinomas in situ (DCIS) were classified into distinct subgroups according to their ER, HER2 and basal markers expression. Luminal DCIS expressed ER and constituted 64.6% of the series; the HER2 overexpressing tumours did not express ER and represented 25.3% of the cases, whereas 10.1% lack the expression of ER and HER2 and expressed at least one basal marker (P-CD, CK5, CK14, p63, vimentin and/or EGFR). These basal-like DCIS were mostly high-grade, with comedo-type necrosis, and consistently showed expression of P-CD and CK5. In conclusion, DCIS with a basal-like phenotype represent a small percentage in our series, being P-CD and CK5, the most useful adjunct markers to distinguish this subset of carcinomas in situ of the breast.

Keywords Basal-like DCIS · P-cadherin · CK5 · CK14 · p63 · Vimentin · EGFR

J. Paredes · F. Milanezi · F. C. Schmitt
Life and Health Science Research Institute (ICVS),
Health Science School, University of Minho,
Braga, Portugal

J. Paredes · N. Lopes · F. Milanezi · F. C. Schmitt (✉)
Institute of Pathology and Molecular Immunology of Porto University (IPATIMUP),
Rua Dr. Roberto Frias s/n 4200-465,
Porto, Portugal
e-mail: fernando.schmitt@ipatimup.pt

F. C. Schmitt
Medical Faculty, Porto University,
Porto, Portugal

Introduction

Breast cancer is a major cause of death among women mainly in the age groups of 35–60 years old. Despite important advances in therapy, more than half of the affected patients undergo relapses [30]. The highly heterogeneous nature of this disease—distinct histological subtypes have markedly different clinical courses and treatment responses—has led to a search for genetic markers to improve therapy and follow-up strategies [1].

Several studies, using cDNA microarrays, have been classifying invasive ductal breast carcinomas not otherwise specified (NOS) in more specific groups according to their genetic and molecular profiles [19, 25, 26]. It is anticipated that global determination of specific gene expression signatures would predict the clinical behaviour of the tumours [1].

One of those groups is constituted by tumours with amplification and consequent overexpression of the oncogene HER2, representing approximately 15% of the invasive ductal carcinomas NOS. The majority of them (≈70%) belong to the luminal-like group (ER positive), which has recently been sub-divided in luminals A and B, being these subgroups related to different responses to hormonal therapy [17]. Additionally, there is a small group

of tumours that falls in the same category of the normal breast samples, which were defined as normal breast-like tumours [19, 25, 26].

Interestingly, 15% of the invasive ductal carcinomas NOS are characterized by high expression of genes that are commonly found in myoepithelial cells, such as basal cytokeratins (CK5, CK6, CK14 and CK17) [25, 26], EGFR, p63 and P-CD [15]. Our interest in this latter subgroup of tumours called basal-like has been increasing, as several reports have shown that the expression of "basal" markers is frequently associated with a poor outcome [29] and short disease-free survival [16] for breast cancer patients. Moreover, in contrast with the other groups of mammary carcinomas, basal-like carcinomas do not have a specific molecular therapy, which demands the study of putative molecular targets that might play a role in these high-grade lesions.

Nielsen et al. [16] recently proposed a definition of basal-like tumours based on immunohistochemical expression. According to these authors, a basal-like breast carcinoma should be negative for ER, progesterone receptor (PgR) and HER2 and positive for CK5/6 and/or EGFR. However, our group has demonstrated that p63 and P-CD proteins, expressed as well in the normal myoepithelial cell layer of the mammary gland, are also upregulated in this subgroup of tumours and, together with CK5, can be considered specific molecular markers of the basal phenotype [15]. Recently, in a paper published by Laakso et al. [13], they concluded that the intratumoral heterogeneity in basal cytokeratin expression (CK5 and CK14) can be used to define two distinct breast cancer subtypes, basal and basoluminal, with distinctive features related to proliferation activity, oncogene and biomarker status and patient survival. In addition, Domagala et al. [7], in 1990, had already called the attention to the association of vimentin expression with high grade breast carcinomas. Livasy et al. [14] have included this intermediary filament in the panel of "basal" biomarkers used to distinguish the basal-like group of breast carcinomas.

Basal-like breast carcinomas have acquired even more interest, as the tumours arising in women harbouring BRCA1 mutations also cluster with this group of lesions [8, 9, 26, 28]. These hereditary tumours are also poorly differentiated, lack ER and HER2 expression and express basal cytokeratins, like CK5 and CK14 [10, 12]. Moreover, Arnes et al. [2] reported that P-CD is associated with BRCA1-related breast cancer.

Ductal carcinoma in situ (DCIS) represents a heterogeneous group of lesions characterized by an abnormal proliferation of duct mammary epithelial cells without microscopic invasion of the periductal stroma [21]. We hypothesize whether there is also a DCIS with a basal phenotype that may be in the origin of the basal-like invasive carcinomas. In fact, our group has demonstrated previously that the majority of high-grade DCIS express P-CD [18]. And, although this hypothesis has been already addressed by three other groups [3, 6, 27], we think that a broader panel might be useful in the identification of pre-invasive basal-like breast lesions.

To test the existence of DCIS lesions with a basal-like phenotype, we examined 79 cases of DCIS to verify the occurrence of the ER/HER2 negative phenotype and to confirm the association between this phenotype and the expression of basal markers we selected, namely, P-CD, CK5, CK14, p63, vimentin and EGFR, characteristically expressed by basal-like invasive breast carcinomas.

Materials and methods

Breast tumour samples

Formalin-fixed, paraffin-embedded tissues of 79 DCIS were consecutively retrieved from the histopathology files of our institute. All cases were reviewed on haematoxylin- and eosin-stained sections by two pathologists (F.S., F.M.). Relevant data that were available for analysis included nuclear grade, necrosis and architecture patterns, ER status, HER2 and P-CD immunohistochemical expression results [18]. DCIS-presenting cells with an unequivocal membranous staining for P-CD were scored as positive, whereas cells with cytoplasmic expression alone were not considered. DCIS cells that showed nuclear staining for ER in at least 10% of the nuclei were considered positive. All the ER negative cases showed complete absence of tumour nuclei staining (with a positive internal control of normal breast epithelial cell nuclei). Tumour cells were considered positive (overexpression) for HER2 when greater than 10% of the cells showed strong membrane staining (equivalent to a score 3+ in the DakoCytomation HercepTest scoring system).

Immunohistochemistry

Two-micra-thick sections were immunostained with primary monoclonal antibodies against CK5, CK14, p63, vimentin and EGFR. Immunostainings for CK5, p63 and vimentin were performed using the streptavidin–biotin–peroxidase technique (LabVision, Fremont, CA, USA), whereas CK14 and EGFR immunostaining used the HRP labelled polymer (DakoCytomation, Carpinteria, CA, USA). Antigen unmasking for vimentin and p63 was carried out using a dilution of 1:100 from a commercially available solution of citrate buffer, pH=6.0 (Vector Laboratories, Burlingame, CA, USA) at 98°C, whereas a dilution of 1:10 from ethylenediaminetetraacetic solution with

pH=9.0 (DakoCytomation) was used for CK5 and CK14. Epitope retrieval for EGFR was performed by proteolytic enzyme digestion (pepsin A, 4 g/l; Sigma-Aldrich) at 37°C. The antigen retrieval times, clone antibodies, dilutions and suppliers are listed in Table 1. After the antigen retrieval procedure, the slides were washed in a phosphate buffer solution (LabVision) and submitted to blockage of the endogenous peroxidase activity by incubation of the slides in a 3% hydrogen peroxide (Panreac, Spain) in methanol (Sigma-Aldrich, Germany) during 10 min. The slides were further incubated with a blocking serum (LabVision Corporation kit) for 15 min and then incubated with the primary antibodies. After washes, the slides were incubated with biotinylated secondary antibody, followed by streptavidin-conjugated peroxidase during 15 min each (LabVision Corporation kit) using DAB solution (3,3-diaminobenzidine tetrahydrochloride) as a chromogen (LabVision Corporation kit). For CK14 and EGFR staining, the secondary antibody was associated with HRP labelled polymer (DakoCytomation) and immediately revealed with DAB. Tissues were then counterstained with Mayer's haematoxylin, dehydrated and coverslipped using a permanent mounting solution (Zymed, San Francisco, CA, USA).

Positive controls were included in all runs for each of the antibodies used. Paraffin sections of normal breast and prostate tissues were used for p63; appendix tissue was used for vimentin and a squamous cell carcinoma of the skin for EGFR. Normal prostate tissue was also used as a positive control for CK5 staining, and normal skin was used for CK14 antibody.

CK5, CK14 and vimentin were considered positive whenever any cytoplasmic staining was observed in the DCIS cells. EGFR was considered positive when any membranous staining was observed, whereas p63 was considered positive whenever nuclear staining was seen.

Statistical analysis

The χ^2 contingency test was used for categorical variables to determine differences between groups. A p value<0.05 was considered as a reflection of a significant association. The StatView 5.0 (SAS Insitute, Cary, NC, USA) software program was used to perform these analyses.

Results

The results obtained are summarized in Table 2 and in Fig. 1. Whereas 64.6% of the DCIS from our series were ER-positive, 53.2% were HER2 positive. Few tumours presented expression of a basal marker: 25% were positive for P-CD, 6.7% for CK5, 19.4% for CK14, 4.1% for p63, 5.4% for vimentin and 8.2% for EGFR. The expression of basal markers was focal rather than diffuse but always showed a moderate to strong immunoreactivity. The morphological analysis of the cases showing positive staining of the basal markers in cells clearly atypical (large nuclei and prominent nucleoli; see Fig. 1) assured that the immunostaining was in the neoplastic cells rather than in entrapped myoepithelial cells, squamous metaplasia or hyperplastic areas.

After analysing the expression of each marker, we subclassified the DCIS based on their ER and HER2 expression (Table 3), as we had previously done with the invasive breast carcinomas [15]. ER-positive DCIS were classified as luminal: ER+/HER2− as luminal A and ER+/HER2+ as luminal B. ER-negative and HER2-positive DCIS were classified as HER2 overexpressing tumours, whereas DCIS that lacked the expression of ER and HER2 but showed expression of at least one basal marker (P-CD and/or CK5 and/or CK14 and/or p63 and /or vimentin and/or EGFR) were classified as basal-like.

Using these criteria, DCIS with a basal-like phenotype comprised 10.1% of the series, whereas luminals A and B represented 50.6 and 14%, respectively. HER2 overexpressing tumours represented 25.3% of the series, and we have not observed DCIS with a null phenotype (Table 3).

We found a statistically significant correlation between these four immunoprofiles and DCIS nuclear grade as well as with the presence or absence of comedo-type necrosis (0.0006 and 0.0026, respectively; Table 4). Grade III DCIS were observed with higher frequency in luminal B (100%),

Table 1 Sources and dilutions of primary antibodies used in this immunohistochemistry study

Antibody	Clone	Manufacturer	Dilution	Time of incubation (min)	Antigen retrieval (min)
ER	1D5	DAKO	1:10	60	30
HER2	CB11	Ventana	1:60	30	20
P-CD	Clone 56	Transduction	1:50	60	30
CK5	XM26	LabVision	1:50	60	30
CK14	LL002	Novocastra	1:400	60	30
p63	4A4	LabVision	1:150	60	30
Vimentin	V9	DakoCytomation	1:150	30	30
EGFR	31G7	Zymed	1:100	30	30

Table 2 Results of immunohistochemistry staining in DCIS cases for the several antibodies used

Molecular marker	Interpretable cases	Positive staining (%)
ER	79	51 (64.6%)
HER-2	79	42 (53.2%)
P-CD	76	19 (25%)
CK5	74	5 (6.7%)
CK14	72	14 (19.4%)
P63	74	3 (4.1%)
Vimentin	74	4 (5.4%)
EGFR	73	6 (8.2%)

basal-like (87.5%) and HER2 overexpressing (85%) subgroups. The luminal A in situ carcinomas were homogeneously distributed along the three histological grades. Comedo-necrosis was observed in 90.9% of the luminal B subgroup, 95% of the HER2 overexpressing DCIS and 87.5% of the basal-like ones. In the luminal A group, we observed a lower percentage (55%) of comedo-necrosis.

The protein expression profiles in luminals A and B, basal-like and HER2 overexpressing tumours were also analysed concerning P-CD, CK5, CK14, p63, vimentin and EGFR (Table 4). Statistically significant differences were only observed for P-CD ($p<0.0001$) and CK5 ($p=0.0319$) expression. Basal-like DCIS demonstrated a clearly higher frequency of P-CD (75%) and CK5 (33.3%) expression when compared with the other basal markers. Interestingly, HER2 overexpressing in situ carcinomas also demonstrate a higher percentage of expression of these two basal markers (45% for P-CD and 10% for CK-5). No significant differences were found concerning CK14, p63, vimentin and EGFR.

The majority of luminal tumours (65% of luminal A and 81.8% of luminal B) was negative for all the basal markers tested; whereas in HER2 overexpressing DCIS this percentage was lower (40%). Although P-CD expression has been found in all tumour subtypes, it was essentially expressed in basal-like (75%) and in HER2 overexpressing

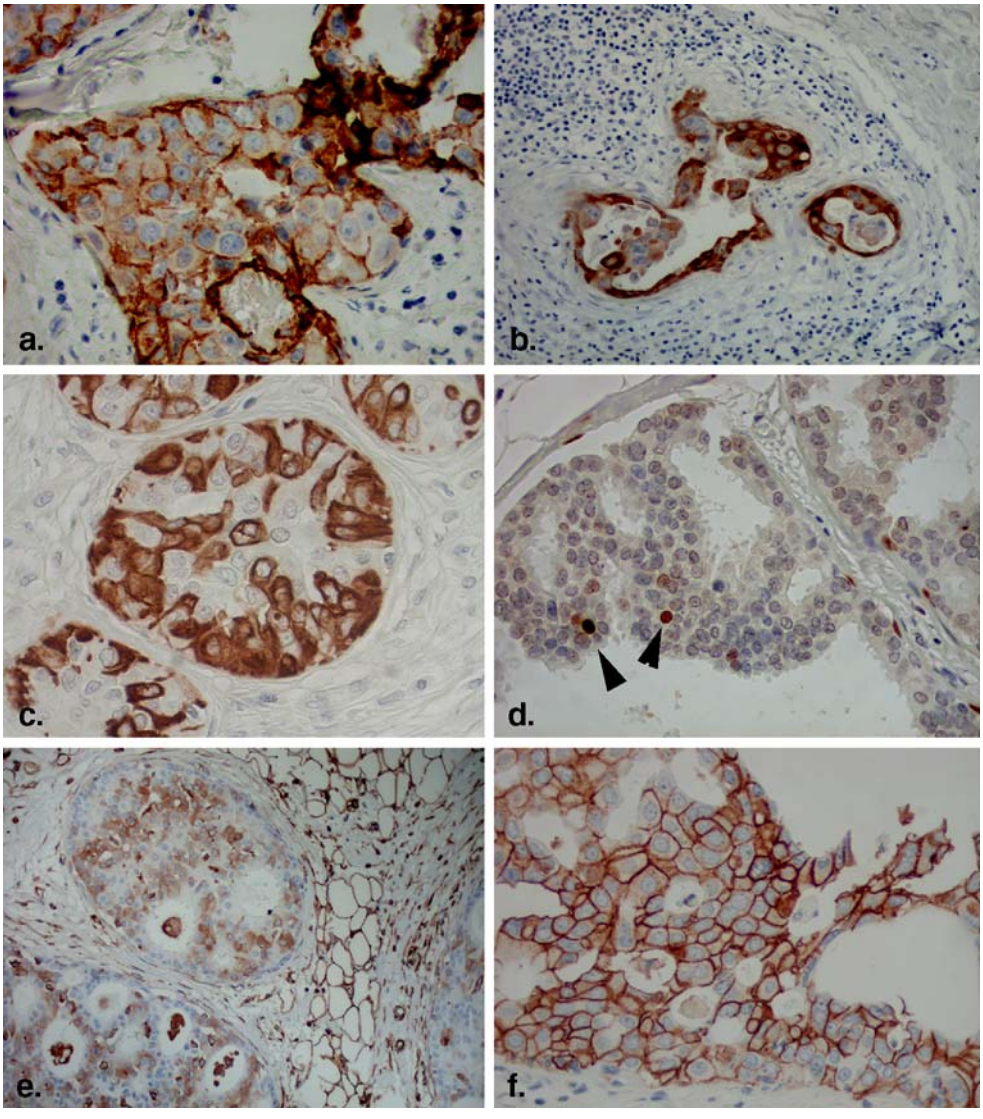

Fig. 1 Immunohistochemical expression of basal markers in DCIS. **a** P-cadherin membrane staining, 400×; **b** CK5 cytoplasmic staining, 200×; **c** CK14 cytoplasmic staining, 400×; **d** p63 nuclear staining (*arrows*), 400×; **e** Vimentin cytoplasmic staining, 200×; **f** EGFR membrane staining, 400×

Table 3 Frequencies of the immunohistochemically defined subtypes of DCIS in informative tumours for the tested markers

Subtype	ER	HER-2	Basal marker	Frequency (%)
Luminal A	Positive	Negative	Positive/negative	40 (50.6%)
Luminal B	Positive	Positive	Positive/negative	11 (14%)
HER-2 overexpressing	Negative	Positive	Positive/negative	20 (25.3%)
Basal-like	Negative	Negative	Positive	8 (10.1%)
Negative	Negative	Negative	Negative	0 (0%)

(45%) tumours. P-CD was the basal marker exclusively found in the majority of HER2 overexpressing cases (40%), being co-expressed with CK5, CK14 and p63 in one case (5%). This particular case was a solid/cribriform Grade III DCIS with comedo-type necrosis. In basal-like tumours, P-CD was the only expressed marker in 25% of the tumours, with simultaneous expression of CK14 in two other cases, with both basal cytokeratins in one of those tumours and together with p63 in one DCIS of this group. The remaining two cases, comprised in the basal-like subtype, were identified by EGFR expression; one case expressed this marker alone and the other showed expression of EGFR and CK5. The majority of the basal-like DCIS cases were micropapillary or comedo-type lesions.

Within luminal tumours, the expression of basal markers was low. In luminal A, there were five tumours that expressed exclusively CK14, three expressed only EGFR, two showed exclusively P-CD, and one showed only vimentin expression. Two luminal DCIS co-expressed CK14 and vimentin from which one also showed P-CD expression and another case co-expressed basal cytokeratins and p63. In luminal B DCIS, we observed two cases with basal markers expression: one showing P-CD positivity and the other showing vimentin and CK14 expression.

Discussion

The analysis of pathological changes together with gene expression can contribute to the understanding of disease mechanisms, the improvement of diagnosis and the identification of novel therapeutic targets [1]. Today, gene expression data generated by array hybridization can be used to group tumour samples into clusters that reflect their

Table 4 Correlation between DCIS nuclear grade, comedo-necrosis and the expression of basal markers and the distinct subtypes of DCIS-defined immunohistochemically

	Luminal A [*n* (%)]	Luminal B [*n* (%)]	HER-2 overexpressing [*n* (%)]	Basal [*n* (%)]	*p* value
Nuclear grade					
I	11 (27.5%)	0 (0%)	0 (0%)	0 (0%)	0.0006
II	13 (32.5%)	0 (0%)	3 (15%)	1 (12.5%)	
III	16 (40.0%)	11 (100%)	17 (85%)	7 (87.5%)	
Comedo-necrosis					
Present	22 (55%)	10 (90.9%)	19 (95%)	7 (87.5%)	0.0026
Absent	18 (45%)	1 (9.1%)	1 (5%)	1 (12.5%)	
P-CD					
Positive	3 (8.1%)	1 (9.1%)	9 (45%)	6 (75%)	<0.0001
Negative	34 (91.9%)	10 (90.9%)	11 (55%)	2 (25%)	
CK5					
Positive	1 (2.6%)	0 (0%)	2 (10%)	2 (33.3%)	0.0319
Negative	37 (97.4%)	10 (100%)	18 (90%)	4 (66.7%)	
CK14					
Positive	8 (22.2%)	1 (11.1%)	2 (10%)	3 (42.9%)	0.2442
Negative	28 (77.8%)	8 (88.9%)	18 (90%)	4 (57.1%)	
P63					
Positive	1 (2.6%)	0 (0%)	1 (5.3%)	1 (12.5%)	0.5486
Negative	37 (97.4%)	9 (100%)	18 (94.7%)	7 (87.5%)	
Vimentin					
Positive	3 (7.9%)	1 (10%)	0 (0%)	0 (0%)	0.5013
Negative	35 (92.1%)	9 (90%)	18 (100%)	8 (100%)	
EGFR					
Positive	3 (8.1%)	0 (0%)	1 (5.3%)	2 (25%)	0.2601
Negative	34 (91.9%)	9 (100%)	18 (94.7%)	6 (75%)	

biological properties. Microarray profiling of invasive mammary carcinomas has identified five distinct subtypes of tumours (luminal A, luminal B, normal breast-like, HER2 overexpressing and Basal-like) that are clearly associated with different clinical outcomes for breast cancer patients [19, 25, 26]. Interestingly, the basal-like subgroup, which is defined by consistent expression of basal markers, includes BRCA1-related hereditary breast cancers and is the one associated with the worst prognosis [2, 9, 28].

In addition, the molecular analysis of invasive breast cancer precursor lesions has supplemented our understanding of breast cancer progression. In the last few years, new pathways of breast cancer evolution have been cleared based on their genotypic–phenotypic correlations. Whereas most of the concepts concerning the morphologically defined breast cancer precursor lesions remain applicable, immunohistochemistry and molecular genetics have altered the way on how breast cancer step model is seen. It is no longer identified as a single pathway but as an intricate sequence of stochastic genetic events, which leads to divergent and deviating pathways towards invasive breast cancer. Some of the lesions along the pathway, like columnar cell lesions, have been repositioned, and the role of others have been questioned [20, 23, 24].

There are evidences that DCIS is a direct precursor lesion of invasive ductal breast cancer, as distinct molecular characteristics found in different grades of invasive carcinomas are also mirrored in pre-invasive lesions of equivalent morphology [4, 5]. Two main branches in breast cancer progression model has been distinguished: one comprising well-differentiated DCIS that progress to grade I invasive ductal carcinomas and the other encompassing poorly differentiated DCIS that progress to high-grade invasive carcinomas [22]. In the "low grade arm", tumours are of low nuclear grade usually ER and PgR positive and negative for HER2 and basal markers with low genetic instability. In contrast, in the "high grade arm", the lesions show a higher degree of nuclear atypia, lack of hormone receptors, expression of either HER2 or basal markers and are genetically advanced lesions, showing a combination of recurrent genomic changes [24]. A more likely precursor to basal-like invasive carcinoma should be a high-nuclear grade DCIS, with similar characteristics of the invasive counterpart.

Recently, Bryan et al. [3], Tang et al. [6] and Dabbs et al. [27] have studied the expression of basal markers in three series of DCIS using a panel of basal cytokeratins, EGFR, p63, vimentin and c-KIT. Bryan et al. [3] found only 6% of DCIS cases with a triple negative phenotype (ER, PgR and HER2 negative) and expression of one or more basal cytokeratins (focal staining) and/or EGFR. Tang et al. [27] demonstrated that the expression patterns of ER, PgR, HER2 and EGFR can identify high-grade DCIS associated with basal/stem cell subtypes. Dabbs et al. [6] showed that a DCIS component of solid, flat or micropapillary type exists in the basal phenotype of breast carcinoma, and it demonstrates the same immunophenotype as the invasive counterpart, typically positive for CK5/6, CK14, CK17, vimentin and EGFR but negative for ER/PgR and HER2.

In our series of 79 DCIS, we included P-CD in the panel of antibodies used to distinguish the basal-like phenotype. In a previous study of our group, P-CD, CK5 and p63 have already demonstrated their ability to distinguish basal-like invasive breast carcinomas [15], whereas the addition of vimentin, CK14 and EGFR was supported by recent studies showing a consistent expression of these proteins in basal-like invasive carcinomas [11, 13, 14, 16].

We have found 10.1% of basal-like DCIS, defined as ER and HER2 negative, with expression of at least one basal marker. Interestingly, if our list of basal markers were restricted to EGFR and CK5, we would loose five cases of basal-like DCIS, two that expressed exclusively P-CD, two that expressed P-CD and CK14 together and one that co-expressed P-CD and p63, comprising 62.5% of the basal-like cases. These findings are similar to those demonstrated in invasive breast carcinomas [15] and confirm the high heterogeneity observed among basal-like breast carcinomas [3], reinforcing the use of an adequate panel of basal/myoepithelial markers. Among the markers used in our study, p63 and vimentin were not consistently expressed and are not considered useful to identify basal-like DCIS.

Similarly to the previous studies on basal-like DCIS, the expression of basal markers was frequently focal in the neoplastic cells [3, 6, 27]. In spite of that, the immunostaining showed a moderate to strong intensity in all markers studied. These results are not surprising; as in invasive breast carcinomas, the focal pattern of expression of basal markers are also described and do not impair the recognition of a basal phenotype [14, 15].

As already stated in the results section, P-CD was also a good marker to discriminate HER-2 overexpressing DCIS, as it was not restricted only to the basal-like subgroup. Indeed, in several studies addressing invasive breast carcinomas, P-CD expression is normally directly associated to HER2 expression, which is in accordance with the results obtained in in situ carcinomas. Although P-CD is an obvious marker of myoepithelial cells in the normal mammary gland, as what happens with the other basal markers, little is known about the regulation of this cadherin expression. It is possible that HER2 amplification and/or overexpression could lead to the constitutive activation of a signalling pathway that mediates P-CD overexpression. This data can be better explored in the future.

As previously demonstrated, the different groups of invasive breast carcinomas recognized by microarray technology can also be identified using immunohistochem-

istry [14–16]. Applying the same rationale to our series of DCIS, we found 64.6% of cases with a luminal phenotype, 25.3% HER2 overexpressing tumours and 10.1% of cases with a basal-like phenotype. Although we have not studied a large series of DCIS, if we compare the level of expression obtained in our study, the results are proportional to the percentages obtained by cDNA microarrays in invasive breast carcinomas. In these studies, the luminal subgroup comprises 65–70% of the cases, the basal-like subgroup comprises less than 15%, and the HER2 overexpressing carcinomas comprises 15–20% of the cases. The recognition of basal-like phenotype implies not only the expression of these markers but also the lack of ER and HER2 reactivity. By using this approach, the expression of some basal markers in the luminal and HER overexpressing DCIS does not impair their categorization in these specific clusters.

In conclusion, this work demonstrates that using a limited number of markers, such as ER, HER2, P-CD, CK5, CK14 and EGFR, we can characterize and distinguish basal-like DCIS, being P-CD and CK5 as the most useful adjunct markers.

Acknowledgement The authors thank Dr. Leda Viegas de Carvalho (M.D., Ph.D.), Santos, São Paulo, Brazil, who kindly provided case material used in this study.

This study was supported by two research grants (Joana Paredes: SFRH/BPD/15319/2005; Nair Lopes: POCTI/CBO/45157/2002) and by a scientific project (POCI/BIA-BCM/59252/2004) both financed by the Portuguese Science and Technology Foundation.

References

1. Ahr A, Ahr A, Holtrich U, Solbach C, Scharl A, Strebhardt K, Karn T, Kaufmann M (2001) Molecular classification of breast cancer patients by gene expression profiling. J Pathol 195:312–320
2. Arnes JB, Brunet JS, Stefansson I, Begin LR, Wong N, Chappuis PO, Akslen LA, Foulkes WD (2005) Placental cadherin and the basal epithelial phenotype of BRCA1-related breast cancer. Clin Cancer Res 11:4003–4011
3. Bryan BB, Schnitt SJ, Collins LC (2006) Ductal carcinoma in situ with basal-like phenotype: a possible precursor to invasive basal-like breast cancer. Mod Path 19:617–621
4. Buerger H, Otterbach F, Simon R, Poremba C, Diallo R, Decker T, Riethdorf L, Brinkschmidt C, Dockhorn-Dworniczak B, Boecker W (1999) Comparative genomic hybridization of ductal carcinoma in situ of the breast—evidence of multiple genetic pathways. J Pathol 187:396–402
5. Buerger H, Otterbach F, Simon R, Schafer KL, Poremba C, Diallo R, Brinkschmidt C, Dockhorn-Dworniczak B, Boecker W (1999) Different genetic pathways in the evolution of invasive breast cancer are associated with distinct morphological subtypes. J Pathol 189:521–526
6. Dabbs DJ, Chivukula M, Carter G, Bhargava R (2006) Basal phenotype of ductal carcinoma in situ: recognition and immunohistologic profile. Mod Pathol 19:1506–1511
7. Domagala W, Wozniak L, Lasota J, Weber K, Osborn M (1990) Vimentin is preferentially expressed in high-grade ductal and medullary, but not in lobular breast carcinomas. Am J Pathol 137:1059–1064
8. Foulkes WD, Stefansson IM, Chappuis PO, Begin LR, Goffin JR, Wong N, Trudel M, Akslen LA (2003) Germline BRCA1 mutations and a basal epithelial phenotype in breast cancer. J Natl Cancer Inst 95:1482–1485
9. Foulkes WD (2004) BRCA1 functions as a breast stem cell regulator. J Med Genet 41:1–5
10. Honrado E, Benitez J, Palacios J (2005) The molecular pathology of hereditary breast cancer: genetic testing and therapeutic implications. Mod Path 18:1305–1320
11. Korsching E Packeisen J, Liedtke C, Hungermann D, Wulfing P, van Diest PJ, Brandt B, Boecker W, Buerger H (2005) The origin of vimentin expression in invasive breast cancer: epithelial–mesenchymal transition, myoepithelial histogenesis or histogenesis from progenitor cells with bilinear differentiation potential? J Pathol 206:451–457
12. Laakso M, Loman N, Borg A, Isola J (2005) Cytokeratin 5/14-positive breast cancer: true basal phenotype confined to BRCA1 tumors. Mod Path 18:1321–1328
13. Laakso M, Tanner M, Nilsson J, Wiklund T, Erikstein B, Kellokumpu-Lehtinen P, Malmström, Wilking N, Bergh J, Isola J (2006) Basoluminal carcinoma: a new biologically and prognostically distinct entity between basal and luminal breast cancer. Clin Cancer Res 12:4185–4191
14. Livasy CA, Karaca G, Nanda R, Tretiakova MS, Olopade OI, Moore DT, Perou CM (2006) Phenotypic evaluation of the basal-like subtype of invasive breast carcinoma. Mod Path 19:264–271
15. Matos I, Dufloth R, Alvarenga M, Zeferino LC, Schmitt F (2005) p63, cytokeratin 5, and P-cadherin: three molecular markers to distinguish basal phenotype in breast carcinomas. Virchows Arch 447:688–694
16. Nielsen TO, Hsu FD, Jensen K, Cheang M, Karaca G, Hu Z, Hernandez-Boussard T, Livasy C, Cowan D, Dressler L, Akslen LA, Ragaz J, Gown AM, Gilks CB, van de Rijn M, Perou CM (2004) Immunohistochemical and clinical characterization of the basal-like subtype of invasive breast carcinoma. Clin Cancer Res 10:5367–5374
17. Oh DS, Troester MA, Usary J, Hu Z, He X, Fan C, Wu J, Carey LA, Perou CM (2006) Estrogen-regulated genes predict survival in hormone receptor-positive breast cancers. J Clin Oncol 24:1656–1664
18. Paredes J, Milanezi F, Viegas L, Amendoeira I, Schmitt F (2002) P-cadherin expression is associated with high-grade ductal carcinoma in situ of the breast. Virchows Arch 440:16–21
19. Perou CM, Sorlie T, Eisen MB, van de Rijn M, Jeffrey SS, Rees CA, Pollack JR, Ross DT, Johnsen H, Akslen LA, Fluge O, Pergamenschikov A, Williams C, Zhu SX, Lonning PE, Borresen-Dale AL, Brown PO, Botstein D (2000) Molecular portraits of human breast tumours. Nature 406:747–752
20. Reis-Filho JS, Lakhani SR (2003) The diagnosis and management of pre-invasive breast disease: genetic alterations in pre-invasive lesions. Breast Cancer Res 5:313–319
21. Reis-Filho JS, Simpson PT, Gale T, Lakhani SR (2005) The molecular genetics of breast cancer: the contribution of comparative genomic hybridization. Pathol Res Pract 201:713–725
22. Roylance R, Gorman P, Harris W, Liebmann R, Barnes D, Hanby A, Sheer D (1999) Comparative genomic hybridization of breast tumors stratified by histological grade reveals new insights into the biological progression of breast cancer. Cancer Res 59:1433–1436
23. Simpson PT, Gale T, Reis-Filho JS, Jones C, Parry S, Sloane JP, Hanby A, Pinder SE, Lee AH, Humphreys S, Ellis IO, Lakhani SR (2005) Columnar cell lesions of the breast: the missing link in

breast cancer progression? A morphological and molecular analysis. Am J Surg Pathol 29:734–746
24. Simpson PT, Reis-Filho JS, Gale T, Lakhani SR (2005) Molecular evolution of breast cancer. J Pathol 205:248–254
25. Sorlie T, Perou CM, Tibshirani R, Aas T, Geisler S, Johnsen H, Hastie T, Eisen MB, van de Rijn M, Jeffrey SS, Thorsen T, Quist H, Matese JC, Brown PO, Botstein D, Eystein Lonning P, Borresen-Dale AL (2001) Gene expression patterns of breast carcinomas distinguish tumor subclasses with clinical implications. Proc Natl Acad Sci USA 98:10869–10874
26. Sorlie T, Tibshirani R, Parker J, Hastie T, Marron JS, Nobel A, Deng S, Johnsen H, Pesich R, Geisler S, Demeter J, Perou CM, Lonning PE, Brown PO, Borresen-Dale AL, Botstein D (2003) Repeated observation of breast tumor subtypes in independent gene expression data sets. Proc Natl Acad Sci USA 100:8418–8423
27. Tang P, Wang X, Schiffhauer L, Wang J, Bourne P, Yang Q, Quinn A, Hajdu S (2006) Expression patterns of ER-{alpha}, PR, HER−2/neu, and EGFR in different cell origin subtypes of high grade and non-high grade ductal carcinoma in situ. Ann Clin Lab Sci 36:137–143
28. Tischkowitz MD, Foulkes WD (2006) The basal phenotype of BRCA1-related breast cancer: past, present and future. Cell Cycle 5:963–967
29. van de Rijn M, Perou CM, Tibshirani R, Haas P, Kallioniemi O, Kononen J, Torhorst J, Sauter G, Zuber M, Kochli OR, Mross F, Dieterich H, Seitz R, Ross D, Botstein D, Brown P (2002) Expression of cytokeratins 17 and 5 identifies a group of breast carcinomas with poor clinical outcome. Am J Pathol 161:1991–1996
30. Yankaskas BC (2005) Epidemiology of breast cancer in young women. Breast Dis 23:3–8

Virchows Arch (2007) 450:81–92
DOI 10.1007/s00428-006-0340-0

ORIGINAL ARTICLE

Analysis of glomerular VEGF mRNA and protein expression in murine mesangioproliferative glomerulonephritis

Christian S. Haas · Valentina Câmpean · Alexander Kuhlmann · Arno Dimmler · Udo Reulbach · Christian Forster · Thomas Aigner · Till Acker · Karl Plate · Kerstin Amann

Received: 18 June 2006 / Accepted: 20 October 2006 / Published online: 22 November 2006
© Springer-Verlag 2006

Abstract Capillary repair is crucial in the healing of glomerulonephritis (GN). The vascular endothelial growth factor (VEGF) has pro-angiogenic properties and plays an important role in glomerular capillary regeneration. Habu Snake Venom (HSV) GN, a murine model for mesangioproliferative GN, was induced in uninephrectomized C57/BL6 mice. Glomerular damage and capillary repair were assessed using morphometry, stereology, and confocal laser scanning microscopy. Mesangiolytic glomeruli were microdissected (days 1,3,7,14) using laser capture microdissection technique. VEGF mRNA expression was analyzed by real-time polymerase chain reaction and compared to intact glomeruli of healthy controls. Spatiotemporal *VEGF* gene and protein expression was determined using nonradioactive in situ hybridization and immunohistochemistry. On day 1, diseased animals developed focal mesangiolysis paralleled by a significant decrease in length density of glomerular capillaries that gradually returned to baseline levels thereafter, indicating capillary growth in response to initial injury. Glomerular VEGF mRNA expression increased on day 3 and returned back to baseline and beyond at day 14 when the glomerular recovery process was completed. Similarly, glomerular VEGF protein expression tended to be higher on day 3. The present study documents temporarily increased glomerular *VEGF* gene and protein expression during the healing of HSV GN, suggesting a potential role of VEGF in the repair of mesangiolytic glomerular damage.

Keywords Habu snake venom glomerulonephritis · Laser capture microdissection · Mouse · Mesangiolysis · Real-time PCR · VEGF

Christian S. Haas and Valentina Câmpean contributed equally to this work.

V. Câmpean · A. Dimmler · C. Forster · K. Amann (✉)
Institute of Pathology, University of Erlangen-Nürnberg,
Krankenhausstr. 8-10,
91054 Erlangen, Germany
e-mail: kerstin.amann@patho.imed.uni-erlangen.de

T. Aigner
Institute of Pathology, University of Leipzig,
Leipzig, Germany

C. S. Haas
Department of Internal Medicine, University of Tübingen,
Tübingen, Germany

U. Reulbach
Department of Psychiatry, University of Erlangen-Nürnberg,
Schwabachanlage 6,
Erlangen, Germany

T. Acker · K. Plate
Edinger Institute, University of Frankfurt,
Frankfurt, Germany

A. Kuhlmann
Department of Internal Medicine,
University of Erlangen-Nürnberg,
Erlangen, Germany

Introduction

Acute glomerular damage in experimental inflammatory glomerular disease is associated with different degrees of destruction of the capillary convolute. Depending on the remodeling and repair processes of the glomerular architecture, this is followed by neovascularization through a coordinate interaction between glomerular cells and various growth factors [22, 26, 36].

The vascular endothelial growth factor (VEGF) is one of the most important and potent angiogenic factors activating endothelial cells (ECs), thus inducing vascular neoformation

[44]. Recently, Ostendorf et al. showed that VEGF mediates EC survival and repair of glomerular capillaries in several models of rat glomerulonephritis (GN) [33, 34]. For example, inhibition of VEGF by a specific aptamer led to more severe glomerular damage in the anti-Thy 1.1 GN model of the rat [33]. Habu Snake Venom (HSV) GN, a murine model of mesangioproliferative GN, is also characterized by initial mesangiolysis, i.e., dissolution of mesangial cells (MCs) and mesangial matrix with subsequent MC migration, proliferation, as well as mononuclear cell infiltration and extracellular matrix accumulation during remodeling with a self-limiting course. Thus, the HSV-induced GN is widely used as a model of inflammatory glomerular disease in mice having much in common with the anti-Thy 1.1 GN model in rats [4, 7, 8]. However, the initial injury, i.e., the degree of mesangiolysis, in HSV is more subtle, and the remodeling process has not been investigated with respect to the neoformation of capillaries in detail so far.

We hypothesized that—as in the anti-Thy 1.1. GN of the rat—VEGF may also play a crucial role in the repair of mesangiolytic glomerular damage in HSV GN. Thus, we investigated the spatiotemporal mRNA and protein VEGF expression pattern in morphologically affected glomeruli during the course of this experimental mesangioproliferative GN. The second aim of the study was to evaluate the practicability of laser capture microdissection (LCM) in combination with real-time polymerase chain reaction (PCR) for the analysis of glomerular *VEGF* gene expression in the diseased mouse kidney. Therefore, we investigated VEGF mRNA expression in microdissected mesangiolytic glomeruli from HSV-injected mice and in normal glomeruli from healthy controls.

We confirmed that LCM combined with real-time PCR is a useful tool and reliable method to quantify *VEGF* gene expression in isolated renal structures even in mesangiolytic glomeruli of mice. Furthermore, we defined spatiotemporal VEGF expression with distinct upregulation after mesangiolysis in HSV GN. Our data argue for a similarly important role of VEGF in the repair of mesangiolysis in murine HSV-induced GN.

Materials and methods

Animals

HSV GN was induced in 18–20 g male C57BL/6 mice (Charles River, Sulzfeld, Germany) by intravenous injection of venom toxin from the Habus snake *Trimeresurus flavoviridis* (6 mg/kg body weight, Sigma-Aldrich Chemicals, Deisenhofen, Germany) 1 week after unilateral nephrectomy, using a modification of previously described protocols [12, 31]. Uninephrectomized mice receiving phosphate-buffered saline intravenously served as controls (day 0). At days 1, 3, 7, and 14 post-induction, five to eight mice per group were killed by perfusion fixation as described previously [12]. For urine collection, animals were placed in metabolic cages for 24 h before perfusion fixation with glutaraldehyde. Successful induction of the nephritis was assessed by detection of hematuria with the dip-stix method (Multistix 10 SG, Bayer Vital GmbH, Fernwald, Germany).

All animals were housed in cages at constant room temperature (20°C) and humidity (70%) under a controlled light–dark cycle. Animals were fed with a standard diet (Altromin, Lage, Germany). All animal experiments were performed according to the German animal protection laws.

Tissue preparation

After determining total organ weight and volume, kidneys were dissected in 1-mm thick slices perpendicular to the longitudinal axis. Tissue sampling for morphometric and stereological analysis was performed using the area-weighted sampling technique as described in detail previously [12]. Two- and 5-μm-thick paraffin sections and 1-μm semi-thin sections (five blocks per animal) were prepared and stained as outlined before [12].

Semiquantitative analysis of mesangiolytic glomerular damage

Focal mesangiolysis, i.e., dissolution or disappearance of the mesangial matrix due to necrosis and apoptosis of MCs, is the hallmark of HSV GN. It is associated with loss of MCs, capillary dilatation, and finally formation of capillary aneurysms in some heavily affected glomeruli. To analyze the extent of mesangiolysis, a semiquantitative score was used on 2-μm-thick periodic acid-Schiff (PAS)-stained paraffin sections. A hundred systematically subsampled glomeruli per animal were investigated using the following scoring system: 0, no changes of capillaries; 1, capillary dilatation <25% of capillary convolute; 2, capillary dilatation >25% of capillary convolute or capillary aneurysm <50% of the capillary convolute; 3, capillary aneurysm comprising 50–75% of the capillary convolute; 4, capillary aneurysm comprising >75% of the capillary convolute [12].

Semiquantitative analysis of mesangial matrix expansion

The degree of mesangial matrix expansion was determined on PAS-stained paraffin sections adopting the semiquantitative scoring systems proposed by el Nahas et al. [13] and Goumenos et al. [18]. Using light microscopy at a magnification of ×400, the score was obtained as a mean of 100 glomeruli in each animal. The severity of matrix

expansion was expressed on an arbitrary scale from 0 to 4 with an individual glomeruli score as follows: grade 0, normal glomerulus; grade 1, presence of mesangial expansion/thickening of the basement membrane; grade 2, mild to moderate segmental hyalinosis/sclerosis involving less than 50% of the glomerular tuft; grade 3, diffuse glomerular hyalinosis/sclerosis >50% of the tuft; and grade 4, diffuse glomerulosclerosis with total tuft obliteration and/or collapse [12].

Immunohistochemistry

For immunohistochemical staining, 5-μm thick paraffin sections were used. Staining for VEGF was performed using a polyclonal rabbit anti-mouse antibody (Santa Cruz, Santa Cruz, CA) at a dilution of 1:500. To reduce nonspecific background staining, sections were incubated for 30 min at 37°C with Powerblock (Biogenex, San Ramon, CA). Samples were then rinsed in Tris-buffered saline, pH 7.6, and subjected to the avidin–biotin system. In brief, slides were incubated with the primary antibody for 60 min at room temperature (RT). Biotinylated goat anti-rabbit IgG were applied for 30 min as secondary antibody (1:200, Biogenex). The sections were incubated with supersensitive-label, alkaline phosphatase-conjugated streptavidin (Biogenex) for 30 min at RT. Each incubation step was followed by thorough rinsing with Tris-buffered saline, and Fast Red substrate (Dako GmbH, Hamburg, Germany) served as chromogen. Finally, sections were counterstained with hematoxylin and evaluated by light microscopy (magnification × 400) for staining intensity of the glomeruli, using the following semiquantitative scoring system from 0 to 4: 0, no expression; 1, weak expression; 2, moderate expression; 3, strong expression; and 4, very strong expression.

Confocal laser scanning microscopy of mesangiolytic glomeruli

To obtain additional information on the three-dimensional structure of a mesangiolytic glomerulus with respect to damage and repair of the capillary convolute during the course of HSV GN, serial images of glomeruli were taken using confocal laser scanning microscopy (TCS SP2, Leica Microsystems, Bensheim, Germany). Subsequently, maximum intensity projection was performed. Using specific projection algorithms, the relevant information from several images was selected and subsequently depicted in a single two-dimensional image. This method is very useful to reconstruct connected structures after a virtual fragmentation in serial sections, e.g., in the glomerulus [35].

To stain the glomerular basement membrane, formalin fixed 12-μm-thick sections were immunostained with a polyclonal rabbit anti-laminin antibody (dilution 1:1,000; Trinova Biochem GmbH, Gießen, Germany) and detected with Alexa Fluor 568-labeled donkey anti-rabbit IgG (Molecular Probes, Leipzig, Germany). Tissue sections were examined by confocal laser scanning microscopy at an excitation wavelength of 543 nm and with a 63× objective lens (HCX PL APO CS 63×1.3 oil). Confocal images were obtained using standard data analysis software of the TCS SP2 system in the z-scan mode as follows: 70 serial horizontal *xy* sections with an interval of 0.17 μm were imaged; the maximum intensity projection of each image was calculated with the analysis software package "3D Visualization and Animation," and eventually viewed in a single image. Subsequently, the rotation and animation mode of the software package allowed viewing the laminin-positive stained capillary convolute of the glomeruli in a three-dimensional fashion.

Analysis of length density and total length of glomerular capillaries

All studies on semi-thin sections were performed in a blinded manner using a magnification of ×1,000 as described elsewhere [2]. In brief, the length density (L_V) of glomerular capillaries, i.e., the length of all capillaries per volume of the glomerular tuft, was analyzed as a three-dimensional parameter of glomerular capillarization according to the standard stereological formula $L_v=2\ Q_A$, with Q_A being the number of capillary transects per area of the glomerular tuft [2].

Laser capture microdissection

Ten-micrometer-thick cryosections were placed on special slides covered with a clear polyethylene membrane (MMI AG, Glottbrugg, Switzerland). LCM was performed on five mesangiolytic glomeruli per animal with glomeruli of non-diseased animals serving as control. The target structures were dissected from adjacent tubulointerstitial tissue at ×200 magnification with the μCut Laser Microdissection System (MMI AG), which was set to the following parameters: laser wave length 337 nm and laser spot diameter 30 μm [27, 38]. Subsequently, dissected glomeruli were transferred into a reaction tube on RNAse-free conditions using adhesion to the tip of a micro fine needle (0.25×8 mm, Becton Dickinson, Heidelberg, Germany).

Real-time PCR

For RNA extraction, five LCM-isolated glomeruli per animal were transferred into a reaction tube containing 7.3 μl 1× real-time buffer (Qiagen, Hilden, Germany) and 0.2 mg/ml Proteinase K. Samples were incubated for 1 h at 54°C. After 5 min denaturing at 95°C, the samples were stored on ice for another 5 min.

First-strand cDNA was synthesized by using Sensiscript Reverse Transcriptase (Qiagen). Cell lysates were places on ice and the following reagents were added: 0.5 μl Sensiscript enzyme (Qiagen), 1 μM dT_{15} primer (TIB-Biomol, Berlin, Germany), 150 ng/μl random hexamers (Promega, Heidelberg, Germany), 1× first-strand buffer (Qiagen), 6 U RNase-Inhibitor (PeqLab, Erlangen, Germany), and 0.5 mM deoxynucleotide triphosphate (Carl Roth, Karlsruhe, Germany) to form a total reaction volume of 10 μl. The reaction was allowed to proceed for 60 min at 37°C, followed by 5 min at 95°C to inactivate the enzyme. After cDNA synthesis, distilled water was added in each probe to a final volume of 40 μl.

TaqMan-PCR was performed with the ABI Prism 7700 Sequence Detection System^R (Perkin Elmer Applied Biosystems, Foster City, CA). After target amplification, an oligonucleotide probe, containing a fluorescent dye (6-carboxyfluorescein) at its 5′-end and a quencher (6-carboxy-tetramethylrhodamine) at its 3′-end, anneals to the amplicon and is displaced and cleaved between the reporter and quencher dyes by the nucleolytic activity of the recombinant Taq-Polymerase. The amount of product resulting in detectable fluorescence at any given cycle within the exponential phase of PCR is proportional to the initial number of template copies. The number of PCR cycles needed to detect the amplicon is therefore a direct measure of template concentration. Intron-overlapping primers and corresponding oligonucleotide probes for VEGF and the housekeeping gene glyceraldehyde-3-phosphate-dehydrogenase (GAPDH) were designed by use of the Primer Express software (Version 1.6, Applied Biosystems, Darmstadt, Germany). The sequences of primers and probes were as follows:

- VEGF (GenBank accession number AF062644, amplicon 68 bp): forward primer (exon 7): 5′-AGG CGA GGC AGC TTG AGT TA-3′; reverse primer (exon 8): 3′-CAG CCT GGC TCA CCG C-5′; probe (exon 7 + exon 8): 5′-FAM-ACG AAC GTA CTT GCA GAT GTG ACA AGC CA-TAMRA-3′
- GAPDH (GenBank accession number J04038, amplicon 75 bp): forward primer (exon 2): 5′-GCC AGC CTC GTC TCA TAG ACA-3′; reverse primer (exon 3): 3′-TGG TAA CCA GGC GTC CGA TA-5′; probe (exon 2 + exon 3): 5′-FAM-TGA AGG TCG GTG TGA ACG GAT TTG GC-TAMRA-3′

Each PCR assay was repeated two times for each cDNA sample. The 25-μl total PCR volume consisted of 5 μl cDNA, 0.3 U Taq polymerase (Eurogentec, Seraing, Belgium), 1× amplification buffer (Eurogentec), 5.5 mM $MgCl_2$, 200 μM deoxynucleotide triphosphate, 1.2 μM ROX (PE ABI, Germany), specific double-labeled probes (Eurogentec) to a final concentration of 100 nM, and forward/reverse primers (MWG-Biotech, Ebersberg, Germany) in the following concentrations: 100/300 nM (VEGF) and 300 nM each (GAPDH). After denaturation for 4 min at 95°C, the PCR assays were carried out for 60 cycles, with denaturation at 95°C for 15 s, annealing and extension at 60°C for 1 min.

Absolute quantification was achieved through the generation of standard curves by serial dilutions of VEGF- and GAPDH-cDNAs in known concentrations, as described in the user manual of ABI Prism 7700 Sequence Detection System^R (standard curve method). The real-time PCR results were calculated as gene expression levels normalized to the GAPDH. To monitor amplification of possible contaminating DNA samples, distilled water served as negative control. mRNA data are depicted as relative expression levels compared to VEGF expression in one of the non-mesangiolytic glomeruli samples.

Nonradioactive in situ hybridization of VEGF mRNA

Nonradioactive in situ hybridization using VEGF sense and antisense probes was performed in three animals per group as detailed before [24]. In detail, cryostat sections (10 μm) were fixed with 3% paraformaldehyde in phosphate-buffered saline, pH 7.0 (5 min, 4°C). Subsequently, sections were dehydrated, air-dried, and stored at −20°C. Probe preparation and labeling was performed as follows. A 583-bp cDNA fragment of the VEGF cDNA (encoding murine VEGF 164) was obtained from a PCR product using rat VEGF-specific primers after reverse transcription of rat kidney total RNA [24]. The segment encoding positions of the mouse *VEGF* gene was inserted into the pBluescript II KS (Stratagene, La Jolla, CA). For preparation of the antisense RNA probe, the plasmid was linearized with *Bam*HI and transcribed using T3 Bacteriophage RNA polymerase. Linearization of the plasmid with *Eco*RI and transcription with T7 RNA Polymerase generated the sense RNA probe. Digoxigenin-labeled RNA probes were synthesized using DIG RNA labeling mix (Boehringer Mannheim GmbH, Mannheim, Germany). The sections were hybridized with 2 ng of labeled probe in buffer in a moist chamber. Hybridization of the probe with native mRNA was allowed for 18 h at 50°C. After several post-hybridization steps, sections were equilibrated in buffer I (Boehringer Mannheim GmbH). Nonspecific background staining was blocked by incubation for 1 h with 0.5% blocking reagent/buffer I (Boehringer Mannheim GmbH). The hybridization products were visualized by enzyme-linked immunoassay using alkaline phosphatase-conjugated sheep anti-digoxigenin-Fab fragments (750 U/ml, Boehringer Mannheim GmbH). After incubation at 4°C overnight, unbound conjugate was removed by two washes in buffer I, followed by equilibration of the sections in buffer II (Boehringer Mannheim GmbH). Nitro-blue tetrazolium and 5-bromo-4-chloro-3-indolyl phosphate served as chromogens. Negative controls included hybridization with the

sense RNA probe, incubation without probe for detection of unspecific binding of the primary antibody, and omission of both probe and primary antibody. Staining intensity was analyzed using the same semiquantitative scoring system (scores 0–4), used for immunohistochemistry, as described above.

Statistics

Data are given as mean±SD or—for semiquantitative analysis of in situ hybridization—as median and range. Nonparametric two-tailed tests were performed to determine statistically significant differences using the software package SPSS 11 (SPSS, Chicago, IL). A p value less than 0.05 was considered as significant.

Results

Animal data

Body and kidney weight in the mice were comparable at all time points after HSV GN induction and in control animals (data not shown).

Urine analysis

Hematuria was present in all mice tested 1 to 2 h after induction of HSV GN, but was only detected in sporadic cases after 24 h or later. The 24-h urinary output showed a significant increase in nephritic mice at day 3 compared to controls (1.54±0.28 ml/24 h vs 0.79±0.43, $p<0.01$), but

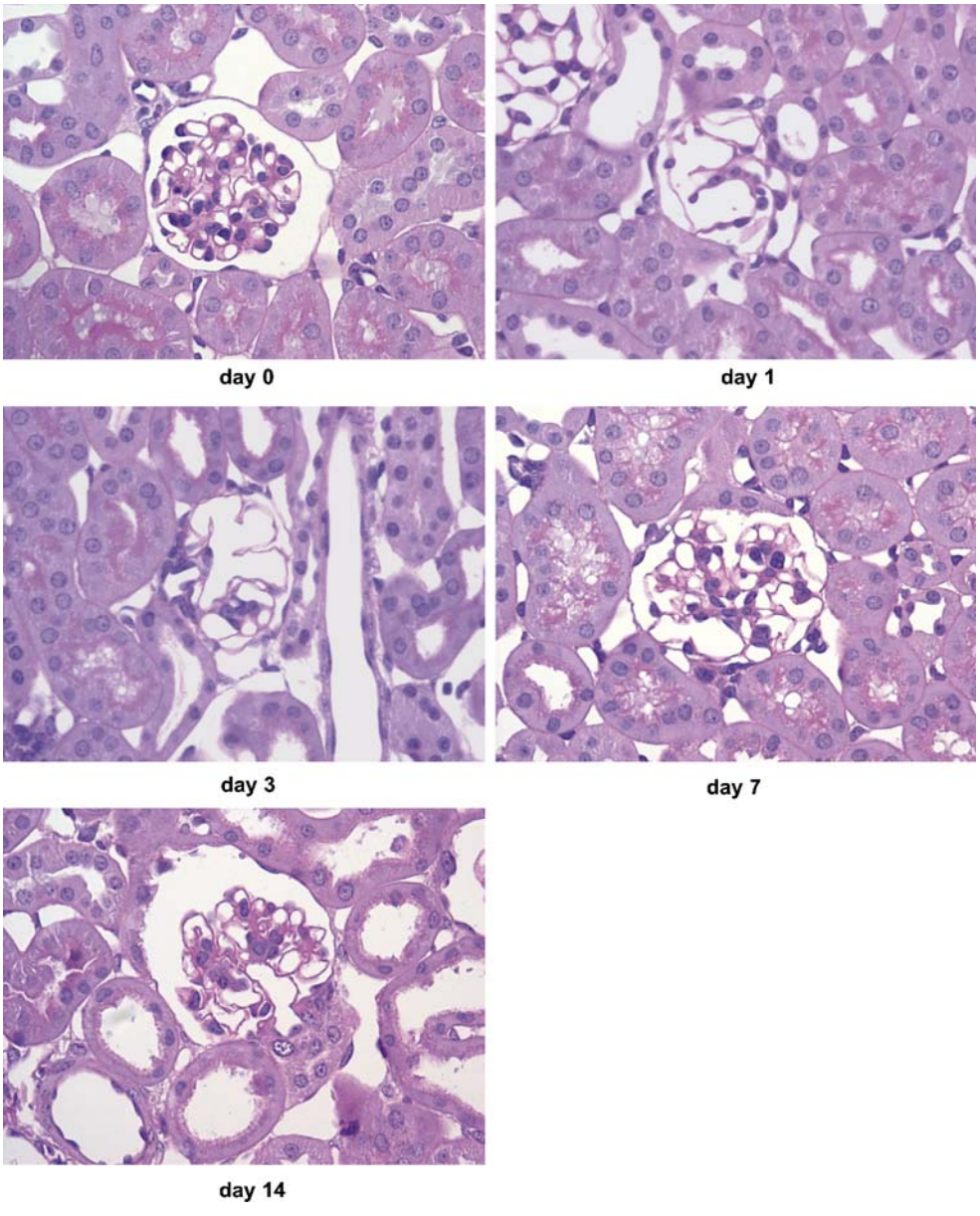

Fig. 1 Mild focal mesangiolytic glomerular damage in HSV-induced GN. Mesangiolytic changes differed significantly at various time points of HSV GN. Mesangiolysis was most prominent at *day 1* post-induction with subsequent decline at *days 3*, *7*, and *14* until complete glomerular reorganization, eventually comparable to glomeruli of healthy control animals (*day 0*)

slightly declined thereafter (data not shown). No proteinuria was present in control mice, while dipstick protein score was positive in almost all nephritic mice (day 1, 2.3±0.8 units; day 3, 2.25±0.4 units; day 7, 1.3±1.2 units; day 14, 1.2±0.9 units), pointing to successful induction of the nephritis.

Mesangiolysis and matrix expansion scores

In HSV GN, mesangiolytic changes as assessed by the mesangiolysis score were significantly different between all five groups (p=0.0001). Mesangiolysis was most prominent at day 1 after induction of the nephritis (p<0.01) with a subsequent decline at the following time points, until reaching baseline levels of control animals again at day 14 (Figs. 1 and 2a). Mesangial matrix expansion increased temporarily in the course of the diseases with significant score differences between the groups (p=0.002), peaking at day 3 (p<0.01) and slowly decreasing thereafter at days 7 and 14 (p<0.05; Fig. 2b).

Glomerular capillary length density

The length density of glomerular capillaries, i.e., the length of all capillaries per glomerular tuft volume, was significantly lower at day 1 compared to control tissue (p<0.005), indicating mesangiolysis with capillary destruction and loss (Fig. 3). However, capillary length density gradually increased from days 3 to 7 and was back to baseline values at day 14, pointing to a capillary repair process that was completed within that period.

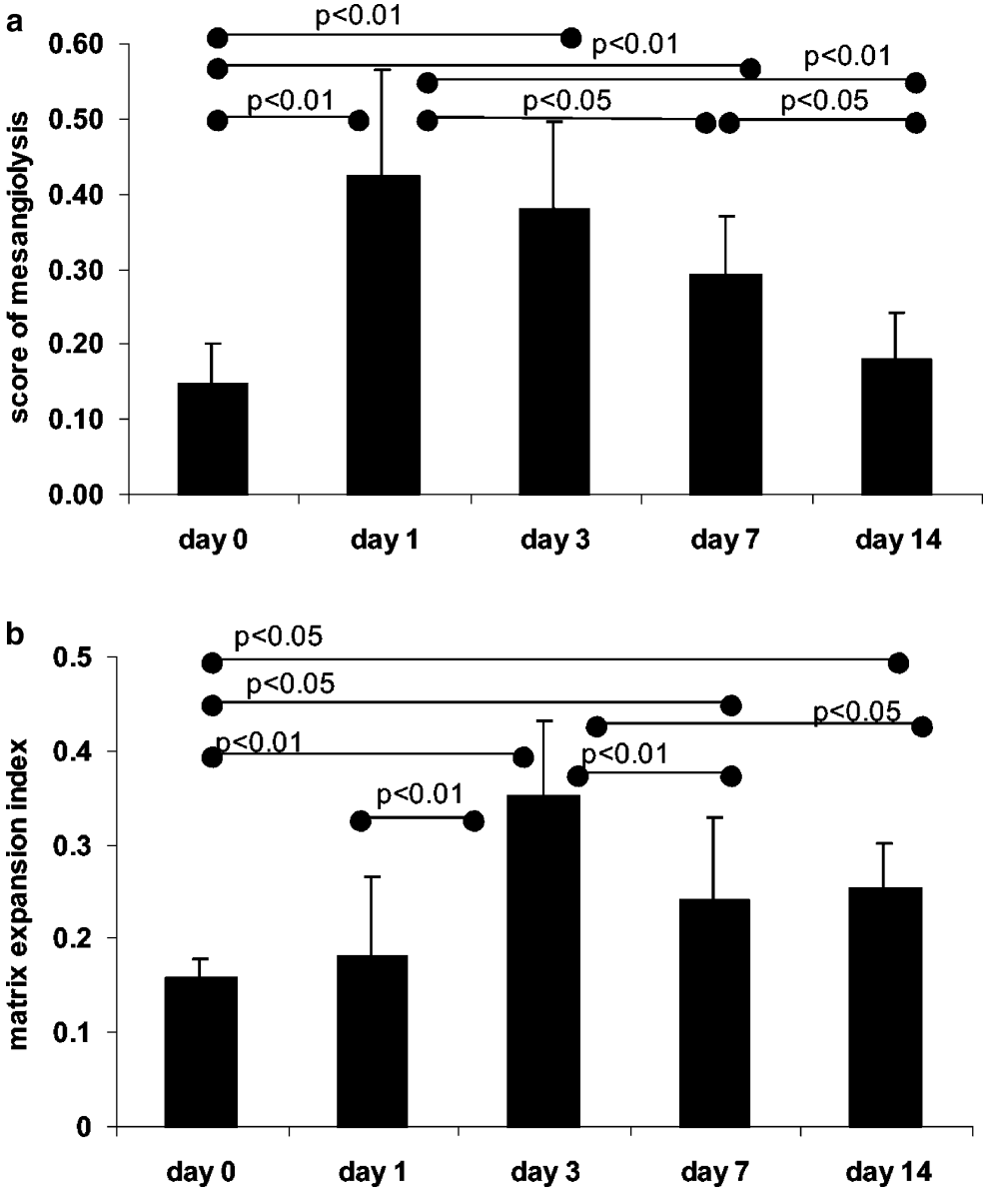

Fig. 2 Semiquantitative analysis of mesangiolysis and mesangial matrix expansion. **a** Mesangiolysis peaked at *day 1* after induction of the nephritis with subsequent decline at the following time points and returned to baseline levels at *day 14*. **b** In contrast, matrix expansion score peaked at *day 3* in response to glomerular damage being still significantly higher at *day 14* than at control *day 0*

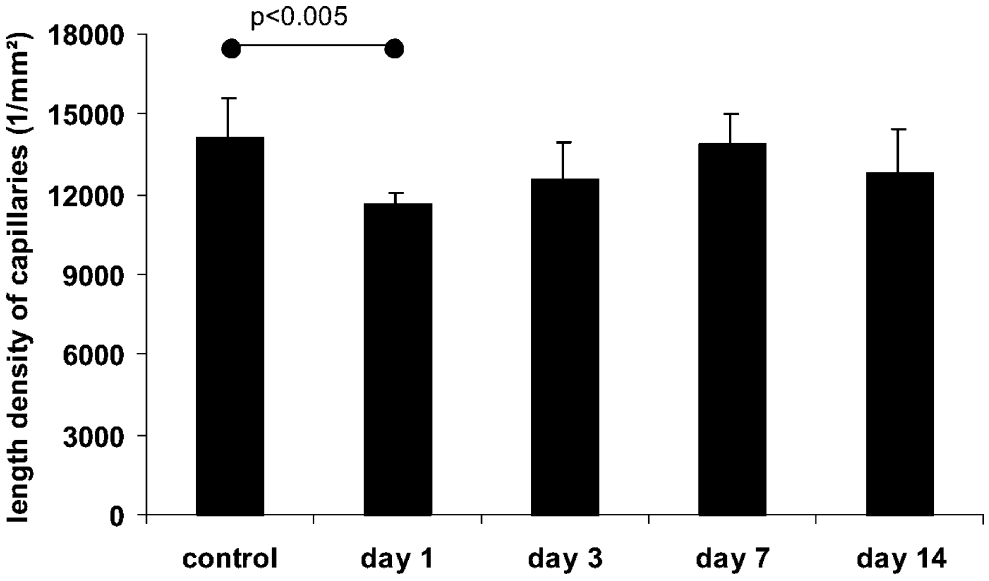

Fig. 3 Glomerular capillary length density. The length density of glomerular capillaries, i.e., the total length of glomerular capillaries per unit of glomerular volume, was significantly reduced at *day 1* of HSV GN, reflecting maximum mesangiolysis. Length density then increased again back to normal values indicating capillary neoformation or lengthening

Confocal laser scanning microscopy

Using the maximum intensity projection method, a mesangiolytic glomerular capillary convolute was reconstructed. At day 3 after HSV GN induction, the integrity of the capillary convolute visualized as laminin positivity was markedly disturbed compared to control glomeruli and showed extensive mesangiolytic damage through 70 consecutive horizontal *xy* sections. A single depiction of the maximum intensity projection of horizontal *xy* sections showed in detail the extent of damage to the capillary convolute (Fig. 4).

VEGF mRNA expression in LCM dissected glomeruli

To test the sensitivity and reproducibility of LCM followed by real-time PCR in isolated structures of the murine kidney, we first performed real-time PCR with various numbers of microdissected glomeruli. We demonstrated a linear correlation between the number of dissected glomeruli and GAPDH mRNA expression and were able to determine *GAPDH* gene expression in only one mouse glomerulus obtained by LCM (data not shown). Note that *GAPDH* gene expression was comparable in all groups.

In HSV-induced glomerular disease, relative *VEGF* gene expression showed a similar course as the semiquantitative mesangiolysis score (Fig. 5), with statistically significant differences in *VEGF* gene expression between all groups (p=0.006). Relative VEGF mRNA expression was 1.24±0.62 in non-mesangiolytic control glomeruli and increased progressively from 1.8±1.12 (day 1) to 2.0±1.15 (day 3) in mesangiolytic glomeruli. Relative VEGF expression then declined again to 1±0.52 at day 7 and was finally back to 0.34±0.17 at day 14.

Glomerular VEGF mRNA expression by nonradioactive in situ hybridization

Glomerular VEGF mRNA expression as determined by nonradioactive in situ hybridization (Fig. 6) showed a

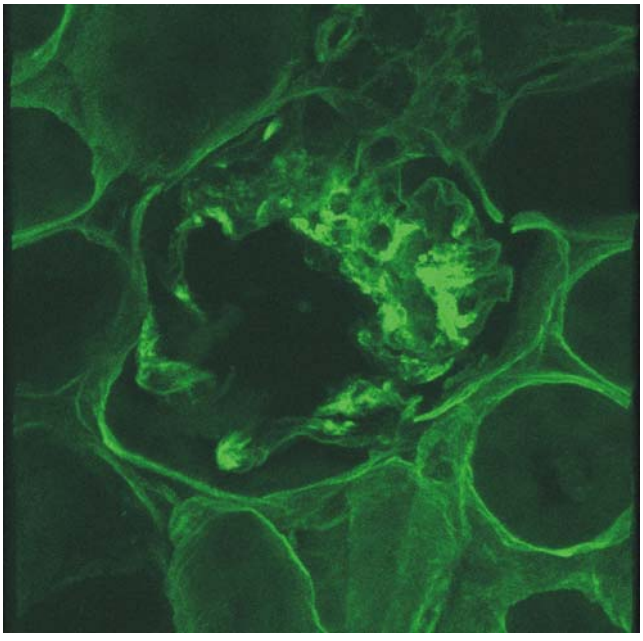

Fig. 4 Confocal laser scanning microscopy for three-dimensional analysis of mesangiolysis in HSV induced GN. A mesangiolytic glomerular capillary convolute at day 3 after HSV injection was reconstructed three-dimensionally with the maximum projection method using confocal laser scanning microscopy after immunofluorescence with an anti-laminin antibody as described in the "Materials and methods" section. The integrity of the capillary convolute was significantly disturbed compared to a control glomerulus and showed extensive mesangiolytic damage through 70 consecutive horizontal *xy* sections in a single depiction of the maximum projection

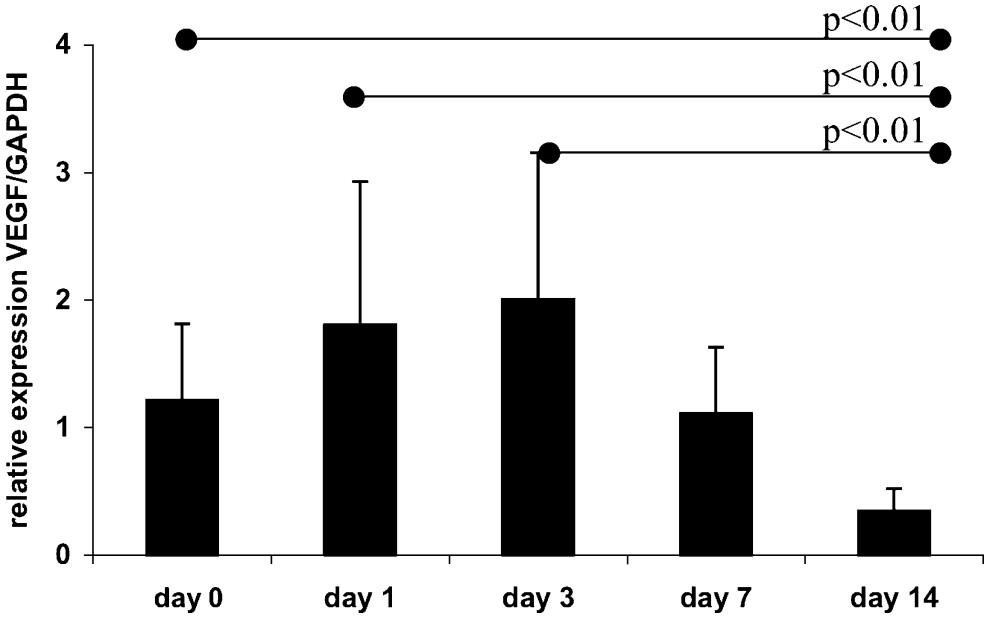

Fig. 5 Relative VEGF mRNA expression in microdissected glomeruli. In HSV GN, analysis of relative *VEGF* gene expression showed a course similar to the semiquantitative mesangiolysis score. VEGF mRNA expression was 1.24±0.62 in non-mesangiolytic glomeruli and increased progressively from 1.8±1.12 (*day 1*) to 2.0±1.15 (*day 3*) in mesangiolytic glomeruli. The relative expression then declined again to 1±0.52 at *day 7* and finally to 0.34±0.17 at *day 14*

similar course to the mRNA expression data obtained by glomerular LCM and subsequent real-time PCR. Normal mouse glomeruli showed only very low VEGF mRNA expression (median score: 1.5, range 1–2) with predominant location in podocytes, while in HSV GN, expression of VEGF mRNA peaked at day 3 (median score: 4, range 4–4), showing intensive staining in podocytes and, to a lesser extent, in some ECs and mesangial cells. Subsequently, VEGF mRNA expression decreased almost to baseline values at day 7 (median score: 2, range 1–3) and day 14 (median score: 2, range 1–3). Sense probe sections showed no specific staining and virtually no background signal.

Glomerular VEGF protein expression by immunohistochemistry

Glomerular VEGF protein expression, as determined by immunohistochemistry, showed a slight increase of expression in mesangiolytic glomeruli at day 1 compared to glomeruli of control tissue. VEGF protein expression was predominantly seen in podocytes and, to a lesser extent, in some ECs and mesangial cells (Fig. 7a). The expression level was only slightly, but not significantly higher, at day 3 compared to the other time points (Fig. 7b).

Discussion

Growth and remodeling of glomerular capillaries after injury seems to be decisive for healing of glomerular diseases. While the role of peritubular capillary damage and repair in the renal recovery process has been thoroughly investigated [5, 25], the sequence of events in glomerular injury and subsequent healing of capillaries during the course of proliferative glomerular disease is much less clear [23, 30]. This is particularly true for HSV-induced murine glomerulonephritis, which is one of the very rare models of inflammatory glomerular disease in mice and might thus also be of interest for disease induction in genetically manipulated mice.

Using stereological techniques and confocal laser scanning microscopy, we studied the extent of damage and repair of the glomerular capillary tuft in HSV-induced GN at several time points after disease onset. Since VEGF is known to play a crucial role in capillary neovascularization after glomerular damage in rats, we were particularly interested in its gene and protein expression during the course of the murine disease. To our knowledge, we found for the first time in the HSV-induced GN that the *VEGF* gene, and to a lesser extent also protein expression, is upregulated in response to capillary damage and loss, and subsequently downregulated again when the capillary healing process had stopped.

VEGF is a potent mitogen that enhances the proliferation of vascular ECs, angiogenesis, and microvascular permeability [15, 44]. At least four VEGF isoforms are known, which interact with the specific tyrosine kinase receptors Flt-1, Flt-4, and KDR/Flk-1 on ECs [10, 39]. In normal fetal and adult kidneys, VEGF mRNA expression was predominantly observed in podocytes and collecting duct cells, while mRNA expression of its receptors has been detected in glomerular ECs and peritubular capillaries [37]. Expression of VEGF as one of the major pro-angiogenic growth factors has been shown to be altered in both human glomerular diseases and experimental animal models. For example, in the rat anti-Thy 1.1 GN followed by unilateral nephrectomy, Wada et al. [43] detected

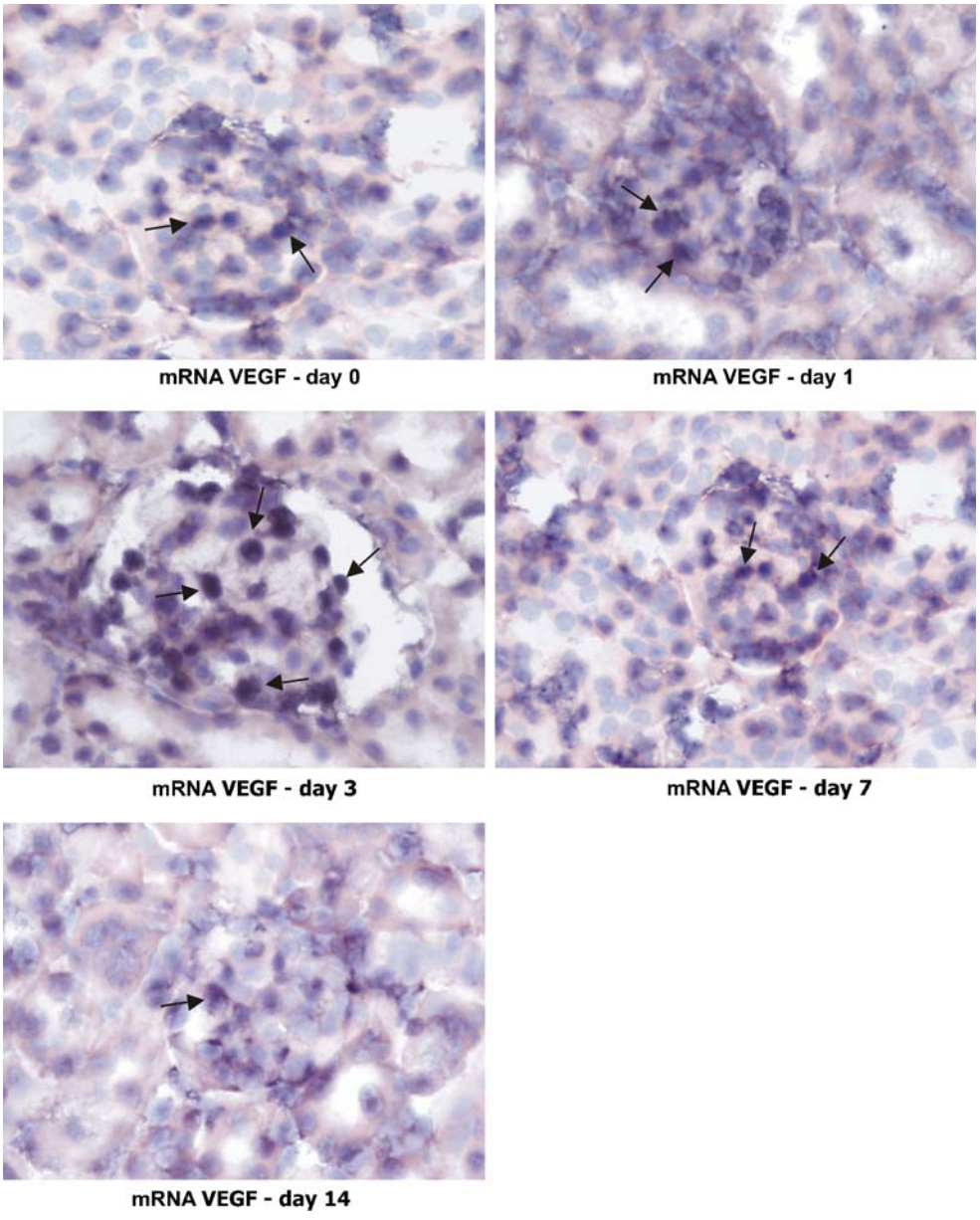

Fig. 6 Glomerular VEGF mRNA expression. Representative pictures of spatiotemporal glomerular VEGF mRNA expression by in situ hybridization. Glomerular VEGF mRNA expression was determined using nonradioactive in situ hybridization. Compared to mRNA expression data obtained by glomerular LCM and subsequent real-time PCR, semiquantitative analysis of VEGF mRNA expression showed a similar course. Normal mouse glomeruli (*day 0*) presented low-level expression of VEGF mRNA, with the signal present primarily in podocytes (*arrows*). Expression of VEGF mRNA increased immediately after induction of the disease (*day 1*) and was most prominent at *day 3*, predominantly in podocytes. Subsequently, VEGF mRNA expression decreased at *day 14* almost to basal values. Sense probe sections demonstrated virtually no background signal

significantly lower glomerular VEGF mRNA expression at day 14 compared to the two-kidney group. In rats, Masuda et al. [30] showed that administration of VEGF in a combined anti-Thy 1.1/HSV-induced GN significantly improved glomerular EC proliferation and capillary repair. VEGF has also been demonstrated to accelerate renal recovery in an experimental model of thrombotic microangiopathy [25], and studies by Ostendorf et al. demonstrated that VEGF is a crucial factor for EC survival and repair in glomerular disease in rats with mesangioproliferative nephritis, passive Heymann nephritis, or puromycin aminonucleoside nephrosis [33]. It is interesting that increased renal expression of both VEGF and its receptor was shown in rodent models of diabetic type 1 and 2 nephropathy [9, 41]. In this context, being a vascular permeability factor, VEGF may be involved in the development of proteinuria, as suggested by a reduction in proteinuria in experimental diabetes after administration of an anti-VEGF antibody [11]. This idea is in line with recent data of Flyvbjerg et al. [17], who demonstrated amelioration of renal changes in obese type 2 diabetic mice by a VEGF neutralizing antibody. The effect of VEGF on proteinuria seems to be much more complex, however, since in a recent study Hara et al. [19] found that blockade of VEGF accelerates proteinuria in rat crescentic glomerulonephritis and this was due to the downregulation of nephrin expression. In our study in HSV GN, however, we did not find a significant correlation between either VEGF mRNA or protein expression and proteinuria, respectively.

Gene expression analysis using real-time PCR is a useful tool in clinical diagnostic procedure and allows highly accurate template quantification from very small tissue

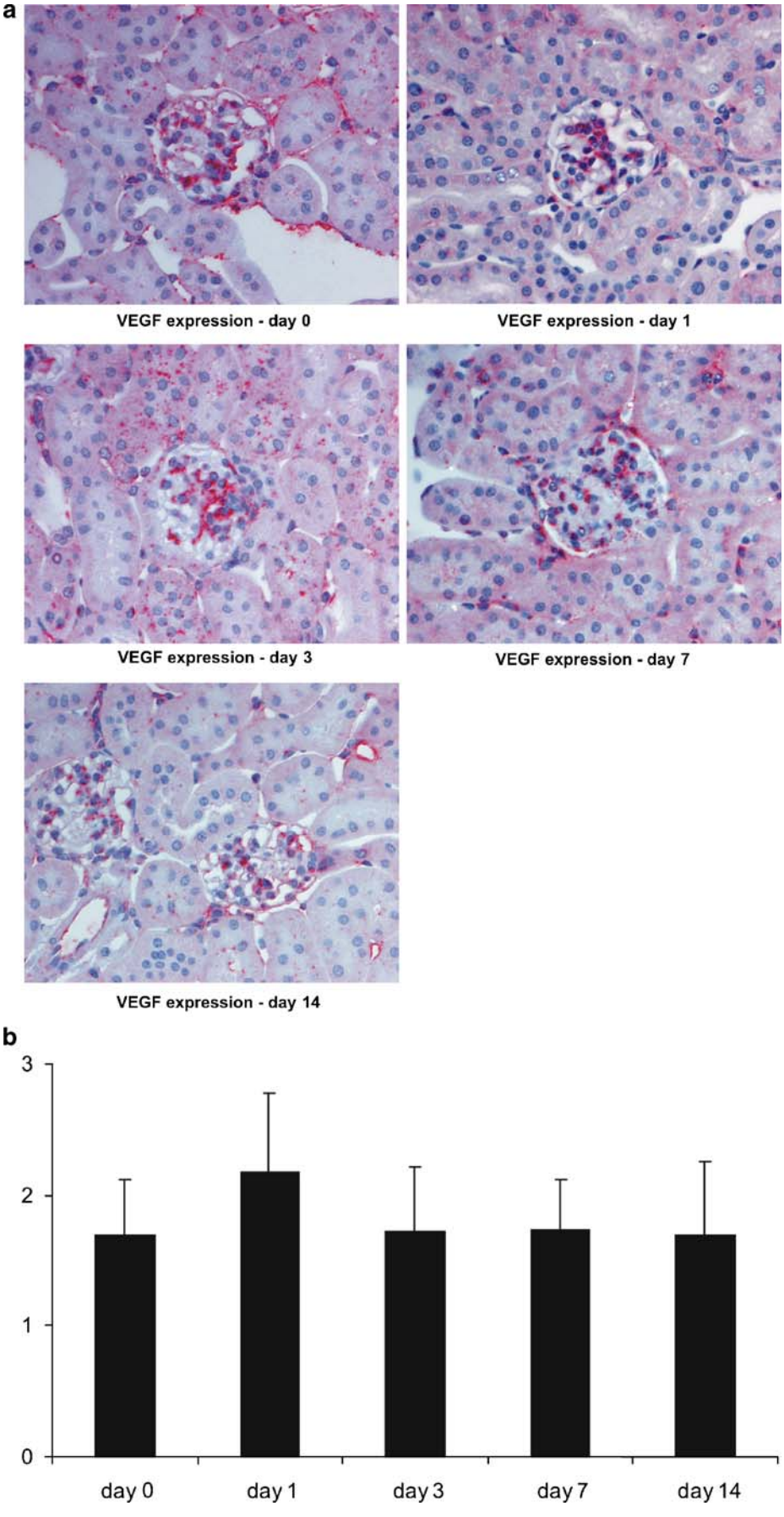

Fig. 7 Glomerular VEGF protein expression. **a** Representative figures of immunohistochemistry for VEGF expression in HSV GN documenting basal expression of VEGF protein in normal mouse glomeruli (*day 0*). VEGF immunopositivity slightly increases within the glomerulus at *day 1* and returns to basal levels at *days 3* and *7* of the disease. **b** Semiquantitative analysis of glomerular VEGF protein expression using a score (0–4). VEGF expression tended to be higher on *day 1* of the disease and returns to basal levels thereafter

samples [1, 3, 14, 40]. The combination of LCM and real-time PCR is a powerful technique to investigate gene expression in specific structures of complex tissues, as shown in several recent studies [6, 12, 16, 21]. In normal rats, Inoue et al. [21] demonstrated the reproducibility of the analysis of glomerular VEGF mRNA expression using LCM and real-time PCR. However, the technique has yet not been evaluated to a greater extent in mouse models of GN. Thus, for the first time, in the murine HSV GN model, we found increased glomerular VEGF mRNA expression after mesangiolytic injury, which subsequently decreased when capillary healing proceeds, suggesting a concurring role of VEGF in the repair process of glomerular capillary damage. This observation is supported by studies in rats demonstrating that glomerular ECs participate in the capillary repair process of experimental GN [22, 26]. The fact that in the present model upregulation of glomerular VEGF mRNA seems to be much stronger than that of VEGF protein expression could have several reasons. It has to be acknowledged that detection of mRNA by either LCM with subsequent TaqMan PCR or in situ hybridization offers a much higher sensitivity than does immunohistochemistry. On the other hand, posttranslational modification of VEGF mRNA leading to differences between mRNA and protein expression can formally not be excluded.

It is noteworthy that VEGF can be released by both resident glomerular cells and infiltrating leukocytes in vivo during glomerular inflammation [20], and epithelial cell, ECs, and MCs [28, 32, 42] cells have been shown to produce VEGF in vitro, but this has never been shown in vivo in healthy glomeruli. Our in situ hybridization data clearly indicate VEGF mRNA expression primarily in podocytes of both intact and damaged glomeruli, whereas VEGF protein expression was confined to podocytes. The latter finding is supported by recent data from Kriz et al. arguing for a crucial role of podocytes in the repair of glomerular damage and particularly capillary neoformation [29].

In conclusion, despite much lesser glomerular damage than in the rat model of anti-Thy 1.1 GN, glomerular *VEGF* gene and protein expression is also temporarily increased during the healing phase of murine HSV GN. Thus, our data support for the first time the idea of VEGF being also important in the murine HSV GN model for angiogenic capillary remodeling and repair with significant mesangiolytic damage.

In addition, our study confirmed that LCM with subsequent real-time PCR is a useful technique to study modulations in gene expression levels under various disease conditions, i.e., in mild mesangiolytic damage in HSV GN, especially in a defined morphological environment, by combining advantages of morphological measurements with quantitative gene expression analysis.

Acknowledgement The work was supported by a DFG grant (SFB 423, project B8/Z2). The authors thank M. Klewer, M. Ramming, S. Söllner, Dr. S. Cho, and Dr. J. Misch for excellent technical assistance.

References

1. Alcorta DA, Prakash K, Waga I, Sasai H, Munger W, Jennette JC, Falk RJ (2000) Future molecular approaches to the diagnosis and treatment of glomerular disease. Semin Nephrol 20:20–31
2. Amann K, Nichols C, Tornig J, Schwarz U, Zeier M, Mall G, Ritz E (1996) Effect of ramipril, nifedipine, and moxonidine on glomerular morphology and podocyte structure in experimental renal failure. Nephrol Dial Transplant 11:1003–1011
3. Anders HJ, Vielhauer V, Kretzler M, Cohen CD, Segerer S, Luckow B, Weller L, Grone HJ, Schlondorff D (2001) Chemokine and chemokine receptor expression during initiation and resolution of immune complex glomerulonephritis. J Am Soc Nephrol 12:919–931
4. Barnes JL, Hevey KA, Hastings RR, Bocanegra RA (1994) Mesangial cell migration precedes proliferation in Habu snake venom-induced glomerular injury. Lab Invest 70:460–467
5. Basile DP, Donohoe D, Roethe K, Osborn JL (2001) Renal ischemic injury results in permanent damage to peritubular capillaries and influences long-term function. Am J Physiol Renal Physiol 281:F887–F899
6. Bohle RM, Hartmann E, Kinfe T, Ermert L, Seeger W, Fink L (2000) Cell type-specific mRNA quantitation in non-neoplastic tissues after laser-assisted cell picking. Pathobiology 68:191–195
7. Bradfield JW, Cattell V, Smith J (1977) The mesangial cell in glomerulonephritis. II. Mesangial proliferation caused by Habu snake venom in the rat. Lab Invest 36:487–492
8. Cattell V, Bradfield JW (1977) Focal mesangial proliferative glomerulonephritis in the rat caused by habu snake venom. A morphologic study. Am J Pathol 87:511–524
9. Cooper ME, Vranes D, Youssef S, Stacker SA, Cox AJ, Rizkalla B, Casley DJ, Bach LA, Kelly DJ, Gilbert RE (1999) Increased renal expression of vascular endothelial growth factor (VEGF) and its receptor VEGFR-2 in experimental diabetes. Diabetes 48:2229–2239
10. de Vries C, Escobedo JA, Ueno H, Houck K, Ferrara N, Williams LT (1992) The fms-like tyrosine kinase, a receptor for vascular endothelial growth factor. Science 255:989–991
11. De Vriese AS, Tilton RG, Elger M, Stephan CC, Kriz W, Lameire NH (2001) Antibodies against vascular endothelial growth factor improve early renal dysfunction in experimental diabetes. J Am Soc Nephrol 12:993–1000
12. Dimmler A, Haas CS, Cho S, Hattler M, Forster C, Peters H, Schocklmann HO, Amann K (2003) Laser capture microdissection and real-time PCR for analysis of glomerular endothelin-1 gene expression in mesangiolysis of rat anti-Thy 1.1 and murine Habu Snake Venom glomerulonephritis. Diagn Mol Pathol 12:108–117
13. el Nahas AM, Bassett AH, Cope GH, Le Carpentier JE (1991) Role of growth hormone in the development of experimental renal scarring. Kidney Int 40:29–34
14. Esposito C, Striker LJ, Patel A, Peten E, Liu ZH, Sakai H, Striker GE (1996) Molecular analysis of glomerular diseases in renal biopsies: initial results of a collaborative international study. The International Study Group for Molecular Study of Kidney Biopsies. Proc Assoc Am Physicians 108:209–217
15. Ferrara N, Houck K, Jakeman L, Leung DW (1992) Molecular and biological properties of the vascular endothelial growth factor family of proteins. Endocr Rev 13:18–32
16. Fink L, Seeger W, Ermert L, Hanze J, Stahl U, Grimminger F, Kummer W, Bohle RM (1998) Real-time quantitative RT-PCR after laser-assisted cell picking. Nat Med 4:1329–1333

17. Flyvbjerg A, Dagnaes-Hansen F, De Vriese AS, Schrijvers BF, Tilton RG, Rasch R (2002) Amelioration of long-term renal changes in obese type 2 diabetic mice by a neutralizing vascular endothelial growth factor antibody. Diabetes 51:3090–3094
18. Goumenos DS, Brown CB, Shortland J, el Nahas AM (1994) Myofibroblasts, predictors of progression of mesangial IgA nephropathy? Nephrol Dial Transplant 9:1418–1425
19. Hara A, Wada T, Furuichi K, Sakai N, Kawachi H, Shimizu F, Shibuya M, Matsushima K, Yokoyama H, Egashira K, Kaneko S (2006) Blockade of VEGF accelerates proteinuria, via decrease in nephrin expression in rat crescentic glomerulonephritis. Kidney Int 69:1986–1995
20. Iijima K, Yoshikawa N, Connolly DT, Nakamura H (1993) Human mesangial cells and peripheral blood mononuclear cells produce vascular permeability factor. Kidney Int 44:959–966
21. Inoue K, Sakurada Y, Murakami M, Shirota M, Shirota K (2003) Detection of gene expression of vascular endothelial growth factor and flk-1 in the renal glomeruli of the normal rat kidney using the laser microdissection system. Virchows Arch 442:159–162
22. Iruela-Arispe L, Gordon K, Hugo C, Duijvestijn AM, Claffey KP, Reilly M, Couser WG, Alpers CE, Johnson RJ (1995) Participation of glomerular endothelial cells in the capillary repair of glomerulonephritis. Am J Pathol 147:1715–1727
23. Janssen U, Eitner F, Kunter U, Ostendorf T, Wolf G, Chaponnier C, Gabbiani G, Kerjaschki D, Floege J (2003) Extracellular actin impairs glomerular capillary repair in experimental mesangioproliferative glomerulonephritis. Nephron Exp Nephrol 93:e158–e167
24. Kelly DJ, Hepper C, Wu LL, Cox AJ, Gilbert RE (2003) Vascular endothelial growth factor expression and glomerular endothelial cell loss in the remnant kidney model. Nephrol Dial Transplant 18:1286–1292
25. Kim YG, Suga SI, Kang DH, Jefferson JA, Mazzali M, Gordon KL, Matsui K, Breiteneder-Geleff S, Shankland SJ, Hughes J, Kerjaschki D, Schreiner GF, Johnson RJ (2000) Vascular endothelial growth factor accelerates renal recovery in experimental thrombotic microangiopathy. Kidney Int 58:2390–2399
26. Kitamura H, Sugisaki Y, Yamanaka N (1995) Endothelial regeneration during the repair process following Habu-snake venom induced glomerular injury. Virchows Arch 427:195–204
27. Kohda Y, Murakami H, Moe OW, Star RA (2000) Analysis of segmental renal gene expression by laser capture microdissection. Kidney Int 57:321–331
28. Kretzler M, Schroppel B, Merkle M, Huber S, Mundel P, Horster M, Schlondorff D (1998) Detection of multiple vascular endothelial growth factor splice isoforms in single glomerular podocytes. Kidney Int Suppl 67:S159–S161
29. Kriz W (2002) Podocyte is the major culprit accounting for the progression of chronic renal disease. Microsc Res Tech 57:189–195
30. Masuda Y, Shimizu A, Mori T, Ishiwata T, Kitamura H, Ohashi R, Ishizaki M, Asano G, Sugisaki Y, Yamanaka N (2001) Vascular endothelial growth factor enhances glomerular capillary repair and accelerates resolution of experimentally induced glomerulonephritis. Am J Pathol 159:599–608
31. Nakao N, Hiraiwa N, Yoshiki A, Ike F, Kusakabe M (1998) Tenascin-C promotes healing of Habu-snake venom-induced glomerulonephritis: studies in knockout congenic mice and in culture. Am J Pathol 152:1237–1245
32. Noguchi K, Yoshikawa N, Ito-Kariya S, Inoue Y, Hayashi Y, Ito H, Nakamura H, Iijima K (1998) Activated mesangial cells produce vascular permeability factor in early-stage mesangial proliferative glomerulonephritis. J Am Soc Nephrol 9:1815–1825
33. Ostendorf T, Kunter U, Eitner F, Loos A, Regele H, Kerjaschki D, Henninger DD, Janjic N, Floege J (1999) VEGF(165) mediates glomerular endothelial repair. J Clin Invest 104:913–923
34. Ostendorf T, Van Roeyen C, Westenfeld R, Gawlik A, Kitahara M, De Heer E, Kerjaschki D, Floege J, Ketteler M (2004) Inducible nitric oxide synthase-derived nitric oxide promotes glomerular angiogenesis via upregulation of vascular endothelial growth factor receptors. J Am Soc Nephrol 15:2307–2319
35. Peti-Peterdi J (2005) Confocal imaging and function of the juxtaglomerular apparatus. Curr Opin Nephrol Hypertens 14:53–57
36. Shimizu A, Masuda Y, Kitamura H, Ishizaki M, Sugisaki Y, Yamanaka N (1998) Recovery of damaged glomerular capillary network with endothelial cell apoptosis in experimental proliferative glomerulonephritis. Nephron 79:206–214
37. Simon M, Grone HJ, Johren O, Kullmer J, Plate KH, Risau W, Fuchs E (1995) Expression of vascular endothelial growth factor and its receptors in human renal ontogenesis and in adult kidney. Am J Physiol 268:F240–F250
38. Tanji N, Ross MD, Cara A, Markowitz GS, Klotman PE, D'Agati VD (2001) Effect of tissue processing on the ability to recover nucleic acid from specific renal tissue compartments by laser capture microdissection. Exp Nephrol 9:229–234
39. Terman BI, Dougher-Vermazen M, Carrion ME, Dimitrov D, Armellino DC, Gospodarowicz D, Bohlen P (1992) Identification of the KDR tyrosine kinase as a receptor for vascular endothelial cell growth factor. Biochem Biophys Res Commun 187:1579–1586
40. Trogan E, Choudhury RP, Dansky HM, Rong JX, Breslow JL, Fisher EA (2002) Laser capture microdissection analysis of gene expression in macrophages from atherosclerotic lesions of apolipoprotein E-deficient mice. Proc Natl Acad Sci USA 99:2234–2239
41. Tsuchida K, Makita Z, Yamagishi S, Atsumi T, Miyoshi H, Obara S, Ishida M, Ishikawa S, Yasumura K, Koike T (1999) Suppression of transforming growth factor beta and vascular endothelial growth factor in diabetic nephropathy in rats by a novel advanced glycation end product inhibitor, OPB-9195. Diabetologia 42:579–588
42. Uchida K, Uchida S, Nitta K, Yumura W, Marumo F, Nihei H (1994) Glomerular endothelial cells in culture express and secrete vascular endothelial growth factor. Am J Physiol 266:F81–F88
43. Wada Y, Morioka T, Oyanagi-Tanaka Y, Yao J, Suzuki Y, Gejyo F, Arakawa M, Oite T (2002) Impairment of vascular regeneration precedes progressive glomerulosclerosis in anti-Thy 1 glomerulonephritis. Kidney Int 61:432–443
44. Yancopoulos GD, Davis S, Gale NW, Rudge JS, Wiegand SJ, Holash J (2000) Vascular-specific growth factors and blood vessel formation. Nature 407:242–248

Virchows Arch (2007) 450:93–101
DOI 10.1007/s00428-006-0331-1

CASE REPORT

A renal cell carcinoma with components of both chromophobe and papillary carcinoma

Michael H. A. Roehrl · Martin K. Selig · G. Petur Nielsen · Paola Dal Cin · Esther Oliva

Received: 11 August 2006 / Revised: 13 October 2006 / Accepted: 16 October 2006 / Published online: 24 November 2006
© Springer-Verlag 2006

Abstract We report a case of a morphologically unusual renal cell carcinoma with features of both chromophobe and papillary carcinoma. Immunohistochemical analysis of high molecular weight cytokeratins (HMWCK), cytokeratin 7 (CK7), cytokeratin 19 (CK19), c-Kit, and α-methylacyl-CoA racemase (AMACR) demonstrated differential profiles for the two components of the tumor, consistent with the respective patterns commonly observed for pure chromophobe and papillary renal cell carcinomas. Specifically, the chromophobe tumor cells expressed CK7 and c-Kit weakly, while HMWCK, CK19, and AMACR were not detectable. In contrast, the papillary tumor cells expressed uniformly HMWCK, CK7, and c-Kit and focally CK19 and AMACR. Fluorescence in situ hybridization analysis of nuclei isolated from paraffin-embedded tumor tissue detected monosomy 1, disomy 7, and monosomy 17, a common and characteristic finding in chromophobe carcinomas, in a majority of, but not all tumor cells, whereas a population characterized by disomy 1, trisomy 7, and trisomy 17, a frequent finding in papillary carcinoma, was not identifiable. Electron microscopic analysis revealed numerous characteristic small cytoplasmic vesicles in the chromophobe areas, which were absent in the papillary component. This case illustrates the rare coexistence of two distinct and admixed histologic types of renal cell carcinoma.

Keywords Renal cell carcinoma · Chromophobe · Papillary · Case report · Immunohistochemistry · Electron microscopy · Fluorescene in-situ hybridization · Histogenesis

M. H. A. Roehrl (✉) · M. K. Selig · G. P. Nielsen · E. Oliva
Department of Pathology and Laboratory Medicine,
James Homer Wright Pathology Laboratories,
Massachusetts General Hospital,
Warren 2, 55 Fruit Street,
Boston, MA 02114, USA
e-mail: michael_roehrl@hms.harvard.edu

P. Dal Cin
Department of Pathology, Brigham and Women's Hospital,
75 Francis Street,
Boston, MA 02115, USA

M. H. A. Roehrl · M. K. Selig · G. P. Nielsen · P. Dal Cin · E. Oliva
Harvard Medical School,
Boston, MA 02115, USA

Introduction

Renal cell carcinomas (RCCs) are usually categorized based on their histologic, immunohistochemical, and ultrastructural features into clear cell, papillary, chromophobe, collecting duct, and unclassified carcinomas [44]. Typically, RCCs are composed of one histologic type that may show spatial variability in specific growth patterns, a variety of which have been observed for each of the major types listed above [37, 44]. In rare instances, two types of RCC are found within the same kidney, usually as synchronous, yet spatially distinct masses [38]. It is unusual to observe more than one morphological type coexistent within the same tumor. Herein, we describe a rare case of RCC that exhibits the features of both chromophobe and papillary carcinoma within the same tumor. To the best of our knowledge, no such cases have been reported in the literature to date.

Clinical history

A 65-year-old woman in good general health presented to her primary care physician with a left-sided abdominal

hernia at a previous laparoscopic port site that appeared to have gradually enlarged over several months. The patient's past surgical history included appendectomy, hysterectomy, and laparoscopic cholecystectomy several years earlier. There was no prior history of malignancy, and her medical history was otherwise unremarkable. The family history was negative for RCC. Her physical exam was within normal limits. An abdominal CT scan revealed a 5-cm mass in the upper pole of the left kidney. The lesion's absorption enhanced from 38 Hounsfield units (HU) to 68 HU after administration of intravenous contrast agent and washed out to a density of 53 HU in the delayed phase images. A subsequent metastatic workup was negative. The patient underwent a left radical nephrectomy with uneventful recovery. Four months after surgery, the patient is well without signs of tumor recurrence.

Materials and methods

Fresh tissue was fixed in buffered formalin and embedded in paraffin. Routine sections were stained with hematoxylin and eosin. Immunohistochemical detection of protein expression was performed on paraffin tissue sections using HRPO-DAB chemistry and alkaline hematoxylin counterstaining (for primary antibodies and concentrations, see Table 1). For electron microscopic analysis, fresh tissue was fixed in Karnovsky's EM fixative [2.5% (v/v) glutaraldehyde, 2.0% (v/v) paraformaldehyde, and 0.025% (v/v) calcium chloride in 0.1 M sodium cacodylate buffer, pH 7.4] and routinely processed for ultrastructural examination. Briefly, samples were post-fixed with osmium, dehydrated in a series of ethanol solutions, stained en bloc with uranyl acetate, and embedded in pure epoxy resin. After representative areas were chosen, thin sections were cut and stained with lead citrate and examined in a Philips 301 electron microscope. Aneuploidy of chromosomes 1, 7, and 17 was assessed by fluorescence in situ hybridization (FISH) to nuclei extracted from 50-μm sections of paraffin-embedded tissue using the centromeric chromosome DNA probes D1Z5, D7Z1, and D17Z1, respectively (Abbott Molecular/Vysis, Des Plaines, IL, USA). Probes D7Z1 and D17Z1 were assessed simultaneously by dual-color FISH, whereas D1Z5 was assessed individually. A total of 400 nuclei (from three representative areas) were evaluated for chromosomes 1 or 7, and 17, respectively.

Table 1 Primary antibodies and concentrations used for immunohistochemistry

Antigen	Manufacturer	Clone	Concentration ($\mu g \cdot ml^{-1}$)
HMWCK	Ventana	34βE12	1.4
CK7	Ventana	OV-TL 12/30	1.0
CK19	Dako	BA17	8.0
c-Kit	Cell Marque	Polyclonal	1.0
AMACR	Zeta	13H4	0.7
EMA	Ventana	E29	1.0
RCC marker	Cell Marque	PN-15	1.0
CD10	Ventana	56C6	1.0
CK5/6	Dako	D5/16 B4	1.2
Vimentin	Ventana	V9	2.0
p53	Ventana	Bp-53-11	2.5

Results

The nephrectomy specimen revealed a 5.4×5.0×3.2-cm, tan-yellow, well-circumscribed mass in the superior pole of the left kidney. The cut surface was predominantly solid and nodular with small cystic areas (Fig. 1). The tumor did not invade the renal pelvis, renal vein, or perirenal fat. The remainder of the kidney was unremarkable.

Microscopic examination revealed that the tumor was composed of an admixture of both chromophobe and papillary RCC (Fig. 2a–f). At low magnification, the two admixed tumor types could be readily distinguished from each other (Fig. 2c,d). Based on surface area estimates of representative tissue sections, approximately 70% of the tumor was composed of chromophobe and 30% of papillary carcinoma, respectively. Areas of chromophobe carcinoma consisted of sheets and wide trabecula of cells intersected by delicate fibrovascular septa (Fig. 2a). The tumor cells were large and polygonal with prominent "plantlike" cell membranes, frequent perinuclear halos, and abundant pale to translucent flocculent pink cytoplasm (Fig. 2e). The cytoplasm stained with Hale's colloidal iron. Cell nuclei were mostly centrally located, hyperchromatic, and wrinkled with an irregular

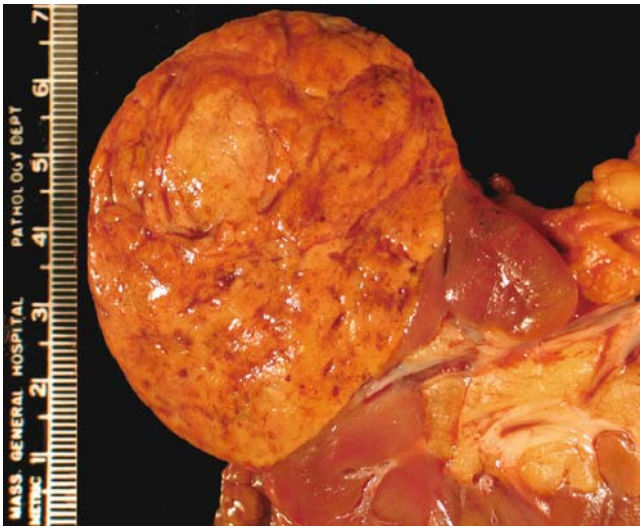

Fig. 1 A well-circumscribed, tan-yellow mass is seen in the superior pole of the left kidney. Note that the cut surface is predominantly solid and nodular with small cystic areas

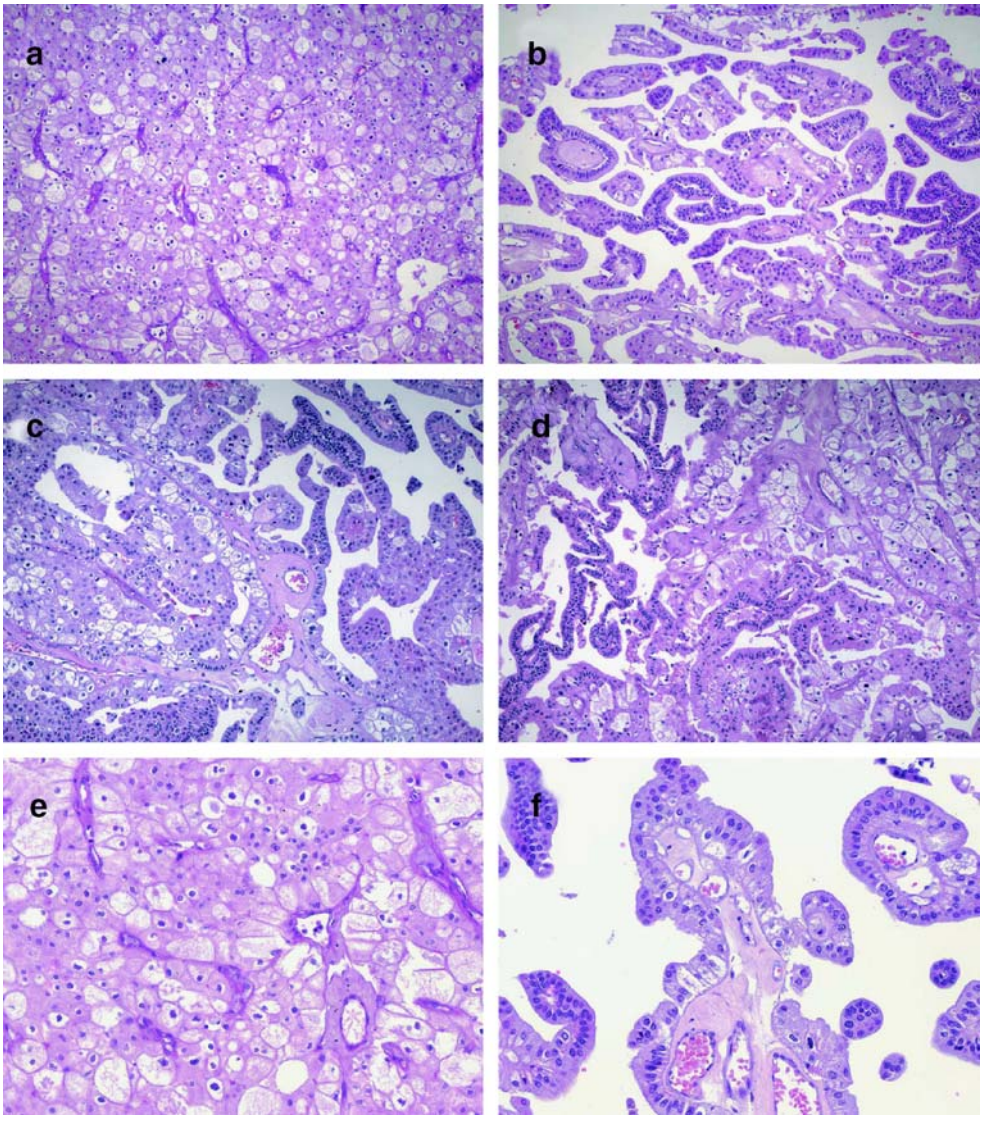

Fig. 2 Histologic appearance of the chromophobe [**a**, **c** (*left*), **d** (*right*), **e**] and papillary [**b**, **c** (*right*), **d** (*left*), **f**] RCC components. Note the close admixture of the two tumor types (**c**, **d**). Areas of chromophobe carcinoma show large, polygonal cells with prominent plant-like cell membranes and abundant pale to translucent flocculent pink cytoplasm intersected by delicate fibrovascular septa. Areas of papillary carcinoma show partially sclerotic fibrovascular cores lined by a single layer of tall or columnar epithelial cells with focal nuclear pseudostratification

nuclear membrane, showing a mild to moderate degree of cytologic atypia, small nucleoli, and low mitotic activity. In contrast, areas of papillary carcinoma were composed of papillae lined by a single layer of epithelial cells with focal nuclear pseudostratification (Fig. 2b,f). The fibrovascular cores were focally sclerotic and edematous with rare psammoma bodies and scattered foamy histiocytes. The tumor cells were predominantly tall or columnar with abundant acidophilic cytoplasm, morphologically most consistent with so-called type 2 papillary carcinoma. The predominantly round nuclei showed mild to moderate cytologic atypia with small nucleoli, and mitotic activity was low. Overall, the tumor was classified as Fuhrman grade 2. All resection margins were microscopically free of tumor (R0), lymphovascular invasion was not detected, and the tumor was staged as pT1b cN0 cM0.

Immunohistochemical analysis of the tumor revealed distinct patterns (Table 2; Fig. 3). The chromophobe areas displayed relatively weak, exclusively membranous and submembranous expression of cytokeratin 7 (CK7) and c-Kit. In contrast, the papillary areas strongly expressed CK7 and c-Kit in both membranous and cytoplasmic compartments. The chromophobe component did not express high molecular weight cytokeratins (HMWCK), cytokeratin 19 (CK19), or α-methylacyl-CoA racemase (AMACR). On the other hand, the papillary areas showed uniform expression of HMWCK and focal expression of CK19 and AMACR. Membranous and cytoplasmic localization of epithelial membrane antigen was demonstrated in both components. Neither component displayed expression of RCC marker, CD10, cytokeratins 5/6, vimentin, or accumulation of p53 protein.

Electron microscopic analysis revealed abundant and ubiquitous cytoplasmic vesicles of approximately 150–300 nm diameter within the chromophobe carcinoma cells (Fig. 4a,b). These vesicles were absent in the papillary carcinoma cells. In contrast, the cytoplasm of the papillary carcinoma cells contained numerous mitochondria with

Table 2 Summary of protein expression patterns of the chromophobe and papillary components

Protein	Chromophobe	Papillary
HMWCK	−	+
CK7	±[a]	+[b]
CK19	−	+[c]
c-Kit	±[a]	+[b]
AMACR	−	+[c]
EMA	+	+
RCC marker	−	−
CD10	−	−
CK5/6	−	−
Vimentin	−	−
p53	−	−

[a] Weak membranous expression
[b] Strong membranous and cytoplasmic expression
[c] Focal expression

lamellar cristae, ribosomes, and rare glycogen and lipid vesicles (Fig. 4c).

Evaluation of numerical chromosomal abnormalities of chromosomes 1, 7, and 17 was performed by three independent FISH analyses of interphase nuclei isolated from three different areas of paraffin-embedded tumor tissue. Chromosomes 7 and 17 were probed simultaneously by two-color FISH. Eight to 37% (mean, 24%) of nuclei showed two hybridization signals from the chromosome 7 probe and one signal from the chromosome 17 probe, respectively. Four chromosome 7 signals and two chromosome 17 signals were observed in 34–55% (mean, 50%) of nuclei. Eight to 38% (mean, 26%) of nuclei displayed two chromosome 7 and 17 signals each. In a separate set of hybridization experiments, a single hybridization signal from chromosome 1 was detected in 10–16% (mean, 13%) of cells, while two hybridization signals were observed in 78–88% (mean, 82%) of nuclei. These findings indicate the presence of a population of hypodiploid tumor cells with monosomy 1, disomy 7, and monosomy 17, a very characteristic observation in chromophobe RCC. The detection of chromosome 7 tetrasomic nuclei may be the result of genomic endoreduplication of this hypodiploid population. No single nuclei with trisomy and/or hexasomy 7/17, the most common chromosomal abnormalities in papillary RCC, were observed. On average, 26% of nuclei had a normal diploid chromosome 7 and 17 karyotype in this FISH assay.

Discussion

The pathologic understanding of adult malignant epithelial renal neoplasms has undergone considerable changes and refinement over the last two decades [6, 18, 34]. Not long ago, only two major histologic types, i.e., "clear cell carcinoma" and "granular cell carcinoma," were recognized [9]. Subsequent morphological, immunohistochemical, ultrastructural, and molecular biological investigations have lead to the discovery of novel distinct disease entities and have resulted in our current understanding and classification of RCC [44]. In particular, papillary RCC was identified early on as a morphologic group possibly associated with a more favorable clinical outcome [29]. Human chromophobe RCC was described in 1985 as an analogy to an earlier *N*-nitrosomorpholine rat model of RCC [45]. Finally, a first series of collecting duct carcinomas was reported in 1986 [17], essentially setting the stage for the current UICC (International Union Against Cancer) classification of RCC [24, 44].

We describe here a case of an unusual RCC in a 65-year-old woman that had the combined histologic features of chromophobe and papillary RCC within the same tumor. We are unaware of a similar, previously reported case. A review of the literature revealed that the cases that bear the closest resemblance to our case are two reports of synchronous chromophobe and papillary RCCs [38]. Both patients in this series had synchronous, spatially distinct, ipsilateral chromophobe (3 and 5.5 cm, respectively) and papillary (3 and 4 cm, respectively) RCCs with radiologic evidence of lung metastases. Unfortunately, the histology of the metastases remains unknown. The original report suggested that a chromophobe carcinoma with synchronous papillary carcinoma may be more aggressive, despite the relatively small sizes of the individual tumors [38]. However, there may be a need to consider that metastatic probability is, to first order, a function of total tumor burden and that simultaneously coexisting carcinomas would very likely increase the overall baseline risk of metastatic disease over each individual tumor alone. Of course, potential differences in metastatic propensity as a function of a tumor's specific histologic subtype also need to be accounted for [14]. Lastly, these two previous cases were significantly different from our present case in that the tumors were spatially separate ipsilateral masses, each composed of exclusively one histologic type of RCC.

Sparse case reports exist of composite collecting duct carcinomas with elements of either clear cell [8, 15], chromophobe [22], or papillary RCC [30]. Furthermore, a case of renal oncocytoma with evolving papillary RCC has been reported [3]. Neoplasms of mixed morphologies can, at times, also result from a collision of transitional cell carcinoma of the renal pelvis and RCC [20] or from metastasis of an extrarenal to a primary renal neoplasm, such as an oncocytoma [4]. Furthermore, an unusual case of combined nephroblastoma, metanephric adenofibroma, and papillary RCC (the latter metastatic to a regional lymph node) has been described [11]. However, none of these cases bear close resemblance with our present case.

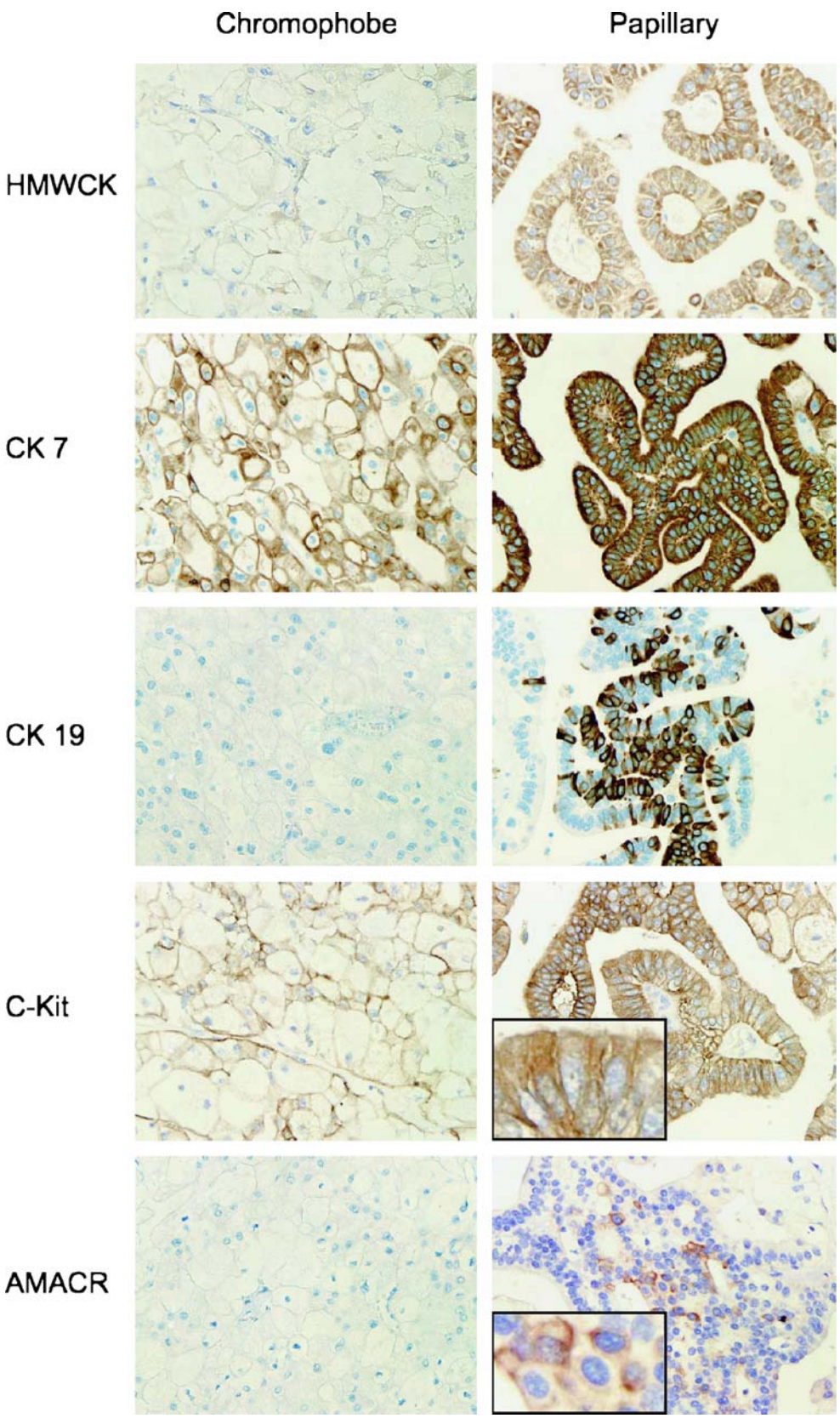

Fig. 3 Comparative immunohistochemical analysis of the chromophobe and papillary components. The chromophobe tumor cells express CK7 and c-Kit weakly, while HMWCK, CK19, and AMACR are negative. In contrast, the papillary tumor cells express uniformly HMWCK, CK7, and c-Kit and focally CK19 and AMACR

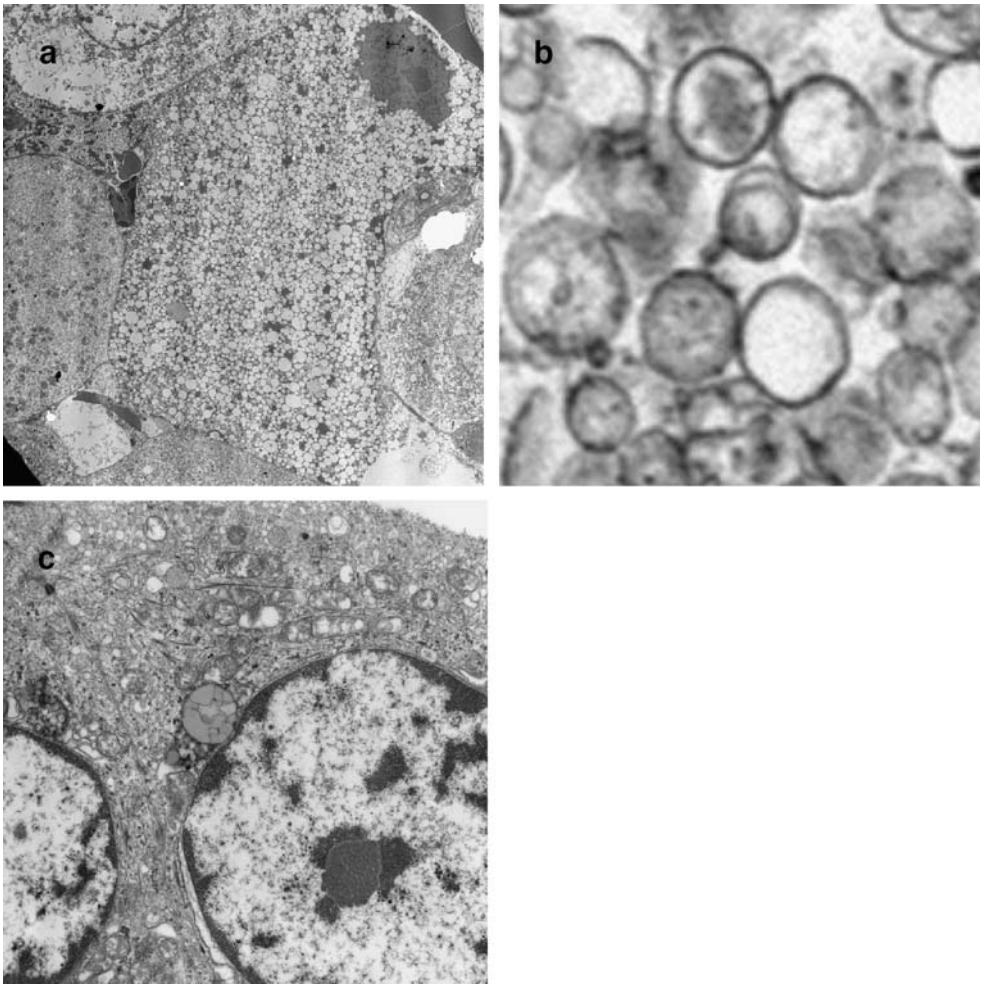

Fig. 4 By electron microscopic analysis (**a** 2,500×, **b** 72,000×, **c** 11,000×), abundant small cytoplasmic vesicles are present in the chromophobe tumor cells (**a**, **b**), but absent in the papillary tumor cells, which contain numerous mitochondria and rare glycogen and lipid vesicles (**c**)

A histologic appearance mimicking both clear cell and papillary RCC morphology may also be observed in association with chromosomal translocations involving Xp11.2 causing *TFE3* gene fusions [7, 11, 31, 32]. These carcinomas predominantly affect children and young adults and tend to show a nested or tubulopapillary morphology with cells characterized by voluminous clear to acidophilic cytoplasm and distinct cell membranes separated by thin fibrovascular septa and prominent psammoma bodies. However, the patient's age and the different histologic appearance of the carcinoma make this diagnosis an unlikely possibility in our case.

Renal tumors of different histologic types and hybrid morphologies have also been described in patients with Birt–Hogg–Dubé (BHD) syndrome [35]. BHD syndrome is an autosomal dominant genodermatosis characterized by cutaneous fibrofolliculomas, pulmonary cysts, and increased risk for renal neoplasia (often multifocal and/or bilateral). Interestingly, renal neoplasms seen in patients with BHD syndrome are most frequently hybrid tumors comprised of admixed elements of both oncocytoma and chromophobe RCC (hybrid oncocytic tumors), followed by pure chromophobe and clear cell RCCs, while pure oncocytomas and, particularly, papillary RCCs are rare [35]. Occasionally, sporadic, non-syndromic hybrid oncocytic tumors have been observed [28]. Based on a negative family history, the absence of cutaneous stigmata, and the fact that no cases of mixed chromophobe/papillary RCC have yet been observed in BHD syndrome, we believe that a syndromic hybrid RCC is a very unlikely scenario in our patient.

Immunohistochemical characterization of protein expression patterns can aid in the differential diagnosis of the various RCC subtypes [27, 33, 37, 42, 46]. Specifically, differences in CK7, c-Kit, and AMACR expression have been found useful for distinguishing chromophobe from papillary carcinomas [27, 42]. Indeed, the papillary component of our case was strongly positive for CK7 and c-Kit (both in membranous and cytoplasmic locations) and focally positive for AMACR (Table 2). In contrast, the chromophobe component was only weakly positive for CK7 and c-Kit (limited to membranous expression) and negative for AMACR. The observed c-Kit expression pattern is consistent with the results of a previous study [27]. Furthermore, HMWCK and CK19 expression were

limited to the papillary component of the tumor. Overall, the observed differences in protein expression are consistent with the specific patterns reported for isolated chromophobe and papillary RCCs, respectively [27, 42].

Electron microscopy has also been found to be a useful tool to distinguish between the different subtypes of RCC [25, 26]. Chromophobe carcinoma cells are characterized by abundant small cytoplasmic vesicles, as seen in our case. In contrast, these vesicles were absent in papillary carcinoma cells. Taken all together, our data strongly support the individual component identities as bona fide chromophobe and papillary RCCs within this single tumor.

Cytogenetic studies have demonstrated that chromophobe RCC is commonly associated with extensive chromosomal losses, most often −1, −2, −6, −10, −13, −17, −21, and −X [12, 13, 39, 43]. In contrast, trisomy or tetrasomy 7 and trisomy 17 are frequent karyotypic alterations in papillary RCC [19, 21, 23, 39]. Yet similar or overlapping chromosomal abnormalities, such as −Y, or normal karyotypes have also been observed in both types [12, 13, 19, 21, 23, 39, 43]. In our case, selective interphase chromosome 1, 7, and 17 enumeration by FISH revealed a major hypodiploid cell population with monosomy 1, disomy 7, and monosomy 17. These findings are characteristic for the presence of a bona fide chromophobe RCC component in our tumor. Approximately 50% of nuclei possessed four chromosome 7 and two chromosome 17 signals, respectively. This finding most likely indicates endoreduplication of chromosome 17 monosomic cells (chromophobe RCC component) and/or may alternatively represent a cell population that is tetrasomic for chromosome 7. The latter has been observed in papillary RCCs, even in the absence of the common trisomy 17 [19, 21, 40]. It is noteworthy that a significant number of analyzed nuclei (26%, as judged by the joint chromosome 7/17 enumeration) did not have FISH-detectable chromosomal abnormalities. While these may include nuclei from intermixed non-neoplastic stromal or inflammatory cells, the finding would also allow for the possibility of a papillary RCC component without numerical alterations detectable by FISH. Taken together, the cytogenetic evaluation of chromosomes 1, 7, and 17 is consistent with the presence of a major component of chromophobe RCC with the classic monosomies 1 and 17. While the most common cytogenetic abnormality in papillary RCC (trisomy 7 and/or 17) was not detected in our case, our FISH analysis does not exclude the presence of a papillary RCC component that is either cytogenetically undetectable or possesses genomic alterations other than the specific aneuploidies screened for.

Based on immunohistochemical, molecular, and cytogenetic observations, it has been proposed that chromophobe RCCs may arise from distal nephron epithelium (intercalated cells of the renal cortex), while papillary RCCs may be derived from proximal nephron epithelium (cells of the distal convoluted tubule) [5, 39]. If this were strictly true, one would have to invoke the possibility that the neoplasm observed in our patient is a collision tumor of two histogenetically independent neoplasms. Given the intimate admixture of chromophobe and papillary components in the neoplasm and the absence of other ipsilateral and contralateral lesions, we consider a true collision tumor a less likely scenario.

Recently, the concept of cancer stem cells has become a focus of investigation in cancer biology and pathophysiology. Cancer stem cells refer generally to a broad group of malignant cells that share the common properties of self-renewal and ability to initiate tumor growth [10, 36]. In solid tumors, cancer stem cells have thus far been identified in breast and central nervous system malignancies [1, 16, 41]. Interestingly, it has been found that within a malignant neoplasm, only a small subpopulation of malignant cells may truly possess stem cell properties [10, 36]. Consequently, cancer stem cells may represent a particularly attractive therapeutic target and are the object of intense current investigative efforts [2]. Along these lines, it is conceivable that our particular RCC may have arisen from a pluripotent cancer stem cell [10, 36] that was capable of recapitulating both proximal and distal nephron histogenesis, either by acquiring dichotomous additional genetic alterations along the way of the two different morphogenic pathways (chromophobe vs papillary) or by undergoing microenvironment-specific differentiation within the tumor. In the former case, one would hypothesize that chromophobe and papillary tumor cells had both common (acquired before dichotomous chromophobe/papillary lineage commitment) and distinct genomic alterations (acquired after lineage commitment). In the latter case, it would be possible that both cell types possessed the same genomic makeup but differed in differentiation due to epigenetic or microenvironmental influences.

In conclusion, we have described an unusual RCC composed of an intimate admixture of chromophobe and papillary carcinoma, with the two components exhibiting distinct morphological, immunohistochemical, and ultrastructural profiles. Unusual cases like the one presented herein may serve as tools to further investigate the origin, relatedness, and classification of renal cell carcinomas.

References

1. Al-Hajj M, Wicha MS, Benito-Hernandez A, Morrison SJ, Clarke MF (2003) Prospective identification of tumorigenic breast cancer cells. Proc Natl Acad Sci USA 100:3983–3988
2. Al-Hajj M, Becker MW, Wicha M, Weissman I, Clarke MF (2004) Therapeutic implications of cancer stem cells. Curr Opin Genet Dev 14:43–47

3. Al-Saleem T, Balsara BR, Liu Z, Feder M, Testa JR, Wu H, Greenberg RE (2005) Renal oncocytoma with loss of chromosomes Y and 1 evolving to papillary carcinoma in connection with gain of chromosome 7. Coincidence or progression? Cancer Genet Cytogenet 163:81–85
4. Altinok G, Guler G, Sahin A (1999) Tumor metastasis to an oncocytoma. Scand J Urol Nephrol 33:416–417
5. Amin MB, Varma MD, Tickoo SK, Ro JY (1997) Collecting duct carcinoma of the kidney. Adv Anat Pathol 4:85–94
6. Amin MB, Amin MB, Tamboli P, Javidan J, Stricker H, de-Peralta Venturina M, Deshpande A, Menon M (2002) Prognostic impact of histologic subtyping of adult renal epithelial neoplasms: an experience of 405 cases. Am J Surg Pathol 26:281–291
7. Argani P, Ladanyi M (2005) Translocation carcinomas of the kidney. Clin Lab Med 25:363–378
8. Auguet T, Molina JC, Lorenzo A, Vila J, Sirvent JJ, Richart C (2000) Synchronus renal cell carcinoma and Bellini duct carcinoma: a case report on a rare coincidence. World J Urol 18:449–451
9. Bennington JL, Beckwith JB (1975) Tumors of the kidney, renal pelvis and ureter. Armed Forces Institute of Pathology, Washington, DC
10. Bjerkvig R, Tysnes BB, Aboody KS, Najbauer J, Terzis AJ (2005) Opinion: the origin of the cancer stem cell: current controversies and new insights. Nat Rev Cancer 5:899–904
11. Bruder E, Passera O, Harms D, Leuschner I, Ladanyi M, Argani P, Eble JN, Struckmann K, Schraml P, Moch H (2004) Morphologic and molecular characterization of renal cell carcinoma in children and young adults. Am J Surg Pathol 28:1117–1132
12. Bugert P, Kovacs G (1996) Molecular differential diagnosis of renal cell carcinomas by microsatellite analysis. Am J Pathol 149:2081–2088
13. Bugert P, Gaul C, Weber K, Herbers J, Akhtar M, Ljungberg B, Kovacs G (1997) Specific genetic changes of diagnostic importance in chromophobe renal cell carcinomas. Lab Invest 76:203–208
14. Cheville JC, Lohse CM, Zincke H, Weaver AL, Blute ML (2003) Comparisons of outcome and prognostic features among histologic subtypes of renal cell carcinoma. Am J Surg Pathol 27:612–624
15. Cho NH, Kim S, Ha MJ, Kim HJ (2004) Simultaneous heterogenotypic renal cell carcinoma: immunohistochemical and karyoptic analysis by comparative genomic hybridization. Urol Int 72:344–348
16. Dontu G, Al-Hajj M, Abdallah WM, Clarke MF, Wicha MS (2003) Stem cells in normal breast development and breast cancer. Cell Prolif 36(Suppl 1):59–72
17. Fleming S, Lewi HJ (1986) Collecting duct carcinoma of the kidney. Histopathology 10:1131–1141
18. Gudbjartsson T, Hardarson S, Petursdottir V, Thoroddsen A, Magnusson J, Einarsson GV (2005) Histological subtyping and nuclear grading of renal cell carcinoma and their implications for survival: a retrospective nation-wide study of 629 patients. Eur Urol 48:593–600
19. Gunawan B, von Heydebreck A, Fritsch T, Huber W, Ringert RH, Jakse G, Fuzesi L (2003) Cytogenetic and morphologic typing of 58 papillary renal cell carcinomas: evidence for a cytogenetic evolution of type 2 from type 1 tumors. Cancer Res 63:6200–6205
20. Hart AP, Brown R, Lechago J, Truong LD (1994) Collision of transitional cell carcinoma and renal cell carcinoma. An immunohistochemical study and review of the literature. Cancer 73:154–159
21. Henke RP, Erbersdobler A (2002) Numerical chromosomal aberrations in papillary renal cortical tumors: relationship with histopathologic features. Virchows Arch 440:604–609
22. Kawano N, Inayama Y, Nakaigawa N, Yao M, Ogawa T, Aoki I, Kitamura H, Nakatani Y, Nagashima Y (2005) Composite distal nephron-derived renal cell carcinoma with chromophobe and collecting duct carcinomatous elements. Pathol Int 55:360–365
23. Kovacs G, Fuzesi L, Emanual A, Kung HF (1991) Cytogenetics of papillary renal cell tumors. Genes Chromosomes Cancer 3:249–255
24. Kovacs G, Akhtar M, Beckwith BJ, Bugert P, Cooper CS, Delahunt B, Eble JN, Fleming S, Ljungberg B, Medeiros LJ, Moch H, Reuter VE, Ritz E, Roos G, Schmidt D, Srigley JR, Storkel S, van den Berg E, Zbar B (1997) The Heidelberg classification of renal cell tumours. J Pathol 183:131–133
25. Krishnan B, Truong LD (2002) Renal epithelial neoplasms: the diagnostic implications of electron microscopic study in 55 cases. Hum Pathol 33:68–79
26. Latham B, Dickersin GR, Oliva E (1999) Subtypes of chromophobe cell renal carcinoma: an ultrastructural and histochemical study of 13 cases. Am J Surg Pathol 23:530–535
27. Lin ZH, Han EM, Lee ES, Kim CW, Kim HK, Kim I, Kim YS (2004) A distinct expression pattern and point mutation of c-kit in papillary renal cell carcinomas. Mod Pathol 17:611–616
28. Mai KT, Dhamanaskar P, Belanger E, Stinson WA (2005) Hybrid chromophobe renal cell neoplasm. Pathol Res Pract 201:385–389
29. Mancilla-Jimenez R, Stanley RJ, Blath RA (1976) Papillary renal cell carcinoma: a clinical, radiologic, and pathologic study of 34 cases. Cancer 38:2469–2480
30. Matei DV, Rocco B, Varela R, Verweij F, Scardino E, Renne G, De Cobelli O (2005) Synchronous collecting duct carcinoma and papillary renal cell carcinoma: a case report and review of the literature. Anticancer Res 25:579–586
31. Meloni AM, Sandberg AA, Pontes JE, Dobbs RM, Jr. (1992) Translocation (X;1)(p11.2;q21). A subtype of renal adenocarcinomas. Cancer Genet Cytogenet 63:100–101
32. Meloni AM, Dobbs RM, Pontes JE, Sandberg AA (1993) Translocation (X;1) in papillary renal cell carcinoma. A new cytogenetic subtype. Cancer Genet Cytogenet 65:1–6
33. Paner GP, Srigley JR, Radhakrishnan A, Cohen C, Skinnider BF, Tickoo SK, Young AN, Amin MB (2006) Immunohistochemical analysis of mucinous tubular and spindle cell carcinoma and papillary renal cell carcinoma of the kidney: significant immunophenotypic overlap warrants diagnostic caution. Am J Surg Pathol 30:13–19
34. Patard JJ, Leray E, Rioux-Leclercq N, Cindolo L, Ficarra V, Zisman A, De La Taille A, Tostain J, Artibani W, Abbou CC, Lobel B, Guille F, Chopin DK, Mulders PF, Wood CG, Swanson DA, Figlin RA, Belldegrun AS, Pantuck AJ (2005) Prognostic value of histologic subtypes in renal cell carcinoma: a multicenter experience. J Clin Oncol 23:2763–2771
35. Pavlovich CP, Walther MM, Eyler RA, Hewitt SM, Zbar B, Linehan WM, Merino MJ (2002) Renal tumors in the Birt–Hogg–Dubé syndrome. Am J Surg Pathol 26:1542–1552
36. Polyak K, Hahn WC (2006) Roots and stems: stem cells in cancer. Nat Med 12:296–300
37. Renshaw AA (2002) Subclassification of renal cell neoplasms: an update for the practising pathologist. Histopathology 41:283–300
38. Renshaw AA, Henske EP, Loughlin KR, Shapiro C, Weinberg DS (1996) Aggressive variants of chromophobe renal cell carcinoma. Cancer 78:1756–1761
39. Reuter VE, Tickoo SK (2004) Adult renal tumors. In: Mills SE, Carter D, Greenson JK, Oberman HA, Reuter VE, Stoler MH (eds) Sternberg's diagnostic surgical pathology. Lippincott Williams & Wilkins, Philadelphia, PA, pp 1955–1999
40. Rigola MA, Casadevall C, Bernues M, Caballin MR, Fuster C, Gelabert A, Egozcue J, Miro R (2002) Analysis of kidney tumors by comparative genomic hybridization and conventional cytogenetics. Cancer Genet Cytogenet 137:49–53
41. Singh SK, Hawkins C, Clarke ID, Squire JA, Bayani J, Hide T, Henkelman RM, Cusimano MD, Dirks PB (2004) Identification of human brain tumour initiating cells. Nature 432:396–401

42. Skinnider BF, Amin MB (2005) An immunohistochemical approach to the differential diagnosis of renal tumors. Semin Diagn Pathol 22:51–68
43. Speicher MR, Schoell B, du Manoir S, Schrock E, Ried T, Cremer T, Storkel S, Kovacs A, Kovacs G (1994) Specific loss of chromosomes 1, 2, 6, 10, 13, 17, and 21 in chromophobe renal cell carcinomas revealed by comparative genomic hybridization. Am J Pathol 145:356–364
44. Störkel S, Eble JN, Adlakha K, Amin M, Blute ML, Bostwick DG, Darson M, Delahunt B, Iczkowski K (1997) Classification of renal cell carcinoma: workgroup No. 1. Union Internationale Contre le Cancer (UICC) and the American Joint Committee on Cancer (AJCC). Cancer 80:987–989
45. Thoenes W, Störkel S, Rumpelt HJ (1985) Human chromophobe cell renal carcinoma. Virchows Arch B Cell Pathol Incl Mol Pathol 48:207–217
46. Tretiakova MS, Sahoo S, Takahashi M, Turkyilmaz M, Vogelzang NJ, Lin F, Krausz T, Teh BT, Yang XJ (2004) Expression of alpha-methylacyl-CoA racemase in papillary renal cell carcinoma. Am J Surg Pathol 28:69–76

Virchows Arch (2007) 450:103–108
DOI 10.1007/s00428-006-0323-1

CASE REPORT

Crystal-storing histiocytosis associated with MALT lymphoma of the ocular adnexa: a case report with review of literature

Takashi Kusakabe · Kazuo Watanabe · Takafumi Mori · Tomohiro Iida · Toshimitsu Suzuki

Received: 28 August 2006 / Accepted: 29 September 2006 / Published online: 17 November 2006
© Springer-Verlag 2006

Abstract We report a case of crystal-storing histiocytosis (CSH) associated with mucosa-associated lymphoid tissue (MALT) lymphoma of the ocular adnexa. The patient was an 81-year-old woman who presented with a 5-month history of a slowly enlarging tumor on her left lower eyelid. The tumor was 2 cm in the largest diameter, involving both inferior oblique and inferior rectus muscles. Histological examination revealed that the tumor was composed predominantly of sheets of spindle-shaped cells resembling striated muscle cells, and scattered aggregates of atypical lymphoid cells at the periphery of the tumor, showing prominent plasmacytoid differentiation. Immunohistochemical and ultrastructural analyses demonstrated that the spindle-shaped cells were CD68-positive histiocytes containing abundant rod-like and/or rectangular crystals in their cytoplasm, consistent with the diagnosis of CSH. The scattered aggregates of atypical lymphoid cells were diagnosed as MALT lymphoma based upon their immunophenotype, featuring diffusely positive staining for CD20, but negative for CD3, CD5, and CD10, and monotypic expression of IgM-kappa in cells with plasmacytoid differentiation. Although CSH is a well-recognized manifestation in lymphoproliferative disorders in the literature, CSH complicated by MALT lymphoma has only very rarely been reported. Given the rarity of this, difficulties in diagnosis may arise especially in cases where histiocytic proliferation overwhelms the underlying lymphoproliferative diseases.

Keywords Crystal-storing histiocytosis · MALT lymphoma · Ocular adnexa

T. Kusakabe (✉) · T. Suzuki
Department of Pathology, Fukushima Medical University, School of Medicine,
1 Hikariga-oka,
Fukushima 960-1295, Japan
e-mail: kabe@fmu.ac.jp

K. Watanabe
Pathology Division, Fukushima Medical University, Fukushima, Japan

T. Mori · T. Iida
Department of Ophthalmology, Fukushima Medical University, School of Medicine,
Fukushima, Japan

Introduction

Crystal-storing histiocytosis (CSH) is a rare manifestation of lymphoproliferative diseases predominantly in cases of B cell neoplasms, which is characterized by intrahistiocytic accumulation of crystallized immunoglobulins (Igs). The most reported cases of CSH are associated with multiple myeloma (MM) or lymphoplasmacytic lymphoma (LPL) typically accompanying paraproteinemia and systemic crystal deposition, although localized CSH with normal serum Ig level in association with mucosa-associated lymphoid tissue (MALT) lymphoma (also called extranodal marginal zone lymphoma) has only rarely been reported. In this study, we describe a case of MALT lymphoma of the ocular adnexa complicated with localized CSH, and review the reported cases of MALT lymphoma-associated CSH in the literature.

Clinical history

The patient was an 81-year-old woman who presented with a 5-month history of a slowly enlarging tumor on her left

lower eyelid, with the largest diameter of 20 mm at the time of first medical examination. She had no significant medical history, including autoimmune diseases such as Sjögren's syndrome. The tumor was elastic, firm, well-demarcated, and movable. Magnetic resonance images, however, revealed an involvement in the inferior oblique and inferior rectus muscles, suggesting malignant potential for the tumor. Ocular involvement was absent, and there was no evidence for paraproteinemia and lymphadenopathy during the clinical course. She underwent excision of tumor without receiving preoperative chemotherapy and radiotherapy. The excised specimen was submitted for histopathological evaluation, and the diagnosis of MALT lymphoma was rendered. Because gallium scan showed a solitary focus of abnormal uptake localized to the left orbital region, the tumor was staged as stage IE according to the Ann Arbor classification for malignant lymphoma. She received postoperative regional radiation therapy and remained free of tumor recurrence for 1 year after the surgery.

Materials and methods

Immunohistochemistry and electron microscopy

The specimen was fixed in 20% formalin and processed routinely. The tissue block was sectioned at a thickness of 4 μm and was placed on silanated slides. Immunohistochemical staining was performed by the labeled streptavidin–biotin complex method, using a commercially available kit (Nichirei, Tokyo, Japan). Primary antibodies used in this study and their final dilutions are listed in Table 1. For electron microscopy, the formalin-fixed tumor tissues were retrieved and refixed in 2% glutaraldehyde and osmium tetroxide, processed into epoxy resin by conventional methods, and examined with a JEM-1200EX transmission electron microscope (Joel, Tokyo, Japan).

Table 1 Antibodies used for immunohistochemistry in paraffin-embedded tissue sections

Antibody specificity	Supplier	Antigen retrieval	Dilution
CD3	Dako[a]	Microwave	1:100
CD5	Novocastra[a]	Microwave	1:100
CD10	Novocastra	Microwave	1:80
CD20	Dako	Microwave	1:50
CD68 (KP-1)	Dako	Protease	1:100
kappa light chain	Dako	Microwave	1:10,000
lambda light chain	Dako	Microwave	1:10,000
IgM	Dako	Microwave	1:3,000
Desmin	Dako	Microwave	1:50
α-SMA	Dako	None	1:100
S-100 protein	Dako	None	1:1,000

[a] Dako, Carpinteria, CA, USA
[a] Novocastra, Burlingame, CA, USA

Results

Macroscopically, the tumor was a tan, poorly demarcated mass measuring 20 mm at its largest diameter, and it involved the inferior oblique muscle. Histopathological examination revealed that the tumor was composed of sheets of large spindle to polygonal cells with abundant eosinophilic cytoplasm containing crystalloid materials, which imparted a striated muscle-like appearance to the cells, and of atypical lymphoid cells infiltrating among the sheets of the crystalloid-storing cells (Fig. 1a,b). Immunohistochemical staining demonstrated that the crystalloid-storing cells were strongly positive for the histiocytic marker CD68 in their cytoplasm (Fig. 1c), but negative for desmin, alpha smooth muscle actin (α-SMA), and S-100 protein (data not shown), indicating that the cells were neither of myogenic nor neurogenic in origin. Lymphoid cells were composed predominantly of both small atypical lymphoid cells and centrocyte-like cells (Fig. 1d) accompanied by scattered plasmacytoid cells, which occasionally had Dutcher bodies or Russell bodies, manifesting the morphological features for MALT lymphoma with plasmacytic differentiation. Immunohistochemical staining confirmed that the lymphoma cells expressed CD20 (Fig. 1e), a pan-B cell antigen marker. Although a small number of CD3-positive reactive T cells were also present, the cells stained with CD5 and CD10 were not identified. Mono-

Fig. 1 Histological section of the surgical specimen. **a** Low power photomicrograph. The tumor consists mainly of sheets of eosinophilic cells admixed with lymphoid aggregates [hematoxylin/eosin (HE), original magnification ×20]. **b** Higher magnification reveals the eosinophilic cells as spindle to epithelioid cells with abundant fibrillar cytoplasm, imparting a striated muscle-like appearance (HE, original magnification ×400). **c** Eosinophilic cells are strongly immunopositive for CD68, confirming their histiocytic nature (original magnification ×400). **d** High power photomicrograph of the lymphoid aggregate discloses small- to intermediate-sized lymphoid cells, atypical nuclei, and moderately abundant pale cytoplasm [HE, original magnification ×400]. **e** Immunostaining for CD20. The lymphoid cells are monotonously CD20-positive, confirming B cell lineage (original magnification ×400). **f**, **g** Immunostaining for IgM (**f**) and light chain kappa (**g**). Focal, monotypic expression of IgM and light chain kappa are seen in the lymphoid aggregates differentiation, showing lymphoplasmacytic differentiation of the lymphoid cells (original magnification ×400). **h**, **i** Immunostaining for IgM (**h**) and light chain kappa (**i**). Weak immunoreactivity for both IgM and kappa, in fibrillary pattern, are also detected in eosinophilic histiocytes (*arrows*), suggesting the phagocytosis of Igs secreted from lymphoma cells (original magnification ×400)

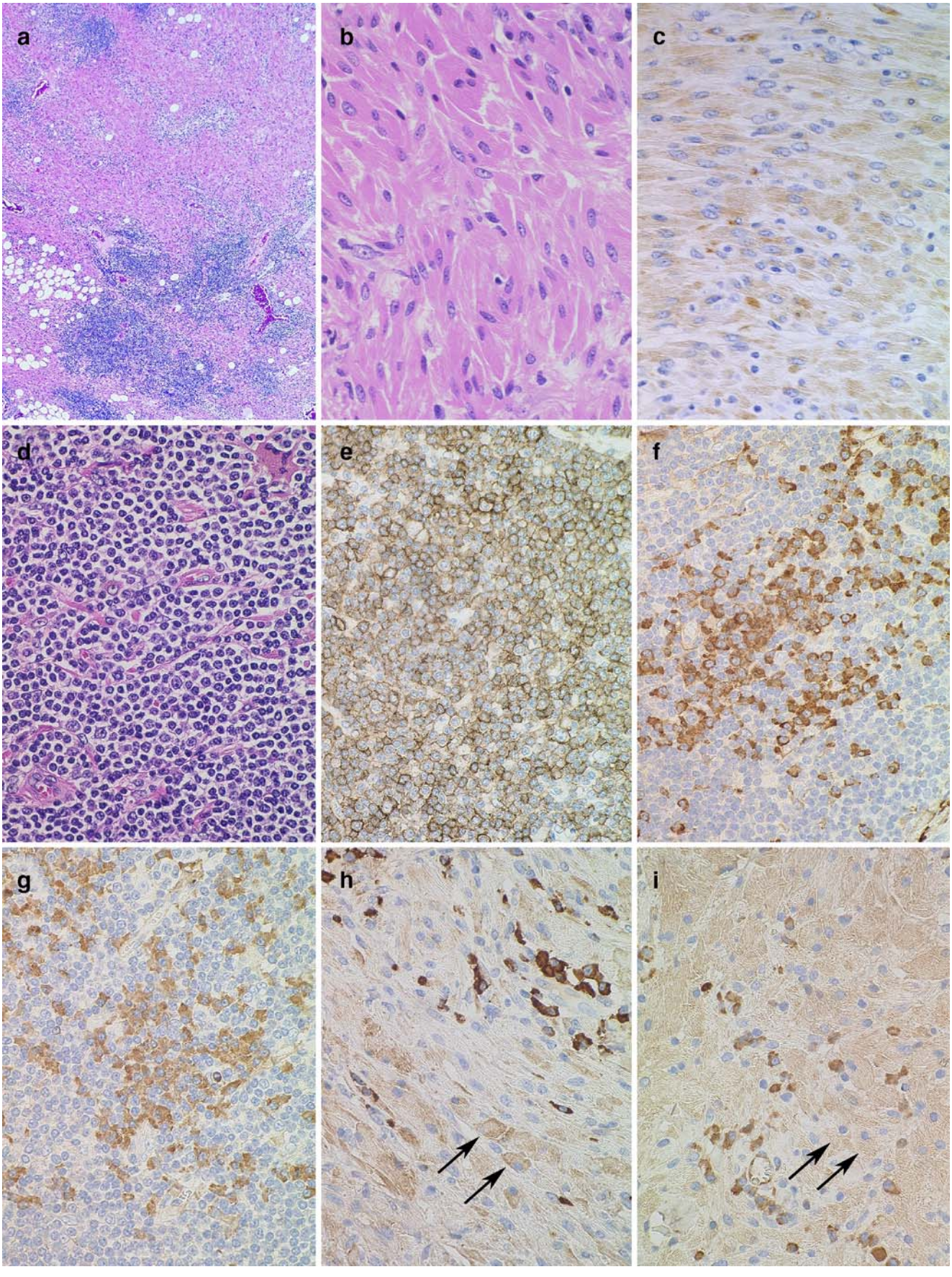
a
b
c
d
e
f
g
h
i

typical expression of IgM-kappa was observed exclusively in the cells with plasmacytoid differentiation (Fig. 1f,g). In addition, some crystalloid-storing histiocytes were also monotypically immunopositive for IgM-kappa (Fig. 1h,i), albeit rather less intensely, suggesting that histiocytes phagocytose the locally secreted Ig molecules from lymphoma cells; the ingested Igs are then crystallized within histiocytes.

The electron microscopy revealed rectangular or rod-shaped crystalloids within the cytoplasm of most histiocytes, but no myofilamentous structures in the cells (Fig. 2). No crystals were seen in lymphoma cells.

Discussion

Ig crystals are occasionally seen in patients with B cell neoplasms. While Ig crystals were usually accumulated within lymphoid cells and hematopoietic tissues [6] or within epithelial cells and connective tissue stroma of various organs and tissues such as the kidney [10], thyroid [10], parotid gland [4], cornea, and conjunctiva [8], massive aggregates of crystal-laden histiocytes (so-called CSH) were also known as a rare phenomenon occurring in lymphoproliferative disorders. Most reported cases of CSH are associated with MM or LPL, although the cases that occurred in some nonneoplastic or reactive conditions have also rarely been described in the literature [1, 13, 18, 20]. Even far less frequent than MM and LPL, MALT lymphoma-associated CSH, as in the present case, has also been reported in five patients to date [2, 5, 17, 21, 22].

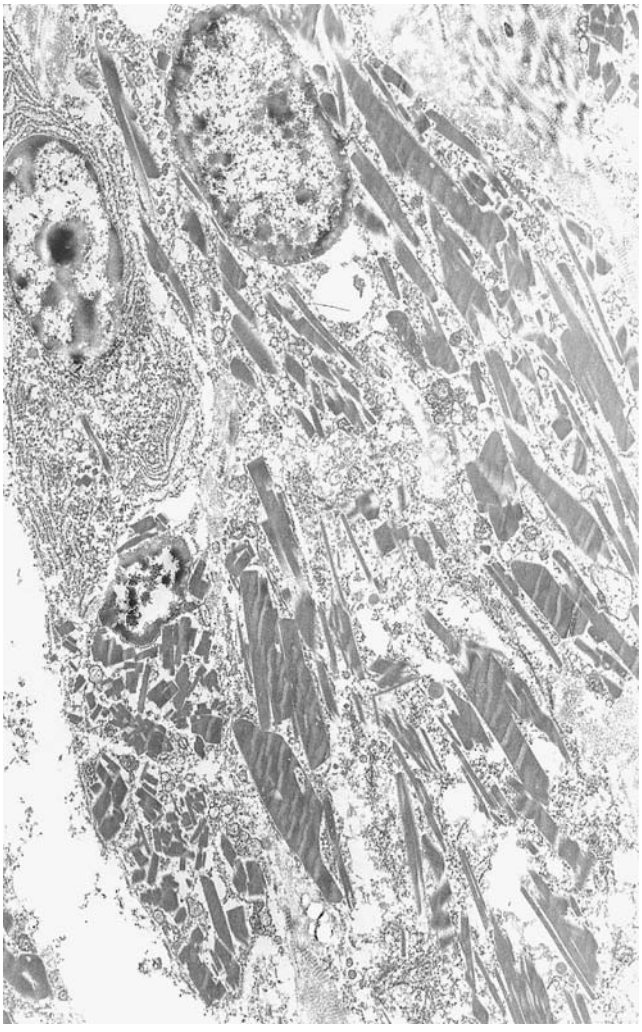

Fig. 2 Electron micrograph demonstrates numerous sharp-edged or polygon-shaped amorphous crystals within the cytoplasm of a histiocyte (original magnification ×6,000)

The mechanism of the Ig crystal formation and its storage in the histiocytes have not been clarified yet. It is interesting to note that the associated light chain in most reported cases of CSH is kappa, though lambda-associated cases have also rarely been described, and there is no relationship among the types of heavy chains. Thus, it is conceivable that sequence abnormalities at specific sites of light chain, especially of kappa light chain, are responsible for crystal formation through some consequent defects such as loss of proteolytic site, high intrinsic stability, or predisposition to the structure forming crystals [7, 16].

It should be noted that MALT lymphoma-associated CSH shows a remarkable predilection for "elderly females." As shown in Table 2, five out of six cases are female, including our patient, although MALT lymphoma affects the gender almost equally (male to female ratio 1:1.2) [19]. Furthermore, a median age at diagnosis of MALT lymphoma among those six cases with CSH is significantly higher (73 years) compared to that among all patients of MALT lymphoma (61 years) [19], giving a striking contrast with 21 reported cases of CSH supervened upon MM (Table 3), the median age of which is considerably younger (60 years) than that of the whole group of patients (68 years in male and 70 in female) [3]. Considering the absence of paraproteinemia in all cases of MALT lymphoma-associated CSH except for one case in which information as to serum paraprotein is not available (Table 2), and that MM commonly presents a monoclonal gammopathy, delayed or early onset of CSH in MALT lymphoma or MM, respectively, seems to depend on the extent of Ig production in tumor cells. Hence, although the abnormalities in light chain are the most likely cause of CSH, overproduction of Ig should also be critical for the pathogenesis. Estrogen depletion, in addition, may be also involved in Ig crystal storage according to the elderly female preponderance in MALT lymphoma-associated CSH. In fact, 17-beta estradiol regulates the expression of genes that function in macrophage activation [11, 15]. It may be, therefore, reasonable to assume that estrogen depletion lowers the enzymatic activities in histiocytes, resulting in the storage

Table 2 MALT lymphoma-associated CSH: summary of clinical and pathologic features of reported cases

Authors	Age (year)	Sex	Involved sites	Ig type	Paraproteinemia
Llobet et al. 1997 [17]	81	F	Parotid gland	IgM, kappa	Not described
Thorson and Hess 2000 [22]	77	F	Parotid gland	lambda	None
Coupland et al. 2002 [2]	62	F	Lacrimal gland	IgM, kappa	None
Sun et al. 2003 [21]	59	M	Lung	Not described	None
Fairweather et al. 2006 [5]	69	F	Lung	kappa	None
Present case	81	F	Eyelid	IgM, kappa	None
Median	73				

of Ig crystals. The enzymes involved in the degradation of Ig, however, are rather nonspecific and are not restricted to their cleavage. Moreover, the hypothesis as to estrogen depletion is invalid in that a series of CSH cases occurred in MM that lacks the elderly female predilection (Table 3). Ig overproduction or estrogen depletion alone does not appear to act as a trigger for CSH, but may help promote the disease.

Given the rarity of this disease, difficulties in diagnosis may arise, especially in cases showing excessive proliferation of crystal-laden histiocytes, which obliterate the underlying neoplastic disease, or enlarged and deformed histiocytes with a fibrillar cytoplasmic appearance, which can lead to misdiagnosis such as rhabdomyoma [14], Gaucher's disease [12], Weber–Christian disease [9], or other forms of histiocytosis. To prevent a serious misdiagnosis, pathologist should keep CSH in mind as a rare complication of lymphoproliferative disease, and when confronted with histologic features suggestive of CSH, it is important to perform immunohistochemical analysis and/or electron microscopy to either confirm or rule out the diagnosis.

Table 3 MM-associated CSH: summary of clinical and pathologic features of reported cases

Authors	Age (year)	Sex	Involved sites	Paraprotein
Glaus 1917	67	F	BM, LN, skin, testes	BJP (urine)
Brass 1948	73	F	BM, liver, spleen	Not described
Engele 1957	38	M	BM, spleen	BJP (urine)
Dedmon 1963	51	M	BM, LN	Not described
Ito 1970	53	F	BM, liver, LN, spleen, adrenals, kidneys	kappa
Kjeldsberg 1977	60	M	BM, liver, spleen	kappa
Terashima 1978	58	M	BM, spleen, liver, LN, and diverse additional	kappa
Itagaki 1981	69	F	BM, systemic	IgG kappa
Mullen 1981	52	M	BM, liver, LN, and diverse additional sites	IgG kappa
Takahashi 1987	60	M	BM, spleen, liver, LN, and diverse additional	IgA kappa
Yamamoto 1991	71	M	BM, spleen, liver, LN, and diverse additional	IgG kappa
Kazzaz 1992	60	M	Lung	kappa
Schaefer 1996	55	M	BM, liver	IgG kappa
Jones 1999	50	M	BM, skull, LN	IgG kappa
	48	M	BM	IgA kappa
	53	M	BM	IgA kappa
	77	F	BM	kappa
	66	M	BM	IgA kappa
Lebeau 2002	73	M	BM, spleen, liver, LN, and diverse additional	IgA kappa
Papla 2004	51	M	BM, liver, spleen	IgG kappa
Tholouli 2005	62	F	BM	IgG kappa
Median	60			

BM Bone marrow, *LN* lymph node(s), *BJP* Bence Jones protein

References

1. Bosman C, Camassei FD, Boldrini R, Piro FR, Saponara M, Romeo R, Corsi A (1998) Solitary crystal-storing histiocytosis of the tongue in a patient with rheumatoid arthritis and polyclonal hypergammaglobulinemia. Arch Pathol Lab Med 122:920–924
2. Coupland SE, Foss HD, Hummel M, Stein H (2002) Extranodal marginal zone B-cell lymphoma of the lacrimal gland associated with crystal-storing histiocytosis. Ophthalmology 109:105–110
3. Devesa SS, Silverman DT, Young JL Jr, Pollack ES, Brown CC, Horm JW, Percy CL, Myers MH, McKay FW, Fraumeni JF Jr (1987) Cancer incidence and mortality trends among whites in the United States, 1947–84. J Natl Cancer Inst 79:701–770
4. El-Nagger AK, Ordonez NG, Batsakis JG (1991) Parotid gland plasmacytoma with crystalline deposits. Oral Surg Oral Med Oral Pathol 71:206–208
5. Fairweather PM, Williamson R, Tsikleas G (2006) Pulmonary extranodal marginal zone lymphoma with massive crystal storing histiocytosis. Am J Surg Pathol 30:262–267
6. Gabriel L, Escribano L, Perales J, Bellas C, Odriozola J, Navarro JL (1985) Multiple myeloma with crystalline inclusions in most hematopoietic cells. Am J Hematol 18:405–411
7. Green ED, Morrison LK, Love PE, DeSchryver-Kecskemeti K, Waltman SR, Smith ME, Scott MG (1990) A structurally aberrant immunoglobulin paraprotein in a patient with multiple myeloma and corneal crystal deposits. Am J Med 88:304–311
8. Grossniklaus HE, Stulting RD, L'Hernault N (1990) Corneal and conjunctival crystals in paraproteinemia. Hum Pathol 21:1181–1183
9. Harada M, Shimada M, Fukayama M, Kaneko T, Kitazume K, Weiss SW (1996) Crystal-storing histiocytosis associated with lymphoplasmacytic lymphoma mimicking Weber–Christian disease: immunohistochemical, ultrastructural, and gene-rearrangement studies. Hum Pathol 27:84–87
10. Hirota S, Miyamoto M, Kasugai T, Kitamura Y, Morimura Y (1990) Crystalline light-chain deposition and amyloidosis in the thyroid gland and kidneys of a patient with myeloma. Arch Pathol Lab Med 114:429–431
11. Hong M, Zhu Q (2004) Macrophages are activated by 17beta-estradiol: possible permission role in endometriosis. Exp Toxicol Pathol 55:385–391
12. Jones D, Renshaw AA (1996) Recurrent crystal-storing histiocytosis of the lung in a patient without a clonal lymphoproliferative disorder. Arch Pathol Lab Med 120:978–980
13. Jones D, Bhatia VK, Krausz T, Pinkus GS (1999) Crystal-storing histiocytosis: a disorder occurring in plasmacytic tumors expressing immunoglobulin kappa light chain. Hum Pathol 30:1441–1448
14. Kapadia SB, Enzinger FM, Heffner DK, Hyams VJ, Frizzera G (1993) Crystal-storing histiocytosis associated with lymphoplasmacytic neoplasms. Report of three cases mimicking adult rhabdomyoma. Am J Surg Pathol 17:461–467
15. Kramer PR, Wray S (2002) 17-Beta-estradiol regulates expression of genes that function in macrophage activation and cholesterol homeostasis. J Steroid Biochem Mol Biol 81:203–216
16. Lebeau A, Zeindl-Eberhart E, Muller EC, Muller-Hocker J, Jungblut PR, Emmerich B, Lohrs U (2002) Generalized crystal-storing histiocytosis associated with monoclonal gammopathy: molecular analysis of a disorder with rapid clinical course and review of the literature. Blood 100:1817–1827
17. Llobet M, Castro P, Barcelo C, Trull JM, Campo E, Bernado L (1997) Massive crystal-storing histiocytosis associated with low-grade malignant B-cell lymphoma of MALT-type of the parotid gland. Diagn Cytopathol 17:148–152
18. Motta L, McMenamin ME, Thomas MA, Calonje E (2005) Crystal deposition in a case of cutaneous Rosai–Dorfman disease. Am J Dermatopathol 27:339–342
19. No authors listed (1997) A clinical evaluation of the International Lymphoma Study Group classification of non-Hodgkin's lymphoma. The Non-Hodgkin's Lymphoma Classification Project. Blood 89:3909–3918
20. Sukpanichnant S, Hargrove NS, Kachintorn U, Manatsathis S, Chanchairujira T, Siritanaratkul N, Akaraviputh T, Thakerngpol K (2000) Clofazimine-induced crystal-storing histiocytosis producing chronic abdominal pain in a leprosy patient. Am J Surg Pathol 24:129–135
21. Sun Y, Tawfiqul B, Valderrama E, Kline G, Kahn LB (2003) Pulmonary crystal-storing histiocytosis and extranodal marginal zone B-cell lymphoma associated with a fibroleiomyomatous hamartoma. Ann Diagn Pathol 7:47–53
22. Thorson P, Hess JL (2000) Transformation of monocytoid B-cell lymphoma to large cell lymphoma associated with crystal-storing histiocytes. Arch Pathol Lab Med 124:460–462

Virchows Arch (2007) 450:109–113
DOI 10.1007/s00428-006-0325-z

CASE REPORT

Synovial tumefactive extramedullary hematopoiesis associated to polycythemia vera

Hugo Alvarez-Argüelles Cabrera · José Luis Carrasco Juan · María Candelaria García Castro · Manuel González Gaitano · Alfonso Bonilla Arjona · Lucio Díaz-Flores

Received: 19 June 2006 / Accepted: 3 October 2006 / Published online: 16 November 2006
© Springer-Verlag 2006

Abstract The case of a 66-year-old male patient with a chronic myeloproliferative type polycythemia vera disorder, who after 2 years of evolution is developing a tumefactive extramedullary hematopoiesis (TEH) located in the synovial of the articulation in the right knee, is described. The tumor histologically consists of a relatively lax and edematous synovial structure diffusely infiltrated by mature and semimature hematopoietic cellular population. The simultaneous study of the bone marrow reveals medullar spaces full of hematopoietic cellularity, with a predominance of megakaryocytic and red series, and with the addition of severe reticulin fibrosis, facts that suggest a progression toward myelofibrosis. The TEH developed in tissues without a reticulum endothelial system is very uncommon. We provide data about the first case located in the synovial membrane and we review the literature regarding this pathologic entity.

H. Alvarez-Argüelles Cabrera · M. C. García Castro · L. Díaz-Flores
Department of Pathology, Canary University Hospital, Tenerife, Canary Islands, Spain

M. González Gaitano
Department of Orthopaedic and Traumatologic Surgery, Canary University Hospital, Tenerife, Canary Islands, Spain

A. Bonilla Arjona
Department of Radiodiagnostic, Canary University Hospital, Tenerife, Canary Islands, Spain

H. Alvarez-Argüelles Cabrera · J. L. Carrasco Juan (✉) · L. Díaz-Flores
Department of Pathology, Faculty of Medicine, La Laguna University, Tenerife, Canary Islands, Spain
e-mail: jcarraju@ull.es

Keywords Synovial tumor · Tumefactive extramedullary hematopoiesis · Extramedullary hematopoietic tumor · Extramedullary hematopoietic proliferation

Introduction

Tumefactive extramedullary hematopoiesis (TEH), or extramedullary hematopoietic tumor, is characterized by one or several masses of a tumoral appearance, which is produced by the nonneoplastic proliferation of hematopoietic cellularity outside the bone marrow [8]. When important fibrosis of the stroma is added, these masses are called fibrous hematopoietic tumors or sclerosing extramedullary hematopoietic tumors [6, 11, 15]. TEH basically appears during the course of a chronic myeloproliferative disorder of an idiopathic myelofibrosis type, and less frequently in chronic myeloid leukemia, polycythemia vera, and essential thrombocythemia [6, 8]. Myeloid metaplasia, the cause of this pathologic entity, has a preference, with regard to its location, for those organs that contain a reticulum endothelial system, such as the spleen, the liver, and lymph nodes, although rare cases of TEH have been reported in the kidney, the adrenal gland, the digestive tract, the central nervous system, the skin, and soft parts [1, 3, 8, 12, 14]. We report the clinical and pathologic study of an unprecedented case of TEH located in the articular synovial of the right knee of a patient with polycythemia vera.

Clinical history

A 66-year-old male patient with a history of gout was diagnosed in 2001 with a chronic myeloproliferative

disorder of a polycythemia vera type and was treated with phlebotomies. The patient was admitted to the University Hospital of the Canary Islands in October 2003 for the study and treatment of a monoarthritis located in the right knee. A mass occupying the knee joint was detected by magnetic resonance (MR) (Fig. 1a), which molded perfectly to the joint without eroding the adjoining bone structures and was of a very similar density to that of the adipose tissue. Besides that, irregular, geographical, and hyperintensive lesions were observed that were located in the epimetaphyseal regions of the distal femur and proximal tibia. After an initial diagnosis of a tumor of the soft parts, neoplasia, or synovial hypertrophy, a decision was made to perform an extirpation of the tumoration and implant a complete knee prosthesis. An apparently well-delimitated, multinodular, reddish brown mass with fine hemorrhagic spots and of a soft consistency, measuring 7×4×3.5 cm (Fig. 1b) is isolated and removed during the surgery. The lesion is sent for its pathologic study together with fragments from the femur and tibia. Later on, in January 2006, a splenectomy was performed on the patient with a diagnosis of splenomegalia associated with myeloid metaplasia. The patient is now 69 years of age and 30 months have passed since the first operation without any signs of local recurrence of the tumoration of the knee.

Materials and methods

The tumor and the bone fragments from the femur and tibia were fixed in 10% buffered formalin, the bone portions were decalcified, and the sections were selected for paraffin embedding for the histological study. Stains of hematoxylin–eosin (HE), Giemsa, periodic acid-Schiff/hematoxylin and Wilder's reticulin were used in the conventional histopathologic study. The immunohistochemical (IH) study was performed with immunoperoxidase on selected and deparaffinized sections, using the automatic Ventana staining system (BIOTEK) with antibodies for factor VIII (clone BGXO16A), CD3 (clone F7.2.38), CD20 (clone L26), CD43 (clone DF-T1), CD45 (clone 2B11+PD7/26), CD68 (clone PG-M1), CK (clone AE1-AE3), and epithelial membrane antigen (clone E29) (products supplied by DAKO).

Results

Morphologically, the tumoration of the knee is composed of clearly delimitated nodules of differing size, separated by fibrovascular septs, where there is a dense cellular infiltration immersed in a lax and heavily vascularized stroma (Fig. 2a,b). Under a higher magnification it is confirmed that the nodules correspond to synovial villi, which have greatly enlarged due to the presence of a diffuse infiltration of hematopoietic cellularity of a mature and semimature appearance, belonging to the three series, although with a predominance of erythroid aggregates and disperse megakaryocytes (Fig. 2c,d). In the somewhat edematous and myxoid interstice, there is a diffuse inflammatory component of a lymphoplasmocitary type, or configuring lymphoid nodes, as well as a certain increase in the fiber framework. The IH study confirms the hematopoietic nature of the infiltrations, which are positive for CD43 and CD45, and the existence of lymphoid nodes with a mixed immunophenotype (positive for CD3 and CD20) (images not shown). Medullar spaces full of mature and semimature hematopoietic cellularity are observed in the femur and tibia bone fragments, with abundant erythroblastic and megakaryocytic nests, as well as a clear reinforcement of the reticulin fiber network (grade 3 reticulin fibrosis) (Fig. 3a,b), findings that explain the images observed in the MR. The pathologic diagnosis given, using these results, is of synovial TEH with chronic follicular synovitis, and the bone marrow was affected by a chronic

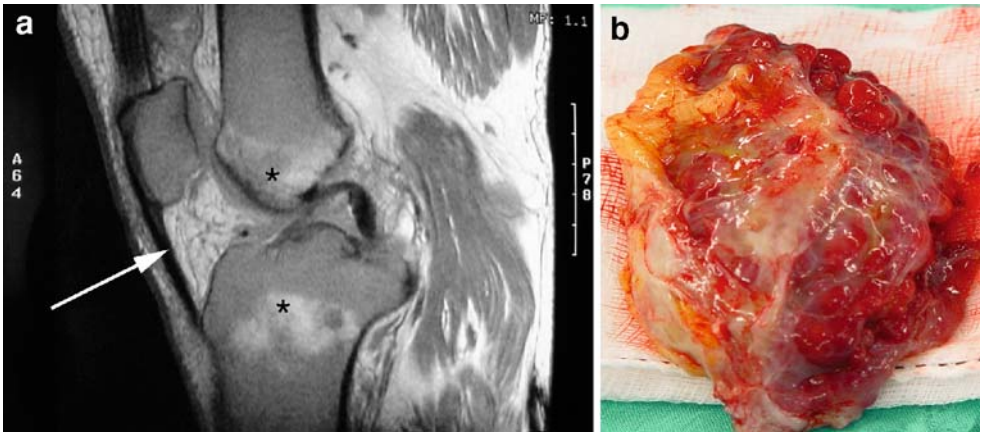

Fig. 1 **a** In the MR, one can see a nondestructive lesion occupying the right knee joint (*arrow*) and the irregular and hyperintensives areas in the epimetaphyseal regions of the distal femur and proximal tibia (*asterisks*). **b** Macroscopic aspect of the tumor after its removal

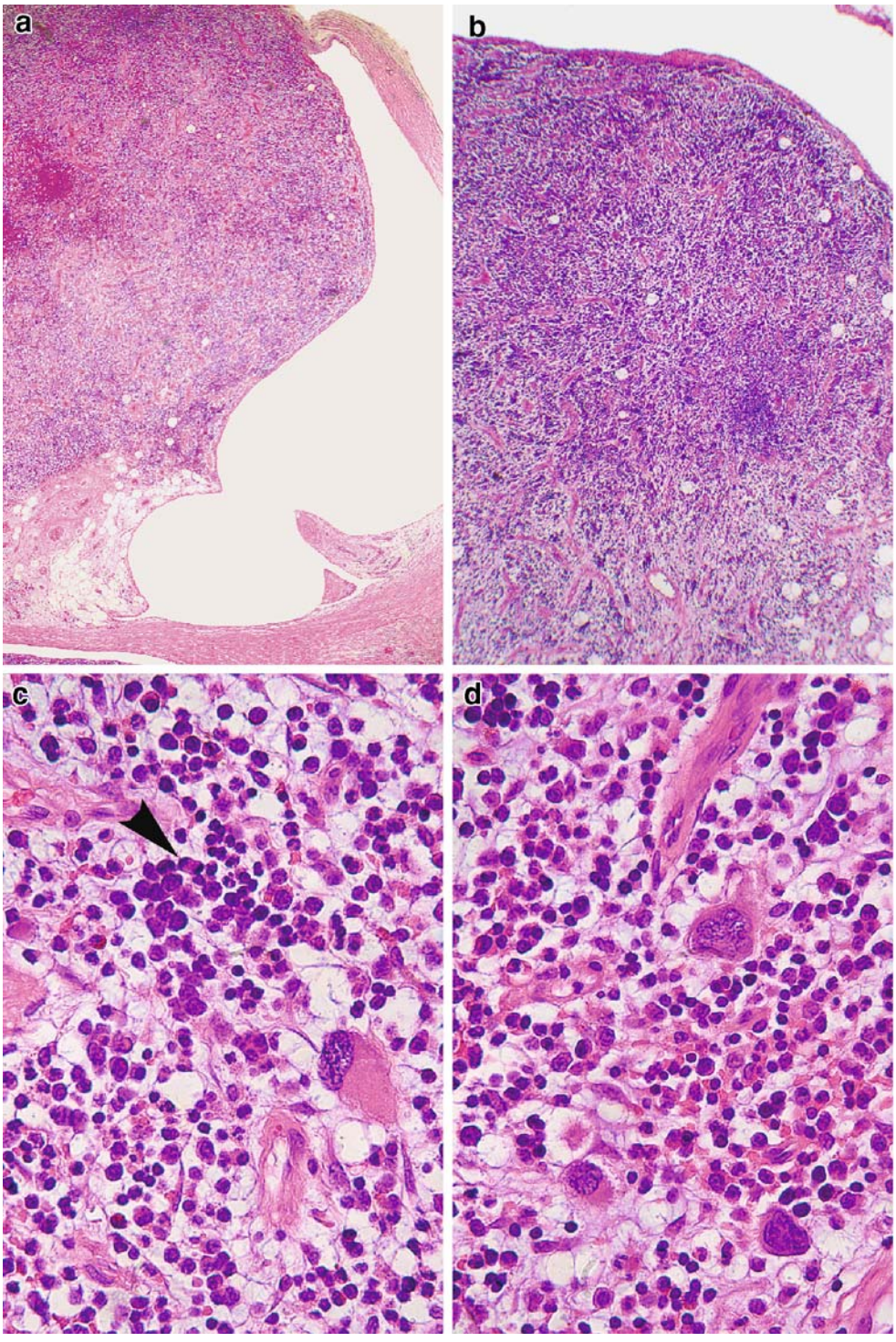

Fig. 2 Microscopic image of the synovial tumoration showing the nodules of which it is composed of (**a**, HE ×25) and the dense cellular infiltrate in them (**b**, HE ×40). The cellular infiltrate corresponds, under greater magnification, to extramedullary hematopoiesis consisting of mature and semimature precursors of the three series, with a predominance of erythroid aggregates with mitotic blast activity (*arrowhead*) (**c**, HE ×400). The megakaryocytes are clearly visible in other areas, which are neither atypical nor form true clusters (**d**, HE ×400)

myeloproliferative disorder compatible with polycythemia vera, in evolution toward myelofibrosis.

Discussion

Myeloid metaplasia, in its pathogenesis, is usually related to a myelofibrosis that progressively causes an ineffective hematopoiesis due to the displacement of stem cells in the bone marrow. Myelofibrosis is preferentially associated with chronic myeloproliferative disorder, mainly idiopathic myelofibrosis, although it can also occur in chronic myeloid leukemia, essential thrombocythemia, and in 2% of polycythemia vera patients. It is thought that in these disorders, the stroma of the bone marrow reacts and thus generates reticulin and collagen fibrosis, angiogenesis, and

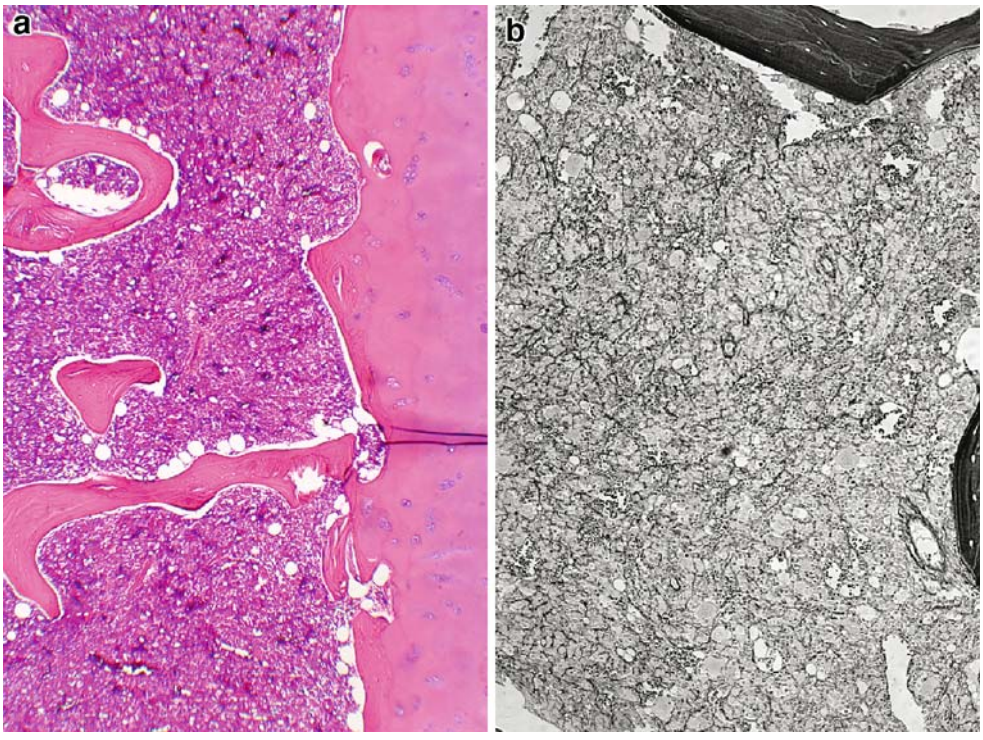

Fig. 3 Images corresponding to femur and tibia bone fragments showing densely cellular medullar spaces (**a**, HE ×40) in which a severe reticulin fibrosis is found (**b**, Wilder's reticulin ×40)

osteosclerosis as a result of the stimulus produced by the diverse cytokines locally secreted by megakaryocytes, monocytes, and platelets [11, 15]. Other entities producing medullar fibrosis include certain lymphoid and myeloid hemopathies, not only neoplastic but also nonneoplastic, metastatic carcinomas, chronic granulomatous infections, connectivepathies, renal osteodystrophy, and some treatments (colony stimulating factor) [3, 8–10, 13]. In general, the resulting extramedullary hematopoiesis affects those organs containing a reticulum endothelial system (spleen, liver, and lymph nodes), although any organ or structure may occasionally be affected, in which case there is a certain predisposition for the serous membranes.

Extramedullary hematopoiesis rarely appears in the form of a single or multiple mass or tumor. This usually occurs when it is in locations that allow an expansion of the process with little accompanying clinical signs, and is known as TEH or extramedullary hematopoietic tumor. There are also cases of TEH simply referred to as "extramedullary hematopoiesis" [1, 3, 8, 12, 14], or by the confusing term "extramedullary myeloid tumor"; nowadays, however, the use of this term is restricted to extramedullary myeloid neoplasias of the granulocytic sarcoma type [7, 8]. With regard to its location, some cases of TEH were reported affecting the serous membranes of the thorax (pleura and pericardium) and of the abdominal cavity (mesentery and epiplon), in the retroperitoneum, kidneys, adrenal glands, uterus, digestive tract, lung, heart, nervous system, skin, subperiostic tissue, and even inside the cardiac and breast tumors [2, 4]. There is a case reported by Heinicke et al. [5] that describes a patient with synovial extramedullary hematopoiesis, secondary to an idiopathic myelofibrosis, showing a clinical picture of arthritis by chronic synovitis (there was chronic follicular synovitis in our patient as well), but which did not develop into a TEH. Therefore, we report the first case of a TEH with a synovial location associated with polycythemia vera.

Regarding the differential diagnosis, determinate features of the described lesion, not only histological (the low presence of fibrosis, the absence of megakaryocytic pleomorphism, and the mixed T and B nature of the accompanying lymphoid nodular infiltrates) but also clinical (its peculiar location in the articular synovial in the knee), makes it possible to differentiate it from other processes such as Hodgkin and non-Hodgkin lymphoma, sclerosing liposarcoma, malignant fibrohistiocytoma, reticulosarcoma, metastatic carcinoma, and myelolipoma [6, 8, 11, 15]. Furthermore, the semimature and nonneoplastic nature of the hematopoietic proliferation in TEH excludes granulocytic-erythroblastic-megakaryocytic sarcoma, also known as tumefactive leukemia or extramedullary myeloid tumor [8].

Finally, we have reported the clinical and pathologic study of a case of TEH that, because its extraordinary location and rarity, suggested clinical diagnoses of a soft tissue tumor, hyperplasia, or synovial neoplasia. In conclusion, a picture of ineffective medullar hematopoiesis by myelofibrosis (evolved from a polycythemia vera) must therefore be considered among the possible causes of tumoration in unusual places.

References

1. Bolaman Z, Polatli M, Cildag O, Kadikoylu G, Culhaci N (2002) Intrathoracic extramedullary hematopoiesis resembling posterior mediastinal tumor. Am J Med 112:739–741
2. Burke AP, Virmani R (1993) Cardiac myxoma. A clinicopathologic study. Am J Clin Pathol 100:671–680
3. Georgiades CS, Neyman EG, Francis IR, Sneider MB, Fishman EK (2002) Typical and atypical presentations of extramedullary hemopoiesis. AJR Am J Roentgenol 179:1239–1243
4. Harbin LJ, Burnett S, Ghilchik M, Lee DM, Rajan P (2002) Extramedullary haematopoiesis in a hyalinized mammary fibroadenoma. Histopathology 41:475–477
5. Heinicke MH, Zarrabi MH, Gorevic PD (1983) Arthritis due to synovial involvement by extramedullary haematopoiesis in myelofibrosis with myeloid metaplasia. Ann Rheum Dis 42:196–200
6. Lane JE, Walker AN, Kulharya A, Marzec T (2002) Cutaneous sclerosing extramedullary hematopoietic tumor in chronic myelogenous leukaemia. J Cutan Pathol 29:608–612
7. Meis JM, Butler JJ, Osborne BM, Manning JT (1986) Granulocytic sarcoma in nonleukemic patients. Cancer 58:2697–2709
8. Nappi O, Boscaino A, Wick M (2003) Extramedullary hematopoietic proliferations, extraosseous plasmocytomas, and ectopic splenic implants (splenosis). Semin Diagn Pathol 20:338–356
9. O'Keane JC, Wolf BC, Neiman RS (1989) The pathogenesis of splenic extramedullary hematopoiesis in metastatic carcinoma. Cancer 63:1539–1543
10. Redmond J 3rd, Kantor RS, Auerbach HE, Spiritos MD, Moore JT (1994) Extramedullary hematopoiesis during therapy with granulocyte colony-stimulating factor. Arch Pathol Lab Med 118:1014–1015
11. Remstein ED, Kurtin PJ, Nascimento AG (2000) Sclerosing extramedullary hematopoietic tumor in chronic myeloproliferative disorders. Am J Surg Pathol 24:51–55
12. Schreibman D, Brenner B, Jacobs R, Ben-Arieh Y, Tatarsky I, Alroy G (1988) Small intestinal myeloid metaplasia. JAMA 259:2580–2582
13. Shigemura N, Akashi A, Nakagiri T (2002) Intrathoracic extramedullary hematopoiesis arising in marble bone disease. Clarifying the genetic disease mechanism. Jpn J Thorac Cardiovasc Surg 50:311–314
14. Sirgi KE, Swanson PE, Gersell DJ (1994) Extramedullary hematopoiesis in the endometrium. Report of four cases and review of the literature. Am J Clin Pathol 101:643–646
15. Yang X, Bhuiya T, Esposito M (2002) Sclerosing extramedullary hematopoietic tumor. Ann Diagn Pathol 6:183–187

Virchows Arch (2007) 450:115–118
DOI 10.1007/s00428-006-0326-y

CASE REPORT

Late recurrence of Wilms' tumour with exclusive skeletal muscle phenotype 23 years after primary diagnosis

Rebecca Senetta · Luigia Macrì · Donatella Pacchioni · Isabella Castellano · Paola Cassoni · Gianni Bussolati

Received: 22 August 2006 / Accepted: 2 October 2006 / Published online: 17 November 2006
© Springer-Verlag 2006

Abstract A late recurrence of Wilms' tumour (WT) 23 years after the primary diagnosis is described. The primary tumour occurred in a 10-month-old girl and showed various degrees of differentiation, including skeletal muscle phenotype. A postoperative chemotherapy was performed. Twenty-three years after the surgery, the tumour relapsed: the lesion was exclusively composed of mature skeletal muscle elements (diffuse and intense desmin reactivity) derived from the primary tumour as confirmed by WT1 immunoreactivity. Chemotherapy and radiotherapy have been reported previously to ablate the immature components of WT; especially, chemotherapy can modify the histological type, reducing the immature elements while leaving mature cells unaffected. We can hypothesise that both morphological and molecular features of the tumour as well as the effect of therapy can influence a tumour relapse in WT. The latter results in a high degree of differentiation and a long disease-free interval after the first diagnosis.

Keywords Wilms' tumour · Late recurrence · Relapse · Skeletal muscle phenotype

Introduction

Wilms' tumour (WT) is the most common primary malignant renal tumour in children.

R. Senetta · L. Macrì · D. Pacchioni · I. Castellano · P. Cassoni · G. Bussolati (✉)
Department of Biomedical Sciences and Human Oncology,
University of Turin,
Via Santena 7,
10126 Turin, Italy
e-mail: gianni.bussolati@unito.it

The association of chemotherapy and radiotherapy to radical nephrectomy has increased the overall survival rate up to 85–90% [3, 6]; however, in spite of these therapeutic improvements, tumour relapses in a subset of patients (15–20%) [12]. Numerous studies have demonstrated that the risk of recurrence can be associated to different features such as histological tumour pattern and loss of heterozygosis (LOH) at 1p and/or 16q, as well as gain of chromosome 1 and other recently described alterations [7, 8, 15, 18]. The recurrence risk is greater within the first 2 years after primary diagnosis (in these patients, the percentage of survival approximately ranges from 24 to 43%), but late relapses have occasionally been reported [1, 10].

We in this study report a case of late recurrence of WT 23 years after primary diagnosis.

Clinical history

In October 2005, a 23-year-old female came to medical attention for abdominal recurrent pain and occlusive status. Physical examination revealed an abdominal soft mass in the periumbilical region; hematochemical analysis showed normal values for gastrointestinal cancer-associated antigens, carcinoembryonic antigen, α-phetoprotein, carbohydrate antigen 19.9 and carbohydrate antigen 125. Abdominal ultrasonography, computed tomography and magnetic resonance imaging disclosed two masses: the first one was placed in the right periumbilical region, whereas the second one, placed in the left retroperitoneal space, caused compression of the wall of the small bowel. A tomography emission of positron showed no signal accumulation. The patient underwent surgical removal of the abdominal and retroperitoneal masses. Nine months after surgical removal, the patient was disease-free.

A left nephrectomy with surgical removal of a WT had been performed 23 years before (in September 1982). A histopathological diagnosis of WT (G2, favourable histology) with differentiation towards epithelial (tubular elements), blastematous and rhabdomyoblastic features was made. No preoperative chemotherapy was performed, but after the surgery, the patient underwent cycles of chemotherapy with actinomycin D and vincristine. The subsequently follow-up was negative for the following 23 years.

Materials and methods

The surgical material was totally examined and accurately sampled. The surgical specimens of both masses were fixed in 4% buffered formaldehyde and embedded in paraffin, and the routine histological sections of 3 μm were prepared and stained with haematoxylin and eosin. Additional sections, collected on poly-L-lysine-coated slides, were used for the immunohistochemistry analysis. Immunohistochemical reactions using antibodies anti-desmin (monoclonal antibody, clone D33, diluted 1:50; DAKO, Glostrup, Denmark), anti-smooth muscle actin (monoclonal antibody, clone 1A4, pre-diluted; Ventana-Diapath, Tucson, AZ, USA) and WT 1 protein (WT-1) (monoclonal antibody, clone 6F-H2, diluted 1:20; IMGENEX) were performed in an automated immunostainer (Ventana BenchMark Auto-Stainer, Ventana Medical Systems, Tucson, AZ, USA).

Results

A left nephrectomy with excision of the renal hilum lymph node and the omentum was performed in September 1982. Grossly, the surgical specimen measured 14×12×8 cm and displayed a pale grey appearance with diffuse hemorrhagic areas; at the cut surface, two different nodes were present: the first one, measuring 6 cm, close to the renal hilum, and the second one, measuring 9 cm, localised at the inferior renal pole. At the histological level (the slides were collected and revised in our institute), the lesion showed various degrees of cell differentiation within the different cell components (epithelial, blastematous and stromal). The tumour cells were organised in nodes either isolated or confluent in clusters and diffusely invading the residual renal parenchyma (Fig. 1a); focally, epithelial cells assumed a pseudo-glandular architecture (Fig. 1b,c). The mesenchymal tumour cells were elongated or rounded with a scanty cytoplasm and voluminous and hyperchromatic nuclei. In some areas, representing about 10% of the tumour, skeletal muscle with elongated cells showing intra-cytoplasmatic cross-striations was present (Fig. 1d). No evidence of nephrogenic rests was found. The renal capsule and the omentum appeared infiltrated by proliferating neoplastic cells. The renal hilum lymph node examined did not display any metastatic cells. A confirmatory diagnosis of WT (G2, favourable histology) with epithelial, blastematous and rhabdomyoblastic differentiation was made (stage III).

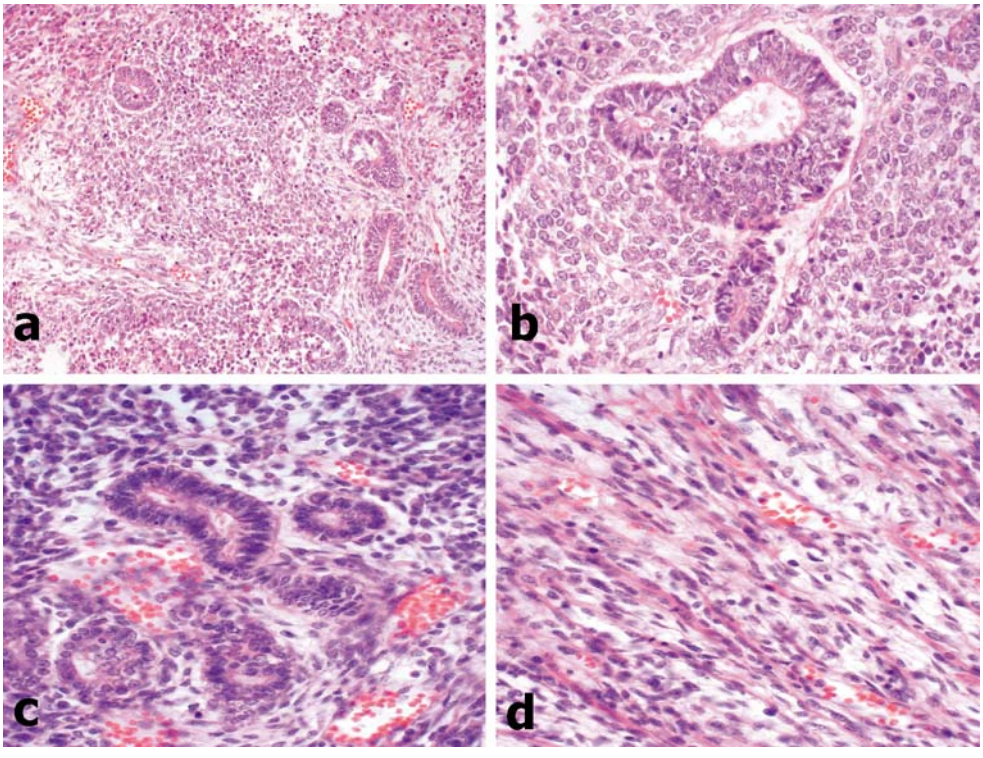

Fig. 1 Histological features of the primary Wilms tumour (surgical removed in September 1982). The tumour showed the coexistence at epithelial (tubular elements), blastematous (**a** 10×, **b** 40×, **c** 20×), and rhabdomyoblastic (**d** 40×) elements; areas of necrosis were also present

The lesion removed in October 2005 was represented by two different surgical specimens: a well-circumscribed mass of abdominal wall, measuring 14×11×2 cm, and a retroperitoneal mass adjacent the small bowel, measuring 11.5×9×3.5 cm. Macroscopically, both lesions were lobulated, encapsulated and showed a stiff-elastic consistency. At cut surface, both lesions appeared yellow–whitish in colour and with a fasciculated appearance. Microscopically, both lesions showed an exclusive benign-appearing stroma component with mature skeletal muscle; no evidence of immature elements or nephrogenic rests was found (Fig. 2a,b). In the lesion adherent to the small bowel, such proliferation of mature skeletal muscle elements was not displaying any infiltrating pattern towards the bowel wall. Such elements were arranged in bundles separated by fibrous tissue and presented intra-cytoplasmatic cross-striations, an eosinophilic cytoplasm and a peripheral nuclear location (Fig. 2b). Necrosis was absent. Immunohistochemical studies showed diffuse and intense desmin (Fig. 2d) and WT-1 (Fig. 2c) reactivity. Cells were negative for smooth muscle actin (which was positive in vascular structures only) and had a low proliferation index (Ki67<1%).

Altogether, the morphological and immunohistochemical features displayed by the two lesions, together with the previous history of WT and the lack of any infiltrating or invading growth pattern, addressed to a diagnosis of late recurrence of WT with exclusive mature skeletal muscle component.

Discussion

Approximately 15–20% of cases of WT relapse, more frequently within the first 2–5 years after the primary diagnosis, are reported; in these cases, the risk of recurrence is mainly related to the morphological and molecular features of the previous tumour [7, 8, 12, 15, 18].

Late recurrences (>5 years after primary diagnosis) of WT are very rare [2, 4, 5, 11, 13, 16, 17], and in all described cases, but one, similar histological patterns between the original and the relapsing tumour are reported with a persistence of immature cells, blastematous elements or nephrogenic rests [2, 4, 11, 13, 16, 17]. In one case only, which was a late (23 years) recurrence, differentiated epithelial cells in absence of immature elements (in contrast of the original tumour showing predominantly blastematous and immature elements) were reported [5]. The case described in this study showed two well-circumscribed lesions with a stiff-elastic consistency, exclusively composed of mature skeletal muscle elements derived from the primary tumour, as confirmed by WT1 immunoreactivity. In addition, absence of necrosis and pleomorphism and the low proliferation index (<1%) further excluded the possible differential diagnosis with a sarcomatous lesion.

Zuppan et al. [19] recently stressed that preoperative chemotherapy is associated to changes of the histological features, thus creating an ambiguity on WT staging according to tumour response. They outlined that the therapy effect is variable depending on the different histological subtypes of WT: some tumours show little

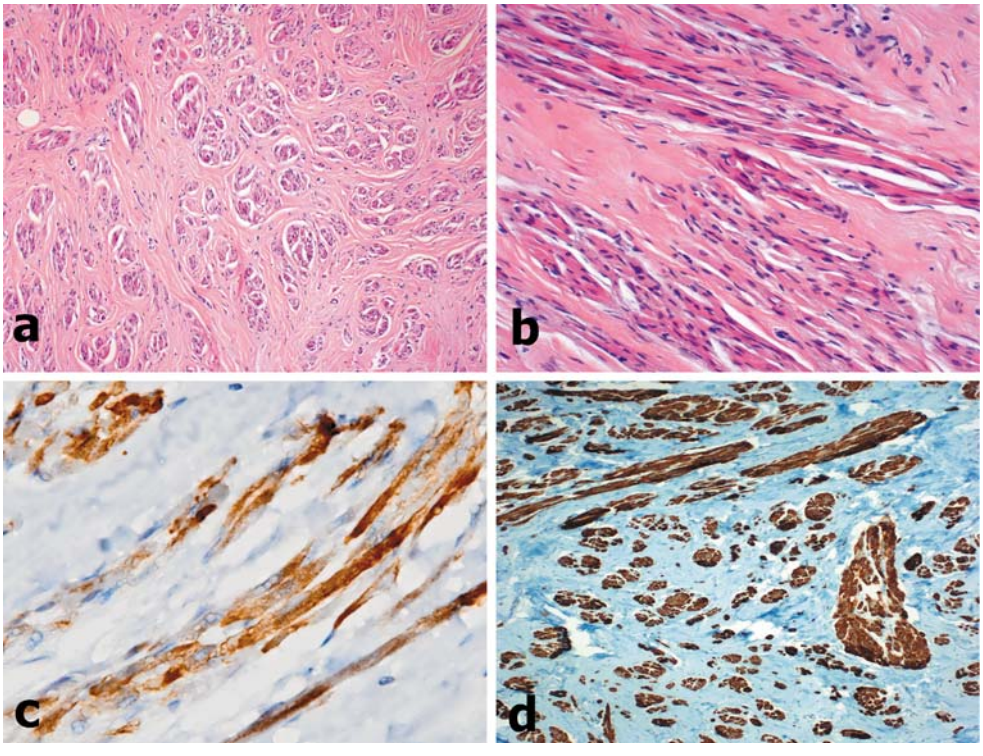

Fig. 2 Histological and immunophenotypical features of the Wilms tumour recurrence (surgical removed in October 2005). The late relapse of Wilms tumour showed an exclusive benign-appearing stroma with the skeletal muscle component without the evidence of immature elements or nephrogenic rests (**a** 10×, **b** 20×). The lesion was immunoreactive for WT-1 (**c** 40×) and desmin in neoplastic muscular cells (**d** 20×)

therapy effects with persistence of abundant and proliferating blastema elements, while others show an "atrophic pattern". Sometimes, the loss of most embryonic elements induced by therapy is accompanied by persistence of mature heterotopic elements such as mature skeletal muscle, cartilage or adipose tissue [19]. Blastematous cells usually show a dramatic response leading to necrosis, whereas mature tubular and skeletal muscle cells tend to persist [14].

We can hypothesise that because preoperative chemotherapy is able to enhance the grade of differentiation, postoperative chemotherapy as well could induce "tumour maturation" and that in our patient, a maturation of residual tumour cells occurred.

Confirmatory evidence to such hypothesis is found in the literature, where a lesion entirely represented by mature skeletal muscle, similar to our relapsing tumour, was reported in the contralateral kidney in two children treated with radiotherapy for WT after surgery [9].

Evidence is therefore accruing that chemotherapy and radiotherapy can ablate the immature components of tumour, operating a sort of selection leading, in some cases, to the exclusive persistence of mature elements [14].

In conclusion, different factors can affect a possible tumour relapse in WT: the morphological and molecular features of the tumour (LOH at 1p and/or 16q, gain 1q, etc.) and/or the therapy effect on the tumour itself. Also, we can consistently hypothesise that two different types of WT recurrences can be recognised: a more undifferentiated one, which usually appears after a short disease-free interval and could be associated to a more aggressive tumour with specific genetic alterations and a worse prognosis, and a second type, eventually related to therapy, presenting a high degree of differentiation and a long disease-free interval after the first diagnosis. The last one generally has an indolent course. The peculiarity of our case consists on the long disease-free interval from the primary tumour, as well as on its morphological well-differentiated features probably induced by chemotherapy.

Acknowledgments Authors wish to thank Dr. Angela Pucci for her technical help and Andrea Grua for the skillful photographic assistance.

This paper was supported by grants from Compagnia di San Paolo "Special Project Oncology".

References

1. Campbell AD, Cohn SL, Reynolds M, Seshadri R, Morgan E, Geissler G, Rademaker A, Marymount M, Kalapurakal J, Haut PR, Duerst R, Kletzel M (2004) Treatment of relapsed Wilms' tumor with high-dose therapy and autologous hematopoietic stem-cell rescue: the experience at Children's Memorial Hospital. J Clin Oncol 22:2885–2890
2. Clausen N (1982) Late recurrence of Wilms' tumor. Med Pediatr Oncol 10:557–561
3. Dome JS, Liu T, Krasin M, Lott L, Shearer P, Daw NC, Billups CA, Wilimas JA (2002) Improved survival for patients with recurrent Wilms tumor: the experience at St. Jude Children's Research Hospital. J Pediatr Hematol Oncol 24:192–198
4. Gibson PJ, Vadeboncoeur CM, Johnston DL (2005) Relapse of Wilms' tumor 13 years after original diagnosis. J Pediatr Hematol Oncol 27:293–294
5. Gottesman JE, Pellettiere EV, Kilmer W (1981) Recurrence of Wilms tumor twenty-three years later. Urology 17:268–269
6. Green DM (2004) The treatment of stages I–IV favorable histology Wilms' tumor. J Clin Oncol 22:1366–1372
7. Grundy PE, Breslow NE, Li S, Perlman E, Beckwith JB, Ritchey ML, Shamberger RC, Haase GM, D'Angio GJ, Donaldson M, Coppes MJ, Malogolowkin M, Shearer P, Thomas PR, Macklis R, Tomlinson G, Huff V, Green DM; National Wilms Tumor Study Group (2005) Loss of heterozygosity for chromosomes 1p and 16q is an adverse prognostic factor in favorable-histology Wilms tumor: a report from the National Wilms Tumor Study Group. J Clin Oncol 23:7312–7321
8. Hing S, Lu YJ, Summersgill B, King-Underwood L, Nicholson J, Grundy P, Grundy R, Gessler M, Shipley J, Pritchard-Jones K (2001) Gain of 1q is associated with adverse outcome in favorable histology Wilms' tumors. Am J Pathol 158:393–398
9. Hughson MD, Hennigar GR, Othersen HB Jr (1976) Cytodifferentiated renal tumors occurring with Wilms' tumors of the opposite kidneys: report of two cases. Am J Clin Pathol 66: 376–389
10. Kalapurakal JA, Dome JS, Perlman EJ, Malogolowkin M, Haase GM, Grundy P, Coppes MJ (2004) Management of Wilms' tumour: current practice and future goals. Lancet Oncol 5:37–46
11. Kim TH, Zaatari GS, Baum ES, Jaffe N, Cushing B, Chard RL Jr, Zwiren GT, Beckwith JB (1985) Recurrence of Wilms' tumor after apparent cure. J Pediatr 107:44–49
12. Li W, Kessler P, Yeger H, Alami J, Reeve AE, Heathcott R, Skeen J, Williams BR (2005) A gene expression signature for relapse of primary Wilms tumors. Cancer Res 65:2592–2601
13. Mikraki V, Yiannoulopoulos G, Moschovi M, Constantinidou-Van Vliet C, Tzortzatou-Stathopoulou F (1996) Late local recurrence of Wilms' tumor. Med Pediatr Oncol 26:71
14. Murphy WM, Grignon JD, Perlman EJ (eds) (2004) Tumors of the kidney, bladder, and related urinary structures. Armed Forces Institute of Pathology (AFIP), Washington, DC, USA
15. Natrajan R, Williams RD, Hing SN, Mackay A, Reis-Filho JS, Fenwick K, Iravani M, Valgeirsson H, Grigoriadis A, Langford CF, Dovey O, Gregory SG, Weber BL, Ashworth A, Grundy PE, Pritchard-Jones K, Jones C (2006) Array CGH profiling of favourable histology Wilms tumours reveals novel gains and losses associated with relapse. J Pathol 210:49–58
16. Perilongo G, Carli M, Fassina A, Colleselli P, Cocito MG, Rebuffi L (1984) Recidiva tardiva di tumore di Wilms. Pediatr Med Chir 6:447–448
17. Gallego-Melcon S, Sanchez de Toledo J, Doste D, Lopez D, Moraga F, Rodriguez C, Vidal T, Bellmunt J (1994) Late recurrent metastasis in Wilms' tumor. Med Pediatr Oncol 23:158–161
18. Williams RD, Hing SN, Greer BT, Whiteford CC, Wei JS, Natrajan R, Kelsey A, Rogers S, Campbell C, Pritchard-Jones K, Khan J (2004) Prognostic classification of relapsing favorable histology Wilms tumor using cDNA microarray expression profiling and support vector machines. Genes Chromosomes Cancer 41:65–79
19. Zuppan CW, Beckwith JB, Weeks DA, Luckey DW, Pringle KC (1991) The effect of preoperative therapy on the histologic features of Wilms' tumor. An analysis of cases from the Third National Wilms' Tumor Study. Cancer 68:385–394

Virchows Arch (2007) 450:119–121
DOI 10.1007/s00428-006-0329-8

CASE REPORT

Cotyledonoid dissecting leiomyoma of the uterus with intravascular growth: report of two cases

Ksenya V. Shelekhova · Dmitry V. Kazakov · Michal Michal

Received: 19 April 2006 / Accepted: 13 October 2006 / Published online: 23 November 2006
© Springer-Verlag 2006

Abstract We present two cases of cotyledonoid dissecting leiomyoma of the uterus with intravascular involvement, which occurred in women aged 73 and 48 years. Grossly and microscopically, both neoplasms had an extrauterine cotyledonoid part and intrauterine dissecting fascicles of disorganized, swirled neoplastic smooth muscle with hydropic degeneration and foci of an intravascular growth (the latter was identified histologically). To our knowledge, the intravascular component of such a neoplasm is a very rare feature that has previously been described only in three cases in the literature.

Keywords Leiomyoma of the uterus · Cotyledonoid · Intravascular · Dissecting · Intravenous leiomyomatosis

Introduction

Cotyledonoid dissecting leiomyoma ("Sternberg tumor") is an unusual type of a benign uterine smooth muscle tumor that combines two main features: an exophytic component of smooth muscle grossly resembling placental tissue and an intrauterine component which irregularly extends into the myometrium between the fascicles of normal smooth muscle cells [1, 3–5, 7, 9]. This is a very rare variant of smooth muscle tumors with a distinctive gross appearance. Approximately 20 cases have been reported in the literature [3–5, 7, 9], and only three cases showed the association of a tumorous tissue with vessels [3]. We describe herein two additional cases of cotyledonoid dissecting leiomyoma of the uterus with intravascular involvement, a very uncommon and infrequent feature to occur in this type of leiomyoma.

K. V. Shelekhova
Department of Pathology, Petrov's Institute of Oncology, Saint-Petersburg, Russia

D. V. Kazakov · M. Michal (✉)
Sikl's Department of Pathology, Charles University, Medical Faculty Hospital, Alej Svobody 80, 30460 Pilsen, Czech Republic
e-mail: michal@medima.cz

Materials and methods

Tissue samples were fixed in 4% formaldehyde and were paraffin-embedded. Sections (5 μm thick) were stained with hematoxylin and eosin.

A panel of immunohistochemical stains included antibodies against CD34 (QBEnd/10, 1:800, Neo Markers), CD31 (JC70A, 1:50, DakoCytomation), factor VIII-related antigen (F8/86, DakoCytomation), α-smooth muscle actin (1A4; 1:1,000, DakoCytomation), muscle-specific actin (HHF35; 1:3,000, DakoCytomation), and desmin (D33, 1:3,000, DakoCytomation).

For electron microscopic investigation, wet glutaraldehyde-fixed tissue was available in one case. It was contrasted in 1% osmium tetroxide and embedded into epoxy resin (Durcupan-Epon). Sections were cut 1 μm thick, stained with toluidine blue, and examined by light microscopy. Appropriate areas were selected, and thin sections were cut and stained with uranyl acetate and lead citrate and were examined with a Philips (Eindhoven, Holland) EM 208S electron microscope.

Fig. 1 Case 2. Gross appearance of the uterus with the exophytic multinodular part of the tumor resembling placental tissue and extending into the broad ligament. The tumorous nodules were originally red in color and appear *brown* here because of long fixation in formalin

Case reports

Case 1 A 73-year-old woman underwent a laparotomy for a uterine mass. Her detailed gynecological history and follow-up were unavailable. Grossly, the tumor measured 8 cm and involved the uterus in the region of the fundus. There were numerous exophytic, rubbery reddish nodules that measured approximately 1.5 cm in diameter, resembled placental tissue, and extended into the broad ligament and projected into the pelvic cavity. Numerous ill-defined yellowish-white subserosal, intramyometrial, and submucosal nodules with a marked hydropic change represented the intrauterine component.

Case 2 A 48-year-old woman, G3, P3 presented with a palpable abdominal mass, for which she underwent a total abdominal hysterectomy and salpingo-oophorectomy. Two years before presentation, the patient was diagnosed with myomatosis of the uterus, and 2 months before surgery, the patient started to experience pain, and the abdominal mass became palpable. She never used hormonal anticonceptives, but in the past, she had had an IUD for 21 years removed 2 years before the diagnosis of myomatosis. The patient was alive and well 2 years after surgery. Macroscopically, the enlarged uterus, measuring 13×10×5 cm, revealed a bulbous tumorous mass measuring 9×4×5 cm, involving the fundus and the cornua, with extension into the broad ligament (Fig. 1). The cut surface of the uterus showed ill-defined intramural nodules of a tumor with variegated coloration. The adnexa were normal both grossly and microscopically.

No intravascular growth was identified on gross examination in either case.

Microscopic and ultrastructural findings

In both cases, there were variably sized micronodules of muscle fascicles, which were composed of disorganized

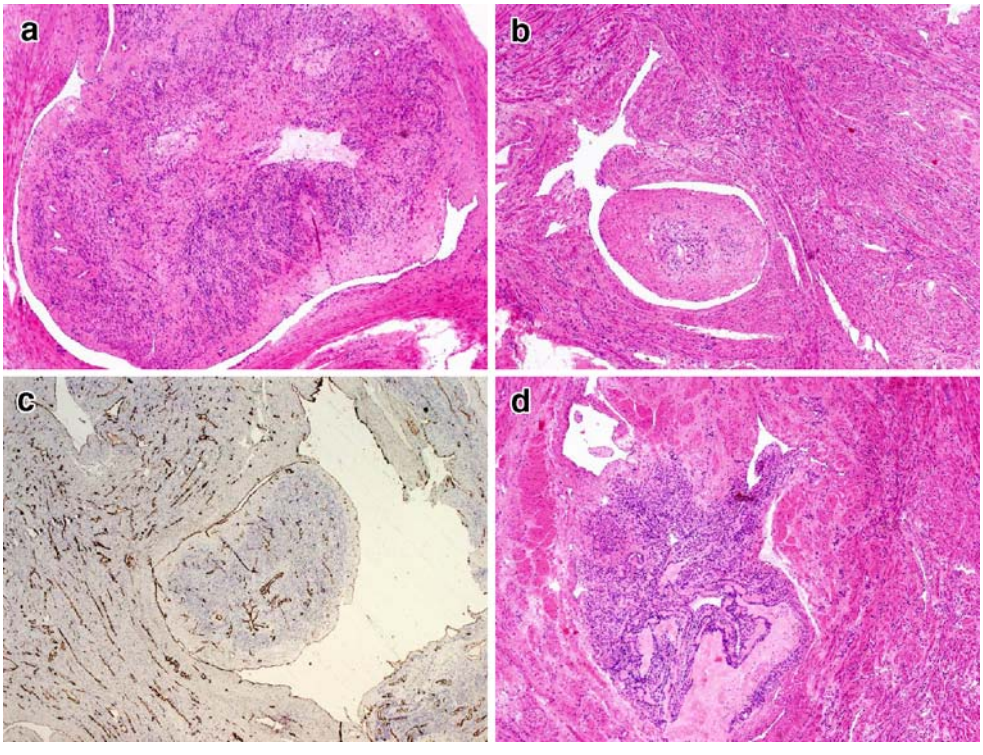

Fig. 2 **a** Case 1. Intravascular extension of leiomyoma. **b** Case 2. Neoplastic leiomyomatous growth into the lumen of the small vein. **c** Case 2. CD31 staining: a tumorous mass in the lumen of the vein. **d** Case 2. Processes of the tumor dissect the myometrium. Note a nodule of swirled smooth muscle surrounded by a hydropic fibrous connective tissue

hypertrophied smooth muscle cells and had a swirled appearance. The tumorous nodules were separated by a connective tissue with marked hydropic change and rich vascularity. Immunohistochemically, the tumor cells exhibited strong staining for desmin and smooth muscle actin.

Within the leiomyomas, we discovered focal intravascular intrusion of the tumor masses. Foci of neoplastic leiomyomatous tissue sometimes entirely filled the lumens of the preexisting veins (Fig. 2a,b). CD31 and factor VIII-related antigen highlighted the endothelial cells of the blood vessels surrounding the foci of the intravascular growth of the leiomyoma (Fig. 2c). In other foci, dissecting tumor areas within the fascicles of normal-appearing myometrium were observed (Fig. 2d). There were neither nuclear atypia nor mitotic figures. No coagulative tumor-cell necrosis was observed. In both cases, mitotic figures were absent or rare (0–1 per 10 high-power fields).

Case 2 was studied ultrastructurally [2]. The tumor was composed of cells that resembled normal smooth muscle cells and showed the characteristic folded nucleus. The cytoplasm contained intermediate filaments and microfilaments with focal densities. There were also abundant collagen fibrils in the matrix.

Discussion

The classification of most benign smooth muscle tumors of the uterus is based on the combination of gross and microscopic features such as growth pattern, histologic appearance, association with vessels, and others [1, 3–7]. Therefore, numerous variants of uterine smooth muscle tumors may be manifestations of a common pathological process.

Roth et al. [7], in 1996, noticed the associations and similarities between intravenous leiomyomatosis, infiltrating leiomyoma, multinodular hydropic leiomyoma, and cotyledonoid dissecting leiomyoma, and in view of these relationships, the authors believed that a cotyledonoid variant of intravenous leiomyomatosis can be anticipated. Indeed, Jordan et al. [3], in 2002, described three cases that demonstrated the features of intravenous leiomyomatosis. The authors regarded this type of leiomyoma as a novel entity and proposed the term “cotyledonoid hydropic intravenous leiomyomatosis”. However, only in one of the three cases reported by Jordan et al. was there an intimate association of the tumorous cells with vessels as detected macroscopically. Earlier, Norris and Pamley suggested that the term “leiomyomatosis” should be applied only to tumors in which intravascular extension could be detected on gross inspection, while lesions with intravascular growth seen only microscopically should be designated as leiomyoma.

An extrauterine cotyledonoid part and intrauterine dissecting fascicles of disorganized, swirled neoplastic smooth muscle with hydropic degeneration and foci of intravascular growth of the tumor characterize both neoplasms described in this report. These features are similar to those detected in previously described cases of Sternberg tumor [4, 5, 7–9]. In our cases, we did not find the intravascular growth macroscopically; hence, following the terminology suggested by Norris and Pamley, we designated both neoplasms reported herein as cotyledonoid dissecting leiomyoma of the uterus with intravascular growth and not as cotyledonoid hydropic intravenous leiomyomatosis.

Foci of an intravascular growth may cause confusion and might imply a malignancy. The tumors however lack nuclear atypia, mitotic activity, or coagulative tumor necrosis, and, besides, well-differentiated smooth muscle cells and the abundance of collagen fibrils in the matrix infer the benign nature of the tumors. However, the small number of reported cases allows no conclusion on the biological course of the lesions. One of our patients was alive and well 2 years after surgery. In the series of Jordan, the follow-up (no evidence of disease at 5 years) was available only for one of the three patients. Further studies are needed to establish the exact biological nature of these tumors.

References

1. Fukunaga M, Ushigome S (1998) Dissecting leiomyoma of the uterus with extrauterine extension. Histopathology 32:160–164
2. Ghadially FN (1985) Diagnostic electron microscopy of the tumours, 2nd edn. Butterworths, London
3. Jordan LB, Al-Nafussi A, Beattie G (2002) Cotyledonoid hydropic intravenous leiomyomatosis: a new variant leiomyoma. Histopathology 40:245–252
4. Kim MJ, Park YK, Cho JH (2002) Cotyledonoid dissecting leiomyoma of the uterus: a case report and review of the literature. J Korean Med Sci 17:840–844
5. Menolascino-Brrata F, Garcia de Barriola V, Navajo de Gomez M, Garcia Tamayo J, Suarez JA, Hernandez Chacon AV (1999) Cotyledonoid dissecting leiomyoma (Sternberg tumor): an unusual form of leiomyoma. Pathol Res Pract 195:435–438
6. Norris HJ, Parmley T (1975) Mesenchymal tumors of the uterus. V. Intravenous leiomyomatosis. A clinical and pathologic study of 14 cases. Cancer 36(6):2164–2178
7. Roth LM, Reed RJ, Sternberg WH (1996) Cotyledonoid dissecting leiomyoma of the uterus: the Sternberg tumor. Am J Surg Pathol 20 (2):1455–1461
8. Roth LM, Reed RJ (2000) Cotyledonoid leiomyoma of the uterus: report of a case. Int J Gynecol Pathol 19(3):272–275
9. Saeed A-Sh, Hanaa B, Faisal AS, Najla A-M (2006) Cotyledonoid dissecting leiomyoma of the uterus: a case report of a benign uterine tumor with sarcomalike gross appearance and review of literature. Int J Gynecol Pathol 25:262–267

Virchows Arch (2007) 450:123–125
DOI 10.1007/s00428-006-0241-2

LETTER TO THE EDITOR

Sporadic subcutaneous angiomyolipoma with expression of estrogen and progesterone receptors

Gaetano Magro · Salvatore Lanzafame

Received: 21 April 2006 / Accepted: 23 May 2006 / Published online: 24 November 2006
© Springer-Verlag 2006

Sir

Angiomyolipoma (AML) is a benign mesenchymal tumor that belongs to the family of the neoplasms with perivascular epithelioid cell differentiation (so-called PEComas) [2]. AML typically involves the kidney, both sporadically or in patients with tuberous sclerosis complex (TSC) [2]. AML may also be seen in association with lymphangioleiomyomatosis (LAM) in patients with or without signs of tuberous sclerosis [6]. Extrarenal AMLs are uncommon and, with the exception of the liver, only rarely they have been reported at other sites, including the bone, colon, heart, lung, parotid gland, skin, adrenal gland, bladder, spermatic cord, uterus, ovary, breast, nasal, oral cavity, retroperitoneum, and mediastinum in patients with or without TSC. Tumors with histological features similar to classic AML and occurring superficially in mucocutaneous sites have been labeled synonimically with the term of "angiomyolipoma or angiolipoleiomyoma", even if they usually occur in men and are not stained with HMB-45 [1, 8]. It has been suggested that these lesions may be better considered as angioleiomyomas with fatty component [1].

AMLs of soft tissues are extremely rare, and the diagnosis of the only four cases reported in literature has not been confirmed by immunostaining with HBM-45 [3–5, 7]. We report a case of subcutaneous AML occurring in the left inguinal region of a 43-year-old woman, without any evidence of associated TSC or lymphangioleiomyomatosis. Tumor was surgically excised and no evidence of recurrence was observed after two-year follow-up period. Grossly, tumor mass, measuring 2 cm in maximum diameter had a lipoma-like appearance. Histological examination revealed an unencapsulated soft tissue tumor composed of an admixture of three different mesenchymal mature tissues: smooth muscle tissue, lipomatous tissue, and blood vessels (Fig. 1a). The smooth muscle component was composed of deeply eosiniphilic spindle cells arranged in intersecting fascicles, intermingling with islands of mature adipocytes (Fig. 1a). In some areas, pale to eosinophilic epitheliod cells, embedded in a fibrous stroma, were arranged in cord-like or trabecular structures (Fig. 1b). Numerous small- to medium-sized thick-walled blood vessels were scattered throughout the tumor (Fig. 1a). Focally, eosinophilic spindle cells were radially oriented around blood vessels, giving the impression of emanating from their smooth muscle layers. Small-sized capillary-like vessels were also focally observed (Fig. 1b). Rare mitoses (1–2 ×10HPF) were seen. Immunohistochemical analyses revealed a diffuse immunoreactivity for vimentin, α-smooth muscle actin (Fig. 1c), desmin, h-caldesmon, and HMB-45 (Fig. 1d) in both spindle and epitheliod smooth muscle cells. It is interesting to note that these cells were diffusely stained with estrogen (ER) and progesterone (PG) receptors (Fig. 1e,f). No immunoreactivity was obtained with pancytokeratins, epithelial membrane antigen, and CD34, while S-100 protein stained adipocytes.

The present paper shows that a tumor with morphological and immunohistochemical features similar to those seen in classical renal AML may occur sporadically in superficial soft tissues. Differential diagnosis mainly included soft tissue myolipoma, and so-called cutaneous–subcutaneous "angiolipoleiomyoma/angioleiomyoma with fatty component" [1, 8]. Although the former tumor may occur in subcutaneous tissue, medium-sized thick-walled blood vessels and immunoreactivity for HMB-45 are

G. Magro (✉) · S. Lanzafame
Dipartimento G.F. Ingrassia, Anatomia Patologica,
Università di Catania,
Catania, Via S. Sofia 87,
95123 Catania, Italy
e-mail: g.magro@unict.it

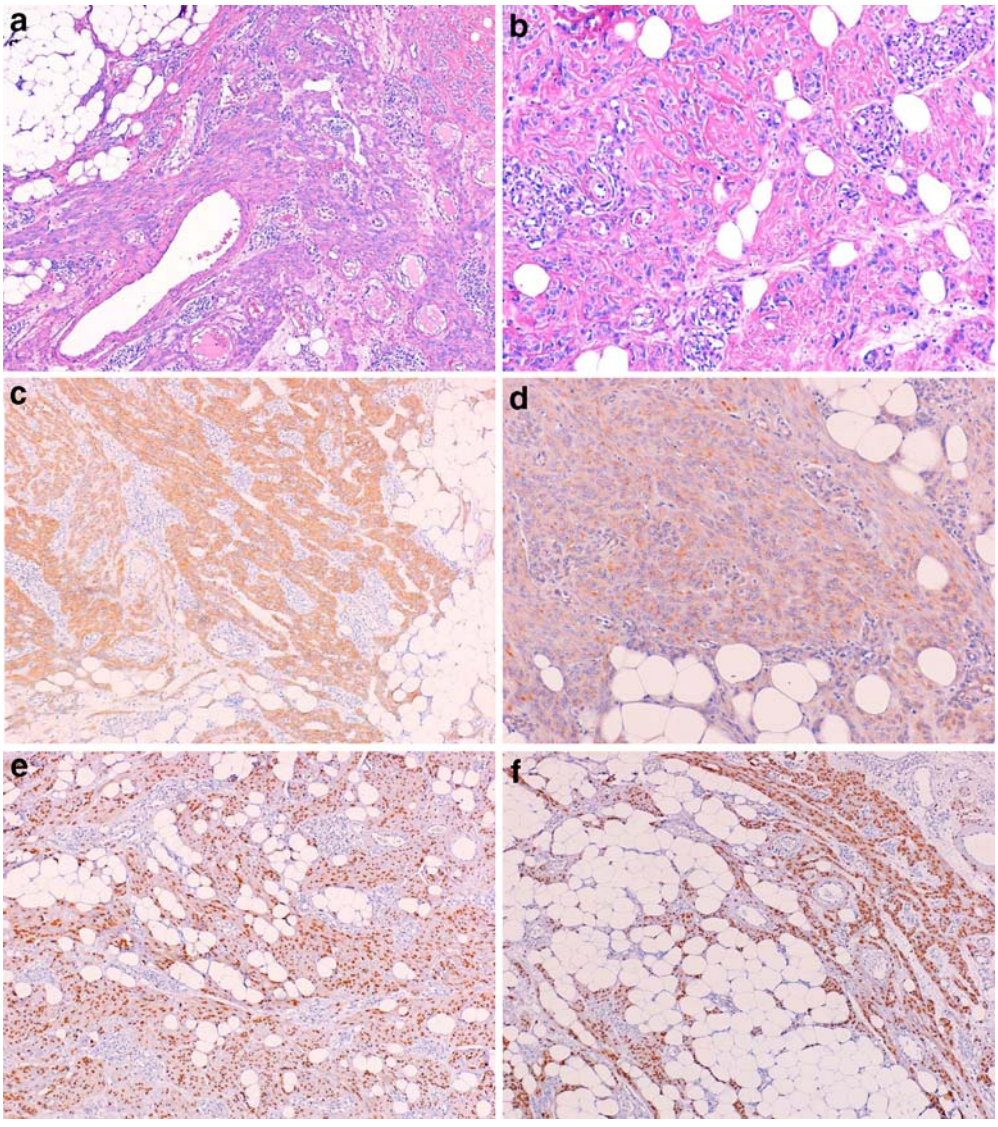

Fig. 1 **a** Tumor was composed of an admixture of smooth muscle cells, adipocytes, and medium-sized blood vessels. **b** Some areas showed epitheliod cells embedded in a fibrous stroma, associated with small islands of adipocytes and nests of small-sized blood vessels. Smooth muscle cells are diffusely stained with α-smooth muscle actin (**c**) and HMB-45 (**d**). A diffuse and strong nuclear immunoreactivity for estrogen (**e**) and progesterone (**f**) receptors is detected in smooth muscle cells

lacking; the latter is a tumor typically occurring in the acral skin or on ear of men, and it is not stained with HMB-45 [1, 8]. Although the diagnosis of classical AML is usually straightford, if such a tumor is in the kidney, potential diagnostic problems may arise when pathologist is faced with this entity in an unexpected location, especially if no medical history of associated tuberous sclerosis is available. We think that subcutaneous AML is not so uncommon than reported, as some tumors, labeled with the terms of "angiolipoleiomyomas or lipoleiomyomas or fibrolipoleiomyomas or even myolipomas" could be reclassified as AMLs by means of immunohistochemistry (HMB-45). In our case, it was noteworthy that smooth muscle cells diffusely expressed both estrogen and progesterone receptors. Although some renal and extrarenal AMLs may variably express ER and PR receptors, the role of steroid hormones in this tumor is still to be clarified. However, the evidence that some renal tumors occasionally grow rapidly during pregnancy, and that both ER and PR receptor expression is more frequent in renal tumors of women with associated LAM [6], suggests that steroid sex hormones may play a role in stimulating the growth of AML. The detection of ER and PR receptors even in a soft tissue AML of a woman with no evidence of LAM or tuberous sclerosis would suggest that steroid hormones could have played an important role in the growth and maintenance of this tumor.

References

1. Beer TW (2005) Cutaneous angiomyolipomas are HMB45 negative, not associated with tuberous sclerosis, and should be considered as angioleiomyomas with fat. Am J Dermatopathol 27:418–421
2. Bonetti F, Pea M, Martignoni G, Zamboni G, Manfrin E, Colombari R, Mariuzzi GM (1997) The perivascular epithelioid cells and related lesions. Adv Anat Pathol 6:343–358
3. Hatori M, Watanabe M, Kokubun S (2005) Angiomyolipoma in the knee—a case report. Ups J Med Sci 110:245–249

4. Huang PC, Chen JT, Ho WL (2000) Clinicopathologic analysis of renal and extrarenal angiomyolipomas: report of 44 cases. Zhonghua Yi Xue Za Zhi (Taipei) 63:37–44
5. Kuroda S, Itoh H, Yamagami T, Kizu O, Murata H, Kusuzaki K, Yamano T, Maeda T (2000) Angiomyolipoma arising in the thigh. Skeletal Radiol 29:293–297
6. Logginidou H, Ao X, Russo I, Henske EP (2000) Frequent estrogen and progesterone receptor immunoreactivity in renal angiomyolipomas from women with pulmonary lymphangioleiomyomatosis. Chest 117:25–30
7. Mahera H, Giamarelou N, Karabela-Bouropoulou V, Samoilis S, Anagnostopoulos D (1997) Soft tissue angiomyolipoma. A case report. Arch Anat Cytol Pathol 45:221–226
8. Makino E, Yamada J, Tada J, Arata J, Iwatsuki K (2006) Cutaneous angiolipoleiomyoma. J Am Acad Dermatol 54:167–171

Virchows Arch (2007) 450:127–129
DOI 10.1007/s00428-006-0297-z

LETTER TO THE EDITOR

Small hepatic vein involvement in IgG multiple myeloma: a very unusual pattern of liver infiltration

Thierry Lazure · Corinne Miceli-Richard · Jérémie Sellam · Monique Fabre · Xavier Mariette · Catherine Guettier

Received: 13 June 2006 / Accepted: 21 August 2006 / Published online: 17 November 2006
© Springer-Verlag 2006

Dear Editor,

We report a unique case of liver involvement in IgG multiple myeloma in a 64-year-old man. The monoclonal plasma cells preferentially surrounded the central hepatic venules whose walls were colonized. As in sinusoidal obstruction syndrome (SOS), the disruption of perivenular sinusoids and small hepatic veins led to lesions of varied ages. Wide hemorrhagic necrosis of perivenular regions and central veins vanishing with perivenular fibrosis were seen throughout the liver. This spread pattern is quite different from the portal, sinusoidal and nodular infiltrations, usually found in liver involvement in multiple myeloma [4].

A 64-year-old man with long past history of IgG kappa monoclonal gammopathy of undetermined significance (MGUS) was admitted to hospital for exploration of hepatomegaly. Clinically, the patient had a homogeneous hepatomegaly without splenomegaly or lymphadenopathy. There was no sign of liver failure nor portal hypertension. Patient did not suffer bone pain. A monoclonal peak in the gamma region on serum protein electrophoresis was subsequently identified as an IgG kappa chain (49 g/l). Levels of IgA and IgM were reduced (0.09 and 0.07 g/l, respectively). Bone marrow aspiration showed 22% dystrophic plasma cells and 1–2% plasmablasts, demonstrating an evolution from MGUS towards plasma cell myeloma. The β2-microglobulin was normal. Bence–Jones protein was present in the urine (0.65 g/24 h) without renal insufficiency. The whole-body computed tomography (CT) scan did not show any lytic bone lesion. The serum calcium level was normal. Blood cell count revealed neutropenia of 1.5×10^9/l, thrombocytopenia with a platelet count of 90×10^9/l and mild anaemia with a haemoglobin concentration of 8.5 g/dl. The count of reticulocytes was low (43×10^9/l). Haptoglobine was ploughed up (0.007 g/l), and the Coombs test (of IgG type) was positive. Haemolytic anaemia was attributed to an autoimmune origin and the lack of regeneration to the infiltration of bone marrow. The liver function tests were indicative of cholestasis with an alkaline phosphatase level of 366 U/l (normal, <130 U/l), a total bilirubine of 25 μmol/l (normal, <17 μmol/l), a gamma glutamate transferase (γGT) of 36 U/l (normal, <60 U/l), an aspartate aminotransferase (AST) of 32 U/l (normal, <40 U/l) and an alanine aminotransferase (ALT) of 20 U/l (normal, <45 U/l). The hepatic Doppler ultrasonography revealed a homogeneous hepatomegaly with a faint hyperechoic pattern. The portal vessels and the hepatic veins were permeable. Hepatoportal blood flow was not inverted. Intra- and extrahepatic bile ducts were normal. There was no hilar or celio-mesenteric adenopathy. The abdominal CT scan did not show a tumor but a heterogeneous enhancement of the liver suggestive of disseminated abnormalities of perfusion, without portal or arterial thrombosis. Ascitis was detected in the Douglas pouch. Corticosteroid treatment alone was initiated for the haemolytic anaemia (1 mg/kg prednisone). The patient left the hospital, and the treatment of myeloma, which was classified stage III (WHO 2001), was scheduled 2 weeks later. However, emergency hospitalization was necessary a few days later for hypothermic shock with back pains, diarrhoea and vomiting, leading to death. An autopsy was performed.

T. Lazure (✉) · M. Fabre · C. Guettier
Service d'Anatomie Pathologique, Hôpital de Bicêtre,
78 rue du Général Leclerc,
F94275 Le Kremlin-Bicêtre, France
e-mail: thierry.lazure@bct.ap-hop-paris.fr

C. Miceli-Richard · J. Sellam · X. Mariette
Service de Rhumatologie, Hôpital Bicêtre,
Université Paris-Sud 11,
Le Kremlin-Bicêtre, France

Macroscopic examination revealed a perforated gastric ulcer, partly fistulised in the transverse colon. The liver weighed 1,975 g (N 1,650 g). Its contours were smooth. The section had a diffuse "nutmeg" pattern. Portal vessels and large sublobular hepatic veins were permeable. The spleen was normal, and there was no lymphadenopathy.

The histopathologic examination highlighted an abnormal plasma cell infiltrate composed of a mixture of mature plasma cells (80%) and plasmablasts (20%) in the bone marrow. The marrow plasmocytosis was about 50%. The kidneys contained scattered interstitial nests of atypical plasma cells, mainly located in the cortex. There was no amyloid deposit. Lymph nodes and spleen were not involved. The liver showed diffuse perivenular lesions of different stages. The chronic lesions were characterized by an obliteration of the central terminal veins by fibrosis that extended in the lobules (Fig. 1). Since portal tracts were uninvolved, bridging perivenular fibrosis from adjacent lobules formed a reverse lobulation. The hepatocytes surrounded by pericellular collagen were atrophic. Nests of atypical plasma cells were scattered in the fibrosis. The mature plasma cells were the most numerous and intermingled with a few plasmablasts. They were stained by CD79a, IgG and kappa and were uniformly negative for lambda, IgA, IgM and IgD. Acute lesions of sinusoidal dilatation and hemorrhagic necrosis coexisted almost everywhere with the chronic lesions. These areas of confluent necrosis were found in the perivenular and midzonal regions (Fig. 2). Central veins were congestive, and their wall was infiltrated by abnormal plasma cells (Fig. 3). The hemorrhagic regions contained atypical plasma cells and a few nests of extramedullary hematopoiesis. Some regenerative nodules similar to those of nodular regenerative hyperplasia were seen. There were neither amyloidosis nor light-chain deposition in liver.

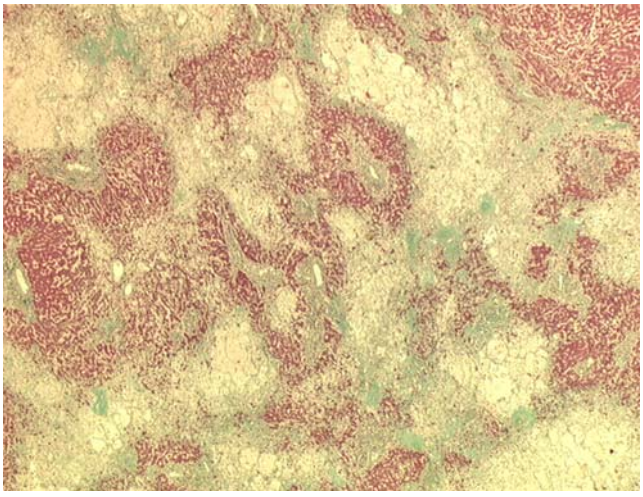

Fig. 2 Prominent perivenular cell necrosis, cell dropout and bridging of necrotic regions between adjacent lobules. Trichrome, ×25

In the literature, extraosseous infiltration by multiple myeloma is found in 25 to 70% of postmortem studies [2, 4]. The sites that are most often involved are spleen, lymph nodes, liver and kidneys. Liver involvement in myeloma seldom reveals the disease but represents the most common hepatic complication [4]. Since it has not been proven to have great therapeutic consequences, an invasive procedure such as liver biopsy is rarely performed. Many cases of liver involvement in multiple myeloma are completely asymptomatic and are discovered only at the time of the autopsy [2]. It has been believed that the liver infiltration was more frequent in the IgA myeloma, but this result was not confirmed in other series [4].

The most frequent clinical symptoms revealing liver involvement by myeloma are hepatomegaly (25 to 60%), jaundice (14%) and ascitis (14%) [2, 4]. The ascitis is probably due to portal hypertension caused either by a

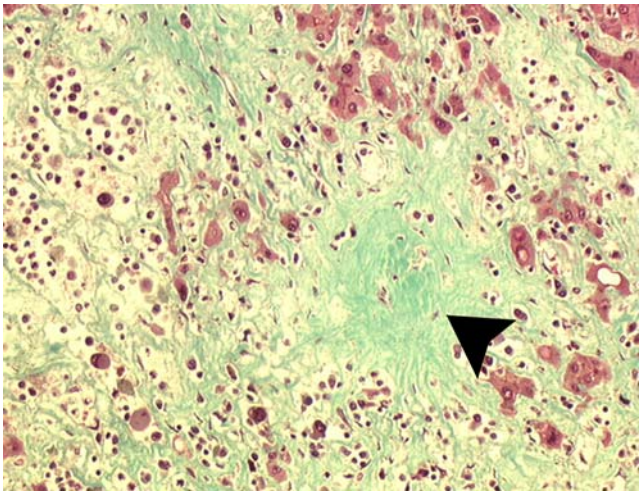

Fig. 1 Perivenular fibrosis with occlusion of the terminal hepatic vein (*arrow*). Some atypical plasma cells are scattered in the fibrosis. Trichrome, ×400

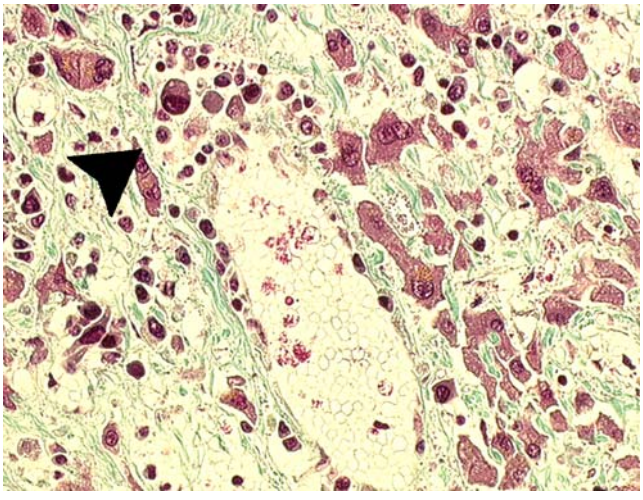

Fig. 3 Small hepatic vein wall disruption by tumoral plasma cells (*arrow*). Trichrome, ×600

sinusoidal block in the massive sinusoidal infiltration or by a pre-sinusoidal block in the event of portal infiltration [4].

Hepatic plasma cell infiltration is accompanied by elevated levels of alkaline phosphatase in 40–85% of cases and constitutes the best predictive biological marker of hepatic involvement. The total bilirubine is increased in 25% of cases. Elevated levels of AST and ALT are found in 25–77 and in 75% of cases, respectively [2]. Fulminant liver failure due to plasma cell infiltration is seldom reported [2]. There is no correlation between laboratory findings and the severity of hepatic lesions, except for the serum alkaline phosphatase level [2, 4]. Abnormal liver function tests may also result from amyloidosis, light-chain deposition disease, extrahepatic cholestasis by infiltration of pancreas or periportal lymph nodes, extramedullary hematopoiesis and liver complications to the treatment of toxic or infectious hepatitis, graft-versus-host disease after allogeneic bone marrow transplantation, SOS, Budd–Chiari syndrome and steatosis [4].

Several patterns of plasma cell infiltration are reported in the liver [2, 4]. They do not depend on the grade and the phenotype of myeloma. The diffuse sinusoidal type is most frequent (60%). Plasma cells lie scattered and/or in small clusters in the sinusoidal lumens. They are free or adhere to the endothelial cells. A perisinusoidal fibrosis is frequently present. The exclusive portal infiltration, as well as the mixed sinusoidal and portal involvement, accounts for approximately 40% of cases. After infiltration of the portal tracts and expansive growth towards central veins and interlobular spaces, nodules of plasma cells become apparent [2, 4]. Exceptional peliotic lesions associated with plasma cells are also reported [1]. To our knowledge, myeloma spreading to the liver with almost exclusive tropism for hepatic terminal venules and perivenular sinusoids has not been previously reported. A SOS coexisting with myelomatous infiltration of the liver is very unlikely because the most common causes of SOS ingestion of pyrrolizidine alkaloids and chemotherapy for neoplasms, with or without bone marrow transplantation [3], are not found in our case. Moreover, a close association between the venular lesions and the presence of tumoral plasma cells was observed. On the contrary, rare hepatic veins not showing endothelial lesions or fibrosis were not infiltrated by plasma cells.

The significance of this infiltration pattern remains obscure. Interactions between endothelial cells and plasma cells may be a possible physiopathological mechanism. Molecules such as VLA-4, LFA-1 and H-CAM present on plasma cells are known to induce the expression of adhesion molecules VCAM-1, ICAM-1, E-selectin and αv integrine on the sinusoidal endothelial cell surface [5, 6]. Other studies showed a "zoning" phenomenon within the hepatic lobule. The expression of adhesion molecules by endothelial cells or hepatocytes under the effect of various stimuli is heterogeneous according to regions of the lobule [6]. Therefore, it can be assumed that the tropism for small central veins is found to be the result of a functional interplay between the plasma cells and the surrounding microenvironment by means of specific adhesion molecules. It has been shown that interactions between liver sinusoidal endothelial cells and tumoral cells result in nitric oxide and other cytotoxic oxidant radicals synthesis and release by endothelial cells [6]. These cytotoxic reagents may finally lead to endothelial cells injury and produce the same effect to that of SOS, i.e. detachment of endothelial cells from lining and embolisation downstream [3]. However, pathogenesis of SOS is quite different. SOS is due to a toxic effect of drugs on sinusoidal endothelial cells involving many factors such as glutathione and nitric oxide depletion, matrix metalloproteinases and vascular endothelial growth factor increase [3].

References

1. Asano S, Wakasa H, Kaise S, Nishimaki T, Kasukawa R (1982) Peliosis hepatis. Report of two autopsy cases with a review of literature. Acta Pathol Jpn 32:861–877
2. Barth C, Bosse A, Andus T (2005) Severe acute cholestatic hepatitis by infiltration of monoclonal plasma cells in multiple myeloma. Z Gastroenterol 43:1129–1132
3. Helmy A (2006) Review article: updates in the pathogenesis and therapy of hepatic sinusoidal obstruction syndrome. Aliment Pharmacol Ther 23:11–25
4. Thomas FB, Clausen KP, Greenberger NJ (1973) Liver disease in multiple myeloma. Arch Intern Med 132:195–202
5. Van Riet I (1999) Homing mechanisms of myeloma cells. Pathol Biol 47:98–108
6. Wang HH, Qiu H, Qi K, Orr FW (2005) Current views concerning the influences of murine hepatic endothelial adhesive and cytotoxic properties on interactions between metastatic tumor cells and the liver. Comp Hepatol 9:4–8

Virchows Arch (2007) 450:131–132
DOI 10.1007/s00428-006-0319-x

LETTER TO THE EDITOR

Reply: mixed germ cell sex cord-stromal tumors of the testis and ovary

Thomas M. Ulbright · Robert H. Young

Received: 22 June 2006 / Accepted: 17 September 2006 / Published online: 16 November 2006
© Springer-Verlag 2006

Dear Editor:

We read with interest the article by Michal et al. [1] describing seven cases of "mixed germ cell sex cord-stromal tumor" of the ovary and testis. Their observations concerning fundamental differences in the nature of this "entity" in the two gonads are in line with our experience. They described morphological, histochemical, and immunohistochemical differences in the germ cell components of the testicular and ovarian cases, noting that, in the testicular cases, the germ cells lacked the "squared-off" cytomorphology of germinoma cells and failed to stain with periodic acid-Schiff and with antibodies directed against the usual markers of neoplastic germ cells (placental alkaline phosphatase, c-kit, and OCT4). These findings contrasted with the germ cell component of the ovarian lesions, which also demonstrated 12p amplification in one case.

The testicular lesions the authors described are similar, if not, in some cases, identical to those we previously reported [2]. We are puzzled, however, by the conclusion of the authors that the testicular lesions are mixed tumors having both neoplastic germ cells and neoplastic sex cord-stromal components. The negative results mentioned above are a powerful argument against the germ cell component being neoplastic; the authors, realizing this contradiction, then hypothesized that the germ cell component is analogous to the germ cells of spermatocytic seminomas. However, convincing evidence to support their hypothesis is not presented. Furthermore, the ages of their patients, averaging 34 years, were similar to the mean of 26 years in our cases, and not what would be expected in a series of tumors related to spermatocytic seminoma. In our cases, we did not identify the "spireme" chromatin characteristic of spermatocytic seminoma, nor did the authors mention this finding in their series.

The authors stated that their cases had "no areas in which the germ cells resembled entrapped cells within testicular tubules or within a sex cord-stromal tumor." They do not, however, provide any actual evidence to support this contention, and in our opinion, no aspect of the appearance of the tumors excludes the possibility of entrapped germ cells in a sex cord-stromal tumor. We do not regard the lack of recognizable tubular configurations of the germ cells as good evidence against entrapment because several of our cases also lacked this finding but had widely scattered germ cells. Still others in our series had foci with tubular-like groupings as well as individually dispersed germ cells throughout the neoplasm. The authors imply that the appearance of the germ cells as "integral" to the tumor means they were not entrapped, but our experience with cases having both widely dispersed individual germ cells as well as tubular groupings of them contradicts this notion. The occurrence of AE1/AE3 cytokeratin expression in the germ cell component of one of their three testicular cases is of interest but could represent a tumor-induced change in

T. M. Ulbright
Department of Pathology,
Indiana University School of Medicine,
Indianapolis, IN, USA

R. H. Young
The James Homer Wright Pathology Laboratories,
Massachusetts General Hospital,
Harvard Medical School,
Boston, MA, USA

T. M. Ulbright (✉)
Clarian Pathology Laboratory,
Room 4014, 350 West 11th Street,
Indianapolis, IN 46202, USA
e-mail: tulbrigh@iupui.edu

nonneoplastic germ cells and, furthermore, was seen in a minority.

In summary, we congratulate the authors on their careful study, but we feel that their conclusions regarding the neoplastic nature of the germ cell component in their testicular cases are not supported by their data. In our opinion, their study not only does not provide objective evidence to rebut our conclusion that these cases represent sex cord-stromal tumors with entrapped, nonneoplastic germ cells but indeed also supports this idea.

References

1. Michal M, Vanecek T, Sima R, Mukensnabl P, Hes O, Kazakov DV, Matoska J, Zuntova A, Dvorak V, Talerman A (2006) Mixed germ cell sex cord-stromal tumors of the testis and ovary. Morphological, immunohistochemical, and molecular genetic study of seven cases. Virchows Archiv 448:612–622
2. Ulbright TM, Srigley JR, Reuter VE, Wojno K, Roth LM, Young RH (2000) Sex cord-stromal tumors of the testis with entrapped germ cells: a lesion mimicking unclassified mixed germ cell sex cord-stromal tumors. Am J Surg Pathol 24:535–542

Virchows Arch (2007) 450:133
DOI 10.1007/s00428-006-0357-4

ANNOUNCEMENTS

© Springer-Verlag 2006

14–17 May 2007
Diagnostic Histopathology of Breast Disease
Hammersmith Hospital (Imperial College), London, UK

A four day long course on the Hammersmith Campus designed for pathologists at Consultant and Senior Trainee level and suitable for the final examination for MRCPath. The course will provide a comprehensive coverage of the histopathology of breast disease, with special emphasis on areas which pose diagnostic difficulties. The course is based, historically, on the extensive referral collection of Professor JG Azzopardi, to which has been added new cases from Charing Cross, Nottingham City and Addenbrooke's Hospitals. The course will be slanted to practical diagnostic pathology with a specific session dealing with problems encountered in core biopsies and a special workshop dealing with the interpretation of HER2 immunostaining. The participants will be given ample time to study histological preparations, followed by illustrated discussions of the cases. In addition there will be several daily talks on specific topics, given by eminent breast pathologists and followed by discussions. The topics will include: new issues in the interpretation of breast biopsies, breast immunohistochemistry, problematic breast lesions, dealing with the gross specimen, fibro-epithelial, spindle cell and papillary lesions, proliferative lesions/carcinoma in-situ, sentinel lymph node biopsy and the impact of molecular genetics on diagnostic breast pathology. The faculty will include Anthony Douglas-Jones, Ian Ellis, Bharat Jassani, Andrew Lee, Sarah Pinder, Jorge Reis-Filho and Sami Shousha.

For further information please contact:
Sandra Lock
Department of Histopathology
Hammersmith Hospital
Du Cane Road
London W12 0NN, UK
Tel: +44 (0)20 8383 3292
Fax: +44 (0)20 8740 7417
E-mail: histopathology.shortcourses@imperial.ac.uk

Virchows Arch (2007) 450:135–141
DOI 10.1007/s00428-006-0355-6

ORIGINAL ARTICLE

Elevated expression of cyclooxygenase-2 is a negative prognostic factor for overall survival in intrahepatic cholangiocarcinoma

Klaus Jürgen Schmitz · Hauke Lang · Jeremias Wohlschlaeger · Henning Reis · Georgios Charalambos Sotiropoulos · Kurt Werner Schmid · Hideo Andreas Baba

Received: 17 August 2006 / Revised: 17 October 2006 / Accepted: 19 November 2006 / Published online: 13 December 2006
© Springer-Verlag 2006

Abstract The production of prostaglandins is regulated by cyclooxygenases (COXs), which also have a role in tumour development and progression in various human malignancies, including cholangiocarcinoma. Limited information is available of the correlation of COX-2 protein expression and prognosis in intrahepatic cholangiocarcinoma (ICC). The aim of the present study was to determine the clinical significance of COX-2 expression in ICC. In addition the correlation of COX-2 expression and apoptosis/proliferation was analysed. COX-2 expression was determined immunohistochemically in 62 resected ICCs. Proliferation was assessed using Ki67-immunohistochemistry, and apoptosis was measured with the TdT-mediated dUTP nick-end-labelling technique. COX-2 was identified as an independent prognostic factor (P=0.028) in resected ICC by survival analysis. High levels of COX-2 expression were found to be associated both with reduced apoptosis and increased proliferation of tumour cells. This study demonstrates the independent prognostic value of the COX-2 expression in resected ICC, thus, offering a potential additional adjuvant therapeutic approach with COX-2 inhibitors.

Keywords Cancer · Mol path · Immunohistochem

K. J. Schmitz · J. Wohlschlaeger · H. Reis · K. W. Schmid · H. A. Baba (✉)
Institute of Pathology and Neuropathology,
University Hospital of Essen, University of Duisburg-Essen,
Hufelandstr. 55,
45147 Essen, Germany
e-mail: hideo.baba@uk-essen.de

H. Lang · G. C. Sotiropoulos
Department of General, Visceral and Transplantation Surgery,
University Hospital of Essen, University of Duisburg-Essen,
Essen, Germany

H. Lang · K. W. Schmid
West German Cancer Centre Essen (WTZE),
Essen, Germany

Introduction

Cholangiocarcinoma (CCC) is composed of cells resembling those of bile ducts. CCC arises either from the extrahepatic duct including the hilar bifurcation or from the intrahepatic ducts. Intrahepatic cholangiocarcinoma (ICC) is less frequent than extrahepatic bile duct carcinoma but second among primary malignant liver tumours after hepatocellular carcinoma. In Western countries, ICC accounts for about 10% of the primary liver malignancies with increasing incidence in the last two decades [24]. The identification of patients with most aggressive ICC might help to optimise surgical treatment and avoid unnecessary surgical therapy. Therefore, it is desirable to identify molecular markers that individually predict tumour behaviour and may facilitate an individualized therapy.

Among the potential prognostic parameters, cyclooxygenase (COX)-2 is of particular interest, as it may also offer the option of treatment with nonsteroidal anti-inflammatory drugs (NSAIDs) [15]. COXs regulate the synthesis of prostaglandins and are, thus, the major target of NSAIDs. Its two isoforms (COX-1 and COX-2) have different expression patterns, with COX-1 being expressed in a broad variety of tissues. COX-2 has been shown to participate in tumour development and progression [11, 21]. Both elevated COX-2 messenger RNA (mRNA) and protein levels were found to be raised in ICC [3, 9]. There exist only few studies dealing with the potential prognostic

value of the COX-2 expression. A small study with only 24 cases of CCC could not prove a significant association with survival; however, this study did not discriminate between extra- and intrahepatic cholangiocarcinoma [12]. Another study on *extrahepatic* cholangiocarcinoma failed to demonstrate a correlation of the COX-2 expression and the patients' outcome in CCC [16]. In the present study, COX-2 expression was determined by immunohistochemistry in one of the largest contemporary series of consecutive resected ICC. The findings were correlated with a broad range of clinicopathological features. Recent observations suggest that COX-2 overexpression may cause a prostaglandin E2-mediated inhibition of apoptosis in CCC. Moreover, COX-2 overexpression was shown to increase cell growth by the activation of E series of prostaglandins (EP receptors) [8, 31]. Thus, apoptosis and proliferation was determined in this series to monitor a putative imbalance between cell death and cell proliferation induced by COX-2 protein overexpression [26].

Materials and methods

Between August 1998 and August 2006, a total of 62 patients with a mean age of 58±11.5 years were available for this study. The study comprised consecutive patients who underwent surgery for liver resection. Patients solely undergoing an explorative laparatomy without subsequent resection were excluded from the study. Patients with hilar cholangiocarcinoma, gallbladder carcinoma, or mixed hepato/-CCC and liver cirrhosis were also excluded from the study. The diagnosis of ICC was based on histology by the examination of the resected liver specimen. The tumours were classified according to the pathologic TNM (pTNM) system (sixth edition) [28]. Detailed clinical data was available including preoperative therapy, operative details, and pathological findings including surgical radicability, tumour staging, and clinical follow-up. One patient suffered from primary sclerosing cholangitis without cirrhosis; hepatolithiasis was not present in any case. Data were completed by August 2006, and minimum follow-up was every six months or until death. The median length of the follow-up was 12 months.

Immunohistochemistry

Immunohistochemistry was performed with an automated staining device (Dako Autostainer, Glostrup, Denmark).

Cyclooxygenase-2

In this study, a monoclonal rabbit anti-human COX-2 antibody (DCS, Hamburg, Germany) was used. Immunohistochemistry was performed on 5-μm-thick paraffin, and antigen retrieval was carried out with 0.01-M citrate buffer at pH 6.1 for 20 min in a hot water bath (95°C). The primary antibody was incubated for 30 min at 1:250 dilution. Antibody demonstration was achieved using the commercially available anti-mouse IgG detection kit (EnVision, DakoCytomation, Carpenteria, CA, USA) The replacement of the primary antibodies by mouse immunoglobin served as negative controls. Positive controls (colorectal carcinoma) were included in each staining series. In ICC, COX-2 was scored according to the amount of positive stained tumour cells. One complete tumour slide was examined for specific cytoplasmic COX-2 immunostaining. If none or less than 10% of the tumour cells showed specific COX-2 immunostaining regardless of staining intensity, the case was classified as negative. The cases with 11–50% of the positively stained tumour cells were classified as moderately positive and tumours with more than 50% stained tumour cells as strongly positive.

Ki67 immunostaining and TdT-mediated dUTP nick-end labelling

Ki67 immunohistochemistry was performed on 5-μm-thick paraffin sections. Dewaxed and rehydrated sections were incubated with hydrogen peroxide to block endogenous peroxidase. After the antigen retrieval in a hot water bath, the prediluted monoclonal anti-Ki67 antibody (Biogenex, San Ramon, USA) was incubated for 30 min; antibody demonstration was performed with the commercially available anti-mouse IgG detection kit (EnVision, DakoCytomation). The replacement of the primary antibodies by mouse immunoglobin served as negative controls.

The growth fraction was defined as the percentage of Ki67-positive, randomly chosen nuclei per 600 tumour cells. In situ DNA fragmentation was established using the terminal desoxyribonucleotide transferase TdT-mediated dUTP nick-end-labelling technique (TUNEL) in paraffin-embedded sections. We used ApoTag™ plus peroxidase in situ apoptosis detection kit (Intergen). The staining procedures were performed according the manufacturer's recommendations. The percentage of the stained apoptotic tumour cells per 600 randomly chosen tumour cells was calculated. To avoid miscounting of the necrotic cells, corresponding H&E sections were examined.

Statistical analysis

COX-2 immunostaining was assessed by two of the authors (K.J.S., H.R.) in a blind-trial fashion without knowledge of the clinical outcome. In case of disagreement, slides were re-evaluated by both investigators until agreement was reached. All data were converted to a PC and statistically

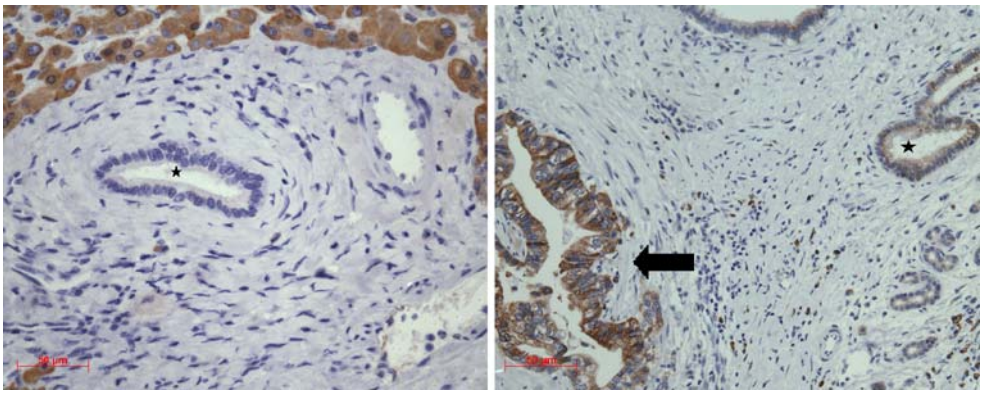

Fig. 1 Immunostaining for COX-2 in noncancerous intrahepatic bile duct epithelial cells. Whereas portal bile ducts distant from the ICC consistently lacked COX-2 immunostaining (*asterisk*, *left side*), bile duct epithelial cells (*asterisk*, *right side*) adjacent to ICC (*arrow*) exhibited cytoplasmic immunoreactivity of varying intensity. Notice the COX-2 protein expression in normal hepatocytes. Original magnification, ×400

analysed using SPSS version 12 for Windows Statistical Package for Social Sciences, Chicago, IL, USA.

The kappa coefficient of the inter-observer agreement was calculated for the semiquantitative COX-2 immunostaining results; the interpretation of the kappa value was performed using the commonly cited scale of Landis and Koch [19]. The interobserver agreement of COX-2 immunostaining was substantial (kappa=0.73). Relationships between ordinal parameters were investigated using the two-tailed χ^2 analysis (or the Fisher's exact test where patient numbers were small). The relationship between categorical data (e.g. COX-2) and numeric data (e.g. number on Ki-67 positive tumour cells) was determined using the ANOVA test. The overall survival (OS) curves were estimated using the Kaplan–Meier method, and any differences in the survival curves were compared by the log-rank test. For multivariate analysis, the COX regression model was used. Overall, 95% confidence intervals were used throughout.

Results

COX-2 immunohistochemistry

The COX-2 immunostaining was located in the cytoplasm of epithelial cells. The plasma cells exhibited a positive cytoplasmic immunostaining, serving as internal control. Noncancerous intrahepatic bile duct epithelial cells next to invasive cancer showed frequently a positive COX-2 immunoreactivity, whereas no COX-2 staining could be detected distant from the tumour (Fig. 1). Hepatocytes near and distant from ICC revealed a positive staining in all cases. In all, 12 (19.4%) tumours were classified as negative, 25 (40.3%) as moderately positive, and 25 (40.3%) as strongly positive. Epithelial tumour cells exhibited a broad range of COX-2 immunoreactivity with a complete lack of staining or a specific and strong granular cytoplasmic COX-2 immunostaining (Fig. 2). COX-2 staining was not associated with any of the investigated clinicopathological parameters (Table 1).

Clinical outcome by COX-2 expression

OS dependent on COX-2 expression was analysed using Kaplan–Meier survival (n=62; p=0.036; Fig. 3). Patients with a strong COX-2 expression exhibited a significantly decreased OS, whereas patients classified as COX-2 negative revealed the most favourable OS. The unfavourable prognostic effect of tumours with elevated COX-2 protein expression remained in the subgroup of patients with primarily R0-resected ICC (n=39; p=0.038).

The parallel univariate survival analysis showed a significant association of the resection status (p<0.001), multifocal tumour growth (p=0.005), higher International Union

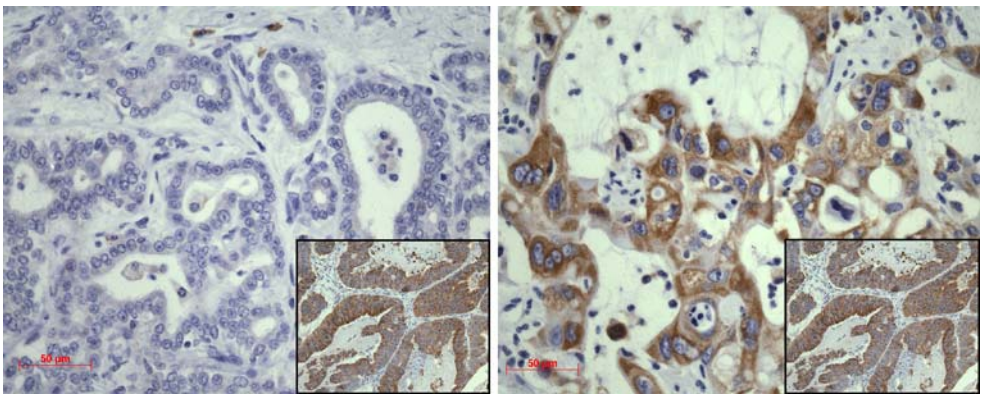

Fig. 2 Representative COX-2 immunostaining results in ICC. Missing COX-2 staining (*left*) in contrast to strong cytoplasmic COX-2 immunoreactivity in ICC tumour cells (*right*). Original magnification, 400×. *Inset*: positive control (colorectal carcinoma) with strong immunostaining

Table 1 COX-2 expression, demographic characteristics, and clinicopathological characteristics in 62 patients of the resected ICC

	All	COX-2 negative	COX-2 moderate	COX-2 strong	*P* values
n (%)	62	12 (19.4)	25 (40.3)	25 (40.3)	
Gender (male/female)		7/5	9/16	10/15	0.422
Mean age at diagnosis (*y*±SD)	58.8±11.5	52±12.1	60.4±9.8	60.6±11.8	0.067
Grading					0.612
G1 (*n*%)	2 (3.2)	0 (0)	2 (100)	0 (0)	
G2 (*n*%)	41 (66.1)	7 (17.1)	15 (36.6)	19 (46.3)	
G3 (*n*%)	19 (30.6)	5 (26.3)	8 (42.1)	6 (31.6)	
UICC stage grouping					0.277
I	16	6 (37.5)	3 (18.8)	7 (43.8)	
II	3	0 (0)	1 (33.3)	2 (66.7)	
IIIA,B,C	38	5 (13.2)	19 (50)	14 (36.8)	
IV	5	1 (20)	2 (40)	2 (40)	
Staging					0.390
T1 (n,%)	21	7 (33.3)	5 (23.8)	9 (42.9)	
T2 (n,%)	7	0 (0)	4 (57.1)	3 (42.9)	
T3 (n,%)	28	4 (14.3)	13 (46.4)	11 (39.3)	
T4 (n,%)	6	1 (16.7)	3 (50)	2 (33.3)	
Lymph vessel infiltration					0.121
L0	47	7 (14.7)	18 (38.3)	22 (46.8)	
L1	15	5 (33.3)	7 (46.7)	3 (20)	
Blood vessel infiltration					0.916
V0	39	8 (20.5)	15 (38.5)	16 (41)	
V1	23	4 (17.4)	10 (43.5)	9 (39.1)	
Nodal status[a]					0.281
0	37	10 (27)	15 (40.5)	12 (32.4)	
1	21	2 (9.5)	10 (47.6)	9 (42.9)	
Distant metastasis					0.999
No	57	11 (19.3)	23 (40.4)	23 (40.4)	
Yes	5	1 (20)	2 (40)	2 (40)	
Solitary tumour[b]	32	7 (21.9)	11 (34.4)	14 (43.8)	0.545
Multifocal tumour	29	5 (17.2)	14 (48.3)	10 (34.5)	
Tumour size	8.1	8.75±4.3	8.3±2.9	7.4±3.6	0.506
Resection status					0.627
R0	39	9 (32.1)	15 (38.5)	15 (38.5)	
R1/2[c]	23	3 (13)	10 (43.5)	10 (43.5)	

P values were calculated using chi-square analysis and ANOVA for continuous variables
[a] Data available for 58 patients; [b] data available for 61 patients; [c] 20 cases were classified R1, only 3 were R2

Against Cancer (UICC) stage (p=0.012), and vascular invasion (p=0.011) with a reduced OS. Table 2 shows the mean OS for all patients in the various subgroups.

To clarify the independent prognostic value of the COX-2 expression in the patients with resected ICC, a multivariate analysis of the relevant parameters was performed. The COX regression analysis revealed the R-classification to be the best prognostic factor for OS followed by the COX-2 expression (Table 3).

COX-2 and apoptosis/proliferation

There were significant lower mean numbers of apoptotic tumour cells per 600 tumour nuclei in tumours with strong COX-2 expression in contrast to tumours with moderate or negative COX-2 immunoreactivity (Table 4). In contrast, the proliferative activity increased in tumours with high levels of COX-2, reflected by a higher mean value of proliferating tumour cells. However, due to a substantial overlap of values, statistical significance was not reached.

Discussion

CCC is a devastating cancer of the hepatic biliary tract. The assessment of the individual prognosis of ICC patients may be helpful to optimise decision making for surgical treatment and avoid unnecessary surgical therapy. At present, surgical therapy remains the only curative treatment for ICC; thus, novel therapeutic strategies for this aggressive cancer are necessary. This study on a large series of 62 patients with resected ICC showed the independent

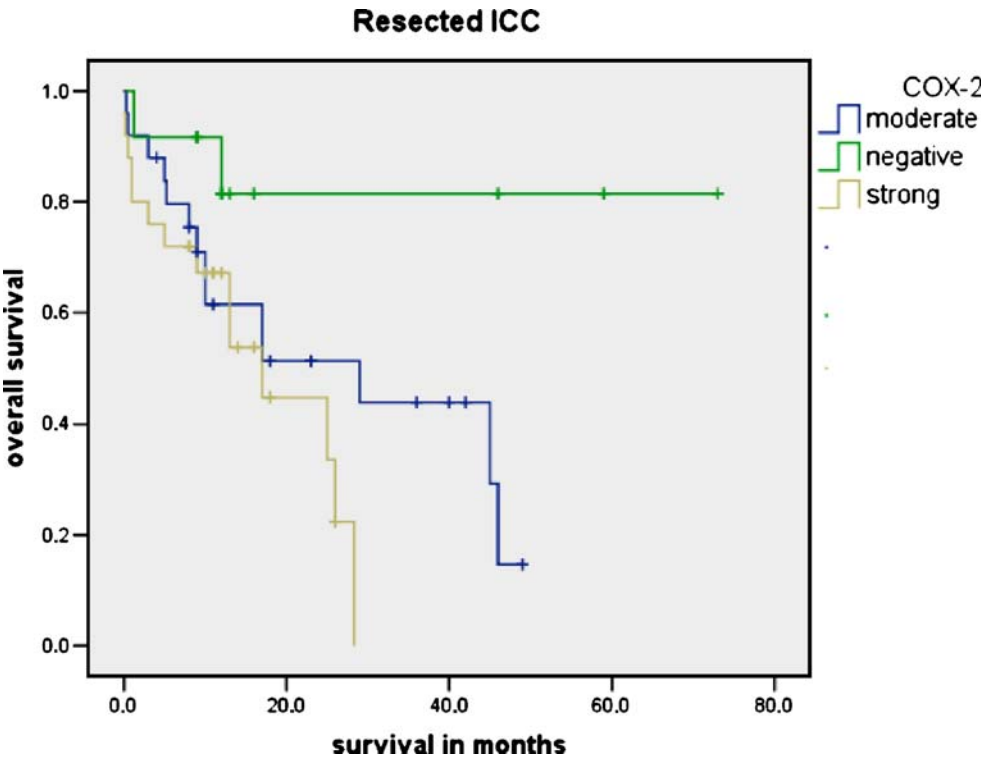

Fig. 3 Kaplan–Meier survival curves in resected intrahepatic cholangiocarcinoma in relation to different COX-2 expression. Tumours with elevated COX-2 levels exhibit a significantly decreased overall survival (p= 0.036, Log Rank test)

prognostic value of immunohistochemically determined COX-2 protein expression, thus, offering a potential additional adjuvant therapeutic approach with COX-2 inhibitors. Elevated COX-2 expression was associated with a marked reduced OS in multivariate analysis. The main advantage of our study is the large number of patients (n= 62) in combination with a high homogeneity of this series composed of consecutively resected ICC. A previous study on *extrahepatic* cholangiocarcinoma failed to demonstrate a relation of COX-2 expression with clinical outcome [16]. This suggests (genetic) differences depending on the site of origin within the biliary tract. Mutations of the *RAS* and *TP53* genes are the most common genetic abnormalities identified both in ICC and cancer of extrahepatic bile duct (BDC) [13, 14, 16, 20, 29]. However, recent studies disclosed genetic differences regarding p53 protein over-expression among carcinomas of the proximal (ICC) and distal bile ducts (BDC), indicating different patterns of the inactivation of tumour-suppressor genes [1]. Because cell line studies suggest COX-2 both as an effector and inhibitor of the tumour suppressor p53 or DNA-damaging agents [4, 7], different genetic patterns in ICC and BDC, with varying induction of COX-2 gene/protein expression, might explain the diverse clinical impact of COX-2 in ICC and BDC.

A small study on 24 patients with CCC failed to show a prognostic significance of the COX-2 expression [12]. However, the power of this study is limited due to two reasons: (1) The authors did not discriminate between extra- and intrahepatic cholangiocarcinoma, and (2) the statistical power of a small series with 24 patients is very low. However, Javle et al. [12] demonstrated in their study that the median survival time of patients with low COX-2 expression was more than twice as high than that of patients with high COX-2 expression. This finding is in accordance with our results identifying COX-2 overexpression as a predictor of reduced OS. Javle et al. found COX-2 to be

Table 2 Mean overall survival in relation to different patient subgroups

Subgroups	Mean overall survival in all ICC patients (months)
All patients	16.5
R0-resected patients	19.7
R1-resected patients	11.4
R2-resected patients	9.3
COX-negative patients	22.8
Moderate COX-2 expression	18.7
Strong COX-2 expression	11.4

Table 3 Multivariate COX regression analysis for overall survival in 62 patients with resected intrahepatic cholangiocarcinoma

	HR (95% CI)	*P* values
pTstage I–II/III–IV	1.63 (0.44–6.02)	0.465
UICC I–II, III–IV	1.20 (0.62–2.35)	0.589
Multifocality, solitary/multifocal	1.26 (0.41–3.89)	0.689
Resection status, R0/R1, R2[a]	3.08 (1.27–7.44)	0.012
Vascular invasion, V0/V1	1.98 (0.88–4.41)	0.095
COX-2, negative/moderate/strong	1.07 (1.07–3.49)	0.028

[a] Twenty cases were classified R1, only three were R2

Table 4 Apoptosis (TUNEL) and proliferative activity (Ki67) in relation to COX-2 expression

	All (mean value/SD)	COX-2 negative	COX-2 moderate/ strong	*P* values
Apoptosis (percentage of positive tumour cells)	2.17±2.40	3.84±4.04	1.76±1.73	0.028
Growth fraction (percentage of Ki67 positive tumour cells)	9.74±7.37	8.55±8.41	9.99±7.34	0.486

P values were calculated using ANOVA for continuous variables

expressed in all 24 ICC, whereas in our study, only 81% of ICC exhibited an either moderate or strong COX-2 expression. Kim et al. [16] found COX-2 to be overexpressed in only 52% of the examined extrahepatic cholangiocarcinomas. These discrepancies are likely to be caused by differences in antigen retrieval and varying scoring systems, emphasizing the relevance of standardized protocols and immunoscores.

Previous studies suggest COX-2 overexpression as an early carcinogenetic event in the human biliary tract and pointed out that COX-2 expression was highest in more differentiated CCC, whereas COX-2 expression decreased with the loss of differentiation [5]. Our study did not reveal a significantly increased COX-2 expression in tumours with higher differentiation. Nevertheless, a detailed analysis of our data rather supports this notion. The group of well and moderately differentiated tumours exhibited the highest amount of cancers classified as strongly COX-2 positive (44.2%) in contrast to ICC with poor tumour differentiation (31.6%). On the other hand, we found the lowest levels of COX-2 expression to be more frequent in poorly differentiated tumours (26.3%) in contrast to well or moderately differentiated ICC (16.5%). The study by Kim et al. [16] on 102 extrahepatic cholangiocarcinoma describes no significant differences in terms of tumour differentiation. In the light of these varying data, one should be careful not to draw premature conclusions about the differential expression COX-2 protein in ICC.

The clinical conditions associated with ICC include parasitic liver fluke infestations, hepatolithiasis, which is frequently observed in clonorchiasis [10], nonbiliary cirrhosis, and primary sclerosing cholangitis [30]. It would be interesting to compare the levels of COX-2 expression in ICC with or without these established associated clinical risk factors. However, our series is not suitable to answer this question because all cases with liver cirrhosis, regardless of its origin, were excluded from our study to maintain the high homogeneity of our cohort and rule out cirrhosis- related influence on patient survival. As a consequence, this series comprises only one patient with associated primary sclerosing cholangitis. Patients with liver fluke infestations and associated hepatolithiasis were not present in this series because our cohort is composed from patients living in western Europe.

Interestingly, we found the up-regulation of COX-2 protein expression not only in cancerous epithelial cells but also in noncancerous epithelial cells adjacent to invasive cancer. Noncancerous epithelial cells distant from the ICC lacked COX-2 immunostaining. This staining pattern is in accordance with the results of Hayashi et al. [9]. The elevated expression of COX-2 in bile duct epithelial cells adjacent to invasive cancer is not surprising, as inflammation often accompanies invasive cancer and inflammatory cytokines such as IL-1α [22], IL-1β [2], or TNF-α are believed to induce COX-2 gene at the transcriptional level [23]. We observed a constant positive specific immunostaining in normal hepatocytes regardless of the distance to the ICC. This finding is in agreement with previous studies documenting elevated COX-2 protein and mRNA expression in nontumourous liver [3, 17].

Against the background of NSAIDs, recent studies have evaluated selective COX- inhibitors for their effect on CCC cells cell growth and invasion in vitro and in nude mice [6, 18, 27, 32, 33]. The treatment with COX-2 inhibitors resulted in induced apoptosis and inhibited proliferation. The mechanisms by which COX-2 contributes to the poor prognosis in variety of human cancers have not been completely elucidated yet. COX-2 has been shown to contribute to both tumourigenesis and the malignant phenotype of tumour cells by different mechanisms, including (1) the inhibition of apoptosis by the activation of the PI3-Kinase/Akt pathway and increased production of PGE2, leading to increased expression of Bcl-2 and attenuation of nitric oxide signalling, (2) increased angiogenesis by increased PGE2 production with subsequent vascular endothelial growth factor production, (3) increased invasiveness by the overexpression of CD44, and (4) increased cell growth by the activation of EP receptors [8, 31]. The above mentioned effect of COX-2 overexpression on apoptosis and proliferation can be confirmed in our study. COX-2 over-expressing ICC revealed a significantly decreased apoptosis and a higher mean value of proliferating tumour cells, although the latter finding did not reach statistical significance. This finding suggests an impaired balance between cell loss and cell gain, resulting in a shift towards tumour net tumour growth due to increased apoptosis. The observed decrease of apoptosis in COX-2 overexpressing ICC might be due to the PGE2-mediated induction of the antiapoptotic protein Bcl-2 and increased NFκB transcriptional activity, which is a key antiapoptotic mediator [25, 26].

In conclusion, this study demonstrates the independent prognostic value of immunohistochemical COX-2 protein

expression in resected ICC, thus, offering a potential additional adjuvant therapeutic approach with COX-2 inhibitors and facilitating an optimised therapeutic strategy. Our results suggest that COX-2 overexpression causes a shift towards increased tumour cell proliferation and decreased apoptosis contributing to the unfavourable clinical course.

Acknowledgement The technical assistance of Dorothe Möllmann, Gabi Ladwig, Renate Kern, and Nicole Cramer und Karin Scholz is gratefully acknowledged.

References

1. Argani P, Shaukat A, Kaushal M, Wilentz RE, Su GH, Sohn TA, Yeo CJ, Cameron JL, Kern SE, Hruban RH (2001) Differing rates of loss of DPC4 expression and of p53 overexpression among carcinomas of the proximal and distal bile ducts. Cancer 91:1332–1341
2. Belvisi MG, Saunders MA, Haddad E, Hirst SJ, Yacoub MH, Barnes PJ, Mitchell JA (1997) Induction of cyclo-oxygenase-2 by cytokines in human cultured airway smooth muscle cells: novel inflammatory role of this cell type. Br J Pharmacol 120:910–916
3. Chariyalertsak S, Sirikulchayanonta V, Mayer D, Kopp-Schneider A, Furstenberger G, Marks F, Muller-Decker K (2001) Aberrant cyclooxygenase isozyme expression in human intrahepatic cholangiocarcinoma. Gut 48:80–86
4. Choi EM, Heo JI, Oh JY, Kim YM, Ha KS, Kim JI, Han JA (2005) COX-2 regulates p53 activity and inhibits DNA damage-induced apoptosis. Biochem Biophys Res Commun 328:1107–1112
5. Endo K, Yoon BI, Pairojkul C, Demetris AJ, Sirica AE (2002) ERBB-2 overexpression and cyclooxygenase-2 up-regulation in human cholangiocarcinoma and risk conditions. Hepatology 36:439–450
6. Han C, Leng J, Demetris AJ, Wu T (2004) Cyclooxygenase-2 promotes human cholangiocarcinoma growth: evidence for cyclooxygenase-2-independent mechanism in celecoxib-mediated induction of p21waf1/cip1 and p27kip1 and cell cycle arrest. Cancer Res 64:1369–1376
7. Han JA, Kim JI, Ongusaha PP, Hwang DH, Ballou LR, Mahale A, Aaronson SA, Lee SW (2002) P53-mediated induction of Cox-2 counteracts p53- or genotoxic stress-induced apoptosis. EMBO J 21:5635–5644
8. Hawk E, Lubet R, Limburg P (1999) Chemoprevention in hereditary colorectal cancer syndromes. Cancer 86:2551–2563
9. Hayashi N, Yamamoto H, Hiraoka N, Dono K, Ito Y, Okami J, Kondo M, Nagano H, Umeshita K, Sakon M, Matsuura N, Nakamori S, Monden M (2001) Differential expression of cyclooxygenase-2 (COX-2) in human bile duct epithelial cells and bile duct neoplasm. Hepatology 34:638–650
10. Hou PC (1955) The pathology of *Clonorchis sinensis* infestation of the liver. J Pathol Bacteriol 70:53–64
11. Howe LR, Subbaramaiah K, Brown AM, Dannenberg AJ (2001) Cyclooxygenase-2: a target for the prevention and treatment of breast cancer. Endocr Relat Cancer 8:97–114
12. Javle MM, Yu J, Khoury T, Chadha KC, Iyer RV, Foster J, Kuvshinoff BW, Gibbs JF, Geradts J, Black JD, Brattain MG (2006) Akt expression may predict favorable prognosis in cholangiocarcinoma. J Gastroenterol Hepatol 21:1744–1751
13. Kang YK, Kim WH, Lee HW, Lee HK, Kim YI (1999) Mutation of p53 and K-ras, and loss of heterozygosity of APC in intrahepatic cholangiocarcinoma. Lab Invest 79:477–483
14. Khan SA, Thomas HC, Toledano MB, Cox IJ, Taylor-Robinson SD (2005) p53 Mutations in human cholangiocarcinoma: a review. Liver Int 25:704–716
15. Khuder SA, Herial NA, Mutgi AB, Federman DJ (2005) Nonsteroidal antiinflammatory drug use and lung cancer: a metaanalysis. Chest 127:748–754
16. Kim HJ, Lee KT, Kim EK, Sohn TS, Heo JS, Choi SH, Choi DI, Lee JK, Paik SW, Rhee JC (2004) Expression of cyclooxygenase-2 in cholangiocarcinoma: correlation with clinicopathological features and prognosis. J Gastroenterol Hepatol 19:582–588
17. Koga H, Sakisaka S, Ohishi M, Kawaguchi T, Taniguchi E, Sasatomi K, Harada M, Kusaba T, Tanaka M, Kimura R, Nakashima Y, Nakashima O, Kojiro M, Kurohiji T, Sata M (1999) Expression of cyclooxygenase-2 in human hepatocellular carcinoma: relevance to tumor dedifferentiation. Hepatology 29:688–696
18. Lai GH, Zhang Z, Sirica AE (2003) Celecoxib acts in a cyclooxygenase-2-independent manner and in synergy with emodin to suppress rat cholangiocarcinoma growth in vitro through a mechanism involving enhanced Akt inactivation and increased activation of caspases-9 and -3. Mol Cancer Ther 2:265–271
19. Landis JR, Koch GG (1977) The measurement of observer agreement for categorical data. Biometrics 33:159–174
20. Levi S, Urbano-Ispizua A, Gill R, Thomas DM, Gilbertson J, Foster C, Marshall CJ (1991) Multiple K-ras codon 12 mutations in cholangiocarcinomas demonstrated with a sensitive polymerase chain reaction technique. Cancer Res 51:3497–3502
21. Liu CH, Chang SH, Narko K, Trifan OC, Wu MT, Smith E, Haudenschild C, Lane TF, Hla T (2001) Overexpression of cyclooxygenase-2 is sufficient to induce tumorigenesis in transgenic mice. J Biol Chem 276:18563–18569
22. Maier JA, Hla T, Maciag T (1990) Cyclooxygenase is an immediate-early gene induced by interleukin-1 in human endothelial cells. J Biol Chem 265:10805–10808
23. Mitchell JA, Belvisi MG, Akarasereenont P, Robbins RA, Kwon OJ, Croxtall J, Barnes PJ, Vane JR (1994) Induction of cyclooxygenase-2 by cytokines in human pulmonary epithelial cells: regulation by dexamethasone. Br J Pharmacol 113:1008–1014
24. Patel T (2001) Increasing incidence and mortality of primary intrahepatic cholangiocarcinoma in the United States. Hepatology 33:1353–1357
25. Poligone B, Baldwin AS (2001) Positive and negative regulation of NF-kappaB by COX-2: roles of different prostaglandins. J Biol Chem 276:38658–38664
26. Sheng H, Shao J, Morrow JD, Beauchamp RD, DuBois RN (1998) Modulation of apoptosis and Bcl-2 expression by prostaglandin E2 in human colon cancer cells. Cancer Res 58:362–366
27. Sirica AE, Lai GH, Endo K, Zhang Z, Yoon BI (2002) Cyclooxygenase-2 and ERBB-2 in cholangiocarcinoma: potential therapeutic targets. Semin Liver Dis 22:303–313
28. Sobin LH, Wittekind C (2002) International union against cancer. TNM classification of malignant tumours, 6th edn. Wiley, New–York
29. Watanabe M, Asaka M, Tanaka J, Kurosawa M, Kasai M, Miyazaki T (1994) Point mutation of K-ras gene codon 12 in biliary tract tumors. Gastroenterology 107:1147–1153
30. Wee A, Ludwig J, Coffey RJ Jr, LaRusso NF, Wiesner RH (1985) Hepatobiliary carcinoma associated with primary sclerosing cholangitis and chronic ulcerative colitis. Hum Pathol 16:719–726
31. Wendum D, Masliah J, Trugnan G, Flejou JF (2004) Cyclooxygenase-2 and its role in colorectal cancer development. Virchows Arch 445:327–333
32. Wu T, Leng J, Han C, Demetris AJ (2004) The cyclooxygenase-2 inhibitor celecoxib blocks phosphorylation of Akt and induces apoptosis in human cholangiocarcinoma cells. Mol Cancer Ther 3:299–307
33. Zhang Z, Lai GH, Sirica AE (2004) Celecoxib-induced apoptosis in rat cholangiocarcinoma cells mediated by Akt inactivation and Bax translocation. Hepatology 39:1028–1037

Virchows Arch (2007) 450:143–149
DOI 10.1007/s00428-006-0352-9

ORIGINAL ARTICLE

KiSS-1 overexpression as an independent prognostic marker in hepatocellular carcinoma: an immunohistochemical study

Katharina Schmid · Xiaowei Wang · Andrea Haitel · Wolfgang Sieghart · Markus Peck-Radosavljevic · Martin Bodingbauer · Susanne Rasoul-Rockenschaub · Fritz Wrba

Received: 26 July 2006 / Revised: 22 October 2006 / Accepted: 12 November 2006 / Published online: 10 January 2007
© Springer-Verlag 2007

Abstract The KiSS-1 gene has been reported to play an important role as a metastasis suppressor gene in various human malignancies. However, there is little information about its possible role in hepatocellular carcinoma (HCC). In this study, we evaluated the prognostic significance of the expression of KiSS-1 and its receptor AXOR12 in 142 HCC tissue specimens by immunohistochemistry. By using a cutoff level of 50%, immunoreactivity of KiSS-1 and AXOR12 was found in 6 (4%) and 11 (8%) HCCs. The expression of KiSS-1 and AXOR12 in HCC correlated with each other (r=0.42, p<0.0001) and with the expression in corresponding, surrounding liver tissue (both r=0.35, p<0.0001). Positive AXOR12 immunoreactivity in HCC correlated with advanced pT-stage of tumors and low tumor grading (r=0.18, p=0.032; r=−0.18, p=0.029). High KiSS-1 expression in HCC had a statistically significant influence on diminished disease-free and overall survival in uni- (p=0.006 and p=0.002) and multivariate analysis (r=2.874, p=0.027 and r=2.913, p=0.026). In this study, we report for the first time that elevated KiSS-1 expression level in HCC correlates with worsened clinical outcome, as an independent prognostic marker for the aggressiveness of HCC.

Keywords Hepatocellular carcinoma · KISS-1 · AXOR12 · Immunohistochemistry · Prognosis

K. Schmid (✉) · A. Haitel · F. Wrba
Department of Clinical Pathology, Medical University of Vienna,
Waehringer Guertel 18-20,
1090 Vienna, Austria
e-mail: katharina.schmid@meduniwien.ac.at

X. Wang · W. Sieghart · M. Peck-Radosavljevic
Department of Internal Medicine IV,
Division of Gastroenterology/Hepatology,
Medical University of Vienna,
Waehringer Guertel 18-20,
1090 Vienna, Austria

X. Wang
Department of Internal Medicine,
China Japan Union Hospital of Jilin University,
Changchun, China

W. Sieghart
Department of Clinical Pharmacology,
Section of Experimental Oncology/Molecular Pharmacology,
Medical University of Vienna,
Vienna, Austria

M. Bodingbauer · S. Rasoul-Rockenschaub
Division of Transplantation Surgery, Department of Surgery,
Medical University of Vienna,
Waehringer Guertel 18-20,
1090 Vienna, Austria

Abbreviations

HCC	hepatocellular carcinoma
OLT	orthotopic liver transplantation
n.s.	nonsignificant

Introduction

Hepatocellular carcinoma (HCC) is one of the most common malignant diseases worldwide. Approximately 560,000 new cases are diagnosed every year, constituting 6% of all new human cancers [17]. It is well accepted that surgery is the only existing curative therapy. During the last decades, orthotopic liver transplantation (OLT) has become the optimal treatment for a subgroup of patients with smaller tumors resulting in fewer deaths due to tumor

recurrence [7, 11, 15]. To improve patients` outcome, it is of great clinical importance to find reliable prognostic markers, which could predict relapse and dissemination of HCC.

The KiSS-1 gene has been reported to be a metastasis suppressor gene in human melanoma and breast carcinoma cells [9, 10]. Its gene product, KiSS-1 (metastin, kisspeptin-54) has been identified as the natural ligand of a G-protein-coupled receptor, termed AXOR12 (hOT7T175, human GPR54) [8, 14, 16]. Highest expression levels of KiSS-1 mRNA were observed in the placenta, with the next highest level in testis and moderate levels in pancreas, liver, and small intestine. For AXOR12 transcripts, the highest expression levels were found in the placenta and the pancreas, with moderate expression in spleen, the peripheral blood leukocyte, testis, and lymph node [9, 16].

To date, only a few clinical studies about KiSS-1 and AXOR12 gene expression in human malignancies are available. Using quantitative real-time reverse transcriptase polymerase chain reaction and/or in situ hybridization, the majority of these study groups observed that down-regulation of KiSS-1 mRNA correlated with tumor progression, while expression patterns of AXOR12 mRNA differed in varying tumor entities: Shirasaki et al. found that KiSS-1 mRNA expression was lost in 50% of advanced stage melanomas [21]. Sanchez-Carbayo and coworkers described lower transcript levels of KiSS-1 in invasive bladder carcinoma compared to superficial tumors and normal urothelium [20]. Masui and colleagues reported that pancreatic cancer tissue specimens showed significantly lower expression of KiSS-1 mRNA than a normal pancreas, whereas AXOR12 mRNA was overexpressed [13]. Ringel and colleagues found overexpression of AXOR12 mRNA in thyroid papillary carcinomas compared to thyroid follicular carcinomas and normal thyroid tissue [19]. Ikegucchi et al. observed that the loss of KiSS-1 and/or AXOR12 gene expression in esophageal squamous carcinoma was a significant predictor of lymph node metastasis [6]. In the study of Dhar et al., down-regulation of KiSS-1 expression was the strongest independent prognostic factor for gastric carcinoma in a multivariate analysis [2]. Conversely, Ikeguchi et al. reported that overexpression of KiSS-1 and AXOR12 genes correlated with tumor progression in HCC [5]. Also, Tracey et al. found that the expression of KiSS-1 increased in patients with aggressive breast cancer [12].

In the present study, we analyzed for the first time the expression of the KiSS-1 gene product and its cognate receptor AXOR12 in HCC specimens by immunohistochemistry. Results were correlated with clinical follow-up to evaluate a possible role between KiSS-1 and AXOR12 expression levels and patient prognosis.

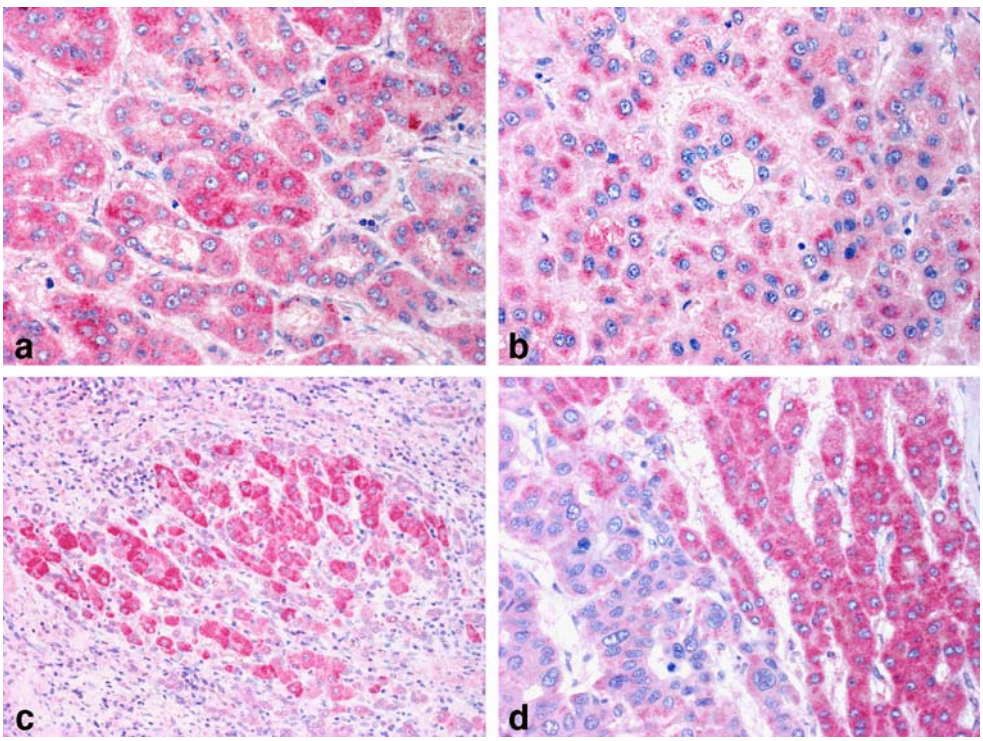

Fig. 1 Four cases with high immunoreactivity of **a** KiSS-1 in HCC, grade 2 (magnification ×200); **b** AXOR12 in HCC, grade 2 (magnification ×200); **c** KiSS-1 in cirrhosis (magnification ×100); **d** AXOR12 in cirrhosis (*right side*) and negative immunostaining of tumor cells (*left side*; magnification ×200)

Table 1 Expression of KiSS-1 and AXOR12 in HCC, in surrounding, cirrhotic liver tissue (both $n=142$) and in normal liver tissue ($n=10$; all cutoff level 50%)

KiSS-1 and AXOR12 expression	Immunoreactivity	
	Negative (weak/absent)	Positive (high)
KiSS-1 expression in HCC	136 (96%)	6 (4%)
KiSS-1 expression in cirrhosis	134 (94%)	8 (6%)
KiSS-1 expression in normal liver	10 (100%)	0 (0%)
AXOR12 expression in HCC	131 (92%)	11 (8%)
AXOR12 expression in cirrhosis	116 (82%)	26 (18%)
AXOR12 expression in normal liver	10 (100%)	0 (0%)

Table 2 Univariate analysis of disease-free and overall survival in 142 patients with HCC

Characteristics	DFS, *p*-value	OS, *p*-value
KiSS-1 overexpression	0.006	0.002
AXOR12 overexpession	n.s.	n.s.
pT (tumor stage)	0.0001	<0.0001
pN (nodal status)	0.009	0.013
pM (distant metastasis)	0.001	0.005
Absence of liver cirrhosis	0.041	0.031
Tumor grading	n.s.	n.s.
Vascular invasion	<0.0001	<0.0001
Resection margin	0.0002	0.0001
Gender	n.s.	n.s.
Loco-regional therapy	n.s.	n.s.
Adjuvant chemotherapy	n.s.	n.s.

Materials and methods

Patients and tissue samples

Our study was comprised of 142 patients who underwent OLT for HCC at the Department of Surgery, Division of Transplantation Surgery, Medical University of Vienna, from 1982 to 2002. Underlying liver diseases were the following: hepatitis C cirrhosis in 49 (35%), alcoholic cirrhosis in 43 (30%), hepatitis B cirrhosis in 15 (11%), cryptogenic cirrhosis in 13 (9%), other causes of cirrhosis (hemochromatosis, primary biliary cirrhosis, and primary sclerosing cholangitis) in 10 (7%), and non-cirrhotic liver in 12 (8%) cases. Before surgery, 20 (14%) patients received percutaneous, endotumoral alcohol instillation intratumoral, and 3 (2%) were treated by transarterial chemoembolization of the tumors. Twenty-one patients undergoing complete tumor ablation after loco-regional therapy before OLT were excluded from our study (no tumor tissue available). After OLT, adjuvant chemotherapy (Doxorubicin) was administered to 21 (15%) patients [18]. In addition, ten cases of non-tumorous, non-cirrhotic liver tissues were included in this study, primarily resected for tumor metastases of colorectal carcinomas.

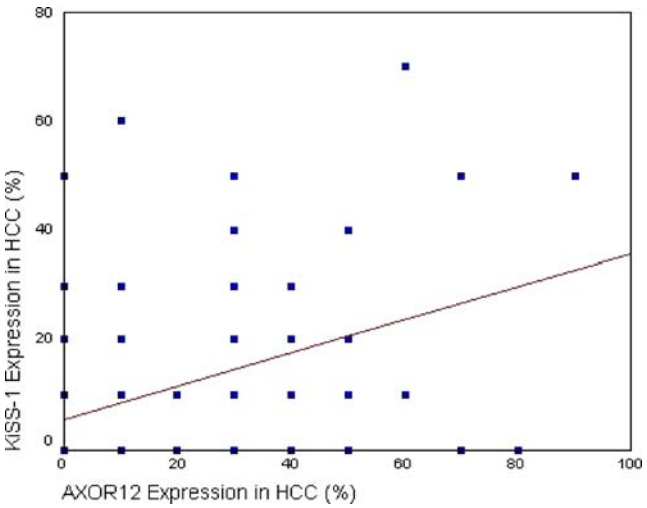

Fig. 2 Correlation of KiSS-1 and AXOR12 immunoreactivity in HCC ($r=0.42$, $p<0.0001$)

After surgery, tissue samples were routinely fixed in 7.5% buffered formalin and embedded in paraffin for routine diagnostics. Tumors were staged according to the International Union Against Cancer (UICC) 2002 issue of the TNM system, while tumor grading was performed as outlined by Edmondson and Steiner [3]. The clinical follow-up of all patients was retrieved from the archives of the Division of Transplantation Surgery, Department of Surgery, Medical University of Vienna. All procedures followed in this study were in accordance with the guidelines of the Human Ethics Committee of the Medical University of Vienna.

Demographics and clinical data

At time of surgery, the mean age of patients (123 males, 19 females) was 54.9+9.3 years. Pathological tumor staging revealed stage pT1 in 13 (9%), pT2 in 22 (16%), pT3 in 29 (20%), and pT4 in 78 (55%) cases. Lymph node metastases were present in two (1%) and distant metastases in three (2%) cases. Tumor grading revealed grade 1 in 27 (19%), grade 2 in 87 (61%), and grade 3 in 28 (20%) cases. Curative surgery was achieved in 134 (94%), while 8 (6%) cases showed tumor infiltrated resection margins (tumor thrombosis of portal and hepatic veins, tumor infiltration of falciform ligament, and/or tumor infiltration into fatty tissue of the liver hilus).

Median follow-up times were 1.2 (disease-free survival) and 2.1 years (overall survival; both range 0 to 16.2 years), respectively. During the observation period, 58 (41%) patients suffered from recurrence of disease and 54 (38%) died of tumor progression, while 47 (33%) patients died of unrelated causes.

Table 3 Multivariate analysis of disease free survival in 142 patients with HCC

Characteristics	*p*-value	*r* (relative risk)
KiSS-1 overexpression	0.027	2.874
AXOR12 overexpression	n.s.	–
pT (tumor stage)	0.039	2.592
pN (nodal status)	n.s.	–
pM (distant metastasis)	n.s.	–
Absence of liver cirrhosis	n.s.	–
Vascular invasion	0.001	2.559
Resection margin	n.s.	–

Immunohistochemistry

One representative tissue block per patient was selected from the archives of the Department of Clinical Pathology, Medical University of Vienna. Special care was taken to include only specimens with sufficient amounts of non-neoplastic tissue surrounding the tumors. Immunohistochemistry of consecutive paraffin sections was performed with antibodies against KISS-1 and AXOR12 (both polyclonal rabbit antibodies, Phoenix Pharmaceuticals, Belmont, California, USA).

For immunostaining, autoclave pretreatment (20 min, 1 bar) of 4 μm paraffin sections was applied. To avoid unspecific staining, sections were blocked with avidin and biotin (Vector, Burlingame, CA, USA) for 15 min each. Afterwards, samples were incubated with primary antibodies for 20 h (overnight) at 4°C first and then incubated for 1 h at 20°C (anti-KISS-1 antibody diluted 1:150, anti-AXOR12 antibody diluted 1:400). This was followed by incubation with biotinylated goat anti-rabbit IgG for 30 min and detection by alkaline phosphatase complex (Biocare Medical, San Diego, CA, USA). Phosphatase reaction product was visualized by a New Fuchsin Kit according to the manufacturer's instructions (Nichirei Corporation, Tokyo, Japan). For negative controls, primary antibodies were substituted by irrelevant rabbit serum, whereas placenta tissue served as positive control.

Two independent observers (K.S., F.W.), uninformed of the patient's clinical and pathological status, evaluated the cytoplasmatic expression of KISS-1 and AXOR12 in HCC, in surrounding, mostly cirrhotic liver tissue, and in normal liver tissue. Immunohistochemical expression of KiSS-1 and AXOR12 was evaluated by creating a system of 10% steps (range, 0–100%). All immunopositive tumor cells in HCC and hepatocytes in surrounding, non-neoplastic liver tissue were counted in at least ten consecutive high-power fields (×400), and the number of positive cells was given as a percentage. The staining was classified as weak or intense. A cutoff level of 50% was chosen because statistical analysis revealed significant correlations between KiSS-1 and AXOR12 expression and clinico-pathological parameters at expression values of >50% with intense staining. Therefore, only samples that exhibited 50% or more intensely stained tumor cells were considered highly immunoreactive and classified as positive samples (Fig. 1). Weakly stained samples and samples showing less than 50% intensely stained tumor cells were considered negative.

Statistical analysis

Correlation of KiSS-1 and AXOR12 immunoreactivity in HCC and their expression in surrounding liver tissue and their correlation to tumor stage and tumor grade were investigated using the Spearman correlation coefficient test. Disease-free and overall survival were assessed using the Kaplan–Meier method, and curves were compared by the log rank test. For multivariate analysis, the Cox proportional hazard regression method (stepwise backwards, Likelihood quotient) was performed; KiSS-1 and AXOR12 expression and all parameters statistically significant in univariate analysis were entered into the regression model. For all tests, a two-tailed p-value of <0.05 was considered significant.

Results

Immunoreactivity of KiSS-1 and AXOR12 and correlation with clinico-pathological parameters

The generally diffuse staining pattern of both, KiSS-1 and AXOR12 antigen showed heterogeneity from focal to more than 80% of the tumors cells and/or heptocytes. Both antigens were located in the cytoplasm. Positive staining of

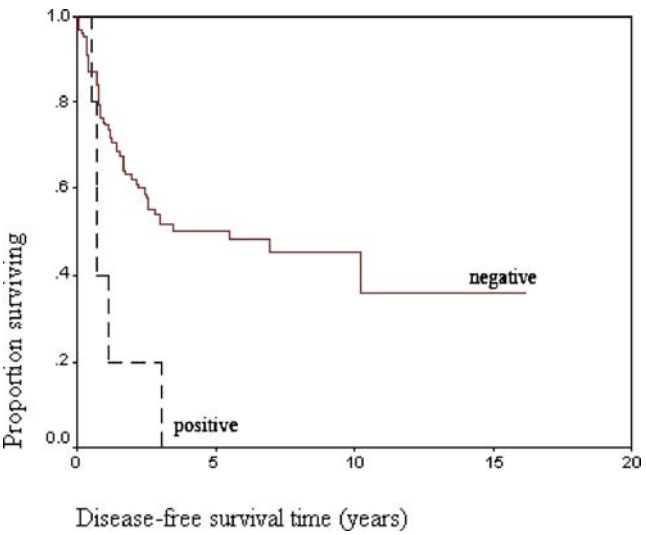

Fig. 3 Kaplan–Meier curves of cumulative disease-free survival of patients with negative and positive immunoreactivity for KiSS-1 (cutoff level 50%)

Table 4 Multivariate analysis of overall survival in 142 patients with HCC

Characteristics	*p*-value	*r* (relative risk)
KiSS-1 overexpression	0.026	2.913
AXOR12 overexpression	n.s.	–
pT (tumor stage)	0.019	4.320
pN (nodal status)	0.011	6.949
pM (distant metastasis)	n.s.	–
Absence of liver cirrhosis	n.s.	–
Vascular invasion	0.002	2.571
Resection margin	n.s	–

KiSS-1 and AXOR12 was seen in 6 (4%) and 11 (8%) cases of HCC. No differences were detected between the central regions of the tumors and areas of transition between malignant and normal-looking tissue. No correlation with underlying liver disease was found.

In most cases, the tumor-surrounding liver tissue was cirrhotic (130 cases, 92%); in our study population in only 12 cases (8%) HCC evolved in normal liver tissue. Cases, in which the corresponding tumor-surrounding liver tissue stained positive for KiSS-1 and AXOR12 in 8 (6%) and 26 (18%) cases, respectively, referred to cirrhotic tissue only (see Table 1 and Fig. 1). The staining of both KiSS-1 and AXOR12 antigen was more intense at the margins of the regenerative nodules than in central proportions of the nodules in cirrhotic liver tissue. In normal liver tissue, KiSS-1 was expressed only weakly in less than 10% of hepatocytes in seven cases (70%) and was absent in three cases (30%), whereas no AXOR12 expression could be observed. Bile duct epithelia were also immunopositive for KiSS-1, but not for AXOR12. Occasionally, endothelial cells in blood vessels stained weakly positive for KiSS-1, but were negative for AXOR12. No staining of KiSS-1 and AXOR12 was present in stroma and inflammatory cells including lymphocytes, macrophages, and plasma cells.

A statistically significant correlation between immunoreactivity of KiSS-1 and AXOR12 in HCC was found (r= 0.42, p<0.0001; see Fig. 2). The expression of KiSS-1 and AXOR12 in HCC also correlated with their expression in surrounding liver tissue (both r=0.35, p<0.0001). In HCC, a statistically significant association between overexpression of AXOR12 and advanced pT-stage and low tumor grade (r=0.18, p=0.032 and r=−0.18, p=0.029) but not with pN- or pM-stage was observed. KiSS-1 immunoreactivity was not associated with tumor stage (including pT-, pN-, and pM-stage) and tumor grade (all p>0.05).

Prognostic significance of KiSS-1 and AXOR12 expression and other clinico-pathological parameters

In univariate analysis, positive immunoreactivity of KiSS-1 in HCC, high pT-, pN-, and pM-tumor stages, absence of liver cirrhosis in the explanted liver, presence of vascular invasion, and tumor infiltrated resection margins were significantly associated with a poorer clinical outcome (disease-free and overall survival), whereas AXOR12 expression, tumor grade, gender, preoperative loco-regional treatment, and adjuvant chemotherapy were not (details outlined in Table 2). In multivariate analysis, KiSS-1 overexpression in HCC, advanced pT-stages, and presence of vascular invasion were shown to be independent prognostic markers for diminished disease-free survival (see Table 3 and Fig. 3). High KiSS-1 expression in HCC, advanced pT- and pN-stage, and the presence of vascular invasion were statistically significant for overall survival (compare Table 4 and Fig. 4).

Discussion

This is the first study investigating the expression of KiSS-1 and its receptor AXOR12 in HCC on the protein expression level by immunohistochemistry. Using a cutoff level of 50%, positive immunoreactivity of KiSS-1 and AXOR12 in HCC was observed in 6 (4%) and 11 (8%) cases, while no intense staining was seen in healthy liver tissue. The KiSS-1 and AXOR12 expression level correlated well with each other and with KiSS-1 and AXOR12 expression in surrounding cirrhotic and non-cirrhotic liver tissue. AXOR12 immunoreactivity was in correlation with pathological tumor grade and stage.

These findings confirm previous studies reporting a coincidence expression of KiSS-1 receptor and its cognate ligand in various tissues [9, 14, 16]. However, Ikeguchi et al. observed overexpression of KiSS-1 and AXOR12 mRNA in 22% and 43% of HCCs, whereas in our study,

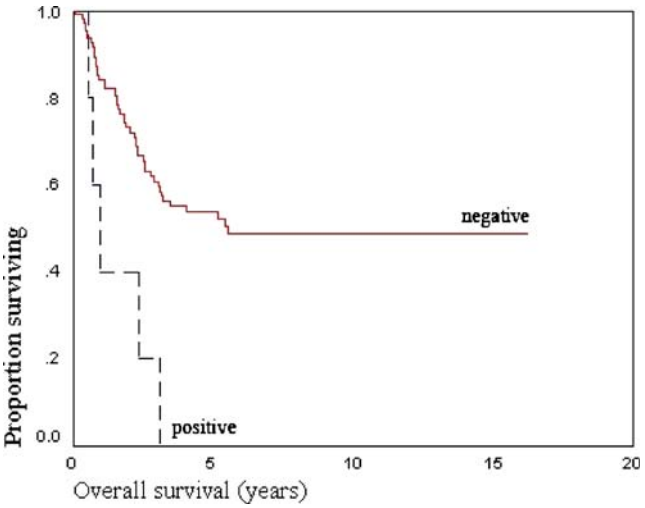

Fig. 4 Kaplan–Meier curves of cumulative overall survival of patients with negative and positive immunoreactivity for KiSS-1 (cutoff level 50%)

high KiSS-1 and AXOR12 expression was seen in only 4 and 8% of cases, respectively [5]. This difference might reflect an additional regulation of KiSS-1/AXOR12 expression at the translational level or by different cleavage variants of the KiSS-1 protein. The KiSS-1 investigated in our study is the major cleavage product, consisting of 54 amino acids (kisspeptin-54). Kotani and colleages recently discovered two other naturally occurring, smaller peptides in the human placenta, termed kisspeptin-14 and kisspeptin-13 [8]. In this context, the main cleavage product KiSS-1 has been found to display greater stability. In contrast, the smaller peptides, kisspeptin-14 and kisspeptin-13, exhibit stronger receptor binding activity [14]. Therefore, further clinical studies to investigate the significance of the different cleavage products of KiSS-1 gene product are warranted.

Furthermore, we demonstrated, by multivariate analysis, that intense KiSS-1 expression in HCC is associated with poor prognosis (i.e., early local recurrence of HCC, followed by lymph node and distant metastases) of patients undergoing OLT. This finding fits to the results of Ikeguchi and coworkers, who reported a worse prognosis of HCC patients with increased KiSS-1 and AXOR12 mRNA levels [5]. In contrast, most of recently published data on KiSS-1 and/or AXOR12 gene expression in other human malignancies report a strong correlation between KiSS-1 and/or AXOR12 gene overexpression and an improved clinical course [2, 6, 13, 19–21]. Mechanisms explaining why the expression of KiSS-1 gene product had an opposite impact on clinical outcome of HCC compared to other malignant tumors remains to be elucidated. Ikeguchi et al. postulated that elevated estrogen levels might modulate the expression patterns of KiSS-1 gene products [5]. Patients with HCC generally suffer from liver cirrhosis and are therefore prone to a hyperestrogenic state. The fact that the KiSS-1/AXOR system in HCC might be influenced by hormonal disorder is supported by the findings of Muir and Horihoshi, who reported that the plasma level of KiSS-1 was 10,000-fold higher in pregnant than in nonpregnant women [4, 14]. Moreover, KiSS-1 mRNA expression levels in placenta were up to 20,000-fold higher than in other normal human tissues.

Interestingly, also in breast carcinoma, an association between increase of KiSS-1 and tumor progression was found by the study group of Martin et al. [12]. It is well-known that one of the most important systemic therapies in breast cancer management is blockade of the estrogen receptor pathway. Conversely, antiestrogenic therapy did not prolong survival in patients with inoperable HCC and had an increasingly negative impact with increasing dose [1]. In this context, one may speculate that patients with overexpression of KiSS-1 in HCC might benefit from such a therapy. However, further studies are needed to clarify the possible link of estrogen signalling and KiSS-1 and AXOR12 expression in tumors.

In summary, this is the first study investigating KiSS-1 and AXOR12 in HCC on the protein level by immunohistochemistry. We showed that KiSS-1 and AXOR12 are expressed in a subset of human HCC. High KiSS-1 expression is an independent prognostic factor for disease-free and overall survival in patients with HCC. Thus, KiSS-1 could serve as an additional molecular marker for assessing the malignant potential of HCC.

References

1. Chow PK, Tai BC, Tan CK, Machin D, Win KM, Johnson PJ, Soo KC (2002) High-dose tamoxifen in the treatment of inoperable hepatocellular carcinoma: a multicenter randomized controlled trial. Hepatology 36:1221–1226
2. Dhar DK, Naora H, Kubota H, Maruyama R, Yoshimura H, Tonomoto Y, Tachibana M, Ono T, Otani H, Nagasue N (2004) Downregulation of KiSS-1 expression is responsible for tumor invasion and worse prognosis in gastric carcinoma. Int J Cancer 111:868–872
3. Edmonson HA, Steiner PE (1954) Primary carcinoma of the liver: a study of 100 cases among 49800 necropsies. Cancer 7:462–503
4. Horikoshi Y, Matsumoto H, Takatsu Y, Ohtaki T, Kitada C, Usuki S, Fujino M (2003) Dramatic elevation of plasma metastin concentrations in human pregnancy: metastin as a novel placenta-derived hormone in humans. J Clin Endocrinol Metab 88:914–919
5. Ikeguchi M, Hirooka Y, Kaibara N (2003) Quantitative reverse transcriptase polymerase chain reaction analysis for KiSS-1 and orphan G-protein-coupled receptor (hOT7T175) gene expression in hepatocellular carcinoma. J Cancer Res Clin Oncol 129:531–535
6. Ikeguchi M, Yamaguchi K, Kaibara N (2004) Clinical significance of the loss of KiSS-1 and orphan G-protein-coupled receptor (hOT7T175) gene expression in esophageal squamous cell carcinoma. Clin Cancer Res 10:1379–1383
7. Island ER, Pomposelli J, Pomfret EA, Gordon FD, Lewis WD, Jenkins RL (2005) Twenty-year experience with liver transplantation for hepatocellular carcinoma. Arch Surg 140:353–358
8. Kotani M, Detheux M, Vandenbogaerde A, Communi D, Vanderwinden JM, Le Poul E, Brézillon S, Tyldesley R, Suarez-Huerta N, Vandeput F, Blanpain C, Schiffmann SN, Vassart G, Parmentier M (2001) The metastasis suppressor gene KiSS-1 encodes kisspeptins, the natural ligands of the orphan G protein-coupled receptor GPR54. J Biol Chem 276:34631–34616
9. Lee JH, Miele ME, Hicks DJ, Phillips KK, Trent JM, Weissman BE, Welch DR (1996) KiSS-1, a novel human malignant melanoma metastasis-suppressor gene. J Natl Cancer Inst 88:1731–1737
10. Lee JH, Welch DR (1997) Suppression of metastasis in human breast carcinoma MDA-MB-435 cells after transfection with the metastasis suppressor gene, KiSS-1. Cancer Res 57:2384–2387
11. Leung JY, Zhu AX, Gordon FD, Pratt DS, Mithoefer A, Garrigan K, Terella A, Hertl M, Cosimi AB, Chung RT (2004) Liver transplantation outcomes for early-stage hepatocellular carcinoma: results of a multicenter study. Liver Transpl 10:1343–1354
12. Martin TA, Wtkins G, Jiang WG (2005) KiSS-1 expression in human breast cancer. Clin Exp Metastasis 22:503–511
13. Masui T, Doi R, Mori T, Toyoda E, Koizumi M, Kami K, Ito D, Peiper SC, Broach JR, Oishi S, Niida A, Fujii N, Imamura M (2004)

Metastin and its variant forms suppress migration of pancreatic cancer cells. Biochem Biophys Res Commun 315:85–92
14. Muir AI, Chamberlain L, Elshourbagy NA, Michalovich D, Moore DJ, Calamari A, Szekeres PG, Sarau HM, Chambers JK, Murdock P, Steplewski K, Shabon U, Miller JE, Middleton SE, Darker JG, Larminie CG, Wilson S, Bergsma DJ, Emson P, Faull R, Philpott KL, Harrison DC (2001) AXOR12, a novel human G protein-coupled receptor, activated by the peptide KiSS-1. J Biol Chem 276:28969–28975
15. Nart D, Arikan C, Akyildiz M, Yuce G, Demirpolat G, Zeytunlu M, Karasu Z, Aydogdu S, Killi R, Yuzer Y, Tokat Y, Kilic M (2003) Hepatocellular carcinoma in liver transplant era: a clinicopathologic analysis. Transplant Proc 35:2986–2990
16. Ohtaki T, Shintani Y, Honda S, Matsumoto H, Hori A, Kanehashi K, Terao Y, Kumano S, Takatsu Y, Masuda Y, Ishibashi Y, Watanabe T, Asada M, Yamada T, Suenaga M, Kitada C, Usuki S, Kurokawa T, Onda H, Nishimura O, Fujino M (2001) Metastasis suppressor gene KiSS-1 encodes peptide ligand of a G-protein-coupled receptor. Nature 411:613–617
17. Parkin DM (2001) Global cancer statistics in the year 2000. Lancet Oncol 2:533–543
18. Pokorny H, Gnant M, Rasoul-Rockenschaub S, Gollackner B, Steiner B, Steger G, Steininger R, Muehlbacher F (2005) Does additional doxorubicin chemotherapy improve outcome in patients with hepatocellular carcinoma treated by liver transplantation? Am J Transplant 5:788–794
19. Ringel MD, Hardy E, Bernet VJ, Burch HB, Schuppert F, Burman KD, Saji M (2002) Metastin receptor is overexpressed in papillary thyroid cancer and activates MAP kinase in thyroid cancer cells. J Clin Endocrinol Metab 87:2399–2402
20. Sanchez-Carbayo M, Capodieci P, Cordon-Cardo C (2003) Tumor suppressor role of KiSS-1 in bladder cancer. Loss of KiSS-1 expression is associated with bladder cancer progression and clinical outcome. Am J Pathol 162:609–617
21. Shirasaki F, Takata M, Hatta N, Takehara K (2001) Loss of expression of the metastasis suppressor gene KiSS-1 during melanoma progression and its association with LOH of chromosome 6q16.3–q23. Cancer Res 61:7422–7425

Virchows Arch (2007) 450:151–159
DOI 10.1007/s00428-006-0342-y

ORIGINAL ARTICLE

Activation of extracellular regulated kinases (ERK1/2) but not AKT predicts poor prognosis in colorectal carcinoma and is associated with *k-ras* mutations

K. J. Schmitz · J. Wohlschlaeger · H. Alakus · J. Bohr · M. A. Stauder · K. Worm · G. Winde · K. W. Schmid · H. A. Baba

Received: 18 July 2006 / Accepted: 26 October 2006 / Published online: 6 December 2006
© Springer-Verlag 2006

Abstract Signal transduction and modulation represent central mechanisms in cellular processes such as cell-cycle regulation, oncogenesis, and apoptosis. The aim of this study was to determine the prognostic relevance of two kinases important in the regulation of cell proliferation and apoptosis in 135 colorectal cancer cases: AKT and extracellular regulated kinases (ERK1/2). We investigated the relationship of phospho-ERK1/2 (pERK1/2) and phospho-AKT (pAKT) with associated parameters (EGFR, COX-2, cyclin-D1), proliferative activity (Ki-67), and apoptosis (TUNEL) using immunohistochemistry. Additionally, the *k-ras* gene was screened for mutations to determine its putative association with ERK1/2 activation. Activation of ERK1/2 but not AKT correlated statistically with the presence of *k-ras* mutations (P=0.015). Survival analysis of phospho-ERK1/2 immunoexpression showed a significant correlation with decreased overall survival (OS). The multivariate Cox regression analysis identified pERK1/2 as an independent prognostic parameter (P=0.005). Activation of ERK1/2 in colorectal cancer may indicate aggressive tumor behavior and may constitute an independent prognostic factor. Furthermore, our data suggest that mutations of the *k-ras* oncogene may induce activation of ERK1/2. We propose immunohistochemical determination of pERK1/2 status as a promising candidate for the identification of high-risk patients who would benefit from new anticancer drugs targeting the ERK pathway.

Keywords Colorectal cancer · Molecular oncology

K. J. Schmitz · J. Wohlschlaeger · J. Bohr · M. A. Stauder · K. Worm · K. W. Schmid · H. A. Baba (✉)
Institute of Pathology and Neuropathology,
University Hospital of Essen,
Hufelandstr. 55,
45122 Essen, Germany
e-mail: hideo.baba@medizin.uni-essen.de

H. Alakus · G. Winde
Department of Gastrointestinal Surgery, Klinikum Herford,
Herford, Germany

K. W. Schmid
West German Cancer Centre Essen (WTZE),
Essen, Germany

Introduction

Colorectal cancer ranks second in terms of both incidence and mortality in industrialized countries. An estimated 945,000 of new colorectal cancer cases occur worldwide each year, and colorectal cancer is responsible for some 492,000 deaths [38]. Colorectal carcinoma is traditionally managed by surgical resection. Chemotherapy has been used in the adjuvant setting for regional metastatic disease, whereas adjuvant chemotherapy for localized nonmetastatic disease remains controversial [43]. Besides the classic 5-fluorouracil (5-FU) adjuvant chemotherapy, further therapeutic options are desirable especially in 5-FU-resistant advanced disease. Recently, protein kinases have emerged as a group of molecular targets with the potential to be cancer specific, allowing the development of a new generation of chemotherapy agents which inhibit these kinases. Promising targets in this context are kinases involved in the MAPK and AKT/PI3K pathway [36].

The ERK signaling pathway is a component of the mitogen-activated protein kinases (MAPK) cascade and is activated by extracellular and intracellular, frequently mitogenic, ligands, including ras proteins and epidermal growth factor (EGF), resulting in increased cellular proliferation in vivo [29, 31] and cell differentiation [33]. ERK1/2, extracellular signal-related kinases—also referred to as

p44 and p42 MAP kinases—are ubiquitously expressed. Constitutive activation of MAP kinases was observed in several human cancer cell lines including colon cancer cell lines and various human cancer tissues [20]. In human colon cancers, infrequent activation of MAP kinases has been demonstrated [32]. A recent study revealed that MAP kinases are frequently expressed in human colorectal tumors in contrast to adjacent normal colonic mucosa [26]. However, up to date, the clinical relevance of activated MAP kinases in colorectal cancer remains unknown.

AKT/protein kinase B plays a critical role in controlling the balance between cell survival and apoptosis [15]. AKT phosphorylation is mediated by phosphatidylinositol-3-OH-kinase (PI3K) [14] in response to various growth/survival factors, including EGF, platelet-derived growth factor, interleukins, and oncogenic *ras* [5, 15, 16]. Upon activation, AKT promotes cell survival by inhibition of apoptosis [6, 11]. Besides its well-known antiapoptotic functions, AKT is involved in cell proliferation [12, 37, 47]. We recently demonstrated AKT phosphorylation as an independent prognostic parameter in breast cancer [34], whereas others found pAKT-associated decreased survival in malignant tumors, including hepatocellular carcinoma, leukemia, breast cancer, pancreatic cancer, and malignant melanoma [10, 28, 44, 45].

Previous studies suggest that AKT is required in human colorectal carcinoma for suppression of cancer cell apoptosis and tumor progression [22] and that the PI3K signaling pathway is involved in the progression of colon adenocarcinoma [23].

To clarify the prognostic relevance of both of these important signaling pathways in colorectal carcinomas, we used tissue microarray (TMA) technology and evaluated pERK1/2 and pAKT immunoexpression in 135 colorectal tumor samples. Moreover, we investigated downstream targets (cyclin D1, cyclooxygenase-2) and upstream activators (EGFR) of these kinases to discover possible biological pathways. In addition, this study focuses on the oncogene *k-ras* and its impact on the ERK and AKT pathways. The *ras* gene product functions upstream of the MAPK pathway and is an important factor in the activation of ERK1/2 [3]. We screened for *k-ras* hot spot mutations in codons 12 and 13, which are frequently observed in colorectal cancer [42] and cause the ras protein to remain in an active state, continuously sending signals downstream [41].

Materials and methods

Patients

This study comprised 135 consecutive colorectal cancer patients, who underwent surgery in the years 1996–1998 according to the recommendations of the German Society of Surgery. Complete clinical records and follow-up information were available in all cases. The minimum follow-up period for patients still alive was 60 months. Surgical material was fixed in formalin and routinely processed. The tumors were classified according to the pTNM System (6th edition), and histopathological diagnosis was made according to the WHO classification of tumors of the rectum and colon [18]. Patients with UICC stages III and IV colorectal carcinoma received in the adjuvant setting a standardized chemotherapy. According to the recommendations of the German Surgical Oncology Working Group (CAO), patients with stages I and II colorectal carcinoma were not advised to any adjuvant treatment. The gender distribution was 68 men (50.4%) and 67 women (49.6%). Information about the tumor site was available for 129 cases, 78 tumors were located at the colon (60.5%), and 51 cases were at the rectum (39.5%). In 130 cases, detailed information about grading, lymph-node status, and distant metastasis was available; the T stage was available in 132 cases.

TMA construction

The most representative tumor area was carefully selected and marked on H&E (hematoxylin-and-eosin-stained) slide. In case of tumor heterogeneity, areas with lowest degree of differentiation were selected. The TMAs were constructed using a manual tissue-array instrument (Beecher Instruments, Silver Spring, MD, USA). Three 0.6-mm-thick tissue cores were taken from each colorectal specimen, and four composite TMA blocks with the primary tumors were designed [4]. One section from each TMA was stained with hematoxylin and eosin. Each block contained normal colon mucosa derived from resection margins of diverticulosis specimen.

Immunohistochemistry of TMA

The primary antibodies used as well as the technical details are summarized in Table 1. Immunohistochemistry was performed on 5-μm-thick paraffin sections. Dewaxed and rehydrated sections were incubated with hydrogen peroxide to block endogenous peroxidase. Immunostainings of phospho-AKT, EGFR, cyclin D1, COX-2, and Ki-67 were carried out with an automated staining device (DAKO Autostainer, Glostrup, Denmark). The staining pERK1/2 protocol for the automated staining device was not established at the time of publication, thus phospho-ERK staining was performed manually. After antigen retrieval antibody in a hot water bath demonstration was achieved using the alkaline phosphatase anti-alkaline phosphatase method (APAAP), the commercially available anti-mouse

Table 1 Antibodies used for immunohistochemistry

Antibody		Pretreatment (manual)	Incubation	Detection	Dilution	Company
Phospho-ERK1/2 [phospho-p44/42Map kinase (Erk1/2) threonine 202; tyrosine 204[a]]	Polyclonal	Hot water bath (95°C), pH 6.1, 45 min	Overnight at 4°C	APAAP	1:1,000	Cell Signaling Technology, Franfurt am Main, Germany
Phospho-AKT [phospho-AKT (1/2/3) serine 473]	Monoclonal	Hot water bath (95°C), pH 6.0, 20 min	30 min	Peroxydase-conjugated streptavidin; DAB	1:20	Cell Signaling Technology
EGFR	Monoclonal	TRS pH 6.1	30 min	EnVision, DakoCytomation	1:100	Zymed Laboratories, CA, USA
Ki-67	Monoclonal	TRS pH 6.1	30 min	EnVision, DakoCytomation	1:1,200	Biogenex, CA, USA
Cyclin-D1	Monoclonal	TRS pH 6.1	30 min	EnVision, DakoCytomation	1:20	Innovative Diagnostik-Systeme GmbH, Hamburg, Germany
COX-2	Monoclonal	TRS pH 6.1	30 min	EnVision, DakoCytomation	1:250	DCS, Hamburg, Germany

[a] Manual staining

IgG detection kit (EnVision, DakoCytomation, Carpenteria, CA, USA) or peroxidase-conjugated streptavidin and diaminobenzidine as chromogen were applied. Replacement of the various primary antibodies by mouse immunoglobin served as negative controls. Positive controls were included in each staining series.

TUNEL

In situ DNA fragmentation was established using the TUNEL (terminal deoxyribonucleotide transferase (TdT)-mediated dUTP nick end labeling) technique in paraffin-embedded sections. We used the ApoTag™ Plus Peroxidase in Situ Apoptosis Detection Kit (Intergen, GA, USA). Staining procedures were performed following the manufacturer's recommendations. Incubation with 20 μg/ml proteinase K solution was modified to 10 min to achieve maximum staining results. Apoptotic count was performed using a light microscope, counting stained apoptotic tumor cells per 10 HPF (400× magnification, area of HPF 0.23 mm^2). Corresponding H&E sections were analyzed to avoid miscounting necrotic cells.

DNA extraction and analysis of *k-ras* mutation

Genomic DNA was extracted from routinely processed paraffin wax blocks, and the DNA was purified with the QIAmp DNA Mini Kit (Quiagen, Hilden, Germany). Further processing was performed according to the recommendations of the supplier. Exon 1 of *k-ras*, harboring the relevant codons 12 and 13, was amplified by polymerase chain reaction (PCR), followed by direct sequencing. The PCR reaction was carried out in a total volume of 50 μl with HotMaster Taq (Eppendorf, Hamburg, Germany) according to the recommendations of the supplier. Amplification was performed in a Primus 25 Thermocycler (MWG, Ebersberg, Germany) with 2 min of initial enzyme activation at 94°C followed by 40 cycles of denaturation at 94°C for 20 s, primer annealing at 55°C for 10 s, and extension at 65°C for 35 s. Sequences of both forward and reverse strands were analyzed on an ABI 3130 Genetic Analyzer (Applied Biosystems, CA, USA) using BigDye Terminator chemistry according to the recommendations of the supplier (Applied Biosystems, Foster City, CA, USA). The sequences of the PCR primers were: forward primer 5′-ATTATAAGGCCTGCTGAAAATGACTGA-3′ and reverse primer 5′-ATATGCATATTAAAACAAGATTTACCTCTA-3′.

Statistical analysis

All semiquantitative immunostainings (phospho-ERK1/2, phospho-AKT, and EGFR) were assessed by two of the authors (KJS, JB) in a blind-trial fashion without knowledge of the clinical outcome. In case of disagreement, slides were evaluated by both, and a final decision was made. All data were converted to a PC and statistically analyzed using SPSS Version 12 for Windows.

The kappa coefficient of interobserver agreement was calculated for semiquantitative pERK1/2, pAKT, and EGFR immunostaining results only; interpretation of the kappa value was performed using the commonly cited scale of Landis and Koch [24]. Interobserver agreement of

pERK1/2 and EGFR was almost perfect (κ=0.81 and 0.88, respectively). Interobserver agreement of pAKT immunostaining was substantial (κ=0.71). Relationships between ordinal parameters were investigated using two-tailed chi-square analysis (or Fisher's exact test where patient numbers were small). The relationship between categorical data (e.g., pERK1/2) and numeric data (e.g., number on Ki-67-positive tumor cells) was determined using the Kruskal–Wallis test. Overall survival (OS) curves were estimated using the Kaplan–Meier method, and any differences in the survival curves were compared by the log-rank test. For multivariate analysis, the Cox regression model was used. Overall, 95% confidence intervals were used throughout.

Results

Immunohistochemical analysis of phospho-ERK1/2 and phospho-AKT

Phospho-ERK1/2 immunohistochemistry of the complete series revealed strong nuclear immunostaining and partly cytoplasmic immunostaining, while nonneoplastic tissue revealed a positive staining, exclusively located at the surface epithelium. Tumors lacking pERK1/2 staining were classified as negative. In all, 115 (85.2%) tumors were classified as negative, and 20 (14.8%) were classified as positive. We refrained from classifying pERK1/2 staining into three categories (negative, moderate, and strong) because further stratification did not provide additional information in survival analysis.

Phospho-AKT immunohistochemistry was available for 133 cases. Loss of discs from slide occurred in two cases. Immunostaining of colorectal tumor tissue revealed a specific cytoplasmic staining, whereas normal mucosal tissue exhibited no staining. Tumors were classified according to their cytoplasmic staining intensity: negative, moderate, and strong. In all, 28 (20.7%) tumors were classified as negative, 77 (57%) as moderate, and 28 (20.7%) as strong. No correlation was observed between pAKT and COX-2 (P=0.185), pERK1/2 (P=0.418), EGFR (P=0.526), cyclin-D1 (P=0.644) or growth fraction (GF) (P=0.299) and apoptosis (P=0.111), respectively.

The relationship of pERK1/2 and pAKT with relevant clinicopathological data is summarized in Table 2. Representative immunohistochemical staining results of pERK1/2 and pAKT are shown in Fig. 1.

Correlation between phospho-ERK1/2 and pAKT immunostaining with survival

In all, 60 patients died of colorectal cancer, and nine were excluded from survival-related statistics, having died from either benign or other malignant neoplasm, for example leukemia after radiation therapy. In the remaining 126 cases, 47 out of 106 (44.3%) patients with a tumor showing negative pERK1/2 immunoreactivity died from colorectal cancer. In contrast, 13 out of 20 (65%) patients with positive pERK1/2 immunoreactivity died from colorectal cancer. OS was inversely associated with a positive pERK1/2 staining status. The impact of pERK1/2 expression and clinicopathological features on patient survival

Table 2 Expression of pERK1/2 and pAKT in relation to clinicopathological data

	N	pERK1/2			pAKT (serine 473)			
		Negative	Positive	*P*-value	Negative	Moderate	Strong	*P*-value
Grade[a]				0.885				0.99
1	31	27 (87.1)	4 (12.9)		3 (10)	22 (73.3)	5 (16.7)	
2	72	60 (83.3)	12 (16.7)		14 (19.7)	40 (56.3)	17 (23.9)	
3	27	23 (85.2)	4 (14.8)		10 (37)	12 (44.4)	5 (18.5)	
T stage[b]				0.231				0.041[c]
pT1	5	3 (60)	2 (40)		1 (20)	2 (40)	2 (40)	
pT2	14	12 (85.7)	2 (14.3)		2 (14.3)	6 (42.9)	6 (42.9)	
pT3	80	71 (88.8)	9 (11.2)		13 (16.5)	53 (67.1)	13 (16.5)	
pT4	33	26 (78.8)	7 (21.2)		12 (21.5)	14 (43.8)	5 (20.8)	
Lymph-node status[a]				0.143				0.443
pN0	63	56 (88.9)	7 (11.1)		10 (16.4)	38 (62.3)	13 (21.3)	
pN+	67	54 (80.6)	13 (19.4)		17 (25.4)	36 (53.7)	14 (20.9)	
Distant metastases[a]				0.534				0.231
pM0	99	84 (84.8)	15 (15.2)		18 (18.6)	58 (59.8)	21 (21.6)	
pM+	31	26 (83.9)	5 (16.1)		10 (32.3)	15 (48.4)	6 (19.4)	

[a] Data available for 130 cases
[b] Data available for 132 cases
[c] Statistically significant

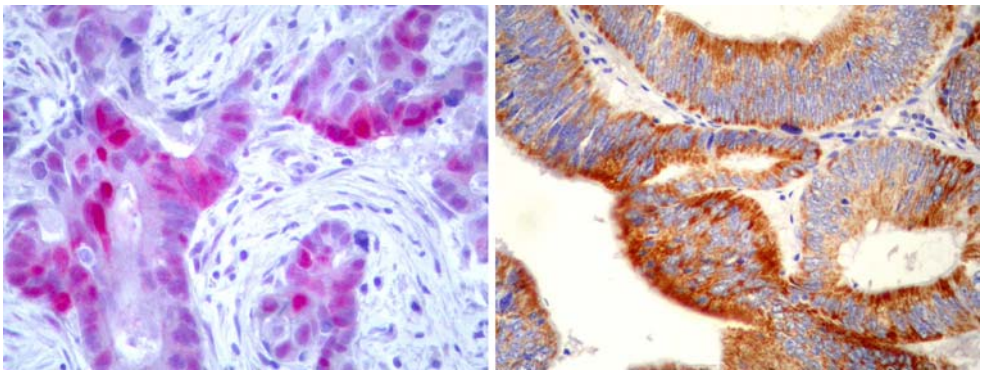

Fig. 1 Light micrograph displaying strong phospho-ERK1/2 (*left*) and strong phospho-AKT (*right*) in colorectal cancer as analyzed by immunohistochemistry

was assessed using univariate Kaplan–Meier survival analysis. Overall disease-specific survival (OS) was inversely associated with different pERK1/2 staining results (Fig. 2a). The 13 patients who had died from ERK1/2-positive colorectal cancer exhibited mainly advanced tumors with local or distant metastases. In detail, all 13 tumors were classified as T3 or T4; 12 tumors (92.3%) exhibited local and 5 tumors (38.5%) presented distant metastases. In contrast, only three (42.9%) of the seven ERK1/2-positive survivors showed T3 or T4 tumors; six (85.7%) were free of local lymph-node metastases, and none developed distant metastases. A comparable distribution was observed in the group of 46 nonsurviving patients with ERK1/2-negative tumors. Nearly all (44; 95.7%) were classified as T3 or T4 tumors; 29 (65.9%) exhibited local and 19 (42.2%) distant metastases. In contrast, 47 (82.5%) of the 57 ERK1/2-negative survivors showed T3 or T4 tumors; 35 (61.4%) were free of local lymph-node metastases, and nearly all patients lacked distant metastases (52; 92.9%). The main difference between ERK1/2-negative nonsurvivors and ERK1/2-positive nonsurvivors is the extent of survival. Whereas the 13 ERK1/2-positive nonsurvivors showed a mean survival time of 16 months until death, the mean survival time of ERK1/2-negative nonsurvivors increased to 23.7 months.

The unfavorable prognostic effect of tumors with elevated pERK1/2 levels increased in the subgroup of lymph-node-positive cases (Fig. 2b), whereas in the subgroup of lymph-node-negative cases, no significance could be detected in univariate Kaplan–Meier analysis. Results of the univariate survival analysis of the remaining parameters are shown in Table 3.

OS and relevant clinicopathological parameters (pERK, histological grading, TNM, lymph-node metastases, and distant metastases) were subjected to multivariate analysis. As a result pERK1/2, tumor size, lymph-node metastasis, and distant metastasis were statistically associated with OS (Table 4).

Correlation of pERK1/2 with COX-2, EGFR, GF, and apoptosis

All cancer specimens, including the cases excluded from survival analysis, were subjected to cyclin-D1, COX-2, EGFR, Ki67, and TUNEL analysis.

A total of 132 tumors were analyzed for COX-2 protein expression; the remaining showed loss of discs. Tumor cells

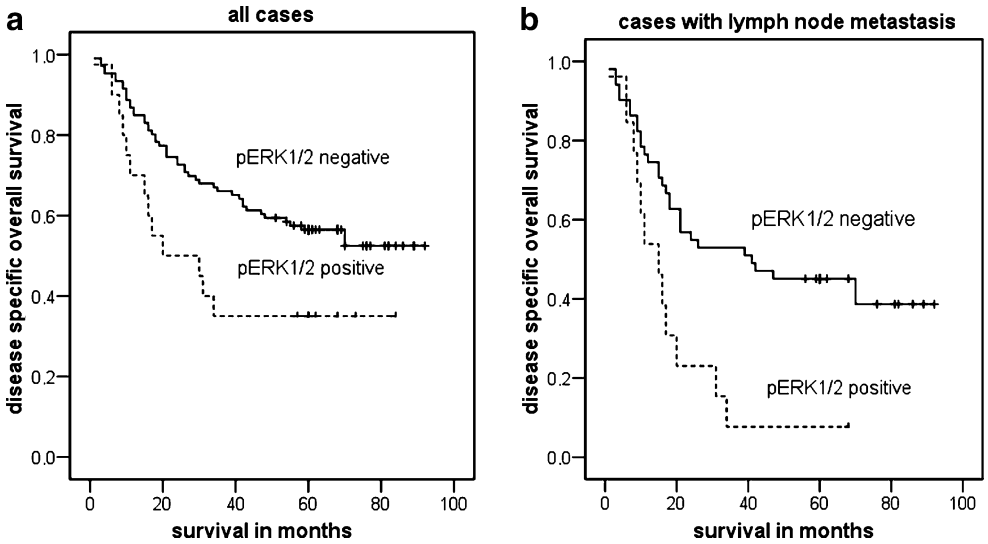

Fig. 2 Kaplan–Meier survival plot (*left*) for disease-specific overall survival in the complete series of 126 colorectal cancers in relation to pERK immunostaining intensity. Log-rank test: $P=0.0299$. Kaplan–Meier survival plot for disease-specific overall survival in colorectal cancer with lymph-node metastasis (*right*). Log-rank test: $P=0.0032$

Table 3 Univariate analysis (Kaplan–Meier, log-rank test) for prognostic significance of pERK1/2, pAKT, histological grading, tumor size, lymph-node metastases, distant metastases, COX-2, cyclin D1, EGFR, and *k-ras*

Parameter	*P*-value
Phospho-ERK1/2 (negative/positive)	0.0299[a]
Phospho-AKT (negative/weak/strong expression)	Not significant
Histological grading (G1–G3)	0.051[a]
Tumor stage (pT1-4)	0.000[a]
Lymph-node metastases (pN0 vs pN+)	0.000[a]
Distant metastases (M0 vs M1)	0.000[a]
COX-2	Not significant
Cyclin-D1	Not significant
EGFR	Not significant
k-ras (mutated vs wild-type)	Not significant

[a] Statistically significant

exhibited a specific cytoplasmic staining pattern. Classification was performed according to the amount of positively stained tumor cells: negative (0–10%) and positive (>10%). In all, 99 (75%) tumors were classified as positive and 33 (25%) as negative. No significant relationship of elevated pERK1/2 with COX-2 expression was observed. COX-2 expression was not associated with EGFR expression, cyclin-D1 immunoreactivity, GF, or apoptotic rate.

EGFR expression was analyzed in 128 tumor samples. Tumor cells revealed a specific cytoplasmic immunoreaction. Classification was performed according to the guidelines of PharmDx™ (DakoCytomation). Tumor samples lacking an immunostaining were classified as negative (0), whereas the remaining were classified as positive. In all, 83 (64.85%) tumors were classified as positive and 45 (35.2%) as negative. EGFR staining intensity was not related to pERK1/2, pAKT, and COX-2 immunostaining results. EGFR-positive tumors revealed a higher amount of proliferating tumor Ki-67-positive cells ($P<0.001$) and an increased apoptotic rate ($P=0.016$).

Table 4 Results of multivariate analysis (Cox regression) to determine the independent prognostic value of different variables in relation to overall survival ($n=126$)

Covariate	Relative risk (e^{β})	95% CI	*P*-value
pERK1/2 (negative vs positive)	2.603	1.336–5.073	0.005[a]
Histological grade (1, 2, 3)	1.027	0.663–1.592	0.904
Tumor stage according to TNM (1, 2, 3, 4)	3.812	2.212–6.571	0.000[a]
Lymph nodes (pN0 vs pN+)	1.798	0.939–3.444	0.030[a]
Distant metastases (M0 vs M1)	3.584	1.962–6.546	0.000[a]

[a] Statistically significant

The GF was defined as the percentage of Ki67-positive nuclei per 300 tumor cells. Statistical analysis showed no significant relationship of growth fraction with pERK1/2, pAKT, or COX-2 immunostaining. The amount of Ki-67-positive tumor cells correlated directly with the percentage of cyclin-D1-positive tumor cells ($P=0.033$). As mentioned above, the growth fraction was significantly increased in EGFR-positive tumors.

There was no relationship between the different pERK1/2 or pAKT immunostaining and the number of apoptotic tumor cells as determined by TUNEL. Statistical analysis revealed no association of the rate of apoptotic cells with COX-2 or cyclin-D1 staining. As mentioned above, EGFR-positive tumors revealed higher amounts of apoptotic cells.

Correlation of pERK1/2 with cyclin-D1

A total of 123 tumors was analyzed for cyclin-D1 protein expression. In 12 cases, the loss of discs from slides occurred. Tumor cells revealed a strong and specific nuclear staining pattern. Tumors were classified according to their amount of stained nuclei: negative (0–10%), weakly positive (11–30%), and strongly positive (>30%). Thirty-eight (30.9%) tumors were classified as negative, 61 (49.6%) tumors as weakly positive, and 24 (19.5%) tumors as strongly positive.

Tumors classified as pERK1/2 negative showed a higher proportion (20.5%) of cyclin-D1-positive tumor cells (mean value), whereas cases with elevated levels of pERK1/2 exhibited a lower proportion (12.7%) of cyclin-D1-positive tumor cells. All cases with a strong expression of cyclin-D1 (>30%) were classified as pERK1/2 negative. Statistical analysis indicates that tumor samples with elevated pERK1/2 expression exhibit significantly lower amounts of cyclin-D1-positive tumor cells (0.042, chi-square analysis).

Mutation of *k-ras* genes

In the present study, mutations were detected in codons 12 and 13 in 36 out of 134 cases (26.9%). Twenty-five mutations were G→A transversions, three mutations were G→T transversions, and eight mutations were G→C transversions. Chi-square analysis showed that tumors with elevated pERK1/2 levels more frequently presented *k-ras* mutations ($P=0.015$). Ten of the 20 (50%) tumor samples with elevated phospho-ERK1/2 levels exhibited a *k-ras* point mutation at codon 12 or 13 in contrast to only 26 of 114 (22.8%) in the group of tumor levels with low pERK1/2 levels. A strong pAKT expression was more frequently found in patients with *k-ras* mutations. In the subgroup of 98 tumors with wild-type *k-ras*, only 19 cases (19.4%)

showed a strong pAKT expression in contrast to nine (26.5%) cases in the subgroup of 34 tumors with mutated *k-ras*. On the other hand, the percentage of pAKT-negative classified tumors was higher in patients with wild-type *k-ras* (22 of 98; 22.4%) in contrast to patients with mutated *k-ras* (6 of 34; 17.6%). Chi-square analysis revealed no statistical significance between the presence of *k-ras* mutations and the expression of pAKT (P=0.639).

Discussion

This study demonstrates for the first time that phosphorylation of ERK1/2 but not AKT predicts poor patient prognosis in colorectal cancers independent of tumor stage, histological grading, and local or distant metastasis. The statistical power of this study is, unfortunately, reduced due to the relatively small number of pERK1/2 positive classified colorectal cancers. Therefore, it is necessary to confirm these promising results in larger cohorts. A detailed analysis of the nonsurviving patients with different pERK1/2 levels revealed that both ERK1/2-positive and ERK1/2-negative nonsurvivors exhibited advanced colorectal cancers with large tumor size and presence of local and/or distant metastasis. However, patients dying from pERK1/2-positive colorectal cancer displayed markedly decreased survival times in contrast to pERK1/2 negative nonsurvivors. Thus, raised pERK1/2 levels seem to enhance aggressiveness of advanced cancer disease rather than initiate or promote tumor growth or metastasis. Analysis of putative upstream mechanisms revealed an association of *k-ras* mutations with ERK1/2 phosphorylation, suggesting a biological link between *k-ras* mutations and activation of this MAPK pathway in colorectal cancer. Our results support the notion that *k-ras* mutations also contribute to activation of the AKT pathway; however, due to the relatively small number of tumors with *k-ras* mutations, significance was not reached. Mutations of *k-ras* are found in approximately 36% of colorectal cancers and are considered to constitute a crucial step in colorectal carcinogenesis [1]. Because *k-ras* mutations occur frequently in colorectal cancer and the RAS/RAF proteins are well-known activators of ERK1/2 [1], phosphorylation of these kinases is likely to reflect the oncogenic potential of *k-ras*. A recent study found *k-ras* mutations to be associated with poor survival in a cohort of 107 colorectal cancers [9], a finding that cannot be confirmed in our study. Although the frequency of *k-ras* mutations in our study (26.7%) was comparable to that described by Conlin et al. (27%), we cannot explain the diverse results. Thus, the prognostic value of *k-ras* remains to be clarified in further studies.

Although there have been previous studies describing elevated pERK1/2 levels in colorectal cell lines [21] and human colorectal cancer tissue [26], the prognostic significance of ERK1/2 activation has not been examined yet. Only few studies focused on the prognostic significance of pERK1/2 in human cancer arriving at contradictory data. Whereas activation of the ERK1/2 pathway in mucoepidermoid carcinoma of the salivary gland was associated with aggressive tumor behavior [19], other studies report pERK1/2 to be a favorable prognostic marker in breast cancer [19, 27] and serous ovarian cancer [17]. We found pERK1/2 not to be related to prognosis in nodal-negative breast cancer [34]. Apparently, activation of the ERK1/2 pathway can initiate cellular processes, resulting in either favorable or worse clinical outcome depending on the tumor type and tumor localization. Keeping the complex signaling network in mind, this is not surprising. In fact, ras/ERK-transduced signals can induce adverse effects, depending on intensity and duration of the signal: a short duration of ERK activation favors a mitogenic response, whereas a long duration primarily stimulates differentiation [46]. To disclose putative pathways contributing to the increased tumor aggressiveness and reduced survival of patients with pERK1/2-positive colorectal cancer, we investigated factors associated with ERK activation and ERK1/2-mediated downstream signaling effects. One of the upstream events which potentially contributes to MAPK activation is the overexpression of EGF receptor [8], but we did not find any linkage of EGFR with pERK1/2.

Within several downstream signaling effects, the ERK pathway is involved in cell proliferation, apoptosis and tumor invasion, and metastasis [13]. Important factors that influence cell proliferation are cyclin-D1 [25] and $p21^{Waf1}$ [13]. In this study, however, we neither were able to demonstrate an increase of cyclin-D1 protein expression nor proliferative activity measured by Ki-67 immunohistochemistry. Surprisingly, cyclin-D1 expression was lower in tumors with elevated pERK1/2, a fact which we cannot sufficiently explain at this time. In addition, we could not detect an association of ERK1/2 activation and tumor-cell apoptosis as measured by TUNEL. Thus, further studies are needed to elucidate the exact mechanism of ERK1/2-induced tumor aggressiveness. Maybe, the consequence of ERK pathway activation on matrix metalloproteinases or vascular endothelial growth factor might contribute to a more aggressive phenotype [13]. Thus, our results suggest that at least in this cohort, the effect of ERK1/2 signaling in tumor invasion and metastasis might be more relevant than its influence on proliferation and apoptosis, but this remains speculative.

Because a study on breast cancer cell lines identified the MAPK pathway as an upstream activator of *COX-2* gene expression [39], we determined the COX-2 protein expression in our cohort. However, COX-2 protein seems not to be linked with ERK1/2 activation.

Among the tumor-cell survival pathways, those mediated by the AKT kinase are the most critical [5, 7]. In human malignancies, AKT is activated in a variety of carcinomas including prostate, ovary, and breast cancer [2, 34, 40]. The prognostic significance of activated AKT (pAKT) in colorectal cancer has not been investigated yet although first studies suggest that AKT is involved in colorectal carcinogenesis [23]. Our data indicate that AKT does not serve as a prognostic parameter in colorectal cancer.

In our study, the clinical impact of ERK1/2 activation was strongest in the subgroup of cancer patients with lymph-node metastases. ERK1/2 activation in these patients might offer a new approach of biochemical therapy due to the existence of ERK-targeted, chemopreventive and chemotherapeutic anticancer drugs. Such elegant drugs are currently being developed [30, 35]. The detection of phosphorylated ERK1/2 in cancer tissue could be a straightforward way to select patients for these treatments.

Acknowledgement The technical assistance of Dorothe Möllmann, Caroline Stang, and Karin Scholz is gratefully acknowledged. K.J. Schmitz and J. Wohlschlaeger contributed equally to this study.

References

1. Andreyev HJ, Norman AR, Cunningham D, Oates JR, Clarke PA (1998) Kirsten ras mutations in patients with colorectal cancer: the multicenter "RASCAL" study. J Natl Cancer Inst 90:675–684
2. Bellacosa A, de Feo D, Godwin AK, Bell DW, Cheng JQ, Altomare DA, Wan M, Dubeau L, Scambia G, Masciullo V (1995) Molecular alterations of the AKT2 oncogene in ovarian and breast carcinomas. Int J Cancer 64:280–285
3. Blenis J (1993) Signal transduction via the MAP kinases: proceed at your own RSK. Proc Natl Acad Sci USA 90:5889–5892
4. Bubendorf L, Nocito A, Moch H, Sauter G (2005) Tissue microarray (TMA) technology: miniaturized pathology archives for high-throughput in situ studies. J Pathol 195:72–79
5. Burgering BM, Coffer PJ (1995) Protein kinase B (c-Akt) in phosphatidylinositol-3-OH kinase signal transduction. Nature 376:599–602
6. Cardone MH, Roy N, Stennicke HR, Salvesen GS, Franke TF, Stanbridge E, Frisch S, Reed JC (1998) Regulation of cell death protease caspase-9 by phosphorylation. Science 282:1318–1321
7. Chan TO, Rittenhouse SE, Tsichlis PN (1999) AKT/PKB and other D3 phosphoinositide-regulated kinases: kinase activation by phosphoinositide-dependent phosphorylation. Annu Rev Biochem 68:965–1014
8. Chen DB, Davis JS (2003) Epidermal growth factor induces c-fos and c-jun mRNA via Raf-1/MEK1/ERK-dependent and -independent pathways in bovine luteal cells. Mol Cell Endocrinol 200:141–154
9. Conlin A, Smith G, Carey FA, Wolf CR, Steele RJ (2005) The prognostic significance of K-ras, p53, and APC mutations in colorectal carcinoma. Gut 54:1283–1286
10. Dai DL, Martinka M, Li G (2005) Prognostic significance of activated Akt expression in melanoma: a clinicopathologic study of 292 cases. J Clin Oncol 23:1473–1482
11. Datta SR, Brunet A, Greenberg ME (1999) Cellular survival: a play in three Akts. Genes Dev 13:2905–2927
12. Diehl JA, Cheng M, Roussel MF, Sherr CJ (1998) Glycogen synthase kinase-3beta regulates cyclin D1 proteolysis and subcellular localization. Genes Dev 12:3499–3511
13. Fang JY, Richardson BC (2005) The MAPK signalling pathways and colorectal cancer. Lancet Oncol 6:322–327
14. Franke TF (1999) A difficult akt to follow. Neural Notes 5:3–7
15. Franke TF, Kaplan DR, Cantley LC (1997) PI3K: downstream AKTion blocks apoptosis. Cell 88:435–437
16. Franke TF, Yang SI, Chan TO, Datta K, Kazlauskas A, Morrison DK, Kaplan DR, Tsichlis PN (1995) The protein kinase encoded by the Akt proto-oncogene is a target of the PDGF-activated phosphatidylinositol 3-kinase. Cell 81:727–736
17. Givant-Horwitz V, Davidson B, Lazarovici P, Schaefer E, Nesland JM, Trope CG, Reich R (2003) Mitogen-activated protein kinases (MAPK) as predictors of clinical outcome in serous ovarian carcinoma in effusions. Gynecol Oncol 91:160–172
18. Hamilton SR, Aaltonen LA (2000) World Health Organization Classification of Tumours. Pathology and genetics of tumours of the digestive system. IARC Press, Lyon
19. Handra-Luca A, Bilal H, Bertrand JC, Fouret P (2003) Extracellular signal-regulated ERK-1/ERK-2 pathway activation in human salivary gland mucoepidermoid carcinoma: association to aggressive tumor behavior and tumor cell proliferation. Am J Pathol 163:957–967
20. Hoshino R, Chatani Y, Yamori T, Tsuruo T, Oka H, Yoshida O, Shimada Y, Ari-i S, Wada H, Fujimoto J, Kohno M (1999) Constitutive activation of the 41-/43-kDa mitogen-activated protein kinase signaling pathway in human tumors. Oncogene 18:813–822
21. Hoshino R, Chatani Y, Yamori T, Tsuruo T, Oka H, Yoshida O, Shimada Y, Ari-i S, Wada H, Fujimoto J, Kohno M (1999) Constitutive activation of the 41-/43-kDa mitogen-activated protein kinase signaling pathway in human tumors. Oncogene 18:813–822
22. Itoh N, Semba S, Ito M, Takeda H, Kawata S, Yamakawa M (2002) Phosphorylation of Akt/PKB is required for suppression of cancer cell apoptosis and tumor progression in human colorectal carcinoma. Cancer 94:3127–3134
23. Khaleghpour K, Li Y, Banville D, Yu Z, Shen SH (2004) Involvement of the PI 3-kinase signaling pathway in progression of colon adenocarcinoma. Carcinogenesis 25:241–248
24. Landis JR, Koch GG (1977) The measurement of observer agreement for categorical data. Biometrics 33:159–174
25. Lavoie JN, L'Allemain G, Brunet A, Muller R, Pouyssegur J (1996) Cyclin D1 expression is regulated positively by the p42/p44MAPK and negatively by the p38/HOGMAPK pathway. J Biol Chem 271:20608–20616
26. Lee SH, Lee JW, Soung YH, Kim SY, Nam SW, Park WS, Kim SH, Yoo NJ, Lee JY (2004) Colorectal tumors frequently express phosphorylated mitogen-activated protein kinase. Acta Pathol Microbiol Immunol Scand 112:233–238
27. Milde-Langosch K, Bamberger AM, Rieck G, Grund D, Hemminger G, Muller V, Loning T (2005) Expression and prognostic relevance of activated extracellular-regulated kinases (ERK1/2) in breast cancer. Br J Cancer 92:2206–2215
28. Min YH, Eom JI, Cheong JW, Maeng HO, Kim JY, Jeung HK, Lee ST, Lee MH, Hahn JS, Ko YW (2003) Constitutive phosphorylation of Akt/PKB protein in acute myeloid leukemia: its significance as a prognostic variable. Leukemia 17:995–997
29. Pearson G, Robinson F, Beers GT, Xu BE, Karandikar M, Berman K, Cobb MH (2001) Mitogen-activated protein (MAP) kinase pathways: regulation and physiological functions. Endocr Rev 22:153–183

30. Rinehart J, Adjei AA, Lorusso PM, Waterhouse D, Hecht JR, Natale RB, Hamid O, Varterasian M, Asbury P, Kaldjian EP, Gulyas S, Mitchell DY, Herrera R, Sebolt-Leopold JS, Meyer MB (2004) Multicenter phase II study of the oral MEK inhibitor, CI-1040, in patients with advanced non-small-cell lung, breast, colon, and pancreatic cancer. J Clin Oncol 22:4456–4462
31. Robinson MJ, Cobb MH (1997) Mitogen-activated protein kinase pathways. Curr Opin Cell Biol 9:180–186
32. Sakakura C, Hagiwara A, Shirahama T, Nakanishi M, Yasuoka R, Fujita Y, Inazawa J, Abe T, Kohno M, Yamagishi H (1999) Infrequent activation of mitogen-activated protein kinase in human colon cancers. Hepatogastroenterology 46:2831–2834
33. Schaeffer HJ, Weber MJ (1999) Mitogen-activated protein kinases: specific messages from ubiquitous messengers. Mol Cell Biol 19:2435–2444
34. Schmitz KJ, Otterbach F, Callies R, Levkau B, Holscher M, Hoffmann O, Grabellus F, Kimmig R, Schmid KW, Baba HA (2004) Prognostic relevance of activated Akt kinase in node-negative breast cancer: a clinicopathological study of 99 cases. Mod Pathol 17:15–21
35. Sebolt-Leopold JS (2000) Development of anticancer drugs targeting the MAP kinase pathway. Oncogene 19:6594–6599
36. Sebolt-Leopold JS, Herrera R (2004) Targeting the mitogen-activated protein kinase cascade to treat cancer. Nat Rev Cancer 4:937–947
37. Shin I, Yakes FM, Rojo F, Shin NY, Bakin AV, Baselga J, Arteaga CL (2002) PKB/Akt mediates cell-cycle progression by phosphorylation of p27(Kip1) at threonine 157 and modulation of its cellular localization. Nat Med 8:1145–1152
38. Stewart BW, Kleihus P (2003) World cancer report. IARC Press, Lyon
39. Subbaramaiah K, Chung WJ, Dannenberg AJ (1998) Ceramide regulates the transcription of cyclooxygenase-2. Evidence for involvement of extracellular signal-regulated kinase/c-Jun N-terminal kinase and p38 mitogen-activated protein kinase pathways. J Biol Chem 273:32943–32949
40. Sun M, Wang G, Paciga JE, Feldman RI, Yuan ZQ, Ma XL, Shelley SA, Jove R, Tsichlis PN, Nicosia SV, Cheng JQ (2001) AKT1/PKBalpha kinase is frequently elevated in human cancers and its constitutive activation is required for oncogenic transformation in NIH3T3 cells. Am J Pathol 159:431–437
41. Vogel US, Dixon RA, Schaber MD, Diehl RE, Marshall MS, Scolnick EM, Sigal IS, Gibbs JB (1988) Cloning of bovine GAP and its interaction with oncogenic ras p21. Nature 335:90–93
42. Vogelstein B, Fearon ER, Hamilton SR, Kern SE, Preisinger AC, Leppert M, Nakamura Y, White R, Smits AM, Bos JL (1988) Genetic alterations during colorectal-tumor development. N Engl J Med 319:525–532
43. Wolmark N, Bryant J, Smith R, Grem J, Allegra C, Hyams D, Atkins J, Dimitrov N, Oishi R, Prager D, Fehrenbacher L, Romond E, Colangelo L, Fisher B (1998) Adjuvant 5-fluorouracil and leucovorin with or without interferon alfa-2a in colon carcinoma: National Surgical Adjuvant Breast and Bowel Project protocol C-05. J Natl Cancer Inst 90:1810–1816
44. Xu X, Sakon M, Nagano H, Hiraoka N, Yamamoto H, Hayashi N, Dono K, Nakamori S, Umeshita K, Ito Y, Matsuura N, Monden M (2004) Akt2 expression correlates with prognosis of human hepatocellular carcinoma. Oncol Rep 11:25–32
45. Yamamoto S, Tomita Y, Hoshida Y, Morooka T, Nagano H, Dono K, Umeshita K, Sakon M, Ishikawa O, Ohigashi H, Nakamori S, Monden M, Aozasa K (2004) Prognostic significance of activated Akt expression in pancreatic ductal adenocarcinoma. Clin Cancer Res 10:2846–2850
46. Yen A, Roberson MS, Varvayanis S, Lee AT (1998) Retinoic acid induced mitogen-activated protein (MAP)/extracellular signal-regulated kinase (ERK) kinase-dependent MAP kinase activation needed to elicit HL-60 cell differentiation and growth arrest. Cancer Res 58:3163–3172
47. Zhou BP, Liao Y, Xia W, Spohn B, Lee MH, Hung MC (2001) Cytoplasmic localization of p21Cip1/WAF1 by Akt-induced phosphorylation in HER-2/neu-overexpressing cells. Nat Cell Biol 3:245–252

Virchows Arch (2007) 450:161–167
DOI 10.1007/s00428-006-0314-2

ORIGINAL ARTICLE

Association of CDK4 and CCND1 mRNA overexpression in laryngeal squamous cell carcinomas occurs without *CDK4* amplification

Alfons Nadal · Pedro Jares · Magda Pinyol · Laura Conde · Coia Romeu · Pedro L. Fernández · Elías Campo · Antonio Cardesa

Received: 22 February 2006 / Accepted: 7 September 2006 / Published online: 1 December 2006
© Springer-Verlag 2006

Abstract CDK4 is involved in the control of G_1–S phase transition as a part of the CCND1/CDK4 complexes. CCND1 and *CDK4* gene alterations have been implicated in the development of different tumors. CCND1 has been associated with progression in laryngeal carcinomas. CDK4 protein overexpression was described associated to CCND1 overexpression in these tumors. However, the mechanisms implicated were not known. We analyzed *CDK4* gene alterations and mRNA expression in a series of carcinomas of the larynx, and the results were compared to CCND1 expression and clinicopathological characteristics of the patients. CDK4 mRNA was overexpressed in 42 out of 60 tumors (70%) associated with CCND1 mRNA overexpression because 15 out of 16 cases with high CCND1 levels showed simultaneous increased levels of CDK4 mRNA (p=0.023) and 12 (87%) of the tumors overexpressing both genes were in stage 4. No *CDK4* gene amplifications, rearrangements, or mutations were detected in any of the tumors, including 24 overexpressed cases. These findings confirm that CDK4 overexpression is a frequent phenomenon in laryngeal carcinomas, which occurs at the transcriptional level but is related neither to gene amplification nor to gene mutation, and suggest that cooperation with CCND1 may be involved in the progression of laryngeal tumors.

Keywords Larynx · Head and Neck · Oncogenes

A. Nadal (✉) · P. L. Fernández · E. Campo · A. Cardesa
Anatomia Patologica, Hospital Clínic, Institut d'Investigacions Biomediques "August Pi i Sunyer" (IDIBAPS),
Villarroel 170,
Barcelona, Spain
e-mail: anadal@clinic.ub.es

A. Nadal · P. L. Fernández · E. Campo · A. Cardesa
Departament de Biologia Cel·lular i Anatomia Patológica,
Universitat de Barcelona,
Casanovas 143,
08036 Barcelona, Spain

P. Jares · M. Pinyol
Genomics Unit, Institut d'Investigacions Biomediques "August Pi i Sunyer"(IDIBAPS), Universitat de Barcelona,
Villarroel 170,
08036 Barcelona, Spain

L. Conde
Fundació Clínic per a la Recerca Biomédica,
Villarroel 170,
08036 Barcelona, Spain

C. Romeu
Hospital de Ntra. Sra. de Meritxell,
Avda. Fiter i Rossell, 1-13,
Escaldes-Engordany, Principat d'Andorra

Introduction

Squamous cell carcinoma (SCC) of the larynx is a malignant neoplasm that shows different incidences throughout the world. The Mediterranean basin shows one of the highest incidences and, in Southern Europe, it is the sixth most common cancer among men [19]. The molecular mechanisms involved in the pathogenesis of these tumors are not well known. In recent years, the participation of cell-cycle regulatory elements in the development and progression of human tumors has gained interest [7]. Particularly, we and others have demonstrated the frequent alterations of different cell-cycle regulatory genes including CCND1, $p16^{INK4a}$, p53, and $p21^{Waf1}$ in laryngeal carcino-

mas [8–10, 18], indicating that deregulation of cell-cycle mechanisms may play an important role in the malignant transformation of laryngeal epithelium.

CDK4 was initially identified as the catalytic subunit present in the G1 CDK/Cyclin D complexes of mammalian cells [16] and, similarly to other G1 regulatory genes, may have oncogenic potential [5]. *CDK4* has been mapped to 12q13, a chromosomal region that includes a number of genes such as MDM2, GADD153, SAS, and GLI, which are frequently amplified in different sarcomas of bone and soft tissues and gliomas [6, 11, 23]. CDK4 overexpression, independent of gene amplification, seems to be a more frequent phenomenon, and it has been observed in different human tumors [13, 15]. Gene mutations in the $p16^{INK4}$ binding domain of CDK4 have been also identified as alternative oncogenic events in rare cases of familial and sporadic malignant melanoma with no alterations of $p16^{INK4}$ gene [4, 24, 26, 27]. The role of CDK4 in the pathogenesis of head and neck carcinomas is not well known, although a putative prognostic value of CDK4 and CCND1 protein overexpression was described in laryngeal carcinomas [2].

To determine whether CDK4 mRNA overexpression was the result of gene amplification, we analyzed CDK4 mRNA expression and gene status in a series of primary SCC of the larynx. The results were compared with clinical and pathological features of the patients and CCND1 mRNA expression levels in the tumors. Our results indicate that CDK4 mRNA is frequently overexpressed in laryngeal carcinomas independently of obvious genetic alterations. CDK4 mRNA deregulation occurs early in the development of the tumors. However, the coordinate overexpression of CDK4 and CCND1 mRNAs could be implicated in the progression of these neoplasms.

Table 1 Clinicopathological characteristics of the patients and CDK4 and CCND1 expression

	Total	With overexpression	
		CDK4	CCND1
Location			
Glottic	18	11 (61%)	2 (11%)
Transglottic	20	13 (65%)	8 (40%)
Supraglottic	16	13 (81%)	2 (13%)
Pyriform sinus	6	5 (83%)	4 (67%)
Grade of differentiation			
1	8	4 (50%)	0
2	13	8 (62%)	4 (31%)
3	33	25 (76%)	10 (30%)
4	6	5 (83%)	2 (33%)
Tumor extension			
T1	4	3 (75%)	0
T2	4	3 (75%)	0
T3	34	21 (62%)	5 (15%)
T4	18	15 (83%)	11 (61%)[a]
Stage			
1	3	2 (66%)	0
2	3	2 (66%)	0
3	28	18 (64%)	4 (14%)
4	26	20 (77%)	12 (46%)[b]

[a] $p<0.001$; Fisher's exact test, T4 vs T1 through T3
[b] $p=0.003$; Fisher's exact test, stage 4 vs stages 1 through 3

Materials and methods

Patients and tissues

Fresh tissue was obtained from 60 patients who underwent surgery for SCC of the larynx at our institution. Tumor and normal samples were dissected from the surgical specimens, snap-frozen in liquid nitrogen, and stored at −80°C until used. The remaining of the specimen was routinely fixed and processed for histopathological analysis. Clinical information was retrieved from the clinical charts of the patients and is summarized in Table 1.

RNA extraction and Northern-blot analysis

Total RNA was isolated from frozen tissues by guanidine isothiocyanate extraction and cesium chloride gradient centrifugation as previously described. Tissue sections were evaluated histologically to ensure that neoplastic cells accounted for, at least, 75% of the total cell number [8]. Fifteen micrograms of total RNA was electrophoresed on a denaturing 1.2% agarose formaldehyde gel and transferred to Hybond-N membranes (Amersham, Buckinghamshire, UK). The membranes were prehybridized, hybridized at 45°C with the full cDNA CDK4 probe [26], and washed at 55°C. Probe was radiolabeled using a random primer DNA labeling kit (Promega, Madison, WI, USA) with α-^{32}P dCTP. Quantification of the hybridization signals was obtained by optical densitometry with the UVP GelBase software package as described elsewhere [8]. Cases with a tumor/normal ratio higher than twofold were considered to overexpress CDK4. After stripping, the membranes were rehybridized with the CCND1 probe and analyzed in the same way.

Quantitative RT-PCR

cDNA was synthesized from 1 μg of DNAase-treated total RNA using random hexamers following the directions of the manufacturer (Taqman Reverse Transcription Reagents, Applied Biosystems). Quantitative PCR was performed to

assess human CCND1 and *CDK4* gene expression using ABI PRISM 7900 Sequence Detector System and Assay on Demand Technology (Applied Biosystems). Assay IDs were Hs00277039_m1 and Hs00364847_m1 for CCND1 and CDK4, respectively. PCR reactions were done using Taqman Universal Master Mix (Applied Biosystems). Amplification conditions were 2 min at 50°C for UNG activation and 10 min at 95°C for TaqGold activation and predenaturation followed by 40 cycles at 95°C for 15 s and 60°C for 1 min. β-Glucoronidase gene (GUS; Applied Biosystems) was used as endogenous control as recommended by the manufacturer.

DNA extraction, Southern-blot, and SSCP analyses

DNA was extracted by conventional methods using proteinase-K digestion and phenol-chloroform extraction. Fifteen micrograms of DNA from normal and tumoral tissue from 31 matched normal and tumor tissues was digested with *Eco*RI and analyzed by Southern blot. All those cases were previously analyzed by Northern blot. Membranes were hybridized with the same probe used for Northern-blot analysis, at 42°C, and exposed at −70°C for 2 weeks.

Exon 2 of *CDK4* was analyzed by nonisotopic SSCP in 38 of the 60 cases analyzed by Northern blot that included the 31 analyzed by Southern blot. A total of 0.5 μg of DNA was used as template in a standard PCR reaction containing PCR buffer, dNTPs 10 mM each, primers 1 mM each, 1 U of *Taq* DNA polymerase, and 5% DMSO in a reaction volume of 50 μl. Primers—modified from Zuo et al. [27]—were 5′-GCTGCAGGTCATACCATCCT-3′ (sense) and 5′-ATCACACCCCACCTATAGG-3′ (antisense). A modification of the touchdown PCR strategy (step-down PCR) was used. Conditions were: a denaturation step of 5 min at 94°C, 4 cycles at 94°C for 45 s (denaturation), at 66°C for 1 min (annealing), and at 72°C for 1 min (extension), 4 cycles with annealing at 63°C, 4 cycles with annealing at 60°C, 4 cycles with annealing at 57°C, and 30 cycles with annealing at 55°C followed by a last step of 5 min at 72°C. Sixteen microliters was digested with *Rsa*I, and 2 μl of the digested product was electrophoresed at room temperature in 15% polyacrylamide gels and silver-stained according to a previously described method [9].

Statistical methods

Categorical data were analyzed by means of contingency tables. Probability was calculated with the Fisher's exact test. Data were analyzed using the SPSS statistical package (SPSS, Chicago, IL, USA). Significance was accepted with an α-risk of 0.05.

Results

CDK4 mRNA expression

CDK4 mRNA expression was analyzed in 60 matched pairs of normal and tumor samples by Northern blot. A single 1.9-kb transcript was detected in all normal tissue samples. Forty-two carcinomas (70%) showed CDK4 mRNA overexpression with a range of two- to 13-fold of their normal counterpart (Fig. 1). Northern-blot results were validated by Q-RT-PCR in a series of nine cases (six with and three without CDK4 overexpression) with a 100% of concordance between Northern blot and Q-RT-PCR (p=0.012, Fisher's exact test). A similar number of tumors overexpressing CDK4 were observed in early and advanced stages. Similarly, no significant differences were observed in CDK4 expression levels according to location or grade of differentiation of the tumors (Table 1). The overall disease-free interval after surgery was independent of CDK4 overexpression. Cases with CDK4 overexpression had a mean disease-free time of 65 vs 56 months for cases without it, for the 47 cases with available follow-up.

CDK4 gene analysis

To determine if the *CDK4* overexpression observed in the tumors was due to genetic alterations, 31 paired normal and tumor samples, previously analyzed for CDK4 overexpression by Northern blot, and including 24 cases with CDK4 overexpression, were examined by Southern blot. The two expected bands of 3.8 and 4.6 kb were observed in all cases. No gene amplification, deletions, or rearrangements were detected in any of the tumors (Fig. 1). In addition, a mutational analysis of *CDK4* exon 2, which included the $p16^{INK4a}$ binding domain, was performed by SSCP in 38 out of the 60 cases analyzed by Northern blot, including all cases analyzed by Southern blot. No altered migration patterns were identified in any of the tumors analyzed.

CCND1 mRNA expression

CCND1 mRNA expression was examined in the same cases (Fig. 2). Sixteen cases showed CCND1 overexpression, with levels ranging from two- to 18-fold of their normal counterparts. Northern-blot results were validated by Q-RT-PCR in a series of ten cases (four with and six without CCND1 overexpression) with a 100% of concordance between both methods (p=0.005, Fisher's exact test; Fig. 3). A significant association was found between CCND1 and advanced stage of disease because 75% of the cases with overexpression were in stage 4 (p=0.003, Fisher's exact test) and between CCND1 and CDK4 mRNA

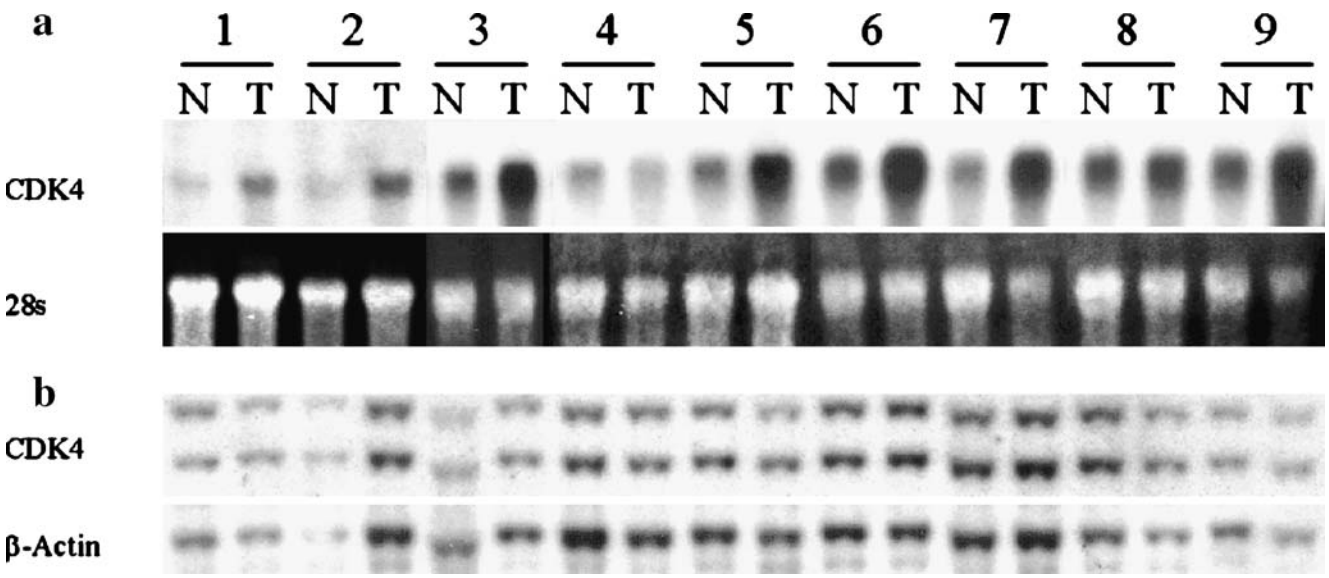

Fig. 1 **a** Northern blot analysis of CDK4 mRNA expression in nine matched samples of normal mucosa (*N*) and squamous cell carcinoma of the larynx (*T*). The numbers of the cases are arbitrary. Tumors 1, 2, 3, 5, 6, 7, and 9 show CDK4 mRNA overexpression, whereas similar expression levels in the normal and tumor samples were detected in cases 4 and 8. Ethidium bromide staining of the membranes after transfer is shown as loading control. **b** Southern blot analysis of the *CDK4* gene of the same cases shown in A. Digestion with *Eco*RI produces two bands of 4.6 and 3.8 kb, respectively. No amplifications, rearrangements, or other gross genetic abnormalities are detected. Differences in intensity are due to unbalanced loading, as shown by the β-actin probe used as loading control

overexpression: 15 of the 16 (94%) tumors with CCND1 overexpression also showed high expression levels of CDK4 (Table 2; p=0.023, Fisher's exact test). Only one case, in stage 3, showed CCND1 overexpression without simultaneous CDK4 upregulation.

Discussion

In this study, we examined the *CDK4* gene structure and mRNA expression in a series of laryngeal carcinomas. CDK4 overexpression was a frequent phenomenon in these tumors (70%), and it was independent of gross structural alterations of the gene. High expression levels were already observed in early-stage tumors, suggesting that CDK4

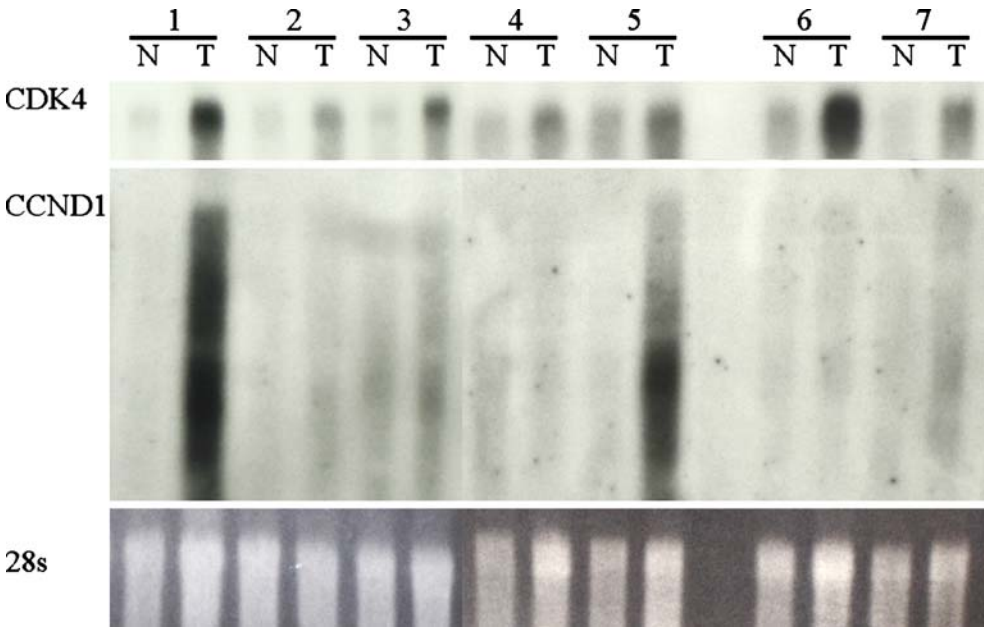

Fig. 2 Comparative analysis of CDK4 and CCND1 expression. The same blots were hybridized with the CDK4 probe (*top*), washed, and rehybridized with the CCND1 probe (*middle*). Ethidium bromide staining of the membranes after transfer is shown as loading control (*bottom*). The two cases with CCND1 overexpression (1 and 5) show also CDK4 overexpression. The case numbers are arbitrary and are not coincidental with those depicted in Fig. 1

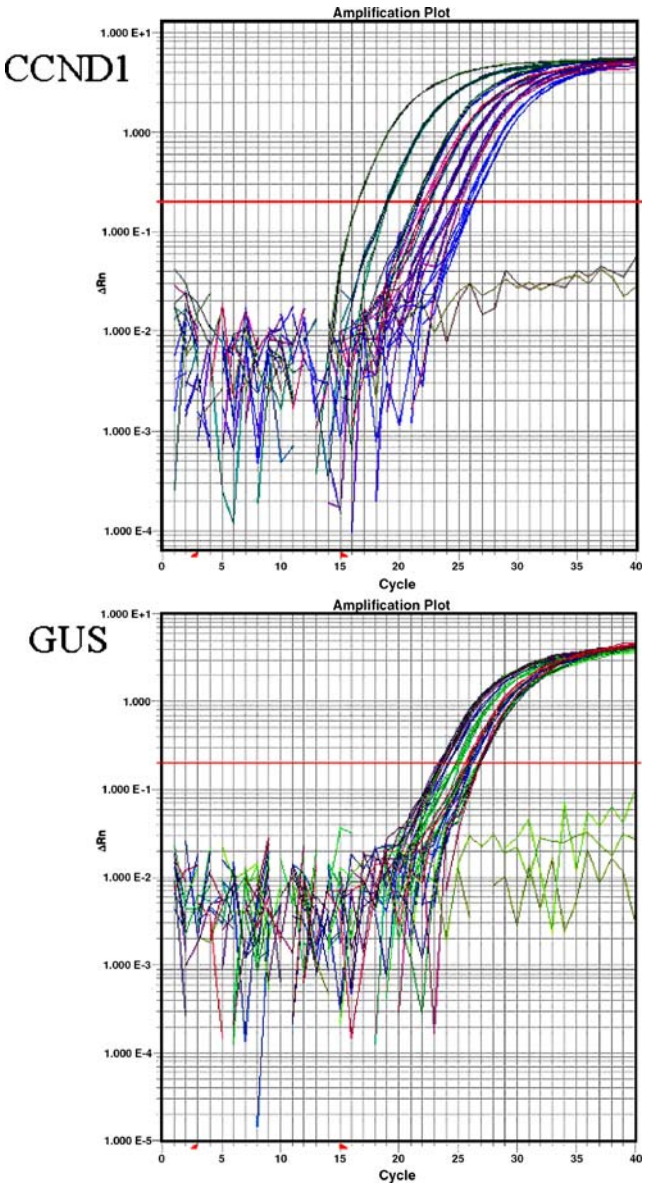

Fig. 3 Amplification plots of Q-RT-PCR of CCND1 (*top*) and GUS (*bottom*). CCND1 curves that appear shifted to the left indicate CCND1 overexpression. Q-RT-PCR was done to ensure that mRNA degradation was not the cause of NB unbalances. GUS curves are tightly packed indicating that mRNA samples contain similar amounts of the control gene in the aliquots used for the analysis

Table 2 Association between CDK4 and CCND1 overexpression

CCND1	CDK4		
	Nonoverexpressed	Overexpressed	Total
Nonoverexpressed	17	27	44
Overexpressed	1	15	16
Total	18	42	60

p=0.023; Fisher's exact test

mRNA upregulation is an early phenomenon in the development of SCC of the larynx. However, the similar incidence of CDK4 mRNA overexpression in early and advanced carcinomas indicates that other factors must be involved in the progression of the tumors.

CDK4 protein overexpression in laryngeal carcinomas was reported by Dong et al. They used immunohistochemistry to detect abnormally high numbers of cells expressing CDK4 protein. They also reported a correlation between CDK4, CCND1, and PCNA (proliferative) indexes and suggested that CDK4 overexpression had prognostic value in overall survival [2]. Unfortunately, we could not investigate CDK4 protein expression in those cases because there was no additional tissue available in a significant fraction of them.

The mechanisms leading to protein overexpression differ from gene to gene. CCND1 overexpression can be explained in most of the cases as the result of gene amplification [8], but this is not a constant for CDK4. *CDK4* amplification was described in sarcoma and glioma cell lines [6, 11], as well as in primary tumors [13, 23], and it is usually associated with CDK4 mRNA overexpression [11, 21]. However, CDK4 mRNA upregulation has been described in the absence of *CDK4* amplification in some high-grade gliomas, peripheral neuroendocrine tumors [21], malignant melanomas [13], and ovarian carcinomas [15]. Similarly, no *CDK4* gene amplifications were detected in our study, including tumors with mRNA overexpression, indicating that other mechanism may be involved in CDK4 deregulation in SCCs of the larynx. The correlation observed by Dong et al. between CDK4 and proliferative indexes could suggest that CDK4 expression was merely a reflection of higher cell proliferation in neoplastic tissues. This is very unlikely because experimental evidence shows that CDK4 levels remain unchanged when mammalian keratinocytes are induced to proliferate [22] or to terminally differentiate [14], in contrast with other cell types such as macrophages [17]. In the present study, we observed that virtually all cases overexpressing CCND1 also showed CDK4 upregulation and were in stage 4. These findings suggest that concomitant overexpression of both genes may be an important phenomenon that can confer a selective growth advantage in the progression of laryngeal carcinomas. This human model parallels in vitro observations indicating that synthesis of both CCND1 and CDK4 is necessary for G1 progression but the rate-limiting factor in CDK activity is often determined by the levels of a cyclin rather than of a kinase [3, 17]. Although differences in expression could be the result of mRNA degradation, we think that this is very unlikely. Q-RT-PCR obtained from the same RNA samples used in Northern-blot analysis shows control gene curves to be densely packed, indicating that there is no significant variation in RNA degradation

between samples, and differences in target signals represent real differences in the target gene mRNA (Fig. 3).

CDK4 itself may have oncogenic activity. However, it has been related to the ability of CDK4 to bind to, and sequester, $p16^{INK4a}$ or other cyclin-dependent kinase inhibitors rather than to its enzymatic activity [5]. Therefore, CDK4 overexpression is proposed as an alternative mechanism to $p16^{INK4a}$ inactivation in the tumorigenesis of different human tumors including malignant melanomas [13] or gliomas [6] because alterations of $p16^{INK4a}$ and CDK4 occur alternatively but not simultaneously in the same tumor. $p16^{INK4a}$ gene is also inactivated in a number of laryngeal carcinomas by mutations or hypermethylation associated with concomitant allelic deletion [9], and these alterations occur in tumors with normal retinoblastoma expression. The CDK4 overexpression observed in our series may also participate in the inactivation of Rb/$p16^{INK4a}$ pathway in laryngeal carcinomas.

An alternative oncogenic mechanism to CDK4 overexpression is the mutation in certain residues of exon 2. Mutations in this region render the CDK4 protein resistant to the inhibitory effect of $p16^{INK4a}$ by preventing the binding of these proteins. Different mutations have been described in occasional human malignant melanomas. However, these alterations seem to be rare in other tumors [1, 24, 26]. Concordant with previous observations in nonmelanoma tumors, no evidence of mutations was found in this series of laryngeal carcinomas.

Several mitogenic agents have been shown to induce CDK4 expression in different tumor models [3, 12, 16, 25]. Particularly, IL6 induces Rb phosphorylation via CDK4 overexpression in multiple myeloma cells [25]. Similarly, androgen treatment increases CDK4 expression both at mRNA and protein levels in an androgen-dependent prostatic cancer cell line [12]. Recently, a switch in *CDK4* promoter response to transcription factors between normal and transformed mammary epithelial cells was described [20]. This widens the putative mechanisms that can alter the cell-cycle regulation in cancer cells and provides an explanation for gene overexpression in the absence of structural alterations of the gene.

In conclusion, our findings indicate that CDK4 mRNA overexpression is a frequent phenomenon in SCCs of the larynx and support a role of this particular CDK in the pathogenesis of these neoplasms. This overexpression, previously detected by others at the protein level, already occurs at mRNA level, indicating that it responds to transcriptional rather than translational mechanisms. The absence of gross genetic alterations suggests the participation of other factors, yet uncharacterized, in the enhanced CDK4 transcription observed in the neoplastic tissues, and, as it has been stated before, this events could reflect changes in the elements that regulate CDK4 transcription from normal to neoplastic cells. The association between CDK4 and CCND1 overexpression suggests a cooperation between these two factors in laryngeal carcinoma progression. CCND1 overexpression occurring upon a background of CDK4 upregulation in the neoplastic cells could produce a selective growth advantage in laryngeal squamous carcinoma progression.

Acknowledgements This study was supported in part by grants from Fondo de Investigación Sanitaria (FIS), Instituto de Salud Carlos III, ref. 030407, Red Temática del Cáncer, Instituto de Salud Carlos III, n°C03/10, and Junta de Comarques de Barcelona de la Asociación Española Contra el Cáncer.

References

1. Coleman KG, Wautlet BS, Morrissey D, Mulheron J, Sedman SA, Brinkley P, Price S, Webster KR (1997) Identification of CDK4 sequences involved in cyclin D1 and p16 binding. J Biol Chem 272:18869–18874
2. Dong Y, Sui L, Sugimoto K, Tai Y, Tokuda M (2001) Cyclin D1–CDK4 complex, a possible critical factor for cell proliferation and prognosis in laryngeal squamous cell carcinomas. Int J Cancer 95:209–215
3. Geng Y, Weinberg RA (1993) Transforming growth factor beta effects on expression of G1 cyclins and cyclin-dependent protein kinases. Proc Natl Acad Sci USA 90:10315–10319
4. Guldberg P, Kirkin AF, Gronbaek K, thor Straten P, Ahrenkiel V, Zeuthen J (1997) Complete scanning of the CDK4 gene by denaturing gradient gel electrophoresis: a novel missense mutation but low overall frequency of mutations in sporadic metastatic malignant melanoma. Int J Cancer 72:780–783
5. Haas K, Staller P, Geisen C, Bartek J, Eilers M, Moroy T (1997) Mutual requirement of CDK4 and Myc in malignant transformation: evidence for cyclin D1/CDK4 and p16INK4A as upstream regulators of Myc. Oncogene 15:179–192
6. He J, Allen JR, Collins VP, Allalunis-Turner MJ, Godbout R, Day RS III, James CD (1994) CDK4 amplification is an alternative mechanism to p16 gene homozygous deletion in glioma cell lines. Cancer Res 54:5804–5807
7. Hunter T, Pines J (1994) Cyclins and cancer. II: Cyclin D and CDK inhibitors come of age. Cell 79:573–582
8. Jares P, Fernandez PL, Campo E, Nadal A, Bosch F, Aiza G, Nayach I, Traserra J, Cardesa A (1994) PRAD1/cyclin D1 gene amplification correlates with messenger RNA overexpression and tumor progression in human laryngeal carcinomas. Cancer Res 54:4813–4817
9. Jares P, Fernandez PL, Nadal A, Cazorla M, Hernandez L, Pinyol M, Hernandez S, Traserra J, Cardesa A, Campo E (1997) p16MTS1/CDK4I mutations and concomitant loss of heterozygosity at 9p2123 are frequent events in squamous cell carcinoma of the larynx. Oncogene 15:1445–1453
10. Jares P, Nadal A, Fernandez PL, Pinyol M, Hernandez L, Cazorla M, Hernandez S, Bea S, Cardesa A, Campo E (1999) Disregulation of p16MTS1/CDK4I protein and mRNA expression is associated with gene alterations in squamous-cell carcinoma of the larynx. Int J Cancer 81:705–711
11. Khatib ZA, Matsushime H, Valentine M, Shapiro DN, Sherr CJ, Look AT (1993) Coamplification of the CDK4 gene with MDM2 and GLI in human sarcomas. Cancer Res 53:5535–5541

12. Lu S, Tsai SY, Tsai MJ (1997) Regulation of androgen-dependent prostatic cancer cell growth: androgen regulation of CDK2, CDK4, and CKI p16 genes. Cancer Res 57:4511–4516
13. Maelandsmo GM, Florenes VA, Hovig E, Oyjord T, Engebraaten O, Holm R, Borresen AL, Fodstad O (1996) Involvement of the pRb/p16/cdk4/cyclin D1 pathway in the tumorigenesis of sporadic malignant melanomas. Br J Cancer 73:909–916
14. Martinez LA, Chen Y, Fischer SM, Conti CJ (1999) Coordinated changes in cell cycle machinery occur during keratinocyte terminal differentiation. Oncogene 18:397–406
15. Masciullo V, Scambia G, Marone M, Giannitelli C, Ferrandina G, Bellacosa A, Benedetti PP, Mancuso S (1997) Altered expression of cyclin D1 and CDK4 genes in ovarian carcinomas. Int J Cancer 74:390–395
16. Matsushime H, Ewen ME, Strom DK, Kato JY, Hanks SK, Roussel MF, Sherr CJ (1992) Identification and properties of an atypical catalytic subunit (p34PSK-J3/cdk4) for mammalian D type G1 cyclins. Cell 71:323–334
17. Matsushime H, Quelle DE, Shurtleff SA, Shibuya M, Sherr CJ, Kato JY (1994) Dtype cyclin-dependent kinase activity in mammalian cells. Mol Cell Biol 14:2066–2076
18. Nadal A, Jares P, Cazorla M, Fernandez PL, Sanjuan X, Hernandez L, Pinyol M, Aldea M, Mallofre C, Muntane J, Traserra J, Campo E, Cardesa A (1997) p21WAF1/Cip1 expression is associated with cell differentiation but not with p53 mutations in squamous cell carcinomas of the larynx. J Pathol 183:156–163
19. Parkin DM, Pisani P, Ferlay J (1993) Estimates of the worldwide incidence of eighteen major cancers in 1985. Int J Cancer 54:594–606
20. Pawar SA, Szentirmay MN, Hermeking H, Sawadogo M (2004) Evidence for a cancer-specific switch at the CDK4 promoter with loss of control by both USF and cMyc. Oncogene 23: 6125–6135
21. Reifenberger G, Reifenberger J, Ichimura K, Meltzer PS, Collins VP (1994) Amplification of multiple genes from chromosomal region 12q1314 in human malignant gliomas: preliminary mapping of the amplicons shows preferential involvement of CDK4, SAS, and MDM2. Cancer Res 54:4299–4303
22. Rodriguez-Puebla ML, Robles AI, Johnson DG, LaCava M, Conti CJ (1998) Synchronized proliferation induced by 12-O-tetradecanoylphorbol-13-acetate treatment of mouse skin: an in vivo model for cell cycle regulation. Cell Growth Differ 9:31–39
23. Sonoda Y, Yoshimoto T, Sekiya T (1995) Homozygous deletion of the MTS1/p16 and MTS2/p15 genes and amplification of the CDK4 gene in glioma. Oncogene 11:2145–2149
24. Tsao H, Benoit E, Sober AJ, Thiele C, Haluska FG (1998) Novel mutations in the p16/CDKN2A binding region of the cyclin-dependent kinase-4 gene. Cancer Res 58:109–113
25. Urashima M, Teoh G, Ogata A, Chauhan D, Treon SP, Hoshi Y, DeCaprio JA, Anderson KC (1997) Role of CDK4 and p16INK4A in interleukin-6-mediated growth of multiple myeloma. Leukemia 11:1957–1963
26. Wolfel T, Hauer M, Schneider J, Serrano M, Wolfel C, Klehmann-Hieb E, De Plaen E, Hankeln T, Meyer zum Buschenfelde KH, Beach D (1995) A p16INK4a-insensitive CDK4 mutant targeted by cytolytic T lymphocytes in a human melanoma. Science 269:1281–1284
27. Zuo L, Weger J, Yang Q, Goldstein AM, Tucker MA, Walker GJ, Hayward N, Dracopoli NC (1996) Germline mutations in the p16INK4a binding domain of CDK4 in familial melanoma. Nat Genet 12:97–99

Virchows Arch (2007) 450:169–177
DOI 10.1007/s00428-006-0350-y

ORIGINAL ARTICLE

ADAM-17 associated with CD44 cleavage and metastasis in oral squamous cell carcinoma

Yasuo Takamune · Tetsuro Ikebe · Osamu Nagano · Hideki Nakayama · Kazutoshi Ota · Takehisa Obayashi · Hideyuki Saya · Masanori Shinohara

Received: 19 July 2006 / Revised: 12 September 2006 / Accepted: 7 November 2006 / Published online: 20 December 2006
© Springer-Verlag 2006

Abstract ADAM-17 (a disintegrin and metalloproteinase 17) is a membrane-anchored protein, which can cleave the ectodomain in a variety of transmembrane proteins. In the in vitro experiments with tumor cells, ADAM-17 is reported to cleave CD44, an adhesion molecule that interacts with hyaluronic acid, to promote tumor cell migration. In the present study, we examined ADAM-17 expression and CD44 cleavage in specimens from 50 patients diagnosed to have oral squamous cell carcinoma (SCC). Each specimen was divided into two pieces, one was studied by immunohistochemistry and the other was subjected to a Western blot. By coordinating the results of both analyses, ADAM-17 expression was evaluated to be high in 23 cases (46%). When CD44 cleavage was also studied by immunohistochemical staining as well as with Western blotting, CD44 cleavage was judged to be positive in 29 cases (58%). When the ADAM-17 expression level was compared with the CD44 cleavage state, most of the cases expressing high levels of ADAM-17 (87%) showed positive CD44 cleavage. The level of ADAM-17 expression was significantly correlated to the nodal metastasis and local recurrence in oral SCC. Our findings suggest that ADAM-17 is involved in CD44 cleavage and contributes to tumor progression in oral SCC.

Keywords ADAM-17 · TACE · CD44 · Squamous cell carcinoma

Y. Takamune · T. Ikebe · O. Nagano · H. Nakayama · K. Ota · T. Obayashi · M. Shinohara
Department of Oral and Maxillofacial Surgery,
Graduate School of Medical Sciences, Kumamoto University,
1-1-1 Honjo,
Kumamoto 860-8556, Japan

O. Nagano · H. Saya
Department of Tumor Genetics and Biology,
Graduate School of Medical Sciences, Kumamoto University,
1-1-1 Honjo,
Kumamoto 860-8556, Japan

T. Ikebe (✉)
Department of Oral and Maxillofacial Surgery,
Fukuoka Dental College,
2-15-1 Tamura, Sawara-ku,
Fukuoka 814-0193, Japan
e-mail: ikb@college.fdcnet.ac.jp

Introduction

Squamous cell carcinoma (SCC) is a major malignant tumor in the oral cavity, and severely lowers a patient's quality of life through the impairment of eating, swallowing, and speaking. Because the prognosis of oral SCC patients are dependent on the metastasis of tumor cells, it is important to clarify the molecules associated with its invasion and metastasis. CD44 is considered to be one of the candidate molecules that are involved in the metastasis of oral SCC. CD44 is a cell surface adhesion molecule which can bind to hyaluronic acid, an extracellular matrix, and regulate a variety of cellular functions such as cell migration, proliferation, cell–cell interaction, and apoptosis [16]. These cellular functions of CD44 imply that a disorder of CD44 expression plays a crucial role in the behaviors of a malignant tumor.

Actually, the downregulation of CD44 expression is reported to correlate with the metastasis and a poor prognosis in various types of carcinoma including oral SCC [4, 6, 7, 20]. CD44 reduction may be caused in part by the cleavage of its extracellular domain (ectodomain), which occurs in many malignant tumors [15]. Because CD44 cleavage is thought to promote cell migration by detaching cells from the extracellular matrices, it may be related to tumor spread and

progression [14]. CD44 cleavage has been observed in many types of tumors including glioma, breast carcinoma, non-small cell lung carcinoma, ovarian carcinoma, and colon carcinoma [15]. Soluble CD44, which is considered to be the CD44 ectodomain released after cleavage, was detected in the serum of patients diagnosed with colon, gastric, or breast carcinoma [8, 19].

Because CD44 cleavage is considered to be involved in tumor invasion and metastasis, then, it is very important to identify the proteases responsible for such actions. The proteases are mainly metalloproteinases (MMPs) because synthetic MMP inhibitors block the cleavage [14]. Among MMPs, membrane-type1 MMP (MT1-MMP) and a disintegrin and metalloprotease domain (ADAM) family are reported to cleave CD44 in vitro [9, 12]. It is reported that a Ca^{2+} influx and TPA will induce the cleavage of CD44 on cultured cells through the use of different proteases [12]. Ca^{2+} influx-induced CD44 cleavage is mediated by ADAM-10, while TPA causes ADAM-17 to cleave CD44 [12]. However, most of the data about the proteases responsible for CD44 cleavage comes from the experiments of culture cells. It remains to be determined which proteases are actually involved in CD44 cleavage in vivo.

ADAM-17 is a member of the ADAM family and was originally identified as a TNFα converting enzyme (TACE) which cleaves a membrane-anchoring precursor form of TNFα to generate a soluble form of TNFα [1, 11]. As a shedase, ADAM-17 is reported to release several cytokines or growth factors from cell membranes and exert a variety of biological functions, some of which may be related to tumor behavior [18].

In the present study, we aimed to clarify the status of ADAM-17 expression and its association with CD44 cleavage in oral SCC by investigating 50 patients' specimens with immunohistochemistry and Western blotting.

Materials and methods

Reagents

Rabbit polyclonal antibodies (Abs) against the cytoplasmic domain of CD44, anti-CD44cyto Ab, were generated as previously described [14]. Monoclonal Abs against the ectodomain of CD44 (BU52) were obtained from Ancell. Rabbit polyclonal anti-ADAM-17 Abs were purchased from Calbiochem.

Tumor specimens

Oral SCC tissue specimens were obtained from 50 patients, which included 26 metastatic cases and 24 nonmetastatic cases, by biopsy before chemotherapy or radiotherapy at the Department of Oral and Maxillofacial Surgery, Kumamoto University Hospital. All the 24 metastatic cases underwent the neck dissection. The term metastatic in this study refers to the patients with positive lymph nodes based on pathological diagnosis after neck dissection. All patients were diagnosed with SCC of the oral cavity as summarized in Tables 1 and 2. During the follow-ups, the local recurrence was found in 15 cases. Mean recurrence-free survival time for local recurrence cases and nonrecurrence cases were 11.5 and 40.2 months, respectively. Each specimen was divided into two pieces; one was used for a Western blot analysis and the other for immunohistochemical staining. For Western blotting, the specimens were frozen and stored at −80°C until homogenization and protein extraction were performed.

Western blot analysis

Tissue specimens were treated with a lysis buffer (50 mM Tris–HCl (pH 7.4), 150 mM NaCl, 1% NP-40, 1 mM Na_3VO_4, protease inhibitor cocktail tablet (Roche, Mannheim, Germany)) and centrifuged at 15,000× *g* to remove any insoluble material. Equal amounts of protein (20 μg) were electrophoresed on 10 or 15% sodium dodecyl sulfate-polycrylamide gel electrophoresis (SDS-PAGE) gels and transferred to nitrocellulose membranes. The membranes were blocked with PBS containing 10% skim milk for 1 h and then incubated with either a 1:1,000 dilution of anti-CD44cyto Ab, a 1:300 dilution of anti-CD44 ectodomain monoclonal Ab (BU52), or a 1:1,000 dilution of anti-ADAM-17 Ab in PBS containing 0.03% Tween 20 for 50 min. Secondary antibodies were horseradish peroxidase-conjugated anti-mouse IgG Ab for anti-CD44cyto Ab and horseradish peroxidase-conjugated anti-rabbit IgG Ab for BU52 Ab or anti-ADAM-17 Ab, respectively. The bound antibodies were visualized by enhanced chemiluminescence Western blotting detection reagents (Amersham Biosciences, UK). The immunoreactivity of the antibodies was confirmed

Table 1 Clinical features of the examined oral SCC patients

	Nodal involvement		
	Negative	Positive	Total
Mean age	70	63.1	66.4
Male to female	14.10	19.17	33.27
Location			
Tongue	8	8	16
Upper gum	5	1	6
Lower gum	5	4	9
Buccal mucosa	5	8	13
Oral floor	1	4	5
Palate	0	1	1
Total	24	26	50

Table 2 Clinical features of the examined oral SCC patients

	Nodal involvement				
	Negative	Positive			Total
	N0	N1	N2	N3	
T scale					
T1	7	1	2	0	10
T2	13	5	10	1	29
T3	1	1	1	0	3
T4	3	0	5	0	8
G status (differentiation)					
G1 (well)	21	4	13	1	39
G2 (moderate)	3	3	5	0	11
Surgical margin					
R0	23	6	17	1	47
R1	1	1	1	0	3
Total	24	7	18	1	50

by using the cell lysates of human glioma cell line U251MG that are reported to show the CD44 cleavage and ADAM-17 expression [12].

Immunohistochemical staining

Four-micrometer-thick histological sections of 4% paraformaldehyde fixed, paraffin embedded SCC tissues were formed, mounted, and air-dried. The sections were deparaffinized in xylene and rehydrated in ethanol, and endogenous peroxidase was blocked by immersion in methanol containing 0.3% hydrogen peroxidase for 30 min. The sections were incubated overnight at 4°C with their respective primary antibodies, then for 30 min at room temperature with the peroxidase-conjugated anti-mouse or anti-rabbit IgG Ab, followed by staining with diaminobenzidine (Histofine MAX-PO kit, Nichirei, Tokyo, Japan).

Evaluation for CD44 cleavage

In the Western blot gels, we regarded a case as CD44-cleavage positive when the band density of a degraded CD44, whose molecular size is approximately 25 kD, is more than 25% of that in the full-length CD44 (85 kD). A case, where the band density of degraded CD44 is less than 25% of that in the full length CD44, was estimated as CD44-cleavage negative. For the immunohistochemical stainings, we used two kinds of anti-CD44 Abs, anti-CD44cyto Ab against the cytoplasmic domain of CD44 and BU52 Ab against its extracellular domain, to detect CD44 cleavage. If CD44 is cleaved, BU52 Ab no longer binds to the cells because the extracellular domain of CD44 is released away from the cell surface, but anti-CD44cyto Ab will still react to the cytoplasmic fragment left behind in the cell. Hence, the area which is positive in anti-CD44cyto Ab staining and negative in BU52 Ab staining is considered to be a CD44 cleavage-positive site in a tumor nest. In the tissue sections, a case was estimated as CD44-cleavage positive when the staining of the ectodomain of CD44 was lost in more than 50% of the area expressing the cytoplasmic domain of CD44. When the ectodomain of CD44 was expressed in more than 50% of the area, we estimated the case as CD44-cleavage negative.

We, then, put together the results of the Western blotting and the immunohistochemimal staining to group the cases into three types of a CD44 cleavage state, positive, questionable, and negative. The positive type of CD44 cleavage includes the cases showing CD44 cleavage that were positive in both the Western blotting and immunohistochemical staining. The questionable type of CD44 cleavage is positive either in the Western blot or immunohistochemical staining. The cases where no CD44 cleavage was seen in either analysis were regarded as negative type.

Evaluation for ADAM-17 expression

When a case showed a 98-kD band of the ADAM-17 mature form in Western blotting, it was designated as a positive case, and otherwise it was a negative case for ADAM-17 expression. For immunohistochemical analysis, we regarded a case as positive for ADAM-17 expression when more than 50% of its tumor nest in all the area of a section was positively stained. When less than 50% of it was stained, it was regarded as a negative case. This judgment was carried out by two independent researchers (T. I. and Y. T.). If their decision did not agree, then a third person (M. S.) judged whether the analysis was positive or negative. Like the CD44 evaluation, then, the results of Western blotting and immunohistochemimal staining were organized to classify the cases into three types of ADAM-17 expression level, high, moderate, and low. The high type of ADAM-17 expression level includes the cases showing that ADAM-17 expression is positive in both the Western blotting and immunohistochemical staining. The moderate type of ADAM-17 expression level is positive in either the Western blotting or immunohistochemical staining. The cases where the ADAM-17 expression was negative in both analyses were evaluated as the low type of ADAM-17 expression level.

Statistical analyses

The chi-square test was used to evaluate the statistical correlation between the ADAM-17 expression level and CD44 cleavage state, between ADAM-17 expression level and nodal metastasis or local recurrence ($p<0.005$), which

was performed with Statview J-4.5 (Abacus Concepts, CA, USA).

Results

Immunohistochemical staining for ADAM-17 expression and CD44 cleavage in oral SCC

Each of the specimens collected from 50 cases of oral SCC was divided into two pieces. One was used to prepare tissue lysates for Western blot analysis, and the other was embedded in paraffin to make serial sections for immunohistochemical staining. The serial sections were stained with anti-ADAM-17 Ab as well as anti-CD44 Abs. All the 50 cases examined were positive for the expression of CD44 cytoplasmic domain. Approximately 95% of the tumor nests expressed CD44 cytoplasmic domain in each case—meaning that almost all the oral SCCs express the cytoplasmic domain of CD44, but its extracellular domain is lost by the cleavage in some cases. Figure 1 shows the serial sections of two representative cases, a CD44 cleavage-negative case (a, b, and c) and a CD44 cleavage-positive case (d, e, and f). Both the expressions of ADAM-17 and CD44 were observed in the tumor nests, rather than in the stromal tissues. At the cellular level, CD44 was expressed in the cell membrane whereas ADAM-17 was seen in the whole cell. In a CD44 cleavage-negative case where both immunostainings with BU52 Ab and anti-CD44cyto Ab were positive, the expression of ADAM-17 was observed to be low (Fig. 1a–c). Importantly, in a CD44 cleavage-positive case where the immunoreactivity with the BU52 Ab was lost, ADAM-17 expression was high at the area where CD44 was considered to be cleaved in the tumor nest (Fig. 1d–f). The extracellular domain of CD44 therefore appeared to be lost in the tumor nests expressing ADAM-17.

We also stained a normal oral mucosa immunohistochemically (Fig. 2). CD44 was expressed in the basal layer and spinous cell layer. The staining for ADAM-17 was only weakly seen in the spinous cell layer.

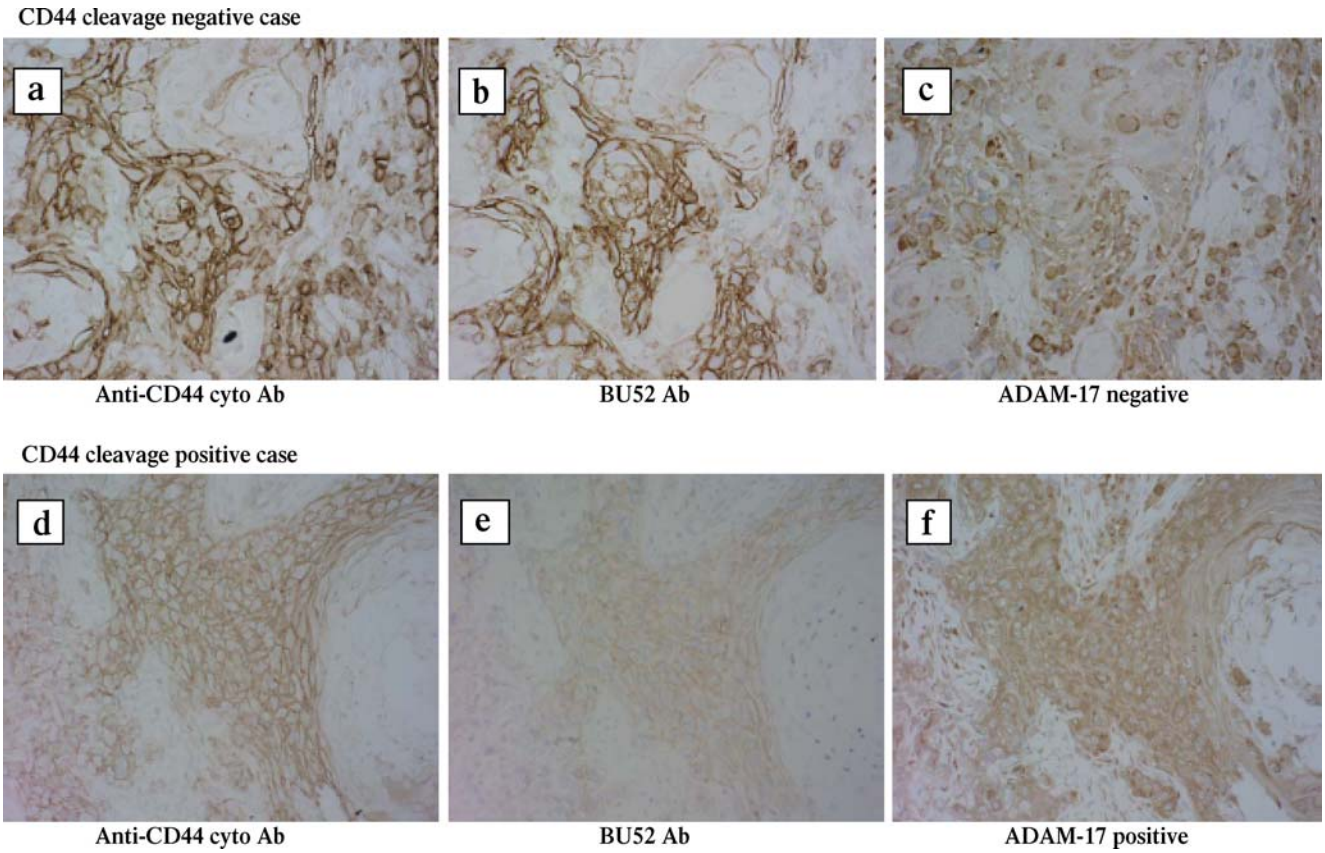

Fig. 1 Locations of CD44 cleavage and ADAM-17 expression in oral SCC tissues. The serial sections were formed from each specimen from oral SCC patients, and then were immunostained with anti-CD44 cyto Ab (an Ab against cytoplasmic domain of CD44) (**a**) (**d**), BU52 Ab (an Ab against extracellular domain of CD44) (**b**) (**e**), and anti-ADAM-17 Ab (**c**) (**f**). Panels **a**, **b**, and **c** are from the serial sections of a patient, and are considered as a CD44 cleavage negative case because the extracellular domain of CD44 (BU52 Ab) is present (**b**). Panels **d**, **e**, and **f** are also from the serial sections of a CD44 cleavage positive patient because the extracellular domain of CD44 is lost (**e**). Panel **f** shows that ADAM-17 is highly expressed in the area where CD44 cleavage is observed. Magnitude ×200

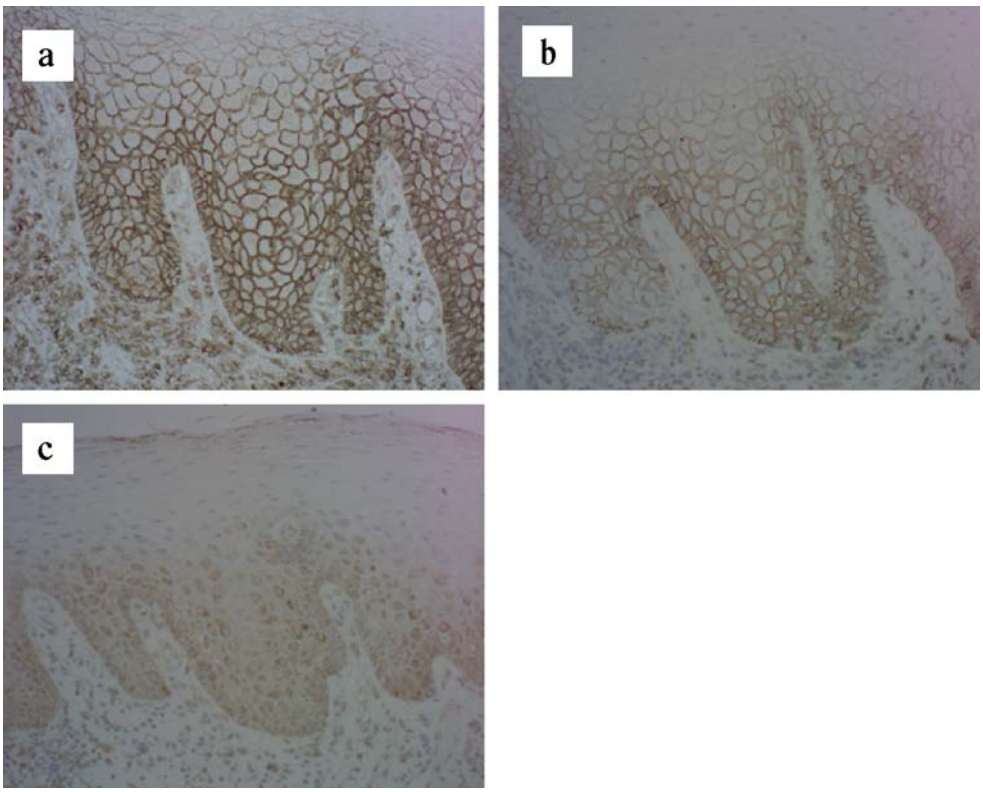

Fig. 2 Locations of CD44 and ADAM-17 in normal oral mucosa. A normal oral mucosa, which is from a nontumorous lesion, was immunostained with anti-CD44 cyto Ab (**a**), BU52 Ab (**b**), and anti-ADAM-17 Ab (**c**). Both of the extracellular domain (**b**) and cytoplasmic domain (**a**) of CD44 is expressed in the basal layer and spinous layer, whereas ADAM-17 expression (**c**) is extremely low. Magnitude ×200

Western blotting analysis for mature ADAM-17 expression and CD44 cleavage in oral SCC

In Western blotting, anti-CD44cyto Ab recognized the cleaved fragment of CD44 (20–25 kD) in 15% SDS-PAGE as well as the full-length CD44 (85 kD) in 10% SDS-PAGE from the tissue lysates of oral SCC (Fig. 3). As described in the "Materials and methods" section, we evaluated CD44 cleavage by comparing the band density of the cleaved fragment with that of full-length CD44 in each case. Figure 3 shows the Western blotting of a keratinocyte cell line HaCaT (lane 1), a normal oral mucosa (lane 2), and six oral SCC cases (five positive cases, one negative case) (lane 3–8). Five out of six oral SCC cases indicate a sharp band of cleaved CD44 fragment. CD44 cleavage was not found in a normal oral mucosa as well as in HaCaT cells although the level of full-length CD44 was also low.

As shown in Fig. 3, the Western blotting with anti-ADAM-17 Ab indicates two bands of a proform (134 kD) and a mature form (98 kD) of ADAM-17. Because a proform of ADAM-17 is needed to be converted to a mature form to acquire proteolytic activity, we focused on the expression of the mature form in the Western blotting for ADAM-17. Compared with the results of CD44 cleavage on Western blotting, a significant band of the ADAM-17 mature form was found in five oral SCC cases with positive CD44 cleavage whereas a CD44-cleavage negative case showed only a faint band of its mature form (Fig. 3). Normal oral mucosa and cultured keratinocytes expressed the less mature form as well as the proform of ADAM-17. The Western blot analysis, thus, suggested that mature ADAM-17 expression is coupled with CD44 cleavage.

Correlation between Western blot analysis and immunohistochemical staining

Table 3 summarizes the results of the 50 cases examined by immunohistochemical staining and Western blotting for ADAM-17 expression (Table 3A) and CD44 cleavage (Table 3B).

For ADAM-17 expression, 23 cases and 10 cases were positive and negative in both analyses, respectively (Table 3A). Thus, both analyses corresponded in 66% of the cases for ADAM-17 expression, although the immunohistochemical staining indicates the total expression of the proform plus the mature form of ADAM-17 and Western blotting accounts for only the mature form of expression.

Like ADAM-17 expression, 29 cases were positive for CD44 cleavage both by immunohistochemical staining and Western blotting, while CD44 cleavage was not detected in 10 cases by either analysis. Both analyses, therefore, corresponded in 78% of the 50 cases for detecting CD44 cleavage.

Relationship between ADAM-17 expression level and CD44 cleavage state

We decided the final evaluation of the ADAM-17 expression level and CD44 cleavage state in each oral SCC case

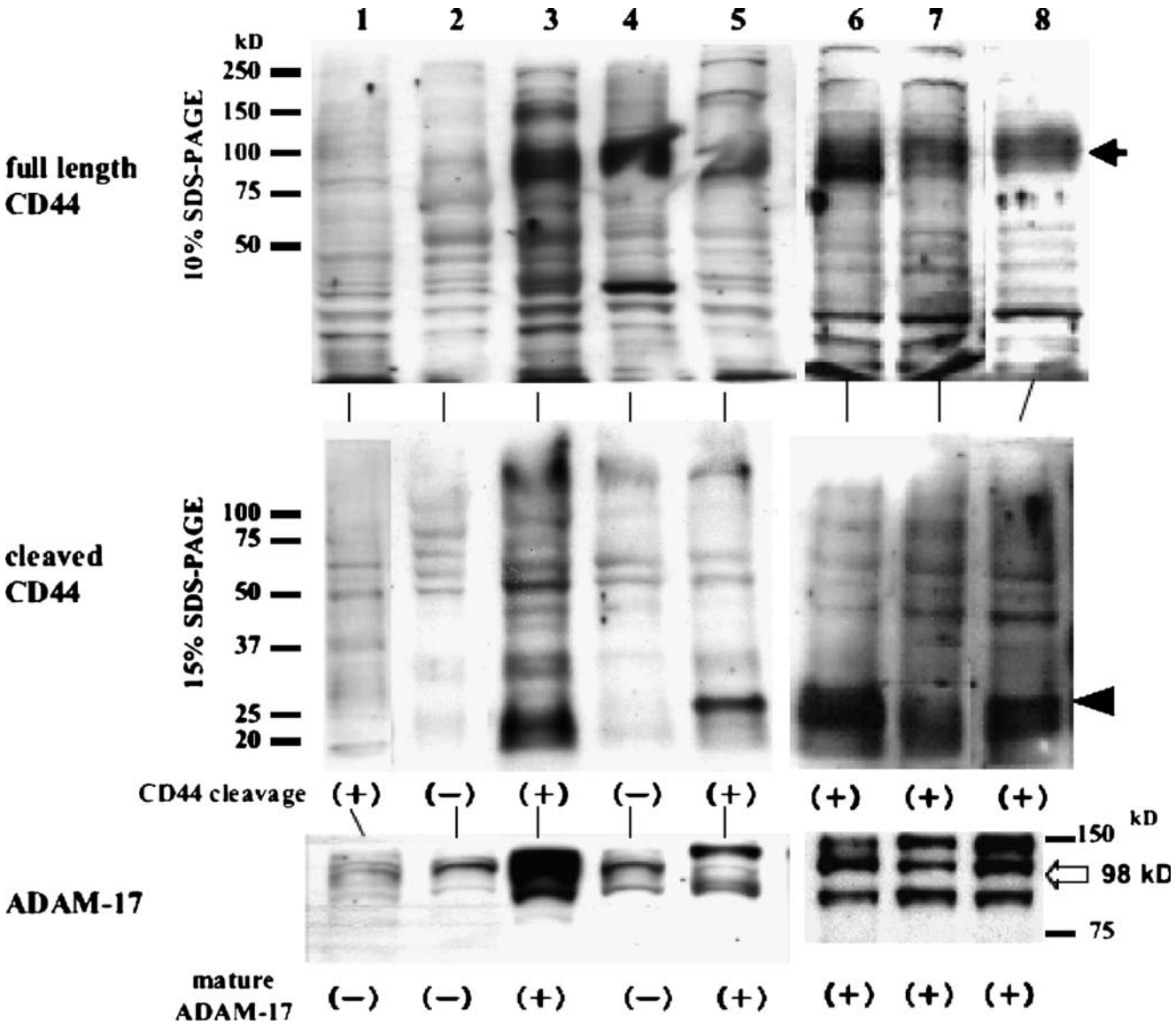

Fig. 3 Western blotting analyses for the comparison between CD44 cleavage and mature ADAM-17 expression in oral SCC tissues. Tissue lysates were prepared from the specimens of oral SCC cases, and subjected to SDS-PAGE. For CD44 detection, 10% SDS-PAGE was used for the full-length CD44 (85 kD) (*upper panel*) while 15% SDS-PAGE was for the cleaved CD44 products (20–25 kD) (*middle panel*). Anti-CD44 cyto Ab was used in the Western blotting. The judgment for CD44 cleavage was determined by the detection of cleaved CD44 bands as described in "Materials and methods" section. The expression of ADAM-17 was also analyzed by Western blotting in the same samples used for CD44 cleavage. The appearance of a mature form of ADAM-17 (98 kD) was regarded as positive in mature ADAM-17 expression. CD44 cleavage was compared with mature ADAM-17 expression in each case. Six representative cases of oral SCC were shown in *lane 3* to *lane 8*. *Lane 1* is from a keratinocyte cell line HaCaT and *lane 2* is from normal oral mucosa. *Arrows* indicate full-length CD44. *Arrowheads* indicate the cleaved CD44 fragment. *Open arrows* indicate the mature form of ADAM-17

by coordinating the results of the immunohistochemical staining and Western blotting. We grouped the level of ADAM-17 expression into three levels, low, moderate, and high, as described in the "Materials and methods" section. Likewise, CD44 cleavage state for each case was classified into three types, negative, questionable, and positive, by comparing the results of the immunohistochemical staining with those of the Western blotting. According to these classifications, Table 4 shows the relationship between the ADAM-17 expression level and the CD44 cleavage state. Most of the cases expressing a high level of ADAM-17 (87%) showed a positive CD44 cleavage. Sixty percent of the cases expressing a low level of ADAM-17 were negative for CD44 cleavage. The ADAM-17 expression level was significantly correlated to the CD44 cleavage state ($p<0.05$) (Table 4).

Table 3 Comparison of the Western blotting analysis and immunohistochemistry findings

Immunohistochemical staining	Western blotting		
	Negative	Positive	Total
(A) Correlation between Western blot analysis and immunohistochemical staining on ADAM-17 expression			
Negative	10	16	26
Positive	1	23	24
Total	11	39	50
(B) Correlation between Western blot analysis and immunohistochemical staining on CD44 cleavage			
Negative	10	9	19
Positive	2	29	31
Total	12	38	50

Involvement of ADAM-17 expression in nodal metastasis and local recurrence

Because ADAM-17 seemed to be associated with CD44 cleavage in oral cancer, the relationship between ADAM-17 and tumor prognostic factors was analyzed. Among 23 cases with high level of ADAM-17 expression, 18 cases (78%) showed nodal involvement (Table 5). In contrast, only 30% of the cases expressing a low level of ADAM-17 were metastatic. A high expression of ADAM-17 was statistically correlated to nodal involvement (Table 5).

The local recurrence rate was 48% in cases expressing high levels of ADAM-17, while cases with a low expression of ADAM-17 showed a 10% rate of local recurrence (Table 6). Local recurrence was also significantly correlated with the ADAM-17 expression level ($p<0.05$) (Table 6).

Discussion

In the present study, two different methods, immunohistochemistry and Western blotting, were combined to evaluate the degrees of CD44 cleavage and ADAM-17 expression more accurately. In addition, the results of CD44 cleavage were compared with those of ADAM-17 expression to clarify their relationship. As a result, an immunohistochemical examination showed the colocalization of ADAM-17-upregulated sites with CD44 cleavage sites while the Western blotting analysis indicated that most of the patients with a mature form of ADAM-17 corresponded to the CD44-cleaved patients. Therefore, two different analyses of the patients' specimens supported the same conclusion that ADAM-17 is involved in CD44 cleavage and tumor spreading in oral SCC. By coordinating the data of ADAM-17 expression with that of CD44 cleavage, the potential of tumor spreading may thus be diagnosed more accurately in oral SCC.

ADAMs are a gene family of multidomain membrane-anchored proteins comprised of more than 30 members in various animal species and are implicated in pathophysiological conditions [18]. ADAM-17/TACE is the most well-studied member of the ADAM family. As a metalloproteinase, ADAM-17 is reported to cleave a variety of substrates including heparin-binding epidermal growth factor (HB-EGF), transforming growth factor α (TGFα), TNF receptor, EGF receptor (EGFR), c-fms, c-kit, p75NTR, growth hormone receptor, interleukin-6 receptor, interleukin-1 receptor, vascular cell adhesion molecule-1, CD40, β-amyloid precursor, L-selectin, collagen VII, MUC1, and Notch [18]. The increased cleavage of such substrates as HB-EGF and TGFα by ADAM-17 is likely to be associated with tumor spread and growth because of their cell growth activity [2, 3, 21]. In this

Table 5 Relationship between ADAM-7 expression and nodal involvement

ADAM-17 expression type	Nodal involvement*		
	Negative	Positive	Total
Low	1 (70%)	3 (30%)	10
Moderate	12 (71%)	5 (29%)	17
High	5 (22%)	18 (78%)	23
Total	24	26	50

*$p<0.005$, Chi-square test

Table 4 Relationship between ADAM-17 expression and CD44 cleavage

ADAM–17 expression type	CD44 cleavage type*			
	Negative	Questionable	Positive	Total
Low	6 (60%)	2 (20%)	2 (20%)	10
Moderate	4 (24%)	6 (35%)	7 (41%)	17
High	0 (0%)	3 (13%)	20 (87%)	23
Total	10	11	29	50

*$p<0.005$, Chi-square test

Table 6 Relationship between ADAM-7 expression and recurrence

ADAM–17 expression type	Local recurrence*		
	Negative	Positive	Total
Low	9 (90%)	1 (10%)	10
Moderate	14 (82%)	3 (18%)	17
High	12 (52%)	11 (48%)	23
Total	35	15	50

*$p<0.005$, Chi-square test

context, several reports have focused on the importance of ADAM-17 upregulation in tumor malignancy. In colon carcinoma, the upregulated expression of ADAM-17 induces the activation of EGFR through the shedding of EGFR ligands [2]. Tanaka et al. [21] demonstrated that the expression of HB-EGF, which is increased in advanced ovarian cancer in comparison to that found in normal ovaries, was significantly correlated with ADAM-17 expression in ovarian cancer. An increased expression of ADAM-17 has also been reported in breast cancer [5] and prostate cancer [10]. The present study is the first report showing the involvement of ADAM-17 in oral, head, and neck SCC.

The present study also demonstrated that CD44 cleavage is enhanced in oral SCC. In various carcinomas, enhanced cleavage of CD44 has been found in the patients' specimens by means of Western blotting with anti-CD44 cytoplasmic domain Ab, which was also used in this study [15]. Tumor cells adhere to hyaluronic acid in the extracellular matrix through cell surface CD44. CD44 cleavage releases tumor cells from the extracellular matrix, promoting tumor cell migration [14]. It however remains to be determined whether CD44 cleavage occurred in oral SCC. As for CD44 in oral SCC, the reduced expression of the specific CD44 variant isoform, for instance CD44 variant 9, has been reported to be related to nodal metastasis in oral SCC [17]. Although the mechanism of how CD44 was reduced in carcinoma is not clarified, our results imply that the CD44 variant reduction is caused by CD44 cleavage. Okamoto et al. [15] reported that the percentage of CD44 cleavage was significantly higher in tumors expressing the CD44 variant isoform than in tumors expressing only the standard CD44 protein in breast, lung, colon, and ovarian carcinomas. The CD44 variant isoform may also be more susceptible to proteolytic cleavage than standard CD44.

Using a cultured glioma cell line in vitro, Nagano et al. [12] demonstrated that TPA-induced cleavage of CD44 was induced by ADAM-17 while calcium-induced CD44 cleavage was mediated by ADAM-10. Nakamura et al. [13] reported that MT1-MMP cleaved CD44 in melanoma cells. Among these metalloproteinases, we focused on ADAM-17's involvement in oral SCC because the preliminary study on the immunostaining for ADAM-10 as well as MT1-MMP did not correspond to the CD44 cleavage sites in the patient specimens with oral SCC, and we confirmed that oral SCC cell lines expressed ADAM-17 (data not shown). In order for tumor cells to invade the surrounding stromal tissues, ADAM-17 was expected to be expressed mainly in the marginal areas of tumor nests. In the immunohistochemically stained sections, however, ADAM-17 appeared to be expressed not only in the marginal areas, but also in the central areas of the tumor nests. Moreover, ADAM-17 seemed to be present in the cytoplasm as well as on the cell surface. Although these immunohistochemical findings about the localization of ADAM-17 did not completely agree to the expected, the Western blotting analyses further support the immunohistochemical findings that the expression level of ADAM-17, which is higher in metastatic oral SCC, coincided with CD44 cleavage in oral SCC. Further study remains to be done to clarify the relationship between the localizations of ADAM-17 and CD44 in cultured SCC cells.

Acknowledgment This work was supported by a grant from the Ministry of Education, Science, and Culture of Japan (to M. Shinohara).

References

1. Black RA, Rauch CT, Kozlosky CJ, Peschon JJ, Slack JL, Wolfson MF, Castner BJ, Stocking KL, Reddy P, Srinivasan S, Nelson N, Boiani N, Schooley KA, Gerhart M, Davis R, Fitzner JN, Johnson RS, Paxton RJ, March CJ, Cerretti DP (1997) A metalloproteinase disintegrin that releases tumour-necrosis factor-α from cells. Nature 385:729–733
2. Blanchot-Jossic F, Jarry A, Masson D, Bach-Ngohou K, Paineau J, Denis MG, Laboisse CL, Mosnier JF (2005) Up-regulated expression of ADAM-17 in human colon carcinoma: co-expression with EGFR in neoplastic and endothelial cells. J Pathol 207:156–163
3. Borrell-Pages M, Rojo F, Albanell J, Baselga J, Arribas J (2003) TACE is required for the activation of the EGFR by TGF-α in tumors. EMBO J 22:1114–1124
4. De Marzo AM, Bradshaw C, Sauvageot J, Epstein JI, Miller GJ (1998) CD44 and CD44v6 downregulation in clinical prostatic carcinoma: relation to Gleason grade and cytoarchitecture. J Hered 34:162–168
5. Fabre-Lafay S, Garrido-Urbani S, Reymond N, Goncalves A, Dubreuil P, Lopez M (2005) Nectin-4, a new serological breast cancer marker, is a substrate for tumor necrosis factor-a-converting enzyme (TACE)/ADAM-17. J Biol Chem 280:19543–19550
6. Fonseca I, Pereira T, Rosa-Santos J, Soares J (2001) Expression of CD44 isoforms in squamous cell carcinoma of the border of the tongue: a correlation with histological grade, pattern of stromal invasion, and cell differentiation. J Surg Oncol 76:115–120
7. Gao AC, Lou W, Dong JT, Isaacs JT (1997) CD44 is a metastasis suppressor gene for prostatic cancer located on human chromosome 11p13. Cancer Res 57:846–849
8. Guo YJ, Liu G, Wang X, Jin D, Wu M, Ma J, Sy MS (1994) Potential use of soluble CD44 in serum as indicator of tumor burden and metastasis in patients with gastric or colon cancer. Cancer Res 54:422–426
9. Kajita M, Itoh Y, Chiba T, Mori H, Okada A, Kinoh H, Seiki M (2001) Membrane-type 1 matrix metalloproteinase cleaves CD44 and promotes cell migration. J Cell Biol 153:893–904
10. Karan D, Lin FC, Bryan M, Ringel J, Moniaux N, Lin MF, Batra SK (2003) Expression of ADAMs (a disintegrin and metalloproteases) and TIMP-3 (tissue inhibitor of metalloproteinase-3) in human prostatic adenocarcinoma. Int J Oncol 23:1365–1371
11. Moss ML, Jin SLC, Milla ME, Burkhart W, Carter HL, Chen WJ, Clay WC, Didsbury JR, Hassler D, Hoffman CR, Kost TA, Lambert MH, Leesnitzer MA, McCauley P, McGeehan G, Mitchell J, Moyer M, Pahel G, Rocque W, Overton LK, Schoenen

F, Seaton T, Su JL, Warner J, Willard D, Becherer JD (1997) Cloning of a disintegrin metalloproteinase that processes precursor tumour-necrosis factor-α. Nature 385:733–736
12. Nagano O, Murakami D, Hartmann D, de Strooper B, Saftig P, Iwatsubo T, Nakajima M, Shinohara M, Saya H (2004) Cell-matrix interaction via CD44 is independently regulated by different metalloproteinases activated in response to extracellular Ca^{2+} influx and PKC activation. J Cell Biol 165:893–902
13. Nakamura H, Suenaga N, Taniwaki K, Matsuki H, Yonezawa K, Fujii M, Okada Y, Seiki M (2004) Constitutive and induced CD44 shedding by ADAM-like proteases and membrane-type 1 matrix metalloproteinase. Cancer Res 64:876–882
14. Okamoto I, Kawano Y, Tsuiki H, Sasaki J, Nakao M, Matsumoto M, Suga M, Ando M, Nakajima M, Saya H (1999) CD44 cleavage induced by membrane-associated metalloprotease plays a critical role in tumor cell migration. Oncogene 18:1435–1446
15. Okamoto I, Tsuiki H, Kenyon LC, Godwin AK, Emlet DR, Holgado-Madruga M, Lanham IS, Joynes CJ, Vo KT, Guha A, Matsumoto M, Ushio Y, Saya H, Wong AJ (2002) Proteolytic cleavage of the CD44 adhesion molecule in multiple human tumors. Am J Pathol 160:441–447
16. Ponta H, Sherman L, Herrlich PA (2003) CD44: from adhesion molecules to signalling regulators. Nature Rev Mol Cell Biol 4:33–45
17. Sato S, Miyauchi M, Takekoshi T, Zhao M, Kudo Y, Ogawa I, Kitagawa S, Fujita M, Takata T (2000) Reduced expression of CD44 variant 9 is related to lymph node metastasis and poor survival in squamous cell carcinoma of tongue. Oral Oncol 36:545–549
18. Seals DF, Courtneidge SA (2003) The ADAMs family of metalloproteinases: multidomain proteins with multiple functions. Genes Dev 17:7–30
19. Sheen-Chen SM, Chen WJ, Eng HL, Sheen CC, Chou FF, Cheng YF (1999) Evaluation of the prognostic value of serum soluble CD44 in patients with breast cancer. Cancer Invest 17:581–585
20. Shtivelman E, Bishop J (1991) Expression of CD44 is repressed in neuroblastoma cells. Mol Cell Biol 11:5446–5453
21. Tanaka Y, Miyamoto S, Suzuki SO, Oki E, Yagi H, Sonoda K, Yamazaki A, Mizushima H, Maehara Y, Mekada E, Nakano H (2005) Clinical significance of heparin-binding epidermal growth factor-like growth factor and a disintegrin and metalloprotease 17 expression in human ovarian cancer. Clin Cancer Res 11:4783–4792

Virchows Arch (2007) 450:179–185
DOI 10.1007/s00428-006-0347-6

ORIGINAL ARTICLE

$CD34^+$ fibrocytes in chronic cystitis and noninvasive and invasive urothelial carcinomas of the urinary bladder

Wilhelm Nimphius · Roland Moll · Peter Olbert · Annette Ramaswamy · Peter J. Barth

Received: 21 July 2006 / Accepted: 31 October 2006 / Published online: 6 December 2006
© Springer-Verlag 2006

Abstract $CD34^+$ fibrocytes are constitutive elements of the connective tissue where they play a role in matrix synthesis and tumor-associated stromal remodeling. Secreted protein, acidic, and rich in cysteine (SPARC) is a pivotal mediator of stromal remodeling precipitated by invasive carcinomas. The present study was undertaken to investigate $CD34^+$ fibrocytes in the stroma of the tumor-free urinary bladder, chronic cystitis, and urothelial carcinomas together with stromal expression of α-smooth muscle actin (α-SMA), CD117, and SPARC. In tumor-free urinary bladder and chronic cystitis, $CD34^+$ fibrocytes were found in the deep lamina propria and tunica muscularis, whereas the superficial lamina propria disclosed a CD34-negative and α-SMA-positive fibrocyte-like cell. Invasive urothelial carcinomas revealed a complete loss of $CD34^+$ fibrocytes and concomitant appearance of α-SMA-reactive myofibroblasts which showed strong expression of SPARC. CD117 expression of tumor-free and tumor-associated stroma revealed no differences. We in this study for the first time describe $CD34^+$ fibrocytes in the urinary bladder and an up-to-now unknown population of α-SMA-positive fibrocytes exclusively occurring in the superficial lamina propria. Stromal remodeling associated with invasive carcinomas in the urinary bladder is characterized by a loss of $CD34^+$ fibrocytes paralleled by a gain of α-SMA-positive myofibroblasts and increased expression of SPARC.

Keywords CD34 · Fibrocyte · Stroma · Urinary bladder · Urothelial carcinoma

W. Nimphius · R. Moll · A. Ramaswamy · P. J. Barth (✉)
Institute of Pathology, University Hospital Giessen and Marburg GmbH, Location Marburg,
Medical Faculty of Philipps-University Marburg,
Baldingerstraße,
35033 Marburg, Germany
e-mail: barthp@med.uni-marburg.de

P. Olbert
Department of Urology, University Hospital Giessen and Marburg GmbH, Location Marburg,
Medical Faculty of Philipps-University Marburg,
Baldingerstraße,
35033 Marburg, Germany

Introduction

$CD34^+$ fibrocytes have been described in the stroma of the upper aerodigestive tract [6], the lung [22] and heart [7], the gastrointestinal tract [4, 20, 21], the cornea [14], the breast [3, 8, 11, 24], and the female genital tract [5], where they constitute the most prevalent cell population. In most of these locations, stromal remodeling associated with invasive carcinomas is characterized by a virtually complete loss of $CD34^+$ fibrocytes, paralleled by a gain of α-smooth muscle actin (α-SMA)-positive myofibroblasts which are not observed in the normal tumor-free stroma [3–6, 8, 11, 20, 24]. Moreover, the carcinoma-associated stromal phenotype change is accompanied by strong expression of secreted protein, acidic, and rich in cysteine (SPARC) [8, 17, 23, 26] and to a lesser extent of CD117 [6]. SPARC and TGFβ act together in the regulation of CD34 and α-SMA expression [1, 2, 14, 25], and SPARC mediates stromal deadhesion which might constitute a pivotal step for tumor invasiveness. $CD34^+$ fibrocytes, originally described by Bucala et al. [10] in 1994, are derived from circulating $CD45^+$ myeloid cells. As shown by several subsequent investigations, $CD34^+$ fibrocytes are involved in wound healing and matrix synthesis, and they appear to act as potent antigen presenting cells [1, 10, 12, 13, 16]. It has therefore been speculated that a loss of $CD34^+$ fibrocytes might be essential for a malignant tumor to escape host

Table 1 Epidemiologic data of patients investigated

Diagnosis	*n*	Male (median age)	Female (median age)	Initial diagnosis	Low grade	High grade
CC	18	12 (71)	6 (81.5)	–	–	–
PUC, pTa	11	6 (57)	5 (77)	7	10	1
UC, pT1	17	14 (70)	3 (85)	15	15	2
UC, pT2	12	11 (69)	1 (95)	10	7	5

CC Chronic cystitis, *UC* urothelial carcinoma, *PUC* papillary urothelial carcinoma

immunosurveillance. Although, meanwhile, many studies as to this cell population have been published, the precise anatomical distribution, histogenesis, function, and fate in the tumor stroma of $CD34^+$ fibrocytes remain in part enigmatic. Up to now, reports concerning the occurrence of $CD34^+$ fibrocytes in the urinary bladder have due to our knowledge not been published. We therefore undertook the present study to investigate whether $CD34^+$ fibrocytes occur in the stroma of the tumor-free urinary bladder, chronic cystitis, and urothelial carcinomas and to what extent the stromal expression of α-SMA, CD117, and SPARC is altered in carcinoma-associated stromal remodeling.

Materials and methods

The present study comprises a total of 58 cystoscopic biopsies of the urinary bladder obtained from 58 patients. In 18 patients (Table 1), biopsies showed chronic cystitis. All patients with chronic cystitis had a pertinent history and clinical presentation. The presumed cause of chronic cystitis was prostatic hyperplasia in men and long-standing ascending infection in women. Biopsies were taken to rule out malignancy and showed a moderate to severe lymphocytic infiltrate of the lamina propria. Squamous metaplasia as well as eosinophilia was each reported in four cases.

Patients with histologically proven urothelial carcinomas in previous or subsequent biopsies were excluded from the chronic cystitis group. Urothelial carcinomas were present in 40 patients. The carcinomas were graded in two tiers according to the WHO (2004); tumor staging was performed according to the UICC TNM classification (2002). Patients' age, gender, and underlying diagnosis are summarized together with the major tumor characteristics in Table 1. Thirty-two of the 40 cases with urothelial carcinomas were initial diagnoses, and the remaining cases were recurrent tumors. In all cases, tumor-free biopsy particles or tumor-free biopsies located remotely from the tumor were available for comparison. However, the tumor-free biopsy particles varied greatly in size because some of them only covered superficial parts of the lamina propria, whereas others included the lamina propria in full thickness and adjacent tunica muscularis. Tissues were fixed in a 10% formalin solution, embedded in paraffin, cut, and stained with H&E and PAS for routine purposes.

Immunohistochemistry

CD34, α-SMA, SPARC, and CD117 were detected immunohistochemically by means of the standard avidin biotin complex (ABC)-peroxidase method (ABC Elite Kit; Vector, Burlingame, CA, USA) using 3,3′-diaminobenzidine (DAB) as chromogen. The primary antibodies and type of tissue pretreatment are listed in Table 2. Microwave pretreatment was performed by heating the deparaffinized and rehydrated sections, immersed in 10 mM sodium citrate buffer (pH 6.0), in a microwave oven at 600 W for three or four times for 5 min (see Table 2).

Double-staining immunohistochemistry

Double-label immunohistochemistry was performed for CD34, shown in brown color, and for α-SMA, shown in green color. In detail, as the first step, sections were stained for CD34 using a microwave oven heating for antigen retrieval and the ChemMate Detection Kit Peroxidase/DAB (DakoCytomation) which included biotinylated secondary antibodies, streptavidin peroxidase, and DAB as chromogen, producing a brown staining reaction. Sections were then again subjected to microwave oven heating (three times for 5 min). After cooling to room temperature, for the

Table 2 Antibodies applied for immunohistochemistry and type of tissue pretreatment

Antibody (clone)	Source	Dilution	Tissue pretreatment
CD34 (Qbend 10)	Dako, Hamburg, Germany	1:50	Microwave 3×5 min, 600 W
CD117	Dako, Hamburg, Germany	1:100	Microwave 3×5 min, 600 W
SPARC	Novocastra, UK	1:40	Microwave 3×5 min, 600 W
α-SMA (ASM-1)	Progen, Heidelberg, Germany	1:200	0.1% trypsin Tris/HCl for 15 min at 37°C

For double-labeling procedure, see the text.

second step, sections were reacted with the monoclonal antibody against α-SMA. Bound antibodies were detected using the same ChemMate Detection Kit as described above, but the staining reaction was based on HistoGreen (Linaris, Wertheim-Bettingen, Germany), producing a green staining reaction. Sections were counterstained using nuclear fast red. Incubations were performed on an automated immunohistochemistry apparatus (Autostainer plus; DakoCytomation). As controls, the primary antibody of the first step (anti-CD34) was substituted by an irrelevant monoclonal antibody while all other steps remained unchanged, or the primary antibody of the second step (anti-α-SMA) was substituted by an irrelevant monoclonal antibody leaving the other steps unchanged. These controls yielded the expected results.

Semiquantitative assessment of immunohistochemistry

Immunoreactivity of CD34, CD117, α-SMA, and SPARC was assessed semiquantitatively in the tumor-free tissue and tumor-associated stroma as previously described [8]. In brief, the percentage of stromal cells expressing the respective antigen was categorized as "0", "+", "++", or "+++" when up to 5%, more than 5% and up to 25%, more than 25% and up to 50%, or more than 50% of stromal cells, respectively, disclosed immunoreactivity. Percentages were assessed by two independent observers, assuming that a microscopic high-power field (objective 40×, microscopic magnification: 400×) harbors 100 stromal cells (range: 75–150). Double-stained (CD34 and α-SMA) slides were assessed qualitatively.

Statistical analyses

Comparison of frequencies was performed using the chi-square test assuming $p<0.01$ to be statistically significant.

Results

Tumor-free urinary bladder

The loose connective tissue of the lamina propria harbored small stromal cells with inconspicuous cytoplasm and slender dendrite-like projections. In the superficial lamina propria, these cells were arranged in parallel to the basal lamina of the covering urothelium and immunohistochemically disclosed α-SMA reactivity (40 of 40) (Fig. 1a), whereas CD34 was not detected (Fig. 1c). Stromal cells within the deeper lamina propria were predominantly located around larger veins and arteries; those located remotely from vessels were haphazardly arranged and disclosed in partly multipolar cytoplasmic projections. In contrast to the superficial lamina propria, stromal cells of the deeper lamina propria were negative for α-SMA (Fig. 1b) and positive for CD34 constituting characteristic $CD34^+$ fibrocytes (Fig. 1d). Accordingly, in the tumor-free lamina propria, $CD34^+$ fibrocytes were found in 23 of 40 cases (Table 3). This value precisely reflects the number of biopsies covering the full thickness of the lamina propria, whereas small superficial biopsies of the lamina propria contained no $CD34^+$ fibrocytes. Fascicles of smooth muscle in the tunica muscularis were surrounded by densely packed $CD34^+$ fibrocytes.

No dual expression of CD34 and α-SMA was found by means of double labeling indicating two distinct populations of α-SMA-positive fibrocytes in the superficial lamina propria (Fig. 1e) and $CD34^+$ fibrocytes in the deep lamina propria and tunica muscularis (Fig. 1f).

CD117 expression was found in a small population of stromal cells within the tumor-free stroma, whereas SPARC positivity appeared in up to 50% of the stromal cells. Strong CD117 staining was also found in mast cells which were scattered throughout the tumor-free lamina propria and tunica muscularis. The smooth muscle within the lamina propria and tunica muscularis was negative for both CD117 and SPARC.

Chronic cystitis

In chronic cystitis cases, the distribution of $CD34^+$ fibrocytes and α-SMA-positive stromal cells was similar compared to that observed in the tumor-free bladder. Double labeling disclosed two distinct populations of $CD34^+$ fibrocytes in the deep and α-SMA-positive stromal cells in the superficial lamina propria. There was also no significant difference as to the number of CD117- and SPARC-reactive stromal cells (Table 3). Compared to the tumor-free samples, the number of mast cells as detected by CD117 appeared to be increased.

Noninvasive papillary urothelial tumors (pTa)

With respect to the expression of CD117 and SPARC, the stroma of noninvasive papillary urothelial tumors disclosed no qualitative or quantitative differences compared to the tumor-free urinary bladder, whereas CD34 expression was completely absent from the stroma of these lesions (Table 3). Moreover, α-SMA-reactive stromal cells were more numerous in the stroma adjacent to and within noninvasive carcinomas, where they disclosed stronger α-SMA reactivity and a myofibroblastic phenotype.

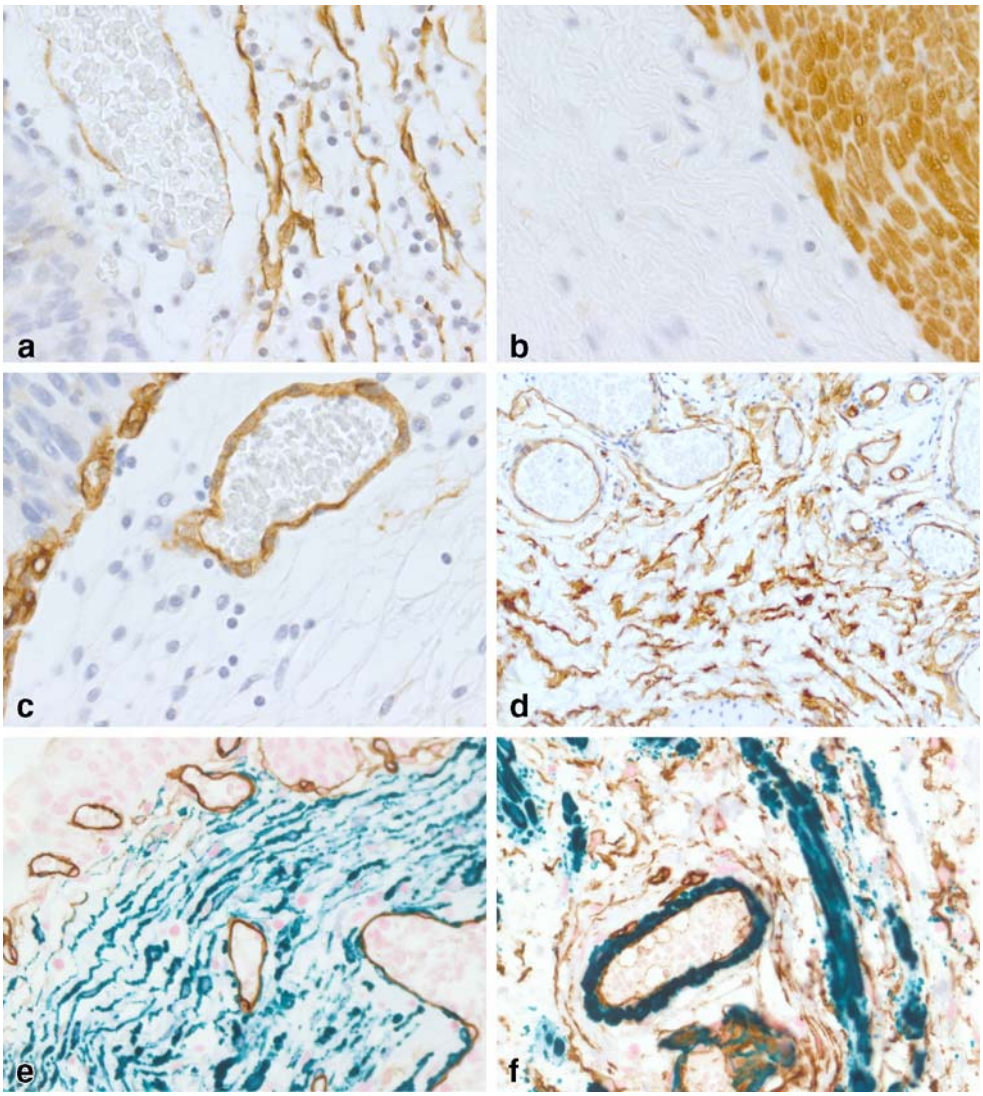

Fig. 1 Stromal cells of the superficial lamina propria exhibit a fibrocyte-like appearance and strong α-SMA positivity (**a**), whereas those of the deep lamina propria and tunica muscularis are negative for α-SMA (**b**). In contrast, the stroma of the superficial lamina propria discloses no reactivity for CD34 (**c**); in the deep lamina propria and tunica muscularis, $CD34^+$ fibrocytes surround the vessels and fascicles of the smooth muscle (**d**). Double labeling discloses a mutually exclusive reactivity of α-SMA (*green*) (**e** superficial lamina propria) and CD34 (*brown*) in the stromal cells (**f** deep lamina propria)

Invasive urothelial carcinomas

As in noninvasive tumors, $CD34^+$ fibrocytes were also completely absent from invasive carcinomas (Fig. 2a, Table 3). The stroma of invasive papillary carcinomas consisted of plump elongated myofibroblasts arranged in parallel or in a herringbone-like pattern. These cells were positive for α-SMA, featuring a characteristic tram-tracking of thick intracytoplasmic α-SMA-positive fibers (Fig. 2b). The stromal cells also mostly disclosed strong SPARC positivity (Fig. 2c), whereas CD117 was only observed in a small subpopulation of tumors displaying no significant difference in comparison to the tumor-free stroma (Table 3). Double labeling showed no dual positivity for α-SMA and CD34 in the carcinoma-associated myofibroblasts (Fig. 2d). Areas of antecedent biopsies were found in four cases and disclosed α-SMA-positive and CD34-negative myofibroblasts which showed weak SPARC positivity. CD117 was not observed in this cell population.

Discussion

The present study is the first to report on $CD34^+$ fibrocytes within the urinary bladder, where they occur in the deep lamina propria and the tunica muscularis. $CD34^+$ fibrocytes, originally described by Bucala et al. in 1994 [10], have meanwhile been shown to be an important and constitutive element of the connective tissue of most organs which have been investigated until now [3–6, 8, 11, 20–22, 24]. The major functions of $CD34^+$ fibrocytes are matrix synthesis and antigen presentation, suggesting a putative role in host response to invasive carcinomas [1, 10, 12, 13].

In addition, the present study reveals a novel cell type located in the superficial lamina propria which is negative for CD34, shows strong α-SMA reactivity, and morphologically resembles fibrocytes. Owing to their morphologic aspect and at least partial reactivity for SPARC and CD117, these cells are distinct from smooth muscle cells and myofibroblasts. Due to their α-SMA expression, it is likely

Table 3 Semiquantitative assessment of CD34, α-SMA, CD117, and SPARC expression in tumor-free biopsies and tumors of different stage

	CD34*			α-SMA*				CD117		SPARC*			
	0	+	++	0	+	++	+++	0	+	0	+	++	+++
Tumor-free *n* (%)	17 (43)	18 **(45)**	5 (12)	0 (0)	20 **(50)**	18 (45)	2 (5)	29 **(73)**	11 (27)	4 (10)	33 **(82)**	3 (8)	0 (0)
Chronic cystitis *n* (%)	5 (28)	10 **(56)**	3 (17)	0 (0)	8 (44)	8 (44)	2 (11)	15 **(83)**	3 (17)	3 (17)	12 **(67)**	3 (17)	0 (0)
pTa *n* (%)	11 **(100)**	0 (0)	0 (0)	2 (18)	1 (9)	5 **(45)**	3 (27)	9 **(82)**	2 (18)	4 (36)	5 **(45)**	2 (18)	0 (0)
pT1 *n* (%)	17 **(100)**	0 (0)	0 (0)	0 (0)	3 (18)	8 **(47)**	6 (35)	17 **(100)**	0 (0)	0 (0)	11 **(65)**	4 (23)	2 (12)
pT2 *n* (%)	12 **(100)**	0 (0)	0 (0)	0 (0)	0 (0)	7 **(58)**	5 (42)	11 **(92)**	1 (8)	0 (0)	4 (33)	7 **(58)**	1 (8)

Highest frequencies in the respective group are set in bold.
*$p<0.01$ (chi-square test)
0 <5%, + >5 and <25%, ++ >25% and <50%, +++ >50% positive stromal cells.

that the superficial stromal cells play a role in providing and maintaining mechanical properties of the lamina propria, whereas $CD34^+$ fibrocytes in the deeper lamina propria are mainly involved in matrix synthesis.

In the cervix uteri and the breast, in situ carcinomas are characterized by a loss of $CD34^+$ fibrocytes in the adjacent stroma [3, 5]. This phenomenon was not observed in the urinary bladder because the superficial lamina propria is devoid of $CD34^+$ fibrocytes. Therefore, the diagnostic value of $CD34^+$ fibrocytes in the diagnosis of carcinomas of the urinary bladder is comparably low. Nevertheless, the presence of $CD34^+$ fibrocytes separates tumor-free urinary bladder and chronic cystitis on one side from invasive and noninvasive carcinomas. In invasive urothelial carcinomas, the stromal composition is similar to that observed in various other carcinomas of whatever histologic type or anatomical location recapitulating the stereotypic transition from the $CD34^+$ α-SMA^- fibrocytes in the tumor-free stroma toward the tumor-associated $CD34^-$ α-SMA^+ myofibroblast [3–6, 8]. This finding is in keeping with Shimasaki et al. [28] who reported myofibroblasts in the stroma of urothelial carcinomas of the urinary bladder.

In squamous cell carcinomas, stromal remodeling is at least in part due to recruitment of additional growth-regulating pathways mediated by CD117 [6]. This is not the case in urothelial carcinomas. However, except for CD117 expression, stromal remodeling in the urinary tract closely resembles that observed in various other organs. Thus, our study confirms the role of SPARC which has been claimed to play a role in stromal invasion by carcinomas. SPARC is a matricellular protein, serving several functions, the most important of which in the present context is induction of stromal de-adhesion [9, 15, 19]. It is interesting to note that in the present study,

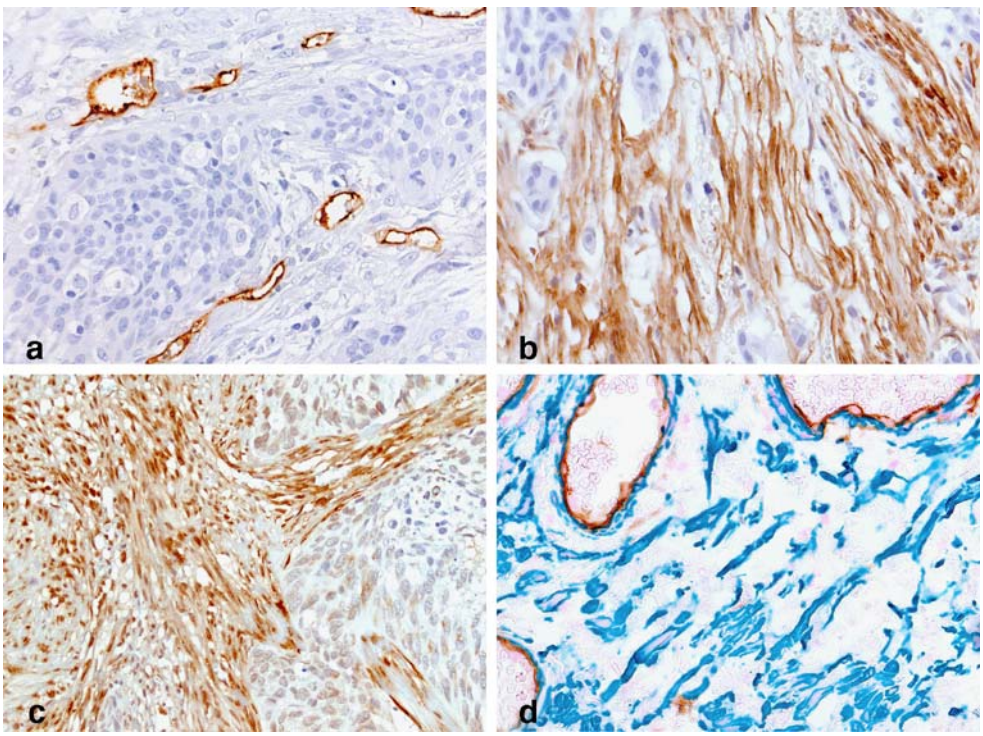

Fig. 2 The stroma of invasive carcinomas shows a complete loss of $CD34^+$ fibrocytes (**a** note preserved CD34 reactivity of endothelial cells) accompanied by a gain of α-SMA-positive myofibroblasts (**b**). Tumor-associated myofibroblasts show a strong reactivity for SPARC (**c**). No coexpression of α-SMA (*green*) and CD34 (*brown*) was observed in the myofibroblasts by means of double labeling (**d**)

SPARC was also observed in the tumor-free lamina propria, reflecting the morphologic aspect of a loose "de-adhesive" stroma. SPARC expression is upregulated by TGFβ and vice versa [2, 25, 27], precipitating many features of carcinoma-associated stromal remodeling as TGFβ has been shown to downregulate CD34 and upregulate α-SMA [1, 14]. Accordingly, immunohistochemical double labeling showed the expression of CD34 and α-SMA to be mutually exclusive in the tumor-free as well as in the tumor-associated stroma. Downregulation of CD34 might further increase stromal de-adhesion induced by SPARC because CD34 signaling has been reported to create and maintain cell–cell contacts and homotypic adherence of mesenchymal cells [18]. Because $CD34^+$ fibrocytes play a pivotal role in matrix synthesis and repair as they are a major source of collagen types I and III [1, 10, 13], a loss of this cell population and the adhesion of stromal cells may constitute an important prerequisite for tumor invasion, tumor cell migration, and subsequent distant tumor spread. This assumption is underlined by the fact that a $CD34^+$ fibrocyte loss develops stereotypically in virtually all invasive carcinomas investigated up to now [3–6, 8, 11, 20–22, 24]. When considering the immunohistochemical analysis of the $CD34^+$ stromal cell population as a diagnostic tool, it should be kept in mind that stromal response to unspecific damage such as previous biopsies is similar to that observed in invasive carcinomas [11]. Therefore, a loss of $CD34^+$ fibrocytes does not prove malignancy although in contrast, the presence of this cell population excludes malignancy with a high degree of probability.

References

1. Abe R, Donnelly SC, Peng T, Bucala R, Metz CN (2001) Peripheral blood fibrocytes: differentiation pathway and migration to wound sites. J Immunol 166:7556–7562
2. Abe K, Hibino T, Mishima H, Shimomura Y (2004) The cytokine regulation of SPARC production by rabbit corneal epithelial cells and fibroblasts in vitro. Cornea 23:172–179
3. Barth PJ, Ebrahimsade S, Ramaswamy A, Moll R (2002) $CD34^+$ fibrocytes in invasive ductal carcinoma, ductal carcinoma in situ, and benign breast lesions. Virchows Arch 440:298–303
4. Barth PJ, Ebrahimsade S, Hellinger A, Moll R, Ramaswamy A (2002) $CD34^+$ fibrocytes in neoplastic and inflammatory pancreatic lesions. Virchows Arch 440:128–133
5. Barth PJ, Ramaswamy A, Moll R (2002) $CD34^+$ fibrocytes in normal cervical stroma, cervical intraepithelial neoplasia III, and invasive squamous cell carcinoma of the cervix uteri. Virchows Arch 441:564–568
6. Barth PJ, Schenck zu Schweinsberg T, Ramaswamy A, Moll R (2004) $CD34^+$ fibrocytes, α-smooth muscle antigen-positive myofibroblasts, and CD117 expression in the stroma of invasive squamous cell carcinomas of the oral cavity, pharynx, and larynx. Virchows Arch 444:231–234
7. Barth PJ, Koster H, Moosdorf R (2005) $CD34^+$ fibrocytes in normal mitral valves and myxomatous mitral valve degeneration. Pathol Res Pract 201:301–304
8. Barth PJ, Moll R, Ramaswamy A (2005) Stromal remodeling and SPARC (secreted protein acid rich in cysteine) expression in invasive ductal carcinomas of the breast. Virchows Arch 446:532–536
9. Bradshaw AD, Sage EH (2001) SPARC, a matricellular protein that functions in cellular differentiation and tissue response to injury. J Clin Invest 107:1049–1054
10. Bucala R, Spiegel LA, Chesney J, Hogan M, Cerami A (1994) Circulating fibrocytes define a new leukocyte subpopulation that mediates tissue repair. Mol Med 1:71–81
11. Chauhan H, Abraham A, Phillips JR, Pringle JH, Walker RA, Jones JL (2003) There is more than one kind of myofibroblast: analysis of CD34 expression in benign, in situ, and invasive breast lesions. J Clin Pathol 56:271–276
12. Chesney J, Bacher M, Bender A, Bucala R (1997) The peripheral blood fibrocyte is a potent antigen-presenting cell capable of priming naive T cells in situ. Proc Natl Acad Sci USA 94:6307–6312
13. Chesney J, Metz C, Stavitsky AB, Bacher M, Bucala R (1998) Regulated production of type I collagen and inflammatory cytokines by peripheral blood fibrocytes. J Immunol 160:419–425
14. Espana EM, Kawakita T, Liu CY, Tseng SC (2004) CD-34 expression by cultured human keratocytes is downregulated during myofibroblast differentiation induced by TGF-beta1. Invest Ophthalmol Vis Sci 45:2985–2991
15. Framson PE, Sage EH (2004) SPARC and tumor growth: where the seed meets the soil? J Cell Biochem 92:679–690
16. Hartlapp I, Abe R, Saeed RW, Peng T, Voelter W, Bucala R, Metz CN (2001) Fibrocytes induce an angiogenic phenotype in cultured endothelial cells and promote angiogenesis in vivo. FASEB J 15:2215–2224
17. Iacobuzio-Donahue CA, Argani P, Hempen PM, Jones J, Kern SE (2002) The desmoplastic response to infiltrating breast carcinoma: gene expression at the site of primary invasion and implications for comparisons between tumor types. Cancer Res 62:5351–5357
18. Majdic O, Stockl J, Pickl WF, Bohuslav J, Strobl H, Scheinecker C, Stockinger H, Knapp W (1994) Signaling and induction of enhanced cytoadhesiveness via the hematopoietic progenitor cell surface molecule CD34. Blood 83:1226–1234
19. Murphy-Ullrich JE (2001) The de-adhesive activity of matricellular proteins: is intermediate cell adhesion an adaptive state? J Clin Invest 107:785–790
20. Nakayama H, Enzan H, Miyazaki E, Kuroda N, Naruse K, Hiroi M (2000) Differential expression of CD34 in normal colorectal tissue, peritumoral inflammatory tissue, and tumour stroma. J Clin Pathol 53:626–629
21. Nakayama H, Enzan H, Miyazaki E, Kuroda N, Naruse K, Kiyoku H, Toi M, Hiroi M (2001) CD34 positive stromal cells in gastric adenocarcinomas. J Clin Pathol 54:846–848
22. Nakayama H, Enzan H, Yamamoto M, Miyazaki E, Hidaka C, Okumichi T, Okumichi A, Kajihara H (2003) CD34-positive stromal cells in primary lung carcinomas. Oncol Rep 10:1313–1316
23. Porter PL, Sage EH, Lane TF, Funk SE, Gown AM (1995) Distribution of SPARC in normal and neoplastic human tissue. J Histochem Cytochem 43:791–800
24. Ramaswamy A, Moll R, Barth PJ (2003) $CD34^+$ fibrocytes in tubular carcinomas and radial scars of the breast. Virchows Arch 443:536–540
25. Reed MJ, Vernon RB, Abrass IB, Sage EH (1994) TGF-beta 1 induces the expression of type I collagen and SPARC, and enhances contraction of collagen gels, by fibroblasts from young and aged donors. J Cell Physiol 158:169–179

26. Ryu B, Jones J, Hollingsworth MA, Hruban RH, Kern SE (2001) Invasion-specific genes in malignancy: serial analysis of gene expression comparisons of primary and passaged cancers. Cancer Res 61:1833–1838
27. Schiemann BJ, Neil JR, Schiemann WP (2003) SPARC inhibits epithelial cell proliferation in part through stimulation of the transforming growth factor-β-signaling system. Mol Biol Cell 14:3977–3988
28. Shimasaki N, Kuroda N, Miyazaki E, Hayashi Y, Toi M, Hiroi M, Enzan H, Shuin T (2006) The distribution pattern of myofibroblasts in the stroma of human bladder carcinoma depends on their invasiveness. Histol Histopathol 21:349–353

Virchows Arch (2007) 450:187–194
DOI 10.1007/s00428-006-0346-7

ORIGINAL ARTICLE

Taxol-resistance-associated gene-3 (TRAG-3/CSAG2) expression is predictive for clinical outcome in ovarian carcinoma patients

Verena Materna · Paweł Surowiak · Irina Kaplenko · Marek Spaczyński · Zhenfeng Duan · Maciej Zabel · Manfred Dietel · Hermann Lage

Received: 8 September 2006 / Accepted: 31 October 2006 / Published online: 10 January 2007
© Springer-Verlag 2007

Abstract An obstacle in chemotherapy of ovarian cancer is the development of drug resistance. Taxol (paclitaxel)-resistance-associated gene-3 (TRAG-3/CSAG2) was found to be overexpressed in a paclitaxel-resistant ovarian carcinoma cell line. However, clinical impact of TRAG-3 in ovarian carcinoma has not been demonstrated previously. For demonstration of potential clinical impact of TRAG-3, immunohistochemistry was applied to determine TRAG-3 protein expression in specimens obtained from ovarian carcinoma patients (n=37) who received a paclitaxel-based chemotherapy at two different time points, initial laparotomy before chemotherapy, and secondary cytoreduction after chemotherapy. The TRAG-3-specific immunohistochemical staining was correlated with clinical outcome. In ovarian carcinoma specimens obtained at the initial laparotomy, an advantage in overall (P<0.001) and progression-free (P=0.003) survival for patients with weak TRAG-3 expression could be demonstrated. Tumor specimens excised at secondary cytoreduction procedure were not predictive for clinical outcome. In summary, TRAG-3 was found to be a prognostic factor for the prediction of clinical outcome after the application of paclitaxel-based chemotherapy.

Keywords Ovarian carcinoma · Paclitaxel · TRAG-3 · CSAG2 · Chemotherapy

V. Materna · P. Surowiak · M. Dietel · H. Lage (✉)
Institute of Pathology, Charité Campus Mitte,
Charitéplatz 1, 10117 Berlin, Germany
e-mail: hermann.lage@charite.de

P. Surowiak · M. Zabel
Department of Histology and Embryology,
Wrocław Medical University,
Chalubińskiego 6a, 50-368 Wrocław, Poland

P. Surowiak
Lower Silesian Center of Oncology,
pl. Hirszfelda 12, 53-413 Wrocław, Poland

I. Kaplenko · M. Spaczyński
Department of Obstetrics and Gynecology,
Poznań University of Medical Sciences,
ul. Polna 33, 60-535 Poznań, Poland

Z. Duan
Division of Hematology/Oncology,
Massachusetts General Hospital,
Jackson 1029, 70 Blossom St., Boston, MA 02114, USA

M. Zabel
Department of Histology and Embryology,
Poznań University of Medical Sciences,
Swięcickiego 6, 60-781 Poznań, Poland

Introduction

About 190,000 new cases and 114,000 deaths from ovarian carcinoma are estimated to occur annually [20]. Most of them (75%) are diagnosed in the stages FIGO III and IV, and affected patients have a 5-year survival rate as poor as 20%. In advanced ovarian carcinoma, combination chemotherapy with platinum-containing drugs and paclitaxel represents the main treatment option, along with surgery. The initial response rate to chemotherapy is high, ranging between 50 and 70%, with 15–20% complete responses. Although a lot of progress has been made in the chemotherapeutic treatment of ovarian carcinoma, acquired drug resistance to currently available antineoplastic agents

remains the major mechanism limiting successful therapy and causes recurrent carcinomas in more than 50% of advanced diseased patients [11, 14].

Paclitaxel is a natural product-based anticancer drug derived from the bark of the Pacific Yew, *Taxus brevifolia.* It inhibits microtubule depolymerization during mitosis followed by cell death. Paclitaxel provides a broad spectrum of antitumor activity including lung, breast, and ovarian cancers [16]. However, treatment with paclitaxel is frequently not curative due to the development of paclitaxel resistance.

The biological mechanisms mediating resistance to paclitaxel include the enhanced activity of the xenobiotics transporter MDR1/P-glycoprotein [1], or alterations in tubulin structure or tubulin expression level [6, 7]. Furthermore, a differential display RT-PCR (DDRT-PCR) approach using a paclitaxel-resistant ovarian carcinoma cell line demonstrated an overexpression of taxol-resistance associated gene 3 (TRAG-3) also designated as CSAG2, in this cell line [4]. Expression analysis revealed a minimal or absent TRAG-3 expression in various normal tissues and elevated expression levels in various cancer-derived cell lines and tissues [2–5, 12, 13, 24, 25]. Transfection experiments using the TRAG-3 encoding cDNA did not mediate a paclitaxel-resistant phenotype to paclitaxel-sensitive cell lines [4]. This observation suggests that TRAG-3 does not directly participate in the paclitaxel-resistant phenotype. TRAG-3 rather may be an essential part of a multi-component mechanism leading to resistance.

The *TRAG-3* encoding gene has been mapped to chromosome Xq28 within a complex for the MAGE (melanoma antigen) family of tumor antigenes [5] and at least four splicing variants have been described [9]. However, the physiological/pathological functions of TRAG-3 have not been elucidated and the mechanisms of involvement in drug resistance remain unclear. Promotor studies and 5-aza-2′-deoxyazacytidine treatment of TRAG-3 non-expressing tumor cell lines showed that TRAG-3 expression is dependent on and can be induced by demethylation [25, 26]. Although diverse cancer specimens, e.g., melanoma and lung and breast cancer were reported to express TRAG-3 on mRNA and/or protein level [2, 4, 24, 25], the influence of its expression on paclitaxel resistance in the meaning of clinical outcome after paclitaxel-based chemotherapy was not investigated so far.

Thus, in the present study, samples of ovarian carcinomas were obtained from first-look laparotomies and from secondary cytoreductions after the chemotherapy from the same patients. TRAG-3 expression levels were correlated with clinical outcome after chemotherapy using paclitaxel-based schemes.

Materials and methods

Patients and histology

Immunohistochemical examination was performed retrospectively on tissue samples taken for routine diagnostic purposes. Thirty-seven patients suffering from ovarian carcinoma, operated on in 1999–2002 in the Department of Obstetrics and Gynecology, Poznań University of Medical Sciences, Poland were qualified for the study. An institutional review board (IRB) approved the study and the patients gave their informed consent before their inclusion into the study. The cases were selected based on availability of tissue and were not stratified for known preoperative or pathological prognostic factors. After the first surgery, all the patients were subjected to chemotherapy using paclitaxel-based schemes (Table 1). Only the FIGO I and the

Table 1 Patient and tumor characteristics

Characteristics	No. (%)[b]
All patients	37 (100)
First surgical treatment	37 (100)
Second surgical treatment	31 (84)
No tumor cells at time of second surgical treatment	6 (16)
Age (mean 51.0)[a]	
≤50	17 (46)
>50	20 (54)
Grade[a]	
1	5 (14)
2	15 (41)
3	17 (46)
FIGO[a]	
I	1 (3)
II	1 (3)
III	35 (95)
Histology[a]	
Serous carcinoma	32 (86)
Endometrioid carcinoma	2 (5)
Mucinous carcinoma	1 (3)
Transitional cell carcinoma	1 (3)
Clear cell carcinoma	1 (3)
Clinical response[c]	
Complete response	16 (43)
Stable disease	5 (14)
Progressive disease	16 (43)
Chemotherapy (in total)	
Cisplatin/paclitaxel	31 (84)
Cisplatin/cyclophosphamide/paclitaxel	3 (8)
Cisplatin/cyclophosphamide/paclitaxel/adriblastin	2 (5)
Carboplatin/paclitaxel	1 (3)

[a] Data are given to first surgical treatment/diagnosis implemented.
[b] Differences in the sum to 100% in groups are due to rounding.
[c] Clinical response to first-line chemotherapy was defined according to the criteria suggested by RECIST (response evaluation criteria in solid tumors) [22].

FIGO II patients achieved optimal cytoreduction after initial surgery.

Thirty-one patients from the same group were subjected also to secondary cytoreduction approximately 6 months after initial surgery. In six cases, no secondary surgery was performed due to advancement of the disease. In six other cases, no tumor cells were detected in the material originating from the secondary cytoreduction (Table 1). The patients were monitored by periodic medical check-ups, CA-125 serum levels, and ultrasonographic and radiological examinations. Tissue samples were fixed in 10% buffered formalin and then embedded in paraffin. In each case, hematoxylin-and-eosin-stained preparations were subjected to histopathological evaluation by two pathologists. The tumors were surgical staged according to the International Federation of Gynecology and Obstetrics [19]. The tumors were graded according to the Silverberg grading system [18].

Immunohistochemistry

Formalin-fixed paraffin-embedded tissue was freshly cut (4 μm). The sections were mounted on Superfrost slides (Menzel Glaeser, Braunschweig, Germany), dewaxed with xylene, and gradually rehydrated. Activity of endogenous peroxidase was blocked by 30 min incubation in 1% H_2O_2. The sections were boiled for 10 min in a microwave oven in Antigen Retrieval Solution (DakoCytomation, Glostrup, Denmark) at 500 W. This was followed by immunological staining using polyclonal rabbit anti-TRAG-3 antibodies (dilution 1:400) [2, 26]. Antibodies were diluted in the antibody diluent with background-reducing components (DakoCytomation, Denmark) and the sections were incubated for 1 h at room temperature.

Subsequently, sections were incubated with biotinylated antibodies and with streptavidin-biotinylated peroxidase complex (each for 15 min at room temperature) (LSAB+, HRP, DakoCytomation). DAB Liquid+ (DakoCytomation) was used as a chromogen, employing 10 min incubation at room temperature. All sections were counterstained using Meyer's hematoxylin. Each reaction was accompanied by a negative control where the specific antibody was substituted by Primary Rabbit Negative Control (DakoCytomation). Control reactions were performed on six samples of healthy human testes and ovaries (archive of the Department of Histology and Embryology, Wrocław Medical University, Poland).

Intensities of immunostaining reactions were appraised using the semi-quantitative immunoreactive score (IRS) in which intensities of the reactions and percentage of positive cells were estimated (Table 2). The final result represented a product of scores given for individual traits and ranged between 0 and 12 [15]. Intensities of immunostaining reactions were evaluated independently by two pathologists. In cases of controversy, a reevaluation was performed with the use of a double-headed microscope.

Table 2 Procedure for evaluation of TRAG-3 expression using an IRS (immunoreactive score) [15]

Percentage of positive cells	Points	Intensity of reaction	Points
No positive cells	0	No reaction	0
<10%	1	Weak	1
10–50%	2	Moderate	2
51–80%	3	Intense	3
>80%	4		

Statistical analysis

Kaplan–Meier statistics and log-rank tests were performed using SPSS software (release 12.0.1; SPSS, Chicago, IL, USA) to estimate the significance of differences in survival times. The length of progression-free survival was defined as the time from the primary surgical treatment until the time of diagnosis of a recurrent tumor or death. The Mann–Whitney U test and χ^2-test were used to investigate the association between gene expression and other findings. All tests were two-sided.

Results

Thirty-seven patients with primary epithelial ovarian carcinoma and a mean age of 51 years were subjected for TRAG-3 protein expression analysis using immunohistochemistry (Table 1). All patients underwent chemotherapeutic treatment with paclitaxel in combination with additional drugs after initial surgery. Most of the patients (84%) received also a secondary surgical treatment. As controls, a healthy human testis, known to be positive for TRAG-3 expression [2, 4], and a healthy human ovary tissue were analyzed by immunohistochemistry (Fig. 1a,b). As expected, the healthy human testis tissue showed a strong cytoplasmic staining reaction, localized in the procreational epithelium.

Varying from that, the healthy human ovary tissue displayed only a weak cytoplasmic reaction in the superficial epithelium. Most of the ovarian carcinoma tissue samples showed different amounts of TRAG-3 protein expression in the cytoplasm (Fig. 1c,d). TRAG-3 expression could not be detected in 6/37 (16%) ovarian carcinoma samples at the time point of the initial laparotomy. However, all 25 patients with secondary surgical treatment and who manifested persistent tumor cells showed TRAG-3 expression.

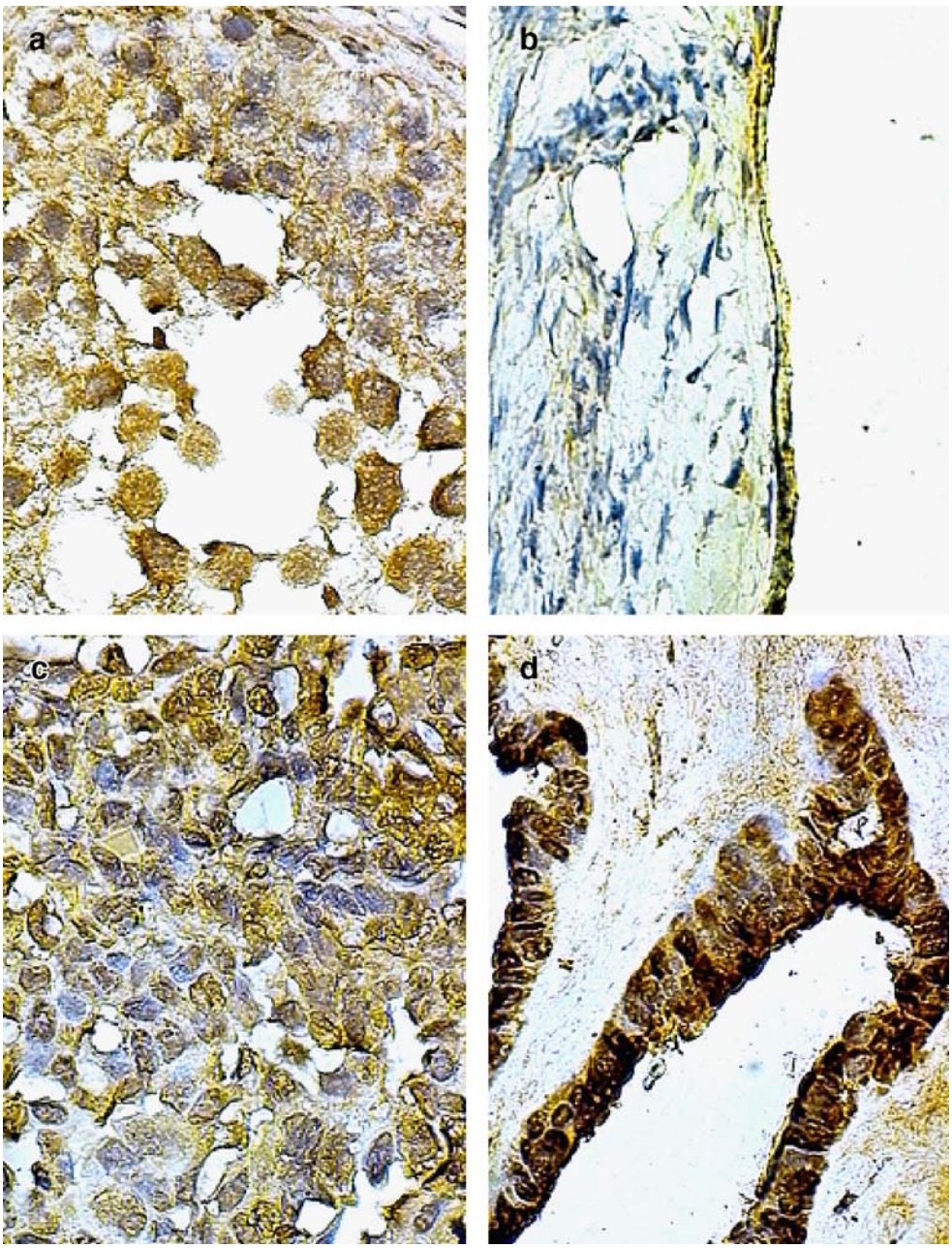

Fig. 1 Immunhistochemical localization of TRAG-3 expression (counterstaining with hematoxylin. **a** Healthy human testis with strong cytoplasmic reaction in the procreational epithelium (×600); **b** healthy human ovarian tissue with weak cytoplasmic reaction in superficial epithelium (×400); **c** and **d** ovarian carcinomas with cytoplasmic localization (×400)

The median score of TRAG-3 protein expression, ranging from 0 to 12 (Table 2), in the analyzed ovarian carcinoma samples was 4 before and 9 after chemotherapy, as determined at the time points of the first-look laparotomy and the secondary cytoreduction. Detailed descriptions of clinical response and TRAG-3 protein expression for all 37 analyzed ovarian carcinoma patients are given in Table 3. There was no difference in TRAG-3 expression between different gradings and ages below and above 50 years. However, patients not responding to chemotherapy showed a significantly higher TRAG-3 expression compared to patients with stable disease or therapy response (P=0.001, Mann–Whitney U test). Using TRAG-3 expression analysis at the time point of the initial laparotomy representing the status before chemotherapy, there was a clear survival advantage for patients expressing weak TRAG-3 protein levels (score 0–8) compared with high levels of TRAG-3 (score 9–12) in overall survival time (P<0.0001) as well as in progression-free survival time (P=0.003).

TRAG-3 expression analysis at the time point of secondary cytoreduction representing the status after chemotherapy was not meaningful for the prediction of disease progression (Fig. 2). For confirmation of these observations in cases of less heterogeneous histological types, the

Table 3 Clinical response and TRAG-3 expression in ovarian carcinoma patients

Code	Age (years)[a]	FIGO stage[a]	Response[b]	Grade[a]	TRAG-3 score (FLL)	TRAG-3 score (SCR)
1	30	1[c]	1	CR	12	n.t.c.
2	48	2[c]	1	PD	12	12
3	52	3	1	CR	6	2
4	54	3	1	CR	2	8
5	52	3	1	SD	3	12
6	40	3	2	CR	0	n.t.c.
7	48	3	2	CR	0	12
8	34	3	2	CR	0	12
9	56	3	2	CR	3	12
10	44	3	2	CR	4	12
11	51	3	2	CR	8	8
12	61	3	2	CR	8	9
13	54	3	2	SD	2	4
14	52	3	2	SD	4	8
15	58	3	2	SD	4	12
16	56	3	2	PD	12	n.t.c.
17	37	3	2	PD	8	8
18	42	3	2	PD	8	4
19	33	3	2	PD	4	no SCR
20	56	3	2	PD	8	no SCR
21	50	3	3	CR	2	n.t.c.
22	47	3	3	CR	4	n.t.c.
23	50	3	3	CR	0	8
24	49	3	3	CR	0	9
25	58	3	3	CR	2	8
26	71	3	3	CR	12	9
27	74	3	3	SD	0	12
28	50	3	3	PD	4	n.t.c.
29	67	3	3	PD	2	4
30	47	3	3	PD	8	12
31	53	3	3	PD	12	12
32	40	3	3	PD	12	12
33	37	3	3	PD	12	9
34	51	3	3	PD	4	no SCR
35	72	3	3	PD	6	no SCR
36	51	3	3	PD	8	no SCR
37	62	3	3	PD	8	no SCR

FLL first-look laparatomy, *SCR* secondary cytoreduction, *n.t.c.* no tumor cells in the obtained tissue from secondary cytoreduction

[a] Data are given to the first surgical treatment/diagnosis implemented.

[b] Clinical response to first-line chemotherapy was defined according to the criteria suggested by RECIST (response evaluation criteria in solid tumors) [22].

[c] Merely FIGO I and FIGO II patients achieved optimal cytoreduction.

analyses were also restricted to the 30 patients suffering from serous ovarian carcinoma in stage FIGO III. Likewise, it could be demonstrated that before chemotherapeutic treatment, there was a clear survival advantage for patients showing weak TRAG-3 protein levels in overall survival time ($P<0.0003$) as well as in progression-free survival time ($P=0.007$). Likewise, the TRAG-3 expression level after chemotherapy had no influence on clinical outcome (Fig. 3).

In accordance with the data obtained at the initial laparotomies, there were no differences in survival depending on age (≤50 vs >50 years) or grading of the tumor specimens. For 33/37 cases, the CA-125 level was determined contemporary to the initial surgical treatment and was elevated compared to the normal range (mean 833.1 units/ml). No differences were found in overall and progression-free survival for patients with lower (<1,000 units/ml) or higher (≥ 1,000 units/ml) initial CA-125 amounts. Due to the relatively small number of analyzed patients and due to the lack of possibly independent factors with significant influence in the performed analyses, we did not perform a multivariate analysis.

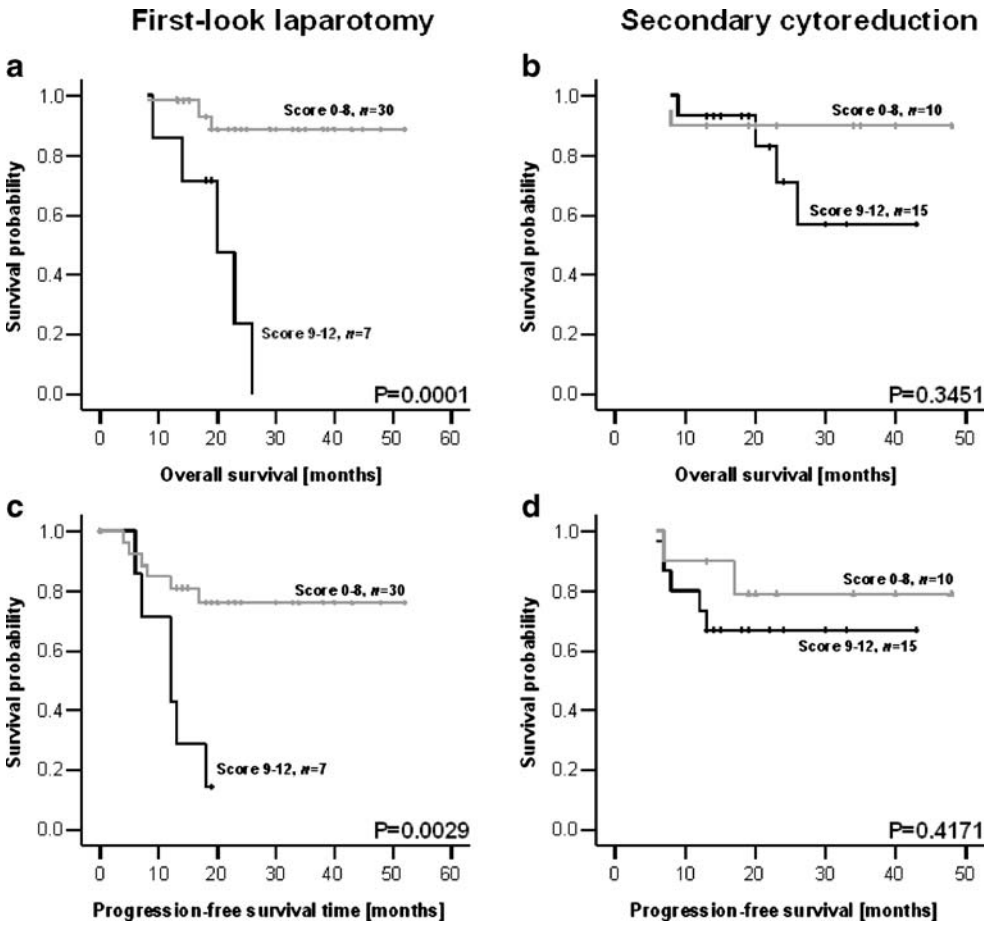

Fig. 2 Kaplan–Meier curves for expression of TRAG-3 and survival in ovarian carcinoma patients. **a** Overall survival time, and **c** progression-free survival time of patients whose tissues were analyzed at the time point of first-look laparotomy; **b** overall survival time, and **d** progression-free survival time of patients whose tissues were analyzed at the time point of secondary cytoreduction. An immunoreactive score (Table 2) was used for dividing patients in groups with low or high TRAG-3 expression levels. *n*, number of patients

Discussion

Due to the inherent difficulties of studying drug-resistance-mediating mechanisms in vivo, a large number of in vitro models have been developed from different neoplasms including ovarian carcinoma. TRAG-3 was identified to be overexpressed in the paclitaxel-resistant human ovarian cancer cell line SKOV-3_{TR} compared to the paclitaxel-sensitive counterpart SKOV-3 by a DDRT-PCR approach [4]. Furthermore, it could be demonstrated that TRAG-3 was overexpressed in additional drug-resistant cell lines of different origin [3, 4]. Although transfection experiments using the TRAG-3-encoding-cDNA sequence did not transfer a paclitaxel-resistant phenotype to drug-sensitive cells, it cannot be excluded that TRAG-3 is part of a multi-component mechanism mediating drug resistance.

Similar to these results using the TRAG-3 encoding cDNA in transfection experiments, transfection of the glypican 3 (GPC3)-encoding cDNA that was found to be overexpressed in a mitoxantrone-resistant gastric carcinoma cell line did not confer a drug-resistant phenotype to drug-sensitive cells [8]. However, an involvement of GPC3 in mitoxantrone resistance could be demonstrated by hammerhead-ribozyme-mediated inhibition of GPC3 expression [23], suggesting that GPC3 is an essential part of a multimodal drug resistance mechanism. Likewise, experiments using the well-known lung resistance protein (LRP) specific cDNA did not lead to drug resistance when transfected into drug-sensitive cell lines [17].

Although it was reported that TRAG-3 is expressed in cancer cell lines of different origin [3–5, 12] and different tumor tissues [2, 5, 13, 24, 25], so far no studies are available in which a potential impact of TRAG-3 expression on clinical outcome including response to anticancer drug treatment was investigated.

As the in vitro analyses indicate that TRAG-3 may be an interesting factor associated with paclitaxel resistance in ovarian carcinoma cells [4], collective patients suffering from advanced ovarian cancer (most of them with stage FIGO III) were analyzed concerning a potential correlation of TRAG-3 expression and their clinical response to paclitaxel-based chemotherapeutic treatment. Specimens of ovarian carcinoma tissue were obtained at two different time points. The initial first-look laparotomy was performed to remove the primary tumor. A paclitaxel-containing chemotherapeutic treatment followed the surgery. Depending on the state of health, a secondary cytoreductive surgery was performed.

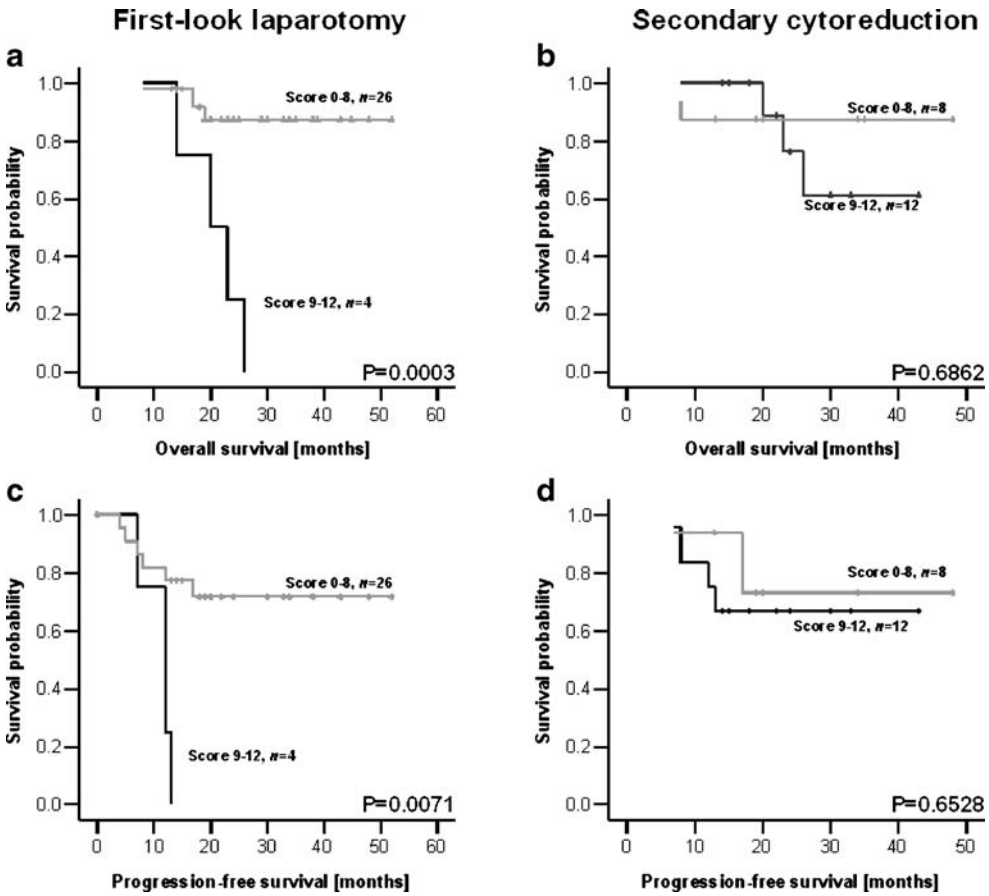

Fig. 3 Kaplan–Meier curves for expression of TRAG-3 and survival of patients with serous ovarian carcinoma cases in stage FIGO III. **a** Overall survival time, and **c** progression-free survival time of patients whose tissues were analyzed at the time point of first-look laparotomy; **b** overall survival time, and **d** progression-free survival time of patients whose tissues were analyzed at the time point of secondary cytoreduction. An immunoreactive score (Table 2) was used for dividing patients in groups with low or high TRAG-3 expression levels. *n*, number of patients

Accordingly, in most of the cases TRAG-3 expression could be measured before and after chemotherapy in the same patients. In this study, the mean TRAG-3 expression level of all analyzed ovarian carcinoma specimens was lower before starting the chemotherapy at the time point of the initial laparotomy compared to the expression measured in tissue samples taken from the secondary cytoreduction. This study then indicates that TRAG-3 expression may be induced by chemotherapeutic treatment.

At the time of the initial laparotomy, immunohistochemical staining with antibodies directed against TRAG-3 was statistically highly significant, predictive for overall survival time as well as progression-free survival time. There was a clear survival advantage for patients with lower amounts of TRAG-3 protein. At the time point of secondary cytoreduction, the same tendency of weak TRAG-3 expression and its association with favorable clinical outcome could be observed, but this trend was not statistically significant. These observations could be confirmed when the statistical analyses were restricted to patients suffering from serous ovarian carcinoma in stage FIGO III. Hence, TRAG-3 may be useful as predictive marker for clinical outcome of ovarian carcinoma patients.

A major mechanism mediating resistance to paclitaxel is the increased expression of the transmembrane transporter MDR1/P-gp [1]. Thus, in an alternative study the impact of MDR1/P-gp on the clinical response to paclitaxel treatment was analyzed in the same tumor specimens [21]. In contrast to TRAG-3 expression, there was no difference in the average expression levels of MDR1/P-gp before and after chemotherapy using paclitaxel-based schemes. Nevertheless, Kaplan–Meier survival analysis demonstrated a survival advantage for progression-free survival for patients with lower MDR1/P-gp expression in tissues obtained by initial laparotomy (P=0.005). However, there was no significant coincidence of higher or lower expression of TRAG-3 and MDR1/P-gp (primary surgery with P=0.618 and secondary with P=0.513). These data are in accordance with a previous study that analyzed the MDR1/P-gp mRNA expression levels in an alternative collection of specimens obtained from ovarian carcinoma patients [10].

In summary, we demonstrated TRAG-3 to be an important factor for the prognosis in ovarian carcinoma patients that may be involved in paclitaxel resistance and should be, therefore, further investigated to clarify the underlying biological function, mode of action, and clinical importance in general.

Acknowledgements This study was supported in part by the "Berliner Krebsgesellschaft e.V." and by grant LA 1039/2-3 of the "Deutsche Forschungsgemeinschaft".

References

1. Ambudkar SV, Kimchi-Sarfaty C, Sauna ZE, Gottesman MM (2003) P-glycoprotein: from genomics to mechanism. Oncogene 22:7468–7485
2. Chen Z, Zhu B, Wu Y (2002) Expression of TRAG-3 antigen in non-small-cell lung carcinomas. Lung Cancer 38:101–102
3. Duan Z, Duan Y, Lamendola DE, Yusuf RZ, Naeem R, Penson RT, Seiden MV (2003) Overexpression of MAGE/GAGE genes in paclitaxel/doxorubicin-resistant human cancer cell lines. Clin Cancer Res 9:2778–2785
4. Duan Z, Feller AJ, Toh HC, Makastorsis T, Seiden MV (1999) TRAG-3, a novel gene, isolated from taxol-resistant ovarian carcinoma cell line. Gene 229:75–81
5. Feller AJ, Duan Z, Penson R, Toh HC, Seiden MV (2000) TRAG-3, a novel cancer/testis antigen, is overexpressed in the majority of melanoma cell lines and malignant melanoma. Anticancer Res 20:4147–4151
6. Giannakakou O, Sackett DL, Kang YK, Zhan Z, Buters JT, Fojo T, Poruchynsky MS (1997) Paclitaxel-resistant human ovarian cancer cells have mutant beta-tubulins that exhibit impaired paclitaxel-driven polymerization. J Biol Chem 272:17118–17125
7. Haber M, Burkhart CA, Regl DL, Madafiglio J, Norris MD, Horwitz SB (1995) Altered expression of Mbeta2, the class II beta-tubulin isotype, in a murine J774.2 cell line with a high level of taxol resistance. J Biol Chem 270:31269–31275
8. Lage H, Dietel M (1997) Cloning and characterization of human cDNAs encoding a protein with high homology to rat intestinal development protein OCI-5. Gene 188:151–156
9. Lin C, Mak S, Meitner PA, Wolf JM, Bluman EM, Block JA, Terek RM (2002) Cancer/testis antigen CSAGE is concurrently expressed with MAGE in chondrosarcoma. Gene 285:269–278
10. Materna V, Pleger J, Hoffmann U, Lage H (2004) RNA expression of MDR1/P-glycoprotein, DNA-topoisomerase I, and MRP2 in ovarian carcinoma patients: correlation with chemotherapeutic response. Gynecol Oncol 94:152–160
11. McGuire WP 3rd, Markman M (2003) Primary ovarian cancer chemotherapy: current standards of care. Br J Cancer 89:53–58
12. Nimmrich I, Erdmann S, Melchers U, Finke U, Hentsch S, Moyer MP, Hoffmann I, Muller O (2000) Seven genes that are differentially transcribed in colorectal tumor cell lines. Cancer Lett 160:37–43
13. Ohta M, Tanaka F, Sadanaga N, Yamaguchi H, Inoue H, Mori M (2006) Expression of the TRAG-3 gene in human esophageal cancer: The frequent synchronous expression of MAGE-3 gene. Oncol Rep 15:1529–1532
14. Ozols RF, Schwartz PE, Eifel PJ (2001) Ovarian cancer, fallopian tube carcinoma and peritoneal carcinoma. In: De Vita Jr. VT, Hellman S, Rosenberg SA (eds) Cancer: principles & practice of oncology, 6th edn. Lippincott-Raven, Philadelphia, pp 1597–1632
15. Remmele W, Stegner HE (1987) Recommendation for uniform definition of an immunoreactive score (IRS) for immunohistochemical estrogen receptor detection (ER-ICA) in breast cancer tissue [Article in German]. Pathologe 8:138–140
16. Rowinsky EK, Donehower RC (1995) Paclitaxel (taxol). N Engl J Med 332:1004–1014
17. Scheffer GL, Wijngaard PL, Flens MJ, Izquierdo MA, Slovak ML, Pinedo HM, Meijer CJ, Clevers HC, Scheper RJ (1995) The drug resistance-related protein LRP is the human major vault protein. Nat Med 1:578–582
18. Shimizu Y, Kamoi S, Amada S, Akiyama F, Silverberg SG (1998) Toward the development of a universal grading system for ovarian epithelial carcinoma. Cancer 82:893–901
19. Sobin LH, Wittekind C (eds) (2002) TNM classification of malignant tumors (UICC). Wiley-Liss, New York
20. Stewart BW, Kleihues P (eds) (2003) World cancer report. IARC, Lyon, pp 220–222
21. Surowiak P, Materna M, Denkert C, Kaplenko I, Spaczynski M, Dietel M, Zabel M, Lage H (2006) Significance of cyclooxygenase 2 and MDR1/P-glycoprotein coexpression in ovarian cancers. Cancer Lett 235:272–280
22. Therasse P, Arbuck SG, Eisenhauer EA, Wanders J, Kaplan RS, Rubinstein L, Verweij J, Van Glabbeke M, van Oosterom AT, Christian MC, Gwyther SG (2000) New guidelines to evaluate the response to treatment in solid tumors. J Natl Cancer Inst 92: 205–216
23. Wichert A, Stege A, Midorikawa Y, Holm PS, Lage H (2004) Glypican-3 is involved in cellular protection against mitoxantrone in gastric carcinoma cells. Oncogene 23:945–955
24. Wu Y, Zhao T, Ni B, Zou L, Liu H, Zhu B (2003) Expression of TRAG-3 in breast cancer. Int J Cancer 107:167–168
25. Yao X, Hu J, Li T, Yang Y, Sun Z, Ulaner GA, Vu TH, Hoffman AR (2004) Epigenetic regulation of the taxol resistance-associated gene TRAG-3 in human tumors. Cancer Genet Cytogenet 151:1–13
26. Zhu B, Chen Z, Cheng X, Wu Y (2002) Induction of TRAG-3 expression in A549 lung adenocarcinoma cell line by 5-aza-2′ deoxyazacytidine. Lung Cancer 38:321–322

Virchows Arch (2007) 450:195–202
DOI 10.1007/s00428-006-0343-x

ORIGINAL ARTICLE

Expression of E-cadherin and its repressor Snail in placental tissue of normal, preeclamptic and HELLP pregnancies

Kareen Blechschmidt · Ioannis Mylonas · Doris Mayr · Barbara Schiessl · Sandra Schulze · Karl-Friedrich Becker · Udo Jeschke

Received: 9 March 2006 / Accepted: 27 October 2006 / Published online: 6 December 2006
© Springer-Verlag 2006

Abstract Incomplete invasion of extravillous trophoblasts (EVT) is thought to be associated with complications of pregnancy. Snail, a zinc-finger transcription factor represses the transcription of the cell adhesion molecule E-cadherin. The aim of this study was to investigate the expression of E-cadherin and Snail in placental tissue with preeclampsia or HELLP. Placental tissues were obtained from five patients with HELLP syndrome, seven patients with preeclampsia and seven patients after a normal term birth and analysed for Snail and E-cadherin immunoreactivity with specific monoclonal antibodies. Immunohistochemical staining of the placental tissue was analysed using an immunoreactivity score for the evaluation of staining intensity. In preeclamptic EVT, Snail immunoreactivity showed a significant 1.7-fold increase, accompanied by a significant 1.9-fold reduction of E-cadherin immunoreactivity. A 1.7-fold increase of Snail and in parallel a 1.3-fold reduction of E-cadherin was observed in EVT of HELLP placentas although without statistical significance. Loss of E-cadherin can be observed during epithelial–mesenchymal transition (EMT), a key process in normal development and trophoblast differentiation. Snail represses the transcription of E-cadherin triggering a complete EMT. Results obtained in this study showed changes of Snail and E-cadherin immunoreactivity in preeclamptic placentas that could be accompanied with an altered EMT in trophoblasts.

Keywords E-cadherin · Snail · HELLP · Preeclampsia · Extravillous trophoblast

K.-F. Becker and U. Jeschke contributed equally to this work.

K. Blechschmidt · K.-F. Becker (✉)
Institute of Pathology, Technical University of Munich,
Trogerstrasse 18,
81675 Munich, Germany
e-mail: kf.becker@lrz.tum.de

I. Mylonas · B. Schiessl · S. Schulze · U. Jeschke
1st Department of Obstetrics and Gynaecology,
Ludwig–Maximilians-University of Munich,
Maistrasse 11,
80337 Munich, Germany

D. Mayr
Institute of Pathology,
Ludwig-Maximilians-University of Munich,
Thalkirchner Street 36,
80337 Munich, Germany

Introduction

A natural model for migration and invasion that shows many similarities to the growth of cancer cells is placental development during embryo implantation. This highly complex but coordinated process relies fundamentally upon the differentiation and organisation of different trophoblastic cell populations with specific functions [7, 18]. Whereas villous trophoblast cells remain in the fetal compartment and undergo terminal differentiation and fusion to form the multinucleate syncytiotrophoblast, extravillous trophoblast cells extensively infiltrate the endomyometrium, anchoring the placenta and modifying maternal spiral arteries [17, 27]. Aberrant differentiation and resulting shallow interstitial and vascular invasion of extravillous cytotrophoblast cells are thought to be associated with complications of pregnancy such as preeclampsia, intrauterine growth restriction and, in severe cases, second trimester miscarriage [28].

Preeclampsia, i.e. hypertension and proteinuria in pregnancy and a variant of severe preeclampsia, the hemolysis, elevated liver enzymes, low platelets (HELLP) syndrome, are amongst the leading causes for maternal and perinatal morbidity and mortality [21, 31, 36, 37, 42]. The etiologic

factors causing these diseases are still not clear, although different risk factors for preeclampsia are known including primiparity, obesity, (family) history of preeclampsia, multiple pregnancies and chronic medical conditions such as long-term hypertension or diabetes [10]. About 6 to 8% of pregnancies are complicated by preeclampsia, and women with early onset of the disease show a severer form of preeclampsia than women with later onset of the disease [21, 36]. The incidence of HELLP syndrome is reported as being 0.17 to 0.85% of all live births with a reported perinatal death rate ranging from 7.4 to 20% [30, 37]. Neither preeclampsia nor HELLP syndrome can be prevented, and treatment of preeclampsia or HELLP syndrome patients often requires immediate delivery, with consequent iatrogenic fetal prematurity [31].

Expression of the homophilic Ca^{2+}-dependent cell adhesion molecule E-cadherin in normal placentas was shown to be high in cytotrophoblast stem cells of anchoring villi and is considered to be down-regulated or absent in the invading extravillous trophoblast (EVT) cells in normal pregnancies [1, 44]. Floridon et al. [11] described a temporary down-regulation of E-cadherin expression in EVT cells during interstitial and endovascular invasion with the potential to restore E-cadherin expression after completion of migration. It was further shown that E-cadherin expression was up-regulated in interstitial and vascular EVTs in placental bed biopsies from patients with preeclampsia [43].

E-Cadherin plays a critical role in the suppression of tumour invasion. E-Cadherin is a caretaker of the epithelial phenotype, and its function is required for the maintenance of stable adherens junctions [26]. Loss of E-cadherin can be observed during epithelial–mesenchymal transition (EMT), a key process in normal development by which epithelial cells acquire a fibroblastoid morphology, accompanied by the loss of epithelial and gain of mesenchymal markers [14, 40]. A key process during embryonic development, which becomes increasingly regarded as a process resembling EMT, is the differentiation of human EVT cells from the adherent to invasive phenotype [41]. Besides its fundamental role during embryonic development, EMT is also an important mechanism during early steps of invasion and metastasis in cancer [12, 38, 39].

The transcription factor, Snail, is thought to act as a key regulator of EMT [2, 5, 6]. Snail belongs to the Snail family of zinc-finger transcription factors and was first described in *Drosophila melanogaster* as a regulator of mesoderm formation [13, 22]. Snail homologues were subsequently found in other species as well, including mouse and human. More recently, Snail has been implicated in the progression of human tumours via its regulatory action on E-cadherin. Snail represses the transcription of E-cadherin by binding to E-box elements found in the E-cadherin promoter, thereby triggering a complete EMT with the acquisition of invasive and tumorigenic properties [2, 5, 9, 24]. Nothing is known so far about the expression pattern of Snail or its role in regulating E-cadherin expression in invading EVT cells.

Recently, we established the first Snail-specific antibody, which now enables immunohistochemical analysis of the active, i.e. nuclear localized, molecule in human tissue samples.

The aim of this study was to investigate the expression pattern of E-cadherin and the transcription factor Snail in placental tissue derived from pregnancies complicated by preeclampsia or HELLP syndrome compared to placentas from normal pregnancy courses.

Materials and methods

Tissue samples

Placental tissues were obtained from 19 women who underwent delivery at the 1st Department of Obstetrics and Gynaecology of the LMU, Munich. Specimens were collected immediately after delivery from five patients with HELLP syndrome (mean date of delivery, 33.8±2.9 weeks of gestation), seven patients with preeclampsia (mean date of delivery, 33±3.2 weeks of gestation) and seven patients after a normal course of pregnancy (mean date of delivery, 38.2±3 weeks of gestation). The study had the approval of the local ethical committee of the LMU, Munich, Germany (No. 158/00), and informed consents from the patients were obtained. The clinical details of the cases enrolled in the study are shown in Table 1.

Table 1 Clinical details on the patients and newborns in the HELLP, preeclamptic and normal control group

	HELLP	Preeclampsia	Normal control
Week of gestation at delivery	33.8 (SD=2.8)	33.18 (SD=0.83)	38.2 (SD=3.9)
Neonatal birthweight (g)	1,796.2 (SD=689.1)	1,409 (SD=547)	3,435 (SD=412.2)
pH umbilical artery	7.332 (SD=0.09)	7.29 (SD=0.06)	7.27 (SD=0.09)
Apgar score at 5 min	9.2 (SD=0.84)	9.36 (SD=0.67)	9.4 (SD=0.9)
Apgar score at 10 min	9.8 (SD=0.5)	9.73 (SD=0.47)	10 (SD=0)

SD standard deviation

Immunohistochemistry

Immunohistochemistry on paraffin sections (7 μm) of the different specimens was done by incubating the slides in methanol/H_2O_2 (30 min) to inhibit endogenous peroxidase activity, followed by washing in phosphate-buffered saline (PBS, pH 7.4, 5 min) and treating with goat serum (20 min, 22°C) to reduce non-specific background staining. Incubation with the primary antibody (Table 2) was done overnight at 4°C. Sections were then thoroughly incubated with the biotinylated secondary anti-mouse or anti-rat antibody (1 hr, 22°C) and avidin-biotinylated peroxidase (45 min, room temperature). Between each step, sections were washed with PBS. Peroxidase-staining reaction was done with diaminobenzidine/H_2O_2 (1 mg/ml; 5 min) and stopped in tap water (10 min). Sections were counterstained in hemalaun (1 min) and then cover-slipped. In controls, the primary antibody was replaced with pre-immune mouse serum with positive and negative controls being included. From each section, five digital images were obtained with a 3CCD colour camera (JVC, Victor Company of Japan, Japan) and a Leitz (Wetzlar, Germany) microscope.

Immunofluorescence double staining

For the identification of E-cadherin and Snail expressing cells, EVT in placental tissue cryosections were examined. All samples were fixed in 5% buffered formalin. Antibodies and antibody dilution used in the experiments are listed in Table 2. Antibodies were diluted with PBS and incubated with the slides overnight at 4°C. After washing, Cy3-labelled goat anti-mouse IgG or Cy2-labelled goat anti-rat IgG (both Dianova), diluted 1:200, served as second antibody. Alternatively, Cy2-labelled goat anti-mouse IgG (Dianova), diluted 1:200, was used as second antibody in some cases. The slides were finally embedded in mounting buffer containing 4′,6-diamino-2-phenylindole, resulting in the staining of the nuclei. Slides were examined with a Zeiss (Jena, Germany) Axiophot photomicroscope. Digital images were obtained with a digital-camera system (Axiocam, Zeiss) and saved on computer.

Table 2 Antibodies used for the study

Antigen	Antibody	Isotype	Dilution	Source
Snail1	Sn9H2	Rat IgG2	1:60	Dr. E. Kremmer GSF—National Research Centre for Environment and Health, Munich
E-Cadherin	HECD-1	Mouse IgG1	1:800	Calbiochem
Cytokeratin 7	OV-TL 12/30	Mouse IgG1	1:30	Novocastra
Cytokeratin-Cy3-labelled	A45-B/B3	Mouse IgG	1:1,000	Micromet

Immunohistochemical evaluation

The intensity and distribution patterns of the staining reaction was evaluated by two blinded, independent observers without knowing the pathological evaluation and diagnosis of each specimen.

Intensity and distribution pattern of the specific immunostaining was evaluated using a semi-quantitative immunoreactivity score (IRS), which was described by Remmele and Stegner [33] in 1987 and was used in previous investigations on estrogen alpha and beta receptor expression in the normal human endometrium. The IRS score was calculated by multiplying staining intensity (SI) and percentage of positivity (PP); in detail, SI is graded as 0=no staining, 1=weak staining, 2=moderate staining and 3=strong staining. Counting approximately 200 cells, the PP is graded as 0=no stained cells, 1=less or equal 10% of cells stained, 2=between 11 and 50% of cells are stained, 3=51–80% of cells are stained and 4=more than 80% of cells are stained.

Statistical analysis

The SPSS/PC software package, version 12.01 (SPSS, Munich, Germany), was used for collection, processing and statistical analysis of all data. Statistical analysis was performed using the Mann–Whitney *U* test for comparison of the means. P values<0.05 were considered statistically significant.

Results

Snail and E-cadherin immunoreactivity in placental tissue

We found a moderate Snail immunoreactivity in EVT cells in the decidua of normal control placentas (Fig. 1a). The immunoreactivity of Snail was significantly increased in EVT of preeclamptic placentas (Figs. 1b and 3a, $p=0.019$). The increase in Snail immunoreactivity was accompanied by a significant reduction of E-cadherin immunoreactivity in preeclamptic EVT compared to normal control placentas (Figs. 2a,b and 3b, $p=0.016$).

An increase of Snail immunoreactivity and, in parallel, a reduction of E-cadherin immunoreactivity were also observed in EVT of HELLP placentas compared to normal control placentas, although there was no statistical significance (Figs. 1c and 2c).

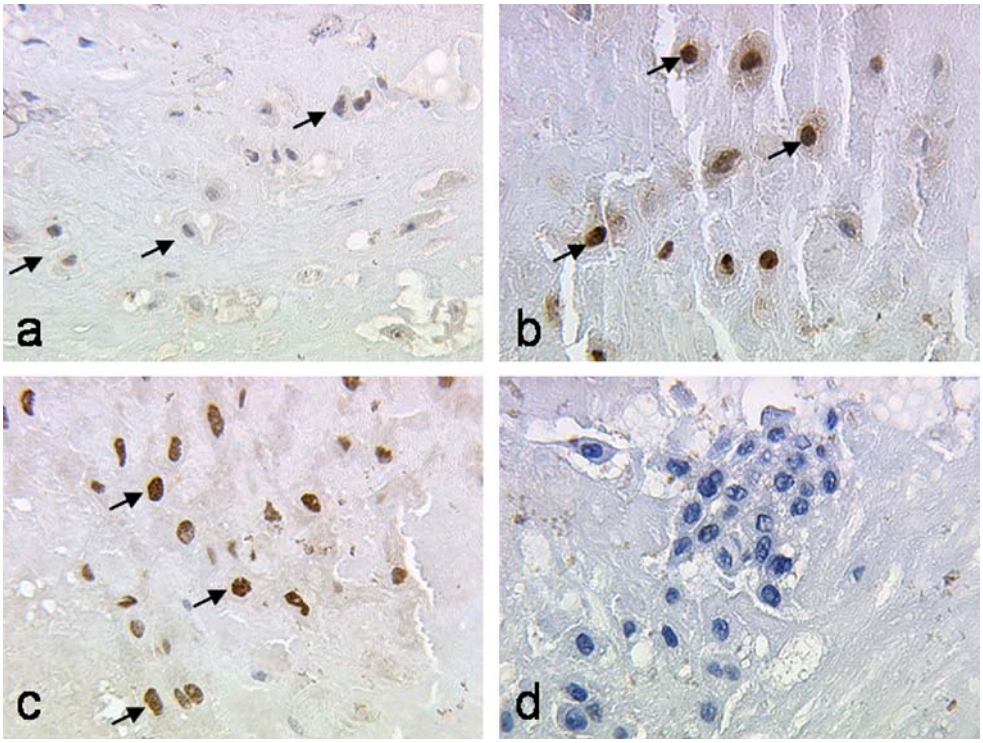

Fig. 1 Snail immunoreactivity in EVT cells (*arrows*): normal placenta (**a**), preeclampsia (**b**) and HELLP (**c**); negative control (the primary antibody was replaced with pre-immune mouse serum; **d**), magnification ×250

For Snail immunoreactivity, the semi-quantitative IRS was 4.07 in normal, 6.71 in preeclamptic and 6.8 in HELLP placentas. This corresponds to an increase of Snail immunoreactivity of approximately 65% in preeclamptic and 67% in HELLP placentas. The IRS score for E-cadherin immunoreactivity was 7.29 in normal, 3.86 in preeclamptic and 5.5 in HELLP placentas. This corresponds to a reduction of E-cadherin immunoreactivity of about 47% in preeclamptic and 25% in HELLP placentas.

We also examined the villous trophoblast for Snail and E-cadherin immunoreactivity. There was a slight increase seen for E-cadherin immunoreactivity in the villous

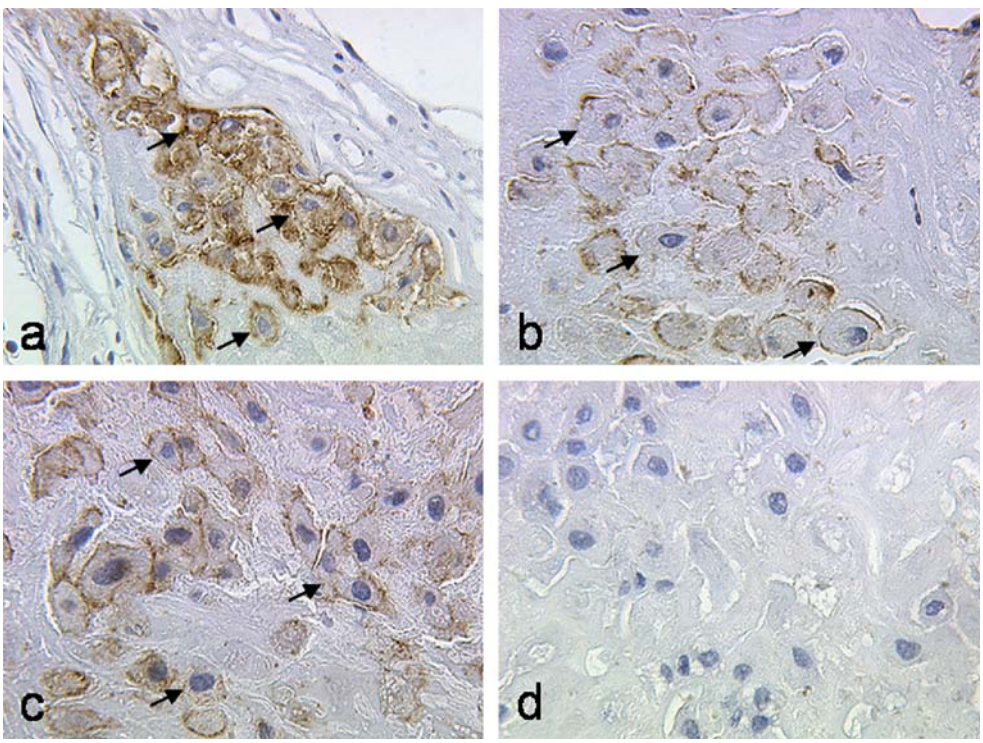

Fig. 2 E-Cadherin immunoreactivity in EVT cells (*arrows*): normal placenta (**a**), preeclampsia (**b**) and HELLP (**c**); negative control (the primary antibody was replaced with pre-immune mouse serum; **d**), magnification ×250

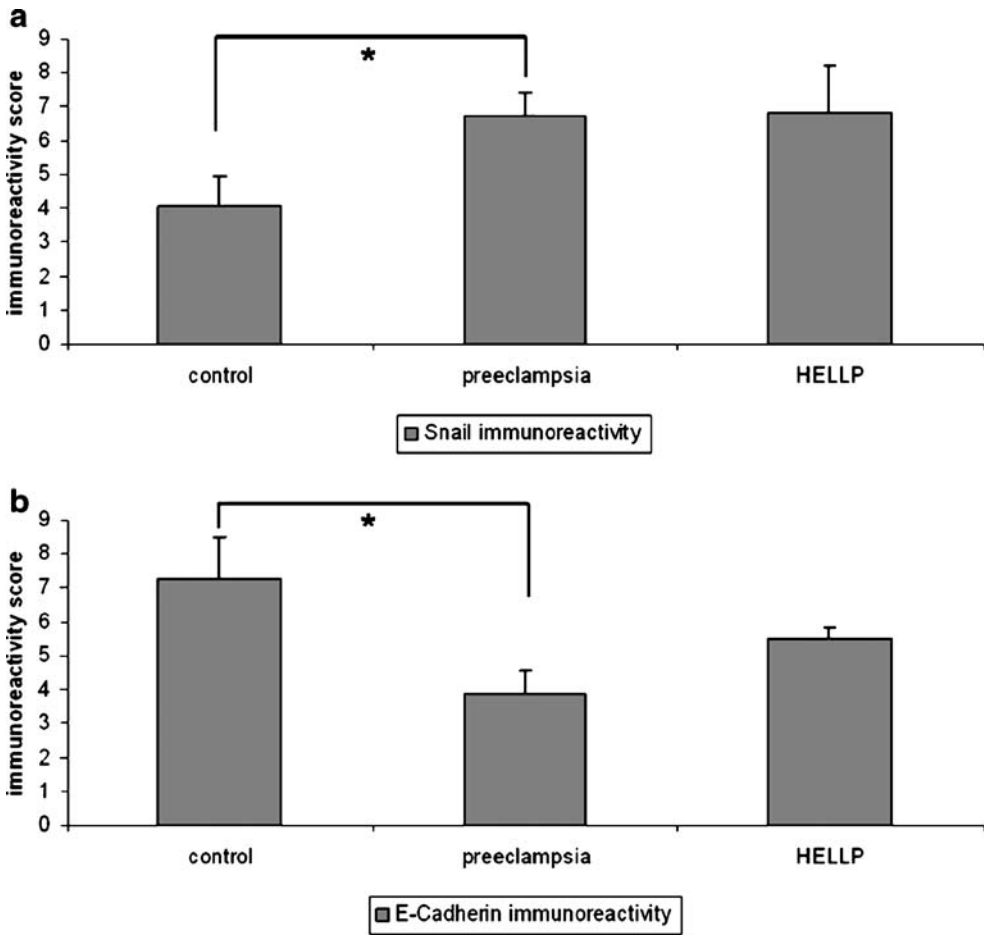

Fig. 3 **a** Staining intensity of Snail in normal term placenta, preeclamptic and HELLP syndrome EVT cells determined by the semi-quantitative immunoreactivity score on the different tissue slides. Data shown represent mean±SEM. Differences in Snail immunoreactivity in normal term placenta and preeclamptic EVT cells (*asterisks*) are statistically significant (p=0.019). **b** Staining intensity of E-cadherin in normal term placenta, preeclamptic and HELLP syndrome EVT cells determined by the semi-quantitative immunoreactivity score on the different tissue slides. Data shown represent mean±SEM. Differences in E-cadherin immunoreactivity in normal term placenta and preeclamptic EVT cells (*asterisks*) are statistically significant (p=0.016)

trophoblast cells of preeclamptic and HELLP placentas compared to the normal control placenta (data not shown). A weak Snail immunoreactivity in villous trophoblast cells was observed in very few cases of normal, preeclamptic and HELLP placentas and showed a slight increase in the pathologic forms of placentas compared to normal control placenta (data not shown). The changes in Snail and E-cadherin immunoreactivity in the villous trophoblast cells of preeclamptic and HELLP placentas compared to normal control placentas showed no statistical significance.

Characterisation of Snail- and E-cadherin-expressing cells in decidual tissue

We wanted to prove that the Snail- and E-cadherin-expressing cells in the decidual tissue of normal, preeclamptic and HELLP placentas are indeed EVT. Therefore, fluorescence double labelling with a cell marker (cytokeratin 7 for trophoblast cells) and with either a Snail- or an E-cadherin-specific antibody was performed. The staining with the monoclonal anti-E-cadherin antibody in combination with the Cy3-labelled anti-cytokeratin 7 antibody showed that the E-cadherin-expressing cells were positive for cytokeratin 7 (Fig. 4a). Cytokeratin 7 positivity was also shown for Snail-expressing cells (Fig. 4b). Thereby, E-cadherin and Snail expressing cells were identified as EVT.

Discussion

Proliferative, non-invasive EVT are found in the proximal and distal parts of the anchoring villi. During EMT, these EVT down-regulate proliferation, become motile and invade the maternal myometrium [8, 34]. This transition in human EVT from the adherent to invasive phenotype correlates with a change of cell-surface-adhesion molecule expression such as E-cadherin [44]. Within this study, we showed that in the decidua of normal control placentas, a strong E-cadherin immunoreactivity and a moderate Snail immunoreactivity was identified in EVT. To prove that Snail- and E-cadherin-expressing cells in the decidual tissue are EVT, fluorescence double labelling with a cell marker (cytokeratin 7 for trophoblast cells; [19, 35]) and with either a Snail- or an E-cadherin-specific antibody was performed. The staining with the monoclonal anti-E-cadherin antibody or the monoclonal anti-Snail antibody in combination with the anti-cytokeratin 7 antibody showed that the E-cadherin/

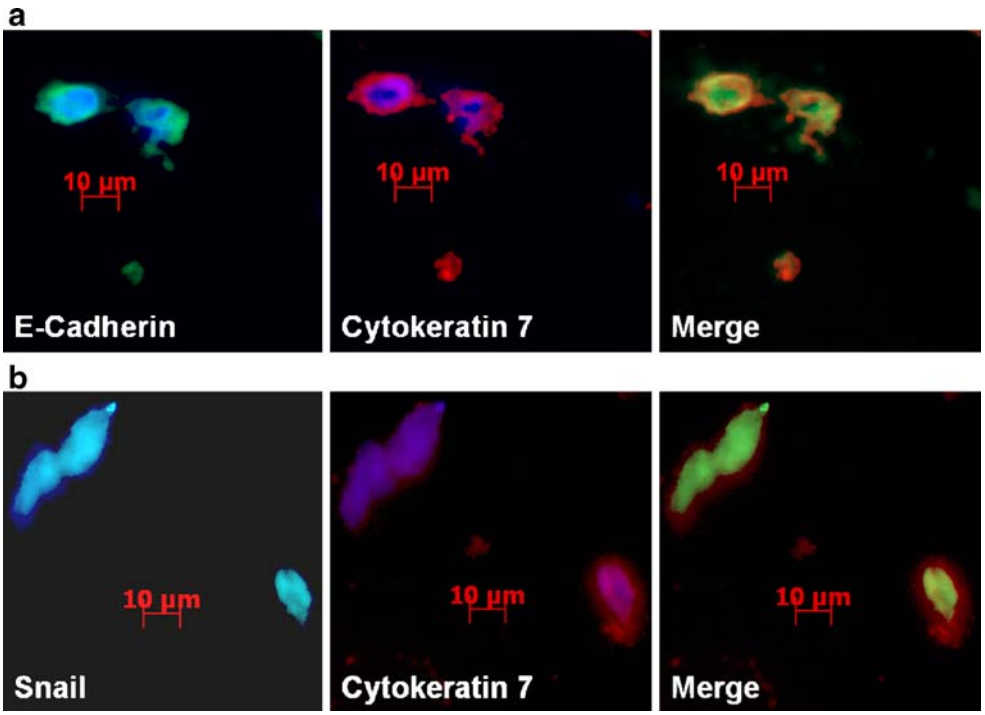

Fig. 4 Immunofluorescence double staining for cytokeratin 7 and E-cadherin (**a**) and for cytokeratin 7 and Snail (**b**), in cryosections of normal control placenta. Cy2 staining is coloured in *green*, whereas Cy3 staining is coloured in *red* (magnification ×400)

Snail expressing cells were also positive for cytokeratin 7 and therefore of trophoblast origin. E-Cadherin in third trimester placental villi anchoring to the superficial basal plate was already described by Floridon et al. [11]. They showed that in the maternal–fetal junction zone, E-cadherin-positive EVTs are found within areas of maternal cells and fibrinoid and were mainly grouped in large aggregates in the third trimester specimens [11]. In the maternal–fetal junction zone, we found a significant reduction of E-cadherin immunoreactivity in preeclamptic EVT compared to normal control placentas. A reduction of E-cadherin immunoreactivity was also observed in EVT of HELLP placentas compared to normal control placentas, although there was no statistical significance. In contrast to our findings, an apparent up-regulation of E-cadherin in EVT in placental bed biopsies from patients with pre-eclampsia has been stated, and a corresponding shallow interstitial and vascular invasion is claimed to be the result in this condition [43]. Shallow invasion in preeclampsia is nonetheless a controversial finding [29]. In addition to the reduced E-cadherin immunoreactivity, we also identified a significant increase in Snail immunoreactivity in pre-eclamptic EVT compared to the normal control. A similar increase in Snail immunoreactivity was seen in HELLP EVT but without statistical significance. Several EMT-inducing developmental regulators repress E-cadherin transcription via interaction with specific E-boxes of the proximal E-cadherin promoter [22, 25]. Most prominent are the Snail-related zinc-finger transcription factors (Snail and Slug) [15, 22]. Snail is considered to be a key regulator of EMT by down-regulating not only E-cadherin expression but also other epithelial marker genes like occludin and claudins [16, 23], which define tight junction components. During EMT, the expression of claudins and occludin is down-regulated likewise E-cadherin. Hereby, the epithelial cells will loose their characteristics, namely, cell polarity and cell adhesion. On the molecular level, down-regulation of the tight junction components is independent of E-cadherin down-regulation; however, one has to speculate that both components will influence each other. Snail also appears to be the major E-cadherin repressor in most studies focusing on tumour progression, but no information on Snail expression in EVT were found in literature so far. This study showed that the immunohistochemical staining patterns of monoclonal antibodies against Snail and E-cadherin, respectively, are inversely correlated and therefore in good agreement with the above-mentioned theory of a repression of E-cadherin by the transcription factor Snail.

Compared to our results, Zhou et al. [43] showed that in preeclamptic placental tissue, cytotrophoblasts in both the villi and decidua showed strong reactivity with anti-E-cadherin, and staining remained strong even on cytotrophoblasts that had penetrated the superficial portions of uterine arterioles. The use of different anti E-cadherin antibodies may at least in part explain the discrepancies in decidual staining. On the other hand, we could also show that E-cadherin expression in the preeclamptic and HELLP villous trophoblast is elevated. For preeclamptic placental tissue, this finding is in agreement with the results of Brown et al. [4] and Benian et al. [3]. These results suggest that

enhanced immunoreactivity of E-cadherin in preeclamptic villous trophoblasts is accompanied with reduced immunoreactivity of this antigen in the EVT. Dysregulation of adhesion molecules that are involved in phenotypic changes associated with epithelial cell transformation are already known from other pathologic forms of pregnancy. Marzioni et al. [20] described down-regulation and/or dysregulation in the expression of ZO-1 and occludin in normal human placenta and in hydatidiform moles. These molecules are also key molecules in cell–cell contacts like E-cadherin. In villous trophoblast cells, a weak Snail immunoreactivity was observed only in one out of seven cases in normal placentas, two out of seven cases in preeclamptic placentas or two out of five cases in HELLP placentas. Therefore, it is difficult to speculate whether Snail is a key molecule for E-cadherin regulation in preeclamptic or HELLP villous trophoblasts.

Impaired invasion of uteroplacental arteries by EVT is a key pathogenic mechanism of preeclampsia. Reister et al. [32] previously demonstrated that reduced trophoblast invasion into uteroplacental spiral arteries was associated with an excess of macrophages in and around these arteries. Macrophages, residing in excess in the placental bed of preeclamptic women, are able to limit EVT invasion of spiral arterial segments through apoptosis mediated by the combination of TNF-alpha secretion and tryptophan depletion. However, the mechanisms by which macrophages are activated and recruited to the placental bed are presently unknown but are likely central to the pathogenesis of preeclampsia.

The data obtained in our study show that in preeclamptic EVT, Snail is up-regulated and E-cadherin is down-regulated. This expression scheme suggests that migration of EVT is not disturbed in preeclampsia, but invasion may be limited by activated macrophages in preeclamptic placentas and induction of apoptosis in EVT. Further investigations on the migration of preeclamptic EVT are necessary to prove these speculations.

In summary, we identified Snail expression in normal and pathologic EVT. Up-regulation of Snail expression in preeclamptic EVT is accompanied with reduced E-cadherin expression in the same cells suggesting a direct regulation of E-cadherin by Snail in EVT. In HELLP EVT, a similar up-regulation of Snail and down-regulation of E-cadherin was observed but without statistical significance.

References

1. Babawale MO, Van Noorden S, Pignatelli M, Stamp GW, Elder MG, Sullivan MH (1996) Morphological interactions of human first trimester placental villi co-cultured with decidual explants. Hum Reprod 11:444–450
2. Batlle E, Sancho E, Franci C, Dominguez D, Monfar M, Baulida J, Garcia De Herreros A (2000) The transcription factor snail is a repressor of E-cadherin gene expression in epithelial tumour cells. Nat Cell Biol 2:84–89
3. Benian A, Madazli R, Aksu F, Uzun H, Aydin S (2002) Plasma and placental levels of interleukin-10, transforming growth factor-beta1, and epithelial-cadherin in preeclampsia. Obstet Gynecol 100:327–331
4. Brown LM, Lacey HA, Baker PN, Crocker IP (2005) E-cadherin in the assessment of aberrant placental cytotrophoblast turnover in pregnancies complicated by pre-eclampsia. Histochem Cell Biol 124:499–506
5. Cano A, Perez-Moreno MA, Rodrigo I, Locascio A, Blanco MJ, del Barrio MG, Portillo F, Nieto MA (2000) The transcription factor snail controls epithelial–mesenchymal transitions by repressing E-cadherin expression. Nat Cell Biol 2:76–83
6. Carver EA, Jiang R, Lan Y, Oram KF, Gridley T (2001) The mouse snail gene encodes a key regulator of the epithelial–mesenchymal transition. Mol Cell Biol 21:8184–8188
7. Cross JC, Werb Z, Fisher SJ (1994) Implantation and the placenta: key pieces of the development puzzle. Science 266:1508–1518
8. Damsky CH, Librach C, Lim KH, Fitzgerald ML, McMaster MT, Janatpour M, Zhou Y, Logan SK, Fisher SJ (1994) Integrin switching regulates normal trophoblast invasion. Development 120:3657–3666
9. De Craene B, Gilbert B, Stove C, Bruyneel E, van Roy F, Berx G (2005) The transcription factor snail induces tumor cell invasion through modulation of the epithelial cell differentiation program. Cancer Res 65:6237–6244
10. Duckitt K, Harrington D (2005) Risk factors for pre-eclampsia at antenatal booking: systematic review of controlled studies. BMJ 330:565
11. Floridon C, Nielsen O, Holund B, Sunde L, Westergaard JG, Thomsen SG, Teisner B (2000) Localization of E-cadherin in villous, extravillous and vascular trophoblasts during intrauterine, ectopic and molar pregnancy. Mol Hum Reprod 6:943–950
12. Gotzmann J, Mikula M, Eger A, Schulte-Hermann R, Foisner R, Beug H, Mikulits W (2004) Molecular aspects of epithelial cell plasticity: implications for local tumor invasion and metastasis. Mutat Res 566:9–20
13. Grau Y, Carteret C, Simpson P (1984) Mutations and chromosomal rearrangements affecting the expression of Snail, a gene involved in embryonic patterning in *Drosophila Melanogaster*. Genetics 108:347–360
14. Hay ED (1995) An overview of epithelio–mesenchymal transformation. Acta Anat 154:8–20
15. Hemavathy K, Ashraf SI, Ip YT (2000) Snail/slug family of repressors: slowly going into the fast lane of development and cancer. Gene 257:1–12
16. Ikenouchi J, Matsuda M, Furuse M, Tsukita S (2003) Regulation of tight junctions during the epithelium–mesenchyme transition: direct repression of the gene expression of claudins/occludin by Snail. J Cell Sci 116:1959–1967
17. Kingdom J, Huppertz B, Seaward G, Kaufmann P (2000) Development of the placental villous tree and its consequences for fetal growth. Eur J Obstet Gynecol Reprod Biol 92:35–43
18. Lala PK, Hamilton GS (1996) Growth factors, proteases and protease inhibitors in the maternal–fetal dialogue. Placenta 17:545–555
19. Manyonda IT, Whitley GS, Cartwright JE (2001) Trophoblast cell lines: a response to the workshop report by King et al. Placenta 22:262–263
20. Marzioni D, Banita M, Felici A, Paradinas FJ, Newlands E, De Nictolis M, Muhlhauser J, Castellucci M (2001) Expression of ZO-1 and occludin in normal human placenta and in hydatidiform moles. Mol Hum Reprod 7:279–285

21. Myatt L, Miodovnik M (1999) Prediction of preeclampsia. Semin Perinatol 23:45–57
22. Nieto MA (2002) The snail superfamily of zinc-finger transcription factors. Nat Rev Mol Cell Biol 3:155–166
23. Ohkubo T, Ozawa M (2004) The transcription factor Snail downregulates the tight junction components independently of E-cadherin downregulation. J Cell Sci 117:1675–1685
24. Peinado H, Ballestar E, Esteller M, Cano A (2004) Snail mediates E-cadherin repression by the recruitment of the Sin3A/histone deacetylase 1 (HDAC1)/HDAC2 complex. Mol Cell Biol 24:306–319
25. Peinado H, Portillo F, Cano A (2004) Transcriptional regulation of cadherins during development and carcinogenesis. Int J Dev Biol 48:365–375
26. Perez-Moreno M, Jamora C, Fuchs E (2003) Sticky business: orchestrating cellular signals at adherens junctions. Cell 112:535–548
27. Pijnenborg R, Dixon G, Robertson WB, Brosens I (1980) Trophoblastic invasion of human decidua from 8 to 18 weeks of pregnancy. Placenta 1:3–19
28. Pijnenborg R, Anthony J, Davey DA, Rees A, Tiltman A, Vercruysse L, van Assche A (1991) Placental bed spiral arteries in the hypertensive disorders of pregnancy. Br J Obstet Gynaecol 98:648–655
29. Pijnenborg R (1998) The origin and future of placental bed research. Eur J Obstet Gynecol Reprod Biol 81:185–190
30. Rath W, Faridi A, Dudenhausen JW (2000) HELLP syndrome. J Perinat Med 28:249–260
31. Rath W, Bartz C (2004) Treatment of severe preeclampsia and HELLP syndrome. Zentralbl Gynakol 126:293–298
32. Reister F, Frank HG, Kingdom JC, Heyl W, Kaufmann P, Rath W, Huppertz B (2001) Macrophage-induced apoptosis limits endovascular trophoblast invasion in the uterine wall of preeclamptic women. Lab Invest 81:1143–1152
33. Remmele W, Stegner HE (1987) Recommendation for uniform definition of an immunoreactive score (IRS) for immunohistochemical estrogen receptor detection (ER-ICA) in breast cancer tissue. Pathologe 8:138–140
34. Shih Ie M, Hsu MY, Oldt RJ 3rd, Herlyn M, Gearhart JD, Kurman RJ (2002) The role of E-cadherin in the motility and invasion of implantation site intermediate trophoblast. Placenta 23:706–715
35. Shiverick KT, King A, Frank H, Whitley GS, Cartwright JE, Schneider H (2001) Cell culture models of human trophoblast II: trophoblast cell lines—a workshop report. Placenta 22(Suppl A): S104–S106
36. Sibai BM, Caritis S, Hauth J (2003) What we have learned about preeclampsia. Semin Perinatol 27:239–246
37. Sibai BM (2004) Diagnosis, controversies, and management of the syndrome of hemolysis, elevated liver enzymes, and low platelet count. Obstet Gynecol 103:981–991
38. Thiery JP, Chopin D (1999) Epithelial cell plasticity in development and tumor progression. Cancer Metastasis Rev 18:31–42
39. Thiery JP (2002) Epithelial–mesenchymal transitions in tumour progression. Nat Rev Cancer 2:442–454
40. Thiery JP (2003) Epithelial–mesenchymal transitions in development and pathologies. Curr Opin Cell Biol 15:740–746
41. Vicovac L, Aplin JD (1996) Epithelial–mesenchymal transition during trophoblast differentiation. Acta Anat 156:202–216
42. Walker JJ (2000) Pre-eclampsia. Lancet 356:1260–1265
43. Zhou Y, Damsky CH, Fisher SJ (1997) Preeclampsia is associated with failure of human cytotrophoblasts to mimic a vascular adhesion phenotype. One cause of defective endovascular invasion in this syndrome? J Clin Invest 99:2152–2164
44. Zhou Y, Fisher SJ, Janatpour M, Genbacev O, Dejana E, Wheelock M, Damsky CH (1997) Human cytotrophoblasts adopt a vascular phenotype as they differentiate. A strategy for successful endovascular invasion? J Clin Invest 99:2139–2151

Virchows Arch (2007) 450:203–210
DOI 10.1007/s00428-006-0356-5

ORIGINAL ARTICLE

Expression of p53/hgf/c-met/STAT3 signal in fetuses with neural tube defects

Maria Trovato · Maria D'Armiento · Luca Lavra · Alessandra Ulivieri · Roberto Dominici · Enrica Vitarelli · Maddalena Grosso · Raffaella Vecchione · Gaetano Barresi · Salvatore Sciacchitano

Received: 19 July 2006 / Revised: 16 November 2006 / Accepted: 25 November 2006 / Published online: 10 January 2007
© Springer-Verlag 2007

Abstract Neural tube defects (NTD) are morphogenetic alterations due to a defective closure of neural tube. Hepatocyte growth factor (HGF)/c-met system plays a role in morphogenesis of nervous system, lung, and kidney. HGF/c-met morphogenetic effects are mediated by signal transducers and activators of transcription (STAT)3 and both HGF and c-met genes are regulated from p53. The aim of our study was to analyze mRNA and protein expressions of p53, HGF, c-met, and STAT3 in fetuses with NTD. By reverse transcriptase-polymerase chain reaction and immunohistochemistry, we analyzed neural tissues from four NTD fetuses and the corresponding non-malformed lungs, kidneys and placentas. We found a reduced mRNA expression of HGF/c-met/STAT3 pathway, in the malformed nervous systems and placentas. The reduced expression of this pathway correlated with the absence of p53 in all these samples. On the contrary, detectable expression levels of p53, HGF, c-met, and STAT3 were observed in non-malformed lungs and kidneys obtained from the same fetuses. Comparable results were obtained by immunohistochemistry, with the exception of p53, which was undetected in all fetal tissues. In conclusion, in NTD fetuses, both the defective neural tube tissue and the placenta have a reduction in all components of the p53/HGF/c-met/STAT3 cascade. This raises the possibility of using the suppression of these genes for early diagnosis of NTD especially on chorionic villus sampling.

Keywords HGF · c-met · STAT3 · NTD · Fetus

Our experiments comply with the current laws of the country in which they were performed.

M. Trovato (✉) · E. Vitarelli · M. Grosso · G. Barresi
Dipartimento di Patologia Umana, Policlinico Universitario,
via Consolare Valeria, 1,
98125 Messina, Italy
e-mail: mariatrovato@tin.it

M. D'Armiento · R. Vecchione
Dipartimento di Scienze Biomorforlogica e Funzionale,
Sezione di Anatomia Patologica, Università Federico II di Napoli,
via Pansini Sergio, 5,
80131 Napoli, Italy

L. Lavra · A. Ulivieri · S. Sciacchitano
Centro di Ricerca Ospedale S.Pietro Fatebenefratelli, AFAR,
via Cassia, 450,
00189 Roma, Italy

R. Dominici · S. Sciacchitano
Istituto di Neurobiologia e Medicina Molecolare, CNR,
Viale Dell' Universita', 11,
00185 Roma, Italy

S. Sciacchitano (✉)
Ospedale Sant'Andrea, II Facoltà di Medicina e Chirurgia,
Università La Sapienza,
Via di Grottarossa, 1035-1039,
00189 Roma, Italy
e-mail: salvatore.sciacchitano@uniroma.it

Introduction

Organogenesis of the nervous system (NS) represents an informative model to elucidate the defects in development responsible for fetal malformations [11]. The morphogenesis of the neuronal component of NS (neurulation) progresses through two phases characterized by distinct events [22]. The first step, named primary neurulation, takes place between the first and fifth week of gestation. This step is concerned with variations of neuronal shape, migration, and the growth of nerve cells. With secondary neurulation, starting at the sixth week of gestation, the

neurons are unable to replicate and may only change in shape or position [7, 22]. The interruption of primary neurulation leads to several types of neural tube defects (NTD) [6, 10, 21]. Genes and cytokines regulating this stage of human neurulation remain largely unknown for the mechanisms leading to defective closure of neural tube [11]. Hepatocyte growth factor/scatter factor (HGF/SF or HGF) and its cognate receptor c-met are two genes necessary for mouse embryonic development [3, 31]. The expression of both HGF and c-met in human normal fetal organs and the low expression of both HGF and c-met in placental tissue of malformed fetuses suggest their role in the normal fetal development and participation in the genesis of organ malformations [16, 30, 32]. Thus, HGF and c-met may be possible candidate primary neurulation genes, and alterations of pathway leading to their inactivation could cause NTD. Organogenesis is driven by the branching morphogenesis, a complex phenomena of cell–cell contacts and cell–extracellular matrix communications [25]. Branching morphogenesis involves cellular changes in cell shape and cell polarization inducing the branching direction. In addition, changes in cell motility, ensure the branching elongation, whereas modifications in cell proliferation stimulate the three-dimensional branching extension [35]. Alterations in the various steps of branching morphogenesis are responsible for the occurrence of defects in organ development [25]. In effect, HGF is one a few cytokines that is able to induce, in c-met expressing cells, branching formation and cellular migration and cellular proliferation [14, 20, 34]. The pathway leading to these effects is partially elucidated: both murine HGF and c-met gene promoters can be activated by wild-type (wt) p53. The HGF/c-met response is mediated through the activation of different specific intracellular transducing effectors [2, 18, 23, 27, 28,], such as a member of the signal transducers and activators of transcription (STAT), namely, STAT3 [4]. The role of HGF and c-met in the development of NS has been investigated exclusively in animal model, whereas only two studies have evaluated the expression of both HGF and c-met in human embryonal NS without any specified malformation [16, 32]. In animal models, it has been suggested that a role of HGF/c-met signaling system in early neural tube development carries out a neurotrophic growth [1, 9, 13, 15, 33]. However, in animal models, the role of HGF/c-met signal has never been correlated with p53 and/or with STAT3. This is the first report studying the complete p53/HGF/c-met/STAT3 pathway in NTD. To clarify the potential role of p53/HGF/c-met/STAT3 pathway in NTD, we examined fetuses showing malformed NS but non-malformed lung, kidney, and placenta; investigating, by reverse transcriptase (RT)-polymerase chain reactors (PCR) and immunohistochemistry, expressions of p53, HGF, c-met, and STAT3, in malformed and non-malformed organs.

Materials and methods

Tissues collection

The protocol we followed to obtain human fetal tissues for this study conformed to Helsinki Declaration (1983). After therapeutic termination of pregnancy, between 16th and 28th week gestational age, four malformed fetuses plus one non-malformed fetus were collected at the Department of Biomorphologic and Functional Science, Human Pathology section, Federico II University of Naples and the Department of Human Pathology of University of Messina. Gestation age, sex, and NTD type of each fetus are indicate in Table 1. All malformed fetuses showed an open lesion containing meninges and dysplastic neuronal cells corresponding to myelomeningocele. This type of NTD was localized in occipital site in three fetuses and thoracic in one. Myelomeningocele was the unique lesion observed in two malformed fetuses whereas in the remaining two it was associated with syndromes such as Arnold Chiari type II or Dandy–Walker. All NTD fetuses had non-malformed lung, kidney, and placenta and a chromosomal map without alterations. Sample tissues of malformed NS and non-malformed NS lung, kidney, and placenta harvested during fetal autopsy were either snap-frozen until RNA extraction, or fixed in 4% formalin and embedded in paraffin.

Total RNA extraction and semiquantitative RT-PCR

Total RNA was isolated from fetal tissue (approximately 30 mg) obtained from malformed NS and non-malformed placenta, lungs, and kidneys using the SV total RNA isolation system (Promega, Madison, WI, USA), according to the manufacturer's recommendations. The extraction yields were quantified using a BioPhotometer (Eppendorf), and nucleic acid quality was assessed by determining the absorbance ratio at 260 and 280 nm. cDNA was synthesized in a total volume of 20 μl of reaction mixture, containing

Table 1 Clinical details of the fetuses

Fetus	Gestational age (week)	Sex	NTD type
1	16th	Male	Occipital myelomeningocele
2	19th	Male	Occipital myelomeningocele associated with Arnold Chiari II malformation
3	24th	Male	Occipital myelomeningocele associated with Dandy–Walker malformation
4	28th	Female	Thoracic myelomeningocele
Control	22th	Female	None

1 μg of total RNA, 0.5 μM each of random hexamers and oligo dT, 1×RT reaction buffer (Qiagen, Milan, Italy), 0.5 mM of each deoxyribonucleotide triphosphate (dNTP), 10 units of ribonuclease inhibitor (Perkin-Elmer, Boston, MA), and 4 units (1 μl) of omniscript RT enzyme (Qiagen). Samples were incubated at 37°C for 2 h, and the reaction was terminated by heating at 93°C for 5 min, followed by rapid chilling on ice.

PCR reaction mixture contained 0.2 μM of each primer set, 0.2 mM of each dNTPs and 1.25 units of Ampli Taq (Perkin-Elmer) and cDNA equivalent of 100 ng of total RNA (2 μl of cDNA) in a total volume of 50 μl.

To amplify p53, HGF, MET, and STAT3 cDNA specific primers were designed using the Primer3 software. Sequences are shown below and their specificity was confirmed by basic local alignment search tool (BLAST) search. p53: 5′-CTGC TCAGATAGCGATGGTCTG-3′ (forward), 5′-TTGTAGTG GATGGTGGTACAGTCA-3′ (reverse; fragment size 162 base pairs [bp]); HGF: 5′-GCACTGAAGATAAAAACC AA-3′ (forward), 5′-GTTTTCTTGCTTTATCAAAA-3′ (reverse; fragment size 118 bp); c-met: 5′-GAGCCAAAGT CCTTTCAT-3′ (forward), 5′-ATCGAATGCAATGGAT GAT-3′ (reverse; fragment size 100 bp); STAT3 5′-GCCAG AGAGCCAGGAGCA-3′ (forward), 5′-ACACAGAT AAACTTGGTCTTCAGGTATG-3′ (reverse; fragment size 100 bp). The cDNAs were amplified using the following cycling conditions: 1 min at 95°C, 1 min at 50–55°C, and 1 min at 72°C. Transcription of the housekeeping 18S gene was carried out using the following primers: 5′-GGAGAGG GAGCCTGAGAAA-3′ (forward) and 5′-CGAAA GAGTCCTGTATTGTTATTTT-3′ (reverse; fragment size 113 bp). p53, HGF, c-met, STAT3, and 18S were amplified from all samples in three separate reactions. Negative controls are included for the entire RT-PCR and for the PCR alone in each reaction.

PCR products were detected by polyacrylamide gel electrophoresis (PAGE) analysis. Amplified DNA was mixed with an equal volume of formamide loading dye (95% formamide, 20 mM ethylenediaminetetraacetic acid [EDTA], 0.05% bromophenol blue and 0.05% xylen cyanol) and loaded onto a gel consisting of 12% acrylamide (19:1 acrylamide:bisacrylamide), 0.089 M Tris (pH 8.3), 0.089 M borate, and 0.002 M EDTA. Samples were electrophoresed at 150 V for 2–4 h and analyzed by silver staining using the silver stain kit (Bio-Rad Lab, Hercules, CA, USA).

Immunohistochemistry

Serial 5-μm sections were cut from selected paraffin-embedded blocks including malformed NS and non-malformed NS, placenta, lungs, and kidneys. One section was stained with hematoxylin–eosin, and four were employed for immunohistochemical methodic using a monoclonal mouse antibody against anti-human p53 protein (DO-7, 1:100; DakoCytomation, Glostrup, Denmark) and polyclonal rabbit antibodies against HGF-α (H-145, 1:100; Santa Cruz Biotechnology, Santa Cruz, CA), c-met (p140 anti h-met, 1:100; Santa Cruz Biotechnology) and STAT3 (h-190, 1:100; Santa Cruz Biotechnology). Briefly, sections were deparaffinized with xylene, rehydrated through a graded series of ethanol solutions to distilled water, and treated with 0.3% (v/v) H_2O_2 in absolute methanol for 30 min to quench the endogenous peroxidase activity. For p53, the antigen retrieval technique as described by Gown et al. [12] was utilized. In particular, a slide was placed in 10 mM citrate buffer (pH 6.0) and heated for 15 min in a microwave oven (Whirlpool AVM 300, power set at 500 W). Microwave exposure was divided into three equal time periods, and at the end of the first cycle, a 50 ml of distilled water was added to the slide holder to prevent loss of fluid from boiling. All four slides were incubated overnight at 4°C with either p53, HGF, c-met, or STAT3 antibody. After overnight incubation, the staining was visualized using the LSAB system (LSAB kit from Dako, Carpinteria, CA). 3,3′-diaminobenzidine (Sigma) activated with 0.05% hydrogen peroxide was used to develop the end products. Sections were counterstained with Mayer's hematoxylin, dehydrated, and mounted. Specificity of the binding was assessed by three kinds of controls: (1) omitting the primary antiserum, (2) replacing it with normal mouse or rabbit serum, or (3) previously absorbing it with its homologous antigen. For each protein, we evaluated the localization of reactivity in each organ, the number of reactive cells per organ, the reactive cell type (epithelial and/or mesenchymal), and the sub-cellular location (membrane and/or cytoplasm and/or nucleus). The number of reactive cells was determined from a population of 1,000 cells/case, using ×50 magnification. Based on the proportion of stained cells, the immunostaining was scored as low (6–20% positive cells), moderate (21–40%) and high (>40%). Immunostaining detected in a cellular percentage under 6% was considered background and scored as absent.

Histological and immunocytochemical evaluations were performed blindly twice by five different pathologists (MD, RV, MT, MG, and GB), with an inter-observer agreement near 100%. The mean value was used as the results to overcome minimal inter-observer discrepancies.

Results

Pathological evaluation of malformed fetuses

Fetus no. 1 showed encephalo-myelomeningocele characterized by a herniation through the occipital/posterior bone

of the cranium that contained degenerative cerebral cortex, covered by meninges.

Fetus no. 2 was affected by Arnold Chiari malformation type II and showed a unique hindbrain herniation with occipital myelomeningocele.

Fetus no. 3 was affected by Dandy–Walker malformation. He showed hydrocephalus, incomplete cerebellar vermis, agenesis of the corpus callosum, a posterior fossa cyst and occipital myelomeningocele.

Fetus no. 4 showed thoracic myelomeningocele with twisted foot.

RT-PCR

Malformed NS was characterized by almost undetectable level of expression of all genes examined. In fact, with the exception of one fetus (Fig. 1, fetus no. 2) that showed detectable level of STAT3 gene expression, no expression was seen in the remaining cases for HGF, c-met, STAT3, and p53.

Reduced expression levels of c-met and STAT3 corresponded to reduced expression levels of p53 in both malformed neural tissue and in placenta. No correlation was seen in the case of HGF that was high in three out of four placental tissues examined.

Non-malformed fetal tissues showed higher expression levels of p53 in three fetuses (Fig. 1, fetus nos. 2, 3, and 4). In these three fetuses the highest expression levels of p53 were always associated with the highest expression levels of STAT3 in both lung and kidney (fetus nos. 2, 3, and 4 of Fig. 1). Further, a quite similar association was observed in the same fetal tissues but involving p53 and c-met expression levels (fetus nos. 2, 3, and 4 of Fig. 1). The remaining fetus (fetus no. 1 of Fig. 1) in which p53 levels were very low in the two non-malformed tissues examined, the expression level of STAT3 and HGF was low too, but c-met was detectable. These data indicate that HGF, c-met and STAT3 may be down-regulated in most of cases of malformed neural tissue.

Immunohistochemistry

Immunohistochemical results are summarized in Table 2 and, representatively, in Fig. 2.

All fetal tissues did not show detectable expression of p53.

I

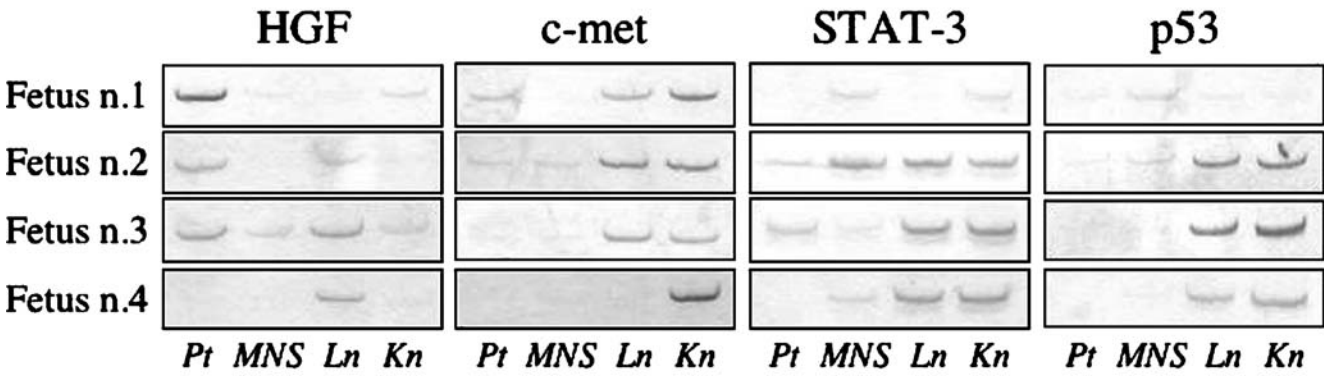

II

	HGF				c-met				STAT3				p53			
	n.1	n.2	n.3	n.4	n.1	n.2	n.3	n.4	n.1	n.2	n.3	n.4	n.1	n.2	n.3	n.4
Placenta	+	+	+	-	-	-	-	-	-	+	+	-	-	-	-	-
MNS	-	-	+	-	-	-	-	-	-	++	-	+	+	-	-	-
Lung	-	+	+	+	+	++	+	-	-	++	++	+++	-	++	++	+
Kidney	-	-	+	-	++	++	+	+++	-	+	+++	+++	-	++	+++	++

RDU	0	0.1 -0.3	0.4 -0.7	0.8 -1.1
	-	+	++	+++

Fig. 1 HGF, c-met, STAT3, and p53 mRNA expressions in the fetuses with neural tube defects. I. RT-PCR products obtained using primers specific for HGF, c-met, STAT3, and p53 were resolved by PAGE and visualized by silver staining. The 18S gene was amplified as control. II. Densitometric analysis of the bands visualized at the polyacrylamide gel. Results are expressed as relative densitometric units (*RDU*), after normalization with the intensity of the band of 18S for each sample. Intensity grade of staining was scored on a four-point scale from 0 to 3+ (0=0 RDU; 1+=0.1–0.3 RDU; 2+=0.4–0.7 RDU; 3+=0.8–1.1 RDU)

Table 2 Immunoexpression of HGF, c-met and STAT3 in fetuses with neural tube defects and non-malformed control fetus

	HGF					c-met					STAT3				
	no. 1	no. 2	no. 3	no. 4	Control	no. 1	no. 2	no. 3	no. 4	Control	no. 1	no. 2	no. 3	no. 4	Control
Placenta	++	+	++	−	+	−	−	−	−	++	−	−	−	−	+
MNS	−	−	−	−	+	−	−	−	−	++	−	−	−	−	+
Lung	−	++	+	++	++	++	++	+++	−	+++	−	++	++	+++	+++
Kidney	−	−	++	−	+	++	++	++	+++	++	−	++	+++	++	+++

− Percentage of immunostained cells at 0–5% (score system, absent), + percentage of immunostained cells at 6–20% (score system, low), ++ percentage of immunostained cells at 21–40% (score system, moderate), +++ percentage of immunostained cells at >40% (score system, high)

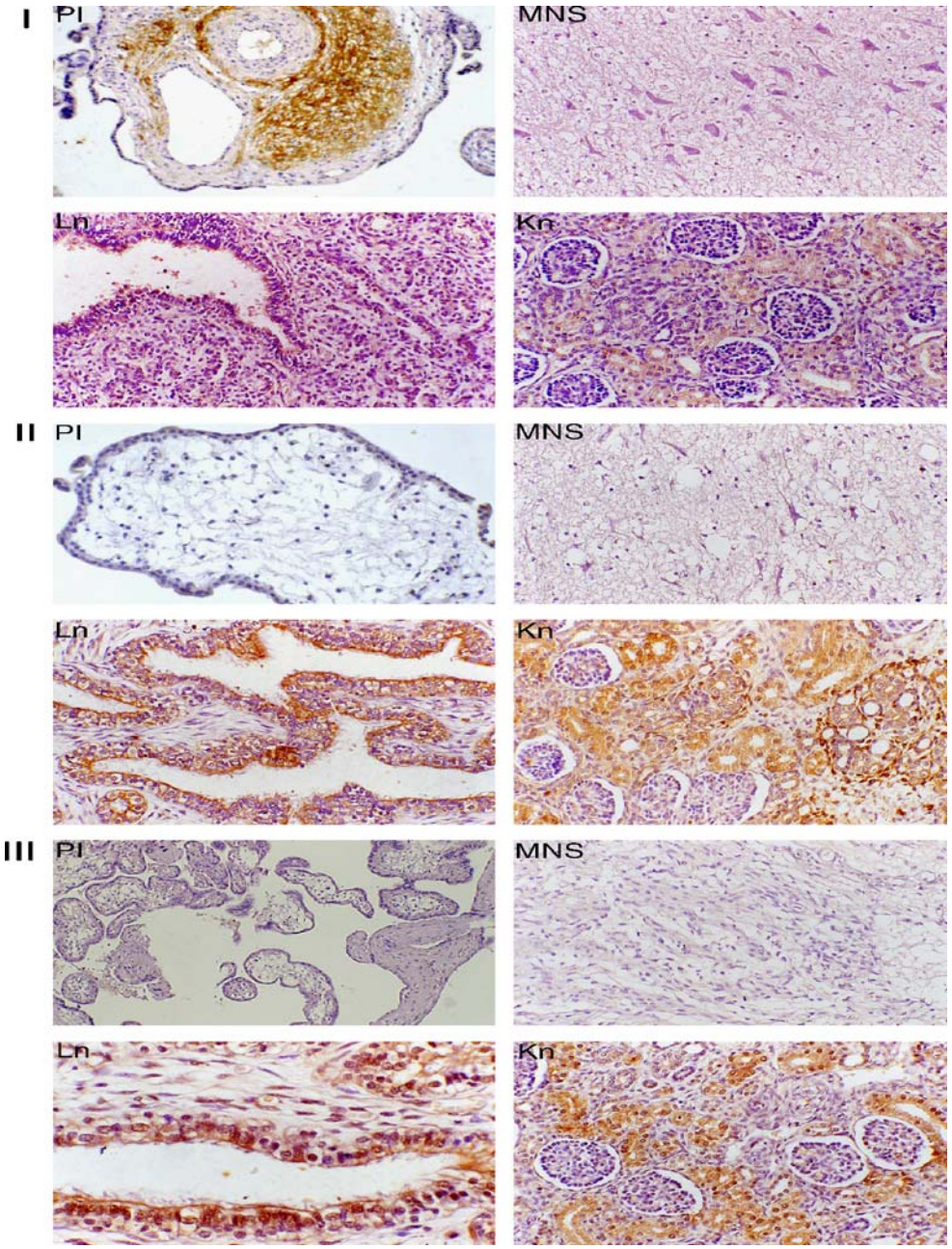

Fig. 2 Immunoexpression of HGF-α, cmet, and STAT3 in malformed and non-malformed tissues of a NTD fetus. **a** Intense HGF-α immunostaining in placenta (*Pl*, magnification ×100), absence of HGF-α immunoreaction in malformed nervous system (*MNS*, magnification ×400), weak HGF-α immunostaining in lung (*Ln*, magnification ×200) and moderate HGF-α immunostaining in kidney (*Kn*, magnification ×200). **b** Absence of c-met immunoreaction in placenta (*Pl*, ×200) and in malformed nervous system (*MNS*, ×200). Very intense c-met immunostaining in lung (*Ln*, ×200) and intense c-met immunoreaction in kidney (*Kn*, ×200). **c** Absence of STAT3 immunostaining in placenta (*Pl*, ×100) and in malformed nervous system (*MNS*, ×200), intense immunostaining in lung (*Ln*, ×400) and very intense immunostaining in kidney (*Kn*, ×200). Intensity grade of staining was scored on a five-point scale from 0 to 4+ (0 = absent; 1 = weak; 2 = moderate; 3 = intense; 4 = very intense)

Non-malformed NS, placenta, lungs, and kidneys of the control fetus were reactive to HGF, c-met and STAT3 (Table 2).

All malformed NS were non-reactive to HGF, c-met, and STAT3 (Table 2) (MNS in Fig. 2a–c). A similar feature was observed in placental tissues of fetuses with NTD, at least for c-met and STAT3 (Table 2) (Pl Fig. 2b and c). However, the placental tissue showed a low or moderate HGF immunoreaction in three cases (Table 2). Similarly to our previous report, HGF immunoreaction was specially localized in cytoplasm of fibroblast and myofibroblast cells (Pl in Fig. 2a) [13].

By contrast with malformed NS and placentas, in the fetuses with NTD the majority of the non-malformed lungs expressed HGF, c-met, and STAT3 (Table 2). The reactivity for HGF, c-met, and STAT3 was predominantly recognized in bronchial columnar epithelial cells (Ln Fig. 2a–c). The immunoreaction for HGF was low or moderate and localized on cytoplasm of epithelial cells (Table 2, Ln in Fig. 2a), whereas the immunostaining for both c-met and STAT3 were moderate or high (Table 2). However, c-met positive immunoreaction was localized on membrane and cytoplasm, whereas STAT3 immunostaining was observed on cytoplasm and nucleus (Ln in Fig. 2b and c).

The non-malformed kidneys of all NTD fetuses reacted to c-met and failed to express STAT3 in one case and HGF in three cases (Table 2). The greatest HGF, c-met, and STAT3 immunoexpression was observed in epithelial cell of uriniferous tubules (Kn in Fig. 2a–c). The HGF expression was moderate, whereas the c-met reactivity was moderate or high likely to the STAT3 immunoreaction (Table 2). The epithelial cells expressed HGF on cytoplasm, c-met on membrane and cytoplasm and STAT3 on cytoplasm and nucleus (Kn in Fig. 2a–c).

Discussion

NTD are failures of closure of the neural tube [11]. They includes two main categories of defects defined as (1) abnormalities of the skull and brain (anencephaly, acrania, and encephalocele) and (2) malformations of the spine (myelomeningocele or spina bifida) [7]. Between these two extremities, there is a wide range of lesions with a variable severity from lethality (anencephaly) to more or less dramatic physical disabilities, i.e., hydrocephalus, no bowel and/or bladder control, paraplegic of lower extremities and twisted foot [8]. This different outcome is depending on the size and location of NTD and the presence of other anomalies [8]. In fact, NTD may occur also associated with malformation syndromes such as Arnold Chiari II or Dandy–Walker [5]. NTD is considered a common human congenital malformation [8, 17, 29]. On a worldwide basis, as many as 10–20 infants per 10,000 births are affected with some type of NTD. Italy's rate falls at the low end of that range [29]. Variations in NTD national incidences are likely correlated with the differences in genetic alterations, nutrition and health status of women, frequency of pre-natal diagnosis resulting in an elective abortion, and exposure to NTD-inducing toxic agents [19]. However, the cause of NTD is not completely clear yet; mostly, NTD are defined as multifactorial disorders derived from chromosomal abnormalities, single gene mutations, maternal diseases, and maternal exposure to teratogens [19]. The identification of genetic alterations as favoring NTD is a critical step for planning preventive strategies reducing NTD risk in reproductive couples.

In this study we report that the myelomeningocele, a common NTD, is associated with a defective expression of HGF/c-met/STAT3 pathway. The failure of expression of the HGF morphogenetic signal seems to be quite characteristic of nervous tissues that haven't completed the normal process of morphogenesis. The correlation between the HGF/c-met/STAT3 pathway and the neural tube defects include: (1) each member the HGF/c-met/STAT3 pathway is expressed in non-malformed NS of the control fetus, whereas the whole pathway is incompletely detected in myelomeningocele tissues. Our results confirm previous studies describing the expression of HGF and c-met in fetal non-malformed brain and spinal cord tissues [16, 32]. However, we complete these studies adding that the non-malformed NS expresses also the transcription factor STAT3 enclosed in the HGF/c-met/STAT3 pathway; (2) the reduced expression of HGF, c-met, and STAT3 in myelomeningocele tissues is independent from the association with malformation syndromes. In fact, we obtained comparable reduced expressions of HGF, c-met, and STAT3 in myelomeningocele alone and in myelomeningocele associated with Arnold Chiari II or Dandy–Walker syndromes; (3) in each fetus with malformed NS, the non-malformed organs such as lung and kidney expressed the components of HGF morphogenetic pathway. All together, these evidences suggest that the HGF signal carries out a role in normal conformation of embryonic lung and kidney too. A similar conclusion has been proposed from other reports [16, 24, 26, 32]: the novelty of our study resides in the particular collection of fetal tissues analyzed. In fact, the fetuses analyzed in this study included non-malformed lungs and kidneys in a context of a fetus with defective closure of neural tube. These types of fetuses allowed us to evaluate the expression of the entire pathway in both malformed and non-malformed organs in the same individual. The results of our study demonstrated that the HGF morphogenetic signal appears to be ubiquitously expressed and its down-regulation may be associated with organ-specific alterations. Therefore, we are able to demonstrate

that the deficient expression of HGF, c-met, and STAT3 in a malformed organ such as NS may coexist with the normal expression of the same pathway in other non-malformed organs belonging to the same fetus. We speculate that HGF, c-met, and STAT3 genes are crucial in early neurulation and alterations of their genetic expression may contribute to NTD.

We have observed a positive correlation between the mRNA expression of p53 and the mRNA expression of HGF/c-met/STAT3 signal in non-malformed organs of the NTD fetuses. Instead, we haven't observed immunohistochemistry expression of p53 in all malformed and non-malformed samples tissues. This discrepancy between molecular biology and immunohistochemistry is probably due to the difficulty in detecting the immunohistochemical expression of wt p53 in non-tumoral tissues. The observation that in the same fetus p53 is expressed in non-malformed lung and kidney but not in myelomeningocele suggests a role of p53 in the genesis of NTD probably associated with the HGF morphogenetic pathway. Because p53 is a known positive regulator of HGF and c-met gene, we postulate that the reduced expression of HGF and c-met in malformed neural tissue may be caused by p53 down-regulation or disruption [18, 27].

Another result of our study was the quite similar decreased expression of c-met, STAT3, and p53 in both placental tissue and myelomeningocele of each NTD fetus. This evidence raises the question of the role of the placenta in normal NS development. We did not observe microscopic placental alterations in any fetus with NTD. This suggests that the placental genetic alterations are independent from placental morphology. Rather, it is more probably that the placenta contains in summary some genetic information that will be expressed in each fetal organ. In the meanwhile, our results may be a contribution in the common diagnostic clinical practice because the placental expression levels of c-met, STAT3, and p53 may recognize and/or to confirm ultrasound myelomeningocele diagnosis.

References

1. Achim CL, Katyal S, Wiley CA, Shiratori M, Wang G, Oshika E, Petersen BE, Li JM, Michalopoulos GK (1997) Expression of HGF and c-met in the developing and adult brain. Dev Brain Res 102:299–303
2. Bhargava M, Joseph A, Knesel J, Halaban R, Li Y, Pang S, Goldberg I, Setter E, Donovan MA, Zarnegar R, Michalopoulos GA, Nakamura T, Faletto D, Rosen EM (1992) Scatter factor and hepatocyte growth factor: activities, properties, and mechanism. Cell Growth Differ 3:11–20
3. Birchmeier C, Sonnenberg E, Weidner KM, Walter B (1993) Tyrosine kinase receptors in the control of epithelial growth and morphogenesis during development. Bioessays 15:185–190
4. Boccaccio C, Ando M, Tamagnone L, Bardelli A, Michieli P, Battistini C, Comoglio PM (1998) Induction of epithelial tubules by growth factor HGF depends on the STAT pathway. Nature 391:285–288
5. Cohen MMJ, Lemire RJ (1992) Syndromes with cephaloceles. Teratologia 25:161–172
6. Copp AJ, Brook FA, Estibeiro JP, Shum AS, Cockroft DL (1990) The embryonic development of mammalian neural tube defects. Prog Neurobiol 35:363–403
7. DeSesso JM, Scialli AR, Holson JF (1999) Apparent lability of neural tube closure in laboratory animals and humans. Am J Med Genet 87:143–162
8. Detrait ER, George TM, Etchevers HC, Gilbert JR, Vekemans M, Speer MC (2005) Human neural tube defects: developmental biology, epidemiology, and genetics. Neurotoxicol Teratol 27:515–524
9. Di Renzo MF, Bertolotto A, Olivero M, Putzolu P, Crepaldi T, Schiffer D, Pagni CA, Comoglio PM (1993) Selective expression of the met/HGF-receptor in human central nervous system microglia. Oncogene 8:219–222
10. Gordon R (1985) A review of the theories of vertebrate neurulation and their relationship to the mechanics of neural tube birth defects. J Embryol Exp Morphol 89:229–255
11. Gos M, Szpecht-Potocka A (2002) Genetic basis of neural tube defects. I. Regulatory genes for the neurulation process. J Appl Genet 43:343–350
12. Gown AM, deWever N, Battifora H (1993) Microwaved-based antigen unmasking. A revolutionary new technique for routine immunohistochemistry. Appl Immunohistochem 1:256–266
13. Honda S, Kagoshima M, Wanaka A, Tohyama M, Matsumoto K, Nakamura T (1995) Localization and functional coupling of HGF and c-met/HGF receptor in rat brain: implication as neurotrophic factor. Brain Res Mol Brain Res 32:197–210
14. Jeffers M, Fiscella M, Webb CP, Anver M, Koochekpour S, Vande Woude GF (1998) The mutationally activated Met receptor mediates motility and metastasis. Proc Natl Acad Sci 95:14417–14422
15. Jung W, Castren E, Odenthal M, Vande Woude GF, Ishii T, Dienes HP, Lindholm D, Schirmacher P (1994) Expression and functional interaction of hepatocyte growth factor–scatter factor and its receptor c-met in mammalian brain. J Cell Biol 126:485–494
16. Kolatsi-Joannou M, Moore R, Winyard PJ, Woolf AS (1997) Expression of hepatocyte growth factor/scatter factor and its receptor, MET, suggests roles in human embryonic organogenesis. Pediatr Res 41:657–665
17. Lemire RJ (1988) Neural tube defects. JAMA 259:558–562
18. Metcalfe AM, Dixon RM, Radda GK (1997) Wild-type but not mutant p53 activates the hepatocyte growth factor/scatter factor promoter. Nucleic Acids Res 25:983–986
19. Mitchell L (2005) Epidemiology of neural tube defects. Am J Med Genet Part C 135C:88–94
20. Montesano R, Matsumoto K, Nakamura T, Orci L (1991) Identification of a fibroblast-derived epithelial morphogen as hepatocyte growth factor. Cell 67:901–908
21. Morrissey RE, Mottet NK (1980) Neural tube defects and brain anomalies: a review of selected teratogens and their possible modes of action. Neurotoxicology 2:125–162
22. Müller F, O'Rahilly R (1987) The development of the human brain, the closure of the caudal neuropore, and the beginning of secondary neurulation at stage 12. Anat Embryol 176:413–430
23. Naldini L, Weidner KM, Vigna E, Gaudino G, Bardelli A, Ponzetto C, Narsimhan RP, Hartmann G, Zarnegar R, Michalopoulos GK, Birchmeierl W, Comoglio PM (1991) Scatter factor and hepatocyte growth factor are indistinguishable ligands for the MET receptor. EMBO J 10:2867–2878

24. Ohmichi H, Koshimizu U, Matsumoto K, Nakamura T (1998) Hepatocyte growth factor (HGF) acts as a mesenchyme-derived morphogenic factor during fetal lung development. Development 125:1315–1324
25. Piscione TD, Rosenblum ND (2002) The molecular control of renal branching morphogenesis: current knowledge and emerging insights. Differentiation 70:227–246
26. Sakurai H, Barros EJ, Tsukamoto T, Barasch J, Nigam SK (1997) An in vitro tubulogenesis system using cell lines derived from the embryonic kidney shows dependence on multiple soluble growth factors. Proc Natl Acad Sci USA 94:6279–6284
27. Seol DW, Chen Q, Smith ML, Zarnegar R (1999) Regulation of the c-met proto-oncogene promoter by p53. J Biol Chem 274:3565–3572
28. Taijima H, Matsumoto K, Nakamura T (1992) Regulation of cell growth and motility by hepatocyte growth factor and receptor expression in various cell species. Exp Cell Res 202:423–431
29. The EUROCAT Working Group (1987) Prevalence of neural tube defects in 16 regions of Europe 1980–1983. Int J Epidemiol 16:246–251
30. Trovato M, Grosso M, Vitarelli E, Benvenga S, Trimarchi F, Barresi G (2002) Immunoexpression of the hepatocyte growth factor (HGF), HGF–receptor (c-met) and STAT3 on placental tissues from malformed fetuses. Histol Histopathol 17:691–698
31. Uehara Y, Minowa O, Mori C, Shiota K, Kuno J, Noda T, Kitamura N (1995) Placental defect and embryonic lethality in mice lacking hepatocyte growth factor/scatter factor. Nature 373:702–705
32. Wang Y, Selden C, Farnaud S, Calnan D, Hodgson HJ (1994) Hepatocyte growth factor (HGF/SF) is expressed in human epithelial cells during embryonic development; studies by in situ hybridisation and Northern blot analysis. J Anat 185:543–551
33. Zarnegar R, Muga S, Rahija R, Michalopoulos G (1990) Tissue distribution of hepatopoietin A: a heparin binding polypeptide growth factor for hepetocytes. Proc Natl Acad Sci USA 87:1252–1256
34. Zarnegar R, Michalopoulos GK (1995) The many faces of hepatocyte growth factor: from hepatopoiesis to hematopoiesis. J Cell Biol 129:1177–1180
35. Zhang YW, Vande Woude GF (2003) HGF/SF-Met signaling in the control of branching morphogenesis and invasion. J Cell Bifochem 88:408–417

Virchows Arch (2007) 450:211–214
DOI 10.1007/s00428-006-0333-z

CASE REPORT

Mediastinal lymphangiomatosis coexisting with occult thymic carcinoma

Jun-ichiro Ikeda · Eiichi Morii · Yasuhiko Tomita · Binglin Zhang · Toshiteru Tokunaga · Masayoshi Inoue · Masato Minami · Meinoshin Okumura · Katsuyuki Aozasa

Received: 31 August 2006 / Accepted: 17 October 2006 / Published online: 22 November 2006
© Springer-Verlag 2006

Abstract Mediastinal lymphangiomatosis in a 70-year-old woman was diagnosed on a medical checkup. The tumor was resistant to sclerotherapy with OK432 or bleomycin. The patient continued on a downhill course and died approximately 3 years after the initial diagnosis. Autopsy revealed a large tumor mass occupying the anterior mediastinum and firmly adhered to the pericardium and the pleura. The tumor consisted of two intermingled lesions: dilated vessels lined with D2-40-positive lymphatic endothelium and CD5-positive atypical cell nests with focal keratinization. The former was diagnosed as lymphangiomatosis and the latter as thymic squamous cell carcinoma. Vascular endothelial growth factor (VEGF)-C, a growth factor for lymphatic endothelial cells, was expressed by the carcinoma, and VEGF-C receptor was expressed by the endothelium of lymphangiomatosis. These findings suggested that VEGF-C derived from the thymic carcinoma induced the lymphangiomatosis lesion in a paracrine manner.

Keywords Lymphangiomatosis · Thymic carcinoma · VEGF-C

J.-i. Ikeda · E. Morii (✉) · Y. Tomita · B. Zhang · K. Aozasa
Department of Pathology, Graduate School of Medicine,
Osaka University,
Yamada-oka 2-2,
Suita 565-0871, Japan
e-mail: morii@patho.med.osaka-u.ac.jp

T. Tokunaga · M. Inoue · M. Minami · M. Okumura
Department of Surgery, Graduate School of Medicine,
Osaka University,
Yamada-oka 2-2,
Suita 565-0871, Japan

Introduction

Lymphangioma usually occurs in the neck and face of children, but is quite rare in the thorax of adults [3, 9]. Lymphangiomatosis, a diffuse, proliferative form of lymphangioma, is typically benign, but association with serious morbidity is not uncommon [1, 3, 5, 6, 9]. Involvement of serosal surfaces and viscera by lymphangiomatosis may result in severe complications such as dyspnea due to compression by the mediastinal or pulmonary mass and pleural or pericardial effusion [1, 3, 9]. Here, we present a case of mediastinal lymphangiomatosis in an elderly patient with concurrent occult thymic carcinoma diagnosed on autopsy adjoining the lymphangiomatosis. To our knowledge, this is the first report of lymphangiomatosis coexisting with thymic carcinoma.

Clinical history

In 2002, an abnormal mediastinal mass was discovered by computed tomography in an asymptomatic 70-year-old Japanese woman during a medical checkup. Two years later, the mass had increased in size. Drainage of chylous fluid from the lesion, together with the findings at lymphangiography, indicated the diagnosis of mediastinal lymphangiomatosis. Sclerotherapy with OK432 was performed, but the amount of chylous fluids in the mediastinum and bilateral pleural cavities increased. The patient was admitted to Osaka University Hospital, Osaka in 2005. Physical examination revealed moist rales in the lower field of the right lung and generalized edema. Neither cutaneous lymphangioma, abdominal mass, nor hepatosplenomegaly were found. Laboratory data showed a leukocyte count of

4,400/μl with normal differential ratio, hemoglobin of 9.5 g/dl, platelet count of 23.2×10^4/μl, and C-reactive protein of 5.8 mg/dl. Sclerotherapy with bleomycin was initiated after progressive dyspnea, due to the large amount of pleural and mediastinal effusion, but no improvement was noted. The patient's condition deteriorated with onset of disseminated intravascular coagulation, oliguria, and hyperbilirubinemia. An autopsy was performed after death on the 37th day after admission.

Materials and methods

All histologic specimens obtained at autopsy were fixed in 10% buffered formalin, embedded in paraffin, sectioned, and stained with hematoxylin and eosin. Immunohistochemistry was performed using the following four antibodies: D2-40 monoclonal antibody against lymphatic endothelial cells (DAKO A/S, Glostrup, Denmark), anti-CD5 monoclonal antibody (DAKO), anti-vascular endothelial growth factor (VEGF)-C polyclonal antibody (Zymed, South San Francisco, CA, USA), and anti-VEGF-receptor-3 (VEGFR-3) polyclonal antibody (Chemicon, Temecula, CA, USA). After antigen retrieval with the Pascal pressurized heating chamber (DAKO), the sections were incubated with D2-40, anti-CD5, anti-VEGF-C, and anti-VEGFR-3 antibody. Antigen detection was completed by treatment with biotin-conjugated anti-mouse or anti-rabbit IgG (Zymed), followed by incubation with the peroxidase-conjugated biotin–avidin complex (Vectastain ABC kit, Vector, Burlingame, CA). As the negative control, sections were incubated with nonimmune serum.

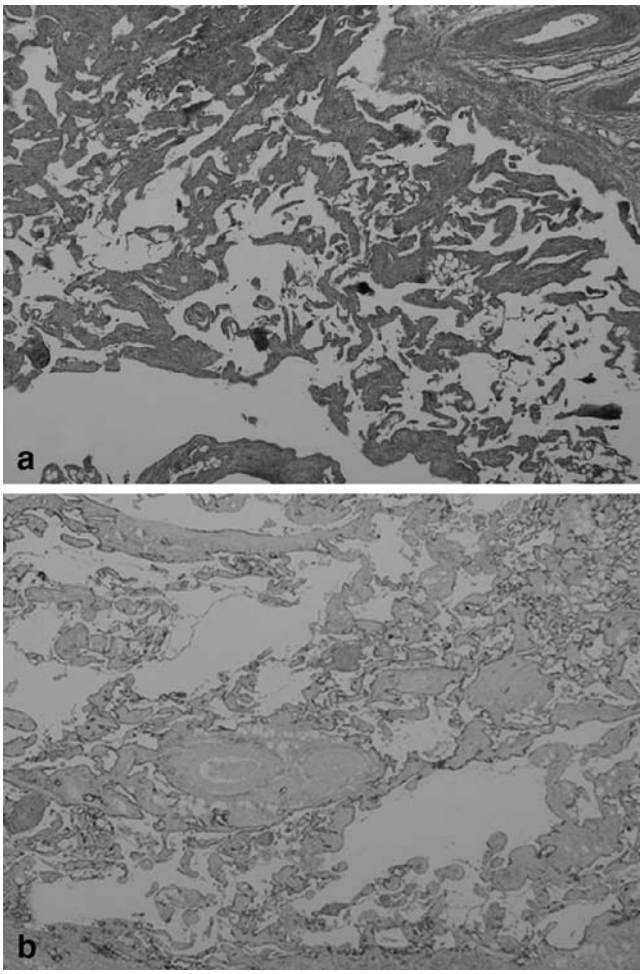

Fig. 1 Lymphangiomatosis in the mediastinum. **a** Numerous irregularly dilated spaces were lined by thin endothelial cells (Hematoxylin and eosin, original magnification, ×40). **b** The endothelial cells showed positive staining for D2-40 that specifically recognizes lymphatic endothelial cells (original magnification, ×40)

Results

At autopsy, a large tumor mass occupied the anterior mediastinum and appeared firmly adhered to the pericardium and the visceral pleura. The size of this tumor was 1,200 mm×800 mm. Histologically, the tumor was composed of dilated vessels lined by thin endothelial cells (Fig. 1a), which showed positive staining for D2-40 (Fig. 1b). These lymphatic vessels showed an infiltrative growth into the surrounding interlobular septa of lung. No metastatic lesion was found. These findings led to a diagnosis of lymphangiomatosis.

Dissection of the lymphangiomatosis in the anterior mediastinum revealed a whitish nodule with a diameter of 30 mm (Fig. 2a). Histologically, numerous cell nests composed of large atypical cells with massive necrotic change in the central area were found in the fibrotic background (Fig. 2b). Obvious keratinization was found in the cell nests, which were positive for CD5. The atypical cell clusters were surrounded with dilated lymphatic vessels in some areas. Histologic and immunohistochemical findings justified the diagnosis of thymic squamous cell carcinoma (SCC). These SCC components were confined to the whitish nodule in the anterior mediastinum and did not invade or metastasize to other organs.

VEGF-C is a growth factor for lymphatic endothelial cells. Overexpression of VEGF-C and its receptor VEGFR-3 in lymphatic endothelial cells is known to trigger lymphangiomatosis in autocrine or paracrine fashion. The immunohistochemical study revealed that the thymic SCC expressed VEGF-C (Fig. 3a), and the endothelial cells in the lymphangiomatosis lesion expressed VEGFR-3 but not VEGF-C (Fig. 3b). To investigate whether VEGF-C expression was common to thymoma/thymic carcinoma, six other thymic tumor cases (types A, AB, B1, and B2 thymomas, and thymic carcinoma) were examined. Among

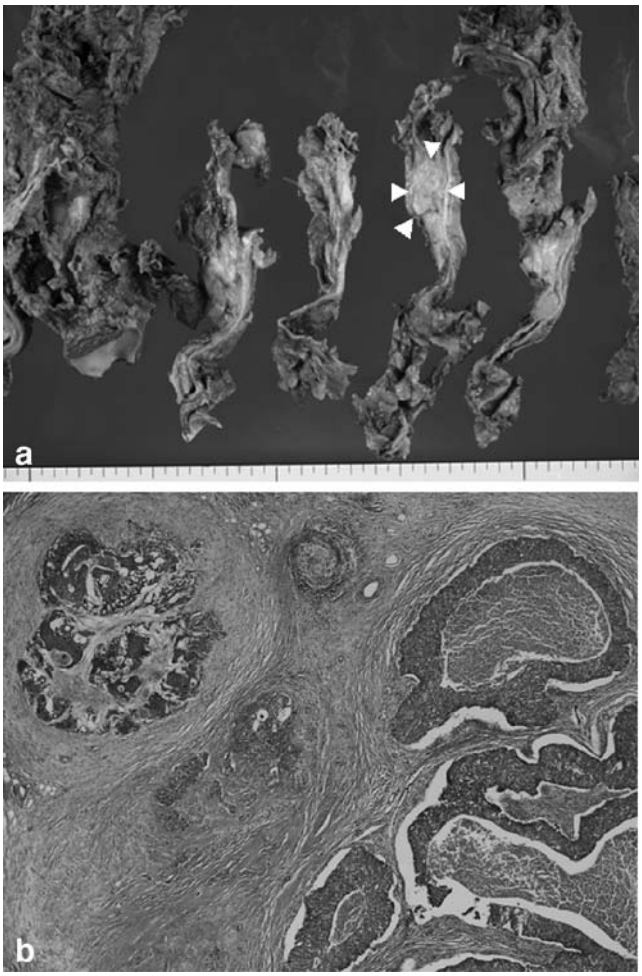

Fig. 2 **a** A whitish nodule (*arrowheads*) was found in the lymphangiomatosis lesion. **b** In the whitish nodule, there was a cohesive proliferation of large atypical cells with necrosis in the central area. Keratinization was occasional in these nests (Hematoxylin and eosin, original magnification, ×40)

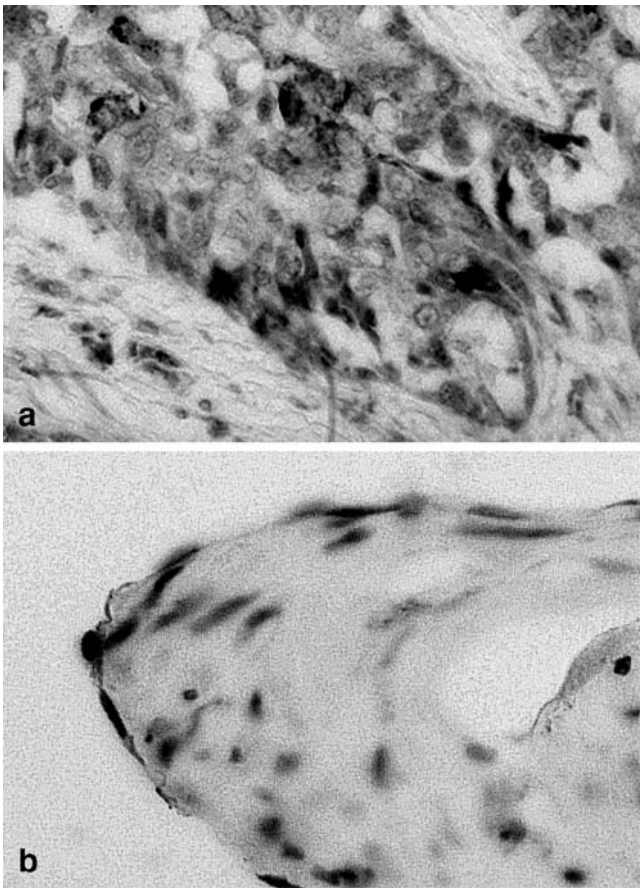

Fig. 3 Expression of VEGF-C in thymic cancer (**a**) and VEGF-C receptor in endothelial cells of lymphangiomatosis (**b**). (Original magnification, ×400)

the six cases, VEGF-C expression was found in three cases but not in the other three cases (Table 1).

Discussion

Lymphangioma usually presents as a localized lesion preferentially developing in the head and face of children; it is usually curable by surgical resection [3, 9]. In contrast, lymphangiomatosis shows diffuse proliferation of lymphatic tissues and is frequently associated with other lymphatic-related abnormalities, such as lymphangiectasis and lymphangioleiomyomatosis [1, 3, 5, 6, 9]. The present case is quite unusual in its late onset age and the lack of other lymphatic-related abnormalities. The invasion to the serosal surfaces and viscera is known to be an unfavorable sign [6, 9]. Indeed, the present lymphangiomatosis lesion firmly adhered to the pericardium and visceral pleura resulting in severe pleural effusion and dyspnea. Treatment with OK432 and bleomycin showed little therapeutic effect on the lymphangiomatosis.

Previous reports [2, 7, 8] show a correlation between the VEGF-C expression level in human carcinomas and their metastatic potential. VEGF-C produced by cancer cells might induce neolymphangiogenesis around a tumor, which could promote metastasis of cancer cells [2, 7, 8]. The overexpression of VEGF-C causes lymphangiomatosis [4]. A previous report suggested that coexpression of VEGF-C

Table 1 Thymic tumors without lymphangiomatosis examined in this study and their VEGF-C expression

Case number	Type of thymic tumor (WHO classification)	VEGF-C expression
1	A	(−)
2	AB	(+)
3	AB	(+)
4	B1	(−)
5	B2	(−)
6	Carcinoma	(+)

and its receptor in lymphatic endothelial cells could be causative for lymphangiomatosis in a paracrine or autocrine fashion [4]. Lymphatic endothelial cells in the lymphangiomatosis lesions of the present case expressed VEGF-C receptor but not its ligand VEGF-C. As the present thymic SCC expressed VEGF-C, this expression may have induced the present lymphangiomatosis.

Among the examined six thymoma/thymic carcinomas, three cases expressed VEGF-C. This was consistent with the previous report that about half of tumors express VEGF-C [7]. In the present study, VEGF-C was expressed in type AB thymoma and thymic carcinoma, but not in type A, B1, and B2 thymomas. No studies have been done on the correlation between VEGF-C expression and thymoma types. Precise examination with a number of thymomas or thymic carcinomas will reveal its correlation.

To our knowledge, this is the first report describing the simultaneous occurrence of lymphangiomatosis and thymic carcinoma. The symptoms relating to the mediastinal disease of this patient began in the sixth decade of life, which is too late for development of lymphangiomatosis. This finding further supports the possibility that VEGF-C produced by the thymic carcinoma cells may induce a proliferation of lymph vessels as, in this case, the lymphangiomatosis lesion surrounded the thymic carcinoma.

Acknowledgement This paper is supported by grants from the Ministry of Education, Culture, Sports, Science and Technology.

References

1. Bermejo Casero EJ, Mongil Poce R, Arrabal Sanchez R, Fernandez de Rota Avecilla A, Benitez Domenech A, Fernandez Bermudez JL (2004) Diffuse thoracic lymphangiomatosis: diagnosis and treatment. Arch Bronconeumol 40:599–601
2. Byrne AM, Bouchier-Hayes DJ, Harmey JH (2005) Angiogenic and cell survival functions of vascular endothelial growth factor (VEGF). J Cell Mol Med 9:777–794
3. Faul JL, Berry GJ, Colby TV, Ruoss SJ, Walter MB, Rosen GD, Raffin TA (2000) Thoracic lymphangiomas, lymphangiectasis, lymphangiomatosis, and lymphatic dysplasia syndrome. Am J Respir Crit Care Med 161:1037–1046
4. Huang HY, Ho CC, Huang PH, Hsu SM (2001) Co-expression of VEGF-C and its receptors, VEGFR-2 and VEGFR-3, in endothelial cells of lymphangioma. Implication in autocrine or paracrine regulation of lymphangioma. Lab Invest 81:1729–1734
5. Konez O, Vyas PK, Goyal M (2000) Disseminated lymphangiomatosis presenting with massive chylothorax. Pediatr Radiol 30:35–37
6. Ramani P, Shah A (1993) Lymphangiomatosis. Histologic and immunohistochemical analysis of four cases. Am J Surg Pathol 17:329–335
7. Salven P, Lymboussaki A, Heikkila P, Jaaskela-Saari H, Enholm B, Alitalo K, Joensuu H (1998) Vascular endothelial growth factors VEGF-B and VEGF-C are expressed in human tumors. Am J Pathol 153:103–108
8. Stacker SA, Achen MG, Jussila L, Baldwin ME, Alitalo K (2002) Lymphangiogenesis and cancer metastasis. Nat Rev Cancer 2: 573–583
9. Takahashi K, Takahashi H, Maeda K, Homma S, Uekusa T, Dambara T, Kira S (1995) An adult case of lymphangiomatosis of the mediastinum, pulmonary interstitium and retroperitoneum complicated by chronic disseminated intravascular coagulation. Eur Respir J 8:1799–1802

Virchows Arch (2007) 450:215–219
DOI 10.1007/s00428-006-0337-8

CASE REPORT

Renal cell carcinoma with t(X;17)(p11.2;q25) in a 6-year-old Taiwanese boy

Chi-Kuan Chen · Chuen Hsueh · Jin-Yao Lai · Iou-Jih Hung · Jacqueline Whang-Peng · Wan-Ping Wang · Hsin-Yi Lai · Jim-Ray Chen

Received: 1 August 2006 / Accepted: 20 October 2006 / Published online: 6 December 2006
© Springer-Verlag 2006

Abstract Pediatric renal cell carcinoma (RCC) associated with ASPL–TFE3 gene fusion resulting from balanced translocation, t(X;17)(p11.2;q25), is a distinctive tumor entity. It is uncommon, and most reported cases have exclusively come from Western societies. We report a case of t(X;17)(p11.2;q25) RCC in a 6-year-old Taiwanese boy. The patient presented with dysuria and intermittent hematuria for 1 year. Nonenhanced CT showed a well-defined homogeneous hyperdensity lesion in the upper pole of the left kidney. This patient refused to receive immediate surgical procedures but had routine follow-ups. After a 9-month follow-up, the patient underwent total nephrectomy with a favorable outcome. Final diagnosis is established based on the characteristic microscopic features, strong nuclear TFE-3 immunoreactivity, and the presence of type 1 TFE3–ASPL fusion gene detected by reverse transcriptase–polymerase chain reactions. No adjuvant therapy is given, and the patient is alive without evidence of disease for 1 year and 6 months.

Keywords Renal cell carcinoma · t(X;17)(p11.2;q25) · ASPL–TFE3 gene fusion

C.-K. Chen · C. Hsueh (✉)
Department of Anatomic Pathology,
Chang Gung Memorial Hospital and Chang Gung University,
Kuei-Shan 333, Tao-Yuan, Taiwan
e-mail: ch9211@adm.cgmh.org.tw

J.-Y. Lai
Department of Pediatric Surgery,
Chang Gung Children's Hospital and Chang Gung University,
Kuei-Shan 333, Tao-Yuan, Taiwan

I.-J. Hung
Department of Hematology/Oncology,
Chang Gung Children's Hospital and Chang Gung University,
Kuei-Shan 333, Tao-Yuan, Taiwan

J. Whang-Peng · W.-P. Wang · J.-R. Chen (✉)
National Institute of Cancer Research,
National Health Research Institutes,
9F, No. 161, Sec. 6, Min-Chun East Road,
Taipei 114, Taiwan
e-mail:jimrchen@nhri.org.tw

H.-Y. Lai
Department of Radiology,
China Medical University Hospital,
Taichung, Taiwan

Introduction

Pediatric renal cell carcinoma (RCC) is rare and represents approximately 2–6% of all solid renal malignancies [8]. According to the 2004 World Health Organization classification of renal tumors, renal carcinomas associated with Xp11.2 translocations/TFE3 gene are a distinct entity with unique morphogenetic characteristics and biological behavior [5]. The tumor affects primarily children and young adults, although a few cases have been described in older patients. There is no apparent gender predilection [5]. Genetically, it is characterized by a number of different translocations involving Xp11.2 chromosome, all of them resulting in gene fusions with the TFE3 gene [5]. At least five genetic variants have been identified including t(X;1)(p11.2;q21) translocation with PRCC–TFE3 fusion [10], t(X;1)(p11.2;p34) translocation with PSF–TFE3 fusion [7], inv(X)(p11;q12) translocation with *NonO* (p54^{nrb})–TFE3 fusion [7], t(X;17)(p11.2;q25) translocation with ASPL–TFE3 fusion [2], and t(X;17)(p11.2;q23) with CLTC–TFE3 fusion [4]. Interestingly, both t(X;17)(p11.2;q25) RCC and alveolar soft part sarcoma contain identical ASPL–TFE3

fusion transcripts, but the t(X;17) translocation is consistently balanced in the former and usually unbalanced in the latter [2]. Histologically, the most distinctive feature is that of a carcinoma with predominantly papillary architecture composed of cells with somewhat voluminous, clear, or slightly eosinophilic cytoplasm. Scattered hyaline nodules and psammomatous bodies can be seen [2, 5]. However, microscopic features can vary among different variants. For example, ASPL–TFE3 tumors have cells with more abundant cytoplasm, more hyaline nodules, and psammomatous bodies, and are less solid than PRCC–TFE3 tumors [2].

By immunohistochemistry, tumor cells express strong nuclear TFE3 immunostaining, which is considered as a supportive diagnostic criterion [3, 5]. These tumors can also be molecularly diagnosed by either cytogenetics or reverse transcriptase–polymerase chain reaction [2, 5, 10]. Most studies of renal carcinomas associated with Xp11.2 translocations/TFE3 gene fusions are limited to case reports and small series from Western societies [2, 3, 5, 6, 11], and to the best of our knowledge, there is no report from Asian countries. In this study, we report a molecularly documented case of t(X;17)(p11.2;q25) RCC in a 6-year-old Taiwanese boy. The diagnosis is established based on the distinctive microscopic features, strong nuclear TFE-3 immunoreactivity, and the presence of type 1 TFE3–ASPL fusion gene detected by reverse transcriptase–polymerase chain reactions (RT–PCRs).

Case report

Clinical history

A 6-year-old boy was admitted to our institution with the chief complaint of dysuria and intermittent hematuria for 1 year. There was no associated flank pain or edema. Urine analysis showed microscopic hematuria without proteinuria or bacteriuria. Renal echo revealed a hyperechoic mass with anechoic rims in the upper pole of the left kidney. Nonenhanced computerized tomography (CT) also showed a well-defined 2.0×1.7 cm homogeneous hyperdensity lesion in the left kidney. This patient refused to receive immediate surgical procedures but had routine follow-ups. After 9 months, a follow-up CT revealed a tumor growth of 2.4×2.4 cm with the development of a 1.6×1.2 cm daughter nodule (Fig. 1a). Neither lymph node nor distant metastasis is found. This tumor was regarded as stage 1 (T1aN0M0) according to the criteria by the American Joint Committee in 2002. He underwent total nephrectomy smoothly with a satisfactory outcome. No adjuvant therapy was given, and he is alive without manifesting disease or any other signs or symptoms for 1 year and 6 months.

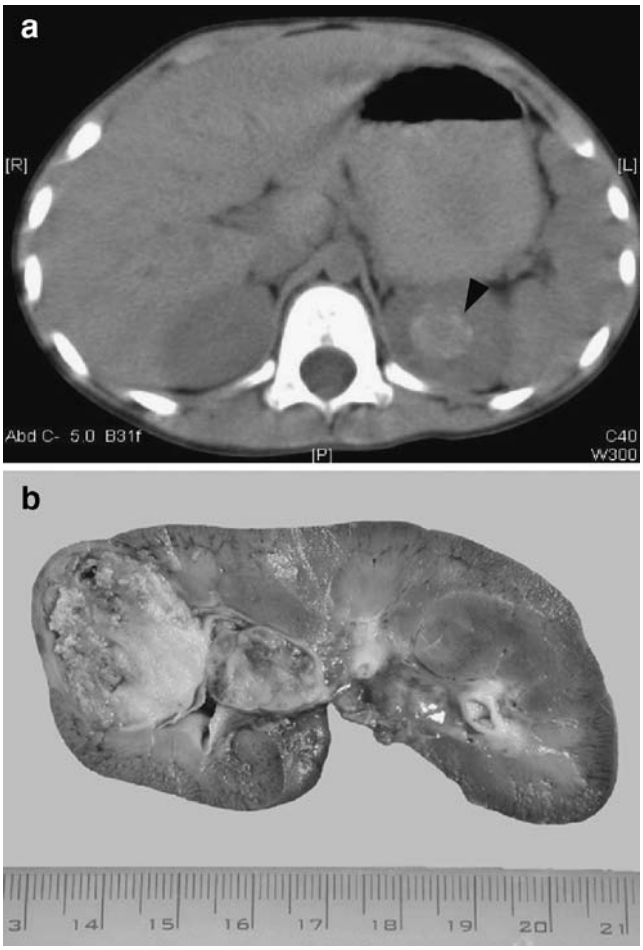

Fig. 1 **a** A follow-up nonenhanced computed tomography performed 9 months after admission demonstrates a 2.4×2.4 cm homogeneous hyperdensity lesion in the upper portion of the left kidney. **b** Grossly, the tumor was well circumscribed with an adjacent daughter nodule. Areas of hemorrhage and necrosis were seen. The renal hilar vessel and capsule were free from tumor

Materials and methods

Immunohistochemistry

Immunohistochemical analysis was performed on formalin-fixed, paraffin-embedded tissue sections. Briefly, 4-μm sections were deparaffinized in xylene and rehydrated in graded ethanol concentrations. Heat-induced antigen retrieval was accomplished by immersing slides in 10-mM citrate buffer pH 6 at 120°C for 10 min in a pressurized heating chamber (Biocare Medical, Concord, CA). Endogenous peroxidase was blocked with 3% aqueous hydrogen peroxide, and nonspecific binding was blocked with 20% protein blocker (Signet Laboratories, Dedham, MA) in Tris-buffered saline. For TFE3 immunostaining, a primary goat anti-human polyclonal TFE3 (P-16) antibody (Santa Cruz Biotechnology, Santa Cruz, CA) was used at

1:300 dilution in a humid container overnight. After washing three times with phosphate-buffered saline (PBS), the slides were then incubated with biotinylated anti-goat IgG antibody (Vector Laboratories, Burlingame, CA) at a dilution of 1:200 followed by three washes of PBS. Signal detection was performed using 3,3′-diaminobenzidine as the chromagen. The slides were counterstained with hematoxilin, cleared in xylene, and mounted with Permount. Negative controls consisted of replacing the primary antibody with PBS.

Molecular analysis

RNA extraction from paraffin sections was performed using a modified protocol [1]. Briefly, a single 10-μm section was deparaffinized at room temperature using xylene and absolute ethanol. After air drying, the tissue was resuspended in 200-μl lysis buffer (20 mM Tris-HCl, pH 7.5; 20 mM ethylenediamine tetraacetic acid; 1% sodium dodecyl sulfate) containing 25 μg/ml proteinase K buffer (Roche Applied Science). After incubation at 55°C for 16–18 h, the lysate was briefly centrifuged, and the clear supernatant was further purified using a Qiagen RNeasy mini spin column (Qiagen GmbH, Germany). The concentration of purified RNA was measured using NanoDrop ND-1000 spectrophotometer (NanoDrop Technologies, Wimington, DE). cNDA synthesis was prepared from 1 μg of total RNA using Ominiscript RT kit (Qiagen GmbH, Germany). To assess the adequacy of RNA for analysis, RT–PCR was performed using primers spanning an intron of the ubiquitously expressed 18S ribosomal RNA, resulting in the amplification of a 315-bp fragment. Negative controls lacking RNA were used in all RT–PCR assays. The amplified fragments were identified by their size on agarose gel electrophoresis. The specificity of all positive results was further confirmed by negative controls containing the target RNA but lacking RT.

The detection of ASPL–TFE3 by PCR was performed as described by Argani et al. [2]. Briefly, detection of an ASPL–TFE3 fusion transcript was performed using a forward primer from ASPL (AAAGAAGTCCAAGTCGG GCCA) and a TFE3 exon 4 reverse primer (CGTTTG ATGTTGGGCAGCTCA). RT–PCR for the reciprocal fusion product, TFE3–ASPL, was performed using an ASPL reverse primer (CACCGTCAGCTCAAAGAAC TC) and a TFE3 forward primer appropriate to the type of ASPL–TFE3 rearrangement in each case: for cases with a type 1 TFE3–ASPL fusion, a TFE3 exon 3 forward primer (TTGATGATGTCATTGATGAGATC), and in cases with a type 2 TFE3–ASPL fusion, a more upstream TFE3 primer (GCTCAAAAGCCAAC CCTTAC). The fusion transcript PCR products were cloned into pGEM-T easy vector (Promega, Madison, WI) using rapid DNA ligation kit (Roche Applied Science). Sequencing was performed using a fluorescent DNA sequencer (Applied Biosystem). DNA sequence analysis was performed by the basic local alignment search tool sequence similarity searches using the National Center for Biotechnology Information database. The ASPL cDNA sequence and junctional sequences of both types of ASPL–TFE3 fusion transcripts have been deposited in GenBank (accession numbers AF324219, AY034077, AY034078).

Results

Histopathologic studies

The left kidney measured about 8.5×4×3.5 cm and weighed 71 g. A 2.4×2×2 cm tumor was located at the

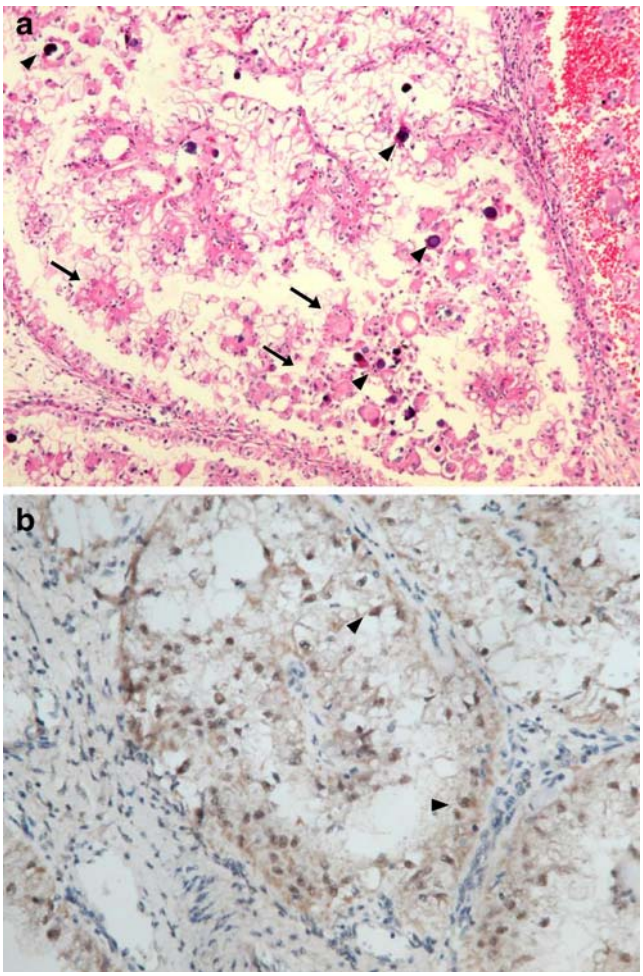

Fig. 2 **a** The hematoxylin and eosin section showed characteristic papillary architectures composed of clear cells with clear, voluminous, and vacuolated cytoplasm. Extensive hyaline nodules (*arrow*) and many psammoma bodies (*arrowhead*) are seen (original magnification, ×200). **b** Tumor cells displayed strong nuclear immunostaining of TFE3 (*arrowhead*), whereas the surrounding stromal cells were negative (original magnification, ×200)

upper pole of the left kidney with an adjacent 1.6×1.2×1 cm daughter nodule (Fig. 1b). The tumor was tan-yellow with areas of necrosis and hemorrhage. There was no gross invasion to the capsule, renal pelvis, hilar vessels, and ureter.

On microscopic examination, the tumor was well circumscribed but unencapsulated. Architecturally, it was composed predominantly of papillary with mixed glandular and pseudopapillary patterns of growth. Tumor cells had clear, voluminous, and vacuolated cytoplasm. Extensive stromal hyaline nodules and many psammoma bodies were seen (Fig. 2a).

Immunohistochemical analysis showed that tumor cells expressed strong nuclear TFE-3 staining, whereas the surrounding mesenchymal cells were negative (Fig. 2b).

Molecular study

RT–PCR analysis using RNA isolated from paraffin sections was successful as judged by the amplification of 18S ribosomal RNA (Fig. 3a). Detection of fusion gene transcripts using different primer combinations showed an approximately 200-bp band in type 1 TEF3–ASPL (Fig. 3a). Sequencing of this PCR product confirmed a 218-bp transcript encoding type 1 TEF3–ASPL rearrangement with an in-frame fusion of TEF3 exon 3 to ASPL (Fig. 3b). No transcript was detected in ASPL–TFE3 and type 2 TFE3–ASPL.

Discussion

Pediatric RCC associated with t(X;17)(p11.2;q25)/ASPL–TFE3 gene fusion is rare, with approximately 30 reports in the literature [2, 5, 11]. Up to now, studies of these tumors are exclusively from Western societies. We report herein a molecularly confirmed t(X;17)(p11.2;q25) RCC in a 6-year-old Taiwanese boy, and to the best of our knowledge, this is the first report from Asian societies. Final diagnosis is established based on the distinctive microscopic features (papillary architecture lined by tumor cells with voluminous, clear to slightly eosinophilic cytoplasm, and prominent hyaline nodules and abundant psammoma bodies), expression of nuclear TFE-3 immunostaining, and the presence of type 1 TFE3–ASPL fusion transcript detected by RT–PCR.

The detection of nuclear TFE3 immunoreactivity by immunohistochemistry is a highly sensitive and specific assay for identifying tumors harboring TFE3 gene fusions [3]. The availability of TFE3 immunostaining can greatly aid in identifying renal carcinomas associated with Xp11.2 translocations/TFE3 gene and in establishing their prevalence in both perspective and retrospective studies. However, it is important to further classify these TFE3-positive renal tumors by cytogenetics and/or RT–PCR due to the presence of different genetic variants [2, 4, 7, 10]. Cytogenetic approach is more technically demanding and expensive compared to RT–PCR and cannot provide detailed information regarding the junctional sequences of

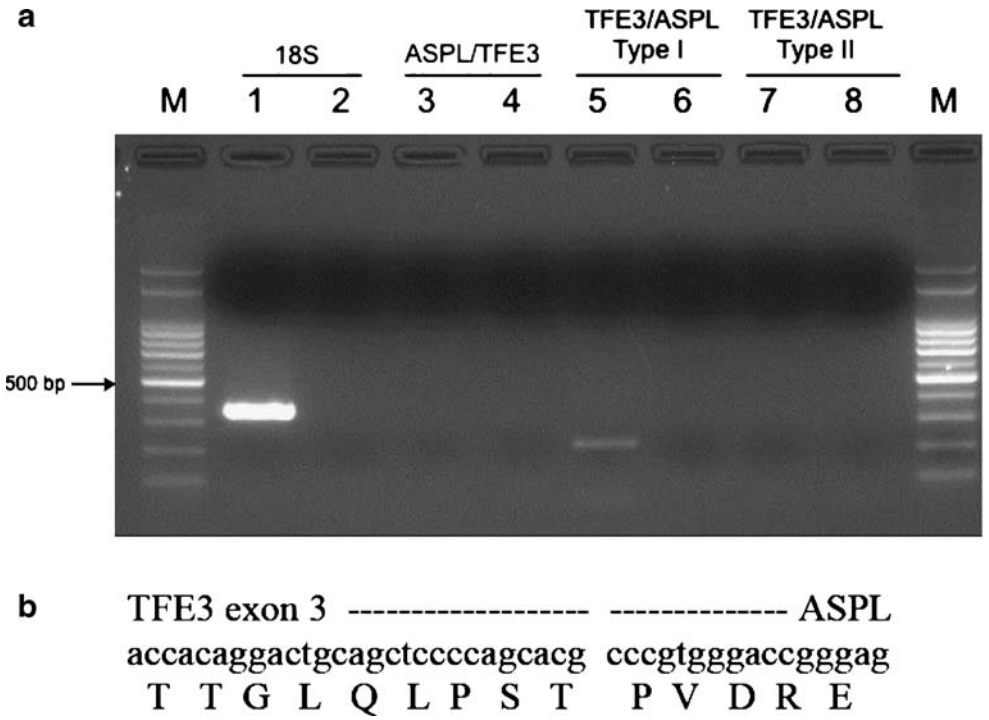

Fig. 3 **a** Analyses of TFE3–ASPL and ASPL–TFE3 fusion transcripts by RT–PCR. RT–PCR was performed as described in the text. Primer combinations were as labeled. 18S ribosomal RNA was used for determining the efficiency of RT. Lane 5 showed a PCR product of type 1 TFE3–ASPL fusion transcript. Lanes 2, 4, 6 and 8 were negative controls. *M* was the marker lane (100 bp). **b** Partial sequences of the PCR product in lane 5 showed in-frame fusion of TFE3 exon 3 to ASPL, corresponding to the junction sequence of type I TFE3–ASPL gene transcript

fusion transcripts. RT–PCR is technically less challenging and can provide the greatest sensitivity, especially for small biopsy specimens. In the case of renal tumor with reciprocal ASPL–TFE3 gene fusions, two subtypes have been detected in each gene rearrangement [2]. In their study, 4 and 1 tumors were shown to contain types 1 and 2 TFE3–ASPL fusion transcript, respectively. Three cases did not have either detectable TFE3–ASPL transcripts. As to ASPL–TFE3 transcript, 7 and 1 tumors had types 1 and 2 gene fusion, respectively. In our report, only type 1 TFE3–ASPL fusion transcript was detected without the detectable ASPL–TFE3 transcript. It seemed that TFE3–ASPL and ASPL–TEF3 transcripts are not mutually present despite reciprocal ASPL–TFE3 gene rearrangement. There is no reasonable explanation for this phenomenon, and differential stability of fusion transcript may be involved. Additionally, it remains to be determined whether these different types of fusion transcript carry clinical significance as noted in alveolar rhabdomyosarcoma [9].

Information regarding the clinical behavior of these tumors is limited due to their rare incidence. It is reported that despite their advanced stage, ASPL–TFE3 renal tumors usually present slow progression with rare instances of metastasis [2]. Among eight cases reported by Argani et al. [2], one 17-year-old female patient died of progressive bony and lymph node metastasis 2 years after surgery, and another 17-year-old girl had lung metastasis after 15 months. The remaining six patients showed no evidence of disease in an average of 4.2-year follow-up (2 months to 10 years). Although the clinical course of this patient is rather indolent, routine follow-up is still mandatory. In summary, the clinical and genetic features of these tumors have begun to emerge; correct distinction of primary renal ASPL–TFE3 tumors from other pediatric RCCs can lead to better understanding of their clinicopathologic differences, which should aid in developing individualized management plans.

Acknowledgment This work is supported by grant CMRPG-32071 to Chun Hseuh and partially supported by NSC 94-3114-P-043-003-Y to Jacqueline Whang-Peng.

References

1. Adams V, Hany MA, Schmid M, Hassam S, Briner J, Niggli FK (1996) Detection of t(11;22)(q24;q12) translocation breakpoint in paraffin-embedded tissue of the Ewing's sarcoma family by nested reverse transcription–polymerase chain reaction. Diagn Mol Pathol 5:107–113
2. Argani P, Antonescu CR, Illei PB, Lui MY, Timmons CF, Newbury R, Reuter VE, Garvin AJ, Perez-Atayde AR, Fletcher JA, Beckwith JB, Ladanyi M (2001) Primary renal neoplasms with the ASPL–TFE3 gene fusion of alveolar soft part sarcoma: a distinctive tumor entity previously included among renal cell carcinomas of children and adolescents. Am J Pathol 159:179–192
3. Argani P, Lal P, Hutchinson B, Lui MY, Reuter VE, Ladanyi M (2003) Aberrant nuclear immunoreactivity for TFE3 in neoplasms with TFE3 gene fusions: a sensitive and specific immunohistochemical assay. Am J Surg Pathol 27:750–761
4. Argani P, Lui MY, Couturier J, Bouvier R, Fournet JC, Ladanyi M (2003) A novel CLTC–TFE3 gene fusion in pediatric renal adenocarcinoma with t(X;17)(p11.2;q23). Oncogene 22:5374–5378
5. Argani P, Ladanyi M (2004) Renal cell carcinomas associated with Xp11.2 translocations/TFE3 gene fusions. In: Eble JN, Sauter G, Epstein JI, Sesterhenn I (ed) WHO Classification of Tumours: pathology and genetics of tumours of the urinary system and male genital organs. IARC, Lyon, pp 37–38
6. Bruder E, Passera O, Harms D, Leuschner I, Ladanyi M, Argani P, Eble JN, Struckmann K, Schraml P, Moch H (2004) Morphologic and molecular characterization of renal cell carcinoma in children and young adults. Am J Surg Pathol 28:1117–1132
7. Clark J, Lu YJ, Sidhar SK, Parker C, Gill S, Smedley D, Hamoudi R, Linehan WM, Shipley J, Cooper CS (1997) Fusion of splicing factor genes PSF and NonO (p54nrb) to the TFE3 gene in papillary renal cell carcinoma. Oncogene 15:2233–2239
8. Cook A, Lorenzo AJ, Salle JL, Bakhshi M, Cartwright LM, Bagi D, Farhat W, Khoury A (2006) Pediatric renal cell carcinoma: single institution 25-year case series and initial experience with partial nephrectomy. J Urol 175:1456–1460
9. Sorensen PH, Lynch JC, Qualman SJ, Triabosco R, Lim JF, Maurer HM, Bridge JA, Crist WM, Triche TJ, Barr FG (2002) PAX3–FKHR and PAX7–FKHR gene fusions are prognostic indicators in alveolar rhabdomyosarcoma: a report from the Children's Oncology Group. J Clin Oncol 20:2672–2679
10. Weterman MA, Wilbrink M, Geurts van Kessel A (1996) Fusion of the transcription factor TFE3 gene to a novel gene, PRCC, in t(X;1)(p11;q21)-positive papillary renal cell carcinomas. Proc Natl Acad Sci USA 93:15294–15298
11. Zambrano E, Reyes-Mugica M (2003) Renal cell carcinoma with t(X;17): singular pediatric neoplasm with specific phenotype/genotype features. Pediatr Dev Pathol 6:84–87

Virchows Arch (2007) 450:221–223
DOI 10.1007/s00428-006-0339-6

CASE REPORT

Sclerosing hemangioma with florid endobronchial and endobronchiolar growth

Yoji Wani · Kenji Notohara · Choutatsu Tsukayama · Norihito Okumura

Received: 5 September 2006 / Accepted: 23 October 2006 / Published online: 22 November 2006
© Springer-Verlag 2006

Abstract Sclerosing hemangioma (SH) with endobronchial growth (SH-EG) is an extremely unusual form of SH. A case of SH-EG in a 47-year-old female is described. She suffered from a productive cough for 4 months. A chest CT scan revealed a well-circumscribed, parenchymal mass with endobronchial lesions continuously extending to the right main bronchus. Right upper sleeve lobectomy was carried out. The tumor was 4.8×3.5 cm in size, tan-brown, and elastically soft. It was located in the pulmonary parenchyma of the right upper lobe and continuously extended to the right upper bronchus. Furthermore, the main tumor also spread into segmental bronchi and peripheral bronchioles. Microscopically, the tumor consisted of round to cuboidal cells with papillary and solid patterns, partly showing sclerosis and hemorrhage. For 2.5 years after surgery, the patient has been well without recurrence or metastasis. Florid intrabronchial extension as seen in this case has never been documented in SH. To form an endobronchial component, it seems to be crucial that the parenchymal SH is located adjacent to the bronchus and involves it, followed by the destruction of the bronchial cartilage.

Y. Wani (✉) · K. Notohara · C. Tsukayama
Department of Pathology, Kurashiki Central Hospital,
1-1-1 Miwa,
Kurashiki 710-8602, Japan
e-mail: yw7144@kchnet.or.jp

N. Okumura
Department of Thoracic Surgery, Kurashiki Central Hospital,
Kurashiki, Japan

Keywords Sclerosing hemangioma · Endobronchial growth · Histopathology · Immunohistochemistry

Introduction

Sclerosing hemangioma (SH) is a female-predominant lung tumor with a distinctive constellation of histologic findings, including solid, papillary, sclerotic, and hemorrhagic patterns [1]. Hyperplastic type II pneumocytes line the surface of the papillary structures and bland round cells growth in the interstitium. SH presents as a well-circumscribed mass in the pulmonary parenchyma, but rarely reveals endobronchial growth. The frequency of SH with endobronchial growth (SH-EG) is only 1 in 100 cases, according to a large study [2]. As far as we know, only three cases of SH-EG were previously described in the English literature [2, 3]. In this report, we describe a case of SH-EG with florid endobronchial and endobronchiolar growth toward both central and peripheral portion.

Case report

A 47-year-old female with no history of smoking presented with a productive cough that had persisted for 4 months. A chest CT scan revealed a well-circumscribed, parenchymal mass with endobronchial lesions continuously extending to the right main bronchus. The peripheral upper lobe showed plate-like atelectasis. A transbronchial fiber optic scope revealed a polypoid mass in the right main bronchus. The bronchoscopic biopsy specimen was diagnosed as being

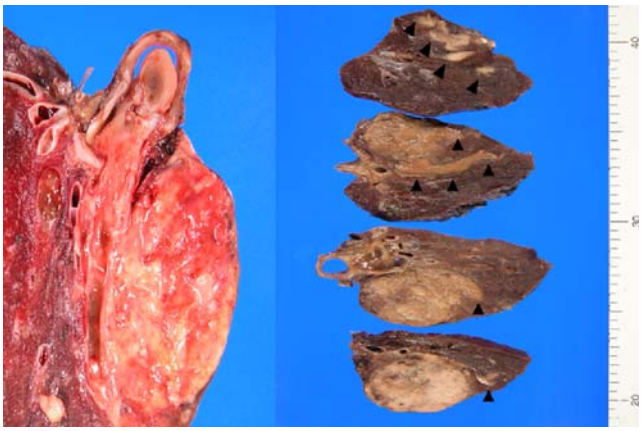

Fig. 1 Cut section showing the main parenchymal tumor with the main bronchial polyp (*left side*) and the extensive intraluminal growth from segmental bronchi to peripheral bronchioli (*right side arrow heads*)

suggestive of malignancy. Right upper sleeve lobectomy, bronchoplasty, and dissection of the lymph nodes were then carried out. For 2.5 years after surgery, the patient has been well without recurrence or metastasis.

Materials and methods

Formalin-fixed paraffin-embedded tissue sections were stained with hematoxylin and eosin for routine examination. Immunohistochemical staining was done with the Envision Plus detection system (DAKO, Japan). Antibodies for cytokeratin AE1/AE3 (Novocastra, UK), cytokeratin 7 (CK7) (DAKO), epithelial membrane antigen (EMA) (DAKO), thyroid transcription factor-1 (TTF-1) (DAKO) estrogen receptor (ER) (Novocastra), progesterone receptor (PR) (Novocastra), CD31 (DAKO), chromogranin A (Novocastra), synaptophysin (DAKO), and thyroglobulin (DAKO) were used.

Pathological findings

Macroscopically, the tumor was 4.8×3.5 cm in size, tan-brown, and elastically soft. It was located in the pulmonary parenchyma of the right upper lobe and continuously extended to the right upper bronchus (Fig. 1). Furthermore, the main tumor also spread into segmental bronchi and peripheral bronchioles.

Microscopically, the tumor consisted of round to cuboidal cells with papillary and solid patterns, partly showing sclerosis and hemorrhage (Fig. 2a). The round epithelioid cells were uniform and bland, with fine chromatin and indistinct nucleoli. Cuboidal surface cells were lining complex papillae, partly with clear cells and multinucleated giant cells. Neither numerous mitotic figures nor atypical mitosis were observed. Foci of cholesterol clefts and aggregation of foamy histiocytes were also seen in the air spaces. The tumor extended to the bronchial lumen, where it was lined by squamous metaplastic epithelium (Fig. 2b), although at the tip of the polyp the epithelium was eroded. At the base of the polyp, tumor cells protruded into the bronchial lumen with destruction of the bronchial cartilage (Fig. 2c). In addition, the tumor extended from middle-sized bronchi to terminal bronchioles

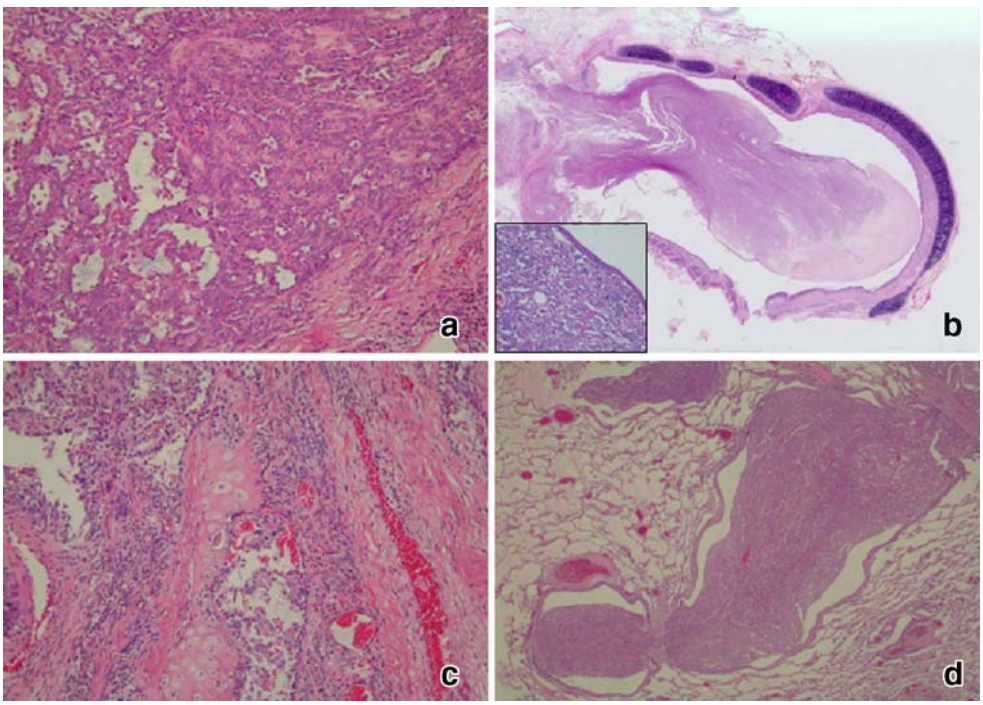

Fig. 2 **a** SH showing papillary growth with sclerosis. (Hematoxylin–eosin, original magnification ×200) **b** Main bronchial polyp covered by a fibrinous cap. Combined overlying metaplastic squamous epithelium and tumor cells are reminiscent of the cutaneous pyogenic granuloma (*inset*). (Hematoxylin–eosin, original magnification ×6.25, inset ×200) **c** SH showing destruction of the bronchial cartilage. (Hematoxylin–eosin, original magnification ×200) **d** SH extending into the peripheral bronchiole and attaching to the wall with minimal destruction.(Hematoxylin–eosin, original magnification ×20)

through airways without any prominent destruction of alveolar structures (Fig. 2d).

Immunohistochemically, both round and surface tumor cells expressed EMA and TTF-1, while expression of cytokeratins (AE1/AE3 and CK7) was limited to the surface cells. Some of the round cells showed expression of PR. ER, CD31, chromogranin A, synaptophysin, and thyroglobulin were negative.

Discussion

Only three cases of SH-EG have ever been reported [2, 3]. In the first case, the tumor, although the data are limited, presented as a peripheral nodule adjacent to the bronchus and extended to the bronchial lumen [2]. The second case was a 5-cm solid, well-circumscribed nodule with an endobronchial polypoid mass 5 mm in size [3]. The third case presented a polypoid mass 2 cm in diameter, which protruded into the left lower bronchial lumen [3]. This mass extended into the lung parenchyma, forming a 1-cm, solid, well-circumscribed nodule. But our case is unique, having an extensive intraluminal growth from the main mass to the right main bronchus and to the peripheral bronchi or bronchioles. Such a form of tumor extension has never been documented in SH. This is the reason why a few cases of SH grow in the bronchial airway remains unknown. There is fundamentally no histological difference between parenchymal and endobronchial components. Judging from the previous and present cases, to form an endobronchial component, it seems to be crucial that the parenchymal SH is located adjacent to a relatively central portion of the bronchus and involves it, followed by the destruction of the bronchial cartilage.

In spite of such unusually extensive and destructive growth, the prognosis is good. All reported patients remain well and are living without signs of disease.

SH-EG may be mistaken for other tumors histologically, particularly on bronchial biopsy. The differential diagnosis includes typical carcinoid (TC), low-grade mucoepidermoid carcinoma, papillary adenoma [4], metastatic carcinoma (in particular, papillary carcinoma of the thyroid [5]), pulmonary adenocarcinoma [6], and hemangioma [7]. The round and well-circumscribed appearance at bronchoscopy—similar to carcinoid—would be atypical for carcinoma. Bland cytology such as less nuclear atypia and scant mitosis favors a diagnosis of SH rather than carcinoma. Careful search may reveal typical dual cell populations of SH. Moreover, the peculiar immunophenotype of the round cells (CK−, EMA+, TTF-1+, and sometimes PR+) can be helpful for the diagnosis. Regarding TC, it would also be ruled out by no expression of neuroendocrine markers such as chromogranin A and synaptophysin. Florid endobronchial extension tends to lead to a wide excision in contrast to peripheral SH. But because SH itself is a benign tumor, accurate diagnosis may allow us to avoid unnecessarily excessive surgery.

In summary, we have reported an unusual SH that showed extensive intraluminal growth from the main mass to the right main bronchus and to the peripheral bronchioles.

References

1. Devouassoux-Shisheboran M, Nicholson AG, Leslie K, Niho S (2004) Sclerosing hemangioma. In: Travis WD, Brambilla E, Muller-Hermelink HK, Harris CC (eds) World Health Organization of Tumours. Tumours of the lung, pleura, thymus and heart. IARC, Lyon, pp 115–117
2. Devouassoux-Shisheboran M, Hayashi T, Linnoila RI, Koss MN, Travis WD (2000) A clinicopathologic study of 100 cases of pulmonary sclerosing hemangioma with immunohistochemical studies. Am J Surg Pathol 24:906–916
3. Devouassoux-Shisheboran M, Fouchardière A, Thivolet-Bèjui F, Sourisseau-Millan, Guerin JC, Travis WD (2004) Endobronchial variant of sclerosing hemangioma of the lung: histological and cytological features on endobronchial material. Mod Pathol 17:252–257
4. Flieder DB (2004) Papillary adenoma. In: Travis WD, Brambilla E, Muller-Hermelink HK, Harris CC (eds) World Health Organization of Tumours. Tumours of the lung, pleura, thymus and heart. IARC, Lyon, pp 84
5. Takata T, Koyanagi K, Uchida S, Ohta Y, Sakakibara N, Miyamoto Y (1989) A case of lung metastasis of thyroid cancer with endobronchial polypoid growth. Gan No Rinsho 35:840–844
6. Kodama T, Watanabe S, Shimosato Y, Yoneyama T, Koide T (1984) Endobronchial polypoid adenocarcinoma of the lung. Histological and ultrastructural studies of five cases. Am J Surg Pathol 8:845–854
7. Park GY, Lee KY, Yoo CG, Kim YW, Han SK, Shim YS (1999) Bronchoscopic findings of endobronchial vascular lesions in patients with haemoptysis. Respirology 4:401–404

Virchows Arch (2007) 450:225–229
DOI 10.1007/s00428-006-0353-8

CASE REPORT

Hepatocellular carcinoma arising from ectopic liver tissue in the pancreas

Diana Cardona · Stephen Grobmyer · James M. Crawford · Chen Liu

Received: 20 July 2006 / Revised: 3 November 2006 / Accepted: 12 November 2006 / Published online: 10 January 2007
© Springer-Verlag 2007

Abstract Liver tissue ectopia is a well-documented phenomenon. Rarely, hepatocellular carcinoma arises from the ectopic liver tissue. In this paper, we report a case of a primary, well-differentiated hepatocellular carcinoma arising from ectopic liver tissue in the pancreas. The patient is a 58-year-old Hispanic man with no history of underlying liver diseases or chronic pancreatic diseases. Patient presented with a several days history of abdominal pain with radiation to his right upper quadrant. Imaging study revealed a 3.7×3.3-cm mass in the distal pancreas. No other lesions were identified. Preoperative fine needle aspiration revealed blood and atypical hepatocytes. The patient underwent distal pancreatectomy and splenectomy for suspected neuroendocrine tumor. Gross examination revealed a well-circumscribed 3.3-cm, beige-tan, pseudolobulated tumor with focal areas of hyperpigmentation. A microscopic examination revealed hepatoid cells arranged in a trabecular pattern with focal bile pigment. Immunohistochemistry study showed that the tumor cells were reactive with hepatocyte antigen (Hep par 1), alpha-1 antitrypsin, but negative for synaptophysin and chromogranin. Immunostain for polyclonal carcinoembryonic antigen showed a typical bile canalicular pattern. These results support that this tumor in the pancreas is hepatocellular carcinoma, most likely arising from ectopic liver tissue within the pancreas.

Keywords HCC · Hepatocellular carcinoma · Ectopic liver

D. Cardona · J. M. Crawford · C. Liu (✉)
Department of Pathology, Immunology, and Laboratory Medicine,
University of Florida College of Medicine,
1600 SW Archer Road,
Gainesville, FL 32610, USA
e-mail: liu@pathology.ufl.edu

S. Grobmyer
Department of Surgery, University of Florida
College of Medicine,
1600 SW Archer Road,
Gainesville, FL 32610, USA

Introduction

Ectopic liver tissue can occur in various locations such as gallbladder, hepatic ligaments, omentum, retroperitoneum and thorax. The diagnosis is typically made incidentally. These lesions often are clinically silent but on rare occasion cause clinical problems such as compression, pain, or bleeding. Ectopic liver tissue can also demonstrate similar diseases that affect the mother liver such as cirrhosis. Out of approximately 100 cases of ectopic liver reported, hepatocellular carcinoma (HCC) was detected in 28 of them [1, 3, 7–9]. These foci of ectopic liver tissue appear to be at an increased risk of undergoing carcinogenesis, for which the underlying mechanism is still not known. Interestingly, the propensity of these tissues to undergo malignant transformation seems to be unrelated to diseases within the mother liver or the presence of viral hepatitis or cirrhosis within the ectopic focus. In the 28 cases of HCC, only 6 had coexistent liver cirrhosis [1]. Several authors postulate that the abnormal arterial supply or venous and biliary drainage within these ectopic foci may increase the tissue's exposure to various carcinogens, thus leading to malignancy [1, 3, 8]. The case we present is HCC arising in ectopic liver tissue in the pancreas, which is the first case reported in the pancreas.

Clinical history

The patient was a 58-year-old obese Hispanic man who presented to the Surgical Oncology Clinic with a history of dull back and flank pain. Before this, he denied any previous episodes of similar abdominal pain, pancreatitis, or liver problems. He denied any jaundice, icterus, nausea, vomiting, or weight loss. His past medical history was significant for diabetes mellitus type 2 and osteoarthritis. The patient reported a 40-pack-year history of smoking and heavy alcohol use. He reportedly had 3–4 drinks per week. Medications include regular use of tramadol, insulin, wellbutrin and hydrocodone. A computed tomography (CT) scan of his abdomen obtained at presentation revealed a 3.7×3.3-cm hyperattenuated lesion within the distal body of the pancreas (Fig. 1a). The pancreas did not demonstrate atrophic changes or pancreatic duct dilation. In addition, no hepatic lesions were identified. Further evaluation included endoscopic ultrasound fine needle aspiration (FNA) of the mass. The aspirate demonstrated blood with groups of reactive hepatocytes with fatty change and was considered unsatisfactory for evaluation secondary to not being representative of the anatomic site (Fig. 1b). The patient was then referred to our institution for surgical intervention. Based on the CT scan appearance, the initial clinical suspicion was of a neuroendocrine tumor. At laparotomy, there was no evidence ascites or of liver disease or metastatic lesions elsewhere. Intraoperative biopsies of the liver were not clinically indicated. The firm mass was palpated in the distal body of the pancreas, and a distal pancreatectomy and splenectomy were performed. The patient is currently alive and without evidence of disease 15 months postoperatively. Follow-up imaging studies have demonstrated no evidence of recurrent disease, and his alpha-fetoprotein (AFP) serum levels have remained in normal range.

Materials and methods

Tissue specimens

The tumor and normal pancreatic tissues were fixed in 10% buffered formalin. Representative tissue sections were collected and then routinely processed. Five micron sections were cut from each paraffin block and stained with hematoxylin and eosin for microscopic examination.

Immunohistochemistry

Immunohistochemistry was performed using the avidin–biotin complex/peroxidase method with antibodies directed against Hep par 1 (monoclonal mouse antihuman hepatocyte, clone CCH1E5; DakoCytomation), polyclonal carcinoembryonic antigen (rabbit antihuman CEA; Dako), alpha-1-antitrypsin (rabbit antihuman A1AT; Dako), cytokeratin 19 (monoclonal mouse antihuman CK19, clone RCK 108; Dako), chromogranin (rabbit antihuman chromogranin A; Dako), and synaptophysin (rabbit antihuman synaptophysin; Dako).

Results

Morphology

On gross examination, the 3.3×2.5×2.5-cm beige-tan mass appeared well-circumscribed with a pseudolobulated appearance and focal areas of hyperpigmentation. The thin fibrous capsule had an average width of 0.1 cm. The remaining pancreatic parenchyma and spleen were grossly unremarkable (Fig. 2a).

A microscopic evaluation demonstrated that the tumor was entirely composed of uniform hepatoid cells arranged

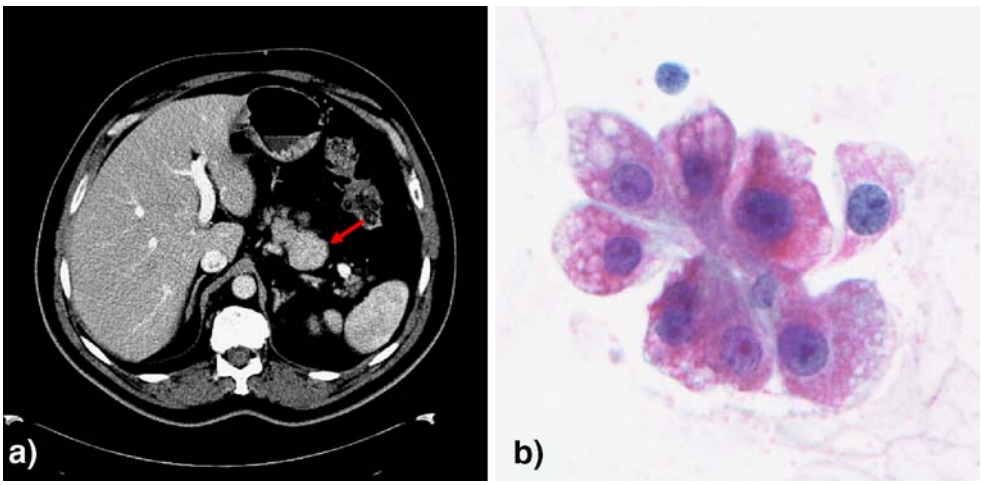

Fig. 1 **a** CT scan of the abdomen. A hyperdensity mass is noted in the distal portion of the pancreas (*arrow*). The liver, spleen, and pancreas show no significant abnormality. **b** CT-guided fine needle aspirate preparation exhibits clusters of cell similar to hepatocytes

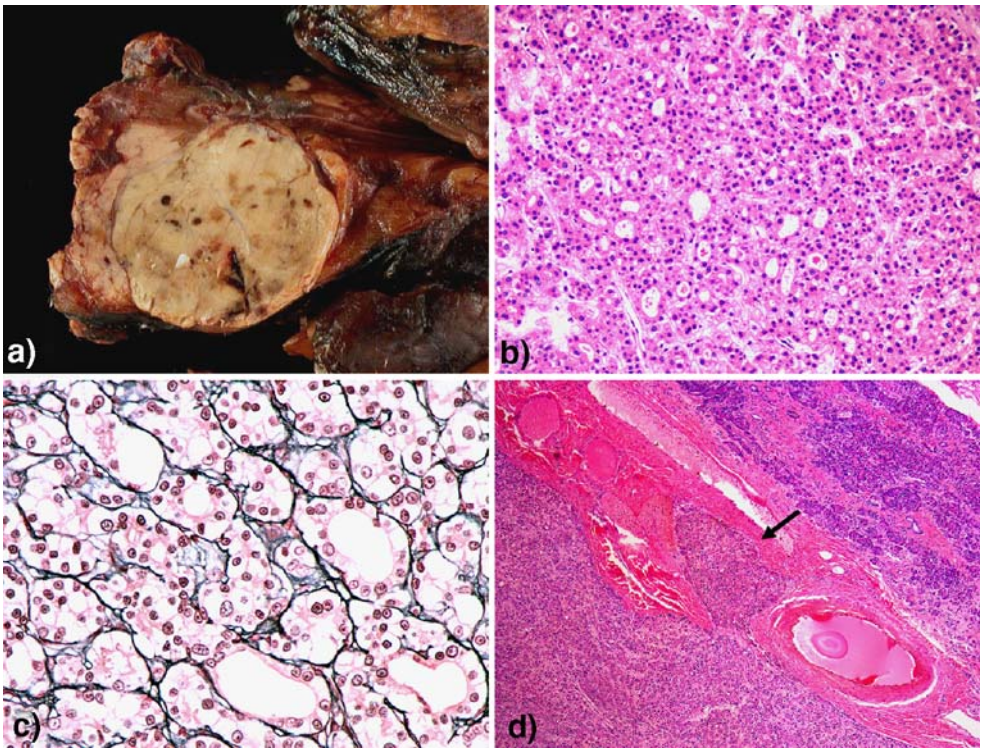

Fig. 2 Pathologic features of the tumor. **a** Gross photograph of the tumor in the distal pancreas. The tumor is solid with lobulated appearance. **b** and **c** Microscopic morphology of the tumor demonstrating both pseudoacinar and trabecular growth patterns, highlighted by the reticulin stain. **d** The tumor was predominantly well circumscribed with a thin capsule; however, a focus of capsular invasion was identified (*arrow*)

in a trabecular pattern with intervening vasculature (Fig. 2b). The reticulin stain highlighted the trabecular pattern with thickened cell plates and the occasional pseudoglandular configuration (Fig. 2c). Some areas showed small cell change, hyperchromasia, and rare mitotic activity. A few cells exhibited yellowish brown pigment, suggestive of bile. An area suspicious for invasion into the capsule was identified (Fig. 2d). The cells in the tumor were similar to the cells in the preoperative FNA cytology specimen.

Immunohistochemical profile

Based on the location and the morphology of the tumor, neuroendocrine tumor was considered as a key differential diagnosis. We therefore performed immunohistochemical staining. The result showed that the tumor cells were negative for synaptophysin and chromogranin, which essentially ruled out neuroendocrine cell tumor. Because the tumor exhibited a trabecular pattern and bile pigment similar to HCC, Hep par 1, A1AT, CK19, AFP immuno-

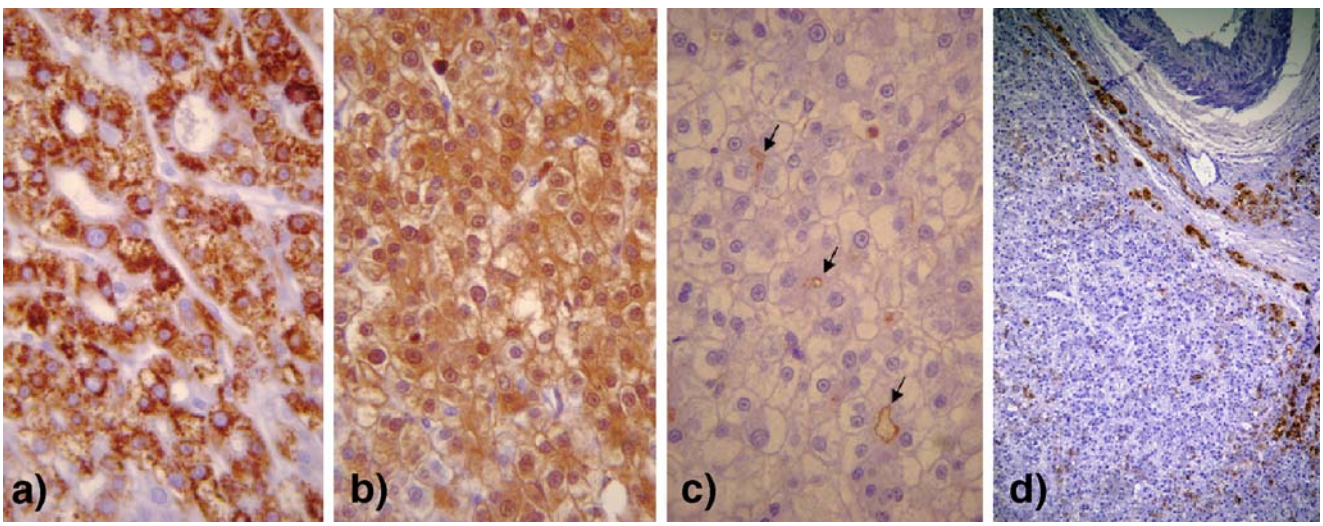

Fig. 3 Immunohistochemistry of the tumor. **a** Immunostain with anti-Hep par 1 antibody; **b** Immunostain with anti-A1AT antibody; **c** Immunostain with anti-polyclonal CEA antibody shows the bile canalicular pattern. **d** Immunostain with CK19 demonstrated remnant bile ductules

histochemistry was performed. The tumor was strongly reactive for Hep par 1 and A1AT but negative for AFP. Polyclonal CEA stain shows bile canalicular pattern. CK19 was focally positive, highlighting remnant bile ductules (Fig. 3). Based on the morphologic appearance of the tumor, loss of normal architecture, thickened cell plates (>3 cells) in a predominantly trabecular pattern and focal infiltrative border, and the molecular marker expression described above, the final diagnosis was well-differentiated HCC arising from ectopic liver tissue within the pancreas.

Discussion

Ectopic livers are defined as islands of normal liver tissue that are not connected to the mother liver. Pedunculated liver tissue is often considered 'ectopic liver' due to the lack of blood, bile, and lymph drainage through the normal liver outflow track. Instead, it drains through an accessory network [1]. Ectopic liver is a rare phenomenon that is usually discovered incidentally at autopsy or laparoscopy. There are approximately 100 reported cases within the gallbladder, hepatic ligament, diaphragm, thorax, retroperitoneum, and omentum. The reported incidence of ectopic or accessory livers ranges from 0.47 to 0.7% with the gallbladder being the most common location [2, 8, 11].

Reviewing embryologic hepatogenesis can help explain the wide range of ectopic liver locations. Normally, the liver forms from an outgrowth of the endodermal caudal foregut and projects into the septum transversum, which is adjacent to the ventral pancreatic bud. This endodermal projection differentiates into the pars hepatica (future liver) and pars cystica (future gallbladder and cystic duct). Solid cords of hepatic cells are sent out from the pars hepatica into the adjacent mesenchyme forming blood sinusoids. The portal triad is complete when the bile canaliculi grow into the liver from the pars cystica. The septum transversum also plays a role in the development of the surrounding connective tissue, diaphragm, and ligaments [4, 10]. Based on this brief review, early or late developmental anomalies of hepatogenesis could explain the broad variety of liver tissue ectopy. One could also theorize that pluripotent endoderm could produce liver tissue de novo elsewhere [4, 5].

More than 100 cases of ectopic liver tissue have been reported. HCC was detected in 28 of those cases. In all of those cases, the mother liver did not have HCC [1, 3, 7–9]. Most cases were reported in patients of Asian decent. There are only a few described in whites. Typically, these patients are men more than the age of 50. However, the youngest case reported was in a 34-year-old woman [8]. The case we presented here is HCC arising in ectopic liver in a 58-year-old white man. This case is unique in that it is the first case of HCC described in pancreatic ectopic liver tissue.

Ectopic liver tissue has an increased propensity of undergoing hepatocarcinogenesis. No obvious insult or strong association with common risk factors has been identified that induce this malignant transformation. In the cases reported in the literature, cirrhosis was identified in only 6 of the 29 cases of HCC reported (including ours) [1, 3, 7–9]. Unfortunately, serologic testing for hepatitis B or C is not available for a majority of reported cases. However, out of 22 cases reported by Arakawa et al. [1], only one patient demonstrated positive hepatitis C markers. These findings indicate that the ectopic liver foci can develop HCC before or in the absence of cirrhosis (a precancerous state), similar to patients with Aflatoxin-B1 exposure [6]. Carcinogenesis is a multistep process that appears to be accelerated within these tissues. It is theorized that due to the lack of normal vascular and ductal systems, the foci of ectopic liver tissue may be metabolically handicapped, leading to longer exposure to various carcinogenic factors [1, 3, 4, 8]. The underlying microenvironment would cause persistent cellular stress, which may result in cell death and compensatory cell proliferation. An increased cell turnover may lead to genetic mutations and subsequent development of carcinoma.

There are four reports with long-term follow-up, in which it appears that surgery is curative. Two out of the four patients were free of disease 4 years postoperatively. In one case, the patient experienced several abdominal recurrences and multifocal liver lesions [8]. In the fourth case, the lesion was originally considered a metastasis, despite the lack of a primary liver lesion. Fortunately, 2 years after the original diagnosis, the lesion was stable and resection was performed [3]. It appears that total resection may portend a good prognosis.

Acknowledgment Special thanks to Mr. Robin Foss, PA, and Ms. Elaine Dooley, MT, for their technical expertise.

References

1. Arakawa W, Kimura Y, Sakata K, Kubo Y, Fukishima T, Okunda K (1999) Propensity of ectopic liver to hepatocarcinogenesis: case reports and a review of the literature. Hepatology 29:57–61
2. Asada J, Onji S, Yamashita Y, Okada S, Morino M, Kanoaka M, Ohta Y (1982) Ectopic liver observed by peritoneoscopy: report of a case. Gastroenterol Endosc 24:309–312
3. Asselah T, Condat B, Cazals-Hatem D, Hassani Z, Bernuau J, Groussard O, Mussot S, Leseche G, Marcellin P, Erlinger S, Valla D (2001) Ectopic hepatocellular carcinoma arising in the left chest wall: a long term follow-up. Eur J Gastroenterol Hepatol 13:873–875
4. Caygill C, Gatenby P (2004) Ectopic liver and hepatocarcinogenesis. Eur J Gastroenterol Hepatol 16:727–729

5. Collan Y, Hakkiluoto A, Hastbacka J (1978) Ectopic liver. Ann Chir Gynaecol 67:27–29
6. Farazi P, DePinho R (2006) Hepatocellular carcinoma pathogenesis: from genes to environment. Nat Rev Cancer 6(9):674–687
7. Kim KA, Park CM, Kim CH, Choi SY, Park SW, Hong SJ, Seol HY, Cha IH (2003) Hepatocellular carcinoma in an ectopic liver: CT findings. Eur Radiol 13:L45–L47
8. Le Bail B, Carles J, Saric J, Balabaud C and Bioulac-Sage P (1990) Ectopic liver and hepatocarcinogenesis. Hepatology 30:585–586
9. Leone N, De Paolis P, Carrera M, Carucci P, Musso A, David E, Brunello F, Fronda G, Rizzetto M (2004) Ectopic liver and hepatocarcinogenesis: report of three cases with four years' follow-up. Eur J Gastroenterol Hepatol 16:731–735
10. Sadler TW (2000) Langman's Medical Embryology, 8th edn. Lippincott Williams and Wilkins, Philadelphia, pp 283–285
11. Sato S, Watanabe M, Nagasawa S, Niigaki M, Sakai S, Akagi S (1998) Laparoscopic observations of congenital anomalies of the liver. Gastrointest Endosc 47(2):136–140

Virchows Arch (2007) 450:231–233
DOI 10.1007/s00428-006-0321-3

LETTER TO THE EDITOR

So-called infantile haemangiopericytoma of the kidney

Françoise Boman · Pierre Leblond · Sophie Taieb · Frédérique Dijoud · Raymonde Bouvier

Received: 19 July 2006 / Accepted: 21 September 2006 / Published online: 17 November 2006
© Springer-Verlag 2006

Dear Editor,

Infantile myofibroma (myofibromatosis) may occur at visceral locations including the kidney [2], and haemangiopericytomas, as well as solitary fibrous tumours, are described as rare primary renal neoplasms [5]. These tumour types may be misdiagnosed as sarcomas, specifically clear cell sarcoma of the kidney, which is a high-risk malignant paediatric tumour.

A 2-month-old boy presented with a well-circumscribed, encapsulated, centrally necrotic, and calcified 7 cm in diameter tumour of the right kidney (Fig. 1). Histologically, tumour tissue was densely cellular and made of tightly packed, elongated polygonal cells with a striking, quasi-exclusive haemangiopericytic vascular pattern (Fig. 2a). The nuclei were oval with finely distributed chromatin and occasional small nucleoli (Fig. 2b). There were 16 mitotic figures in ten high-power fields and no abnormal mitotic figure. Some spindle cells with more eosinophilic cytoplasm (<1% of tumour tissue) were focally present in the peripheral parts of the tumour and, very scarcely, at some distance from the fibrous capsule, which circumscribed the tumour. Immunohistochemically, tumour cells were positive for CD34 (Fig. 2c), vimentin, and MIB1 (Ki67 index, 14%); they were negative for CD99, Bcl2, pan-actin HHF-35, smooth muscle actin, desmin, myogenin, cytokeratin KL1, cytokeratin AE1/3, epithelial membrane antigen, CD10, CD56, chromogranin A, synaptophysin, S100 protein, CD117, ALK, and E-cadherin. No ETV6/NTRK3 transcript could be demonstrated by reverse transcriptase polymerase chain reaction (RT-PCR), which was performed twice with appropriate controls.

A retrospective study of 13 specimens of spindle cell paediatric renal tumours using the same primary antibodies was performed. Specimens included three clear cell sarcomas of the kidney, two stromal and four blastematous predominant nephroblastomas, two classical or mixed mesoblastic nephromas, and two metanephric stromal tumours. All tumours contained numerous vessels that expressed CD34. Clear cell sarcomas expressed vimentin and varied in their expression of Bcl2, CD56, and CD117. Nephroblastomas varied in their expression of mesenchymatous and epithelial markers, Bcl2, and CD56. Mesoblastic nephromas expressed vimentin and smooth muscle actin. Metanephric stromal tumours expressed vimentin (two of two cases) and CD117 (one case). The percentage of tumour nuclei immunoreactive for MIB1 varied from 3% (in a metanephric stromal tumour) to 91% (in a blastematous predominant nephroblastoma). In the case reported here, the renal tumour displayed morphological and immunohistochemical features distinct from those of clear cell sarcoma and nephroblastoma. Immunoreactivity for epithelial markers

F. Boman (✉)
Department of Pathology, University Hospital of Lille,
Site Eurasanté, CHRU de Lille,
59037 Lille Cedex, France
e-mail: f-boman@chru-lille.fr

P. Leblond
Department of Paediatrics, Centre Oscar Lambret,
Lille, France

S. Taieb
Department of Radiology, Centre Oscar Lambret,
Lille, France

F. Dijoud
Department of Pathology, Hôpital Debrousse,
Lyon, France

R. Bouvier
Department of Pathology, Hôpital Edouard Herriot,
Lyon, France

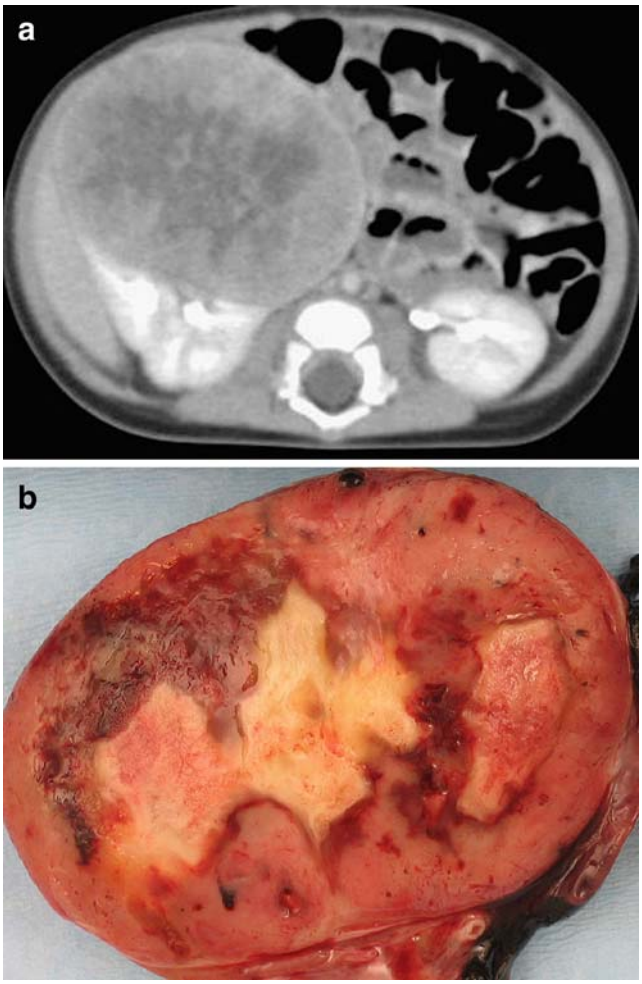

Fig. 1 **a** Computed tomography scan; **b** macroscopy of a well-circumscribed, encapsulated, centrally necrotic, and calcified 7 cm in diameter tumour of the right kidney

and fusion genes diagnostic for synovial sarcoma could not be demonstrated in this tumour. The age of the patient and histologic features raised the likelihood of congenital mesoblastic nephroma, but the ETV6-NTRK3 fusion gene characteristic of this tumour (and congenital/infantile fibrosarcoma) could not be demonstrated, and immunoreactivity for CD34 was inconsistent with this diagnosis. Metanephric stromal tumours most commonly present in infancy may display a number of architectural patterns including a haemangiopericytomatous pattern and, like an increasing number of tumours in various locations, is often immunoreactive for CD34 [1], but morphological features suggestive of this rare, benign tumour were not present.

The tumour reported here was most consistent with a very cellular infantile myofibroma(tosis) or an immature solitary fibrous tumour. Myofibroma and myofibromatosis are terms to denote the solitary (myofibroma) or multicentric (myofibromatosis) occurrence of benign neoplasms composed of contractile myoid cells arranged around thin-

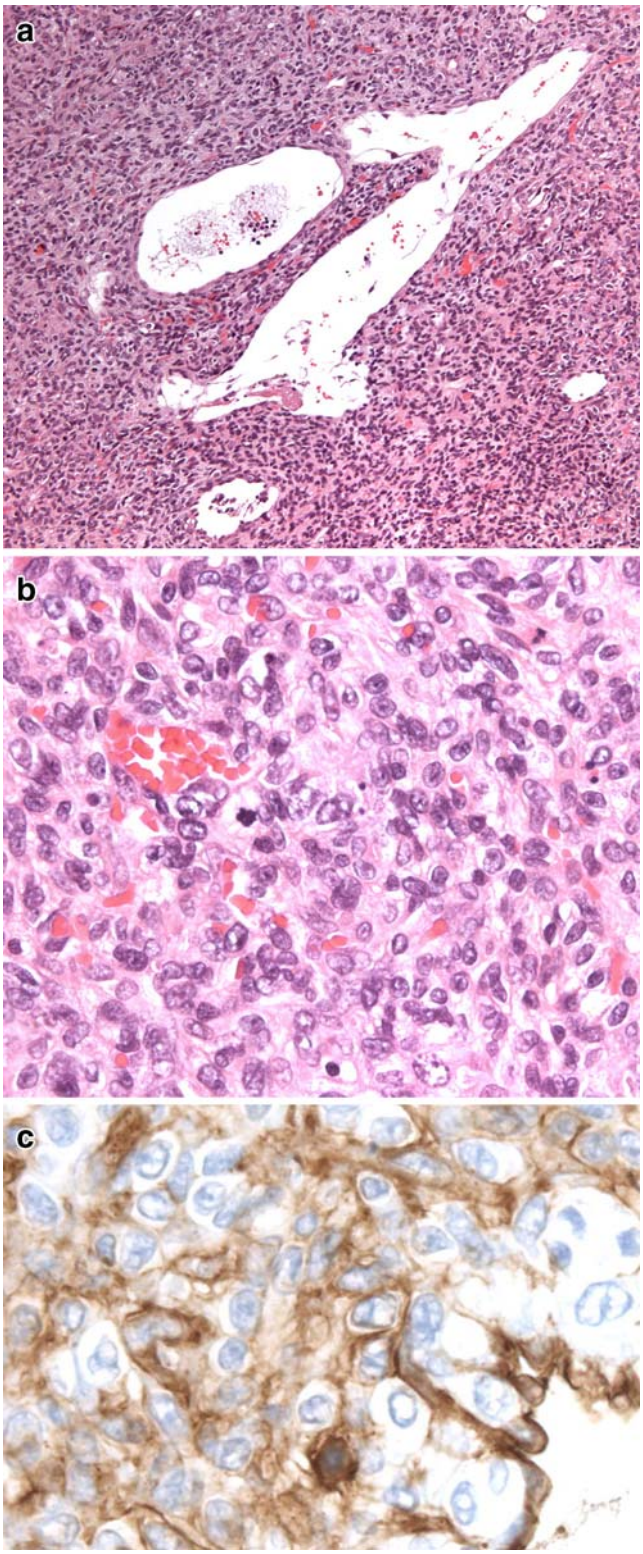

Fig. 2 **a** Low-power magnification showing a densely cellular proliferation with a striking haemangiopericytic vascular pattern. **b** At higher magnification, tightly packed elongated cells with oval nuclei, finely distributed chromatin, occasional small nucleoli, and scattered mitotic figures. **c** CD34 immunoreactivity of tumour cells and endothelial cells

walled blood vessels. Myofibroma(tosis) forms a morphological continuum with myopericytoma and the so-called infantile haemangiopericytoma. Most cases are described in infants. They often have central necrotic areas or cystic spaces. Histologically, they are characterized by multinodularity and zonation, a haemangiopericytoma-like component which can predominate, myofibroblastic cells, frequent presence of intravascular growth, and variable mitotic activity and necrosis. Both components are immunoreactive for vimentin and smooth muscle actin, whereas the myofibroblastic component is more strongly positive for pan-actin HHF-35 [2]. It has been suggested that most cases of the so-called infantile haemangiopericytoma are actually cases of myofibroma(tosis), and that haemangiopericytomas include fibrous-to-cellular solitary fibrous tumours [3, 4]. Solitary fibrous tumours are circumscribed but nonencapsulated. Histologically, bland spindle cells are arranged in various patterns including short storiform and a haemangiopericytoma-like vascular pattern. Cells are immunoreactive for CD34 and vimentin and variably reactive for actin, smooth muscle actin, and desmin. All solitary fibrous tumours primary to the kidney have behaved in a benign manner [5]. In the tumour reported here, a spindle cell component with eosinophilic cytoplasm, although very minor (<1%), and the absence of features seen in typical solitary fibrous tumour (alternating hypocellular and hypercellular areas and thick eosinophilic collagen bands) favoured the diagnosis of myofibroma versus solitary fibrous tumour. We concluded that the very unusual haemangiopericytoma-like renal tumour reported here was most probably a rare example of an immaturely appearing, smooth muscle-actin-negative and CD34-positive solitary infantile myofibroma of the kidney, most importantly presumably benign, although related to solitary fibrous tumours with worrying features such as high cellularity, mitotic activity, and necrosis. The lesion was completely excised, and no post-operative treatment was given. Its course was uneventful (at 7-month follow-up).

Acknowledgments We thank Olivier Delattre for performing RT-PCR studies and Elizabeth Perlman, Cheryl Coffin, and Jean-Michel Coindre for reviewing the slides.

References

1. Argani P, Beckwith B (2000) Metanephric stromal tumor: report of 31 cases of a distinctive pediatric renal neoplasm. Am J Surg Pathol 24:917–926
2. Fletcher CDM, Unni KK, Mertens F (eds) (2002) Pathology and genetics of tumours of soft tissue and bone. World Health Organization Classification of Tumours. IARC, Lyon
3. Gengler C, Guillou L (2006) Solitary fibrous tumour and haemangiopericytoma: evolution of a concept. Histopathology 48:63–74
4. Mentzel T, Calonje E, Nascimento AG, Fletcher CD (1994) Infantile hemangiopericytoma versus infantile myofibromatosis. Study of a series suggesting a continuous spectrum of infantile myofibroblastic lesions. Am J Surg Pathol 18:922–930
5. Murphy WM, Grignon DJ, Perlman EJ (eds) (2004) Tumors of the kidney, bladder, and related urinary structures. AFIP Atlas of Tumor Pathology, series 4. American Registry of Pathology, Washington, DC

Virchows Arch (2007) 450:235–237
DOI 10.1007/s00428-006-0322-2

LETTER TO THE EDITOR

Primary intravascular myxoid leiomyosarcoma of the femoral vein presenting clinically as deep vein thrombosis: a case report

Manish Mani Subramaniam · Miguel Martinez-Rodriguez · Samuel Navarro · Jorge Guijarro Rosaleny · Antonio Llombart Bosch

Received: 12 August 2006 / Accepted: 1 October 2006 / Published online: 16 November 2006
© Springer-Verlag 2006

Sir:

Primary venous leiomyosarcomas of the extremities involving the common femoral vein and superficial femoral vein are rare and are described in the literature mostly in the form of single case reports or small series [3]. Clinically, vascular leiomyosarcomas of the lower extremities may present with features of deep vein thrombosis, thereby causing delay in appropriate surgical intervention. Myxoid variants of leiomyosarcomas were originally described in the uterus [2], while they are extremely rare and underrecognized in soft tissues [4, 5]. We report here a case of intravascular myxoid leiomyosarcoma of the femoral vein, which we believe is the first reported case of myxoid leiomyosarcoma of venous origin in English literature, although previously, only one such case of arterial origin has been recorded.

A 29-year-old female patient was referred to the department of vascular surgery with complaints of right lower extremity swelling and calf tenderness of 1 month duration. The Doppler-ultrasound and CT scan of the right lower extremity were suggestive of deep vein thrombosis of the right common femoral and external iliac vein. Following an unsuccessful oral anticoagulant therapy for 3 months, she was rehospitalized for further investigations. On second admission, the arteriogram of the right femoral axis showed abnormal vascularization involving the superficial and deep femoral vein (Fig. 1a), while angio-CT scan (Fig. 1b) and magnetic resonance angiography (MRA) demonstrated an intraluminal space-occupying lesion in the right common femoral vein, upper one-third of the superficial femoral and extending into the right external iliac vein. Subsequently, complete resection of the tumor and the involved veins, venous bypass, and implantation of polytetrafluoroethylene grafts were performed.

The resected vascular segment measuring 18 cm in length with variable transverse diameters ranging from 2.3 to 3.8 cm showed a coarsely nodular solid intraluminal growth completely occluding the entire lumen acquiring the configuration of the vessel. Cut section revealed a yellow-white, pinkish-gray tumor with lobular architecture and a fleshy appearance. Focal areas of hemorrhagic necrosis and cystic degeneration were also seen. Microscopically, the tumor exhibited typical interlacing sweeping bundles of spindle-shaped cells with elongated, blunt-ended nuclei and eosinophilic fibrillary cytoplasm (Fig. 1d). Extensive foci of myxoid matrix tending to disperse the fascicular architecture accounting to >50% of examined tissue and focal necrosis were also noted (Fig. 1c). The cellular picture varied from areas exhibiting benign spindle cells to highly cellular foci showing nuclear pleomorphism, bizarre-shaped nuclei, and mitotic figures of 10/10 HPF (Fig. 1e). The tumor was scored as grade 2 according to the Federation Nationale des Centres de Lutte Contre le Cancer system.

Supported by a grant (PI-04/0822) from the Fondo de Investigaciones Sanitarias (Instituto Carlos-III, Madrid, Spain), Prognosis and therapeutic targets of Ewing's family of tumors FP6 contract number 503036, and a personal grant (Manish Mani Subramaniam) from the Hospital Clinic of University and the Spanish Association Against Cancer of Valencia, Spain.

M. M. Subramaniam · M. Martinez-Rodriguez · S. Navarro · A. L. Bosch (✉)
Department of Pathology, Medical School, University of Valencia,
Avda. Blasco Ibañez, 17,
46010 Valencia, Spain
e-mail: antonio.llombart@uv.es

J. G. Rosaleny
Department of Radiodiagnosis,
Hospital Clinic of University of Valencia,
Valencia, Spain

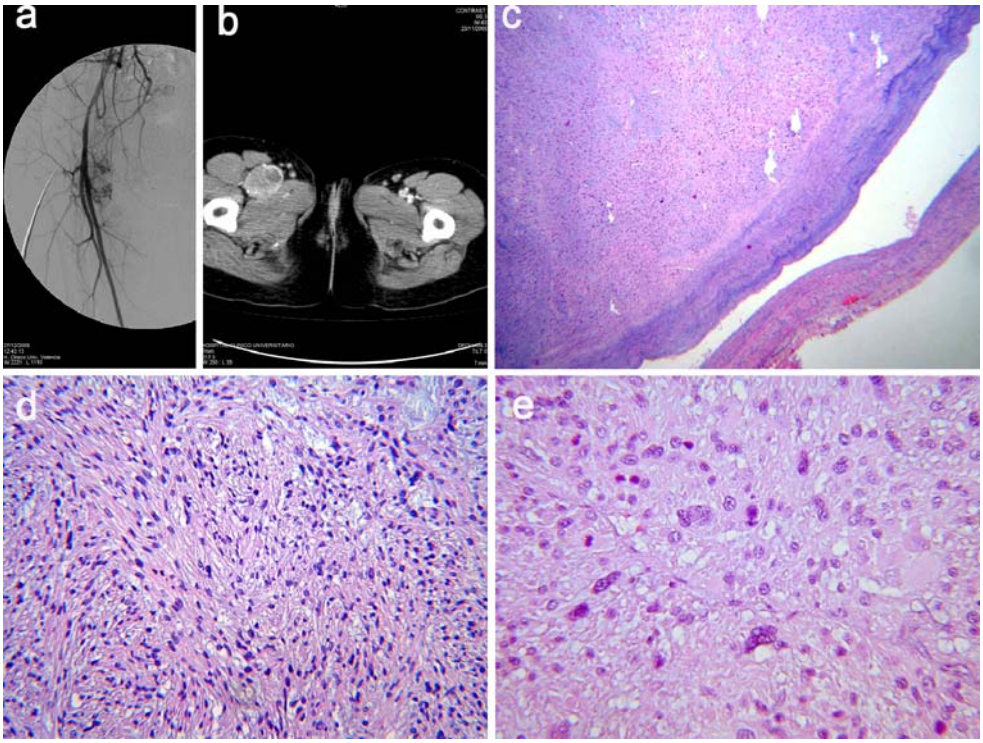

Fig. 1 **a** Arteriogram of the right femoral axis showing the formation of abnormal vascular network involving the superficial and deep femoral vein. **b** Angio-CT scan of the right femoral–iliac axis using intravenous contrast medium demonstrates an intraluminal tumor in the dilated right common femoral vein. **c** Low-power view shows an intraluminal tumor with extensive myxoid change arising from the vascular wall (hematoxylin–eosin, original magnification ×40). **d** The neoplasm revealed intersecting fascicles of spindle cells with elongated blunt-ended nuclei, perinuclear vacuolization and acidophilic fibrillary cytoplasm (original magnification ×200). **e** Higher magnification of the tumor exhibiting nuclear pleomorphism, bizarre anaplastic nuclei, and mitotic figures

Immunohistochemically, the tumor cells displayed intense cytoplasmic positivity for alpha smooth muscle actin (clone 1A4, DAKO) (Fig. 2a), desmin (D33, DAKO) (Fig. 2b), vimentin (V9, Novocastra), and moderate staining of caldesmon (h-CD, DAKO) (Fig. 2c). S100 and cytokeratin were negative. CD34 expression in the endothelial cells highlighted the vessel of origin of the tumor. The proliferation index detected by Ki-67 (MIB-1, DAKO) was 65%. Based on the above findings, a grade-2 myxoid leiomyosarcoma, most probably arising in the wall of the right common femoral vein and extending into the external iliac vein, was diagnosed.

Vascular leiomyosarcomas usually occur in the inferior vena cava [6], whereas leiomyosarcomas of femoral vein are a rare entity. To date, fewer than approximately 40 cases have been reported [1]. Clinical presentations of venous leiomyosarcoma are usually an enlarged limb or palpable mass, edema, and an ill-defined pain [3]. Our case was initially masqueraded by clinical and radiological signs of deep vein thrombosis. However, angio-CT scan and MRA demonstrated the intraluminal tumor in the femoral vein, proving them to be gold standard tests in the evaluation of venous tumors of the extremities. These imaging techniques avoid subjecting the patient to preoperative incisional biopsy, thereby preventing the risk of tumor dissemination [1]. Myxoid leiomyosarcomas of soft tissue are usually more low-grade tumors than conventional soft tissue leiomyosarcoma. Extensive sampling is necessary to demonstrate the presence of myxoid change occupying more than 50% of the tumor tissue [5]. Although myxoid leiomyosarcomas were thought to be of poor prognosis based on the observations in small numbers of cases, the myxoid phenotype per se does not have prognostic relevance [5]. However, accurate diag-

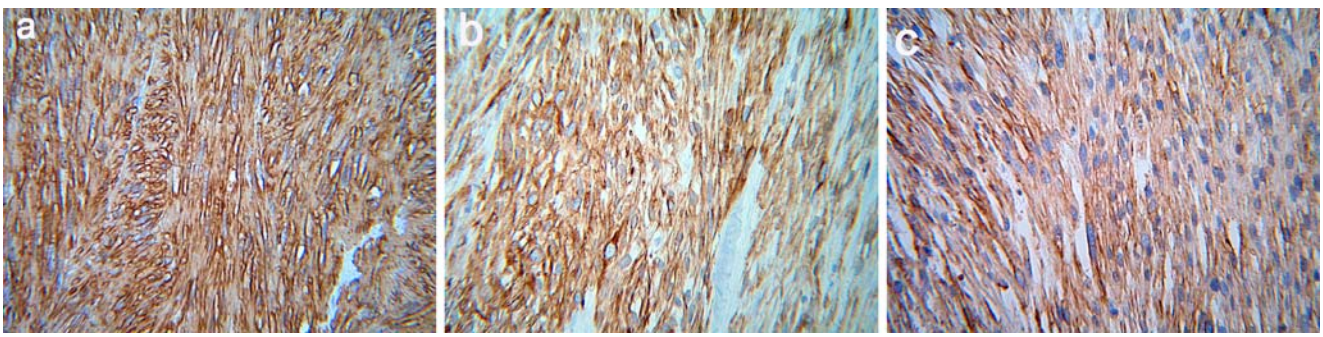

Fig. 2 The spindle tumor cells positive showing diffuse intense cytoplasmic staining for alpha smooth muscle actin (**a**), desmin (**b**), and caldesmon (**c**) (smooth muscle actin, desmin, and caldesmom immunostains; original magnification ×400)

nosis is critical because therapies may differ widely for entities in its differential diagnosis, such as hemangioendothelioma, a thrombus showing myxoid change or a vascular leiomyoma with myxoid change. Low mitotic activity is a common feature observed in myxoid leiomyosarcomas [5]. Features such as detectable mitotic activity, necrosis, and/or atypia in a smooth muscle tumor are indicative of malignancy and help to distinguish it from myxoid leiomyoma, which usually lacks mitotic activity [5]. Vascular leiomyosarcomas can cause distant metastasis mainly in the lung and liver and, rarely, to the scalp [3]. In our case, no metastasis was detected. Primary vascular leiomyosarcoma has a more aggressive behavior and poorer prognosis than its soft tissue counterpart [3]. The ideal treatment seems to be a complete surgical excision, with selective venous reconstruction as performed in our case and systemic chemotherapy in cases of metastasis. In conclusion, we present a case of primary intravenous myxoid leiomyosarcoma of the common femoral and superficial femoral veins for its extremely rare occurrence. In addition, vascular surgeons should be aware of intraluminal tumors as an uncommon cause in a patient presenting with a clinical picture of deep vein thrombosis.

References

1. Berlin O, Stener B, Kindblom LG, Angervall L (1984) Leiomyosarcomas of venous origin in the extremities. A correlated clinical, roentgenologic, and morphologic study with diagnostic and surgical implications. Cancer 54:2147–2159
2. Botsis D, Koliopoulos C, Kondi-Pafitis A, Creatsas G (2006) Myxoid leiomyosarcoma of the uterus in a patient receiving tamoxifen therapy: a case report. Int J Gynecol Pathol 25:173–175
3. Gow CH, Liaw YS, Chang YL, Chang YC, Yang RS (2005) Primary vascular leiomyosarcoma of the femoral vein leading to metastases of scalp and lungs. Clin Oncol (R Coll Radiol) 17:201
4. Grabellus F, Sheu SY, Schmidt B, Flasshove M, Kuhnen C, Ruchholtz S, Taeger G, Schmid KW (2006) Recurrent high-grade leiomyosarcoma with heterologous osteosarcomatous differentiation. Virchows Arch 448:85–89
5. Rubin BP, Fletcher CD (2000) Myxoid leiomyosarcoma of soft tissue, an underrecognized variant. Am J Surg Pathol 24:927–936
6. Shimoda H, Oka K, Otani S, Hakozaki H, Yoshimura T, Okazaki H, Nishida S, Tomita S, Oka T, Kawasaki T, Mori N (1998) Vascular leiomyosarcoma arising from the inferior vena cava diagnosed by intraluminal biopsy. Virchows Arch 433:97–100

Virchows Arch (2007) 450:239–241
DOI 10.1007/s00428-006-0328-9

LETTER TO THE EDITOR

Cystic endosalpingiosis of the appendix

Marion J. Pollheimer · Sebastian Leibl · Verena S. Pollheimer · Manfred Ratschek · Cord Langner

Received: 4 August 2006 / Accepted: 11 October 2006 / Published online: 17 November 2006
© Springer-Verlag 2006

Sir,

Endosalpingiosis usually occurs in the pelvic and abdominal peritoneum and may involve the serosal surfaces of the uterus and its adnexa. Histologically, the lesion is characterized by the presence of benign glands lined by tubal-type epithelium, containing ciliated and secretory cells. By definition, endometrial stroma is absent, thus distinguishing the lesion from endometriosis [1].

To the best of our knowledge, only two cases of appendiceal endosalpingiosis have been reported so far [2, 3]. In this study, we present another case, describe its characteristic histological appearance, and discuss the criteria to separate this peculiar lesion from other nonneoplastic or neoplastic conditions potentially affecting the vermiform appendix.

Case report

An 82-year-old female presented with acute abdominal pain due to perforated sigmoid diverticular disease and subsequent purulent pelvic peritonitis. Laparotomy was performed with excision of the diseased colonic segment, on-table lavage, and appendectomy.

Grossly, the resected sigmoid colon showed acute diverticulitis with pericolic abscess formation and suppurative peritoneal exudate. The vermiform appendix measured 7 cm in length and the serosa appeared dull and lusterless. The cut surface disclosed a polycystic tumor, centrally located at the tip of the appendix, measuring 0.8 cm in largest diameter.

On microscopic examination, the tumor consisted of multiple cysts of varying size (Fig. 1a), lined by a single layer of either cuboidal or flattened serous cells (Fig. 1b). Occasional ciliated cells (Fig. 1c, arrowheads) and secretory cells, characteristic of tubal-type epithelium, were present. Accompanying the cysts, a paucicellular fibrovascular stroma was found but no densely packed spindle-shaped cells nor hemosiderin-laden macrophages, suggestive of endometrial-type stroma, were identified. Neither cytological nor architectural abnormalities were noted, and mitotic figures were absent.

By immunohistochemistry, the lining cells of the cysts were diffusely decorated with pancytokeratin (AE1/AE3) and epithelial membrane antigen (EMA) antibodies. They showed expression of cytokeratin 7 (Fig. 1d), but were negative for cytokeratin 20. In addition, most cells were estrogen receptor positive (Fig. 1e), while progesterone receptor staining was present only in a minority of nuclei. No CD10-positive endometrial stromal elements were identified. With respect to mucin expression, MUC1 immunoreactivity was present in virtually all lining cells (Fig. 1f), whereas no staining for MUC2, the characteristic mucin of gastrointestinal epithelial cells, was observed (Fig. 1g). Similarly, all applied markers of mesothelial (calretinin, D2-40) and neuroendocrine (chromogranin A, synaptophysin) differentiation as well as Vimentin, CEA, and CA125 were negative. Hence, a final diagnosis of appendiceal endosalpingiosis was made.

M. J. Pollheimer · S. Leibl · V. S. Pollheimer · M. Ratschek · C. Langner (✉)
Institute of Pathology, Medical University of Graz,
Auenbruggerplatz 25,
8036 Graz, Austria
e-mail: cord.langner@meduni-graz.at

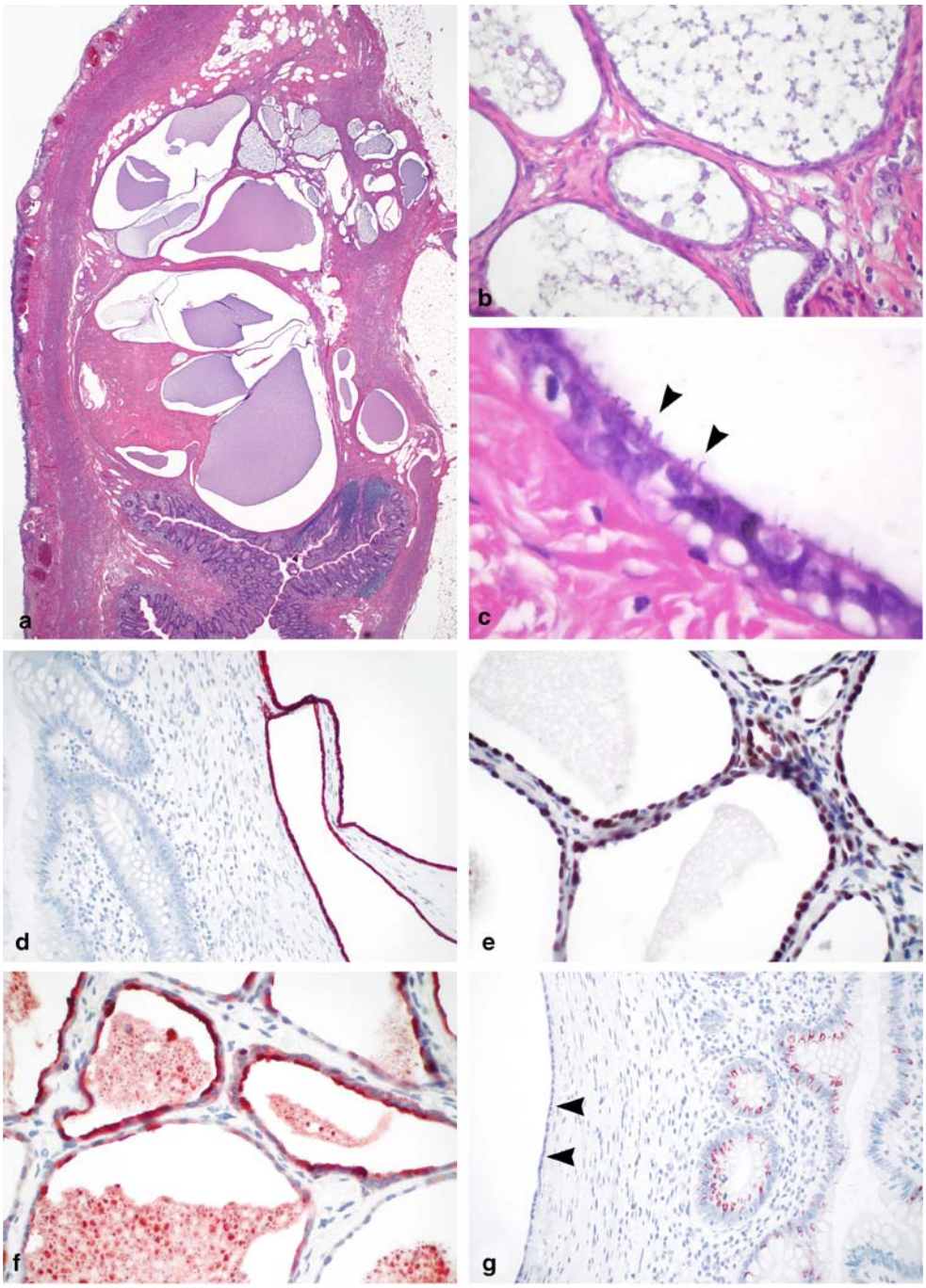

Fig. 1 Longitudinal section of the vermiform appendix showing a polycystic tumor, centrally located at the tip (**a**, ×25). The cysts are lined by a single layer of cuboidal and flattened tubal-type epithelium (**b**, ×100) with occasional ciliated cells (**c**, *arrowheads*, ×500). By immunohistochemistry, lining cells diffusely express cytokeratin 7 (**d**, ×75), estrogen receptor (**e**, ×100), and MUC1 (**f**, ×100), but lack MUC2 immunostaining (**g**, *arrowheads*, ×75)

Discussion

Only little is known about the clinical significance of endosalpingiosis. The presentation reaches from peritoneal nodular changes mimicking peritoneal tuberculosis or peritoneal carcinomatosis to cystic omental or pelvic masses. With respect to symptomatology, most authors, however, agree that endosalpingiosis commonly is an incidental finding, associated with additional pelvic pathology, rather than being a cause of pelvic pain itself [1]. Accordingly, endosalpingiosis in our patient as well as in the two other cases reported was an incidental finding [2, 3].

Differential diagnosis includes several distinct entities, the most important being appendiceal endometriosis and mesothelial inclusion cysts. In addition, several neoplastic or nonneoplastic lesions originating from local intestinal epithelium have to be ruled out.

Endometriosis of the appendix has been observed in up to 2.6% of surgically excised appendices and in 13.6 to 18% of women with intestinal endometriosis [4]. Diagnosis is based on the unequivocal demonstration of endometrium-

type stroma. Problems may arise when tubal metaplasia is present within the ectopic endometrium and stromal elements are scarce. In these cases, CD10 immunostaining may help to identify endometrial stromal cells [5].

Mesothelial inclusion cysts or benign cystic mesothelioma is an infrequent lesion that commonly localizes to the pelvic peritoneal surface of women in their thirties and forties, presenting as an isolated and localized lesion, a multifocal but still localized or as diffuse mass. Histologically, the cysts are lined by single layered, flattened to cuboidal cells. Immunostaining for mesothelial markers, such as calretinin or D2-40, confirms their mesothelial origin. Likewise, adenomatoid tumors show mesothelial differentiation; their stroma may additionally express myogenic markers.

Cystic lesions originating from local gastrointestinal epithelium may be neoplastic, such as cystadenoma or cystadenocarcinoma, or nonneoplastic, such as mucocele formation secondary to obstruction of the appendix, in nature. In general, the lining epithelium reveals attributes of gastrointestinal differentiation, such as positivity for cytokeratin 20, MUC2, or CDX-2. Rare cystic neuroendocrine tumors are characterized by their well-known expression of general neuroendocrine or specific hormonal markers.

In conclusion, the present case illustrates an example of endosalpingiosis of the vermiform appendix. Although uncommon, pathologists should include this lesion in the differential diagnosis of cystic appendiceal tumors.

References

1. Heinig J, Gottschalk I, Cirkel U, Diallo R (2002) Endosalpingiosis—an underestimated cause of chronic pelvic pain or an accidental finding? A retrospective study of 16 cases. Eur J Obstet Gynecol Reprod Biol 103:75–78
2. Cajigas A, Axiotis CA (1990) Endosalpingiosis of the vermiform appendix. Int J Gynecol Pathol 9:291–295
3. McCluggage WG, Clements WDB (2001) Endosalpingiosis of the colon and appendix. Histopathology 39:639–650
4. Misdraji J, Graeme-Cook F (2004) Miscellaneous conditions of the appendix. Sem Diagn Pathol 21:151–163
5. Sumathi VP, McCluggage WG (2002) CD10 is useful in demonstrating endometrial stroma at ectopic sites and in conforming a diagnosis of endometriosis. J Clin Pathol 55:391–392

Virchows Arch (2007) 450:243–244
DOI 10.1007/s00428-006-0338-7

LETTER TO THE EDITOR

Expression of epidermal growth factor receptor (EGFR) is frequent in inflammatory bowel disease (IBD)-associated intestinal cancer

Magali Svrcek · Jacques Cosnes · Emmanuel Tiret · Malika Bennis · Yann Parc · Jean-François Fléjou

Received: 19 June 2006 / Accepted: 23 October 2006 / Published online: 23 November 2006
© Springer-Verlag 2006

Sir,

Epidermal growth factor receptor (EGFR), which is part of the human epidermal receptor family of tyrosine kinase receptors, is expressed by a variety of cells, including normal and tumoural epithelial cells of the gastrointestinal tract [3]. EGFR appears to be a key element in colorectal carcinogenesis. Its activation induces cellular growth, cell differentiation, proliferation and migration. EGFR expression is present in approximately 60–80% of sporadic colorectal cancer (CRC) [5]. EGFR inhibitors, such as monoclonal antibodies or small molecules inhibiting tyrosine kinase activity, have been developed and several clinical trials have demonstrated their efficacy in patients with advanced CRC [4].

Patients with inflammatory bowel disease (IBD) face an increased risk of CRC in ulcerative colitis (UC) and Crohn's disease (CD), and of small intestinal cancer (SIC) in CD. The molecular events underlying IBD-associated CRC seem to be different from sporadic CRC. Only a few studies have assessed the expression of EGFR in IBD-associated intestinal neoplasms [1].

We studied 7 SIC and 16 CRC in patients with CD and 49 CRC in patients with UC. The specimens, obtained from surgical resections between 1990 and 2004, were selected from the files of the Pathology Department of Saint-Antoine Hospital, AP-HP, Paris, France. Immunohistochemical study of EGFR expression was also performed on dysplastic lesions (n=10) and lymph node metastases (n=2). Immunohistochemical staining was carried out with the EGFR pharmDx kit (DakoCytomation, Trappes, France), used according to the manufacturer's instructions. Only complete or incomplete membranous staining of tumoural cells was considered as positive. EGFR expression was assessed according to both the percentage of reactive tumour cells and the mean intensity of the membranous staining (1+, weak reactivity; 2+, moderate reactivity and 3+, strong reactivity). EGFR reactivity in the region of deepest tumour invasion was also assessed.

Positive immunohistochemical staining of any intensity was detected in all SIC, in 13/16 (81%) CRC in patients with CD and in 43/49 (88%) CRC in patients with UC. Four SIC (57%) and eight CRC (50%) in patients with CD and seven CRC in patients with UC (24%) had 2+ or 3+ EGFR reactivity in more than 50% of the cells. In more than half of the cases, neoplastic cells were stained with a greater intensity in the region of deepest tumour invasion,

M. Svrcek (✉) · J.-F. Fléjou
AP-HP, Hôpital Saint-Antoine,
Service d'Anatomie et Cytologie Pathologiques,
184, rue du Faubourg Saint-Antoine,
75571 Paris Cedex 12, France
e-mail: magali.svrcek@sat.aphp.fr

M. Svrcek · J. Cosnes · E. Tiret · M. Bennis · Y. Parc · J.-F. Fléjou
Université Paris6, Faculté de Médecine Pierre et Marie Curie,
Paris, France

M. Svrcek · J.-F. Fléjou
Inserm, U762, CEPH,
Paris, France

J. Cosnes
AP-HP, Hôpital Saint-Antoine,
Service de Gastroentérologie et Nutrition,
184, rue du Faubourg Saint-Antoine,
75571 Paris Cedex 12, France

E. Tiret · M. Bennis · Y. Parc
AP-HP, Hôpital Saint-Antoine, Service de Chirurgie Viscérale,
184, rue du Faubourg Saint-Antoine,
75571 Paris Cedex 12, France

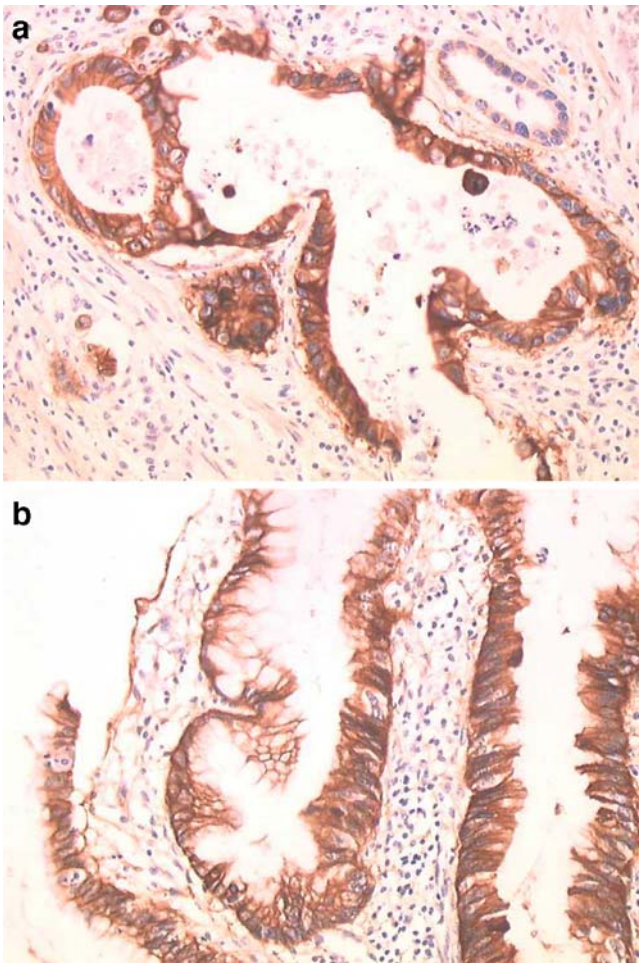

Fig. 1 **a** Strong (3+) intensity of EGFR reactivity in a colorectal adenocarcinoma complicating UC (haematoxylin and dimethylaminoazobenzene, ×200). **b** The intensity of EGFR reactivity was similar (3+) in the associated high-grade dysplasia (haematoxylin and dimethylaminoazobenzene, ×200)

both in SIC and CRC. The staining was of similar intensity within dysplastic lesions and the corresponding adenocarcinomas (Fig. 1) and within lymph node metastases and the primary adenocarcinoma.

Thus, our study shows that a very high percentage of IBD-associated intestinal cancers display immunohistochemical positivity for EGFR. Expression occurs at an early stage, i.e. is present in premalignant lesions, as described in sporadic CRC [6]. The high percentage of strongly reactive EGFR cells in the region of deepest tumour invasion may point towards a role of EGFR in metastatic spread. Until now, only patients with evidence of EGFR-expressing cancer were included in clinical trials using anti-EGFR-targeted therapy, based on findings from preclinical studies that EGFR expression is a prerequisite for the efficiency of this therapy. Although, up to now, clinical trials have not included IDB-associated cancers, these patients do receive anti-EGFR therapies if indicated, just like patients with sporadic CRC. As the rate of immunohistochemical expression of EGFR within IBD-associated CRC and sporadic CRC appears to be similar, EGFR now also emerges as a target for anticancer therapy in IBD-associated intestinal cancers.

Tumour EGFR status can be quantified by several techniques, including immunohistochemistry, fluorescent in situ hybridisation, chromogenic in situ hybridisation, and polymerase chain reaction. In practice, immunohistochemistry has been the most commonly used method for clinical trials. However, recent data suggest that the selection of patients for a monoclonal antibody-based treatment must not be based on the extent of EGFR immunostaining in the tumour, as the response is apparently unrelated to the immunohistochemical positivity [2]. EGFR-negative sporadic CRC patients, as defined by immunohistochemical analysis, may also respond to anti-EGFR-based therapy [2].

Further research into the role of EGFR in IBD-associated colorectal carcinogenesis will certainly help to define the use of anti-EGFR-targeted therapy and to develop selection criteria for this treatment.

References

1. Alexander RJ, Panja A, Kaplan-Liss E, Mayer L, Raicht RF (1995) Expression of growth factor receptor-encoded mRNA by colonic epithelial cells is altered in inflammatory bowel disease. Dig Dis Sci 40:485–494
2. Chung KY, Shia J, Kemeny NE, Shah M, Schwartz GK, Tse A, Hamilton A, Pan D, Schrag D, Schwartz L, Klimstra DS, Fridman D, Kelsen DP, Saltz LB (2005) Cetuximab shows activity in colorectal cancer patients with tumors that do not express the epidermal growth factor receptor by immunohistochemistry. J Clin Oncol 23:1803–1810
3. Ciardiello F, Tortora G (2003) Epidermal growth factor receptor (EGFR) as a target in cancer therapy: understanding the role of receptor expression and other molecular determinants that could influence the response to anti-EGFR drugs. Eur J Cancer 39: 1348–1354
4. Cunningham D, Humblet Y, Siena S, Khayat D, Bleiberg H, Santoro A, Bets D, Mueser M, Harstrick A, Verslype C, Chau I, Van Cutsem E (2004) Cetuximab monotherapy and cetuximab plus irinotecan in irinotecan-refractory metastatic colorectal cancer. N Engl J Med 351:337–345
5. Goldstein NS, Armin M (2001) Epidermal growth factor receptor immunohistochemical reactivity in patients with American Joint Committee on Cancer stage IV colon adenocarcinoma: implications for a standardized scoring system. Cancer 92:1331–1346
6. O'Dwyer PJ, Benson AB (2002) Epidermal growth factor receptor-targeted therapy in colorectal cancer. Semin Oncol 29:10–17 (Suppl)

Virchows Arch (2007) 450:245–246
DOI 10.1007/s00428-006-0336-9

LETTER TO THE EDITOR

Epithelioid angiosarcoma of the bladder after irradiation for endometrioid adenocarcinoma

A. Kulaga · A. Yilmaz · R. P. Wilkin · K. Trpkov

Received: 16 October 2006 / Accepted: 20 October 2006 / Published online: 6 December 2006
© Springer-Verlag 2006

Dear Editor,

Angiosarcomas of the urinary bladder are uncommon and only 11 cases have been reported in the literature [1–3]. Of the previously reported cases, angiosarcoma developed in three patients after radiation treatment for prostate cancer (one patient) [2] and for gynecological malignancies (two patients) [3]. We report a patient who developed primary epithelioid angiosarcoma of the urinary bladder 14 years after radiation treatment for uterine endometrioid adenocarcinoma. To our knowledge, this is only the second epithelioid angiosarcoma documented in the urinary bladder.

An 83-year-old female presented with painless microhematuria. Fourteen years ago, the patient underwent hysterectomy and bilateral salpingo-oophorectomy for endometrioid adenocarcinoma of the uterus (FIGO grade I, stage I), followed by external beam irradiation. No exposure to other chemical agents was documented in the clinical history. On ultrasonography, a bladder wall lesion was identified. On cystoscopy, there was a sessile nodular mass at the posterolateral bladder wall, and transurethral bladder resection (TURB) was performed. The patient's clinical condition deteriorated rapidly and she developed bilateral leg edema and ascites. Abdominal CT scan revealed peritoneal carcinomatosis. The patient died 3 months after the presentation, and no autopsy was performed.

Pathology of the TURB showed a high-grade neoplasm that infiltrated extensively underneath the normal urothelium into lamina propria (Fig. 1a) and into muscularis propria (Fig. 1b). Neoplastic cells exhibited sheet-like growth pattern and focal coagulative necrosis. The neoplasm was composed of epithelioid cells with indistinct cell borders, oval to round nuclei, and prominent nucleoli. Brisk mitotic activity and abnormal mitoses were readily seen. Vasoformative areas were not apparent, but rare intracytoplasmic lumina were present (Fig. 1b, arrow). Tumor immunoprofile was in keeping with angiosarcoma and neoplastic cells demonstrated diffuse immunoreactivity for vimentin and vascular endothelial marker CD31 (Fig. 2a). Other endothelial markers (factor VIII and CD34) were negative. Neoplastic cells were also negative for pancytokeratin (Fig. 2b), EMA, S-100, and HMB-45.

Angiosarcomas are rare mesenchymal neoplasms that arise most often in the skin and are less common in the deep soft tissues. Epithelioid angiosarcoma is a variant of angiosarcoma that can be mistaken for an epithelial neoplasm, as it is composed of "epithelioid" cells containing large vesicular nuclei [4]. Epithelioid appearance has been documented previously in only one angiosarcoma of the urinary bladder [1]. The association of a high-grade epithelioid angiosarcoma with prior radiotherapy is also unusual, because the majority of radiation-associated angiosarcomas are conventional, rather than epithelioid,

A. Kulaga · A. Yilmaz · K. Trpkov
Department of Pathology, Rockyview General Hospital,
Calgary, Alberta, Canada

R. P. Wilkin
Department of Urology, Rockyview General Hospital,
Calgary, Alberta, Canada

A. Kulaga · A. Yilmaz · R. P. Wilkin
Calgary Laboratory Services, University of Calgary,
Calgary, Alberta, Canada

K. Trpkov
Department of Anatomical Pathology,
Rockyview General Hospital,
7007-14 Street S.W.,
Calgary, Alberta T2V 1P9, Canada

K. Trpkov (✉)
Department of Pathology, Calgary Laboratory Services,
Calgary, Alberta, Canada
e-mail: kiril.trpkov@cls.ab.ca

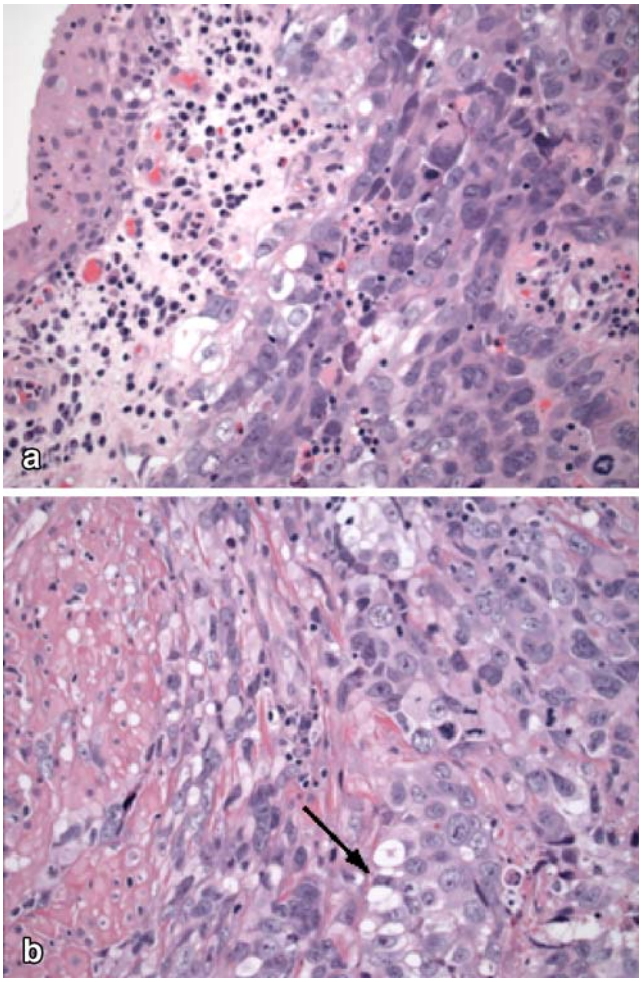

Fig. 1 Epithelioid neoplastic cells form solid sheets that infiltrate underneath the normal urothelium, which can be seen in the *top left corner* (**a**) [hematoxylin and eosin (H&E)×400]. Neoplastic cells infiltrate into bladder muscularis propria and demonstrate focal cytoplasmic lumina (*arrow*) (**b**) (H&E ×400)

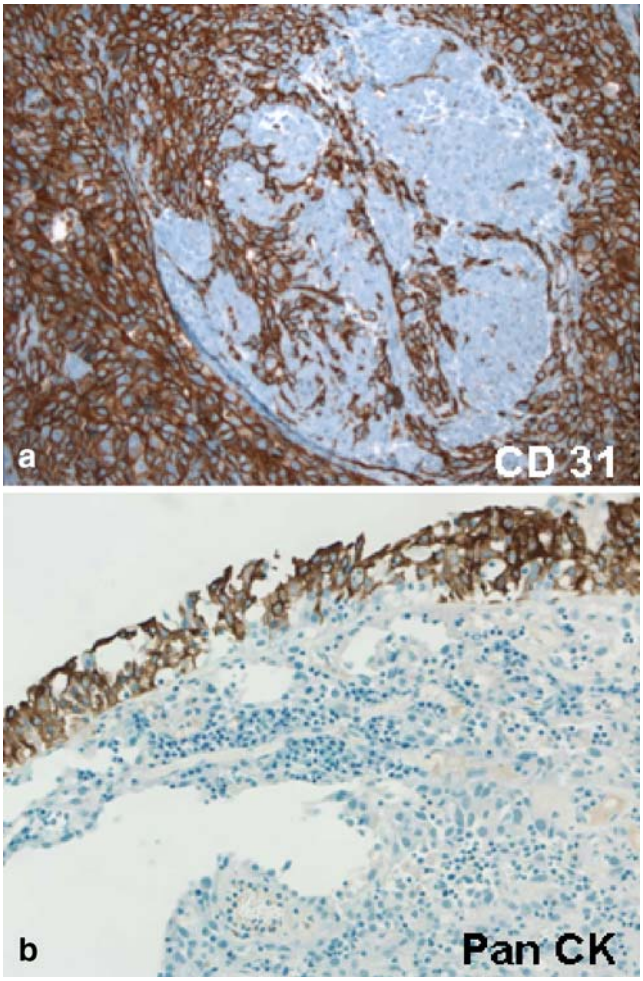

Fig. 2 Neoplastic cells demonstrate strong and uniform immunoreactivity for vascular endothelial marker CD31 (**a**) (H&E ×200). Normal urothelium is reactive for pancytokeratin, while neoplastic cells are negative (**b**) (H&E ×200)

and they usually appear as surface, rather than visceral tumors. Angiosarcomas of the urinary bladder typically pursue an aggressive clinical course.

Of 11 patients with bladder angiosarcomas with documented follow-up (including the present case), eight died with a mean survival time of 7.9 months. Three patients had no evidence of recurrence or metastases after 8, 29, and 30 months of follow-up. Optimal therapy for bladder angiosarcoma remains to be determined and, given the aggressive nature of the disease, may include a multimodal aggressive treatment with a combination of radical surgery, if the tumor is resectable, followed by radiotherapy and chemotherapy.

References

1. Engel JD, Kuzel TM, Moceanu MC, Oefelein MG, Schaeffer AJ (1998) Angiosarcoma of the bladder: a review. Urology 52: 778–784
2. Navon JD, Rahimzadeh M, Wong AK, Carpenter PM, Ahlerig TE (1997) Angiosarcoma of the bladder after therapeutic irradiation for prostate cancer. J Urol 157:1369–1370
3. Morgan MA, Moutos DM, Pippitt CH Jr, Suda RR, Smith JJ, Thurnau GR (1989) Vaginal and bladder angiosarcoma after therapeutic irradiation. South Med J 82:1434–1436
4. Fletcher CDM, Beham A, Bekir S, Clarke AMT, Marley NJE (1991) Epithelioid angiosarcoma of deep soft tissue: a distinctive tumor readily mistaken for an epithelial neoplasm. Am J Surg Pathol 15:915–924

Virchows Arch (2007) 450:247–248
DOI 10.1007/s00428-007-0374-y

ANNOUNCEMENTS

Announcements

© Springer-Verlag 2007

14–17 May 2007
Diagnostic Histopathology of Breast Disease
Hammersmith Hospital (Imperial College), London, UK

A four day long course on the Hammersmith Campus designed for pathologists at Consultant and Senior Trainee level and suitable for the final examination for MRCPath. The course will provide a comprehensive coverage of the histopathology of breast disease, with special emphasis on areas which pose diagnostic difficulties. The course is based, historically, on the extensive referral collection of Professor JG Azzopardi, to which has been added new cases from Charing Cross, Nottingham City and Addenbrooke's Hospitals. The course will be slanted to practical diagnostic pathology with a specific session dealing with problems encountered in core biopsies and a special workshop dealing with the interpretation of HER2 immunostaining. The participants will be given ample time to study histological preparations, followed by illustrated discussions of the cases. In addition there will be several daily talks on specific topics, given by eminent breast pathologists and followed by discussions. The topics will include: new issues in the interpretation of breast biopsies, breast immunohistochemistry, problematic breast lesions, dealing with the gross specimen, fibro-epithelial, spindle cell and papillary lesions, proliferative lesions/carcinoma in-situ, sentinel lymph node biopsy and the impact of molecular genetics on diagnostic breast pathology. The faculty will include Anthony Douglas-Jones, Ian Ellis, Bharat Jassani, Andrew Lee, Sarah Pinder, Jorge Reis-Filho and Sami Shousha.

For further information please contact:
Sandra Lock
Department of Histopathology
Hammersmith Hospital
Du Cane Road
London W12 0NN, UK
Tel: +44 (0)20 8383 3292
Fax: +44 (0)20 8740 7417
E-mail: histopathology.shortcourses@imperial.ac.uk

May 18–20, 2007
Postgraduate Course
Molecular Pathology
Graz, Austria

Course Directors
Gerald Höfler, MD, Department of Pathology, Medical University Graz, Austria Falko Fend, MD, Department of Pathology, Technical University Munich, Germany

Course Objectives
This course is designed for pathologists, molecular biologists and technicians with special interest in diagnostic molecular pathology. It features lectures and practical aspects (wet lab course). Topics include DNA/RNA isolation from formalin-fixed paraffin embedded tissue, translocation analysis, clonality analysis (IgH, TCR), microsatellite instability (HNPCC) and quantification of RNA transcripts. The course language will be English.

Course Fee: 400,-€ The course fee includes hands on participation in the wet lab course, a comprehensive handout, coffee breaks, lunch and dinner (Saturday), buffet lunch (Sunday) and guided city walk.

Attendance is limited to 30 participants!

Registration / more information:
To register please use the form on our homepage:
http://pathologie.meduni-graz.at/Pathologie/veranstaltungen.htm
or send your registration to
Edith Kleinferchner
Department of Pathology
Medical University Graz
Auenbruggerplatz 25
8036 Graz, Austria;
Fax 0043-(0)316-385-3432
E-mail: edith.kleinferchner@meduni-graz.at

Since attendance is limited acceptance to the course will be acknowledged and a bill will be mailed.

7–8 June 2007
Thyroid Pathology for the Practising Pathologist
15 rue de l'Ecole de Médecine
Paris, France

A 2-day course will take place in Paris under the auspices of the French Division of the I.A.P. This course will be given in English by Prof. J. Rosai (Milano), Prof. M. Sobrinho-Simoes (Porto) and Prof. R. Heimann (Brussels). It will consist of lectures alternating with slide reviews and a slide seminar over a multiheaded microscope. The cases of the seminar will be sent on CD before the meeting.
The audience will be limited to 30 participants.

Course fees: 410 euros (340 euros for members of any I.A.P. division). The fees include registration, hand-out, CD of the slide seminar and coffee breaks.

For further information, please contact:
Mrs M. Fontanière, Administrative Secretary,
French Division of the I.A.P.
32 Cours Albert Thomas,
69008, Lyon, France
Fax: 33 4 78754311
E-mail: academie.pathologie@wanadoo.fr

24–27 July, 2007
Practical Pulmonary Pathology
London, UK

This course is designed to provide histopathology and cytopathology trainees and consultants with an opportunity to study diagnostic lung pathology in a comprehensive manner. It comprises lectures and practical microscopy sessions, the latter making up roughly half the time and consisting of individual study of a unique collection of cases.

For further information and application forms please contact:
Professor B Corrin,
Brompton Hospital,
London SW3 6NP, UK
Fax +44 20 7351 8293
E-mail: b.corrin@ic.ac.uk

27–31 August 2007 (Part I+II), 29–31 October 2007 (Part III)
Postgraduate Course Lung, Pleural & Mediastinal Diseases,
Department of Pathology,
Medical University, Graz, Austria

Course Director: Helmut Popper, MD (Graz)

Course Objectives:
This three-part course (common and rare lung and pleural, and mediastinal diseases) is designed for trainees as well as for experienced colleagues. Lectures as well as microscopy sessions alternate for each part. Clinical lectures and case studies are also included in selected lung diseases. Each part can be booked separately.

Course fee:
Part I (Common diseases) Aug 27–29, 2007€ 240,00
Part II (Mediastinal diseases) Aug 30–31, 2007€ 240,00
Part III (Rare diseases) Oct 29–31, 2007€ 240,00
Whole 8-day course (Part I + II + III) € 600,00
Two parts (Part I + II or Part I + III or Part II + III) € 450,00

For more information and registration please contact:
Edith Kleinferchner
Department of Pathology, Medical University Graz
Auenbruggerplatz 25
8036 Graz, Austria
Fax: 0043 (0)316 385-3432
e-mail:edith.kleinferchner@meduni-graz.at
http://pathologie.meduni-graz.at/Pathologie/veranstaltungen.htm

Virchows Arch (2007) 450:249–260
DOI 10.1007/s00428-006-0348-5

ORIGINAL ARTICLE

Expression microarray analysis of papillary thyroid carcinoma and benign thyroid tissue: emphasis on the follicular variant and potential markers of malignancy

S. P. Finn · P. Smyth · S. Cahill · C. Streck · E. M. O'Regan · R. Flavin · J. Sherlock · D. Howells · R. Henfrey · M. Cullen · M. Toner · C. Timon · J. J. O'Leary · O. M. Sheils

Received: 27 July 2006 / Accepted: 2 November 2006 / Published online: 25 January 2007
© Springer-Verlag 2007

Abstract The most common sub-variant of papillary thyroid carcinoma (PTC) is the so-called follicular variant (FVPTC), which is a particularly problematic lesion and can be challenging from a diagnostic viewpoint even in resected lesions. Although fine needle aspiration cytology is very useful in the diagnosis of PTC, its accuracy and utility would be greatly facilitated by the development of specific markers for PTC and its common variants. We used the recently developed Applied Biosystems 1700 microarray system to interrogate a series of 11 benign thyroid lesions and conditions and 14 samples of PTC (six with classic morphology and eight with follicular variant morphology). TaqMan® reverse transcriptase-polymerase chain reaction was used to validate the expression portfolios of 50 selected transcripts. Our data corroborates potential biomarkers previously identified in the literature, such as LGALS3, S100A11, LYN, BAX, and cluster of differentiation 44 (CD44). However, we have also identified numerous transcripts never previously implicated in thyroid carcinogenesis, and many of which are not represented on other microarray platforms. Diminished expression of metallothioneins featured strongly among these and suggests a possible role for this family as tumour suppressors in PTC. Fifteen transcripts were significantly associated with FVPTC morphology. Surprisingly, these genes were associated with an extremely narrow repertoire of functions, including the major histocompatibility complex and cathepsin families.

Keywords Papillary thyroid carcinoma · Biomarker · Follicular variant · Microarray · TaqMan® PCR

S. P. Finn · P. Smyth · S. Cahill · R. Flavin · J. J. O'Leary · O. M. Sheils
Department of Histopathology, University of Dublin, Trinity College, Dublin, Ireland

E. M. O'Regan · M. Toner
Dublin Dental School and Hospital, Dublin, Ireland

C. Timon
Department of Otolaryngology, St. James's Hospital, Dublin, Ireland

M. Cullen
Department of Endocrinology, St James's Hospital, Dublin, Ireland

C. Streck · J. Sherlock · D. Howells · R. Henfrey
Applied Biosystems, Foster City, CA, USA

O. M. Sheils (✉)
Department of Histopathology, Institute of Molecular Medicine, Trinity Centre for Health Sciences, St. James's Hospital, Dublin 8, Ireland
e-mail: osheils@tcd.ie

Introduction

Papillary thyroid carcinoma (PTC) is the most common endocrine malignancy and encompasses a variety of morphological/architectural variants, all of which are characterized by a distinctive nuclear appearance. In recent years, PTC has become an important paradigm of solid tumour molecular pathogenesis principally arising from intensive investigation prompted by the Chernobyl accident.

The discovery of ret rearrangements [12, 13, 35] and their association with radiation [42] was followed by the demonstration of the BRAF V600E mutation [21, 30]

found more commonly associated with sporadic PTC in non-radiation exposed populations [22, 32]. In the past, our group and others have noted an association between classic morphology and the BRAF V600E mutation and between variant morphology and ret rearrangements particularly ret/PTC-3 [11, 39]. Similarly ret/PTC-3 appears to strongly correlate with the solid/follicular variant seen commonly in children exposed to the Chernobyl fallout [42]. Nevertheless, the utility of these genetic lesions to diagnostic pathology and clinical practice has remained negligible.

Recently, gene expression microarray technology has been used to attempt to identify clinically relevant biomarkers of malignancy related to the thyroid [2, 6, 9, 10, 20, 28]. The discovery of such a biomarker or panel of biomarkers allied to the gold standard triage method of fine needle aspiration cytology (FNAC) would represent a significant advancement in the treatment of the solitary thyroid nodule.

An intriguing but commonly occurring variant of PTC is known as follicular variant (FVPTC). This lesion, which by definition retains the classic nuclear features of PTC, shows no evidence of the architectural papillae. FVPTC may be a controversial lesion due to interobserver variation in its pathological diagnosis [25]. Further, the occurrence of follicular patterned lesions with poorly or incompletely developed nuclear features may occur, which are easily dismissed as benign thyroid nodules. This has led to the controversial designation "well-differentiated tumour of uncertain malignant potential" for tumours of this type [45].

It is clear that this is a complex and contentious area, and that further work needs to be done to ascertain the underlying molecular biology of this particular variant. Recently, inroads into elucidation of molecular pathways underpinning PTC have been carried out using microarray studies. The overriding objective of these investigations was to identify clinically useful biomarkers. However, the majority of these studies have analysed PTC as though it were a homogenous singular entity without deference in a detailed manner to sub-variants and, in particular, the most common variant (FVPTC). The identification of specific biomarkers of FVPTC and a deeper understanding of its origins are clearly warranted.

The aim of this expression microarray study using a novel microarray platform was twofold: to identify markers that distinguish PTC from benign thyroid tissue and lesions and, secondly, to identify potential markers and further explore the molecular pathology of FVPTC.

Materials and methods

Patients and tissue samples

Tissue from 25 thyroid resections was collected prospectively from patients undergoing partial or total thyroidectomy for a variety of reasons at St. James's Hospital, Dublin. The study had approval of the local ethics committee and informed consent was obtained from each patient by the clinical team before surgery. Small samples (<1 cm) were divided and immediately snap-frozen in liquid nitrogen for storage at −80°C until use. Histopathological examination of formalin-fixed paraffin-embedded sections was performed by two pathologists (SF and MT) for diagnostic categorisation. Classification of neoplastic tissue was made according to a recognised system [24]. The cohort comprised 11 benign lesions or conditions including follicular adenoma, nodular goitre, normal thyroid tissue, and Graves's thyroiditis. The remaining 14 samples were diagnosed as PTC and comprised six classical morphology PTC and eight FVPTC (see Table 1). Immediately before RNA extraction, frozen sections were cut and stained to confirm the presence of representative lesional tissue with morphology corresponding to that noted in the diagnostic formalin-fixed paraffin-embedded sections.

RNA isolation and characterization

Samples were ground in liquid nitrogen and homogenised in RLT buffer (Qiagen, UK). RNA was then extracted using

Table 1 Sample cohort

Identifier	Diagnosis
N1	Normal thyroid tissue
N2	Normal thyroid tissue
N3	Lymphocytic thyroiditis
N4	Nodular hyperplasia
N5	Follicular adenoma
N6	Nodular hyperplasia with focal lymphocytic thyroiditis
N7	Nodular hyperplasia
N8	Follicular adenoma
N9	Nodular hyperplasia
N10	Follicular adenoma
N11	Grave's thyroiditis
T1	Solid/FVPTC
T2	FVPTC
T3	PTC classic morphology
T4	FVPTC-oxyphil
T5	FVPTC
T6	FVPTC
T7	PTC classic morphology
T8	FVPTC
T9	PTC classic morphology
T10	FVPTC
T11	PTC classic morphology
T12	FVPTC
T13	PTC classic morphology
T14	PTC classic morphology

List of the 11 benign and 14 malignant lesions that were used in this study.
FV follicular variant; *PTC* papillary thyroid carcinoma

the RNeasy Mini Kit with optional on-column RNase-free DNase digestion (Qiagen) according to the manufacturer's instructions. RNA quantity was determined using UV spectrophotometry. RNA quality was assessed using the RNA 6000 Nano LabChip® Kit in conjunction with the Agilent 2100 Bioanalyzer (Agilent Technologies, Waldbronn, Germany).

Microarray analysis

Applied Biosystems Human Genome Survey Arrays were used to analyse the transcriptional profiles of thyroid RNA samples in this study. Digoxigenin-UTP-labelled cRNA was generated and linearly amplified from 5 μg of total RNA using Applied Biosystems Chemiluminescent RT-IVT Labelling Kit v 2.0 using manufacturer's protocol. 10 μg of labelled cRNA were hybridized to each pre-hybed microarray in a 1.5-ml volume at 55°C for 16 h. Array hybridization and chemiluminescence detection were performed using Applied Biosystems Chemiluminescence Detection Kit following manufacturer's protocol. Images were collected for each microarray using the 1700 analyser. Images were auto-gridded and the chemiluminescent signals were quantified, corrected for background and spot, and spatially normalized.

TaqMan® PCR validation

Sufficient RNA remained from 20 of the initial 25 samples for TaqMan® polymerase chain reaction (PCR) validation in a series of 50 targets. RNA was reverse transcribed using a High Capacity cDNA Archive Kit (Applied Biosystems, CA, USA). Primers and probes for TaqMan® PCR were obtained by using Applied Biosystems' pre-designed TaqMan® Gene Expression Assays. PCR was carried out using an ABI PRISM 7900 Sequence Detection System (Applied Biosystems). Analysis of relative gene expression data was performed using the ΔΔCT method [23] with glyceraldehyde-3-phosphate dehydrogenase (GAPDH) as an endogenous control/reference assay.

Statistical analysis

Microarrays were analysed using Spotfire DecisionSite™ for Functional Genomics (Spotfire AB, Goteborg, Sweden) and R version 1.9.1, a free language and environment for statistical computing and graphics (R Development Core Team, 2004). Arrays were initially normalized, and genes were deemed undetectable and, therefore, excluded from final gene lists if they had a signal-to-noise ratio of less than three (S/N<3) in greater than 18 of the 25 arrays.

An ANOVA test was used to generate p values for statistical differences between groups. Their p values were then adjusted for multiple comparisons using the technique described by Benjamini and Yekutieli [3]. Genes were deemed statistically different between groups if they had an adjusted $p<0.05$ and an average fold-change difference of greater than 2. Hierarchical clustering was performed based on the statistically different genes to determine whether samples grouped appropriately. Gene ontology analysis was performed using an online database known as the Panther classification system (http://www.pantherdb.org). Correlations between microarray and TaqMan® expression data were measured using the Pearson coefficient.

Results

Unsupervised clustering of all 25 samples demonstrated clustering into two major groups (data not shown) comprising the N group and the T group (see Table 1). There was no tendency for FVPTC to cluster independently with classic morphology PTC, confirming the close relationship of these variants of PTC. To identify potential markers of malignancy, ANOVA with false discovery rate correction was used to compare the benign and malignant thyroid cohorts. A p value cut-off of <0.05 and fold-change difference of ≥2 yielded 236 statistically significant probes. Of these, 172 corresponded to fully annotated probes and are listed in Table 2.

Supervised hierarchical clustering was performed on the 25 arrays based on the 236 statistically significant probes to determine whether the samples would segregate appropriately. The resulting heat map can be observed in Fig. 1. Benign lesions and tumours clustered together with the exception of one tumour sample that clustered with the benign group (T5).

A binomial statistics tool was used to compare classifications of multiple clusters of lists to a reference list (i.e. the complete human genome) to statistically determine over- or under-representation of Panther classification categories. Biological processes over-represented in the up-regulated PTC cohort included tumour suppressor, oncogenesis, DNA replication, cell cycle, and cell adhesion ($p<0.0001$). Genes involved in homeostasis and other homeostasis activities were highly over-represented in the down-regulated cohort ($p<0.000001$).

ANOVA tests were used to determine which genes were differentially regulated in the FVPTC cohort only. Fifteen genes were identified, including cluster of differentiation 14 (CD14), CD74, CTSC, CTSH, CTSS, DPP6, ETHE1, human leucocyte antigen A (HLA-A), HLA-DMA, HLA-DPB1, HLA-DQB1, HLA-DRA, osteoclast stimulating factor 1 (OSTF1), TDO2, and a previously uncharacterized gene (noname).

Microarray results were validated using a reverse transcription reaction followed by TaqMan® PCR for 50 gene targets. The ΔΔCT method [23] was used to analyse

Table 2 Genes differentially expressed in malignant vs benign thyroid tissue

Gene Name	Gene Symbol	Adjusted *p* value	1700 probe ID
Genes up-regulated in malignant vs benign			
Active BCR-related gene	ABR	0.014482	154399
Adaptor-related protein complex 2, alpha 1 subunit	AP2A1	0.0312	115368
Apoptosis, caspase activation inhibitor	AVEN	0.030998	203738
BCL2-associated X protein	BAX	0.009782	146510
BH3 interacting domain death agonist	BID	0.021424	131216
Brain abundant, membrane attached signal protein 1	BASP1	0.024214	198318
Brain acyl-CoA hydrolase	BACH	0.014566	133876
Bromodomain adjacent to zinc finger domain, 1A	BAZ1A	0.03538	209809
Calcium/calmodulin-dependent protein kinase I	CAMK1	0.041887	157712
Cathepsin S	CTSS	0.046544	105790
CD44 antigen (homing function and Indian blood group system)	CD44	0.044181	133604
Chemokine (C-X-C motif) ligand 16	CXCL16	0.043234	199059
Chromosome 1 open reading frame 38	C1orf38	0.049072	202924
CLIP-170-related protein	CLIPR-59	0.023629	102205
Docking protein 1, 62 kDa (downstream of tyrosine kinase 1)	DOK1	0.041898	204989
Epidermodysplasia verruciformis 1	EVER1	0.003348	175569
FXYD domain containing ion transport regulator 5	FXYD5	0.01444	154607
FXYD domain containing ion transport regulator 5	FXYD5	0.023629	112771
Galactose-4-epimerase, UDP	GALE	0.047363	141143
Genethonin 1	GENX-3414	0.016836	124360
Hypothetical gene BC008967	BC008967	0.015683	108526
Hypothetical protein FLJ10849	FLJ10849	0.013822	224983
Hypothetical protein FLJ22531	FLJ22531	0.024391	145918
Hypothetical protein MGC4607	MGC4607	0.006507	211836
Intercellular adhesion molecule 1 (CD54), human rhinovirus receptor	ICAM1	0.028746	109070
Jun dimerization protein p21SNFT	SNFT	0.043301	144215
Lectin, galactoside-binding, soluble, 3 (galectin 3)	LGALS3	0.034491	179836
Major vault protein	MVP	0.0312	212354
Matrix metalloproteinase 14 (membrane-inserted)	MMP14	0.038682	152076
Milk fat globule-EGF factor 8 protein	MFGE8	0.02392	144588
Mst3 and SOK1-related kinase	MST4	0.042028	112198
neuronal cell adhesion molecule	NRCAM	0.011178	106462
Phospholipase D3	PLD3	0.034491	143388
Promyelocytic leukemia	PML	0.016018	217558
Protein inhibitor of activated STAT protein PIASy	PIASY	0.00536	153434
Protein tyrosine phosphatase, receptor type, E	PTPRE	0.048653	221568
Rho GDP dissociation inhibitor (GDI) beta	ARHGDIB	0.043853	143589
S100 calcium binding protein A11 (calgizzarin)	S100A11	0.019933	145550
Similar to rat tricarboxylate carrier-like protein	BA108L7.2	0.025387	179870
SP110 nuclear body protein	SP110	0.0312	113484
Stimulated by retinoic acid gene 6	FLJ12541	0.043234	193986
Syndecan 3 (N-syndecan)	SDC3	0.048804	143980
Tax interaction protein 1	TIP-1	0.006673	119665
TBC1 domain family, member 2	TBC1D2	0.029907	205982
Tenascin C (hexabrachion)	TNC	0.032355	143831
Thymosin, beta 4, Y chromosome	TMSB4Y	0.040937	193911
Tissue inhibitor of metalloproteinase 1 (erythroid potentiating activity, collagenase inhibitor)	TIMP1	0.032306	134692
Topoisomerase (DNA) II alpha 170 kDa	TOP2A	0.040937	135302
Transforming growth factor, beta 1	TGFB1	0.016836	170749
Transgelin 2	TAGLN2	0.031971	172296
Tyrosine 3-monooxygenase/tryptophan 5-monooxygenase activation protein, eta polypeptide	YWHAH	0.039009	188379
v-yes-1 Yamaguchi sarcoma viral related oncogene homolog	LYN	0.016175	194134

Table 2 (continued)

Gene Name	Gene Symbol	Adjusted *p* value	1700 probe ID
Genes down-regulated in malignant vs benign			
Aldehyde oxidase 1	AOX1	0.003227	106573
Ankyrin 2, neuronal	ANK2	0.035357	155780
Aspartate beta-hydroxylase	ASPH	0.002064	221656
Aspartate beta-hydroxylase	ASPH	0.019666	114180
ATPase, Cu++ transporting, beta polypeptide	ATP7B	0.044511	198852
Brain-specific protein p25 alpha	p25	0.023629	120622
Casein kinase	LOC149420	0.022382	149347
Cellular retinoic acid binding protein 1	CRABP1	0.008315	100295
Centromere protein J	CENPJ	0.0312	164563
Ceroid-lipofuscinosis, neuronal 5	CLN5	0.011021	205999
Chloride channel Kb	CLCNKB	0.040418	176266
Chondroitin beta1,4 *N*-acetylgalactosaminyltransferase	ChGn	0.013148	101140
Chromosome 11 open reading frame 8	C11orf8	0.001977	174025
Chromosome 11 open reading frame 8	C11orf8	0.004148	108279
Chromosome 21 open reading frame 4	C21orf4	0.0042	156895
Clusterin-like 1 (retinal)	CLUL1	0.019631	186062
Component of oligomeric golgi complex 3	COG3	0.003664	129212
Coxsackie virus and adenovirus receptor	CXADR	0.004648	108284
Crystallin, alpha B	CRYAB	0.030418	190274
Cytosolic sialic acid 9-*O*-acetylesterase homolog	CSE-C	0.040993	213856
Dicarbonyl/L-xylulose reductase	DCXR	0.001977	103350
DnaJ (Hsp40) homolog, subfamily B, member 4	DNAJB4	0.043853	103618
ERO1-like beta (*S. cerevisiae*)	ERO1LB	0.013962	207998
Extracellular link domain containing 1	XLKD1	0.039738	195865
Family with sequence similarity 13, member A1	FAM13A1	0.019631	116936
Fatty acid binding protein 4, adipocyte	FABP4	0.014832	150137
Fc fragment of IgG binding protein	FCGBP	0.001965	118361
Fibroblast growth factor receptor 2	FGFR2	0.0042	110548
FLJ35740 protein	FLJ35740	0.020224	101102
Friedreich ataxia region gene X123	X123	0.032602	133505
Glutamate-ammonia ligase (glutamine synthase)	GLUL	0.014649	175147
Glycine amidinotransferase (L-arginine/glycine amidinotransferase)	GATM	0.013962	111904
Glycoprotein M6A	GPM6A	0.011739	215326
Growth hormone receptor	GHR	0.017721	190306
HLA complex group 4	HCG4	0.025807	191199
Hypothetical protein BC009561	LOC119710	0.003227	211319
Hypothetical protein BC019238	LOC120379	0.013438	201200
Hypothetical protein FLJ13204	FLJ13204	0.003227	145066
Hypothetical protein FLJ13842	FLJ13842	0.016448	208504
Hypothetical protein FLJ14054	FLJ14054	0.049072	202017
Hypothetical protein FLJ20154	FLJ20154	0.014428	143310
Hypothetical protein FLJ20513	FLJ20513	0.019493	154130
Hypothetical protein FLJ32110	FLJ32110	0.015507	229492
Hypothetical protein FLJ32343	FLJ32343	0.012208	116902
Hypothetical protein FLJ33516	FLJ33516	0.03965	224600
Hypothetical protein FLJ37549	FLJ37549	0.001956	218577
Hypothetical protein FLJ39378	FLJ39378	0.005853	163223
Hypothetical protein FLJ40021	FLJ40021	0.023629	174198
Hypothetical protein LOC134285	LOC134285	0.018694	163671
Hypothetical protein MGC10946	MGC10946	0.022382	195982
Hypothetical protein MGC14425	MGC14425	0.015445	161569
Hypothetical protein MGC17299	MGC17299	0.026062	168452
Hypothetical protein MGC17943	MGC17943	0.0042	147296
Hypothetical protein MGC23980	MGC23980	0.018694	224619

Table 2 (continued)

Gene Name	Gene Symbol	Adjusted *p* value	1700 probe ID
Hypothetical protein MGC24047	MGC24047	0.001956	138122
Hypothetical protein MGC33607	MGC33607	0.033547	100645
Ionized calcium binding adapter molecule 2	IBA2	0.0042	179489
KIAA0390 gene product	KIAA0390	0.014832	119936
KIAA0703 gene product	KIAA0703	0.032602	146652
Lectin, mannose-binding, 1	LMAN1	0.031092	179632
Leiomodin 1 (smooth muscle)	LMOD1	0.022352	120404
Likely ortholog of rat SNF1/AMP-activated protein kinase	SNARK	0.044605	157942
LIM domain kinase 2	LIMK2	0.002409	151439
Low density lipoprotein-related protein 1B (deleted in tumors)	LRP1B	0.00536	209464
Low density lipoprotein-related protein 2	LRP2	0.040937	114919
Matrilin 2	MATN2	0.0042	167316
Metallothionein 1A (functional)	MT1A	0.013822	204773
Metallothionein 1A (functional)|metallothionein 1E (functional)|metallothionein 1K| metallothionein 2A	MT1A|MT2A| MT1E|MT1K	0.027037	146368
Metallothionein 1A (functional)|metallothionein 1E (functional)|metallothionein 2A| metallothionein 1K	MT1A|MT2A| MT1K|MT1E	0.043841	182305
Metallothionein 1A (functional)|metallothionein 2A|metallothionein 1K| metallothionein 1E (functional)	MT1A|MT1K| MT1E|MT2A	0.011739	223856
Metallothionein 1B (functional)	MT1B	0.019631	174119
Metallothionein 1F (functional)	MT1F	0.024726	144569
Metallothionein 1G	MT1G	0.0192	164525
Metallothionein 1G	MT1G	0.03965	171539
Metallothionein 1J	MT1J	0.008315	227956
Metallothionein 1X	MT1X	0.008335	119685
Metallothionein 1X	MT1X	0.010748	173072
Metallothionein IV	MT4	0.007447	223241
Methionine adenosyltransferase II, alpha	MAT2A	0.014428	158350
Mitogen-activated protein kinase 4	MAPK4	0.042306	131252
Myc-induced nuclear antigen, 53 kDa	MINA53	0.011959	130284
NIMA (never in mitosis gene a)- related kinase 11	NEK11	0.001965	194628
Otospiralin	LOC150677	0.018694	182360
PDZ/coiled-coil domain binding partner for the rho-family GTPase TC10	PIST	0.013822	103651
Phospholipase A2 receptor 1, 180 kDa	PLA2R1	0.004029	134379
Phospholipase C-like 1	PLCL1	0.022657	206894
Phosphotidylinositol transfer protein, beta	PITPNB	0.014428	122698
Polycystic kidney and hepatic disease 1 (autosomal recessive)-like 1	PKHD1L1	0.0042	199896
Polymerase (DNA directed) iota	POLI	0.003227	167492
Potassium channel, subfamily K, member 9	KCNK9	0.000849	108648
Potassium channel-interacting protein 4	KCNIP4	0.011447	147058
Potassium inwardly-rectifying channel, subfamily J, member 13	KCNJ13	0.008972	124187
pp21 Homolog	LOC51186	0.004326	127636
Pre-B cell leukemia transcription factor 4	PBX4	0.030311	199118
Protein kinase, cAMP-dependent, catalytic, beta	PRKACB	0.023863	198878
Protein phosphatase 4, regulatory subunit 2|hypothetical protein LOC151987	PPP4R2|LOC151987	0.011338	200919
RAB23, member RAS oncogene family	RAB23	0.000659	122394
Ras association (RalGDS/AF-6) domain family 6	RASSF6	0.048804	119072
Sarcoglycan, delta (35 kDa dystrophin-associated glycoprotein)	SGCD	0.011178	120415
Serum deprivation response (phosphatidylserine binding protein)	SDPR	0.011021	156433
SH3 and multiple ankyrin repeat domains 2	SHANK2	0.043996	193906
Solute carrier family 26, member 7	SLC26A7	0.0042	225067
Solute carrier family 26, member 7	SLC26A7	0.005853	213530
Solute carrier family 5 (iodide transporter), member 8	SLC5A8	0.031284	231731
SPARC related modular calcium binding 2	SMOC2	0.021505	135930
Syndecan 2 (heparan sulfate proteoglycan 1, cell surface-associated, fibroglycan)	SDC2	0.001258	209676
Syntaxin 12	STX12	0.01117	199949

Table 2 (continued)

Gene Name	Gene Symbol	Adjusted *p* value	1700 probe ID
T-box 22	TBX22	0.024297	177517
Thioredoxin-like, 32 kDa	TXNL	0.001102	192552
Thyroid stimulating hormone receptor	TSHR	0.02176	108606
Tissue inhibitor of metalloproteinase 4	TIMP4	0.023629	184795
Trefoil factor 3 (intestinal)	TFF3	0.004648	114445
Trefoil factor 3 (intestinal)	TFF3	0.014428	100949
UDP-*N*-acetyl-alpha-D-galactosamine/polypeptide *N*-acetylgalactosaminyltransferase 9 (GalNAc-T9)	GALNT9	0.031284	161042
WEE1 homolog (*S. pombe*)	WEE1	0.024101	123533
WW domain containing oxidoreductase	WWOX	0.012208	224298
WW domain containing oxidoreductase	WWOX	0.024101	135080
Zinc finger protein 258	ZNF258	0.013962	225961
Zinc finger protein 36, C3H type-like 2	ZFP36L2	0.018837	210469

Two-tail ANOVA with p value correction yielded 173 probes (52 up-, 121 down-regulated in PTC) significantly different ($p<0.05$) between the malignant and benign thyroid tissues.

relative gene expression data. GAPDH was used as an endogenous control, and T12 was chosen as an arbitrary calibrator sample. Gene expression profiles for TaqMan® PCR were plotted in conjunction with those for microarray results in Fig. 2. Pearson co-efficient was used to directly compare data from microarray analysis and TaqMan® RT-PCR. Table 3 depicts genes differentially expressed in both benign vs malignant and FVPTC vs classic morphology PTC.

Discussion

The primary aim of this study was to generate an overview of molecular markers of malignancy in PTC with a view to identifying discriminators between common sub-types (classic PTC and FVPTC), using genome-wide expression microarray technology validated by TaqMan® RT-PCR. To this end, lesions that were well characterized histologically were selected.

The application of microarray analysis designed to identify transcripts strongly associated with each group of interest yielded a gene list of 173 genes that were differentially expressed between cohorts. Significant down-regulation of Coxsackie virus receptor was recorded in the malignant cohort of thyroid lesions. The Coxsackievirus B and adenovirus receptor (CAR) plays a dual role as a homotypic junctional adhesion protein and as a viral receptor. It is biologically plausible that altered expression may impact on the morphology peculiar to PTC given its association with cellular adhesion. CAR has been shown to be differentially expressed in various human adenocarcinomas, and differential expression may represent a new factor in thyroid tumourigenesisigenesis [27].

Rab 23 expression was also down regulated in the malignant cohort. The Rab small G protein family is composed of approximately 40 members. Many of them are ubiquitous and are expressed and participate in transport processes, such as endocytosis and exocytosis [26]. Other gene targets demonstrating significant down-regulation in the malignant group were syndecans 2 and 3. Syndecans are transmembrane proteoglycans expressed on adherent cells. Changes in syndecan expression have been postulated to influence cell adhesion, migration, and the structure of focal contacts and the cytoskeleton [8].

The abundance of metallothionein genes in the cohort of genes down-regulated in PTC is interesting partly because of the sheer number of isoforms detected (Table 2). There have been many studies showing increased metallothionein expression in a plethora of cancer types but few showing decreased expression [4, 7, 33]. Although previous microarray experiments showed metallothionein genes to be down-regulated in thyroid tumours to a certain extent [2, 9, 16], none have detected so many as the current study.

Apart from microarray experiments, there has been little reported in the literature regarding metallothioneins in thyroid cancer. An early report by Nartey et al. [31] showed metallothioneins to be expressed actively in certain human thyroid neoplastic tissues but not in normal thyroid tissue, which would seem to contradict the current authors' findings. In contrast to this, a later immunohistochemical study showed an absence of metallothionein expression in 13 of 20 PTCs [36]. Interestingly, in three of the seven positive PTCs, metallothionein positivity was restricted to areas of follicular differentiation. In one of the only recent studies, Huang et al. [17] followed up their initial microarray experiment by showing that MT1G is down regulated in PTC via hypermethylation. The biological significance

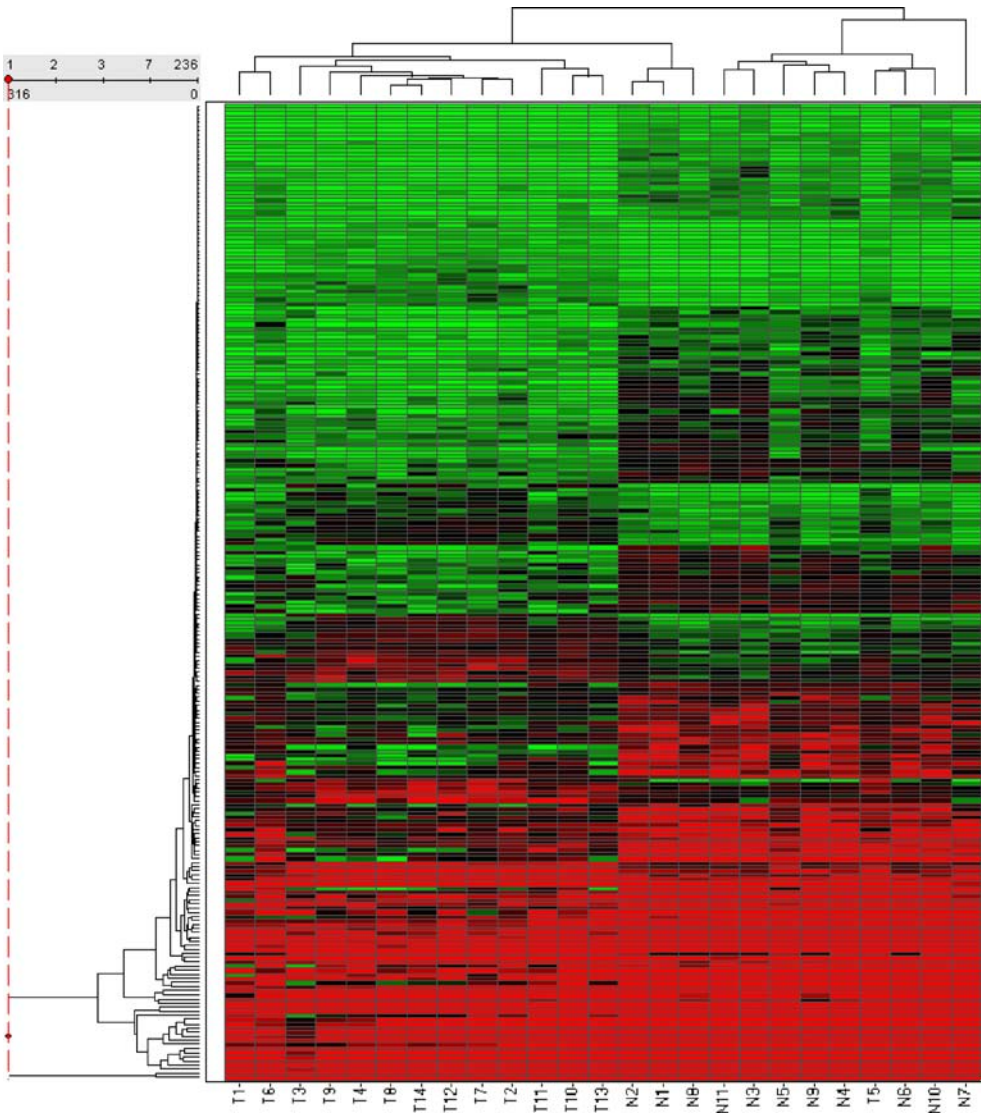

Fig. 1 Hierarchical clustering of samples. This heat map shows the clustering of the 25 samples based on the 236 probes found to be differentially regulated in benign vs malignant thyroid tissue. Clustering was performed using the unweighted pair group method with arithmetic mean, with Euclidian distance as the similarity measure. Average value was used as the ordering function

of low metallothionein expression in thyroid tumours is therefore still poorly understood; however, it is interesting to speculate that metallothioneins may have roles as tumour suppressors in thyroid carcinoma.

Many genes identified, such as *LGALS3* [9, 16, 20], *LYN* [46], *TFF3* [2, 9, 16], *CRABP1* [9, 16], *BAX* [2], *MAPK4* [28], *CD44* [16], *TIMP1* [20], *FGFR2* [9], and *S100A11* [20, 40], have been previously reported in both microarray and conventional experiments in thyroid cancer. The data generated in this study corroborates the importance of several biological processes in the progression of thyroid neoplasia. For example, S100A11 expression was up regulated in the PTC cohort compared with benign lesions, paralleling the increased protein expression of this gene target identified at the protein level using immunohistochemistry [29]. S100A11 has also been suggested as a biomarker of malignancy in the context of colorectal carcinoma as long ago as 1995 [41].

Correlation of highlighted features with the current state of knowledge of the molecular pathology of thyroid neoplasia goes some way towards providing an external validation of the data obtained from the AB1700 system. However, additional validation using TaqMan® RT-PCR was performed.

In general, microarray and TaqMan® data correlated well with approx. 80% of comparisons having $p<0.05$. Candidate genes were selected contingent on results identified as over-represented biological processes (oncogenesis, cell cycling, DNA replication, and homeostasis) using the Panther binomial statistics tool as opposed to the more traditional method of selecting the most highly disregulated genes. This may account for the poor correlation observed with certain genes. Some genes, such as TFF3 and FGFR2, had excellent correlation between microarray and TaqMan® results, whereas others, such as BAX and TSHR, showed poor correlation despite previous studies implicating them

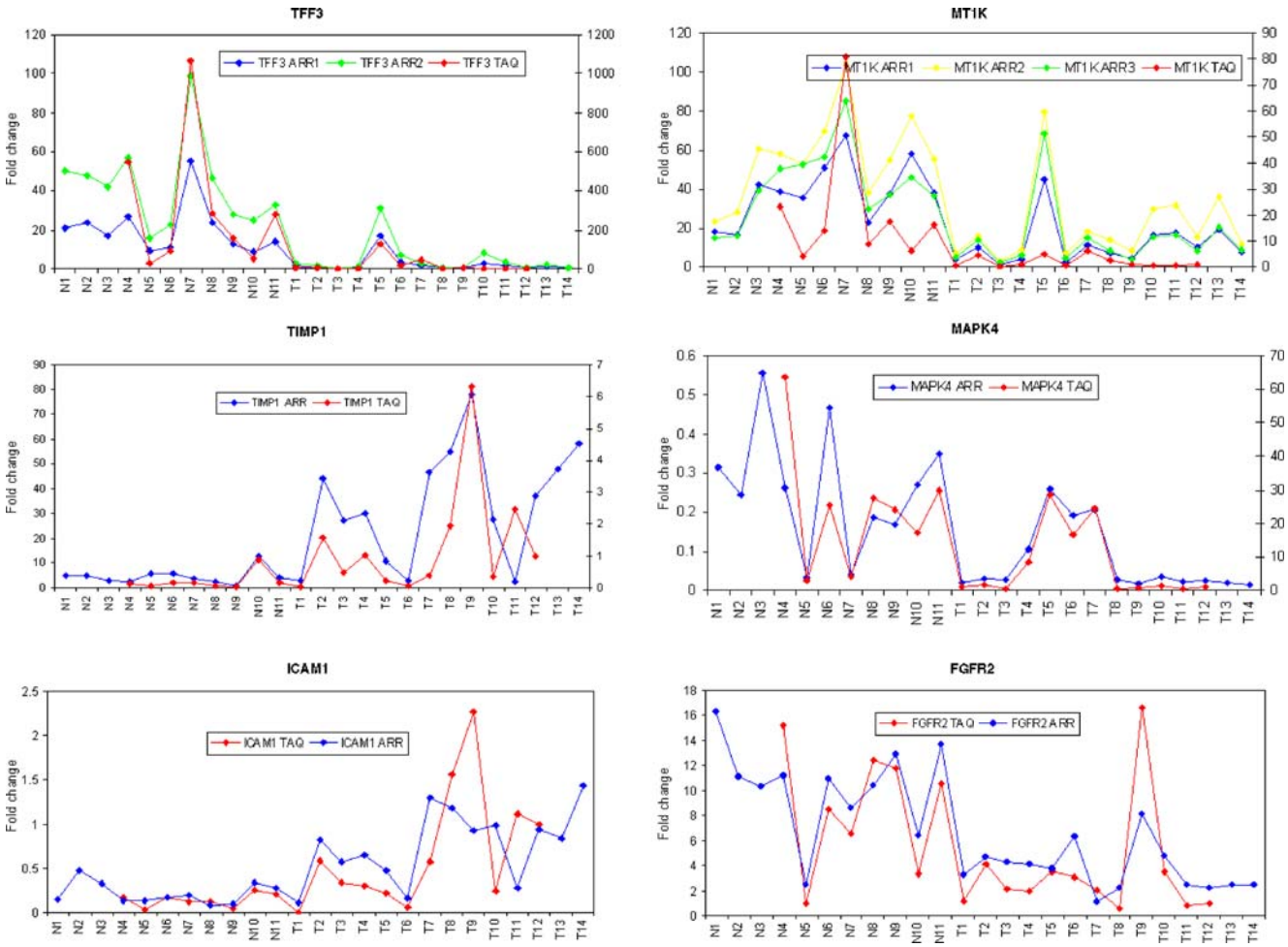

Fig. 2 TaqMan® PCR validation of microarray experiments. Profile charts of gene expression levels comparing results obtained by microarray analysis (n=25) to TaqMan® PCR analysis (n=20) for six genes. Plots for those genes with multiple probes are also displayed where appropriate

in thyroid cancer [15, 38]. Where there was discordance in the data, it could be accounted for by differences in the sequences targeted by the TaqMan® target sequences and the microarray probe. In those cases, the array and predesigned TaqMan assays interrogated different exons or alternative splice variants. This finding highlights the importance of matching the targets to be validated from microarray data sets.

Analysis of differentially expressed transcripts in the FVPTC revealed many transcripts showing similar expression level patterns in both FVPTC and classic morphology PTC. Examples of these transcripts are included in Table 2. In addition, somewhat surprisingly, unsupervised clustering of all samples showed no tendency for FVPTC to cluster independently of classic morphology PTC, emphasizing the very close relationship of these PTC variants (data not shown). However, analysis of differentially expressed genes in FVPTC exclusive of those identified in classic morphology PTC revealed 15 genes exhibiting differential expression in FVPTC compared with benign lesions and conditions outwith of classic morphology PTC. These genes displayed a narrow gamut of function represented by the transcripts involved (Table 3). TaqMan® RT-PCR was performed for all of these targets to confirm the array findings and correlation with the array data was strong (see Table 3).

Aberrant expression of two major groups of transcripts was noted in FVPTC. Relatively increased expression of class 1 major histocompatibility complex (MHC) genes (HLA-A) and aberrant expression of class 2 MHC genes (HLA-DMA, HLA-DPB-1, HLA-DQB-1, HLA DRA) and associated genes (e.g. CD74 represents the invariant membrane bound moiety of class II HLA molecules and regulates the biology and functions of MHC class II molecules and CD14 is a surface marker of monocytes/macrophages) were the most significant findings. Additionally, relatively up-regulated expression of members of the cathepsin family (cathepsin C, cathepsin H, cathepsin S, and TDO2) was striking in the FVPTC group. HLA expression is generally associated with immune functions

Table 3 Correlation between TaqMan® and microarray data

Gene	Pearson's *r* coefficient	two-tailed *p*
Genes differentially expressed in FVPTC vs classic PTC		
CD14	0.83	<0.0001
CD74[a]	0.87	<0.0001
	0.74	0.0002
CTSC	0.53	0.0170
CTSH	0.71	0.0005
CTSS	0.62	0.0037
DPP6	0.76	0.0001
ETHE1	0.30	0.2008
HLA-A	0.77	<0.0001
HLA-DMA	0.75	0.0001
HLA-DPB1	0.96	<0.0001
HLA-DQB1[a]	0.70	0.0006
	0.63	0.0031
HLA-DRA	0.82	<0.0001
NONAME	−0.02	0.9323
OSTF1	0.15	0.5171
TDO2	0.68	0.0009
Genes differentially expressed in benign vs malignant		
BAX	0.20	0.3997
CAMK1	0.17	0.4771
CD44	0.57	0.0094
CTSS	0.62	0.0037
CXADR	0.36	0.1152
FGFR2	0.84	<0.0001
GALE	0.54	0.0138
ICAM1	0.62	0.0038
LYN	0.45	0.0483
MAPK4	0.76	<0.0001
MMP14	0.36	0.1175
MT1F	0.92	<0.0001
MT1K[a]	0.68	0.0011
	0.69	0.0007
	0.70	0.0006
MT1X[a]	0.88	<0.0001
	0.88	<0.0001
RAB23	0.70	0.0006
S100A11	0.61	0.0041
SDC2	0.34	0.1415
SDC3	0.57	0.0087
TFF3[a]	0.97	<0.0001
	0.96	<0.0001
TGFB1	0.56	0.0098
TIMP1	0.73	0.0003
TIMP4	0.80	<0.0001
TOP2A	0.07	0.7769
TSHR	0.18	0.4440

Gene expression profiles for TaqMan® PCR and microarray results were compared using the Pearson coefficient.

[a] Genes have more than one probe ID on microarray

such as T cell interaction and antigen presentation. The presence of prominent HLA transcript expression, especially among class 2 in FVPTC, is intriguing. One potential cause of this was that tumour-infiltrating leucocytes were responsible for this finding. However, haematoxylin–eosin (H&E)-stained slides of each case were reviewed to specifically identify the degree of tumour infiltration by leucocytes. Although a mild lymphocytic infiltrate was noted in some cases, there was no apparent over representation of lymphocytes in the follicular variant compared to benign lesions and classic morphology PTC. This raises the clear possibility that the findings represent aberrant increased expression of class 2 HLA transcripts by the epithelium of FVPTC. This is an unexpected finding, as over-expression of MHC class 2 molecules would be expected to increase tumour immunogenicity. A similar aberrant expression of HLA transcripts has been recently described in ovarian neoplasms [34]. Rangel et al. [34] concluded over-expression of HLA-DRA might represent a novel biomarker for malignancy, and this also seems biologically plausible in the FVPTC setting. A recent paper has also described HLA-DRA expression in ret/PTC-activated papillary thyroid carcinoma but not in surrounding normal thyroid follicles [19]. Yu et al. [47] showed discordant expression of (CD74Ii) and HLA-DR in Hashimoto thyroiditis, an autoimmune condition associated with increased incidence of PTC and sharing molecular features such as ret/PTC expression [18, 37]. Hwang et al. [19] have drawn attention to aberrant expression of HLA-DRA in ret/PTC-activated PTC. Expression of HLA-DRA may in some way explain the propensity for PTC to metastasize to lymph nodes and often apparently reside there without markedly worsening prognosis.

Cathepsins C (dipeptidyl-peptidase I), H, and S showed up-regulation in FVPTC compared to benign lesions. Cathepsins are a family of proteases that play an important role in protein degradation. They are key players in the proliferative, invasive, and metastatic potential of malignant tumour cells. Their expression in the relatively biologically indolent FVPTC is intriguing, and it remains possible that cathepsins have cellular roles outside of those involved in invasion and dissemination of tumour cells as indeed has been suggested by others [43]. For example, cathepsin L has recently been shown to play a role in nuclear transcriptional activation, and cathepsins are now recognized to play a role in MHC class II antigen presentation [44]. OSTF1 has no defined role in carcinogenesis, although outside of its role in ossification, it is also known to have roles in signal transduction and protein binding, which may be relevant to carcinogenesis and, particularly, FVPTC. A recent paper highlights the role of bone mineralization proteins including osteopontin and osteoclast stimulating factors as potential biomarkers of malignant tumours in general [1]. Indeed, in addition to elevated OSTF1 expression, increased expression of osteopontin was seen in PTC (data not shown); however, in our data, osteopontin does not appear to be specifically up-regulated

in FVPTC, and this finding has also been noted by other researchers [14]. In any case, osteopontin is known to be a downstream effector of ret/PTC [5] and mutated BRAF [14], where it acts in association with CD44, another transcript showing increased expression in both classic morphology PTC and FVPTC.

A particular focus of this study was to compare transcriptome profiles for PTCs with classic morphology and FVPTC given the propensity for FVPTC lesions to prove problematic from a diagnostic perspective. Although the study confirms the close relationship between the two most common variants of PTC, a narrow portfolio of genes and, in particular, gene functions was elucidated in the FVPTC cohort. The targets identified are easily amenable to analysis by more established techniques such as TaqMan® RT-PCR, with associated potential as additional markers for application in the FNAC setting. Clearly, the potential biomarkers identified in this study will require prospective evaluation in the context of real clinical diagnostic situations in the future to consolidate their merit as adjunctive tests in the diagnostic setting and to validate their altered expression states in the pathobiology of PTC development.

Acknowledgement Dr. Smyth and Dr. Finn contributed equally to this study.

References

1. Amatschek S, Koenig U, Auer H, Steinlein P, Pacher M, Gruenfelder A, Dekan G, Vogl S, Kubista E, Heider KH, Stratowa C, Schreiber M, Sommergruber W (2004) Tissue-wide expression profiling using cDNA subtraction and microarrays to identify tumor-specific genes. Cancer Res 264:844–856
2. Barden CB, Shister KW, Zhu B, Guiter G, Greenblatt DY, Zeiger MA, Fahey TJ 3rd (2003) Classification of follicular thyroid tumors by molecular signature: results of gene profiling. Clin Cancer Res 9:1792–1800
3. Benjamini Y, Yekutieli D (2001) The control of the false discovery rate in multiple testing under dependency. Ann Stat 29:1165–1188
4. Cai L, Wang GJ, Xu ZL, Deng DX, Chakrabarti S, Cherian MG (1998) Metallothionein and apoptosis in primary human hepatocellular carcinoma (HCC) from northern China. Anticancer Res 18:4667–4672
5. Castellone MD, Celetti A, Guarino V, Cirafici AM, Basolo F, Giannini R, Medico E, Kruhoffer M, Orntoft TF, Curcio F, Fusco A, Melillo RM, Santoro M (2004) Autocrine stimulation by osteopontin plays a pivotal role in the expression of the mitogenic and invasive phenotype of RET/PTC-transformed thyroid cells. Oncogene 23:2188–2196
6. Cerutti JM, Delcelo R, Amadei MJ, Nakabashi C, Maciel RM, Peterson B, Shoemaker J, Riggins GJ (2004) A preoperative diagnostic test that distinguishes benign from malignant thyroid carcinoma based on gene expression. J Clin Invest 113:1234–1242
7. Deng DX, Chakrabarti S, Waalkes MP, Cherian MG (1998) Metallothionein and apoptosis in primary human hepatocellular carcinoma and metastatic adenocarcinoma. Histopathology 32:340–347
8. Ding K, Lopez-Burks M, Sanchez-Duran JA, Korc M, Lander AD (2005) Growth factor-induced shedding of syndecan-1 confers glypican-1 dependence on mitogenic responses of cancer cells. J Cell Biol 171:729–738
9. Finley DJ, Arora N, Zhu B, Gallagher L, Fahey TJ 3rd (2004) Molecular profiling distinguishes papillary carcinoma from benign thyroid nodules. J Clin Endocrinol Metab 89:3214–3223
10. Finley DJ, Zhu B, Barden CB, Fahey TJ 3rd (2004) Discrimination of benign and malignant thyroid nodules by molecular profiling. Ann Surg 240:425–436
11. Finn SP, Smyth P, O'Leary J, Sweeney EC, Sheils O (2003) Ret/PTC chimeric transcripts in an Irish cohort of sporadic papillary thyroid carcinoma. J Clin Endocrinol Metab 88:938–941
12. Fusco A, Grieco M, Santoro M, Berlingieri MT, Pilotti S, Pierotti MA, Della Porta G, Vecchio G (1987) A new oncogene in human thyroid papillary carcinomas and their lymph-nodal metastases. Nature 328:170–172
13. Grieco M, Santoro M, Berlingieri MT, Melillo RM, Donghi R, Bongarzone I, Pierotti MA, Della Porta G, Fusco A, Vecchio G (1990) PTC is a novel rearranged form of the ret proto-oncogene and is frequently detected in vivo in human thyroid papillary carcinomas. Cell 60:557–563
14. Guarino V, Faviana P, Salvatore G, Castellone MD, Cirafici AM, De Falco V, Celetti A, Giannini R, Basolo F, Melillo RM, Santoro M (2005) Osteopontin is overexpressed in human papillary thyroid carcinomas and enhances thyroid carcinoma cell invasiveness. J Clin Endocrinol Metab 90:5270–5278
15. Hermann S, Sturm I, Mrozek A, Klosterhalfen B, Hauptmann S, Dorken B, Daniel PT (2001) Bax expression in benign and malignant thyroid tumours: dysregulation of wild-type P53 is associated with a high Bax and P21 expression in thyroid carcinoma. Int J Cancer 92:805–811
16. Huang Y, Prasad M, Lemon WJ, Hampel H, Wright FA, Kornacker K, LiVolsi V, Frankel W, Kloos RT, Eng C, Pellegata NS, de la Chapelle A (2001) Gene expression in papillary thyroid carcinoma reveals highly consistent profiles. Proc Natl Acad Sci USA 98:15044–15049
17. Huang Y, de la Chapelle A, Pellegata NS (2003) Hypermethylation, but not LOH, is associated with the low expression of MT1G and CRABP1 in papillary thyroid carcinoma. Int J Cancer 104:735–744
18. Hunt JL, Baloch ZW, Barnes L, Swalsky PA, Trusky CL, Sesatomi E, Finkelstein S, LiVolsi VA (2002) Loss of heterozygosity mutations of tumor suppressor genes in cytologically atypical areas in chronic lymphocytic thyroiditis. Endocr Pathol 13:321–330
19. Hwang ES, Kim DW, Hwang JH, Jung HS, Suh JM, Park YJ, Chung HK, Song JH, Park KC, Park SH, Yun HJ, Kim JM, Shong M (2004) Regulation of signal transducer and activator of transcription 1 (STAT1) and STAT1-dependent genes by RET/PTC (rearranged in transformation/papillary thyroid carcinoma) oncogenic tyrosine kinases. Mol Endocrinol 18:2672–2684
20. Jarzab B, Wiench M, Fujarewicz K, Simek K, Jarzab M, Oczko-Wojciechowska M, Wloch J, Czarniecka A, Chmielik E, Lange D, Pawlaczek A, Szpak S, Gubala E, Swierniak A (2005) Gene expression profile of papillary thyroid cancer: sources of variability and diagnostic implications. Cancer Res 65:1587–1597
21. Kimura ET, Nikiforova MN, Zhu Z, Knauf JA, Nikiforov YE, Fagin JA (2003) High prevalence of BRAF mutations in thyroid cancer: genetic evidence for constitutive activation of the RET/PTC–RAS–BRAF signaling pathway in papillary thyroid carcinoma. Cancer Res 63:1454–1457
22. Lima J, Trovisco V, Soares P, Maximo V, Magalhaes J, Salvatore G, Santoro M, Bogdanova T, Tronko M, Abrosimov A, Jeremiah S, Thomas G, Williams D, Sobrinho-Simoes M (2004) BRAF mutations are not a major event in post-Chernobyl childhood thyroid carcinomas. J Clin Endocrinol Metab 89:4267–4271

23. Livak KJ, Schmittgen TD (2001) Analysis of relative gene expression data using real-time quantitative PCR and the 2(−Delta Delta C(T)) Method. Methods 25:402–408
24. Lloyd R, DeLellis R, Heitz P, Eng C (eds) (2004) Pathology and genetics of tumours of endocrine Organs. IARC Press
25. Lloyd RV, Erickson LA, Casey MB, Lam KY, Lohse CM, Asa SL, Chan JK, DeLellis RA, Harach HR, Kakudo K, LiVolsi VA, Rosai J, Sebo TJ, Sobrinho-Simoes M, Wenig BM, Lae ME (2004) Observer variation in the diagnosis of follicular variant of papillary thyroid carcinoma. Am J Surg Pathol 28:1336–1340
26. Marcos I, Borrego S, Antinolo G (2003) Molecular cloning and characterization of human RAB23, a member of the group of Rab GTPases. Int J Mol Med 12:983–987
27. Marsee DK, Vadysirisack DD, Morrison CD, Prasad ML, Eng C, Duh QY, Rauen KA, Kloos RT, Jhiang SM (2005) Variable expression of Coxsackie–adenovirus receptor in thyroid tumors: implications for adenoviral gene therapy. Thyroid 15:977–987
28. Mazzanti C, Zeiger MA, Costouros NG, Umbricht C, Westra WH, Smith D, Somervell H, Bevilacqua G, Alexander HR, Libutti SK (2004) Using gene expression profiling to differentiate benign versus malignant thyroid tumors. Cancer Res 64:2898–2903
29. Mitselou A, Vougiouklakis TG, Peschos D, Dallas P, Boumba VA, Agnantis NJ (2002) Immunohistochemical study of the expression of S-100 protein, epithelial membrane antigen, cytokeratin and carcinoembryonic antigen in thyroid lesions. Anticancer Res 22:1777–1780
30. Namba H, Nakashima M, Hayashi T, Hayashida N, Maeda S, Rogounovitch TI, Ohtsuru A, Saenko VA, Kanematsu T, Yamashita S (2003) Clinical implication of hot spot BRAF mutation, V599E, in papillary thyroid cancers. J Clin Endocrinol Metab 88:4393–4397
31. Nartey N, Cherian MG, Banerjee D (1987) Immunohistochemical localization of metallothionein in human thyroid tumors. Am J Pathol 129:177–182
32. Nikiforova MN, Ciampi R, Salvatore G, Santoro M, Gandhi M, Knauf JA, Thomas GA, Jeremiah S, Bogdanova TI, Tronko MD, Fagin JA, Nikiforov YE (2004) Low prevalence of BRAF mutations in radiation-induced thyroid tumors in contrast to sporadic papillary carcinomas. Cancer Lett 209:1–6
33. Ofner D, Maier H, Riedmann B, Bammer T, Rumer A, Winde G, Bocker W, Jasani B, Schmid KW (1994) Immunohistochemical metallothionein expression in colorectal adenocarcinoma: correlation with tumour stage and patient survival. Virchows Arch 425:491–497
34. Rangel LB, Agarwal R, Sherman-Baust CA, Mello-Coelho V, Pizer ES, Ji H, Taub DD, Morin PJ (2004) Anomalous expression of the HLA-DR alpha and beta chains in ovarian and other cancers. Cancer Biol Ther 3:1021–1027
35. Santoro M, Carlomagno F, Hay ID, Herrmann MA, Grieco M, Melillo R, Pierotti MA, Bongarzone I, Della Porta G, Berger N, Peix JL, Paulin C, Fabien N, Vecchio G, Jenkins RB, Fusco A (1992) Ret oncogene activation in human thyroid neoplasms is restricted to the papillary cancer subtype. J Clin Invest 89:1517–1522
36. Schmid KW, Greeff M, Hittmair A, Totsch M, Ofner D, Dockhorn-Dworniczak B, Bocker W, Jasani B (1994) Metallothionein expression in normal, hyperplastic, and neoplastic thyroid follicular and parafollicular C cells using monoclonal antimetallothionein antibody E9. Endocr Pathol 5:114–122
37. Sheils OM, O'Leary JJ, Uhlmann V, Lattich K, Sweeney EC (2000) ret/PTC-1 activation in Hashimoto thyroiditis. Int J Surg Pathol 8:185–189
38. Sheils OM, Sweeney EC (1999) TSH receptor status of thyroid neoplasms-TaqMan RT-PCR analysis of archival material. J Pathol 188:87–92
39. Smyth P, Finn S, Cahill S, O'Regan E, Flavin R, O'Leary JJ, Sheils O (2005) ret/PTC and BRAF act as distinct molecular, time-dependant triggers in a sporadic Irish cohort of papillary thyroid carcinoma. Int J Surg Pathol 13:1–8
40. Stolf BS, Abreu CM, Mahler-Araujo MB, Dellamano M, Martins WK, de Carvalho MB, Curado MP, Diaz JP, Fabri A, Brentani H, Carvalho AF, Soares FA, Kowalski LP, Hirata R Jr, Reis LF (2005) Expression profile of malignant and non-malignant diseases of the thyroid gland reveals altered expression of a common set of genes in goiter and papillary carcinomas. Cancer Lett 227:59–73
41. Tanaka M, Adzuma K, Iwami M, Yoshimoto K, Monden Y, Itakura M (1995) Human calgizzarin; one colorectal cancer-related gene selected by a large scale random cDNA sequencing and Northern blot analysis. Cancer Lett 89:195–200
42. Thomas GA, Bunnell H, Cook HA, Williams ED, Nerovnya A, Cherstvoy ED, Tronko ND, Bogdanova TI, Chiappetta G, Viglietto G, Pentimalli F, Salvatore G, Fusco A, Santoro M, Vecchio G (1999) High prevalence of RET/PTC rearrangements in Ukrainian and Belarussian post-Chernobyl thyroid papillary carcinomas: a strong correlation between RET/PTC3 and the solid-follicular variant. J Clin Endocrinol Metab 84:4232–4238
43. Turk B, Turk D, Turk V (2000) Lysosomal cysteine proteases: more than scavengers. Biochim Biophys Acta 1477:98–111
44. Villadangos JA, Bryant RA, Deussing J, Driessen C, Lennon-Dumenil AM, Riese RJ, Roth W, Saftig P, Shi GP, Chapman HA, Peters C, Ploegh HL (1999) Proteases involved in MHC class II antigen presentation. Immunol Rev 172:109–120
45. Williams ED (2000) Two proposals regarding the terminology of thyroid tumors. Int J Surg Pathol 8:181–183
46. Yano Y, Uematsu N, Yashiro T, Hara H, Ueno E, Miwa M, Tsujimoto G, Aiyoshi Y, Uchida K (2004) Gene expression profiling identifies platelet-derived growth factor as a diagnostic molecular marker for papillary thyroid carcinoma. Clin Cancer Res 10:2035–2043
47. Yu M, Xu M, Savas L, Khan A (1998) Discordant expression of Ii and HLA-DR in thyrocytes: a possible pathogenetic factor in Hashimoto's thyroiditis. Endocr Pathol 9:201–208

Virchows Arch (2007) 450:261–266
DOI 10.1007/s00428-006-0349-4

ORIGINAL ARTICLE

Expression of transcription factors and precursor cell markers during regeneration of β cells in pancreata of rats treated with streptozotocin

Katharina Tiemann · Roswitha Panienka · Günter Klöppel

Received: 30 June 2006 / Accepted: 7 November 2006 / Published online: 18 January 2007
© Springer-Verlag 2007

Abstract An understanding of β cell regeneration is needed if we are to develop new treatment modalities in diabetes mellitus. Lineage tracing studies have shown that all pancreatic cell types, including β cells, arise from PDX-1-expressing precursor cells. We studied β cell regeneration by analyzing the immunocytochemical expression of the transcription factors, PDX-1, PBX-1, and MEIS2, and that of the potential precursor cell markers, c-Kit and nestin, using the model of streptozotocin (STZ)-induced diabetes in rats. The pancreata were examined 3, 7, and 14 days after STZ administration. PDX-1 expression, but not that of MEIS2 and PBX-1, transiently increased on day 7. c-Kit expression was found to be upregulated in islet cells at all points in time, while nestin expression was lacking. Ki-67 labeling was increased in islets on days 3 and 7. These results suggest that temporary upregulation of PDX-1 and prolonged overexpression of c-Kit may play a role during β cell regeneration.

Keywords Islet cell neogenesis · Beta cell regeneration · Transcription factors · Streptozotocin · Diabetes

Supported by a grant from the Deutsche Forschungsgemeinschaft (PE 732/2-1).

K. Tiemann (✉) · R. Panienka · G. Klöppel
Department of Pathology, University of Kiel,
Michaelisstr.11,
24105 Kiel, Germany
e-mail: k.peters@path.uni-kiel.de

Introduction

The regenerative capacity of the adult human pancreas appears to be limited. In experimental settings, however, adaptive β cell growth has been demonstrated in response to various stimuli and insults [3, 14, 15, 17, 19, 20]. In previous investigations using the pancreatic duct ligation (PDL) model, we found β cell neogenesis to be associated with the timing of the expression of transcription factors and putative stem cell markers [11]. Especially duct cells expressed c-Kit, nestin, and PDX-1. Here, we extend our studies to the pancreata of streptozotocin (STZ)-treated rats, an experimental model of β cell regeneration, to determine the expression patterns of the transcription factors PDX-1, PBX-1, and MEIS2, and that of c-Kit and nestin under these conditions. This should help us to identify the cells or compartments that are responsive to the stimulus and, therefore, should have a high regenerative capacity. The regeneration of β cells in STZ-treated pancreata has already been demonstrated in neonatal rats [19]. In adult rats with STZ diabetes, it has been postulated that, in contrast to the PDL model, ductal cells are not the main source for a regeneration of β cells [4, 7].

We investigated the expression patterns of the transcription factor PDX-1, which is necessary for pancreatic development during embryogenesis and persists in β cells and a few acinar cells during adult life [8]; the transcription factor PBX-1, the inactivation of which leads to pancreatic hypoplasia [5]; and MEIS2, which is able to alter the activity of PDX-1 [16]. We expected to find a rise in expression of these transcription factors in the cells of all pancreatic compartments in association with concomitant c-Kit (CD117) and nestin expression. These two markers have been reported to be associated with pancreatic ducts and islets during pancreatic regeneration [6, 10, 12, 21]. Finally,

we wanted to gain insights into the different modes of regeneration in the pancreas of STZ-treated diabetic rats in comparison with other models.

Materials and methods

Animals and tissue processing

In the STZ group (n=20), 3-month-old Wistar rats received a single intraperitoneal injection of 100 μg STZ (Sigma, St. Louis, MO, USA) per gram body weight, dissolved in citrate buffer, pH 4.5, as described previously [19]. Animals were killed 3, 7, and 14 days after treatment. Pancreata were dissected, fixed in 4% paraformaldehyde, and embedded in paraffin, with the head and tail portion embedded separately. Due to the division of the pancreas, 16 tissue blocks for day 3 and 12 tissue blocks each for days 7 and 14 were obtained. Head portions of pancreata of non-STZ-treated age-matched rats served as controls.

Immunohistochemistry

The tissue sections from both the head and tail portions of the STZ-treated rats were immunostained with the primary antibodies against PDX-1 (a kind gift of Christopher V.E. Wright, Vanderbilt University Medical Center, Nashville, TN, USA, dilution 1:200), antibodies against PBX-1 and MEIS2 (Santa Cruz Biotechnology, Santa Cruz, CA, USA, dilution 1:20 and 1:30, respectively), nestin (BD PharMingen, Heidelberg, Germany, dilution 1:50), c-Kit (Santa Cruz Biotechnology, dilution 1:20), insulin (BioGenex, San Ramon, CA, USA, dilution 1:40), and Ki-67 (DAKO, Glostrup, Denmark, dilution 1:25), using the avidin–biotin complex method (Vectastain ABC kit, ELITE, Vector, Burlingame, CA, USA).

Briefly, deparaffinized, rehydrated, 3–4-μm sections were cooked in a pressure cooker for 3.5 min using citrate buffer, pH 6.0. After washing, endogenous peroxidase was blocked for 20 min with H_2O_2 blocking reagent (DAKO-Cytomation, Hamburg, Germany). Nonspecific staining was blocked by incubation with serum for 15 min. All

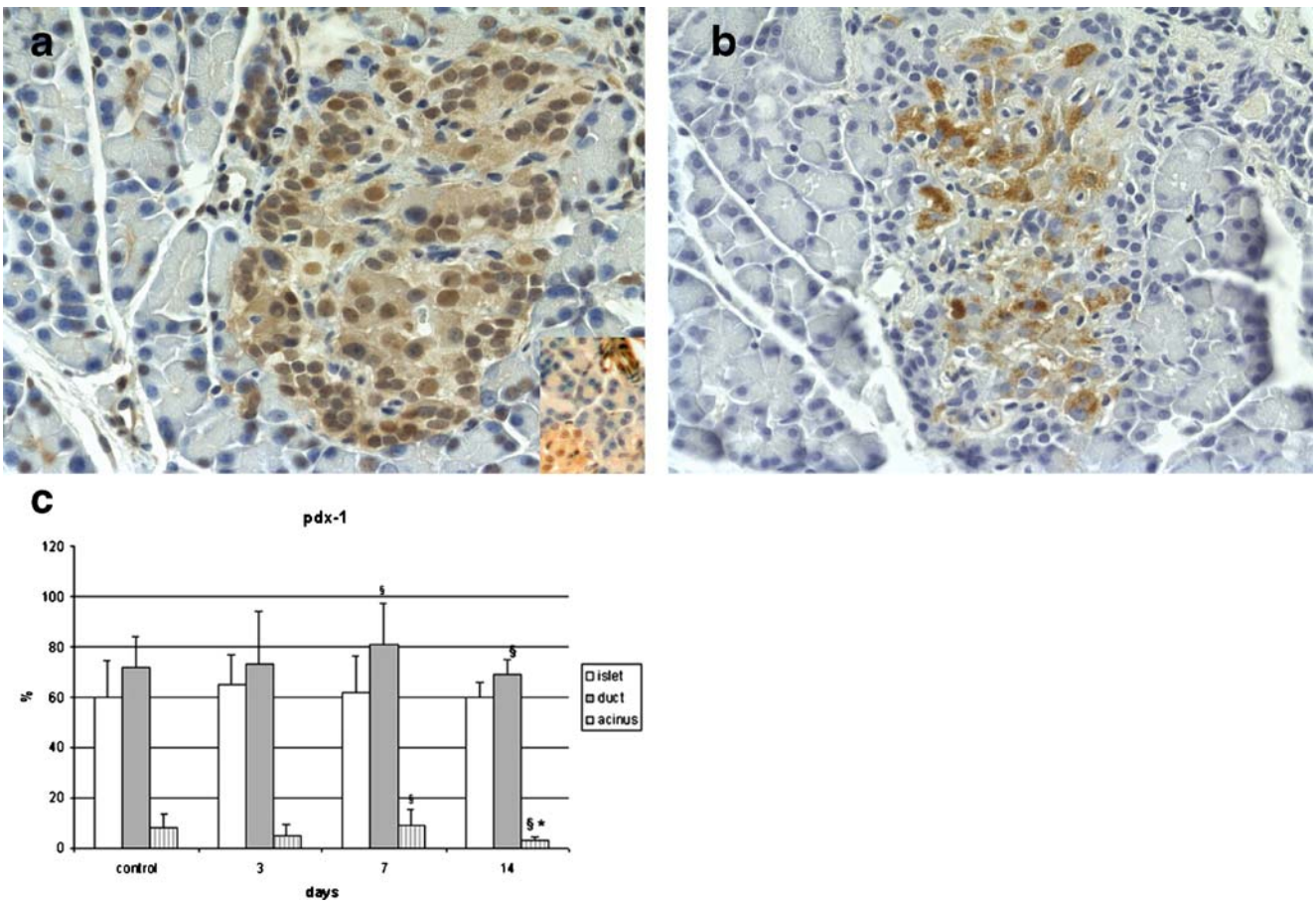

Fig. 1 Expression of PDX-1 (**a**) compared to insulin staining (**b**) in the pancreas on day 7 after STZ administration, and quantitative analysis of the percentage of PDX-1-positive cells (**c**); significant differences are marked with an *asterisk* (compared to the control) and *section marks* (comparison of day 7 with day 14). *Insert* in **a**: control

sections were incubated with a tested dilution of the primary antibody for 45 min and with the biotinylated secondary antibody for 30 min. Staining was visualized using diaminobenzidine (substrate kit, Vector) as chromogen. Controls were performed by omitting the primary antibody or secondary antibody. No staining was observed under the negative control conditions. Normal pancreatic tissue served as control for PDX-1, PBX-1, MEIS2, and insulin. Other antibodies were tested on adequate tissue specimens, as applicable in routine immunohistochemistry.

Quantitative analysis

In the immunostained sections at least 200 cells per compartment (islet, duct, acini) were counted. Counting was performed at least twice by two independent observers.

Statistical analysis

Values are expressed as mean±SD. Statistical significance was determined by using a two-tailed unpaired Student's *t* test. Differences were considered to be statistically significant if $p<0.05$.

Results

Histopathology

The morphology of the pancreas did not show any significant changes in H&E-stained sections. Only few islets showed a weak inflammatory reaction. On day 3 after STZ administration, the number of insulin-positive cells in the islets decreased from a large number to a few cells. During the subsequent days, the number of insulin-positive β cells in the islets increased; the islets became more prominent and, concomitantly, an increase in islet size was observed. Furthermore, clusters of extraislet endocrine cells were observed, defined by scattered insulin immunoreactive cells, that were not associated with ducts.

Expression of PDX-1, PBX-1, and MEIS2

PDX-1 expression increased in pancreatic duct cells and acinar cells until day 7 and had decreased significantly by day 14 to levels below those of day 3. Islet cells showed constant PDX-1 expression, which was not restricted to β cells (Fig. 1a–c). PBX-1 expression (Fig. 2a) also showed a

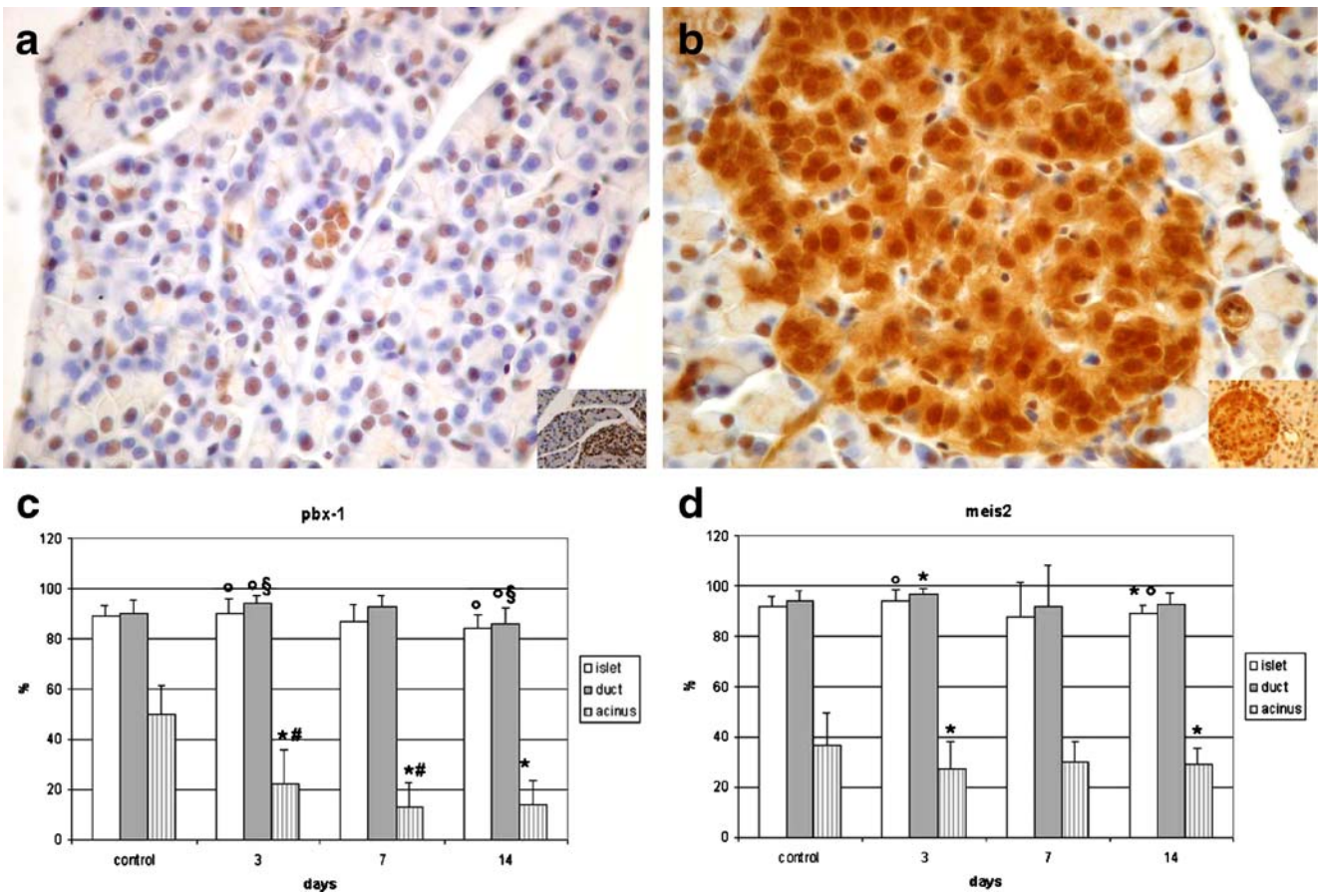

Fig. 2 Expression of PBX-1 (**a**) and MEIS2 (**b**) on day 7 after STZ treatment and respective quantitative analysis (**c** and **d**), statistically significant differences are marked marked with *asterisks* (compared to the control), *sharp signs* (day 3 compared to day 7), *open circles* (comparison of days 3 and 14), and *section marks* (comparison of day 7 to day 14). *Inserts* in **a** and **b** shows control pancreas

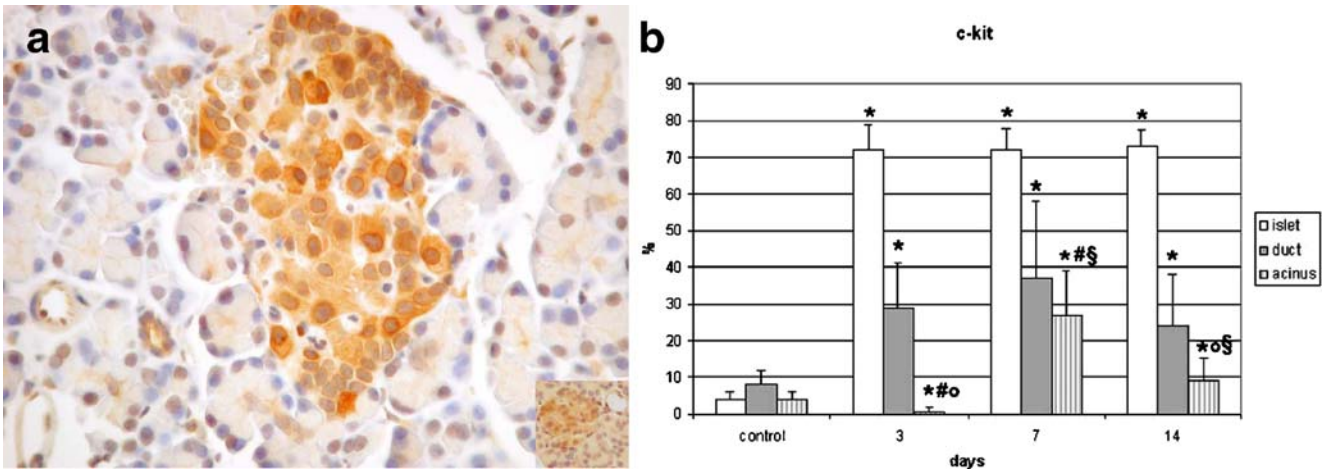

Fig. 3 c-Kit expression in the pancreas on day 7 after STZ administration (**a**, *insert* shows control), and quantitative analysis of the percentage of c-Kit-positive cells in the different compartments compared to the control (**b**, significant differences are marked as in Fig. 2c and d)

decrease over time, which was most evident in acinar cells (22±14% positive cells on day 3 and 14±9% positive cells on day 14), while the expression level was always lower than in the control. MEIS2 expression (Fig. 2b) decreased significantly in islet cells during the observation period (from 94±5% to 89±3%, $p=0.007$). All three transcription factors were expressed in the nuclei.

Expression of c-Kit and nestin

Islet cells consistently showed cytoplasmic overexpression of c-Kit compared to the control. In ductal and acinar cells, the expression peaked on day 7 and decreased thereafter. c-Kit expression was lower in acinar cells on day 3 than in the controls (Fig. 3a,b). No expression of nestin was seen on either day, a pattern identical to the controls.

Ki-67 labeling

Ki-67 labeling revealed that proliferation was significantly increased in the islet cells on days 3 and 7 compared to day 14 (both $p<0.0001$). Proliferation was also increased in ductal and acinar cells on day 3 compared to days 14 and 7, respectively (Fig. 4a,b). The level at day 14 equalizes that of a normal pancreas.

Discussion

A main aim of stem cell therapy in type 1 or type 2 diabetes is to replenish the insulin-producing cell pool. For this, our understanding of the factors controlling the growth and renewal of β cells needs to be improved. We used an animal model to study β cell regeneration under diabetic

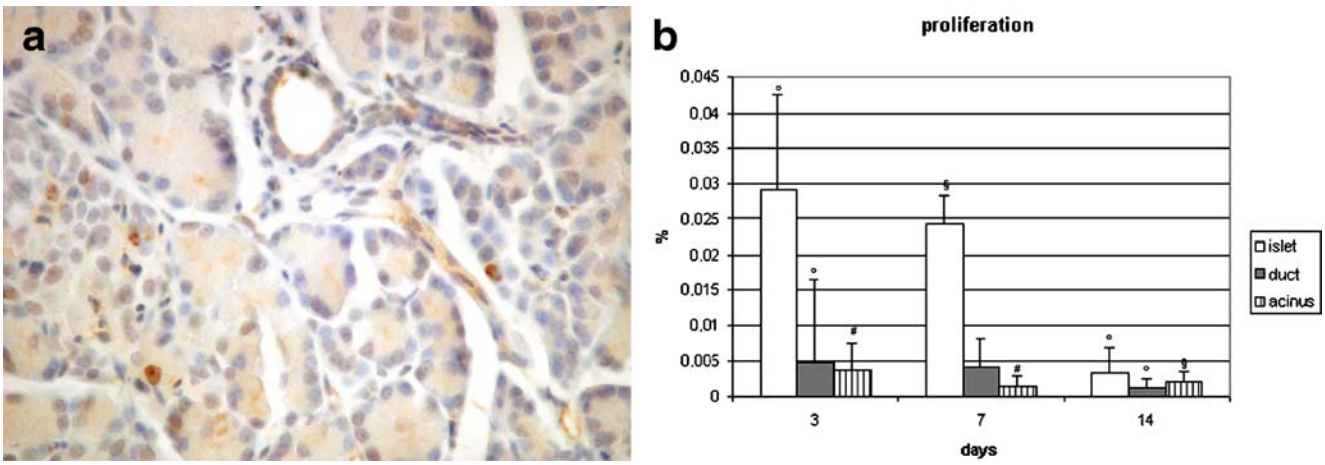

Fig. 4 Proliferation, demonstrated by Ki-67 staining, on day 7 after STZ administration (**a**) and quantitative analysis of proliferation (**b**, significant differences are marked as in Fig. 2c and d)

conditions and traced the expression of transcription factors and putative progenitor cell markers during β cell regeneration after degranulation by STZ. The reappearance of the β cells was associated with a temporary overexpression of PDX-1 in all compartments of the pancreas and the occurrence of a population of c-Kit-positive cells in the islets. Three days after STZ treatment, PDX-1 was found to be overexpressed not only in islet cells but also, and especially, in ductal cells and acinar cells. This PDX-1 expression was temporary because on day 14 it was already no longer demonstrable. The fact that all cellular lineages in the pancreas expressed PDX-1 after selective damage of the β cells by STZ could suggest that all cell compartments are involved in the regeneration of β cells by neogenesis and reduplication and that the expression pattern recapitulates early embryogenesis when PDX-1-positive cells give rise to both endocrine and exocrine cell lineages. Although the PDX-1 and PBX-1 expression decreased over time in the ductal and acinar cell compartments, this pattern does not contradict the hypothesis that these compartments are involved in the regeneration of β cells. A decrease in expression might be a sign either for reestablishment of a sufficient β cell mass or for the limited potential of neogenetic stimuli. The latter hypothesis is supported by the minimally elevated proliferation rate of these cells. The generally low acinar PBX-1 expression compared to the control might be due to the experimental setting in which the control was achieved, using the head portion of rats treated with PDL.

In contrast to our expectations, neither PBX-1 nor MEIS2 showed a similar expression pattern to PDX-1. Whereas in obese nondiabetic patients, PBX-1 overexpression with cytoplasmic sequestration into ductal cells has been observed along with islet neogenesis [9], this phenomenon was not seen in STZ-treated rats. On the other hand, PBX-1 and MEIS2 have been observed in acinar cell lines, thereby mediating an “acinar type” of PDX-1 activity. At least the phenomenon of decreasing levels of PBX-1 expression in acinar cells may be due to this pattern. PBX-1 might therefore be associated with the transdifferentiation of β cells into progenitor cells, as speculated by other authors [1].

c-Kit-positive cells have previously been found in close association with pancreatic ducts. c-Kit-expressing cells have a potential for further differentiation [12]. In STZ-treated rats, the number of c-Kit-positive cells increased in all cell compartments of the pancreas in comparison to controls. Whereas the percentage of c-Kit-overexpressing islet cells remained high, in ductal and acinar cells the expression intensity fluctuated and decreased. This finding, together with an elevated proliferation rate, suggests that the islet cells are the most important compartment for β cell regeneration. We previously demonstrated the coexpression of c-Kit with CK20 and PDX-1 during β cell neogenesis after PDL [11]. In these conditions, the c-Kit-positive cells were identified especially as ductal cells. This comparison reveals that, in the two models, different pathways for the regeneration of β cells predominate. In STZ diabetes in rats, regeneration is largely due to the replication of β cells that survive destruction, while in the duct ligation model, β cell neogenesis from ductal cells occurs. This comparison nicely indicates that c-Kit is a marker of pluripotent precursor cells in the pancreas. Because c-Kit expression also occurred in acinar cells, it is possible that these cells also have the capability to differentiate into other β cells [2]. Because the number of c-Kit-positive cells in compartments other than islets rose on day 7, when transcription factor expression begins to decline, it can be concluded that c-Kit up-regulation is a downstream event after transcription factor activation.

Since recent studies suggested that nestin is also involved in regenerative processes in the endocrine pancreas, we expected to find overexpression in STZ-treated rats. Surprisingly, however, there was no nestin expression at all. This observation contrasts with the results of Nagasao et al. [10] in STZ-treated neonatal rats. They found that 1% of the cells were nestin-positive 3 and 7 days after administration of STZ. These contradictory findings might be either due to the different antibodies used or to the age of the animals. The complete lack of nestin-positive cells in our series may be due to the destruction of a nestin-positive subpopulation by STZ. On the other hand, nestin expression may be induced by cytokine activity. This hypothesis explains why we were able to show nestin expression in a PDL model [11] but not in the STZ model, in which destruction of β cells is not associated with an inflammatory, cytokine-inducing reaction. This is further evidence for the concept that nestin is not useful as a stem cell marker [13]. Nevertheless, nestin-positive cells might be necessary for the environment and the maintenance of the islets [18]. It is known that the number of new β cells after STZ treatment is limited. For the development of new islet-like structures, not only β cell precursors but also environmental factors are needed. Nestin-positive cells may belong to these supporting factors. By destroying these supporting, nestin-positive cells, regeneration may be stopped at a certain level. It may therefore not be possible to replenish the β cell pool to the level prior to destruction.

In conclusion, our results suggest that, besides the expression of transcription factors like PDX-1, the expression of c-Kit is important for β cell regeneration in an STZ model of diabetes mellitus, whereas nestin is not needed for the development of new β cells.

Acknowledgements This work was supported by a grant from the Deutsche Forschungsgemeinschaft (PE 732/2-1). We are grateful to Rennian Wang, M.D., for providing tissue and helpful discussions.

References

1. Bouckenooghe T, Vandewalle B, Moerman E, Danze PM, Lukowiak B, Muharram G, Kerr-Conte J, Gmyr V, Laine B, Pattou F (2005) Expression of progenitor cell markers during expansion of sorted human pancreatic beta cells. Gene Expr 12:83–98
2. Bouwens L, Rooman I (2005) Regulation of pancreatic beta-cell mass. Physiol Rev 85:1255–1270
3. Fernandes A, King LC, Guz Y, Stein R, Wright CV, Teitelman G (1997) Differentiation of new insulin-producing cells is induced by injury in adult pancreatic islets. Endocrinology 138:1750–1762
4. Jörns A, Klempnauer J, Tiedge M, Lenzen S (2001) Recovery of pancreatic beta cells in response to long-term normoglycemia after pancreas or islet transplantation in severely streptozotocin diabetic adult rats. Pancreas 23:186–196
5. Kim SK, Selleri L, Lee JS, Zhang AY, Gu X, Jacobs Y, Cleary ML (2002) Pbx1 inactivation disrupts pancreas development and in Ipf1-deficient mice promotes diabetes mellitus. Nat Genet 30:430–435
6. Kim SY, Lee SH, Kim BM, Kim EH, Min BH, Bendayan M, Park IS (2004) Activation of nestin-positive duct stem (NPDS) cells in pancreas upon neogenic motivation and possible cytodifferentiation into insulin-secreting cells from NPDS cells. Dev Dyn 230:1–11
7. Kodama S, Toyonaga T, Kondo T, Matsumoto K, Tsuruzoe K, Kawashima J, Goto H, Kume K, Kume S, Sakakida M, Araki E (2005) Enhanced expression of PDX-1 and Ngn3 by exendin-4 during beta cell regeneration in STZ-treated mice. Biochem Biophys Res Commun 327:1170–1178
8. McKinnon CM, Docherty K (2001) Pancreatic duodenal homeobox-1, PDX-1, a major regulator of beta cell identity and function. Diabetologia 44:1203–1214
9. Muharram G, Beucher A, Moerman E, Belaich S, Gmyr V, Vandewalle B, Pattou F, Kerr-Conte J (2005) Endocrine pancreatic tissue plasticity in obese humans is associated with cytoplasmic expression of PBX-1 in pancreatic ductal cells. Biochem Biophys Res Commun 333:1153–1159
10. Nagasao J, Yoshioka K, Amasaki H, Mutoh K (2004) Expression of nestin and IGF-1 in rat pancreas after streptozotocin administration. Anat Histol Embryol 33:1–4
11. Peters K, Panienka R, Li J, Klöppel G, Wang R (2005) Expression of stem cell markers and transcription factors during the remodeling of the rat pancreas after duct ligation. Virchows Arch 446:56–63
12. Rachdi L, El Ghazi L, Bernex F, Panthier JJ, Czernichow P, Scharfmann R (2001) Expression of the receptor tyrosine kinase KIT in mature beta-cells and in the pancreas in development. Diabetes 50:2021–2028
13. Selander L, Edlund H (2002) Nestin is expressed in mesenchymal and not epithelial cells of the developing mouse pancreas. Mech Dev 113:189–192
14. Sharma A, Zangen DH, Reitz P, Taneja M, Lissauer ME, Miller CP, Weir GC, Habener JF, Bonner-Weir S (1999) The homeodomain protein IDX-1 increases after an early burst of proliferation during pancreatic regeneration. Diabetes 48:507–513
15. Sumi S, Gu Y, Hiura A, Inoue K (2004) Stem cells and regenerative medicine for diabetes mellitus. Pancreas 29:e85–e89
16. Swift GH, Liu Y, Rose SD, Bischof LJ, Steelman S, Buchberg AM, Wright CV, MacDonald RJ (1998) An endocrine–exocrine switch in the activity of the pancreatic homeodomain protein PDX1 through formation of a trimeric complex with PBX1b and MRG1 (MEIS2). Mol Cell Biol 18:5109–5120
17. Taguchi M, Yamaguchi T, Otsuki M (2002) Induction of PDX-1-positive cells in the main duct during regeneration after acute necrotizing pancreatitis in rats. J Pathol 197:638–646
18. Treutelaar MK, Skidmore JM, Dias-Leme CL, Hara M, Zhang L, Simeone D, Martin DM, Burant CF (2003) Nestin-lineage cells contribute to the microvasculature but not endocrine cells of the islet. Diabetes 52:2503–2512
19. Wang RN, Bouwens L, Klöppel G (1994) Beta-cell proliferation in normal and streptozotocin-treated newborn rats: site, dynamics and capacity. Diabetologia 37:1088–1096
20. Wang RN, Rehfeld JF, Nielsen FC, Klöppel G (1997) Expression of gastrin and transforming growth factor-alpha during duct to islet cell differentiation in the pancreas of duct-ligated adult rats. Diabetologia 40:887–893
21. Yashpal NK, Li J, Wang R (2004) Characterization of c-Kit and nestin expression during islet cell development in the prenatal and postnatal rat pancreas. Dev Dyn 229:813–825

Virchows Arch (2007) 450:267–271
DOI 10.1007/s00428-006-0344-9

ORIGINAL ARTICLE

Sertoli–Leydig cell tumours of the ovary and testis: a CGH and FISH study

I. Verdorfer · D. Horst · A. Höllrigl · H. Rogatsch · G. Mikuz

Received: 22 June 2006 / Accepted: 27 October 2006 / Published online: 18 January 2007
© Springer-Verlag 2007

Abstract We present two malignant cases of Sertoli–Leydig cell tumours (SLCT) of the testis and one ovarian SLCT with benign behaviour. The DNA copy number changes affected chromosome 1, 8, 9p, 10, 11, 12, 16, 19, 22 and X. The present study is the first molecular–cytogenetic analysis of Sertoli–Leydig cell tumours of the testis.

Keywords Comparative genomic hybridisation · Fluorescence in situ hybridisation · Sertoli–Leydig cell tumours · Sex-cord stromal tumours

Introduction

The Sertoli–Leydig cell tumours (SLCT) are exceptionally rare sex-cord stromal tumours of the testis [10, 18]. There are, however, some few cytogenetic studies of SLCT of the ovary, which revealed genetic aberrations affecting the sex chromosome [1, 3, 4]. Trisomy 8 was detected in a metastasizing ovarian SLCT as sole karyotypic aberration [7]. A case of virilising ovarian SLCT in a 14-year old black girl showed chromosomal rearrangements of chromosome 5, 18, trisomy 6 and 12 [15]. Cytogenetic studies of such tumours located in the testis have never been reported. We analysed therefore the chromosomal aberrations of two testicular and one ovarian SLCT.

I. Verdorfer (✉) · D. Horst · A. Höllrigl · G. Mikuz
Institute of Pathology, Medical University of Innsbruck,
Muellerstrasse 44,
6020 Innsbruck, Austria
e-mail: Irmgard.Verdorfer@i-med.ac.at

H. Rogatsch
Institute of Pathology, LKH Klagenfurt,
9020 Klagenfurt, Austria

Materials and methods

Tumour specimens and immunohistochemistry

Three SLCT, retrieved from the files of the Institute of Pathology Innsbruck (Medical University Innsbruck, Austria) were examined. Tissue sections were stained with haematoxylin and eosin, profiled immunohistochemically and classified according to the WHO classification of testicular tumours [12].

Comparative genomic hybridisation

Comparative genomic hybridisation (CGH) analysis was performed as previously described [17]. Briefly, tumour DNA and reference DNA were labelled with biotin-16-dUTP and digoxigenin-11-dUTP, respectively, by nick translation using a commercially available nick translation kit (Roche, Mannheim, Germany). The probe mixture of 500 ng tumour DNA, 500 ng reference DNA, 20 μg human Cot-1 DNA (Gibco BRL, Life Technologies, Germany) and 10 μg salmon sperm DNA (Eppendorf, Germany) was denatured for 5 min at 75°C and pre-annealed for 20 min at 37°C. The probe mixture was hybridised on a normal, denatured lymphocyte metaphase slide and hybridised 3 days in a humidified chamber. For detection, the slides were stained with avidin–fluorescein isothiocyanate (Vector Labs, Burlingame, CA, USA) and with anti-digoxigenin–rhodamin (Roche, Mannheim, Germany), followed by counter-staining with 4,6-diamino-2-phenylindole (DAPI; Serva, Germany). The slides were evaluated using a fluorescence microscope (Zeiss Axioplan) equipped with a CCD camera (JAI M300), specific filter sets and CGH software (ISIS, MetaSystems, Germany).

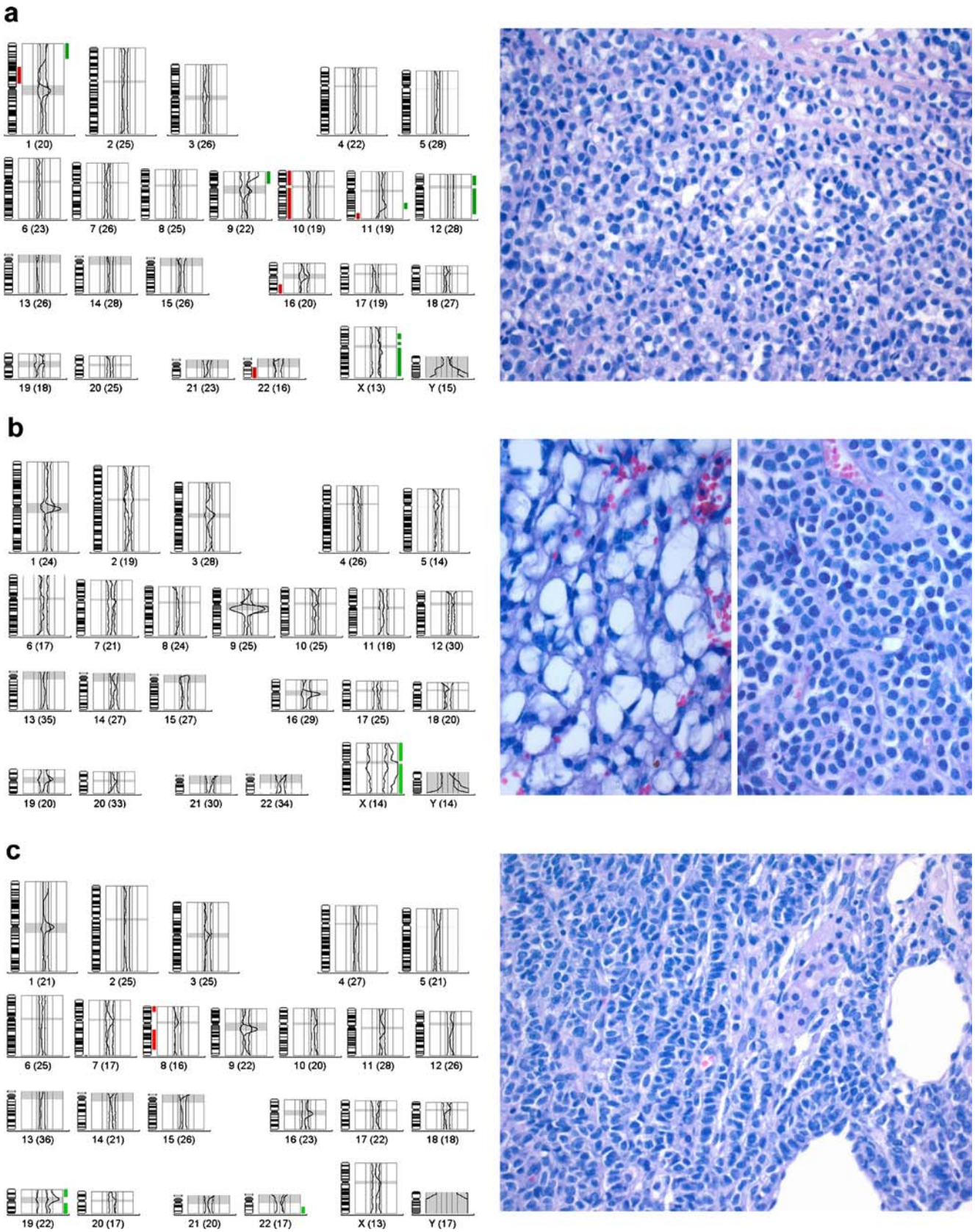
a
1 (20)
2 (25)
3 (26)
4 (22)
5 (28)
6 (23)
7 (26)
8 (25)
9 (22)
10 (19)
11 (19)
12 (28)
13 (26)
14 (28)
15 (26)
16 (20)
17 (19)
18 (27)
19 (18)
20 (25)
21 (23)
22 (16)
X (13)
Y (15)
b
1 (24)
2 (19)
3 (28)
4 (26)
5 (14)
6 (17)
7 (21)
8 (24)
9 (25)
10 (25)
11 (18)
12 (30)
13 (35)
14 (27)
15 (27)
16 (29)
17 (25)
18 (20)
19 (20)
20 (33)
21 (30)
22 (34)
X (14)
Y (14)
c
1 (21)
2 (25)
3 (25)
4 (27)
5 (21)
6 (25)
7 (17)
8 (16)
9 (22)
10 (20)
11 (28)
12 (26)
13 (36)
14 (21)
15 (26)
16 (23)
17 (22)
18 (18)
19 (22)
20 (17)
21 (20)
22 (17)
X (13)
Y (17)

◀ **Fig. 1** CGH profiles (*left*) and the corresponding histology of the tumours (*right*, H&E, ×40). **a** Case 1 (lung metastasis) showed alterations on chromosome 1p, 9p, 10, 11q, 12, 16q, 22q and X. Histomorphological features were nested tumour formations, eosinophilic cytoplasm, oval to spindle-shaped nuclei. **b** Case 2 with gain of chromosome X. The malignant tumour showed morphologies of a lipid-rich Sertoli-cell component (*left*) and a nested Leydig-cell component (*right*). **c** Case 3 with partial loss of chromosome 8 and gain on chromosome 19 and 22. The benign tumour showed Sertoli-cells in a trabecular arrangement and islands of Leydig-cells

Gains or losses were calculated as significant by the evaluation software if fluorescence ratio showed borderline values of 0.8 and 1.25, respectively. Pericentromeric, heterochromatic regions, telomeric regions and chromosome Y were excluded from the evaluation.

Fluorescence in situ hybridisation

To evaluate the CGH results, fluorescence in situ hybridisation (FISH) on paraffin-embedded sections was performed according to the manufacturer's protocol. Tissue sections (5 μm) were mounted on adhesion slides and dried at 70°C for 30 min. The inter-phase preparation and hybridisation were performed according to the protocol of the manufacturer (Abbott/Vysis, Downers Grove, IL, USA). DNA probes for the centromeric region for chromosome X/Y, 8, two LSI probes for 9p21 and 22q11.2 (Abbott/Vysis) and a locus specific probe on 12q14-15 (YAC probe 745a10, kindly provided by Dr. Kalscheuer, Max Planck Institute, Berlin) were used. At least 100 nuclei in each case were examined.

Results

Pathologic and immunohistochemical findings

Microscopically case 1 (lung metastasis lung metastasis from a 66-year-old male patient) showed uniform cells, arranged in nested tumour formations, with eosinophilic cytoplasm, oval to spindle-shaped cells with not overtly prominent nuclei and an increased mitotic rate (26 mitotic figures/10 HPF). Only the Leydig cell component showed formation of metastases (Fig. 1a, right). The second malignant tumour of the testis from a 75-year-old patient (case 2) showed morphologies of lipid-rich Sertoli-cell components (Fig. 1b, left) and a nested Leydig-cell component (Fig. 1b, right). The tumour showed vascular invasion and an increased mitotic rate (33 mitotic figures/10 HPF).

The cells of case 3 (ovarian SLCT from a 74-year-old woman) appeared bland and uniform; the benign tumour showed Sertoli cells in a trabecular arrangement and islands of Leydig cells. Immunohistochemical analysis showed positivity of the Leydig-cell component of the benign tumour (case 3) for α-inhibin and calretinin whilst both components stained negative for Melan A (A 103). Both malignant tumours (case 1 and 2) were completely negative for these markers (Table 1).

CGH and FISH analysis

All analysed cases showed chromosomal imbalances. Case 1 showed gains and losses involving 10 chromosomes or chromosomal regions. The second case showed gain on the entire chromosome X as sole aberration. The third case was with loss of the entire chromosome 8 and gain of chromosome 19 and 22. CGH profiles and histomorphological features of the tumours are shown in Fig. 1. The FISH results were in agreement with the CGH data. Results of CGH and FISH data are given in Table 2.

Discussion

Sertoli–Leydig tumours of the ovary and the testis are scarce neoplasm [9] exceptionally rare in the testis [10, 18]. Only few cytogenetic studies of ovarian sex-cord stromal tumours and no chromosomal analysis in SLCT of the testis are reported in the literature. The present CGH analysis in two male patients with SLCT is the first study of genetic aberrations in these tumours, affecting entire chromosomes (or chromosome regions) on 1p, 8, 9p, 11q, 12, 16q, 19, 22 X.

Trisomy 8 has been described in fibrosarcomas of the ovary as one of several aberrations [16]. Manegold et al. [7] found trisomy 8 as sole karyotypic aberration in an ovarian metastasizing SLCT. These findings are in contrast to our CGH data. One of the three analysed tumours showed loss and no gain of chromosome 8 (Fig. 1c, left) as part of other chromosomal imbalances.

Simple numeric changes, patriculary trisomy 12 and monosomy 22, have been described as recurrent findings in ovarian sex-cord stromal tumours [13], including granu-

Table 1 Patients' profile

Case	Age/Sex	Clinical behaviour	IHC profile		
			α-inhibin	Melan A	Calretinin
1[a]	66 years/m	M	–	–	–
2	75 years/m	M	–	–	–
3	74 years/f	B	L+, S–	–	L+, S–

B Benign, *M* malignant, *m* male, *f* female, + positive staining, – negative staining, *L* Leydig-cell component, *S* Sertoli-cell component
[a] Lung metastasis

Table 2 Results of CGH and FISH

Case	DNA copy number changes		FISH results of target anomalies [% analysed nuclei]
	Losses	Gains	
1[a]	1p31.3p12, 10	1pterp32.3, 9p	3–9 (mainly 3–4) copies of 9p21 [44]
	11q23.3qter	11q14.2q23.1	3–4 copies of 12q14q15 [50]
	16q21qter, 22	12, X[b]	2–5 copies of X [38] and 2–3 copies of Y [19], mainly XXY or XXYY
2		X	2–3 copies of X and loss of Y [80], (mainly XX)
3	8[b]	19, 22q	3 to 4 copies of 22q11.2 [30]

[a] Lung metastasis
[b] Imbalance with a clear shift, but the CGH profile shows only a partially significant imbalance (partially reaching the threshold)

losa-stromal cell tumours [14], fibrothecomas [16], in sclerosing stromal tumours [5] and ovarian tumours [6, 11]. Also, the CGH and interphase FISH study by Mayr et al. [8] on ovarian granulosa cell tumours corroborate these previous reports of the prevalence of trisomy and monosomy 22. Truss et al. [15] found trisomy 12 in a virilizing ovarian SLCT as part of a number of other aberrations, including an overexpression of the BCL-2 gene, caused by rearrangement of chromosome 18 with a clonal karyotype 48XX,der(5)t(5;18)(p13;q12),+6,+12,der(18)r(5;18)(p15.3p13;p11.3q12).

We found gain of entire chromosome 12 and monosomy 22 in case 1 by CGH. However, a discrepant result regarding chromosome 22 was seen in case 3: not monosomy 22 but gain of chromosome 22 was detected. The FISH analysis confirmed this, showing three to four signals for 22q11.2 in 30% of the analysed nuclei (Table 2). De Giorgi et al. [1] presented a case of ovarian SLCT with endometrioid-like yolk sac tumour in a 26-year-old patient with a 46,XX karyotype with Y-chromosomal material insertion into chromosome 1. A well-differentiated SLCT of the ovary in a 48-old-year Japanese woman with symptoms of virilisation and a 45,X/46XX/47XXX karyotype is reported by Hitosugi et al. [3]. Another Sertoli–Leydig cell tumour in a woman with XO/XX/XXX-mosaicism is reported by Glaser et al. [2]. We provide the first molecular-cytogenetic analysis of testicular SLCT, identifying gain of chromosome X in both analysed cases (case 1 and 2) by CGH. FISH analysis showed two to three copies of chromosome X in both cases; in one of them, loss of chromosome Y was observed in 80% of the analysed nuclei.

In conclusion, aberrations on chromosome 12 and on sex chromosomes suggest associations with oncogenetic mechanisms in these groups of neoplasms. However, the characterisation of SLCT in this study represents an additional contribution to the poorly explored SLCT of the ovary and testis.

Acknowledgements The present case report is part of a study of Leydig cell tumours, supported by the Austrian Cancer Society/Tyrol.

References

1. De Giorgi U, Turci D, Crisanti E, Cantù MG, Cappellini A, Marangolo M (2003) Ovarian Sertoli–Leydig cell tumor, endometrioid-like yolk sac tumor, and Y-chromosomal material. Oncology 64:370–373
2. Glaser D, Nienhaus H, Kohler R, Walther G, Pawlowitzki IH (1988) A sex cord stromal tumour in a woman with X0/XX/XXX-mosaicism. Arch Gynecol Obstet 243:115–118
3. Hitosugi M, Matsuoka Y, Irimajiri S, Fukuda J (1997) Sertoli–Leydig cell tumour complicated by X chromosomal mosaicisms. Clin Endocrinol (Oxf) 47:619–622
4. Hittmair A, Zelger BG, Obrist P, Dirnhofer S (1997) Ovarian Sertoli–Leydig cell tumor: a SRY gene-independent pathway of pseudomale gonadal differentiation. Hum Pathol 28:1206–1210
5. Kawauchi S, Tsuji T, Kaku T, Kamura T, Nakano H, Tsuneyoshi M (1998) Sclerosing stromal tumor of the ovary: a clinicopathologic, immunohistochemical, ultrastructural, and cytogenetic analysis with special reference to its vasculature. Am J Surg Pathol 22:83–92
6. Lindgren V, Waggoner S, Rotmensch J (1996) Monosomy 22 in two ovarian granulosa cell tumors. Cancer Genet Cytogenet 89:93–97
7. Manegold E, Tietze L, Günther K, Fleischer A, Amo-Takyi BK, Schröder W, Handt S (2001) Trisomy 8 as sole karyotypic aberration in an ovarian metastasizing Sertoli–Leydig cell tumor. Human Pathol 32:559–562
8. Mayr D, Kaltz-Wittmer C, Arbogast S, Amann G, Aust DE, Diebold J (2002) Characteristic pattern of genetic aberrations in ovarian granulosa cell tumors. Mod Path 15:951–957
9. Panagiotou JP, Polychronopoulou S, Sofou K, Vanvliet-Constantinidou C, Papandreou E, Haidas S (2006) Second and third malignant solid tumor in a girl with ovarian Sertoli–Leydig tumor. Pediatr Blood Cancer 46:654–656
10. Perito PE, Ciancio G, Civantos F, Politano VA (1992) Sertoli–Leydig cell testicular tumor: case report and review of sex cord/gonadal stromal tumor histogenesis. J Urol 148:883–885
11. Persons DL, Hartmann LC, Herath JF, Keeney GL, Jenkins RB (1994) Fluorescence in situ hybridization analysis of trisomy 12 in ovarian tumors. Am J Clin Pathol 102:775–779
12. Sesterhenn IA, Cheville J, Wooward PJ, Damjanov I, Jacobsen GK, Nistal M, Paniagua R, Renshaw AA (2004) Germ cell tumours. In: Eble JN, Sauter G, Epstein JI, Sesterhenn IA (eds) Pathology and genetics: tumours of the urinary system and male genital organs. IARC Press, Lyon, pp 251–258
13. Shashi V, Golden WL, von Kap-Herr C, Andersen WA, Gaffey MJ (1994) Interphase fluorescence in situ hybridization for trisomy 12 on archival ovarian sex cord-stromal tumors. Gynecol Oncol 55:349–354

14. Taruscio D, Carcangiu ML, Ward DC (1993) Detection of trisomy 12 on ovarian sex cord stromal tumors by fluorescence in situ hybridization. Diagn Mol Pathol 2:94–98
15. Truss L, Dobin SM, Rao A, Donner LR (2004) Overexpression of the BCL2 gene in a Sertoli–Leydig cell tumor of the ovary: a pathologic and cytogenetic study. Cancer Genet Cytogenet 148: 118–122
16. Tsuji T, Kawauchi S, Utsunomija T, Nagata Y, Tsuneyoshi M (1997) Fibrosarcoma versus cellular fibroma of the ovary: a comparative study of their proliferative activity and chromosome aberrations using MIB-1 immunostaining, DNA flow cytometry, and fluorescence in situ hybridization. Am J Surg Pathol 21:52–59
17. Wolff E, Girod S, Liehr T, Vorderwulbecke U, Ries J, Steininger H, Gebhart E (1998) Oral squamous cell carcinomas are characterized by a rather uniform pattern of genomic imbalances detected by comparative genomic hybridisation. Oral Oncol 34:186–190
18. Young RH (1993) Sertoli–Leydig cell tumors of the ovary: review with emphasis on historical aspects and unusual variants. Int J Gynecol Pathol 12:141–147

Virchows Arch (2007) 450:273–278
DOI 10.1007/s00428-006-0354-7

ORIGINAL ARTICLE

Overexpression of laminin-5 γ2 chain in clear cell carcinoma of the ovary

Noriko Kato · Shun-ichi Sasou · Shin-ichi Teshima · Tei-ichi Motoyama

Received: 15 August 2006 / Revised: 25 October 2006 / Accepted: 20 November 2006 / Published online: 18 January 2007
© Springer-Verlag 2007

Abstract One of the characteristic microscopic features of ovarian clear cell carcinoma (CCC) is the densely hyaline basement membrane material expanding the stroma. The biological significance of this material, however, has remained unclear. Recent studies have shown that laminin-5 (LN-5), a major component of the epithelial basement membrane, plays a more active role in cell migration or tumor invasion. In the present study, 20 CCCs and 5 borderline clear cell tumors were examined for LN-5 expression immunohistochemically, using an antibody against LN-5 γ2 chain. All of the 20 CCCs showed a focal or diffuse immunoreactivity with the LN-5 γ2 chain in the tumor stroma; whereas, borderline clear cell tumors rarely showed a stromal immunoreactivity. Cytoplasmic accumulation of the LN-5 γ2 chain was far less common than stromal accumulation, suggesting an accelerated secretion in CCC. In vitro, CCC cell lines showed a significant increase in cell migration over excessive LN-5, and the migration was blocked by an antibody against integrin α3. These results indicate that an interaction between CCC cells and extracellularly accumulated LN-5 is responsible for cell migration and the subsequent stromal invasion of CCC.

N. Kato (✉) · T. Motoyama
Department of Pathology,
Yamagata University School of Medicine,
2-2-2 Iida-nishi,
Yamagata 990-9585, Japan
e-mail: nkato@med.id.yamagata-u.ac.jp

S. Sasou
Department of Pathology, Yamagata Prefectural Central Hospital,
Yamagata, Japan

S. Teshima
Department of Pathology, Douai Memorial Hospital,
Tokyo, Japan

Keywords Clear cell carcinoma · Borderline clear cell tumor · Ovary · Laminin-5 γ2 chain · Migration

Introduction

Stromal hyalinization is a characteristic histological feature of clear cell carcinoma (CCC) of the ovary [17, 20]. Previous studies have shown that it is caused by the deposition of basement membrane materials, including laminin (LN), which is excessively produced by tumor cells [12, 22]. The biological significance of this deposition, however, has remained unclear, as little had been known about the type and function of LN.

Recently, it has been shown that LN not only composes the basement membrane but also plays a more active role in cell migration. The LN molecules consist of three chains of α, β, and γ, and more than 15 LN isoforms with different combinations of the α1–α5, β1–β3, and γ1–γ3 chains have been identified [13]. Of the many LN isoforms, laminin-5 (LN-5; α3β3γ2) is a major component of epithelial basement membrane [2, 19]. Notably, LN-5 is overexpressed by keratinocytes at the wound edge [14] or by tumor cells of the invasive front or tumor–stroma interface of many carcinomas [7, 8, 16, 18, 21], indicating that LN-5 plays an important role in cell migration. In vitro, LN-5 stimulates human cancer cells to form marked lamellipodia, leading to enhanced cell migration and invasion [3, 5]. Considering these facts, it is very interesting to know the LN-5 expression and its role in ovarian CCC.

In the present study, we first immunohistochemically examined surgically resected CCCs for LN-5γ2 chain expression. Subsequently, three CCC cell lines were analyzed in vitro to examine the role of LN-5.

Materials and methods

Surgical specimens

Twenty CCCs and five borderline clear cell tumors (four pure borderline tumors and one with minor foci of CCC) were examined. The diagnostic criteria for borderline tumor is that the tumor shows an atypical or even carcinomatous epithelium without invasion or just with microinvasion (one focus or more 10 mm^2 or less in area) [17, 20]. Of 20 CCCs, 15 were stage I, 3 were stage II, and 2 were stage III, according to the criteria of the International Federation of Gynecology and Obstetrics (FIGO) [1]. The histologic grade (FIGO) was 2 (15 cases) and 3 (5 cases). Three patients died of the tumor, whereas 17 are alive with recurrence (2 patients) or without recurrence (15 patients) for 1–6 years after surgery. For comparison, ten serous adenocarcinomas and ten endometrioid adenocarcinomas of the ovary were examined. All of them were obtained from surgery, fixed in 10% formalin, and embedded in paraffin.

Cell culture

Three ovarian CCC cell lines (JHOC-5, HAC-2, and SMOV-2) were used. JHOC-5 was kindly provided by Dr. H. Ishikawa (Tokyo Jikei Medical School, Tokyo, Japan), and HAC-2 was a generous gift from Dr. M. Nishida (Kasumigaura Medical Center, Tsuchiura, Japan). SMOV-2 was obtained from the Immunobiological Laboratory, Takasaki, Japan. All cell lines were cultured in RPMI1640 supplemented with 10% fetal bovine serum (FBS) in a humidified 5% CO_2 atmosphere at 37°C.

Immunohistochemistry

Immunohistochemistry was performed on paraffin-embedded tissue sections. A mouse monoclonal antibody raised against human LN γ2 chain, a LN subunit characteristic to LN-5 (D4B5, dilution 1:100; Chemicon International, Temecula, CA, USA), was used. For antigen retrieval, paraffin-embedded sections were digested with 0.1% protease type XXVII (Sigma, St Louis, MO, USA) for 10 min at 37°C. The slides were exposed to 10% non-immunized rabbit serum in phosphate-buffered saline (PBS) for 10 min to block nonspecific bindings of the antibody. Then, the slides were incubated with anti-LN-5 γ2-chain antibody at 4°C overnight. The immunohistochemical reactions were visualized using a Histofine SAB-PO kit (Nichirei, Tokyo, Japan). Immunoreactivity was evaluated for distribution (stromal or cytoplasmic) and pattern (diffuse or focal) of staining. The staining was considered positive if the intensity was equal to or more than that of basement membrane. The Fisher's exact probability test was used to analyze the statistical significance of the relationship between LN-5 γ2-chain expression and the clinicopathological variables. Differences were considered significant if P values were less than 0.05.

Cell migration assay

Cell migration was assayed as reported previously [11]. Transwell filters with 8-μm pores (Corning Incorporated, Corning, NY, USA) were precoated on the underside with rat recombinant LN-5 (10 μg/ml; Chemicon International). Low ionic strength (0.05 M) carbonate buffer, pH 9.6, was used to precoat the rat recombinant LN-5 on the underside of the filters. Filters were coated for 16 h at 37°C in a humid 5% CO_2 atmosphere. Filters were then washed with PBS and air-dried before use in the migration assay. Control filters were treated similarly in carbonate buffer without LN-5. One hundred microliters of cell suspension (4×10^5 cells/ml in RPMI1640 containing 10% FBS) was inoculated in the upper transwell chamber and incubated at 37°C for 16 h in a humidified atmosphere containing 5% CO_2. The cells were stained with Giemsa, and those that migrated to the underside were quantified by counting six microscopic fields from duplicate filters.

Inhibition assay

The cells were pre-incubated with function-blocking monoclonal antibody against human integrin α_3 (P1B5; 1:100; Chemicon International) at room temperature for 20 min before inoculating the cells onto the filters.

Results

LN-5 expression in CCC

All of the 20 CCCs showed a diffuse (9 cases) or focal (11 cases) immunoreactivity with the LN-5 γ2 chain in the tumor stroma. The stromal immunoreactivity was observed in either the central or peripheral part of the tumor and was much more accentuated in the area of papillary architecture than in the area of tubulocystic or solid architecture (Fig. 1a,b). Eight CCCs also showed a focal immunoreactivity with the LN-5 γ2 chain in the cytoplasm including the hyaline globules (Fig. 1c). In contrast, four pure borderline clear cell tumors showed neither stromal nor cytoplasmic immunoreactivity with the LN-5 γ2 chain, although the basement membrane was weakly positive for it (Fig. 1d). In one borderline tumor with minor foci of CCC, most of the borderline area did not show stromal nor cytoplasmic immunoreactivity with the LN-5 γ2 chain, but

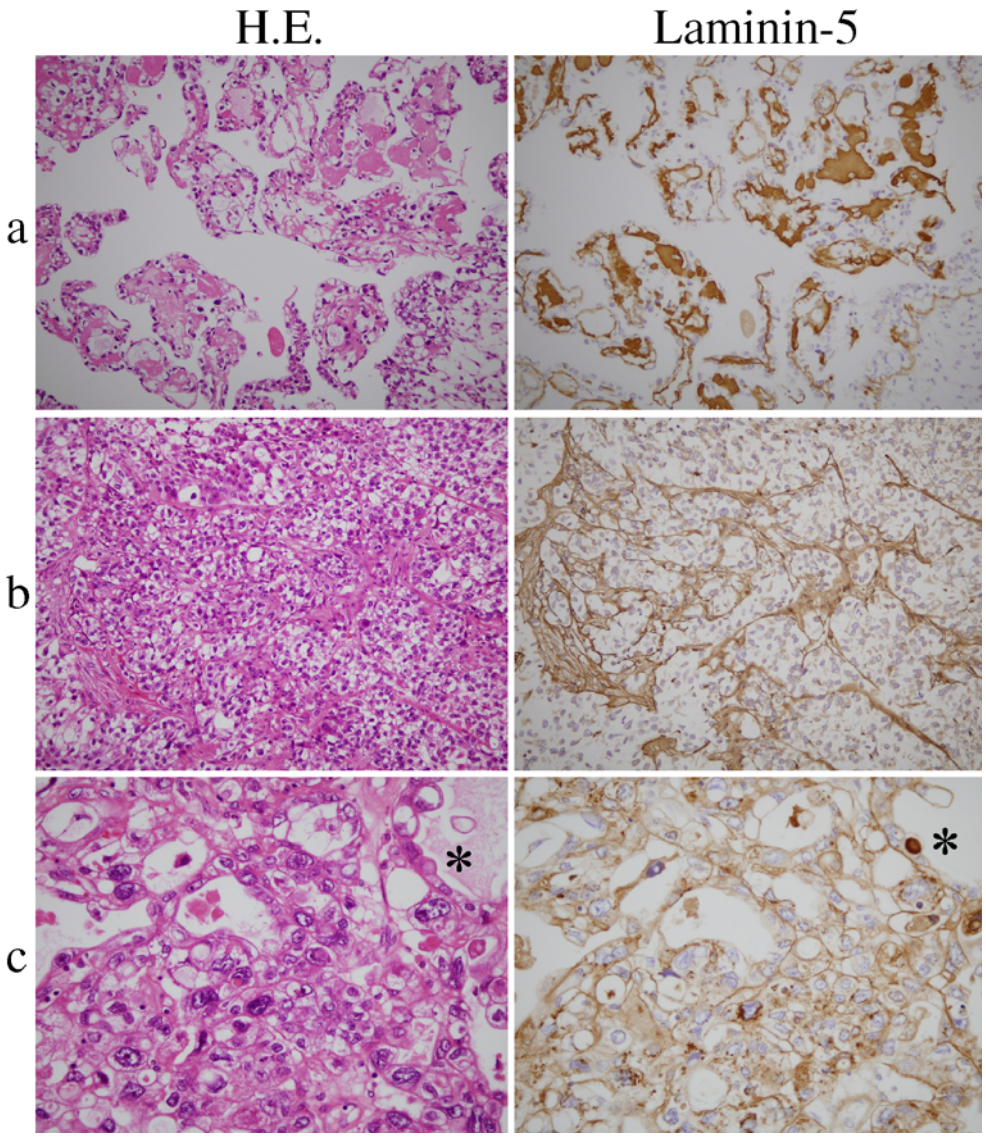

Fig. 1 Expression of laminin-5 (LN-5) γ2 chain in CCC and borderline clear cell tumor of the ovary. In CCC, the stroma of papillary cores (a) showed more intense immunoreactivity with LN-5 γ2 chain than that of the surrounding solid nests (**b**). Immunoreactivity in the cytoplasm, including the hyaline globules (*asterisks*), was focally found (**c**). In pure borderline clear cell tumor, neither stromal nor cytoplasmic immunoreactivity with LN-5 γ2 chain was observed, although the basement membrane was weakly positive for it (**d**). In one borderline tumor with minor foci of CCC, the borderline area (*Bor.*), which was adjacent to the foci of CCC (*Ca.*) also showed a stromal immunoreactivity with LN-5 γ2 chain (**e**). *Left*, HE and *right*, SAB with hematoxylin counterstain; original magnification, **a**, **b**, and d, ×20, **c** and **e** (*right*), ×40, **e** (*left*), ×10

the area that was just adjacent to the foci of CCC showed a stromal immunoreactivity, as well as the foci of CCC (Fig. 1e). In CCCs, the different expression pattern of LN-5 γ2 chain, that is, diffuse or focal, did not correlate with FIGO stage (I/II or III, P=0.51), histologic grade (2 or 3, P=0.40), or patient survival (alive or dead, P=0.46). None of the ten serous adenocarcinomas nor the ten endometrioid adenocarcinomas showed stromal immunoreactivity with LN-5 γ2 chain, although the basement membrane was continuously or discontinuously positive for it in nine serous and seven endometrioid adenocarcinomas, respectively.

Migration of CCC cells on LN-5

When LN-5 was precoated on the underside of transwell filters, all three CCC cell lines showed a significant increase of migration through the pores (Table 1 and Fig. 2).

Inhibition by anti-integrin α3 antibody

Migration of CCC cells on LN-5 was decreased after pretreatment of the cells with antibody against integrin α_3 (Fig. 3).

Discussion

Densely hyaline material expanding the stroma is one of the characteristic features of ovarian CCC [17, 20]. Previous studies demonstrated that it was composed of basement membrane materials, including LN, which was produced by tumor cells [12, 22]. At that time, however, little was

Fig. 1 (continued)

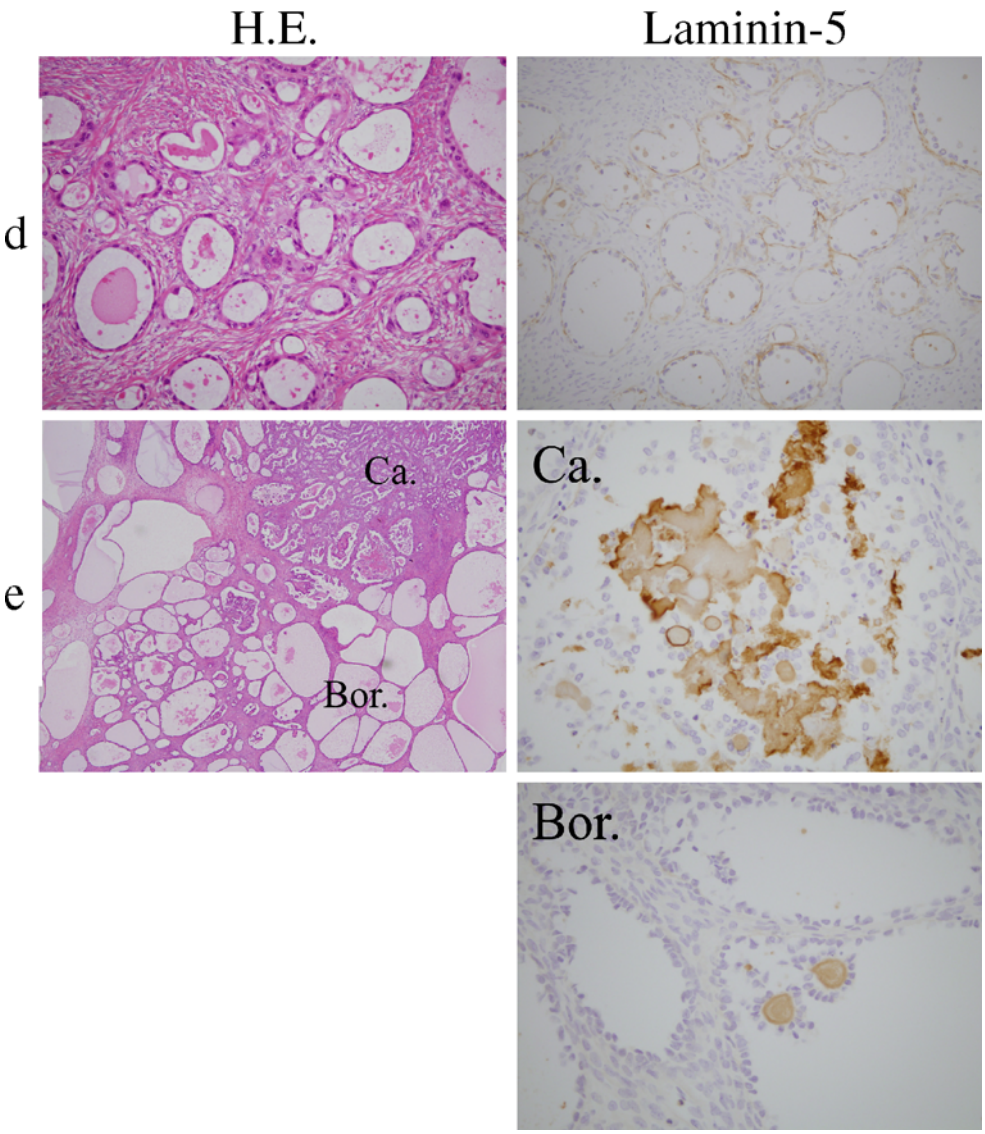

known about the structure and function of LN. The biological significance of this deposition has remained unclear. Recent studies on the extracellular matrix molecules led to the identification of more than 15 LN isoforms with different combinations of the α1–α5, β1–β3, and γ1–γ3 chains and their function. Among them, LN-5, which is composed of α3, β3, and γ2 chains, is a major component of the epithelial basement membrane [2, 19] and regulates not only cell adhesion but also cell migration in wound healing or tumor invasion [3, 5, 7, 8, 14, 16, 18, 21]. In various types of carcinomas, LN-5 was overexpressed in the cytoplasm of tumor cells located at the invasive front or tumor–stroma interface [7, 8, 16, 18, 21]. It is likely that LN-5 is also involved in ovarian CCC, but there are no data on LN-5 expression in CCC.

In the present study, we first examined 20 CCCs for LN-5 expression immunohistochemically. For comparison, five borderline clear cell tumors were examined. We used a monoclonal antibody against the LN-5 γ2 chain, because the γ2 chain is found only in LN-5 [13]. All 20 CCCs showed a focal or diffuse immunoreactivity with the LN-5 γ2 chain in the stroma, regardless of the histological

Table 1 Migration of clear cell carcinoma (JHOC-5, HAC-2 and SMOV-2) cells on laminin-5 (LN-5) precoated filters

Cell line	Migrated cells per HPF	
	Non-coated	LN-5-precoated
JHOC-5	3.2±1.7	98.9±10.5
HAC-2	3.7±1.1	80.8±9.0
SMOV-2	1.3±1.3	44.8±6.1

Filters were precoated on the underside with a high concentration (10 μg/ml) of rat recombinant LN-5. After washing and air drying, filters were used in the migration assay. Data represent the mean number of migrated cells per high power (×400) field plus or minus the standard error of the mean.

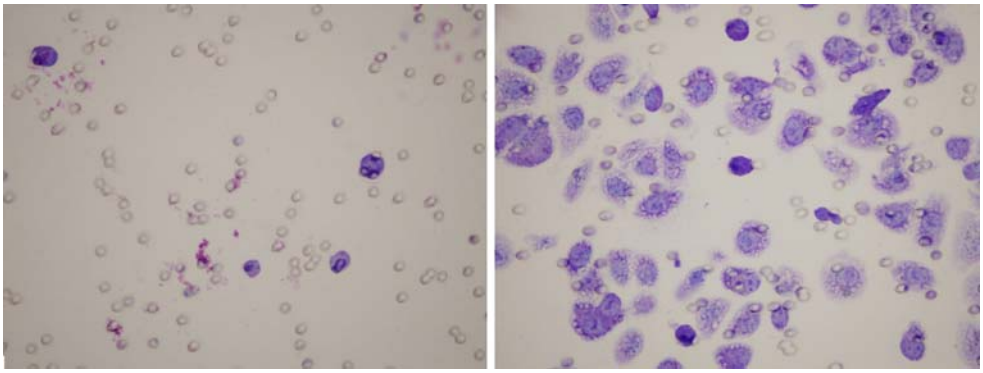

Fig. 2 Migration of a CCC cell line (HAC-2) on laminin-5 (LN-5)-precoated filters. HAC-2 on the LN-5 precoated filter (*right*) showed an increase of migration as compared with that on the non-coated filter (*left*) (Giemsa, original magnification ×40)

architecture. In contrast, four pure borderline clear cell tumors did not show any stromal immunoreactivity with the LN-5 γ2 chain. Considering the fact that the borderline clear cell tumor is distinguished from CCC by the absence of stromal invasion [17, 20], it is suggested that the stromal accumulation of LN-5, either γ2 monomer or α3β3γ2 trimer, is related to the stromal invasion of CCC. Interestingly, one borderline tumor with minor foci of CCC showed a stromal immunoreactivity with the LN-5 γ2 chain, not only in the CCC foci but also in the borderline area that was just adjacent to the CCC, whereas most of the borderline area never showed a stromal immunoreactivity with it, suggesting that the stromal accumulation of LN-5 is responsible for stromal invasion. In CCCs, the cytoplasmic accumulation of LN-5 γ2 chain was not evident or far less common than stromal accumulation. In many carcinomas of various organs, including the colon, stomach, tongue, or urinary bladder, LN-5 accumulation has not been observed in the stroma but in the cytoplasm of tumor cells, which are located at the tumor–stroma interface [7, 8, 16, 18]. The stromal accumulation of LN-5 has not been reported in serous or endometrioid adenocarcinomas of the ovary either [10], which is also confirmed by the present study. It seems that ovarian CCC is unique for the stromal accumulation of LN-5 γ2 chain. The production and secretion of LN-5 might be much more accelerated in ovarian CCC than in many other carcinomas. The expression pattern of LN-5 γ2 chain (i.e., diffuse or focal) did not correlate with the tumor stage or patient prognosis. In ovarian CCCs, the stromal accumulation of LN-5γ2 chain could be an indicator of stromal invasion but less likely to be indicators of tumor progression or patient prognosis.

To examine if the accumulated LN-5 in the extracellular space influences the cell migration of CCC, three CCC cell lines were investigated in vitro. LN-5 accumulation in these cell lines has been confirmed by heterotransplantation into nude mice (data not shown). A high concentration (10 μg/ml) of rat recombinant LN-5, which is interchangeable to human LN-5, was precoated on the filter, then the cells were inoculated on it, and cell migration was evaluated. All three CCC cell lines showed a significant increase of cell migration through the filter pores when LN-5 was precoated on the underside of the filter, whereas they rarely migrated without LN-5. This result indicates that CCC cells can take advantage of extracellularly

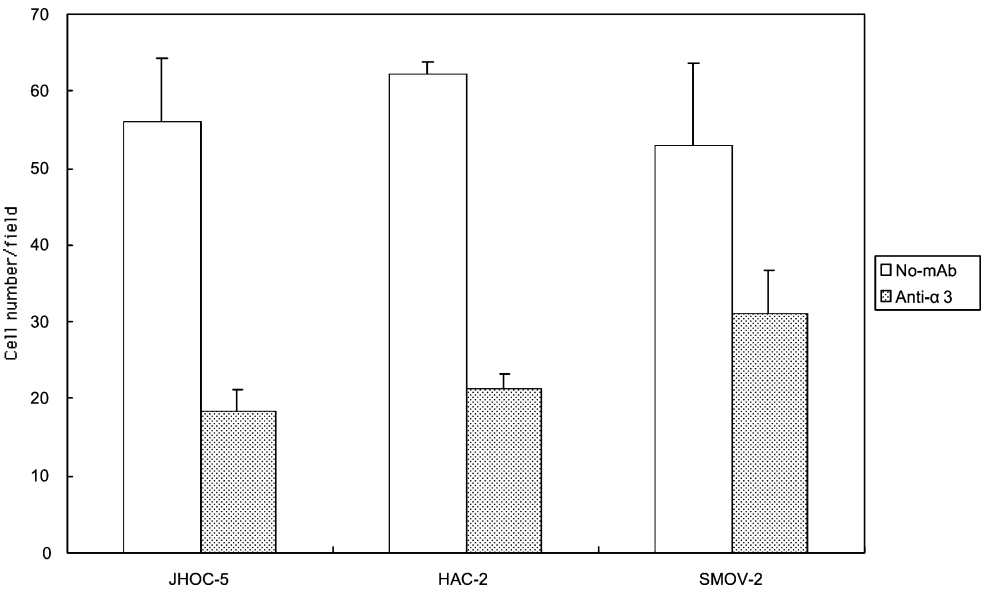

Fig. 3 Effect of anti-integrin α3 monoclonal antibody on the migration of CCC cells. The cells were preincubated with anti-integrin α3 antibody (×100), then innoculated on the laminin-5 (10 μg/ml) precoated filters. All three CCC cell lines (JHOC-5, HAC-2, and SMOV-2), which were preincubated with anti-integrin α3 monoclonal antibody (anti-α3), showed a decrease of migration, compared with those without preincubation (No-mAb). Data represent the mean number of migrated cells per high power (×400) field plus or minus the standard error of the mean

accumulated LN-5 for their migration. It is most likely that the interaction between tumor cells and accumulated LN-5 in the stroma is, at least, one of the important mechanisms for the stromal invasion of ovarian CCC.

It has been shown that integrin α3β1 is one of the major receptors for LN-5 [2]. Interaction of LN-5 with integrin α3β1 induces intracellular signal transduction to support cell migration, as well as cellular survival and proliferation, by activating many signal mediators such as focal adhesion kinase, protein kinase C, and phosphatidylinositol 3-kinase [6, 14]. In the present study, the migration of CCC cells on the excessive LN-5 was effectively blocked by an antibody to the human integrin α3 subunit, suggesting that the cell migration of CCC is supported by interaction with integrin and following intracellular signal transduction. Alternatively, recent studies have shown that the cell motility activity of LN-5 is also regulated by the proteolytic processing of the LN-5 chains. In particular, the cleavage of the γ2 chain by MMP-2 or MT1-MMP increases the cell motility activity of LN-5 [4, 9, 15]. In ovarian CCC, the proteolytic processing of LN-5 chains might also be involved in the cell migration, especially in the case that the accumulated LN-5 is not composed of complete α3β3γ2 trimer but of γ2 monomer, which does not contain any integrin-binding site. Further study is needed to clarify whether CCC cells secret the γ2 chain as a trimer or as a monomer and if the MMP-2 or MT1-MMP activity is elevated in CCC.

In conclusion, the stromal accumulation of the LN-5 γ2 chain is common in ovarian CCC but rare in borderline clear cell tumors. The infrequent intracytoplasmic accumulation of the LN-5 γ2 chain suggests an accelerated secretion in ovarian CCC. In vitro, CCC showed a significant increase of cell migration over excessive LN-5. Interaction between CCC cells and extracellularly accumulated LN-5 is responsible for the cell migration and probably for the stromal invasion of CCC.

References

1. Benedet JL, Bender H, Jones HW III, Ngan HY, Pecorelli S (2000) FIGO staging classifications and clinical practice guidelines in the management of gynecologic cancers. FIGO committee on gynecologic oncology. Int J Gynaecol Obstet 70:209–262
2. Carter WG, Ryan MC, Gahr PJ (1991) Epigrin, a new cell adhesion ligand for integrinα3β1 in epithelial basement membranes. Cell 65:599–610
3. Fukushima Y, Ohnishi T, Arita N, Hayakawa T, Sekiguchi K (1998) Integrinα3β1-mediated interaction with laminin-5 stimulates adhesion, migration and invasion of malignant glioma cells. Int J Cancer 76:63–72
4. Giannelli G, Falk-Marzillier J, Schiraldi O, Steler-Stevenson WG, Quaranta V (1997) Induction of cell migration by matrix metalloprotease-2 cleavage of laminin-5. Science 277:225–228
5. Kariya Y, Tsubota Y, Hirosaki T, Mizushima H, Puzon-McLaughlin W, Takada Y, Miyazaki K (2003) Differential regulation of cellular adhesion and migration by recombinant laminin-5 forms with partial deletion or mutation within the G3 domain of α3 chain. J Cell Biochem 88:506–520
6. Kariya Y, Miyazaki K (2004) The basement membrane protein laminin-5 acts as a soluble cell motility factor. Exp Cell Res 297:508–520
7. Kiyoshima K, Oda Y, Kinukawa N, Naito S, Tsuneyoshi M (2005) Overexpression of laminin-5 γ2 chain and its prognostic significance in urothelial carcinoma of urinary bladder: association with expression of cyclooxygenase 2, epidermal growth factor, and human epidermal growth factor 2. Hum Pathol 36:522–530
8. Koshikawa N, Moriyama K, Takamura H, Mizushima H, Nagashima Y, Yanoma S, Miyazaki K (1999) Overexpression of laminin gamma2 chain monomer in invading gastric cancel cells. Cancer Res 59:5596–5601
9. Koshikawa N, Giannelli G, Cirulli V, Miyazaki K, Quaranta V (2000) Role of cell surface metalloprotease MT1-MMP in epithelial cell migration over laminin-5. J Cell Biol 148:615–624
10. Maata M, Butzow R, Luostarinen J, Petajaniemi N, Pihlajaniemi T, Salo S, Miyazaki K, Autio-Harmainen H, Virtanen I (2005) Differential expression of laminin isoforms in ovarian epithelial carcinomas suggesting different origin and providing tools for differential diagnosis. J Histochem Cytochem 53:1293–1300
11. McCarthy JB, Furcht LT (1984) Laminin and fibronection promote the haptotactic migration of B16 mouse melanoma cells in vitro. J Cell Biol 98:1474–1480
12. Mikami Y, Hata S, Melamed J, Moriya T, Manabe T (1999) Basement membrane material in ovarian clear cell carcinoma: correlation with growth pattern and nuclear grade. Int J Gynecol Pathol 18:52–57
13. Miyazaki K (2006) Laminin-5 (laminin-332): unique biological activity and role in tumor growth and invasion. Cancer Sci 97:91–98
14. Nguyen BP, Gil SG, Carter WG (2000) Deposition of laminin 5 by keratinocytes regulates integrin adhesion and signaling. J Biol Chem 275:31896–31907
15. Ogawa T, Tsubota Y, Maeda M, Kariya Y, Miyazaki K (2004) Regulation of biological activity of laminin-5 by proteolytic processing of γ2 chain. J Cell Biochem 92:701–714
16. Ono Y, Nakanishi Y, Ino Y, Niki T, Yamada T, Yoshimura K, Saikawa M, Nakajima T, Hirohashi S (1999) Clinicopathologic significance of laminin-5 gamma2 chain expression in squamous cell carcinoma of the tongue: immunohistochemical analysis of 67 cases. Cancer 85:2315–2321
17. Prat J (2004) Clear cell tumors. In: Prat J (ed) Pathology of the ovary. Saunders, Philadelphia, pp 153–162
18. Pyke C, Salo S, Ralfkiaer E, Romer J, Dano K, Tryggvason K (1995) Laminin-5 is a marker of invading cancer cells in some human carcinomas and is coexpressed with the receptor for urokinase plasminogen activator in budding cancer cells in colon adenocarcinomas. Cancer Res 55:4132–4139
19. Rousselle P, Lunstrum GP, Keene DR, Burgeson RE (1991) Kalinin: an epithelium-specific basement membrane adhesion molecule that is a component of anchoring filaments. J Cell Biol 114:567–576
20. Scully RE, Young RH, Clement PB (1998) Clear cell tumors. In: Rosai J (ed) Tumor of the ovary, maldeveloped gonads, fallopian tube, and broad ligament. Atlas of tumor pathology, 3rd series, fascicle 23. AFIP, Washington, DC, pp 141–151
21. Soini Y, Maatta M, Salo S, Tryggvason K, Autio-Harmainen H (1996) Expression of the lamininγ2 chain in pancreatic adenocarcinoma. J Pathol 180:290–294
22. Wong WSF, Wong YF, Ng YTA, Huang PD, Chew EC, Ho TH, Chang MZA (1990) Establishment and characterization of a new human cell line derived from ovarian clear cell carcinoma. Gynecol Oncol 38:37–45

Virchows Arch (2007) 450:279–285
DOI 10.1007/s00428-006-0362-7

ORIGINAL ARTICLE

Nuclear metallothionein expression correlates with cisplatin resistance of ovarian cancer cells and poor clinical outcome

Paweł Surowiak · Verena Materna · Adam Maciejczyk · Marek Pudełko · Ewa Markwitz · Marek Spaczyński · Manfred Dietel · Maciej Zabel · Hermann Lage

Received: 26 September 2006 / Revised: 7 December 2006 / Accepted: 18 December 2006 / Published online: 19 January 2007
© Springer-Verlag 2007

Abstract Elevated metallothionein (MT) expression in ovarian cancers treated with cisplatin-based schemes represents an unfavorable prognostic index. MT expression is significantly higher in tumor samples obtained after chemotherapy. The present study aimed at examining MT expression in ovarian carcinoma cells sensitive (A2780) or resistant (A2780RCIS) against platinum drug treatment as well as examining effects of exposure to cisplatin on MT expression. Subcellular expression of MT was evaluated also in samples originating from 73 ovarian tumors. Cisplatin-resistant A2780RCIS cells were exposed to increasing cisplatin concentrations, and the subcellular expression of MT was determined by immunocytochemistry. The studies demonstrated that cisplatin-resistant A2780RCIS cells exposed to cisplatin typically manifested a nuclear MT expression. The study demonstrated also that exposure to cisplatin was paralleled by growing MT expression in cell nuclei. The nuclear expression of MT was also found to be specific for ovarian cancers of poor clinical outcome. No relationship could be demonstrated between cytoplasmic expression of MT and clinical variables. Nuclear MT expression is induced by cisplatin and seems to protect DNA in the cells from toxic effects of the drug.

Keywords Ovarian cancer · Cisplatin resistance · Metallothionein · Nuclear expression

P. Surowiak · V. Materna · M. Dietel · H. Lage (✉)
Institute of Pathology, Charité Campus Mitte,
Charitéplatz 1,
10117 Berlin, Germany
e-mail: hermann.lage@charite.de

P. Surowiak · M. Zabel
Department of Histology and Embryology,
University School of Medicine,
ul. Chałubińskiego 6a,
50-356 Wrocław, Poland

P. Surowiak · A. Maciejczyk · M. Pudełko
Lower Silesian Centre of Oncology,
pl. Hirszfelda 12,
53-413 Wrocław, Poland

E. Markwitz · M. Spaczyński
Department of Obstetrics and Gynaecology,
University School of Medicine,
ul. Polna 33,
60-535 Poznań, Poland

M. Zabel
Department of Histology and Embryology,
University School of Medicine,
ul. Święcickiego 6,
60-781 Poznań, Poland

Introduction

Due to their location, ovarian cancers are diagnosed frequently at an advanced clinical stage. In such cases, surgical operation is used to be followed by chemotherapy [3, 7]. Therefore, the principal cause of therapeutic failures in cases of ovarian cancer involves the phenomenon of multidrug resistance to cytostatic drugs [10]. At present, most of the therapeutic procedures are based on platinum-containing drugs in conjunction with paclitaxel or topotecan [3]. Detailed analysis of the resistance to platinum-containing drugs should permit to formulation of predictive tests, permitting to apply alternative drugs in cases which are resistant to platinum-containing drugs. Also, recognition of the mechanisms responsible for resistance to

platinum-containing drugs may create the potential to overcome the resistance phenomenon.

In our earlier studies [14], we have shown that elevated expression of metallothionein (MT) in samples of ovarian cancer postsurgically treated with cisplatin-based schemes represents an unfavorable prognostic index. We have demonstrated also that MT expression is significantly lower in samples originating from primary laparotomies (PLs) as compared to samples originating from post-chemotherapy secondary cytoreductions (SCRs) [14]. The relationship between MT expression and resistance to platinum-containing drugs is used to be explained by the potential of MT to bind molecules of the drug [6]. Data on predictive value of immunohistochemical estimation of MT have been divergent [12, 13, 16].

In the present study, using immunocytochemistry, we examined MT expression in ovarian cancer cells sensitive or resistant to cisplatin as well as the effects of exposure of the cells to various concentrations of cisplatin on the expression of MT. MT expression was reevaluated in the earlier described immunohistochemical preparations originating from 73 ovarian tumors [14]. Upon the reevaluation, attention was paid to subcellular localization of MT.

Materials and methods

Cell lines and cell culture

Human ovarian carcinoma cells A2780 [9] were grown in Leibovitz L-15 medium (Biowhittaker, Walkersville, MD, USA) supplemented with 10% fetal calf serum (FCS) (GIBCO/BRL, Grand Island, NY, USA), 1 mM L-glutamine, 6.25 mg/l fetuin, 80 IE/l insulin, 2.5 mg/ml transferrin, 0.5 g/l glucose, 1.1 g/l $NaHCO_3$, 1% minimal essential vitamins, and 20,000 kIE/l trasylol in a humidified atmosphere of 5% CO_2 at 37°C. The cisplatin-resistant cell line A2780RCIS was derived from the ovarian carcinoma cell line A2780 as described previously [9]. To ensure maintenance of cisplatin-resistant phenotype of A2780RCIS cells, the medium was supplemented with 10 μg/ml [33.3 μM] cisplatin (GRY-Pharm, Kirchzarten, Germany).

Cell proliferation assay

Chemoresistance was tested using a proliferation assay based on sulforhodamine B (SRB) staining as described previously [5, 9]. Briefly, 800 cells per well were seeded in 96-well plates in triplicates. After 24 h attachment, cisplatin was added in dilution series for a 5-day incubation before SRB staining was performed. IC_{50} values were calculated from three independent experiments for each cell line.

Analysis of cisplatin effects on expression of MT

Cisplatin-resistant ovarian cancer cells, A2780RCIS, were cultured for 3 days on microscope slides in the presence of the following concentrations of cisplatin: 0, 11.1, 22.2, 33.3, and 66.6 μM (GRY-Pharm, Kirchzarten, Germany). The cells were cultured in the above-listed conditions. After 3 days, the cells were fixed in ice-cold methanol–acetone mixture (1:1) for 10 min. The experiments were run in triplicates.

Immunocytochemistry

Immunostaining of MT was performed using A2780, A2780RCIS, and cisplatin-exposed A2780RCIS cell lines. Cells were grown on microscope slides and fixed in ice-cold methanol–acetone mixture (1:1) for 10 min. After rehydration, immunostaining reactions were performed using the monoclonal mouse antibodies (clone E9) detecting isoforms 1 and 2 of MT (DakoCytomation, Denmark) at 1:100 dilution in Antibody Diluent, Background Reducing (DakoCytomation, Denmark). The cells were incubated with an antibody for 1 h at room temperature. Subsequently, they were incubated with biotinylated antibodies (15 min, room temperature) and with the streptavidin-biotinylated peroxidase complex (15 min, room temperature) (LSAB+, HRP, DakoCytomation, Denmark). NovaRed (Vector Laboratories, UK) was used as a chromogen, employing 10 min incubation at room temperature. All the slides were counterstained using Meyer's hematoxylin. Every reaction was accompanied by the negative control in which specific antibody was substituted by the Primary Mouse Negative Control (DakoCytomation, Denmark).

Scoring of immunostaining results

MT-specific staining reactions were localized by two experienced histologists. In cases of divergencies, the evaluation was repeated using double-headed microscope. Immunostaining reactions were evaluated using a simplified scale, providing merely a score for the intensities of the reactions (0, total absence of staining; 1, faint staining only; 2, moderate staining; 3, strong, intense staining) and subcellular localization—cytoplasmic and nuclear. The intensity of the studied antigen expression was also measured using a digital imaging system, Lucia-G/F (Nikon, Japan). In every case, in four microscopic fields (×200), the mean saturation feature was measured. The final result was the mean value of measured parameters.

Table 1 Chemosensitivity to cisplatin and metallothionein (MT) expression in A2780 and A2780RCIS human ovarian carcinoma cell lines

Cell line	IC_{50} [μM]	Cisplatin concentration [μM]	MT cytoplasmic [score]	MT nuclear [score]	MT overall [mean saturation]
A2780	2.0	0.00	2	0	11.02
A2780RCIS	16.5	33.3	1	2	21.24
A2780RCIS	–	0.00	1	1	15.44
A2780RCIS	–	11.1	2	1	15.67
A2780RCIS	–	22.2	2	1	19.97
A2780RCIS	–	33.3	1	2	21.24
A2780RCIS	–	66.6	1	3	32.76

Reevaluation of MT immunostaining in sections from ovarian cancers

The reevaluation of MT immunolocalization was conducted by two independent pathologists in preparations originating from 43 PLs and 30 SCRs performed in the same patients. Only a single FIGO I and a single FIGO II patient received optimal cytoreduction. All FIGO III patients did not receive an optimal cytoreduction. The semiquantitative IRS scale was employed [11]. Clinical details of the patients and

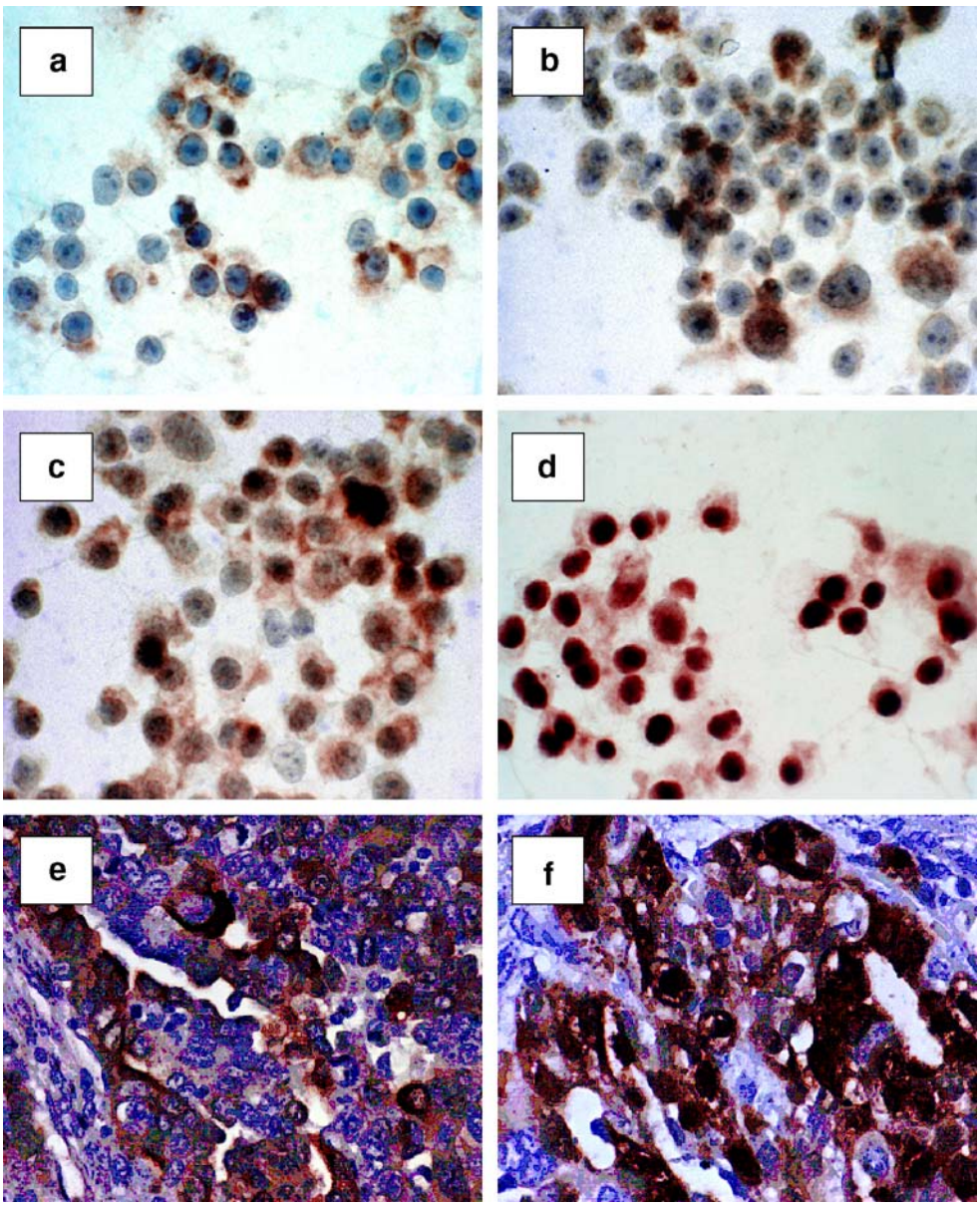

Fig. 1 Metallothionein expression as detected by immunocytochemistry in **a** A2780 cells, **b** A2780RCIS cells, **c** A2780RCIS cells exposed to 33.3 μM of cisplatin, **d** A2780RCIS cells exposed to 66.6 μM of cisplatin, and **e** cytoplasmic and **f** nuclear expression in ovarian carcinomas (hematoxylin, ×400)

Table 2 Correlation between nuclear (MTn) and cytoplasmic (MTc) metallothionein expression and various clinicopathological parameters (*P* values, Chi-square test)

Characteristics	MTn at PL	MTn at SCR	MTc at PL	MTc at SCR
Histological type[a]	0.3454	–	0.1099	–
Grade[a]	0.9668	–	0.2426	–
CA-125 at PL[b]	0.6336	0.7239	0.3426	0.1838
CA-125 at SCR[b]	0.3925	0.3983	0.5578	0.0054
Age[b]	0.7121	0.1979	0.9543	0.1452
Clinical response	0.0073	0.0117	0.9907	0.1186
Relapse	0.0020	0.0040	0.9412	0.1247
Death	<0.001	0.0106	0.7992	0.4732

PL Primary laparotomy, *SCR* secondary cytoreduction
[a] The relationships between metallothionein expression at SCR on one hand and histological type and grade on the other were not examined.
[b] Spearman's rank correlation

methods of immunohistochemical reactions were described previously [14].

Statistical analysis

Statistical analysis was performed using the Statistica 98 PL software (StatSoft, Tulsa, Ok) and SPSS software (release 12.0.1.; SPSS Inc., Chicago, IL). The intensity of MT expression in individual cell lines, as estimated using the Lucia software, was compared employing the *U* test of Mann–Whitney. The survival analysis was restricted to FIGO III patients who received a platinum-drug-containing chemotherapy. By this approach, the potential impact of tumor stage and alternative anticancer drugs should be prevented. Statistical analysis of the data pertaining to clinical material was conducted as described previously [14].

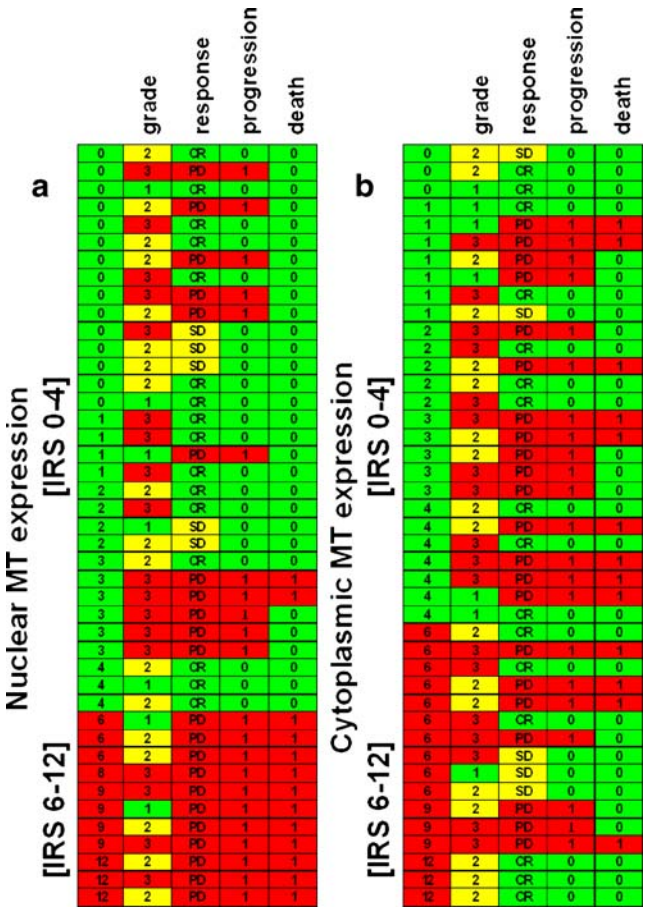

Fig. 2 Nuclear (**a**) and cytoplasmic (**b**) metallothionein (MT) expression at primary laparotomy and clinical and pathological data on the patients

Results

MT expression and sensitivity to cisplatin

At the first stage, values of IC_{50} were estimated for cisplatin and ovarian cancer cells sensitive (A2780) or resistant (A2780RCIS) to cisplatin. The value was 2.0 μM for A2780 cell line and 16.5 μM for A2780RCIS cell line (Table 1). The *U* test of Mann–Whitney demonstrated that the mean saturation of the colored product yielded by the immunocytochemical reactions with antibodies reactive with MT was significantly higher in the case of A2780RCIS cells than in A2780 cells (P=0.02). Also, a subjective appraisal of the studied preparations demonstrated stronger expression of MT in cell nuclei than in cytoplasm of the cisplatin-resistant cells, A2780RCIS (Table 1, Fig. 1). No MT expression in cell nuclei could be detected in A2780 cells (Table 1, Fig. 1).

Exposure to cisplatin and expression of MT

The *U* test of Mann–Whitney demonstrated higher MT expression in A2780RCIS cells exposed to 22.2, 33.3, or 66.6 μM cisplatin as compared to the cells cultured in the medium containing no cytostatic drugs (P=0.04, 0.003, and <0.001, respectively). Subjective appraisal of the reaction intensity demonstrated that exposure to cisplatin resulted in

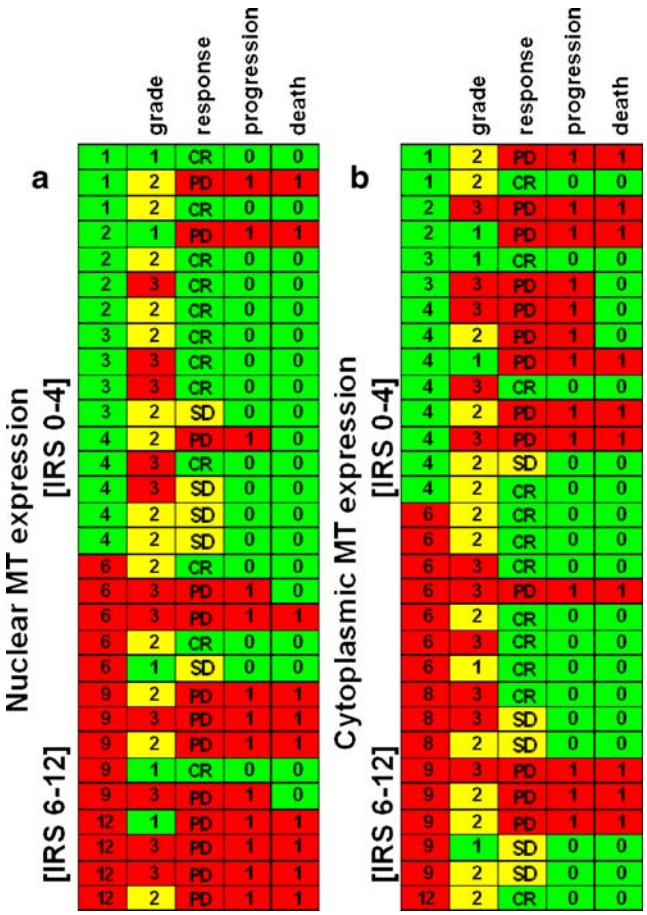

Fig. 3 Nuclear (**a**) and cytoplasmic (**b**) metallothionein (MT) expression at secondary cytoreduction and clinical and pathological data on the patients

an increasing nuclear expression of MT in A2780RCIS cells (Table 1, Fig. 1). Incubation with 66.6 μM cisplatin was followed by a very pronounced MT expression in cell nuclei of A2780RCIS cells (Fig. 1).

MT expression in clinical specimens of ovarian carcinoma

In the case of studied ovarian cancers, reaction of a nuclear (MTn) and cytoplasmic (MTc) localization was found, which was of variable intensity in individual cases (Fig. 1). The mean overall immunoreactivity score of MTn expression amounted to 4.26±3.24 SD (min. 0, max. 12) in PL material and 5.57±2.75 SD (min. 0, max. 12) in SCR material. In the case of MTc, mean overall immunoreactivity score of MTc expression amounted to 3.26±3.76 SD (min. 0, max. 12) in PL material and 5.53±3.61 SD (min. 0, max. 12) in SCR material.

At the first stage of statistical analysis, the Mann–Whitney *U* test was employed to compare overall immunoreactivity score of MT expression at PL and SCR. Both in the case of Mtn and in MTc, the expression in PL material was found to be significantly lower than that in SCR material ($P<0.001$).

Using the Chi-square test, relationships were examined between overall immunoreactivity score of MT expression on one hand and histological type of the tumor and grade on the other. The calculations demonstrated that higher expression of MTn (at PL and at SCR) was typical for cases with progression of the neoplastic process, relapse and death (Table 2, Figs. 2 and 3). In the case of MTc, a negative correlation was demonstrated between MTc at SCR and CA-125 serum levels at SCR (Table 2).

Kaplan–Meier analysis performed on the entire studied group and on the subgroup of 35 patients at FIGO III treated using platinum-containing schemes demonstrated that higher expression of MTn both at PL and at SCR was typical for cases with significantly shorter overall and progression-free survival (Table 3). In the case of MTc, only in the subgroup of patients at FIGO III treated using platinum-containing schemes that the higher expression of MTc at SCR was found to be typical for cases with shorter progression-free survival (Table 3).

Discussion

Although MTs are primarily cytoplasmic proteins, there are those localized in the nuclei under several pathological and physiological conditions, such as in malignant tumor cells,

Table 3 Analysis of relationship between nuclear (MTn) and cytoplasmic (MTc) metallothionein expression (scores 0–4 vs 5–12) and survival rates of the studied patients in the entire group and subgroup of FIGO III patients treated with platinum-based drugs and paclitaxel (log-rank test)

	MTn at PL	MTn at SCR	MTc at PL	MTc at SCR
Entire group				
Overall survival	$P<0.0001$[a]	$P=0.0317$[a]	$P=0.4681$	$P=0.2412$
Progression-free survival	$P<0.0001$[a]	$P=0.0103$[a]	$P=0.4497$	$P=0.0601$
FIGO III patients				
Overall survival	$P<0.0001$[a]	$P=0.0228$[a]	$P=0.4363$	$P=0.1954$
Progression-free survival	$P=0.0001$[a]	$P=0.0116$[a]	$P=0.5224$	$P=0.0325$[a]

PL Primary laparotomy, *SCR* secondary cytoreduction

[a] Patients with higher metallothionein expression had worse survival rates.

fetal liver, cells in a high glucose medium, and proliferating cells [1, 2, 4]. So far, no relationship has been examined between subcellular localization of MT and its prognostic or predictive value.

MTs are known to be responsible for the resistance of tumor cells to platinum-containing drugs [6]. In our previous study, we have described MT expression in 73 samples of ovarian cancer, originating from patients treated with platinum-based schemes [14]. We have detected both cytoplasmic and nuclear presence of MT but, following the established routine, we have examined merely the relationships between overall immunoreactivity score of MT expression and clinical and pathological variables in the patients. Elevated MT expression in the patients has been found to characterize patients with shorter overall survival and patients in whom relapse has been noted [14]. We have noted also that in samples obtained after chemotherapy (secondary cytoreductions), MT expression has been significantly higher than in samples originating from the period before chemotherapy (primary laparotomies) [14]. The data on the relationship between MT expression in ovarian cancer and survival of patients treated with platinum-containing drugs are divergent, with some investigators noting the relationship and the other failing to detect it [12–14, 16].

In this study, we have examined MT expression in cells of ovarian cancer sensitive or resistant to cisplatin. The cisplatin-resistant A2780RCIS cells have been shown to exhibit higher overall MT expression. In contrast to the sensitive A2780 cells, they have manifested mainly nuclear expression of MT. Exposure of studied cells to growing concentrations of cisplatin has been shown to be paralleled by increasing intensity of MT expression, mainly in cell nuclei. At the highest of the examined concentrations of cisplatin, 66.6 μM, cell nuclei of ovarian cancer cells manifested a very strong expression of MT. Our studies have proven that MT expression in tumor cell nuclei increases in the course of exposure to cisplatin and is typical for cells resistant to the drug. Therefore, in studies on the prognostic and predictive value of MT expression in tumors, the expression in cell nuclei and in cytoplasm should be analyzed separately. Possibly, such an approach will reduce discrepancies in the results on MT. In the present study, we have shown for the first time that exposure to cisplatin results in translocation of MT to cell nuclei. Most probably, this represents the mechanism which protects DNA of tumor cells from toxic effects of the drug. Kondo et al. [8] in their in vitro studies demonstrated that nuclear expression of MT may be typical for cisplatin-resistant cells. Also, Cherian and Apostolova [4] noted that MT may manifest in cell nuclei of tumor cells, particularly in sites of intense proliferation. Takahashi et al. [15] suggested that MTn protects cell nuclei in the course of progression through the cell cycle. Until now, the prognostic and predictive value of subcellular MT localization has not been examined. Reevaluation of immunohistochemical reactions performed in our earlier study [14] has demonstrated that, in contrast to MTc, MTn expression is typical of ovarian cancer cases with lower overall and progression-free survival rates.

Summing up, in the present study, we have shown that nuclear expression of MT increases under the effect of exposure to cisplatin. We have demonstrated also that nuclear localization of MT is typical of ovarian cancer cells resistant to cisplatin and of cancers with less favorable clinical response to chemotherapy and lower survival rates. Thus, nuclear expression of MT seems to represent a very interesting novel and unfavorable prognostic and predictive factor.

References

1. Apostolova MD, Chen S, Chakrabarti S, Cherian MG (2001) High-glucose-induced metallothionein expression in endothelial cells: An endothelin-mediated mechanism. Am J Physiol Cell Physiol 281:C899–C907
2. Apostolova MD, Cherian MG (2000) Delay of M-phase onset by aphidicolin can retain the nuclear localization of zinc and metallothionein in 3T3-L1 fibroblasts. J Cell Physiol 183:247–253
3. Averette HE, Hoskins W, Nguyen HN, Boike G, Flessa HC, Chmiel JS, Zuber K, Karnel LH, Winchester DPSO (1993) National survey of ovarian carcinoma. 1. A patient care evaluation study of the American College of Surgeons. Cancer 71:1629–1638
4. Cherian MG, Apostolova MD (2000) Nuclear localization of metallothionein during cell proliferation and differentiation. Cell Mol Biol 46:347–356
5. Györffy B, Surowiak P, Kiesslich O, Denkert C, Schäfer R, Dietel M, Lage H (2006) Resistance prediction profile for eleven anticancer agents at clinical concentrations based on the gene expression pattern of thirty cell lines. Int J Cancer 118:1699–1712
6. Hagrman D, Goodisman J, Dabrowiak JC, Souid AK (2003) Kinetic study on the relation of cisplatin with metallothionein. Drug Metab Dispos 31:916–923
7. Holschneider CH, Berek JS (2000) Ovarian cancer: epidemiology, biology, and prognostic factors. Sem Surg Oncol 19:3–10
8. Kondo Y, Kuo SM, Watkins SC, Lazo JS (1995) Metallothionein localization and cisplatin resistance in human hormone-independent prostatic tumor cell lines. Cancer Res 55:474–477
9. Kowalski P, Surowiak P, Lage H (2005) Reversal of different drug-resistant phenotypes by an autocatalytic multitarget multiribozyme directed against the transcripts of the ABC transporters MDR1/P-gp, MRP2, and BCRP. Molec Ther 11:508–522
10. Lage H (2003) ABC-transporters: implications on drug resistance from microorganisms to human cancers. Int J Antimicrob Agents 22:188–199
11. Remmele W, Stegner HE (1987) Recommendation for uniform definition of an immunoreactive score (IRS) for immunohistochemical estrogen receptor detection (ER-ICA) in breast cancer tissue. Pathologe 8:138–140
12. Siegsmund MJ, Marx C, Seeman O, Schummer B, Steidler A, Toktomambetova L, Kohrmann KU, Rassweiler J, Alken P (1999)

Cisplatin-resistant bladder carcinoma cells: enhanced expression of metallothioneins. Urol Res 27:157–163
13. Siu LL, Banerjee D, Khurana RJ, Pan X, Pflueger R, Tannock IF (1998) The prognostic role of p53, metallothionein, P-glycoprotein, and MIB-1 in muscle-invasive urothelial transitional cell carcinoma. Clin Cancer Res 4:559–565
14. Surowiak P, Materna V, Kaplenko I, Spaczynski M, Dietel M, Lage H, Zabel M (2005) Augmented expression of metallothionein and glutathione S-transferase pi as unfavorable prognostic factors in cisplatin-treated ovarian cancer patients. Virchows Archiv 447:626–633
15. Takahashi Y, Ogra Y, Suzuki KT (2005) Nuclear trafficking of metallothionein requires oxidation of a cytosolic partner. J Cell Physiol 202:563–569
16. Wrigley E, Verpaget HW, Jayson GC, McGown AT (2000) Metallothionein expression in epithelial ovarian cancer: effect of chemotherapy and prognostic significance. J Cancer Res Clin Oncol 126:717–721

Virchows Arch (2007) 450:287–295
DOI 10.1007/s00428-006-0359-2

ORIGINAL ARTICLE

The expression of receptor for advanced glycation end products is associated with angiogenesis in human oral squamous cell carcinoma

Tomonori Sasahira · Tadaaki Kirita · Ujjal K. Bhawal · Masayuki Ikeda · Akira Nagasawa · Kazuhiko Yamamoto · Hiroki Kuniyasu

Received: 6 June 2006 / Revised: 10 December 2006 / Accepted: 11 December 2006 / Published online: 19 January 2007
© Springer-Verlag 2007

Abstract The receptor for advanced glycation end products (RAGE) is associated with cancer progression in several human cancers. In this study, we examined the roles of RAGE in the angiogenesis of oral squamous cell carcinoma (OSCC). RAGE concentration was examined in 20 OSCC tumors by enzyme-linked immunosorbent assay (ELISA). The microvessel density (MVD) and lymph vessel density (LVD) were examined by immunostaining. Concentrations of vascular endothelial growth factor (VEGF) and VEGF-C were examined in tumor tissues by ELISA. Tumoral RAGE concentration was associated with higher tumor MVD (P=0.0123) and tumor VEGF concentration (P=0.0344), but not with LVD and VEGF-C concentration. Treatment with RAGE ligand, high-mobility group box (HMGB)-1 increased the secretion of VEGF but not that of VEGF-C in human OSCC cell lines, HSC-3 and HSC-4. The effect of HMGB-1 was abrogated by RAGE down-regulation by antisense *S*-oligodeoxynucleic acid. These results suggest that RAGE expression is closely associated to angiogenesis in OSCC.

T. Sasahira · U. K. Bhawal · H. Kuniyasu (✉)
Department of Molecular Pathology, Nara Medical University,
840 Shijo-cho,
Kashihara, Nara 634-8521, Japan
e-mail: cooninh@zb4.so-net.ne.jp

T. Kirita · K. Yamamoto
Department of Oral and Maxillofacial Surgery,
Nara Medical University,
840 Shijo-cho,
Kashihara, Nara 634-8521, Japan

M. Ikeda · A. Nagasawa
Miyoshi Central Hospital,
Miyoshi, Japan

Keywords RAGE · Angiogenesis · VEGF · OSCC

Abbreviations

RAGE	receptor for advanced glycation end products
OSCC	oral squamous cell carcinoma
HMGB	high mobility group box
VEGF	vascular endothelial growth factor
ELISA	enzyme-linked immunosorbent assay

Introduction

Oral squamous cell carcinoma (OSCC) is the sixth commonest cancer in the world [20]. Especially in India and Sri Lanka, OSCC is the commonest cancer, accounting for at least 40% of all malignancies [5, 21]. The overall 5-year survival rate for patients with OSCC is the lowest among major cancers and has not changed during the past two decades [17]. Malignant potential of OSCC is closely associated with local expansion and lymph node metastasis [14]. Extended local invasion involves surrounding important structures, which makes it difficult to complete tumor resection and reduce cancer curability [23].

Angiogenesis is one of the major factors in the progression of OSCC [11, 14, 24]. Several angiogenetic factors are recruited in OSCC: vascular endothelial growth factor (VEGF), basic fibroblast growth factor (bFGF), interleukin (IL)-8, and platelet-derived endothelial growth factor; their roles on angiogenesis in OSCC are reported in [1, 13, 26, 32]. These factors are significantly associated with tumor microvessel density (MVD); VEGF is especially relevant [13, 26].

We previously reported that the expression of receptor for advanced glycation end products (RAGE) is closely associ-

ated with metastasis in various human cancers: gastric, colorectal, prostate, and malignant transformation of colorectal adenoma [6–10, 22]. RAGE activation accelerates cancer cell migration and invasion. [7, 8, 10]. In OSCC, RAGE also plays a pivotal role in cell growth and invasion [2]. The intracellular signaling pathways of RAGE induce the VEGF expression for the binding to advanced glycation end products (AGE); that is, the other ligand of RAGE and the activated nuclear factor-kB (NF-kB) in vascular endothelial cells [19], and causes abnormal vascularities in diabetes complication [34, 35]. However, an angiogenic role of RAGE is not well elucidated in cancer. In this study, we investigated the relationship between RAGE expression in OSCC and angiogenesis and lymphangiogenesis, and examined the effect of HMGB1 (a RAGE ligand) on the expression of VEGF and VEGF-C in human OSCC cell lines.

Materials and methods

Patients and tumor specimens

Twenty OSCC patients (ten men, ten women; aged 49 to 83 with a mean of 69.1 years old) were randomly selected from Nara Medical University Hospital, Kashihara, Japan, and Miyoshi General Hospital, Miyoshi, Japan. The tissues were obtained from cancer and from the surrounding non-cancerous mucosa before any treatment, in which histological contents were confirmed by the microscopical examination of the frozen sections. The surrounding mucosa was used as a non-cancer control. Informed consent was obtained from each patient. Their tumors were classified according to the UICC TNM classification system [29]. It was confirmed clinically that any patient has no metastasis to distant organs, such as the lung, liver, and bone. Histopathological grading was classified according to the World Health Organization (WHO) criteria [33]. In 11 out of 20 cases, lymph node metastasis was confirmed by histopathological examination. Their medical records and prognostic follow-up data were obtained from the patient database maintained by the hospitals.

ELISA for RAGE, VEGF, and VEGF-C

Enzyme-linked immunosorbent assay (ELISA) was used for the measurement of protein concentrations of RAGE (R&D Systems, Minneapolis, MN, USA), VEGF (Calbiochem, Darmstadt, Germany), and VEGF-C (Bender MedSystems GmbH, San Bruno, CA, USA). A small piece (approximately 10 mm^3) of tumor tissue was obtained from each case, frozen with liquid nitrogen, and stored at −80°C. The tissues were homogenized in lysis buffer (50-mM Tris HCl, pH 7.5, 5-mM EDTA, 1-mM EGTA, 2% nonidet-40, 10 μg/ml leupeptin, 50 μg/ml phenylmethylsulfonyl fluoride), and centrifuged (5,000×*g*). The supernatant (10 μg) was used for ELISA. The assay was performed according to the provider's instructions with triplicate. The experiment was repeated twice.

Immunohistochemistry

Immunohistochemistry was performed as previously described [10]. Formalin-fixed, paraffin-embedded specimens were used and an immunoperoxidase technique was done after antigen retrieval with pepsin (DAKO, Carpinteria, CA, USA) treatment for 20 min. After blocking endogenous peroxidase activity with 3% H_2O_2-methanol for 15 min, the specimens were rinsed with phosphate-buffered saline (PBS). Anti-RAGE antibody (clone C-20, Santa Cruz Biotechnology, Santa Cruz, CA, USA), CD34 antibody (DAKO), D2-40 antibody (reacting with lymphatic endothelium-specific *O*-linked sialoglycoprotein, Signet Laboratories, Dedham, MA, USA), anti-VEGF antibody (Santa Cruz Biotechnology), and anti-VEGF-C antibody (Zymed Laboratories, South San Francisco, CA, USA) diluted by 0.5 μg/ml were used as primary antibodies. After a 2-h incubation at room temperature, the specimens were rinsed with PBS and incubated at room temperature for 1 h with secondary antibody conjugated to peroxidase (1:200; anti-goat IgG antibody, Medical and Biological Laboratories, Nagoya, Japan). After rinsing with PBS, all specimens were color-developed with diaminobenzidine (DAB) solution (DAKO). The immunostaining of all specimens was performed simultaneously to ensure the same antibody reaction and DAB exposure conditions.

Evaluation of immunoreactivity

Immunoreactivity in vascular endothelial cells in the same specimen was used as a "built-in" positive control for RAGE immunoreactivity [10]. The vascular density was measured on anti-CD34-(for blood vessels) or anti-D2-40-(for lymph vessels)immunostained specimens. To quantify MVD or lymph vessel density (LVD), 15 random 0.8-mm^2 fields selected from the entire tumor area were examined under a 200-fold magnification by microscopy by three pathologists (T. S., U. K. B., and H. K.) independently in a masked fashion. The average value of the vessel densities in the three areas with maximum density (hot spot) was represented as the MVD or LVD in the tumor tissues [12].

Cell culture

Human OSCC cell lines, HSC-3 and HSC-4 cells, and MKN45 human gastric cancer cells (kindly provided by Dr. W. Yasui, Hiroshima University Graduate School, Hiroshima,

Japan) were studied. The MKN45 cells that do not express RAGE were used as negative controls for in vitro experiments [10]. The cell lines were routinely maintained in Roswell Park Memorial Institute (RPMI)-1640 (Sigma Chemical) containing 10% fetal bovine serum (FBS; Sigma Chemical) under 5% CO_2 in air at 37°C. The cells were treated with human recombinant HMGB1 (hrHMGB1, Abnova, Taipei City, Taiwan) for 24 h. The cultured medium was used for ELISA on VEGF or VEGF-C.

Preparation of conditioned medium

For measurement of VEGF and VEGF-C concentrations in cell culture media by HSC-3 and HSC-4 cells, 1×10^4 cells were cultured in 1 ml of RPMI-1640 for 48 h that was supplemented by 10% FBS for avoiding cell stresses from low serum concentration. Then, the cultured medium was filtered with 0.2-μm push filter (Millipore, Bedfold, MA, USA) and used for ELISA.

Reverse transcriptase-polymerase chain reaction

The RAGE messenger RNA (mRNA) expression was assessed with reverse transcriptase–polymerase chain reaction (RT-PCR) using 0.5 μg of total RNA extracted by RNeasy kit (Qiagen, Hilden, Germany). The primer sets for RAGE amplification are the upper 5′-GGG CTC TTC ACA CTG C-3′ and lower 5′-ACT GCT CCA CCT TCT G-3′ (GenBank accession no. BC020669; synthesized by Sigma Genosys, Ishikari, Japan). PCR products were electrophoresed in 2% agarose gel and stained with ethidium bromide. β-actin mRNA was also amplified for internal controls (GenBank accession no. NM_001101).

Antisense phosphorothioate(*S*)-oligodeoxynucleaotide assay

The 18-mer *S*-oligodeoxynucleotide (*S*-ODN) for antisense sequence from the 6th to 18th nucleotide of RAGE complementary DNA was synthesized and purified by

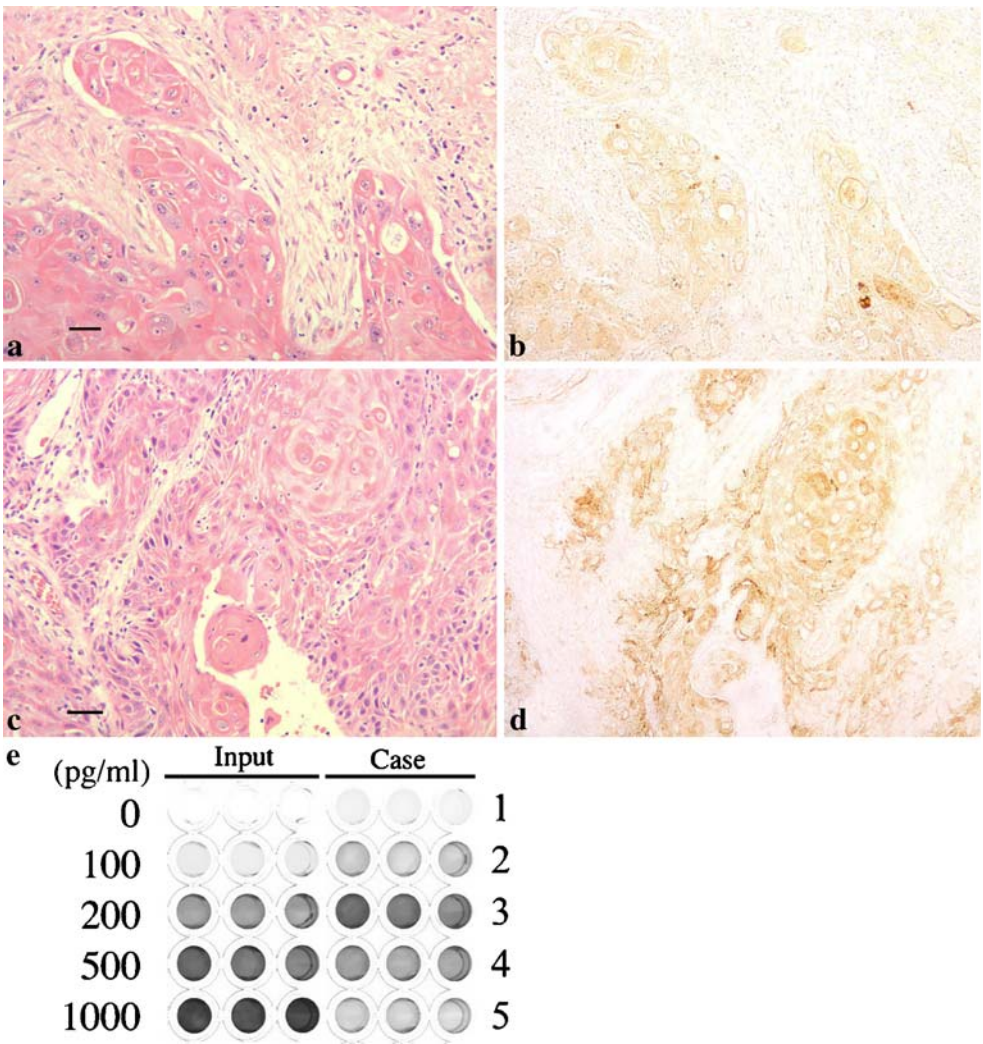

Fig. 1 Expression of RAGE in OSCC (**a**–**d**). Immunohistochemical analysis of RAGE in OSCC cases. RAGE immunoreactivity is found in the membrane and cytoplasm of cancer cells. **a**, **b** A case with moderate RAGE immunoreactivity (**b**). Well-differentiated SCC (**a**; H & E) invading into subepithelial tissue (*bar*=200 μm). **c**, **d** A case with strong RAGE immunoreactivity (**d**). Well-differentiated SCC (**c**; H & E) invading into the muscle layer (*bar*= 200 μm). **e** RAGE concentration in five representative tumor tissues. RAGE protein concentration is examined by ELISA in lysates of the tumor tissues. To examine RAGE in tumors, 10 μg of tissue lysate was used for ELISA. Then concentration "pg/ml" is equivalent to "pg/ 10 μg lysate." RAGE concentrations of cases in (**a**) and (**b**) are 85.8 pg/10 μg lysate (*case 2*) and 42.4 pg/10 μg lysate (*case 3*), respectively

reverse-phase high-performance liquid chromatography (Sigma Genosys). The sequence was 5′-CTG CTT CCT TCC AGG GTC-3′(GenBank accession no. BC020669). The sense sequence 18-mer was for negative control. Each cell line was pretreated with 3 μM of antisense or sense *S*-ODN for 6 days with medium exchanges and additions of antisense or sense *S*-ODN every 2 days. After then, the cells were used for further experiments.

Statistical analyses

The correlation of variables was performed using a non-parametric two-tailed Mann–Whitney *U* test. All statistical analyses were carried out with StatView version 4.5 (SAS Institute, Cary, NC, USA). *P* values less than 0.05 were regarded as statistically significant.

Results

RAGE expression in OSCC

RAGE expression was examined by immunohistochemistry and ELISA (Fig. 1, Tables 1, and 2). The immunoreactivity for RAGE was detected in the cell membrane and cytoplasm of tumor cells (Fig. 1b and d). No RAGE immunoreactivity was observed in the corresponding mucosal or glandular epithelia. RAGE proteins in the frozen tumor tissues of the 20 cases were measured by ELISA (Fig. 1e). The cases examined were listed in Table 1. The RAGE concentration was higher in T1–T2 cases (75±12) than that in T3–T4 cases (57±19; $P=0.0408$, Table 2), whereas the RAGE concentration in N1–N2 cases (70±13) was not significantly different from that in N0 cases (53±21). We did not find any correlations between RAGE concentration and age, sex, or histological differentiation.

Relation of RAGE expression with angiogenesis or lymphngiogenesis in OSCC

We next compared RAGE expression with angiogenesis or lymphangiogenesis in OSCC. MVD and LVD were evaluated by immunohistochemistry with CD34 and D2-40 antibodies (Fig. 2a and b). The LVD and VEGF-C concentration were significantly different between the cases of N0 and N1–N2 or the cases of stage I–II and stage III–IV ($P=0.0012$ and $P=0.0057$, respectively; Table 2). In 9 of 20

Table 1 Cases examined and the results

Number	Sex	Age	Histology[a]	TNM[b]	Stage[b]	MVD[c]	LVD[d]	RAGE[e]	VEGF[e]	VEGF-C[e]
1	M	59	Well	T1N0M0	I	56	36	57.3	112	59
2	F	66	Well	T2N0M0	II	223	50	79.8	486	89
3	F	53	Mod	T2N0M0	II	265	61	88.0	433	154
4	M	70	Mod	T2N0M0	II	138	98	64.6	168	154
5	F	83	Well	T2N0M0	II	19	52	25.7	69	94
6	F	81	Mod	T2N0M0	II	27	65	41.6	78	146
7	F	78	Mod	T2N0M0	II	64	72	34.8	233	111
8	F	79	Well	T2N0M0	II	31	82	42.4	105	204
9	M	66	Well	T2N0M0	II	59	79	46.2	136	178
10	F	77	Well	T2N1M0	III	198	110	82.4	308	221
11	F	69	Well	T2N1M0	III	42	183	49.7	88	306
12	M	60	Well	T2N1M0	III	121	142	74.0	304	250
13	F	70	Well	T2N1M0	III	89	108	55.5	255	166
14	M	63	Well	T3N1M0	III	207	95	78.9	367	122
15	M	63	Well	T3N1M0	III	72	101	66.2	134	243
16	M	68	Mod	T3N1M0	III	69	122	61.9	102	198
17	M	75	Mod	T2N2M0	IV	61	197	61.0	156	433
18	F	49	Mod	T4N1M0	IV	191	40	89.8	406	102
19	M	73	Well	T4N1M0	IV	94	174	85.8	121	297
20	M	80	Mod	T4N2M0	IV	162	235	66.0	225	401

[a] Histology: *well* well-differentiated squamous cell carcinoma, *mod* moderately differentiated squamous cell carcinoma [33]

[b] Clinical TNM classification and stage [29]. *T1* Tumor 2 cm or less; *T2* tumor more than 2–4 cm; *T3* tumor more than 4 cm; *T4* tumor invading adjacent structures; *N0* no regional lymph node metastasis; *N1* metastasis in a single ipsilateral lymph node (3 cm or less); *N2* metastasis in a single ipsilateral lymph node (3–6 cm) multiple ipsilateral lymph nodes (none more than 6 cm), or contralateral lymph nodes (none more than 6 cm); *M0* no distant metastasis; *Stage I* T1N0M0; *Stage II* T2N0M0; *Stage III* T3N0M0 or T1-3N1M0; *Stage IV* T4N0-1M0 or T1-4N2

[c] *MVD* Microvessel density (per mm^2); maximum values from 15 examined fields

[d] *LVD* Lymph vessel density (per mm^2); maximum values from 15 examined fields

[e] Concentration was measured in tumor tissues by ELISA (pg/10 μg tissue lysate) in triplicate. The value was the average of the triplicate measurement (each SD was less than 10% in all cases)

Table 2 Relation of clinical parameters with vessel densities or concentrations of RAGE, VEGF, and VEGF-C

	Number	MVD[a]	LVD[b]	RAGE[c]	VEGF[c]	VEGF-C[c]
Sex						
M	10	104±52	128±60	66±11	183±89	233±118
F	10	115±94	82±42	59±24	246±159	159±69
Age						
<=69	10	131±83	91±48	69±15	257±158	170±80
70<=	10	88±61	119±62	56±20	172±81	223±118
Histology[d]						
Well	12	101±71	101±47	62±19	207±133	186±82
Mod	8	122±82	111±70	63±19	225±131	212±130
T factor[e]						
T1–T2	14	100±79	95±49	57±19*	209±133	183±98
T3–T4	6	133±62	128±68	75±12*	226±132	227±112
N factor[e]						
N0	9	98±90	66±19**	53±21	202±155	132±47***
N1–N2	11	119±60	137±56**	70±13	224±112	149±105***
Stage[e]						
I–II	9	98±90	66±19**	53±21	202±155	132±47***
III–IV	11	119±60	137±56**	70±13	224±112	149±105***

[a] *MVD* Microvessel density (per mm^2); maximum values from 15 examined fields
[b] *LVD* Lymph vessel density (per mm^2); maximum values from 15 examined fields
[c] Concentration was measured in tumor tissues by ELISA (pg/10 μg tissue lysate) in triplicate. The value was the average of the triplicate measurement (each SD was less than 10% in all cases).
[d] Histology: *well* well-differentiated squamous cell carcinoma, *mod* moderately differentiated squamous cell carcinoma [33]
[e] Clinical TNM classification and stage [29]. *T1* Tumor 2 cm or less; *T2* tumor more than 2–4 cm; *T3* tumor more than 4 cm; *T4* tumor invading adjacent structures; *N0* no regional lymph node metastasis; *N1* metastasis in a single ipsilateral lymph node (3 cm or less); *N2* metastasis in a single ipsilateral lymph node (3–6 cm) multiple ipsilateral lymph nodes (none more than 6 cm), or contralateral lymph nodes (none more than 6 cm); *M0* no distant metastasis; *Stage I* T1N0M0; *Stage II* T2N0M0; *Stage III* T3N0M0 or T1-3N1M0; *Stage IV* T4N0-1M0 or T1-4N2
*P=0.0408
**P=0.0012
***P=0.0057

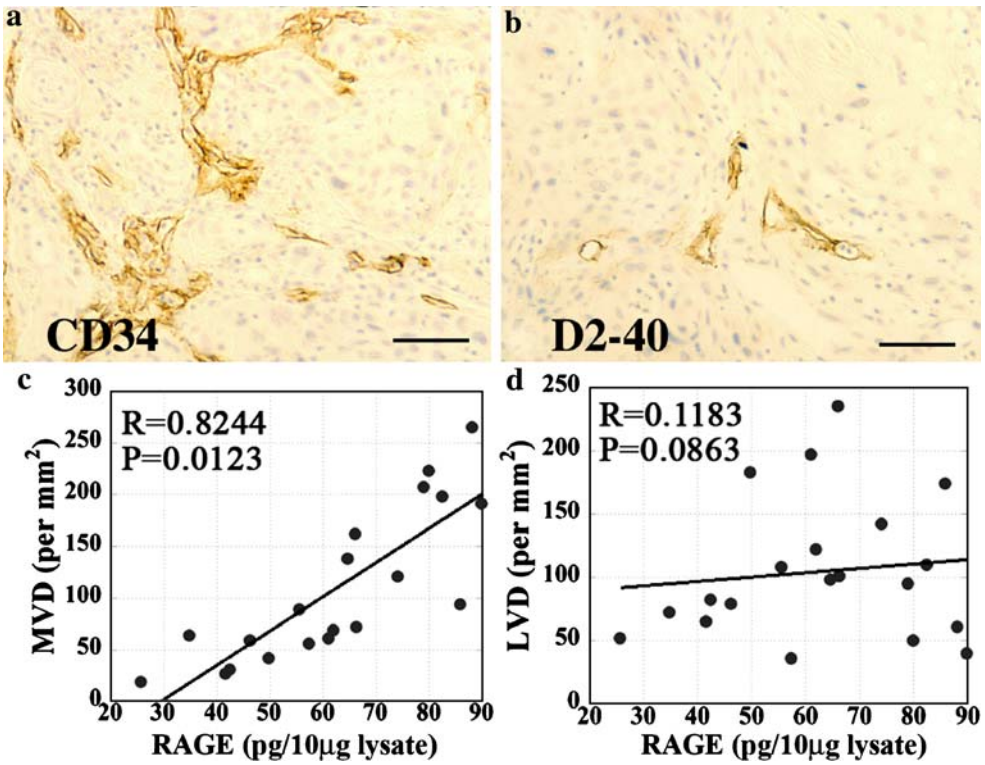

Fig. 2 Relation of RAGE expression with MVD or LVD in OSCC (**a**). Tumor vasculature is examined by CD34 immunostaining (*bar*=200 μm). **b** Lymph vessels are examined by D2-40 immunostaining (*bar*=200 μm). **c** Association of RAGE expression with MVD. **d** Association of RAGE expression with LVD. **c**, **d** Significance of the correlation was tested by the Mann–Whitney *U* test

cases, the maximum values of both MVD and LVD were located at the invasive front. The tumoral concentration of RAGE was compared with MVD and LVD and tested by the Mann–Whitney *U* test (Fig. 2c and d). A significant correlation was observed between RAGE concentration and MVD (P=0.0123, Fig. 2c), whereas no correlation was observed between RAGE concentration and LVD (P=0.0863, Fig. 2d).

We also compared the RAGE expression with the VEGF or VEGF-C expression in OSCC. The expressions of VEGF and VEGF-C were examined by immunohistochemistry and ELISA (Fig. 3a and b). Tumoral concentration of RAGE was compared with the concentration of VEGF or VEGF-C (Fig. 3c and d). RAGE concentration was significantly associated with VEGF expression (P=0.0344, Fig. 3c). In contrast, VEGF-C expression was not associated with RAGE concentration (P=0.0921, Fig. 3d). The expression of VEGF and VEGF-C was significantly associated with MVD (P=0.0024) and LVD (P=0.00016), respectively.

Effects of hrHMGB1 on the secretion of VEGF and VEGF-C in OSCC cell lines

We examined the effect of HMGB1, the major ligand for RAGE in neoplasm [7], on the secretion of VEGF and VEGF-C in HSC-3 and HSC-4 human OSCC cells. The MKN45 human gastric carcinoma cells were also examined for RAGE-negative control (Fig. 4a,d, and g) [10]. The secretion of VEGF under treatment with hrHMGB1 was increased in a dose-dependent manner in RAGE-positive HSC-3 and HSC-4 cells (Fig. 4b and c), but not in RAGE-negative MKN45 cells (Fig. 4d) [10]. The HSC-3 and HSC-4

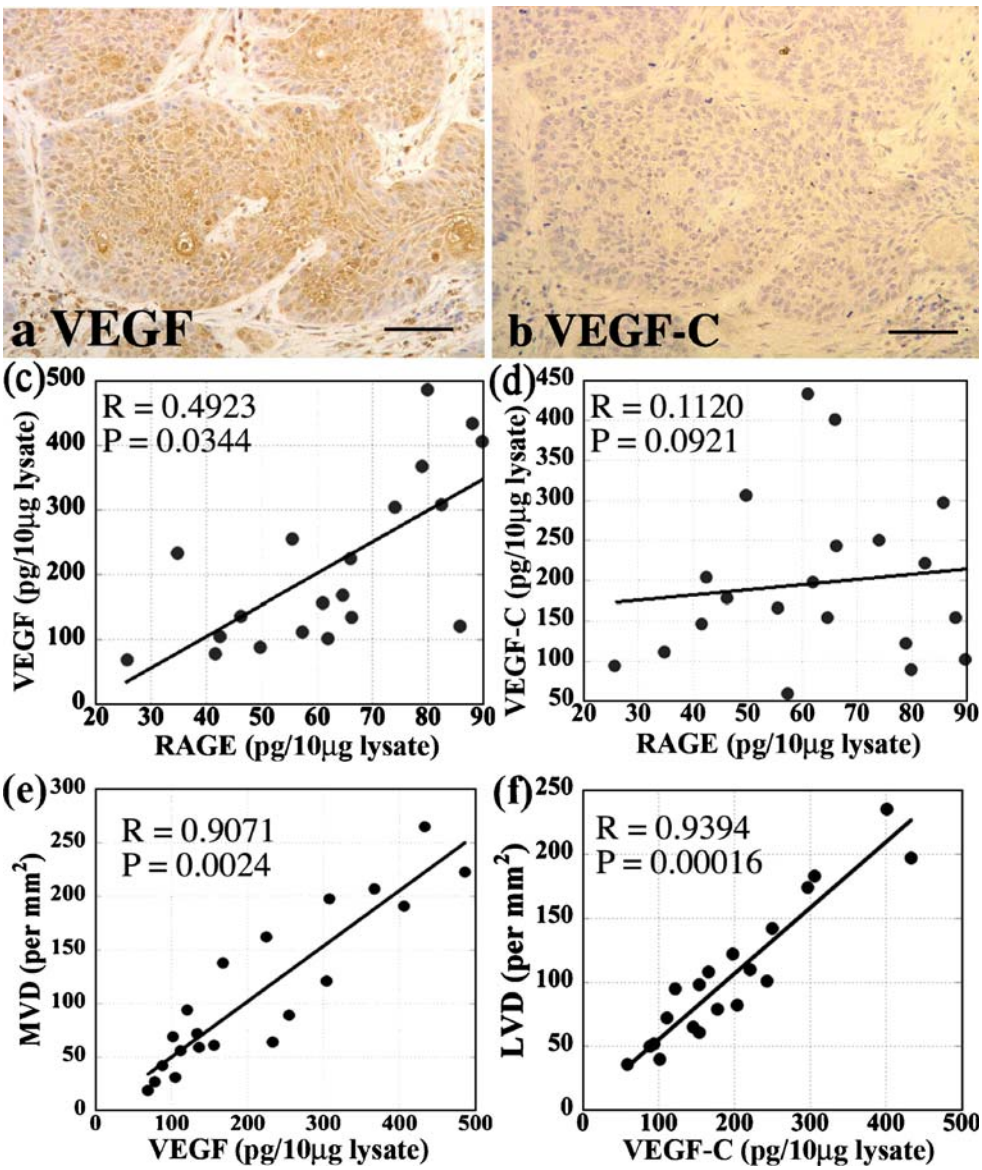

Fig. 3 Relation of RAGE expression with the expression of VEGF or VEGF-C in OSCC (**a**, **b**). Expression of VEGF (**a**) and VEGF-C (**b**) is confirmed in tumor cells by immunohistochemistry (*bar*=200 μm). **c** Association of RAGE expression with tumoral VEGF concentration detected by ELISA. **d** Association of RAGE expression with tumoral VEGF-C concentration detected by ELISA. **e**, **f** Association of expression of VEGF or VEGF-C with MVD or LVD, respectively. **c**–**f** Significance of the correlation was tested by the Mann–Whitney *U* test

cells expressed RAGE under exposure to RAGE sense *S*-ODN that was suppressed by exposure to RAGE antisense *S*-ODN (Fig. 4a). In RAGE sense *S*-ODN-exposed HSC-3 and HSC-4 cells, the VEGF secretion was increased to 162±18% and 184±24%, respectively, by HMGB1 (40 μg/ml) treatment, whereas the RAGE antisense *S*-ODN abrogated the HMGB1-induced VEGF increase. The HSC-3and HSC-4 cells exposed to RAGE antisense *S*-ODN showed significantly lower VEGF secretion (105±9% and 99±8%, respectively) than those in RAGE sense *S*-ODN cells (P=0.0010 and P=0.0008, respectively). In contrast, the secretion level of VEGF-C was not affected under treatment with the various concentration of hrHMGB1 in HSC-3, HSC-4, and MKN45 cells (Fig. 4e–g). The exposure to RAGE antisense *S*-ODN abrogated VEGF secretion by hrHMGB1 treatment (Fig. 4b and c) but had no effect on the VEGF-C secretion in both cell lines (Fig. 4e and f). In contrast, RAGE antisense *S*-ODN or hrHMGB1 did not affect the secretion of VEGF and VEGF-C in RAGE-negative MKN45 cells.

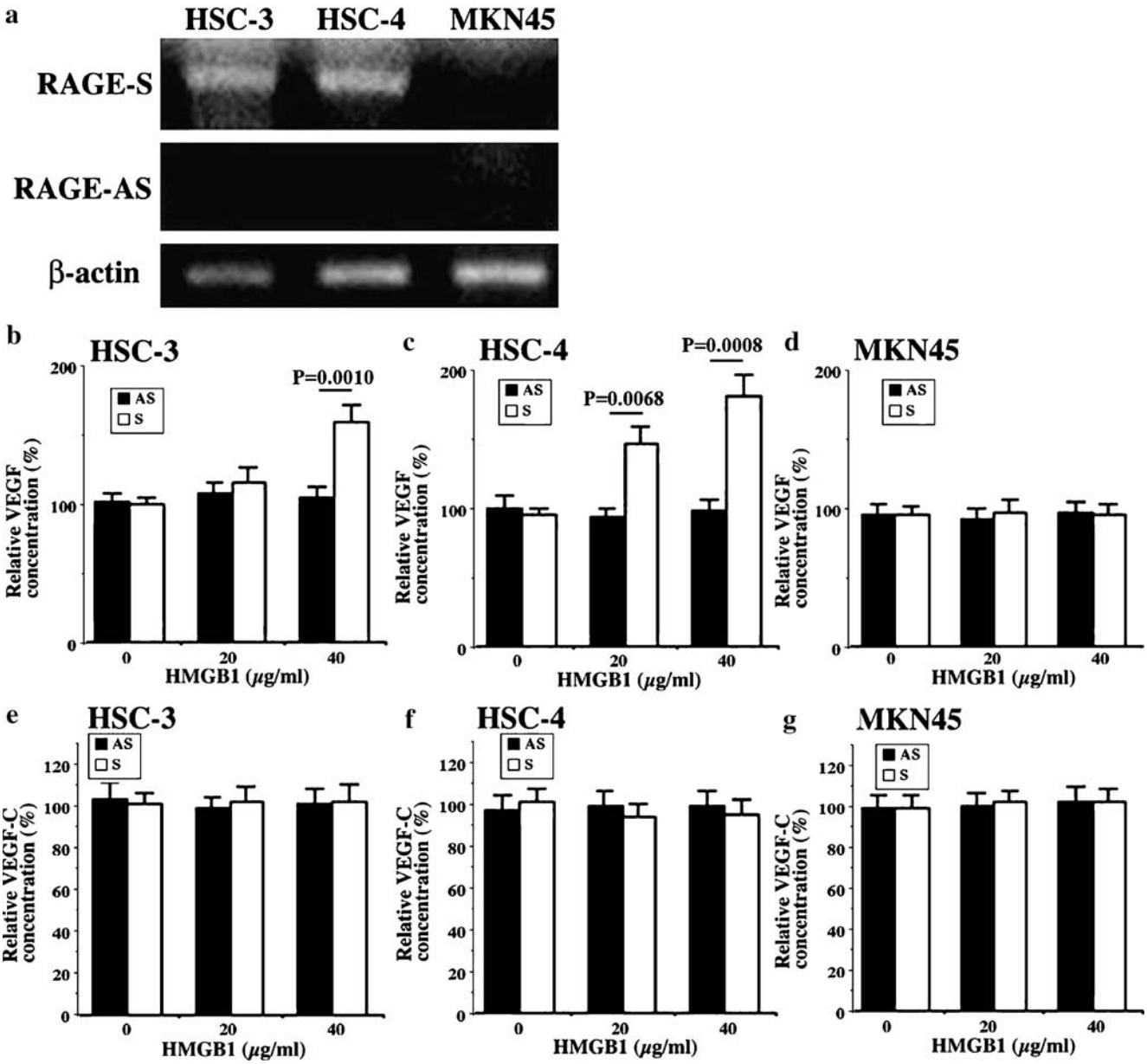

Fig. 4 Effect of human recombinant HMGB1 on the secretion of VEGF or VEGF-C in human HSC-3 and HSC-4 OSCC cells (**a**). RAGE mRNA expression in HSC-3 and HSC-4 cells exposed to RAGE antisense or sense *S*-ODNs detected by RT-PCR. MKN45 cells were also treated as a RAGE-negative control. β-actin was served for internal control. **b**–**d** VEGF secretion by hrHMGB1-treated HSC-3 (**b**), HSC-4 (**c**), and RAGE-negative MKN45 cells (**d**) exposed to RAGE antisense or sense *S*-ODNs detected by ELISA. **e**–**g** VEGF-C secretion by HMGB1-treated HSC-3 (**e**), HSC-4 (**f**), and MKN45 cells (**g**) exposed to RAGE antisense or sense *S*-ODNs detected by ELISA. **b**–**g** *Error bar*, SD that was calculated from the triplicate assay repeated twice (**b**, **c**)

Discussion

Advanced OSCC is tended to local expansion and lymph node metastasis [14]. We examined a role of RAGE for tumor angiogenesis in OSCC. RAGE protein concentration in OSCC tumor tissues is significantly correlated with MVD and VEGF concentration but not with LVD and VEGF-C concentration. In vitro examination showed that a RAGE ligand, HMGB1, induces VEGF secretion but not VEGF-C in HSC-3 and HSC-4 human OSCC cell lines. Differential induction of VEGF from VEGF-C by RAGE activation by HMGB1 might explain why RAGE expression is not associated with lymphangiogenesis. The lymph node metastasis of cancer is strongly associated with lymphangiogenesis [27]. We confirmed that there is no correlation between RAGE expression and nodal metastasis of OSCC (data not shown).

RAGE is associated with abnormal neovascularization in diabetic retinopathy [34]. In that condition, AGE generated under hyperglycemic and oxidative conditions works as a RAGE ligand [3, 34, 35]. Activated RAGE induces VEGF expression transcriptionally through the activation of nuclear factor kappa B (NFkB), AP-1, and HIF-1α [19, 30]. The induction of VEGF-C is resulted by the activation of p38 mitogen-activated protein kinase (MAPK) and NFkB [31]. The activation profile of MAPK might be associated with the differential response to RAGE ligand on VEGF/VEGF-C induction. There is a difference in VEGF induction between AGE and HMGB1 [7]. AGE–bovine serum albumin (BSA) is a more pronounced effect on VEGF expression than HMGB1 in colorectal cancer cell lines. Further examination is necessary on the difference of intracellular signaling associated with different responses to the ligands.

VEGF-A and VEGF-B are commonly expressed with or without nodal metastasis, whereas VEGF-C and VEGF-D are associated with lymph node metastasis [18, 28]. Actually, the expression of VEGF and VEGF-C was significantly associated with MVD and LVD, respectively, in this study. VEGF-C also participates relevantly in angiogenesis [16]. One of the suggested mechanisms is that binding affinity to the receptors of VEGF-C is different on the lymphoendothelial and vasculoendothelial cells for the proteolytic processing of VEGF-C [4].

The roles of RAGE on cancer development might be different in the different tumor types. RAGE overexpression is significantly associated with lymph node metastasis in gastric, colorectal, and prostate cancer [8–10]. In contrast, RAGE expression is associated with the differentiation of the normal and cancer tissues in the lung [25]. RAGE is also associated with cellular differentiation of erythroleukemia [15]. In OSCC, RAGE expression was associated with tumor growth but not histological differentiation or nodal metastasis. Thus, the roles of RAGE might depend on the histological types of tumors or on the intracellular signaling pathways of RAGE. Furthermore, details of RAGE functions are needed to examine in each cancer involving OSCC.

The results presented in this study showed that RAGE has a role for VEGF expression in tumors that is closely associated with tumor angiogenesis. Complicated combinations of factors are connected with tumor angiogenesis, such as hypoxia-inducible factor, nitric oxide, and other cytokines/growth factors as limited to VEGF-associated factors. RAGE is one of the relevant factors of the angiogenesis in OSCC and might suggest a therapeutic target on cancer progression.

Acknowledgment The authors thank Mrs. Kaori Isobe for the expert assistance with the preparation of this manuscript. This work was supported in part by the grant-in-aid for scientific research from the Japan Society for the Promotion of Science, Japan.

References

1. Alcalde RE, Terakado N, Otsuki K, Matsumura T (1997) Angiogenesis and expression of platelet-derived endothelial cell growth factor in oral squamous cell carcinoma. Oncology 54:324–328
2. Bhawal UK, Ozaki Y, Nishimura M, Sugiyama M, Sasaki N, Kuniyasu H, Kato Y (2005) Association of expression of receptors for advanced glycation end-products (RAGE) and invasive and metastatic activity of oral squamous cell carcinoma. Oncology 69:246–255
3. Brownlee M (2000) Negative consequences of glycation. Metabolism 49:9–13
4. Joukov V, Pajusola K, Kaipainen A, Chilov D, Lahtinen I, Kukk E, Saksela O, Kalkkinen N, Alitalo K (1996) A novel vascular endothelial growth factor, VEGF-C, is a ligand for the Flt4 (VEGFR-3) and KDR (VEGFR-2) receptor tyrosine kinases. EMBO J 15:1751
5. Kaura J, Srivastava A, Ralhan R (1994) Overexpression of p53 protein in betel-and tobacco-related human oral dysplasia and squamous-cell carcinoma in India. Int J Cancer 58:340–345
6. Kuniyasu H (2005) The molecular pathology of gastric cancer. In: Kuriyama S, Yoshiji H (eds) New perspectives in cancer research and therapy 2005. Research Signpost, Kerala, pp 85–98
7. Kuniyasu H, Chihara Y, Kondo H (2003) Differential effects between amphoterin and advanced glycation end products on colon cancer cells. Int J Cancer 104:722–727
8. Kuniyasu H, Chihara Y, Kondo H, Ohmori H, Ukai R (2003) Amphoterin induction in prostatic stromal cells by androgen deprivation is associated with metastatic prostate cancer. Oncol Rep 10:1863–1868
9. Kuniyasu H, Chihara Y, Takahashi T (2003) Co-expression of receptor for advanced glycation end products and the ligand amphoterin associates closely with metastasis of colorectal cancer. Oncol Rep 10:445–448
10. Kuniyasu H, Oue N, Wakikawa A, Shigeishi H, Matsutani N, Kuraoka K, Ito R, Yokozaki H, Yasui W (2002) Expression of receptors for advanced glycation end-products (RAGE) is closely associated with the invasive and metastatic activity of gastric cancer. J Pathol 196:163–170
11. Kuniyasu H, Tahara E (2001). Molecular pathology of esophageal cancer. In: Kelsen DP, Daly J, Kern S, Levin B, Tepper J (eds)

Gastrointestinal oncology: principles and practices. Lippincott, Williams & Wilkins, Cherlottesville, pp 237–249
12. Kuniyasu H, Yasui W, Shinohara H, Yano S, Ellis LM, Wilson MR, Bucana CD, Rikita T, Tahara E, Fidler IJ (2000) Induction of angiogenesis by hyperplastic colonic mucosa adjacent to colon cancer. Am J Pathol 157:1523–1535
13. Li C, Shintani S, Terakado N, Klosek SK, Ishikawa T, Nakashiro K, Hamakawa H (2005) Microvessel density and expression of vascular endothelial growth factor, basic fibroblast growth factor, and platelet-derived endothelial growth factor in oral squamous cell carcinomas. Int J Oral Maxillofac Surg 34:559–565
14. Lopez-Graniel CM, Tamez de Leon D, Meneses-Garcia A, Gomez-Ruiz C, Frias-Mendivil M, Granados-Garcia M, Barrera-Franco JL (2001) Tumor angiogenesis as a prognostic factor in oral cavity carcinomas. J Exp Clin Cancer Res 20:463–468
15. Melloni E, Sparatore B, Patrone M, Pessino A, Passalacqua M, Pontremoli S (1995) Identity in molecular structure between "differentiation enhancing factor" of murine erythroleukemia cells and the 30 kD heparin-binding protein of developing rat brain. Biochem Biophys Res Commun 210:82–89
16. Miyata Y, Kanda S, Ohba K, Nomata K, Hayashida Y, Eguchi J, Hayashi T, Kanetake H (2006) Lymphangiogenesis and angiogenesis in bladder cancer: prognostic implications and regulation by vascular endothelial growth factors-A, -C, and -D. Clin Cancer Res 12:800–806
17. Nagler RM (2002) Molecular aspects of oral cancer. Anticancer Res 22:2977–2980
18. Nakazato T, Shingaki S, Kitamura N, Saito C, Kuwano R, Tachibana M (2006) Expression level of vascular endothelial growth factor-C and -A in cultured human oral squamous cell carcinoma correlates respectively with lymphatic metastasis and angiogenesis when transplanted into nude mouse oral cavity. Oncol Rep 15:825–830
19. Okamoto T, Yamagishi S, Inagaki Y, Amano S, Koga K, Abe R, Takeuchi M, Ohno S, Yoshimura A, Makita Z (2002) Angiogenesis induced by advanced glycation end products and its prevention by cerivastatin. FASEB J 16:1928–1930
20. Parkin DM, Bray F, Ferlay J, Pisani P (2001) Estimating the world cancer burden: Globocan 2000. Int J Cancer 94:135–156
21. Paterson IC, Eveson JW, Prime SS (1996) Molecular changes in oral cancer may reflect and ethnic origin. Eur J Cancer B Oral Oncol 32B:150–153
22. Sasahira T, Akama Y, Fujii K, Kuniyasu H (2005) Expression of receptor for advanced glycation end products and HMGB1/amphoterin in colorectal adenomas. Virchows Arch 446:411–415
23. Sawair FA, Irwin CR, Gordon DJ, Leonard AG, Stephenson M, Napier SS (2003) Invasive front grading: reliability and usefulness in the management of oral squamous cell carcinoma. J Oral Pathol Med 32:1–9
24. Schliephake H (2003) Prognostic relevance of molecular markers of oral cancer—a review. Int J Oral Maxillofac Surg 32:233–245
25. Schraml P, Shipman R, Colombi M, Ludwig CU (1994) Identification of genes differentially expressed in normal lung and non-small cell lung carcinoma tissue. Cancer Res 54:5236–5240
26. Shang ZJ, Li ZB, Li JR (2005) VEGF is up-regulated by hypoxic stimulation and related to tumour angiogenesis and severity of disease in oral squamous cell carcinoma: in vitro and in vivo studies. Int J Oral Maxillofac Surg 35:533–538
27. Shayan R, Achen MG, Stacker SA (2006) Lymphatic vessels in cancer metastasis: bridging the gaps. Carcinogenesis 27:1729–1738
28. Shintani S, Li C, Ishikawa T, Mihara M, Nakashiro K, Hamakawa H (2004) Expression of vascular endothelial growth factor A, B, C, and D in oral squamous cell carcinoma. Oral Oncol 40:13–20
29. Sobin LH, Wittekind C (2003) UICC TNM classification of malignant tumours. Wiley, New York
30. Treins C, Giorgetti-Peraldi S, Murdaca J, Van Obberghen E (2001) Regulation of vascular endothelial growth factor expression by advanced glycation end products. J Biol Chem 276:43836–43841
31. Tsai PW, Shiah SG, Lin MT, Wu CW, Kuo ML (2003) Up-regulation of vascular endothelial growth factor C in breast cancer cells by heregulin-β1. A critical role of p38/nuclear factor-κ B signaling pathway. J Biol Chem 278:5750–5759
32. Watanabe H, Iwase M, Ohashi M, Nagumo M (2002) Role of interleukin-8 secreted from human oral squamous cell carcinoma cell lines. Oral Oncol 38:670–679
33. WHO (1988) International histological classification of tumours. Springer, Berlin Heidelberg New York
34. Yamagishi S, Takeuchi M, Inagaki Y, Nakamura K, Imaizumi T (2003) Role of advanced glycation end products (AGEs) and their receptor (RAGE) in the pathogenesis of diabetic microangiopathy. Int J Clin Pharmacol Res 23:129–134
35. Yamamoto Y, Yamagishi S, Yonekura H, Doi T, Tsuji H, Kato I, Takasawa S, Okamoto H, Abedin J, Tanaka N, Sakurai S, Migita H, Unoki H, Wang H, Zenda T, Wu PS, Segawa Y, Higashide T, Kawasaki K, Yamamoto H (2000) Roles of the AGE–RAGE system in vascular injury in diabetes. Ann NY Acad Sci 902:163–170

Virchows Arch (2007) 450:297–302
DOI 10.1007/s00428-006-0360-9

ORIGINAL ARTICLE

Aurora-B expression and its correlation with cell proliferation and metastasis in oral cancer

Guangying Qi · Ikuko Ogawa · Yasusei Kudo · Mutsumi Miyauchi · B. S. M. S. Siriwardena · Fumio Shimamoto · Masaaki Tatsuka · Takashi Takata

Received: 22 October 2006 / Revised: 13 December 2006 / Accepted: 15 December 2006 / Published online: 19 January 2007
© Springer-Verlag 2007

Abstract Aurora-B kinase is a chromosomal passenger protein and is essential for chromosome segregation and cytokinesis. Aurora-B overexpression in various cancer cells induces chromosomal number instability to produce multinuclearity and relates to metastasis. Here, we examined the expression of Aurora-B in oral squamous cell carcinoma (OSCC) to elucidate the relationship between Aurora-B expression and clinico-pathological findings by immunohistochemistry. Aurora-B expression was observed in normal oral squamous epithelia and OSCC cases, but the number of positive cells was significantly higher in OSCC than in normal squamous epithelium ($p<0.01$). The labeling index of Aurora-B was significantly correlated with lymph node metastasis ($p<0.01$) and histological grades of differentiation ($p<0.01$). We also compared Aurora-B expression with Ki-67 expression and a positive correlation was found ($p<0.0001$). Moreover, Aurora-B expression is significantly more frequent in multinuclear tumor cells than in total tumor cells. In summary, we found that Aurora-B expression was well correlated with cell proliferation, induction of multinuclear cells, histological differentiation, and metastasis in OSCC. These findings suggest that Aurora-B may be involved in tumor progression and that Aurora-B can be a new diagnostic and therapeutic target for OSCC.

Keywords Oral squamous cell carcinoma · Aurora-B · Cell proliferation · Metastasis · Multinuclear cells

G. Qi · Y. Kudo · M. Miyauchi · B. S. M. S. Siriwardena · T. Takata (✉)
Department of Oral and Maxillofacial Pathobiology, Division of Frontier Medical Science, Graduate School of Biomedical Sciences, Hiroshima University, 1-2-3 Kasumi, Minami-ku, Hiroshima 734-8553, Japan
e-mail: ttakata@hiroshima-u.ac.jp

I. Ogawa
Center of Oral Clinical Examination, Hiroshima University Hospital, Hiroshima, Japan

F. Shimamoto
Graduate School of Human Life and Environmental Science, Prefectural University of Hiroshima, Hiroshima, Japan

M. Tatsuka
Department of Molecular Radiobiology, Research Institute of Radiation Biology for Medicine, Hiroshima University, Hiroshima, Japan

Introduction

Aurora-B kinase is a chromosomal passenger protein and is essential for chromosome segregation and cytokinesis [1, 25, 27, 28], localized on the centromeres from prophase through the metaphase–anaphase transition [1, 3, 12, 21, 23, 25]. The Aurora-B protein expression level peak is at G2-M phase [28], and phosphorylation of histone H3 at ser-10 by Aurora-B is required for proper chromosome dynamics during mitosis [3, 12, 21, 23, 25]. However, overexpression throughout the cell cycle has been found in a number of cancer cell lines [25]. Little is known about the dynamics and functions of overexpressed Aurora-B during interphase. It has also been demonstrated that Aurora-B overexpression in normal human diploid fibroblasts (NHDF), induces multinuclearity, leading to genetic instability, possibly due to defects in mitotic progression [23, 25]. Aurora-B expression is associated with cell proliferation and prognosis in thyroid, prostate, and endometrial

carcinomas [15, 16, 24] and Duke's stages in colorectal cancer [14]. However, the expression of Aurora-B in oral squamous cell carcinoma (OSCC) tissues is undetermined. The aim of our study is to investigate the relationship of Aurora-B protein expression with cell proliferation, histological differentiation, and nodal metastasis in OSCC. Furthermore, the relationship between overexpression of Aurora-B and multinuclearity of tumor cells is also examined in OSCC.

Materials and methods

Patients and tissues samples

Forty cases of OSCC (26 men and 14 women), including 11 cases with lymph node metastasis, were selected from the pathological files of Hiroshima University Hospital, Japan, and University of Peradeniya, Sri Lanka. At the time of diagnosis, their ages ranged from 23 to 86 years (mean, 58.1 years). Histologically, 12 cases were classified as well, 19 were moderately, and 9 were poorly differentiated squamous cell carcinomas according to the criteria of the Japanese Society for Head and Neck Cancer. In addition, six samples of normal oral mucosa were examined as a normal control. For immunohistochemical examination, tissues were fixed in 10% buffered formalin and embedded in paraffin.

Immunohistochemistry

Immunohistochemical staining was carried out with a monoclonal antibody for Aurora-B protein (Transduction, San Diego, CA, USA, 1:50) after antigen retrieval by microwave treatment in citrate buffer (pH 6.0) and detection by streptoabidin–biotin peroxidase system using LSAB kit (DAKO, Kyoto, Japan). In addition, to determine the proliferative cell compartments and correlate them with Aurora-B expression, we examined Ki-67 expression using anti-Ki-67 monoclonal antibody (DAKO, 1:50). The sections were incubated with primary antibodies at 4°C overnight.

Evaluation of immunohistochemical results

A labeling index, percentage of nuclear stained cells, of Aurora-B or Ki-67 was determined by the examination of at least 500 cells in three representative and intensely stained areas. In addition, for the evaluation of a relationship between multinuclearity and Aurora-B expression, we calculated a percentage of Aurora-B positivity of multinuclearity tumor cells in 10 selected cases (five well differentiated and five poorly differentiated) and four metastasized lymph nodes and compared it to Aurora-B labeling index in each case. As differences of number of multinuclear tumor cells were considerable between well and poorly differentiated tumors, we examined 50–100 multinuclear tumor cells in at least three fields.

Statistical analysis

The Statcel software package was used. The T test was used for comparison of the data between two groups. Regression analysis was used to investigate the correlation between Aurora-B expression and cell proliferation activity measured by Ki-67 index. A p value that was less than 0.05 was considered to indicate statistical significance.

Results

Aurora-B expression in normal oral epithelium and in OSCC

We examined the expression of Aurora-B in normal oral epithelium and OSCC by immunohistochemistry. We found that nuclear expression of Aurora-B was detected in all cases of normal oral and OSCC. Expression in chromosome was also observed in mitotic cells. However, expression patterns and frequency of Aurora-B-positive cells were different between the normal epithelium and OSCC. In the normal epithelium, sporadic cells in the basal and parabasal layers occasionally exhibited weak staining (Fig. 1a), but, in OSCC, Aurora-B-positive cells were more frequently detected. The mean Aurora-B expression was 16.5±8.5% in OSCC and 4.4±1.9% in normal epithelium. Aurora-B expression level was significantly higher in OSCC than in normal epithelium ($p<0.01$). In well differentiated OSCC cases, Aurora-B-positive cells were observed predominantly in the periphery of the tumor nests (Fig. 1b), while in poorly differentiated OSCC cases, Aurora-B-positive cells were present throughout the tumor nests (Fig. 1c).

Correlation of Aurora-B expression with cell proliferation

Next, we compared the expression of Ki-67 with Aurora-B expression in both normal oral epithelium and OSCC. Expression patterns of Ki-67 and Aurora-B appeared to be similar in the serial section of the same cases, but Ki-67 was more frequently expressed in tumor cells (Fig. 1d–f, Table 1). Increase of Aurora-B-positive rate was accompanied by a proportional increase of Ki-67 index. There was a linear correlation between the Aurora-B score and the Ki-67 ($R=0.69$, $p<0.0001$).

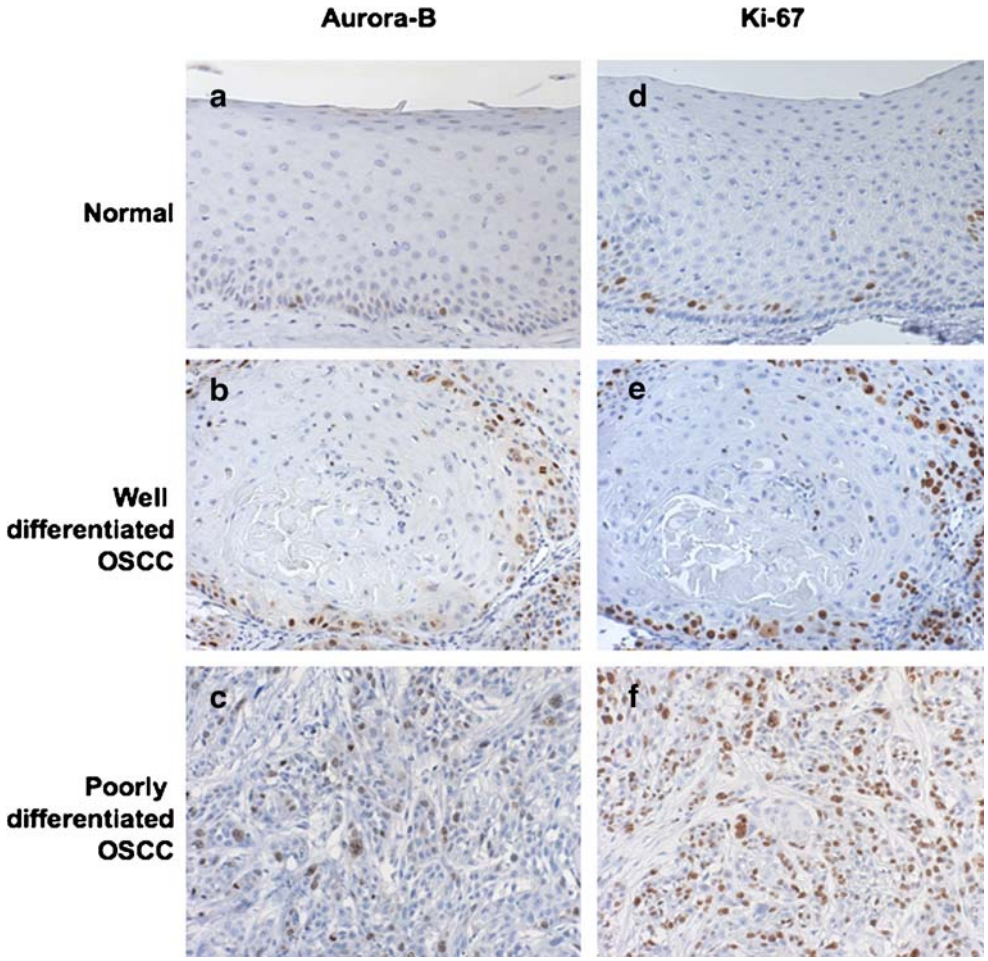

Fig. 1 Immunohistochmical staining for Aurora-B (**a**–**c**) and Ki-67 (**d**–**f**) in normal oral mucosa and OSCC. In the normal epithelium, sporadic cells in the basal and parabasal layers occasionally exhibit weak staining (**a**), but, in OSCC, Aurora-B-positive cells are more frequently detected. In well differentiated OSCC cases, Aurora-B-positive cells are observed predominantly in the periphery of the tumor nests (**b**), while in poorly differentiated OSCC cases, Aurora-B-positive cells are present throughout the tumor nests (**c**). Expression patterns of Ki-67 and Aurora-B appear to be similar in the serial section of the same cases, but Ki-67 is more frequently expressed in tumor cells (**e**, **f**)

Correlation of Aurora-B expression with histological grades of differentiation and lymph node metastasis

We examined the correlation among Aurora-B expression, histological grades of differentiation, and lymph node metastasis. The mean labeling index of Aurora-B was 9.03±5.50% in well differentiated, 17.8±6.7% in moderate differentiated, and 23.6±8.1% in poorly differentiated OSCC cases. Interestingly, the mean labeling index of Aurora-B was significantly higher in poorly differentiated OSCC cases. Moreover, the labeling index of Aurora-B was significantly higher in cases with lymph node metastasis (22.1±10.1%) than in cases without lymph node metastasis (14.3±6.9%) ($p<0.01$, Table 2). We compared the percentage of Aurora-B-positive cells in each histological type of nodal metastasis-positive and -negative cases (Table 2). The

Table 1 Analysis of Aurora-B and Ki-67 expression in the normal oral epithelium and OSCC

	No. of cases	Average of positive cells (%)	
		Aurora B	Ki-67
Normal	6	4.4±1.9[a]	13.7±2.9[a]
Cancer	40	16.5±8.5[a]	49.7±18.1[a]

[a] $P<0.01$

Table 2 Correlation between clinicopathological factors (histological type and lymph node metastasis) and expression of Aurora-B in OSCC

		No. of cases	Average of Aurora-B positive cells (%)
Histological differentiation	Well	12	9.0±5.5[b]
	Moderate	19	17.8±6.7[a,b]
	Poor	9	23.6±8.1[a,b]
Lymph node metastasis	Negative	29	14.3±6.9[b]
	Positive	11	22.1±10.1[b]
Lymph node metastasis			
Negative	Well	11	9.6±5.4[a,b]
	Moderate	13	16.0±6.3[a,b]
	Poor	5	20.4±5.4[b]
Positive	Well	1	3.3
	Moderate	6	21.8±6.4
	Poor	4	27.6±9.9

[a] $P<0.05$; [b] $P<0.01$

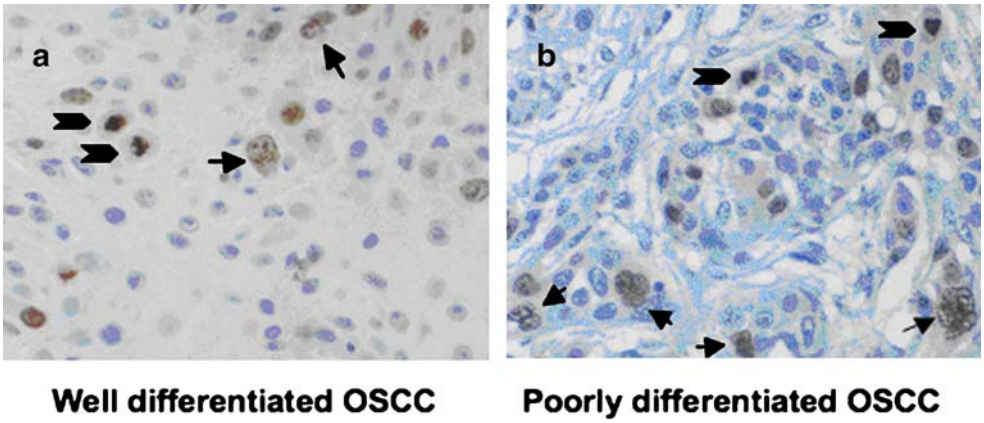

Fig. 2 The correlation between Aurora-B expression and multinuclear cells. Strong expression of Aurora-B is observed in multinuclear cells (*arrow*) and in mitotic cells (*arrow head*) in well differentiated (**a**) and poorly differentiated OSCC (**b**)

percentage of Aurora-B-positive cells in each histological type of nodal metastasis-positive cases was higher than those of nodal metastasis-negative cases. Increased percentage of Aurora-B-positive cells was observed with histological differentiation both in cases with and without lymph node metastasis.

Difference of Aurora-B labeling index between total tumor cells and multinuclear tumor cells

It has previously been demonstrated that Aurora-B overexpression in NHDF induces multinuclearity [23, 25]. Therefore, we examined the difference of Aurora-B labeling index between total tumor cells and multinuclear tumor cells in primary and metastasized OSCC. As we expected, a strong expression of Aurora-B was observed in multinuclear cells (Fig. 2a,b). The percentage of Aurora-B expression was higher in multinuclear cells than in total tumor cells in both primary and metastasized OSCC (35.9±6.59 vs 21.2±10.91 in primary OSCC and 29.5±7.9 vs 43.1±4.4 in metastasized OSCC) ($p<0.05$). Especially, the difference was significant in well differentiated OSCC cases (Table 3). Interestingly, average of Aurora-B-positive cells in metastasized OSCC is higher than that in primary OSCC (Table 3).

Discussion

Characteristic features of human solid tumors and many hematological malignancies are chromosomal instability (CIN), the rate of change of whole chromosomal gains/losses, aneuploidy, and the state of altered chromosome number. Recent studies have clearly shown that CIN and aneuploidy, long considered late progression events of established tumors, are in fact early molecular changes currently seen [17]. Aurora-B kinase is a chromosomal passenger protein and is essential for chromosome segregation by phosphorylating mitotic histone H3 as one of histone H3 kinase [27]. The phosphorylation status of histone H3 may be balance by Aurora-B kinase activity and protein phosphatase 1 (PP1) phosphatase activity [10]. Overexpression of Aurora-B produces multinuclearity and increases ploidy, which is important during human cancer development [23, 25]. Here, we examined the expression of Aurora-B in OSCC, which is one of the most common types of human cancer, with an annual incidence of more than 500,000 cases worldwide. We demonstrated that Aurora-B expression level was significantly higher in OSCC than in normal epithelium. Aurora-B expression was well associated with histological differentiation. In well differentiated OSCC cases, Aurora-B-positive cells were

Table 3 Analysis of Aurora B expression in total tumor cells and in multinuclear cells in OSCC

		Average of Aurora-B-positive cells (%)	*P* value
Primary OSCC (10 cases)	Total cells	21.2±10.9	<0.01
	Multinuclear cells	35.9±6.6	
Well differentiated OSCC (5 cases)	Total cells	12.6±5.9	<0.01
	Multinuclear cells	32.8±6.3	
Poorly differentiated OSCC (5 cases)	Total cells	29.8±7.0	>0.05
	Multinuclear cells	39.0±5.8	
Metastasized OSCC (4 cases)	Total cells	29.5±7.9	<0.05
	Multinuclear cells	43.1±4.4	

observed predominantly in the periphery of the tumor nests. On the other hand, strong Aurora-B expression was observed throughout the nests in poorly differentiated OSCC cases. We also found that the number of multinuclear cells was higher in poorly differentiated than in well differentiated cases (Table 3). Interestingly, the percentage of Aurora-B-positive cells was higher in multinuclear cells than in total cells. Although it has previously been demonstrated that Aurora-B overexpression induces multinuclearity and increases ploidy [23, 25], the correlation between DNA ploidy and Aurora-B expression is still unclear. Therefore, we will examine the correlation between DNA ploidy and Aurora-B expression in the future. We suggest that Aurora-B may be involved in developing malignant phenotypes such as poor differentiation including multinuclear cells [23]. These observations are supported by previous findings that Aurora-B expression was correlated with differentiation of other types of tumor including colon cancers [14], prostate cancers [16], endometrial cancers [15], seminomas and thyroid carcinomas [6, 22, 24]. In addition, Aurora-B expression was well correlated with clinical staging of these tumors. In the present study, we found that Aurora-B expression was well associated with lymph node metastasis in OSCC. Moreover, average of Aurora-B-positive cells in metastasized lymph node is higher than that in primary site (Table 3). The detailed mechanism of metastasis caused by Aurora-B overexpression is still unknown. In the future, we would like to examine the correlation between Aurora-B overexpression and migration or invasion in OSCC cells.

Here we found that the expression of Aurora-B was strongly associated with Ki-67 index. Other groups also reported that Aurora-B was associated with Ki-67 expression in other types of cancer [15, 16, 24]. These results indicate that Aurora-B expression is well correlated with cell proliferation. Aurora-B has been identified as a major regulator of cytokinesis. Aurora-B associates with TACC and MgcRac1GAP at the last stage of M phase [7, 20] and with the other chromosome passenger proteins, survivin, inner centromere protein (INCENP), and Borealin [8]. INCENP tightly associates with Aurora-B, probably regulating its activity. Survivin, a conserved inhibitor-of-apoptosis-like protein, is a third member of the Aurora-B complex [3, 4, 9]. In cancer cells, the high appearance of survivin and INCENP is observed as well as Aurora-B [2]. Survivin dynamics increases at centromeres during G2/M phase transition and is regulated by microtubule-attachment and Aurora-B kinase activity [4]. We had already found that high expression of survivin is an early event during oral carcinogenesis and may provide a useful tool for the identification of precancerous lesions at higher risk of progression into invasive carcinoma [18]. Survivin expression often increased in poorly differentiated tumors and is correlated with poor prognosis in OSCC [19]. Aurora-B kinase exists in a complex with survivin and INCENP and its kinase activity is stimulated by survivin binding and phosphorylation [5]. Survivin may promote tumorigenesis and progression by suppressing the antiproliferate effect of p53 tumor suppressor activated by Aurora-B overexpression in normal cells and glioblastoma cells containing intact p53 gene [11]. A recent finding shows that the activity of survivin, Aurora-B, and INCENP are responsible for oncogenic Ras-mediated cell transformation and lead to an accelerated growth of tumor cells [13, 26]. However, the molecular mechanism of Aurora-B is not completely clear in cancer prognoses.

In conclusion, Aurora-B expression was well correlated with cell proliferation, induction of multinuclear cells, histological differentiation, and metastasis in OSCC, suggesting that Aurora-B may be involved in tumor progression of OSCC. We suggest that Aurora-B can be a new diagnostic and therapeutic target for OSCC.

References

1. Adams RR, Carmena M, Earnshaw WC (2001) Chromosomal passengers and the (aurora) ABCs of mitosis. Trends Cell Biol 11:49–54
2. Adams RR, Eckley DM, Vagnarelli P, Wheatlev S, Gerloff DL, Mackav AM, Svinqen PA, Kaufmann SH, Earnshaw WC (2001) Human INCENP colocalizes with the Aurora-B/AIRK2 kinase on chromosomes and is overexpressed in tumour cells. Chromosome 110:65–74
3. Adams RR, Maiato H, Earnshaw WC, Carmena M (2001) Essential roles of Drosophila inner centromere protein (INCENP) and aurora B in histone H3 phosphorylation, metaphase chromosome alignment, kinetochore disjunction, and chromosome segregation. J Cell Biol 153:865–880
4. Beardmore VA, Ahonen LJ, Kallio MJ (2004) Survivin dynamics increases at centromeres during G2/M phase transition and is regulated by microtubule-attachment and Aurora B kinase activity. J Cell Sci 117:4033–4042
5. Bolton MA, Lan W, Powers SE, McCleland ML, Kuang J, Stukenberg PT (2002) Aurora B kinase exists in a complex with survivin and INCENP and its kinase activity is stimulated by survivin binding and phosphorylation. Mol Biol Cell 13:3064–3077
6. Chieffi P, Troncone G, Caleo A, Libertini S, Linardopoulos S, Tramontano D, Portella G (2004) Aurora B expression in normal testis and seminomas. J Endocrinol 181:263–270
7. Delaval B, Ferrand A, Conte N, Larroque C, Hernandez-Verdun D, Prigen C, Birnbaum D (2004) Aurora B-TACC1 protein complex in cytokinesis. Oncogene 23:4516–4522
8. Gassmann R, Carvalho A, Henzing AJ, Rucchaud S, Hudson DF, Honda R, Niqq EA, Gerloff DL, Earnshaw WC (2001) Borealin: a novel chromosomal passenger required for stability of the bipolar mitotic spindle. J Cell Biol 166:179–191
9. Giet R, Glover DM (2001) Drosophila Aurora-B kinase is required for Histone H3 phosphorylation and Condesin recruitment during chromosome condensation and to organize central spindle during cytokinesis. J Cell Biol 152:669–681
10. Hsu JY, Sun ZW, Li X, Reuben M, Tatchell K, Bishop DK, Grushcow JM, Brame CJ, Caldwell JA, Hunt DF, Lin R, Smith

MM, Allis CD (2000) Mitotic phosphorylation of histone H3 is governed by Ipl1/aurora kinase and Glc7/PP1 phosphatase in budding yeast and nematodes. Cell 102:279–291
11. Jung JK, Kim TK, Lee JS, Oh SY, Kwak S, Jin X, Sohn JY, Song MK, Sohn YW, Lee JB, Chung YG, Choi YK, You S, Kim H (2005) Survivin inhibits anti-growth effect of p53 activated by aurora B. Biochem Biophys Res Commun 336:1164–1171
12. Kaitna S, Pasierbek P, Jantsch M, Loidl J, Glotzer M (2002) The aurora B kinase AIR-2 regulates kinetochores during mitosis and is required for separation of homologous chromosomes during meiosis. Curr Biol 12:798–812
13. Kanda A, Kawai H, Suto S, Kitajima S, Sato S, Takata T, Tatsuka M (2005) Aurora-B/AIM-1 kinase activity is involved in Ras-mediated cell transformation. Oncogene 24:7266–7272
14. Katayama H, Ota T, Jisaki F, Ueda Y, Tanaka T, Odashima S, Suzuki F, Terada Y, Tatsuka M (1999) Mitotic kinase expression and colorectal cancer progression. J Natl Cancer Inst 91:1160–1162
15. Kurai M, Shiozawa T, Shih HC (2005) Expression of Aurora kinases A and B in normal, hyperplastic, and malignant human endometrium: Aurora B as a predictor for poor prognosis in endometrial carcinoma. Hum Pathol 36:1281–1288
16. Lee EC, Frolov A, Li R, Ayala G, Greenberg NM (2001) Targeting Aurora kinases for the treatment of prostate cancer. Cancer Res 66:4996–5002
17. Li JJ, Li SA (2006) Mitotic kinases: the key to duplication, segregation, and cytokinesis errors, chromosomal instability, and oncogenesis. Pharmacol Ther 111:974–984
18. Lo Muzio L, Pannone G, Leonardi R, Staibano S, Mignogna MD, De Rosa G, Kudo Y, Takata T, Altieri DC (2003) Survivin, a potential early predictor of tumor progression in the oral mucosa. J Dent Res 82:923–928
19. Lo Muzio L, Pannone G, Staibano S, Mignogna MD, Rubini C, Mariggio MA, Procaccini M, Ferrari F, De Rosa G, Altieri DC (2003) Survivin expression in oral squamous cell carcinoma. Br J Cancer 89:2244–2248
20. Minoshima Y, Kawashima T, Hirose K, Tonozuka Y, Kawajiri A, Bao YC, Deng X, Tatsuka M, Narumiya S, May WS Jr, Nosaka T, Semba K, Inoue T, Satoh T, Inagaki M, Kitamura T (2003) Phosphorylation by aurora B converts MgcRacGAP to a RhoGAP during cytokinesis. Dev Cell 4:549–560
21. Murata-Hori M, Wang YL (2002) The kinase activity of aurora B is required for kinetochore microtubule interactions during mitosis. Curr Biol 12:894–899
22. Nikiforov YE (2005) Editorial: anaplastic carcinoma of the thyroid—will aurora B light a path for treatment? J Clin Endocrinol Metab 90:1243–1245
23. Ota T, Suto S, Katayama H, Han ZB, Suzuki F, Maeda M, Tanino M, Terada Y, Tatsuka M (2002) Increased mitotic phosphorylation of histone H3 attributable to AIM-1/Aurora B overexpression contributes to chromosome number instability. Cancer Res 62:5168–5177
24. Sorrentino R, Libertini S, Pallante PL, Troncone G, Palombini L, Bavetsias V, Spalletti-Cernia D, Laccetti P, Linardopoulos S, Chieffi P, Fusco A, Portella G (2005) Aurora B over expression associates with the thyroid carcinoma undifferentiated phenotype and is required for thyroid carcinoma cell proliferation. J Clin Endocrinol Metab 90:928–935
25. Tatsuka M, Katayama H, Ota T, Tanaka T, Odashima S, Suzuki F, Terada Y (1998) Multinuclearity and increased ploidy caused by overexpression of the aurora B and Ipl1-like midbody-associated protein mitotic kinase in human cancer cells. Cancer Res 58:4811–4816
26. Temme A, Rieber EP, Schmitz M, Moreqenroth A, Weiqie B, Rieqer MA, Kiessling A, Rieber EP (2005) Increased p21(ras) activity in human fibroblasts transduced with survivin enhances cell proliferation. Biochem Biophys Res Commun 327:765–773
27. Terada Y (2001) Role of chromosomal passenger complex in chromosome segregation and cytokinesis. Cell Struct Funct 26:653–657
28. Terada Y, Tatsuka M, Suzuki F, Yasuda Y, Fujita S, Otsu M (1998) AIM-1: a mammalian midbody-associated protein required for cytokinesis. EMBO J 17:667–676

Virchows Arch (2007) 450:303–310
DOI 10.1007/s00428-006-0361-8

ORIGINAL ARTICLE

High *PRL-3* expression in human gastric cancer is a marker of metastasis and grades of malignancies: an in situ hybridization study

U. A. Miskad · S. Semba · H. Kato · Y. Matsukawa · Y. Kodama · E. Mizuuchi · N. Maeda · K. Yanagihara · H. Yokozaki

Received: 13 October 2006 / Revised: 26 November 2006 / Accepted: 19 December 2006 / Published online: 18 January 2007
© Springer-Verlag 2007

Abstract *Phosphatase of regenerating liver (PRL)-3*, encoding a 22-kD low molecular weight tyrosine phosphatase, has been reported to be associated with metastasis of colorectal carcinoma. We assessed the levels of *PRL-3* mRNA expression to know whether its up-regulation was involved in progression and metastasis of gastric carcinoma. Levels of *PRL-3* expression in 94 human gastric adenocarcinomas and 54 matched lymph node metastases were detected by in situ hybridization and compared with clinicopathological characteristics including prognosis. High *PRL-3* expression was detected in 36.2% of primary gastric carcinoma (with nodal metastasis, 55.6%; without nodal metastasis, 10%; $P<0.001$) and in 74.1% of lymph node metastases. The incidence of high *PRL-3* expression in lymph node metastasis was significantly higher than in primary tumors ($P<0.044$). Moreover, high expression of *PRL-3* was closely associated with tumor size, lymphatic invasion, venous invasion, extent of lymph node metastasis, and tumor stage. These results suggest that high *PRL-3* expression may participate in the progression and metastasis of gastric carcinoma. *PRL-3* might be a novel molecular marker for aggressive gastric cancer.

U. A. Miskad · S. Semba · H. Kato · Y. Matsukawa · Y. Kodama · E. Mizuuchi · N. Maeda · H. Yokozaki (✉)
Division of Surgical Pathology, Department of Biomedical Informatics, Kobe University Graduate School of Medicine, 7-5-1 Kusunoki-cho,
Chuo-ku, Kobe 650-0017, Japan
e-mail: hyoko@med.kobe-u.ac.jp

K. Yanagihara
Central Animal Laboratory,
National Cancer Center Research Institute,
Tokyo 104-0045, Japan

Keywords *PRL-3* · Gastric carcinoma · *in situ* hybridization · Lymph node metastasis

Introduction

Gastric cancer incidence and mortality has fallen dramatically over the last 50 years in many regions, but remains the second most common cancer worldwide [1, 23]. Metastasis of gastric cancer to the lymph nodes, peritoneum, and/or other organs is often responsible for highest mortality rate because the primary tumors can usually be surgically removed [4, 9]. Involvement of regional lymph nodes is an important prognostic factor for gastric carcinoma, i.e., if lymph nodes are found to be negative for metastasis by thorough pathologic examination, more than 50% of the patients may be expected to survive for 5 years; otherwise, the survival rate drops to less than 10% [4, 8]. Mechanisms of gastric cancer metastasis are not fully clarified because of the involvement of multiple steps with the accumulation of altered expression of a number of different genes [29]. Although many molecular factors participating in metastasis have been identified from studies that use microarray expression profiling [9], much remains to be learned about the process to provide a new therapeutic target for these metastatic lesions.

Protein tyrosine phosphatases (PTPs) play fundamental roles in regulating diverse proteins that participate essentially in every aspect of cellular physiological and pathogenic processes [33]. Phosphatase of regenerating liver (PRL)-1, PRL-2, and PRL-3 represents a novel class of PTPs superfamily members in possessing a unique COOH-terminal prenylation motif with PTP active site signature sequence CX_5R [5, 30]. PRL phosphatases were found to

be associated with the early endosome and plasma membrane in their prenylated state, while nuclear localization of these enzymes may occur in the absence of prenylation [31]. All are proteins of about 20-kD and share 75% amino acid sequence similarity [6, 30]. *PRL-1* was originally identified as an immediate early gene whose expression was induced in mitogen-stimulated cells and regenerating liver [16]. Overexpression of PRL-1 and PRL-2 transformed mouse fibroblasts and hamster pancreatic epithelial cells in culture and promoted tumor growth in nude mice, suggesting that it may participate in the tumorigenesis [5, 6].

PRL-3 has been found to enhance growth of human embryonic kidney fibroblasts [14]. Among normal human adult tissues, it is expressed predominantly in the heart and skeletal muscle cells with lower expression in the pancreas, and this expression pattern is distinct from the wider expression of PRL-1 and PRL-2 [14]. Gene expression profiling using serial analysis of gene expression (SAGE) revealed that among 144 up-regulated genes detected in liver samples of metastatic colorectal cancer, *PRL-3* was the only gene consistently overexpressed in all cancer metastasis cases examined with lower levels in non-metastatic tumors and normal colorectal epithelium [24]. Overexpression of *PRL-3* was reported to be associated with human colorectal cancer metastasis and *PRL-3* was apparently expressed in colorectal cancer metastases to any organ [2, 11]. In addition, stable transfection of wild-type *PRL-3* in non- or less metastatic CHO or mouse melanoma B16 cells has been reported to induce the acquisition of metastasis-associated phenotypes and to confer metastatic ability, whereas a catalytically inactive PRL-3 mutant greatly reduced the effect on promoting cell migration [28, 32]. Moreover, specific anti-sense oligodeoxynucleotide and phosphatase inhibitors could reverse the acquired higher migratory ability with exogenously overexpressed PRL-3 [28].

Conversely, transient down-regulation of *PRL-3* expression in DLD-1 human colon cancer cells with a specific small interfering RNA-abrogated cellular motility in vitro and in vivo hepatic colonization after infection into the nude mice spleen, suggesting the possible contribution of PRL-3 to the establishment of liver metastasis, especially at the step in which cancer cells leave the circulation to extravasate into the liver tissue [11]. Moreover, stable knockdown of PRL-3 by artificial microRNA in SGC7901 human gastric cancer cells effectively suppressed the growth of experimental peritoneal metastases in nude mice independent of cellular proliferation [13]. These experimental evidences support the significant role of overexpressed and catalytically active PRL-3 in cancer metastasis.

We previously conducted an immunohistochemical analysis of human gastric carcinomas using anti-PRL-3 antibody and reported that high expression of PRL-3 immunoreactivity was frequently detected in those with lymph node metastasis [15]. However, we could not eliminate the possibility of cross-reaction of the antibody to PRL-1 and/or PRL-2. To clarify this, in the present study, we investigated the levels of *PRL-3* mRNA expression by highly specific in situ hybridization (ISH) in the primary gastric carcinoma tissues and corresponding non-neoplastic mucosa and matched regional lymph node metastases and correlated with clinicopathological features and prognosis of the patients.

Materials and methods

Tissue samples

A total of 152 formalin-fixed and paraffin-embedded surgical specimens of primary human gastric carcinomas and lymph node metastases were collected from the Department of Pathology, Kobe University Hospital. They consisted of 54 cases of primary tumors along with matched lymph node metastases and 40 cases of primary tumors without lymph node metastasis. Four cases with liver metastasis and peritoneal metastasis were also available. They consisted of 68 men and 26 women with an age range of 34–87 years and mean of 66.82 years. Informed consent was obtained from all patients. We classified gastric carcinomas according to the criteria of the Japanese Classification of Gastric Carcinoma [10].

Oligonucleotide probe and ISH

The expression levels of PRL-3 in tissue sections were analyzed using ISH as described elsewhere with some modifications [3, 11]. Specific antisense oligonucleotide DNA probe was designed complementary to the mRNA transcript of *PRL-3* gene, based on published reports of the cDNA sequences. The sequence of probe was 5′ GTTGATGGCTCCGCGGCG-Brigati Tail-3′ with 72.2% GC content. The specificity of the oligonucleotide sequences was initially determined by a GenBank/European Molecular Biology Laboratory database search using the Genetics Computer Group sequence analysis program (Genetics Computer Group, Madison, WI, USA) based on the FastA algorithm [18] that showed 100% homology with the target gene and minimal homology with non-specific mammalian gene sequences. DNA probe was synthesized with six biotin molecules (hyperbiotinylated) at the 3′ end via direct coupling using standard phosphormidine chemistry (Invitrogen, Carlsbad, CA, USA) [17].

ISH was carried out using the Microprobe manual staining system (Fisher Scientific, Pittsburgh, PA, USA). Tissue sections (4 μm) of formalin-fixed, paraffin-embed-

ded specimens were mounted on Silane-coated ProbeOn slides (Fisher Scientific). The slides were placed in the Microprobe slide holder, dewaxed, dehydrated, and followed by enzymatic digestion with pepsin (Dako, Carpinteria, CA, USA). Hybridization of the probe was carried out for 90 min at 45°C, and the samples were then washed three times with 2x SSC for 2 min at 45°C. The samples were incubated for 30 min in alkaline phosphatase-labeled avidin (Biomeda, Foster City, CA, USA) at 45°C, briefly rinsed in 50 mM Tris–HCl (pH 7.6), rinsed for 1 min with alkaline phosphatase enhancer, and incubated for 20 min with the chromogen substrate FastRed (Biomeda) at 45°C. Hybridization of the samples with a biotinylated poly$(dT)_{20}$ oligonucleotide was used to verify the integrity of mRNA in each sample.

To analyze the specificity of the hybridization signal, we performed the following controls: (1) RNase pretreatment of tissue sections, (2) competitive assay with sense probe, (3) treatment of the samples in the absence of the biotinylated probe to control endogenous alkaline phosphatase, and (4) use of chromogen in the absence of any oligonucleotide probes. A markedly decreased or absent signal was obtained under all of these conditions. For evaluation of staining, normal gastric epithelium, smooth muscle cells of the vessels and infiltrated inflammatory cells were used as internal controls. Staining in more than 25% cancer cells obviously exceeding the internal controls was regarded as "high expression" and negative or no increase of staining in cancer cells compared with them was judged as "low/none expression." The grades of *PRL-3* expression were determined by three independent observers (U.A.M., S.S., H.K.) unaware of the clinical and histological diagnoses. All of the sections were scored twice to confirm the reproducibility of the results and any discordant result was settled by using a conference microscope.

Immunohistochemistry

We determined Ki-67 labeling index and apoptotic body index immunohistochemically as described elsewhere [25], using monoclonal antibody against Ki-67 antigen (Dako, Japan; 1:100 dilution) and polyclonal antibody against single-stranded DNA (ssDNA, Dako; 1:100 dilution), respectively. The Ki-67 labeling index and apoptotic body index were calculated by counting the number of positive cells (%) in a total of 1,000 or more tumor cells observed in ten representative high-power fields. Values were presented as the mean ± SD (standard deviation).

Statistical methods

The relationships between the results of the ISH study and clinicopathological variables were tested by χ^2 test and Mann–Whitney *U* test. Survival analysis was computed by the Kaplan–Meier method and compared by log-rank test. A *P* value less than 0.05 was regarded as statistically significant.

Results

We examined the expression and localization of *PRL-3* in 148 cases of gastric carcinoma and lymph node metastasis by using ISH method that facilitated the study of paraffin-embedded specimens. We confirmed that all samples had intense histochemical reaction with poly$(dT)_{20}$ probe, indicating that the mRNA was well preserved (Fig. 1a–c). Negative to weak *PRL-3* expression was detected in non-neoplastic gastric mucosa including foveolar epithelia, fundic and pyloric glandular cells. Weak to moderate expression was also detected in smooth muscle cells of the vessels and in some inflammatory cells, such us lymphocytes and plasma cells. However, in the tumor cells, *PRL-3* expression was varied and observed heterogeneously among the cases. Prominent hybridization indicating high *PRL-3* expression was detected in 34 (36.2%) of 94 primary gastric carcinoma cases examined.

Representative results of *PRL-3* ISH staining are shown in Fig. 1d–i. We then analyzed the relationship between expression of *PRL-3* and clinicopathological parameters of gastric carcinoma. Results are summarized in Table 1. High expression of *PRL-3* was significantly associated with gender (P=0.010), tumor size (P=0.017) and stage of tumor (P=0.008). Also, a similar correlation was observed with cancer progression, such as lymphatic invasion (P< 0.001), venous invasion (P=0.012) and extent of lymph node metastasis (P<0.001). Although not statistically significant, the incidence of *PRL-3* expression tended to be associated with depth of tumor invasion (P=0.051). Additionally, high expression of *PRL-3* was also associated with the high level of Ki-67 labeling index (P=0.032) and low level of apoptotic bodies (P=0.030). There was no significant correlation between *PRL-3* expression and age or histological type.

As shown in Table 2, among primary gastric carcinomas, the incidence of cases with high *PRL-3* expression was significantly frequent in carcinomas with nodal metastasis (30 [55.6%] of 54 cases) than in those without nodal metastasis (4 [10%] of 40 cases; (P<0.001). Simultaneously, we also investigated the expression of *PRL-3* in regional lymph node metastases. Interestingly, out of 54 cases with lymph node metastases, high *PRL-3* expression was detected in 40 cases (74.1%). The frequency of high *PRL-3* expression was increased in matched lymph node metastases in comparison with primary gastric carcinomas (P=0.044). Moreover, high *PRL-3* expression was also

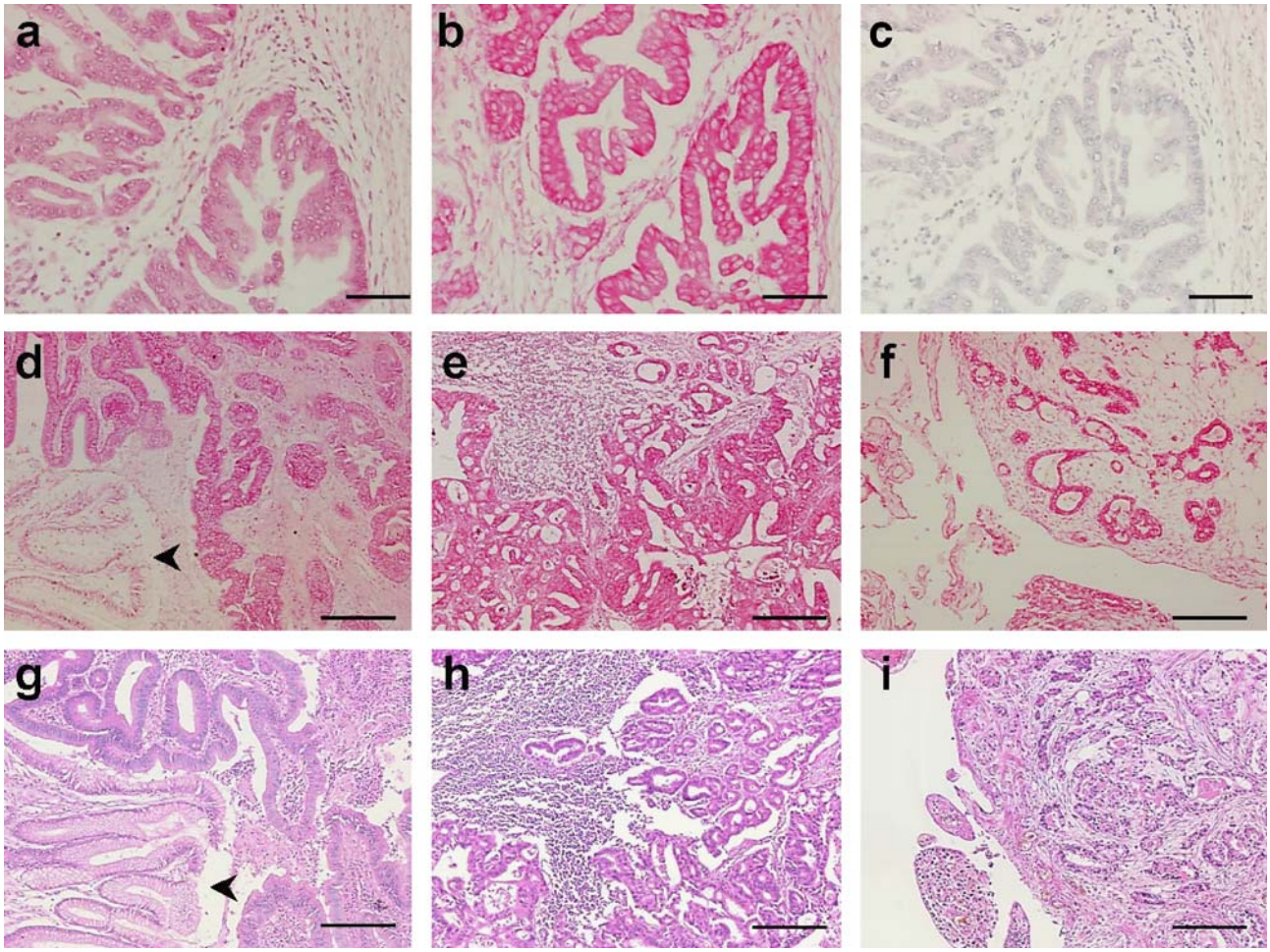

Fig. 1 In situ hybridization (ISH) analysis of *PRL-3* mRNA expression in human gastric cancer tissues. Hybridization with a biotinylated poly(dT)$_{20}$ oligonucleotide probe (**a**) is performed to verify the integrity of mRNA. A positive ISH reaction of *PRL-3* with the specific antisense probe (**b**) in this assay provides red staining in the cytoplasm. Negative chromogen reaction is confirmed with the sense oligonuculeotide probe (**c**) with the same specimen as (**a**) or (**b**). Bars: 100 μm. Representative results of *PRL-3* ISH in primary gastric cancer (**d**), metastatic cancer in regional lymph node of the stomach (**e**) and peritoneal metastasis (**f**). Consecutive sections stained with hematoxylin and eosin are displayed in (**g**), (**h**), and (**i**). High levels of *PRL-3* expression is detected in cancer cells, while non-neoplastic gastric mucosa ([*d*], [*g*]; *arrow head*) demonstrated negative to low expression. *Bars*: 200 μm

detected in other metastatic sites, such as liver and peritoneum.

Finally, we checked the survival rate of gastric cancer patients after surgery. The cases with high expression of *PRL-3* showed a tendency to have a worse prognosis than the cases with low/none expression of *PRL-3*, although it was not statistically significant (P=0.165) (Fig. 2).

Discussion

Histochemical evaluation of PRL-3 expression in human cancer tissues has been reported mainly on colorectal carcinomas. Bardelli et al. developed ISH methods for the study of paraffin-embedded colorectal cancer sections and reported that *PRL-3* expression was elevated in nearly all metastatic lesions derived from colorectal cancers, regardless of the site of metastasis, while they observed little or no *PRL-3* mRNA expression in normal colon, non-metastatic primary cancers, or metastatic lesions derived from cancers of pancreas, stomach or esophagus [2]. On the other hand, Kato et al., also using ISH methods on paraffin-embedded specimens, detected *PRL-3* expression in primary colorectal cancers of which the frequency of up-regulated *PRL-3* expressions in cases with liver or lung metastasis was statistically higher than that in cases without either type of metastasis [11]. Peng et al. prepared a specific monoclonal antibody against human PRL-3 and detected its immunoreactivity in 7% of normal colorectal epithelia, 23.9% of primary colorectal cancers, 53.7% of metastatic lymph nodes, and 66.7% of liver metastases [19, 20].

Table 1 Expression of *PRL-3* in human gastric carcinomas and its correlation with clinicopathological parameters, Ki-67 labeling index and apoptotic body index

	Number of cases	*PRL-3* expression[a]				*P* value[d]
		High		Low/none		
		n	(%)	*n*	(%)	
Total	94	34	(36.2)	60	(63.8)	
Sex						
Male	68	30	(44.1)	38	(55.9)	0.010*
Female	26	4	(15.4)	22	(84.6)	
Age						
≤65	38	13	(34.2)	25	(65.8)	0.745
>65	56	21	(37.5)	35	(62.5)	
Histology[b]						
Well	53	23	(43.4)	30	(56.6)	0.097
Poorly	41	11	(26.8)	30	(73.2)	
Tumor size[c]						
≤40 mm	43	10	(23.3)	33	(76.7)	0.017*
>40 mm	51	24	(47.1)	27	(52.9)	
Lymphatic invasion						
ly (−)	33	4	(12.1)	29	(87.9)	<0.001**
ly (+)	61	30	(49.2)	31	(50.8)	
Venous invasion						
v (−)	41	9	(22.9)	32	(78.1)	0.012*
v (+)	53	25	(47.2)	28	(52.8)	
Depth of invasion[b]						
T1	33	6	(18.2)	27	(81.8)	0.051
T2	23	12	(52.2)	11	(47.8)	
T3	28	12	(42.9)	16	(57.1)	
T4	10	4	(40)	6	(60)	
Extent of lymph node metastasis[b]						
N0	40	4	(10)	36	(90)	<0.001**
N1	27	16	(59.3)	11	(40.7)	
N2	18	8	(44.4)	10	(55.6)	
N3	9	6	(66.7)	3	(33.3)	
Tumor stage[b]						
I	38	6	(15.8)	32	(84.2)	0.008*
II	14	6	(42.9)	8	(57.1)	
III	28	15	(53.6)	13	(46.4)	
IV	14	7	(50)	7	(50)	
Ki-67 labeling index (mean±SD)[e]		45.96±9.82		40.49±11		0.032*
Apoptotic body index (mean±SD)[e]		13.07±5.05		17.31±8.2		0.030*

[a] The levels of *PRL-3* expression were determined by ISH. Grades of *PRL-3* staining were classified as high, low, or negative as described in the text.

[b] According to the criteria of the Japanese Classification of Gastric Carcinoma [10]. Well, well-differentiated type including papillary adenocarcinoma, well-differentiated tubular adenocarcinoma and moderately differentiated tubular adenocarcinoma; poorly, poorly differentiated type including solid-type poorly differentiated adenocarcinoma, non-solid type poorly differentiated adenocarcinoma, signet-ring cell carcinoma, and mucinous adenocarcinoma. Depth of carcinoma invasion and extent of lymph node metastasis were classified into T1–T4 and N0–N3, respectively.

[c] Tumor size was divided into two groups according to the maximum diameter.

[d] Statistical analyses were performed by χ^2 test and Mann–Whitney *U* test. A *P* value less than 0.05 was regarded as statistically significant. **P*<0.05, ***P*<0.001.

[e] Ki-67 labeling index and apoptotic body index were determined by counting the number of positive cells (%) in a total of 1,000 or more tumor cells observed in ten representative high-power fields (×400). *SD* Standard deviation

Table 2 Expression of *PRL-3* in human gastric carcinomas and lymph node metastasis

	Number of cases	*PRL-3* expression[a]				*P* value[b]
		High		Low/none		
		n	(%)	*n*	(%)	
Primary gastric carcinomas	94					
with nodal metastases	54	30	(55.6)	24	(44.4)	<0.001**
without nodal metastasis	40	4	(10)	36	(90)	
Gastric carcinomas with nodal metastases						
Primary gastric carcinomas	54	30	(55.6)	24	(44.4)	0.044*
Matched lymph node metastases	54	40	(74.1)	14	(25.9)	

[a] The levels of *PRL-3* expression were determined by ISH. Grades of *PRL-3* staining were classified as high, low or negative as described in the text.

[b] Statistical analysis was performed by χ^2 test. A *P* value less than 0.05 was regarded as statistically significant. *$P<0.05$, **$P<0.001$.

Previously, we conducted immunohistochemical analysis of PRL-3 on human gastric cancer tissues using commercial antibody and reported that overexpression of PRL-3 immunoreactivity in primary gastric carcinoma was closely associated with lymphatic invasion, extent of lymph node metastasis and tumor stage [15]. However, as PRL-3 shares 78% and 75% amino acid sequence similarity with PRL-1 and PRL-2, respectively [12], we could not exclude the possibility of the cross-reaction of the anti-PRL-3 antibody used in the previous study to other PRL family phosphatases.

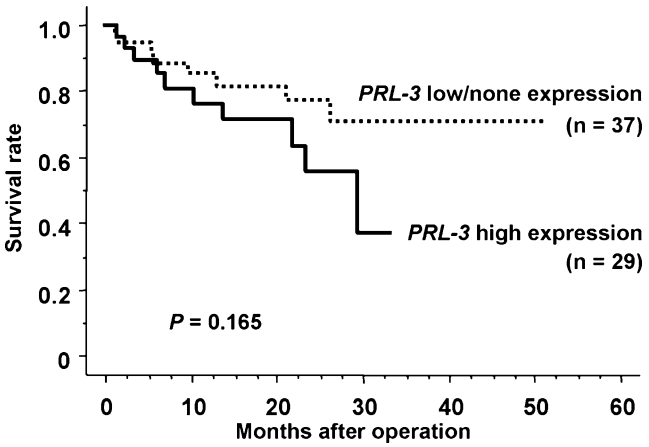

Fig. 2 Kaplan–Meier analysis of gastric cancers. Cancer-related survival rates of patients whose gastric cancer tissue showed high (*solid line*) or low/none (*hatched line*) expression of *PRL-3* mRNA assessed by ISH. Patients with gastric cancers expressing high levels of *PRL-3* showed a tendency to have much worse prognosis than those with primary gastric tumors exhibiting low/none *PRL-3* expression ($P=0.165$)

The present ISH study, highly specific for the detection of *PRL-3* mRNA, on the same gastric cancer specimens as was investigated in the previous immunohistochemical analysis [15] confirmed the *PRL-3* expression in primary as well as metastatic gastric cancer cells. Interestingly, a high level of *PRL-3* expression in primary gastric carcinoma tissue was closely associated not only with clinicopathological factors characterized by immunohistochemistry (i.e., lymphatic invasion, extent of lymph node metastasis, and tumor stage) [15], but also with tumor size, venous invasion, and either higher levels of Ki-67 labeling index as well as lower levels of apoptotic body index. Moreover, high expression of *PRL-3* was significantly frequent in primary gastric carcinoma with nodal metastasis than those without nodal metastasis that was also observed in the previous study [15]. Consistent with the elevated expression of *PRL-3* in colorectal cancer metastasis [2, 11, 20, 24], the frequency of high *PRL-3* expression was significantly increased in matched lymph node metastases than in primary gastric tumors.

The growth-promoting effect of ectopically overexpressed PRL-3 in HEK293 human embryonic kidney epithelial cells [14] and mouse B16 melanoma cells [28] have been reported. Although enhanced cell cycle progression and down-regulation of $p21^{cip1/waf1}$, a cyclin-dependent kinase inhibitor, by PRL-1 or PRL-2 typrosine phosphatases, was demonstrated in D27 hamster pancreatic ductal epithelial cells [27], effect of overexpressed PRL-3 on the cell cycle or apoptosis has not been elucidated yet. These findings suggest that high *PRL-3* expression might not only have important roles in invasion and metastasis, but also play some role in cellular proliferation and/or growth of human gastric cancer.

Elevated PRL-3 protein or mRNA expression in the primary tumor has been reported to associate with prognosis, including disease-free- and overall-survival, of colorectal and breast cancer patients [11, 20, 22, 26]. The present study demonstrated that patients with high expression of *PRL-3* in their primary gastric cancer tissue tended to have worse prognosis than those with low or negative PRL-3 expression, while we could not obtain a significant statistical difference.

These results overall suggest that overexpression of PRL-3 may contribute to the progression and metastasis of human gastric carcinoma. Histochemical detection of PRL-3 expression may serve as a good marker for the prediction of grade of malignancy. Inhibition of prenylation and/or inactivating the catalytic function of PRL-3 phosphatase could block or reduce the cellular properties of invasion and metastasis [32]. Therefore, elucidation of precise biological function of PRL-3 may provide an attractive molecular

target for gastric cancer control. Although it has been reported that PRL-3 interacted with integrin $\alpha 1$ [21] and regulated Rho family GTPases [7], further investigations will be required to clarify the exact pathway(s) of PRL-3-driven cancer metastasis.

Acknowledgement This study was supported by Grants-in-Aid for Cancer Research from the Ministry of Health, Labor and Welfare of Japan (14-7). It is also supported in part by Grants-in-Aid for Scientific Research (B) (14370070) and Exploratory Research (18659096) from the Ministry of Education, Culture, Sports, Science and Technology of Japan. Grant from the Terry Fox Run Foundation for Cancer Research was also indebted. The authors thank to Prof. Hiroki Kuniyasu (Department of Molecular Pathology, Nara Medical University) for valuable discussion and technical assistance.

References

1. Alberts SR, Cervantes A, van de Velde CJ (2003) Gastric cancer: epidemiology, pathology and treatment. Ann Oncol 14(Suppl 2): ii31–ii36
2. Bardelli A, Saha S, Sager JA, Romans KE, Xin B, Markowitz SD, Lengauer C, Velculescu VE, Kinzler KW, Vogelstein B (2003) PRL-3 expression in metastatic cancers. Clin Cancer Res 9:5607–5615
3. Bucana CD, Radinsky R, Dong Z, Sanchez R, Brigati DJ, Fidler IJ (1993) A rapid colorimetric in situ mRNA hybridization technique using hyperbiotinylated oligonucleotide probes for analysis of mdr1 in mouse colon carcinoma cells. J Histochem Cytochem 41:499–506
4. Buchholtz TW, Welch CE, Malt RA (1978) Clinical correlates of resectability and survival in gastric carcinoma. Ann Surg 188:711–715
5. Cates CA, Michael RL, Stayrook KR, Harvey KA, Burke YD, Randall SK, Crowell PL, Crowell DN (1996) Prenylation of oncogenic human PTP_{CAAX} protein tyrosine phosphatases. Cancer Lett 110:49–55
6. Diamond RH, Cressman DE, Laz TM, Abrams CS, Taub R (1994) PRL-1, a unique nuclear protein tyrosine phosphatase, affects cell growth. Mol Cell Biol 14:3752–3762
7. Fiordalisi JJ, Keller PJ, Cox AD (2006) PRL tyrosine phosphatases regulate rho family GTPases to promote invasion and motility. Cancer Res 66:3153–3161
8. Hawley PR, Westerholm P, Morson BC (1970) Pathology and prognosis of carcinoma of the stomach. Br J Surg 57:877–883
9. Hippo Y, Yashiro M, Ishii M, Taniguchi H, Tsutsumi S, Hirakawa K, Kodama T, Aburatani H (2001) Differential gene expression profiles of scirrhous gastric cancer cells with high metastatic potential to peritoneum or lymph nodes. Cancer Res 61:889–895
10. Japanese Gastric Cancer Association (1998) Japanese Classification of Gastric Carcinoma—2nd English Edition. Gastric Cancer 1:10–24
11. Kato H, Semba S, Miskad UA, Seo Y, Kasuga M, Yokozaki H (2004) High expression of *PRL-3* promotes cancer cell motility and liver metastasis in human colorectal cancer: a predictive molecular marker of metachronous liver and lung metastases. Clin Cancer Res 10:7318–7328
12. Kim KA, Song JS, Jee J, Sheen MR, Lee C, Lee TG, Ro S, Cho JM, Lee W, Yamazaki T, Jeon YH, Cheong C (2004) Structure of human PRL-3, the phosphatase associated with cancer metastasis. FEBS Lett 565:181–187
13. Li Z, Zhan W, Wang Z, Zhu B, He Y, Peng J, Cai S, Ma J (2006) Inhibition of PRL-3 gene expression in gastric cancer cell line SGC7901 via microRNA suppressed reduces peritoneal metastasis. Biochem Biophys Res Commun 348:229–237
14. Matter WF, Estridge T, Zhang C, Belagaje R, Stancato L, Dixon J, Johnson B, Bloem L, Pickard T, Donaghue M, Acton S, Jeyaseelan R, Kadambi V, Vlahos CJ (2001) Role of PRL-3, a human muscle-specific tyrosine phosphatase, in angiotensin-II signaling. Biochem Biophys Res Commun 283:1061–1068
15. Miskad UA, Semba S, Kato H, Yokozaki H (2004) Expression of PRL-3 phosphatase in human gastric carcinomas: close correlation with invasion and metastasis. Pathobiology 71:176–184
16. Mohn KL, Laz TM, Hsu JC, Melby AE, Bravo R, Taub R (1991) The immediate-early growth response in regenerating liver and insulin-stimulated H-35 cells: comparison with serum-stimulated 3T3 cells and identification of 41 novel immediate-early genes. Mol Cell Biol 11:381–390
17. Park CS, Manahan LJ, Brigati DJ (1991) Automated molecular pathology: one hour in situ hybridization. J Histotechnol 14:219–229
18. Pearson WR, Lipman DJ (1988) Improved tools for biological sequence comparison. Proc Natl Acad Sci USA 85:2444–2448
19. Peng L, Li Y, Meng L, Shou C (2004) Preparation and characterization of monoclonal antibody against protein tyrosine phosphatase PRL-3. Hybrid Hybridomics 23:23–27
20. Peng L, Ning J, Meng L, Shou C (2004) The association of the expression level of protein tyrosine phosphatase PRL-3 protein with liver metastasis and prognosis of patients with colorectal cancer. J Cancer Res Clin Oncol 130:521–526
21. Peng L, Jin G, Wang L, Guo J, Meng L, Shou C (2006) Identification of integrin alpha1 as an interacting protein of protein tyrosine phosphatase PRL-3. Biochem Biophys Res Commun 342:179–183
22. Radke I, Gotte M, Kersting C, Mattsson B, Kiesel L, Wulfing P (2006) Expression and prognostic impact of the protein tyrosine phosphatases PRL-1, PRL-2, and PRL-3 in breast cancer. Br J Cancer 95:347–354
23. Roder DM (2002) The epidemiology of gastric cancer. Gastric Cancer 5(Suppl 1):5–11
24. Saha S, Bardelli A, Buckhaults P, Velculescu VE, Rago C, St Croix B, Romans KE, Choti MA, Lengauer C, Kinzler KW, Vogelstein B (2001) A phosphatase associated with metastasis of colorectal cancer. Science 294:1343–1346
25. Semba S, Itoh N, Ito M, Youssef EM, Harada M, Moriya T, Kimura W, Yamakawa M (2002) Down-regulation of PIK3CG, a catalytic subunit of phosphatidylinositol 3-OH kinase, by CpG hypermethylation in human colorectal carcinoma. Clin Cancer Res 8:3824–3831
26. Wang L, Peng L, Dong B, Kong L, Meng L, Yan L, Xie Y, Shou C (2006) Overexpression of phosphatase of regenerating liver-3 in breast cancer: association with a poor clinical outcome. Ann Oncol 17:1517–1522
27. Werner SR, Lee PA, DeCamp MW, Crowell DN, Randall SK, Crowell PL (2003) Enhanced cell cycle progression and down regulation of $p21^{Cip1/Waf1}$ by PRL tyrosine phosphatases. Cancer Lett 202:201–211
28. Wu X, Zeng H, Zhang X, Zhao Y, Sha H, Ge X, Zhang M, Gao X, Xu Q (2004) Phosphatase of regenerating liver-3 promotes motility and metastasis of mouse melanoma cells. Am J Pathol 164:2039–2054
29. Yokozaki H, Yasui W, Tahara E (2001) Genetic and epigenetic changes in stomach cancer. Int Rev Cyt 204:49–95

30. Zeng Q, Hong W, Tan YH (1998) Mouse PRL-2 and PRL-3, two potentially prenylated protein tyrosine phosphatases homologous to PRL-1. Biochem Biophys Res Commun 244:421–427
31. Zeng Q, Si X, Horstmann H, Xu Y, Hong W, Pallen CJ (2000) Prenylation-dependent association of protein-tyrosine phosphatases PRL-1, -2, and-3 with the plasma membrane and the early endosome. J Biol Chem 275:21444–21452
32. Zeng Q, Dong JM, Guo K, Li J, Tan HX, Koh V, Pallen CJ, Manser E, Hong W (2003) PRL-3 and PRL-1 promote cell migration, invasion, and metastasis. Cancer Res 63:2716–2722
33. Zhang ZY, Zhou B, Xie L (2002) Modulation of protein kinase signaling by protein phosphatases and inhibitors. Pharmacol Ther 93:307–317

Virchows Arch (2007) 450:311–319
DOI 10.1007/s00428-006-0363-6

ORIGINAL ARTICLE

MYH, *OGG1*, *MTH1*, and *APC* alterations involved in the colorectal tumorigenesis of Korean patients with multiple adenomas

Jin C. Kim · In H. Ka · Yoo M. Lee · Kum H. Koo · Hee C. Kim · Chang S. Yu · Se J. Jang · Yong S. Kim · Han I. Lee · Kang H. Lee

Received: 1 November 2006 / Revised: 16 December 2006 / Accepted: 20 December 2006 / Published online: 25 January 2007
© Springer-Verlag 2007

Abstract This study was done to characterize base excision repair (*BER*) genes and adenomatous polyposis coli (*APC*) alterations in the tumorigenesis of multiple colorectal adenomas in Korean patients. In total, 217 adenomas (mean number=10) and 117 cancers were available from 143 patients. The heterozygous genotype of *OGG1* c.1-18*G>T* was closely associated with multiple adenoma families ($P<0.001$), while *MYH* A359V mutation exhibited a tendency ($P=0.053$). *MYH* R170G mutation was exclusively identified in one patient. The *G:C>T:A* transversion or attenuated familial adenomatous polyposis (AFAP) mutations of *APC* was identified in the specific genotypes of *BER* variants. Tubular adenomas or adenomas with none-to-mild dysplasia were significantly associated with polymorphic genotypes of *OGG1* IVS4-15 and S326C. In addition, large and pedunculated adenomas were more frequent in patients with *G:C>T:A* transversion and AFAP mutations of *APC*, respectively. However, *BER* variants were not associated with mismatch repair or altered p53 protein expression. Conclusively, two novel mutations of *MYH* and a novel *OGG1* polymorphism seemed to be associated with multiple colorectal adenomas in Korean families, differing from those in other ethnic groups. Some *BER* variants involved in specific *APC* mutations are associated with characteristics of histogenesis other than altered mismatch repair or p53 pathway.

Keywords Colorectal adenoma · Multiple · *APC* · *BER* · Mismatch repair · p53

J. C. Kim · I. H. Ka · Y. M. Lee · K. H. Koo · H. C. Kim · C. S. Yu
Department of Surgery, University of Ulsan College of Medicine, Seoul, South Korea

J. C. Kim (✉) · I. H. Ka · Y. M. Lee · K. H. Koo · H. C. Kim · C. S. Yu · S. J. Jang
Laboratory of Cancer Biology and Genetics,
Asan Institute for Life Sciences,
388-1 Poongnap-2-Dong Songpa-Ku,
Seoul, South Korea
e-mail: jckim@amc.seoul.kr

S. J. Jang
Department of Pathology,
University of Ulsan College of Medicine,
Seoul, South Korea

Y. S. Kim
Division of Molecular Therapeutics,
Korean Research Institute of Bioscience and Biotechnology,
Daejeon, South Korea

H. I. Lee
Department of Surgery, Catholic University of Daegu,
Daegu, South Korea

K. H. Lee
Department of Surgery, Hanyang University Hospital,
Seoul, South Korea

Introduction

Recently, 5–30% of attenuated familial adenomatous polyposis (AFAP) patients were shown to have specific *MYH* mutations [4, 30]. Compared with familial adenomatous polyposis (FAP), the typical AFAP phenotype is characterized by fewer adenomas (less than 100), more proximal colonic adenomas, later age of onset for colon adenomas and cancer, and a limited extracolonic manifestation [3, 17]. Thus, AFAP was originally characterized as a subset of polyposis with a phenotype distinct from FAP, but the definition now involves the number of adenomas. The

incidence of AFAP may account for up to 10% of FAP patients [32]. Specific mutations in *MYH* were identified in AFAP patients, but no pathogenic change was identified in the other base excision repair (*BER*) genes, namely, *OGG1* and *MTH1*. Few studies have examined *BER* mutations in patients with multiple adenomas that are not classed as FAP or AFAP [7, 19].

The BER pathway has an important role in the repair of mutations caused by reactive oxygen species [4]. The 8-oxo-dGTP, which is an oxidized form of dGTP, is highly mutagenic and one of the main endogenous sources for spontaneous genomic instability [22, 24]. In *Escherichia coli* and human cells, three proteins are known to be involved in defending cellular DNA against the mutagenic effects of 8-oxo*G*: MutT (human homolog, MTH1), which has nucleoside triphosphatase activity and hydrolyzes 8-oxo-dGTP to 8-oxo-dGMP; MutM (human homolog, OGG1), which is involved in direct repair by 8-oxoguanine DNA glycosylase; and MutY (human homolog, MYH), which is involved in repair of A to 8-oxoG mismatches due to its adenine glycosylase activity [24]. Two mutational hot spots such as *MYH* codons 165 and 382 possibly affect the catalytic core of glycosylase [4]. Regarding other *BER* variants, the well-documented polymorphism in exon 7 of *OGG1* (S326C) equivocally affects glycosylase activity in the repair of 8-oxo*G*. Otherwise, two different single nucleotide polymorphisms (SNPs) in human *MTH1* gene, i.e., IVS1-1 *T*>*C* and V83M, which probably affect expression or function of the human MTH1 protein, were identified [22]. However, it remains to be shown whether these SNPs increase the risk of developing colorectal adenomas or carcinomas [10, 24].

Routinely used mutation-detection techniques have identified adenomatous polyposis coli (*APC*) germline mutations in approximately 70% of patients with classic FAP and 10% of patients with AFAP [18, 20, 33]. APC is identified as a nucleocytoplasmic shuttling protein [6, 26]. Somatic mutations in *APC* were found in 34–70% of sporadic colorectal tumors that are clustered in the central region of the open reading frame, spanning codons 1286–1513 of exon 15 [21]. Otherwise, AFAP mutations are known to often involve germline mutations in specific regions of the *APC* gene: the 5′-end, the 3′-end, and the alternatively spliced region of exon 9 [17, 31]. Colorectal tumors from individuals with biallelic *MYH* mutations are associated with a significant excess of somatic *G*:*C*>*T*:*A* mutations of *APC*, compared with sporadic and FAP-associated tumors [13]. This confirms that germline *MYH* mutations predispose individuals to colorectal adenomas and carcinomas rather than to the sporadic lesions. Simultaneous inactivation of *E. coli MutM* and *MutY* markedly increases the frequency of spontaneous *G*:*C*>*T*:*A* mutations, and deficiency in *E. coli MutT* leads to a 1,000-fold increase in *T*:*A*>*G*:*C* transversions compared with a control [23].

Several studies have reported contradictory results about the reciprocal interaction of mismatch repair (MMR) and *BER* mutations in colorectal tumorigenesis. Some authors have reported cooperation between MYH-mediated BER and MMR [9]. The MYH protein interacts with the MSH2/MSH6 heterodimer via MSH6, thereby stimulating DNA-binding and glycosylase activities of MYH with an 8-oxo*G*:*A* mismatch. By contrast, another study has indicated that the BER and MMR pathways may be mutually exclusive, which is consistent with the report that 8-oxo*G* repair is defective in some microsatellite stable cells of colorectal cancers [24]. One study has found a significant negative association between *APC* or *p53* mutations and microsatellite instability: Mutations are more commonly found in microsatellite stable tumors than instable ones [27].

To date, few studies investigated the alterations of both *BER* and *APC* in multiple adenomas that are not associated with FAP or AFAP. The present study therefore focused on characterizing the genetic alterations involved in the tumorigenesis of multiple colorectal adenomas in Korean patients. We examined the relationships between *BER* and *APC* alterations together with MMR and altered p53 expression, as well as histologic features. Our findings should help determine risk factors and the discrete genetic changes involved in development of multiple adenomas.

Materials and methods

Tissue samples

A total of 143 Korean patients with multiple colorectal adenomas (number of adenomas ≥2) were consecutively and prospectively enrolled between 1999 and 2005 at the Asan Medical Center (Seoul, Korea). Of the 143 patients, 121 were men and 22 were women, with a mean age of 62 years (25–89 years). Invasive carcinoma (infiltration into the submucosa or deeper layers) was found in 116 patients, and 31 (21.7%) patients had multiple primary cancers, including more than one colorectal cancer. The mean number of adenomas in each patient was 10 (range 2–83), and 43, 45, and 55 patients had 2–4, 5–9, and 10 or more adenomas, respectively. A family history of colorectal neoplasm or any solid cancer was identified in first-degree relatives for 18 patients and in second-degree relatives for 37 patients (12.6 and 25.9% of the total, respectively). All neoplastic tissues were confirmed by histologic identification, and 217 adenomas and 117 carcinomas were available for genetic analysis. Peripheral blood lymphocytes from patients, their first-degree relatives (n=80), and healthy control subjects (n=300) were also obtained for DNA

extraction. The healthy controls from general Korean population were consecutively recruited from our Health Evaluation Center, confirming no family history of cancer by the personal recall. Patients who were diagnosed with hereditary nonpolyposis colorectal cancer, FAP or AFAP, and who were treated preoperatively with radiotherapy were excluded from the study. The mean period of follow-up was 39 months (range 10–84 months). All samples were acquired with the patients' informed consent and the study was conducted with the approval of the Institutional Review Board for Human Genetic and Genomic Research in accordance with the declaration of Helsinki.

BER alterations

Single-strand conformation polymorphism polymerase chain reaction (SSCP-PCR) was performed on genomic DNA of peripheral blood lymphocytes. All exons and exon–intron boundaries were separately amplified in 16 *MYH* fragments (exons 1–16), four *MTH1* fragments (exons 2–5), and 11 *OGG1* fragments (exons 1–8), using previously reported primers (http://www.uwcm.ac.uk) [1]. It is difficult to accurately discriminate between heterozygous and homozygous mutants by denaturing high-performance liquid chromatography (DHPLC), so SSCP-PCR was used for *BER* assays. The amplification protocol consisted of an initial denaturation step at 94°C for 5 min, followed by 35 cycles of denaturation at 94°C for 45 s, annealing at the optimal temperature (54–57°C for 45 s), and extension at 72°C for 45 s, with a final extension at 72°C for 7 min. PCR products were separated by electrophoresis on 10% nondenaturing polyacrylamide gels at 20 mA for 18 h. DNA bands of distinct mobility were detected by silver staining. Aberrant bands identified by SSCP-PCR were sequenced using a genetic analyzer (ABI 3730, PE Applied Biosystems, Foster, CA, USA) using forward and reverse primers. Reverse sequences were repeatedly verified as the forward sequencing primers located close to the mutation site.

APC mutations

An automated DHPLC instrument (WAVE™, Transgenomic, Omaha, NE, USA) was used to examine mutations of the *APC* exons 1–14 in genomic DNA of peripheral blood lymphocytes and tumors. The universal Touchdown PCR protocol was used for all amplicons using specific primers and a standard protocol [38]. Briefly, hybridized PCR products were denatured at 95°C for 5 min with gradual cooling of 1.5°C per cycle to allow efficient heteroduplex formation. Samples were injected onto a DNASep column and eluted with a mixture of buffer A [0.1 M of triethylammonium acetate (TEAA)] and buffer B (0.1 M of TEAA and 25% acetonitrile) at a flow rate of 0.9 ml/min. The mobile phase gradient and running column temperature for optimal heteroduplex separation were determined using WAVEMARKER 3.4 S/W. Abnormal DNA elution patterns were identified by the presence of one or more additional eluting peaks in the chromatogram.

We used the protein truncation test (PTT) to identify the translation-terminating mutation in exon 15. Four primer pairs designed in our laboratory were used to amplify whole reading frames of exon 15, including overlapping base sequences of 1959–3789, 3084–5100, 4782–7009, and 6300–8668 (sequence details available on request). PCR amplification comprised a denaturation cycle at 94°C for 4 min, followed by 35 cycles of 1 min at 94°C, 1.5 min at 55°C, and 2 min at 72°C. PCR products were introduced into the TnT T7 rabbit reticulocyte system (Promega, Southampton, UK) with ^{35}S incorporation (Amersham, Buckinghamshire, UK). Products were resolved by 15% sodium dodecyl sulfate polyacrylamide gel electrophoresis and visualized by autoradiography. Aberrant eluting peaks and bands identified by DHPLC and PTT were also directly sequenced. Specific primers from 17 overlapping segments of exon 15 were used for sequencing, corresponding to the aberrant PTT bands [20].

Immunohistochemistry

Paraffin-embedded tissue cores of carcinomas were used for the construction of tissue microarray, arrayed onto recipient paraffin blocks using a precision instrument (Beecher Instrument, Sun Prairie, WI, USA). Tissue array blocks containing core cylinders were subjected to immune staining based on the labeled streptavidin–biotin method, using DAKO LSAB® kit (DAKO, Carpinteria, CA, USA) and monoclonal antibodies to hMLH1 (G168-15), hMSH2 (G219-1129) (BD Pharmingen, San Diego, CA, USA), and p53 (DO-7) (DAKO, Glostrup, Denmark). For all samples with negative immune staining on a tissue microarray, the whole tissue sections were repeatedly assayed. The percent cells positively stained was divided into two groups for hMLH1 and hMSH2 (i.e., − for ≤10% and + for >10% nuclear staining) and altered p53 (i.e., low for ≤10% and high for >10%), respectively.

Statistical methods

Respective alleles and genotypes were compared among them or with various clinicopathological parameters by cross-table analysis using Fisher's exact or Pearson's χ^2 tests, depending on statistical validity. Numerical values for independent groups were tested by unpaired Student's *t* test or ANOVA with least squares deviation verification. Adenoma/recurrence-free intervals were compared using

the Kaplan–Meier method with a log-rank test. Recurrence factors were then verified using a Cox regression model. Hardy–Weinberg equilibrium and genotypic disequilibrium were assessed using Genepop S/W (Raymond & Rousset, version 3.4; http://wbiomed.curtin.edu.au). The linkage between *BER* variants was assessed by linear regression analysis. The significance level was adjusted at 5% for each analysis, and all calculations were performed using SPSS software (version 13, SPSS, Chicago, IL, USA).

Results

Clinicopathological characteristics

Multiple primary colorectal cancers and stages I and II colorectal cancers were significantly more common in patients with five or more adenomas than in patients with fewer than five adenomas (P=0.002 and 0.029, respectively) (Table 1). Patients with 20 or more adenomas were younger than patients with fewer than 20 (mean age±SD 50±13 years vs 64±9 years, P<0.001). The number of colorectal tumors was significantly greater in patients with a family history of colorectal tumors than those without it (P<0.001). Excluding patients who underwent total colectomy, the mean adenoma/recurrence-free interval was significantly shorter in patients with ten or more adenomas than in patients with less than ten adenomas (16±2 m vs 29±2 m, P=0.003).

BER variants in patients and healthy controls

Eleven *BER* alterations were identified: P18L, G25D, R170Q, Q324H, and A359V in *MYH*; c.1-18 *G>T*, c.1-23 *A>G*, IVS4-15 *C>G*, and S326C in *OGG1*; and IVS1-1 *T>C* and V83M in *MTH1* (novel and trend or significant alterations are shown in Table 2 and Fig. 1). Two heterozygous *MYH* variants (R170Q and A359V) were novel mutations, and two heterozygous *OGG1* variants (c.1-18 *G>T* and c.1-23 *A>G*) were novel polymorphisms. The R170Q mutation in *MYH* was only identified in one male patient with seven adenomas, whereas the A359V *MYH* mutation tended to be more frequent in patients with ten or more adenomas and their first-degree relatives than healthy control (P=0.053). Another novel pathogenic SNP in *OGG1* (c.1-18 *G>T*) was identified with a heterozygous *GT* genotype that was approximately five times more common in patients and their first-degree relatives than in healthy control individuals (P<0.001). All SNPs identified in our study constituted Hardy–Weinberg equilibrium with their respective reference alleles in patients, their first-degree relatives, and healthy controls. It is interesting to note that a close linkage between alleles was identified in half of the *BER* variants: 100% between P18L and G25D genotypes in *MYH*, 84.1% between IVS4-15 *C>G* and S326C genotypes in *OGG1* (R^2=0.659, P<0.001), and 96.6% between IVS1-1 *T>C* and V83M genotypes in *MTH1* (R^2=0.702, P<0.001).

Table 1 Clinicopathological features according to the number of adenomas

Clinicopathological features	Number of adenomas			*P* value
	2–4, *n*=43	5–9, *n*=45	≥10, *n*=55	
Sex, M/F	34/9	37/8	50/5	0.236
Age, <50/≥50	6/37	5/40	6/49	0.882
FH of CRC/adenoma, −/+	39/4	39/6	47/8	0.728
Adenomas,[a] *n*=217				
Growth, S/P	34/14	44/22	77/26	0.522
Size, <10/≥10 mm	32/16	43/23	72/31	0.799
Site, right/left	14/34	33/33	43/60	0.083
Histology, T and TV/V	40/8	57/9	91/12	0.699
Dysplasia, 0–1/1–2	40/8	59/7	86/17	0.524
Concurrent cancer,[a] *n*=117				
Patients with multiple cancers	3	11	16	0.002
AJCC stage,[b] I–II/III–IV	20/20	24/15	30/8	0.029
Site, right/left	8/32	16/23	11/27	0.123
Differentiation, WD + MD/PD	36/4	36/3	33/5	0.73

[a] Number represents adenomas or carcinomas included in the genetic and histologic examination of this study.
[b] Cancer staging according to the American Joint Committee on Cancer (AJCC) (sixth edition, 2001).
FH Family history in first- and second-degree relatives, *CRC* colorectal cancer, *Growth S/P* sessile/pedunculated, *Histology T* and *TV/V* tubular and tubulovillous/villous, *Dysplasia 0–1/2–3* none–mild/moderate–severe, *Differentiation WD + MD/PD* well + moderately/poorly differentiated, *Site*, *right/left* cecum-splenic flexure of transverse colon/splenic flexure of transverse colon–rectum

Table 2 Germline *BER* variants and genotype/allele frequencies, shown novel and trend or significance

Gene	Exon (intron)	Nucleotide change	Consequence	Genotype/allele	Frequency (%)		P value
					P + R, *n*=223	Control, *n*=300	
MYH	7	c.509*G>A*	R170Q	*GG*	222 (99.6)	300 (100)	0.426
				GA	1 (0.4)	0	
				G frequency	0.998	1	0.426
				HWE exact *P*	NA	NA	
MYH	12	c.1076*C>T*	A359V	*CC*	218 (97.8)	299 (99.7)	0.053
				CT	5 (2.2)	1 (0.3)	
				C frequency	0.989	0.998	0.054
				HWE exact *P*	1	NA	
OGG1		c.1-18*G>T*	NA	*GG*	200 (89.7)	294 (98)	<0.001
				GT	23 (10.3)	6 (2)	
				G frequency	0.987	0.992	<0.001
				HWE exact *P*	1	1	
OGG1		c.1-23*A>G*	NA	*AA*	217 (97.3)	295 (98.3)	0.306
				AG	6 (2.7)	5 (1.7)	
				A frequency	0.992	0.987	0.307
				HWE exact *P*	1	1	

Genetic nomenclature according to den Dunnen JT and Antonarakis [5].
BER Base excision repair, *P* + *R*, patients and their first-degree relatives, *HWE* Hardy–Weinberg equilibrium, *NA* not assessed

APC mutations identified and associated with *BER* variants

Somatic *APC* mutations were identified in 89 of 217 adenomas (41%) and 53 of 117 carcinomas (46.3%). In the same patient, identical mutation between adenoma and carcinoma was identified in 18 of 31 patients (58%). Mutations in adenomas occurred throughout the *APC* sequence, whereas those in carcinomas were found in exons 5–14 and in the 3′-end of exon 15 (to codon 1049) (Fig. 2). The frequency of mutations found in the mutation "hot spots" of AFAP—the 5′-end to codon 175, exon 9, and the 3′-end to codon 1596 of *APC*—did not differ significantly between adenomas and carcinomas (17.6 vs 22.6%, respectively). Mutation patterns of tumors included missense, nonsense, deletion, insertion mutations, splicing-site alterations, and mixed-type mutations, which had frequencies of 16.7, 30.6, 9, 16, 43.1, and 25%, respectively. A 48-year-old patient with five adenomas and rectal cancer carried germline mutation of *G*:*C*>*T*:*A* transversion (S631I and Y642F), but no truncating germline mutation was identified in all patients and their first-degree relatives.

G:*C*>*T*:*A* transversions in *APC* were identified in 16 tumors carrying six germline *BER* variants (Table 3). Among concurrent occurrences of *BER* variants, *OGG1* or *MTH1* polymorphic genotypes were interestingly associated with *G*:*C*>*T*:*A* transversions without MYH Q324H genotype in seven tumors. The AFAP mutations were closely associated with the *CC* genotype of *MYH* Q324H (P=0.025), and with the *AA* genotype of *OGG1* c.1-23 (P=0.041). However, these genotypes were not associated with *APC* mutations of the mutation cluster region in FAP.

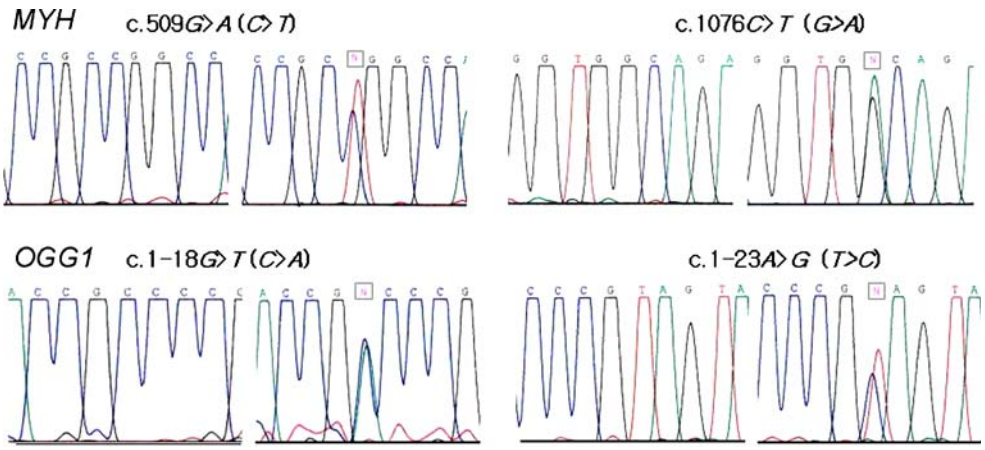

Fig. 1 Novel mutations (*MYH* c.509*G>A* and c.1076*C>T*) and polymorphisms (*OGG1* c.1-18*G>T* and c.1-23*A>G*) identified. Reverse sequences (*in parenthesis*) are shown as the forward sequencing primers located close to the mutation site

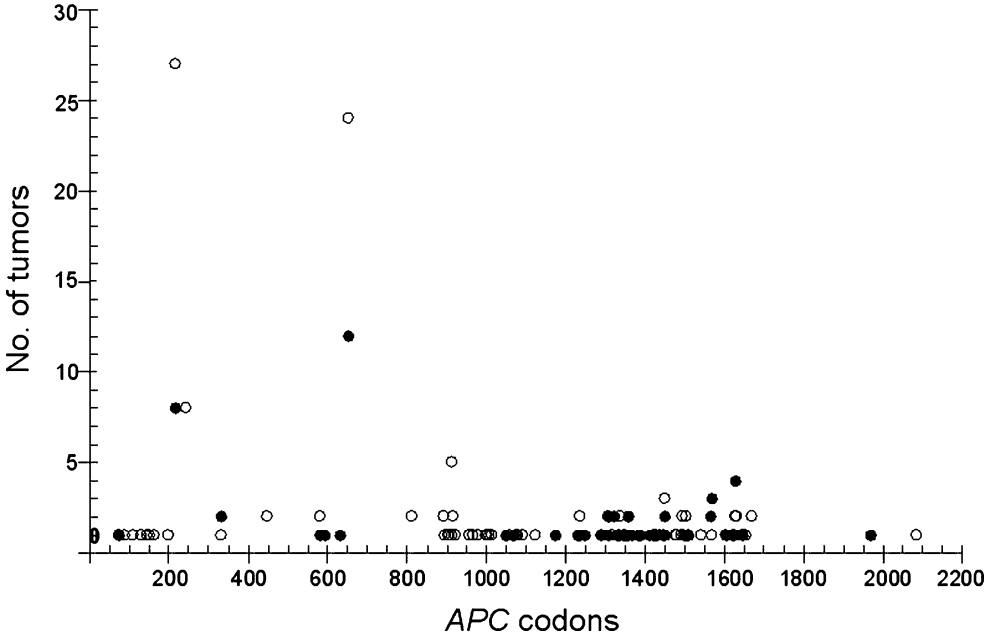

Fig. 2 Mutation distributions along all codons of *APC* in the colorectal adenomas (*open circles*) and carcinomas (*filled circles*) in patients with multiple adenomas. Splicing site variants are marked between the relevant codons. In the same patient, identical mutation between adenoma and carcinoma was identified in 18 of 31 patients

Clinicopathological correlations

Tubular adenomas or adenomas with none-to-mild dysplasia were significantly associated with polymorphic genotypes of *OGG1* IVS4-15 and S326C (Table 4). Large adenomas (diameter ≥10 mm) or pedunculated adenomas tended to be associated with *MTH1* IVS1-1 polymorphic genotypes. In addition, large adenomas were also found in patients with *G*:*C*>*T*:*A* transversion mutations of *APC* (P=0.039) and pedunculated adenomas were more frequent in those with AFAP mutations of *APC* (P=0.05). Neither hMLH1 nor hMSH2 expression was identified in 17 of 143 tumors (11.9%), including carcinomas and adenomas with high-grade dysplasia. This lack of expression was significantly associated with poorly differentiated cancers, right-sided cancers, and cancers with a young age of onset. However, hMLH1 or hMSH2 expression was not associated with *BER* variants or *APC* mutations. Overexpression of altered p53 in carcinomas was significantly associated with moderate-to-severe dysplasia and villotubular or villous adenomas (P=0.011 and 0.031, respectively), but was inversely correlated with *APC* mutations in adenomas (P=0.022). Altered p53 expression was not associated with *BER* variants.

Table 3 *G*:*C*>*T*:*A APC* mutations in colorectal tumors from patients with germline *BER* variants

ID	Sample	*BER* variants	*APC* mutations	
			Nucleotide change	Consequence
AC–17	Adenoma-1	*OGG1* (IVS4-15, S326C)	c.3925*G*>*T*	E1309X
	Adenoma-2	*OGG1* (IVS4-15, S326C)	c.4529*G*>*T*	S1510T
	Carcinoma	*OGG1* (IVS4-15, S326C)	c.4529*G*>*T*	S1510T
AC–24	Carcinoma	*MYH* (Q324H), *OGG1* (IVS4-15, S326C)	c.1897 *G*>*T*	E633X
AC–27	Adenoma	*MYH* (Q324H), *OGG1* (IVS4-15, S326C)	c.4892 *G*>*T*	S1631I
AC–30	Carcinoma	*OGG1* (IVS4-15, S326C)	c.3964 *G*>*T*	E1322X
MA–59	Adenoma	*MYH* (Q324H), *OGG1* (IVS4-15, S326C)	c.4892*G*>*T*	S1631T
AC–76	Adenoma	*MTH1* (IVS1-1, V83M)	c.3925*G*>*T*	E1309X
	Carcinoma	*MTH1* (IVS1-1, V83M)	c.3925*G*>*T*	E1309X
MA–85	Adenoma	*MYH* (Q324H), *OGG1* (IVS4-15, S326C)	c.3275*G*>*T*	E1080D
MA–89	Adenoma	*MYH* (Q324H), *OGG1* (IVS4-15, S326C)	c.4426*G*>*T*	A1476F
AC–94	Adenoma	*MYH* (Q324H)	c.3175*G*>*T*	E1059X
AC–95	Carcinoma	*MYH* (Q324H)	c.3964*G*>*T*	E1322X
AC–97	Adenoma	*MYH* (Q324H), *OGG1* (IVS4-15, S326C)	c.436*G*>*T*	L162F
AC 105	Carcinoma	*OGG1* (c.1-18, IVS4-15, S326C)	c.4057*G*>*T*	E1353X
AC–106	Carcinoma	*MYH* (Q324H), *OGG1* (IVS4-15, S326C)	c.3747*C*>*A*	C1249X

BER Base excision repair

Table 4 Biologic characteristics of adenomas regarding respective genotypes of *BER* variants

BER variants and genotypes	Adenoma no., <15/≥15	Size, <10/≥10 mm	Growth, S/P	Histology, T or TV/V	Dysplasia, 0–1/2–3
MYH P18L/G25D[a]					
CC/GG	118/20	144/68	153/59	184/28	182/31
CT,TT/GA,AA	2/3	3/2	2/3	4/1	4/1
P value	0.03	0.519	0.142	0.515	0.551
OGG1 IVS4-15					
CC	24/3	21/16	23/14	28/9	26/11
CG,GG	96/20	126/54	132/48	160/20	160/21
P value	0.325	0.086	0.122	0.035	0.008
OGG1 S326C					
CC	25/2	22/16	23/15	29/9	28/10
CG,GG	95/21	125/54	132/47	159/20	158/22
P value	0.14	0.109	0.077	0.042	0.029
MTH1 IVS1-1					
TT	109/21	136/59	143/52	169/26	165/30
TC	11/2	11/11	12/10	19/3	21/2
P value	0.652	0.054	0.058	0.589	0.309

[a] The same genotypes of *MYH* P18L and G25D occur concurrently in the same individual.

BER Base excision repair, *Growth S/P* sessile/pedunculated, *Histology T* and *TV/V*, tubular and tubulovillous/villous, *Dysplasia 0–1/2–3* none–mild/moderate–severe

Discussion

Some investigations reported that 25% of patients with at least ten adenomas have MYH polyposis, whereas others have found no MYH polyposis in patients with 1–19 polyps [3, 28, 33]. Accordingly, many cases of AFAP could not be defined as MYH polyposis, but the genetic alterations involved in tumorigenesis were not fully investigated in these cases of multiple adenomas. The *MYH* mutations in the AFAP families, which are frequently observed among Caucasians (Y165C and G382D) or other races of Indian (E466X) and Pakistani (Y90X), were not identified in our study. This finding is similar to other studies involving Korean, Japanese, and Jewish populations [15, 19, 25], and indicates a marked ethnic or regional segregation in MYH polyposis. However, we found two novel heterozygous *MYH* mutations: R170Q and A359V. *MYH* R170Q mutation was exclusively identified in one patient and A359V mutation tended to be identified in patients and their relatives. These mutations may be associated with multiple adenomas, but need to be further verified as predictive biomarkers in the large population covering various ethnic groups. For single *MYH* mutations associated with colorectal cancer, several investigations have suggested that this heterozygosity may confer a slightly increased risk of cancer [8, 25, 34]. The other three *MYH* variants in our study were previously identified as nonpathogenic SNPs [29].

In our study, a novel SNP in *OGG1*, c.1-18 *G>T*, was identified and the heterozygous *GT* genotype was found to be significantly associated with multiple adenoma families, possibly indicating a predictive SNP in these patients. Many studies suggest *OGG1* mutations have a limited effect on tumorigenesis, but the effect of this novel SNP in the promoter site remains to be determined [2, 30]. One study proposed that *OGG1* might be inactivated in tumors by transcription repression due to methylation of its promoter region containing many *CpG* sites [2]. Other three *OGG1* variants did not cosegregate with multiple adenoma patients in our study. Among them, c.1-23 *A>G* was a novel SNP, whereas IVS4-15 *C>G* and S326C had previously been identified as some of the most common polymorphisms in other studies [2, 37]. Several contrary issues were also raised in terms of mutagenesis ability of S326C missense variant [11, 36].

Cancerous tissues in humans have significantly increased levels of *MTH1* transcripts [14], presumably due to the consequence of oxidative stress. In our study, two SNPs in *MTH1*, IVS 1-1 *T>C* and V83M, were identified and shown to be closely linked. The IVS 1-1 *T>C* SNP in exon 2, which is tightly linked to the other SNP (V83M), is known to create an additional alternative in-frame *AUG* in B-type *MTH1* mRNAs producing p26, the fourth MTH1 polypeptide [22]. This polypeptide also has a mitochondrial-targeting signal, which is likely to be one of the risk factors for cancer or neuronal degeneration. Although one Japanese study reported a slightly higher frequency of homozygous Met83 mutants in patients including hepatocellular and lung cancers [22], we did not find any association of this variant with multiple adenoma families.

In our study, mutations of adenomas evenly occurred throughout all codons, and mutations in carcinomas were found in exons 5–14 and in the region from the 3′-end to codon 1049 of exon 15. AFAP is known to often involve germline mutations in specific regions of the *APC* gene, so-called AFAP mutations such as at the 5′-end (codons 1–177, exons 1–4), 3′-end (distal to codon 1580), and the alternatively spliced region of exon 9 (codons 311–408) [17, 31]. One study screened 164 unrelated British multiple adenoma patients (the numbers of adenomas ranged from 3–100) for germline *APC* mutations and found that 10% had mutations [18]. In our study, no truncating germline mutation was identified and somatic mutations were not clustered at the AFAP mutation sites. Thus, *APC* mutation patterns in multiple adenomas differ from those of known MYH polyposis. During DNA replication, 8-oxo-dGTP can be inserted into the nascent strand opposite adenine and cytosine in the template and leads to *G*:*C* to *T*:*A* transversion mutations [22]. In our study, the somatic *G*:*C*>*T*:*A* transversion in *APC* was identified in patients carrying six germline *BER* variants, showing exclusive linkage among some polymorphic sites of *BER*. Although an exclusive linkage was identified between these polymorphic sites in other previous studies [2, 22], our study is the first to find compound heterozygous variants of *OGG1* or *MTH1* associated with *G*:*C*>*T*:*A* transversions. We found AFAP mutations of *APC* to be associated with specific genotypes of *BER* variants, possibly causing multiple adenomas in addition to known MYH polyposis.

A younger age of onset was associated with increased numbers of adenomas, which is in agreement with other studies [4, 28]. Several polymorphic variants of *BER* were closely associated with specific growth, histologic type, and dysplasia of adenomas in our study. Furthermore, the same biological features were also found in adenomas with *G*:*C*>*T*:*A* transversions and AFAP mutations of *APC* in our study. Collectively, specific *BER* variants associated with AFAP mutations may play important roles in the tumorigenesis and growth of multiple adenomas. Histologically well-documented characteristics associated with p53 and MMR expression were found as in the other studies [16, 35]. In our study, excluding the patients who underwent total colectomy, the mean adenoma/recurrence-free interval was significantly shorter in patients with ten or more adenomas than in those with fewer adenomas, indicating that patients with ten or more adenomas should be closely monitored. Many investigators recommend prophylactic colectomy as a standard treatment option due to the risk of overlooking colorectal cancer during surveillance in patients with AFAP [17, 30].

In our study, hMLH1 or hMSH2 expression was not associated with *BER* or *APC* alterations. In addition, tumors with altered p53 overexpression were not associated with changes in hMLH1 or hMSH2 expression. Other investigation demonstrated inverse relationships between microsatellite instability and mutations in *APC* and *p53* [27]. The BER and MMR pathways seem to be mutually exclusive in our study, consistent with other previous studies on defective 8-hydroxyguanosine repair in microsatellite stable colorectal cancer cells [24, 34]. In our study, overexpression of altered p53 in carcinomas was inversely correlated with *APC* mutations in adenomas, but was not correlated with *BER* variants. A recent study reported that in a transgenic mouse that expressed mutant *KRAS2* none of the intestinal tumors showed evidence of *APC* alteration, although some showed *p53* alteration [12]. Taken together, these data indicate that three pathways, BER–APC, p53, and MMR alterations, may function independently in a significant number of multiple adenomas.

In conclusion, in Korean patients, two novel mutations in *MYH* (R170Q and A359V) and a SNP in *OGG1* (c.1-18*G*>*T*) seem to be associated with multiple colorectal adenomas, which need to be verified as potential biomarkers in the further investigation. Some variants of *BER* involved in AFAP mutations and *G*:*C*>*T*:*A* transversions of *APC* were associated with characteristic features in the histogenesis of adenomas. In addition, the three pathways involved in colorectal tumorigenesis, BER–APC, p53, and MMR alterations, may function independently in a significant number of cases of multiple adenomas.

Acknowledgement This study was supported from the Basic Research Program of the Korea Science and Engineering Foundation (grant no. R01-2006-000-10021-0).

References

1. Al-Tassan N, Chmiel NH, Maynard J, Fleming N, Livingston AL, Williams GT, Hodges AK, Davies DR, David SS, Sampson JR, Cheadle JP (2002) Inherited variants of MYH associated with somatic G:CT:A mutations in colorectal tumors. Nat Genet 30:227–232
2. Boiteux S, Radicella JP (2000) The human OGG1 gene: structure, functions, and its implication in the process of carcinogenesis. Arch Biochem Biophys 377:1–8
3. Burt RW, Leppert MF, Slattery ML, Samowitz WS, Spirio LN, Kerber RA, Kuwada SK, Neklason DW, Disario JA, Lyon E, Hughes JP, Chey WY, White RL (2004) Genetic testing and phenotype in a large kindred with attenuated familial adenomatous polyposis. Gastroenterology 127:444–451
4. Cheadle JP, Sampson JR (2003) Exposing the MYtH about base excision repair and human inherited disease. Hum Mol Genet 12: R159–R165
5. den Dunnen JT, Antonarakis SE (2000) Mutation nomenclature extensions and suggestions to describe complex mutations: a discussion. Hum Mutat 15:7–12
6. Fagman H, Larsson F, Arvidsson Y, Meuller J, Nordling M, Martinsson T, Helmbrecht K, Brabant G, Nilsson M (2003) Nuclear accumulation of full-length and truncated adenomatous

polyposis coli protein in tumor cells depends on proliferation. Oncogene 22:6013–6022
7. Farrington SM, Tenesa A, Barnetson R, Wiltshire A, Prendergast J, Porteous M, Campbell H, Dunlop MG (2005) Germline susceptibility to colorectal cancer due to base-excision repair gene defects. Am J Hum Genet 77:112–119
8. Fleischmann C, Peto J, Cheadle J, Shah B, Sampson J, Houlston RS (2004) Comprehensive analysis of the contribution of germline MYH variation to early-onset colorectal cancer. Int J Cancer 109:554–558
9. Gu Y, Parker A, Wilson TM, Bai H, Chang DY, Lu AL (2002) Human MutY homolog, a DNA glycosylase involved in base excision repair, physically and functionally interacts with mismatch repair proteins human MutS homolog 2/human MutS homolog 6. J Biol Chem 277:11135–11142
10. Hansen R, Saebo M, Skjelbred CF (2005) GPX Pro198Leu and OGG1 Ser326Cys polymorphisms and risk of development of colorectal adenomas and colorectal cancer. Cancer Lett 229:85–91
11. Janssen K, Schlink K, Gotte W, Hippler B, Kaina B, Oesch F (2001) DNA repair activity of 8-oxoguanine DNA glycosylase 1 (OGG1) in human lymphocytes is not dependent on genetic polymorphism Ser326/Cys326. Mutat Res 486:207–216
12. Janssen KP, el-Marjou F, Pinto D, Sastre X, Rouillard D, Fouquet C, Soussi T, Louvard D, Robine S (2002) Targeted expression of oncogenic K-ras in intestinal epithelium causes spontaneous tumorigenesis in mice. Gastroenterology 123:492–504
13. Jones S, Emmerson P, Maynard J, Best JM, Jordan S, Williams GT, Sampson JR, Cheadle JP (2002) Biallelic germline mutations in MYH predispose to multiple colorectal adenoma and somatic G:C>T:A mutations. Hum Mol Genet 11:2961–2967
14. Kennedy CH, Cueto R, Belinsky SA, Lechner JF, Pryor WA (1998) Overexpression of hMTH1 mRNA: a molecular marker of oxidative stress in lung cancer cells. FEBS Lett 429:17–20
15. Kim IJ, Ku JL, Kang HC, Park JH, Yoon KA, Shin Y, Park HW, Jang SG, Lim SK, Han SY, Shin YK, Lee MR, Jeong SY, Shin HR, Lee JS, Kim WH, Park JG (2004) Mutational analysis of OGG1, MYH, MTH1 in FAP, HNPCC and sporadic colorectal cancer patients: R154H OGG1 polymorphism is associated with sporadic colorectal cancer patients. Hum Genet 115:498–503
16. Kim JC, Lee KH, Ka IH, Koo KH, Roh SA, Kim HC, Yu CS, Kim TW, Chang HM, Gong GY, Kim JS (2004) Characterization of mutator phenotype in familial colorectal cancer patients not fulfilling Amsterdam criteria. Clin Cancer Res 10:6159–6168
17. Knudsen AL, Marie Luise Bisgaard ML, Steffen Bülow S (2003) Attenuated familial adenomatous polyposis (AFAP). A review of the literature. Familial Cancer 2:43–55
18. Lamlum H, Al Tassan N, Jaeger E, Frayling I, Sieber O, Reza FB, Eckert M, Rowan A, Barclay E, Atkin W, Williams C, Gilbert J, Cheadle J, Bell J, Houlston R, Bodmer W, Sampson J, Tomlinson I (2000) Germline APC variants in patients with multiple colorectal adenomas, with evidence for the particular importance of E1317Q. Hum Mol Genet 9:2215–2221
19. Miyaki M, Iijima T, Yamaguchi T (2005) Germline mutations of the *MYH* gene in Japanese patients with multiple colorectal adenomas. Mutat Res 578:430–433
20. Miyoshi Y, Ando H, Nagase H, Nishisho I, Horii A, Miki Y, Mori T, Utsunomiya J, Baba S, Petersen G, Hamilton SR, Kinzler KW, Vogelstein B, Nakamura Y (1992) Germ-line mutations of the APC gene in 53 familial adenomatous polyposis patients. Proc Natl Acad Sci USA 89:4452–4456
21. Nagase H, Nakamura Y (1993) Mutations of the APC (adenomatous polyposis coli) gene. Hum Mutat 2:425–434
22. Nakabeppu Y (2001) Molecular genetics and structural biology of human MutT homolog, MTH1. Mutat Res 477:59–70
23. Nohmi T, Kim SR, Yamada M (2005) Modulation of oxidative mutagenesis and carcinogenesis by polymorphic forms of human DNA repair enzymes. Mutat Res 591:60–73
24. Parker AR, O'Meally RN, Sahin F, Su GH, Racke FK, Nelson WG, DeWeese TL, Eshleman JR (2003) Defective human MutY phosphorylation exists in colorectal cancer cell lines with wild-type MutY alleles. J Biol Chem 278:47937–47945
25. Peterlongo P, Mitra N, Chuai S, Kirchhoff T, Palmer C, Huang H, Nafa K, Offit K, Ellis NA (2005) Colorectal cancer risk in individuals with biallelic or monoallelic mutations of MYH. Int J Cancer 114:505–507
26. Rosin-Arbesfeld R, Townsley F, Bienz M (2000) The APC tumour suppressor has a nuclear export function. Nature 406:1009–1012
27. Salahshor S, Kressner U, Pahlman L, Glimelius B, Lindmark G, Lindblom A (1999) Colorectal cancer with and without microsatellite instability involves different genes. Genes Chromosomes Cancer 26:247–252
28. Sampson JR, Dolwani S, Jones S, Eccles D, Ellis A, Evans DG, Frayling I, Jordan S, Maher ER, Mak T, Maynard J, Pigatto F, Shaw J, Cheadle JP (2003) Autosomal recessive colorectal adenomatous polyposis due to inherited mutations of MYH. Lancet 362:39–41
29. Shinmura K, Yamaguchi S, Saitoh T, Kohno T, Yokota J (2001) Somatic mutations and single nucleotide polymorphisms of base excision repair genes involved in the repair of 8-hydroxyguanine in damaged DNA. Cancer Lett 166:65–69
30. Sieber OM, Lipton L, Crabtree M, Heinimann K, Fidalgo P, Phillips RK, Bisgaard ML, Orntoft TF, Aaltonen LA, Hodgson SV, Thomas HJ, Tomlinson IP (2003) Multiple colorectal adenomas, classic adenomatous polyposis, and germ-line mutations in MYH. N Engl J Med 348:791–799
31. Sieber OM, Segditsas S, Knudsen AL, Zhang J, Luz J, Rowan AJ, Spain SL, Thirlwell C, Howarth KM, Jaeger EE, Robinson J, Volikos E, Silver A, Kelly G, Aretz S, Frayling I, Hutter P, Dunlop M, Guenther T, Neale K, Phillips R, Heinimann K, Tomlinson IP (2006) Disease severity and genetic pathways in attenuated familial adenomatous polyposis vary greatly, but depend on the site of the germline mutation. Gut 55:1440–1448
32. Vasen HF (2000) Clinical diagnosis and management of hereditary colorectal cancer syndromes. J Clin Oncol 18:S81–S92
33. Venesio T, Molatore S, Cattaneo F, Arrigoni A, Risio M, Ranzani GN (2004) High frequency of MYH gene mutations in a subset of patients with familial adenomatous polyposis. Gastroenterology 126:1681–1685
34. Wang L, Baudhuin LM, Boardman LA, Steenblock KJ, Petersen GM, Halling KC, French AJ, Johnson RA, Burgart LJ, Rabe K, Lindor NM, Thibodeau SN (2004) MYH mutations in patients with attenuated and classic polyposis and with young-onset colorectal cancer without polyps. Gastroenterology 127:9–16
35. Wheeler JM (2005) Epigenetics, mismatch repair genes and colorectal cancer. Ann R Coll Surg Engl 87:15–20
36. Yamane A, Kohno T, Ito K, Sunaga N, Aoki K, Yoshimura K, Murakami H, Nojima Y, Yokota J (2004) Differential ability of polymorphic OGG1 proteins to suppress mutagenesis induced by 8-hydroxyguanine in human cell in vivo. Carcinogenesis 25:1689–1694
37. Yoshimura K, Hanaoka T, Ohnami S, Ohnami S, Kohno T, Liu Y, Yoshida T, Sakamoto H, Tsugane S (2003) Allele frequencies of single nucleotide polymorphisms (SNPs) in 40 candidate genes for gene-environment studies on cancer: data from population-based Japanese random samples. J Hum Genet 48:654–658
38. Zhou XL, Eriksson U, Werelius B, Kressner U, Sun XF, Lindblom A (2004) Definition of candidate low risk APC alleles in a Swedish population. Int J Cancer 110:550–557

Virchows Arch (2007) 450:321–328
DOI 10.1007/s00428-007-0370-2

ORIGINAL ARTICLE

Co-expression of EGF receptor, TGFα and S6 kinase is significantly associated with colorectal carcinomas with distant metastases at diagnosis

Marco Tampellini · Marina Longo · Susanna Cappia · Elisa Bacillo · Irene Alabiso · Marco Volante · Luigi Dogliotti · Mauro Papotti

Received: 25 August 2006 / Revised: 1 December 2006 / Accepted: 5 January 2007 / Published online: 30 January 2007
© Springer-Verlag 2007

Abstract Autocrine tumour growth factor alpha (TGFα)/epidermal growth factor receptor (EGFR) stimulation in colorectal carcinoma (CRC) cells regulates cell adhesion and invasiveness via ribosomal protein S6 kinase (S6K) phosphorylation in pre-clinical studies. The aim of this study was to evaluate whether TGFα and EGFR expression might be correlated with a higher metastatic behaviour in human tumours. Paraffin-embedded material was retrospectively collected from 101 primitive CRCs including all stage IV patients at diagnosis treated at our Institution from 1999 to 2004 (50 cases, Group B) and 51 stage II–III control cases (Group A). EGFR and TGFα expression, together with signalling molecules (including signal transducer and activator of transcription [STAT3], serine–treonine kinase [Akt], mitogen-activated protein kinase [MAPK], mammalian target of rapamycin [mTOR] and S6K) in selected samples, was evaluated by immunohistochemistry using the EGFR Dako antibody. A total of 68/101 (67.3%) cases were EGFR positive and 79/101 (78.2%) cases were TGFα positive. EGFR/TGFα co-expression differed significantly ($p=0.02$) between Group A and Group B tumours (23/51, 45.1% vs 34/50, 68.0%, respectively), whereas no differences in STAT, Akt, mTOR expression was evident between the two groups. Conversely, there was a significantly higher expression of phosphorylated S6K in stage IV cases (Group B) than in the controls (Group A; 70.4% vs 38.7%; $p=0.02$). In agreement with in vitro data, EGFR, TGFα and S6K co-expression in human CRC was significantly higher in patients with advanced stage at diagnosis.

Keywords Colorectal carcinoma · Immunohistochemistry · EGFR · TGFα · Metastases · S6K

Abbreviations

EGFR	epidermal growth factor receptor
TGFα	tumour growth factor alpha
S6K	ribosomal protein S6 kinase
CRC	colorectal cancer
STAT3	signal transducer and activator of transcription
Akt	serine–treonine kinase
MAPK	mitogen-activated protein kinase
mTOR	mammalian target of rapamycin

Work supported by grants from the Italian Ministry of University (ex 60% to MT, and LD) and the Regione Piemonte, Project CIPE2005, no. A70 to MP.

Presented in part at the 2006 ASCO Annual Meeting, Atlanta, GA, June 2–6.

M. Tampellini (✉) · M. Longo · I. Alabiso · L. Dogliotti
Division of Medical Oncology, Department of Clinical & Biological Sciences, University of Turin at San Luigi Hospital, Regione Gonzole 10,
10043 Orbassano, Turin, Italy
e-mail: marco.tampellini@unito.it

S. Cappia · E. Bacillo · M. Volante · M. Papotti
Division of Pathology, Department of Clinical & Biological Sciences, University of Turin at San Luigi Hospital, Orbassano, Turin, Italy

Introduction

Colorectal carcinoma (CRC), one of the most common types of cancer in Western countries, carries significant morbidity and mortality [3, 12]. The clinical outcome is heterogeneous. Up to 30% of patients bear distant metastases at the time of diagnosis, and another 35% will develop distant spread with tumour progression. Although tumour

stage at diagnosis is a key indicator of prognosis for individual patients, in those with intermediate stages of disease (e.g. Dukes B), survival may vary markedly despite similar clinico-pathological features [11, 14]. Given that other factors probably interfere with tumour growth control and prognosis, a more appropriately defined profile of each tumour is needed to tailor the therapeutic strategy accordingly.

Several molecules and markers have been proposed to select high-risk CRC cases and to provide prognostic indications. Numerous genetic and phenotypic analyses [9, 20] have studied receptors regulating tumour cell growth. The epidermal growth factor receptor (EGFR) is a transmembrane glycoprotein activated by several ligands, including EGF and tumour growth factor alpha (TGFα), which by phosphorylation, initiate a transduction signalling cascade that, in turn, regulates tumour cell growth, differentiation and dissemination. EGFR overexpression was detected in several human cancers, and a significant prognostic value was identified in breast, prostate, lung and oral carcinomas, among others [15]. In CRC, EGFR overexpression was shown to be associated with disease recurrence and decreased survival [14]. Increased EGFR mRNA content was found to be predictive of metastatic potential [13]. The effects and interactions of EGFR ligands, i.e. EGF and TGFα, were also studied in vitro models of CRC where TGFα was shown to activate autocrine circuits with its receptor and determine growth factor independence of CRC cells [2, 22]. In addition, TGFα has been shown to regulate cell adhesion by multiple signalling via specific phosphorylation sites of S6 kinase by activating the extracellular signal-regulated kinase (ERK)/mitogen-activated protein kinase (MAPK) pathway [16, 17]. Furthermore, S6 kinase is known to regulate cell growth and survival by inducing protein synthesis components and inactivating the pro-apoptotic molecule BAD [8]. In clinical studies, TGFα was found to be overexpressed in CRC presenting with synchronous metastases [5], whereas no correlation with serine–treonine kinase (Akt) and MAPK status was evident between primary tumours and metastasis [18]. Further data on the downstream signalling in vivo human models are lacking. To fill this gap, a better understanding of the ligand-receptor-induced downstream signalling cascade is needed.

In recent years, the approval of tailored therapy, targeting EGFR-positive tumours with the monoclonal antibody cetuximab, has attracted new interest in EGFR immunohistochemistry in primary or recurrent CRC as a certified method to select candidate patients for targeted therapy. EGFR can be detected by various methods. Immunohistochemistry—the easiest and least expensive—has shown good correlation with EGFR mRNA analysis [7]. Several antibodies have been developed to reveal the EGFR protein at the membrane level. To date, only the Dako Pharma kit [19] has been officially approved by the US Food and Drug Administration (FDA) as the optimal procedure to detect EGFR in CRC (FDA protocol BL 125084/0, dated February 12th, 2004). No cut-off level has been set for EGFR positivity so that even cases with very few immunoreactive cells can be eligible for cetuximab treatment. Interestingly, some responses have also been recorded in EGFR negative tumours [4]. For this reason, a standardised, highly sensitive (and specific) procedure for EGFR determination is needed.

The aim of this retrospective study was to analyse EGFR expression in relation to that of its ligand TGFα and to explore the activation of the downstream signalling pathway in two patient subsets with CRC tumours: those with limited disease (stage II–III) vs those with distant metastases (stage IV) at diagnosis.

Materials and methods

Materials A total of 101 CRC cases were investigated. From 1999 to 2004, 52 cases of CRC patients that presented with distant metastases at diagnosis at the Division of Medical Oncology of the San Luigi Hospital and University of Turin were retrospectively collected. After a review of the clinical and pathological data, 50 cases were retained for this study in which both histopathological material and complete clinical and follow-up data were available. Two cases were excluded as they were lost to follow-up. All had distant metastases in either the liver (39 cases) or the lung. All patients underwent large bowel resection. In addition, 51 cases with limited tumour stages II and III were collected in the same period in which no distant metastases were present at diagnosis (but 16 developed during disease progression 3–27 months after the operation). The study population was divided into two groups according to tumour stage at diagnosis: Group A comprised 51 patients with stage II and III disease, Group B comprised 50 patients with stage IV tumours. Clinical and pathological parameters were age, sex, tumour location and size, tumour grade and stage, lymph node metastases, type of treatment administered. The study design was approved by our Hospital Institutional Review Board.

Methods All cases were reviewed by two of us (MV, MP) and the pathological parameters re-assessed (including tumour type, grade, stage). A representative paraffin block taken from the deepest areas of invasion of each tumour was selected. Sections serial to that stained with hematoxylin and eosin were collected onto charged slides for immunohistochemistry. An automated immunoperoxidase procedure was employed (Dako Autostainer, DakoCytoma-

tion, Glostrup, Denmark) using standard detection methods based on biotin-free reagents (peroxidase conjugated dextran polymers, EnVision, DakoCytomation). Before starting the immune reaction, endogenous peroxidase activity was blocked with hydrogen peroxide, and antigen retrieval was obtained by protease pre-treatment for EGFR and TGFα and microwaving (citrate buffer pH 6) for the other antibodies tested. Diaminobenzidine was used as chromogen to reveal immune reaction.

Antibodies The primary antibodies for the first 30 cases were monoclonal antibodies to EGFR from different sources: EGFR pharmDX clone 2-18C9 (DakoCytomation), EGFR clone 111.6 diluted 1:50 (Neomarkers-Lab Vision, Fremont, CA), EGFR clone 31G7 diluted 1:200 (Zymed Laboratories, San Francisco; Fig. 1a–c). As the correlation coefficients for Zymed and Neomarkers vs Dako were 0.76 ($p<0.0001$) and 0.54 ($p<0.01$), respectively, all the study samples were immunostained with the Dako kit. All cases were also stained for TGFα (clone 213-4,4 diluted 1:200, Calbiochem, Darmstadt, Germany). Selected cases were stained for downstream signalling molecules of the EGFR pathway (Fig. 2): signal transducer and activator of transcription (STAT3; clone F-2 to the native form, diluted 1:100, Santa Cruz Technology, Santa Cruz, CA); Akt (Ser 473; clone 736E11 to the phosphorylated form, diluted 1:50, Cell Signalling Technology, Beverly, MA); MAP Kinase (clone P44/42 to the phosphorylated form, diluted 1:250, Cell Signalling Technology); mammalian target of rapamycin (mTOR; clone 7C10 to the native form, diluted 1:50, Cell Signalling Technology); p-mTOR (clone 49F9 to the phosphorylated form, diluted 1:50, Signalling Technology); S6 Kinase (Thr 389; clone 1A5 to the phosphorylated form, diluted 1:300, Cell Signalling Technology).

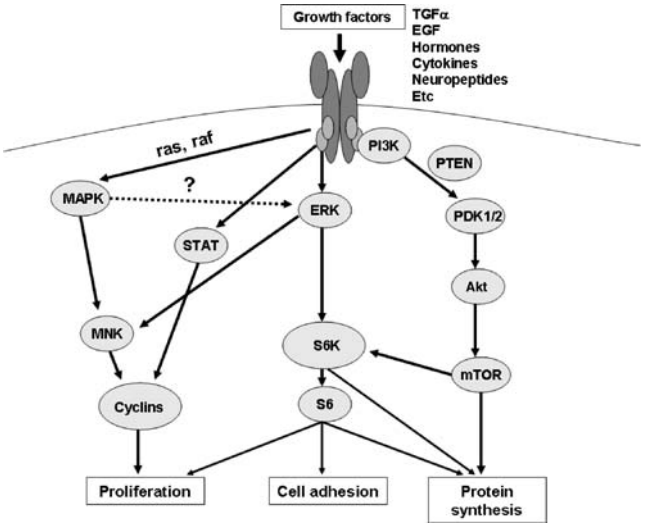

Fig. 2 EGFR/TGFα downstream signalling pathway. *PI3K*: phosphatidylinositol 3-kinase; *PTEN*: phosphatase and tension homolog deleted on chromosome 10; *PDK*: 3-phosphoinositide-dependent protein kinase; *Akt*; *mTOR*; *MAPK*; *ERK*; *STAT*; *S6K*; MNK: MAPK-interacting kinase

Scoring system and statistical evaluation All immunostainings were blindly evaluated by three independent observers (ML, SC, MP). Immune reaction intensity and marker

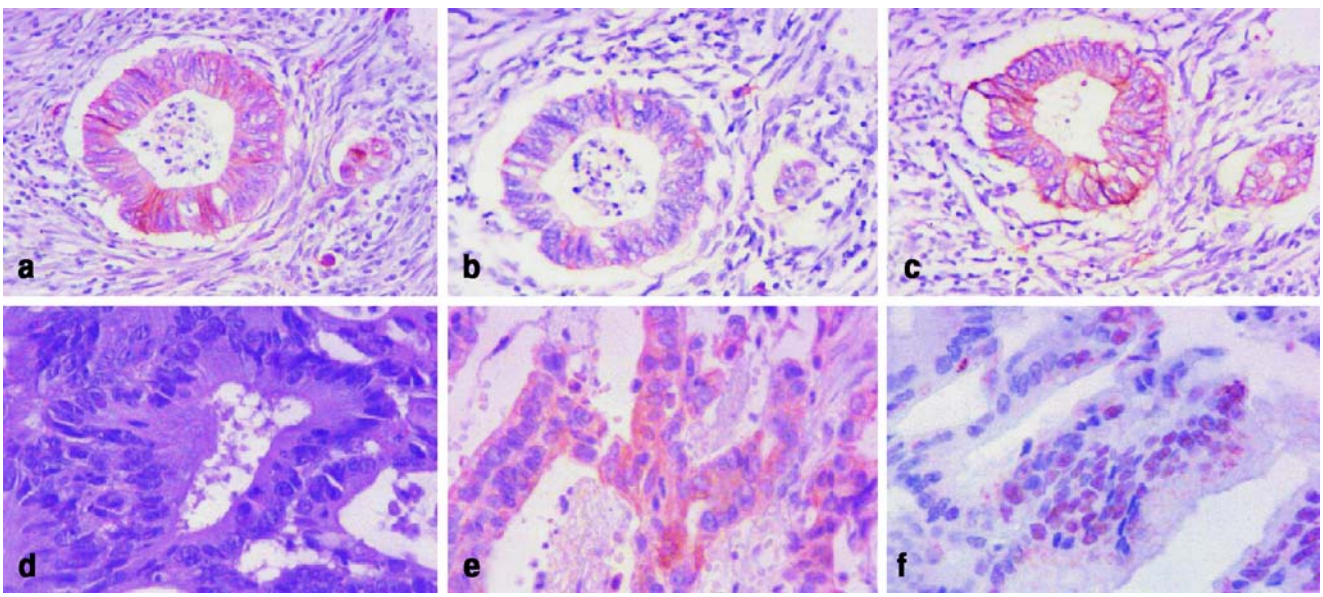

Fig. 1 Immunoreactivity for EGFR in serial sections of a colorectal carcinoma with metastases at diagnosis (case no. 13) using three different antibodies from Dako (**a**), Neomarkers (**b**) and Zymed (**c**). In this case, the immunoreactivity is comparable in the same area using different antibodies (immunoperoxidase, 200×, nuclei counterstained with haemalum). A colorectal carcinoma (case no. 66, **d**) with a strong TGFα cytoplasmic expression (**e**) and S6K nuclear expression in the same area (**f**) (**d**: hematoxylin and eosin; **e**, **f**: immunoperoxidase; 400×)

extension throughout the tumour cells were graded on a 4-point semi-quantitative scale. Intensity was graded as absent (0), weak (1), moderate (2) or strong (3). Marker extension was assigned a score of 1–4: negative (0), reactivity in 1–25% of cells (1), in 26–50% (2), in 51–75% (3), in 76–100% (4). As in similar scoring systems described in the literature [21], the intensity and the extension values of each reaction were summed to produce a final value (0–7). The cases were then divided into a four-tier score system: 0 (no reaction), 1 (weak and focal reaction, values 1–2), 2 (moderate reaction, values 3–5), 3 (intense and/or diffuse reaction, values 6–7). In the statistical analysis, negative and positive cases were compared (any score, 1, 2 or 3). A cut-off value was then selected, where cases scored 1 (focal reaction) were conflated with the negative cases; these (scores 0+1 cases) were compared against the positive cases (scores 2 and 3). The results were statistically evaluated by the chi-square test with Yates' correction, when necessary. Correlation coefficients were computed according to the Spearman method. Non-parametric comparisons for unpaired variables were performed with the Mann–Whitney U test. All statistical computations were performed using SPSS and STATISTICA for Windows software.

Results

Patients Patient characteristics are shown in Table 1. The two groups were similar in gender, age and tumour location. Group B had a higher proportion of grade 3 tumours (30 vs 9.8%; $p=0.02$) and T4 tumours (38 vs 5.9%; $p=0.0002$).

EGFR was positive in 68/101 (67.3%) CRC cases (Table 1). Reactivity was either focal or diffuse and localised on the surface of the tumour cells. Twenty-eight cases had score 1, 24 had score 2 and 16 had score 3. No difference according to tumour grade at diagnosis was evident. However, a trend was noted between grade 2 (26/72 [36.1%] patients) and grade 3 (10/18 [55.6%] patients) tumours when cases with EGFR scores 2 and 3 were pooled together ($p=0.1$). Moreover, no difference in EGFR staining was recorded when patients were grouped by tumour infiltration at diagnosis (T stage; $p=0.99$). No difference was found within Group A patients (stage II and III; 16/27 [59.2%] and 14/24 [58.3%], respectively) testing EGFR positive. The EGFR expression profiles for the two groups are summarised in Table 2 and Fig. 3. EGFR was expressed in 30/51 (58.8%) low-stage cases (Group A) and in 38/50 (76%) stage IV cases (Group B; $p=0.06$). Analysis of EGFR intensity and extension showed that only 14/51 (27.4%) of low-stage cases (Group A) had diffuse (scores 2 and 3) EGFR staining, whereas higher EGFR scores (2 and 3) were recorded in 26/50 (52.0%) cases with advanced disease (Group B). This difference was statistically significant ($p=0.01$). In the patients with no distant metastases at diagnosis (stage II–III, Group A) but who later developed metastases during follow-up, only 6/16 (37.5%) cases were EGFR positive and showed mostly focal staining. This figure differs significantly from that observed in the patients with metastases at diagnosis, indicating that CRCs with synchronous metastases probably have an EGFR profile different from both non-progressing and progressing cases at follow-up.

TGFα was expressed in 79/101 (78.2%) cases (Table 1), showing a focal or a diffuse pattern in 34 and 45 cases, respectively (Fig. 1e). The reactivity was intense cytoplasmic, and the peritumoural normal mucosa was generally negative. TGFα expression profiles are summarised in Table 3 and Fig. 3. No differences were found between stage II and III patients (19/27 [70.4%] and 18/24 [75%]) testing TGFα positive or when grouped according to

Table 1 Clinico-pathological data and immunohistochemical findings in 101 resected CRC in stage II–III (Group A) or IV (Group B)

	Entire population	Group A (II/III)	Group B (IV)
Feature			
No. of cases	101	51	50
Gender (M/F)	61/40	35/16	26/24
Age (median, years)	66.7	68.9	64.2
Tumour location			
Right/Transverse	30	15	15
Left	48	27	21
Rectum	23	9	14
Tumour grade (1+2/3)	81/20	46/5	35/15
T at diagnosis 1/2/3/4	3/6/70/22	3/5/40/3	0/1/30/19
N at diagnosis 0/1/2	34/32/35	27/15/9	7/17/26
Tumour stage (II/III/IV)	27/24/50	27/24/0	0/0/50
EGFR+ no. (%)	68 (67.3)	30 (58.8)	38 (76.0)
TGFα no. (%)	79 (78.2)	37 (72.5)	42 (84.0)
EGFR+ and TGFα no. (%)	57 (56.4)	23 (45.1)	34 (68.0)

Table 2 EGFR immunoreactivity according to tumour stage at diagnosis

Stage at diagnosis	EGFR score ($p=0.04$)			
	0	1	2	3
Group A (St II/III)	21 (41.2)	16 (31.4)	11 (21.6)	3 (5.8)
Group B (St IV)	12 (24.0)	12 (24.0)	13 (26.0)	13 (26.0)

Data are expressed as absolute number of patients and percentage of the corresponding group.

Table 3 TGFα immunoreactivity according to tumour stage at diagnosis

Stage at diagnosis	TGFα score (p=0.09)			
	0	1	2	3
Group A(St II/III)	14 (27.5)	19 (37.3)	12 (23.5)	6 (11.7)
Group B(St IV)	8 (16.0)	15 (30.0)	12 (24.0)	15 (30.0)

Data are expressed as absolute number of patients and percentage of the corresponding group.

tumour grade or T stage. Thirty-seven cases out of 51 (72.5%) in Group A and 42/50 (84.0%) samples in Group B were positive (p=0.16). Diffuse (scores 2 and 3) TGFα immunostaining was found in 18/51 (35.3%) patients from Group A and in 27/50 (54.0%) from Group B (p=0.06). TGFα reactivity was noted in 11/16 (68.8%) stage II–III patients who developed distant metastasis during follow-up. Analysis of diffuse immunostaining in the same sub-group showed that 7/16 (43.8%) tested positive.

Co-expression Variable degrees of co-expression intensity were found in 57/101 cases (56.4%; Fig. 4); 11 cases lacked both receptor and ligand immunoreactivity. Of the CRC patients with stage II–III tumours at diagnosis (Group A), 23/51 (45.1%) presented TGFα/EGFR co-expression, whereas 34/50 (68.0%) of Group B patients were concomitantly positive (p=0.02); diffuse TGFα/EGFR co-expression (scores 2 and 3) was found in 6/51 (11.8%) in Group A and 16/50 (32.0%) in Group B (p=0.01) patients. In stage II–III patients at diagnosis but who later developed distant metastases, 4/16 (25.0%) co-expressed EGFR and TGFα; the reactivity was weak and/or focal in all cases. No correlation was found between EGFR and/or TGFα expression and any of the clinico-pathological parameters (including age, sex, tumour location and size and lymph node metastases).

Signalling molecules Randomly selected cases (Table 4) were immunostained for downstream molecules of the EGFR pathways (Table 5, Fig. 2). Generally, positivity to Akt was low (8/50, 16.0% cases), whereas positivity to the other signalling molecules was higher by comparison (40.0% to MAPK, 78.0% to STAT3, 53.4% to ribosomal protein S6 kinase [S6K], 75.0% to mTOR, 87.5% to the phosphorylated form of mTOR). Analysed by tumour stage at diagnosis, no evident differences emerged between STAT3, MAPK, mTOR and p-mTOR. A non-statistically significant trend for higher Akt immunostaining was noted in Group B compared with Group A (4/16 [25.0%] vs 4/34 [11.8%]). There was a higher proportion of samples expressing S6K in Group B (19/27, 70.4%) than in Group A (12/31, 38.7%; p=0.02). This difference was maintained

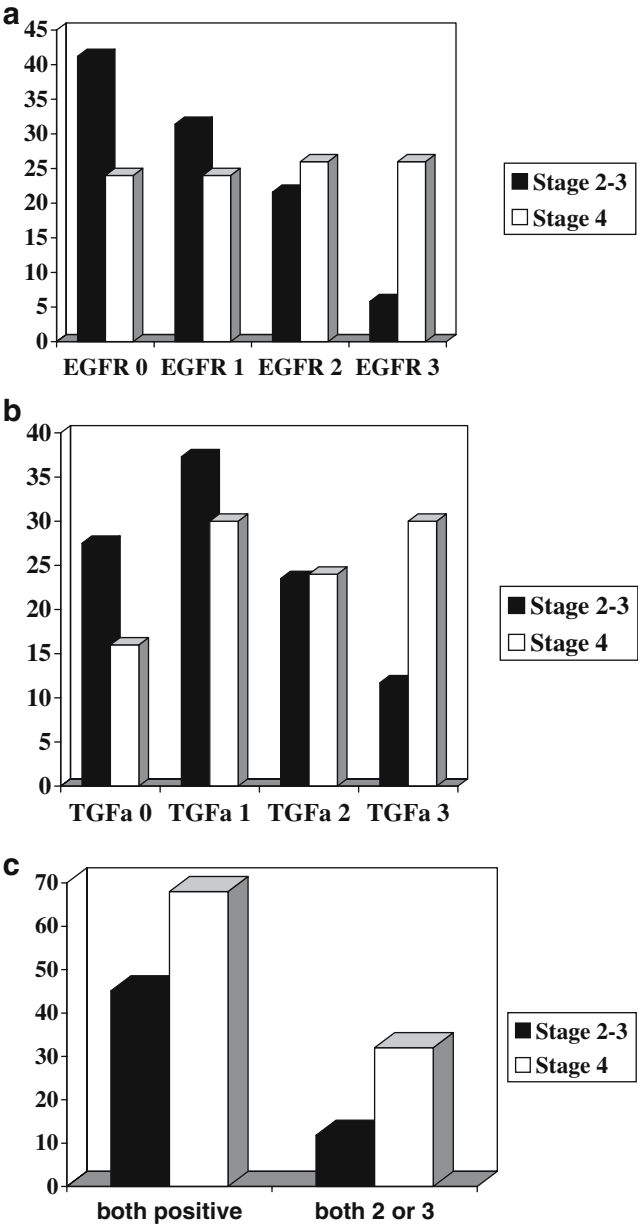

Fig. 3 EGFR- (**a**) and TGFα- (**b**) positive staining according to score and tumor stage at diagnosis (X^2p, 0.04 and 0.09, respectively). Concomitant EGFR and TGFα positivities were subsequently extrapolated (**c**). p Value for concomitant positivity was 0.2; p value for concomitant scores 2 and 3 positivities was 0.01. Data are expressed as percentage of patient population

even when stage T4 tumours with similar percentages of S6K reactivity were excluded, demonstrating that its activation is independent of local tumour invasiveness (Group B 11/15 [73.3%] vs Group A 10/29 [34.5%]; p=0.03).

No significant correlation was found between EGFR, TGFα and STAT3, Akt, mTOR or p-mTOR. MAPK positivity was found in 16/20 (80.0%) of EGFR positive cases and in 18/30 (60.0%) of EGFR negative tumours (p= 0.2). When tumours with only focal EGFR immunostaining and the negative ones were pooled together (i.e. at a cut-off

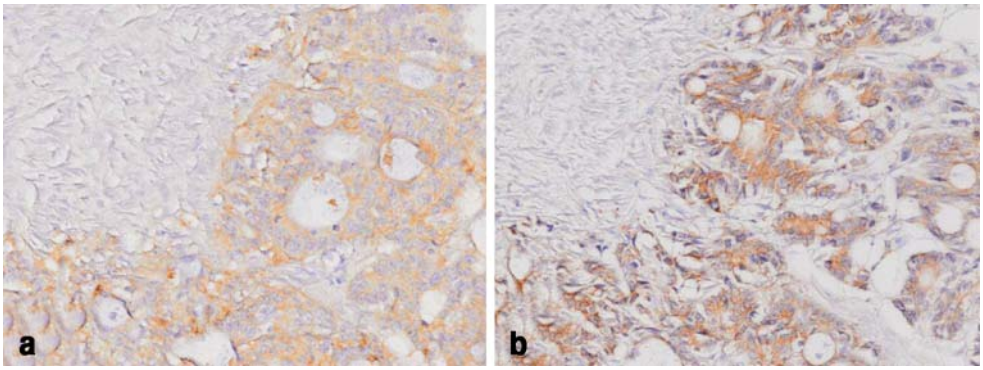

Fig. 4 In these serial sections of a colorectal carcinoma (case no. 45), the invasive front of the adenocarcinoma into the subserosal adipose tissue has a positive staining for both EGFR (**a**) and TGFα (**b**) in most tumor cells (immunoperoxidase, 200×; nuclei counterstained with haemalum)

of 25% tumour cells positive and/or weak reaction), MAPK positivity was noted in 10/30 (33.3%) low-EGFR expressing cases and in 13/20 (65.0%) tumours with high EGFR expression (scores>2; $p=0.02$). Tumours with diffuse (scores 2 or 3) co-expression of EGFR and TGFα were MAPK positive in 9/15 (60.0%) cases, whereas this was the case in only 5/20 (25.0%) samples with low EGFR/TGFα expression ($p=0.03$).

The phosphorylated form of S6K was found in 25/42 (59.5%) EGFR positive cases and in 6/16 (37.5%) EGFR negative tumours ($p=0.1$; Fig. 1f). When the patients were grouped by EGFR immunostaining score, 11/29 (37.9%) of those with negative/focal (score 0 or 1) and 20/29 (69.0%) of those with diffuse (score 2 or 3) immunostaining demonstrated the phosphorylated form of S6K ($p=0.01$). In 14/18 (77.8%) tumours with diffuse (score 2 or 3) EGFR and TGFα, co-expression were S6K positive, whereas only 7/20 (35.0%) of those with negative/focal (score 0 or 1) resulted positive ($p=0.02$).

Of the 46 samples tested for both MAPK and S6K, 20 (43.5%) were concomitantly negative and 14 (30.4%) concomitantly positive, with a general concordance of 73.9% (Spearman $r=0.5$, $p=0.02$; $X^2p=0.03$). Correlative data for EGFR, MAPK and S6K staining are summarised in Table 6.

Table 4 Characteristics of the cases tested for downstream molecules

Characteristics	
Feature	
No. of cases	50
Median age (years) (range)	68 (41.5–85.2)
Gender (M/F)	30/20
Tumor location	
Right/Transverse	15
Left	26
Rectum	9
Tumor grade 1+2/3	42/8

Discussion

In this study, we have shown that co-expression of immunoreactive EGFR and TGFα is significantly higher in CRC with synchronous distant metastases at diagnosis than in CRC presenting at a lower tumour stage, irrespective of the subsequent type of evolution with disease progression to distant spread or long disease-free survival. Colonic tumours with an early metastatic behaviour presented a higher proportion of S6K expressing cells.

Patients in Group B (i.e. those with distant metastases at diagnosis) presented a higher proportion of pT4 tumours than their counterparts. A hypothetical delay in the diagnosis of these patients might be the explanation for the higher tumour aggressiveness in this group. It should be underlined, however, that patients in Group B also presented a higher proportion of grade 3 tumours, suggesting that an intrinsic aggressiveness independent of the time of diagnosis might explain this discrepancy. Moreover, the results of EGFR, TGFα and S6K were similar when patients with pT4 tumours were excluded from the statistical analysis. These findings indicate that EGFR/TGFα/S6K activation might lie at the basis of a higher metastatic behaviour of cancer cells.

Immunohistochemistry—the easiest method to identify EGFR in pathology specimens for pharmacotherapeutic purposes—has several limitations. Antigen preservation in old cases is problematic, as long-standing filing of paraffin blocks has been shown to reduce EGFR immunoreactivity [1]. The cases presenting our series were filed for no more than 8 years, and the immunoreactivity seemed relatively well preserved in all specimens and with different antibodies. Another drawback to the procedure is its intrinsic sensitivity, which is unable to identify low EGFR protein expressing cases. This potentially scarce sensitivity may also explain the recent observation of EGFR negative cases of CRC that responded to cetuximab therapy [4]. Nonetheless, a recent study has shown that the copy number of the EGFR receptor mRNA is a predictor of response to cetuximab therapy [10]. A final consideration concerns

Table 5 Downstream molecule immunostaining

	Entire population		Group A (II/III)		Group B (IV)		*p*
	No. tested		No. tested		No. tested		
Molecule							
STAT 3	50	39 (78.0)	34	26 (76.5)	16	13 (81.2)	ns
Akt	50	8 (16.0)	34	4 (11.8)	16	4 (25.0)	ns
MAPK	50	20 (40.0)	34	13 (38.2)	16	7 (43.8)	ns
mTOR	50	24 (75.0)	34	19 (55.9)	16	8 (50.0)	ns
p-mTOR	50	28 (87.5)	34	24 (70.6)	16	11 (68.8)	ns
S6K	58	31 (53.4)	31	12 (38.7)	27	19 (70.4)	0.02

Data are expressed as absolute number of positive samples and relative percentage in brackets

selection of the tumour area to assess and score EGFR reactivity, as EGFR assessed in the deepest areas of tumour invasion seem to better correlate with decreased survival [6]; in fact, these areas usually contain the largest amount of strongly positive (3+) cells. In our cases, representative tissue blocks were selected on the basis of this observation, and the scoring was obtained in the areas of highest labelling. Incidentally, these areas were also those with the strongest TGFα expression.

In our opinion, a major matter of interest is the concurrent expression of TGFα, and possibly of other ligands, as an indirect indication of receptor activity. Additional information on receptor system functionality may be gained by analysing downstream signalling molecules. We tested the presence of phosphorylated key molecules and found that most were present, although none is exclusive to the EGFR receptor system. Tumours with a metastatic behaviour ab initio presented a higher proportion of cells with EGFR and TGFα co-expression, activation of the MAPK pathway and phosphorylation in Thr-389 of the S6K protein. This finding is consistent with in vitro data demonstrating the TGFα-mediated regulation of cell adhesion via the ERK/MAPK pathway and the activation of ribosomal S6K [17]. No correlations were found between the metastatic behaviour of the tumour, EGFR/TGFα expression and Akt, mTOR and STAT3. The Akt staining rate in our series was lower than that reported elsewhere [18]. This was probably due to a different phosphorylation site (Ser-473) recognised by the monoclonal antibody used in our study. Even so, a higher proportion of tumours expressed mTOR and its phosphorylated form. These findings need further validation in larger series.

Table 6 Correlative data for EGFR, MAPK and S6K staining (46 cases)

	MAPK	
	Negative	Positive
EGFR 0–1		
S6K negative	13 (28.3)	3 (6.5)
S6K positive	5 (10.9)	4 (8.7)
EGFR 2–3		
S6K negative	7 (15.2)	1 (2.2)
S6K positive	3 (6.5)	10 (21.7)

Data are expressed as absolute number of positive staining (and percentage of the entire group)

The observation that the co-expression of TGFα and EGFR is significantly higher in CRC with synchronous metastases at diagnosis is novel, although a previous report has indicated that TGFα alone was overexpressed in cancers with synchronous metastases [5]. This is not surprising given the known association of EGFR and TGFα expression with biological and clinical aggressiveness of CRC demonstrated in vitro models [16, 17]. What was unexpected was the partially different profile of ligand/receptor expression in CRC that presented in stage II and III and developed distant metastases at follow-up; these cases were expressing EGFR and TGF at a frequency overlapping that of the lower stage control instead of that of advanced CRC at diagnosis. This may indicate that EGFR is implicated in tumour progression of a fraction of CRCs characterised by a markedly aggressive behaviour ab initio and an early capacity for distant dissemination, at variance with other CRCs that follow a less aggressive and/or slower course. Whether this finding may be useful for selecting candidates for early treatment with EGFR inhibitors at the time of CRC diagnosis remains to be ascertained with specifically designed clinical trials. Probably, those with metastatic CRC at diagnosis may be better candidates for EGFR targeted treatments with cetuximab in first-line chemotherapy based on the significantly higher expression of both the ligand (TGFα) and the receptor in their tumours.

In conclusion, in our series, the fraction of CRC with distant metastases at diagnosis significantly expressed higher amounts of immunoreactive EGFR, its ligand (TGFα) and S6K. This finding could hold interest when planning treatments targeting the EGFR as first-line therapy at the time of diagnosis of advanced colorectal carcinomas (immediately after surgery, if applicable) and prompt new experiments focusing on the role of therapeutic agents targeting downstream molecules.

References

1. Atkins D, Reiffen KA, Tegtmeier CL, Winther H, Bonato MS, Storkel S (2004) Immunohistochemical detection of EGFR in paraffin-embedded tumour tissue: variation in staining intensity due to choice of fixative and storage time of tissue sections. J Histochem Cytochem 52:893–901
2. Awwad RA, Sergina N, Yang H, Ziober B, Willson JK, Zborowska E, Humphrey LE, Fan R, Ko TC, Brattain MG, Howell GM (2003) The role of transforming growth factor alpha in determining growth factor independence. Cancer Res 63:4731–4738
3. Black RJ, Bray F, Ferlay J, Parkin DM (1997) Cancer incidence and mortality in the European Union: cancer registry data and estimates of national incidence for 1990. Eur J Cancer 33:1075–1107
4. Chung KY, Shia J, Kemeny NE, Shah M, Schwartz GK, Tse A, Hamilton A, Pan D, Schrag D, Schwartz L, Klimstra DS, Fridman D, Kelsen DP, Saltz LB (2005) Cetuximab shows activity in colorectal cancer patients with tumours that do not express the epidermal growth factor receptor by immunohistochemistry. J Clin Oncol 23:1803–1810
5. De Jong KP, Stellema R, Karrenbeld A, Koudstaal J, Gouw AS, Sluiter WJ, Peeters PM, Slooff MJ, De Vries EG (1998) Clinical relevance of transforming growth factor alpha, epidermal growth factor receptor, p53, and Ki67 in colorectal liver metastases and corresponding primary tumours. Hepatology 28:971–979
6. Goldstein NS, Armin M (2001) Epidermal growth factor receptor immunohistochemical reactivity in patients with American Joint Committee on Cancer stage IV colon adenocarcinoma: implications for a standardized scoring system. Cancer 92:1331–1346
7. Hanawa M, Suzuki S, Dobashi Y, Yamane T, Kono K, Enomoto N, Ooi A (2006) EGFR protein overexpression and gene amplification in squamous cell carcinomas of the esophagus. Int J Cancer 118:1173–1180
8. Harada H, Andersen JS, Mann M, Terada N, Korsmeyer SJ (2001) p70S6 kinase signals cell survival as well as growth, inactivating the pro-apoptotic molecule BAD. Proc Natl Acad Sci USA 98:9666–9670
9. Hemming AW, Davis NL, Kluftinger A, Robinson B, Quenville NF, Liseman B, LeRiche J (1992) Prognostic markers of colorectal cancer: an evaluation of DNA content, epidermal growth factor receptor, and KI 67. J Surg Oncol 51:147–152
10. Moroni M, Veronese S, Benvenuti S, Marrapese G, Sartore-Bianchi A, Di Nicolantonio F, Gambacorta M, Siena S, Bardelli A (2005) Gene copy number for epidermal growth factor receptor (EGFR) and clinical response to antiEGFR treatment in colorectal cancer: a cohort study. Lancet Oncol 6:279–286
11. O'Connell JB, Maggard MA, Ko CY (2004) Colon cancer survival rates with the new American Joint Committee on Cancer sixth edn. staging. J Natl Cancer Inst 96:1420–1425
12. Parkin DM, Pisani P, Ferlay J (1999) Estimates of the worldwide incidence of 25 major cancers in 1990. Int J Cancer 80:827–841
13. Radinsky R, Risin S, Fan D, Dong Z, Bielenberg D, Bucana CD, Fidler IJ (1995) Level and function of epidermal growth factor receptor predict the metastatic potential of human colon carcinoma cells. Clin Cancer Res 1:19–31
14. Resnick MB, Routhier J, Konkin T, Sabo E, Pricolo VE (2004) Epidermal growth factor receptor, c-met, beta-catenin, and p53 expression as prognostic indicators in stage II colon cancer: a tissue microarray study. Clin Cancer Res 10:3069–3075
15. Salomon DS, Brandt R, Ciardiello F, Normanno N (1995) Epidermal growth factor-related peptides and their receptors in human malignancies. Crit Rev Oncol Hematol 19:183–232
16. Sawhney RS, Sharma B, Humphrey LE, Brattain MG (2003) Integrin α_2 and extracellular signal-regulated kinase are functionally linked in highly malignant autocrine transforming growth factor-α-driven colon cancer cells. J Biol Chem 278:19861–19869
17. Sawhney RS, Cookson MM, Sharma B, Hauser J, Brattain MG (2004) Autocrine transforming growth factor α regulates cell adhesion by multiple signalling via specific phosphorylation sites of p70S6 kinase in colon cancer cells. J Biol Chem 279:47379–47390
18. Scartozzi M, Bearzi I, Berardi R, Mandolesi A, Pierantoni S, Casinu S (2006) Epidermal growth factor receptor (EGFR) downstream signaling pathway in primary colorectal tumours and related metastatic sites: optimizing EGFR target treatment options. Proceedings of the American Society of Clinical Oncology Gastrointestinal cancers symposium, San Francisco, CA, Jan 26–28
19. Spaulding DC, Spaulding BO (2002) Epidermal growth factor receptor expression and measurement in solid tumours. Semin Oncol 29:45–54
20. Westra JL, Plukker JT, Buys CH, Hofstra RM (2004) Genetic alterations in locally advanced stage II/III colon cancer: a search for prognostic markers. Clin Colorectal Cancer 4:252–259
21. Xu C, McLeod H (2004) Pharmacogenomic profiling of the PI3K/PTEN-AKT-mTOR pathway in common human tumours. Int J Oncol 24:893–900
22. Ziober BL, Willson JK, Humphrey LE, Childress-Fields K, Brattain MG (1993) Autocrine transforming growth factor-α is associated with progression of transformed properties in human colon cancer cells. J Biol Chem 268:691–698

Virchows Arch (2007) 450:329–333
DOI 10.1007/s00428-006-0364-5

ORIGINAL ARTICLE

Comparison of clinical and post-mortem findings in intensive care unit patients

Calliope Maris · Benoît Martin · Jacques Creteur · Myriam Remmelink · Michael Piagnerelli · Isabelle Salmon · Jean-Louis Vincent · Pieter Demetter

Received: 7 August 2006 / Revised: 27 October 2006 / Accepted: 27 December 2006 / Published online: 25 January 2007
© Springer-Verlag 2007

Abstract The autopsy has long been regarded as an important tool for clinical confrontation, education and quality assurance. The aims of this study were to examine the correlation between the clinical diagnosis and autopsy findings in adult patients who died in an intensive care unit (ICU) and to identify the types of errors in diagnosis to improve quality of care. Autopsies from 289 patients who died in the ICU during a 2-year period were studied. Post-mortem examination revealed unexpected findings in 61 patients (21%) including malignancy, pulmonary embolism, aspergillosis, myocardial or mesenteric infarction and unsuspected bacterial, viral or fungal infection. These unexpected findings were classified as Goldman class I errors in 17 (6%), class II in 38 (13%) and class III in six (2%) cases. Although the incidence of unexpected findings with clinical significance was low, post-mortem examination remains a valuable source of pertinent information that may improve the management of ICU patients.

Keywords Autopsy · Intensive care · Diagnostic discrepancy · Post-mortem examination

C. Maris · B. Martin · M. Remmelink · I. Salmon (✉) · P. Demetter
Department of Pathology, Erasme University Hospital,
808 Route de Lennik,
Brussels 1070, Belgium
e-mail: isalmon@ulb.ac.be

J. Creteur · M. Piagnerelli · J.-L. Vincent
Department of Intensive Care, Erasme University Hospital,
Free University of Brussels,
Brussels, Belgium

Introduction

During the past 30 years, autopsy rates have decreased worldwide [2, 40, 49] partly because of the availability of new and more effective technologies for diagnostic procedures, particularly in terms of imaging techniques. Other reasons have also been suggested, including reluctance to ask relatives for their consent and fear of medico-legal implications [23, 30]. Pathologists themselves have sometimes become reluctant to perform autopsies because of the possible infectious risks and the lack of evidence of the usefulness of the autopsy examination [20, 27, 30]. Delays in the communication of autopsy results by pathologists may also contribute to the reduced autopsy rates [32, 33, 42].

However, studies on autopsies have demonstrated their usefulness not only in determining the exact cause of death but also in visualising how a patient responded to treatment. The autopsy is often considered a fundamental element of quality control in medicine, being the ultimate audit of clinical practice [26, 28, 51]. The persisting discordance between clinical and autopsy diagnoses is also an argument for continuing to perform autopsies [9, 17, 34, 36]. Studies carried out during the past 20 years have failed to show a significant increase in diagnostic agreement between ante- and post-mortem diagnoses; this persistent discord is observed in all groups of patients (neonatal, paediatric, elderly and psychiatric patients) and in all hospitals, whether affiliated to a university or not [7, 14, 15, 22, 24–26, 44, 50, 52, 53]. The autopsy also provides an excellent basis for teaching students the fundamentals of anatomy and the manifestations of disease. It provides important information on the effects of newer drugs on normal and on diseased tissues [3, 37, 47] and is a valuable tool for detecting and evaluating emerging diseases [28, 29].

Published discrepancy rates between ante- and post-mortem diagnoses vary between 10 and 50% depending on the criteria for post-mortem examination, the completeness of the post-mortem examination, the methods used to evaluate the differences and the population studied [7, 8, 26, 34, 41, 43, 45, 53]. Despite all the supportive measures available for the treatment of critically ill patients, the difficulty in obtaining an adequate medical history from these patients and the speed at which their critical condition develops can prevent the ICU physician from making a diagnosis that, if established, would probably prevent the death of these patients [19]. The objective of the present study was to compare pre- and post-mortem diagnostic findings and to determine the types of errors in an ICU-patient population to improve quality control of future care.

Patients and methods

We reviewed the clinical and post-mortem findings of all patients who died in the Department of Intensive Care of Erasme University Hospital between January 1, 2004 and December 31, 2005 and who underwent post-mortem examination. This department includes five medico-surgical ICUs with 3,000 admissions a year and a 13% mortality rate. Complete body autopsies were performed within 48 h of death, and the procedure included macroscopic and microscopic assessment of all internal organs and the brain when indicated (neurological alterations or specific concerns regarding central nervous system pathology). As recommended by the Association of Directors of Anatomic and Surgical Pathology [1], post-mortem examinations were performed after a written Quality Control and Quality Assurance plan for our Department of Pathology. Data obtained from the charts included age, sex, length of ICU and hospital stay and major clinical findings, including the presumed cause of death and underlying diseases. Autopsy diagnoses included histological and immunohistochemical findings as listed in the final autopsy reports. To avoid subjectivity in the interpretation of histological findings, a second staff pathologist had been consulted in doubtful cases.

The comparisons between ante- and post-mortem diagnoses were classified as major and minor discrepancies or as a complete agreement according to the classification proposed by Goldman et al. [17]. According to this classification, a class I discrepancy is a missed major diagnosis that would have changed patient management and might have resulted in cure or prolonged survival. A class II discrepancy includes a missed major diagnosis that would not have modified ongoing patient care. A class III discrepancy refers to a missed minor diagnosis associated with the terminal disease but not directly responsible for death, and a class IV discrepancy refers to other missed minor diagnoses. In Goldman class V, there is a complete agreement between clinical and post-mortem diagnoses. In case of multiple unexpected findings, only the most severe level of discrepancy was considered.

Statistical analysis included a chi-square test or Fisher's exact test to compare categorical variables and a Student's t test to compare mean values. A p value less than 0.05 was considered as statistically significant.

Results

Study population

Of the total of 786 patients who died in the 2-year period, 289 (37%) had a post-mortem examination. Refusal of the family was the most frequent reason for not performing an autopsy. For the autopsy cases, the male to female ratio was 1.5, and the median age was 71 years (range, 19–95 years). Of the autopsy population, 19.5% had been admitted to the ICU immediately after surgery. Among the non-surgical patients, the main reason for admission was neurological problems.

The characteristics of these patients are presented in Table 1.

Comparison of clinical and post-mortem diagnoses

Post-mortem examinations revealed unexpected findings in 61 (21%) patients, which were class I in 17 (6%), class II in 38 (13%) and class III in six (2%) patients. The major discrepancies (class I and II) are presented in Table 2 and included fungal, bacterial and viral infection, pulmonary embolism, mesenteric infarction, acute pancreatitis, major haemorrhage and myocardial infarction. Minor findings included non-metastatic malignancy, kidney infarction and lymphangioleiomyomatosis.

Major discrepancies were detected more frequently in the 68 (23.5%) patients staying more than 10 days than in those staying fewer than 10 days in the ICU (31% vs 15%,

Table 1 Characteristics of patients undergoing post-mortem examination after dying in the ICU

Characteristics of patients	
No. of patients	289
Age (years)	71 (19–95)
Male/Female	172/117
Hospital stay (days)	6 (0–167)
ICU stay (days)	3 (0–97)
Patients admitted directly after surgery	57
Patients admitted directly after cardiac surgery	17

Data for age, hospital stay and ICU stay are presented as median (range).

Table 2 Major discrepancies (Goldman class I and II) found at post-mortem examination of 289 patients who died in the ICU

	Causes	No. of discrepancies
Class I	Aspergillosis	7
	Pulmonary embolism	3
	Other infection (viral, fungal)	2
	Acute pancreatitis	2
	Myocardial infarction	2
	Mesenteric infarction	1
Class II	Malignancy	12
	Myocardial infarction	6
	Infection (viral, fungal)	5
	Infection (bacterial)	5
	Cerebral haemorrhage	4
	Cirrhosis	2
	Pulmonary embolism	1
	Abdominal haemorrhage	1
	Other	2

p=0.008; Table 3). No statistical difference was observed with regard to sex or age.

Discussion

Our autopsy rate of 37% is greater than the minimal rate of 25% considered adequate [54] and close to the 35% considered as ideal [55]. Post-mortem examination revealed unexpected findings in 21% of our patients, with important diagnoses like malignancy, various types of infection, myocardial or mesenteric infarctions and pulmonary embolism. These unexpected findings were considered as class I in 6% and as class II in 13% of the cases. These results are comparable with our previous study [13] where the discrepancy rate was 23%. Other studies have reported major diagnostic discrepancies in 5–40% of all hospitalised patients and in 7–32% of ICU patients [7, 10, 11, 15, 31, 43, 46, 48, 50]. These differences among studies may be explained not only by different ICU populations but also by differences in the indications for autopsy. Studies from hospitals in which autopsies are predominantly performed in complicated cases may be expected to show higher discrepancy rates [39]. On the other hand, Ong et al. [38] reported a rate as low as 3% for missed major (class I) diagnoses in a study that included only trauma- and burn-related deaths in the ICU.

Table 3 Discrepancies with regard to sex, age and length of stay in the ICU

		Class I and II	Class III–V	p value
Sex	Male	34	138	0.76
	Female	21	96	
Age	<60 years	11	68	0.24
	>60 years	44	166	
ICU stay	<10 days	34	187	0.008
	>10 days	21	47	

Several autopsy studies have reported that infections, particularly fungal infections, are the most common discrepant finding [34, 35, 43, 45, 46]. The methods available to diagnose fungal infections in patients do not reliably differentiate colonization from systemic infection, and blood cultures (indicating invasive infection) are negative in 50% of patients with invasive candidiasis [16]. The often rapid fatal outcome after ICU admission suggests that colonization with fungi can occur before ICU admission [12].

In our present series, unexpected fungal infections were identified in only nine patients. Infections were the most frequently missed major diagnoses in the study by Nadrous et al. [35], with a total of 26 missed infections, of which 13 were fungal. Of these fungal infections, three were categorised as type I discrepancies. Silfvast et al. [46] reported that five of the eight class I discrepancies in their analysis of 346 autopsy reports on ICU patients were infections that occurred in patients already being treated for another infection, highlighting the difficulties in diagnosing infections in ICU patients. Previous studies have suggested that transplant recipients may be more prone to missed infections [34, 50]. Mort and Yeston [34] found that 85% of missed diagnoses in a surgical population had an infectious aetiology. Although it may be argued that terminal infections, especially disseminated aspergillosis, would not have been treated more effectively by earlier diagnosis, as new therapies emerge [21], it remains important to recognise atypical presentations of infection, especially in immunocompromised patients. In the present series, 19 of 55 major discrepancies (class I and class II) were of an infectious origin. With regard to the post-surgical patients, three of nine major discrepancies were infections; in these three cases, invasive aspergillosis was detected, and in one of the three patients, immunohistochemistry revealed the presence of cytomegalovirus in lung and colon tissues and of herpes simplex virus in the oesophagus. This patient, however, was immunocompromised with a known non-Hodgkin's lymphoma.

Early autopsy studies (before 1970) reported clinically undiagnosed malignancies in 18–35% of patients [5]. Since then, newer diagnostic techniques and improved clinical acumen gained from previous autopsy studies have contributed to a decline in the rate of detection of undiagnosed neoplastic diseases to as low as 4% in a series by Goldman et al. [18]. In the present series, 12 cases of malignancy were identified as major discrepancies. Likewise, we detected four cases of clinically undiagnosed pulmonary embolism, emphasising the importance of maintaining a

high index of suspicion for theses diagnoses in the critically ill [6, 7, 50].

Myocardial infarction is also a commonly missed major diagnosis. Perkins et al. [39] found that only 55% of patients undergoing a post-mortem examination had an electrocardiogram performed at any stage during their ICU stay. These authors suggested that the index of suspicion for ischaemic heart disease is inappropriately low in the critically ill patient. Although an electrocardiogram is performed almost every day in our ICU, post-mortem examination still revealed myocardial infarction as a major discrepancy in eight patients.

We found a higher rate of major discrepancies in patients staying more than 10 days in the ICU. Mort and Yeston [34] reported that patients staying more than 48 h were more likely to have a major discrepancy than those who died within 48 h of ICU admission. Other studies, however, have reported no relation between the length of stay and post-mortem findings [4, 10, 15, 35, 39].

There are several limitations of this study, including that this is a retrospective analysis and that the diagnostic work-up of each individual was not critically reviewed; it is possible that variability in the investigation influenced the incidence of missed diagnoses. The strength of the study is the large number of patients hospitalised in a large medico-surgical department of intensive care. Nevertheless, these findings from an academic hospital may not be applicable to other units.

In conclusion, this study reveals a number of significant discrepancies between clinical diagnoses before death and post-mortem findings, even in a large academic institution. Our observations reinforce the importance of the post-mortem examination in identifying suspected or unexpected diagnoses, even in patients receiving close monitoring and intensive care. The post-mortem examination should not be seen as a means of providing evidence of clinical malpractice but rather as a positive educational tool to improve patient care in an attempt to reduce the number of clinically missed diagnoses; autopsy should be considered in every patient who dies in the ICU.

Acknowledgement The authors declare that the experiments comply with the current laws of Belgium.

This work has been carried out with the support of grants awarded by the "Fondation Yvonne Boël" (Brussels, Belgium).

References

1. Association of Directors of Anatomic and Surgical Pathology (1991) Recommendations on quality control and quality assurance in anatomic pathology. Am J Surg Pathol 15:1007–1009
2. Baker PB, Zarbo RJ, Howanitz PJ (1996) Quality assurance of autopsy face sheet reporting, final autopsy report turnaround time, and autopsy rates: a College of American Pathologists Q-Probes study of 10,003 autopsies from 418 institutions. Arch Pathol Lab Med 120:1003–1008
3. Baron JH (2000) Clinical diagnosis and the function of the autopsy. J R Soc Med 93:463–466
4. Battle RM, Pathak D, Humble CG, Key CR, Vanatta PR, Hill RB, Anderson RE (1987) Factors influencing discrepancies between premortem and postmortem diagnoses. JAMA 258:339–344
5. Bauer FW, Robbins SL (1972) An autopsy study of cancer patients. I. Accuracy of the clinical diagnoses (1955 to 1965) Boston City Hospital. JAMA 221:1471–1474
6. Berlot G, Dezzoni R, Viviani M, Silvestri L, Bussani R, Gullo A (1999) Does the length of stay in the intensive care unit influence the diagnostic accuracy? A clinical-pathological study. Eur J Emerg Med 6:227–231
7. Blosser AS, Zimmerman HE, Stauffer JL (1998) Do autopsies of critically ill patients reveal important findings that were clinically undetected? Crit Care Med 26:1332–1336
8. Boers M, Nieuwenhuyzen Kruseman AC, Eulderink F, Hermans J, Thompson J (1988) Value of autopsy in internal medicine: a 1-year prospective study of hospital deaths. Eur J Clin Investig 18:314–320
9. Burton EC, Troxclair DA, Newman WP 3rd (1998) Autopsy diagnoses of malignant neoplasms: how often are clinical diagnoses incorrect? JAMA 280:1245–1248
10. Combes A, Mokhtari M, Couvelard A, Trouillet JL, Baudot J, Hénin D, Gibert C, Chastre J (2004) Clinical and autopsy diagnoses in the intensive care unit: a prospective study. Arch Intern Med 164:389–392
11. Dhar V, Perlman M, Vilela MI, Haque KN, Kirpalani H, Cutz E (1998) Autopsy in a neonatal intensive care unit: utilization patterns and associations of clinicopathologic discordances. J Pediatr 132:75–79
12. Dimopoulos G, Piagnerelli M, Berre J, Eddafali B, Salmon I, Vincent JL (2003) Disseminated aspergillosis in intensive care unit patients: an autopsy study. J Chemother 15:71–75
13. Dimopoulos G, Piagnerelli M, Berre J, Salmon I, Vincent JL (2004) Post mortem examination in the intensive care unit: still useful? Intensive Care Med 30:2080–2085
14. Egervary M, Szende B, Roe FJ, Lee PN (2000) Accuracy of clinical diagnosis of lung cancer in Budapest in an institute specializing in chest diseases. Pathol Res Pract 196:761–766
15. Fernandez-Segoviano P, Lazaro A, Esteban A, Rubio JM, Iruretagoyena JR (1988) Autopsy as quality assurance in the intensive care unit. Crit Care Med 16:683–685
16. Geha DJ, Roberts GD (1994) Laboratory detection of fungemia. Clin Lab Med 14:83–97
17. Goldman L, Sayson R, Robbins S, Cohn LH, Bettmann M, Weisberg M (1983) The value of the autopsy in three medical eras. N Engl J Med 308:1000–1005
18. Goldman L (1984) Diagnostic advances v the value of the autopsy. 1912–1980. Arch Pathol Lab Med 108:501–505
19. Gut AL, Ferreira AL, Montenegro MR (1999) Autopsy: quality assurance in the ICU. Intensive Care Med 25:360–363
20. Haber SL (1996) Whither the autopsy? Arch Pathol Lab Med 120:714–717
21. Herbrecht R, Denning DW, Patterson TF, Bennett JE, Greene RE, Oestmann JW, Kern WV, Marr KA, Ribaud P, Lortholary O, Sylvester R, Rubin Rh, Wingard JR, Stak P, Durand C, Caillot D, Thiel E, Chandrasekar PH, Hodges MR, Schlamm HT, Troke PF, De Pauw B, Invasive Fungal Infections Group of the European Organisation for Research and Treatment of Cancer and the Global Aspergillus Study Group (2002) Voriconazole versus amphotericin B for primary therapy of invasive aspergillosis. N Engl J Med 347:408–415
22. Juvin P, Teissiere F, Brion F, Desmonts JM, Durigon M (2000) Postoperative death and malpractice suits: is autopsy useful? Anesth Analg 91:344–346

23. Kamal IS, Forsyth DR, Jones JR (1997) Does it matter who requests necropsies? Propective study of clinical audit on rate of requests. BMJ 314:1729
24. Kumar P, Taxy J, Angst DB, Mangurten HH (1998) Autopsies in children: are they still useful? Arch Pediatr Adolesc Med 152:558–563
25. Kumar P, Angst DB, Taxy J, Mangurten HH (2000) Neonatal autopsies: a 10-year experience. Arch Pediatr Adolesc Med 154:38–42
26. Landefeld CS, Chren MM, Myers A, Geller R, Robbins S, Goldman L (1988) Diagnostic yield of the autopsy in a university hospital and a community hospital. N Engl J Med 318:1249–1254
27. Lundberg GD (1996) College of American Pathologists Conference XXIX on restructuring autopsy practice for health care reform: let's make this autopsy conference matter. Arch Pathol Lab Med 120:736–738
28. Lundberg GD (1998) Low-tech autopsies in the era of high-tech medicine: continued value for quality assurance and patient safety. JAMA 280:1273–1274
29. Marche C (1990) The autopsy and AIDS. Evaluation and perspectives. Ann Pathol 10:225–228
30. Marwick C (1995) Pathologists request autopsy revival. JAMA 273:1889–1891
31. McPhee SJ, Bottles K (1985) Autopsy: moribund art or vital science? Am J Med 78:107–113
32. McPhee SJ, Bottles K, Lo B, Saika G, Crommie D (1986) To redeem them from death. Reactions of family members to autopsy. Am J Med 80:665–671
33. McPhee SJ (1996) Maximizing the benefits of autopsy for clinicians and families. What needs to be done. Arch Pathol Lab Med 120:743–748
34. Mort TC, Yeston NS (1999) The relationship of pre mortem diagnoses and post mortem findings in a surgical intensive care unit. Crit Care Med 27:299–303
35. Nadrous HF, Afessa B, Pfeifer A, Peters SG (2003) The role of autopsy in the intensive care unit. Mayo Clin Proc 78:947–950
36. Nichols L, Aronica P, Babe C (1998) Are autopsies obsolete? Am J Clin Pathol 110:210–218
37. O'Grady G (2003) Death of the teaching autopsy. BMJ 327:802–803
38. Ong AW, Cohn SM, Cohn KA, Jaramillo DH, Parbhu R, McKenney MG, Barquist ES, Bell MD (2002) Unexpected findings in trauma patients dying in the intensive care unit: results of 153 consecutive autopsies. J Am Coll Surg 194:401–406
39. Perkins GD, McAuley DF, Davies S, Gao F (2003) Discrepancies between clinical and postmortem diagnoses in critically ill patients: an observational study. Crit Care 7:R129–R132
40. Potet F (1996) Autopsy. A method for evaluating the quality of care. Ann Pathol 16:409–413
41. Rao MG, Rangwala AF (1990) Diagnostic yield from 231 autopsies in a community hospital. Am J Clin Pathol 93:486–490
42. Roberts WC (1978) The autopsy: its decline and suggestion for its revival. N Engl J Med 299:332–338
43. Roosen J, Frans E, Wilmer A, Knockaert DC, Bobbaers H (2000) Comparison of premortem clinical diagnoses in critically ill patients and subsequent autopsy findings. Mayo Clin Proc 75:562–567
44. Salib E, Tadros G, Ambrose A (2000) Autopsy in elderly psychiatric inpatients: a retrospective review of autopsy findings of deceased elderly psychiatric inpatients in north Cheshire 1980–1996. Med Sci Law 40:20–27
45. Sarode VR, Datta BN, Banerjee AK, Banerjee CK, Joshi K, Bhusnurmath B, Radotra BD (1993) Autopsy findings and clinical diagnoses: a review of 1,000 cases. Human Pathol 24:194–198
46. Silfvast T, Takkunen O, Kolho E, Andersson LC, Rosenberg P (2003) Characteristics of discrepancies between clinical and autopsy diagnoses in the intensive care unit: a 5-year review. Intensive Care Med 29:321–324
47. Slavin G, Kirkham N, Underwood JCE, Molt JM, Hopkins A, Jackson BT, Windsor CWO (1991) The autopsy and audit. Report of the Joint Working Party of the Royal College of Pathologists, the Royal College of Physicians of London and the Royal College of Surgeons of England. Royal College of Pathologists, London
48. Sonderegger-Iseli K, Burger S, Muntwyler J, Salomon F (2000) Diagnostic errors in three medical areas: a necropsy study. Lancet 355:2027–2031
49. Start RD, Firth JA, Macgillivray F, Cross SS (1995) Have declining clinical necropsy rates reduced the contribution of necropsy to medical research? J Clin Pathol 48:402–404
50. Tai DY, El-Bilbeisi H, Tewari S, Mascha EJ, Wiedemann HP, Arroliga AC (2001) A study of consecutive autopsies in a medical ICU: a comparison of clinical cause of death and autopsy diagnosis. Chest 119:530–536
51. The Royal College of Pathologists of Australasia Autopsy Working Party (2004) The decline of the hospital autopsy: a safety and quality issue for healthcare in Australia. Med J Aust 180:281–285
52. Tse GM, Lee JC (2000) A 12-month review of autopsies performed at a university-affiliated teaching hospital in Hong Kong. Hong Kong Med J 6:190–194
53. Twigg SJ, McCrirrick A, Sanderson PM (2001) A comparison of post mortem findings with post hoc estimated clinical diagnoses of patients who die in a United Kingdom intensive care unit. Intensive Care Med 27:706–710
54. Yalamarthi S, Ridley S, Barker T (1998) Agreement between ante-mortem diagnoses, death certificates and post-mortem causes of death in critically ill patients. Clin Intensive Care 9:100–104
55. Yesner R, Robinson MJ, Goldman L, Reichert CM, Engel L (1985) A symposium on the autopsy. Pathol Annu 20:441–477

Virchows Arch (2007) 450:335–341
DOI 10.1007/s00428-006-0351-x

ORIGINAL ARTICLE

Inhibition of estrogen-induced pituitary tumor growth and angiogenesis in Fischer 344 rats by the matrix metalloproteinase inhibitor batimastat

Slawomir A. Mucha · Gabriela Meleń-Mucha · Andrzej Godlewski · Henryk Stepień

Received: 21 June 2006 / Revised: 12 October 2006 / Accepted: 13 November 2006 / Published online: 18 January 2007
© Springer-Verlag 2007

Abstract The development of estrogen-induced pituitary prolactinoma in Fischer 344 (F344) rats is associated with enhanced neovascularization. Based on the significance of matrix metalloproteinases (MMPs) for tumor growth and angiogenesis, we have studied the effect of batimastat (BB-94), a synthetic MMPs inhibitor (MMPI) on the progression of prolactin-secreting pituitary adenoma in rats. Pituitary tumors were induced in male F344 rats by s.c. implantation of Silastic tubes containing diethylstilbestrol (DES). The effects of chronic treatment with BB-94 (30 mg/kg b.w.) on pituitary weight, cell proliferation, apoptosis and vascular density were evaluated. We have stated that chronic treatment with batimastat caused a significant reduction in the pituitary weight. Batimastat has been found to decrease cell proliferation evaluated by a number of PCNA-positive stained cell nuclei. A marked increase in the apoptotic index within the pituitary was observed in the study group. Moreover, the density of microvessels identified by CD31 was reduced in the group treated with BB-94. The results of our study provide evidence for an inhibitory effect of batimastat, a synthetic MMPI, on the growth and angiogenesis in an experimental model of human prolactinoma. The ability of BB-94 to suppress established pituitary tumor growth suggests a possible application of MMPIs in the treatment of pituitary adenomas.

Keywords Pituitary · Prolactinoma · Proliferation · Apoptosis · Angiogenesis

Andrzej Godlewski died during the preparation of the manuscript.

S. A. Mucha (✉)
Department of Clinical Endocrinology,
Medical University of Lodz,
Sterling Street 3,
91-425 Lodz, Poland
e-mail: mucha.sla@wp.pl

G. Meleń-Mucha
Department of Immunoendocrinology,
Medical University of Lodz,
Sterling Street 3,
91-425 Lodz, Poland

A. Godlewski
Department of Cytology, Histology and Embryology,
Medical University of Lodz,
Narutowicza Street 60,
90-136 Lodz, Poland

H. Stepień
Department of Immunoendocrinology,
Medical University of Lodz,
Sterling Street 3,
91-425 Lodz, Poland

Introduction

It is well known that the process of neovascularization plays a central role in the growth of solid tumors [12]. Angiogenesis is controlled by the balance between stimulatory and inhibitory factors and by the interaction of endothelial cells with extracellular matrix (ECM) components, particularly with the proteoglycans. These enzymes, called matrix metalloproteinases (MMPs), form a diversified group of Zn^{2+}-dependent endopeptidases that degrade most of the components of the ECM to allow cell invasion, migration and new tissue formation [44]. The activity of MMPs is regulated by endogenous tissue inhibitors of MMPs (TIMPs) [24]. Inhibition of MMP activity represents a promising non-cytotoxic approach to the therapy for cancer. In fact, new treatment strategies specifically targeted towards MMPs have been developed. Consequently, synthetic MMPs inhibitors (MMPIs) are undergoing

active investigation as possible anti-tumor and anti-metastatic agents, including assessment in clinical trials [15].

Although most prolactinomas are benign and do not metastasize to distant sites, they may cause local invasion [1, 31]. It has been suggested that the interactions with the ECM might be an important factor in pituitary tumorigenesis [27]. Normal pituitary gland and pituitary adenomas differentially express ECM components [10, 11]. MMPs were found in the majority of different pituitary tumors, but their levels of expression were unrelated to tumor grade or to their invasive phenotype. On the other hand, a good inverse correlation between TIMP-2 and TIMP-3 expression levels and tumor grade has been observed [2]. Moreover, high expression of MMPs and low levels of TIMP-1 in human pituitary adenomas have been reported [25]. These studies have demonstrated that pituitary MMPs (e.g. MMP-2 and MMP-9) may contribute to the regulation of cell proliferation and hormone secretion through the release of growth factors. Other observations suggest a role for MMP-9 in the pituitary tumor recurrence and invasiveness [38].

One of the first synthetic MMPIs to be identified was batimastat (BB-94), which possesses potent activity against most of the major MMPs [5, 36]. Batimastat is almost completely insoluble, and consequently, the only way it can be administered is by direct injection into various body cavities (peritoneal and pleural cavities). There is now a large body of evidence showing the effects of BB-94 in various experimental models of human cancer [5]. Moreover, its effective use in some clinical situations has also been reported [45].

Chronic treatment of F344 rats with natural or synthetic estrogen is known to result in the development of lactotrope hyperplasia and, consequently, prolactin-secreting anterior pituitary tumors [28, 33]. Moreover, estrogen-induced pituitary tumorigenesis is associated with an enhanced formation of blood vessels [9, 30]. Our study was aimed to explore the effects of batimastat on diethylstilbestrol-induced pituitary prolactinoma growth and angiogenesis in F344 rats.

Materials and methods

Materials

Batimastat [4-9N-(hydroxyamino)-2R-isobutyl-3S-(thienylthiomethyl)-succinyl]-L-phenylalanine-N-methylamide was kindly obtained from Dr. H. R. Mills (British Biotech, Oxford, UK). According to the producer's data sheet, BB-94 was dissolved in phosphate-buffered saline containing 0.01% (v/v) Tween-80 (pH 7.2), vortexed, placed in a sonic water bath for 10 min and then treated with a sonic probe at 100 Hz for approximately 5 min until a uniform suspension was achieved.

Animals and induction of prolactinoma

Young (4 weeks old) male Fischer 344 rats were obtained from Harlan Olac (Bicester Oxon, England). They were housed in group cages in a controlled 12-h light/12-h dark environment and with free access to water and food. The animals underwent chronic estrogen treatment using Silastic tubes (Dow Corning, Midland, MI) filled with a solution of diethylstilbestrol (DES; Stilboestrolum, Polfa, Poland) in 95% ethanol [28]. The capsules were implanted s.c. in the lumbar region of each rat under anesthesia to induce pituitary tumors [35, 43]. Empty Silastic capsules were implanted as controls.

Experimental protocol and preparation of tissues

Five weeks after implantation of capsules, daily i.p. injections of batimastat (BB-94) at a dose of 30 mg/kg b. w. were started. Control animals received i.p. injections of 0.9% NaCl. All injections were made once a day for 21 days. Twelve hours after the last injection, all rats were weighted and killed by decapitation. Pituitary glands were carefully isolated, weighted and cut into two similar parts. One half of the tumor was fixed in zinc fixative (0.1 M Tris buffer pH 7.4, 0.5 g calcium acetate, 5.0 g zinc acetate and 5.0 g zinc chloride) for immunohistochemistry of CD31; the other one in 4% neutral buffered formalin for the rest of immunohistochemical procedures (PCNA and apoptosis) and then embedded in paraffin. The sections of the pituitary glands at a thickness of 5 μm were mounted on normal gelatine-coated glass slides (for H&E staining and for PCNA immunohistochemistry) or on aminopropyl-triethoxysilane (APES)-treated super frost glass slides (for detecting apoptosis and CD31).

Immunohistochemistry

The determination of the proliferating cell nuclear antigen (PCNA) was applied as an index of cell proliferation [4]. Immunohistochemistry was performed using a monoclonal, mouse anti-h PCNA antibodies (clone PC-10, 1529; Dako, Carpinteria, CA) for 10 min. Sections were heated in citrate buffer (pH 6.0) in a microwave oven (700 W) for 10 min, chilled at room temperature for 20 min and washed in distilled water and in Tris/HCl buffer (pH 7.4). Then, they were exposed to anti-mouse immunoglobulins, followed by streptavidin-peroxidase conjugat (Dako; K0609) and 3,3′-diaminobenzidine (DAB) as a chromogen. For staining controls, the identical procedure was performed without the primary antibody.

Apoptosis was visualized by the terminal deoxynucleotidyl transferase (TdT)-mediated dUTP nick-end labeling (TUNEL) method. The laboratory protocol was adopted from Gavrieli et al. [14] and was performed by means of the in situ cell death detection kit, POD (Roche Diagnostics

GmbH, Mannheim, Germany) according to the manufacturer's instruction, with our own necessary modifications [22]. Briefly, the tissue sections were adhered to slides pretreated with silane and heated for about 30 min at the temperature of 60°C to avoid section detachment, and then, they were deparaffinized and rehydrated. After the step including TdT, the specimens were additionally saturated in 5% normal sheep serum to diminish the background. At the end, the color reaction with DAB lasted for about 5 min. A negative control was performed by omitting TdT. After that, the tissue sections were counterstained with hematoxylin for about 40 s and mounted in Geltol Permanent (Aqueous Mounting Medium; Immunon).

Intrapituitary vessels were visualized by anti-CD31 antibodies (clone TLD-3A12, PECAM-1; Pharmingen, San Diego, CA), a marker of endothelial cells [8]. Sections were microwaved at 100°C for 10 min in a citrate buffer (pH 6.0) and left to cool for 20 min at room temperature. During hydratation, 0.5% iodine in 80% ethanol was employed instead of 80% ethanol and, after 50% ethanol, 5% sodium thiosulphate bath during 5 min was included. The sections were washed vigorously in bidistilled water; endogenous peroxidase was blocked by 3% H_2O_2 bath (5 min). The iodination of samples was used for removing zinc salts precipitates. Immunohistological detection of microvessels was achieved with commercially available mouse anti-rat monoclonal CD31 antibody in a dilution of 1:30 to 1:50 (72 h, 4°C). After incubation, typical procedure was employed with the use of complex LSAB (Dako). Control samples exposed to secondary antibody alone showed no specific staining.

Image analysis

Digital images were acquired from the light microscope (Olympus BX40, Japan) at ×200 magnification via CCD colour camera (CC20P; Videotronic GmbH, Germany) and analyzed using a computer system (MultiScanBase v.8.08; Computer Scanning System, Warsaw, Poland). The labeling index (LI), determined as a number of PCNA-positive nuclei per at least 8,000 anterior pituitary cells per group, was counted and expressed as a percentage. The apoptotic index (AI) was evaluated as a number of cells containing apoptotic bodies or nuclei assessed per 1,000 randomly scored pituitary cell nuclei and was expressed in per mil. The evaluation of AI was based not only on TUNEL staining but also on typical features of apoptotic cells such as chromatin condensation, nuclear fragmentation, cell shrinkage, separation from the neighbouring cells and the presence of dispersed irregular granules-apoptotic bodies [46]. Vessel density was assessed by counting CD31-positive blood vessels per microscopic image [41, 42] and defined as the number of manually counted vessel profiles per field. The areas of tumor tissue containing the highest number of capillaries per area (hot spots) were chosen, avoiding areas of gross hemorrhage or necrosis. A single countable vessel was defined as any endothelial cell or group of cells that was clearly separate from other vessels, without the necessity of a vessel lumen or red blood cells within the lumen. All sections have been examined by two independent observers (SAM and GMM) who have not been informed about the pretreatment of the rats.

Statistical analysis

Pituitary tumor weight was evaluated by using the Fisher's least significant difference procedure. The data from immunohistochemical procedures were statistically analyzed using an analysis of variance followed by the Mann–Whitney's test, and a $P<0.05$ was considered significant.

Results

Effects of DES and BB-94 on pituitary weight

Prolonged estrogen administration to F344 rats leads to lactotroph hyperplasia followed by pituitary adenoma. Table 1 presents the results of the effects of batimastat on rat pituitary weight, which was relative to the tumor mass. At the end of the experiment (8 weeks after the implantation of capsules containing DES), pituitary weight was significantly higher than in the control group. Treatment with batimastat for 21 days caused a significant decrease in the pituitary weight, corresponding to a 53% of growth suppression. As demonstrated, batimastat stopped further pituitary growth, but did not diminish the pituitary enlargement caused by 5 weeks of DES treatment.

Cell proliferation, apoptosis and angiogenesis in treated DES-induced tumors

Changes in the PCNA LI in the anterior pituitary gland caused by DES, BB-94, and in the control group are shown

Table 1 Effects of DES and BB-94 (30 mg/kg) on pituitary weight in F344 rats in vivo. Data are expressed as means±SD ($n=10$ animals)

Group	Pituitary weight (mg)	P value
Control	8.9±0.85	
DES (5 weeks)	30.58±5.59	<0.05[a]
DES (8 weeks)	48.31±16.79	<0.05[a]
DES + BB-94	27.86±9.44	NS[b]
		<0.05[c]

[a] Compared with control group
[b] Compared with DES-treated group (5 weeks)
[c] Compared with DES-treated group (8 weeks)
NS non significant

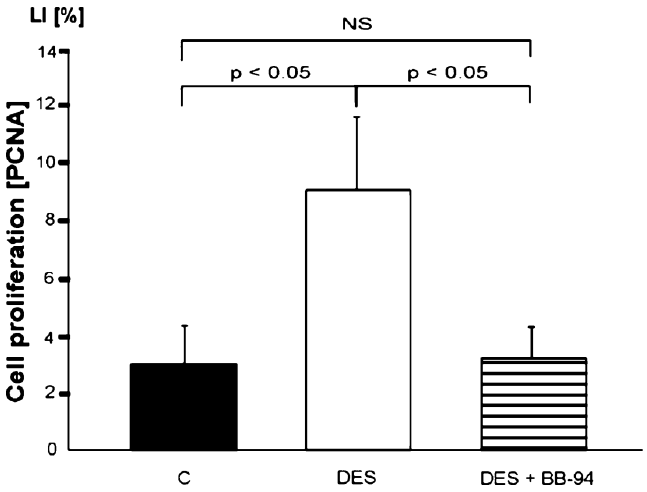

Fig. 1 Effects of BB-94 (30 mg/kg) on anterior pituitary cell proliferation (PCNA) in DES-induced prolactinoma in F344 rats. Daily treatment with 0.9% NaCl solution (control rats) or BB-94 (30 mg/kg) was started 5 weeks after s.c. implantation of Silastic tubes containing DES. After the next 21 days, pituitary tumors were resected, fixed, and paraffin-embedded. The number of mitotic pituitary cells was smaller in BB-94-treated rats as compared with animals from DES group. *Bars* represent the means±SD of ten animals

in Fig. 1. After chronic estrogen treatment, the number of proliferating cells highly increased (9.06±2.52%) as compared with control rats (3.05±1.37%). In the group administered with batimastat, a significant decrease in PCNA LI was found (3.21±1.13%, $P<0.01$; Fig. 4).

Analysis of apoptosis by TdT labeling of fragmented DNA showed very low AI in control rat pituitaries (0.7±0.45‰; Figs. 2 and 4). We have found an increase in apoptosis in pituitary tumor cells of batimastat-treated animals (6.51±1.86‰), as compared with that in DES-treated group (1.5±0.67‰; $P<0.05$).

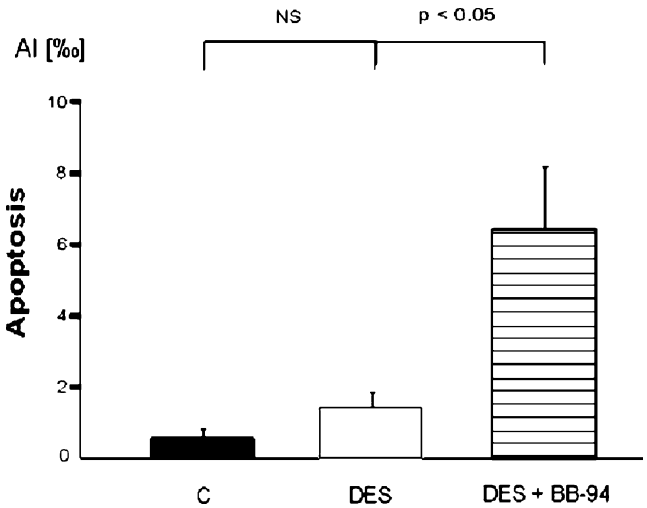

Fig. 2 Batimastat (30 mg/kg) exerts proapoptotic activity in DES-induced prolactinoma in F344 rats. A higher frequency of apoptotic cells was found in tumors from BB-94-treated animals as compared with DES-treated rats. *Bars* represent the means±SD of ten animals

The effects of estrogens and the tested substance on the vasculature in the anterior pituitary were evaluated using CD31 immunostaining (Figs. 3 and 4). The vascular density in estrogen-induced pituitary tumors was significantly higher (8.0±2.28) than in the group with implanted empty Silastic tubes and treated with 0.9% NaCl solution (4.64±1.68; $P<0.05$). Evaluation of the number of vessels per microscopic area has shown a significant inhibition of the pituitary angiogenesis in the rats treated for 21 days with batimastat (5.86±1.35; $P<0.05$).

Discussion

In our study, we have demonstrated for the first time the potential of batimastat, a synthetic MMP inhibitor, to inhibit the growth of diethylstilbestrol-induced rat pituitary tumor, which serves as an experimental model of human prolactinoma. Prolactin-secreting pituitary adenomas comprise the most prevalent type of pituitary tumor in humans [23], and the medical therapy with dopamine agonists (e.g. bromocriptine, cabergoline and quinagolide) is sufficient in most cases of prolactinoma [3]. However, there are often significant side effects, which lead to the drug withdrawal. On the other hand, about 5–10% of patients with prolactinoma exhibit resistance to bromocriptine [26]. Additionally, there is no effective medical therapy for non-functioning pituitary adenomas and high recurrence rate after neurosurgical treatment of these tumors has been observed [17]. Thus, the search for new therapeutic agents for the treatment of different pituitary tumors seems justified.

In the present work, treatment of estrogen-induced prolactinoma with batimastat for 21 days resulted in a

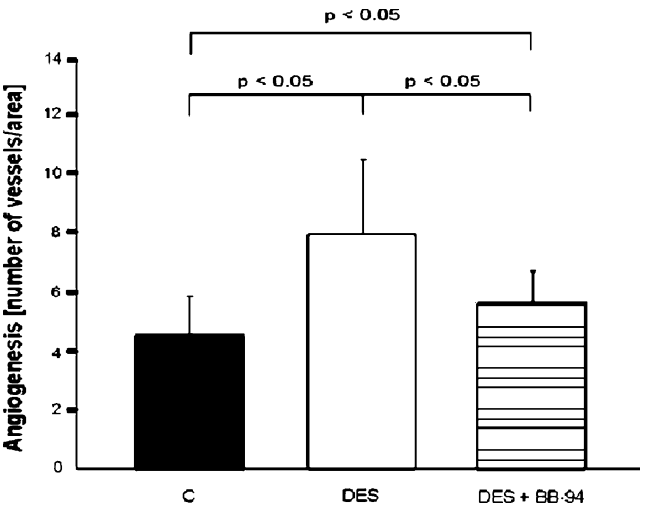

Fig. 3 Inhibitory effect of batimastat (30 mg/kg) on angiogenesis (expressed as a number of vessels per area) in DES-induced rat pituitary prolactinoma. Tumor vessel density in prolactinomas decreased after 21 days of treatment with BB-94. *Bars* represent the means±SD of ten animals

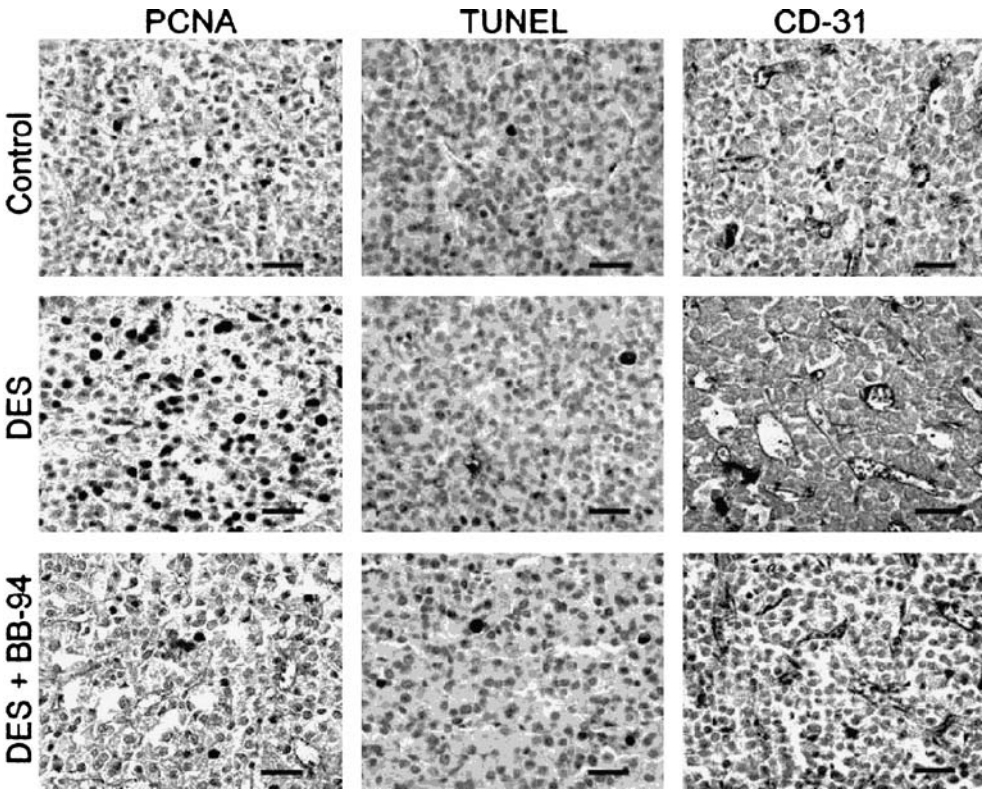

Fig. 4 The expression of proliferation was analyzed by IHC in sections immunostained for PCNA. Paraffin sections of tumor samples were assayed for apoptosis using terminal deoxynucleotidyl transferase (TdT)-mediated dUTP nick-end labeling (TUNEL) technique. Microvessel density in the treatment groups was measured by counting the average number of CD31-positive blood vessels per X400 field. Shown are representative pictures at the light microscope from experimental groups. *Scale bars* represent 50 μm

significant reduction in pituitary weight, which corresponds to the tumor mass. However, there was no difference between pituitary weight in the group administered with BB-94 and the group before treatment (after 5 weeks only on estrogen). Hence, the treatment with batimastat for 3 weeks has been found to inhibit further tumor growth.

The results of the study showed that batimastat inhibited cell proliferation within pituitary tumors. We have also found that BB-94 increased apoptotic index, which might also be responsible, at least in part, for the observed anti-tumor activity of this MMPI. Although recent studies have enhanced our understanding of pathways that regulate apoptosis, there is no reason to believe that all anti-neoplastic agents induce this process. The effect of batimastat on apoptosis has been earlier demonstrated only in a few papers, but it seems to be divergent depending on the experimental condition [13, 19]. Interestingly, apoptosis has not been found to play a role in the involution of a human prolactinoma, in contrast to the suppression of cell proliferation, which mainly contributes to tumor shrinkage [34]. Moreover, Levy [21] has suggested that increased cell proliferation, rather than decreased apoptosis, is the principal contributor to tumor growth in the majority of pituitary adenomas in rats. It is well known that in both rat and human pituitary tumors, low levels of apoptotic activity are commonly found. In this study, we have also demonstrated low apoptotic activity in normal male rat pituitaries, as well as in estrogen-induced pituitary tumors.

To test the hypothesis that inhibition of angiogenesis contributed to the observed anti-tumor effects of tested substances on estrogen-induced prolactinoma in F344 rats, we have assessed microvascular density by staining with an anti-CD31 antibody. It has been found that BB-94 decreased the number of vessel profiles, which confirms the anti-angiogenic activity of the tested agent also within the pituitary adenomas. Our results strongly support earlier data on a possible involvement of some matrix metalloproteinases (e.g. MMP-2 and MMP-9) in the control of pituitary tumor growth [25]. Additionally, Turner et al. [38] have found that MMP-9 expression was related to tumor invasiveness in prolactinomas and was associated with non-functioning tumor regrowth. It is well known that MMPs dissolve ECM components and may initiate and promote angiogenesis [29], which has been implicated in the process of growth and spread of solid tumors [12]. Interestingly, it has been found in humans that in contrast to tumors from other tissues such as prostate and breast, pituitary adenomas were less vascularized than the normal pituitary gland [16, 38]. On the other hand, studies on the relationship between angiogenesis, tumor size, and the type of a pituitary adenoma are controversial [reviewed in 39].

By analyzing the proliferation and apoptotic indexes, as well as microvessel density of resected pituitary adenomas, we were able to assess at least some of the mechanisms of anti-tumor activity of batimastat. The results of this study clearly indicated that the pituitary tumor growth

suppression by BB-94 was accompanied by a reduced proliferation rate, an increased apoptosis, and a decrease in vascularity. Although the means by which BB-94 inhibited tumor growth have not been established in other experimental studies, cytostatic and/or anti-angiogenic activity of the drug has been suggested [6, 7, 18, 20, 32, 37, 40, 47]. Ten years ago, we found that TNP-470, a fumagillin analog, inhibited tumor growth in the same experimental model of a pituitary adenoma also through the inhibition of cell proliferation and angiogenesis [35]. Although an increasing body of evidence exists demonstrating the crucial role of angiogenesis in the formation and growth of solid tumors, potential mechanisms involved in the regulation of tumor vascularization within the pituitary and the influence of pro-angiogenic factors and endogenous inhibitors of angiogenesis are still unclear.

In conclusion, our work provides the first evidence that batimastat, a synthetic MMPI, is effective in inhibiting the growth of estimated estrogen-induced rat pituitary tumors in vivo. Batimastat appears to exert its anti-tumor activity through a combined anti-proliferative, anti-angiogenic and pro-apoptotic effect. Moreover, in our, as well as in other studies, the administration of batimastat was not associated with any detectable signs of local or systemic toxicity. The ability of batimastat to suppress established pituitary tumor growth might suggest a novel application of synthetic MMPIs in the management of pituitary adenomas.

Acknowledgement This study was supported by a grant from the State Committee for Scientific Research of Poland (KBN) to H. S. (No 4 P05A 04215). All experiments were performed according to our institutional and National Institutes of Health (NIH) guidelines for care and use of research animals.

References

1. Asa SL, Ezzat S (1998) The cytogenesis and pathogenesis of pituitary adenomas. Endocr Rev 19:798–827
2. Beaulieu E, Kachra Z, Mousseau N, Delbecchi L, Hardy J, Beliveau R (1999) Matrix metalloproteinases and their inhibitors in human pituitary tumors. Neurosurgery 45:1432–1441
3. Bevan JS, Webster J, Burke CW, Scanlon MF (1992) Dopamine agonists and pituitary tumor shrinkage. Endocr Rev 13:220–240
4. Bravo R, Frank R, Blundell PA, MacDonald-Bravo H (1987) Cyclin/PCNA is the auxiliary protein of DNA polymerase-δ. Nature 326:515–517
5. Brown PD, Giavazzi R (1995) Matrix metalloproteinase inhibition—a review of anti-tumor activity. Ann Oncol 6:967–974
6. Chirivi RGS, Garofalo A, Crimmin MJ, Bawden LJ, Stoppacciano A, Brown PD, Giavazzi R (1994) Inhibition of the metastatic spread and growth of B16-BL6 murine melanoma by a synthetic matrix metalloproteinase inhibitor. Int J Cancer 58: 460–464
7. Davies B, Brown P, East N, Crimmin MJ, Balkwill FR (1993) A synthetic matrix metalloproteinase inhibitor decreases tumor burden and prolongs survival of mice bearing human ovarian carcinoma xenografts. Cancer Res 53:2087–2091. Erratum: Cancer Res 53:3652
8. DeLisser HM, Christofidou-Solomidou M, Strieter RM, Burdick MD, Robinson CS, Wexler RS, Kerr JS, Garlanda C, Merwin JR, Madri JA, Albelda SM (1997) Involvement of endothelial PECAM-1/CD31 in angiogenesis. Am J Pathol 151:671–677
9. Elias KA, Weiner RI (1984) Direct arterial vascularization of estrogen-induced prolactin-secreting anterior pituitary tumors. Proc Natl Acad Sci USA 81:4549–4553
10. Farnoud MR, Farhadian F, Samuel JL, Derome P, Peillon F, Li JY (1995) Fibronectin isoforms are differentially expressed in normal and adenomatous human anterior pituitaries. Int J Cancer 61:27–34
11. Farnoud MR, Veirana N, Derome P, Peillon F, Li JY (1996) Adenomatous transformation of the human anterior pituitary is associated with alterations in integrin expression. Int J Cancer 67:45–53
12. Folkman J (1971) Tumor angiogenesis: therapeutic implications. N Engl J Med 285:1182–1186
13. Gastman BR, Atarshi Y, Reichert TE, Saito T, Balkir L, Rabinowich H, Whiteside TL (1999) Fas ligand is expressed on human squamous cell carcinomas of the head and neck, and it promotes apoptosis of T lymphocytes. Cancer Res 59:5356–5364
14. Gavrieli Y, Sherman Y, Ben-Sasson SA (1992) Identification of programmed cell death in situ via specific labeling of nuclear DNA fragmentation. J Cell Biol 119:493–501
15. Heath EI, Grochow LB (2000) Clinical potential of matrix metalloprotease inhibitors in cancer therapy. Drugs 59:1043–1055
16. Jugenburg M, Kovacs K, Jugenburg I, Scheithauer BW (1998) Angiogenesis in endocrine neoplasms. Endocr Pathol 8:259–272
17. Katznelson L, Alexander JM, Klibanski A (1993) Clinically nonfunctioning pituitary adenomas. J Clin Endocrinol Metab 76:1089–1094
18. Knox JD, Bretton L, Lynch T, Bowden GT, Nagle RB (1998) Synthetic matrix metalloproteinase inhibitor, BB-94, inhibits the invasion of neoplastic human prostate cells in a mouse model. Prostate 35:248–254
19. Lei H, Kalluri R, Furth EE, Baker AH, Strauss JF 3rd (1999) Rat amnion type IV collagen composition and metabolism: implications for membrane breakdown. Biol Reprod 60:176–182
20. Lein M, Jung K, Le DK, Hasan T, Ortel B, Borchert D, Winkelmann B, Schnorr D, Loenings SA (2000) Synthetic inhibitor of matrix metalloproteinases (batimastat) reduces prostate cancer growth in an orthotopic rat model. Prostate 43:77–82
21. Levy A (1999) Mitosis and apoptosis in anterior pituitary gland: tumour formation or hyperplasia? Baillieres Best Pract Res Clin Endocrinol Metab 13:353–365
22. Meleń-Mucha G, Winczyk K, Pawlikowski M (1998) Somatostatin analogue octreotide and melatonin inhibit bromodeoxyuridine incorporation into cell nuclei and enhance apoptosis in the transplantable murine colon 38 cancer. Anticancer Res 18:3615–3620
23. Minderman T, Wilson CB (1994) Age-related and gender-related occurrence of pituitary adenomas. Clin Endocrinol 41:359–364
24. Murphy G, Docherty AJP (1992) The matrix metalloproteinases and their inhibitors. Am J Respir Cell Mol Biol 7:120–125
25. Páez Pereda M, Ledda MF, Goldberg V, Chervin A, Carrizo G, Molina H, Müller A, Renner U, Podhajcer O, Arzt E, Stalla GK (2000) High levels of matrix metalloproteinases regulate proliferation and hormone secretion in pituitary cells. J Clin Endocrinol Metab 85:263–269
26. Pellegrini I, Rasolonjanahary R, Gunz G, Bertrand P, Delivet S, Jedynak CP, Kordon C, Peillon F, Jaquet P, Enjalbert A (1989) Resistance to bromocriptine in prolactinomas. J Clin Endocrinol Metab 69:500–509
27. Pereda MP, Goldberg V, Chervin A, Carizzo G, Molina A, Andrada J, Sauer J, Renner U, Stalla GK, Arzt E (1996)

Interleukin-2 (IL-2) and IL-6 regulate *c-fos* protooncogene expression in human pituitary adenoma explants. Mol Cell Endocrinol 124:33–42
28. Phelps C, Hymer WC (1983) Characterization of oestrogen-induced adenohypophyseal tumors in the Fischer 344 rat. Neuroendocrinology 37:23–31
29. Sang QX (1998) Complex role of matrix metalloproteinases in angiogenesis. Cell Res 8:171–177
30. Schechter J, Ahmad N, Elias K, Weiner R (1987) Estrogen-induced tumors: changes in the vasculature in two strains of rat. Am J Anat 179:315–323
31. Scheithauer BW, Kovacs KT, Laws ER, Randall RV (1986) Pathology of invasive pituitary tumors with special reference to functional classification. J Neurosurg 65:733–744
32. Sledge GW Jr, Qulali M, Goulet R, Bone EA, Fife R (1995) Effect of matrix metalloproteinase inhibitor batimastat on breast cancer regrowth and metastasis in athymic mice. J Natl Cancer Inst 87:1546–1550
33. Spady TJ, McComb RD, Shull JD (1999) Estrogen action in the regulation of cell proliferation, cell survival, and tumorigenesis in the rat anterior pituitary gland. Endocrine 11:217–233
34. Stefaneanu L, Kovacs K, Scheithauer BW, Kontogeorgos G, Riehle DL, Sebo TJ, Murray D, Vidal S, Tran A, Buchfelder M, Fahlbusch R (2000) Effect of dopamine agonists on lactotroph adenomas of the human pituitary. Endocr Pathol 11:341–352
35. Stepień H, Grochal M, Zieliński KW, Mucha S, Kunert-Radek J, Kulig A, Stawowy A, Pisarek H (1996) Inhibitory effects of fumagillin and its analogue TNP-470 on the function, morphology and angiogenesis of an oestrogen-induced prolactinoma in Fischer 344 rats. J Endocrinol 150:99–106
36. Talbot DC, Brown PD (1996) Experimental and clinical studies on the use of matrix metalloproteinase inhibitors for the treatment of cancer. Eur J Cancer 32:2528–2533
37. Taraboletti G, Garofalo A, Belotti D, Drudis T, Borsotti P, Scanziani E, Brown PD, Giavazzi R (1995) Inhibition of angiogenesis and murine hemangioma growth by batimastat, a synthetic inhibitor of matrix metalloproteinases. J Natl Cancer Inst 87:293–298
38. Turner HE, Nagy Z, Esiri MM, Harris AL, Wass JAH (2000) Role of matrix metalloproteinase 9 in pituitary tumor behavior. J Clin Endocrinol Metab 85:2931–2935
39. Turner HE (2001) Pituitary tumor angiogenesis. Endocrinologist 11:465–469
40. Wang X, Fu X, Brown PD, Crimmin MJ, Hoffman RM (1994) Matrix metalloproteinase inhibitor BB-94 (batimastat) inhibits human colon tumor growth and spread in a patient-like orthotopic model in nude mice. Cancer Res 54:4726–4728
41. Weidner N, Semple JP, Welch WR, Folkman J (1991) Tumor angiogenesis and metastasis: correlation in invasive breast carcinoma. N Engl J Med 324:1–8
42. Weidner N (1995) Current pathologic methods for measuring intratumoral microvessel density within breast carcinoma and other solid tumors. Breast Cancer Res Treat 36:169–180
43. Wiklund J, Wertz N, Gorski J (1981) A comparison of estrogen effects on uterine and pituitary growth and prolactin synthesis in F344 and Holtzman rats. Endocrinology 109:1700–1707
44. Woessner JF Jr (1991) Matrix metalloproteinases and their inhibitors in connective tissue remodeling. FASEB J 5:2145–2154
45. Wojtowicz-Praga S, Low J, Marshall J, Ness E, Dickson R, Barter J, Sale M, McCann P, Moore J, Cole A, Hawkins MJ (1996) Phase I trial of a novel matrix metalloproteinase inhibitor batimastat (BB-94) in patients with advanced cancer. Invest New Drugs 14:193–202
46. Wyllie AH (1993) Apoptosis (The 1992 Frank Rose Memorial Lecture). Br J Cancer 67:205–208
47. Zervos EE, Norman JG, Gower WR, Franz MG, Rosemurgy AS (1997) Matrix metalloproteinase inhibition attenuates human pancreatic cancer growth in vitro and decreases mortality and tumorigenesis in vivo. J Surg Res 69:367–371

Virchows Arch (2007) 450:343–348
DOI 10.1007/s00428-006-0277-3

CASE REPORT

Primary nasopharyngeal mucoepidermoid carcinoma in Japanese patients: two case reports with histochemical and immunohistochemical analysis and a review of the literature

Kimihide Kusafuka · Yoshinori Takizawa · Yoshiyuki Iida · Mitsuru Ebihara · Tetsuro Onitsuka · Toru Kameya

Received: 2 March 2006 / Accepted: 17 July 2006 / Published online: 22 November 2006
© Springer-Verlag 2006

Abstract Mucoepidermoid carcinoma is a common neoplasm of the salivary glands. Salivary gland-type neoplasms are very rare in the nasopharynx, and there are only few reports on mucoepidermoid carcinoma of the nasopharynx. Two additional cases of mucoepidermoid carcinoma arising from the nasopharynx are reported here. Case 1: the patient was a 57-year-old Japanese woman who had bloody sputum. Case 2: the patient was a 51-year-old Japanese woman who underwent resection of a nasopharyngeal tumor. Histologically, both tumors were also low-grade mucoepidermoid carcinomas with clear cells. Histochemically, the gland-like nests and mucous cells were positive for mucin staining. Immunohistochemically, the lesions were positive for cytokeratins (CKs), p63, and MUC1, but negative for alpha-smooth muscle actin and EBER mRNA. The Ki-67 labeling indices of the two tumors were 10.4% and 4.3%, respectively. The two present cases and a review of the English literature indicate that salivary gland-type neoplasms arising from the nasopahrynx are extremely rare. The prognosis of salivary gland-type carcinomas of the nasopharynx is still unknown.

Keywords Mucoepidermoid carcinoma · Nasopharynx · MUC · Immunohistochemistry · Epstein–Barr virus

K. Kusafuka (✉) · T. Kameya
Pathology Division, Shizuoka Cancer Center Hospital,
1007 Shimonagakubo, Nagaizumi-cho,
Sunto-gun, Shizuoka 411-8777, Japan
e-mail: k.kusafuka@scchr.jp

Y. Takizawa · Y. Iida · M. Ebihara · T. Onitsuka
Division of Head and Neck Surgery,
Shizuoka Cancer Center Hospital,
1007 Shimonagakubo, Nagaizumi-cho,
Sunto-gun, Shizuoka 411-8777, Japan

Introduction

Mucoepidermoid carcinoma (MEC) is a common malignancy in the salivary glands, especially, in the major salivary glands and intra-oral minor salivary glands [8]; in addition this neoplasm was known to arise from other sites, including the lung, nasal cavity and paranasal sinuses.

Lymphoepithelioma is commonly found in the nasopharynx, and is known to be associated with Epstein–Barr virus (EBV) infection, usually originating from the nasopharyngeal mucosa [8]. Salivary gland-type tumors originating in the nasopharynx are very rare, and only a few cases of papillary adenocarcinoma, adenoid cystic carcinoma and mucoepidermoid carcinoma were reported [2, 8, 9, 12, 14]. The histogenesis and the prognosis of salivary gland-type malignant tumors are still uncertain.

We describe two cases of nasopharyngeal MEC and, based on a review of the literature, discuss the histological, histochemical, and immunohistochemical findings.

Clinical history

Case 1 A 57-year-old woman, with bloody sputum upon coughing, consulted a nearby hospital for a detailed examination, and was found to have a nasopharyngeal lesion. The biopsy material was diagnosed as adenoid cystic carcinoma, and she was immediately hospitalized in the Division of Head and Neck Surgery, Shizuoka Cancer Center, Japan. Clinically, a well-circumscribed, dome-like mass was found in the left nasopharynx. CT scan showed a mass in the left nasopharynx and magnetic resonance imaging (MRI) showed a low intensity mass upon T1 and T2 weighted imaging (Fig. 1). No lesion was found in the major or minor salivary glands. According to the World

Health Organization (WHO) classification, the clinical stage was estimated to be cT1N0M0 (stage IA) due to the expansion of the tumor to the left ear canal without evidence of the destruction of the skull base. After approximately 1 month, tumor resection was performed, and the excised mass was 2.0×2.0 cm in size. MRI from the head to the lower neck showed no evidence of lymph node enlargement. The patient remains on follow-up and showed no signs of either local recurrence or lymph node or distant metastasis 3 months postoperatively.

Case 2 A 51-year-old woman suffered from throat obstruction, and was accordingly admitted to a nearby hospital where she was found to have a 2.0×2.0-cm mass in the posterior wall of the nasopharynx. The biopsy material was diagnosed as clear cell carcinoma, not otherwise specified. No lesion was seen in the major or minor salivary glands. After 4 months, tumor resection was performed. Since the upper bilateral and sagittal surgical margins were positive, she was hospitalized in the Division of Head and Neck Surgery, Shizuoka Cancer Center, Japan, for additional treatment, after approximately 1 month. The biopsy material in our institution showed no tumor in the nasopharynx. Follow-up was continued after approximately 2 months and there was no sign of recurrence or metastasis.

Fig. 1 Magnetic resonance imaging (MRI) of the nasopharynx (Case 1). A polypoid mass with high T1 intensity

Materials and methods

Two cases of nasopharyngeal MEC were reviewed by two pathologists (K.K. and T.K.). They were examined histologically, histochemically and immunohistochemically. Immunostaining was performed on formalin-fixed paraffin-embedded tissue using the ENVISION system (DakoCytomation, Carpinteria, CA, USA). The primary antibodies used in this examination are summarized in Table 1. Moreover, in situ hybridization analysis of EBER mRNA was performed (probe: EBV RNA probe Y5200, and PNA detection kit K5201: DakoCytomation, USA).

Results

Macroscopic findings

Case 1 The resected specimen showed a polypoid mass with erosive surface that was approximately 2.0×3.0×1.7 cm in size, with partial resection of the left ear canal. On the cut surface, the tumor showed a grayish-white, well-circumscribed appearance, and erosion of the covering epithelium (Fig. 2).

Case 2 As this case was a consultation case, we could not obtain macroscopic images of the resected specimen.

Microscopic findings

Case 1 The tumor was 2.0×2.9×1.6 cm in size. The main lesion was underneath the eroded membranous mucosa of the nasopharynx, and showed a nesting pattern with multiple well-circumscribed squamous nests containing numerous clear cells, some of which contained intracytoplasmic mucin (Fig. 3a). Microcystic structures were frequently seen. This case was diagnosed as MEC. Mild nuclear atypia and low mitotic figures were observed. No necrosis was seen. No keratinization of squamous nests was found. According to the WHO classification, this tumor was estimated to be low-grade mucoepidermoid carcinoma. The specimen was incompletely excised due to the presence of tumor cells on the surgical margin of the stalk. The mucous cells and the microcystic structures were positive for mucin staining (mucicarmin, periodic acid-Schiff (PAS)–Alcian blue and diastase-digestive PAS–Alcian blue stainings), while the squamous cells contained glycogen granules, which were positive for PAS stain but negative for diastase-digestive PAS stain (Fig. 3b). Inflammatory cells were observed in the fibrous stroma. The covering epithelium was columnar epithelium, with partial erosion. The tumor cells did not invade the left ear canal.

Table 1 Antibodies used for markers in immunostaining

	Reactivity	Antigen retrieval	Supplier
Monoclonal antibodies			
Clone			
34βE12	[a]HMWK Cytokeratin 1,5,10,14	Autoclave[b]	DakoCytomation (Carpinteria, CA,USA)
AE-1/3	Pan-cytokeratin cocktail	Autoclave	Signet Laboratories (Dedhem, MA, USA)
CAM5.2	Cytokeratin 7,8	Autoclave	Beckton Dickinson (San Jose, CA, USA)
OV-TL-12/30	Cytokeratin 7	Autoclave	DakoCytomation
Ks19.1	Cytokeratin 19	Autoclave	Progen Biotechnik (Heidelberg, Germany)
IT-Ks20.8	Cytokeratin 20	Autoclave	Progen Biotechnik
E29	Epithelial membrane antigen		Takara Bio (Otsu, Japan)
CEM010	Carcinoembryonic antigen		DakoCytomation
116NS199	Carbohydrate antigen19-9		DakoCytomation
NCL-GCDFP-15	Gross cystic disease fluid protein-15	Autoclave	Novocastra Laboratories (Newcastle upon Tyne, UK)
HECD-1	E-cadherin	Autoclave	DakoCytomation
DO-7	p53	Autoclave	DakoCytomation
4A4	p63	Autoclave	LAB Vision (Fremont, CA, USA))
1A4	α-smooth muscle actin	Autoclave	DakoCytomation
NCL-clone Ma695	MUC1	Autoclave	Novocasatra Laboratories
NCL-clone Ccp58	MUC2	Autoclave	Novocastra Laboratories
NCL-clone CLH2	MUC5AC	Autoclave	Novocastra Laboratories
NCL-clone CLH5	MUC6	Autoclave	Novocastra Laboratories
MIB-1	Ki-67	Autoclave	DakoCytomation
Polyclonal antibody			
Rabbit	S-100 protein		DakoCytomation

[a] HMWK, high-molecular-weight keratin; [b] autoclave in 0.1 mol/L citrate buffer, pH 6.0

Case 2 The tumor was 2.0×1.8 cm in size. The main lesion was underneath the eroded membranous mucosa of the nasopharynx, and showed the development of tumor nests with well-circumscribed epithelial components including numerous clear cells (Fig. 3c). The tumor had marked hyalinized stroma around the tumor nests, and some epithelial cells consisted of intermediate cells. Mild cellular atypia and low mitotic figures were observed. No necrotic areas were seen, and no keratinization or goblet cells were observed. The mucin staining, which was rarely observed, was positive in the intracytoplasmic lumen (Fig. 3d). PAS staining showed abundant glycogen in the clear cells. The surgical margins were positive. According to the WHO classification, the final diagnosis was a clear cell variant of MEC with low-grade malignancy. When the biopsy was performed at our institution, the biopsy material was diagnosed as showing no residual tumor in the nasopharynx.

Immunohistochemical findings

Case 1 Most of the tumor cells showed diffuse strong positivity for pan-cytokeratin (CK), high-molecular-weight keratin, CK7, CK19, and p63 product, while the squamous cells showed stronger positivity for CKs than clear cells and mucous cells (Fig. 4a,b). The tumor cells were also focally positive for CK7/8, CK14 and p53 product, whereas they were negative for CK20, alpha-smooth muscle actin (ASMA), S-100 protein, E-cadherin, and gross cystic disease fluid protein-15. Diffuse positivity for MUC1, and focal positivity for MUC5AC and MUC6, were observed, whereas the tumor cells were negative for MUC2 (Fig. 4c). The tumor cells that were positive for MUC immunostaining consisted of clear cell components of this tumor. The Ki-67 labeling index was 10.4% in the most strongly

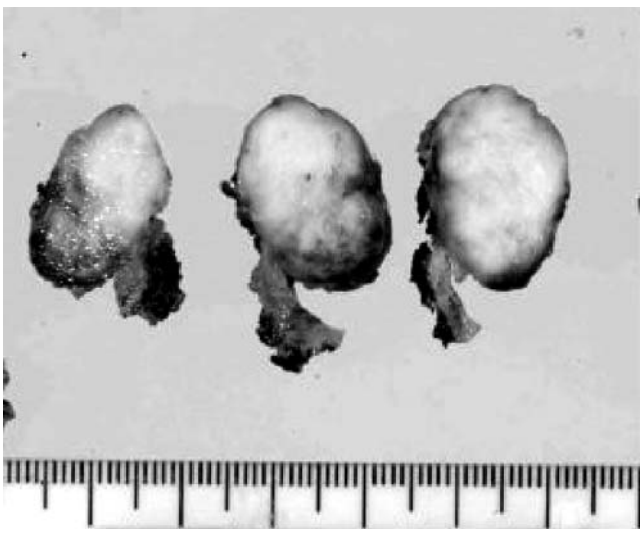

Fig. 2 Macroscopic features of the resected specimen (Case 1). A grayish-white polypoid tumor with erosion of the surface mucosa

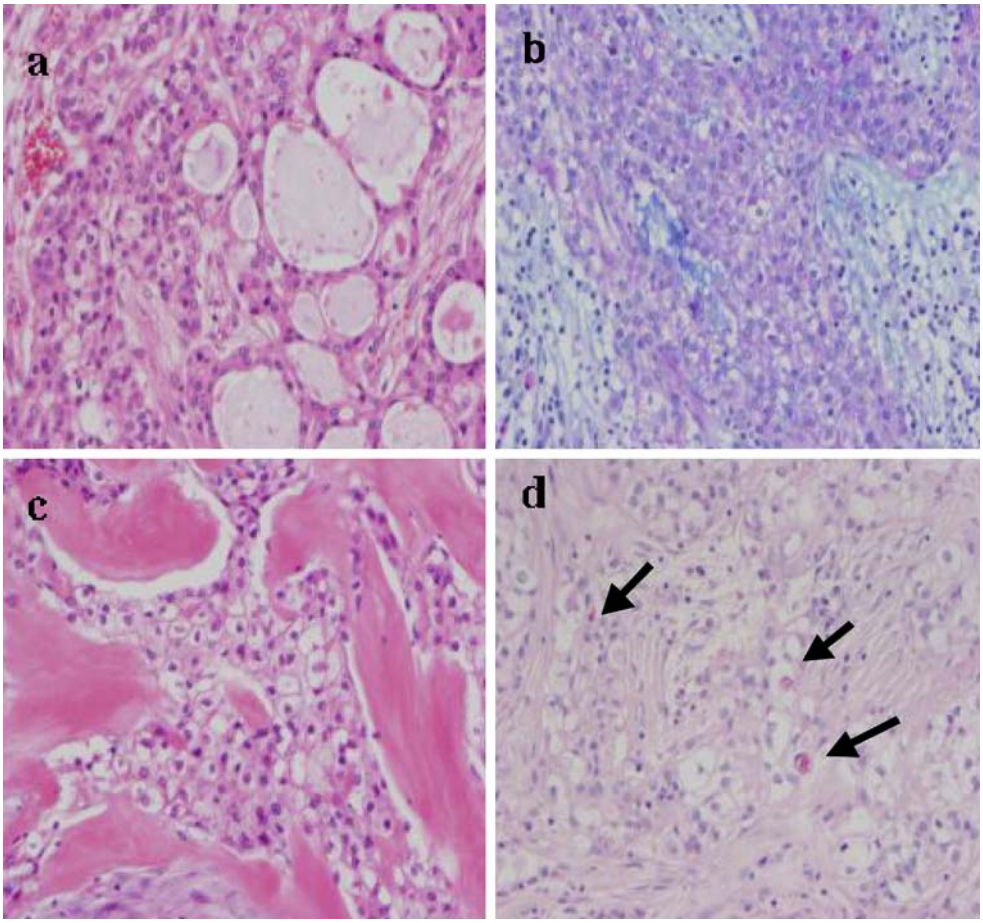

Fig. 3 Microscopic features of the resected specimen (Cases 1 and 2). **a**) Tumor nests of epidermoid cells and intermediate cells with hyalinous stroma are seen (Case 1). Note the admixture of clear cells. Also note the microcystic structure (hematoxylin and eosin stain). **b**) Intracytoplasmic glycogen is seen in the clear cells of the tumor nests (Case 1) (PAS and Alcian blue staining). **c**) Tumor nests of clear cells and intermediate cells which are circumscribed by marked hyalinized stroma are seen (Case 2) (hematoxylin and eosin stain). **d**) The tumor cells are positive for mucin staining in the intracytoplasmic lumen (Case 2) (arrows)

labeled part (hot spot) of this tumor (Fig. 4d). Although we detected EBER mRNA in the nasal NK/T lymphoma tissue as the positive control, we could find no signal for EBER mRNA (data not shown).

Case 2 The immunoprofile was similar to that of Case 1. Briefly, the tumor cells were positive for CKs, but negative for ASMA, S-100 protein, and E-cadherin. The tumor cells were focally positive for p63. Diffuse positivity for MUC1 and focal positivity for MUC6 were observed, while the tumor cells were negative for MUC2 and MUC5 (Fig. 4e). The Ki-67 labeling index was 4.3% in the most strongly labeled part (hot spot) of this tumor. In situ hybridization analysis for EBER showed no signals for tumor cells, stromal cells, or inflammatory cells (Fig. 4f).

Discussion

MEC arising from the nasopharynx is rare. To our knowledge, 19 cases of primary nasopharyngeal MEC, including the present cases, were reported. The male to female ratio is 11:8, and the mean age is 45.4 years old (range is 15 to 65 years old). Table 2 summarizes the clinical features, histological types and prognosis of the cases of salivary gland-type neoplasms of the nasopharynx reported in the English-language literature, including the present cases.

Neoplasms of the minor salivary glands are much less common than parotid tumors, accounting for roughly 15% of all salivary neoplasms. However, 50% of the minor salivary gland tumors are malignant [4, 5]. The frequency of minor salivary glands in the nasopharynx is low relative to that of the oral cavity, oropharynx, or sinonasal tract; therefore, adenocarcinomas are much less common in this location than elsewhere in the upper aerodigestive tract. Spiro et al. reported that the frequency of nasopharyngeal salivary gland-type neoplasms was approximately 2.0% in their minor salivary gland tumor series [13]. Recently, Kuo and Tsang reported 15 cases of salivary gland-type nasopharyngeal carcinoma, among which they found that MEC was the most common type (8 cases: 53%) [9]. On the other hand, in another study, the most common histological subtype was reported to be adenoid cystic carcinoma, accounting for 65% of the total, while MEC and adenocarcinoma, not otherwise specified, each accounted for approximately 15% [3, 4]. In 1975, Schmid and

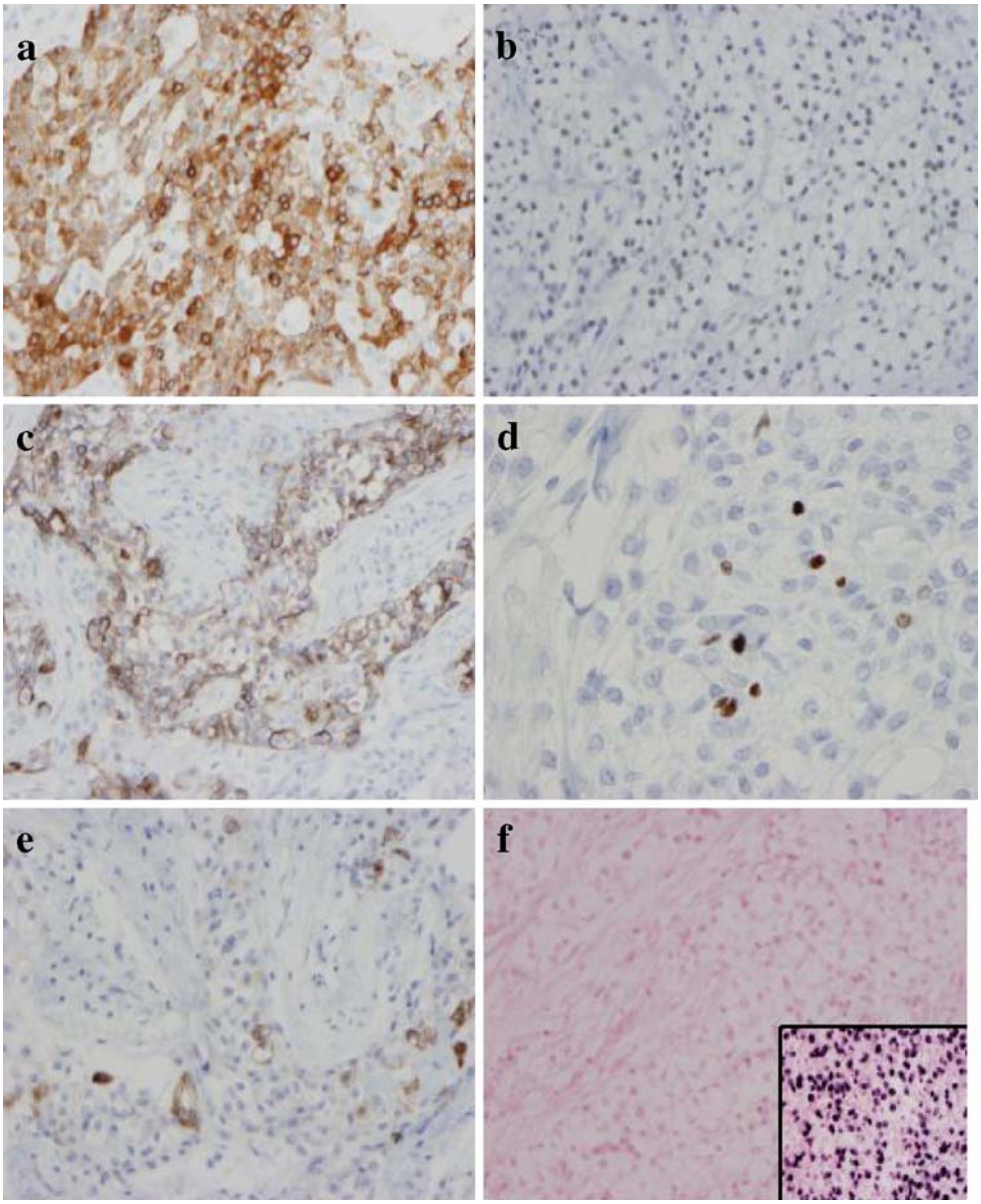

Fig. 4 Immunohistochemical features of the resected specimens. Immunoreactivity for high-molecular-weight keratin (**a**) and p63 (**b**) was observed in the tumor nests (Case 1). Immunoreactivity for p63 was seen diffusely in the nuclei of the clear cells of the tumor nests. Strong immunoreactivity for MUC1 was observed in the clear cells of the tumor nests (Case 1) (**c**). The tumor cells (Case 1) showed nuclear immunoreactivity for Ki-67 (**d**). Focal immunoreactivity for MUC6 was seen in the clear cells of the tumor nests (Case 2) (**e**). The tumor cells (Case 2) showed no signals for EBER in situ hybridization (Case 2) (**f**). Inset: strong positivity for EBER in situ hybridization is seen in the nasal NK/T lymphoma tissue used as a positive control

Table 2 Reported cases of primary nasopharyngeal salivary gland-type carcinoma

Reference	No. of Cases	Mean age (range)	Sex	Histological type	Follow-up
Kuo and Tsang [9]	15	50 (15–74)	11M 4F	MEC (*n*=8) ACC (*n*=2) AC (*n*=5)	NED (*n*=7) DOD (*n*=6) Lost (*n*=2)
Brown et al. [2]	3	46.3 (45–49)	2M 1F	MEC (*n*=3)	NED (*n*=2) DOD (*n*=1)
Schramm et al. [12]	23	43.6 (18–73)	11M 12F	ACC (*n*=11) MEC (*n*=8) AC (*n*=4)	NED (*n*=11) AWD (*n*=3) DOD (*n*=9)
van Hasselt et al. [6]	1	28	M	PapAC (*n*=1)	NED
Wenig et al. [14]	9	37 (11–64)	5M 4F	PapAC (*n*=9)	NED (*n*=9)
Present cases	2	57/51	F/F	MEC (*n*=2)	NED (*n*=2)

M, male; F, female; MEC, mucoepidermoid carcinoma; ACC, adenoid cystic carcinoma; AC, adenocarcinoma, not otherwise specified; PapAC, papillary adenocarcinoma; NED, no evidence of disease; AWD, alive with disease; DOD, dead of disease

Neuwirt first reported cases of MEC in rare locations [11], and in 1990, Li reported the salivary gland-type neoplasms originating in the nasopharynx [10]. The exact proportion of salivary gland-type neoplasms in the nasopahrynx has been uncertain, but MEC of the nasopharynx is much rarer than lymphoepithelioma and squamous cell carcinoma, which are common in the nasophaynx [8]. Previous reports indicated that MECs of the nasopharynx can be low-grade or high-grade [2, 9]. According to the Ki-67 labeling indices, the tumors in the present study had low proliferating activities, indicating low-grade malignancy. As the tumor cells in the present cases had clear cytoplasm and glycogen, the tumors were diagnosed as clear cell variants of MEC. The immunoprofiles of the present cases were similar to those of the conventional MEC of the major salivary glands: positive for mucin staining, cytokeratins, and EMA, but negative for myoepithelial markers including ASMA and S-100 protein [8].

Recently, the immunohistochemical expression of mucins (MUC1, MUC2, MUC4, MUC5AC, MUC5B, MUC6, MUC7) in salivary MECs was reported. High expression of MUC1 was related to high histological grades, high recurrence and metastasis rates and shorter disease-free intervals, whereas high MUC4 expression was mainly related to low-grade tumors, low recurrence rates and a longer disease-free intervals [1]. Salivary MEC expresses MUC1, MUC4, MUC5AC and MUC5B and less frequently MUC6, and rarely MUC2 and MUC7. Both of the present cases expressed MUC1 diffusely and MUC5AC and MUC6 focally, whereas they were negative for MUC2. Unfortunately, we could not examine the expression of MUC4, MUC5B, and MUC7. At follow-up approximately 2 and 6 months after surgery, there were no signs of lymph node metastasis or recurrence.

The frequency of nasopharyngeal carcinomas and EBV infection is very different between South China and other countries [7, 8]. Kuo and Tsang reported that salivary gland-type nasopharyngeal carcinomas are associated with Epstein–Barr virus (EBV) infection, as demonstrated by EBER in situ hybridization and PCR analysis of the LMP-1 gene [7, 9]. We performed the EBER in situ hybridization analysis, but both of the present cases were negative for EBER mRNA.

In conclusion, here we report two cases of nasopharyngeal MEC characterized by histochemical, immunohistological and genetic analyses. Nasopharyngeal MEC, which may originate from the minor salivary glands in the nasopahrynx, is extremely rare in Japan. As the Ki-67 labeling index was low, the high expression of MUC1 in the present tumors may not have been related to high-grade malignancy.

Acknowledgments The authors thank Mr. Isamu Hayashi, Mr. Kazuhiro Kawabata, Mr. Yoichi Watanabe, Ms. Yukiko Fukazawa, Mr. Kiyoshi Tone, Mr. Koji Muramatsu, Ms. Kaori Nagata, Ms. Sayaka Tokushige, Mr. Hiroshi Tashiro, Ms. Tsukumi Yabuzaki, Mr. Eiichiro Simmori, Ms. Sachiyo Ohno, Mari Hiyoshi, and Mr. Masataka Honda, the staff of the Division of Pathology, Shizuoka Cancer Center, Shizuoka, Japan, for the technical assistance. We are grateful to Mr. Koji Sugawara, the staff of the Photo Center, Shizuoka Cancer Center, Shizuoka, Japan, for the help with the preparation of the figures.

References

1. Alos L, Lujan B, Castillo M, Nadal A, Carreras M, Caballero M, de Bolos C, Cardesa A (2005) Expression of membrane-bound mucins (MUC1 and MUC4) and secretory mucins (MUC2, MUC5AC, MUC5B, MUC6 and MUC7) in mucoepidermoid carcinomas of salivary glands. Am J Surg Pathol 29:806–813
2. Brown J, Choi EC, Fee WE Jr (1999) Nasopharyngectomy for recurrent high-grade mucoepidermoid carcinoma after radiation failure. Otolaryngol Head Neck Surg 120:564–566
3. Ellis ER, Million RR, Medenhall WM, Parsons JT, Cassisi NJ (1988) The use of radiation therapy in the management of minor salivary gland tumors. Int J Radiat Oncol Biol Phys 15:613–617
4. Garden AS, Weber RS, Ang KK, Morrison WH, Matre J, Peters LJ (1994) Postoperative radiation therapy for malignant tumors of minor salivary glands. Cancer 73:2563–2569
5. Gates GA (1982) Current concepts in otolaryngology: malignant neoplasms of the minor salivary glands. N Engl J Med 306:718–722
6. van Hasselt CA, Ng HK (1991) Papillary adenocarcinoma of the nasopharynx. J Laryngol Otol 105:853–854
7. Hu LF, Zabarovsky ER, Chen F, Cao SL, Ernberg I, Kein G, Winberg G (1991) Isolation and sequencing of the Epstein–Barr virus BNLM-1 gene (LMP1) from a Chinese nasopharyngeal carcinoma. J Gen Virol 72:2399–2409
8. Kuo TT, Chan JKC, Wenig BM, Eveson JW (2005) Nasopharyngeal adneocarcinoma and salivary gland-type carcinoma. In: Barnes L, Eveson JW, Reichart P, Sidransky D (eds). World Health Organization Classification Tumours: Pathology & Genetics Head and Neck Tumours. WHO Publications Center, Albany, NY, USA, IARC Press, Lyon, p98
9. Kuo TT, Tsang NM (2001) Salivary gland type nasopharyngeal carcinoma: a histologic, immunohistochemical, and Epstein–Barr virus study of 15 cases including a psammomatous mucoepidermoid carcinoma. Am J Surg Pathol 25:80–86
10. Li TS (1990) Minor salivary gland tumors of the nasopharynx. Zhonghua Zhongliu Zazhi 12:127–129
11. Schmid E, Neuwirth H (1975) On mucoepidermoid tumors with rare locations in laryngological areas (author's transl). Laryngol Rhinol Otol 54:290–296(German)
12. Schramm VL Jr, Imora MJ (2001) Management of nasopharyngeal salivary gland malignancy. Laryngoscope 111:1533–1544
13. Spiro RH, Koss LG, Hajdu SI, Strong EW (1973) Tumors of minor salivary origin. A clinicopathologic study of 492 cases. Cancer 31:117–129
14. Wenig BM, Hyams VJ, Heffner DK (1988) Nasopharyngeal papillary adenocarcinoma: a clinicopathologic study of a low-grade carcinoma. Am J Surg Pathol 12:946–953

Virchows Arch (2007) 450:349–353
DOI 10.1007/s00428-006-0345-8

CASE REPORT

Extrauterine endometrial stromal sarcoma with *JAZF1/JJAZ1* fusion confirmed by RT-PCR and interphase FISH presenting as an inguinal tumor

Katsuaki Sato · Yoshimichi Ueda · Junichi Sugaya · Mamoru Ozaki · Masanori Hisaoka · Shogo Katsuda

Received: 31 March 2006 / Accepted: 30 October 2006 / Published online: 18 January 2007
© Springer-Verlag 2007

Abstract Endometrial stromal sarcomas are rare malignant mesenchymal tumors that usually develop in the uterine corpus and occasionally arise at various extrauterine sites. This report describes the first case of primary extrauterine endometrial stromal sarcoma arising in the extraperitoneal portion of the round ligament presenting as a solitary inguinal mass in a 46-year-old woman. The patient presented gradually growing tumor in the right inguinal region. Local tumor resection was performed and no recurrence or metastasis was found at 15 months after the operation. Histological examination revealed that the tumor comprised uniform, spindle-shaped cells with blunt nuclear figure and scattered small arteries, and infiltrated into adjacent tissue. No endometriosis was morphologically identified in the lesion. Immunohistochemically, the tumor cells were positive for CD10, estrogen receptor, progesterone receptor, α-smooth muscle actin, and calponin. We confirmed *JAZF1*/*JJAZ1* fusion by reverse transcription–polymerase chain reaction and the corresponding chromosomal translocation by interphase fluorescence in situ hybridization on paraffin sections. It is essential that the inguinal region should be recognized as a possible primary site of endometrial stromal sarcoma, and the detection of a *JAZF1*/*JJAZ1* fusion can be useful when the diagnosis is not confirmed by microscopic observation or immunohistochemistry for the tumor arising in extrauterine sites.

Keywords Endometrial stromal sarcoma · Inguinal hernia · Round ligament · *JAZF1*/*JJAZ1* · Interphase FISH

K. Sato (✉) · Y. Ueda · S. Katsuda
Department of Pathophysiological and Experimental Pathology,
Kanazawa Medical University,
1-1 Daigaku, Uchinada, Kahoku,
Ishikawa 920-0293, Japan
e-mail: sato-k@kanazawa-med.ac.jp

J. Sugaya
Department of Surgical Oncology, Kanazawa Medical University,
Ishikawa, Japan

M. Ozaki
Division of Human Genetics, Medical Research Institute,
Kanazawa Medical University,
Ishikawa, Japan

M. Hisaoka
Department of Pathology and Oncology, School of Medicine,
University of Occupational and Environmental Health,
Kitakyushu, Japan

Introduction

Endometrial stromal sarcoma (ESS) is a rare type of uterine tumor that accounts for less than 10% of uterine sarcomas [10]. The World Health Organization's classification of tumors of the breast and female genital organs subclassified endometrial stromal tumors into three categories: endometrial stromal nodule, low-grade ESS, and undifferentiated endometrial sarcoma (UES) [3]. The tumors traditionally called high-grade ESS were recently reclassified as UES due to their lack of specific differentiation and histological resemblance to endometrial stroma [3]. Accordingly, ESS only means low-grade ESS. ESS was distinguished from the endometrial stromal nodule based on the presence of an infiltrative growing character or vascular invasion in ESS [4, 5, 7, 8].

Recently, a fusion of two zinc finger genes, *JAZF1* and *JJAZ1*, caused by a reciprocal translocation t(7;17)(p15;q21) was detected in more than 80% of ESS cases [4, 5, 7, 8]. Furthermore, *JAZF1*/*PHF1* or *EPC1*/*PHF1* fusion also presented in a small number of ESS cases [9]. Diagnosis of

ESS has been dependent on histological findings supported by immunohistochemical examination. However, it could be difficult to get to a definite diagnosis for monophasic spindle cell tumors, especially when an unusual location was involved. Molecular detection of specific fusion transcripts could overcome these problems and should become a potent diagnostic tool for ESS.

ESS's usually develop as primary uterine tumor, but ESS's of extrauterine origin, such as the ovary, fallopian tube, pelvic cavity, abdominal cavity, omentum, retroperitoneum, vagina, vulva, and sigmoid colon, have been reported [2, 6]. The round ligament passes through the inguinal canal and comprises mainly smooth muscle, fibrous tissue, blood vessels, and nerves [12]. Most round ligament tumors are leiomyomas or fibromas, and there is no previous report of ESS arising in the inguinal portion of the round ligament.

We described the first case of primary extrauterine ESS arising from the round ligament in the inguinal canal, unassociated with endometriosis, with a confirmed *JAZF1*/*JJAZ1* fusion by reverse transcription–polymerase chain reaction (RT-PCR) and interphase fluorescence in situ hybridization (FISH) analysis.

Clinical history

A 46-year-old woman, para 3 and gravida 3, presented with an indolent mass in the right inguinal region. Her menstrual cycle was regular, and her gynecologic history was unremarkable. Physical examination suggested an inguinal hernia. The MRI showed a demarcated 3.0-cm solid mass in the right inguinal canal (Fig. 1a), and no significant lesion in the uterus. Tumor resection was performed. At the operation, the tumor was not covered with a hernia sac nor adhered to the peritoneum but attached to the extraperitoneal portion of the round ligament. There was no evidence of recurrence or metastasis 15 months after surgery.

Materials and methods

Surgically resected specimen was fixed in 10% neutral-buffered formalin, cut into 6 tissue blocks of 5 mm in thickness, and embedded in paraffin. Sections, 4-μm thick, were used for hematoxylin and eosin staining, immunohistochemical studies, molecular analysis, and interphase FISH.

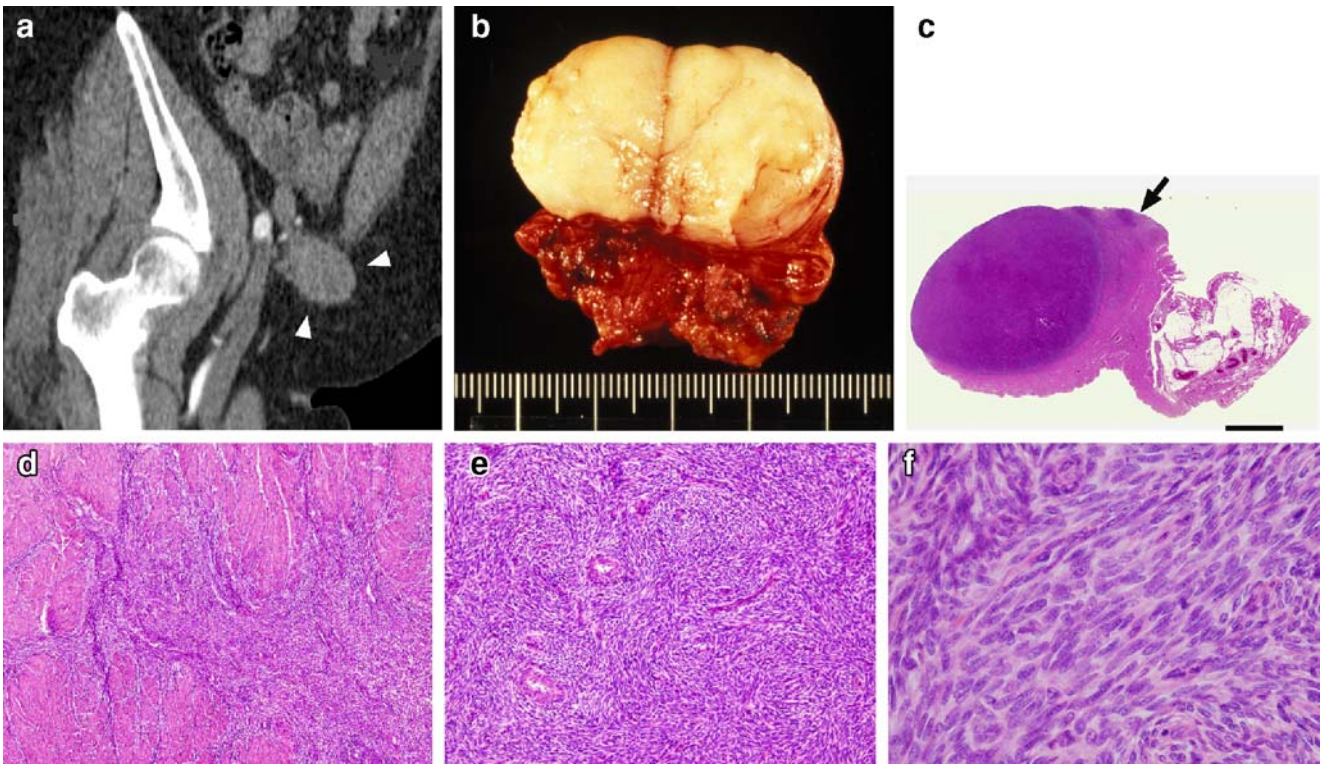

Fig. 1 **a** MRI showing a mass (*arrow head*) in the right inguinal canal. **b** Macroscopic appearance of the cut surface of the tumor showing a yellow-white tumor. **c** Panoramic view of the tumor demonstrating invasion to adjacent tissue (*arrow*). H & E staining; scale bar, 5 mm. **d** The tumor cells infiltratively growth into the adjacent smooth muscle tissue of the round ligament. H & E staining (original magnification ×40). **e** The tumor is densely cellular, and whorls around small arteries are observed. H & E staining (original magnification ×100). **f** The tumor cells are uniform, short, and spindle shaped. H & E staining (original magnification ×400)

Immunohistochemistry

Immunohistochemical examinations were performed on deparaffinized thin sections using the standard avidin–biotin–peroxidase complex method with an automated immunostainer (Ventana Medical System, Tucson, AZ, USA). Primary antibodies against following antigens were used: low molecular weight cytokeratin (CAM5.2, prediluted, Becton–Dickinson, San Jose, CA, USA), high molecular weight cytokeratin (34βE12, 1:75, Dako, Glostrup, Denmark), vimentin (V9, 1:100, Dako), α-smooth muscle actin (1A4, 1:200, Dako), desmin (D33, 1:100, Dako), calponin (CALP, 1:75, Dako), high-molecular-weight caldesmon (h-caldesmon; h-CD, 1:100, Dako), bcl-2 (124, 1:50, Dako), E-cadherin (NCH-38, 1:100, Dako), epithelial membrane antigen (EMA; E29, 1:100, Dako), CD10 (56C6, 1:20, Novocastra, Newcastle upon Tyne, UK), CD34 (NU-4A1, 1:100, Nichirei, Tokyo, Japan), CD117 (c-kit; polyclonal, 1:80, Dako), estrogen receptor (1D5, 1:50, Dako), progesterone receptor (PgR636, 1:800, Dako), calretinin (polyclonal, prediluted, Invitrogen, Carlsbad, CA, USA), inhibin-α (R1, 1:50, Dako), S-100 protein (2A10, Immuno-Biological Laboratories, Gunma, Japan), and Ki-67 (MIB-1, 1:50, Dako). Antigen retrieval was carried out with appropriate methods for each antibody.

Molecular analysis

Three sections cut from paraffin-embedded tissue were prepared for RT-PCR. The RNA extraction and RT-PCR to identify the *JAZF1*/*JJAZ1* fusion was carried out as previously described using the following primers: JAZF1-369-FW (5′-CCACCCATCACCCCCTCCT-3′) and JJAZ1-400-RV (5′-TGCTATGAGATTCCGAGTTC-3′) [5]. To confirm the *JAZF1*/*JJAZ1* fusion, PCR products extracted from a corresponding band in agarose gel were analyzed by direct sequencing. The RT-PCR for detection of *SYT*/*SSX* fusion transcripts, frequently observed in synovial sarcoma, were performed as reported elsewhere [11, 13].

Interphase fluorescence in situ hybridization

The interphase FISH was performed on the paraffin-embedded tissue sections. The probes used were derived from bacterial artificial chromosomes (BAC). BAC clones were commercially purchased from Invitrogen. To detect chromosomal translocations, *JAZF1/JJAZ1* fusion, the probes were selected as follows: RP11-350G16 encompassing the entire *JAZF1* gene mapping to 7p15 and CTD-3205H10 fully covering the *JJAZ1* gene mapping to 17q21 according to the mapping data at the NCBI map viewer website (http://www.ncbi.nlm.nih.gov/mapview/static/MVstart.html). RP11-350G16 and CTD-3205H10 were labeled with digoxigenin and biotin, respectively, with Nick translation mix (Roche Diagnostics, Basel, Switzerland). The slides were deparaffinized in xylene and rehydrated in ethanol. The slides were pretreated by microwaving in 10-mmol citrate buffer (pH 6.0) at 90°C for 15 min. The extracellular matrix in the tissue section was digested using 0.2% pepsin (in 0.01 NHCl) for 10 min at 37°C. The DNA in the tissue sections and the probes were codenatured for 10 min at 90°C, and incubated in a humidified box at 37°C for 48 h. Digoxigenin-labeled probes were detected with rhodamine-conjugated antidigoxigenin antibody, and biotinylated probes were detected with conjugated avidin (Alexa Fluor 488, Molecular Probes, Eugene, OR, USA). The nuclei were counterstained with mounting medium containing 4′,6-diamidino-2-phenylindole (Vector, Burlingame, CA, USA). The probe signals were detected using a fluorescence microscope with a digital camera, with rhodamine as red and Alexa Fluor 488 as green label. For each slide, more than 100 nuclei of tumor cells were analyzed. The composed images were reconstructed with Adobe Photoshop 6.0 software (Adobe, San Jose, CA, USA).

Results

Macroscopically, the tumor was demarcated, adhered to fibromuscular tissue of the round ligament, and had a maximum diameter of 3 cm. The cutting surface of the tumor displayed a yellow-white color and had an elastic hard consistency (Fig. 1b). No necrosis or hemorrhage was apparent.

Microscopically, the tumor cells infiltrated the adjacent smooth muscle tissue of the round ligament at the periphery, 10 mm away from the main mass (Fig. 1c and d). The tumor was highly cellular, and whorls of the tumor cells around small arteries were observed (Fig. 1e). The tumor cells were uniform and spindle-shaped, and had bland nuclei and indistinct cytoplasmic margins (Fig. 1f). Mitotic figures were rare. There was no evidence of vascular invasion or endometriosis throughout the entire specimen.

Immunohistochemically, the tumor cells were positive for CD10, estrogen receptor, progesterone receptor, bcl-2, vimentin, α-smooth muscle actin, and calponin but negative for low and high molecular weight cytokeratin, desmin, h-caldesmon, E-cadherin, EMA, CD34, CD117, calretinin, inhibin-α, and S-100 protein. Less than 1% of tumor cells were positive for Ki-67.

The RT-PCR for the detection of the *JAZF1*/*JJAZ1* fusion transcript showed a fusion product at the expected level of 93 bp as previously reported (Fig. 2a). The fusion of *JAZF1* and *JJAZ1* genes was confirmed by direct sequencing (Fig. 2b). No *SYT–SSX1* or *SYT–SSX2* fusions were detected.

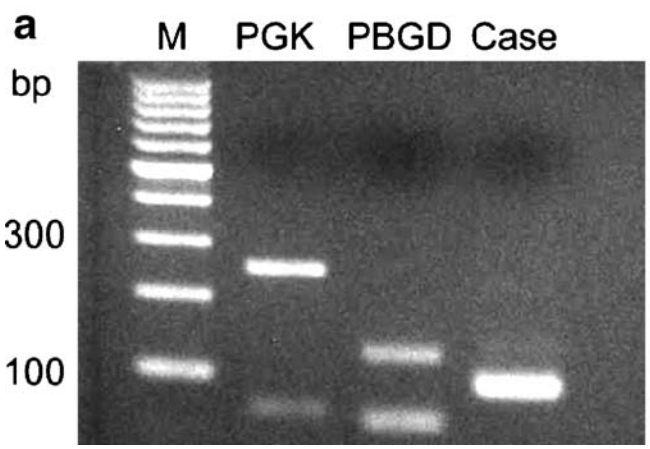

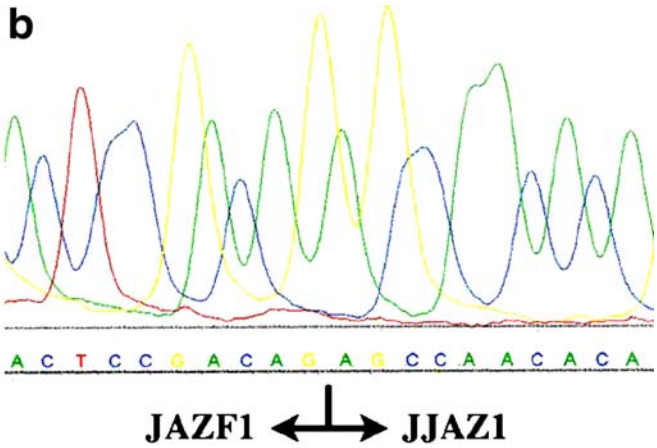

Fig. 2 Detection of the *JAZF1*/*JJAZ1* fusion transcript. **a** Fusion transcript is amplified and identified in the expected range of 93 bp. **b** Partial chromatogram showing the junction of the *JAZF1*/*JJAZ1* fusion gene (*arrows*). *M* 100-bp DNA ladder, *PGK* phosphoglycerate kinase (247 bp, internal control), *PBGD* porphobilinogen deaminase (127 bp, internal control), *Case* RNA extracted from the present tumor

The interphase FISH revealed a *JAZF1*/*JJAZ1* fusion as a result of a reciprocal translocation between 7p15 and 17q21 (Fig. 3).

Discussion

ESS's usually arise in the uterine corpus and are composed of uniform ovoid to slightly spindle-shaped cells. However, these tumors occasionally present elongated spindle-shaped cells that are hard to distinguish from various spindle cell tumors and may be confused with other tumors. In this case, histological diagnosis was difficult because the tumor developed in the extrauterine site, the inguinal region, and comprised uniform, elongated spindle-shaped cells.

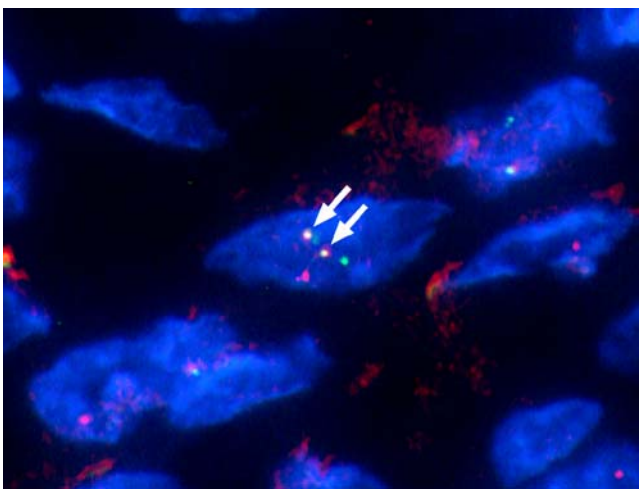

Fig. 3 Interphase FISH analysis on a paraffin section. Two fusion spots (merge signal, *arrows*), one red spot and one green spot, indicate *JAZF1*/*JJAZ1* fusion originating from a reciprocal translocation between 7p15 and 17q21

Immunohistochemical findings supported the differential diagnosis for spindle cell tumor. The present tumor was positive for CD10, estrogen receptor, progesterone receptor, α-smooth muscle actin, calponin but negative for desmin and h-caldesmon. These findings supported the diagnosis of ESS. Monophasic fibrous synovial sarcoma (MFSS) is a representative spindle-shaped soft tissue tumor that resembles ESS histologically, demonstrating *SYT*/*SSX1* or *SYT*/*SSX2* chimera gene in more than 90% of the cases [13]. In this case, although these chimera genes were not revealed by RT-PCR using RNA extracted from paraffin-embedded tissues, the diagnosis of MFSS could not completely be excluded from these negative results only.

Previous studies examining the genetic aspects of ESS's revealed frequent chromosomal abnormalities of 6p, 7p, and 17q [8]. In recent years, a specific chromosomal rearrangement t(7;17)(p15;q21) resulting in a *JAZF1*/*JJAZ1* fusion transcript was reported in ESS [4, 5, 7, 8]. The *JAZF1*/*JJAZ1* fusion in ESS was described in 5 of 5 cases by Koontz et al. [7], 1 of 3 cases by Micci et al. [8], 3 of 13 cases including variant types by Huang et al. [4], and 16 of 20 cases by Hrzenjak et al. [5]. Micci et al. [9] identified ESS cases with two other genetic alterations, t(6;7)(p21;p15) leading to a *JAZF1*/*PHF1* fusion gene and t(6;10;10)(p21;q22;p11) causing a *EPC1/PHF1* fusion gene. The *JAZF1*, *JJAZ1*, and *PHF1* genes all encode zinc finger domains often found in DNA-binding proteins, and fusion genes previously reported in ESS, *JAZF1*/*JJAZ1*, *JAZF1*/*PHF1*, and *EPC1/PHF1* could express unusual proteins with zinc finger motifs. Wild-type *JAZF1* is expressed in normal endometrium, and loss of expression for normal *JAZF1* was demonstrated in some ESS cases [7]. The function of the *JAZF1* gene has not been elucidated, but it has been suggested that *JAZF1* might have a role in tumor suppression, and abnormal fusion proteins with DNA-

binding activities could deregulate the transcriptional process of other genes [7, 9]. The recognition of the *JAZF1*/*JJAZ1* fusion gene was crucial and unique in diagnosing ESS. The detection of these chimera genes should become a specific diagnostic tool, especially when the ESS arises at an extrauterine site. In this case, *JAZF1*/*JJAZ1* fusion was confirmed by RT-PCR and interphase FISH.

Primary ESS's have been reported in various extrauterine locations [2, 6]. Irvin et al. [6] reported a case of ESS that occurred in the endometriosis of the vulva in association with the extrapelvic portion of the round ligament; however, an ESS arising from the round ligament in the inguinal canal has not been described. Some cases of extrauterine ESS included endometriosis, but many of the extrauterine ESS's described in the literature have been unassociated with endometriosis [2]. There are many reports of inguinal endometriosis often presenting as an inguinal hernia, and approximately 90% of these cases have right-side lesion [1]. The present case showed a right groin mass, but there was no endometriosis within the lesion as determined by histological examination.

In conclusion, it is important to recognize that ESS can develop in extrauterine sites such as the inguinal region, and the detection of *JAZF1*/*JJAZ1* fusion can be useful when the diagnosis is not definitive by other studies including light microscopy and immunohistochemistry.

Acknowledgment The authors thank Hideaki Ninomiya and Yoshitame Yanaida (Department of Pathology, Kanazawa Medical University Hospital, Ishikawa, Japan) for the immunohistochemistry. This work was supported by a grant for promoted research from Kanazawa Medical University (S2006-3).

References

1. Candiani GB, Vercellini P, Fedele L, Vendola N, Carinelli S, Scaglione V (1991) Inguinal endometriosis: pathogenetic and clinical implications. Obstet Gynecol 78:191–194
2. Chang KL, Crabtree GS, Lim-Tan SK, Kempson RL, Hendrickson MR (1993) Primary extrauterine endometrial stromal neoplasms: a clinicopathologic study of 20 cases and a review of the literature. Int J Gynecol Pathol 12:282–296
3. Hendrickson MR, Tavassoli FA, Kempson RL, McCluggage WG, Haller U, Kubik-Huch RA (2003) Mesenchymal tumours and related lesions. In: Tavassoli FA, Devilee P (eds) World Health Organization classification of tumours. Pathology and genetics of tumours of the breast and female genital organs. IARC, Lyon, pp 233–244
4. Huang HY, Ladanyi M, Soslow RA (2004) Molecular detection of *JAZF1–JJAZ1* gene fusion in endometrial stromal neoplasms with classic and variant histology: evidence for genetic heterogeneity. Am J Surg Pathol 28:224–232
5. Hrzenjak A, Moinfar F, Tavassoli FA, Strohmeier B, Kremser ML, Zatloukal K, Denk H (2005) *JAZF1*/*JJAZ1* gene fusion in endometrial stromal sarcomas: molecular analysis by reverse transcriptase–polymerase chain reaction optimized for paraffin-embedded tissue. J Mol Diagn 7:388–395
6. Irvin W, Pelkey T, Rice L, Andersen W (1998) Endometrial stromal sarcoma of the vulva arising in extraovarian endometriosis: a case report and literature review. Gynecol Oncol 71:313–316
7. Koontz JI, Soreng AL, Nucci M, Kuo FC, Pauwels P, van Den Berghe H, Cin PD, Fletcher JA, Sklar J (2001) Frequent fusion of the *JAZF1* and *JJAZ1* genes in endometrial stromal tumors. Proc Natl Acad Sci USA 98:6348–6353
8. Micci F, Walter CU, Teixeira MR, Panagopoulos I, Bjerkehagen B, Saeter G, Heim S (2003) Cytogenetic and molecular genetic analyses of endometrial stromal sarcoma: nonrandom involvement of chromosome arms 6p and 7p and confirmation of *JAZF1*/*JJAZ1* gene fusion in t(7;17). Cancer Genet Cytogenet 144:119–124
9. Micci F, Panagopoulos I, Bjerkehagen B, Heim S (2006) Consistent rearrangement of chromosomal band 6p21 with generation of fusion genes *JAZF1*/*PHF1* and *EPC1*/*PHF1* in endometrial stromal sarcoma. Cancer Res 66:107–112
10. Moinfar F, Gogg-Kamerer M, Sommersacher A, Regitnig P, Man YG, Zatloukal K, Denk H, Tavassoli FA (2005) Endometrial stromal sarcomas frequently express epidermal growth factor receptor (EGFR, HER-1): potential basis for a new therapeutic approach. Am J Surg Pathol 29:485–489
11. Okamoto S, Hisaoka M, Daa T, Hatakeyama K, Iwamasa T, Hashimoto H (2004) Primary pulmonary synovial sarcoma: a clinicopathologic, immunohistochemical, and molecular study of 11 cases. Hum Pathol 35:850–856
12. Smith P, Heimer G, Norgren A, Ulmsten U (1993) The round ligament: a target organ for steroid hormones. Gynecol Endocrinol 7:97–100
13. Tsuji S, Hisaoka M, Morimitsu Y, Hashimoto H, Shimajiri S, Komiya S, Ushijima M, Nakamura T (1998) Detection of SYT-SSX fusion transcripts in synovial sarcoma by reverse transcription–polymerase chain reaction using archival paraffin-embedded tissues. Am J Pathol 153:1807–1812

Virchows Arch (2007) 450:355–358
DOI 10.1007/s00428-007-0371-1

CASE REPORT

Primary mediastinal anaplastic alk-1-positive large-cell lymphoma of T/NK-cell type expressing CD20

J. Gonin · H. Kadiri · S. Bensaci · A. Le Tourneau · T. J. Molina · J. Diebold · D. J. Abdellouche · J. Audouin

Received: 31 July 2006 / Revised: 13 December 2006 / Accepted: 9 January 2007 / Published online: 25 January 2007
© Springer-Verlag 2007

Abstract We describe an unusual case of ALK-1-positive primary mediastinal lymphoma with the morphology of an anaplastic large-cell lymphoma (ALCL) of T/NK cell type but expressing CD20. This tumour had T/NK morphology and immunophenotype, as demonstrated by its expression of CD30, EMA, ALK-1, CD7 and TiA-1 and the lack of expression of B-cell markers other than CD20. The significance of such a co-expression of a B cell-associated antigen in a case of ALCL of T/NK cell type is discussed.

Keywords Anaplastic ALK-1 positive large-cell lymphoma T/NK · Aberrant CD20 expression · Mediastinum lymphoma

Introduction

CD20 is a membrane protein involved in regulating B-cell activation. It is considered to be a specific marker for cells of the B lineage [3]. We report, here, a case of anaplastic large-cell lymphoma (ALCL) of the T/NK type expressing CD20 and discuss, based on a short review of the literature, the significance of this expression.

J. Gonin · H. Kadiri · A. Le Tourneau · T. J. Molina · J. Diebold (✉) · J. Audouin
Service Central d'Anatomie et Cytologie Pathologiques, "Jacques Delarue", Hôtel-Dieu,
1, place du parvis Notre-Dame,
75181 Paris Cedex 04, France
e-mail: anapath.hd@htd.aphp.fr

S. Bensaci · D. J. Abdellouche
Département de pathologie, Centre Hospitalier,
Sétif, Algéria

Clinical history

In 2002, an 11-year-old boy was referred to the Pathology Department of Hôtel-Dieu Hospital (Paris, France) from Setif Hospital (Setif, Algeria). This Algerian boy presented with a 1-month history of cough, chest pain, and weight loss, with no sign of immunodepression. Thoracic computed tomography (CT)-scan revealed a 14×7 cm mass located in the postero-inferior mediastinum, invading the subcutaneous and paravertebral spaces. This mass compressed the left bronchus, causing segmental atelectasia. There were no signs of bone lysis or mediastinal adenopathy. A biopsy was performed on this mass.

Materials and methods

Tissues were fixed in 10% formalin, embedded in paraffin and cut into 5 μm sections, which were stained with haematein–eosin, Giemsa stain and impregnated with silver by the Gordon–Sweet method. Immunohistochemical studies were performed on paraffin sections, using the three-step immunoperoxidase method with microwave pretreatment (Table 1).

Results

Histology

We received one paraffin block with two fragments, each measuring 1 cm and showing the same histological pattern. Both presented a diffuse infiltrate, masking the normal tissue. This infiltrate consisted of medium to large cells with an abundant pale cytoplasm (Fig. 1a). The nuclei

Table 1 Summary of immunohistochemistry materials and results

Antigen	Name	Source	Result
CD30	Ber-H2	Dako, Glostrup, Denmark	+ Membranous and Golgi punctate pattern
EMA	E29	Dako	+ Membranous and cytoplasmic
ALK-1	ALK-1	Dako	+ Cytoplasmic and nuclear
CD20	L26	Dako	+ Membranous
CD79a	JCB117	Dako	−
Kappa	Polyclonal	Dako	−
Lambda	Polyclonal	Dako	−
CD7	272	Tebu, Le Perray en Yvelines, France	+ 30–40% of tumour cells
TiA-1	TiA-1	Immunotech, Luminy, France	+ cytoplasmic granular
Granzyme B	GRANZ-B	Tebu	+ 10% of tumour cells, cytoplasmic granular
CD2	AB75	Tebu	−
CD3	polyclonal	Dako	−
CD5	4C7	Tebu	−
CD8	114B	Dako	−
CD56	1B6	Tebu	−
CD57	NK1	Dako	−
Bcl2	124	Dako	−
Cytokeratins	KL1	Immunotech	−
LMP-1	CS1/4	Dako	−

contained finely dispersed chromatin and one or two prominent nucleoli. The nuclei varied considerably in shape: round, ovoid, bilobulated and horseshoe-shaped or multilobulated (Fig. 1b). Some large multinucleated cells were also present. Mitotic figures were frequent. A few small lymphocytes and histiocytes were scattered between the tumour cells. Small necrotic areas were also dispersed throughout the infiltrate. In some places, the tumour had been destroyed by large areas of ischaemic necrosis.

Immunohistochemistry

The tumour cells strongly expressed CD30 (Fig. 2a) and EMA. Punctate ALK-1 staining was observed around the nucleus (Golgi apparatus) in most cells, but well-defined nuclear staining was observed in some cells, suggesting nucleophosmin-ALK-1 rearrangement [1] (Fig. 2b). Approximately 30 to 40% of the tumour cells expressed CD7 (Fig. 2c). All expressed TiA-1. Only a few (10%) showed strong granzyme B expression. The demonstration of perforin was not interpretable, probably due to the fixative which has been used (Bouin's solution) and also to the very low number of tumour cells present on the remaining section. However, all the other T/NK markers studied were negative (CD2, CD3, CD5, CD4, CD8). Surprisingly, the membranes of all the tumour cells were strongly stained for CD20 (Fig. 2d), whereas CD79a staining was negative. Staining for the kappa and lambda immunoglobulin light chains was also negative. The expression of Pax5 gene

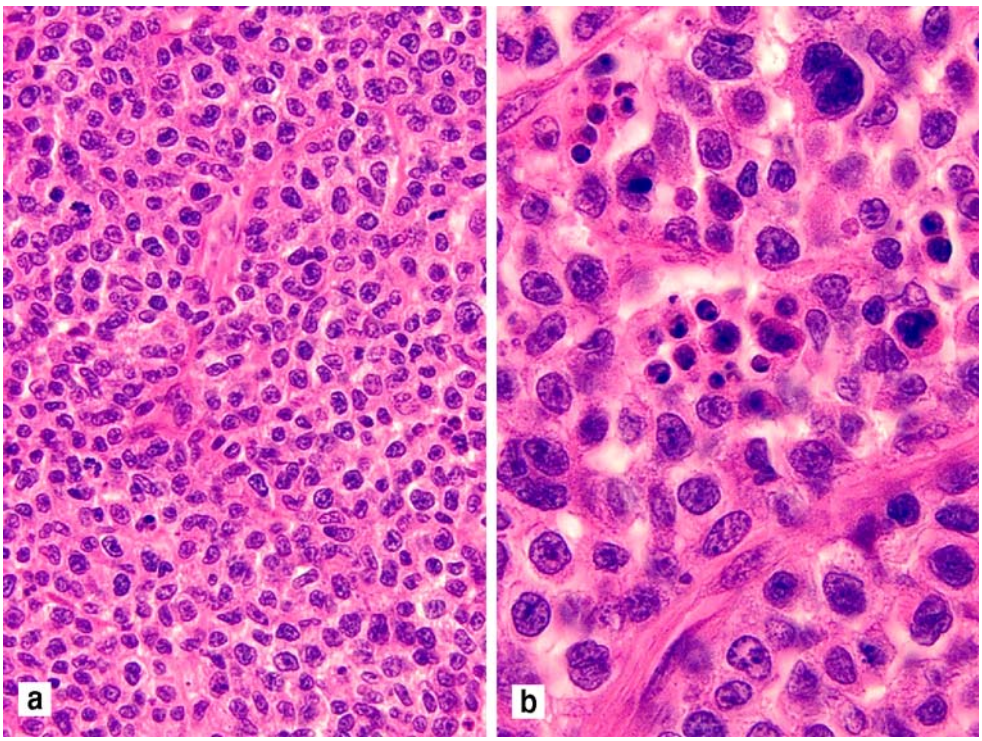

Fig. 1 Haematein and eosin. **a** G×40. Diffuse infiltration by large cells with irregular nuclei. **b** G×100. Note the presence of cells with multilobulated nuclei and with a horseshoe-shaped nucleus

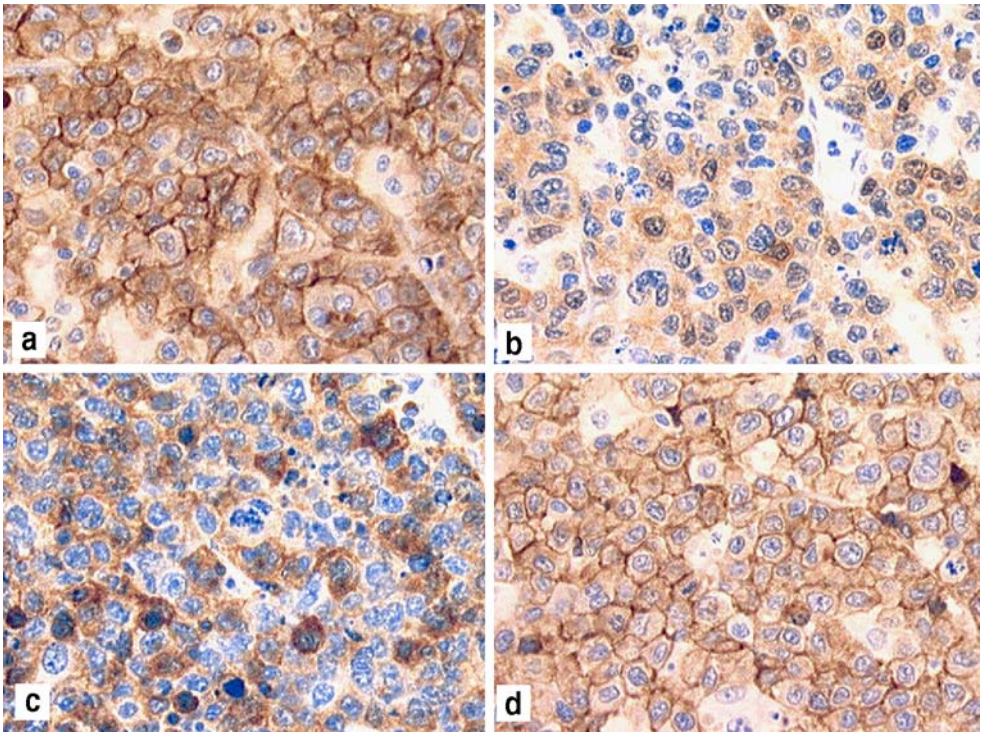

Fig. 2 Immunoperoxidase: G× 100. The tumour cells express CD30 with a cytoplasmic and a Golgi staining (**a**), ALK-1 with a cytoplasmic, membranous and sometimes nuclear staining (**b**), CD7 with a cytoplasmic staining (**c**) and CD20 on the membrane (**d**)

product, a good marker for a B cell origin, could not be evaluated due to the absence of material. Moreover, the Bouin fixation strongly decreases the chance to detect such nuclear antigen by immunohistochemistry.

Molecular biology

Polymerase chain reaction (PCR) was carried out on formalin-fixed and paraffin-embedded tissue, to check for B and T rearrangement. Unfortunately, this approach was unsuccessful due to DNA degradation as a result of fixation.

Discussion

We report a case of mediastinal large-cell lymphoma presenting the morphology of a T/NK anaplastic large-cell lymphoma defined according to the WHO classification [7, 9]. The immunophenotype of this tumour was also typical, with the neoplastic cells expressing CD30, EMA and ALK-1. The T/NK origin of the tumour is demonstrated by the expression of CD7, TiA1 and granzyme B, with no staining observed for any other T-cell marker. However, this T/NK ALCL also strongly expressed one B cell-associated antigen, CD20. We were unable to demonstrate the T-cell origin of the tumour by molecular biological analysis of paraffin-embedded tissue because the fixation process had resulted in nucleic acid degradation. Unfortunately, the absence of results for perforin and Pax5 gene product did not help us to confirm a T cell origin or to demonstrate a B cell origin of the tumour cells.

The mediastinal site of this tumour does not rule out a diagnosis of ALCL of T/NK origin, as several similar cases have been reported in adults and children. In the GELA (*Groupe d'Etude des Lymphomes de l'Adulte*) series [12], mediastinal involvement was found in 24% of ALCL of T/NK-cell type.

Differential diagnoses for our case include ALCL of B-cell phenotype, a rare condition [5]. ALCL of B-cell phenotype have a similar anaplastic morphology and express CD20. However, they also express other B-cell markers, such as CD79a, and no T-cell markers. They may be positive for CD30 in some cases, and they lack EMA. They also differ from ALCL of T/NK origin in having no ALK-1 protein or typical translocation. They are now regarded as a cytological variant of diffuse large-cell lymphomas of B-cell type (DLBCL) [5].

DLBCL expressing ALK-1 is the second main differential diagnosis, but can easily be ruled out on the basis of morphology and phenotype. Histologically, this type of lymphoma shows a mixture of large immunoblasts and plasmablasts, but lacks the hallmark cells of ALCL. These DLBCL do not express CD30, CD20 or T cell-associated antigens, but do, as in our case, express EMA and ALK-1. However, ALK-1 is generally exclusively cytoplasmic, due to clathrin-ALK-1 rearrangement [4] and is only rarely cytoplasmic and nuclear, as in our case.

Finally, our case should also be distinguished from peripheral T/NK-cell lymphoma, which may aberrantly

express some B cell-associated antigens, particularly CD20 and even CD79a [13], but without the morphology and immunophenotype of ALCL.

We must also consider the likelihood of CD20 expression by malignant T cells. First, it is unlikely that a molecule other than CD20 reacted with the L26 monoclonal antibody, as shown in previous studies of T-cell neoplasias expressing CD20 [10, 14]. Indeed, in such cases, the malignant cells were shown to be CD20-positive with two different monoclonal antibodies directed against different epitopes of the CD20 molecule.

Second, some cases of peripheral T/NK cell lymphoma may result from the neoplastic proliferation of a normal subset of peripheral T cells expressing CD20 [10]. Such cells, accounting for 12% of normal T cells are known as CD20dimT lymphocytes and display weaker membrane CD20 expression than B lymphocytes on flow cytometry [6]. They are present in the bone marrow [2] and have been associated with clonal T-cell proliferation in flow cytometry studies, suggesting clonal transformation of the CD20dim subset into peripheral T/NK cells [8, 11].

As a last possibility, the malignant T/NK cells may display aberrant CD20 expression as an aberrant characteristic frequently observed in malignancy. Based on the available evidence, we diagnosed this tumour as a cytotoxic T/NK ALCL expressing CD20.

This case also demonstrates that the use of a single marker, such as CD20, as a specific marker of the B-cell lineage may, in some cases, lead to the misclassification of cell lineage, particularly in the absence of CD3 expression.

References

1. Adam P, Katzenberger T, Seeberger H, Gattenlöhner S, Wolf J, Steinlein C, Schmid M, Müller-Hermelink HK (2003) A case of a diffuse large B-cell lymphoma of plasmablastic type associated with the t(2,5)(p23,q35) chromosome translocation. Am J Surg Pathol 27:1473–1476
2. Algino KM, Thomasson RW, King DE, Montiel MM, Craig FE (1996) CD20 (pan B antigen) expression on bone marrow-derived T cells. Am J Clin Pathol 106:78–81
3. Dorken B, Moller P, Pezzutto A, Schwartz-Albiez R, Moldenhauer G (1989) B-cell antigens: CD20. In: Knapp W, Dorken B, Gilks WR, Rieber EP, Schmidt RE, Stein H, Von Dem Borne AEGK (eds) Leukocyte typing IV: white cell differentiation antigens. Oxford University Press, Oxford, pp 46–48
4. Gascoyne RD, Lamant L, Martin-Subero JI, Lestou VS, Harris NL, Müller-Hermelink HK, Seymour JF, Campbell LJ, Horsman DE, Auvigne I, Espinos E, Siebert R, Delsol G (2003) ALK-positive diffuse large B-cell lymphoma is associated with clathrin-ALK rearrangements: report of 6 cases. Blood 102:2568–2573
5. Haralambieva E, Pulford KA, Lamant L, Pileri S, Roncador G, Gatter KC, Delsol G, Mason DY (2000) Anaplastic large-cell lymphomas of B-cell phenotype are anaplastic lymphoma kinase (ALK)-negative and belong to the spectrum of diffuse large B-cell lymphomas. Br J Haematol 109:584–591
6. Hultin LE, Hausner MA, Hultin PM, Giorgi JV (1993) CD2O (pan B cell) antigen is expressed at a low level on a subpopulation of human T lymphocytes. Cytometry 14:196–204
7. Jaffe ES, Harris NL, Stein H, Vardiman JW (eds) (2001) World Health Organization classification of tumours. Pathology and genetics of tumours of haematopoietic and lymphoid tissues. IARC, Lyon
8. Mohrmann RL, Arber DA (2000) CD20-positive peripheral T-cell lymphoma: report of a case after nodular sclerosis Hodgkin's disease and review of the literature. Mod Pathol 13:1244–1252
9. Pulford K, Lamant L, Morris SW, Butler LH, Wood KM, Stroud D, Delsol G, Mason DY (1997) Detection of anaplastic lymphoma kinase (ALK) and nucleolar protein nucleophosmin (NPM)-ALK proteins in normal and neoplastic cells with the monoclonal antibody ALK1. Blood 89:1394–1404
10. Quintinilla-Martinez L, Preffer F, Rubin D, Ferry JA, Harris NL (1994) CD20+ T-cell lymphoma. Neoplastic transformation of a normal T-cell subset. Am J Clin Pathol 102:483–489
11. Takami A, Saito M, Nakao S, Asakura H, Nozue T, Onoe Y, Yachie A, Shiobara S, Matsuda T (1998) CD20-positive T-cell chronic lymphocytic leukaemia. Br J Haematol 102:1327–1329
12. Tilly H, Gaulard P, Lepage E, Dumontet C, Diebold J, Plantier I, Berger F, Symann M, Petrella T, Lederlin P, Brière J for the Groupe d'Etudes des Lymphomes de l'Adulte (1997) Primary anaplastic large-cell lymphoma in adults: clinical presentation, immunophenotype, and outcome. Blood 90:3727–3734
13. Yao X, Teruya-Feldstein J, Raffeld M, Sorbara L, Jaffe ES (2001) Peripheral T-cell lymphoma with aberrant expression of CD79a and CD20: a diagnostic pitfall. Mod Pathol 14:105–110
14. Yokose N, Ogata K, Sugisaki Y, Mori S, Yamada T, An E, Dan K (2001) CD20-positive T-cell leukemia/lymphoma: case report and review of the literature. Ann Hematol 80:372–375

Virchows Arch (2007) 450:359–360
DOI 10.1007/s00428-007-0366-y

LETTER TO THE EDITOR

Comments on the reporting of lymph nodes and tumour budding in the checklist of colorectal carcinoma

Paolo Greco · Gaetano Magro

Received: 24 December 2006 / Revised: 29 December 2006 / Accepted: 2 January 2007 / Published online: 30 January 2007
© Springer-Verlag 2007

Dear Sir:

We have read with interest the paper of Jass et al. [3] about the recommendations for the reporting of surgically resected specimens of colorectal carcinoma. We would like to comment on two controversial issues dealing with the number and the size of lymph nodes to be recovered and with the reporting of tumour budding.

Although we admit that there is no unacceptable low number of lymph nodes for an individual dissection, we do not agree with the authors when they state that 12–15 (lymph nodes) is the mean number giving an indication of good practice in a series of colorectal cancer dissections [3]. There is no general consensus about this number if other authors, recently reporting colorectal cancer guidelines, propose a mean number of 15–18 lymph nodes [6]. Recently, we have published in Virchows Archiv a paper showing that in pT3 rectal cancer, 12–15 lymph nodes are insufficient for a correct staging [2]. In that prospective study, we first showed that if the mean number of lymph nodes recovered increased from 17.8 to 26.8, after a second sampling of the same surgically resected specimens, metastases were detected in 18.7% of patients that had been originally understaged [2]. Our results are in line with those previously obtained by other authors showing that most lymph-node metastases (about 80–90% of cases) of colorectal cancer are detected if about 26–30 lymph nodes are recovered [2].

P. Greco (✉) · G. Magro
Department G.F. Ingrassia, Anatomia Patologica,
Azienda Ospedaliero-Universitaria Policlinico di Catania,
Via S. Sofia 87,
95123 Catania, Italy
e-mail: paolo.greco@policlinico.unict.it

Jass et al. do not provide any comment about the possibility that some patients with colorectal cancer have only a single metastatic lymph node. In a large series of colorectal cancers reported by Goldstein [1], about 30% of pT3N+ patients had a single metastatic lymph node, and the percentage of specimens with one lymph-node metastasis increased from 41.62 to 80.36% when the number of lymph nodes increased from 11–15 to more than 21, respectively. Notably, in our study, we obtained similar results, as all restaged pT3N+ patients had only a single metastatic lymph node, which was found in specimens in which a minimum number of 19 lymph nodes had been originally detected [2]. Accordingly, we propose that at least 20 lymph nodes should be recovered as an acceptable mean number in a series of colorectal cancer dissections.

Apart from the number, in our opinion, the size of the lymph nodes to be recovered is crucial for a correct staging of colorectal cancer. It is known that a significative number of metastatic lymph nodes are small in size and can be easily missed during manual dissection. This is confirmed by our previously mentioned study showing that all restaged pT3N+ patients had a single metastatic lymph node measuring less than 5 mm in greatest diameter [2].

Another important issue refers to tumour budding. The authors state that tumour budding should be merely reported as present or absent [3]. Although we generally agree in reporting tumour budding, however, we point out that there is no general consensus about the definition and quantification. While Jass et al. regard tumour budding as single isolated cancer cells or a cluster composed of four cells at the invasive front [3], others include in the definition a cluster composed of five cells or even generic small clusters (number of cells not established) of undifferentiated cancer cells, also known as solitary trabecular forms [5]. There is no general consensus even about the

quantification of tumour budding, if the methods to assess them vary between different pathologists, resulting in cutoffs (low vs high budding) not defined uniformly, with difficulties in the comparison of prognostic information. Accordingly, we think that a more general agreement about the definition and quantification of tumor budding is mandatory in the future if this proposed novel, prognostic morphological parameter could be reliably applied by all pathologists.

Finally, we would like to conclude the present letter with a speculative consideration about a potential relationship between tumor budding and cancer stem cells, which is recently identified in colorectal cancer [7]. Given their ability to detach from the original tumor mass, and their association with poor prognosis, infiltrative invasive margins, vascular invasion, lymph-node metastases and distant metastases, it has been recently suggested that tumour budding may have the properties of cancer stem cells [4]. If this hypothesis will be confirmed, the role of pathologists will be crucial for future therapeutic strategies of colorectal cancer.

References

1. Goldstein NS (2002) Lymph node recoveries from 2427 pT3 colorectal resection specimens spanning 45 years: recommendations for a minimum number of recovered lymph nodes based on predictive probabilities. Am J Surg Pathol 26:179–189
2. Greco P, Andreola S, Magro G, Belli F, Giannone G, Gallino GF et al (2006) Potential pathological understaging of pT3 rectal cancer with less than 26 lymph nodes recovered: a prospective study based on a resampling of 50 rectal specimens. Virchows Arch 449:647–651
3. Jass JR, O'Brien MJ, Riddell RH, Snover DC (2006) Recommendations for the reporting of surgically resected specimens of colorectal carcinoma. Virchow Arch DOI 10.1007/s00428-006-0302-6
4. Jass JR (2007) Classification of colorectal cancer based on correlation of clinical, morphological and molecular features. Histopathology 50:113–130
5. Prall F (2007) Tumour budding in colorectal carcinoma. Histopathology 50:151–162
6. Quirke P, Morris E (2007) Reporting colorectal cancer. Histopathology 50:103–122
7. Ricci-Vitiani L, Lombardi DG, Pilozzi E, Biffoni M, Todaro M, Peschle C De Maria R (2007) Identification and expansion of human colon-cancer-initiating cells. Nature 445:111–115. DOI 10.1038/nature05384

Virchows Arch (2007) 450:361–363
DOI 10.1007/s00428-006-0365-4

LETTER TO THE EDITOR

Sertoli cell tumor of the testis, not otherwise specified, presenting extensive hemorrhage and overexpression of α-methylacyl-CoA racemase (AMACR/P504S)

Katsuaki Sato · Hironori Tachibana · Shojiroh Morinaga · Yoshimichi Ueda · Shogo Katsuda

Received: 27 October 2006 / Revised: 18 December 2006 / Accepted: 27 December 2006 / Published online: 25 January 2007
© Springer-Verlag 2007

Dear Editor,

Sertoli cell tumors are rare, accounting for approximately 1% of testicular tumors, and mostly benign. Sertoli cell tumors are subclassified as Sertoli cell tumors, not otherwise specified (NOS), with two rare variants: large cell calcifying Sertoli cell tumor and sclerosing Sertoli cell tumor. α-Methylacyl-CoA racemase (AMACR/P504S) is an enzyme engaging in β-oxidation of branched-chain fatty acids and bile acid synthesis. AMACR has been reported to be frequently expressed in prostatic carcinoma and colorectal adenocarcinoma, and occasionally in other types of carcinoma [5]. To the best of our knowledge, there have been no reported cases of Sertoli cell tumors demonstrating AMACR overexpression. In this study, we report a case of Sertoli cell tumor, NOS, presenting widespread hemorrhage and immunohistochemical AMACR overexpression.

A 49-year-old man presented with a gradually enlarging painless mass in his left testis. No hormone-related symptoms were noted, and his past and familial histories were unremarkable. Ultrasonographic examination demonstrated a 6-cm tumor and left radical orchiectomy was performed. Torsion of the spermatic cord was not observed during surgery. There was no evidence of recurrence or metastasis 2 years after surgery.

Macroscopically, the tumor was located in the testis and the cut surface displayed extensive hemorrhage. Viable tumor tissue, yellow–white in color, remained only at the periphery and fibrous capsules were detected (Fig. 1a). There was no tumor invasion of the tunica albuginea. Microscopically, tumor cells with bland nuclei and an eosinophilic or clear cytoplasm proliferated in various patterns: trabecular (Fig. 1b), tubular, solid, and spirally (Fig. 1c). Lipid droplets in the cytoplasm and hyalinized stroma were locally found. Mitotic figures were not evident. No lymphovascular invasion, dense sclerotic stroma, or calcification was seen in the tumor. No infarct area was identified around the tumor. Immunohistochemical examination using anti-AMACR monoclonal antibody (clone 13H4, Dako, Glostrup, Denmark, 1/300) showed AMACR overexpression diffusely in the viable tumor tissue with a finely granular pattern in the cytoplasm (Fig. 1d). Calretinin, CD10, cytokeratin (CAM5.2), inhibin-α, melan-A, and S-100-α protein were also diffusely positive in the cytoplasm. Restricted CD56 expression was observed in the tubular structures, but no chromogranin A or synaptophysin were detected. Mesothelial markers, cytokeratin 5/6, D2-40, HBME-1, mesothelin, podoplanin, thrombomodulin, and WT-1 protein were all negative. In our previously reported cases of large cell calcifying Sertoli cell tumor and Leydig cell tumor [3], no AMACR overexpression was detected.

The present tumor showed extensive hemorrhage which is rarely observed in Sertoli cell tumors [4]. Viable tissue was limited to the tumor margin, making the histological diagnosis difficult. Uniform tumor cells with minimal cytological atypia and a partially vacuolated cytoplasm proliferated in a trabecular, tubular or solid pattern. This

K. Sato (✉) · Y. Ueda · S. Katsuda
Department of Pathophysiological and Experimental Pathology,
Kanazawa Medical University,
1-1 Daigaku, Uchinada, Kahoku,
Ishikawa 920-0293, Japan
e-mail: sato-k@kanazawa-med.ac.jp

H. Tachibana
Department of Urology, Kanazawa Medical University,
Ishikawa, Japan

S. Morinaga
Department of Pathology, Kitasato Institute Hospital,
Tokyo, Japan

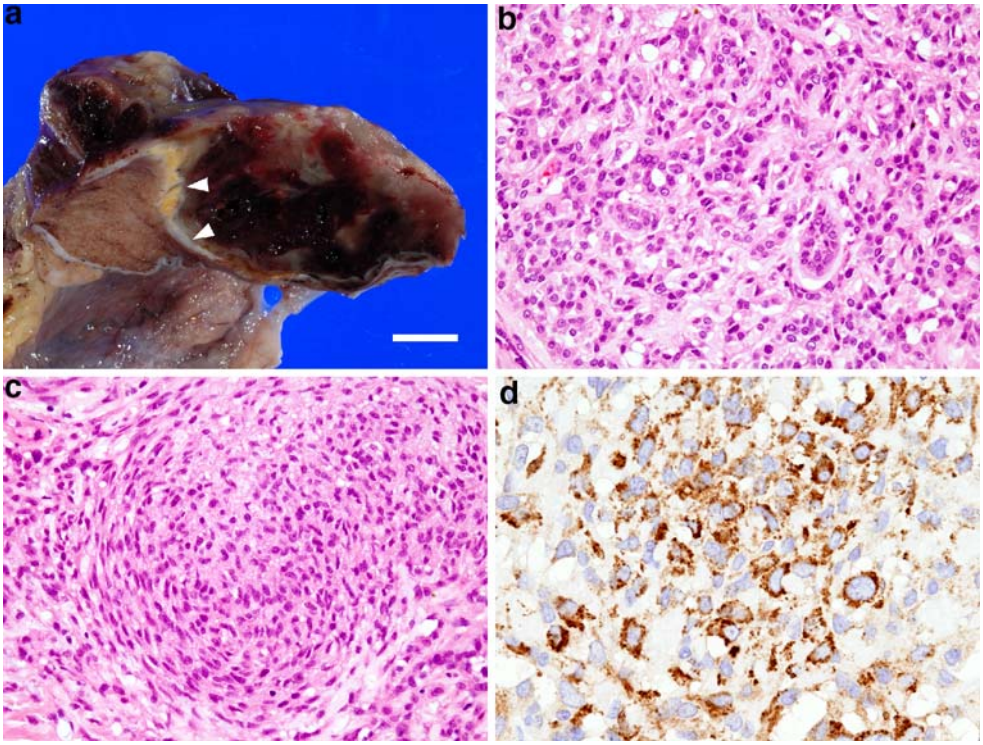

Fig. 1 **a** Cut surface of the tumor showed a demarcating tumor restricted to the testis comprising of extensive hemorrhage and yellow–white viable tissue confined to the periphery (*arrow head*). Scale bar: 1 cm. **b** Tumor cells with bland cytological atypia were arranged in trabecular and tubular patterns. Lipid droplets in the cytoplasm were locally seen. H&E staining (×200). **c** Spindle-shaped cells were spirally organized. H&E staining (×200). **d** Immunohistochemistry for AMACR demonstrated overexpression with a finely granular pattern in the cytoplasm (×400)

apparently simulates an adenomatoid tumor, which is of mesothelial origin and usually arises from the epididymis but can develop into tunica albuginea and grow intratesticularly. In this case, there were no smooth muscle component or lymphocytic aggregates in the stroma, characteristic of adenomatoid tumor. Furthermore, immunohistochemically, the current tumor cells expressed no mesothelial markers other than calretinin, but were reactive for inhibin-α, S-100 protein, melan A, and cytokeratin (CAM5.2). These findings are consistent with those of previously reported cases of Sertoli cell tumors. Neuroendocrine markers are occasionally revealed in sex cord stromal tumors of the testis. In the present case, CD56 was identified only in the tubular structures, but chromogranin A and synaptophysin were negative.

AMACR is globally used as a reliable marker of prostatic adenocarcinoma, but expression has also been demonstrated in various other neoplasms [5]. In the testis, no AMACR overexpression has been detected in normal tissue or germ cell tumors [1], and there have been no studies in sex-cord stromal tumors. The present tumor cells revealed finely granular cytoplasmic expression of AMACR as seen in prostatic adenocarcinoma. Our previously reported cases of large cell calcifying Sertoli cell tumor and Leydig cell tumor [3] were immunohistochemically reevaluated and tested negative for AMACR.

AMACR is involved in β-oxidation of branched-chain fatty acids in mitochondria and peroxisomes, and overexpression may cause changes in energy metabolism in tumor cells, or vice versa. Recently, Langner et al. [2] reported that tumors presenting foci of necrosis exhibit marked AMACR immunostaining in urothelial carcinoma of the upper urinary tract. The extensive hemorrhage in the present case was not due to hemorrhagic infarct because there was no evidence of torsion of the spermatic cord during surgery or necrotic area in the histological specimens. However, extensive hemorrhage might influence on energy metabolism and AMACR expression of tumor cells.

Further examinations are needed to clarify if AMACR expression is specific for Sertoli cell tumors, NOS, and whether AMACR immunohistochemistry is useful for discriminating between Sertoli cell tumors, NOS, and other testicular tumors.

Acknowledgement The authors thank Dr. Shinichi Teshima (Department of Pathology, Fraternity Memorial Hospital, Tokyo, Japan) and Dr. Hiroshi Ishikura (Department of Molecular Pathology, Chiba University Graduate School of Medicine, Chiba, Japan) for kindly useful comments, and Takayuki Nakata (Department of Pathology, Kanazawa Medical University Hospital, Ishikawa, Japan) for immunohistochemistry.

References

1. Jiang Z, Fanger GR, Woda BA, Banner BF, Algate P, Dresser K, Xu J, Chu PG (2003) Expression of α-methylacyl-CoA racemase (P504S) in various malignant neoplasms and normal tissues: a study of 761 cases. Human Pathol 34:792–796
2. Langner C, Rupar G, Leibl S, Hutterer G, Chromecki T, Hoefler G, Rehak P, Zigeuner R (2006) Alpha-methylacyl-CoA racemase

(AMACR/P504S) protein expression in urothelial carcinoma of the upper urinary tract correlates with tumour progression. Virchows Arch 448:325–330
3. Sato K, Ueda Y, Sakurai A, Ishikawa Y, Okamoto S, Ikawa H, Katsuda S (2005) Large cell calcifying Sertoli cell tumor of the testis: comparative immunohistochemical study with Leydig cell tumor. Pathol Int 55:366–371
4. Young RH, Koelliker DD, Scully RE (1998) Sertoli cell tumors of the testis, not otherwise specified: a clinicopathologic analysis of 60 cases. Am J Surg Pathol 22:09–721
5. Zhou M, Chinnaiyan AM, Kleer CG, Lucas PC, Rubin MA (2002) Alpha-Methylacyl-CoA racemase: a novel tumor marker over-expressed in several human cancers and their precursor lesions. Am J Surg Pathol 26:926–931

Virchows Arch (2007) 450:365–367
DOI 10.1007/s00428-006-0324-0

LETTER TO THE EDITOR

A case of acquired renal cystic disease (ACDK) with oncocytosis, a dominant nodule (oncocytoma), multiple adenomas and a microscopic papillary renal cell carcinoma associated with crescentic glomerulonephritis

C. L. Menéndez · A. Pobes · M. G. Corte Torres · E. Fuente · A. M. Merino · B. Corrales · M. Argüelles

Received: 29 August 2006 / Accepted: 29 September 2006 / Published online: 17 November 2006
© Springer-Verlag 2006

Sir,

A 76-year-old female patient suffering from long-term arterial hypertension had a nephrotic syndrome in 1997, being diagnosed of membranous glomerulonephritis clinically and with biopsy. She was resistant to steroids and azathioprine. Then, her treatment was changed to Mycophenolate Mofetil. In 2005, she had anuria, abdominal discomfort and acral edema. Serologic studies were negative. Hemodyalisis, besides steroids and cyclofosphamide treatment were started. Her renal function was worsening and a new biopsy showed a crescentic glomerulonephritis with epithelial crescents, severe tubulointerstitial changes and focal tubular hyperplasia. IF studies were identical to the previous biopsy and consistent with membranous glomerulonephritis (granular peripheral glomerular deposits of Ig G, C3 and C1q). EM is not available. CT scan and MRI displayed multiple renal cysts suggesting ACDK with a 2.5 cm solid nodule and a total right nephrectomy was performed. The removed kidney (Fig. 1) had multiple cysts, numerous minute nodules and a tan-green 2.5 cm mass. Studied by routine methods and immunohistochemistry (cytogenetics and EM are not available), a crescentic GN with many obsolescent glomeruli was found (Fig. 2). There were prominent tubulointerstitial changes: severe tubular atrophy, frequent tubular hyperplasia and oncocytic changes, sometimes papillary;

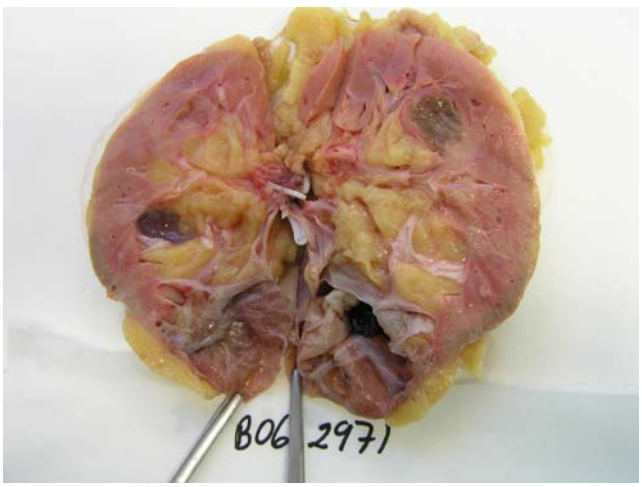

Fig. 1 Nephrectomy specimen: differently sized cysts, minute white nodules and a tan mass

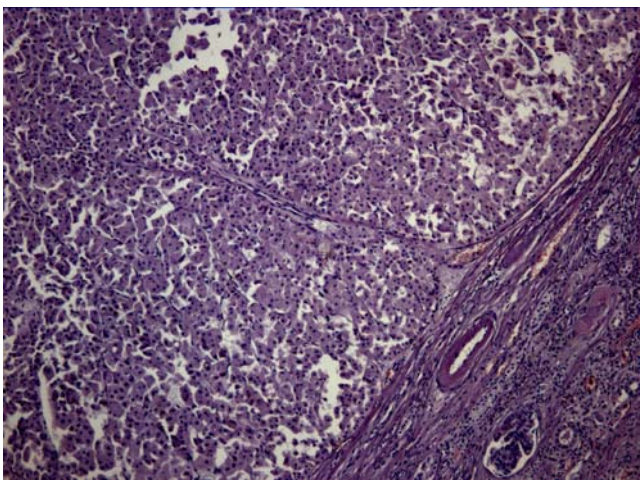

Fig. 2 Dominant mass: typical oncocytoma (top) (H & E)

C. L. Menéndez (✉) · A. Pobes · M. G. Corte Torres · E. Fuente · A. M. Merino · B. Corrales · M. Argüelles
Pathology Department, Hospital de Cabueñes, Gijón, 33203 Asturias, Spain
e-mail: carluznr@telecable.es

A. Pobes
Nephrology Department, Hospital de Cabueñes, Gijón, 33203 Asturias, Spain

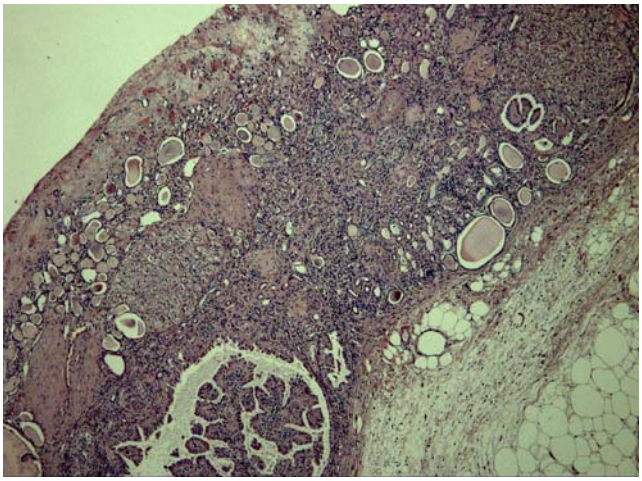

Fig. 3 A cyst wall, oncocytic nodules (oncocytosis) and papillary adenomas (top) (H & E)

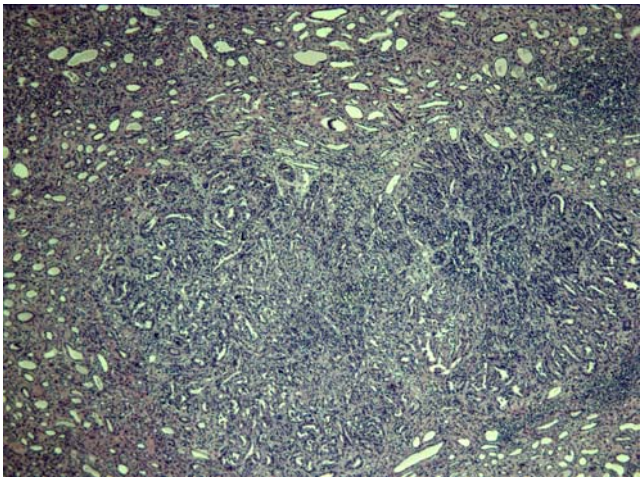

Fig. 5 Microscopic tubular and spindle cell nodular proliferation (H & E)

multiple oncocytic nodular aggregates (EMA+, CK7+, C-kit+, Vim−), occasionally with a hybrid morphology related to chromophobe cells and papillary adenomas (Fig. 3) [6, 7], one microscopic papillary renal cell carcinoma (1 cm) with slender papillae and type 1 and 2 epithelial cells (CK 7+,CD10+), a microscopic tubular and spindle cell nodule reminiscent of mucinous tubular and spindle cell carcinoma (WHO 2004) (CD10−, EMA+, AMACR+, CK7+, Vim−) (Fig. 4) [4] and a classic Oncocytoma (EMA+, C-kit+, CD10−, CK7− and MIB1 <4%) (Fig. 5); besides there were occasional tubulointerstitial oxalosis (Fig. 2), not intratumoral [5], some calcium deposits, cysts with or without epithelial layering (oncocytic frequently)and clustered microcystic lesions. IF studies didn't differ from previous ones (granular Ig G, C3 and C1q deposits along glomerular capillaries without additional changes).

We are facing an ACDK secondary to membranous glomerulopathy evolving during 8 years with no dialysis until the end. ACDK is related to diverse renal neoplasias, usually papillary renal cell carcinoma [3, 6] and some special forms of clear renal cell carcinomas, very rarely to oncocytoma [2]. This case shows an unusual whole spectrum of macro-microscopic tumors, mainly oncocytic [3, 7] probably having the same progenitor lesion (intercalated cells–distal nephron) and the very uncommon association with crescentic GN, most unlikely due to membranous GN but to ACDK (a well-known premalignant condition) with different epithelial neoplasias as a paraneoplastic syndrome in a setting of immunosuppression. In the case of just one tumor, the disappearance of crescentic GN after tumor removal would prove its relationship with the neoplasia (sometimes this doesn't happen) [1], but here this hypothesis can't work because there are multiple lesions.

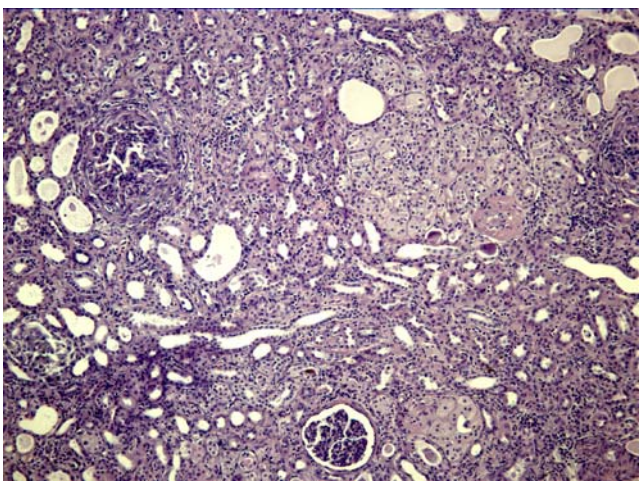

Fig. 4 Oncocytosis, crescentic GN and oxalosis (bottom left) (H & E)

References

1. Feriozzi S, Giannakakis K, Ranalli TV, Pofi E, Gomes V, Ancarani E (2006) Renal oncocytoma associated with necrotizing glomerulonephritis. Ren Fail 28(2):181–183
2. Hashimoto T, Togo Y, Yasuda K, Fukui K, Nagkai J, Nakao A, Higuchi Y, Maruyama T, Yamamoto S, Kondo N, Nojima M, Takiuchi H, Mori Y, Hirota S, Shimai H (2005) Oncocytoma associated with acquired cystic disease of kidney (ACDK): a case report. Hinyokika Kiyo 51(11):747–749
3. Leroy X, Lemaitre L, De La Taille A, Hazzan M, Delepaul B, Couturier J, Gosselin B (2001) Bilateral renal oncocytosis with renal failure. Arch Pathol Lab Med 125:683–685
4. Paner GP, Srigley JR, Radhakrishnan A, Cohen C, Skinnider BF, Tickoo SK, Young AN, Amin MB (2006) Immunohistochemical analysis of mucinous tubular and spindle cell carcinoma and papillary renal cell carcinoma of the kidney. significant immunophenotypic overlap warrants caution. Am J Surg Pathol 30:13–19
5. Sule N, Yakupoglu U, Shen SS, Krishnan B, Yang G, Lemer S, Sheikh-Hamad D, Truong LD (2005) Calcium oxalate deposi-

tion in renal cell carcinoma associated with acquired cystic kidney disease: a comprehensive study. Am J Surg Pathol 29 (4):443–451

6. Tickoo SK, dePeralta-Venturina MN, Harik LR, Worcester HD, Salama ME, Young AN, Moch H, Amin MB (2006) Spectrum of epithelial neoplasms in end-stage renal disease. An experience from 66 tumor-bearing kidneys with emphasis on histologic patterns distinct from those in sporadic adult renal neoplasia. Am J Surg Pathol 30:141–153
7. Tickoo SK, Reuter VE, Amin MB, Srigley JR, Epstein JI, Min KW, Rubin MA, Ro JY (1999) Renal oncocytosis: a morphologic study of fourteen cases. Am J Surg Pathol 23(9):1094–1101

Virchows Arch (2007) 450:369–370
DOI 10.1007/s00428-007-0387-6

ANNOUNCEMENTS

Announcements

© Springer-Verlag 2007

14–17 May 2007
Diagnostic Histopathology of Breast Disease
Hammersmith Hospital (Imperial College), London, UK

A four day long course on the Hammersmith Campus designed for pathologists at Consultant and Senior Trainee level and suitable for the final examination for MRCPath. The course will provide a comprehensive coverage of the histopathology of breast disease, with special emphasis on areas which pose diagnostic difficulties. The course is based, historically, on the extensive referral collection of Professor JG Azzopardi, to which has been added new cases from Charing Cross, Nottingham City and Addenbrooke's Hospitals. The course will be slanted to practical diagnostic pathology with a specific session dealing with problems encountered in core biopsies and a special workshop dealing with the interpretation of HER2 immunostaining. The participants will be given ample time to study histological preparations, followed by illustrated discussions of the cases. In addition there will be several daily talks on specific topics, given by eminent breast pathologists and followed by discussions. The topics will include: new issues in the interpretation of breast biopsies, breast immunohistochemistry, problematic breast lesions, dealing with the gross specimen, fibro-epithelial, spindle cell and papillary lesions, proliferative lesions/carcinoma in-situ, sentinel lymph node biopsy and the impact of molecular genetics on diagnostic breast pathology. The faculty will include Anthony Douglas-Jones, Ian Ellis, Bharat Jassani, Andrew Lee, Sarah Pinder, Jorge Reis-Filho and Sami Shousha.

For further information please contact:
Sandra Lock
Department of Histopathology
Hammersmith Hospital
Du Cane Road
London W12 0NN, UK
Tel: +44 (0)20 8383 3292
Fax: +44 (0)20 8740 7417
E-mail: histopathology.shortcourses@imperial.ac.uk

May 18–20, 2007
Postgraduate Course
Molecular Pathology
Graz, Austria

Course Directors
Gerald Höfler, MD, Department of Pathology, Medical University Graz, Austria Falko Fend, MD, Department of Pathology, Technical University Munich, Germany

Course Objectives
This course is designed for pathologists, molecular biologists and technicians with special interest in diagnostic molecular pathology. It features lectures and practical aspects (wet lab course). Topics include DNA/RNA isolation from formalin-fixed paraffin embedded tissue, translocation analysis, clonality analysis (IgH, TCR), microsatellite instability (HNPCC) and quantification of RNA transcripts. The course language will be English.

Course Fee: 400,-€ The course fee includes hands on participation in the wet lab course, a comprehensive handout, coffee breaks, lunch and dinner (Saturday), buffet lunch (Sunday) and guided city walk.

Attendance is limited to 30 participants!

Registration / more information:
To register please use the form on our homepage:
http://pathologie.meduni-graz.at/Pathologie/veranstaltungen.htm
or send your registration to
Edith Kleinferchner
Department of Pathology
Medical University Graz
Auenbruggerplatz 25
8036 Graz, Austria;
Fax 0043-(0)316-385-3432
E-mail: edith.kleinferchner@meduni-graz.at

Since attendance is limited acceptance to the course will be acknowledged and a bill will be mailed.

7–8 June 2007
Thyroid Pathology for the Practising Pathologist
15 rue de l'Ecole de Médecine
Paris, France

A 2-day course will take place in Paris under the auspices of the French Division of the I.A.P. This course will be given in English by Prof. J. Rosai (Milano), Prof. M. Sobrinho-Simoes (Porto) and Prof. R. Heimann (Brussels). It will consist of lectures alternating with slide reviews and a slide seminar over a multiheaded microscope. The cases of the seminar will be sent on CD before the meeting.
The audience will be limited to 30 participants.

Course fees: 410 euros (340 euros for members of any I.A.P. division). The fees include registration, hand-out, CD of the slide seminar and coffee breaks.

For further information, please contact:
Mrs M. Fontanière, Administrative Secretary,
French Division of the I.A.P.
32 Cours Albert Thomas,
69008, Lyon, France
Fax: 33 4 78754311
E-mail: academie.pathologie@wanadoo.fr

24–27 July, 2007
Practical Pulmonary Pathology
London, UK

This course is designed to provide histopathology and cytopathology trainees and consultants with an opportunity to study diagnostic lung pathology in a comprehensive manner. It comprises lectures and practical microscopy sessions, the latter making up roughly half the time and consisting of individual study of a unique collection of cases.

For further information and application forms please contact:
Professor B Corrin,
Brompton Hospital,
London SW3 6NP, UK
Fax +44 20 7351 8293
E-mail: b.corrin@ic.ac.uk

27–31 August 2007 (Part I+II), 29–31 October 2007 (Part III)
Postgraduate Course Lung, Pleural & Mediastinal Diseases,
Department of Pathology,
Medical University, Graz, Austria

Course Director: Helmut Popper, MD (Graz)

Course Objectives:
This three-part course (common and rare lung and pleural, and mediastinal diseases) is designed for trainees as well as for experienced colleagues. Lectures as well as microscopy sessions alternate for each part. Clinical lectures and case studies are also included in selected lung diseases. Each part can be booked separately.

Course fee:
Part I (Common diseases) Aug 27–29, 2007€ 240,00
Part II (Mediastinal diseases) Aug 30–31, 2007€ 240,00
Part III (Rare diseases) Oct 29–31, 2007€ 240,00
Whole 8-day course (Part I + II + III) € 600,00
Two parts (Part I + II or Part I + III or Part II + III) € 450,00

For more information and registration please contact:
Edith Kleinferchner
Department of Pathology, Medical University Graz
Auenbruggerplatz 25
8036 Graz, Austria
Fax: 0043 (0)316 385-3432
e-mail:edith.kleinferchner@meduni-graz.at
http://pathologie.meduni-graz.at/Pathologie/veranstaltungen.htm

Virchows Arch (2007) 450:371–378
DOI 10.1007/s00428-007-0367-x

ORIGINAL ARTICLE

Search for residual prostate cancer on pT0 radical prostatectomy after positive biopsy

Roberta Mazzucchelli · Francesca Barbisan · Adriano Tagliabracci · Antonio Lopez-Beltran · Liang Cheng · Marina Scarpelli · Rodolfo Montironi

Received: 6 November 2006 / Revised: 17 December 2006 / Accepted: 1 January 2007 / Published online: 7 February 2007
© Springer-Verlag 2007

Abstract Reported incidence of no residual prostate cancer (i.e. pathological stage pT0) on radical prostatectomy ranges from 0.07 to 4.2%. The incidence is higher after neoadjuvant endocrine treatment. The aim of this study was to search for residual cancer on radical prostatectomy (RP) specimens when an initial sampling failed to find the cancer in patients with positive biopsy. Our database of 1,328 consecutive patients whose biopsies and RP specimen were both examined at the Polytechnic University-United Hospitals of the Marche Region between March 1995 and June 2006 was reviewed. The radical prostatectomies were grossly completely sampled and examined with the whole mount technique. We identified eight patients (i.e. 0.6%; three untreated and five hormonally treated preoperatively, i.e. 0.3 and 0.8%, respectively, of the total number of RPs included in the study) with positive biopsy and with no residual cancer in the initial routine histological examination of the RP. The RP of this group of eight was subjected to additional sectioning and evaluation of the paraffin blocks of the prostatectomy, also after block-flipping, immunostaining with an antibody against CAM 5.2, p63, PSA, and alpha-methylacyl-CoA racemase, and DNA specimen identity analysis. There were no cases with a false positive biopsy diagnosis, and cancer was not overlooked or missed in the initial routine histological examination of any of the 8 pT0 RPs. A minute focus of cancer (the diameter was always below 2.0 mm) was found on the additional sections in five. In particular, cancer was found after block-flipping in one of them. In an additional case, cancer was eventually discovered after immunostaining tissue sections for cytokeratin CAM 5.2, for p63 and PSA. In the remaining two cases (one untreated and the other hormonally treated), cancer was not found (0.15% of the 1,328 RPs included in the study); the review of the description of the macroscopic appearance of the RP and of its slides revealed that part of the peripheral zone corresponding to the site of the positive biopsy was missing, i.e. not removed from the patient at the time of the operation at least in one of the two. DNA specimen analysis confirmed the identity of the biopsy and prostatectomy in both. An extensive search for residual cancer reduces the number of pT0 RPs after a positive biopsy from 0.6 to 0.15%. It is recommended to have the needle biopsy reviewed, carefully look again at the radical prostatectomy, do deeper sections and then flip certain paraffin blocks. In addition, atypical foci should be stained for basal cell markers and often AMACR, especially in hormone-treated cases. If a block is missing part of the peripheral zone (capsular incision), this should be commented on. DNA analysis for tissue identity should be performed when the other steps have been taken without finding cancer.

R. Mazzucchelli · F. Barbisan · M. Scarpelli · R. Montironi (✉)
Section of Pathological Anatomy and Histopathology,
School of Medicine, United Hospitals,
Polytechnic University of the Marche Region (Ancona),
I-60020 Torrette,
Ancona, Italy
e-mail: r.montironi@univpm.it

A. Tagliabracci
Legal Medicine, School of Medicine,
Polytechnic University of the Marche Region (Ancona),
Ancona, Italy

A. Lopez-Beltran
Unit of Anatomic Pathology, Cordoba University Medical School,
Cordoba, Spain

L. Cheng
Department of Pathology and Laboratory Medicine,
Indiana University School of Medicine,
Indianapolis, IN, USA

Keywords Prostate cancer · Residual prostate cancer · Vanishing cancer

Introduction

In 1995, Goldstein et al. [9] introduced the term *vanishing cancer phenomenon* referring to cases with minute or no cancer on radical prostatectomy after a positive biopsy. They reported 13 patients with minimal (11 patients) or no (two patients) cancer in prostatectomy specimens. In two cases with no residual cancer on RP, they confirmed the identity of the biopsy and the prostatectomy tissue by DNA matching.

The Johns Hopkins Hospital group documented a fivefold increase in the incidence of no residual cancer on prostatectomy in patients in whom both biopsies and prostatectomies were performed at that institution between 1997 and 2005 (0.07% in 1997, 0.13% in 2004 and 0.34% in 2005) [5, 7, 30]. In their first study, they also documented two cases, one in which the biopsy review revealed only high-grade PIN and in which a diagnosis of cancer had been established in another institution, and a second case in which the possibility of specimen switching could not be ruled out due to DNA mismatch between the biopsy and the prostatectomy. Most recently, they have reported a series of 46 patients, 11 with no residual cancer on prostatectomy and 35 with minute cancer, and in 40 cases, they documented specimen identity [5]. In five of the six remaining cases, the results could not be interpreted due to technical problems, and in one case, the tissue from the biopsy with cancer did not match the tissue from the radical prostatectomy.

Bostwick and Bostwick [4] found that 38 patients with no cancer on prostatectomy, identified among 6,843 radical prostatectomies performed at Mayo Clinic during a 30-year period, showed no disease recurrence or progression after a mean follow-up of 10 years. In their experience, the incidence of vanishing cancer declined tenfold, comparing prostatectomies performed before 1980 (2.1% incidence) to a more recent time interval from 1993 to 1995 (0.2% incidence). They have estimated the current incidence of vanishing cancer at 2 per 1,000 radical prostatectomies [4].

Recently, Trpkov et al. [28] found an incidence of no residual cancer on prostatectomy of 0.67% after ten-core positive biopsy. They concluded that in most cases, finding no residual cancer on prostatectomy after additional sectioning and evaluation may indicate minimal patient disease. Very recently Zynger et al. [32] reported that their frequency of finding no residual cancer in RP specimens has increased from 0% in 2002 to 4.2% in 2006. In Canada, Srigley [25] has estimated the incidence of no residual cancer after positive biopsy in his practice at less than 0.5%.

In Germany, the incidence of pT0 in patients with prostate cancer without neoadjuvant treatment was analysed by Herkommer et al. [13]. Based on a database of 3,609 patients, no residual prostate cancer was found in 0.8% after RP. Most men in this pT0 series had previous TURP or open prostatectomy, which may have eliminated prostate cancer, whereas in two patients, cytology was used for primary diagnosis. Only in 0.3% of men with positive prostate needle biopsies was no residual tumour detected in the prostatectomy specimen [13]. The incidence of pT0 patients in a very recent French study was reported to be 0.5% [6].

No residual cancer may also result from preoperative endocrine therapy [11, 12, 15, 16, 19, 24, 26]. The incidence of pT0 after neoadjuvant endocrine therapy for prostate cancer is reported to be higher than in untreated patients [11]. Kollermann et al. [16] analysed a group of 174 men who underwent prolonged androgen deprivation therapy and observed a pT0 in 36 of 174 men (21%).

Several questions are addressed to explain why cancer is not present in a small proportions of prostatectomies. Cancer is missed during the examination of the RP, all prostatectomy tissue is not sampled, and the cancer is overdiagnosed in the biopsy. Pathologists face additional challenges in eliminating the possibility of laboratory error resulting in specimen (blocks, slides) mislabelling or switching and excluding an information system error resulting in specimen mix-up [28].

The aim of this paper was to report the results of a search for residual cancer on RP after an initial stage pT0 evaluation in eight patients with positive biopsy.

Materials and methods

We reviewed our database of 1,328 consecutive patients whose biopsies and RP specimen were examined between March 1995 and June 2006 at the five Pathological Anatomy Services associated with the Polytechnic University-United Hospitals of the Marche Region, Ancona, Italy. Most of the biopsies and all the RPs of this series of 1,328 patients were reported by the same pathologist (RM). Seven hundred patients were untreated before the operation, whereas 628 had received neoadjuvant endocrine treatment for approximately 3 to 6 months.

The biopsies and RPs were routinely processed as follows. The core biopsies from each site were submitted in separate containers. In brief, during biopsy processing, no more than two biopsy cores were embedded in paraffin blocks, and all blocks were sectioned at 3 μm and were stained with haematoxylin–eosin (HE). All cores were sectioned in two separate levels represented on separate slides, with each slide containing three additional sections [28].

All radical prostatectomy specimens (tissue was not harvested for research) were fixed en bloc in 10% buffered formalin for at least 24 h and were grossly completely sampled using a standard protocol [17, 18, 28]. In particular, each specimen was painted over the surface with India ink. The seminal vesicles were amputated at the prostate junction and were grossly completely sampled. The remainder of the specimen was serially cut with a domestic electric food slicer calibrated and set to deliver slices which are 3–4 mm in thickness, representing transverse planes parallel to the initial apical and basal sections. Each prostate slide was processed into complete whole mount section, and one HE slide was routinely sectioned per block. The apical and basal transverse 2- to 3-mm margins were sectioned perpendicularly to assess the prostatic apical and basal margins. Prostatectomies were grossly sectioned in 8.5 slices (mean; range, 6–16), and 15.3 slides (mean; range, 10 to 20) were generated per prostatectomy. Slides from pelvic lymph nodes were not included in the reported number of examined slides.

We identified eight patients with positive 6- to 12-core biopsy and with no residual cancer (pathological stage pT0) in the initial routine histological examination of the RP and successively subjected to additional sectioning and evaluation.

Search for residual cancer

Since 1995, a special cancer searching protocol has been applied to those RPs in which an initial routine-based examination does not show residual cancer [18]. As mentioned earlier, this is basically done in those cases whose biopsies and RP specimen are both examined at the Ancona institution.

The following successive steps were undertaken by two pathologists (RM and RMa). The procedure was usually stopped at the step where cancer is found.

1. The diagnostic needle biopsies were reviewed to exclude the possibility of a false positive biopsy diagnosis and to assess the approximate location of the biopsy with tumour, such as apex, mid-zone and base, both left and right.
2. The slides of the surgical specimens were reviewed for residual cancer that was initially overlooked or missed.
3. If the prostate was not totally embedded, the remaining prostate tissue was processed in toto. If the prostate was completely sampled, then this step was skipped. This type of information was usually contained in the pathology form where the all the steps of the processing procedure were recorded. The information was further confirmed by searching the specimen's container for residual pieces. As we routinely sample completely all prostatectomies, this step was skipped.
4. Additional deeper sections (i.e. three to five sections) of the prostatectomy area (paraffin block) corresponding to the location of the core with cancer were re-cut. Further sections were also obtained from all the other paraffin blocks.
5. Additional deeper sections (i.e. three to five sections) of the area corresponding to the location of the positive core as well as of all the remaining blocks were re-cut after block-flipping.
6. Immunostains for p63 and alpha-methylacyl-CoA racemase (AMACR) were performed to evaluate suspicious foci (When these two were not yet available, we used 34betaE12 immunostaining).
7. Immunostain for cytokeratin CAM 5.2, for p63 and for PSA (prostate specific antigen) was performed to identify the so-called "minimal residual cancer" especially in patients receiving neoadjuvant hormonal therapy [17].
8. Review the description of the macroscopic appearance of external and cut surfaces of the surgical specimen as well as inspect the contour of the tissue sections on the slides for hint or clues that might indicate that part of the tissue was missing either due to the surgical procedure or for technical reasons.
9. DNA specimen analysis was performed on formalin-fixed tissue to confirm the identity of the biopsies and prostatectomies whenever necessary.

Table 1 Patients' clinical data

Patient no.	Age (years)	PSA Prebiopsy (ng/ml)	Digital rectal examination	TRUS	Gland volume (cc)
1	68	9.0	Abnormal	Normal	47.9
2	71	5.4	Normal	Abnormal	31.4
3	64	6.1	Normal	Normal	28.1
4	67	1.25	Abnormal	Normal	93.5
5	60	5.9	Normal	Normal	36.6
6	66	3.0	Abnormal	Normal	47.9
7	58	3.9	Normal	Abnormal	29.3
8	66	6.5	Normal	Normal	36.6
Mean (range)	65 (58–71)	5.1 (1.25–9.0)			43.9 (28.1–93.5)

PSA Prostate-specific antigen; *TRUS* transrectal ultrasound

Table 2 Biopsy findings

Patient no.	No. of positive cores	Gleason score	Cancer length (% of involvement)	Positive core location
1	1/12	3+3=6	5	Right apex
2	1/10	3+4=7	10	Right apex
3	1/6	3+3=6	5	Left mid-zone
4	1/6	3+3=6	5	Right mid-zone
5	1/6	3+3=6	5	Right mid-zone
6	1/12	3+3=6	10	Left mid-zone
7	1/10	3+3=6	5	Right mid-zone
8	1/12	3+3=6	5	Left base

Fig. 2 Paraffin blocks, original sections and additional sections before and after block-flipping in case no. 1. **a** Is the right apex. **b** Is the left apex. **c** Includes the whole mount sections of the body of the prostate. **d** Is the right and left base. **e** Includes the seminal vesicles and deferens. A1 is the paraffin block. A2 is the original H-E-stained section. A3 includes the additional sections before block-flipping. A4 refers to the additional sections after block-flipping (Block-flipping was done only for **a** and **b**). The *dotted area* (see also the *red arrow*) on the A4 slides is that of the cancer. It corresponds to the lesion of the biopsy seen in Fig. 1. The same identification procedure applies to **b**. Concerning **c** and **d** the paraffin blocks, the original sections and the additional sections (block-flipping was not done) are shown. For **e** the paraffin blocks and the original sections are shown. (Other slides contain some annotations and abbreviations to indicate additional findings, slide orientation, and section order, etc.)

DNA specimen identity analysis

Tested samples in an individual case included the biopsy core with cancer and a random block for the corresponding RP. The tissue was obtained as a direct section from formalin-fixed and paraffin-embedded blocks. DNA was extracted from paraffin-embedded tissue using the QIAmp DNA mini kit (Qiagen) according to manufacturer's protocol (Promega, Madison, WI, USA). Fifteen microsatellites and amelogenin locus were co-amplified by the AmpFlSTR identifiler kit (Applied Biosystems, Foster City, CA), and the amplified fragments were electrophorized on an ABIPrism3130 genetic analyzer (Applied Biosystems). Fragment sizing and allele designation were established by GeneMapperID v3.2 software (Applied Biosystems), and genetic profiles from both biopsy and prostatectomy samples were compared.

Results

Residual cancer was not found in eight RPs after an initial routine examination. They represent 0.6% of the 1,328 consecutive patients. Three (0.2%) of them were from the group of untreated patients, whereas five (0.4%) were from those who had received neoadjuvant treatment. The latter figure represents 0.8% of the treated patients.

Patients' clinical data are summarised in Table 1. The mean age of the patients was 65 years (range, 58–71 years). Mean serum PSA pre-biopsy was 5.1 ng/ml (range, 1.25–9.0 ng/ml). Mean gland volume was 43.9 ml (range, 28.1–93.5 ml). Digital rectal examination was abnormal in 37% of patients, and 25% of patients had abnormal transrectal ultrasound.

Patients' biopsy findings are shown in Table 2. In all patients, carcinoma was found in one core. Seven patients demonstrated biopsy Gleason score of 6 (3+3), whereas in one, it was 7 (3+4). Cancer occupied approximately 5% of the core length (Fig. 1) in 6 and 10% of the core in two. The positive biopsy location was variable, and there was no side predilection.

Search for residual cancer

There were no cases with a false positive biopsy diagnosis (step 1). Cancer was not overlooked or missed in any of the eight prostatectomies (step 2). Each prostate had been totally embedded (step 3).

Cancer was found on deeper sections (steps 4 and 5) in five cases. Cancer was in the right and left apex, respectively, in two of them. Cancer was in the mid-zone in another two, one in the left and the other in the right. The fifth was in the left base. In particular, the cancer found in

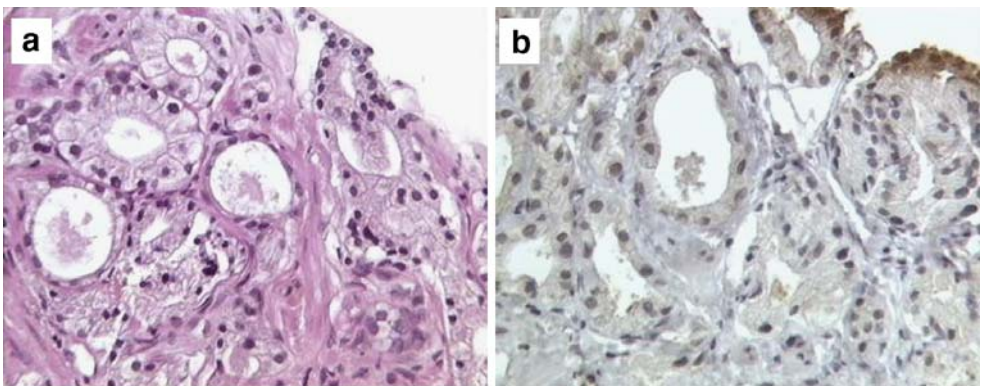

Fig. 1 Biopsy finding of a small groups of atypical acini (**a**) devoid of basal cells (**b**). Section immunostained for p63 (case no. 5). The diagnosis is acinar adenocarcinoma, Gleason score 3+3=6. (The prostatectomy findings are those seen in Fig. 2)

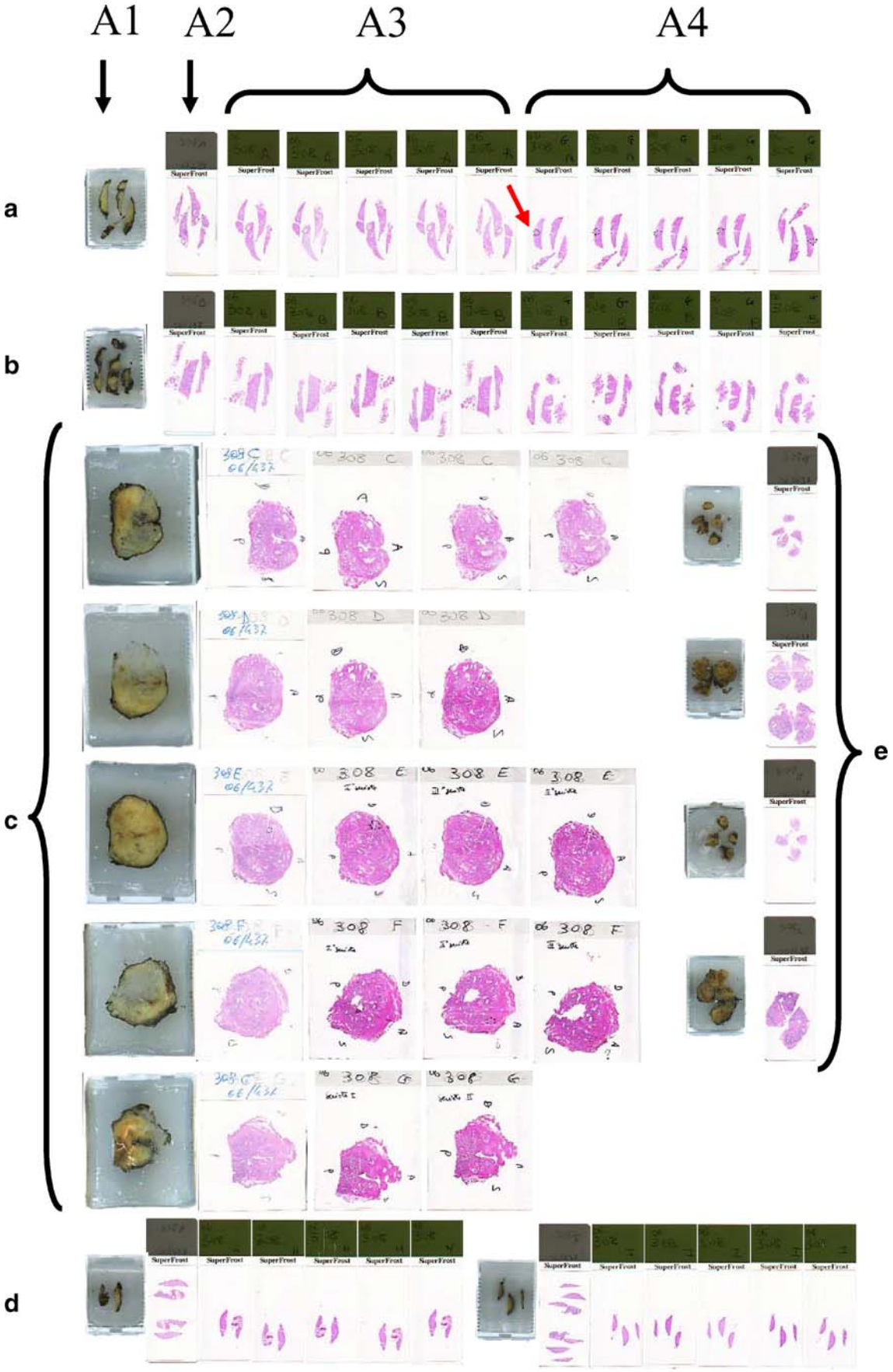
A1
A2
A3
A4
a
b
c
d
e

the right apex was discovered after block-flipping (i.e. step 5; Fig. 2). The location corresponded to site of the positive biopsy in four cases. Two out of five cases were from the untreated group and showed a Gleason score of 3+3=6. Three cases had the morphologic appearance of cancer with evident regressive changes due to endocrine therapy. The diameter of the tumour, measured on the slides, was always below 2.0 mm. In one of the three treated cases, an additional focus of cancer was seen at a distance from to that of the positive biopsy.

The definitive diagnosis was established on steps 6 and 7 in an additional case (the patient was hormonally treated before RP) where cancer was not seen in the additional sections even after block-flipping. Immunohistochemistry for p63 and AMACR was applied to a small suspicious focus of crowded acini. There were a few scattered p63 positive (basal) cells, whereas AMACR was negative. The focus was considered to be benign (i.e. atrophy). Cancer was discovered after immunostaining for cytokeratin CAM 5.2, for p63 and PSA. It was represented by scattered isolated cells positively immunostained with the antibody against CAM 5.2 (Fig. 3) and with PSA and negative for p63 (Fig. 3). The diameter of the focus was 1.0 mm. The block selected for immunohistochemistry corresponded to an H&E-stained slide with hypercellular stroma. There was no exact correspondence with the site of the positive biopsy.

In the remaining two cases (one untreated and the other treated preoperatively), cancer was not found on steps 4 through 7. The review of the description of the macroscopic appearance and the inspection of the contour of the tissue sections on the slides revealed that part of the peripheral zone of the prostate was missing (Fig. 4). This corresponded to the location of the positive biopsy (step 8). DNA specimen analysis confirmed the identity of the biopsy and prostatectomy in both cases (step 9; Table 3).

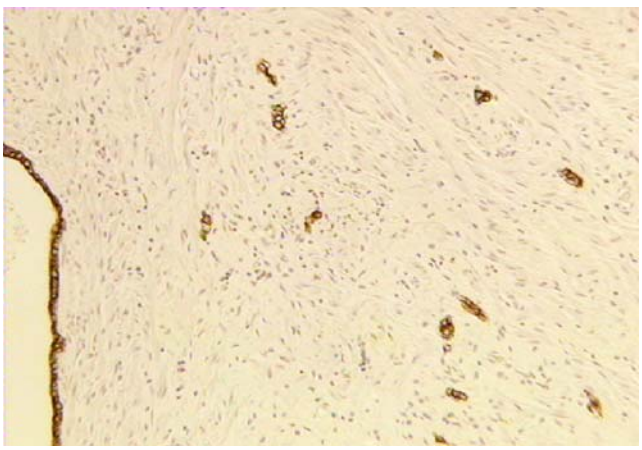

Fig. 3 Cancer is discovered after immunostaining for cytokeratin CAM 5.2 (case no. 6). It is represented by *scattered* isolated cells. The same cells are negative for the basal cell marker p63 and positive for PSA. Part of an atrophic duct is also present

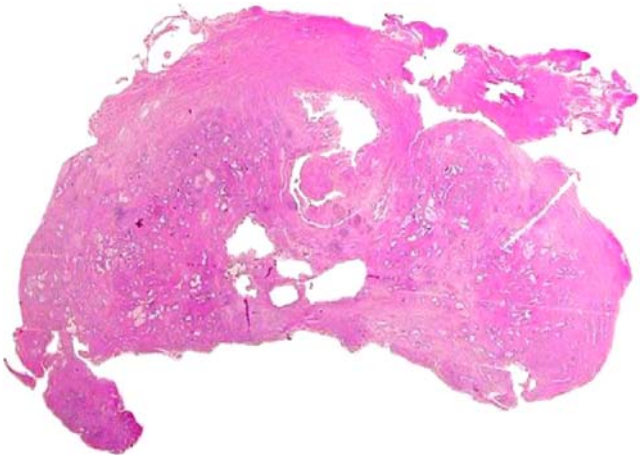

Fig. 4 Whole mount section (case no 7). Part of the peripheral zone, posteriorly, is missing

Incidentally, prostate tissue was documented clinically in one of the two patients (patient no. 7, hormonally treated before operation; the same patient whose prostate is shown in Fig. 4). In particular, a biopsy of the residual fragment showed normal prostate tissue and adenocarcinoma with features identical to those seen in the preoperative biopsy.

Discussion

Reported incidence of no residual cancer on RPs ranges from 0.07 to 4.2% (1–11, 20). It is higher after neoadjuvant hormonal treatment [16].

There are multiple reasons why cancer may not be found on RP after a positive biopsy. In some cases, the cancer may be minute and completely removed by the initial procedure, either needle biopsy or transurethral resection of prostate. Small cancers may be removed from the RP during the technical preparation of the specimen, such as leveling of the paraffin blocks. Small cancer foci can also

Table 3 Results of the search for residual cancer

Patient no.	Neoadjuvant treatment	Cancer found	ID test done
1	No	In recut	No
2	No	In recut	No
3	Yes	In recut	No
4	Yes	In recut	No
5	Yes	In recut after block-flipping	No
6	Yes	After cytokeratin stain	No
7	Yes	Not in RP[a]	Yes, identical
8	No	No	Yes, identical

[a] A post-operative biopsy of the residual prostate fragment in the patient showed normal prostate tissue and adenocarcinoma with features identical to those seen in the preoperative biopsy.

be completely obscured if the patient has undergone antiandrogen therapy or the RP shows extensive inflammation or granulomatous inflammation. Other reasons include false-positive diagnosis on the initial biopsy, resulting in cancer overdiagnosis, or false-negative diagnosis rendered on the RP. Review of the material by a second pathologist or a specialist in urological pathology can often resolve the latter scenario. Lastly, errors may occur either before a specimen is submitted for pathological assessment or in the pathology laboratory. These errors include switching of patients' requisitions, mislabelling or switching of specimen containers, mislabelling or switching slides or blocks and information system errors (e.g. incorrect case entry in the information system or mixed accession numbers) [28].

In our study, the incidence of RPs with no residual cancer after an initial routine examination of the 1,328 specimens was 0.6%. This figure includes both untreated and hormonally treated patients. The incidence was 0.2 and 0.4%, respectively, of the total number of RPs included in the study, or 0.4% (3 out 700 untreated patients) and 0.8% (5 out 628 treated patients) when the two groups were considered separately. The former is well in the range of values reported in the literature for untreated patients and very close to the figure published by Herkommer et al. [11, 13]. The latter value seen in our treated patients is much lower than that observed by Kollermann et al. [16].

Additional sectioning and evaluation of the cases can reduce the number of pT0 RPs after a positive biopsy. In particular, the current study showed that the final incidence was 0.15% and included only two RPs with missing parts, probably due to incomplete removal of the prostate. One of these two patients was hormonally treated preoperatively.

Our findings on the role of immunohistochemistry to detect residual PCa cells are in agreement with previous studies. Gleave et al. [8] found that 50% of the cases that exhibited no residual cancer on routine pathologic assessment had remaining foci of cancer discovered by immunostaining. Without the aid of additional step sections and immunostaining for cytokeratin, these cases would have been reported as being stage pT0 [2].

DNA identity on formalin-fixed tissue from the paraffin blocks is a useful test to establish specimen identity and to exclude the possibility of laboratory error when no residual cancer is found on RP after a positive biopsy. In particular, DNA analysis is a useful test that eliminates the possibility of specimen mishandling or switching by establishing the identity of the tissue from the positive biopsy and the RP. It can be performed in the formalin-fixed tissue from the paraffin blocks. Different methods are used to investigate tissue specimen identity. These include immunolabeling of blood group antigens [22], sex chromosome targeting using fluorescence in situ hybridization [21] and microsatellite analysis. According to some authors, microsatellite analysis is the gold standard for investigating tissue identity [1, 10, 23, 28, 31].

In our study, the clinical and the biopsy data in patients with no initial residual cancer on radical prostatectomy after positive biopsy are similar to the findings from a recent study in patients with single-core positive biopsies and minimal cancer on biopsy [28, 29]. The majority of patients with no residual cancer on prostatectomy demonstrated minute cancer foci in one or two biopsy cores with Gleason score of 6, which, in many cases, may reflect minimal disease [28]. Rare small-volume cancers of higher grade may also be encountered [28]. Follow-up investigations have, in general, shown that no pT0 patient has clinical or biologic evidence of prostate cancer recurrence or progression [6, 14, 20, 27].

There are four aspects that we have not explored in our study. One is that the carcinoma could be lost in facing off of the paraffin blocks. We are fully aware of this potential problem. Our technicians are instructed so that they have to collect tissue sections and not waste material when the paraffin blocks are levelled off. The second is whether the time, effort and expense of the sampling described in this paper are warranted on a routine basis for all pT0 cases. We have not done any analysis in these respects due to the fact that the number of cases is very small and that time and expense do not represent an issue of concern in our institution. The third is what degree of sampling would be necessary to serially section through the entire prostate. Probably thousands of sections would be required, and we were prepared to cut as many sections as needed to find cancer. The fourth is whether there is an outcome difference when the initial pT0 carcinomas are detected after more thorough sampling vs pT0 cases without additional sampling. This was not addressed in our study because the basic aim was to avoid that a pT0 report is rendered to the clinician and to the patient, thus triggering a potential legal issue with all the problems related to it.

There are few observations in the literature on pT0 cases and preoperative diagnosis of cancer made in TURP specimens. The real incidence of no residual cancer after cancer detected by TURP material is not known and is reported to be seen in 6 to 39% of cases [9], presumably due to tumour ablation during the initial resection. However, studies of this phenomenon are limited by variations in the number of tissue sections submitted for histological evaluation and by the small number of cases [3].

Conclusions and recommendations

The current study showed that an extensive search for residual cancer reduces the number of pT0 RPs after a positive biopsy. To achieve this, it is recommended to have

the needle biopsy reviewed, carefully look again at the radical prostatectomy, do deeper sections and then flip certain paraffin blocks. In addition, atypical foci should be stained for basal cell markers and often AMACR, especially in hormone-treated cases. If a block is missing part of the peripheral zone (capsular incision), this should be commented on. DNA analysis for tissue identity should be performed when the other steps have been taken without finding cancer.

References

1. Abeln EC, van Kemenade FD, van Krieken JH, Cornelisse CJ (1995) Rapid identification of mixed up bladder biopsy specimens using polymorphic microsatellite markers. Diagn Mol Pathol 4:286–291
2. Bazinet M, Zheng W, Begin LR, Aprikian AG, Karakiewicz PI, Elhilali MM (1997) Morphologic changes induced by neoadjuvant androgen ablation may result in underdetection of positive surgical margins and capsular involvement by prostatic adenocarcinoma. Urology 49:721–725
3. Blackwell KL, Bostwick DG, Myers RP, Zincke H, Oesterling JE (1994) Combining prostate specific antigen with cancer and gland volume to predict more reliably pathological stage: the influence of prostate specific antigen cancer density. J Urol 151:1565–1570
4. Bostwick DG, Bostwick KC (2004) 'Vanishing' prostate cancer in radical prostatectomy specimens: incidence and long-term follow-up in 38 cases. BJU Int 94:57–58
5. Cao D, Hafez M, Berg K, Murphy K, Epstein JI (2005) Little or no residual prostate cancer at radical prostatectomy: vanishing cancer or switched specimen? A microsatellite analysis of specimen identity. Am J Surg Pathol 29:467–473
6. Descazeaud A, Zerbib M, Flam T, Vieillefond A, Debre B, Peyromaure M (2006) Can pT0 stage of prostate cancer be predicted before radical prostatectomy? Eur Urol 50:1248–1253
7. DiGiuseppe JA, Sauvageot J, Epstein JI (1997) Increasing incidence of minimal residual cancer in radical prostatectomy specimens. Am J Surg Pathol 21:174–178
8. Gleave ME, Goldenberg SL, Jones EC, Bruchovsky N, Kinahan J, Sullivan LD (1996) Optimal duration of neoadjuvant androgen withdrawal therapy before radical prostatectomy in clinically confined prostate cancer. Semin Urol Oncol 14(Suppl 2):39–47
9. Goldstein NS, Bégin LR, Grody WW, Novak JM, Qian J, Bostwick DG (1995) Minimal or no cancer in radical prostatectomy specimens: report of 13 cases of the "vanishing cancer phenomenon". Am J Surg Pathol 19:1002–1009
10. Gras E, Matias-Guiu X, Catasus L, Arguelles R, Cardona D, Prat J (2000) Application of microsatellite PCR techniques in the identification of mixed up tissue specimens in surgical pathology. J Clin Pathol 53:238–240
11. Hammerer P (2004) pT0 after radical prostatectomy: overtreatment for insignificant prostate cancer? Eur Urol 45:35
12. Hellstrom M, Haggman M, Brandstedt S, de la Torre M, Pedersen K, Jarlsfeldt I, Wijkstrom H, Busch C (1993) Histopathological changes in androgen-deprived localized prostatic cancer. A study in total prostatectomy specimens. Eur Urol 24:461–465
13. Herkommer K, Kuefer R, Gschwend JE, Hautmann RE, Volkmer BG (2004) Pathological T0 prostate cancer without neoadjuvant therapy: clinical presentation and follow-up. Eur Urol 45:36–41
14. Kollermann J, Caprano J, Budde A, Weidenfeld H, Weidenfeld M, Hopfenmuller W, Helpap B (2003) Follow-up of nondetectable prostate carcinoma (pT0) after prolonged PSA-monitored neoadjuvant hormonal therapy followed by radical prostatectomy. Urology 62:476–480
15. Kollermann J, Feek U, Muller H, Kaulfuss U, Oehler U, Helpap B, Kollermann MW (2000) Nondetected tumor (pT0) after prolonged, neoadjuvant treatment of localized prostatic carcinoma. Eur Urol 38:714–720
16. Kollermann J, Hopfenmuller W, Caprano J, Weidenfeld H, Weidenfeld M, Helpap B (2004) Prognosis of stage pT0 after prolonged neoadjuvant endocrine therapy of prostate cancer: a matched-pair analysis. Eur Urol 45:42–45
17. Montironi R, Mazzucchelli R, van der Kwast T (2003) Morphological assessment of radical prostatectomy specimens. A protocol with clinical relevance. Virchows Arch 442:211–217
18. Montironi R, van der Kwast T, Boccon-Gibod L, Bono AV, Boccon-Gibod L (2003) Handling and pathology reporting of radical prostatectomy specimens. Eur Urol 44:626–636
19. Murphy WM, Soloway MS, Barrows GH (1991) Pathologic changes associated with androgen deprivation therapy for prostate cancer. Cancer 68:821–828
20. Prayer-Galetti T, Gardiman M, Sacco E, Fracalanza S, Betto G, Pinto F (2007) The finding of no tumor (pT0) in patients submitted to radical retropubic prostatectomy for clinically localized prostate cancer. Anal Quant Cytol Histol (in press)
21. Riopel MA, Yu IT, Hruban RH, Lazenby AJ, Griffin CA, Perlman EJ (1995) Ideas in pathology: whose tumor is this? FISHing for the answer. Mod Pathol 8:456–457
22. Ritter JH, Sutton TD, Wick MR (1994) Use of immunostains to ABH blood group antigens to resolve problems in identity of tissue specimens. Arch Pathol Lab Med 118:293–297
23. Shibata D (1993) Identification of mismatched fixed specimens with a commercially available kit based on the polymerase chain reaction. Am J Clin Pathol 100:666–670
24. Smith DM, Murphy WM (1994) Histologic changes in prostate carcinomas treated with leuprolide (luteinizing hormone-releasing hormone effect). Distinction from poor tumor differentiation. Cancer 73:1472–1477
25. Srigley JR (2003) No cancer in the radical prostatectomy specimen: an approach to a surgical pathologist's dilemma. In: Microtutorial: a systematic approach to prostate needle biopsies. Canadian Association of Pathologists Annual Meeting. Prince Edward Island, Charlottetown, Section V: 32–36 (July 6)
26. Tetu B, Srigley JR, Boivin JC, Dupont A, Monfette G, Pinault S, Labrie F (1991) Effect of combination endocrine therapy (LHRH agonist and flutamide) on normal prostate and prostatic adenocarcinoma. A histopathologic and immunohistochemical study. Am J Surg Pathol 15:111–120
27. Thwaini A, Anjum F, Kaluba J, Shergill IS, Lewi HJE (2004) 'Vanishing' prostate cancer in radical prostatectomy specimens: incidence and long-term follow-up in 38 cases [letter/comment]. BJU Int 94:1145–1146
28. Trpkov K, Gao Y, Hay R, Yimaz A (2006) No residual cancer on radical prostatectomy after positive 10-core biopsy: incidence, biopsy findings, and DNA specimen identity analysis. Arch Pathol Lab Med 130:811–816
29. Trpkov K, Tsui J, Mancevska J, Faris P, Yilmaz A (2005) Single core positive and minimal prostate cancer (PCa) on needle biopsy: correlation with tumor volume and clinically insignificant cancer. Mod Pathol 18(Suppl 1):167A
30. Truskinovsky AM, Sanderson H, Epstein JI (2004) Characterization of minute adenocarcinomas of prostate at radical prostatectomy. Urology 64:733–737
31. Worsham MJ, Wolman SR, Zarbo RJ (2001) Molecular approaches to identification of tissue contamination in surgical pathology sections. J Mol Diagnostics 3:11–15
32. Zynger DL, Dimov ND, Yang XJ (2006) Trends in carcinoma volume in 1612 radical prostatectomies: increased evidence of minimal and no residual cancer. Mod Pathol 19(Suppl 3):90A

Virchows Arch (2007) 450:379–385
DOI 10.1007/s00428-007-0386-7

ORIGINAL ARTICLE

Expression changes of the MAD mitotic checkpoint gene family in renal cell carcinomas characterized by numerical chromosome changes

Mafalda Pinto · Maria J. Soares · Nuno Cerveira · Rui Henrique · Franclim R. Ribeiro · Jorge Oliveira · Carmen Jerónimo · Manuel R. Teixeira

Received: 15 December 2006 / Accepted: 8 February 2007 / Published online: 28 February 2007
© Springer-Verlag 2007

Abstract Papillary and chromophobe renal cell carcinomas are characterized by multiple trisomies and monosomies, respectively, but the molecular mechanisms behind the acquisition of these numerical chromosome changes are unknown. To evaluate the role of mitotic checkpoint defects for the karyotypic patterns characteristic of these two renal cell cancer subtypes, we analyzed the messenger RNA expression levels of the major mitotic checkpoint genes of the budding uninhibited by benzimidazole family (*BUB1*, *BUBR1*, *BUB3*) and of the mitotic arrest deficiency family (*MAD1*, *MAD2L1*, *MAD2L2*) by real-time quantitative polymerase chain reaction in 30 renal cell cancer samples (11 chromophobe and 19 papillary) and 36 normal kidney tissue samples. *MAD1*, *MAD2L1*, and *MAD2L2* showed significant expression differences in tumor tissue compared to controls. Chromophobe tumors presented underexpression of *MAD1*, and *MAD2L2*, whereas papillary tumors showed overexpression of *MAD2L1*. The expression level of the BUB gene family did not differ significantly from that of normal kidney. We conclude that expression changes in mitotic arrest deficiency genes (*MAD1*, *MAD2L1*, and *MAD2L2*) play a role in renal carcinogenesis characterized by multiple numerical chromosome abnormalities.

Keywords Kidney cancer · Chromophobe · Papillary · Mitotic checkpoint · Gene expression · MAD gene family

M. Pinto · M. J. Soares · N. Cerveira · F. R. Ribeiro · C. Jerónimo · M. R. Teixeira (✉)
Department of Genetics, Portuguese Oncology Institute,
Rua Dr António Bernardino de Almeida,
4200-072, Porto, Portugal
e-mail: mteixeir@ipoporto.min-saude.pt

R. Henrique
Department of Pathology, Portuguese Oncology Institute,
Rua Dr António Bernardino de Almeida,
4200-072, Porto, Portugal

R. Henrique · C. Jerónimo · M. R. Teixeira
Department of Pathology and Molecular Immunology, Institute of Biomedical Sciences Abel Salazar, University of Porto,
Largo Professor Abel Salazar,
2-4099-003, Porto, Portugal

J. Oliveira
Department of Urology, Portuguese Oncology Institute,
Rua Dr António Bernardino de Almeida,
4200-072, Porto, Portugal

C. Jerónimo
Fernando Pessoa University School of Health Sciences,
Rua Carlos da Maia,
296-4200-150, Porto, Portugal

Introduction

Renal cell carcinoma (RCC) accounts for approximately 3% of all adult malignancies and 90–95% of all neoplasms arising in the kidney [20]. RCC is a heterogeneous disease that includes several histologically and genetically distinct subtypes [13], the most common of which are the clear cell (75%), papillary (10–15%), and chromophobe (5%) carcinomas [13, 21]. Whereas the clear cell and papillary RCC originate from the proximal tubules, the chromophobe counterpart originates from the collecting tubule [22]. As opposed to clear cell RCC, which presents the defining deletion of the short arm of chromosome 3 and other structural chromosome changes, papillary RCC typically presents different combinations of trisomies of chromosomes 7, 12, 16, 17, and/or 20, and chromophobe RCC is characterized by multiple monosomies of chromosomes 1,

2, 6, 10, 13, 17, and/or 21 [21]. The mechanism behind such characteristic patterns of numerical chromosome abnormalities in kidney carcinogenesis is not known.

Aneuploidy can arise as a consequence of a defect in the mitotic spindle checkpoint, a highly conserved mechanism that ensures that sister chromatids are equally divided upon duplication of the cell [10–12, 16]. Several studies have shown evidence that mutations and/or reduced levels of mitotic checkpoint proteins can cause checkpoint malfunction and chromosomal instability (CIN) and thereby contribute to tumor formation. In yeast, mutations in genes involved in chromosome segregation and regulation of mitotic spindle checkpoint can result in aneuploidy [24], whereas analysis of mice with reduced levels of mitotic arrest deficient-like 2 gene (*Mad2*), budding uninhibited by benzimidazoles 1 homolog beta gene (*Bubr1*), or budding uninhibited by benzimidazoles 3 homolog gene (*Bub3*) has shown that all these mice have significant increases in the number of aneuploid fibroblasts [15].

Cahill et al. [2] cloned two human homologues of yeast budding uninhibited by benzimidazoles 1 (Bub1) homolog gene, *hBUB1*, and *hBUBR1* and reported that the two genes were mutated, although rarely, in CIN colorectal cancers, providing the first evidence that gene mutations can result in defective spindle checkpoint in humans and thus be responsible for aneuploidy in human cancers. Moreover, mutations in human *BUB1* gene have demonstrated a dominant negative effect by disrupting the mitotic checkpoint [2] and *MAD2* haploinsufficiency has been shown to cause premature anaphase and CIN in mammalian cells [15]. Sequence alterations in some mitotic checkpoint genes have been reported in carcinomas arising in several different organs, such as those of the bladder (*MAD2*) [8], breast (mitotic arrest deficient-like 1, (*MAD1*) [23], colon (*BUB1*) [2, 9, 19], lung (*BUB1*) [5], prostate (*MAD1*) [23], and thyroid (*BUB1*) [17]. However, the relatively low mutation frequency in mitotic checkpoint genes (2–33%) does not explain the CIN phenotype often seen in those carcinomas, indicating that alternative mechanisms may be operative. Indeed, recent studies have shown that nonmutational silencing of human *BUB1* and *BUBR1* genes is more common than mutational inactivation, contributing to the development of aneuploidy in human colorectal cancers [17, 19]. Moreover, several breast cancer cell lines with the CIN phenotype have been reported to have decreased expression of *MAD2L1*, yet without the presence of mutations or promoter hypermethylation [18, 26].

As papillary and chromophobe RCC are characterized by multiple numerical chromosome alterations (trisomies and monosomies, respectively), we asked whether or not expression changes in the mitotic checkpoint genes *BUB1*, *BUBR1*, *BUB3*, *MAD1*, *MAD2L1*, and *MAD2L2* might be involved in the development of these two types of kidney carcinomas.

Materials and methods

Patients and sample collection

From a consecutive series of RCC prospectively collected at the Portuguese Oncology Institute—Porto, Portugal, 19 papillary and 11 chromophobe primary carcinomas were studied (diagnosed from 2001 to 2005). The institutional review board of the Portuguese Oncology Institute—Porto, approved the project and patients were enrolled in this study after informed consent. For control purposes, non-neoplastic renal tissue distant from RCC (with chromophobe, papillary, or clear cell histology) was obtained from 36 patients who underwent radical nephrectomy before any other kind of treatment. Tissue samples intended for genetic analysis were promptly snap-frozen in isopentane immediately after surgery and stored at −80°C. The remaining tissues were formalin-fixed and subsequently processed for paraffin embedding. Sections were cut and hematoxylin/eosin stained for histopathological evaluation. Five-micron-thick sections were cut and stained for the identification of the areas of carcinoma and normal tissue. These procedures comprised the diagnosis, grading, and pathological staging (2003 TNM staging system).

RNA extraction and cDNA synthesis

Total RNA was extracted from all samples using the FastRNA Green Kit (Qbiogene, Carlsbad, CA) for 45 s with a speed rating of 6.0 in a FastPrep FP120 Instrument (Qbiogene). RNA quality was checked on 0.8% agarose gels. Reverse transcription was performed with the SuperScript III First-Strand Synthesis System for reverse transcription polymerase chain reaction (RT-PCR; Invitrogen, Carlsbad, CA) following the manufacturer's instructions.

Quantitative RT-PCR

We have evaluated messenger RNA (mRNA) expression of *BUB1*, *BUBR1*, *BUB3*, *MAD1*, *MAD2L1*, and *MAD2L2* by means of quantitative real-time RT-PCR in altogether 66 samples, comprising 36 nonneoplastic renal tissue samples obtained from RCC patients (control), 19 papillary RCC, and 11 chromophobe RCC. Real-time RT-PCR was performed on a TaqMan® ABI PRISM 7000 Sequence Detection System (Applied Biosystems, Foster City, CA). Primers and probes for the budding uninhibited by benzimidazole gene family (*BUB1*, *BUBR1*, and *BUB3*) and for the mitotic arrest deficiency genes (*MAD1*, *MAD2L1,* and *MAD2L2*; Table 1) were designed using the Primer Express Software (version 2.0; Applied Biosystems). To use as the internal reference gene, commercially available TaqMan® reagents with optimized primer and probe concentrations for human

Table 1 Primers and probes used for expression analysis of the mitotic checkpoint genes *BUB1*, *BUBR1*, *BUB3*, *MAD1*, *MAD2L1*, and *MAD2L2*

Primer/Probe	Sequence 5′→3′	Amplicon size (bp)
BUB1_F	GGAGACATCCCATGAGGATCTG	
BUB1_R	CCTACACTTGGCCCCATACG	77
BUB1_probe	TCCCAGGAAAGGTCCGAGGTTAATCCA	
BUBR1_F	TCAACAGAAGGCTGAACCACTAGA	
BUBR1_R	CCAACAGAGTTTGCCGAGACA	82
BUBR1_probe	CCAGCACCGACAATTCCAAGCTCG	
BUB3_F	GACTTACGGAACATGGGTTACGT	
BUB3_R	TGCAGCGAGTCTGGTATTTCA	116
BUB3_probe	CAGCAGCGCAGGGAGTCCAGC	
MAD1_F	CTGCGTGAGAAAGAGGACAGTCT	
MAD1_R	CCGAGATCCTCCCCTTCAGT	69
MAD1_probe	CCCAGGCTGGCGAGACCATCAAC	
MAD2L1_F	CGGGAGCGCCGAAATC	
MAD2L1_R	ACGCTGATATAAAATGCTGTTGATG	63
MAD2L1_probe	TGGCCGAGTTCTTCTCATTCG	
MAD2L2_F	CGTGCCGGTCCAGATGTC	
MAD2L2_R	AGTGCAGCGTGTCCTGGATAT	61
MAD2L2_probe	TGCCACCCGGAGCTGAATCA	

All probes were FAM (5′) and TAMRA (3′) labeled.
F Forward; *R* reverse

hypoxanthine ribosyltransferase (*HPRT*) were purchased from Applied Biosystems (Applied Biosystems).

Complementary (cDNA) generated from each sample was split in equal parts for the measurement of the expression of all six mitotic checkpoint genes under study as well as the endogenous control gene *HPRT*. PCR was performed according to the manufacturer's specifications (Applied Biosystems) in separate wells for each primer/probe set and each sample was run in triplicate. The 20 μl total volume final reaction mixture consisted of 1 μM of each primer, 0.25 μM of probe, 1 μl of TaqMan® Universal PCR Master Mix (Applied Biosystems), and 9 μl of cDNA (with approximately the same concentration in each case). Controls consisting of bidistilled H_2O were negative in all runs. PCR was performed using the following conditions: 50°C for 2 min, 95°C for 10 min, followed by 50 cycles at 95°C for 15 s and 60°C for 1 min. Each plate included multiple nontemplate controls and serial dilutions of a positive control to construct the standard curve.

To determine the relative mRNA expression levels of each of the six genes in each sample, the values of the target gene were normalized against the values of the internal reference gene *HPRT* to obtain a ratio. Thus, expression data of each sample is given as the mean quantity of each gene divided by the mean quantity of the endogenous control *HPRT* gene for the same sample.

Statistical analysis

The normalized expression values of papillary and chromophobe carcinomas were compared with those of normal kidney tissue samples using the Bonferroni-adjusted Mann–Whitney *U* test. Relationship between clinical variables was assessed using either the χ^2 or Fisher's exact test, according to the categorization of the data. All analyses were performed using SPSS version 11.0 (SPSS, Chicago, IL).

Results

A summary of the clinical and histopathological data of the samples is presented in Table 2. Normalized median

Table 2 Clinicopathological features of the 30 renal cell carcinomas analyzed

	Chromophobe	Papillary
Patients (*n*)	11	19
Mean age (range; years)	62 (43–76)	65 (46–83)
Sex (M:F)	4:7	14:5
Metastasis (%)	0	5
pT stage (%)		
1a	9	16
1b	18	47
2	55	21
3a	18	16
3b	0	0
3c	0	0
4	0	0
Fuhrman grade (%)		
1	0	5
2	18	42
3	27	48
4	55	5

Table 3 Normalized median expression levels (with 95% confidence intervals, 95% CI) for six mitotic checkpoint genes in normal kidney tissue and chromophobe and papillary renal cell carcinomas

Gene	Normal	Chromophobe RCC		Papillary RCC	
	Median (95% CI)	Median (95% CI)	*p*	Median (95% CI)	*p*
BUB1	0.01(0.01–0.04)	0.12(0.01–0.07)	ns	0.01(0–0.60)	ns
BUBR1	0.04(0.01–0.26)	0.28(0–0.15)	ns	0.23(0–1.74)	ns
BUB3	21.72(0–815.19)	0.60(0–53.78)	ns	3.12(0–33.07)	ns
MAD1	62.79(72.31–271.85)	0.86(0–14.95)	<0.0001	22.25(0–606.77)	ns
MAD2L1	0.02(0.02–0.12)	0.28(0–0.44)	ns	0.14(0–25.31)	0.0002
MAD2L2	0.80(0.72–4.41)	0.24(0.11–0.66)	0.0017	1.11(0–7.84)	ns

RCC Renal cell cancer; *CI* confidence interval; *ns* non-significant.

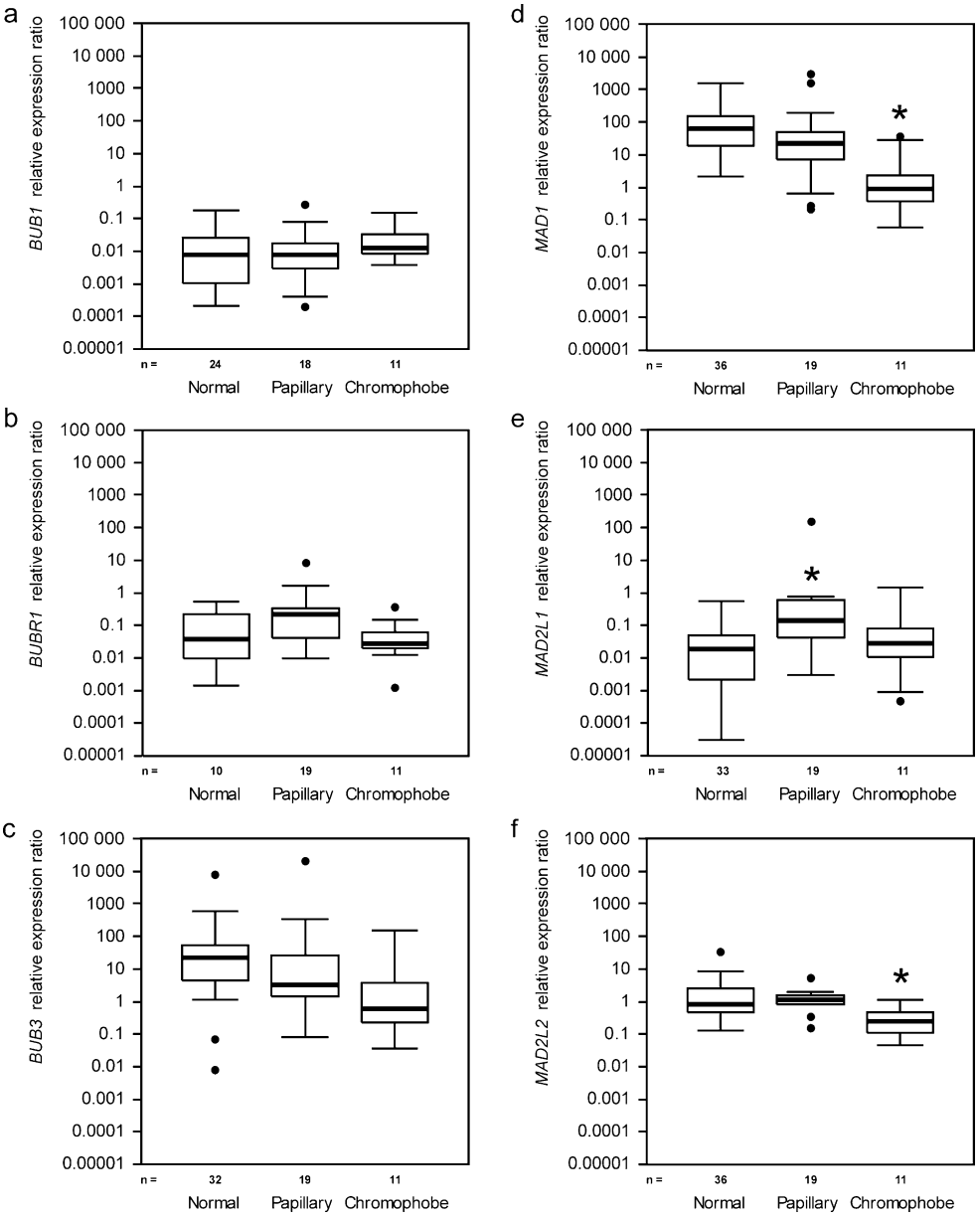

Fig. 1 Distribution of the relative expression level (Log 10 transformed) in normal tissue, chromophobe RCC, and papillary RCC for *BUB1* (**a**), *BUBR1* (**b**), *BUB3* (**c**), *MAD1* (**d**), *MAD2L1* (**e**), and *MAD2L2* (**f**). *Filled circles*, outliers; *asterisks*, statistically significant difference compared to normal controls

expression levels (with 95% confidence intervals) for the mitotic checkpoint genes *BUB1*, *BUBR1*, *BUB3*, *MAD1*, *MAD2L1*, and *MAD2L2* in normal kidney tissue and chromophobe and papillary RCC are presented in Table 3. Three of the six genes showed significant expression differences in tumor tissue compared to controls (*MAD1*, *MAD2L1*, and *MAD2L2*), with each tumor type we have studied presenting abnormal expression in at least one gene (Fig. 1). More specifically, chromophobe RCC presented underexpression of *MAD1* and *MAD2L2* (p=<0.0001 and p=0.0017, respectively; Fig. 1d and f, respectively), whereas papillary RCC showed overexpression of *MAD2L1* (p=0.0002; Fig. 1e). No significant expression changes were detected for *BUB1*, *BUBR1*, or *BUB3* as compared to normal kidney tissue (Fig. 1a, b, and c, respectively). No significant associations were observed between expression alterations and tumor grade or stage.

Discussion

Mitotic checkpoint genes have drawn considerable attention for their possible role in CIN in cancer, as it has been shown that even a partial reduction in function for one of these genes can have a profound effect on mitotic stability and maintenance of genomic integrity. With this in mind, we reasoned that expression changes in genes involved in chromosome segregation could at least in part be responsible for the aneuploidies characteristic of two of the main histological subtypes of RCC, namely, chromophobe and papillary RCC. We have evaluated the relative transcript levels of *BUB1*, *BUBR1*, *BUB3*, *MAD1*, *MAD2L1*, and *MAD2L2* genes in these two tumor types and compared them with those of normal kidney tissue. To the best of our knowledge, this is the first study of this kind performed in renal cancer and is also one of the first studies to analyze the coordinated expression of these six mitotic checkpoint genes.

Both chromophobe and papillary carcinomas proved to have a significant difference in the expression of at least one of the six mitotic checkpoint genes, as compared to nonneoplastic samples (Table 3). Our data thus indicate that altered expression of genes involved in chromosome segregation may play a role in the development of the numerical cytogenetic changes that characterize chromophobe (multiple monosomies) and papillary (multiple trisomies) RCC. Interestingly, only genes from the mitotic arrest deficiency group (*MAD1*, *MAD2L1*, and *MAD2L2*) were shown to have expression changes in these tumor types, whereas the expression level of the three genes from the budding uninhibited by benzimidazole gene family (*BUB1*, *BUBR1*, and *BUB3*) did not significantly differ from normal kidney tissue. As the literature data existent for other tumors is skewed towards the genes *BUB1* and *BUBR1* [2, 9, 6, 7, 19, 24], it is unknown whether or not this pattern of mitotic checkpoint gene expression is specific for these types of kidney cancer or a more general trend in neoplasias characterized by aneuploidy.

We report for the first time *MAD1* and *MAD2L2* underexpression in chromophobe RCC (Fig. 1d and f, respectively). Underexpression of these two genes has not been reported before in this or other tumor types, as the few studies concerning *MAD1* or *MAD2L2* dealt more with mutation screening rather than expression analysis [2, 23]. Recently, Yuan et al. [27] reported overexpression of *MAD1* and *MAD2L2* in genetically unstable breast cancer cell lines and in high-grade primary breast cancer tissues, as compared to stable (and checkpoint proficient) cell lines and normal breast tissue. Although we have observed an association between *MAD1* and *MAD2L2* underexpression and a tumor type characterized by multiple whole chromosome losses, further studies are necessary to establish a causal relationship.

Point mutations and/or hypermethylation are uncommon mechanisms causing *MAD1* and *MAD2L2* underexpression in kidney or other tumors. An alternative explanation might be the involvement of other proteins in the mitotic checkpoint complex, such as *BUB2*, *MPS1*, *CENP-E*, as well as other still unknown proteins that might work as repressors. Furthermore, several studies have shown that removing the kinase activity of some of the mitotic checkpoint proteins weakens or abolishes mitotic checkpoint signaling and diminishes or prevents kinetochore recruitment of other checkpoint proteins [1, 3]. Thus, in case proteins responsible for the recruitment of *MAD1* and/or *MAD2L2* are not (totally) functional, the recruitment of these two proteins may be abolished or diminished and its expression decreased. Moreover, transcriptional repression of *MAD1* by both wild-type and mutant *p53* has been reported [4].

Overexpression of *MAD2L1* was the only significant change in papillary RCC, although we emphasize that our findings concern transcriptional expression and not translational expression. However, other authors have correlated transcriptional and translational overexpression for different mitotic checkpoint genes [27]. Our data are in accordance with other studies that have also shown overexpression of *MAD2L1*, both in primary tumors from several neoplasias (e.g., breast, colon, and gastric) as well as in breast cancer cell lines [14, 25, 27]. Yuan et al. [27] have recently proposed the hypothesis that overexpression of some of the mitotic checkpoint genes could represent a compensation for other defects in the mitotic spindle checkpoint. As a total loss of checkpoint function would be catastrophic for the cell, it seems reasonable that cells would have such a compensatory mechanism to prevent a total chaos at

mitosis. However, they found an increased expression level of eight different mitotic checkpoint genes, whereas we found only in one. The compensatory system seems reasonable when it includes all or at least a significant amount of the genes involved, which is not the case in our study. Another hypothesis these authors have advanced is that overexpression of checkpoint genes themselves would lead to CIN, as overexpression of wild-type *BUB1* or *MAD3* gene leads to CIN in yeast [24]. However, the data at hand are not sufficient to establish a causal relationship between *MAD2L1* overexpression and the multiple trisomies that characterize papillary RCC.

As the two types of renal tumors analyzed in this study are characterized by numerical chromosome alterations, we hypothesized that the expression changes of the MAD gene family of mitotic checkpoint genes could be related to a dose effect caused by gain or loss of whole chromosomes in the cancer cells, but the data supporting this hypothesis are scarce. Although it could be argued that *MAD2L2* underexpression could be related to the monosomy of chromosome 1 commonly observed in chromophobe RCC (*MAD2L2* is located on 1p36), the argument does not hold for the expression changes of *MAD1* or *MAD2L1* as none of these genes is located in chromosomes commonly affected by numerical changes in these tumor types. The data we present are therefore more compatible with expression changes in mitotic checkpoint genes causing chromosome numerical abnormalities than the other way around.

We conclude that expression changes in mitotic arrest deficiency genes (*MAD1*, *MAD2L1*, and *MAD2L2*) play a role in renal carcinogenesis characterized by multiple numerical chromosome abnormalities. Moreover, the type of expression change and the mitotic checkpoint genes affected differ between a tumor type characterized by multiple monosomies (chromophobe RCC) and a tumor type characterized by multiple trisomies (papillary RCC). Further studies are warranted to determine the mechanism (s) leading to the expression changes we uncovered and to establish a causal relationship between mitotic checkpoint defects and the specific patterns of chromosome changes that define these subsets of RCC.

Acknowledgments This study was supported by the Fundação para a Ciência e a Tecnologia (FCT; Projecto de Investigação Plurianual do Centro de Investigação do IPO-Porto [03-05]). FRR (grant SFRH/BD7067/2001) and MP (grant SFRH/BPD/14506/2003) are research fellows of FCT.

References

1. Abrieu A, Magnaghi-Jaulin L, Kahana JA, Peter M, Castro A, Vigneron S, Lorca T, Cleveland DW, Labbe JC (2001) Mps1 is a kinetochore-associated kinase essential for the vertebrate mitotic checkpoint. Cell 106:83–93
2. Cahill DP, Lengauer C, Yu J, Riggins GJ, Willson JK, Markowitz SD, Kinzler KW, Vogelstein B (1998) Mutations of mitotic checkpoint genes in human cancers. Nature 392:300–303
3. Chen RH (2004) Phosphorylation and activation of Bub1 on unattached chromosomes facilitate the spindle checkpoint. EMBO J 23:3113–3121
4. Chun AC, Jin DY (2003) Transcriptional regulation of mitotic checkpoint gene MAD1 by p53. J Biol Chem 278:37439–37450
5. Gemma A, Seike M, Seike Y, Uematsu K, Hibino S, Kurimoto F, Yoshimura A, Shibuya M, Harris CC, Kudoh S (2000) Somatic mutation of the hBUB1 mitotic checkpoint gene in primary lung cancer. Genes Chromosomes Cancer 29:213–218
6. Grabsch H, Takeno S, Parsons WJ, Pomjanski N, Boecking A, Gabbert HE, Mueller W (2003) Overexpression of the mitotic checkpoint genes BUB1, BUBR1, and BUB3 in gastric cancer-association with tumour cell proliferation. J Pathol 200:16–22
7. Grabsch HI, Askham JM, Morrison EE, Pomjanski N, Lickvers K, Parsons WJ, Boecking A, Gabbert HE, Mueller W (2004) Expression of BUB1 protein in gastric cancer correlates with the histological subtype, but not with DNA ploidy or microsatellite instability. J Pathol 202:208–214
8. Hernando E, Orlow I, Liberal V, Nohales G, Benezra R, Cordon-Cardo C (2001) Molecular analyses of the mitotic checkpoint components hsMAD2, hBUB1 and hBUB3 in human cancer. Int J Cancer 95:223–227
9. Imai Y, Shiratori Y, Kato N, Inoue T, Omata M (1999) Mutational inactivation of mitotic checkpoint genes, hsMAD2 and hBUB1, is rare in sporadic digestive tract cancers. Jpn J Cancer Res 90:837–840
10. Jallepalli PV, Lengauer C (2001) Chromosome segregation and cancer: cutting through the mystery. Nat Rev Cancer 1:109–117
11. Kops GJ, Foltz DR, Cleveland DW (2004) Lethality to human cancer cells through massive chromosome loss by inhibition of the mitotic checkpoint. Proc Natl Acad Sci USA 101:8699–8704
12. Kops GJ, Weaver BA, Cleveland DW (2005) On the road to cancer: aneuploidy and the mitotic checkpoint. Nat Rev Cancer 5:773–785
13. Kovacs G, Akhtar M, Beckwith BJ, Bugert P, Cooper CS, Delahunt B, Eble JN, Fleming S, Ljungberg B, Medeiros LJ, Moch H, Reuter VE, Ritz E, Roos G, Schmidt D, Srigley JR, Storkel S, van den Berg E, Zbar B (1997) The Heidelberg classification of renal cell tumours. J Pathol 183:131–133
14. Li GQ, Zhang HF (2004) Mad2 and p27 expression profiles in colorectal cancer and its clinical significance. World J Gastroenterol 10:3218–3220
15. Michel LS, Liberal V, Chatterjee A, Kirchwegger R, Pasche B, Gerald W, Dobles M, Sorger PK, Murty VV, Benezra R (2001) MAD2 haplo-insufficiency causes premature anaphase and chromosome instability in mammalian cells. Nature 409:355–359
16. Musacchio A, Hardwick KG (2002) The spindle checkpoint: structural insights into dynamic signalling. Nat Rev Mol Cell Biol 3:731–741
17. Ouyang B, Knauf JA, Ain K, Nacev B, Fagin JA (2002) Mechanisms of aneuploidy in thyroid cancer cell lines and tissues: evidence for mitotic checkpoint dysfunction without mutations in BUB1 and BUBR1. Clin Endocrinol 56:341–350
18. Percy MJ, Myrie KA, Neeley CK, Azim JN, Ethier SP, Petty EM (2000) Expression and mutational analyses of the human MAD2L1 gene in breast cancer cells. Genes Chromosomes Cancer 29:356–362
19. Shichiri M, Yoshinaga K, Hisatomi H, Sugihara K, Hirata Y (2002) Genetic and epigenetic inactivation of mitotic checkpoint genes hBUB1 and hBUBR1 and their relationship to survival. Cancer Res 62:13–17

20. Stewart BW, Kleihues P (2003) World cancer report. IARC, Lyon
21. Storkel S, Eble JN, Adlakha K, Amin M, Blute ML, Bostwick DG, Darson M, Delahunt B, Iczkowski K (1997) Classification of renal cell carcinoma: workgroup no. 1. Union Internationale Contre le Cancer (UICC) and the American Joint Committee on Cancer (AJCC). Cancer 80:987–989
22. Thoenes W, Storkel S, Rumpelt HJ (1986) Histopathology and classification of renal cell tumors (adenomas, oncocytomas and carcinomas). The basic cytological and histopathological elements and their use for diagnostics. Pathol Res Pract 81:125–143
23. Tsukasaki K, Miller CW, Greenspun E, Eshaghian S, Kawabata H, Fujimoto T, Tomonaga M, Sawyers C, Said JW, Koeffler HP (2001) Mutations in the mitotic check point gene, MAD1L1, in human cancers. Oncogene 20:3301–3305
24. Warren CD, Brady DM, Johnston RC, Hanna JS, Hardwick KG, Spencer FA (2002) Distinct chromosome segregation roles for spindle checkpoint proteins. Mol Biol Cell 13:3029–3041
25. Wu CW, Chi CW, Huang TS (2004) Elevated level of spindle checkprotein MAD2 correlates with cellular mitotic arrest, but not with aneuploidy and clinicopathological characteristics in gastric cancer. World J Gastroenterol 10:3240–3244
26. Yoon DS, Wersto RP, Zhou W, Chrest FJ, Garrett ES, Kwon TK, Gabrielson E (2002) Variable levels of chromosomal instability and mitotic spindle checkpoint defects in breast cancer. Am J Pathol 161:391–397
27. Yuan B, Xu Y, Woo JH, Wang Y, Bae YK, Yoon DS, Wersto RP, Tully E, Wilsbach K, Gabrielson E (2006) Increased expression of mitotic checkpoint genes in breast cancer cells with chromosomal instability. Clin Cancer Res 12:405–410

Virchows Arch (2007) 450:387–395
DOI 10.1007/s00428-006-0358-3

ORIGINAL ARTICLE

Prognostic value of PIK3CA and phosphorylated AKT expression in ovarian cancer

Joachim Woenckhaus · Klaus Steger · Klaus Sturm · Karsten Münstedt · Folker E. Franke · Irina Fenic

Received: 1 October 2006 / Revised: 30 November 2006 / Accepted: 1 December 2006 / Published online: 15 February 2007
© Springer-Verlag 2007

Abstract Disrupted phosphatidylinositol 3-kinase (PI3K) activity and its effect on the downstream target AKT plays an important role in malignant diseases. Gain and/or amplification of PIK3CA gene, encoding the catalytic subunit of phosphatidylinositol 3-kinase (p110α) and its increased expression are associated with enhanced PI3K activity in ovarian cancer cell lines. In this study, ovarian carcinomas with documented clinical outcome were assessed for genetic aberrations at the 3q26.3 locus, including PIK3CA, by fluorescence in situ hybridization. PIK3CA amplification was evaluated by quantitative real-time PCR with respect to a control gene situated at 3q13. The expression of p110α, phosphorylated AKT (pAKT) and the proliferation marker Ki-67 were immunohistochemically investigated. PIK3CA amplification and Ki-67 index were strong predictors for an early tumour-associated death. p110α expression correlated with 3q26.3 gain and Ki-67 index but not with the patient outcome. No relationship could be observed between p110α and pAKT or between pAKT and disease outcome. It is interesting to note that cases with a nuclear pAKT immunoreactivity showed a trend of improved overall survival. Our results underline the prognostic significance of PIK3CA in ovarian carcinoma and argue against a simple linear model of PIK3CA gain/amplification followed by PI3K activation and consecutive AKT phosphorylation in ovarian carcinoma.

Keywords PIK3CA · pAKT · Ovarian carcinoma · Prognosis

J. Woenckhaus · K. Sturm · F. E. Franke
Institute of Pathology, University of Giessen and Marburg, Giessen, Germany

K. Münstedt
Clinic of Obstetrics and Gynaecology, University of Giessen and Marburg, Giessen, Germany

K. Steger · I. Fenic (✉)
Clinic of Urology and Children Urology, University of Giessen and Marburg, Rudolf-Buchheim Street 7, 35392 Giessen, Germany
e-mail: ifenic@gmx.de

Introduction

Ovarian carcinoma is the most lethal gynaecological malignancy because most tumours are detected in advanced stages. Depending on the type and grade of malignancy, alterations of various tumour suppressors and oncogenes, such as KRAS, PTEN, BCL2/HER2/neu, p53, AKT2, p16, MYC and TGF-β are involved in the tumourigenesis of ovarian carcinoma [27]. The identification of molecular markers predicting the clinical outcome becomes more and more important for a better adjustment of patients' treatment. In a recent study [19], it was shown that cell proliferation assessed by the Ki-67 index in the early stages of ovarian carcinomas is a prognostic marker outweighing other established parameters in the prediction of the disease-specific survival.

PIK3CA (Gene Bank NM_006218) located at the 3q26.3 locus was implicated as an oncogene in ovarian carcinoma [26]. Over-representation of 3q26ter is one of the most frequent aberrations and is supposed to be an early event in the ovarian tumourigenesis [2, 5, 25], whereas other authors suggested an association with disease progression [31]. Amplification of the 3q26.3 locus was described as an independent predictor of clinical tumour behaviour and long-term outcome in head and neck squamous cell

carcinoma [28]. However, its prognostic significance in ovarian carcinoma is still unclear. PIK3CA encodes the catalytic sub-unit p110α of phosphatidylinositol 3-kinase class IA (PI3K), which forms dimers with the regulatory sub-unit p85 of the same enzyme. Increased PI3-kinase activity could be caused by gene-dependent over-expression of p110α [15, 26]. PI3K triggers the activation of the downstream target serine–threonine kinase AKT by inducing phosphorylation of the Thr-308 and Ser-473 sites (pAKT) in the plasma membrane through 3-phosphoinositide-dependent kinases (PDKs) [1, 16]. The PI3K/AKT pathway promotes the inhibition of apoptosis and cell cycle progression [6, 14, 20]. It was recently shown that an increased PI3KCA transcription contributes to chemotherapy (cisplatin) resistance in ovarian cancer cell lines [11].

To date, mainly in vitro data exist about the PI3K/AKT pathway in ovarian carcinoma and there is only sparse information about the prognostic relevance of the genomic status of PIK3CA in combination with pAKT expression analysis. Therefore, we assessed quantitatively the status of PIK3CA gene and compared the p110α protein expression with that of its major downstream target kinase AKT in a series of clinically documented ovarian carcinomas.

Materials and methods

Patients and tissues

The tissue and patient data were used in accordance with the declaration of Helsinki and the International Conference of Harmonisation—Good Clinical Practice. The anonymity of the patients investigated was preserved according to the data protection rules of the Human Medical Faculty, Giessen and the German state Hessen.

Seventy-four cases of ovarian carcinomas with documented clinical outcome were selected from the paraffin tumour archive of the Institute of Pathology, Giessen, Germany. The material included primary carcinomas, which underwent surgery between 1980 and 1996 at the Department of Obstetrics and Gynaecology, Giessen, Germany. Follow-up was done every 3 months within 3 years after diagnosis, every 6 months up to 5 years and annually thereafter. The last update was performed in July 2006. Clinical–pathological factors assessed included patient age, FIGO stage as described by the Union International Contre le Cancer (UICC) [30], histological grading, tumour type (Table 1). Volume of ascites, residual tumour size and success of therapy were included as additional prognosis factors. The response to therapy was documented in terms of complete remission, partial remission, stable disease or progressive disease. The histological diagnosis was re-evaluated on haematoxylin and eosin (HE) stained sections according to the WHO classification [10]. All cases showed reliable antigen preservation verified by Ki-67 immunostaining. The area with the highest proliferative activity was selected for tissue microarrays (cylinders, 4 mm in diameter). Sections were cut for fluorescence in situ hybridization (thickness 5–7 μm) and for immunohistochemistry (2–4 μm).

DNA extraction and quantitative real-time PCR (qPCR)

DNA was extracted from formalin-fixed paraffin-embedded tissue. Twelve sections (thickness 5 μm) in each case were taken on glass slides and deparaffinized in xylol (3×5 min). The first and last sections were routinely stained with hematoxylin and eosin and were used to sort the appropriate cases for DNA extraction. Of the 74 cases, only 50 contained sufficient tumour tissue (at least 50% in both control slides) for a reliable evaluation of PIK3CA gene status. The extraction was carried out with the QIAamp DNA Mini Kit (Qiagen, Germany) according to the manufacturer's instructions.

PIK3CA copy number was evaluated by qPCR (Icycler, BioRad, Germany) using qPCR™ mastermix for SYBR-green (Eurogentec, Germany) and primers to genomic sequences of PIK3CA (forward, 5′-CATTTGCTCCAA ACTGACCA-3′; reverse, 5′-AGAGATTGGCATG CTGTCGA-3′) and TRAT1 (forward, 5′-CATGTCAGG TAAGTGGCATT-3′; reverse, 5′-GGGTCTTCTCGTTAG GACTTAG-3′). TRAT1, situated on chromosome 3q13, served as reference genes for the evaluation of PIK3CA status; the variation of PIK3CA copy number with respect to TRAT1 was specified as "amplification". The amount of PIK3CA-specific template was estimated in each carcinoma with respect to the control gene. Non-carcinomatous tissue (at least three cases per assay) was

Table 1 Clinical–pathological features of ovarian carcinomas and distribution of the analysed cases

	Age		FIGO stage				Histological grading			Tumour type				
	<50	≥50	I	II	III	IV	1	2	3	Serous	Mucinous	Endometrioid	Clear cell	Undifferentiated
Number of cases	17	57	22	21	24	7	3	28	43	39	8	6	9	12
Total	74		74				74			74				

employed to normalize the data using the ΔΔCt method (Perkin Elmer, USA). Each case was repeated in triplicate and the mean value was calculated. For statistical evaluation, the cases were sub-divided into three groups with respect to the PIK3CA amplification values (0–2 no amplification; 2–3 moderate amplification, >3 high level amplification).

Fluorescence in situ hybridization (FISH)

The YAC DNA clone 914e08 containing the PIK3CA gene was obtained from the CEPH mega YAC library (RZPD, Berlin, Germany). The YAC DNA was amplified and labelled as described previously [35]. The tissue microarray slides were pre-treated 10 min in phosphate buffer saline (PBS) at 80°C followed by 30 min digestion with 0.5% proteinase K in PBS at 37°C. Co-hybridization of the digoxigenin-labelled telomeric probe D3Z1 (Appligene Oncor) with the biotinylated probe 3q26.3 and visualization were performed as described previously [35]. Signals were visualized with a Zeiss Axiophot fluorescence microscope (Zeiss, Oberkochen, Germany) using the Pinstel filter set 83000 Chroma. Digitisation and documentation were done with the Mac Probe System (PSI, Chester, UK). The FISH results were verified independently by a second observer. Of 74 cases, only 32 showed sufficient FISH signals and could be evaluated for 3q26.3 gain and amplification. Between 151 and 204 (mean 155) cells with D3Z1-centromeric and 3q26.3-YAC signals, respectively, were analyzed in each case. The 3q26.3 gain was calculated by dividing the total number of YAC signals by the total number of cells per case. The 3q26.3 amplification was calculated by dividing the total number of YAC signals by the total number of centromeric signals per case. For statistical analyses, the cases were sub-divided into three groups with respect to the 3q26.3 gain values (0–2 no gain; 2–4 moderate gain; ≥4 high level gain) and the 3q26.3 amplification values (0–2 no amplification; 2–3 moderate amplification, >3 high level amplification).

Immunohistochemistry

Commercially available antibody raised against Ki-67 (monoclonal mouse, clone mib-1, DAKO), p110α (polyclonal rabbit, Cell Signaling, USA) and pAKT Ser-473 (monoclonal mouse, clone 587F11, Cell Signaling, USA) were used. Slides were de-waxed in xylene, rehydrated through a graded ethanol series and washed in Tris buffer saline (TBS). Endogenous peroxidase was blocked by incubation for 10 min in 3% hydrogen peroxide in methanol. Antigen retrieval was performed in 0.01 mol/l sodium citrate buffer, pH 6, for 25 min at 98°C in a microwave oven. Primary antibodies were diluted in DAKO antibody diluent according to the manufacturer's instructions and incubated overnight at 4°C. The reactions were detected using the DAB detection kit (DAKO). Negative controls for p110α were treated identically excepting the use of the primary antibody, whereas for phosphorylated AKT the primary antibody was pre-incubated with its blocking protein (Cell Signaling, USA). Seventy-one cases showed a reliable staining for p110α and 64 cases for pAKT. Immunohistochemistry was evaluated using the immunoreactive score (IRS) as described previously [18]. The IRS is the product of the intensity of immunostaining (none=0; weak=1; moderate=2; strong=3) and the percentage of positive tumour cells (none=0; <10%=1; 10–50%=2; 51–80%=3; >80%=4). Nuclear and cytoplasmic pAKT staining was distinguished and scored as mainly cytoplasmic (C) or mainly nuclear (N). For the statistical analyses of p110α and pAKT expression, IRS values of 0–3 were scored as 1 (poor expression), IRS values of 4–8 as 2 (moderate expression) and IRS values of 9–12 as 3 (strong expression). For the Ki-67 index, 500 nuclei in areas of maximal nuclear positivity were assessed for each case and given as the percentages of positive nuclei.

Data management and statistics

The effect of each variable on tumour-specific survival was evaluated by Kaplan–Meier analysis. The influence of the Ki-67 index, PIK3CA amplification, 3q26.3 gain, p110α-expression, cytoplasmic pAKT-expression and nuclear pAKT-expression on disease-specific survival were further analysed by Kaplan–Meier residual survival analysis. The residual survival, reflecting the theoretical survival without the effect of established influence factors (tumour stage, tumour grading, volume of ascites, residual tumour size and success of therapy), was calculated by multiple regression analysis with respect to the abovementioned factors [17]. To avoid negative results, the number 9 was added to all residuals. The association between variables was assessed by Chi-square test, Fisher's exact test or Spearman's rank correlation coefficient. All analyses were performed using the SPSS software for Windows™, release 11.0. A probability of error less than 5% was regarded as significant.

Results

qPCR

The PIK3CA amplification related to TRAT1 ranged between 0.75 and 12.1 (mean value 1.99). From 50 cases evaluated, 11 (22%) harboured amplifications (Fig. 1): 3 (6%) showed high level, 8 (16%) moderate and 39 (78%)

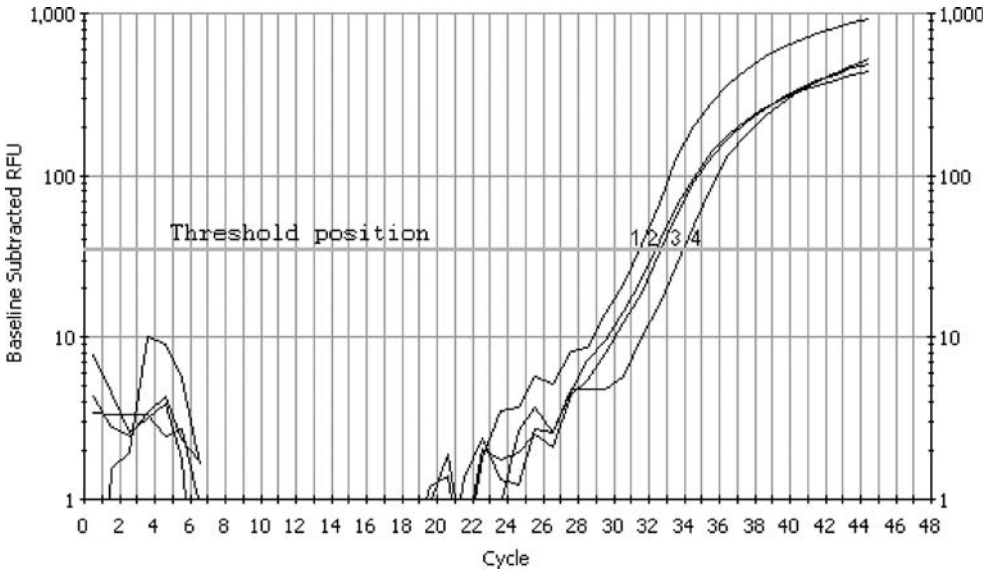

Fig. 1 Representative amplification curves of genomic DNA obtained from a non-tumoural tissue (*2*: PIK3CA, *3*: TRAT1, ΔCt=−0.3) and from an ovarian carcinoma (*1*: PIK3CA, *4*: TRAT1, ΔCt=−2.5)

no amplification of PIK3CA. The association of PIK3CA amplification with clinical–pathological data revealed that 8 out of 30 patients with poorly differentiated (26%) and 3 out of 19 patients (16%) with moderately differentiated carcinomas harboured amplifications. Only one case was better differentiated and showed no amplification. For assessing the association with tumour staging, the cases were grouped upon FIGO stage in three categories: FIGO I, II, III and IV. Six of 14 patients with FIGO stage I (43%), 3 out of 17 with FIGO stage II (17%), 2 out of 15 cases with FIGO stage III (13%) and none of the 4 cases with FIGO stage IV harboured amplifications. These results suggest that PIK3CA genomic amplification is an early event in the development of poorly differentiated (high grade) ovarian carcinomas. However, the associations between PIK3CA amplification and either tumour grade or stage were not statistically significant (Fisher's exact test $p=0.269$, Chi-square test $p=0.074$, respectively). No connection between PIK3CA amplification and either patient age or histological tumour type could be found.

FISH

The average 3q26.3 copy number gain related to the cell number in each case ranged between 1.40 and 6.86 (mean value 2.99). From 32 cases analysed, 25 (78%) harboured 3q26.3 gains: 3 out of 32 cases (9.4%) showed high level, 22 out of 32 cases (68.8%) showed moderate (Fig. 2) and 7 cases (21.9%) displayed no gain. Concerning the associations between 3q26.3 gain and clinical–pathological data, no obvious connection with FIGO stage, tumour grading, age of patients or tumour type could be observed. Spearman's rank correlation coefficient showed direct

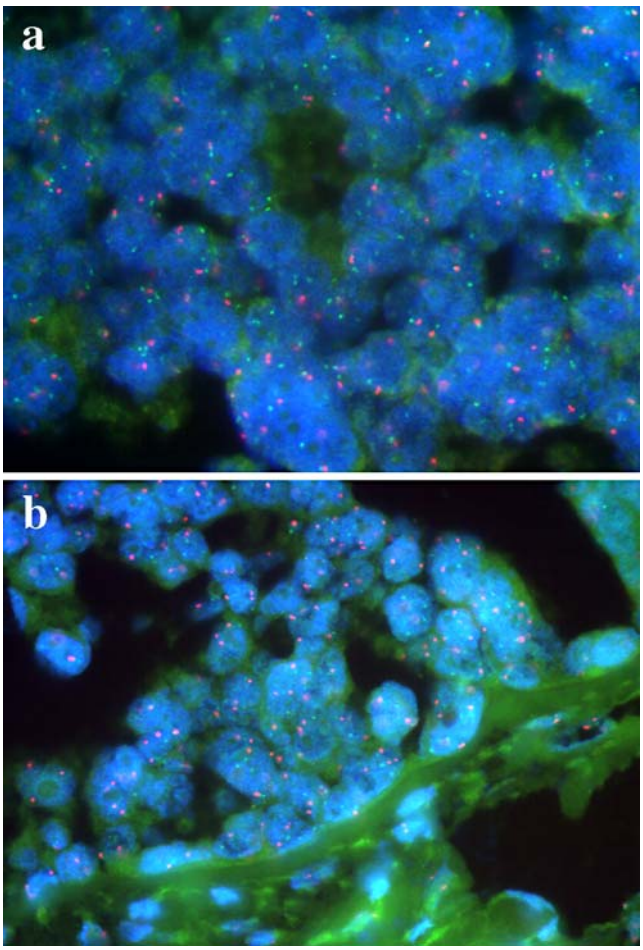

Fig. 2 Ovarian carcinomas showing the YAC DNA probe 914e08 (*green signals*) and the D3Z1 probe (*red signals*). **a** Significant 3q26.3 gain (3.2 YAC signals/cell); **b** modest 3q26.3 gain (2.2 YAC signals/cell). Original magnification ×60 (**a**), ×40 (**b**)

correlations between 3q26.3 gain and PIK3CA amplification assessed by qPCR (rs=0.429, p=0.020).

The 3q26.3 amplification related to chromosome 3 centromeric signals ranged between 0.98 and 2.20 (mean value 1.34). From 32 cases, only 2 (6%) displayed amplifications and both were moderate.

Immunohistochemistry

Ki-67 was positive in 74 cases. The range of Ki-67 positive tumour cells was between 2% and 85% (mean value 36.8%). Concerning the Ki-67 index, the cases were subdivided into three groups: 0–14%, 15–59% and 60–85% positive cells. Immunohistochemistry for p110α and pAKT protein expression was performed in 71 and 64 informative cases, respectively. p110α showed a predominantly cytoplasmic and in some cases an accentuated membranous staining, whereas a nuclear and/or cytoplasmic staining was observed for pAKT (Ser-473) (Fig. 3). p110α expression was strong in 23 (32.4%), moderate in 35 (49.2%) and poor in 13 (18.3%) out of 71 carcinomas (median IRS 8, range: 1–12). Two distinct scores could be calculated for pAKT: the IRS for cytoplasmic pAKT (median IRS 4, range: 0–12) and the IRS for the nuclear pAKT (median 0, range: 0–9). Four cases (6.2%) displayed a strong, 32 (50%) a moderate and 28 (43.8%) a poor cytoplasmic pAKT staining. Only one case showed a strong nuclear pAKT expression. Therefore, IRS for the nuclear pAKT was dichotomised as follows: 16 cases (25%) with a moderate-to-strong expression, 48 cases (75%) with a poor nuclear immunoreactivity. No significant associations were found between immunohistochemical expressions of pAKT or p110α and clinical–pathological data including FIGO stage, tumour grading, patient age or tumour type. Ki-67 index, however, correlated with tumour grade (rs=0.445, p<0.001) and therapy success (rs=0.318, p=0.007). Direct correlations were found between 3q26.3 gain and p110α expression (rs=0.556, p=0.001). The expression data together with PIK3CA genomic modifications and their connection with clinical–pathological data are summarized in Table 2.

Survival analysis

The median survival time showed associations with PIK3CA amplification and enhanced Ki-67 index. Patients with high level PIK3CA amplification showed a reduced median survival compared to those harbouring moderate level and no amplification (1.29, 4.89 and 6.72 years, respectively). Similarly, patients displaying 60–85% Ki-67 positive cells had a reduced median survival than those with 15–59% and under 15% positive cells (2.72, 5.16 and 12.43 years, respectively). Inverse correlations were found

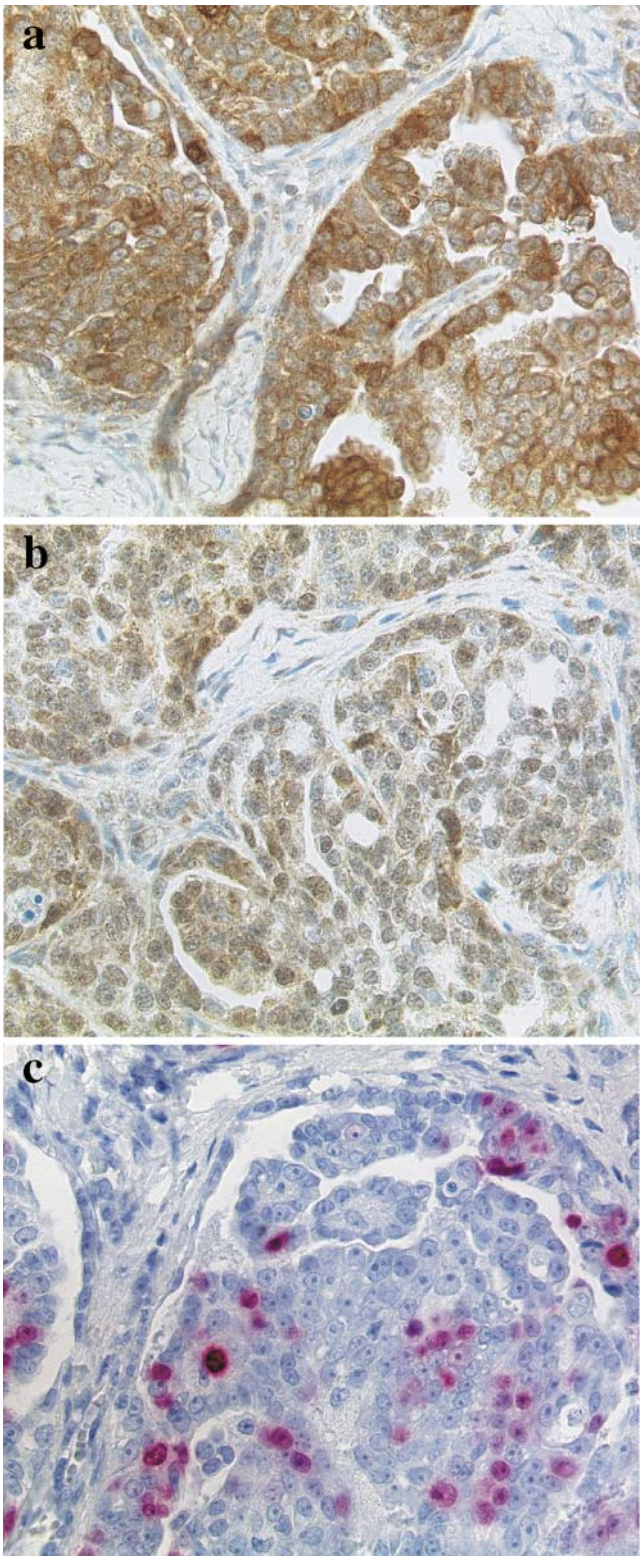

Fig. 3 **a** Strong expression of p110α protein (IRS 9); **b** the same case with pAKT staining showing a moderate nuclear signals (IRS 6) and a poor cytoplasmic staining (IRS 3); **c** corresponding Ki-67 positive cells (Ki-67 index: 21%). Original magnification ×20

Table 2 PIK3CA genomic modifications and expression data in connection with the clinical–pathological features

	Gain (FISH)		Amplification (qPCR)		p110 expression			pAKT expression (C)			pAKT expression (N)		Ki-67 expression		
	<2	≥2	<2	≥2	Poor	Moderate	Strong	Poor	Moderate	Strong	Poor	Moderate-to-strong	Poor	Moderate	Strong
Age															
<50	2	4	9	2	5	4	5	4	8	1	12	1	4	10	3
≥50	6	20	30	9	8	31	18	23	25	3	36	15	9	35	13
FIGO stage															
I	4	4	8	6	4	14	4	8	10	1	16	3	4	13	5
II	1	7	14	3	2	11	7	9	8	1	13	5	2	13	6
III–IV	3	13	17	2	7	10	12	10	15	2	19	8	7	19	5
Histological grading															
G1 and G2	3	9	17	3	8	12	8	12	12	2	18	8	10	19	2
G3	5	15	22	8	5	23	15	15	21	2	30	8	3	26	14
Tumour type															
Serous	5	13	22	3	8	17	11	15	18	1	25	9	10	21	8
Mucinous	1	1	3	2	2	4	2	3	2	2	5	2	2	5	1
Endometrioid	1	2	1	3	2	1	3	1	5	0	6	0	0	5	1
Clear cell	1	2	5	2	0	7	2	5	2	0	5	2	1	7	1
Undifferentiated	0	6	8	1	1	6	5	3	6	1	7	3	0	7	5
Number of cases analysed	32		50		71			64			64		74		

between disease-specific survival and PIK3CA amplification (p=0.0030), Ki-67 index (p=0.0049), FIGO stage (p=0.0015), residual tumour size (p<0.0001) and success of therapy (p<0.0001). The residual Kaplan–Meier analysis revealed PIK3CA amplification (p=0.0016) and Ki-67 index (p=0.0097) as strong predictors for an early tumour-associated death (Fig. 4). No significant associations were found between p110α or pAKT expression and disease-specific survival. However, by residual survival analysis, the nuclear expression of pAKT showed a tendency to associate to a better patient survival (p=0.0936). The results of the univariate and residual Kaplan–Meier analyses are summarised in Tables 3 and 4, respectively.

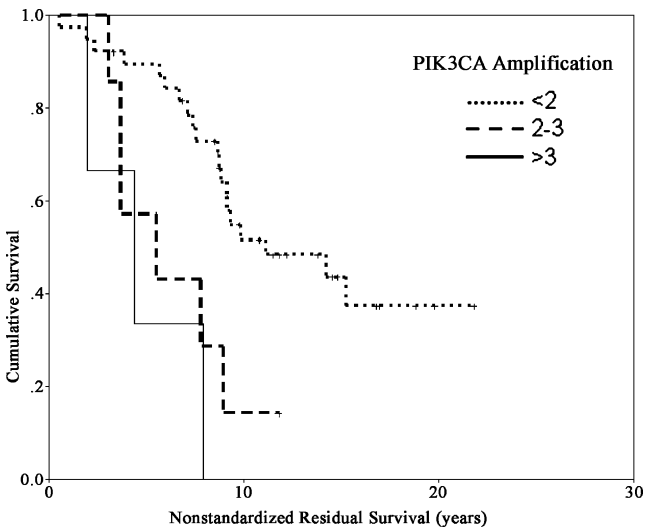

Fig. 4 Residual Kaplan–Meier analysis showing PIK3CA amplification as strong predictor for an early tumour-associated death

Discussion

PI3KCA was identified as an oncogene leading to increased PI3-kinase and protein kinase B (AKT) activity in ovarian cancer [26]. In this study, we investigated by FISH and/or qPCR the status of PIK3CA in 50 cases of ovarian carcinoma. To discriminate between an over-expression restricted to PIK3CA (amplification) and an over-expression due to polysomy of chromosome 3 (gain), we introduced a probe for the centromeric region of chromosome 3 in the FISH technique and TRAT1 as reference gene in the qPCR technique. Eleven out of 50 cases investigated by qPCR (22%) harboured amplifications. The FISH analysis detected amplifications in only 2 out of 32 analysed cases (6.2%). Discrepancies between qPCR and FISH methods were previously observed in a study assessing HER2/neu gene in osteosarcomas [12] and could be due to tissue heterogeneity and intra-tumoural clonal differences. On the other hand, more than 25% of FISH signals are lost in tissue sections because of artificial nuclear truncation [22]. Furthermore, it is possible that the

Table 3 Univariate Kaplan–Meier analysis of prognostic factors (disease-specific survival)

Variable	Log–rank statistic	*df*	*p* value
3q26.3 gain (FISH)	0.57	2	0.7505
PIK3CA aplification (qRTPCR)	11.63	2	**0.0030**
p110α expression	1.18	2	0.5550
pAKT expression (cytoplasmic)	0.50	2	0.7780
pAKT expression (nuclear)	0.80	1	0.3702
Ki-67 index	10.64	2	**0.0049**
Age (<50 vs >50 years)	1.62	1	0.2028
Histological type	9.38	4	0.0522
Tumour grading	2.64	2	0.2678
Tumor stage (FIGO)[a]	25.07	8	**0.0015**
Residual tumour size	32.29	2	**<0.0001**
Volume of ascites	3.56	2	0.1682
Success of therapy	64.43	3	**<0.0001**

Significant *p* values are in bold.
df: degrees of freedom.
[a] Extended FIGO stage including the following sub-categories: 1a, 1c, 2a, 2b, 2c, 3a, 3b, 3c, 4 (1b was represented only once and therefore excluded from the analysis).

FISH method is not able to recognise changes limited to very short regions, as the 3q26.3-YAC probe used in this study cover approximately 1,700 kilobases. In turn, the qPCR technique, amplifying a DNA fragment of only 92 bases, could be more sensitive for modifications restricted to PIK3CA and its proximate surroundings. In line with our results, a recent study employing qPCR detected PIK3CA amplifications in 24.6% of 182 screened ovarian cancers [3].

PIK3CA amplification assessed by qPCR correlated with the FISH results for 3q26.3 gain ($p=0.02$), suggesting that at least in some cases, PIK3CA is amplified as a result of genomic gains affecting the entire 3q26.3 locus. However, the PIK3CA amplification was significantly associated with a shorter disease-specific survival, whereas the 3q26.3 gain did not. This could be due to the limited number of cases assessed by FISH, but may also reflect that PIK3CA is selectively amplified in aggressive tumours. Under the multifactorial survival analysis implying established prognostic factors, PIK3CA amplification maintained its significant influence on patient survival. Moreover, all statistical evaluations revealed that PIK3CA amplification has a similar or even better prognostic significance as some established factors, such as FIGO stage or Ki-67 index. These findings emphasise the implication of PIK3CA as an oncogene with prognostic importance in ovarian carcinoma [2, 8, 25, 31]. Previous studies employing comparative genomic hybridization did not find 3q26.3 gain as a significant prognostic factor in ovarian cancer [4, 5, 7]. This could be due to the fact that, similarly to FISH, the CGH method is not sensitive for aberrations limited to small genomic segments. Therefore, qPCR method seems to be more appropriate when assessing genetic aberrations restricted to a single gene.

Table 4 Residual Kaplan–Meier analysis of prognostic factors (disease-specific survival)

Variable	Log–rank statistic	*df*	*p* value
3q26.3 gain (FISH)	2.20	2	0.3334
PIK3CA amplification (qRTPCR)	12.85	2	**0.0016**
p110α expression	0.90	2	0.6381
pAKT expression (cytoplasmatic)	0.13	2	0.9350
pAKT expression (nuclear)	2.81	1	0.0936
Ki-67 index	9.27	2	**0.0097**

Significant *p* values are in bold.
df: degrees of freedom.

To investigate the functional implication of PIK3CA gain, we evaluated immunohistochemically the expression of p110α and active AKT (pAKT). p110α correlated with gains at the 3q26.3 locus, but not with PIK3CA amplification or patient outcome. This could be due to transcriptional or post-transcriptional mechanisms, which finely tune the expression level of the catalytic sub-unit of PI3K. It is possible that p110α is only transiently over-expressed in tumour cells that exhibit PIK3CA amplification and as a consequence, difficult to detect by immunohistochemistry. Therefore, the gene status is likely to be more reliable than the protein expression for the prognosis. No relationship could be observed between the protein expression of p110α and pAKT nor between pAKT and clinicopathologic variables or disease outcome. According to previous findings [24], we found no association between pAKT and cell proliferation estimated by Ki-67. It is known that PI3K is able to promote cell survival via AKT-independent signalling pathways, such as those implicating the serum and glucocorticoid kinase (SGK) and the cytokine-independent survival kinase (CISK) [23]. Therefore, our results hint to multiple downstream PI3K-effectors, which cross talk in ovarian tumourigenesis [34].

Immunohistochemical analyses of pAKT showed a remarkable nuclear and mixed cytoplasmic–nuclear immunoreactivity. This observation is in line with similar findings in ovarian, breast and prostate cancers [9, 21, 32, 34]. In vitro studies showed that AKT is activated by membrane localisation and later translocated to the cytosol and nucleus [1, 16]. The function of the nuclear activated AKT is not clear. There is evidence that AKT determines the activation or inactivation of certain molecules in the nucleus, such as fatty acid synthase [32], transcriptional factors of the FOXO family [33], estrogen and androgen hormone receptors [3, 13], always leading to cell survival. However, in our study, the positive nuclear pAKT immunoreactivity in tumour cells showed a tendency of association with a rather improved survival. These results

are in line with previous findings in malignant melanomas [29] and may reflect the existence of inactivation/degradation mechanisms of AKT kinase after translocation into the nucleus, at least in certain tumour cells or tumour types. It is interesting to note that Wang et al. [34] observed a positive correlation between protein expression of pAKT and that of the phosphatase PTEN in ovarian carcinomas. The latter is the main inactivator of the PI3K/AKT survival pathway. Similar data were reported for breast cancer [21]. In this context, it is tempting to speculate that the translocation of active (phosphorylated) AKT into the nuclei does not only bring the kinase in contact to its specific nuclear substrates but is also required for a physiological spatial regulation, which finally leads to the inactivation of AKT by phosphatases.

In summary, the results of this study underline the prognostic significance of PIK3CA in ovarian carcinoma and argue against a simple linear model of PIK3CA gain/amplification followed by p110α over-expression leading to an activation of the PI3K/AKT signal cascade. The real-time quantitative PCR is a reliable method for investigating the PIK3CA amplification in archive material, which could evolve as a sensitive tool for the prognosis and treatment decision in ovarian carcinoma.

Acknowledgement This work was supported, in part of the FISH examinations, by the German Human Genome project grant no. 01KW99087.

References

1. Andjelković M, Alessi DR, Meier R, Fernandez A, Lamb NJC, Frech M, Cron P, Cohen P, Lucocq JM, Hemmings BA (1997) Role of translocation in the activation and function of protein kinase B. J Biol Chem 272:31515–31524
2. Arnold N, Hagele L, Walz L, Schempp W, Pfisterer J, Bauknecht T, Kiechle M (1996) Overrepresentation of 3q and 8q material and loss of 18q material are recurrent findings in advanced human ovarian cancer. Genes Chromosomes Cancer 16:46–54
3. Campbell IG, Russell SE, Choong DC, Montgomery KG, Ciavarella ML, Hooi CSF, Cristiano BE, Pearson RB, Phillips WA (2004) Mutation of the PIK3CA gene in ovarian and breast cancer. Cancer Res 64:7678–7681
4. Cheng KW, Lahad JP, Kuo WL, Lapuk A, Yamada K, Auersperg N, Liu J, Smith-McCune K, Lu KH, Fishman D, Gray JW, Mills GB (2004) The RAB25 small GTPase determines aggressiveness of ovarian and breast cancers. Nat Med 10:1251–1256
5. Diebold J (2001) Phenotype–genotype–correlation in ovarian neoplasia. Verh Dtsch Ges Pathol 85:153–160
6. Franke TF, Kaplan DR, Cantley LC (1997) PI3K: downstream AKTion blocks apoptosis. Cell 88:435–437
7. Hauptmann S, Denkert C, Koch I, Petersen S, Schluns K, Reles A, Dietel M, Petersen I (2002) Genetic alterations in epithelial ovarian tumors analyzed by comparative genomic hybridization. Hum Pathol 30:632–641
8. Iwabuchi H, Sakamoto M, Sakunaga H, Ma YY, Carcangiu ML, Pinkel D, Yang-Feng TL, Gray JW (1995) Genetic analysis of benign, low-grade, and high-grade ovarian tumors. Cancer Res 55:6172–6180
9. Kirkegaard T, Witton CJ, McGlynn LM, Tovey SM, Dunne B, Lyon A, Barlett JM (2005) AKT activation predicts outcome in breast cancer patients treated with tamoxifen. J Pathol 207:139–146
10. Lee KR, Tavassoli FA, Prat J, Dietel M, Gersell DJ, Karseladze AI, Hauptmann S, Rutgers J, Russell P, Buckley CH, Pisani P, Schwartz P, Goldgar DE, Silva E, Caduff R, Kubik-Huch RA (2003) Surface epithelial–stromal tumours. In: Fattaneh A, Devilee P (eds) World Health Organization and classification of tumours: pathology and genetics: tumours of the breast and female genital organs. IARC Press, Lyon, pp 113–197
11. Lee S, Choi EJ, Jin C, Kim DH (2005) Activation of PI3K/Akt pathway by PTEN reduction and PIK3CA mRNA amplification contributes to cisplatin resistance in an ovarian cancer cell line. Gynecol Oncol 97:26–34
12. Lee WI, Bacchni P, Bertoni F, Maeng YH, Park YK (2004) Quantitative assessment of HER2/neu expression by real-time PCR and fluorescent in situ hybridization analysis in low-grade osteosarcoma. Oncol Rep 12:125–128
13. Lin HK, Yeh S, Kang HY, Chang C (2001) Akt suppresses androgen-induced apoptosis by phosphorylating and inhibiting androgen receptor. Proc Natl Acad Sci USA 98:7200–7205
14. Luo J, Sobkiw CL, Logsdon NM, Watt JM, Signoretti S, O'Connell F, Shin E, Shim Y, Pao L, Neel BG, Depinho RA, Loda M, Cantley L (2005) Modulation of epithelial neoplasia and lymphoid hyperplasia in PTEN+/− mice by the p85 regulatory subunits of phosphoinositide 3-kinase. Proc Natl Acad Sci USA 19:10238–10243
15. Ma YY, Wei SJ, Lin YC, Lung JC, Chang TC, Whang-Peng JM, Liu JM, Yang DM, Yang WK, Shen CY (2000) PIK3CA as an oncogene in cervical cancer. Oncogene 19:2739–2744
16. Meier R, Alessi DR, Cron P, Andjelković M, Hemmings BA (1997) Mitogenic activation, phosphorylation, and nuclear translocation of protein kinase Bbeta. J Biol Chem 272:30491–30497
17. Munstedt K, Kovacic M, Zygmunt M, von Georgi R (2003) Impact of hemoglobin levels before and during chemotherapy on survival of patients with ovarian cancer. Int J Oncol 23:837–843
18. Munstedt K, Steen J, Knauf AG, Buch T, von Georgi R, Franke FE (2000) Steroid hormone receptors and long term survival in invasive ovarian cancer. Cancer 15:1783–1791
19. Munstedt K, von Georgi R, Franke FE (2004) Correlation between MIB1-determined tumour growth fraction and incidence of tumour recurrence in early ovarian carcinomas. Cancer Invest 22:185–194
20. Osaki M, Oshimura M, Ito H (2004) PI3K–Akt pathway: its functions and alterations in human cancer. Apoptosis 9:667–676
21. Panigrahi AR, Pinder SE, Chan SY, Paish EC, Robertson JF, Ellis IO (2004) The role of PTEN and its signalling pathways, including AKT, in breast cancer; an assessment of relationships with other prognostic factors and with outcome. J Pathol 4:93–100
22. Qian J, Bostwick DG, Takahashi S, Borell TJ, Brown JA, Lieber MM, Jenkins RB (1996) Comparison of fluorescence in situ hybridization analysis of isolated nuclei and routine histological sections from paraffin-embedded prostatic adenocarcinoma specimens. Am J Pathol 194:1193–1199
23. Scheid MP, Woodgett JR (2001) PKB/AKT: functional insights from genetic models. Nat Rev Mol Cell Biol 2:760–768
24. Schmitz KJ, Otterbach F, Callies R, Levkau B, Holscher M, Hoffmann O, Grabellus F, Kimming R, Schmidt KW, Baba HA (2004) Prognostic relevance of activated Akt kinase in node-negative breast cancer: a clinicopathological study of 99 cases. Mod Pathol 17:15–21

25. Sham JS, Tang TC, Fang Y, Sun L, Qin LX, Wu QL, Xie D, Guan XY (2002) Recurrent chromosome alterations in primary ovarian carcinoma in Chinese women. Cancer Genet Cytogenet 133:39–44
26. Shayesteh L, Lu Y, Kuo WL, Godfrey T, Collins C, Pinkel D, Powell B, Mills GB, Gray JW (1999) PIK3CA is implicated as an oncogene in ovarian cancer. Nat Genet 21:99–102
27. Shih IeM, Kurman R (2004) Ovarian tumourigenesis: a proposed model based on morphological and molecular genetic analysis. Am J Pathol 164:1511–1518
28. Singh B, Stoffel A, Gogineni S, Poluri A, Pfister DG, Shaha AR, Pathak A, Bosl G, Cordon-Cardo C, Shah JP, Rao PH (2002) Amplification of the 3q26.3 locus is associated with progression to invasive cancer and is a negative prognostic factor in head and neck squamous cell carcinomas. Am J Pathol 161:365–371
29. Slipicevic A, Holm R, Nguyen MT, Bohler PJ, Davidson B, Florenes VA (2005) Expression of activated Akt and PTEN in malignant melanomas: relationship with clinical outcome. Am J Clin Pathol 124:528–536
30. Sobin LH, Wittekind C (eds) (2002) TNM classification of malignant tumours, 6th edn. International Union Against Cancer, Wiley, New York
31. Suzuki S, Moore DH 2nd, Ginzinger DG, Godfrey TE, Barclay J, Powell B, Pinkel D, Zaloudek C, Lu K, Mills G, Berchuck A, Gray JW (2000) An approach to analysis of large-scale correlations between genome changes and clinical endpoints in ovarian cancer. Cancer Res 60:5382–5385
32. Van de Sande T, Roskams T, Lerut E, Joniau S, Van Poppel, Verhoeven G, Swinnen JV (2005) High-level expression of fatty acid synthase in human prostate cancer tissues is linked to activation and nuclear localization of Akt/PKB. J Pathol 206:214–219
33. Vogt PK, Jiang H, Aoki M (2005) Triple layer control: phosphorylation, acetylation and ubiquitination of FOXO proteins. Cell Cycle 4:908–913
34. Wang Y, Kristensen GB, Helland A, Nesland JM, Borresen-Dale AL, Holm R (2005) Protein expression and prognostic value of genes in the erb-b signaling pathway in advanced ovarian carcinomas. Am J Clin Pathol 124:392–401
35. Woenckhaus J, Steger K, Werner E, Fenic I, Gamerdinger U, Dreyer T, Stahl U (2002) Genomic gain of PIK3CA and increased expression of p110alpha are associated with progression of dysplasia into invasive squamous cell carcinoma. J Pathol 198:335–342

Virchows Arch (2007) 450:397–403
DOI 10.1007/s00428-007-0381-z

ORIGINAL ARTICLE

Expression of aberrant mucins in lobular carcinoma with histiocytoid feature of the breast

Satomi Kasashima · Atsuhiro Kawashima · Yoh Zen · Satoru Ozaki · Masako Kobayashi · Akihiko Tsujibata · Hiroshi Minato

Received: 31 October 2006 / Revised: 4 February 2007 / Accepted: 5 February 2007 / Published online: 28 February 2007
© Springer-Verlag 2007

Abstract The clinicopathological profiles of histiocytoid carcinoma of the breast have not been well examined because of their rarity and heterogenous groups of ductal and lobular origin. A large foamy or granular cytoplasm of histiocytoid carcinoma was characterized by abundant mucin, but the properties of mucin in histiocytoid carcinoma have also not been well investigated. We selected eight cases of histiocytoid features of invasive lobular carcinoma (HLC) and compared with 14 age- and tumor size-matched cases of classical invasive lobular carcinoma (CLC). Mucin profiles were significantly different between the two groups: a fair number of HLC cases were immunopositive for MUC2 and MUC5AC (75 and 50%, respectively); in contrast, almost all CLC cases showed both as negative. Both groups were immunopositive for MUC1 and negative for MUC4 and MUC6. The prognosis of HLC was significantly worse than CLC; HLC showed shorter disease-free time than CLC (p=0.0262). In particular, HLC with MUC2 and MUC5AC expressions showed significantly shorter disease-free time and survival time than lobular carcinoma without the expressions of MUC2 and MUC5AC (p=0.0055 and p=0.0060, respectively). Therefore, the expression of 'non-mammary mucins', such as MUC2 and MUC5AC in HLC, is characteristic and indicates the more malignant transformation of tumor cells and poorer prognosis.

Keywords Invasive lobular carcinoma · Histiocytoid feature · Mucin · Hormone receptor

S. Kasashima (✉) · Y. Zen · S. Ozaki · H. Minato
Pathology Section, Kanazawa University Hospital,
13-1 Takara-machi,
Kanazawa, Ishikawa 920-8641, Japan
e-mail: satokasa@med.kanazawa-u.ac.jp

Y. Zen
e-mail: yzen@med.kanazawa-u.ac.jp

S. Ozaki
e-mail: s-ozaki@med.kanazawa-u.ac.jp

H. Minato
e-mail: hminato@med.kanazawa-u.ac.jp

S. Kasashima · A. Kawashima
Pathology Section, Kanazawa Medical Center,
Kanazawa, Japan

A. Kawashima
e-mail: kawasima@kinbyou.hosp.go.jp

M. Kobayashi
Pathology Section, Kanazawa Municipal Hospital,
Kanazawa, Japan
e-mail: ayumu_masako@ybb.ne.jp

A. Tsujibata
Pathology Section, Komatsu Municipal Hospital,
Kanazawa, Japan
e-mail: tujibata@mtf.biglobe.ne.jp

Breast carcinoma with histiocytoid and/or myoblastomatoid features is rare [2, 3, 6, 7, 10, 11, 14–16, 18, 20, 21, 24–27, 37–40] and has been diagnosed by its characteristic morphology: large abundant granular and foamy cytoplasm and less atypical nuclei, regardless of its origin [16, 21]. The clinicopathological features of histiocytoid carcinoma have not been well clarified on account of its rarity and heterogeneity including ductal and lobular carcinomas. Several cases of histiocytoid ductal carcinoma are recognized as a variant of apocrine carcinoma due to the high expression of gross cystic disease fluid protein (GCDFP)-15 [6, 7, 21].

The histiocytoid features of invasive lobular carcinoma (HLC) are characterized by abundant mucin in the cytoplasm, but mucin profiles have not been well examined [6,

16, 37]. Mucins are a large family of glycoproteins expressing various epithelial cell types and malignant counterparts, and a number of core mucins (MUC1-9, MUC11-13, and MUC15-17) have been identified and categorized into membranous associated mucins (MUC1, MUC3, MUC4, MUC12, and MUC17), gel-forming mucins (MUC2, MUC5AC, MUC5B, and MUC6), and a soluble mucin (MUC17) [19, 32]. Mucin profiles of adenocarcinoma have been related to etiology, histologic characteristics, tumor progression, and prognosis [19, 32]. The abnormal expression of 'non-mammary mucins' (MUC2, MUC5, MUC6) in breast carcinoma has been also reported to be a potential prognostic indicator [28, 35, 42]. In addition, MUC4 expression in tumor cells may be a poorer progenitor factor because MUC4 has been reported to act as an intramembrane ligand for thyrosine kinase c-erbB-2 (Her2/neu), altering tumor growth [8].

In this study, we investigated mucin profiles of HLC and CLC by immunohistochemistry of MUC1, MUC2, MUC4, MUC5AC, and MUC6 and also examined differences between HLC and CLC in the immunoreactivity of GCDFP-15, estrogen receptor (ER), progesterone receptor (PgR), androgen receptor (AR), Her2/neu, and cyclin D1.

Materials and methods

From the surgical pathology files of our hospitals, from 1990 to 2005, 1,585 consecutive cases of breast carcinoma were reviewed to select invasive lobular carcinomas. Hematoxylin and eosin stained slides made from each tumor block (average four slides per each tumor) were reviewed, all invasive lobular carcinoma cases exhibited diffuse or multifocal infiltration or dissociated cells with admixture in a single file linear pattern and targetoid or solid cell nests. There was no tubular formation. The diagnosis of lobular carcinoma was confirmed by negative immunostaining for E-cadherin (clone HECD-1, 1:100, Takara, Ootsu, Japan) [31]. We selected eight cases of HLC satisfying the diagnostic criteria of HLC described by previous reports [16, 24, 38–40]: most tumor cells (at least 90%) had a granular to foamy large cytoplasm with vacuoles and an occasional intracytoplasmic lumina and small, round to oval nuclei, fine chromatin, and inconspicuous nucleoli (Fig. 1). As age- and tumor size-matched controls, we selected 14 cases of CLC.

Immunohistochemical staining was done on formalin-fixed, paraffin-embedded, serial 4-μm thick sections mounted on precoated slides by an immunoperoxidase method using the avidin–biotin complex. Primary antibodies included E-cadherin, MUC1 (clone DF3, 1:100, Toray Fuji Bionics, Tokyo, Japan), MUC2 (clone Ccp58, 1:100, Novocastra Laboratories, Newcastle, UK), MUC4

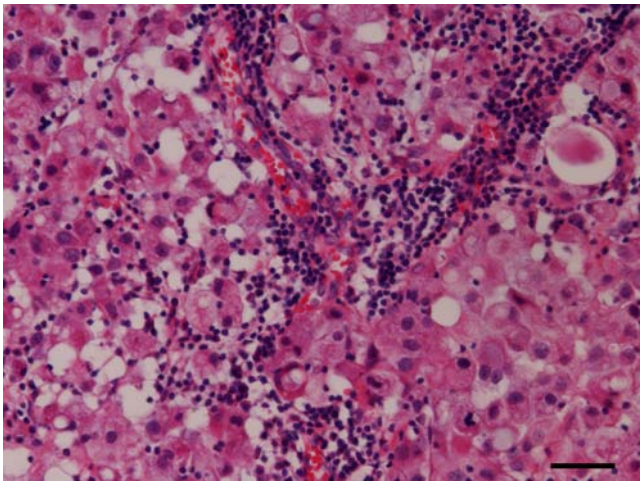

Fig. 1 Histological findings of HLC. Tumor cells show abundant cytoplasm with intracellular mucin accumulation and small round nuclei, with moderate infiltration of lymphocytes (Case 1; hematoxylin and eosin staining; *scale bar* = 100 μm)

(clone 1G8, 1:50, Zymed, South San Francisco, USA), MUC5AC (clone CLH2, 1:100, Novocastra), MUC6 (clone CLH5, 1:50, Novocastra), GCDFP-15 (clone D6, 1:80, Signet Laboratories, Massachusetts, USA), ER (clone 1D5, 1:100, DAKO, Glostrup, Denmark), PgR (clone PgR636, 1:100, DAKO), AR (clone AR411, 1:100, DAKO), Her2/neu (K5205, 1:100, DAKO), and Cyclin D1 (clone DCS-6, 1:20, Novocastra). Antigen retrieval for MUC2 and MUC5AC was carried out by microwave treatment in sodium citrate buffer (pH 6.0) for 20 min, for MUC4 by heating for 20 min at 80°C in sodium citrate buffer (pH 8.0), and for ER, PgR, AR, and cyclin D1 by pressure cooking in EDTA buffer (pH 6.0) for 5 min. The staining procedure was carried out using a Ventana standardized automated system (Ventana Medical Systems, Tucson, AZ) according to the manufacturer's protocols. For MUC1, MUC2, MUC4, MUC5AC, and MUC6, we considered more than 5% of tumor cell staining as positive [9, 34, 35]. For GCDFP-15, ER, PgR, AR, and cyclin D1, we considered 10% or more labeling as positive, similar to the standardized criteria using hormone receptors [36]. Her2/neu scoring was done according to the manufacturer's guidelines (from 0 to 3+). Her2/neu scores of 2+ and 3+ were regarded as strongly positive.

Fischer's exact probability test was utilized to compare each group using the parameters of the positive rate of immunohistochemical status and the frequency of lymph node metastasis. Moreover, we analyzed the association of each group with survival using the Kaplan–Meier plot and log rank test (mental-Cox) and also Breslow–Gehan–Wilcoxon for all parameters. For all calculations, the StatView 5.0 Macintosh program (SAS Institute, Cary, NC, USA) was used. A p value less than 0.05 was considered significant.

Table 1 Clinical and pathological findings of histiocytoid feature of invasive lobular carcinoma

Case	Age (years)	Stage	Size (mm)	LN	Treatment	Follow-up	LCIS	Fibrosis	Lymphocyte infiltration	Lymphatic invasion	Vascular invasion
1	62	IIB	44	11/11	RM-AD, ChT/HT/RT	12 mo LR, 25 mo DOD	+	+	++	++	+
2	66	IIB	35	5/7	RM-AD	2 mo LR, 36 mo DOD	+	−	+	++	−
3	50	IIB	30	39/39	RM-AD, ChT/HT/RT	24 mo LR, DM, 37 mo DOD	+	+	+	+++	−
4	88	IIIA	75	4/5	RM-AD, HT	75 mo NED	−	−	++	++	+
5	62	IIB	22	–	RM-AD	Lost	−	+	+++	+	−
6	62	IIIA	50	0/7	RM-AD, ChT/HT/RT	16 mo LR, 48 mo AWD	+	+	+++	++	−
7	54	IIIA	30	1/13	RM-AD, ChT/HT/RT	6 mo NED	−	+	+	+++	+
8	42	IIIA	35	1/4	RM-AD, ChT/HT/RT	108 mo NED	−	++	+++	+	+

LN Lymph node metastasis; *LCIS* lobular carcinoma in situ; *RM-AD* radical mastectomy and axillary lymph nodes dissection; *ChT* chemotherapy; *HT* hormone therapy; *RT* radiation therapy; *mo* months; *NED* no evidence of disease; *AWD* alive with disease; *DOD* death on disease; *LR* local recurrence; *DM* distant metastasis; (*minus sign*) no evidence; (*single plus sign*) mild; (*double plus sign*) moderate; (*triple plus sign*) severe.

Results

The clinicopathological features of HLC are summarized in Table 1. The mean age of HLC and CLC patients was 60.8 years (range 42–88 years) and 62.0 years (range 43–80 years), respectively. Median tumor size was 42-mm diameter in HLC (range 22–75 mm) and 44 mm in CLC (range 20–90 mm), respectively. All patients underwent radical or modified mastectomy with dissection of axillary lymph nodes. Five HLC patients received a combination of adjuvant chemotherapy, radiation, and hormone therapy, and three CLC patients received chemotherapy. Lymph node metastasis was observed in six HLC cases (85.7%) and four CLC cases (28.6%), respectively. In particular, in four HLC cases (Cases 1–4; 57.1%), massive lymph node metastasis was seen but not in CLC cases. Despite the higher incidence of lymph node involvement in HLC, the differences between the two groups were not statistically significant ($p=0.635$) because of the small number of cases.

Using follow-up data on seven HLC cases and all CLC patients with a mean interval of 49 months, local recurrence and/or distant metastasis occurred in four HLC patients (Cases 1–3, 6; 57.1%) within 13.5 months and in only one CLC patient (7.1%) after 18 months. The disease-free time of HLC was significantly worse than that of CLC ($p=0.0262$). For all survival times, three HLC patients (Cases 1–3; 42.9%) died with average follow-up periods of 32.7 months. Only one CLC patient (7.1%) died at 28 months. The survival time of HLC was shorter than that of CLC but was not significantly different ($p=0.1047$).

Histologically, considerable lymphocytic infiltration was seen in five HLC cases (62.5%) and in one CLC case (7.1%). Two HLC cases contained signet-ring cells in approximately 10% of tumor cells. Moderate to severe lymphatic invasion was often observed in HLC, whereas only mild lymphatic invasion was seen in five cases of CLC (35%).

The immunohistochemical findings of HLC are summarized in Table 2. MUC1 immunoreactivity was present in both groups. MUC1 of carcinoma cells was stronger than that of normal epithelium. The pattern of staining was heterogeneous, and most carcinoma cells showed MUC1 expression in the cytoplasm and cell membrane (Fig. 2a). Both groups were negative for MUC4 and MUC6. We detected MUC2 reactivity in six HLC cases (Cases 1–5, 8; 75%). Only one CLC case (7.1%) was weakly positive for MUC2. MUC5AC was immunostained in four HLC cases (Cases 1–4) but not in any case of CLC. The expression

Table 2 Immunohistochemical findings of histiocytoid feature of invasive lobular carcinoma

Case	MUC1	MUC2	MUC4	MUC5AC	MUC6	ER	PgR	AR	GCDFP-15	Her2/neu	Cyclin D1
1	+++	++	−	+	−	−	−	−	+++	−	−
2	+++	++	−	++	−	−	−	++ weak	+++	+	−
3	+++	++	−	+++	−	−	−	−	+++	++	−
4	+++	+	−	+	−	−	−	−	+++	−	−
5	+++	+	−	−	−	−	−	−	+++	−	+
6	+++	−	−	−	−	−	−	−	+++	+	−
7	+++	−	−	−	−	+	−	−	+++	++	−
8	+++	+	−	−	−	+++	+++	++	++	−	+

ER Estrogen receptor; *PgR* progesterone receptor; *AR* androgen receptor; *GCDFP* gross cystic disease fluid protein; (*minus sign*) 0%; (*single plus sign*) 1–9%; (*double plus sign*) 10–50%; (*triple plus sign*) 51–100%

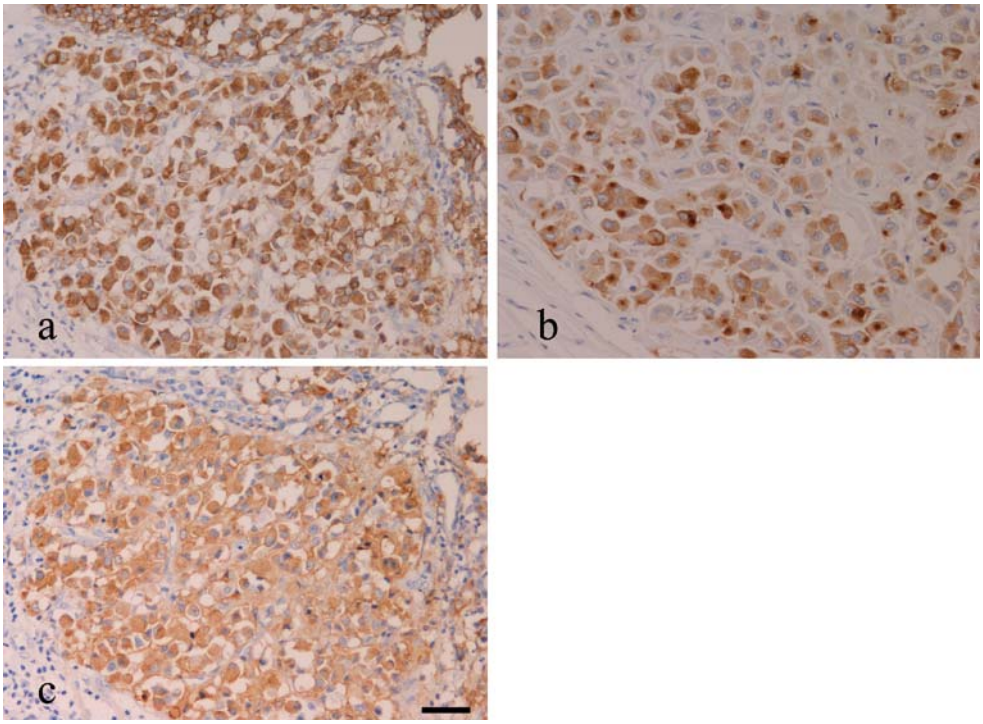

Fig. 2 Immunohistochemical findings of mucin of HLC. **a** Tumor cells are diffusely and strongly positive for MUC1 in the membrane and entire cytoplasm in HLC (Case 3). **b** About 20% of all tumor cells in HLC are immunopositive for MUC2 (Case 1). **c** Tumor cells in HLC express MUC5AC diffusely in the cytoplasm (Case 3; *scale bar* = 100 μm)

rates of MUC2 and MUC5AC in HLC were significantly higher than those in CLC (p=0.0023 and p=0.0096, respectively). Immunopositivity for MUC2 and MUC5AC was observed in vacuoles of cytoplasm or diffusely in the cytoplasm and, in several cases, in the cell membrane (Fig. 2b and c). The positive rate for MUC2 and MUC5AC varied by case (5–50% of total tumor cells) and one HLC case (Case 3) in which about half of all carcinoma cells were strongly positive for MUC5AC. Co-expression of MUC2 and MUC5AC was seen in the same cases of HLC (Cases 1–4). The disease-free time and survival time of HLC patients with MUC2 expression were significantly shorter than those with invasive lobular carcinomas without MUC2 expression (p=0.0357 and p=0.0300, respectively). Similarly, HLC patients with MUC5 expression showed significantly worse disease-free time and survival time than those with invasive lobular carcinomas without MUC5 expression (p=0.0055 and p=0.0060, respectively).

All HLC expressed GCDFP-15. HLC showed a low positive rate of ER, PgR, AR, and cyclin D1 (12.5, 12.5, 25, and 0%, respectively). On the other hand, most CLC frequently expressed ER, PgR, AR, and cyclin D1 (63.4, 50, 50, and 71.3%, respectively) but frequently lacked GCDFP-15 (7.2%). Seven of nine AR-positive CLC cases (77.8%) showed the co-expression of ER and PgR. There were significant differences between HLC and CLC in the positive rates of ER, cyclin D1, and GCDFP-15 (p=0.031, p=0.017, and p<0.001, respectively); CLC had a higher number of positive cases of PgR and AR, but this was not statistically significant (p=0.1673 and p=0.1827, respectively). We found no significant differences in the expression rate of Her2/neu between two groups.

Discussion

Histiocytoid or myoblastomotoid carcinoma is an uncommon variant of breast carcinoma, and only about 50 cases have been reported in the English literature [2, 3, 6, 7, 10, 11, 14–16, 18, 20, 21, 24–27, 37–40]. Histiocytoid or myoblastomotoid carcinoma is characterized by the tumor cells resembling reactive histiocytes with bland uniform appearance, abundant foamy to granular cytoplasm, and small, round to ovoid inactive-looking nuclei. In addition, histiocytoid cytological features were emphasized by the diffuse infiltration of inflammatory cells and/or fibrous stroma in several previous cases [21, 24, 26, 38] and in our cases. Since Hood et al. [24] first described this tumor in 1973 and used the term 'histiocytoid carcinoma' for a tumor mainly composed of histiocyte-like cells, histiocytoid carcinomas have been reported for a mixture of ductal and lobular carcinomas [16, 21, 24, 39]; however, several authors consider a number of cases of histiocytoid carcinoma as being of lobular origin because of the lack of E-cadherin expression, in addition to infiltrating in single file or a targetoid pattern and the coexistence of in situ lobular carcinoma component [2, 11, 14, 18, 26, 38, 40].

In addition, other variants have been reported as invasive lobular carcinoma: a solid variant and alveolar variant, which are classified according to their histological growth

pattern, pleomorphic lobular carcinoma (PLC), according to cytomorphological features and mixed variant [17]. HLC can overlap other variants of lobular carcinoma. Our HLC cases are often arranged in irregularly shaped solid nests and resemble the solid variant of invasive lobular carcinoma. A few reports previously described that HLC is a lobular carcinoma showing solid or medullary growth patterns [20, 26]. Others described HLC as PLC with apocrine metaplasia [16, 37]. PLC has been recognized as a distinct variant of lobular carcinoma and is characterized by significantly worse prognosis defined as striking nuclear anaplasia and frequent mitoses, showing BR nuclear Grade 3 [4, 5, 15, 41]. According to cytomorphological classification, HLC would be a non-CLC subgroup, which often means PLC in the broad sense [4, 17]; however, HLC nuclei are uniform, relatively small, and with low atypia, showing BR nuclear Grade 1 or 2; therefore, usually it is easy to distinguish HLC from PLC [16]. In this study, we noticed the lobular carcinoma characterized by abundant foamy cytoplasm with an accumulation of mucin and selected this subtype as HLC.

The prognosis of histiocytoid carcinoma is still controversial, several prior reports indicated that histiocytoid carcinoma has a relatively unfavorable prognosis, that is, lymph node metastases [3, 14, 21, 39] and remote metastases [2, 11, 14, 24, 38, 40]. Moreover, the clinical course of HLC remains unclear due to no sequential studies of HLC [3, 20, 21, 27], except Eusebi et al. [16] who explained that a number of HLC cases were not particularly aggressive behavior. Recently, several reports of HLC showed excellent prognosis, with no lymph node metastasis and no recurrence during a follow-up period of 6–61 months, probably because these cases were of rather small tumor size (12 to 30 mm maximum diameter) and early stage (stage I) [3, 20, 26, 37]. In this study, in comparison with age- and tumor size-matched CLC cases, HLC patients exhibited more frequent lymph node metastasis, shorter relapse-free survival, and a higher mortality rate despite adequate radiotherapy and chemotherapy. These differences were nearly insignificant statistically. Similar to other variants of lobular carcinoma [12], in particular PLC [4, 15, 41], we indicated that HLC also has a poorer outcome than CLC. Indeed, more serial studies still need to be carried out to assess the detail of survival of HLC, due to the small number of cases of this report.

In the first reported cases of histiocytoid carcinoma by Hood et al. [24], mucin production was detected in the vacuoles by Alcian blue and mucicarmine stains, and these tumors were designated as mucus-secreting histiocytoid carcinomas; however, to date, little is known about the characteristics of mucin in HLC [6, 16, 37]. MUC2 is the major secretory glycoprotein in normal tissue and is largely observed in intestinal goblet cells and airway surface epithelia [23] but not in normal mammary tissue [1]. In contrast to the absence of MUC2 in CLC cases, one of our novel findings was the high percentage (75%) of MUC2 expression in HLC. In previous reports, only a few cases (6–8%) of breast carcinoma showed MUC2 expression, except for frequent MUC2 expression in mucinous carcinoma [28, 34, 35, 42]. The intracytoplasmic presence of MUC2 in HLC is different from mucinous carcinoma, in which MUC2 is positive in the abundant mucous lake. Generally, MUC5AC is found mainly in the mucosal layer of the cardia, fundus of the stomach [23], and is not detected in normal breast tissues [28, 34, 35]. MUC5AC expression has been reported in a few cases of mucinous carcinoma; however, little is known about other types of breast carcinoma [1, 34]. In this study, we demonstrated the presence of MUC5AC in about half of all HLC cases. Therefore, the expression of MUC2 and MUC5AC in HLC is characteristic because no association has been found between the expression of different mucins and breast tumor types, apart from MUC2 and MUC6 expression in mucinous carcinoma [1, 28, 35]. Recently, signet-ring cell carcinoma of the breast, which contains mucin as intracytoplasmic vacuoles [29], was described as having no expression of MUC2 and MUC5AC [9], probably according to relatively less accumulation of mucin. In invasive breast carcinoma, except for mucinous carcinoma, MUC2 and MUC5AC expression was considered to have pathological or ectopic secretion, associated with aggressive tumor behavior, similar to frequent lymph node metastasis [35, 42]. Similarly, in our study, the patients with MUC2 and/or MUC5AC expression had a significantly worse outcome than those with invasive lobular carcinoma without MUC2 and/or MUC5AC. The ectopic expression of MUC5AC in conjunction with MUC2 in the same HLC cases demonstrates a dedifferentiated nature. Therefore, we suggested that the expression of ‘non-mammary mucins’, such as MUC2 and MUC5AC in HLC, indicates the more malignant transformation of tumor cells and leads to poor prognosis. Indeed, more work needs to be carried out to determine the association of these mucins in invasive lobular carcinoma.

MUC1 is present in the apical membrane of most epithelial tissues, especially in normal mammary tissue [1, 23, 34]. Many studies have shown the overexpression of MUC1 in most breast carcinomas, but these have been investigated in mainly ductal carcinomas [34, 35, 38, 42]. In this study, frequent MUC1 expression was also detected in both groups of lobular carcinoma. MUC4 is a membrane mucin expressed in the protective layer of the breast epithelium [8]. MUC4 and c-erbB-2 (Her2/neu) mediate intracellular signaling pathways that are linked to the repression of apoptosis and either to the proliferation or differentiation of tumor cells [8]; therefore, previous studies

have suggested that MUC4 may have a prognostic value in breast and other carcinomas [8]. However, we did not detect any expression of MUC4 in both groups of CLC and HLC and no relationship with the prognosis. In contrast to the high expression rate (95%) of MUC4 in invasive ductal carcinoma in a previous report [35], lack of MUC4 in invasive lobular carcinoma may be characteristic and is in agreement with the low expression of Her2/neu in invasive lobular carcinoma [4]. The different expression pattern of MUC1 and MUC4 suggest the possibility of different signaling functions of membrane mucins. MUC6 is located in the gastric pyloric glands and key proteins for producing mucin, likely MUC2 and MUC5AC [23]. We detected a lack of MUC6 in CLC and HLC, while MUC6 has been previously observed in about 15–20% of invasive ductal carcinoma and 70% of mucinous breast carcinoma [28, 35].

The high immunopositivity of GCDFP-15 in HLC has often been described [3, 16, 20, 21, 27, 37], but it has been rarely detected in CLC [5, 15, 30]. Quite a high percentage of ER and PgR expression in CLC has been shown [36], but in HLC, ER or PgR expression has often been lacking [3, 20, 37, 38]. Our results agreed with these findings. These profiles of immunoreactivity in HLC also resembled PLC; that is, most PLC reports showed a frequent expression of GCDFP-15 and lack of ER and PgR expression [5, 15, 31]. Recently, Riva et al. [36] reported frequent AR expression, as well as ER and PgR, in CLC. Similarly, in the present report, many cases (64%) of CLC were also positive for AR, coexistent with ER and PR. Antithetically, in HLC, we observed a low positive rate (25%) of AR, although previous reports of HLC did not examine AR expression, except Augros et al. [3] who described three HLC cases with AR expression in more than 70% of tumor cells. Although AR reactivity in HLC is still controversial, we demonstrated that the lack of sex steroid hormone receptors in HLC is also one of the characteristics and is different from CLC and ductal GCDFP-15-positive carcinomas such as apocrine carcinomas [22]. The majority of CLC is reported to overexpress cyclin D1 protein [13, 33]. The association of the overexpression of cyclin D1 and ER positivity was described in several studies of breast carcinoma [13, 33], which was in agreement with the frequent immunoreactivity of cyclin D1 and ER in CLC in this report. None of our HLC cases showed cyclin D1.

In conclusion, HLC is characterized by the frequent expression of abnormal mucin of MUC2 and MUC5AC. We consider that the lack of all hormone receptors (ER, PgR, AR) and cyclin D1 and clinically unfavorable prognosis in HLC are also characteristic and distinct from CLC. In addition, the aberrant and unique expression of non-mammary mucin, such as MUC2 and MUC 5AC, in HLC would indicate a worse prognosis.

References

1. Adsay NV, Merati K, Nassar H, Shia J, Sarkar F, Pierson CR, Cheng JD, Visscher DW, Hruban RH, Klimstra DS (2003) Pathogenesis of colloid (mucinous) carcinoma of exocrine organs: coupling of gel-forming mucin (MUC2) production with altered cell polarity and abnormal cell stroma interaction may be the key factor in morphogenesis and indolent behavior of colloid carcinoma in the breast and pancreas. Am J Surg Pathol 27:571–578
2. Allenby PA, Chowdhury LN (1986) Histiocytic appearance of metastatic lobular breast carcinoma. Arch Pathol Lab Med 110:759–760
3. Augros M, Buenerd A, Devouassoux-Shisheboran M, Berger G (2004) Infiltrating lobular carcinoma of the breast with histiocytoid features: three cases. Ann Pathol 24:259–263
4. Bane AL, Tjan S, Parkes RK, Andrulis I, O'Malley FP (2005) Invasive lobular carcinoma: to grade or not to grade. Mod Path 18:621–628
5. Bentz JS, Yassa N, Clayton F (1998) Pleomorphic lobular carcinoma of the breast: clinicopathologic features of 12 cases. Mod Path 11:814–822
6. Camesselle-Teijeiro J, Alfonsin-Barreiro N, Allegue F, Caeiro M (1997) Apocrine carcinoma with signet ring cells and histiocytoid features. A potentially confusing axillary tumor. Pathol Res Pract 193:713–720
7. Cangiarella J, Mazzei EO, Weg N, Limaya A, Waisman J (2003) Aspiration biopsy in a case of apocrine adenocarcinoma with foam cells. Diagn Cytopathol 26:320–323
8. Carraway KL, Price-Schiavi SA, Komatsu M, Jepson S, Perez A, Carraway CAC (2001) MUC4/Sialomucin complex in the mammary gland and breast cancer. J Mammary Gland Biol Neoplasia 6:323–337
9. Chu PG, Weiss LM (2004) Immunohistochemical characterization of signet-ring cell carcinoma of the stomach, breast and colon. Am J Clin Pathol 121:884–892
10. Cohen H, Szvalb S, Bickel A, Maly B, Munichor M (1997) Myoblastomatoid carcinoma of the breast. Diagn Cytopathol 16:145–148
11. Dabski K, Mikgrom H, Stoll HL Jr (1985) Breast carcinoma metastatic to eyelids: case report and review of the literature. J Surg Oncol 29:233–236
12. DiCostanzo D, Rosen PP, Gareen I, Franklin S, Lesser M (1990) Prognosis in infiltrating lobular carcinoma. An analysis of classical and variant tumors. Am J Surg Pathol 14(1):12–23
13. van Diest PJ, Michalides RJAM, Jannink I, van der Valk P, Peterse HL, de Jong JS, Meijer CJLM, Baak JPA (1997) Cyclin D1 expression in invasive breast cancer. Am J Pathol 150:705–771
14. Eisenberg BL, Bagnall JW, Harding CT III (1986) Histiocytoid carcinoma: a variant of breast carcinoma. J Surg Oncol 31:271–274
15. Eusebi V, Betts C, Haagensen DE, Gugliotta P, Bussolati G, Azzopardi JG (1984) Apocrine differentiation in lobular carcinoma of the breast. A morphologic, immunologic, and ultrastructural study. Hum Pathol 15:134–140
16. Eusebi V, Foschini MP, Bussolati G, Rosen PP (1995) Myoblastomatoid (histiocytoid) carcinoma of the breast. A type of apocrine carcinoma. Am J Surg Pathol 19:553–562
17. Fechner RE (1975) Histologic variants of infiltrating lobular carcinoma of the breast. Hum Pathol 6(3):373–378
18. Filotico M, Trabucco M, Gallone D, Buonsanto A, Senatore S (1983) Histiocytoid carcinoma of the breast. A problem of differential diagnosis of the pathologist. Report of a case. Pathologica 75:429–433
19. Fowler J, Vinall L, Swallow D (2001) Polymorphism of the human muc genes. Front Biosci 6:D1207–D1215

20. Fujiwara M, Horiguchi M, Mori S, Yokoyama K, Horiguchi H, Fukuzawa M, Fujiwara H, Yano Y, Satoh H, Kamma H (2005) Histiocytoid breast carcinoma: solid variant of invasive lobular carcinoma with decrease expression of both E-cadherin and Vd44 epithelial variant. Pathol Int 55:353–359
21. Gupta D, Croitoru CM, Ayala AG, Sahin AA, Middlelton LP (2002) E-cadherin immunohistochemical analysis of histiocytoid carcinoma of the breast. Ann Diagn Pathol 6:141–147
22. Hall RE, Clements JA, Birrell SN, Tilley WD (1998) Prostate-specific antigen and gross cystic disease fluid protein-15 are co-expressed in androgen receptor-positive breast tumors. Br J Cancer 78(3):360–365
23. Ho SB, Niehans GA, Lyftogt C, Yan PS, Cherwitz DL, Gum ET, Dahiya R, Kim YS (1993) Heterogeneity of mucin gene expression in normal and neoplastic tissues. Cancer Res 53:641–651
24. Hood CI, Front RL, Zimmerman LE (1973) Metastatic mammary carcinoma in the eyelid with histiocytoid appearance. Cancer 31:793–800
25. Jakobiec FA, Austin P, Iwamoto T, Trokel SL, Marquardt MD, Harrison W (1983) Primary infiltrating signet ring carcinoma of the eyelids. Opthalmology 90:291–299
26. Kitamura H, Shimizu S, Matsukawa H, Arita E (1996) Histiocytoid breast carcinoma: a case report with immunohistochemical and ultrastructural studies. Breast Cancer 3:57–63
27. Kostopoulos I, Barbanis S, Mylona E, Papadopoulos S, Papadimitriou C (2003) Histiocytoid breast carcinoma. A case report of an uncommon histologic variant of lobular carcinoma. Ann Pathol 23:249–252
28. Matsukita S, Nomoto M, Kitajima S, Tanaka S, Goto M, Irimura T, Kim YS, Sato E, Yonezawa S (2003) Expression of mucins (MUC1, MUC2, MUC5AC and MUC6) in mucinous carcinoma of the breast: comparison with invasive ductal carcinoma. Histopathology 42:26–36
29. Merino M, Livolsi V (1981) Signet-ring cell carcinoma of the female breast. A clinicopathologic analysis of 24 cases. Cancer 48:1830–1837
30. Middleton LP, Palacios DM, Bryant BR, Krebs P, Otis CN, Merino MJ (2000) Pleomorphic lobular carcinoma: morphology, immunohistochemistry, and molecular analysis. Am J Surg Pathol 24(12):1650–1656
31. Moll R, Mitze M, Frixen UH, Birchmeier W (1993) Differential loss of E-cadherin expression in infiltrating ductal and lobular breast carcinomas. Am J Pathol 143:1731–1742
32. Moniaux N, Escande F, Porchet N, Aubert JP, Batra SK (2001) Structural organization and classifications of the human mucin genes. Front Biosi 6:D1192–D1206
33. Oyama T, Kashiwabara K, Yoshimoto K, Arnold A, Koerner F (1998) Frequent overexpression of the cyclin D1 oncogene in invasive lobular carcinoma of the breast. Cancer Res 58:2876–2880
34. Pereira MB, Dias AJ, Reis CA, Schmitt FC (2001) Immunohistochemical study of the expression of MUC5AC and MUC6 in breast carcinomas and adjacent breast tissues. J Clin Pathol 54:210–213
35. Rakha WA, Boyce RWG, El-Rehim DA, Kurien T, Green AR, Paish EC, Robertson JFR, Ellis IO (2005) Expression of mucins (MUC1, MUC2, MUC3, MUC4, MUC5AC and MUC6) and their prognostic significance in human breast cancer. Mod Path 1–10
36. Riva C, Dainese E, Caprara G, Rocca PC, Massarelli G, Tot T, Capella C, Eusebi V (2005) Immunohistochemical study of androgen receptors in breast carcinoma. Evidence of their frequent expression in lobular carcinoma. Virchows Arch 447(4):695–700
37. Shimizu S, Kitamura H, Nakamura T, Fujisawa J, Matsukawa H (1998) Histiocytoid breast carcinoma: histological, immunohistochemical, ultrastructural, cytological and clinicopathological study. Pathol Int 48:549–556
38. Senatore S, Trabucco M, Gallone D, Filotico M (1986) Metastatic histiocytoid carcinoma of the breast. Pathologica 78:71–78
39. Stefanszyn MA, DeVita EG, Flanagan JC (1987) Breast carcinoma. Metastatic to the orbit. Ophthalmic Plastic Reconstr Surg 3:43–47
40. Walford N, Velden JT (1989) Histiocytoid breast carcinoma: an apocrine variant of lobular carcinoma. Histopathology 14:515–522
41. Weidner N, Semple JP (1992) Pleomorphic variant of invasive lobular carcinoma of the breast. Hum Pathol 23:1167–1171
42. Xu Y, Kimura N, Yoshida R, Lin H, Yoshinaga K (2001) Immunohistochemical study of MUC1, MUC2 and human gastric mucin in breast carcinoma: relationship with prognostic factors. Oncol Rep 8:1177–1182

Virchows Arch (2007) 450:405–410
DOI 10.1007/s00428-007-0382-y

ORIGINAL ARTICLE

Liver histology in patients with sporadic acute hepatitis E: a study of 11 patients from South-West France

Jean-Marie Peron · Marie Danjoux · Nassim Kamar · Réda Missoury · Hélène Poirson · Jean-Pierre Vinel · Jean-Michel Mansuy · Christophe Bureau · Jacques Izopet · Pierre Brousset · Janick Selves

Received: 13 October 2006 / Revised: 19 January 2007 / Accepted: 29 January 2007 / Published online: 28 February 2007
© Springer-Verlag 2007

Abstract Hepatitis E virus is a ribonucleic acid (RNA) enterically transmitted virus that causes both epidemics and sporadic cases of acute hepatitis E in many countries of Asia and Africa. Domestically acquired (non-travel-associated) hepatitis E has been reported recently in many industrialized countries including the USA, Europe, and Japan. There is little information available on liver histology in these patients. We report a series of 11 patients with sporadic acute hepatitis E and needle liver histology in South-West France. Hepatitis E was diagnosed based on elevated transaminases (>10 upper limit normal) and the presence of specific serum antibodies (immunoglobulin-G class, present in all 11 patients) and/or viral RNA detection in serum and/or stools. Acute hepatitis lesions were observed in all cases with marked necro-inflammatory activity in nine patients. Confluent necrosis was present in five cases. Anisocaryosis and Kupffer's cell aggregates with siderosis were observed in most of the 11 patients. Cholangitis was frequent (9/11 cases). Cholestasis was observed in eight cases. Pseudo-glandular pattern was present in only one case but without zonal repartition. Characteristic pathological signs of acute hepatitis E were severe intralobular necrosis, polymorph inflammation, and acute cholangitis with numerous neutrophils.

Keywords Hepatitis E · Liver histology · Cholangitis · Cholestasis

J.-M. Peron (✉) · H. Poirson · J.-P. Vinel · C. Bureau
Service d'Hépato-Gastro-Entérologie,
CHU Purpan and INSERM U-531, Université Paul Sabatier,
Toulouse 31400, France
e-mail: peron.jm@chu-toulouse.fr

M. Danjoux · R. Missoury · P. Brousset · J. Selves
Service d'Anatomie Pathologique, CHU Purpan
and INSERM U-563, Centre de Physiopathologie
de Toulouse Purpan,
Toulouse 31300, France

N. Kamar
Service de Néphrologie, CHU Rangueil,
Avenue J Poulhes,
31059 Toulouse, France

J.-M. Mansuy · J. Izopet
Laboratoire de Virologie, CHU Purpan,
31059 Toulouse, France

Introduction

The hepatitis E virus (HEV) is a ribonucleic acid (RNA) virus transmitted by the fecal–oral route. It is responsible for acute hepatitis predominantly in developing countries including Central America, Africa, subcontinental India, Asia, and the Southeast Pacific [4]. In these countries, infection occurs both sporadically and in large outbreaks often through contaminated water. Histological data in these patients are scarce and gathered mainly from three outbreaks [6–9].

Recently, it has become clear that sporadic hepatitis E occurs in persons in Western countries who have no evidence of exposure to HEV strains from countries where the infection is endemic [11]. The largest series of patients with autochthonous hepatitis E have been described in the Barcelona area and the Toulouse area on both sides of the Pyrénées mountains [1–15]. Evidence exists that some animals can be reservoirs for HEV. This may explain some sporadic cases in industrialized countries. There is no information available on liver histology in these patients with acute non-travel-associated hepatitis E.

We report a series of 11 patients with sporadic acute hepatitis E and needle liver histology in South-West France.

Materials and methods

Patients

From March 1997 to March 2004, 11 consecutive patients were diagnosed with acute hepatitis E and had a concomitant liver biopsy. It was performed because of clinical suspicion of underlying chronic liver disease or uncertain etiology of the acute episode of hepatitis despite thorough diagnostic evaluation. All biological samples were collected from patients at the Toulouse University Hospital. All patients were hospitalized. Hepatitis E was diagnosed based on elevated transaminases (>10 upper limit normal) and the presence of specific serum antibodies and/or viral RNA detection in serum and/or stools.

All sera were negative for hepatitis B virus antigen, antibodies and deoxyribonucleic acid (DNA), hepatitis C virus antibodies and RNA, immunoglobulin-M (IgM) class antibodies to hepatitis A virus (HAV), cytomegalovirus and Epstein–Barr virus. Anti-smooth muscle and anti-liver kidney microsome type 1 antibodies were also negative. Antinuclear antibodies were negative except for two patients (patient 1, 1/400; patient 2, 1/160).

Toxic and drug-induced hepatitis was ruled out on medical history. Alcohol abuse was defined as more than 40 g of alcohol per day.

Serological testing

Immunoglobulin-G (IgG) class antibodies to HEV were detected with an enzyme immunoassay (Abbott HEV EIA, Laboratoire Abbott, Rungis, France). This enzyme immunoassay (EIA) uses two recombinant proteins "SG-3" from open reading frame 2 (ORF2) and "8–5", the full length of ORF3 from the Burmese strain (genotype I) expressed in *Escherichia coli*. Anti-HEV IgM antibodies were not tested, as no commercial kits for identifying them were available in France at the time of the study.

Anti-HAV IgM antibody detection was performed with an automated EIA (Axsym HAVAB-M, Laboratoires Abbott, Rungis, France). For both EIAs, data were analyzed according to the manufacturers' instructions.

HEV genome detection

Genome was drawn from serum and stools. After extraction, purification of the nucleic acid (High Pure Viral Nucleic Acid Kit, Roche Diagnostics, Meylan, France) and reverse transcription in complementary DNA (Moloney murine leukemia virus reverse transcriptase, Invitrogen), a real-time polymerase chain reaction (PCR) assay was performed using the TaqMan format for the real-time LightCycler technology [5]. Primer pairing was done from the ORF2 region (viral capsid) to perform the amplification of a 189-base product [primer sense 5′-GACAGAAT TRATTTCGTCGGCTGG-3′, primer anti-sense 5′-TGYTGGTTRTCATAATCCTG-3′, fluorogenic probe 5′-(6-Fam) GTYGTCTCRGCCAATGGCGAGCXT (Tamra)-3′].

Real-time PCR was carried out in a Light Cycler™ capillary using Fast Start™ DNA Master Hybridization probes (Roche Diagnostics). The reaction, data acquisition, and analysis were done using Light Cycler™ instrument software.

Histology

Each biopsy was serially sectioned and stained with hematoxylin, Masson's trichrome, and Perls' stains. Evaluation of several histological criteria was made by two observers (JS and RM). The stage of fibrosis and the grade of activity were evaluated using the METAVIR scoring system (A0: no activity, A1: mild activity, A2: moderate activity, A3: severe activity and F0: no fibrosis, F1: portal fibrosis without septa, F2: few septa, F3: numerous septa without cirrhosis, and F4: cirrhosis) [12]. The following histological criteria were examined and semiquantitatively scored (none=0, mild=1, moderate=2, and severe=3): portal plasmocytes, lymphocytes and neutrophil polynuclears, piecemeal necrosis, lobular inflammation, and lobular necrosis. The same score was applied for other lobular or portal lesions: steatosis, hepatocellular ballooning, Mallory bodies, Kupffer's cell aggregates, bile ducts damage (epithelial alteration or bile duct lymphocyte infiltration), and ductular proliferation. Cholestasis and phlebitis were reported as absent or present. Hepatosiderosis was scored with the Searle's score. Diagnostic criteria for alcoholic hepatitis were the presence of steatohepatitis and alcohol abuse on anamnesis.

Statistical analysis

Statistical analysis was performed using the SPSS package of statistical programs (SPSS, Chicago, IL, USA). Results were expressed as mean±SD, unless otherwise specified.

Results

Clinical and biological features

Eleven patients, three females and eight males, diagnosed with acute hepatitis E from March 1997 to March 2004 had

Table 1 Baseline characteristics of the patients

Variable	Patient 1	Patient 2	Patient 3	Patient 4	Patient 5	Patient 6	Patient 7	Patient 8	Patient 9	Patient 10	Patient 11
Age (year)	71	38	74	51	61	69	58	51	46	78	76
Sex (M/F)	F	F	M	F	M	M	M	M	M	M	M
Alcohol abuse (>40 g/day)	No	No	Yes	Yes	No	No	No	Yes	No	Yes	Yes
Travel outside of France (within 3 months)	Yes[a]	No	No	Yes[b]	No	No	No	No	No	No	No
Death	Yes	No	No	Yes	No	No	No	No	No	No	Yes
Aspartate transaminase AST (<35 IU/l)	1,950	2,550	60	1,590	1,170	340	1,128	207	239	3,760	5,304
Alanine transaminase ALT (<45 IU/l)	1,710	3,150	105	1,290	2,160	1,313	1,281	54	171	3,483	4,625
Alkaline phosphatase (100–280 IU/l)	868	1,708	364	273	952	448	924	340	802	491	448
Gamma glutamyl transferase (11–60 IU/l)	150	360	156	70	264	564	312	431	29	294	120
Bilirubin (μmol/l)	391	227	561	663	39	54	153	17	91	307	629
Accelerin (%)	86	82	76	44	75	136	152	100	140	156	51
HEV genome detection	Yes	NE	NE	Yes	No	Yes	No	NE	Yes	Yes	Yes
Histological evaluation[c]—fibrosis	F4	F1	F4	F4	F1	F2	F0	F1	F1	F4	F4
Histological evaluation[c]—activity	A3	A3	A1	A3	A3	A2	A3	A1	A3	A3	A3

NE not evaluated
[a] La Réunion Island
[b] Portugal
[c] The stage of fibrosis and the grade of activity were evaluated using the METAVIR scoring system (A0: no activity, A1: mild activity, A2: moderate activity, A3: severe activity, F0: no fibrosis, F1: portal fibrosis without septa, F2: few septa, F3: numerous septa without cirrhosis, F4: cirrhosis).

a liver biopsy. Their main clinical and biological features are shown in Table 1. All patients were positive for HEV IgG. HEV RNA was detected in the serum or stools of six patients. In three patients, no specimens were available for genomic testing. Mean±SD age was 61±13. Overall, 45% of the patients were active drinkers. Mean aspartate aminotransferase, alanine aminotransferase, alkaline phosphatase, gamma glutamyl transferase, bilirubin and accelerin were, respectively, 1,663±1,659 IU/l, 1,758±1,486 IU/l, 693±420 IU/l, 265±148 IU/l, 284±244 μmol/l, and 99±40%. Three patients died of severe liver failure (patients 1, 4, and 11).

HEV contamination

One patient travelled to Portugal 1 month before jaundice. All but one lived in the Midi-Pyrénées region located in the south west part of France. Patient 1 lived in La Réunion Island in the Indian Ocean of the south-east coast of Madagascar.

Table 2 Histological features of the five cases with cirrhosis

Patients	Fibrosis	Activity	Piecemeal necrosis[a]	Lobular necrosis[a]	Steatosis[a]	Ballooning[a]	Mallory bodies[a]	Neutrophil polynuclears[a]	Ductular proliferation[a]	Acute alcohol hepatitis[b]	Biliary damage[a]
1	F4	A3	2	3	0	0	0	3	3	No	1
3	F4	A1	1	1	1	1	0	1	2	Mild	1
4	F4	A3	1	3	1	1	0	3	3	Mild	2
10	F4	A3	1	3	1	1	1	3	3	Moderate	2
11	F4	A3	1	3	1	2	1	3	3	Moderate	3

[a] Semiquantitative score: none=0, mild=1, moderate=2, severe=3
[b] Diagnosis of acute alcohol hepatitis was made for patients with steatohepatitis and alcohol abuse on anamnesis.

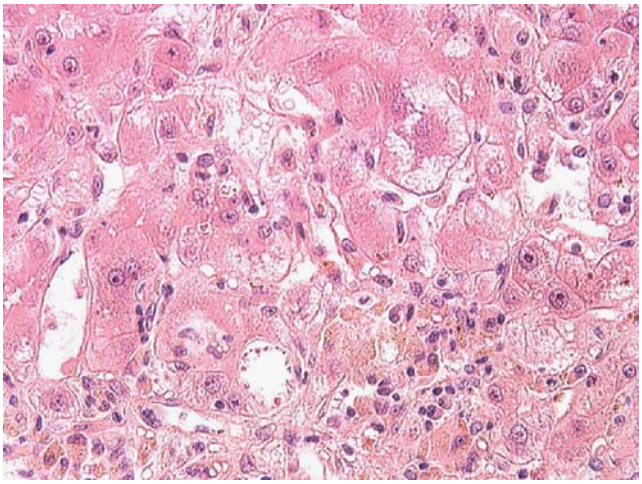

Fig. 1 Alcoholic cirrhosis and acute hepatitis E. Acidophilic necrosis of hepatocytes, ballooning without Mallory bodies, plasmocytic inflammation, and Kupffer's cell aggregates are consistent with acute viral hepatitis E. Steatohepatitis is mild (×400)

Patient 9 had a dog, patient 11 had a cat, and patient 7 had both a cat and a dog. None of the others had household pets. None were hunters nor had contacts with pigs, sheep, cattle, or goats. No distinct geographical or epidemiological pattern was found (data not shown). There was no history of acute hepatitis in family or colleagues at work or at home.

Histological examination

Liver biopsy was transjugular in five cases. The size of biopsy was sufficient for good histological evaluation in all 11 cases. Acute hepatitis lesions were observed in all cases with marked necro-inflammatory activity (A2 or A3) in nine patients. Confluent necrosis was present in five cases, but there was no panlobular necrosis. Anisocaryosis and Kupffer's cell aggregates with siderosis were observed in most of the 11 patients, consistent with acute hepatitis. There was no viral inclusion or epithelioid granuloma and no phlebitis.

Histological analysis revealed micronodular cirrhosis in five cases (patients 1, 3, 4, 10, and 11). This group of patients is described in Table 2. Among these, four had a history of exaggerated alcohol consumption and histological lesions of acute alcoholic hepatitis: steatosis and ballooning (patients 3, 4, 10, and 11) with Mallory bodies in two (patients 10 and 11). In these four patients, acidophilic necrosis was more important than steatohepatitis (Fig. 1). Antinuclear antibodies were positive (1/400) in the fifth patient (patient 1). This patient died, and no definite diagnosis was made concerning cirrhosis.

Patients without associated acute alcoholic hepatitis are described in Table 3. Important spotty or confluent necrosis of hepatocytes with polymorph inflammation in the lobule, consistent with acute viral hepatitis, was observed in these patients (Fig. 2). In portal tracts, inflammation was marked with numerous neutrophils in almost all cases. In two patients (patients 1 and 2), moderate piecemeal necrosis was also seen, and antinuclear antibodies were positive (1/400 and 1/160).

Cholangitis was frequent (9/11 cases; Tables 2 and 3). In most cases, it corresponded to acute cholangitis with epithelial alteration, bile duct infiltration by inflammatory cells, and ductular proliferation with neutrophils (Fig. 3). In two patients (patients 2 and 8), biliary lesions corresponded to mild lymphocytic cholangitis with no true epithelial destruction (Fig. 4). Cholestasis was observed in eight cases; it was more severe in cases associated with acute alcoholic hepatitis. Pseudo-glandular pattern was present in only one case but without zonal repartition (patient 11).

Discussion

There is little information to date on detailed histological appearances in domestically acquired hepatitis E in industrialized countries. The most extensive histopathological studies of hepatitis E were carried out on specimens from patients during the outbreaks in Delhi in 1955–1956 [6], Kashmir in 1978–1979 [9], and Ghana West Africa in

Table 3 Histological lesions of patients without associated acute alcoholic hepatitis

Patients	Fibrosis	Activity	Piecemeal necrosis[a]	Portal lymphocytes[a]	Lobular necrosis[a]	Lobular inflammation[a]	Portal neutrophils[a]	Biliary damage[a]	Ductular proliferation[a]	Cholestasis[a]
1	F4	A3	2	2	3	3	3	1	3	0
2	F1	A3	2	3	3	3	3	1	1	1
5	F1	A3	1	2	3	3	3	2	2	0
6	F2	A2	0	1	2	1	1	0	1	1
7	F0	A3	1	3	3	3	2	0	0	2
8	F1	A1	0	2	1	1	1	1	0	0
9	F1	A2	0	1	2	2	3	1	3	1

[a] Semi-quantitative score: none=0, mild=1, moderate=2, severe=3

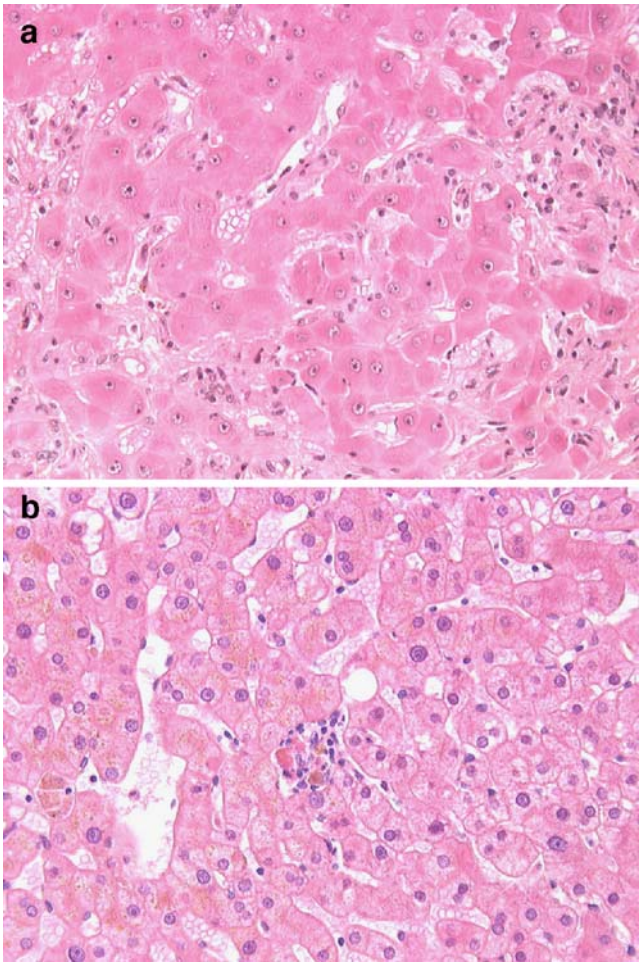

Fig. 2 Features of necrosis in acute hepatitis E. **a** Confluent necrosis in the lobule. Acidophilic necrosis of hepatocytes is marked with important polymorphic inflammation in sinusoids (×400). **b** Spotty necrosis. Foci of acidophilic bodies with mild inflammation are scattered in the lobule (×100)

1962–1963 [13]. Both classic and cholestatic types of acute viral hepatitis have been reported, similar to those of hepatitis A [5]. In fatal cases, extensive necrosis and collapse of the parenchyma are also described [9]. We did not observe such extensive hepatitis lesions probably because the samples of this series are biopsies removed from patients who are alive and not after autopsy.

Most of our cases corresponded to classic acute hepatitis with spotty or confluent necrosis including acidophilic bodies, swollen hepatocytes, and polymorphic parenchymal and portal inflammation. Histological cholestasis is common in acute hepatitis, but marked cholestasis in zone 3 with pseudo-glandular acinar transformation and bile duct proliferation are considered to be typical features of cholestatic type hepatitis E [10]. We found that mild cholestasis was frequent, but pseudo-glandular pattern was observed in only one case. However, this patient had cirrhosis with alcohol hepatitis, so this pattern should be interpreted with caution. Interface hepatitis was observed in

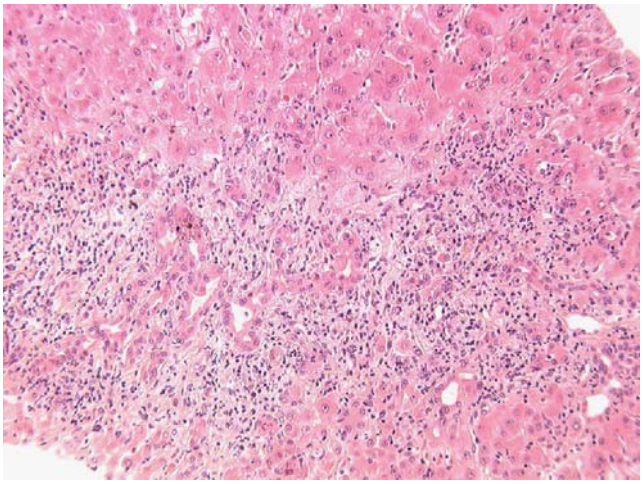

Fig. 3 Acute cholangitis in hepatitis E. The portal tract is edematous with marked inflammation, numerous neutrophils, and ductular proliferation (×200)

two patients of this series to be always associated with intense lesions of acute lobular necrosis. Interestingly, these two patients had positive antinuclear antibodies, raising the question of viral E infection and autoimmune hepatitis. One of the two patients had cirrhosis of unknown etiology, but a definitive diagnosis of autoimmune hepatitis could not be made. Some authors have reported a rare association of past exposure to hepatitis E and the occurrence of autoimmune hepatitis or primary biliary cirrhosis, suggesting a possible role in the development of autoimmune liver disease, similar to that seen in hepatitis A [14, 17]. However, no histological data about these cases are available.

Recently, a case of acute hepatitis E with lymphocytic destructive cholangitis was reported [18]. In our series, acute cholangitis was frequent, whereas lymphocytic cholangitis was rare without true lymphocytic destruction of the duct. In human liver, HEV replicates in the cytoplasm of hepatocytes. However, two experimental animals studies

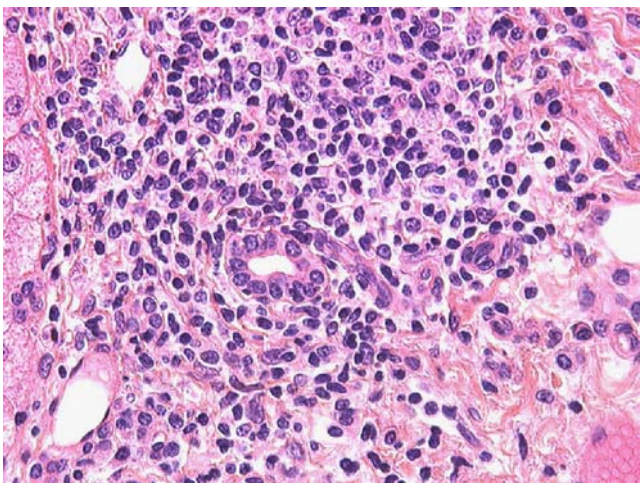

Fig. 4 Lymphocytic cholangitis. Marked lymphocytic inflammation and mild biliary damage are seen within the portal tract (×400)

showed that HEV can be detected in biliary epithelial cells [3, 8]. This may explain, in part, this particular bile duct involvement that characterizes some cases of hepatitis E.

In our series, three patients died. There is a recruitment bias; the more severe patients had a liver biopsy. Nevertheless, prognosis of sporadic hepatitis E can be severe and probably more severe than in patients with endemic hepatitis E in part because it occurs in older patients [2, 7, 15, 16]. They frequently have underlying liver disease and, at least in France, chronic alcohol consumption [11]. Alcohol consumption may facilitate infection with HEV or more likely aggravate the consequence of viral hepatitis.

In conclusion, characteristic pathological signs of acute non-travel-associated hepatitis E were severe intralobular necrosis, polymorph inflammation, and acute cholangitis in portal tract with numerous neutrophils.

References

1. Buti M, Clemente-Casares P, Jardi R, Formiga-Cruz M, Schaper M, Valdes A, Rodriguez-Frias F, Esteban R, Girones R (2004) Sporadic cases of acute autochthonous hepatitis E in Spain. J Hepatol 41:126–131
2. Chau TN, Lai ST, Tse C, Ng TK, Leung VKS, Lim W, Ng M (2006) Epidemiology and clinical features of sporadic hepatitis E as compared with hepatitis A. Am J Gastroenterol 101:292–296
3. Choi S, Chae C (2003) Localisation of swine hepatitis E virus in liver and extrahepatic tissues from naturally infected pigs by in situ hybridization. J Hepatol 38:827–832
4. Emerson SU, Purcell RH (2004) Running like water—the omnipresence of hepatitis E. N Engl J Med 351:2367–2368
5. Ferell LD, Theise ND, Scheuer PJ (2002) Acute and chronic viral hepatitis. In: MacSween RNM (ed) Pathology of the liver. Churchill Livingston, London, pp 313–362
6. Gupta DN, Smetana HF (1957) The histopathology of viral hepatitis as seen in the Delhi epidemic (1955–56). Indian J Med Res 45(Suppl):101–113
7. Ija S, Arnold E, Banks M, Bendall RP, Cramp ME, Cunningham R, Dalton HR, Harrison TJ, Hill SF, MacFarlane J, Meigh RE, Shafi S, Sheppard MJ, Smithson J, Wilson MP, Teo CG (2005) Non-travel-associated hepatitis E in England and Wales: demographic, clinical, and molecular epidemiological characteristics. J Infect Dis 192:1166–1172
8. Kawai HF, Koji T, Iida F, Kaneko S, Kobayashi K, Nakane PK (1999) Shift of hepatitis E virus RNA from hepatocytes to biliary epithelial cells during acute infection of rhesus monkey. J Virol Hepatitis 6:287–297
9. Khuroo MS (1980) Study of an epidemic of non-A, non-B hepatitis: possibility of another human hepatitis virus distinct from post-transfusion non-A non-B type. Am J Med 68:818–823
10. Krawczynski K (1993) Hepatitis E. Hepatology 17:932–941
11. Mansuy JM, Péron JM, Abravanel F, Poirson H, Dubois M, Miedouge M, Vischi F, Alric L, Vinel JP, Izopet J (2004) Hepatitis E in the south west of France in individuals who have never visited an endemic area. J Med Virol 74:419–424
12. The French METAVIR Cooperative Study Group (1994) Intraobserver and inter observer variations in liver biopsy interpretation in patients with chronic hepatitis C. Hepatology 20:15–20
13. Morrow RH, Smetana HF, Sai FT, Edgcomb JH (1968) Unusual features of viral hepatitis in Accra, Ghana. Ann Intern Med 68:1250–1264
14. Nagasaki F, Ueno Y, Mano Y, Igarashi T, Yahagi K, Niitsuma H, Okamoto H, Shimosegawa T (2005) A patient with clinical features of acute hepatitis E viral infection and autoimmune hepatitis. Tohoku J Exp Med 206:173–179
15. Péron JM, Mansuy JM, Poirson H, Bureau C, Dupuis E, Alric L, Izopet J, Vinel JP (2006) Hepatitis E is an autochthonous disease in industrialized countries: analysis of 23 patients in South-West France over a 13-month period and comparison with hepatitis A. Gastroenterol Clin Biol 30:757–762
16. Su CW, Wu JC, Huang YS, Huo TI, Huang YH, Lin CC, Chang FY, Lee SD (2002) Comparison of clinical manifestations and epidemiology between acute hepatitis A and acute hepatitis E in Taiwan. J Gastroenterol Hepatol 17:1187–1191
17. Sylvan SP, Hellstrom UB, Hampl H, Kapprell HP, Troonen H (1995) Hepatitis E in patients with chronic autoimmune liver disease. JAMA 273:377–378
18. Wendum D, Nachury M, Yver M, Leman M, Flejou JF, Janin A, Berthau P (2005) Acute hepatitis E: a cause of lymphocytic destructive cholangitis. Human Pathol 36:436–843

Virchows Arch (2007) 450:411–417
DOI 10.1007/s00428-007-0388-5

ORIGINAL ARTICLE

Prevalence of *Toxocara*-induced liver granulomas, detected by immunohistochemistry, in a series of autopsies at a Children's Reference Hospital in Vitoria, ES, Brazil

Carlos Musso · Jane S. Castelo · Ana M. C. Tsanaclis · Fausto E. L. Pereira

Received: 26 October 2006 / Revised: 5 January 2007 / Accepted: 12 February 2007 / Published online: 28 February 2007
© Springer-Verlag 2007

Abstract The aim of this investigation was to study the frequency of *visceral larva* migrans (VLM) granulomas in autopsies at a Children's Reference Hospital in Vitoria, ES Brazil, where anti-*Toxocara* antibodies are frequently detected in the serum of children admitted at the hospital. Two liver fragments from 310 autopsies of children aged between 1 and 15 years were paraffin embedded, and sections were stained with hematoxylin and eosin and submitted to detection of *Toxocara* antigens using a rabbit anti-*Toxocara* serum. Among the 24 cases with granulomatous lesions, ten had eosinophil-rich granulomas positively stained with the anti-*Toxocara* serum. Some were typical epithelioid granulomas, with a positive reaction in multinucleated giant cells, epithelioid cells, or necrotic debris. The results showed that VLM granulomas are the most frequent granulomatous hepatitis in children in our county. This agrees with the high prevalence of anti-*Toxocara* antibodies in the serum of children admitted to the Children's Reference Hospital. The 3.2% frequency of liver VLM granulomas in autopsies is less than the 30–39% frequency of positive serology in these children, probably reflecting the low larval burden in infected children.

Keywords *Toxocara* · Visceral larva migrans · Hepatic granulomas · Eosinophil-rich granulomas · Toxocariasis

C. Musso (✉) · F. E. L. Pereira
Núcleo de Doenças Infecciosas, Centro Biomédico, UFES,
Av Marechal Campos 1468,
29040-091 Vitória, ES, Brazil
e-mail: carmusso@veloxmail.com.br

J. S. Castelo
Hospital Infantil Nossa Senhora da Glória,
Alameda Mary Ubirajara 205, Sta. Lúcia,
29050-030 Vitória, ES, Brazil

A. M. C. Tsanaclis
Department of Pathology, Medical School and Health Sciences,
Sherbrooke University,
3001, 12e Avenue Nord,
Sherbrooke J1H 5N4, Canada

Introduction

Anti-*Toxocara* antibodies are frequently detected in children and adolescents, especially in people living in developing tropical countries. However, the relevance of the presence of these antibodies is not fully understood. The classical clinical syndromes of *Toxocara* infection, visceral and ocular larva migrans, are not so frequent in children in countries with a high prevalence of anti-*Toxocara* antibodies [4, 15], although a covert, under-diagnosed form of visceral larva migrans syndrome has been reported [19].

In Vitoria, Espirito Santo State, Brazil, prevalence of anti-*Toxocara* antibodies ranged from 31 to 39% in random samples of children admitted at a Children's Reference Hospital (Hospital Infantil Nossa Senhora da Gloria—HINSG) [9, 12]. Although the classical visceral larva migrans syndrome has been diagnosed at the HINSG, its prevalence is not known. However, a high prevalence of anti-*Toxocara* antibodies has been reported there in children with pyogenic liver abscesses and different staphylococcal infections [10, 11]. In addition, a study of 22 autopsied cases of pyogenic liver abscess in children from the HINSG demonstrated eosinophil-rich granulomas in the liver in six children (27.2 %), in which *Toxocara* antigens were detected by a polyclonal anti-*Toxocara* serum [16]. These observations are an indication

that active *Toxocara* infection is not uncommon there, and it is frequently associated with staphylococcal infections.

In an attempt to know the prevalence of eosinophil-rich granulomas related to *Toxocara* infection, the authors decided to investigate the frequency of these liver granulomas in a sample of 310 autopsies, using a polyclonal anti-*Toxocara* serum to identify *Toxocara* antigens by immunohistochemistry.

Materials and methods

From January 1991 to August 1998, 2,020 autopsies, representing 78% of the infantile deaths during this period, were performed at the HINSG. The sample used in the present study was the same as that used in a case control study to investigate the role of visceral larva migrans as a risk factor for infectious meningitis. This sample was made up of 310 autopsies of children, aged 1–15 years, of which 132 presented meningitis (representing all cases of meningitis dead during the period) and 178 did not. The randomization of cases without meningitis was carried out by selecting one or two autopsies of children with the same age, adjacent to the register number of the meningitis case. As the prevalence of *Toxocara* granulomas in the central nervous system was the same in both groups [13] and the prevalence of anti-*Toxocara* antibodies was similar in children with or without meningitis admitted to the HINSG [12], this sample may be considered an unbiased sample of autopsies in children aged 1–15 years, performed at the HINSG.

Two fragments of liver from the right and left lobes, from each autopsy, were paraffin embedded. Five-micrometer sections (five sections/block) were conventionally stained by hematoxylin and eosin (H&E), and six sections from the same blocks were submitted to immunohistochemical detection of *Toxocara* larvae and antigens. Grocott and Ziehl–Nielsen staining methods were used in all cases of granulomatous hepatitis.

The anti-*Toxocara* serum was elicited in rabbits after oral administration of infective *T. canis* eggs according to Smith et al. [18]. An avidin–biotin–peroxidase kit from Sigma Chemical (St. Louis, MO) was used to stain paraffin sections according to the manufacturer's instructions. No previous adsorption with antigens of other nematodes was done to the rabbit serum. For this reason, cross-reactivity with other nematode larvae was not eliminated.

Results

There were 174 boys and 136 girls in the sample studied, without significant differences in ages (4.8±4.1 and 4.2± 3.5 years, respectively; $p=0.204$). Age, gender, and the underlying causes of death diagnosed at autopsy in 310 children are depicted in Table 1.

Granulomas were observed in 25 cases, where ten cases were identified as eosinophil-rich granulomas, positively stained with anti-*Toxocara* serum, and 13 cases as the granulomas of other infectious diseases (schistosomiasis in six, tuberculosis in five, paracoccidioidomycosis and histoplasmosis in one case for each). There was one case with a foreign body granuloma, produced by a sliver of wood, and the etiology of the granuloma could not be established in one case.

The liver granulomas stained with the anti-*Toxocara* serum presented morphological patterns, similar to those already described in both humans and experimental infections with *Toxocara canis* [1, 3, 7]. Some were typical epithelioid granulomas, with multinucleated giant cells and epithelioid cells forming a palisade around the necrotic debris or amorphous eosinophilic material (Fig. 1a,e), suggestive of the Splendore–Hoeppli phenomenon (eosinophilic material formed by necrotic debris and immunoglobulin, most frequently found surrounding schistosome eggs, microfilariae, nematode larvae, and a variety of fungi). These granulomas were oval shaped and frequently coalescent (Fig. 1a). The eosinophilic core material exhibited a peculiar screw-like morphology (Fig. 1c). Eosinophils and mononuclear cells were frequently seen around or intermixed with the macrophages in the outer layer of the granulomas where proliferating fibroblasts were also frequent. A positive anti-*Toxocara* immunohistochemical reaction was observed in all the eosinophil-rich granulomas, in the necrotic debris or in the amorphous eosinophilic material and in the epithelioid cells around them (Fig. 1b,f,g). In one case, the epithelioid granuloma presented fragments of a larva, deeply stained by the anti-*Toxocara* antiserum, amid the necrotic material (Fig. 1g). The cross-sectional diameter of this larva was 17.5 μm, compatible with a *Toxocara* larva according to the morphometric criteria presented by Nichols [14]. Diffuse-exuded eosinophils were also abundant in the portal traits far from the granulomas (Fig. 1d), and Charcot–Leyden crystals were frequently observed among these eosinophils (insert in Fig. 1d). In other cases, healed granulomas exhibited a faintish dot-like stain with the anti-*Toxocara* serum in the central area (Fig. 1h,i). Other granulomas were seen as less-organized macrophages with few loosely arranged epithelioid cells and some multinucleated giant cells mixed with numerous eosinophils and Charcot–Leyden crystals. The macrophages showed a positive histochemical reaction in these granulomas. Curiously, a focal positive staining with the anti-*Toxocara* antiserum was also observed in the cytoplasm of proliferating terminal bile ductules, notwithstanding the presence of granulomas. Figure 1 shows some microscopic patterns described above.

Table 1 Underlying cause of death, age, and gender in 310 autopsied children in which the presence of granulomas in the liver was investigated

Underlying cause of death (ICD-10)	Number	Gender			
		Male		Female	
		Number	Age±SD	Number	Age±SD
Menigitis					
Bacterial meningitis (G00)	98	45	5.3±4.1	53	33.6±3.1
Tuberculous meningitis (G01* A39.0+)	21	12	4.1±4.3	9	4.2±3.1
Viral meningitis (G02* A87.9)	13	9	7.3±4.6	4	3.7±3.7
Bacterial Pneumonitis (J13–J15)	20	11	2.0±1.8	9	1.7±1.3
Staphyloccus aureus septicemia (A41.1)	26	18	6.2±4.6	8	8.0±1.9
Diarrhoea and gastrenteritis of presumed infectious origin (A09)	10	5	1.0±0.0	5	1.0±0.0
Viral hepatitis (B15–B19)	6	4	2.0±0.8	2	1.5±0.7
Ascariasis complications (B77)	3	0	1.7±1.2	3	4.3±4.1
HIV disease resulting in infectious and parasitic diseases (B20)	3	3	–	0	–
Tuberculosis (A15)	2	0	–	2	11.5±3.5
Malignant neoplasms					
Lymphoid, hematopoietic and related tissue (C81–C96)	16	10	4.8±3.8	6	6.2±3.9
Brain (C71)	6	5	6.2±4.4	1	8.0±0.0
Soft tissue (C49)	6	4	2.0±0.8	2	1.5±0.7
Kidney (C64)	5	4	5.3±3.9	1	4.0±0.0
Adrenal medulla (C74.1)	3	2	7.5±6.3	1	13.0±0.0
Bone (C40)	2	2	12.5±2.1	0	–
Congenital malformations (Q00–Q99)	25	17	2.8±2.2	8	4.7±4.4
Other disorders of the nervous system (G90–G99)	15	3	6.0±4.3	12	4.8±3.9
Malnutrition (E40–E46)	9	6	1.7±0.5	3	1.0±0.0
Glomerular and tubulointersticial diseases (N1–N16)	4	3	5.7±3.2	1	6.0±0.0
Status asthmaticus (J46)	4	3	5.3±4.9	1	11.0±0.0
Insulin-dependent diabetes mellitus (E10)	4	3	5.7±3.9	1	6.0±0.0
Miscellaneous diseases	9	5	6.6±4.3	4	4.1±3.1
Total	310	174	4.8±4.1	136	4.2±3.5

The mean age of the children with *Toxocara* positive granulomas was 2.8±2.0 years in seven girls and 6.3±5.8 years in three boys. The frequency of granulomas in girls (7/136, 5.1%), although higher than in boys (3/174, 1.7%), was not statistically significant (Fisher exact test, $p=0.111$).

Gender distribution, age, and underlying cause of death of children in which eosinophil-rich granulomas were detected in the liver are depicted in Table 2. Except for eosinophilia (more than 600 eosinophils/mm^3) in six cases, no signs or symptoms related with *Toxocara* infection were observed in those children.

Ascaris eggs and fragments of adult *Ascaris* worms in the bile ducts (two cases) were heavily stained with anti-*Toxocara* antiserum (Fig. 2c).

No positive staining with the anti-*Toxocara* antiserum was observed in the granulomas produced by *Schistosoma mansoni* eggs (Fig. 2a,b), *Mycobacterium tuberculosis*, or *Histoplasma capsulatum*. It is interesting to stress that in all six cases with schistosoma hepatic granulomas, the embrionated eggs, the egg shell, or its fragments never showed any staining with the anti-*Toxocara* serum. However, the cytoplasm of proliferating terminal bile ductules (Fig. 2d) and the cells of *Paracoccidioides brasiliensis* (Fig. 2e) and *Candida* sp. (Fig. 2f) were stained with the anti-*Toxocara* serum.

Discussion

As discussed previously, the studied sample may be considered an unbiased sample from autopsies performed at the HINSG because infectious meningitis was demonstrated not to be a condition associated with *Toxocara* infection [12, 13]. The number of cases is large enough to detect children with *Toxocara* infection, if an expected frequency of at least 30% of positive serology for *Toxocara* in children admitted there is considered [9, 12].

The frequency of 3.2% eosinophil-rich granulomas with positive staining with the anti-*Toxocara* serum may be considered high and is in agreement with the frequency of anti-*Toxocara* antibodies reported in children admitted at the HINSG.

This study is the first observation on the prevalence of eosinophil-rich liver granulomas in an autopsy series in

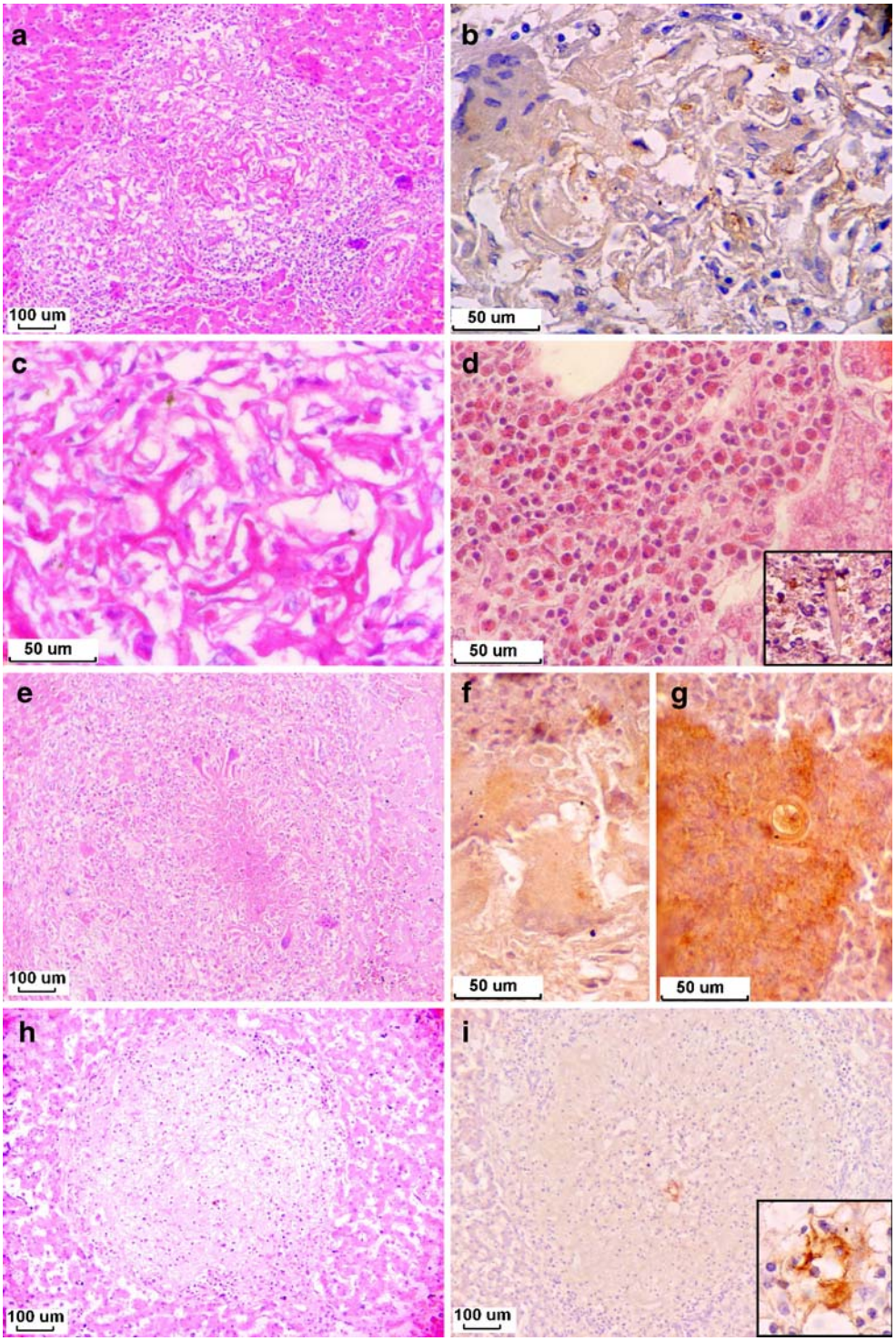

Fig. 1 **a** Three portal-confluent epithelioid granulomas centered with eosinophilic material (Splendore–Hoeppli phenomenon); H&E. **b** Epithelioid granuloma with positive staining for *Toxocara* antigens in the cytoplasm of giant cells, histiocytes, and intercellular space. **c** Detail of a central area of an epithelioid granuloma showing screw-like core morphology of eosinophilic material; H&E. **d** Liver portal tract with intense eosinophilic infiltrate; H&E. *Insert* showing Charcot–Leyden crystal observed in an eosinophil-rich granuloma stained for *Toxocara* antigens that are seen in debris between eosinophils. **e** Oval-shaped necrotizing epithelioid granuloma. Stellate central necrosis surrounded by a palisade of histiocytes and giant cells; H&E. **f** Same necrotizing granuloma positive for *Toxocara* antigens, mainly in the central necrotic material and palisade of histiocytes. **g** Intact segment of *Toxocara* larvae and necrotic material deeply stained with anti-*Toxocara* serum. **h** Healed sclerotic granuloma with evanescent inflammatory portal tract infiltrate; H&E. **i** The same healed granuloma faintly stained for *Toxocara* antigens. In the *insert*, high magnification of the central area showing intense immunoreaction

which immunohistochemistry was performed to detect *Toxocara* antigens. The only observation of prevalence of liver granulomas in a series of autopsies was made in Merida (Venezuela) where Salfelder et al. [17] found 221 (5.18 %) different granulomas in the liver in 4,263 autopsies, including children and adults. In this series, there were 47 eosinophil-rich granulomas (1.54% cases in 3,051 autopsies of patients older than 13 months). However, these authors did not investigate the cause of the eosinophil-rich granulomas. Apart from discussing the assumption of their allergic etiology, they admit possible parasitic origin because of the high frequency of intestinal nematodes and the similarity with the granulomas described in *visceral larva migrans*. It is interesting to observe that the frequency of liver granulomas reported in this study was similar to that observed in Merida, Venezuela [17] (7.74 and 5.18%,

Table 2 Age, gender, and underlying cause of death in ten children in which eosinophil-rich granulomas were detected in the liver

Age (year)	Gender	Basic cause of death
1	F	Bacterial meningitis
7	F	Bacterial meningitis
2	F	Bacterial meningitis
2	F	Ascariasis complication
2	M	Staphylococcal septicemia
4	F	Bacterial endocarditis
2	F	Staphylococcal septicemia
4	M	Bacterial meningitis
13	M	Rheumatic fever
2	F	Bacterial meningitis

Mean of ages: M=6.3±5.8, F=2.8±2.0; p=0.222

respectively; prevalence ratio 1.49; p=0.074), but the frequency of eosinophil-rich granulomas was higher (3.22 and 1.54%, respectively; prevalence rate=2.09; p=0.050).

There was also a high frequency of intestinal nematodes identified in the study herewith. During the opening of the gastrointestinal lumen, 87 autopsied children (28.1%) bore at least one type of nematode, mainly *Ascaris lumbricoides* (78 cases). Because of the fact that the anti-*Toxocara* serum was not adsorbed with other helminths antigens, it is possible to admit that some granulomas stained with this antiserum could be originated from the larvae of other helminths, specially *Ascaris*, whose larvae naturally migrate through the liver. In fact, in two cases reported here, the *Ascaris* eggs and fragments of the *Ascaris* worm were stained with the anti-*Toxocara* serum. However, the only larva observed in one granuloma had a cross-sectional diameter compatible with the *Toxocara* larva.

The relationship of eosinophil-rich granulomas of the liver with *Toxocara* infection was recently reported by Kaplan et al. [7] after reviewing 43 cases from the files of the Armed Forces Institute of Pathology, USA, including all

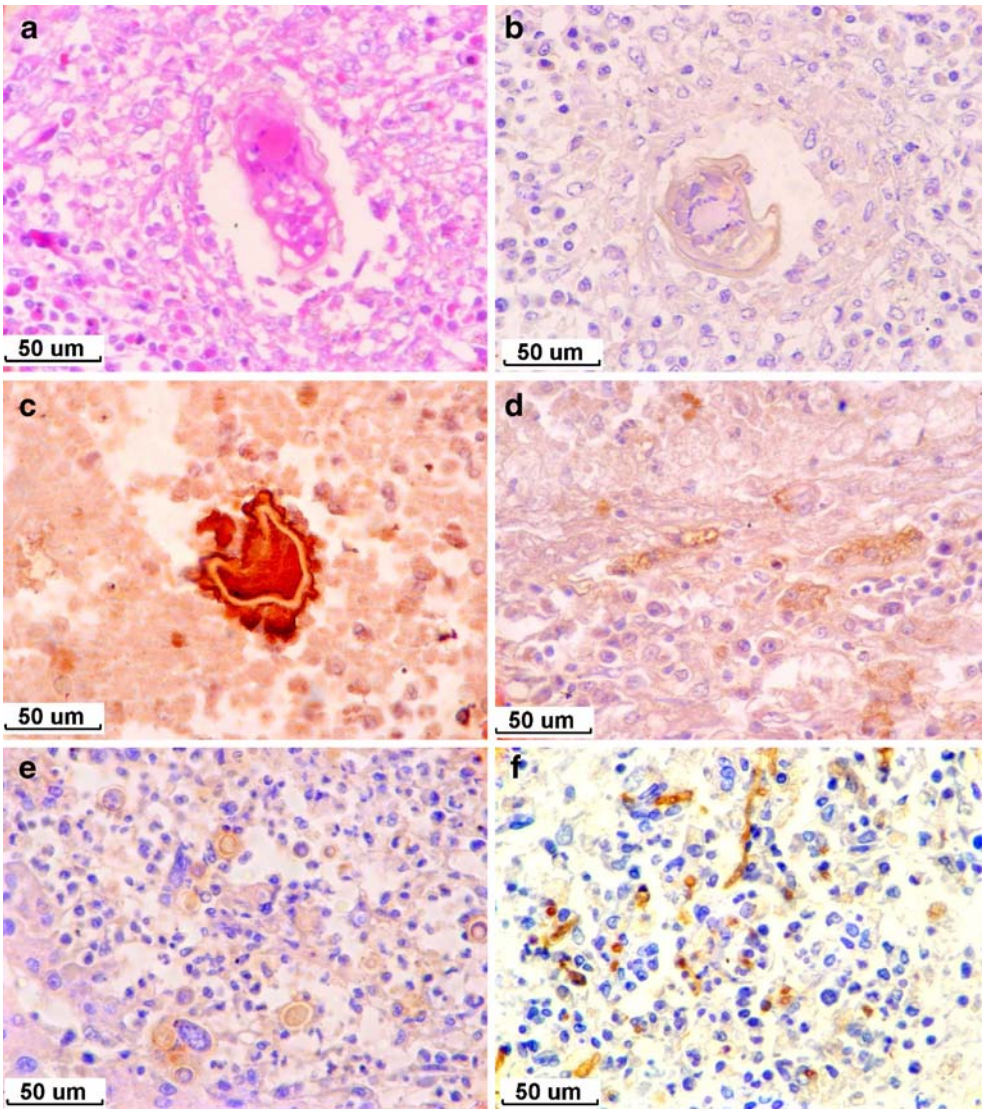

Fig. 2 **a** *Schistosoma mansoni* exudative granuloma with numerous eosinophils; H&E. **b** Negative staining of *S. mansoni* granuloma after immunohistochemistry with the anti-*Toxocara* serum. The faint mahogany-brown eggshell color is the natural color of this structure. **c** *Ascaris* egg deeply stained with the anti-*Toxocara* serum. **d** Cytoplasm of proliferating biliary ductules positively stained with the anti-*Toxocara* serum. **e**, **f** Cross-reactivity of the anti-*Toxocara* serum, respectively, with *P. brasiliensis* and *Candida* sp.

ages from 12 months to 77 years. Sixty percent were asymptomatic, and the lesions were incidental findings during laparotomy or autopsies. In symptomatic patients, abdominal pain and fever were the main complaints. They found 13 cases (30%) confirmed to have *Toxocara* infection, demonstrated by immunohistochemistry with the anti-*Toxocara* serum (eight cases) or by investigation of anti-*Toxocara* antibodies in the serum (five cases).

The frequency of 3.2% eosinophil-rich granulomas with positive staining with the anti-*Toxocara* serum may be considered high and is in agreement with the frequency of anti-*Toxocara* antibodies reported in children admitted at the HINSG. However, the absence of signs and symptoms of visceral larva migrans in these children and the small number of symptomatic cases diagnosed at HINSG are suggestive of a frequent low larval burden in the infected children in our country.

If 30% was the expected prevalence of positive serology for *Toxocara* infection in autopsied children, based on previously reported data [9, 12], at least 93 children in the studied sample would have anti-*Toxocara* antibodies. The *larva migrans* granulomas were detected in only ten cases representing around 10% of the 93 possibly infected cases. Thus, it is possible to admit that the presence of active lesions induced by *Toxocara*, in a sufficient number to be detected in a routine histological examination, is not so frequent in infected children, probably because of the low larval burden. Because of this, the clinical manifestations of *visceral larva migrans* are not so commonly diagnosed, despite the high prevalence of positive serology in children in Vitoria.

The morphology of the eosinophil-rich granulomas described herewith was similar to that previously reported. The observed oval-shaped and frequently coalescent granulomas are an indirect evidence of the serpiginous larval track sectioned at different levels. Moreover, the eosinophilic core material in some granulomas exhibited a peculiar screw-like morphology. This morphological pattern lead us to suppose that during migration, the undulating or helical larval movement, so as to obtain thrust for tissue invasion, leave behind them a spiral tunnel with this screw-like core. The serpiginous appearance of these granulomas contrast with granulomas produced by worm eggs, such as schistosoma eggs, in which a spherical epithelioid macrophage halo is formed around the egg.

Although all eosinophil-rich granulomas revealed positively stained material after the anti-*Toxocara* immunohistochemistry, only one granuloma presented fragments of larva in the central area. One explanation for the low frequency of larvae in the granulomas would be the natural migration of larvae through the liver, leaving behind them serpiginous granulomas that represent the larval track. Probably, if a large number of serial sections were applied in each case, it would be possible to increase the finding of larval remains in the granulomas as observed by Kaplan et al. [7].

The staining of *Paracoccidioides brasiliensis* cells, pseudo-hyphae of *Candida* sp., and proliferating bile ductules may be explained as a cross-reaction or a nonspecific binding of an avidin–peroxidase complex to proteins of these fungi and ductular cells. Phosphatidiletahnolamine-binding proteins shared by some yeasts are expressed by *Toxocara* larvae [6] and may be responsible for the cross-reacting epitopes. In addition, cytoskeleton proteins from helminths may share epitopes with the cytoskeleton proteins of fungi and the mammalian epithelial cells [2, 5]. This would justify not only the cross-reaction with fungi but also the staining of terminal bile ductules observed in some cases. The nonspecific binding of avidin to cell wall proteins of fungi, as demonstrated by Masuoka et al. [8], seems to be unreliable because the control slides, treated with avidin–peroxidase, without the primary antibodies (the anti-*Toxocara* serum), did not stain the cell wall of *Candida* or *Paracoccidioides*.

Pyogenic infections were more frequent in children with *Toxocara* granulomas than in children in which these granulomas were not found (3/10, 30% and 23/300, 7.6%, respectively; prevalence rate=3.94, p=0.042), confirming previous observations demonstrating a significant association of *Toxocara* infection with pyogenic liver abscess in children [10, 11].

In conclusion, the data reported here demonstrate that *Toxocara* granulomas are frequent in the liver of children autopsied at a Children's Reference Hospital in the city of Vitoria, although this frequency is around ten times less than the 30–39% prevalence of anti-*Toxocara* antibodies found in the serum of children admitted to this same hospital. The discrepancy between the frequency of liver granulomas and the frequency of anti-*Toxocara* antibodies in serum may be an indirect evidence that *Toxocara* infection is frequently a mild infection, justifying the low frequency of classical visceral or ocular *larva migrans* in children admitted at the Children's Reference Hospital in Vitoria.

References

1. Beaver PC (1956) Larva migrans. Exp Parasitol 5:587–621
2. Chandrashekar R, Curtis KC, Weil GJ (1995) Molecular characterization of a parasite antigen in sera from onchocerciasis patients that is immunologically cross-reactive with human keratin. J Infect Dis 171:1586–1592
3. De Brito T, Chieffi PP, Peres BA, Santos RP, Gayotto LCC, Vianna MR, Porta G, Alves VA (1994) Immunohistochemical detection of *Toxocara* antigen in human biopsies. Int J Surg Pathol 2:117–124

4. Despommier D (2003) Toxocariasis: clinical aspects, epidemiology, medical ecology, and molecular aspects. Clin Microbiol Rev 16: 265–272
5. Fuchs E, Marchuk D (1983) Type I and type II keratins have evolved from lower eukaryotes to form the epidermal intermediate filaments in mammalian skin. Proc Natl Acad Sci USA 80: 5857–5861
6. Gems D, Ferguson CJ, Robertson BD, Nieves R, Page AP, Blaxter ML, Maizels RM (1995) An abundant, trans-spliced mRNA from *Toxocara canis* infective larvae encodes a 26-kDa protein with homology to phosphatidylethanolamine-binding proteins. Biol Chem 270:18517–18522
7. Kaplan KJ, Goodman ZD, Ishak KG (2001) Eosinophilic granuloma of the liver: a characteristic lesion with relationship to *visceral larva migrans*. Am J Surg Pathol 25:1316–1321
8. Masuoka J, Guthrie LN, Hazen KC (2002) Complications in cell-surface labelling by biotinylation of *Candida albicans* due to avidin conjugate binding to cell-wall proteins. Microbiology 148 (Pt 4):1073–1090
9. Moreira-Silva SF, Leao ME, Mendonca HF, Pereira FE (1998) Prevalence of anti-*Toxocara* antibodies in a random sample of inpatients at a children's hospital in Vitoria, Espirito Santo, Brazil. Rev Inst Med Trop Sao Paulo 40:259–261
10. Moreira-Silva SF, Leite AL, Brito EF, Pereira FE (2002) Nematode infections are risk factors for staphylococcal infection in children. Mem Inst Oswaldo Cruz 97:395–399
11. Moreira-Silva SF, Pereira FE (2000) Intestinal nematodes, *Toxocara* infection, and pyogenic liver abscess in children: a possible association. J Trop Pediatr 46:167–172
12. Musso C, Lemos EM, Tsanaclis AMC, Pereira FEL (2006) Toxocara infection is not associated with viral or bacterial central nervous system infection in children. Neuropediatrics 37:126–129
13. Musso C, Castelo JS, Tsanaclis AMC, Pereira FE (2006) Visceral larva migrans granulomas in liver and central nervous system of children who died of bacterial or viral meningitis. Clin Neuropathol 25:288–290
14. Nichols RL (1956) The etiology of visceral larva migrans. I. Diagnostic morphology of infective second-stage *Toxocara* larvae. J Parasitol 42:349–362
15. Pawlowski Z (2001) Toxocariasis in humans: clinical expression and treatment dilemma. J Helminthol 75(4):299–305
16. Pereira FE, Musso C, Castelo JS (1999) Pathology of pyogenic liver abscess in children. Pediatr Dev Pathol 2:537–543
17. Salfelder K, De Liscano TR, De Mendelovici M (1973) Visceral eosinophilic granulomas. Beitr Pathol 149:420–428
18. Smith HV, Quinn R, Bruce RG, Girdwood WA (1982) Development of the serological response in rabbits infected with *Toxocara canis* and *Toxascaris leonina*. Trans R Soc Trop Med Hyg 76:89–94
19. Taylor MR, Keane CT, O'Connor P, Mulvihill E, Holland C (1988) The expanded spectrum of toxocaral disease. Lancet 1:692–695

Virchows Arch (2007) 450:419–424
DOI 10.1007/s00428-007-0383-x

ORIGINAL ARTICLE

Aurora-A/STK-15 is a predictive factor for *recurrent* behaviour in non-invasive bladder carcinoma: a study of 128 cases of non-invasive neoplasms

E. Compérat · P. Camparo · R. Haus · E. Chartier-Kastler · B. Radenen · F. Richard · F. Capron · V. Paradis

Received: 7 December 2006 / Revised: 25 January 2007 / Accepted: 25 January 2007 / Published online: 28 February 2007
© Springer-Verlag 2007

Abstract Aurora-A, a member of serine/threonine kinase, is implied in mitosis and centrosome maturation. Increasing levels of Aurora-A have been shown to be present in several malignancies and especially in bladder cancer. No immunohistochemical marker has shown to be able to predict the clinical outcome of patients with superficial bladder cancer, except MIB-1, as a predictive marker of relapse and progression. The aim was to investigate the expression of Aurora-A and MIB-1 in tissue micro arrays of superficial bladder cancer representative of pTa papillary urothelial neoplasm with different degrees of aggressiveness (low malignant potential [PUNLMP], non-invasive papillary urothelial carcinoma low grade [NILGC], non-invasive papillary urothelial carcinoma high grade [NIHGC] and carcinoma in situ). We analysed predictive values of both markers, their specificity and sensitivity in tumor recurrence. Aurora-A was a sensitive marker to predict tumor recurrence especially for pTa (PUNLMP, NILGC; PUNLMP $p<0.001$, NILGC $p<0.001$) with statistical significant correlation between immunohistochemical staining and clinical outcome. MIB-1 expression displayed statistical difference $p=0.002$ in the PUNLMP group and $p=0.03$ in the NILGC group. Aurora-A is a more sensitive marker than MIB-1 to predict relapse in pTa bladder neoplasias. The combination of both markers seems to have a very powerful predictive value of recurrence ($p<0.001$).

Keywords Aurora-A · MIB-1 · STK-6 · Bladder cancer · Superficial tumors

E. Compérat · E. Chartier-Kastler · F. Richard · F. Capron
Service Central d'Anatomie et Cytologie Pathologiques
et d'Urologie, Hôpital La Pitié-Salpêtrière,
83, Bd de l'Hôpital,
75013 Paris, France

E. Compérat (✉) · V. Paradis
Faculté de Pharmacie, Unité CNRS, UMR 8149,
4, Av de l'Observatoire,
Paris V, France
e-mail: evacomperat@yahoo.fr

P. Camparo · R. Haus
Service Central d'Anatomie et Cytologie Pathologiques
et d'Urologie, Département d'Epidemiologie et de Santé Publique
Nord, Hôpital d'Instruction des Armées Val-de Grace,
74, boulevard Port Royal,
75230 Paris, France

B. Radenen
Service Central d'Anatomie et Cytologie Pathologiques,
Groupe hospitalier Cochin-Saint Vincent de Paul,
Faculté de médecine Paris V,
27, rue du Faubourg Saint Jaques,
75679 Paris, Cedex 14, France

Introduction

Urothelial carcinoma (UC) of the bladder is an important cause of morbidity and mortality in the world. In France, about 7,800 new cases are detected every year, and 3,000 patients die every year from their disease [8, 13]. Four main groups of UC are distinguished according to clinical behaviour and prognosis, the stage and the grade being the most important prognostic factors [8, 21]. Although distinction between superficial pTa tumors, which do not invade the subepithelial connective tissue, and pT1 tumors, which invade the subepithelial connective tissue even via few cells, is not always evident, it might also be tricky to separate low grade from high grade pTa tumors.

Superficial bladder neoplasias (pTa) are divided into three groups depending on their grade. Each group is associated with various risks of relapse. The World Health Organization (WHO) classification 2004 separates papillary urothelial

neoplasms of low malignant potential (PUNLMP) showing a relapse rate from 35 to 47% [22, 29, 30]. The second group concerns non-invasive papillary urothelial carcinoma low grade (NILGC) with a recurrence rate varying from 48 to 71% [3, 30]. The third group is called non-invasive papillary urothelial carcinoma high grade (NIHGC) with a recurrence rate of about 65% [30]. It is of note that around 20% of pTa NIHGC tumors progress towards pT2 stage with muscular invasion and poor clinical outcome [8, 28].

To date, although many investigations have been made, few immunohistochemical markers showed their relevance to predict clinical outcome with high specificity and sensitivity [1, 8]. One of the most performing markers potentially useful in daily practice is a marker for cellular proliferation, Ki-67 index (MIB-1). MIB-1 is a nuclear protein complex expressed in the G1, S, G2 and M phases of the cell cycle of proliferating cells and absent in resting cells [16]. Immunohistochemical investigations have shown that MIB-1 expression is predictive of the recurrence of bladder cancer, especially in PUNLMP [6, 7, 9, 27]. Nevertheless, increased and diffused labelling of MIB-1 is also observed in non-invasive and invasive high grade carcinomas [24].

Aurora-A is a member of the serine/threonine kinase (located on 20q13) and is essential for mitosis. Aurora-A begins to accumulate on the centrosomes around the S-phase. During mitosis, it is heavily concentrated on the centrosomes at the spindle poles and is detectable along the spindle cells microtubules [15]. Aurora-A regulates spindle cell assembly in mitosis and centrosome maturation. Therefore, Aurora-A plays a role in cell division and has a key role in maintaining genomic integrity to avoid the development of cancer [15]. In recent studies, Sen et al. [28] have shown that Aurora-A overexpression activates genetic pathways that involve centrosome amplification and results in the misaggregation of chromosomes. Their study showed that urothelial tumors with high levels of Aurora-A amplification had a major increase in chromosome copy number and in their total nuclear DNA content. In that study, increased expression of Aurora-A was linked to clinical aggressiveness and poor overall survival of the patients.

The aim of our study was to investigate and compare Aurora-A and MIB-1 expression to assess their relevance as markers of disease recurrence in bladder cancers. For this purpose, we studied immunohistochemistry superficial bladder cancers and in situ carcinoma cases by tissue micro arrays (TMA) approach that enables the analysis of phenotypic features of tumoural tissues in a large series of samples [2, 23].

Materials and methods

This multicentric retrospective study concerned 128 patients who underwent transurethral resection for non-invasive bladder tumours between 1997 and 2004 in our establishments (Hôpital La Pitié-Salpêtrière and Val-de-Grâce, Paris). All the patients were untreated, and the examined bladder specimen was their first neoplastic episode. Patients with progression into a higher stage after the first episode were excluded, *because we were specially interested in recurrence*. We excluded benign urothelial neoplasms as well as reactive atypia or reactive dysplasia.

All tumour specimens and TMAs with immunohistochemical staining were evaluated by two experimented pathologists in an independent manner (EC and PC). The nuclear grading and the pT stage were adjusted according to the WHO guidelines 2004 into the following groups : pTa (distinguishing PUNLMP, NILGC and NIHGC) and in situ carcinoma (C*is*) [8].

TMAs were confected for each of the following histological group: pTa tumours PUNLMP, NILGC, NIHGC and C*is*, respectively. Three cylindrical core biopsies of 0.6 cm in diameter were taken from each tumour. At least 100 malignant cells/per tumour were examined. Four-micrometer TMA sections were deparaffinised and rehydrated; in addition, immunohistochemistry was performed using the modified streptavidin-biotin-peroxidase method and diaminobenzidine as chromogen. An antigenic retrieval, if necessary, was used. The panel of antibodies included AURORA-A (1/150, Santa Cruz, CA) and MIB-1 (1/50; Dako, Denmark). Aurora-A staining was considered positive when perinuclear reinforcement or intracytoplasmic vesicles could be observed in at least 10% of the tumoural cells. Regarding MIB-1, we evaluated the percentage of cells having nuclear staining. MIB-1 staining of more than 10% was considered as positive according to the literature [2, 27]. Normal tissue was not evaluated, as immunostaining with Aurora-A as well as MIB-1 is generally negative in these samples. Positive controls with invasive bladder cancers overexpressing *constantly Aurora-A antibody* and negative controls without antibody application were systematically performed.

Statistical methods

Analysis was made with a SAS logiciel. The Fisher exact test was performed to compare categorical variables with

Table 1 Number and percent (%) of patients with superficial bladder cancers without and with relapse according to the stage and grade of the tumor

Stage, grade	No relapse (%)	Relapse (%)
pTa, PUNLMP	13/35 (37)	22/35 (63)
pTa, NILGC	22/60 (37)	38/60 (63)
pTa, NIHGC	3/23 (13)	20/23 (87)
C*is*	5/10 (50)	5/10 (50)

Table 2 Comparison between the number of positive pTa tumors with Aurora-A and MIB-1 according to the presence of relapse

Aurora-A			MIB-1		
PUNLMP ($p<0.001$)			PUNLMP ($p<0.001$)		
	Positive	Negative	Positive	Negative	Total
Relapse	12 (92%)	1 (8%)	7 (54%)	6 (46%)	13 (100%)
No Relapse	5 (23%)	17 (77%)	1 (5%)	21 (95%)	22 (100%)
NILGC ($p<0.001$)			NILGC ($p=0.03$)		
Relapse	37 (97%)	1 (3%)	16 (42%)	22 (58%)	38 (100%)
No Relapse	5 (23%)	17 (77%)	3 (14%)	19 (86%)	22 (100%)
NIHGC ($p=0.05$)			NIHGC(p=n.s.)		
Relapse	20 (100%)	0 (0%)	13 (65%)	7 (35%)	20 (100%)
No Relapse	2 (67%)	1 (33%)	1 (33%)	2 (67%)	3 (100%)
C*is* (p=n.s.)			C*is* (p=n.s.)		
Relapse	5 (100%)	0 (0%)	2 (50%)	2 (50%)	4*(100%)
No Relapse	4 (80%)	1 (20%)	1 (20%)	4 (80%)	5 (100%)

n.s. Non significant
* One case could not be interpreted, loss of material

the status of Aurora-A and MIB-1 expression. Multivariate analysis was also performed by statistical regression (case/relapse and case/no relapse), including Aurora-A, MIB-1 and the tumoural grade.

Results

The patients consisted of 85 men and 43 women of mean age 68.3 years (range, 52–91). Follow-up, available for all patients, ranged from 11 to 108 months (mean 58.7 months,), this series included 35 cases of PUNLMP, 60 cases of NILGC, 23 cases of NIHGC and ten cases of C*is*. Increased frequency in relapse was observed in the group of higher-grade tumours (NIHGC, 87%; NILGC, 63.3%; PUNLMP, 37.1%; and C*is*, 50%). Detailed results are reported in Table 1.

Aurora-A expression in non-invasive bladder cancers

Taking all 128 cases together, 90 cases (17 PUNLMP [49%], 42 NILGC [70%], 22 NIHGC [87%] and nine C*is* [90%]) showed significant Aurora-A immunostaining. Relapsing tumours displayed Aurora-A overexpression in 58 versus 12% of tumours without relapse, whatever their tumour grade ($p=0.001$). When analysing Aurora-A expression and the incidence of recurrence, according to the grade, significant different results could be seen only between the group of PUNLMP and NILGC ($p<0.001$; Table 2). For both groups, sensitivity, specificity and negative predictive values of Aurora-A staining were 92, 77 and 94%, respectively (Table 3).

Among the 35 PUNLMP cases, Aurora-A immunostaining displayed perinuclear intracytoplasmic staining in 12/13 (92%) cases with recurrence compared to 5/22 cases (23%)

Table 3 Predictive values, sensitivity and specificity of Aurora-A and MIB-1 staining in pTa and C*is* tumors according to the stage

PUNLMP	Aurora-A (%)	MIB-1 (%)	NILGC (%)	Aurora-A (%)	MIB-1 (%)
PPV	71	87		88	87
NPV	94	78		94	78
Sensitivity	92	54		92	54
Specificity	77	95		77	95
NIHGC	Aurora-A	MIB-1	Cis	Aurora-A	MIB-1
PPV	91	84		55	66
NPV	100	46		100	66
Sensitivity	100	42		100	50
Specificity	33	86		20	80

PPV Positive predictive value; *NPV* negative predictive value; *Ss* sensitivity; *Sp* specificity

without relapse ($p<0.001$). In the group of 60 NILGC, 37/38 cases (97%) with recurrence displayed strong Aurora-A staining compared to the 5/22 without relapse (23%), which were positive ($p<0.001$; Figs. 1 and 2). Among the 23 patients with NIHGC, all cases (20/20) with relapse displayed positive immunostaining with Aurora-A compared to the group without recurrence, whereas 2/3 (67%) cases stained positively with Aurora-A. This difference was not statistically significant. In the last group of ten C*is*, all cases with relapse (50%) were considered as positive compared to 4/5 cases (80%) without recurrence. No statistical significant results could be found between Aurora-A staining and clinical outcome.

MIB-1 expression in non-invasive bladder cancers

Among all 128 examined cases, 38 samples (eight PUNLMP [23%], 19 NILGC [32%], 14 NIHGC [61%] and three C*is* [30%]) with relapsing tumours displayed significant MIB-1 immunolabelling. Only 4.7% of cases without recurrence displayed MIB-1 expression (Table 2).

MIB-1 staining in the PUNLMP group was positive in 7/13 cases (54%) with recurrence and in 1/22 cases (5%) without recurrence ($p=0.002$). In cases of NILGC with recurrence, MIB-1 staining was positive in 16/38 cases (42%) versus 3/22 cases (14%) without recurrence ($p=0.03$). Furthermore, in NIHGC cases, positive MIB-1 expression was seen in 13/20 cases (65%) with recurrence. In the group without relapse, 1/3 cases (33%) was marked positively by the MIB-1 antibody. Such difference was not statistically significant. At last, in C*is*, MIB-1 was expressed in 2/4 cases (50%) with recurrence, one case could not be interpreted by the loss of material. In cases without relapse, MIB-1 showed positive expression in one out of five cases (20%; $p=$ n.s.).

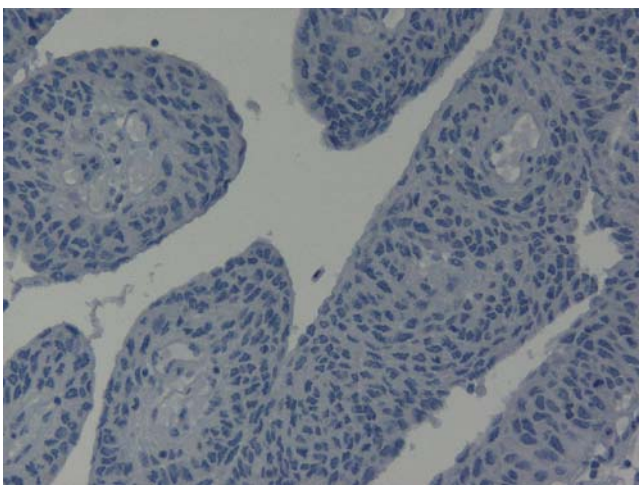

Fig. 1 Weak Aurora—a cytoplasmic staining without reinforcement in a pTa tumor without relapse

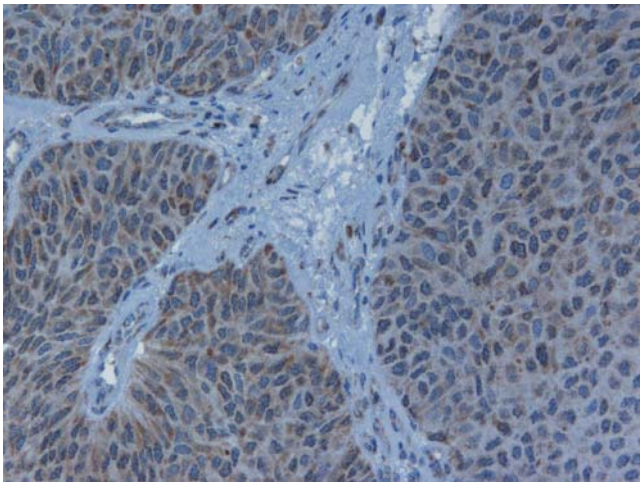

Fig. 2 Cytoplasmic Aurora—a reinforcement in a NILGC with recurrence

Comparison of AURORA-A and MIB-1 expression in non-invasive bladder cancers

Multivariate analysis including MIB-1, Aurora-A and tumour grade showed a strong relationship between Aurora-A and MIB-1 expression ($p<0.001$). The risk to develop a tumour with recurrence was higher (90.2%) in the group of pTa tumours, expressing both markers or expression of at least one marker (MIB-1 and/or Aurora-A) whatever their grade, than in tumours without any expression of both antibodies (2.9%; Table 4). In addition, tumors with positive Aurora-A expression displayed higher risk of relapse than those with MIB-1 expression. These results suggest that Aurora-A appears to be a more sensitive marker for relapsing tumors than MIB-1, especially in PUNLMP and NILGC.

When comparing MIB-1 versus Aurora-A staining in the PUNLMP group, both markers were found to be positive in 7/13 (54%) cases with recurrence. Concerning the NILGC group, Aurora-A, MIB-1 staining and clinical outcome, 16/60 cases (26%) with relapse displayed positive expression of both tested antibodies. When comparing the expression of Aurora-A and MIB-1 in the group of NIHGC, both antibodies stained positively in 13/20 cases (65%). In patients without recurrence, positivity of both antibodies

Table 4 Proportion of relapse and odds ratio according to the different expressions of Aurora-A and/or MIB-1

	Number	Proportion of relapse (%)	Odds ratio	*p* Value
MIB1− STK6−	35	2.9	1	–
MIB1+ STK6−	3	33.3	16.9	0.07
MIB1− STK6+	47	74.5	99.1	<0.0001
MIB1+ STK6+	41	90.2	314.5	<0.0001

was seen in 2/3 cases (67%). Comparisons between Aurora-A and MIB-1 in the C*is* group showed concordant results in two out of five relapsing tumours (40%; Tables 2 and 3).

Taken all 128 cases together, Aurora-A expression showed to be a statistically predictive factor for recurrence (p=6.10^{-7}) as well as MIB-1 (p=3.10^{-6}) and histological grade (p=0.001). Aurora-A positive cases had higher predictive potential for recurrence than MIB-1 positive specimen.

Discussion

In this study, we were interested in non-invasive bladder tumours that represent 70–80% of bladder tumours. That peculiar group represents a very heterogeneous entity according to their degree of tumoural differentiation and their potential of recurrence with high and significant recurrence rate for NIHGC [5, 12, 18, 24]. Therefore, the choice of treatment and follow-up of patients with NILGC and NIHGC are still challenged. In that context, surrogate markers that are able to identify inside the group of pTa tumors, those associated with a high risk of recurrence, are clearly needed [26, 28].

One of those markers could be Aurora-A. Indeed, Sen et al. [28] observed Aurora-A amplification in human bladder cancer with more aggressive behaviour. Our retrospective study, demonstrating that Aurora-A immunostaining in bladder pTa tumor specimen is a good predictive factor of recurrence especially in PUNLMP and NILGC, is in accord with these data. Our results suggest that Aurora-A expression might be a useful indicator of the choice of patients' follow-up, and specially routine controls should be less frequent in cases of Aurora-A negative tumours. This might be especially true in patients with PUNLMP and NILGC, whereas Aurora-A staining seems to be less useful in NIHGC and Cis. Several authors have shown implication of Aurora-A in carcinogenesis, demonstrating overexpression in human gastric carcinoma cell lines, primary gastric carcinoma and hepatocellular carcinoma [4, 10, 11, 14, 25]. As a matter of fact, Aurora-A regulates spindle cell assembly in mitosis and interferes in centrosome maturation. During cell division, Aurora-A plays a key role in maintaining genomic integrity to avoid the development of cancer [15]. Few studies were interested in Aurora-A expression in bladder cancer. However, Frazier et al. [9], who explored bladder cancer cells, suggested that the overexpression of Aurora-A contributes to tumour progression by promoting chromosomal instability leading to aneuploidy.

As MIB-1 was proposed as a reliable marker of proliferation, progression and relapse in bladder cancer, we wondered whether Aurora-A expression provided more benefit than MIB-1 expression in the evaluation of relapses independently from grade. Several authors have shown that MIB-1 tumours have worse clinical outcome and a higher risk of recurrence [26]. Santos et al. have insisted on high MIB-1 levels as a significant factor of risk of relapse especially in superficial bladder tumours [19]. In our study, MIB-1 staining is not as able as Aurora-A to predict recurrence of bladder cancer in our series. Interestingly, cases with positive staining of both Aurora-A and MIB-1 had statistical significant higher risk of relapse, and both expression markers improved the predictive power. In our study, many patients relapsed, even in low grade groups such as PUNLMP and NILGC. The reason might be that the follow-up of patients included in our study was very long, up to 9 years in several cases. Nevertheless, our results support the hypothesis that Aurora-A is a major target gene in bladder cancer development as it seems to play a role already in early phases such as PUNLMP. We suggest that Aurora-A has an increased implication in bladder cancer and already seems to play a role in the early stages of the disease. No statistical significant results were found in NIHGC and C*is*. Concerning NIHGC, our results showed that 100% of cases with recurrence display positive perinuclear Aurora-A immunostaining. Aurora-A has been proven to be a very sensitive marker in this group, although specificity is less important.

At least, we would like to insist on the difficulties of the interpretation of the results of our C*is* group, as there were few cases. Moreover, TMA for superficial C*is* samples might not be the best way to examine C*is*. Tumoural cells are few, only superficial, and it is sometimes difficult to have enough tumoural cells for immunohistochemical examination.

Our data strongly support the hypothesis that overexpression of Aurora-A is an important factor in bladder cancer development and might be useful as an independent factor for predicting clinical outcome. In the early stages of bladder carcinoma, expression of both markers has a very important positive predictive value. Further investigations, especially prospective studies with a larger cohort, would be interesting to elucidate the value of Aurora-A staining in superficial bladder neoplasias.

References

1. Alsheikh A, Mohamedali Z, Jones E, Masterson J, Gilks CB (2001) Comparison of the WHO/ISUP classification and cytokeratin 20 expression in predicting the behavior of low-grade papillary urothelial tumors. World/Health Organization/International Society of Urologic Pathology. Mod Pathol 14(4):267–272
2. Cahill DP, Lengauer C, Yu J, Riggins GJ, Willson JK, Markowitz SD et al (1998) Mutations of mitotic checkpoint genes in human cancers. Nature 392(6673):300–303

3. Chopin DK, Gattegno B (2002) Superficial bladder tumors. Eur Urol 42(6):533–541
4. Ducat D, Zheng Y (2004) Aurora kinases in spindle assembly and chromosome segregation. Exp Cell Res 301(1):60–67
5. Duchrow M, Schluter C, Wohlenberg C, Flad HD, Gerdes J (1996) Molecular characterization of the gene locus of the human cell proliferation-associated nuclear protein defined by monoclonal antibody Ki-67. Cell Prolif 29(1):1–12
6. Dybowski B, Kupryjanczyk J, Rembiszewska A, Pykalo R, Borkowski A (2003) P27(Kip1) and Ki-67 expression analysis in transitional cell carcinoma of the bladder. Urol Res 31(6):397–401
7. Dyrskjot L, Zieger K, Kruhoffer M, Thykjaer T, Jensen JL, Primdahl H et al (2005) A molecular signature in superficial bladder carcinoma predicts clinical outcome. Clin Cancer Res 11 (11):4029–4036
8. Eble JN, Sauter G, Epstein JI, Sesterhenn IA (2004) Tumours of the urinary system and male genital organs. IARC, Lyon, France
9. Fraizer GC, Diaz MF, Lee IL, Grossman HB, Sen S (2004) Aurora-A/STK15/BTAK enhances chromosomal instability in bladder cancer cells. Int J Oncol 25(6):1631–1639
10. Frank I, Cheville JC, Blute ML, Lohse CM, Karnes RJ, Weaver AL et al (2004) Prognostic value of p53 and MIB-1 in transitional cell carcinoma of the urinary bladder with regional lymph node involvement. Cancer 101(8):1803–1808
11. Gattegno B, Chopin D (2001) Natural history of superficial bladder tumors. Prog Urol 11(5):963–990
12. Gritsko TM, Coppola D, Paciga JE, Yang L, Sun M, Shelley SA et al (2003) Activation and overexpression of centrosome kinase BTAK/Aurora-A in human ovarian cancer. Clin Cancer Res 9 (4):1420–1426
13. Helpap B (2001) Nonepithelial neoplasms of the urinary bladder. Virchows Arch 439(4):497–503
14. Helpap B, Schmitz-Drager BJ, Hamilton PW, Muzzonigro G, Galosi AB, Kurth KH et al (2003) Molecular pathology of non-invasive urothelial carcinomas (part I). Virchows Arch 442(4):309–316
15. Holmang S, Andius P, Hedelin H, Wester K, Busch C, Johansson SL (2001) Stage progression in Ta papillary urothelial tumors: relationship to grade, immunohistochemical expression of tumor markers, mitotic frequency and DNA ploidy. J Urol 165(4):1124–1128, discussion 1128–1130
16. Holmang S, Johansson SL (2002) Stage Ta-T1 bladder cancer: the relationship between findings at first follow-up cystoscopy and subsequent recurrence and progression. J Urol 167(4):1634–1637
17. Jeng YM, Peng SY, Lin CY, Hsu HC (2004) Overexpression and amplification of Aurora-A in hepatocellular carcinoma. Clin Cancer Res 10(6):2065–2071
18. Jourdan F, Sebbagh N, Comperat E, Mourra N, Flahault A, Olschwang S et al (2003) Tissue microarray technology: validation in colorectal carcinoma and analysis of p53, hMLH1, and hMSH2 immunohistochemical expression. Virchows Arch 443(2):115–121
19. Kamada K, Yamada Y, Hirao T, Fujimoto H, Takahama Y, Ueno M et al (2004) Amplification/overexpression of Aurora-A in human gastric carcinoma: potential role in differentiated type gastric carcinogenesis. Oncol Rep 12(3):593–599
20. Knowles MA (2001) What we could do now: molecular pathology of bladder cancer. Mol Pathol 54(4):215–221
21. Lebret T, Bohin D, Kassardjian Z, Herve JM, Molinie V, Barre P et al (2000) Recurrence, progression and success in stage Ta grade 3 bladder tumors treated with low dose bacillus Calmette–Guerin instillations. J Urol 163(1):63–67
22. Li D, Zhu J, Firozi PF, Abbruzzese JL, Evans DB, Cleary K et al (2003) Overexpression of oncogenic STK15/BTAK/Aurora A kinase in human pancreatic cancer. Clin Cancer Res 9(3):991–997
23. Mai KT, Elmontaser G, Perkins DG, Yazdi HM, Stinson WA, Thijssen A (2004) Histopathological and immunohistochemical study of papillary urothelial neoplasms of low malignant potential and grade associated with extensive invasive low-grade urothelial carcinoma. BJU Int 94(4):544–547
24. Nocito A, Bubendorf L, Maria Tinner E, Suess K, Wagner U, Forster T et al (2001) Microarrays of bladder cancer tissue are highly representative of proliferation index and histological grade. J Pathol 194(3):349–357
25. Reis-Filho JS, Simpson PT, Martins A, Preto A, Gartner F, Schmitt FC (2003) Distribution of p63, cytokeratins 5/6 and cytokeratin 14 in 51 normal and 400 neoplastic human tissue samples using TARP-4 multi-tumor tissue microarray. Virchows Arch 443(2):122–132
26. Richter J, Jiang F, Gorog JP, Sartorius G, Egenter C, Gasser TC et al (1997) Marked genetic differences between stage pTa and stage pT1 papillary bladder cancer detected by comparative genomic hybridization. Cancer Res 57(14):2860–2864
27. Sanchez-Carbayo M (2004) Recent advances in bladder cancer diagnostics. Clin Biochem 37(7):562–571
28. Sen S, Zhou H, Zhang RD, Yoon DS, Vakar-Lopez F, Ito S et al (2002) Amplification/overexpression of a mitotic kinase gene in human bladder cancer. J Natl Cancer Inst 94(17):1320–1329
29. Shariat SF, Kim J, Raptidis G, Ayala GE, Lerner SP (2003) Association of p53 and p21 expression with clinical outcome in patients with carcinoma in situ of the urinary bladder. Urology 61 (6):1140–1145
30. Yang A, Schweitzer R, Sun D, Kaghad M, Walker N, Bronson RT et al (1999) p63 is essential for regenerative proliferation in limb, craniofacial and epithelial development. Nature 398(6729):714–718

Virchows Arch (2007) 450:425–431
DOI 10.1007/s00428-007-0385-8

ORIGINAL ARTICLE

Molecular-cytogenetic characterisation of sex cord-stromal tumours: CGH analysis in sertoli cell tumours of the testis

I. Verdorfer · A. Höllrigl · U. Strasser · M. Susani · A. Hartmann · H. Rogatsch · G. Mikuz

Received: 13 December 2006 / Revised: 16 January 2007 / Accepted: 28 January 2007 / Published online: 28 February 2007
© Springer-Verlag 2007

Abstract Sertoli cell tumours (SCT) are rare and poorly explored neoplasias, and the genetic features of these uncommon tumours are largely unknown. Data about chromosomal aberrations in human SCT of the testis are very rare. We present in this paper the first molecular-cytogenetic study of SCT of the testis. DNA was isolated from paraffin-embedded tumour material from 11 patients with unilateral SCT. We used comparative genomic hybridisation to investigate changes in DNA copy number. The detected DNA imbalances showed variation from case to case, indicating a high genetic heterogeneity. Chromosomal aberrations were detected in 9 of the 11 tumours evaluated, with 13 losses versus 14 gains. The most frequent aberrations detected were gain of chromosome X (5 of 11 cases) followed by losses of entire or part of chromosomes 2 and 19 in three cases. This study suggests a high variability in histomorphological and genetic patterns. Only gain of the entire chromosome X seems to be a frequent aberration in these tumours. Further studies of these tumour types are necessary to clarify the significance of chromosomal alterations in carcinogenesis of SCT.

Keywords Sertoli cell tumours · CGH · FISH · Molecular cytogenetic

I. Verdorfer (✉) · A. Höllrigl · U. Strasser · H. Rogatsch · G. Mikuz
Institute of Pathology, Medical University of Innsbruck,
Muellerstrasse 44,
6020 Innsbruck, Austria
e-mail: Irmgard.Verdorfer@i-med.ac.at

M. Susani
Department of Clinical Pathology,
Medical University of Vienna,
AKH, 1090 Vienna, Austria

A. Hartmann
Institute of Pathology, University of Regensburg,
93053 Regensburg, Germany

H. Rogatsch
Institute of Pathology, LKH Klagenfurt,
9020 Klagenfurt, Austria

Introduction

Sertoli cell tumours (SCT) are rare sex cord-stromal tumours, occurring in male and female gonads, but they are more common in the testis, accounting for 1% of all testicular tumours [32]. About 100 SCT have been described in the literature so far, only 20 of them in children [27]. The majority of SCT in the testis are sporadic, but they can be associated with genetic syndromes such as Carney syndrome, androgen insensitivity syndrome and Peutz-Jeghers syndrome [8, 9, 23]. Most of the SCT are benign; approximately 20% of cases manifest malignant behaviour [6].

The histomorphology of SCT varies from highly differentiated cases with more or less well-developed tubular structures lined by recognizable Sertoli cells to undifferentiated, diffuse growing cases with only few distinct cytomorphological characteristics. The cytomorphology of the tumour cells of the large-cell calcifying SCT, for example, displays greater similarity to the Leydig than to the Sertoli cells. SCT also do not have a specific immunostaining profile: they react mostly positive with vimentin antibodies (90%), followed by cytokeratin (80%) and to a variable extent with inhibin (30–90%), calretinin (33%) and S100 (30–60%) [2, 3, 12, 17, 20]. The tumour cells are invariably negative for placental alkaline phosphatase (PLAP), alpha-fetoprotein and human chorion gonadotropin. The mitotic activity can be rather high (>5

mitotic figures/10 high power fields, HPF) in about 15% of cases [33]. Most of these neoplasms are classified as not otherwise specified (NOS) tumours. However, the rare "large-cell calcifying Sertoli cell tumour" (LCCSCT) and the sclerosing SCT have been accepted as variants in the WHO 2004 classification [25].

The genetic features of these uncommon tumours are largely unknown. Consequently, it is of great importance to elucidate the pathogenesis of these tumours by cytogenetic and molecular biological investigations.

Materials and methods

Tumour specimens and immunohistochemistry

Eleven patients with diagnosed unilateral SCT were examined, obtained from the Institute of Pathology Innsbruck (Austria), Institute of Pathology Regensburg (Germany) and the Department of Clinical Pathology Vienna (Austria), including nine testicular SCT and one ovarian SCT, and one patient had signs of hermaphroditism. The age of the patients ranges from 5 months to 76 years (mean age 37.8 years). The tumours were classified according to the WHO classification of testicular tumours [25]. Ten cases were classified as "SCT, NOS", and one SCT was diagnosed as lipid rich/sclerosing variant.

Tissue sections were stained with haematoxylin and eosin, profiled immunohistochemically with antibodies against vimentin (DAKO, Austria, dilution 1:250, microwave 750 W, in distilled water for 10 min), α-inhibin (SEROTEC, Biomedica, Austria, dilution 1:80, autoclave 1 bar, in citrate buffer for 30 min), cytokeratin (BECTON DICKINSON, Austria, CAM 5.2, dilution 1:5, microwave 750 W in distilled water for 10 min), calretinin (ZYMED, Szabo-Scandic, Austria, dilution 1:25 without pre-treatment), PLAP (DAKO, Austria, dilution 1:10, pronase for 8 min) and Melan A (DAKO, Austria, dilution 1:100, autoclave 1 bar in citrate buffer for 30 min) using an automated immunostainer (Nexes, Ventana, Tucson, AZ, USA).

Comparative genomic hybridisation

DNA from formalin-fixed, paraffin-embedded tumour material was extracted according to standard protocols. A standard comparative genomic hybridisation (CGH) technique was performed according to a protocol described previously [31].

Briefly, tumour- and reference DNA was labelled by nick translation with either biotin or digoxigenin (Roche Diagnostics, Mannheim, Germany). After co-precipitation with human Cot-1 DNA (Roche Diagnostics, Mannheim, Germany), hybridisation was carried out to normal human metaphase cells for 3 days at 37°C. For detection, the slides were stained with avidin-fluorescein isothiocyanate (Vector Labs Burlingame, CA) and anti-digoxigenin-rhodamine (Roche Diagnostics, Mannheim, Germany). CGH experiments using reverse labelling were repeated with DNA of different gender in most of our cases, and the hybridisation patterns of X were used for assessment of the quality of hybridisation. Evaluation of the CGH preparations was performed using a fluorescence microscope (ZEISS Axioplan, Germany) equipped with a charge-coupled device camera (JAI M300) and the ISIS software (Metasystems, Altlussheim, Germany). Gains or losses were calculated as significant by the evaluation software if fluorescence ratio values were less than 0.8 and more than 1.25. Pericentromeric, heterochromatic regions, telomeric regions and chromosome Y were excluded from the evaluation.

Fluorescence in situ hybridisation

In parallel, fluorescence in situ hybridization (FISH) was applied to define the size of the aberrant cell population and to evaluate the CGH results. Tissue sections (2–5 μm) were mounted on adhesion slides and dried at 70°C overnight. The slide and probe preparation were performed according to the protocol of the manufacturer (Vysis, Downers Grove IL, USA). DNA probes for the centromeric regions for chromosomes X/Y, 2, 3, 8 and 17 and locus-specific identifier (LSI) probes for 20q13 and 22q11.2 were used. At least 100 nuclei in each case were examined.

Results

Histopathology and immunohistochemical findings

The cellular features and growth patterns of the 11 tumours showed several distinct types and varied from case to case (Fig. 1). Immunohistochemical analyses showed positive staining for vimentin (in all six analysed cases), cytokeratin (in six of seven cases), α-inhibin (in four of five cases), calretinin (in all three analysed cases) and negative staining for PLAP and Melan A. A summary of clinical, histology and immunohistochemical data is presented in Table 1.

Two malignant testicular SCT were analysed in this study. The first tumour (case 7) was a poorly differentiated tumour, with large necrosis, cellular polymorphism with spindle or polygonal cells and positive staining for calretinin and cytokeratin. The second malignant and poorly differentiated tumour (case 8) showed similarities to Leydig cells. The immunostaining (α-inhibin and Melan A negative), however, did not support the diagnosis of a Leydig cell tumour. The tumour was categorized as poorly differentiated tumour with diffuse lymphatic and parenchyma invasion.

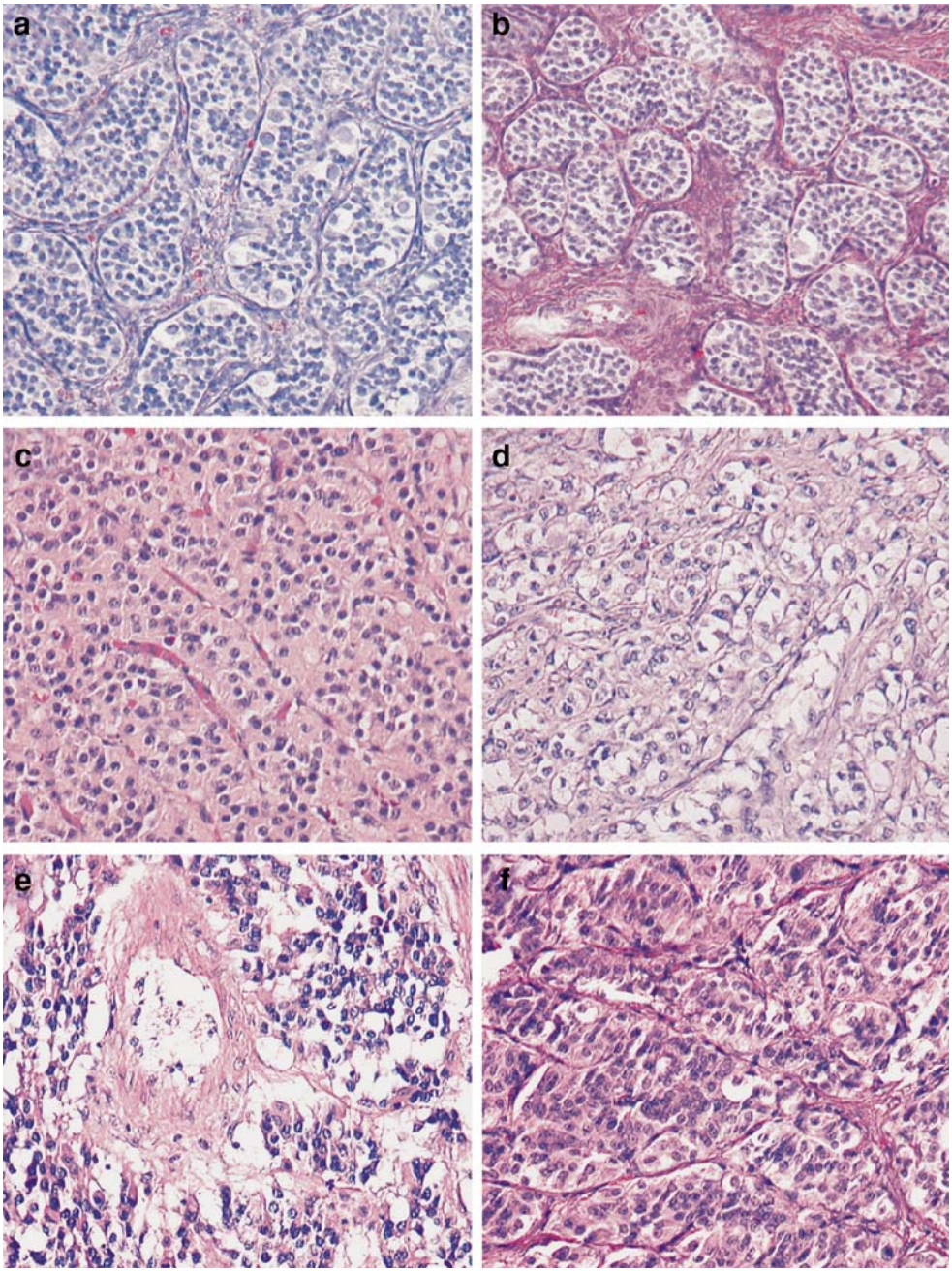

Fig. 1 **a**–**f** Histomorphological features of different cases of SCT. **a** Case 5; **b** case 3; **c** case 7, a malignant, poorly differentiated tumour showed large necrosis and cellular polymorphism with spindle or polygonal cells; **d** case 8, the second malignant tumour in our study showed similarities to Leydig cells. The immunostaining (α-inhibin and Melan A negative), however, did not support the diagnosis of a Leydig cell tumour. The tumour categorized as poorly differentiated tumour with diffuse lymphatic and parenchyma invasion; **e** case 2; and **f** case 1. Haematoxylin and eosin stain, magnification ×100

Comparative genomic hybridisation and fluorescence in situ hybridization results

Chromosomal anomalies were detected in 9 of the 11 analysed tumour specimens without predominance for losses or gains (14 gains versus 13 losses). Most cases showed few copy number changes, affecting one to three chromosomes. The most frequent findings were gains of chromosome X in five cases, followed by loss of entire or part of chromosome 2 and chromosome 19 in three cases. A summary of CGH and FISH results are given in Table 2 and Fig. 2.

In two of our patients, testicular SCT (case 7 and 8) with malignant behaviour were diagnosed. Case 8 displayed the largest number of changes. DNA copy number changes, affecting 14 chromosomes or chromosome regions, were involved, including losses on 1p, 3, 5, 6, 11, 13, 14 and 21 and gains on 1q, 8, 17, 20, 22 and X. Our FISH analyses (Table 2) confirmed loss of chromosome 3 and gains of chromosomes 8, 17, 20q13, 22q11.2 and X. Loss of Y was observed as additional aberration in 73% of the analysed nuclei. The second malignant case (case 7) showed gain of the entire chromosome 2 as sole aberration. None DNA copy-

Table 1 Summary of clinical, histological and immunohistochemical data

Case	Histology	B/M	Age/sex	IHC profile					
				Vimentin	α-Inh	Cytok	Cal	PLAP	Melan A
1	NOS	B	43 years/M	+	/	+	/	−	/
2	NOS	B	35 years/M	+	/	−	/	−	−
3	NOS	B	70 years/M	w+	/	w+	/	/	/
4	NOS	B	5 months/M	+	+	f+	/	−	/
5	NOS	B	5 months/M	/	/	/	/	/	/
6	NOS	B	66 years/F[a]	/	/	/	/	/	/
7	**NOS, p.d.**	**M**	**66 years/M**	**/**	**+**	**+**	**+**	**/**	**/**
8	**NOS, p.d.**	**M**	**76 years/M**	**+**	**−**	**+**	**/**	**/**	**−**
9	NOS	B	4 years/M	/	/	/	/	/	/
10	NOS	B	21 years/F	f+	f+	/	+	/	−
11	S/L	B	34 years/M	/	f+	f+	+	/	−

B/M Benign/malignant, *IHC* immunohistochemistry, *α-inh* α-inhibin, *cytok* cytokeratin, *cal* calrentinin, *PLAP* placental alcaline phosphatase, *NOS* not otherwise specified, *S/L* lipid rich/sclerosing variant, *HPF* high power field, *p.d.* poor differentiated, / not done, + positive, *w+* weak positive, *f+* focal positive, − negative, *bold type* malignant cases

[a] Patient with signs of hermaphroditism

number changes were found in two cases. Case 6, a tumour from a phenotypic female patient with signs of hermaphroditisms, was one of them. The FISH analysis in this tumour detected XY signals in 90% of the analysed nuclei.

Discussion

SCT of the testis are extremely rare tumours with a great variability in their morphology. In most cases, however, a tubular differentiation permits a correct classification. Even in less differentiated cases with solid growth pattern, few tubules can be detected in most instances. In cases with entirely solid pattern, the diagnosis is made when the appearance is inconsistent with any other plausible diagnosis [29], which is also supported by appropriate immunostains.

Cytogenetic data about human SCT of the testis are very rare. Aly et al. [1] reported loss of chromosome Y as the sole aberration in a 5-year-old boy with malignant SCT. In one of our malignant tumours (case 8), we observed loss of

Table 2 Summary of CGH and FISH analyses of all analysed Sertoli cell tumours

Case	CGH results		FISH results (% analysed nuclei, number of copies)	
	Losses	Gains	Losses	Gains
1	None	X[a]		X and Y (36 and 14, mainly XXY/XXYY)
2	None	None		Not done
3	2p11.3–q32.1	19p, X	2 (60, 1)	X and Y (12 and 75, mainly XYY)
4	1[a], 2	X	2 (46, 1)	X and Y (15 and 6, mainly XXYY/XXY)
5	2p16–q34	19	2 (39, 1)	
6	None[b]	None		XY (90)
7	**None**	**2**		**2 (75, mainly 3 to 5)**
8	**1p, 3, 5, 6, 11, 13,14, 21**	**1q, 8, 17, 20, 22, X**	**Y (73)** **3 (44, 0–1)**	**X (70, mainly XX)** **8 (67, mainly 3 to 4)** **17 (55, mainly 3 to 4)** **20q13 (77, mainly 3 to 4)** **22q11.2 (70, mainly 3 to 4)**
9	17	None	17 (69, 1)	
10	None	19		Not done
11	None	X		X and Y (44 and 26, mainly XXYY/XX)

Bold type Malignant testicular SCT

[a] Imbalance with a clear shift, but the CGH profile shows only a partially significant imbalance (partially reaching the threshold).

[b] Patient with signs of hermaphroditism. The patient showed a female phenotype; the CGH analysis with a female reference DNA showed loss of chromosome X. A repeated analysis with a male reference DNA showed no imbalances on chromosome X. XY karyotype was found in tumour tissue of this patient by FISH.

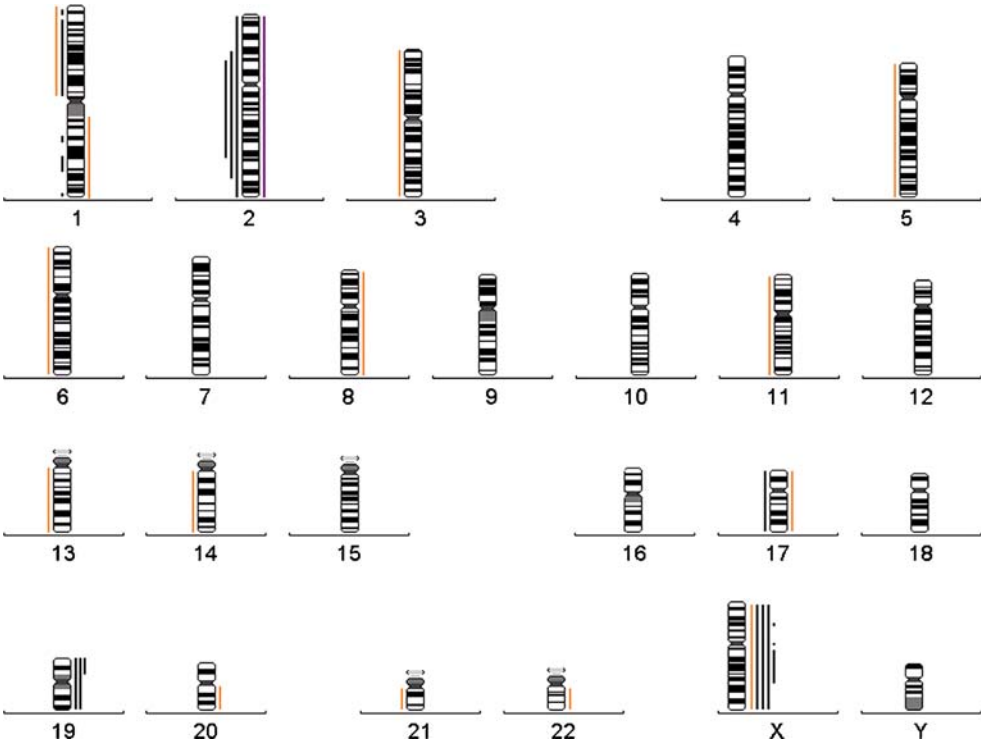

Fig. 2 Summary of chromosomal imbalances detected by CGH in nine Sertoli cell tumours; *vertical lines on the right side* of the ideogram indicate gain, and those on the *left*, loss of genetic material. Each *line* represents gain or loss in a single case; DNA copy number changes in our two malignant testicular tumours are indicated as *orange lines* (case 8) and *lilac line* (case 7)

chromosome Y in 73% of the nuclei by FISH but not as sole abnormality (Table 2). The second malignant case (case 7) showed gain of the entire chromosome 2 by CGH and FISH.

Few genetic data are reported in SCT of the ovary [11, 12, 21]. Formation of an isochromosome 1q is reported by Pejovic et al. [22] as the sole karyotypic abnormality in a peritoneal metastasis of an ovarian SCT. In one of our malignant cases (besides other aberrations), loss of 1p and gain of 1q were detected, suggesting an isochromosome 1q. Only a single CGH analysis of an ovarian SCT is reported in the literature [21], with amplification of 1q21.3–q31 and 6q and a deletion of 7q32–q35.

Copy-number changes on chromosome X is a frequent aberration in testicular germ cell tumours [7, 14, 18, 30], reported also in Sertoli-Leydig cell tumours [4, 7]. Gain of chromosome X, detected in 5 of 11 cases (45%), was the most frequent aberration in our CGH study. In most of the analysed tumour tissues, we found tripartite mosaicisms (XY/XXY/XXYY) by FISH.

LCCSCT, a rare variant of SCT [16, 24, 28] is associated with Carney syndrome, an autosomal dominant syndrome characterised by multiple neoplasias [8, 23]. Matyakhina et al. [19] reported 2p16 abnormalities (amplifications and deletions) in a series of Carney complex tumours, including a LCCSCT without 2p abnormalities, but with a mutation in the PRKAR1A tumour suppressor gene. However, it is of interest that three of our tumours (cases 3, 4 and 5) showed entire or partial loss of chromosome 2 material.

Thirty percent of patients with sex cord tumours have Peutz-Jeghers syndrome, another autosomal dominant disorder, characterised by multiple gastrointestinal hamartomatous polyps, mucocutaneous pigmentation and increased risk of various neoplasms [9]. Germline mutations of the STK11 gene, located at 19p13.3, are responsible for the Peutz-Jeghers syndrome. The study by Kato et al. [13] showed loss of heterozygosity (LOH) on 19p13.3 in ovarian sex cord-stromal tumours. According to the authors, this gene seems not to be involved in the pathogenesis of sporadic sex cord-stromal tumours. The LOH at 19p13.3 indicates other gene alterations in this chromosomal region. These findings are in contrast with our CGH results, which demonstrate gain of chromosome 19 or 19p in three of our cases.

SCT with malignant behaviour are very rare. About 25 cases of malignant SCT are reported in the literature [6, 15, 26, 28]. The criteria for malignancy in SCT are not precisely determined because of great histomorphological variation [27, 33]. A tumour diameter >5 cm, necrosis, nuclear atypia, vascular invasion and a high mitotic count (five of ten HPF) are accepted criteria of malignancy [25, 26, 33]. One of the two 5-month-old patients (case 4) had an increased number of mitotic figures (about seven of ten HPF). Despite the high mitotic activity and the early onset of disease, a malignant behaviour of this tumour was not predictable. Unfortunately, no information about the size of the tumour was available for this retrospective series of cases.

The risk of sex cord neoplasms is increased in patients with testicular feminisation. Testicular feminisation (or androgen insensitivity syndrome) is a rare form of male pseudohermaphroditism, characterised by primary amenorrhoea, sparse hair coat ("hairless women"), female phenotype and male genotype [5, 10]. Such patients have a congenital resistance of the effects of androgens, caused by a mutation in the AR-gene, which is located on the chromosomal region Xq11-12. We analysed tumour tissue of a 66-year-old patient with female phenotype (case 6). The CGH analysis with a female reference DNA showed loss of chromosome X. In a repeated analysis with male reference DNA, no imbalance on chromosome X was detected. The FISH analysis showed XY signals. The constitutional karyotype was not analysable. Unfortunately, no information about the nature of the genetic syndrome in this patient was available. According to the new WHO classification [25], tumours occurring in androgen insensitivity syndrome or androgenital syndrome should be classified under tumour-like lesions. The fact that no genetic changes were identified in this patient's lesion may help indicate this. In summary, similar to the high variability of the histomorphological patterns of SCT, the chromosomal alterations are very heterogeneous. The significance of genetic lesions remains unclear. However, our study presents evidence of morphological and molecular heterogeneity and forms a basis for future analyses of these tumour types.

References

1. Aly MS, Dal Cin P, Moerman P, De Wever I, Devriendt K, Brock P, Casteels-Van-Daele M, Van den Berghe H (1993) Loss of the Y-chromosome in a malignant sertoli tumor. Cancer Genet Cytogenet 65:104–106
2. Augusto D, Leteurtre E, De La Taille A, Gosselin B, Leroy X (2002) Calretinin: a valuable marker of normal and neoplastic Leydig cells of the testis. Appl Immunohistochem Mol Morphol 10:159–162
3. Conkey DS, Howard GC, Grigor KM, McLaren DB, Kerr GR (2005) Testicular sex cord-stromal tumours: the Edinburgh experience 1988–2002, and a review of the literature. Clin Oncol 17:322–327
4. Glaser D, Nienhaus H, Kohler R, Walther G, Pawlowitzki IH (1988) A sex cord stromal tumour in a woman with X0/XX/XXX-mosaicism. Arch Gynecol Obstet 243:115–118
5. Gurer IE, Demirkiran AE, Sare M (2000) Sertoli cell tumor in two sibs with testicular feminization syndrome. Turk J Med Sci 30:385–387
6. Henley JD, Young RH, Ulbright TM (2002) Malignant sertoli cell tumors of the testis: a study of 13 examples of a neoplasm frequently misinterpreted as seminoma. Am J Surg Pathol 26:541–550
7. Hitosugi M, Matsuoka Y, Irimajiri S, Fukada J (1997) Sertoli-Leydig cell tumour complicated by X chromosomal mosaicism. Clin Endocrinol (Oxf) 47:619–622
8. Jayasena SN, Ariyasinghe JT, Gunawardena DM, Gunawardena SA, de Silva MV (2005) Large-cell calcifying sertoli cell tumour of the testis detected at screening of a family with Carney syndrome. Urol Int 75:365–367
9. Kara C, Kutlu AO, Tosun MS, Apaydin S, Senel F (2005) Sertoli cell tumor causing prepubertal gynecomastia in a boy with Peutz-Jeghers syndrome: the outcome of 1-year treatment with the aromatase inhibitor testolactone. Horm Res 63:252–256
10. Karabulut N, Karabulut A, Pakdemirli E, Sabir N, Soysal SK, Soysal ME (2002) Stromal tumor of the sex cord in a woman with testicular feminization syndrome: imaging features. Am J Roentgenol 178:1496–1498
11. Kato N, Fukase M, Motoyama T (2004) Expression of a transcription factor, SOX9, in Sertoli-stromal cell tumors of the ovary. Int J Gynecol Pathol 23:180–181
12. Kato N, Fukase M, Ono I, Matsumoto K, Okazaki E, Motoyama I (2001) Sertoli-stromal cell tumor of the ovary: immunohistochemical, ultrastructural, and genetic studies. Hum Pathol 32:796–802
13. Kato N, Romero M, Catasus L, Prat J (2004) The STK11/LKB1 Peutz-Jegher gene is not involved in the pathogenesis of sporadic sex cord-stromal tumors, although loss of heterozygosity at 19p13.3 indicates other gene alteration in these tumors. Hum Pathol 35:1101–1104
14. Kawakami T, Okamoto K, Sugihara H, Hattori T, Reeve AE, Ogawa O, Okada Y (2003) The roles of supernumerical X chromosome and XIST expression in testicular germ cell tumors. J Urol 169:1546–1552
15. Kolon TF, Hochman HI (1997) Malignant sertoli cell tumor in a prepubescent boy. J Urol 158:608–609
16. Kratzer S, Ulbright T, Talermann A, Srigley JR, Roth LM, Wahle GR, Moussa M, Stephens JK, Millos A, Young RH (1997) Large cell calcifying Sertoli cell tumor of the testis: contrasting features of six malignant and six benign tumors and a review of the literature. Am J Surg Pathol 21:1271–1280
17. Kuroda N, Senzaki T, Yamasaki Y, Miyazaki E, Hayashi Y, Toi M, Hiroi M, Enzan H (2004) Sertoli cell tumor of the testis (not otherwise specified) with the expression of neuroendocrine markers and without the expression of inhibin-α. Pathol Int 54:719–724
18. Looijenga LH, Oosterhuis JW (2004) Clinical value of the X chromosome in testicular germ-cell tumours. Lancet 363:6–8
19. Matyakhina L, Pack S, Kirschner LS, Pak E, Mannan P, Jaikumar J, Taymans SE, Sandrini F, Carney JA, Stratakis CA (2003) Chromosome 2 (2p16) abnormalities in Carney complex tumours. J Med Genet 40:268–277
20. Oliva E, Alvarez T, Young RH (2005) Sertoli cell tumors of the ovary: a clinicopathologic and immunohistochemical study of 54 cases. Am Surg Pathol 29:143–156
21. Patael-Karasik Y, Daniely M, Gotlieb WH, Ben-Baruch G, Schiby J, Barakai G, Goldman B, Aviram A, Friedman E (2000) Comparative genomic hybridization in inherited and sporadic ovarian tumors in Israel. Cancer Genet Cytogenet 121:26–32
22. Pejovic T, Heim S, Alm P, Iosif S, Himmelmann A, Skjaerris J, Mitelman F (1993) Isochromosome 1q as the sole karyotypic abnormality in a Sertoli cell tumor of the ovary. Cancer Genet Cytogenet 65:79–80
23. Sandrini F, Stratakis C (2003) Clinical and molecular genetics of Carney complex. Mol Genet Metab 78:83–92
24. Sato K, Ueda Y, Sakurai A, Ishikawa Y, Okamoto SY, Ikawa H, Katsuda S (2005) Large cell calcifying Sertoli cell tumor of the testis: comparative immunohistochemical study with Leydig cell tumor. Pathol Int 55:366–371
25. Sesterhenn IA, Cheville J, Woodward PJ, Damjanov I, Jacobsen GK, Nistal M, Paniagua R, Renshaw AA (2004) Sex cord/gonadal stromal tumours. In: Eble JN, Sauter G, Epstein JI,

Sesterhenn IA (eds) Pathology and genetics. Tumours of the urinary system and male genital organs. IARC, Lyon, pp 250–258
26. Talerman A (1971) Malignant sertoli cell tumor of the testis. Cancer 28:446–455
27. Talon I, Moog R, Kauffmann I, Grandadam S, Becmeur F (2005) Sertoli cell tumor of the testis in children: reevaluation of a rarely encountered tumor. J Pediatr Hematol Oncol 27:491–494
28. Tanaka Y, Yamaguchi M, Ijiri R, Kondo I (1999) Malignant large cell calcifying sertoli cell tumor with endocrine overactivity. J Urol 161:1575
29. Ulbright TM, Amin MB, Young RH (1999) Tumors of the testis, adnexa, spermatic cord, and scrotum. AFIP atlas of tumor pathology, 3rd series, Fascicle 25. Washington, DC
30. Verdorfer I, Rogatsch H, Tzankov A, Steiner H, Mikuz G (2004) Molecular cytogenetic analysis of human spermatocytic seminomas. J Pathol 204:277–281
31. Wolff E, Girod S, Liehr T, Vorderwulbecke U, Ries J, Steininger H, Gebhart E (1998) Oral squamous cell carcinomas are characterized by a rather uniform pattern of genomic imbalances detected by comparative genomic hybridisation. Oral Oncol 34:186–190
32. Young RH (2005) Sex cord-stromal tumors of the ovary and testis: their similarities and differences with consideration of selected problems. Mod Pathol 18:81–98
33. Young RH, Koelliker DD, Scully RE (1998) Sertoli cell tumors of the testis, not otherwise specified: a clinicopathologic analysis of 60 cases. Am J Surg Pathol 22:709–721

Virchows Arch (2007) 450:433–439
DOI 10.1007/s00428-007-0379-6

ORIGINAL ARTICLE

Expression of sex steroid hormone receptors in C cell hyperplasia and medullary thyroid carcinoma

Claire Bléchet · Pierre Lecomte · Loïc De Calan · Patrice Beutter · Serge Guyétant

Received: 7 December 2006 / Revised: 29 January 2007 / Accepted: 31 January 2007 / Published online: 28 February 2007
© Springer-Verlag 2007

Abstract Previous studies have shown that C cells are twice as numerous in male than in female thyroids and that C cell hyperplasia (CCH) is much more frequent in men. These findings suggest regulation involving sex steroid hormones through the expression of sex steroid hormone receptors on C cells. To investigate this hypothesis, we performed an immunohistochemical study of estrogen receptors α (ERα) and β (ERβ), progesterone receptors (PR), and androgen receptors (AR) on specimens from a series of 40 patients operated on for a medullary thyroid carcinoma (MTC; n=28; female 18, male 10) and/or CCH (n=19; female 6, male 13). ERβ was the only receptor to be consistently expressed in CCH (100%) and MTC (96.5%), whereas ERα was never expressed. PR and AR were rarely expressed in MTC (7 and 14%, respectively). AR was expressed in half the CCH cases (53%), with a trend to male predominance (61% in men vs 33% in women). Our study is the first to describe ERβ expression in CCH. In addition, our findings suggest that CCH, and possibly MTC, might be influenced by sex steroid hormones, namely, estrogens and androgens, through the expression of ERβ and AR on C cells.

Keywords C cell · C cell hyperplasia · Medullary thyroid carcinoma · Estrogen receptors · Androgen receptors

C. Bléchet
Service d'Anatomie et Cytologie Pathologiques,
Hôpital Bretonneau, CHRU de Tours, Tours, France

P. Lecomte
Service d'Endocrinologie, Hôpital Bretonneau,
CHRU de Tours, Tours, France

L. De Calan
Service de Chirurgie Digestive et Endocrinienne,
Hôpital Trousseau, CHRU de Tours, Tours, France

P. Beutter
Service d'Oto-rhino-laryngologie, Hôpital Bretonneau,
CHRU de Tours, Tours, France

S. Guyétant (✉)
Service d'Anatomie et Cytologie Pathologiques,
Hôpital Trousseau, CHRU de Tours,
37044 Tours Cedex 9, France
e-mail: guyetant@med.univ-tours.fr

C cell hyperplasia (CCH) was first recognized in multiple endocrine neoplasia type 2 (MEN2) and familial medullary thyroid carcinoma (MTC) patients. In these genetically determined conditions, CCH precedes and accompanies MTC through a sequence described by Wolfe et al. [41] more than 30 years ago, which has been named neoplastic CCH. Many authors have highlighted the fact that this condition does not fit the definition of hyperplasia but is closer to premalignant states. Since 1980, CCH has been reported in a number of conditions such as hypercalcemia [42], hyperparathyroidism [38], hypergastrinemia, cimetidine treatment, autoimmune thyroiditis [15], and in the presence of a nearby thyroid tumor of follicular origin [1]. In these situations, CCH may be secondary to an exterior stimulus, thus closer to the definition of hyperplasia. Because it has no documented neoplastic potential, it is called "reactive" CCH [33]. During the 1990s, several authors reported that CCH also occurred in a substantial part of the normal adult population ("physiological" CCH) [16, 35]. Moreover, the extension of routine calcitonin serum measurement in endocrinology has led to the identification of an increasing number of patients with mild or moderate hypercalcitoninemia unrelated to MTC, but in whom pathological analysis evidenced reactive or physiological CCH [11, 17]. In a previous quantitative autopsy study of 47 thyroids, we observed that 12 men (41%) and

only 2 women (15%) had CCH [16]. In this study, C cell density was twice as high in men as in women. This difference between genders may be related to the fact that, in normal adults, basal serum calcitonin is significantly higher in males than in females. This has been confirmed in routine practice: Most physiological CCH cases revealed by increased serum calcitonin levels occur in males [11, 17, 18, 22].

The male predominance of physiological CCH suggests possible sex steroid hormone regulation. The biological effects of sex steroid hormones are mainly mediated through interactions with their native receptors. These receptors, including the estrogen receptor (ER), progesterone receptor (PR), and androgen receptor (AR), belong to the superfamily of nuclear receptors. They function as dimers and activate transcription in a ligand-dependent manner by interacting with the responsive element in the promoter region of the target genes [12, 27]. Very little information is available regarding possible sex steroid hormone regulation of both pathological and normal C cells, or regarding possible differential gender expression. Some authors have shown that estrogens and progesterone could influence in vitro and in vivo calcitonin secretion and stimulate MTC cell growth in culture [13, 43], and others have suggested that testosterone might also influence calcitonin secretion in men [10]. Zhai et al. [44] found using immunohistochemistry that AR was expressed in 80% of 45 MTC and 2 of 8 CCH in men. Several studies have shown that ERα was not present in normal C cells [9, 23, 37]. In the 1990s, a second ER was cloned and named ERβ to distinguish it from the original receptor [25, 26]. In humans, ERβ is expressed in a number of normal (e.g., breast, ovary, colon, and prostate) [3, 26, 37] and neoplastic tissues (breast cancer) [21]. Taylor et al. [37] found ERβ expression in human thyroid C cells and follicular cells by immunolocalization.

The aim of the present study was to evaluate the expression of sex steroid receptors, namely, ERα, ERβ, PR, and AR, in a series of patients with CCH and MTC, and to compare their expression in male and female specimens.

Materials and methods

Patients

Forty-three consecutive cases of CCH and/or MTC were gathered from the files of the Pathology Departments of our institution between September 1994 and June 2003. Three cases (CMT) were excluded (partial thyroid specimen and incomplete histological sampling) leaving a series of 40 patients. The medical records were reviewed to collect the following data: age at diagnosis, gender, basal calcitonin level using immunoradiometric assay (calcitonin radioimmunoassay, Brahms, Germany) and pentagastrin infusion test when necessary (according to the French Endocrine Tumor Group [GTE] recommendations) [14], associated thyroid or endocrine disease, prior familial disease, sporadic or inherited MTC, germline mutation on the RET proto-oncogene, and renal failure (if present). CCH unassociated with MTC, RET mutation, and prior familial disease was considered sporadic CCH.

All the experiments complied with French laws for research.

Thyroid specimens

All thyroid specimens were formalin-fixed and sampled according to the GTE recommendations. Each lobe was horizontally sliced, and the whole thyroid was embedded in paraffin. The histological slides of each block, stained with hematoxylin–eosin–saffron (HES) and with calcitonin antibody, were reviewed. The presence of CCH was assessed using previously described criteria [15]: CCH was diagnosed if at least three low-power fields, corresponding to ×100 magnification, contained more than 50 C cells. According to the predominant growth pattern, CCH was morphologically subclassified into focal, diffuse, or nodular, as defined by Rosai et al. [34]. We also classified CCH as neoplastic or physiological, according to the criteria of Perry et al. [33]: Neoplastic CCH was defined by the presence of intrafollicular C cells with nuclear pleomorphism, easily recognizable on HES sections, whereas physiologic CCH was composed of bland C cells that could easily be overlooked on standard HES-stained sections.

Immunohistochemistry for sex steroid hormone receptors

In each case, the most representative block for MTC and/or CCH was selected, and serial 4 μm thick tissue sections were used for immunohistochemistry. Tissue sections were deparaffinized, rehydrated, and subjected to water bath heat antigen retrieval in an ethylenediamine tetraacetic acid buffer (MS-Unmasker, pH 7.8, DiaPath) for 20 to 40 min or in a citrate buffer, when necessary. The primary antibodies, their characteristics, and pretreatments are summarized in Table 1. The polyclonal anti-ERβ 385P is a rabbit immune serum that recognizes a sequence close to C terminus of ERβ1 protein (wild-type ligand-binding isoform of ERβ) and does not recognize other isoforms (ERβ2–5). Immunostaining was performed with the Lab Vision Autostainer (Lab Vision, Fremont, USA) using a biotin–streptavidin–peroxidase detection system with diaminobenzidine as chromogen (ChemMate™ detection kit, Dako, Denmark) for calcitonin, ERα, PR, and AR and EnVision (Dako) for

Table 1 Antibodies clone, source, dilution, and pretreatment

Antibody	Clone	Source	Dilution	Pretreatment
Erα	1D5	Dako	1/50	Heat antigen retrieval
Erß	Polyclonal 385P	BioGenex	1/50	Heat antigen retrieval
PR	PgR636	Dako	1/50	Heat antigen retrieval
AR	AR441	Dako	1/50	Heat antigen retrieval

ERβ. Slides were hematoxylin counterstained. Tissue sections used as positive controls comprised breast cancer for ERα, ERβ, and PR and skin for AR. Negative controls were obtained by omitting the primary antibodies, replaced by mouse immunoglobulins or buffer. The percentages of immunostained cells (in normal or hyperplastic C cells, MTC, and follicular cells) were evaluated by two of the authors (CB, SG) using a semiquantitative scale to define five groups as follows: 0=no staining; 1+=>0 to <5% stained cells; 2+=5 to <20% stained cells; 3+=20 to <50% stained cells; 4+=>50% stained cells.

Statistics

The nonparametric Mann–Whitney test was used to compare the frequency of sex steroid hormone receptor expression in different groups. p values were considered significant when ≤0.05.

Results

Clinical findings

Of the 40 patients, 28 had MTC: 6 patients (4 men and 2 women, mean age 20.5 year) had familial MTC (genetically proved) with CCH in 5/6 cases, and 22 patients (6 men and 16 women, mean age 52 year) had sporadic MTC, associated with CCH in 2 cases. The sex ratio (male/female) was 1:1.8 for all MTC and 1:2.6 for sporadic MTC. Twelve patients had a sporadic CCH (9 men and 3 women, mean age 50 year). Clinical data and morphological features of MTC and CCH are detailed in Table 2. It is noteworthy that chronic renal failure was identified in a high proportion of patients with sporadic CCH (5:12 patients).

Immunohistological expression of sex steroid hormone receptors

ERβ was found in hyperplastic C cells, MTC, and follicular cells, but not ERα. ERα immunoreactivity was not detected in normal or hyperplastic C cells in MTC nor in follicular cells (data not shown). ERβ was detected in all CCH cases (19/19; Fig. 1a) and in 26/28 MTC (Fig. 1b). It was consistently expressed in normal follicular cells. A strong nuclear and cytosolic ERβ signal was detected in more than 50% of cells (score 4+) in 20/28 MTC (72%), in 18/19 CCH (94.5%), and in 20/40 follicular cells (50%; Fig. 1a–b).

PR was expressed in only a minority of cells in CCH, MTC, and follicular cells. There was a weak positive nuclear PR signal in five CCH (17%; Fig. 1c) and in two MTC (7%), usually in a minority of cells (score 1+ or 2+), except for a score of 4+ in MTC (Fig. 1d). Only one thyroid showed immunostaining for PR in follicular cells.

AR was expressed in CCH and in a few cases of MTC. A positive nuclear AR signal was detected in 10/19 CCH (53%, Fig. 1e). Nuclear immunostaining was strong or moderate and represented 20 to 50% of C cells (Fig. 1e) in three cases (score 3+) and less than 20% of C cells in seven cases (score 2+). A positive nuclear AR signal was detected in two cases of MTC (7%, Fig. 1f) and in follicular cells in six patients (15%). In these cases, the staining was heterogeneous and always present in a minority of cells (score 2+ or less).

Table 3 summarizes the expression profile of sex steroid hormone receptors in CCH and MTC.

There was no difference in ERα, ERβ, or PR expression according to gender in MTC (Table 4). AR was more often expressed in men than women (p=0.01), but its expression was only identified in four men (two MEN2 and two sporadic MTC; Table 4). ERα, ERβ, and PR expression was similar in men and in women in CCH (Table 5). AR expression tended to be more frequent in men (8/13, 61%) than in women (2/6, 33%) but the difference was not statistically significant. Similar results were obtained among

Table 2 Main clinical and pathological data in sporadic and familial CCH and MTC

		Age (median)	Gender (M/F)	Renal failure	CCH	Neoplastic/ Physiologic CCH	Focal CCH	Diffuse CCH	Nodular CCH
MTC	n=28	(11–77) 51	10/18	–	7	6/1	–	2	5
Sporadic MTC	n=22	(32–77) 52	6/16	–	2	1/1	–	2	–
Familial MTC	n=6	(11–62) 21	4/2	–	5	5/0	–	–	5
Sporadic CCH	n=12	(32–64) 54	9/3	5	12	1/11	3	5	4

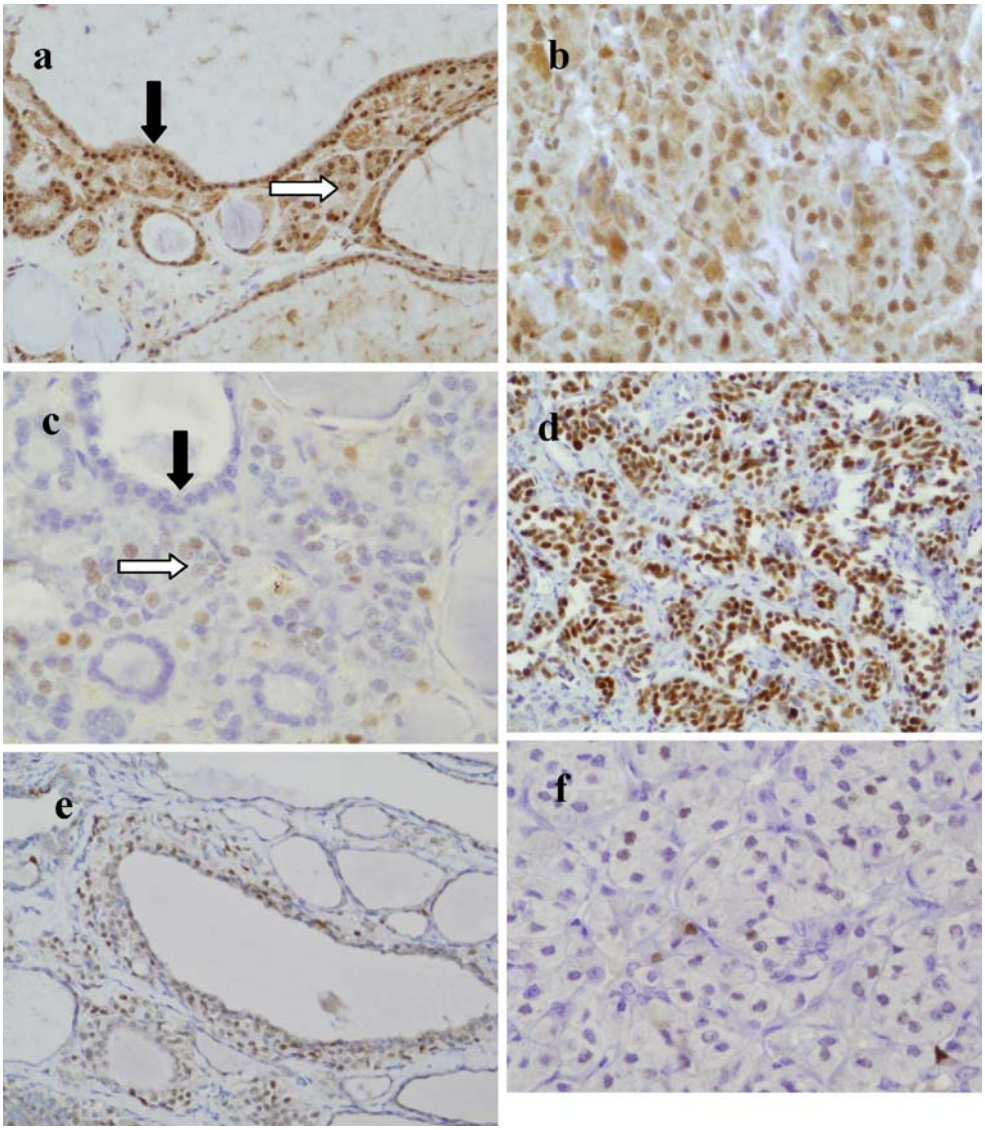

Fig. 1 ERβ, PR, and AR expression in CCH, MTC, and normal follicular cells. **a** ERβ expression in a male sporadic diffuse CCH: nuclear and cytosolic immunostaining in thyroid follicles (*black arrow*) and in C cells (*white arrow*). Original magnification, ×200. **b** ERβ expression in a male sporadic MTC: nuclear and cytosolic immunostaining in neoplastic C cells. Original magnification, ×400. **c** PR expression in a male sporadic nodular CCH: nuclear immunostaining in C cells (*white arrow*) and absence of signal in thyroid follicles (*black arrow*). Original magnification, ×400. **d** PR expression in a male sporadic MTC: nuclear immunostaining. Original magnification, ×200. **e** AR expression in a male sporadic nodular CCH: nuclear immunostaining in C cells. Original magnification, ×200. **f** AR expression in a male sporadic MTC: nuclear immunostaining of neoplastic cells. Original magnification, ×400

sporadic CCH cases: AR expression was more frequent in men (7/9, 66%) than in women (1/3, 33%), but the difference was not significant. In addition, we observed no difference in staining intensity in these different subpopulations. ER and PR expression was not different between men and women in thyroid follicles (Table 6). All positive controls (breast cancer for ERα, ERβ, and PR and sebaceous glands of skin for AR) showed more than 50% of immunostained cells (score 3+). The negative controls showed no staining.

Table 3 Expression profile of sex steroid hormone receptors in CCH and MTC

	CCH (n=19)	MTC (n=28)
ERβ+ AR+ PR+	4/19	1/28
ERβ+ AR+ PR−	6/19	2/28
ERβ+ AR− PR+	1/19	1/28
ERβ+ AR− PR−	8/19	23/28
ERβ− AR+ PR−	0/19	1/28

ERβ+, *PR*+, or *AR*+ >5% of immunostained cells

Table 4 Sex steroid hormone receptors expression according to gender in MTC

	Women (n=18)	p values	Men (n=10)
ERα+	0/18	ns*	0/10
ERβ+	18/18	ns*	9/10
PR+	0/18	ns*	2/10
AR+	0/18	p=0.01	4/10

Erα+, *ERβ*+, *PR*+, or *AR*+ >5% of immunostained cells
*Non significant

Table 5 Sex steroid hormone receptors expression according to gender in CCH

	Women (n=6)	p values	Men (n=13)
ERα+	0/6	ns*	0/10
ERβ+	6/6	ns*	13/13
PR+	1/6	ns*	4/13
AR+	2/6 (33%)	ns*	8/13 (61%)

ERα+, *ERβ+*, *PR+*, or *AR+* >5% of immunostained cells
*Non significant

Discussion

In this study, we showed that normal, hyperplastic, and neoplastic C cells possess ERβ, but not ERα. To our knowledge, this report represents the first identification of ERβ in CCH. In addition, we confirmed that ERβ is consistently expressed in follicular cells, but not ERα. Our results are consistent with recent studies concerning the expression of ER in normal C cells and follicular cells [23, 37]. The presence of ERα in normal thyroid C cells has been a matter of debate for many years, and reports on this subject are often dated. In 1986, Greenberg et al. [13] showed that calcitonin secretion was responsive to 17 β-estradiol (E2) in the rat. In 1988, Yang et al. [43] reported estrogen growth stimulation and tamoxifen growth inhibition of a tumor cell line derived from human MTC, suggesting the presence of ER in C cells. In the 1990s, several studies were unable to detect ERα in normal or neoplastic C cells by immunohistochemistry, while others detected very low concentrations of ER in one of seven human MTC by steroid binding analysis [2, 6, 23]. These apparent contradictions may be explained in part by the presence of ERβ in C cells but not ERα. Egawa et al. [7] showed the presence of ERα and ERβ mRNA in 6/6 MTC, with no difference in transcript expression between normal and neoplastic tissues for both receptors. However, this study did not give any information on ER protein expression and on the type of cells involved in ER mRNA synthesis [7]. In a more recent study by Kawabata et al. [23], ERα immunoreactivity was not detected in normal follicular cells or C cells but was detected in various thyroid disease conditions, including some of the 20 MTC tested (fourteen women and six men). These authors detected ERα in MTC in women but not in men, whereas ERβ was detected in both. These results partly differ from ours, in which none of 28 MTC presented ERα immunoreactivity whereas all but one expressed ERβ. Unfortunately, the work of Kawabata et al. did not focus on C cell pathology and comparison with our series is difficult because much information is lacking: For example, the number of MTC immunoreactive for ERα and ERβ and staining intensity are not specified. Both studies used the same anti-ERα antibody (monoclonal antibody ER1D5). It must be noted that the ERα-labeling index reported by Kawabata et al. was very low (mean 5.5%) and almost identical to our cut-off for positive immunoreactivity (5% of immunostained cells). However, we did not identify any ERα immunoreactivity in MTC or C cells. In the study of Kawabata et al., the mean number of cells stained with ERβ in MTC was 24%. In our study, the immunostaining for ERβ was stronger and more homogenous in most MTC and CCH (score 4+ in 72% of MTC and in 94.5% of CCH). The type of antibody used may explain these differences: Kawabata et al. used a personal ERβ antibody, whereas the antibody that we used is a commercial polyclonal anti-ERβ antibody (anti-ERβ 385P). In an evaluation of multiple different ERβ antibodies on formalin-fixed paraffin embedded tissue, anti-ERβ 385P was considered to be one of the best antibodies [40]. We also used a labeling system (EnVision™) that was previously considered to be more sensitive for ERβ immunostaining [4]. In addition to the nuclear staining, we found a consistent cytoplasmic staining for ERβ. This cytoplasmic staining was reported previously, and as it is abolished using blocking peptide, it is probably a real staining and not an artifact [5, 36, 37]. The signification of cytoplasmic ER localization is unclear and may represent localization of ER in mitochondria [5] or an ERβ1 isoform lacking the DNA binding domain. In view of previous reports on estrogen growth stimulation (and tamoxifen growth inhibition) on C cells, our results suggest that these effects might be mediated through direct binding of estrogens to ERβ. The higher prevalence of follicular thyroid carcinoma in women has been explained by such an effect of estrogens on ERβ [29]. Similarly, the growth stimulation effect of estrogen on C cells might also contribute to the higher prevalence of sporadic MTC in women (in comparison with men). However, more information is needed to confirm this hypothesis.

Table 6 Sex steroid hormone receptors expression according to gender in follicular epithelial cells

	Women (n=21)	p value	Men (n=19)
ERα +	0/21	ns*	0/19
ERβ +	21/21	ns*	19/19
PR +	0/21	ns*	1/19
AR +	1/21	ns*	5/19

ERα+, *ERβ+*, *PR+*, or *AR+* >5% of immunostained cells

Our study shows that AR was expressed in half the CCH cases (53%, 8 men/2 women) and was rarely expressed in MTC (4/28 cases [14%], 4 men). These findings suggest that the genomic effect of AR (linked to higher androgen levels in men) might be at least partially responsible for the increased frequency of sporadic CCH in men. The presence

of AR was also studied by Zhai et al. [44] in a series of MTC and CCH. The authors identified AR in 80% of 43 cases of MTC and in 25% of 8 cases of MTC or MEN-2-associated CCH. No significant difference in AR expression was identified between genders in their study, but the series did not contain any sporadic CCH, which is the main context where male predominance exists, and according to the authors, the autopsy series probably gave false negative results due to postmortem degradation of the receptor. Our study revealed that AR was often present in sporadic CCH (7/12 cases, 58.3%) and seemed to be more often expressed in men. Since our first study in 1997 showing male predominance of CCH in healthy subjects [16], a number of studies have confirmed this finding [11, 17, 19]. Nonetheless, very few reports are available in the literature to explain this phenomenon. In 1987, Garcia-Ameijeras et al. [10] analyzed the relationship between basal and poststimulatory calcitonin levels and free testosterone and concluded that the elevated calcitonin levels and enhanced response found in normal men compared to normal women were influenced by the higher testosterone levels found among men. Although our findings showed a tendency to increased expression of AR in men (61% vs 33%), our CCH series was probably too small to reach statistical significance. The fact that 5/12 (42%) patients in our sporadic CCH population had chronic renal failure may also have biased this result. This particular population warrants attention: The identification of a slight increase in basal calcitonin in patients treated by chronic hemodialysis has been well documented in the literature (between 20 to 29% patients with chronic renal failure have a basal calcitonin level above 10 pg/ml [28, 32]), without demonstrating a higher risk of MTC [8, 24, 39]. In two small autopsy series, Santeusanio et al. [35] identified CCH in 6/8 patients with chronic renal failure, and Tomita and Millard [38] identified CCH in 7/12 patients. However, no correlation with serum calcitonin levels was available in these autopsy studies, and as such patients are rarely surgically treated, very little information is available on this subject. Kotzmann et al. [24] identified an increase in basal serum calcitonin in 44 of 150 patients (29%) treated with chronic hemodialysis and in 48 of 800 (6%) patients receiving kidney transplantation. Pentagastrin-stimulated calcitonin concentrations exceeded 100 pg/ml in four patients and seven patients, respectively. Thyroidectomy was performed in eight patients and revealed MTC in two cases and CCH in six [24]. Our results confirm these findings and show that even mild hypercalcitoninemia in patients with chronic renal failure is associated with CCH. In our study, only one (of five) patient with chronic renal failure expressed AR in CCH. The mechanism of CCH in this particular context may be different from other forms of physiological CCH.

We also evaluated PR expression in CCH and MTC. Its interactions with ER in reproductive tissues are well documented [30]. In a previous study, Colomer et al. [6] demonstrated the presence of very low concentrations of PR in five of seven cases of human MTC using steroid-binding analysis and enzyme immune assay. Progesterone receptors were focally detected by immunohistochemistry (less than 1% of cells) in all cases [6]. In the present study, PR immunoreactivity (more than 5% of cells) was present in only two cases of MTC (5%) and five of CCH (26%), suggesting that PR does not play an important role in MTC, although it may interact with ERβ in some CCH.

In summary, our study shows that normal, hyperplastic, and neoplastic C cells often express AR and consistently express ERβ, but not ERα. The presence of AR in C cells may interact with high levels of androgen in men and partly explain the high frequency of sporadic CCH observed in males. Further investigations are needed to confirm this hypothesis. In addition, the consistent expression of ERβ in CCH and MTC may be significant: Indeed, sex steroid hormone receptors have been detected in a variety of nonhormone-dependent tumors [3, 20, 31], in which they can have a prognostic impact and/or therapeutic value. This high level of expression of ERβ on C cells might contribute to the higher frequency of sporadic MTC observed in women.

References

1. Albores-Saavedra J, Monforte H, Nadji M, Morales AR (1988) C-cell hyperplasia in thyroid tissue adjacent to follicular cell tumors. Hum Pathol 19:795–799
2. Bur M, Shiraki W, Masood S (1993) Estrogen and progesterone receptor detection in neoplastic and non-neoplastic thyroid tissues. Mod Pathol 6:469–472
3. Campbell-Thompson M, Lynch IJ, Bhardwaj B (2001) Expression of estrogen receptor (ER) subtypes and ERbeta isoforms in colon cancer. Cancer Res 61:632–640
4. Carder PJ, Murphy CE, Dervan P, Kennedy M, McCann A, Saunders PT, Shaaban AM, Foster CS, Witton CJ, Bartlett JM, Walker RA, Speirs V (2005) A multi-centre investigation towards reaching a consensus on immunohistochemical detection of ERbeta in archival formalin-fixed paraffin embedded human breast tissue. Breast Cancer Res Treat 92:287–293
5. Ceresini G, Morganti S, Graiani V, Saccani M, Milli B, Usberti E, Valenti G, Ceda G, Corcione L (2006) Estrogen receptor (ER)-β, but not ER-α, is present in thyroid vessels: immunohistochemical evaluations in multinodular goiter and papillary thyroid carcinoma. Thyroid 16:1215–1220
6. Colomer A, Martinez-Mas JV, Matias-Guiu X, Llorens A, Cabezas R, Prat J, Garcia-Ameijeiras A (1996) Sex-steroid hormone receptors in human medullary thyroid carcinoma. Mod Pathol 9:68–72
7. Egawa C, Miyoshi Y, Iwao K, Shiba E, Noguchi S (2001) Quantitative analysis of estrogen receptor-α and -β messenger RNA expression in normal and malignant thyroid tissues by real-time polymerase chain reaction. Oncology 61:293–298
8. Elisei R, Bottici V, Luchetti F, Di Coscio G, Romei C, Grasso L, Miccoli P, Iacconi P, Basolo F, Pinchera A, Pacini F (2004)

Impact of routine measurement of serum calcitonin on the diagnosis and outcome of medullary thyroid cancer: experience in 10,864 patients with nodular thyroid disorders. J Clin Endocrinol Metab 89:163–168
9. Frolich A, Christensen L, Andersen J (1990) Estrogen receptors appear undetectable in the C-cells of the human thyroid gland. Bone 11:393–396
10. Garcia-Ameijeiras A, De La Torre W, Rodriguez-Espinosa J, Perez-Perez A, De Leiva A (1987) Does testosterone influence the post-stimulatory levels of calcitonin in normal men? Clin Endocrinol (Oxf) 27:545–552
11. Gibelin H, Essique D, Jones C, Levillain P, Marechaud R, Kraimps JL (2005) Increased calcitonin level in thyroid nodules without medullary carcinoma. Br J Surg 92:574–578
12. Gobinet J, Poujol N, Sultan C (2002) Molecular action of androgens. Mol Cell Endocrinol 198:15–24
13. Greenberg C, Kukreja SC, Bowser EN, Hargis GK, Henderson WJ, Williams GA (1986) Effects of estradiol and progesterone on calcitonin secretion. Endocrinology 118:2594–2598
14. Groupe d'étude des tumeurs endocrines (2003) Cancers Médullaires de la Thyroïde et Néoplasies Endocriniennes Multiples de type 2: recommandations pour la prise en charge diagnostique et thérapeutique. In: Groupe d'étude des tumeurs endocrines (ed) http://www.sf-endocrino.net/index1.php?pageID=sommaire_gte
15. Guyetant S, Wion-Barbot N, Rousselet MC, Franc B, Bigorgne JC, Saint-Andre JP (1994) C-cell hyperplasia associated with chronic lymphocytic thyroiditis: a retrospective quantitative study of 112 cases. Hum Pathol 25:514–521
16. Guyetant S, Rousselet MC, Durigon M, Chappard D, Franc B, Guerin O, Saint-Andre JP (1997) Sex-related C-cell hyperplasia in the normal human thyroid: a quantitative autopsy study. J Clin Endocrinol Metab 82:42–47
17. Guyetant S, Josselin N, Savagner F, Rohmer V, Michalak S, Saint-Andre JP (2003) C-cell hyperplasia and medullary thyroid carcinoma: clinicopathological and genetic correlations in 66 consecutive patients. Mod Pathol 16:756–763
18. Guyetant S, Blechet C, Saint-Andre JP (2006) C-cell hyperplasia. Ann Endocrinol (Paris) 67:1–8
19. Iacobone M, Niccoli-Sire P, Sebag F, De Micco C, Henry JF (2002) Can sporadic medullary thyroid carcinoma be biochemically predicted? Prospective analysis of 66 operated patients with elevated serum calcitonin levels. World J Surg 26:886–890
20. Ishibashi H, Suzuki T, Suzuki S, Moriya T, Kaneko C, Takizawa T, Sunamori M, Handa M, Kondo T, Sasano H (2003) Sex steroid hormone receptors in human thymoma. J Clin Endocrinol Metab 88:2309–2317
21. Jensen EV, Cheng GJ, Palmieri C, Saji S, Makela S, Van Noorden S, Wahlstrom T, Warner M, Coobes RC, Gustafsson JA (2001) Estrogen receptors and proliferation markers in primary and recurrent breast cancer. Proc Natl Acad Sci U S A 98:15197–15202
22. Kaserer K, Scheuba C, Neuhold N, Weinhausel A, Vierhapper H, Haas OA, Niederle B (1998) C-cell hyperplasia and medullary thyroid carcinoma in patients routinely screened for serum calcitonin. Am J Surg Pathol 22:722–728
23. Kawabata W, Suzuki T, Moriya T, Fujimori K, Naganuma H, Inoue S, Kinouchi Y, Kameyama K, Takami H, Shimosegawa T, Sasano H (2003) Estrogen receptors (alpha and beta) and 17beta-hydroxysteroid dehydrogenase type 1 and 2 in thyroid disorders: possible in situ estrogen synthesis and actions. Mod Pathol 16:437–444
24. Kotzmann H, Schmidt A, Scheuba C, Kaserer K, Watschinger B, Soregi G, Niederle B, Vierhapper H (1999) Basal calcitonin levels and the response to pentagastrin stimulation in patients after kidney transplantation or on chronic hemodialysis as indicators of medullary carcinoma. Thyroid 9:943–947
25. Kuiper GG, Enmark E, Pelto-Huikko M, Nilsson S, Gustafsson JA (1996) Cloning of a novel receptor expressed in rat prostate and ovary. Proc Natl Acad Sci USA 93:5925–5930
26. Kuiper GG, Gustafsson JA (1997) The novel estrogen receptor-beta subtype: potential role in the cell- and promoter-specific actions of estrogens and anti-estrogens. FEBS Lett 410:87–90
27. Levin ER (2001) Cell localisation, physiology, and nongenomics actions of estrogen receptors. J Appl Physiol 91:1860–1867
28. Lissak B, Baudin E, Cohen R, Barbot N, Meyrier A, Niccoli P, Bouyge N, Modigliani E (1998) Pentagastrin testing in patients with renal insufficiency: normal responsivity of mature calcitonin. Thyroid 8:265–268
29. Manole D, Schildknecht B, Gosnell B, Adams E, Derwahl M (2001) Estrogen promotes growth of human thyroid tumor cells by different molecular mechanisms. J Clin Endocrinol Metab 86:1072–1077
30. Mulac-Jericevic B, Conneely OM (2004) Reproductive tissue selective actions of progesterone receptors. Reproduction 128:139–146
31. Nasser SM, Faquin WC, Dayal Y (2003) Expression of androgen, estrogen, and progesterone receptors in salivary gland tumors. Frequent expression of androgen receptor in a subset of malignant salivary gland tumors. Am J Clin Pathol 119:801–806
32. Niccoli P, Brunet P, Roubicek C, Roux F, Baudin E, Lejeune PJ, Berland Y, Conte-Devolx B (1995) Abnormal calcitonin basal levels and pentagastrin response in patients with chronic renal failure on maintenance hemodialysis. Eur J Endocrinol 132:75–81
33. Perry A, Molberg K, Albores-Saavedra J (1996) Physiologic versus neoplastic C-cell hyperplasia of the thyroid: separation of distinct histologic and biologic entities. Cancer 77:750–756
34. Rosai J, Carcangu ML, DeLellis RA (1992) C-cell hyperplasia. In: Rosai J, Carcangu ML, DeLellis RA (eds) Tumours of the thyroid gland. Armed Forced Institute of Pathology, Washington, DC, pp 247–258
35. Santeusiano G, Iafrate E, Partenzi A, Mauriello A, Autelitano F, Spagnoli LG (1997) A critical reassessment of the concept of C-cell hyperplasia of the thyroid. A quantitative immunohistological study. Appl Immunohistochem 5:160–172
36. Skliris G, Parkes A, Limer J, Burdall S, Carder P, Speirs V (2002) Evaluation of seven oestrogen receptor β antibodies for immunohistochemistry, western blotting, and flow cytometry in human breast tissue. J Pathol 197:155–162
37. Taylor AH, Al-Azzawi F (2000) Immunolocalisation of oestrogen receptor beta in human tissues. J Mol Endocrinol 24:145–155
38. Tomita T, Millard DM (1992) C-cell hyperplasia in secondary hyperparathyroidism. Histopathology 21:469–474
39. Vierhapper H, Raber W, Bieglmayer C, Kaserer K, Weinhausl A, Niederle B (1997) Routine measurement of plasma calcitonin in nodular thyroid diseases. J Clin Endocrinol Metab 82:1589–1593
40. Weitsman G, Skliris G, Ung K, Peng B, Younes M, Watson P, Murphy L (2006) Assessment of multiple different estrogen receptor-beta antibodies for their ability to immunoprecipitate under chromatin immunoprecipitation conditions. Breast Cancer Res Treat 100:23–31
41. Wolfe HJ, Melvin KE, Cervi-Skinner SJ, Saadi AA, Juliar JF, Jackson CE, Tashjian AH Jr (1973) C-cell hyperplasia preceding medullary thyroid carcinoma. N Engl J Med 289:437–441
42. Wolfe HJ, DeLellis RA, Scott RT, Tashjian AH Jr (1975) C-cell hyperplasia in chronic hypercalcemia in man. Am J Pathol 78:20a
43. Yang K, Pearson CE, Samaan NA (1988) Estrogen receptor and hormone responsiveness of medullary thyroid carcinoma cells in continuous culture. Cancer Res 48:2760–2763
44. Zhai QH, Ruebel K, Thompson GB, Lloyd RV (2003) Androgen receptor expression in C-cells and in medullary thyroid carcinoma. Endocr Pathol 14:159–165

Virchows Arch (2007) 450:441–447
DOI 10.1007/s00428-007-0372-0

ORIGINAL ARTICLE

Study of the reactive dendritic cells in small B-cell lymphoproliferations of the skin

Amélie Carbonnelle · Nadine Martin-Garcia · Nicolas Ortonne · Liliane Laroche · Martine Bagot · Valérie Molinier-Frenkel · Janine Wechsler

Received: 17 August 2006 / Revised: 4 January 2007 / Accepted: 12 January 2007 / Published online: 15 February 2007
© Springer-Verlag 2007

Abstract Distinguishing between low-grade primary cutaneous B-cell lymphoma (LG-pCBCL) and cutaneous lymphoid hyperplasia (CLH) based on histological features is often difficult. CLH lesions contain numerous reactive cells of the histiocyte lineage [Langerhans cells (LC), dermal dendritic cells (DDC), and macrophages], which are also often present in CBCL. The aim of this study was to determine whether immunohistochemical detection of those cells could help differentiate between CLH and LG-pCBCL. We determined the percentages of those histiocytic cells in the dermal infiltrates of 45 cases of cutaneous lymphoproliferations comprising 16 CLH and 29 LG-pCBCL (19 follicle-center cell lymphomas and 10 marginal zone lymphomas) by immunohistochemical labeling with antibodies to CD1a, FXIIIa, and CD68 to respectively detect LC, DDC, and macrophages. To avoid observer-dependent bias, an automated morphometric analysis method was used to recognize immunoreactive cells and calculate their percentages within the infiltrate. $FXIIIa^+$ cells were significatively more frequent in CLH than in LG-pCBCL, whereas $CD1a^+$ and $CD68^+$ cell frequencies were comparable in the two groups. The results of our study suggest that DDC might play an important role in the genesis of cutaneous lymphomas.

Keywords Dermathopathology · Lymphoma · Morphometry

Abbreviations

CLH	cutaneous lymphoid hyperplasia
CTCL	cutaneous T cell lymphoma
DC	dendritic cell
DDC	dermal dendritic cell
FCL	follicle-center cell lymphoma
LC	Langerhans cell
LG-pCBCL	low-grade primary cutaneous B cell lymphoma
MF	mycosis fungoides
MZL	marginal zone lymphoma

Introduction

Distinguishing between low-grade primary cutaneous B-cell lymphoma (LG-pCBCL) and cutaneous lymphoid hyperplasia (CLH) represents a challenging diagnostic difficulty in dermatopathology. CLH, also called pseudo-lymphoma, lymphocytoma cutis, or lymphadenosis benigna

A. Carbonnelle · N. Martin-Garcia · N. Ortonne · J. Wechsler
Département de Pathologie, Hôpital Henri Mondor, VI AP-HP, Université Paris XII,
Créteil, France

L. Laroche
Service de Dermatologie, Hôpital Avicenne,
Bobigny, France

M. Bagot
Service de Dermatologie, Hôpital Henri Mondor, VI AP-HP, Université Paris XII,
Créteil, France

V. Molinier-Frenkel
Service d'Immunologie Biologique, Hôpital Henri Mondor, VI AP-HP, Université Paris XII,
Créteil, France

J. Wechsler (✉)
Department of Pathology, Hôpital Henri Mondor,
51, avenue du Maréchal de Lattre de Tassigny,
94010 Créteil cedex, France
e-mail: janine.wechsler@hmn.ap-hop-paris.fr

cutis, refers to a heterogeneous group of benign reactive T- and B-cell lymphoproliferative processes of diverse etiologies (arthropod bites, infectious agents, drug- or allergen-derived antigens, or trauma) that clinically and histologically simulate lymphomas. According to the World Health Organization and European Organization for Research on the Treatment of Cancer (WHO–EORTC) classification of primary cutaneous lymphoma, LG-CBCL comprises two subgroups: follicle-center cell lymphomas (FCL) and marginal zone lymphomas (MZL) [18]. Other CBCLs are high-grade lymphomas: large B-cell lymphoma, leg-type; FCL, diffuse type; large B-cell lymphoma, other; and intravascular large B-cell lymphoma. These high-grade cutaneous lymphomas do not represent a diagnostic problem with CLH because they are composed of large cells.

Differentiation between LG-pCBCL and CLH based on histological features can be very difficult. Traditional histological criteria for malignancy include cellular monomorphism, cytological atypia, and diffuse dermal infiltration [10], but lesions present atypical features that make a definitive diagnostic difficult, if not impossible. Determination of light-chain immunoglobulin restriction may be a decisive diagnostic tool but is difficult to achieve in the absence of plasma cells and has no absolute value [12, 15]. Recent advances in molecular genetics have emerged as an important tool to overcome these diagnostic dilemmas, particularly the determination of clonality of lymphoid infiltrates. In the past, these techniques required fresh, unfixed tissue for optimal application. Nowadays, they can be performed on fixed, routinely processed specimens. However, the demonstration of clonality does not necessarily indicate malignancy. Indeed, several pseudolymphomas with clonal lymphoid proliferations have been reported [1, 5, 11, 17, 20].

Reactive cells are known to be frequent in LG-pCBC [8, 14] and often mask tumor cells. They comprise small T lymphocytes and cell of the histiocyte lineage [macrophages and dendritic cells (DC)]. Among the reactive cells, macrophages and DC could help distinguish between CLH and LG-pCBCL. Indeed, these cells play major roles in antigen processing and presentation to T cells and might do so in lymphoproliferations. DC in skin comprise $CD1a^{+}FXIIIa^{-}$ Langerhans cells (LC), mostly present in the epidermis, and $CD1a^{-}FXIIIa^{+}$ dermal dendritic cells (DDC), mostly found in the upper dermis.

DC number and distribution have been thoroughly studied in T-cell infiltrates. Indeed, it has been shown that LC and DDC were more abundant in mycosis fungoides (MF) lesions [4] and that the number of $CD1a^{+}$ cells was possibly useful for the differential diagnosis between cutaneous T-cell lymphoma (CTCL) and pseudo-CTCL [9]. In contrast, DC have not been extensively studied in B-cell infiltrates. The number of DC in benign versus malignant B-cell lymphoproliferations was evaluated in only one study that demonstrated a distinct pattern of CD1a labeling in B-cell lymphoma versus pseudolymphoma infiltrates that might be of value in the differential diagnosis of these skin disorders [13]. Macrophages in cutaneous infiltrates have not been extensively studied. Only one study showed that macrophages are more numerous in CLH than in B- or T-cell lymphoma [14].

In this study, we investigated the percentages of DDC, LC, and macrophages in cutaneous lymphoproliferations using an automated morphometric analysis method to recognize and

Table 1 Clinical, molecular, and immunohistochemical data for 16 CLH patients

Number	Age	Sex	Site	Initial treatment	GR	Kappa/ lambda	CD1a (%)	FXIIIa (%)	CD68 (%)
1	47	F	Temple	Topical corticosteroid	−	−	1.6	0	15.6
2	44	M	Ear	Plaquenil	NA	NA	0.1	1	13.6
3	48	F	Lip	Surveillance	−	NA	0.4	ND	10.8
4	56	F	Cheek	Unknown	−	NA	1	3.7	9.4
5	24	M	Nose	Surveillance	NA	NA	3	0	25.4
6	10	M	Leg, shoulder	Antiseptic	−	−	ND	1.6	30.2
7	14	F	Ankle	Topical corticosteroid	−	NA	6.9	1.4	10.3
8	46	M	Face	Topical corticosteroid antibiotic	−	−	4.4	0.9	18.3
9	44	F	Thorax, hand, head neck	Topical corticosteroid	−	NA	0	2.7	7.6
10	62	M	Thorax	Topical corticosteroid	−	−	6.6	3.3	14.6
11	58	M	Thorax	Unknown	−	NA	ND	9.73	14.1
12	25	F	Leg	Surveillance	+	NA	8.7	14.1	16.6
13	32	M	Arm	Unknown	−	Kappa	ND	1.8	6.9
14	71	F	Eyebrow	Topical corticosteroid	+	NA	ND	0	6.6
15	67	F	Thorax	Topical corticosteroid	+	−	0.6	0	22.1
16	65	F	Arm	Antibiotic	−	NA	0	ND	13.9

F Female; *M* male; *NA* not available; − absent; + present; *ND* not done (below detection limit); *GR* gene rearrangement

Table 2 Clinical, histological, molecular, and immunohistochemical data for 19 FCL patients

Number	Age	Sex	Site	Initial treatment	Cell size	GR	Kappa/ lambda	CD1a (%)	FXIIIa (%)	CD68 (%)
1	70	F	Thigh	Radiation	Small	NA	NA	ND	0	8.2
2	74	F	Arm	Radiation	Small	−	Kappa	8.7	1.1	16.6
3	49	M	Cheek	Radiation	Small	+	Lambda	6.9	1.6	10.3
4	80	M	Scalp	Chemotherapy, radiation	Small	+	NA	0	0	14,7
5	58	F	Neck	Radiation	Large	+	NA	0.3	0	8,6
6	57	M	Back, side, sus umbilical	Topical corticosteroids	Small	NA	NA	0.5	0	5,2
7	68	F	Shoulder	Excision	Large	+	NA	0	0	5,8
8	58	M	Scalp	Radiation	Large	+	NA	8.4	0.9	3.2
9	50	M	Leg	Excision	Large	+	NA	0	0.6	6.9
10	39	M	Temple	Radiation	Small	+	NA	3	0	25.4
11	59	M	Lower back	Excision	Small	+	NA	0	0	13.9
12	78	F	Breast	Radiation	Large	+	NA	0.8	0	18.8
13	42	F	Scalp	Topical corticosteroids	Large	+	NA	7.9	0	11.9
14	68	F	Scalp and neck	Chemotherapy, topical corticosteroids	Small	+	NA	0	0	5
15	73	M	Nose	Radiation	Small	+	NA	3.4	0	9.8
16	44	M	Scalp, back and thorax	Chemotherapy	Large	+	NA	0	1.4	10.5
17	64	F	Thigh	Topical corticosteroids	Small	+	NA	1.4	1.7	5
18	57	M	Chest, arm	Topical corticosteroids	Small	+	NA	4.6	0	22.7
19	44	F	Temple	Radiation	Small	−	Lambda	0.3	2.3	8.6

F Female; *M* male; *NA* not available; − absent; + present; *ND* not done (below detection limit); *GR* gene rearrangement

count immunoreactive cells. Hypothesizing that secondary to persistent antigenic stimulation arises from CLH, we advanced that histiocytic cells should be more abundant in CLH than LG-pCBCL, and we attempted to determine whether the immunohistochemical detection of the histiocytic cells could be helpful in differentiating between CLH and LG-pCBCL.

Materials and methods

Specimens

Forty-five cutaneous lymphoproliferations were retrieved from our department pathology files by means of a computer search for cases that had been coded CLH, FCL, or MZL between 1996 and 2003. The patients originated from two dermatology departments. Clinical data were available for all of them. The diagnoses were 16 CLH and 29 LG-pCBCL, comprising 19 FCL and 10 MZL, according to WHO–EORTC classification. All the skin specimens showed nodular or diffuse dermal lymphocytic infiltrates and were reviewed by the pathologists of the French Study Group for Cutaneous Lymphomas. All cases were classified according to classical morphological and immunohistochemical criteria using the routine B-cell markers CD 20, CD 79a, Bcl6, and CD 138 [8].

Table 3 Clinical, molecular, and immunohistochemical data from MZL patients

Age	Sex	Site	Initial treatment	GR	Kappa/lambda	CD1a(%)	FXIIIa(%)	CD68(%)
78	F	Arm	Surveillance	−	Kappa	0.8	1.6	11
73	M	Leg	Radiation	+	Kappa	ND	1.2	1.2
57	M	Back	Topical corticosteroid + oral corticotherapy	ND	Lambda	ND	0.42	22.5
59	F	Back	Topical corticosteroid	ND	Kappa	7.9	0	11.9
52	M	Arm	Topical corticosteroid	+	Kappa	0.2	1.5	13
81	F	Arm, back and shoulder	Topical corticosteroid	+	Kappa	0	0.7	10.7
79	F	Arm	Excision, topical corticosteroid	−	Kappa	8.4	2.7	3.2
72	M	Back, buttock	Radiation	−	Kappa	ND	0	14.7
73	F	Cheek	Surveillance	+	ND	0	0	7.6
39	M	Shoulder	Excision	+	−	9.9	1.37	13.9

F Female; *M* male; *NA* not available; − absent; + present; *ND* not done (below detection limit); *GR* gene rearrangement

Morphology and immunochemistry

All tissue samples had been formalin-fixed and paraffin-embedded for standard morphology and immunohistochemistry. The primary antibodies used were directed against CD68 (monoclonal, clone KP1 diluted 1/50; Dako, Glustrup, Denmark), CD1a (monoclonal, clone 010, pre-diluted; Immunotech, Coulter, France) and Factor XIIIa (rabbit polyclonal diluted 1:200; Nordic Laboratories, Tilburg, The Netherlands), followed by immunoperoxidase labeling according to the alkaline phosphatase-conjugated avidin–biotin-complex procedure (Vectastain kit, Vector Laboratories, Burlingame, CA, USA). Antigen retrieval was performed in citrate buffer at pH 6 (ChemMate, Dako) in a 900 W microwave oven (Whirlpool VIP 20, Benton Harbor, USA; 3×5 min) before CD68 or CD1a antibody incubation.

Morphometric analysis

Immunoreactive cells were detected using a fully automated image analysis system including a microscope (Nikon E400, Tokyo), an XYZ motorized stage with a four-slide holder mounted on the microscope, a motorized filter wheel, a CCD high-resolution monochrome camera (Hamamatsu, C8484, Iwata City, Japan), a PC Pentium 4, and the Morphoscan software (provided by Imstar, Paris, France; http://www.imstar.fr). For slide scanning, the area to be scanned was selected as the zone where the infiltrate was densest. Nine color images of 1,280×1,024 pixels at 1.7 μm resolution (400× magnification) within this selected area were captured using superposition of the three-color filters (red, green, and blue). The immunoreactive cells ($CD1a^+$, $FXIIIa^+$, or $CD68^+$) were detected using the green filter. The total number of cells composing the infiltrate (lymphocytes and histiocytic cells) was determined with the red filter by the MorphoScan module software for automated recognition of each cell's contour according to its density and morphological criteria.

Statistical analysis

Statistical analysis was conducted using software package Staview (Abacus Concepts, Berkeley, CA, USA). For each marker (CD1a, FXIIIa, or CD68), the percentage of positive cells detected within the dermal infiltrate was calculated for each specimen as the number of positive cells/total number of infiltrating cells, and the mean percent was calculated for each of the three groups (CLH, FCL, and MZL). One-way analysis of variance and Fisher's exact test were used to establish differences among the three subgroups. Student's *t* test was applied to determine for the differences between CLH and LG-pCBCL (FCL + MZL). A difference was considered statistically significant when $P<0.05$.

Results

For CLH, FCL, and MZL, clinical, molecular, and immunohistochemical data are detailed respectively in Tables 1, 2 and 3.

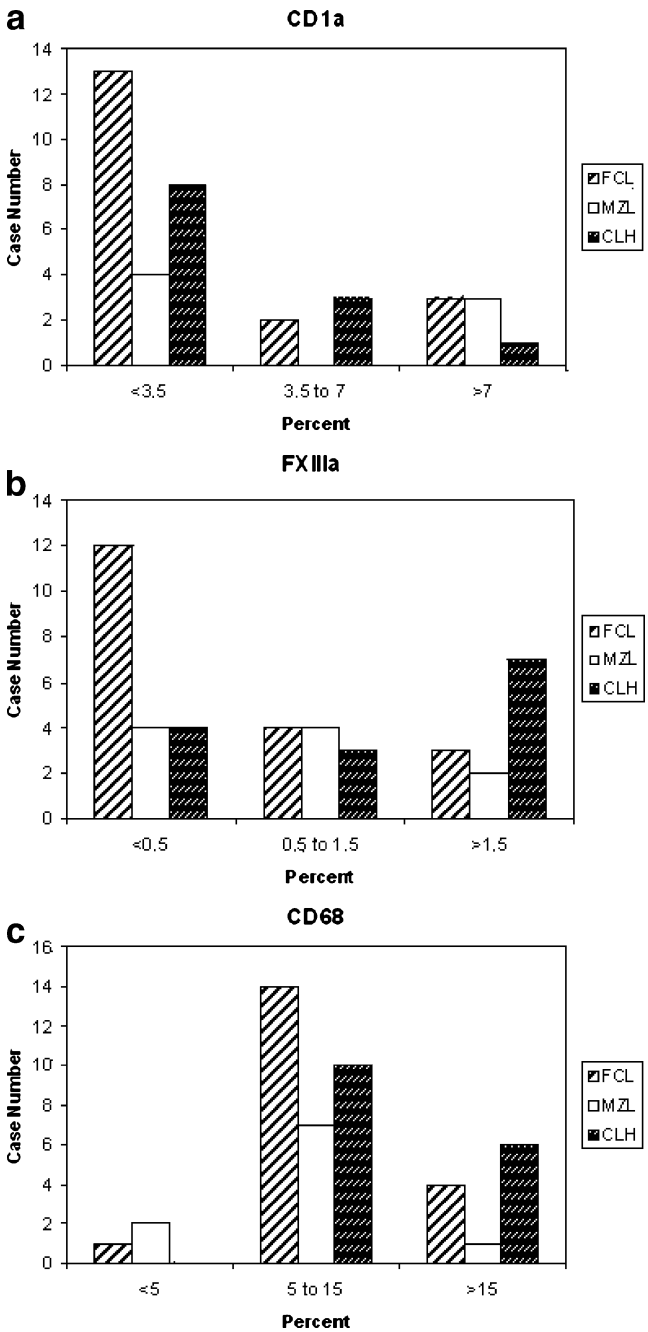

Fig. 1 Distribution of the percentages of $CD1a^+$ (**a**), $FXIIIa^+$ (**b**), and $CD68^+$ (**c**) cells in the dermal infiltrates according to the diagnosis of CLH, FCL, and MZL

Table 4 Mean percentages of $CD1a^+$, $CD68^+$, and $FXIIIa^+$ cells in the CLH, FCL, MZL, and LG-pCBCL (MZL + FCL) dermal infiltrates

	LCH	FCL	MZL	LG-pCBCL
CD1a	2.8	2.6	3.9	3.3
CD68	14.3	11.1	11	11
FXIIIa	2.9	0.5	0.9	0.7

CD1a Labeling

$CD1a^+$ cells showed a dendritic shape. They were often larger than epidermal $CD1a^+$ cells and were dispersed within the dermal infiltrate, with often a peri annexal concentration. Only few cells were localized out of the infiltrate.

For all the three groups, most samples had <3.5% immunoreactive cells (Fig. 1a). The mean $CD1a^+$ cell percentages were equal in the three groups (Table 4). The mean percentage for LG-pCBCL did not differ significantly from that of CLH (P=0.90). Eight samples (one FCL, three MZL, and four CLH) showing weak immunoreactivity below the detection limit were not taken into account to calculate the mean percentage. An example of software-scanned immunohistochemical labeling of CD1a in an FCL is shown in Fig. 2a and b.

FXIIIa labeling

Most $FXIIIa^+$ cells were fusiform with an elongated nucleus. Larger cells with plump cytoplasm and round nucleus were also often present. The cells were dispersed within the dermal infiltrate and were more numerous at the periphery of the infiltrate. A small number of sparse $FXIIIa^+$ cells were also present out of the infiltrate.

Most MZL and FCL samples had <0.5% immunoreactive cells, whereas most CLH specimens had >1.5% immunoreactive cells (Figs. 1b and 3). The mean percentage was higher for CLH than FCL or MZL (Table 4). The mean CLH percentage was significantly higher than that of LG-pCBCL (P=0.0072). In two CLH specimens, the immunoreactivity was weak and below the detection limit; they were not taken into account to calculate the mean percentages. Typical light microscopy images of immunohistochemical labeling of FXIIIa in FCL and CLH infiltrates are shown in Fig. 4a and b.

CD68 labeling

$CD\ 68^+$ cells were not only mainly located within the dermal infiltrate, but were also numerous out of the infiltrate. They appeared dispersed and often aggregated within the infiltrate.

Most FCL, MZL, and CLH samples had between 5 and 15% immunoreactive cells (Fig. 1c). Software-scanned images of $CD68^+$ cells in a CLH lesion are shown in Fig. 2c and d. The mean $CD68^+$ cell percentage was higher for CLH than FCL and or MZL (Table 4), but no significant difference was observed (P=0.0655).

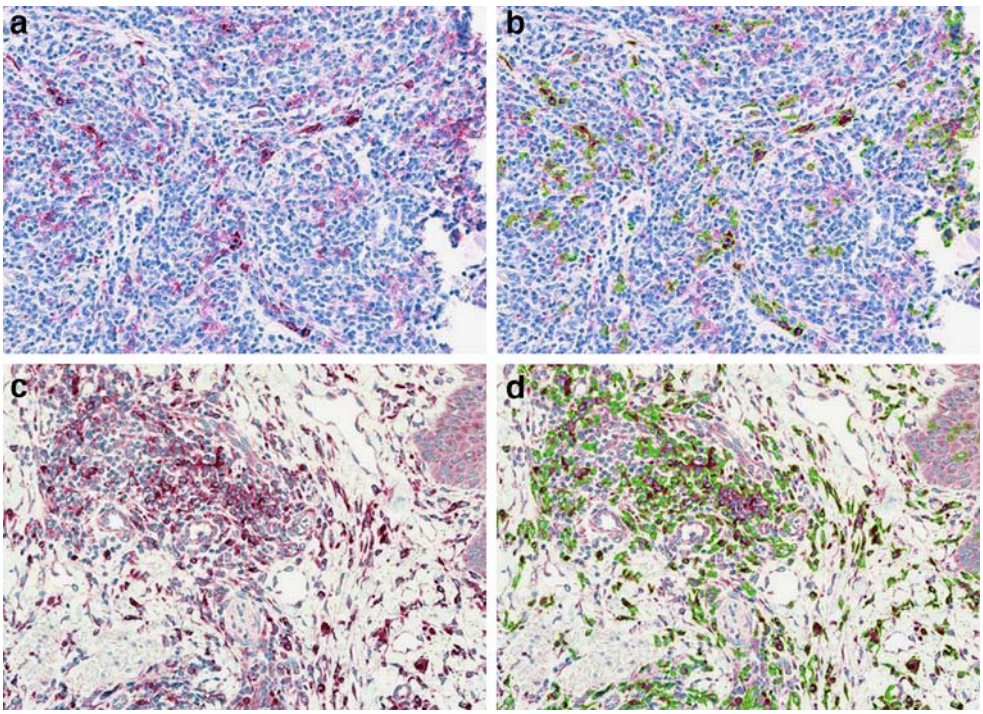

Fig. 2 Detection of $CD1a^+$ cells in FCL (**a**, **b**) and $CD68^+$ cells in CLH (**c**, **d**). Panels **a** and **c** show the areas of the slides scanned by the software; $CD1a^+$ (**b**) and $CD68^+$ (**d**) cells detected by the software in the scanned area are surrounded by *green*

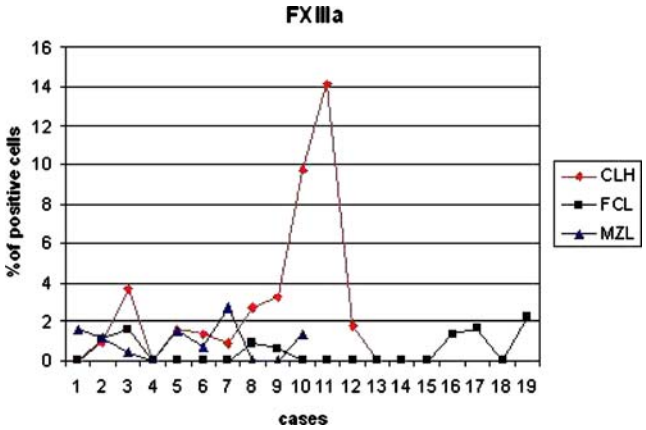

Fig. 3 FXIIIa$^+$ reactivity in CLH, FCL, and MZL cases

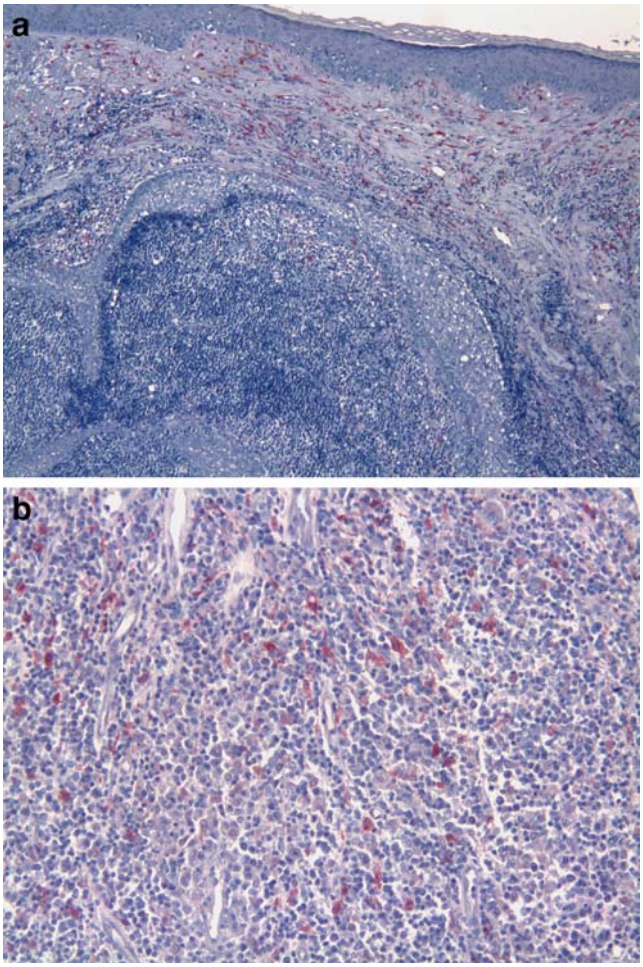

Fig. 4 Immunolabeling of anti FXIIIa. In FCL (**a**), no FXIIIa$^+$ cell was seen within the infiltrate, only a few positive cells were observed in the reticular dermis surrounding it. In CLH (**b**), numerous FXIIIa$^+$ cells were located within and around the infiltrate

Discussion

Differentiating benign from malignant cutaneous infiltrates is difficult in dermatopathology. In the present study, we investigated the respective percentages of LC, DDC, and macrophages in the dermal infiltrates of CLH and LG-pCBCL (MZL and FCL) using immunohistochemical methods and morphometric analysis. We found that FXIIIa$^+$ cells, corresponding to DDC, were significantly more frequent in CLH than in LG-pCBCL infiltrates. Nevertheless, Fig. 3 shows that, whereas FCL clearly display lower percentage of positive cells, some cases of MZL display a relative overlap with cases of CLH. In contrast, the percentages of CD1a$^+$ and CD68$^+$ cells within the infiltrates did not differ significantly for CLH and LG-pCBCL.

DDC constitute a heterogeneous population of antigen-presenting cells, distinct from LC, that are located in the upper part of the reticular dermis and have a perivascular distribution [16]. DDC have been implicated in dermal inflammation and MF lesions [2, 4], and FXIIIa$^+$ cells are expanded in the upper dermis of MF and psoriasis lesions [4]. Notably, the presence and possible implication of DDC in B-cell infiltrates had not been studied previously. Our findings suggest that DDC might play a role in B-cell lymphoproliferations throughout a persistent antigenic stimulation. Some authors have previously suggested that there is a spectrum of B-cell lymphoproliferative diseases. Indeed, CLH patients may progress occasionally to overt cutaneous lymphoma [6, 7]. Nihal et al. detected clonality in 27 of 44 CLH cases that they called "clonal CLH." One of these "clonal CLH" cases developed overt CBCL. The same dominant IgH gene rearrangement was present in the initial CLH and the subsequent CBCL lesions, indicating that "clonal CLH" may undergo clonal evolution to CBCL [7]. However, only few cases of "clonal CLH" progress to lymphoma and most cases disclose a benign evolution. The progression of CLH to lymphoma might be influenced by the host histiocytic reaction. Indeed, the persistent antigenic stimulation mediated by DDC might induce an unbalanced proliferation of lymphoid cells. As a consequence, an oligoclonal phase might emerge, before genetic instability with somatic mutations and evolution into a clonal malignancy [20]. Based on that hypothesis, the number of DC should decrease with malignant evolution. Previously, Wirt et al. [19] evaluated LC presence in the epidermis and dermis in cutaneous pseudolymphomas and found it enhanced. Others suggested that the abundance of CD1a$^+$ cells might be useful in the differentiation between CTCL and pseudo-CTCL [9]. Drijkoningen et al. [3] quantified DC (LC and DDC) and their distributions in benign and malignant cutaneous lymphoproliferations. They found that DC were more numerous in T-cell infiltrates than B-cell infiltrates. Moreover, in T-cell infiltrates, they noted different DC distributions in malignant and inflammatory infiltrates, with larger, more loosely arranged DC aggregates seen in malignant lesions. Smolle J et al. [14] investigated the distribution of non-lymphoid accessory cells in 35 lymphoproliferative disease specimens using

immunohistochemical methods. They found that DC were abundant in cutaneous B- and T-cell lymphomas and associated with T lymphocytes, especially T-helper cells. Macrophages were also plentiful in both B- and T-cell lymphomas and pseudolymphomas, but were more abundant in cutaneous pseudolymphomas than in B- or T-cell lymphomas. Schmuth et al. [13] found $CD1a^+$ cells to be significantly more enhanced in CLH than in T- or B-cell lymphomas. We found that only the percentage of $FXIIIa^+$ cells was increased in CLH, while that of $CD1a^+$ cells did not differ significantly between CLH and LG-pCBCL. One explanation for this discrepancy might be that we had too few cases. Indeed, for eight of the samples tested, CD1a immunoreactivity was below the detection limit of the software. Another explanation might be that those authors had included secondary and primary B-cell lymphomas, which usually have few reactive cells. In contrast, we chose to focus on LG-pCBCL, which are responsible for the majority diagnostic difficulties. Moreover, we also determined the percentages of non-lymphoid reactive cells using an automated morphometric analysis, which is not observer-dependent.

In conclusion, we found that the percentage of $FXIIIa^+$ cells was significantly higher in CLH versus LG-pCBCL. Nevertheless, because of the presence of a relative overlap between CLH and MZL cases, the FXIIIa immunostaining might not be useful for the routine diagnosis of individual cases.

Besides, the results of our study suggest that DDC might play an important role in the genesis of cutaneous lymphomas.

Acknowledgments We thank Olivier Hongtuanha and Charles Homsi (IMSTAR company) for technical help.

References

1. Bouloc A, Delfau-Larue MH, Lenormand B, Meunier F, Wechsler J, Thomine E, Revuz J, Farcet JP, Joly P, Bagot M (1999) Polymerase chain reaction analysis of immunoglobulin gene rearrangement in cutaneous lymphoid hyperplasias. French Study Group for Cutaneous Lymphomas. Arch Dermatol 135:168–172
2. Cerio R, Griffiths CE, Cooper KD, Nickoloff BJ, Headington JT (1989) Characterization of factor XIIIa positive dermal dendritic cells in normal and inflamed skin. Br J Dermatol 121:421–431
3. Drijkoningen M, de Wolf-Peeters C, Snauwaert J, de Greef H, Desmet V (1987) Immunohistochemical study of epidermal Langerhans cells and dermal dendritic cells in benign and malignant skin lesions characterized by a dermal lymphoid infiltrate consisting either of B-cells or T-cells. Virchows Arch A Pathol Anat Histopathol 411:337–343
4. Fivenson DP, Nickoloff BJ (1995) Distinctive dendritic cell subsets expressing factor XIIIa, CD1a, CD1b and CD1c in mycosis fungoids and psoriasis. J Cutan Pathol 22:223–228
5. Flaig MJ, Schuhmann K, Sander CA (2000) Impact of molecular analysis in the diagnosis of cutaneous lymphoid infiltrates. Semin Cutan Med Surg 19:87–90
6. Gilliam AC, Wood GS (2000) Cutaneous lymphoid hyperplasias. Semin Cutan Med Surg 19:133–141
7. Nihal M, Mikkola D, Horvath N, Gilliam AC, Stevens SR, Spiro TP, Cooper KD, Wood GS (2003) Cutaneous lymphoid hyperplasia: a lymphoproliferative continuum with lymphomatous potential. Hum Pathol 34:617–622
8. Pimpinelli N, Romagnoli P, Moretti S, Giannotti B (1988) Non-lymphoid accessory cells in the cutaneous infiltrate of B-cell lymphomas. An immunohistochemical and ultrastructural study. Br J Dermatol 118:353–362
9. Rijlaarsdam JU, Scheffer E, Meijer CJ, Willemze R (1992) Cutaneous pseudo-T-cell lymphomas. A clinicopathologic study of 20 patients. Cancer 69:717–724
10. Ritter JH, Adesokan PN, Fitzgibbon JF, Wick MR (1994) Paraffin section immunohistochemistry as an adjunct to morphologic analysis in the diagnosis of cutaneous lymphoid infiltrates. J Cutan Pathol 21:481–493
11. Ritter JH, Wick MR, Adesokan PN, Fitzgibbon JF, Zhu X, Humphrey PA (1997) Assessment of clonality in cutaneous lymphoid infiltrates by polymerase chain reaction analysis of immunoglobulin heavy chain gene rearrangement. Am J Clin Pathol 108:60–68
12. Schmid U, Eckert F, Griesser H, Steinke C, Cogliatti SB, Kaudewitz P, Lennert K (1995) Cutaneous follicular lymphoid hyperplasia with monotypic plasma cells. A clinicopathologic study of 18 patients. Am J Surg Pathol 19:12–20
13. Schmuth M, Sidoroff A, Danner B, Topar G, Sepp NT (2001) Reduced number of CD1a+ cells in cutaneous B-cell lymphoma. Am J Clin Pathol 116:72–78
14. Smolle J, Kaudewitz P, Burg G, Kresbach H, Kerl H (1985) Significance of non-lymphoid ('accessory') cells in malignant lymphomas and pseudolymphomas of the skin. Br J Dermatol 113:677–85
15. Slater DN (1992) Diagnostic difficulties in 'non-mycotic' cutaneous lymphoproliferative diseases. Histopathology 21:203–213
16. Valladeau J, Saeland S (2005) Cutaneous dendritic cells. Semin Immunol 17:273–83
17. Wechsler J, Bagot M, Henni T, Le Couedic JP, Gaulard P, Zafrani ES (1995) Gene analysis in 18 cases of cutaneous lymphoid infiltrates of uncertain significance. Arch Pathol Lab Med 119:157–162
18. Willemze R, Jaffe ES, Burg G, Cerroni L, Berti E, Swerdlow SH, Ralfkiaer E, Chimenti S, Diaz-Perez JL, Duncan LM, Grange F, Harris NL, Kempf W, Kerl H, Kurrer M, Knobler R, Pimpinelli N, Sander C, Santucci M, Sterry W, Vermeer MH, Wechsler J, Whittaker S, Meijer CJ (2005) WHO–EORTC classification for cutaneous lymphomas. Blood 105:3768–3785
19. Wirt DP, Grogan TM, Jolley CS, Rangel CS, Payne CM, Hansen RC, Lynch PJ, Schuchardt M (1985) The immunoarchitecture of cutaneous pseudolymphoma. Hum Pathol 16:492–510
20. Wood GS, Ngan BY, Tung R, Hoffman TE, Abel EA, Hoppe RT, Warnke RA, Cleary ML, Sklar J (1989) Clonal rearrangements of immunoglobulin genes and progression to B-cell lymphoma in cutaneous lymphoid hyperplasia. Am J Pathol 135:13–19

Virchows Arch (2007) 450:449–453
DOI 10.1007/s00428-007-0376-9

ORIGINAL ARTICLE

D2-40 labeling in lymphangiomyoma/lymphangiomyomatosis of the soft tissue: further evidence of lymphangiogenic tumor histogenesis

Torsten Hansen · Kathrin Katenkamp · Fernando Bittinger · C. James Kirkpatrick · Detlef Katenkamp

Received: 25 September 2006 / Revised: 4 December 2006 / Accepted: 23 January 2007 / Published online: 15 February 2007
© Springer-Verlag 2007

Abstract We examined ten cases of extrapulmonary lymphangioleiomyoma/lymphangioleiomyomatosis (LAM; all patients female; median age 46.5 years) for immunohistochemical labeling with a monoclonal antibody against podoplanin (D2-40), which is specific for lymphatic endothelial lining. We found positive staining in thin-wall branching vessels reflecting the lymphatic nature of tumor vessels in all cases tested. In contrast, perivascular (HMB-45 positive) myoid cells were not detected by D2-40. The D2-40 labeling confirms the current concept of lymphangiogenic origin of the tumor vessels in LAM. In addition, this study makes a further contribution to the immunohistochemical mapping of this antibody in vascular tumors. Finally, the use of this commercially available antibody provides an additional help in the differential diagnosis of LAM from other soft tissue tumors.

Keywords Lymphangio(leio)myoma · Lymphangio(leio)myomatosis · *Podoplanin* · D2-40 · Lymphatic tumor vessels

Introduction

Lymphangio(leio)myoma is a rare disorder that nearly always affects women, mostly in the premenopausal period [5, 17]. This tumor may occur as a localized form or as a widespread multisystem disease, then called lymphangio(leio)myomatosis (LAM). Lymphangio(leio)myoma/LAM belongs to the tumor family of so-called perivascular epithelioid cell tumors (PEComas), i.e., they show perivascular epithelioid cell differentiation [6, 10]. Besides LAM, this group comprises angiomyolipoma as well as pulmonary and extrapulmonary clear cell "sugar" tumors. The concept of this tumor family is based on perivascular epithelioid cells with myomelanocytic origin [6, 10, 17]. Therefore, these cells show a characteristic positivity for smooth-muscle actin and variably desmin as well as for the (pre-)melanosomal marker HMB-45 and/or melan-A [6, 10].

LAM is different from the other PEComas in that it always contains large numbers of thin-walled branching vessels, sometimes surrounded by lymph follicles [6, 16, 17]. It was therefore proposed that these vessels are of lymphatic origin. This was confirmed by the fact that especially extrapulmonary LAMs are very often closely associated with lymph nodes or large lymphatic vessels such as the thoracic duct [16]. In addition, Kumasaka et al. [13] showed strong expression of vascular endothelial growth factor receptor-3 (VEGFR-3) in the vessels of LAM. This molecule has been demonstrated to be a marker for lymphatic endothelial cells in human tissues. Kumasaka et al. furthermore showed extensive lymphangiogenesis in association with the myoid cells [13].

Besides VEGFR-3, a new monoclonal antibody, D2-40, plays an increasing role in the routine diagnostics of vascular soft-tissue tumors. D2-40 is directed against an oncofetal antigen (M2A antigen) [15]. This protein was subsequently identified on the surface of rat glomerular podocytes, and because it was found to be involved in the flattening of foot processes in puromycin-induced nephro-

T. Hansen (✉) · F. Bittinger · C. J. Kirkpatrick
Institute of Pathology, Johannes Gutenberg University of Mainz,
Langenbeckstr. 1,
55101 Mainz, Germany
e-mail: hansen@pathologie.klinik.uni-mainz.de

K. Katenkamp · D. Katenkamp
Institute of Pathology, Friedrich-Schiller-University of Jena,
Jena, Germany

sis, it was named podoplanin [18]. Recently, D2-40 has been shown to react with a fixation-resistant epitope on lymphatic endothelium [12]. It is now considered to be the best commercially available antibody for the delineation of lymphatic endothelial cells, and has been tested for several vascular tumors [12]. Although positivity has been found for lymphangioma [8, 11], Kaposi's sarcoma [8, 11], kaposiform hemangioendothelioma [4], hobnail hemangioma [7], and a subset of angiosarcomas [8, 11], labeling could not be demonstrated for hemangiomas, epitheloid hemangioendotheliomas, angiolipomas, and glomus tumors [8, 11]. Recently, sinonasal-type hemangiopericytoma could be further separated from the family of solitary fibrous tumors/hemangiopericytomas by the fact that the former commonly revealed strong labeling, whereas the latter did not at all [9]. However, until now, there are no reports concerning D2-40 labeling in LAM. We therefore analyzed LAM for D2-40 staining to contribute to immunohistochemical mapping of D2-40 in soft-tissue tumors and to confirm the lymphatic origin of this distinct tumor entity.

Materials and methods

The records from the Soft Tissue Tumor Registry of the Institute of Pathology in Jena and the records of the Institute of Pathology in Mainz were searched for cases coded as LAM of the soft tissue from 1995 to the present. We found ten cases (listed in Table 1) with a median age of 46.5 years. All patients were female. Tumors were mostly localized in the retroperitoneum (n=8), whereas one case was found in subcutaneous fat tissue of the neck, and one case was from the mediastinum. All tumors except one (patient no. 3) were found to diffusely involve soft tissues leading to the diagnosis of "lymphangioleiomyomatosis."

All specimens were prepared for routine histology using hematoxylin and eosin staining according to standard protocols. In brief, all tumors evaluated showed bundles of myoid cells, which were mostly arranged in a fascicular pattern. These bundles were surrounded by thin-walled and branching vessels (Fig. 1). Thus, these tumors showed the common and recently recapitulated morphological features of LAM [10].

Immunohistochemical staining was performed according to previous protocols [9] using the alkaline phosphatase-antialkaline phosphatase method. Besides D2-40, tissue specimens were investigated for expression of CD31, HMB-45, and α1-smooth-muscle actin (ASMA). Primary antibodies applied for immunohistochemical analysis are summarized in Table 2. D2-40 (Signet, Dedham, USA) was applied in a 1:400 dilution. Pretreatment by microwave (600 W, 3×5 min) was performed before the immunohistochemical procedure. Labeling was semiquantitatively analyzed and scored by one investigator (T.H.) as follows: no vessels/cells positive (=0), less than 20% of vessels/cells positive (=1), greater than 20% and less than 50% of vessels positive (=2), and greater than 50% of vessels positive (=3). Slides were evaluated and photographed by a Zeiss microscope (type Axiophot, Zeiss, Jena, Germany; digital camera Camedia, Olympus, Hamburg, Germany).

Results

In all cases, the typical morphological features of LAM were found as summarized above and shown in Fig. 1. Analysis of the immunohistochemical staining is summarized in Table 1. Strong expression of ASMA was demonstrated in the majority of myoid cells in nearly all patients (with more than 50% of cells positive in eight cases). In addition, this molecule was also strongly labeled in smooth muscle cells in the blood vessels (Fig. 2). By contrast, staining for HMB-45 was less intensive in the myoid cells. Most commonly, a diffuse staining pattern

Table 1 Patients' characteristics and scoring of the immunohistochemical labeling

Patient no.	Age	Sex	Localization	D2-40	CD31	ASMA	HMB-45
1	35	F	Retroperitoneum (neighborhood of vena cava)	2	2	3	1
2	75	F	Retroperitoneum (neighborhood of A. ilicia com)	3	3	3	ND
3	43	F	Retroperitoneum (NFS)	1	3	3	1
4	35	F	Retroperitoneum (NFS)	2	2	2	2
5	41	F	Mediastinum (between esophagus and parietal/visceral pleura)	2	ND	3	2
6	ND	F	Retroperitoneum (neighborhood of iliacal lymph nodes)	3	ND	3	2
7	51	F	Retroperitoneum (neighborhood of the left renal hilus)	2	ND	3	1
8	32	F	Retroperitoneum (NFS)	3	3	3	1
9	41	F	Retroperitoneum (lateral pelvis)	3	1	3	1
10	66	F	Right neck	3	2	2	1

ASMA α1-smooth-muscle actin, *F* female, *ND* no data; *NFS* not further specified

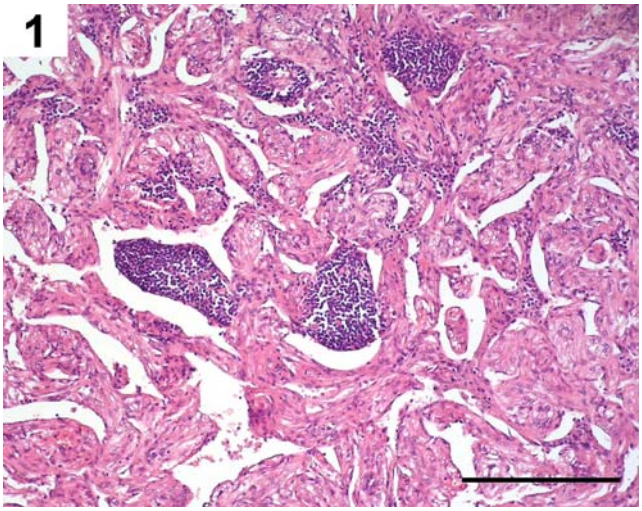

Fig. 1 Histological overview shows multiple branching vessels arranged around bundles of myoid cells as well as lymph follicles (HE; patient no. 9; *bar*=200 μm)

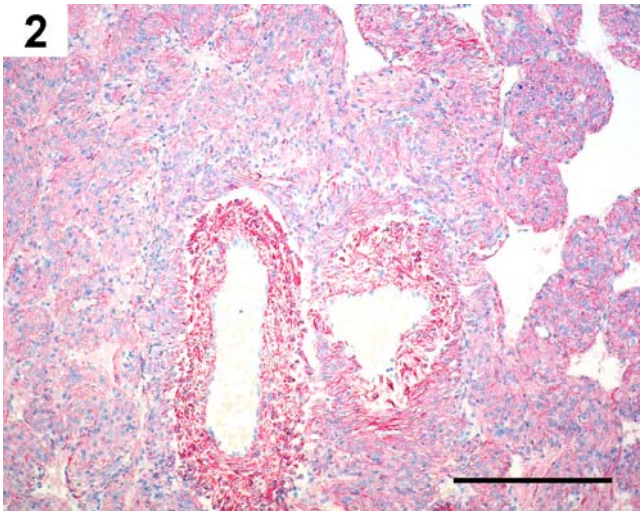

Fig. 2 Immunohistochemical staining of smooth-muscle actin (*red*) reveals strong positivity in the myoid cells as well as in the media of two larger blood vessels (APAAP method; *center* of the picture; patient no. 8; *bar*=200 μm)

occurred in bundles of myoid cells, whereas vascular smooth muscle cells generally did not display HMB-45 positivity (Fig. 3). Moreover, CD31 was detected in the majority of thin-walled branching vessels between the myoid cells (see Table 1). Typically, linear staining pattern was seen. In addition, positivity for CD31 was also found in numerous blood vessels again exhibiting a linear staining (Fig. 4).

D2-40 labeled vessels occurred in all cases examined. In particular, the staining reaction was found exclusively in the thin-walled branching vasculature (Fig. 5). By contrast, neither fascicular bundles of myoid cells nor lymphocytes arranged in follicles in the vicinity of the bundles revealed any positivity. In the vessels, we commonly observed a linear staining of the thin cytoplasm of the endothelial cells, although nuclei were typically spared (Fig. 5). Some blood vessels were interspersed between myoid bundles and thin-walled vessels. These did not reveal positivity for D2-40 (Fig. 5). Semiquantitative analysis revealed five LAMs with more than 50% of vessels positive; four cases were found with more than 20% and less than 50% of vessels positive, whereas there was only one patient (no. 3) with less than 20% of the vessels positive. In the vicinity of the tumors, there were some residual thin-walled vessels without intraluminal erythrocytes, which were interpreted as lymphatic vessels, and which revealed D2-40 labeling as well (Fig. 6). However, residual blood vessels did not show any positivity for this marker.

Table 2 Data on the primary antibodies used for this study

Marker (manufacturer)	Clone	Dilution	Pretreatment
ASMA (Dako, Glostrup, Denmark)	Clon 1A4	1:600	None
CD31 (Dako)	JC70A	1:50	MW
D2-40 (Signet)	D2-40	1:400	MW
HMB-45 (Dako)	HMB-45	1:200	Trypsin

ASMA α1-smooth-muscle actin, *MW* microwave pretreatment (600 W, 3×5 Min)

Discussion

In contrast to the other tumors comprising the group of the so-called "PEComas," LAM shows large numbers of thin-walled branching vessels, which have been suggested to be of lymphatic origin [6, 16, 17]. D2-40 is a (relatively novel) monoclonal antibody directed against podoplanin, which

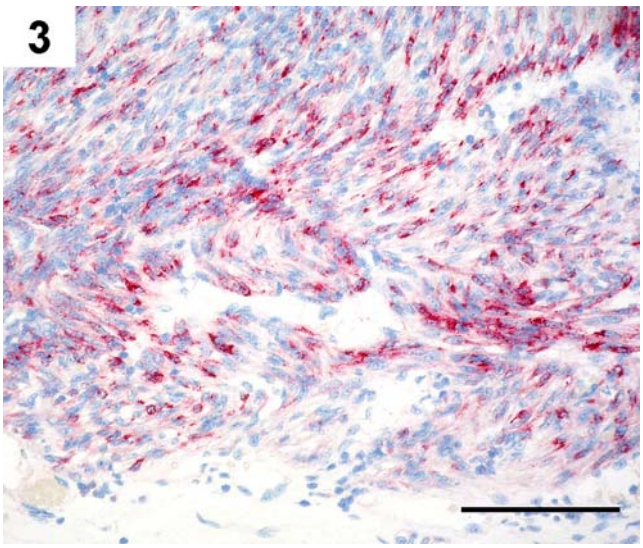

Fig. 3 HMB-45 (*red*) reveals a focally distributed strong expression in the myoid cells (APAAP method; patient no. 5; *bar*=100 μm)

Fig. 4 CD31 (*red*) is detected in numerous vessels: Besides the thin-walled branching vessels between myoid cell bundles, there is also a blood vessel (*arrow*) with a strong linear positivity at the luminal side reflecting the endothelial lining (APAAP method; patient no. 8; *bar*= 100 μm)

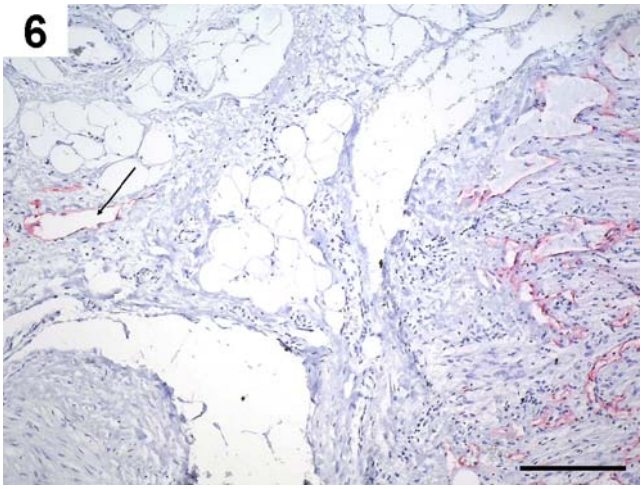

Fig. 6 D2-40 (*red*) is also labeled in the residual lymphatic vessels (*arrow*). LAM is revealed at the *right* part of the image (APAAP method; patient no. 7; *bar*=200 μm)

has been shown to be specific for lymphatic endothelial lining [8–11]. In the present study, we investigated the D2-40 in LAMs to further contribute to the immunohistochemical mapping of this antibody for vascular tumors, and moreover, to confirm the lymphatic origin of this distinct tumor entity. We examined (extrapulmonary) cases of LAM of the soft tissue only, because previous examinations by Matsui et al. [16] showed distinct differences between pulmonary and extrapulmonary LAMs, principally regarding the histological features.

In nearly all LAM cases, D2-40 strongly labeled a large numbers of vessels both in the tumor areas as well as in surrounding vessels in the neighborhood of the tumor. Histological differences between negative and positive vessels were not found. It is known that D2-40 in some cases does not reveal a homogenous labeling of lymphatics. Furthermore, D2-40 does not detect lymph vessels only, but also reacts with several other cell types such as mesothelial cells, myofibroblasts, and some kinds of gonadal tumors (for review see Ordonez [18]). However, in comparison with the other commercially available vascular markers, D2-40 is generally accepted as an antibody that does react with lymphatic-derived vascular tumors with the highest sensitivity. In our study, CD31 showed strong expression with lymph vessels, but on the other hand, this molecule was also labeled in numerous blood vessels (which is a typical staining pattern as described previously [19]). Taken together, these firstly presented data of D2-40 in LAM contribute to the immunohistochemical mapping of this marker in vascular soft-tissue tumors. They are in line with the general view that lymphangiogenic origin of vascular tumors can be ascertained by this marker.

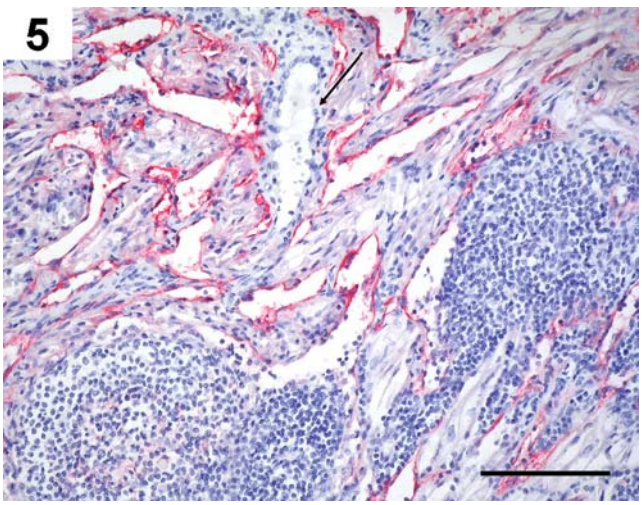

Fig. 5 Immunohistochemical labeling of D2-40 (*red*) demonstrates cytoplasmic staining in numerous positive thin-walled vessels. Note negative blood vessel (*arrow*; APAAP method; patient no. 9; *bar*= 100 μm)

The LAM cases presented in our study show a similar local distribution as those in the study of Matsui et al. [16]. Thus, extrapulmonary LAMs can be observed in three major locations: the mediastinum, the upper retroperitoneum, and the pelvic cavity (a cervical localization, as presented in our study, has been described only in one prior case [1]). In general, the specific histological features of LAM lead to the correct diagnosis. Because of the presented restricted locations, a few distinct tumor entities have to be excluded: In the case of the localization in the upper retroperitoneum (especially in the neighborhood of the kidneys), one has to bear in mind that leiomyomas of the kidney, particularly of the renal capsule, can show reactivity for HMB-45 [2], and thus can be misinterpreted as a tumor of the PEComa family. In contrast to LAM, lymph vessels do not comprise major portions of renal

leiomyomas, and therefore, D2-40 can aid in the differentiation between both diseases.

Because extrapulmonary LAMs are closely associated or even embedded in the regional (pelvic or iliacal) lymph nodes, metastasis of leiomyosarcoma is a further differential diagnosis. In fact, data concerning the incidence of lymph node metastasis in patients with uterine sarcomas are controversial, reaching from 45% (9/20 patients) of uterine stage I sarcomas in the study of Chen [3] to 0% (0/27 patients) of lymph node metastases of stage I/II uterine leiomyosarcomas in the study of Leitao et al. [14]. Nevertheless, for purposes of microscopical diagnosis, one should consider this possible pitfall, which can be solved by careful examination for signs of atypia (as a common finding for leiomyosarcoma) on the one hand, and numerous D2-40 positive branching lymphatic vessels arranged between myoid bundles without signs of atypia (as a common finding for LAM) on the other hand.

In summary, we examined ten cases of extrapulmonary LAM for labeling of D2-40 and contributed to the further immunohistochemical mapping of this marker. D2-40 positivity was revealed in all LAMs tested and confirms the current concept of lymphangiogenic origin of the tumor vessels in this neoplasm. Furthermore, the use of this commercially available antibody provides an additional help in the differential diagnosis of LAM from other soft-tissue tumors.

Acknowledgements We thank Mrs. Bergholz, Mrs. Dietrich, and Mrs. Pelzer (Institute of Pathology, Jena) as well as Mrs. Roth (Institute of Pathology, Mainz) for the excellent technical assistance.

We are very grateful to all pathologists who sent case material and clinical details from patients included in this study.

References

1. Betlejewski S, Burduk D, Szukalski J (2004) Lymphangioma and lymphangiomyomatosis—the same lesion? Otolaryngol Pol 58:903–906
2. Bonsib S (1996) HMB-45 reactivity in renal leiomyomas and leiomyosarcomas. Mod Path 9:664–669
3. Chen SS (1989) Propensity of retroperitoneal lymph node metastasis in patients with stage I sarcoma of the uterus. Gynecol Oncol 32:215–217
4. Debelenko LV, Perez-Atayde AR, Mulliken JB, Liang MG, Archibald TH, Kozakevich HP (2005) D2-40 immunohistochemical analysis of pediatric vascular tumors reveals positivity in kaposiform hemangioendothelioma. Mod Path 18:1454–1460
5. Fiore MG, Sanguedolce F, Lolli I, Piscitelli D, Ricco R (2005) Abdominal lymphangioleiomyomatosis in a man with Klinefelter syndrome: the first reported case. Ann Diagn Pathol 9:96–100
6. Folpe AL (2002) Neoplasms with perivascular epithelioid cell differentiation (PEComas). In: Fletcher CDM, Unni KK, Mertens F (eds) WHO classification of tumours of soft tissue and bone. IARC, Lyon, pp 221–222
7. Franke FE, Steger K, Marks A, Kutzner H, Mentzel T (2004) Hobnail hemangiomas (targetoid hemosiderotic hemangiomas) are true lymphangiomas. J Cutan Pathol 31:362–367
8. Fukunaga M (2005) Expression of D2-40 in lymphatic endothelium of normal tissues and in vascular tumors. Histopathology 46:396–402
9. Hansen T, Katenkamp K, Katenkamp D (2006) D2-40 staining in sinonasal-type hemangiopericytoma—further evidence of distinction from conventional hemangiopericytoma and solitary fibrous tumor. Virchows Arch 448:459–462
10. Hornick JL, Fletcher CDM (2006) PEComa: what do we know so far? Histopathology 48:75–82
11. Kahn HJ, Bailey D, Marks A (2002) Monoclonal antibody D2-40, a new marker of lymphatic endothelium, reacts with Kaposi's sarcoma and a subset of angiosarcomas. Mod Path 15:434–440
12. Kaiserling E (2004) Immunohistochemical identification of lymph vessels with D2-40 in diagnostic pathology. Pathologe 25: 362–374
13. Kumasaka T, Seyama K, Mitani K, Sato T, Souma S, Kondo T, Hayashi S, Minami M, Uekusa T, Fukuchi Y, Suda K (2004) Lymphangiogenesis in lymphangioleiomyomatosis. Its implication in the progression of lymphangioleiomyomatsosis. Am J Surg Pathol 28:1007–1016
14. Leitao MM, Sonoda Y, Brennan MF, Barakat RR, Chi DS (2003) Incidence of lymph node and ovarian metastases in leiomyosarcoma of the uterus. Gynecol Oncol 91:209–212
15. Marks A, Sutherland DR, Bailey D, Iglesias J, Law J, Lei M, Yeger H, Banerjee D, Baumal R (1999) Characterization and distribution of an oncofetal antigen (M2A antigen) expressed on testicular germ cell tumors. Br J Cancer 80:569–578
16. Matsui K, Tatsuguchi A, Valencia J, Yu ZX, Bechtle J, Beasley MB, Avila N, Travis WD, Moss J, Ferrans VJ (2000) Extrapulmonary lymphangioleiomyomatosis (LAM): clinicopathologic features in 22 cases. Human Pathol 31:1242–1248
17. Miettinen M (ed) (2003) Diagnostic soft tissue pathology. Churchill Livingstone, Philadelphia, pp 248–249
18. Ordonez NG (2006) Podoplanin: a novel diagnostic immunohistochemical marker. Adv Anat Pathol 13:83–88
19. Pusztaszeri MP, Seelentag W, Bosman FT (2006) Immunohistochemical expression of endothelial markers CD31, CD34, von Willebrand factor, and fli-1 in normal human tissues. J Histochem Cytochem 54:385–395

Virchows Arch (2007) 450:455–461
DOI 10.1007/s00428-007-0375-x

ORIGINAL ARTICLE

Cytological diagnosis of malignant mesothelioma—improvement by additional analysis of hyaluronic acid in pleural effusions

L. Welker · M. Müller · O. Holz · E. Vollmer · H. Magnussen · R. A. Jörres

Received: 17 November 2006 / Revised: 9 January 2007 / Accepted: 19 January 2007 / Published online: 15 February 2007
© Springer-Verlag 2007

Abstract Cytology allows the diagnosis of malignant mesothelioma (MM) from effusions with high specificity but low sensitivity. Conversely, elevated levels of hyaluronic acid (HA) in effusions are sensitive indicators of MM, although specificity is insufficient. We studied whether the cytological diagnosis of MM could be improved by HA analysis. HA was analysed in patients with histologically confirmed MM (n=162), adenocarcinoma or other malignant tumours (n=100) and in 90 patients with benign pleural diseases. In 77 out of 162 effusions, all, and in 33 some, cytological criteria of MM were satisfied. The cut-off value of HA showing maximum diagnostic reliability (86%) regarding MM was 30 mg/l (sensitivity 87%, specificity 86%). A HA value of 100 mg/l yielded 39 and 98%, respectively. Seventy three out of 77 patients with cytological findings indicative of MM showed HA levels greater than 30 mg/l as well as 27 of 33 patients with suspicious lesions. These 100 patients were correctly recognised as having MM. The addition of HA analysis to cytology, requiring all or some criteria of MM as positive, increased sensitivity for MM from 48 to 71–91%, whereas specificity only slightly decreased to 94–96%. We conclude that the combined cytological and HA analysis of pleural effusions had the potential to improve the diagnosis of MM.

Keywords Hyaluronic acid · Malignant mesothelioma

L. Welker · M. Müller · O. Holz · H. Magnussen · R. A. Jörres
Hospital Großhansdorf,
Center for Pneumology and Thoracic Surgery,
Großhansdorf, Germany

M. Müller
Medical Clinic, Clinical Center Itzehoe,
Itzehoe, Germany

E. Vollmer
Research Center Borstel, Clinical and Experimental Pathology,
Borstel, Germany

R. A. Jörres
Institute and Outpatient Clinic for Occupational
and Environmental Medicine, LMU,
Munich, Germany

L. Welker (✉)
Cytological Laboratory, Hospital Großhansdorf,
Center for Pneumology and Thoracic Surgery,
Wöhrendamm 80,
22927 Großhansdorf, Germany
e-mail: l.welker@gmx.net

Introduction

Asbestos-related malignant mesothelioma (MM) shows increasing incidence over the last decade [13, 14, 19], although it is still not a common disease. Its diagnosis is usually based on clinical history with special emphasis on occupational history, thoracic imaging, pleural puncture and biopsy. In case of inconclusive cytological or histological findings, more invasive procedures such as thoracoscopy, video-assisted thoracic surgery or thoracotomy are performed. The early diagnosis of MM is difficult, and not rarely a delay of several months occurs between the onset of the symptoms and diagnosis. At the time of presentation, 54–85% of patients with MM suffer from a pleural effusion [2] as a major clinical sign that often initiates the diagnostic process.

Cytology has as a major task the distinction between reactive alterations of mesothelial cells and malignant transformations such as adenocarcinoma, MM or other

malignant tumours [17, 18]. Although the morphological criteria for MM ensure a high specificity of routine cytology (Fig. 1), sensitivity is low [1, 16, 18] as most effusions satisfy only part of the respective criteria. Hyaluronic acid (HA) has been proposed as a biochemical marker of MM as early as 1939 [12], whereby elevated levels in pleural fluid are indicative of MM. Other diseases however, such as empyema, can also lead to elevated values thus reducing the specificity of HA analysis [3, 4, 8, 15].

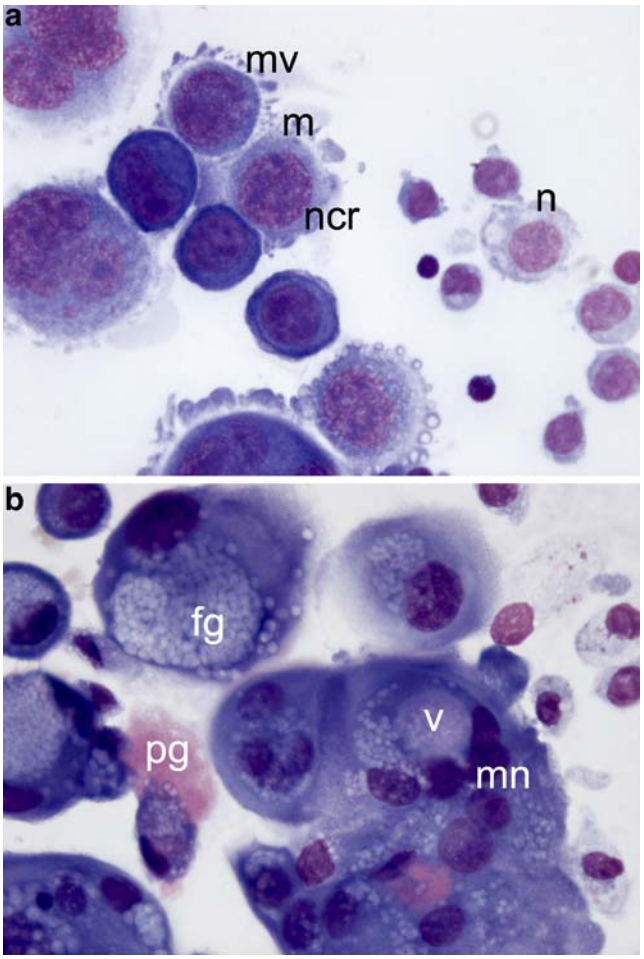

Fig. 1 Giemsa staining of cellular smears from MM (720×). There are several characteristic features to be observed as follows: (1) The cellular pattern is dominated by mesothelial cells looking like "caricatures" of reactive mesothelial cells; (2) bi- and multinucleate (*mn*) cells are common; (3) Giemsa smears show background staining in the form of minute pink granules (*pg*); (4) instead of two dissimilar populations as common in malignant effusions, there is a continuous transition between normal-looking mesothelial cells (*n*) and those recognised as malignant (*m*); (5) individual cells are tending to have larger, always round nuclei and a larger cytoplasm than reactive mesothelial cells with a lower nucleo-cytoplasmic ratio (*ncr*), the nucleus often being eccentrically placed nearby a single vacuole; (6) Giemsa-stained mesothelioma cells show two differently coloured areas within the cytoplasm and a pink border because of microvilli (*mv*); (7) in some cases, foamy vacuolation (*v*) and/or clusters of fat granules (*fg*) are present; (8) clusters of mesothelial cells tend to be unusually large and numerous

On the other hand, empyema can be easily identified by cytology. This suggests that a proper combination of cytology and HA analysis could take benefit from the sensitivity and specificity of the two approaches.

HA levels determined by fluid chromatography or colourimetry [4, 6, 11, 19] are known to be different from those obtained by immunological methods used today. This difference influences the choice of cut-off values. For immunological measurements, a value of 100 mg/l has been proposed [5, 7, 10, 15], although it has not been validated in a large sample. Thus, there is a need for exploring the most suitable cut-off value if the measurement of HA is evaluated either separately or in combination with routine cytology that is considered indispensable in the diagnosis of pleural effusions.

Based on these considerations, we studied whether it is possible to improve the sensitivity of the cytological diagnosis of MM while keeping its specificity by taking into account HA levels in pleural fluid. For this purpose, HA data as determined by immunoassay were analysed in a large group of patients (n=352, including n=162 patients with histologically confirmed MM). The power of cytology was additionally examined in the set of 2,516 patients from which the group taken for HA analysis had been recruited.

Materials and methods

Patients

Between 1997 and 2005, 3,289 effusions from 2,516 patients (1,694 men, 822 women; mean age, 64.6; range 15–93 years) were collected. In case of repeated assessments in one patient, the first one was taken for analysis.

HA was measured in a sample of 352 of the 2,516 patients, including 162 patients with a histologically confirmed final diagnosis of MM. For control, we randomly recruited 100 patients with histologically verified malignant tumours and 90 patients with benign pleural diseases, 77 of which were histologically proven. Based on the final diagnosis, the control patients were further classified into four groups as follows: 67 patients with adenocarcinoma (AD), 33 with other malignant tumours (OT), 20 with empyema (E) and 70 with reactive effusions (RE). Each patient's final diagnosis was based on all available histological and/or clinical findings except cytology and HA data.

HA measurement and cytological analysis

Immediately after receipt, pleural fluid samples were centrifuged at 2,000 U/min for 5 min. Supernatants were immediately frozen and stored at −20°C. Measurements

were performed within 6 months using an immunoassay according to the manufacturer's instructions (Pharmacia, Freiburg, Germany). From the sediment, smears were prepared, fixed in 95% methanol and stained with Giemsa for microscopy. The diagnosis of "epithelial type MM" was based on well-described cytological features (Fig. 1) [14, 17, 18].

Data analysis

Median values and quartiles of HA concentrations were computed, and log-transformed HA data were compared between final diagnoses by one-way ANOVA and the Newman–Keuls post hoc test. Relative frequencies, sensitivity, specificity and diagnostic reliability were computed as usual. Sensitivity and specificity were compared between different criteria by the McNemar test or the one-sided test of proportions, if appropriate. To describe the information content of cytology from a different point of view, posterior probabilities of diagnoses according to Bayes were additionally computed [20], whereby the relative frequencies of final diagnoses were taken as estimates of prior probabilities. This type of analysis was restricted to cytology, as the result could be checked in the total population of 2,516 patients. This allowed to assess whether it was dependent on the selection of patients of the MM or control group. Using the full range of cut-off values of HA, a receiver operating characteristic (ROC) curve was computed. Statistical significance was assumed for $p<0.05$.

Results

Cytological analysis of pleural effusions

Sensitivity and specificity

A cytological inspection showed a sensitivity of 47.5% and a specificity of 98.9% for the detection of MM, if all cytological criteria were required (Table 1). When this was

Table 1 Sensitivity and specificity of cytology, HA analysis and their combination in MM diagnosis

	Final diagnosis				Sensitivity	Specificity
	MM		Other			
	Yes	No	Yes	No	(%)	(%)
Cytology alone	n=162		n=190			
All criteria for MM satisfied	77	85	2	188	47.5	98.9
Criteria only partially satisfied[a]	33/33	129/52	13/13	177/175	20.4/38.8	93.2/93.1
All or some criteria satisfied	110	52	16	175	67.9*	92.1*
HA analysis alone	n=162		n=190			
HA >30 mg/l	141	21	27	163	87.0	85.8
HA >70 mg/l	81	81	10	180	50.0	94.7
HA >100 mg/l	63	99	4	186	38.9	97.9
All cytological criteria satisfied	n=77		n=2			
HA >30 mg/l	73	4	0	2	94.8	100[b]
HA >100 mg/l	39	38	0	2	50.6	100[b]
All or some criteria satisfied	n=110		n=16			
HA >30 mg/l	100	10	1	15	90.9***	93.8***
HA >100 mg/l	50	60	0	16	45.5	100
HA >30 mg/l	n=141		n=27			
All criteria for MM satisfied	73	68	0	27	51.8	100.0
Criteria only partially satisfied	27	114	1	26	19.0	96.3
All or some criteria satisfied	100	41	1	26	70.9**	96.3**
HA >100 mg/l	n=63		n=4			
All or some criteria fulfilled	50	13	0	4	79.4	100.0[b]

The table presents the results of the analyses considering either cytology and HA in separation or cytology and HA in different complementary combinations to reveal the superiority of their combined use.

*$p<0.05$, **$p<0.001$ compared to "all criteria satisfied"

***$p<0.001$ compared to 100mg/l

[a] First number referring to samples of 352 patients and the second number to the same sample without patients in whom all criteria of MM were satisfied (n=273).

[b] Not reliable because of the small number of patients.

relaxed to the condition that either all or some criteria were satisfied, sensitivity and specificity were significantly different from the former values ($p<0.05$ each, Table 1).

Post hoc analysis according to Bayes

This computation was first performed in patients in whom HA measurements were available ($n=352$). The prior probability for MM increased from 46.0 to 97.4%, when all cytological criteria for MM were required, and to 72.3%, when only some criteria were required, that is, alterations were suspicious (S) of MM but inconclusive (Table 2). Conversely, the cytological diagnosis of AD or OT reduced the likelihood of MM to 16.9%, whereas the likelihood for AD and OT was raised compared to prior probabilities when cytology showed a malignancy of this type but no MM (Table 2).

The same analysis was performed in the total population of 2,516 patients with pleural effusions including those without HA measurement. This population comprised 266 patients with histologically verified MM, 557 with AD, 431 with OT, 163 with E, 1,058 with RE and 41 patients suffering from effusions of uncertain dignity (UD). Thus, the relative frequency of MM in this population was lower than in the sub-group in which HA had been measured. Correspondingly, the likelihood for MM increased from 10.6 to 93.8% when all cytological criteria for MM were satisfied (Table 3). Cytology correctly recognised 122 of the 266 patients with MM, whereas in eight patients with a cytological diagnosis of MM, the final diagnosis turned out to be OT ($n=2$), AD or RE ($n=3$ each). The corresponding sensitivity was 46.4% and specificity 94.1%, similar to the values observed in the sub-group of 352 patients. When only some cytological criteria were satisfied, the likelihood of MM increased to only 36.9%.

Hyaluronic acid in pleural effusions

Differences between groups

HA concentrations as measured in patients with different diagnoses are shown in Fig. 2. ANOVA and post hoc comparisons revealed HA levels to be significantly higher in MM compared to all other diagnoses ($p<0.01$ each). In addition, HA levels in empyema were higher than in AD, OT and RE ($p<0.05$ each). The histological sub-type could be determined in 143 patients with MM. Epitheloid MM showed the highest, and sarcomatoid MM showed the lowest values of HA; however, the differences between sub-types were not statistically significant (Table 4).

Optimal cut-off value of hyaluronic acid concentration

As illustrated by the ROC curve (Fig. 3), the highest diagnostic reliability of MM diagnosis was found at 30 mg/l, corresponding to a sensitivity of 87.0% and a specificity of 85.8% (Table 1). A cut-off value of 100 mg/l led to a lower sensitivity and a higher specificity that were significantly different between the two cut-off values ($p<0.0001$ each).

Combination of cytology and hyaluronic acid analysis

In the sub-group of patients in whom all cytological criteria of MM were satisfied, sensitivity for MM was raised by requiring HA greater than 30 mg/l from 47.5 to 94.8% ($p<0.0001$; Table 1); there was also a gain compared to HA analysis alone ($p=0.03$). If all or some criteria required for MM were satisfied, sensitivity still increased from 47.5 to 90.9% ($p<0.0001$) by using the 30 mg/l cut-off value for HA, whereas specificity was essentially unchanged

Table 2 Prior vs posterior probabilities according to Bayes (in %)

Final diagnosis	*n*	Prior	Cytological diagnosis						HA
			MM	AD/OT	S	E	RE	MM/S	>30 mg/l
MM	162	46.0	97.4	16.9	72.3	4.5	29.1	88.0	84.7
AD	67	19.0	1.3	57.7	4.3	0.0	17.2	2.4	1.8
OT	33	9.4	1.3	25.4	10.6	13.6	4.5	4.8	1.6
E	20	5.7	0.0	0.0	2.1	72.7	2.2	0.8	4.8
RE	70	19.9	0.0	0.0	10.6	9.1	47.0	4.0	7.2
∑	352	100.0	78	71	47	22	134	125*	169

Data refer to the diagnosis of different pleural diseases by cytology in patients in whom HA had been analysed. Slashes indicate that either the first or the second cytological diagnosis was true in the respective category.

∑ Sum of absolute numbers underlying the data of the respective column (except for column "prior" where the sum of prior probabilities is given).

*Total number representing the sum of the total numbers from the MM and S column.

Table 3 Prior vs posterior probabilities according to Bayes (in %)

Data refer to the diagnosis of different pleural diseases by cytology in all patients studied over a period of 9 years.
UD Effusion of uncertain dignity
*Total number representing the sum of the total numbers from the MM and S column.

Final diagnosis	*n*	Prior	Cytological diagnosis					
			MM	AD/OT	S	E	RE	MM/S
MM	266	10.6	93.8	3.3	36.9	1.1	5.4	63.3
AD	557	22.1	2.3	61.3	10.7	2.6	6.5	6.3
OT	431	17.1	1.5	35.0	14.8	4.7	10.9	7.9
E	163	6.5	0.0	0.0	0.8	82.1	0.4	0.4
RE	1058	42.1	2.3	0.4	4.9	9.5	76.6	3.6
UD	41	1.6	0.0	0.0	32.0	0.0	0.1	15.5
∑	2516	100.0	130	732	122	190	1342	252*

(Table 1). There was, however, no gain in sensitivity when introducing the 100 mg/l cut-off value. A complementary picture was obtained when performing cytology requiring all or some criteria to be satisfied in the sub-group showing HA levels greater than 30 mg/l (Table 1). Sensitivity was slightly lowered from 87.0 to 70.9% ($p<0.0001$), but specificity raised from 85.8 to 96.3% ($p<0.0001$). In patients demonstrating levels greater than 100 mg/l, sensitivity of MM diagnosis reached 79.4%, if all or some cytological criteria for MM were satisfied (Table 1). This was higher ($p=0.0001$) than the sensitivity of 38.9% observed when an HA level greater than 100 mg/l was required without taking into account cytology (Table 1). To statistically compare specificities, absolute numbers were too low.

Discussion

The results of this study indicate that the combined use of cytology and HA analysis is capable of improving the detection of MM from pleural effusions. Cytology showed a high specificity for MM, in the presence of limited sensitivity, and a cut-off value of 30 mg/l of HA turned out to be the best with regard to diagnostic reliability. When both methods were combined, HA levels allowed to correctly identify a great proportion of those samples that were cytologically suspicious but did not satisfy all of the required criteria of MM. Fully positive cytological evidence was also supported by HA analysis, corresponding to a marked increase in sensitivity, with minor change in specificity. Thus, the combined use of the two procedures appeared to be a reasonable approach in the diagnosis of MM from effusions.

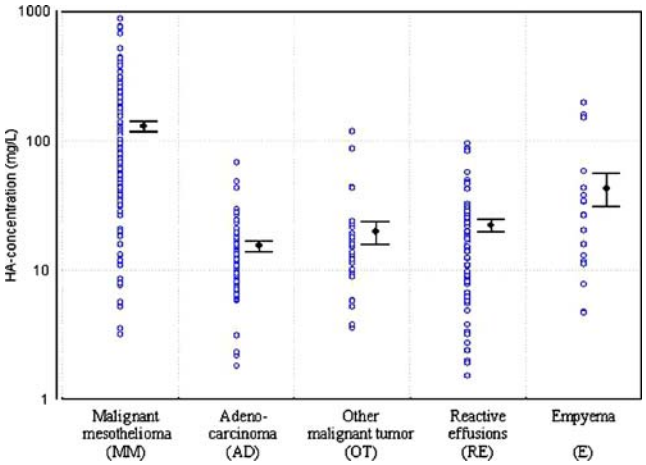

Fig. 2 Concentration of hyaluronic acid in pleural effusions of patients with different pleural diseases. *Filled circles* and *bars* indicate geometric mean values and standard errors of mean, respectively. HA levels were significantly higher in MM compared to all other diagnoses ($p<0.01$ each). In addition, HA levels in empyema were higher than those of AD, OT and RE ($p<0.05$, each)

In contrast to a specificity close to 100%, the sensitivity of cytology in diagnosing MM was less than 50% (Table 1). To evaluate the information contained in the data from a different point of view, we also computed the changes from before posterior probabilities as a function of cytological findings. This type of analysis was additionally performed in a large unselected group of 2,516 patients with pleural effusions that had been collected over a period of 9 years. The results obtained in the sub-group of patients having HA measurements were corroborated in this population, and a cytological finding indicative of MM raised the probability of MM from about 11 to 94%, again underlining the high specificity of the method (Table 3).

One reason for the low sensitivity of cytology seemed to be the high proportion of suspicious effusions, in which only some of the cytological criteria for MM were satisfied. This corresponds to the well-known morphological heterogeneity in MM [4, 17]. Based on this, the cytological diagnosis of MM has been depicted as not sufficiently reliable for clinical use [9], and many clinicians were reluctant to accept cytology for this purpose. In the meantime, the data base of cytologists has significantly broadened owing to the increasing incidence of MM. The high specificity of cytology, as underlined by our results, is valuable because a positive diagnosis in the presence of occupational exposure to asbestos can have important consequences beyond clinical treatment. Although immunocytochemistry has not been used in this study, such

Table 4 HA concentrations (mg/l) in pleural effusions for histological subtypes of MM

Subtype	*n*	Median	Lower quartile	Upper quartile	Minimum	Maximum
Epithelial	100	68.3	39.1	178.8	3.2	883.0
Sarcomatoid	6	48.8	11.7	95.2	5.2	302.0
Biphasic	37	62.0	43.6	113.3	11.6	278.0
Other	19	86.6	41.6	191.0	3.5	752.0

methods have the potential to raise sensitivity. The analysis of HA levels in pleural effusions can be considered as one step in this direction.

HA levels observed by us were similar to those found previously in patients with either MM or AD or benign pleural diseases [7]. We also confirmed that HA levels in MM were significantly higher than in AD [4, 5, 10, 15]. Little is known on HA levels in sub-types of MM as only small numbers of patients have been studied previously [19]. In our data, there was a tendency towards lower levels in sarcomatoid MM compared to other forms.

Only data on HA that have been obtained by immunological assays can be compared with our measurements. Using cut-off values of 100 mg/l of HA, sensitivity and specificity for recognising MM have been determined in small groups of 15–41 patients with MM [5, 7, 15]. Specificity ranged from 90 to 94% and sensitivity from 31 to 73%. Applying the 100-mg/l value to the data from 162 patients with MM and 190 control patients, we found estimates of sensitivity and specificity that were most similar to those reported by Fuhrman et al. [7]. Diagnostic reliability was highest at 30 mg/l, corresponding to a sensitivity of 87% and a specificity of 86%. However, the use of diagnostic reliability for identifying cut-off values has its trade off when putting special emphasis on specificity or sensitivity. Specificity at 30 mg/l was probably still too low for using HA analysis alone in the diagnosis of MM. We took this as an entry point where cytology came into play.

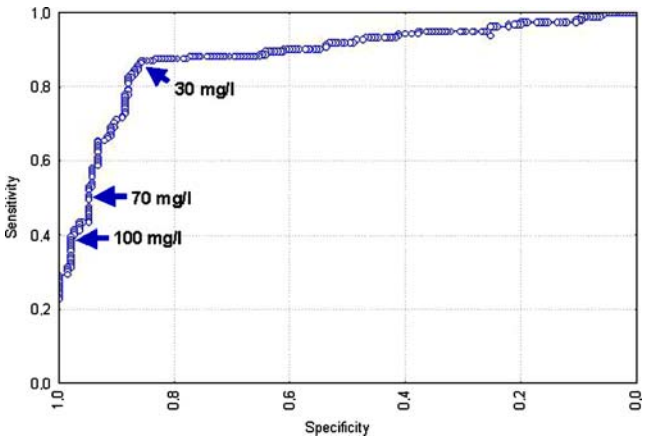

Fig. 3 ROC curve corresponding to the full range of different cut-off levels of hyaluronic acid for the diagnosis of malignant mesothelioma vs all other diseases. For orientation, three different cut-off values are indicated by *arrows*

When requiring all cytological criteria of MM to be positive and additionally an HA level greater than 30 mg/l, sensitivity increased markedly compared to cytology but was also raised compared to HA analysis alone (Table 1). This finding underlined the potential of HA determination if previous information from cytology was available. When testing for HA in patients with either full or partial cytological evidence for MM, sensitivity was also raised to about 91%, whereas specificity was still 94% (Table 1). If performed separately, neither cytology nor HA analysis reached this level of sensitivity at a comparable specificity of about 95%. Similar findings were obtained when adding full or partial cytological evidence for MM to the evidence obtained from the determination of HA levels. The gain in sensitivity compared to cytology was impressive in both sub-groups showing HA levels of either >30 or >100 mg/l (Table 1).

The information from the data was also reflected in the analysis of probabilities as a correlate of the positive and negative predictive value of cytology, particularly its high specificity. As judged from Tables 2 and 3, the implications for clinical practice may even have been underestimated, as the group of patients in whom HA values were available was enriched in MM compared to the set of 2,516 patients who might be considered as more of representatives for clinical practice. Among other effects, this enrichment in MM implied less room for improvement in predicting MM by the combination of the two procedures. When using the 30-mg/l cut-off value in combination with fully or partially satisfied cytological criteria, the probability of MM increased from 84 to a posterior value of 99% (data not shown). This small change reflected the already high probability of MM in patients showing elevated HA levels and conversely.

Based on these results, one might draw tentative conclusions towards a rational combination of cytology with HA analysis in clinical practice. The decision on HA measurement will rely on the clinical evidence collected and the cytological result, as far as cytology is routine in the diagnosis of pleural effusions. If cytological criteria are fully positive for MM, HA analysis could help by further increasing the already high specificity of cytology by adding assuring evidence. Nearly one third of patients with

MM, however, showed only partial cytological evidence in terms of suspicious lesions not satisfying all criteria of MM (Table 1). HA measurement seemed particularly advantageous in these patients. If values are greater than 30 or even 100 mg/l, patients could be considered as having MM with a high degree of certainty, and further diagnostic procedures to verify MM could be considered dispensable. This seems to be the major conclusion from our study. If cytology indicates the presence of adenocarcinoma or other tumours, HA analysis might also help owing to its high specificity for MM, if values turn out to exceed 100 mg/l (Table 1), although HA seems less informative than in the case of cytology suggesting MM. All other conditions render further (Bioptic) diagnostic procedures indispensable, as usual. The potential clinical benefits of the proposed scheme have, of course, to be assessed in independent studies. To avoid a bias arising if the results of cytology and HA analysis are used for establishing the final diagnosis, studies would still have to rely on histology in combination with clinical findings as the present analysis did.

In conclusion, the results of this study underlined the very high specificity of cytology in the diagnosis of MM. Regarding hyaluronic acid in pleural effusions, a cut-off value of 30 mg/l showed high sensitivity and a value of 100 mg/l high specificity but low sensitivity comparable to cytology. Finally, in case of positive cytological evidence for MM as well as in those cases in which only some cytological criteria of mesothelioma were satisfied, the combination of cytology and the 30-mg/l cut-off value of hyaluronic acid markedly raised sensitivity while maintaining a high specificity. Thus, the combined use of both procedures has the potential to facilitate the diagnostic process in MM without being likely to introduce unbearable expenses.

Conflict of interest statement

L Welker	None declared
M Müller	None declared
O Holz	None declared
E Vollmer	None declared
H Magnussen	None declared
RA Jörres	None declared

References

1. Achatzy R, Beba W, Ritschler R, Worn H, Wahlers B, Macha HN, Morgan JA (1989) The diagnosis, therapy and prognosis of diffuse malignant mesothelioma. Eur J Cardiothorac Surg 3:445–447
2. Antman K, Shemin R, Ryan L, Klegar K, Osteen R, Herman T, Lederman G, Corson J (1988) Malignant mesothelioma: prognostic variables in a registry of 180 patients, the Dana–Farber Cancer Institute and Brigham and Women's Hospital experience over two decades, 1965–1985. J Clin Oncol 6:147–153
3. Antony VB (2003) Immunological mechanisms in pleural disease. Eur Respir J 21:539–544
4. Atagi S, Ogawara M, Kawahara M, Sakatani M, Furuse K, Ueda E, Yamamoto S (1997) Utility of hyaluronic acid in pleural fluid for differential diagnosis of pleural effusions: likelihood ratios for malignant mesothelioma. Jpn J Clin Oncol 27:293–297
5. Dahl IM, Solheim OP, Erikstein B, Müller E (1989) A longitudinal study of the hyaluronan level in the serum of patients with malignant mesothelioma under treatment. Hyaluronan as an indicator of progressive disease. Cancer 64:68–73
6. Friman C, Hellström PE, Juvani M, Riska H (1977) Acid glycosaminoglycans (mucopolysaccharides) in the differential diagnosis of pleural effusion. Clin Chim Acta 76:357–361
7. Fuhrman C, Duche JC, Chouaid C, Abd Alsamad I, Atassi K, Monnet I, Tillement JP, Housset B (2000) Use of tumor markers for differential diagnosis of mesothelioma and secondary pleural malignancies. Clin Biochem 33:405–410
8. Hillerdal G, Lindqvist U, Engström-Laurent A (1991) Hyaluronan in pleural effusions and in serum. Cancer 67:2410–2414
9. Martensson G (1990) Diagnosing malignant pleural mesothelioma. Eur Respir J 3:985–986
10. Martensson G, Thylen A, Lindquist U, Hjerpe A (1994) The sensitivity of hyaluronan analysis of pleural fluid from patients with malignant mesothelioma and a comparison of different methods. Cancer 73:1406–1410
11. Matzel W (1985) Biochemical and cytological features of diffuse mesotheliomas of the pleura. Arch Geschwulstforsch 55:259–64
12. Meyer K, Chaffee E (1939) Hyaluronic acid in pleural fluid associated with malignant tumour involving pleura and peritoneum. Pro Soc Exp Biol Med 42:797–800
13. Parker C, Neville E (2003) Lung cancer * 8: management of malignant mesothelioma 1. Thorax 58:809–813
14. Peto J, Decarli A, La Vecchia C, Levi F, Negri E (1999) The European mesothelioma epidemic. Br J Cancer 79:666–672
15. Pettersson T, Froseth B, Riska H, Klockars M (1988) Concentration of hyaluronic acid in pleural fluid as a diagnostic aid for malignant mesothelioma. Chest 94:1037–1039
16. Renshaw AA, Dean BR, Antman KH, Sugarbaker DJ, Cibas ES (1997) The role of cytologic evaluation of pleural fluid in the diagnosis of malignant mesothelioma. Chest 111:106–109
17. Spriggs AI, Boddington MM (1994) Atlas of serous fluid cytopathology. A guide to the cells of pleural, pericardial, peritoneal and hydrocele fluid. In: Gresham GA (ed) Current histopathology series, vol 14. Kluwer, Dordrecht (1989)
18. Stevens MW, Leong AS, Fazzalari NL, Dowling KD, Henderson DW (1992) Cytopathology of malignant mesothelioma: a stepwise logistic regression analysis. Diagn Cytopathol 8:333–341
19. Thylen A, Hjerpe A, Martensson G (2001) Hyaluronan content in pleural fluid as a prognostic factor in patients with malignant pleural mesothelioma. Cancer 92:1224–1230
20. Welker L, Jörres RA, Costabel U, Magnussen H (2004) Predictive value of BAL cell differentials in the diagnosis of interstitial lung diseases. Eur Respir J 24:1000–1006

Virchows Arch (2007) 450:463–470
DOI 10.1007/s00428-007-0378-7

ORIGINAL ARTICLE

Perivascular epithelioid cell neoplasms (PEComas): four malignant cases expanding the histopathological spectrum and a description of a unique finding

Ilan Weinreb · David Howarth · Eleanor Latta · Danny Ghazarian · Runjan Chetty

Received: 18 December 2006 / Revised: 24 January 2007 / Accepted: 26 January 2007 / Published online: 15 February 2007
© Springer-Verlag 2007

Abstract Four cases of malignant PEComas were stained with smooth muscle actin, muscle specific actin, desmin, human melanoma black-45, melan-A, microphthalmia transcription factor, S100 and cyclin D1. One case was studied by electron microscopy (EM). Tumour locations were the thigh, elbow, retroperitoneum and bladder in association with a urachal cyst. There were two men and two women; the average age was 51.3 years, and the size ranged from 5.0–23.0 cm. In three cases, 50–95% of the tumour was composed of pleomorphic sarcomatous areas. All cases had at least focal clear-cell areas. One case showed a continuous single layer of perivascular clear cells remote from the tumour, transitioning to invasive nests and to PEComa. EM demonstrated these cells in apposition to and in direct contact with the abluminal surface of the basal lamina of the capillaries. We suggest the term "pecosis" for these areas. All cases were positive for two or more melanocytic markers and for at least one actin. S100 and desmin were focally positive in one case. Cyclin D1 was positive in 3:4 cases. Four cases of malignant PEComa are described with the existence of a unique lesion (pecosis) in one case. These tumours may manifest largely as sarcomas appearing to be undifferentiated and should be considered in their differential diagnosis.

Keywords Pecoma · Myomelanocytic tumour · Perivascular epithelioid cell · Pecosis

I. Weinreb (✉) · D. Ghazarian · R. Chetty
Department of Pathology, University Health Network,
200 Elizabeth Street, 11th Floor,
Toronto, ON M5G 2C4, Canada
e-mail: weinrebi@yahoo.ca

D. Howarth
Department of Pathology and Laboratory Medicine,
Mount Sinai Hospital,
Toronto, ON, Canada

E. Latta
Department of Pathology, St. Michael's Hospital,
Toronto, ON, Canada

I. Weinreb · D. Howarth · E. Latta · D. Ghazarian · R. Chetty
Department of Laboratory Medicine and Pathobiology,
University of Toronto,
Toronto, ON, Canada

Introduction

The perivascular epithelioid cell tumour (PEComa) family is a well-accepted and distinctive group, initially described by Bonetti et al. [5] who also first proposed the theoretical cell of origin [16, 23]. This terminology applies to angiomyolipomas of the kidney and liver, clear cell sugar tumours, lymphangioleiomyomatosis of the lung and tumours of the soft tissue and viscera with either spindled or epithelioid morphology and dual myomelanocytic differentiation [14–16]. The growing list of sites of occurrence include gastrointestinal, gynecological, genitourinary, extremities and the skin, as well as single reports in the oral cavity, skull base, orbit and prostate [16, 23, 24, 27, 28, 32]. The putative cell of origin (perivascular epithelioid cell) has not been identified to date in normal tissues, nor has a precursor lesion been described. Malignant PEComas are being increasingly reported as well [4, 7, 8, 10, 11, 13, 16, 21, 22, 28, 32, 33]. Folpe et al. [16] suggested criteria for malignancy including a size of >8.0 cm, mitotic count of >1 per 50 high power fields (HPFs) and necrosis, and these help to stratify PEComas into benign, uncertain malignant potential and malignant. Occasional cases with overt sarcomatous areas have been described and mim-

icked other malignancies, and these may, therefore, escape recognition [1].

To study these issues further, we examined four malignant PEComas with overt sarcomatous areas that mimicked other pleomorphic sarcomas. We also report the first example of a PEComa arising in a urachal remnant. This case had a unique lesion remote from the tumour, for which we suggest the term "pecosis" and discuss its possible implications. We also examine the role of cyclin D1 over-expression by immunohistochemistry, which has been reported previously in a single example of a malignant PEComa of the colon [43].

Materials and methods

A search of the computer records of our archives for malignant cases belonging to the "PEComa" family was undertaken. All cases listed as malignant examples of PEComa, angiomyolipoma, clear-cell sugar tumour and myomelanocytic tumour were collected. Only cases that were histologically malignant (according to the criteria established by Folpe et al. [16]) were included. All four surgical specimens were fixed in neutral buffered formalin. Hematoxylin and eosin stains were performed on 3- to 4-μ thick sections of formalin-fixed paraffin-embedded tissue. Immunohistochemical stains were performed in sections from one or more representative paraffin blocks from each case, using the ultra-streptavidin–horseradish peroxidase (HRP) detection system (ID Labs Biotechnology, London, Ontario, Canada). Colour development was performed using the NovaRed substrate kit (Vector Labs, Burlingame, California, USA). The following antibodies were employed: AE1/AE3 (Dako, 1:800), EMA (Ventana, prediluted), smooth muscle actin (SMA; Dako, 1:200), muscle specific actin (MSA; Dako, 1:100), desmin (Dako, 1:200), S100 (Dako, 1:200), melan-A (Ventana, prediluted), human melanoma black-45 (HMB-45; Ventana, prediluted), microphthalmia transcription factor (MiTF; Neomarkers, 1:50) and cyclin D1 (Neomarkers, 1:80). Immunopositivity was assessed as follows: +++, >75% of tumour cells labelling; ++, 50–75% of tumour cells labelling; +, 25–50% of tumour cells labelling; focal +, 0–25% of tumour cells labelling.

Electron microscopy was performed on one case with the areas of "pecosis" on the tissue extracted from a paraffin block (urachal case). Molecular analysis on one case was performed from the paraffin-embedded tissue to exclude the presence of the *t*(12;22) translocation present in clear-cell sarcoma of the tendons and aponeuroses.

Results

Clinical findings

The clinical findings are summarised in Table 1. There were four patients in total, two men and two women with an average age of 51.3 years and an age range of 39–69 years. They were found in the elbow, retroperitoneum, a urachal remnant and the left thigh. The tumours ranged in size from 5.0 to 23.0 cm with an average size of 10.7 cm. Follow-up information was available on three of the cases, with one patient lost to follow-up. Of these three cases, two are alive and well with no evidence of disease 8 and 11 months after resection. One patient with the retroperitoneal mass is alive with brain and lung metastases 4 years after surgery. No patient had the tuberous sclerosis complex or a current or subsequent history of melanoma.

Histopathologic findings

All four cases showed sheets of cells arranged in fascicles, nests or both and had infiltrative borders with invasion of the surrounding soft tissues. Focal areas of perivascular accentuation were seen in all cases and, in some cases, was a prominent feature. The cells ranged from small epithelioid and spindle cells to large pleomorphic malignant giant cells. The cytoplasm varied from clear to eosinophilic and granular. Melanin pigment was seen in one case by H&E alone and by melanin special staining (Fontana–Masson) in a second. Three cases showed dense stromal hyalinization.

Case 1 (retroperitoneal) had >95% epithelioid and giant cell morphology, reminiscent of a myogenic sarcoma or undifferentiated malignant tumour and was noted grossly to be wrapping around the ureter, but not invading it. The tumour showed nested architecture with a fine fibrovascular compartmentalization. There were focal areas of perivas-

Table 1 Clinicopathological features

Case	Age	Gender	Site	Size (cm)	Histologic pattern	Follow-up
1	49	F	Retroperitoneal	7.0	Myogenic sarcoma-like	AWD (brain and lung metastases)
2	68	M	Left thigh	7.8	Dedifferentiation	NED×11 months
3	49	F	Elbow	5.0	Fibrosarcoma-like	Lost to follow-up
4	39	M	Urachal	23.0	Myomelanocytic	NED×8 months

AWD Alive with disease, *NED* no evidence of disease recurrence

cular epithelioid clear cells (Fig. 1a). Marked pleomorphism was noted; the mitotic count was 28 mitotic figures (MFs) per 10 HPFs including atypical forms, and there were large areas of geographic necrosis. A large thick-walled vein identified as the inferior vena cava was noted to have a large tumour embolus within it.

Case 2 (left thigh), which grossly involved and surrounded a large neurovascular bundle, showed a predominant spindled eosinophilic and clear cell pattern. There were large areas of necrosis with the preservation of cells nearest the blood vessels (Fig. 1b). Little-to-no-cellular pleomorphism was evident in most of the tumour, but there was a high mitotic count of 42 MFs per 10 HPFs. In addition, there was an abrupt transition from the entirely clear-spindled areas to an undifferentiated patternless sarcoma with prominent intra-tumoural chronic inflammation

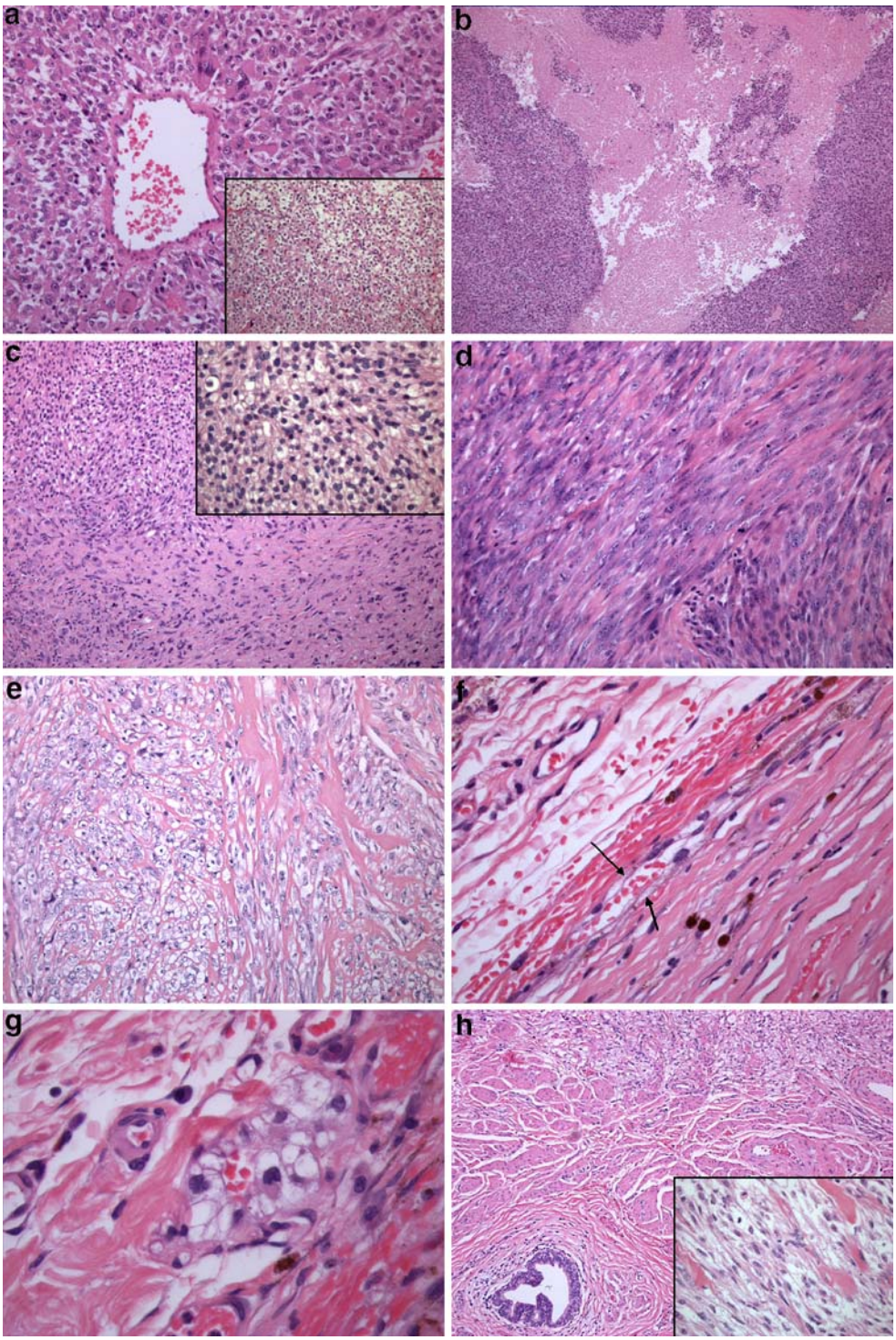

Fig. 1 **a** A pleomorphic sarcomatous PEComa mimicking a myogenic sarcoma, containing focal perivascular clear cell areas (*inset*), which is an important clue to the diagnosis (case 1; 200×). **b** Geographic necrosis in the case arising in the thigh (case 2; 50×). **c** The same case as in **b** (case 2) demonstrating an abrupt transition of clear cell areas to a more undifferentiated, sarcoma pattern (100×). *Inset*, higher power of clear cell areas. **d** Case 3, arising in the elbow with a fibrosarcoma-like pattern representing 50% of the tumour (200×). **e** The same case (case 3) with clear cell areas within hyalinized fibrous tissue representing the other 50% of the tumour arising in the elbow (200×). **f** Longitudinal section of a capillary involved by "pecosis" in case 4. *Arrows* point to the subtle clear cells lining the vascular space that correspondingly stain for HMB-45. Note the cytoplasmic melanin pigment at the *top right corner* of image (400×). **g** The same case demonstrating an additional example of "pecosis" within the urachal cyst wall (630×). **h** The urachal PEComa (case 4) showing infiltration of the bladder wall by clear cells in the *top half* of the picture. Note the uninvolved urachal remnant at the *bottom half* of the picture (100×). *Inset*, high power of classic PEComa

(Fig. 1c). The post radiotherapy resection specimen showed mainly the undifferentiated sarcoma pattern with involvement and occlusion of the superficial femoral vein.

Case 3 (elbow) showed a tumour-infiltrating skeletal muscle and fibroadipose tissue in a fascicular and herringbone, "fibrosarcoma-like" pattern (Fig. 1d). In addition, there were areas of dense hyalinization and a single file arrangement of epithelioid clear cells entrapped within the fibrous tissue in approximately 50% of the tumour (Fig. 1e). The mitotic count was 20 MFs per 10 HPFs including atypical forms, and there was focal single-cell necrosis. Multi-nucleated malignant giant cells were noted within the tumour, and there was focal vascular invasion by tumour cells.

In case 4 (urachal cyst), the umbilicus and the dome of the bladder were resected in continuity with a 23.0-cm cystic lesion. Within the cyst was a 5.0-cm mural mass. Several centimeters away from the main tumour mass, at the umbilical end of the specimen, there were isolated capillaries surrounded by a single layer of clear cells (pecosis; Fig. 1f,g). These clear cells showed fine dusty melanin pigment in their cytoplasm. They were noted to have little to no nuclear atypia and no nucleoli. The involved capillaries merged to form complex interconnecting vascular spaces that were also surrounded by a single continuous layer of clear cells. There was no invasion between these individual vascular channels, but the lesion gradually merged with focal invasive nests within the stroma of the cyst wall. The invasive nests converged to form the mural tumour mass with the classical clear, spindled morphology of a "myomelanocytic tumour" (Fig. 1h). At the bladder end of the cyst, the tumour showed focal evidence of dedifferentiation: discohesive, pleomorphic eosinophilic cells containing larger nuclei and prominent nucleoli, focal single cell necrosis and isolated mitotic figures. No vascular invasion was noted.

Immunohistochemical findings

The immunohistochemical profile of the four cases is summarised in Table 2. All four cases showed strong and diffuse staining with at least two melanocytic markers (Fig. 2a). All but one of the cases were S100 negative; the positive case occurred in the urachal remnant and was patchy (20% of cells labelling). This case was *t*(12;22) negative (see later). All cases showed actin positivity with three of the cases showing multiple myoid marker positivity as well (Fig. 2b). The most frequent and strongest staining myoid marker present was SMA. A single case was focally positive for desmin. The case with the "pecosis" showed strong HMB-45 and MiTF positivity of the clear cells in apposition to the thin endothelial lined spaces (Fig. 2c). Only focal keratin or EMA staining was seen (one case each).

Cyclin D1 staining was present in three of the four cases, with strong nuclear positivity in the tumour cells, suggesting its over-expression. In case 2 (thigh) where there was an abrupt transition to an undifferentiated sarcoma pattern, the cyclin D1 staining was absent in the clear-cell portion of the tumour and present in the area of dedifferentiation. All other positive tumours showed diffuse staining. The retroperitoneal tumour was cyclin D1 negative. The urachal tumour showed cyclin D1 staining in the main tumour mass but not in the peri-capillary "pecosis". The degree of cyclin D1 staining increased from the early invasive nests to the main tumour mass.

Ultra-structural analysis

Electron microscopy was performed on the "pecosis" and mural mass of case 4 from the paraffin-embedded tissue. It showed single perivascular epithelioid cells surrounding endothelial-lined vascular channels in a single continuous layer (Fig. 3a). These cells were found to be in direct apposition to the abluminal surface of the basement membrane of these capillaries with no stroma in-between (Fig. 3b). No invasive nests were seen in-between these capillaries. The invasive areas in the mural mass showed primitive cellular junctions, but no melanosomes or pre-melanosomes were seen.

Molecular analysis

Case 4 (focally S100 positive) was also tested by RT-PCR for the recurrent *t*(12;22) translocation (EWS/ATF-1 fusion

Table 2 Immunohistochemical results

Case	SMA	MSA	Desmin	Melan-A	HMB-45	S-100	MiTF	Cyclin D1
1	Focal +	−	−	+++	++	−	Not done	−
2	+++	++	−	+++	−	−	+++	+++[a]
3	++	Focal +	−	++	++	−	+++	+++
4	+++	++	Focal +	Focal +	+++	Focal +	+++	+++[b]

+++, >75% of tumour cells labelling; ++, 50–75% of tumour cells labelling; +, 25–50% of tumour cells labelling; focal +, 0–25% of tumour cells labelling

[a] Cyclin D1 staining in undifferentiated areas only

[b] Cyclin D1 staining in tumour but not in "pecosis"

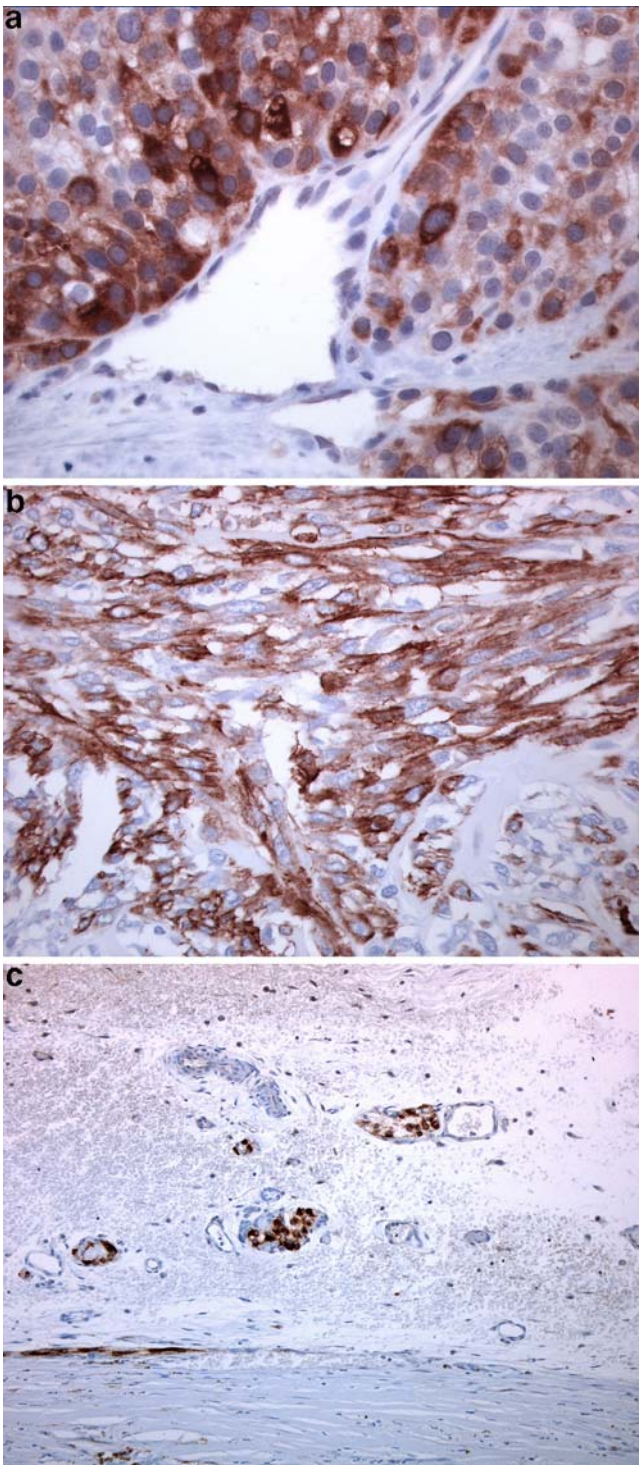

Fig. 2 **a** Melan-A staining of the retroperitoneal tumour (case 1) with an increase in staining intensity noted in a perivascular locale (400×). **b** Strong SMA staining of the elbow PEComa (case 3; 400×). **c** HMB-45 staining numerous capillaries within the cyst wall containing foci of "pecosis" in case 4. Note the perivascular staining and the lack of invasive tumour nests in-between capillaries (100×)

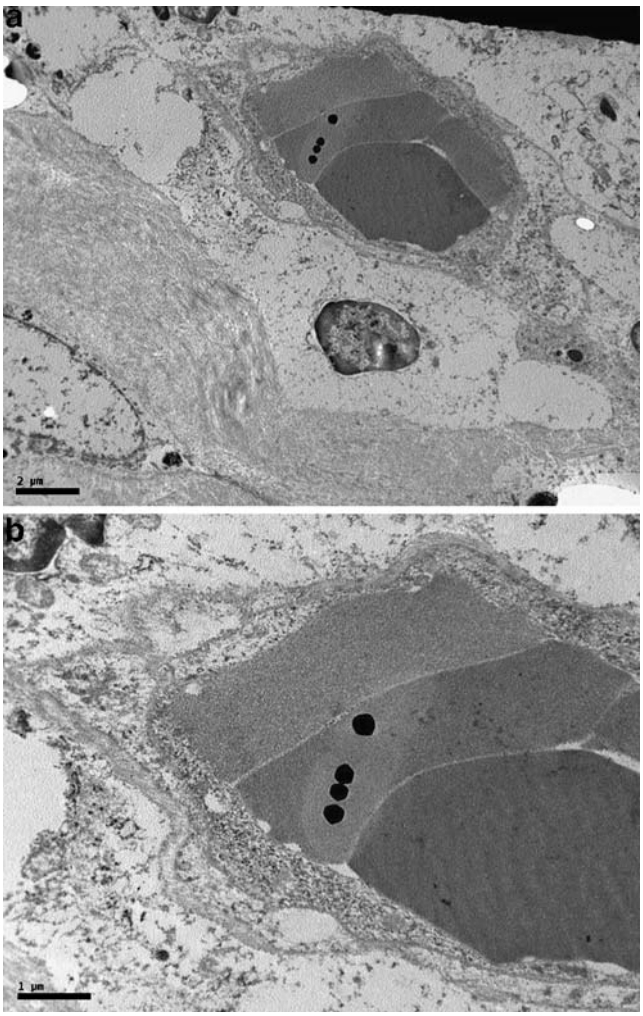

Fig. 3 **a** Electron microscopy demonstrating "pecosis" within the urachal cyst wall. Note the PEC cells surrounding the capillary in a single layer. **b** Higher power image of the same capillary showing the cells in direct apposition to the basal lamina

transcript seen in clear cell sarcoma/melanoma of soft parts) and was negative.

Discussion

It appears clear that the PEComa family of tumours represent a unique and distinct group arising from the perivascular epithelioid cell [16, 23, 31]. The first suggestion of this possible origin is credited to Bonetti et al. [5, 6, 35, 36], based on a series of observations in clear-cell sugar tumours, angiomyolipomas and lymphangioleiomyomatosis of the lung. The perivascular accentuation of tumour and the intimate association with vessel walls is a prominent feature and a useful clue to the diagnosis. The differential diagnosis includes leiomyosarcoma, malignant melanoma, clear-cell sarcoma of tendons and aponeuroses and any other tumour with focal or prominent clear-cell change.

PEComas have now been reported in almost every body site including visceral and somatic soft tissues [23]. The majority has been reported in women, and only a few are associated with tuberous sclerosis [12, 16, 23, 31, 41].

Malignant PEComas are being increasingly reported as well [4, 7, 8, 10, 11, 13, 16, 21, 22, 28, 32, 33]. Criteria for malignancy have been suggested recently and include size greater than 8.0 cm, mitotic count >1 per 50 HPFs and necrosis, with benign, uncertain malignant potential and malignant categories based on zero, one or two of these criteria, respectively [16]. Infiltrative edges, cellularity and nuclear pleomorphism may be secondary features suggesting aggressive behaviour [16, 23]. An occasional case may even have no features of malignancy and still show clinical aggressiveness [16]. No case described in the skin has behaved aggressively to date, suggesting that site may also determine behaviour in PEComas [9, 23, 30]. An occasional case may have frankly sarcomatous areas and mimic other sarcomas [1].

All four malignant cases in this series contained at least focal clear-cell areas, and three had a large sarcomatous component. These latter cases were initially suspected to be other sarcomas, but based on the clear cell areas, malignant PEComas were considered. Myomelanocytic marker expression was found to be prominent, including in the sarcomatous areas. Controversy exists regarding the minimum criteria for the diagnosis of malignant PEComa [38]. In a study of uterine tumours demonstrating epithelioid morphology, clear cell areas and HMB-45 positivity, Silva et al. [38] argued that this group represented smooth muscle tumours with focal melanocytic differentiation and not PEComas. This was based largely on the fact that the tumours looked like typical leiomyosarcomas with spindled and epithelioid areas and stained with desmin. It is also noteworthy that only focal HMB-45 staining was seen, unlike the diffuse expression in our cases. More than 30% of PEComas showed at least focal desmin staining in the study by Folpe et al. [16], and this does not exclude the diagnosis of PEComa. Other authors have reported uterine, cervical and broad ligament tumours of the kind Silva et al. described as PEComas, and at least two cases were associated with tuberous sclerosis [2, 8, 10, 12, 13, 17–21, 25, 26, 41]. We suggest that tumours with diffuse myomelanocytic differentiation should be regarded as being related to the PEComa family irrespective of site of origin or desmin positivity. It is the characteristic immunophenotype that warrants separating these tumours from classic leiomyosarcoma that exhibit only muscle differentiation.

In addition to leiomyosarcoma, other malignant neoplasms have also to be considered. The most important of these (melanoma and clear cell sarcoma) can be differentiated based on S100 positivity; however, up to 18% of PEComas express S100 as well [16]. Important clues to the diagnosis of PEComa in this context include perivascular accentuation of tumour cells, actin positivity, negative history for melanoma, visceral location of tumour and absence of the *t*(12:22) translocation. Although S100 negative melanomas have rarely been described, we feel tumours with diffuse melanocytic marker positivity, S100 negativity and actin immunoreactivity are PEComas based on morphology and immunophenotype. Despite this, an occasional case will still defy classification. The single case in our series with patchy S100 (20% cells staining) expression showed typical histology for a PEComa in most of the tumour, was diffusely actin positive, lacked a history of melanoma, had a visceral location and lacked the *t* (12;22) translocation.

Malignant PEComas that are entirely undifferentiated may also exist and, in the absence of the aforementioned features, will escape recognition. Such lesions warrant a search for conspicuous clear cell areas and perivascular growth, as well as being investigated with a panel of myomelanocytic markers if the histological appearance is appropriate. However, purely undifferentiated sarcomas without clear cell areas do not warrant additional investigation. Pitfalls in this diagnosis include aberrant staining of cells with melanocytic markers. In our experience, diffuse and multiple melanocytic marker expression is highly reliable for melanocytic differentiation. Focal or weak positivity can be disregarded, however, and do not warrant the diagnosis of PEComa. All of our cases were diffusely and strongly positive with at least two melanocytic markers (excluding S100), which is not a finding in other sarcomas in our experience. Other modalities such as cytogenetics may help to refine these diagnostic categories in the future. Cytogenetic alterations have been described in PEComas, including losses on chromosome 16p, the location of the tuberous sclerosis complex 2 gene (TSC2) [31].

There is no known precursor lesion for PEComas, and the so-called PEC has not been identified in normal tissue. The presumed perivascular location and actin positivity of the cells may argue for a pericyte origin, but pericytic differentiation has never been suggested, to our knowledge, in ultra-structural studies. We report the first description of one case with a perivascular lesion, for which we propose the term “pecosis”, arising in a urachal cyst. In addition, we have encountered a benign PEComa located in the skin that also exhibited this phenomenon. The “pecosis” showed a gradual transition to an invasive PEComa with the usual features and, focally, to a poorly differentiated malignant neoplasm. This may imply that “pecosis” was a precursor to the PEComa in this case. Bladder PEComas have been reported previously [31, 34], but this is the first case specifically proven to arise within a urachal cyst and

display "pecosis" remote to the main tumour. An alternative explanation for "pecosis" may be malignant tumour extension along capillaries away from the tumour rather than a precursor. Although this is a possibility, the lack of atypia in these cells (Fig. 1f) compared to the main tumour, lack of cyclin D1 expression (positive in tumour) and lack of any invasive nests in these areas argue against this. More cases showing "pecosis" need to be identified to resolve this issue. If "pecosis" is found to be a precursor lesion, it is still possible that most PEComas arise de novo and not from a precursor, and that this is a rare phenomenon.

The term "pecosis" should not be confused with "pecomatosis", a term first applied to a single case in the literature that demonstrated numerous aggregates of PEC cells in the lamina propria of small bowel, myometrium and ovarian hilum in a tuberous sclerosis patient with a cervical PEComa [12]. These aggregates were felt not to be metastases of the cervical tumour, but rather a "field effect" in the abdomen. These pecomatosis aggregates were not confined to the walls of capillaries in a single continuous layer and are best regarded as microscopic benign PEComas.

Other than the tuberous sclerosis connection that does not appear to be important in the pathway to most PEComas, little is known of genes that may be involved in the pathogenesis of these tumours. A single malignant case in the colon was shown to over-express cyclin D1 by immunohistochemistry [43]. Cyclin D1 is a cell cycle regulator necessary for the transition through the G1→S checkpoint [3, 37, 42]. It is normally expressed transiently and may be constitutively expressed in many neoplasms including melanoma [40]. Soucek et al. [39] have shown cyclin D1 abnormalities associated with the loss of the TSC2 gene. Two of the three cyclin D1 positive cases in our series showed a diffuse expression in both classical and malignant areas, whereas one was positive only in the sarcomatous areas. If cyclin D1 has a role in the genesis of PEComa, it is not well understood and it warrants further study.

In conclusion, we have described four additional cases of malignant PEComa, all of which had pleomorphic areas and three of which showed significant sarcomatous areas. Malignant PEComa should be considered in the light microscopic differential diagnosis for all pleomorphic sarcomas. The recent report of focal HMB-45 positivity in undifferentiated soft tissue sarcomas should not be regarded as malignant PEComas in our opinion, and reflex melanocytic marker staining of these tumours is unwarranted [29]. At least, focal light microscopic suspicion of PEComa and diffuse myomelanocytic marker positivity is required to support this diagnosis. We also describe the first PEComa arising in a urachal remnant. One case of "pecosis", a lesion of uncertain etiology is described. Finally, cyclin D1 was strongly expressed in three of the four cases and may have a role in the genesis of these tumours.

References

1. Agaimy A, Wunsch PH (2006) Perivascular epithelioid cell sarcoma (malignant PEComa) of the ileum. Pathol Res Pract 202:37–41
2. Azad NS, Aziz AB, Pervez S, Kayani N (2006) Uterine perivascular epithelioid cell tumour presenting as a cervical mass. J Pak Med Assoc 56:83–84
3. Beijersbergen RL, Bernards R (1996) Cell cycle regulation by the retinoblastoma family of growth inhibitory proteins. Biochim Biophys Acta 1287:103–120
4. Bonetti F, Martignoni G, Colato C, Manfrin E, Gambacorta M, Faleri M, Bacchi C, Sin VC, Wong NL, Coady M, Chan JK (2001) Abdominopelvic sarcoma of perivascular epithelioid cells. Report of four cases in young women, one with tuberous sclerosis. Mod Pathol 14:563–568
5. Bonetti F, Pea M, Martignoni G, Zamboni G (1992) PEC and sugar. Am J Surg Pathol 16:307–308
6. Bonetti F, Pea M, Martignoni G, Zamboni G, Iuzzolino P (1991) Cellular heterogeneity in lymphangiomyomatosis of the lung. Hum Pathol 22:727–728
7. Chen IY, Yang SF, Chen FM, Chai CY (2005) Abdominopelvic perivascular epithelioid cell tumor with overt malignancy: a case report. Kaohsiung J Med Sci 21:277–281
8. D'Andrea V, Lippolis G, Biancari F, Ruco LP, Marzullo A, Wedard BM, Di Matteo FM, Sarmiento R, Dibra A, De Antoni E (1999) A uterine pecoma: a case report. G Chir 20:163–164
9. de Saint Aubain Somerhausen N, Gomez Galdon M, Bouffioux B, Courtin C, Theunis A, Vogeleer MN, Myant N (2005) Clear cell 'sugar' tumor (PEComa) of the skin: a case report. J Cutan Pathol 32:441–444
10. Dimmler A, Seitz G, Hohenberger W, Kirchner T, Faller G (2003) Late pulmonary metastasis in uterine PEComa. J Clin Pathol 56:627–628
11. Evert M, Wardelmann E, Nestler G, Schulz HU, Roessner A, Rocken C (2005) Abdominopelvic perivascular epithelioid cell sarcoma (malignant PEComa) mimicking gastrointestinal stromal tumour of the rectum. Histopathology 46:115–117
12. Fadare O, Parkash V, Yilmaz Y, Mariappan MR, Ma L, Hileeto D, Qumsiyeh MB, Hui P (2004) Perivascular epithelioid cell tumor (PEComa) of the uterine cervix associated with intraabdominal "PEComatosis": A clinicopathological study with comparative genomic hybridization analysis. World J Surg Oncol 19:35
13. Fink D, Marsden DE, Edwards L, Camaris C, Hacker NF (2004) Malignant perivascular epithelioid cell tumor (PEComa) arising in the broad ligament. Int J Gynecol Cancer 14:1036–1039
14. Folpe AL, Goodman ZD, Ishak KG, Paulino AF, Taboada EM, Meehan SA, Weiss SW (2000) Clear cell myomelanocytic tumor of the falciform ligament/ligamentum teres: a novel member of the perivascular epithelioid clear cell family of tumors with a predilection for children and young adults. Am J Surg Pathol 24:1239–1246
15. Folpe AL, McKenney JK, Li Z, Smith SJ, Weiss SW (2002) Clear cell myomelanocytic tumor of the thigh: report of a unique case. Am J Surg Pathol 26:809–812
16. Folpe AL, Mentzel T, Lehr HA, Fisher C, Balzer BL, Weiss SW (2005) Perivascular epithelioid cell neoplasms of soft tissue and gynecologic origin: a clinicopathologic study of 26 cases and review of the literature. Am J Surg Pathol 29:1558–1575
17. Fukunaga M (2004) Perivascular epithelioid cell tumor of the uterus: a case report. Int J Gynecol Pathol 23:287–291

18. Fukunaga M (2005) Perivascular epithelioid cell tumor of the uterus: report of four cases. Int J Gynecol Pathol 24:341–346
19. Gan MF, Jin M, Yu CK, Cai JF (2006) Perivascular epithelioid cell tumor (PEComa) of the uterine. Zhonghua Binglixue Zazhi 35:314–315
20. Gao Z, Bhuiya T, Anderson A (2004) Perivascular epithelioid cell tumour (PEComa) of the uterus associated with malignant neoplasm of the female genital tract. J Obstet Gynaecol 24:600–604
21. Greene LA, Mount SL, Schned AR, Cooper K (2003) Recurrent perivascular epithelioid cell tumor of the uterus (PEComa): an immunohistochemical study and review of the literature. Gynecol Oncol 90:677–681
22. Harris GC, McCulloch TA, Perks G, Fisher C (2004) Malignant perivascular epithelioid cell tumour ("PEComa") of soft tissue: a unique case. Am J Surg Pathol 28:1655–1658
23. Hornick JL, Fletcher CD (2006) PEComa: what do we know so far? Histopathology 48:75–82
24. Iyengar P, Deangelis DD, Greenberg M, Taylor G (2005) Perivascular epithelioid cell tumor of the orbit: a case report and review of the literature. Pediatr Dev Pathol 8:98–104
25. Jeon IS, Lee SM (2005) Multimodal treatment using surgery, radiotherapy, and chemotherapy in a patient with a perivascular epithelioid cell tumor of the uterus. J Pediatr Hematol/Oncol 27:681–684
26. Kim HJ, Lim SJ, Choi H, Park K (2006) Malignant clear-cell myomelanocytic tumor of broad ligament—a case report. Virchows Arch 448:867–870
27. Koutlas IG, Pambuccian SE, Jessurun J, Manivel JC, Gopalakrishnan R (2005) Perivascular epithelioid cell tumor of the oral mucosa. Arch Pathol Lab Med 129:690–693
28. Lehman NL (2003) Malignant PEComa of the skull base. Am J Surg Pathol 28:1230–1232
29. Mai KT, Belanger EC (2006) Perivascular epithelioid cell tumour (PEComa) of the soft tissue. Pathology 38:415–420
30. Mentzel T, Reisshauer S, Rutten A, Hantschke M, Soares de Almeida LM, Kutzner H (2005) Cutaneous clear cell myomelanocytic tumour: a new member of the growing family of perivascular epithelioid cell tumours (PEComas). Clinicopathological and immunohistochemical analysis of seven cases. Histopathology 46:498–504
31. Pan CC, Jong YJ, Chai CY, Huang SH, Chen YJ (2006) Comparative genomic hybridization study of perivascular epithelioid cell tumor: molecular genetic evidence of perivascular epithelioid cell tumor as a distinctive neoplasm. Hum Pathol 37:606–612
32. Pan CC, Yang AH, Chiang H (2003) Malignant perivascular epithelioid cell tumor involving the prostate. Arch Pathol Lab Med 127:96–98
33. Parfitt JR, Bella AJ, Izawa JI, Wehrli BM (2006) Malignant neoplasm of perivascular epithelioid cells of the liver. Arch Pathol Lab Med 130:1219–1222
34. Parfitt JR, Bella AJ, Wehrli BM, Izawa JI (2006) Primary PEComa of the bladder treated with primary excision and adjuvant interferon-alpha immunotherapy: a case report. BMC Urol 22:20
35. Pea M, Bonetti F, Zamboni G, Martignoni G, Fiore-Donati L, Doglioni C (1991) Clear cell tumor and angiomyolipoma. Am J Surg Pathol 15:199–202
36. Pea M, Bonetti F, Zamboni G, Martignoni G, Riva M, Colombari R, Mombello A, Bonzanini M, Scarpa A, Ghimenton C (1991) Melanocyte-marker-HMB-45 is regularly expressed in angiomyolipoma of the kidney. Pathology 23:185–188
37. Sherr CJ, Roberts JM (1995) Inhibitors of mammalian G1 cyclin-dependent kinases. Genes Dev 9:1149–1163
38. Silva EG, Deavers MT, Bodurka DC, Malpica A (2004) Uterine epithelioid leiomyosarcomas with clear cells: reactivity with HMB-45 and the concept of PEComa. Am J Surg Pathol 28:244–249
39. Soucek T, Pusch O, Wienecke R, DeClue JE, Hengstschlager M (1997) Role of the tuberous sclerosis gene-2 product in cell cycle control. Loss of the tuberous sclerosis gene-2 induces quiescent cells to enter S phase. J Biol Chem 272:29301–29308
40. Utikal J, Udart M, Leiter U, Peter RU, Krahn G (2005) Additional cyclin D (1) gene copies associated with chromosome 11 aberrations in cutaneous malignant melanoma. Int J Oncol 21:597–605
41. Vang R, Kempson RL (2002) Perivascular epithelioid cell tumor ('PEComa') of the uterus: a subset of HMB-45-positive epithelioid mesenchymal neoplasms with an uncertain relationship to pure smooth muscle tumors. Am J Surg Pathol 26:1–13
42. Weinberg RA (1995) The retinoblastoma protein and cell cycle control. Cell 81:323–330
43. Yamamoto H, Oda Y, Yao T, Oiwa T, Kobayashi C, Tamiya S, Kawaguchi K, Hino O, Tsuneyoshi M (2006) Malignant perivascular epithelioid cell tumor of the colon: report of a case with molecular analysis. Pathol Int 56:46–50

Virchows Arch (2007) 450:471–474
DOI 10.1007/s00428-007-0377-8

CASE REPORT

Expression of the breast differentiation antigen NY-BR-1 in a phyllodes tumor of the vulva

Olivier T. Giger · Elena Lacoste · Christoph Honegger · Barbara Padberg · Holger Moch · Zsuzsanna Varga

Received: 5 December 2006 / Accepted: 25 January 2007 / Published online: 21 February 2007
© Springer-Verlag 2007

Abstract We describe a phyllodes tumor of borderline malignancy in the labium majus of a 49-year-old woman. The histogenetic origin of phyllodes tumors in the vulva is controversial. Strong immunoreactivity for NY-BR-1, a novel breast differentiation antigen, was demonstrated within the epithelial components of the phyllodes tumor. A similar expression pattern was observed in mammary-like glands of the vulva. These findings provide further evidence that phyllodes tumors of the vulva might derive from mammary-like glands in the labium majus or from ectopic breast tissue.

Keywords Vulva · Phyllodes tumor · NY-BR-1 · Mammary-like glands

Introduction

Mammary glands are modified apocrine glands arising along the mammary ridges, which appear on either side of the body in the fourth week of embryonal development, persisting only for a week. Remnants of these ridges can result in an arborising mesh of canals, giving rise to aberrant lactiferous ducts at anatomical sites other than the breast in the form of ectopic breast tissue. A fully formed mammary gland arising in the vulvar region was first described in 1872 by Hartung in a 30-year-old woman at the left labium majus. Since then, various benign and malignant variants of epithelial mammary tumors have been described, and ectopic mammary glands have been regarded as the tissue of origin of these neoplasms.

It has been reported that histologic changes in the ectopic breast tissue are, in general, similar to hormon-induced lesions in the breast occurring during puberty and early pregnancy [9]. Benign or malignant tumors of the vulva other then squamous neoplasms occur very rarely [20]. Whether proliferative processes mimicking breast lesions in the anogenital region evolve from remnants of the mammary ridges or originate from local adnexal structures, e.g. eccrine, sebaceous and apocrine glands of the skin, from mammary-like glands (MLGs) of the vulva, or whether they arise in neoplastically transformed ectopic breast tissue are still a question of debate.

In this report, we present a rare case of a phyllodes tumor in the vulva. We show that the recently described breast differentiation antigen NY-BR-1 is expressed in this tumor at an extramammary site as well as in MLGs of the vulva.

Clinical history

A 49-year-old hysterectomized, smoking (60 package years) but otherwise healthy perimenopausal patient presented with a rapidly growing mass at the labium majus near the clitoris on the right side. The patient was treated with 17-β-estradiole for menopausal symptoms. The symptoms were spotting and discharge. The lesion, which developed within 5 weeks, measured 3.7 cm in diameter and appeared sharply circumscribed. The tumor was excised surgically. A second resection was performed 2 months after the first tumor excision.

O. T. Giger (✉) · B. Padberg · H. Moch · Z. Varga
Institute of Surgical Pathology, University Hospital of Zurich,
Schmelzbergstrasse 12,
CH 8091 Zurich, Switzerland
e-mail: Olivier.giger@hispeed.ch

E. Lacoste · C. Honegger
Department of Gynecology, Hospital Uster,
Uster, Switzerland

Materials and methods

The surgical specimen was fixed in 4% buffered formalin and submitted entirely for histology. Two-micrometer sections from the paraffin-embedded tissue were taken for immunohistochemistry and haematoxylin and eosin (H&E) staining (Superfrost Plus, Menzel, Braunschweig, Germany). Immunostaining for mAb NY-BR-1 [21]; Ludwig Institute, New York) was performed on Ventana Benchmark (Ventana Medical Systems, Tucson, AZ) at a dilution of 1:400 (concentration, 2 μg/ml), MIB-1 (DAKO Diagnostics, dilution 1:20), CD34 (Serotec, dilution 1:50), estrogen receptor (6F11, Ventana dispenser), and progesterone receptor (1A6, Ventana dispenser).

Results

On gross examination, the specimen appeared as a polypoid firm lesion, with an uneven surface. The polyp was covered by normal epidermis. The cut surface was light gray, showing a firm sharply demarked tumor of 3.7 cm in diameter (Fig. 1).

The histological examination of the tumor revealed a subcutaneous mass consisting of a predominant stromal component, interrupted by leaf-like spaces lined by an epithelial component with bilayered epithelia consisting of myoepithelial and secretory cells, which directly harbored to the surface and covered the same one superficially. The surface of the tumor was focally ulcerated, without direct infiltration through neoplastic cells (Fig. 2).

The lining was predominantly composed of secretory (apocrine)-type epithelia and resembled mammary glandular epithelia. The secretory epithelial cells demonstrated a strong nuclear and cytoplasmatic immunoreactivity to NY-BR-1 and a 100% nuclear immunoreactivity for estrogen and progesterone receptors. No atypia or significant mitotic activity was present in the epithelial tumor component. The stroma was hypercellular with spindle-shaped, moderately pleomorphic cells with pale elongated nuclei and scanty cytoplasm. Focally, the mitotic activity of the stroma was increased (three to four mitoses per ten high-power fields, HPF). The proliferation index was 5% (MIB-1, Ki67). The neoplastic stroma demonstrated a stronger immunoreactivity for CD34 than the surrounding subcutaneous connective tissue. There was a small intraductal papilloma within the polypoid lesion. Overtly polymorphic stromal cells, necrosis or brisk mitotic activity exceeding ten mitoses per ten HPF were absent. Therefore, the tumor was diagnosed as a phyllodes tumor with "borderline" malignancy.

Fig. 1 Phyllodes tumor of the vulva. Overview (H&E). Typical leaf-like pattern (scale bar=1 cm)

Eccrine glands and MLGs were observed adjacent to the tumor. The latter also showed nuclear and cytoplasmic reactivity for NY-BR-1.

Because of the incomplete resection and the unpredictable behavior of "borderline" phyllodes tumors, a second resection was performed 2 months after the primary excision. The resection specimen contained MLGs, regenerative tissue with foreign body reaction but no remnants of the phyllodes tumor.

Discussion

In this report, we describe a phyllodes tumor of the vulva and discuss its histogenesis in the light of its expression of the novel breast differentiation antigen NY-BR1.

Various benign and malignant tumors resembling breast neoplasms have been described in the vulvar region [1–3, 5, 6, 8, 9, 15, 16, 20]. It has been suggested that these tumors derive from ectopic breast tissue or from MLG.

Cystosarcoma phyllodes of the breast, today preferentially named phyllodes tumor, was first described by Johannes Müller in 1838 [7]. According to our knowledge, five phyllodes tumors [4, 14, 17, 18] of the vulva and one phyllodes tumor of the perineum [13] have been reported. More than two dozen fibroadenomas of the vulva have been described, and it has been discussed whether these neoplasms arise from skin adherence glands or from ectopic mammary tissue.

The epithelial cells of the present tumor demonstrate strong cytoplasmic and nuclear NY-BR-1 immunoreactivity. NY-BR-1 is a novel mammary differentiation antigen. It was recently identified by SEREX analysis of a metastatic breast carcinoma patient [10–12]. The NY-BR-1 gene has been mapped to chromosome 10p11–12 and is composed of 37 exons. It encodes a peptide of Mr 150,000 to 160,000, which is regarded as a putative transcription factor. NY-BR-

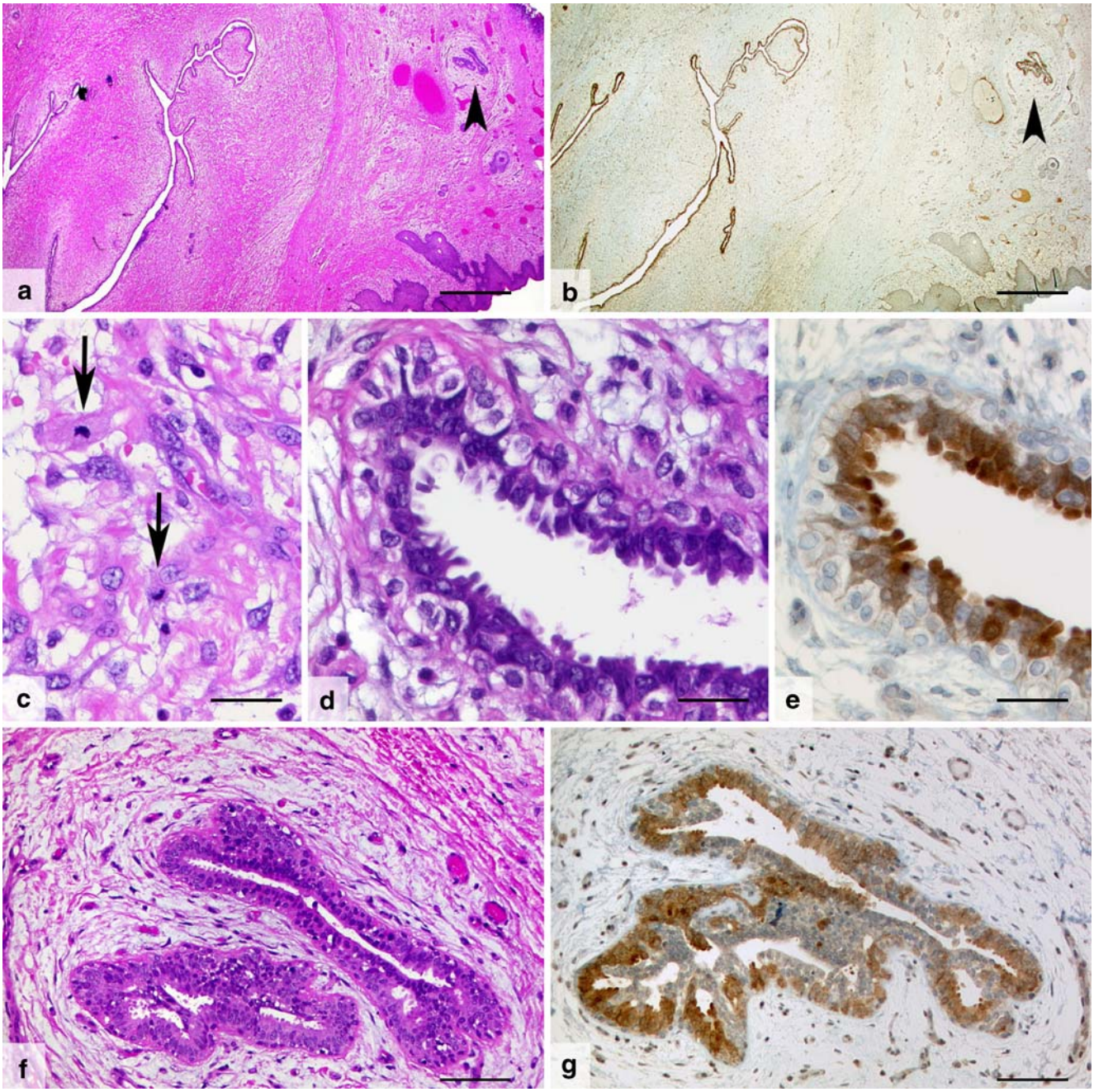

Fig. 2 Phyllodes tumor of the vulva. Histology and immunohistochemistry. *A–B* Mammary-like glands in the vicinity of the phyllodes tumor (*arrowhead*) HE (**a**) and NY-BR-1 immunohistochemistry (**b**; A–B scale bar=1 mm). *C–E* Detail of stroma with increased mitotic activity. *Arrows* indicate two mitoses in one HPF (**c**); Bilayered epithelium consisting of myoepithelial- and secretory-cell layers (**d**); NY-BR-1 immunoreactivity in cytoplasm and nuclei of secretory ductal cells (**e**; C–D scale bar=20 μm). Legend to figures: *F–G* MLG in the surroundings of the phyllodes tumor. HE (**f**) and NY-BR-1 (**g**; F–G scale bar=0.15 mm)

1 mRNA expression was found in a high percentage of breast cancers (84%) and normal breast tissue and at a much lower level in normal adult testis but not in other normal tissues [10]. We have recently demonstrated strong protein expression in mammary glands and in carcinomas of the breast using immunohistochemistry [21]. Our findings suggest that the novel monoclonal NY-BR-1 antibody can be used as a surrogate marker for tumors of breast origin.

The NY-BR-1 expression is a strong argument for a derivation of the phyllodes tumor of the vulva from MLGs or from ectopic breast tissue. Further evidence for a derivation of the phyllodes tumor from MLGs is its location at the inner side of the labium majus and the

prominent MLGs in the immediate surroundings. Van der Putte [19, 20] suggests that vulvar neoplasms resembling breast tumors most probably arise in MLGs. He observed that many of these lesions (a) greatly resemble but are not identical to corresponding lesions of the breast, (b) occur also in the perineum and around the anus but rarely elsewhere on the skin and (c) are elements of discussion concerning their derivation that focus on eccrine or apocrine glands or their precursor cells rather than on mammary tissue. He further argues that these features reflect basic elements of the MLGs that are directly related to eccrine glands and show apocrine metaplasia. Some MLGs reveal a mammary-type histology as the predominant feature.

The behavior of phyllodes tumors is difficult to predict by histology alone. In the breast, phyllodes tumors are classified into benign, borderline and malignant according to mitotic rate, nuclear pleomorphism and presence of necrosis.

Because of the increased mitotic activity, the tumor of our patient was classified as "borderline." After incomplete excision of the lesion, an additional resection was performed to prevent local recurrence.

In summary, we present a phyllodes tumor of the vulva with strong expression of the breast differentiation antigen NY-BR-1. MLGs of the vulva also express this antigen and were abundantly present in close vicinity to the tumor. Therefore, we speculate that at least some phyllodes tumors of the vulva are derived from such glands, although we cannot exclude that ectopic mammary glands are also the origin of such vulvar tumors.

References

1. Baisre A, Heller DS, Lee J, Zheng P (2002) Fibroadenoma of the vulva. A report of two cases. J Reprod Med 47(11):949–951
2. Baykal C, Tulunay G, Usubutun A, Kucukali T, Ozer S, Demir OF (2004) Fibrocystic disease of vulvar ectopic breast tissue. Case report and review of the literature. Gynecol Obstet Investig 58(3):151–154
3. Boscaino A, Sapere P, De Rosa GD (1996) Fibroadenoma of the vulva. Report of a case. Pathologica 88(5):444–446
4. Chulia MT, Paya A, Niveiro M, Ceballos S, Aranda FI (2001) Phyllodes tumor in ectopic breast tissue of the vulva. Int J Surg Pathol 9(1):81–83
5. Degrell I (1979) Fibroadenoma in an accessory breast. A case of polythelia and fibroadenoma in the left breast region and a perivulvar accessory breast. Fortschr Med 97(29):1269–1270 [in German]
6. Erb-Gremillet S, Gunther M, Amiaux F, Parache RM (1999) Breast-like carcinoma of the vulva. Ann Pathol 19(2):124–127 [in French]
7. Fiks A (1981) Cystosarcoma phyllodes of the mammary gland—Müller's tumor. For the 180th birthday of Johannes Müller. Virchows Arch A Pathol Anat Histopathol 392(1):1–6
8. Foushee JH, Pruitt AB Jr (1967) Vulvar fibroadenoma from aberrant breast tissue. Report of 2 cases. Obstet Gynecol 29 (6):819–823
9. Grossl NA (2000) Supernumerary breast tissue: historical perspectives and clinical features. South Med J 93(1):29–32
10. Jager D, Stockert E, Gure AO, Scanlan MJ, Karbach J, Jager E, Knuth A, Old LJ, Chen YT (2001) Identification of a tissue-specific putative transcription factor in breast tissue by serological screening of a breast cancer library. Cancer Res 61(5):2055–2061
11. Jager D, Unkelbach M, Frei C, Bert F, Scanlan MJ, Jager E, Old LJ, Chen YT, Knuth A (2002) Identification of tumor-restricted antigens NY-BR-1, SCP-1, and a new cancer/testis-like antigen NW-BR-3 by serological screening of a testicular library with breast cancer serum. Cancer Immun 2:5
12. Jager D, Taverna C, Zippelius A, Knuth A (2004) Identification of tumor antigens as potential target antigens for immunotherapy by serological expression cloning. Cancer Immunol Immunother 53 (3):144–147
13. Kazakov DV, Bisceglia M, Mukensnabl P, Michal M (2005) Pseudoangiomatous stromal hyperplasia in lesions involving anogenital mammary-like glands. Am J Surg Pathol 29(9):1243–1246
14. Mariappan MR, Lagera JE, Fadare O, Sibley RK (2006) A 69-year-old woman with a vulvar lesion. Phyllodes tumor of the vulva. Arch Pathol Lab Med 130(1):e11–e12
15. Marshall MB, Moynihan JJ, Frost A, Evans SR (1994) Ectopic breast cancer: case report and literature review. Surg Oncol 3 (5):295–304
16. Prasad KR, Kumari GS, Aruna CA, Durga K, Kameswari VR (1995) Fibroadenoma of ectopic breast tissue in the vulva. A case report. Acta Cytol 39(4):791–792
17. Tbakhi A, Cowan DF, Kumar D, Kyle D (1993) Recurring phyllodes tumor in aberrant breast tissue of the vulva. Am J Surg Pathol 17(9):946–950
18. Tresserra F, Grases PJ, Izquierdo M, Cararach M, Fernandez-Cid A (1998) Fibroadenoma phyllodes arising in vulvar supernumerary breast tissue: report of two cases. Int J Gynecol Pathol 17 (2):171–173
19. van der Putte SC (1991) Anogenital "sweat" glands. Histology and pathology of a gland that may mimic mammary glands. Am J Dermatopathol 13(6):557–567
20. van der Putte SC (1994) Mammary-like glands of the vulva and their disorders. Int J Gynecol Pathol 13(2):150–160
21. Varga Z, Theurillat JP, Filonenko V, Sasse B, Odermatt B, Jungbluth AA, Chen YT, Old LJ, Knuth A, Jager D, Moch H (2006) Preferential nuclear and cytoplasmic NY-BR-1 protein expression in primary breast cancer and lymph node metastases. Clin Cancer Res 12(9):2745–2751

Virchows Arch (2007) 450:475–477
DOI 10.1007/s00428-007-0368-9

LETTER TO THE EDITOR

Intravascular myopericytoma of the oral mucosa: a rare histologic variant in an uncommon location

Fumio Ide · Kumi Obara · Hiroyuki Yamada · Kenji Mishima · Ichiro Saito

Received: 15 September 2006 / Revised: 25 December 2006 / Accepted: 2 January 2007 / Published online: 30 January 2007
© Springer-Verlag 2007

Dear Editor:

Myopericytoma (MPC) belongs to a family of benign tumors showing a myoid/pericytic line of differentiation [8]. The most common anatomic setting for MPC is the skin and superficial soft tissues of distal extremities. With increased recognition, a wider distribution is described [10]; however, an intraoral lesion appears never to have been recorded.

The patient was a 45-year-old woman with a painless, slowly expanding mass that had been present in her right buccal mucosa for more than 2 years. Clinical examination revealed a freely movable, 2-cm spherical nodule with a purplish hue in the submucosal space (Fig. 1a). The smooth-surfaced tumor attached to the buccal fat pad was excised, and 9 years later, there was no evidence of recurrence.

Microscopically, the lesion presented as a discrete intravenous solid mass filling the distended lumen (Fig. 1b). It was focally attached to the attenuated vessel wall by the stalk, and both internal elastic lamella and smooth muscle layer were interrupted at this site. The luminal aspect of the tumor was covered by a single layer of endothelium. There was no formation of thrombus. The tumor was typified by a hemangiopericytomatous growth pattern of thin-walled branching vessels, ranging from slit-like capillary size (Fig. 1c) to gaping cavernous spaces (Fig. 1d). A multilayered, concentric perivascular orientation of myoid-appearing oval-to-spindle cells was easily identified (Fig. 1e). Often, myoid tumor cells spun off from the thick-walled vessels (Fig. 1f), and at high magnification, intervascular sweeping fascicles of elongated cells with abundant eosinophilic cytoplasm and cigar-shaped nuclei showed morphology of smooth muscle differentiation (Fig. 1g). Also of note were scattered nodules of glomoid cytomorphology. Tumor cells, irrespective of their shape, expressed immunopositivity for α-smooth muscle actin (Fig. 1h) and h-caldesmon (Fig. 1i), but were desmin negative (Fig. 1j). No reactivity for CD34 was obtained in tumor cells. Ultrastructurally, prominent external lamina, numerous pinocytotic vesicles, thin filaments with dense bodies, and attachment plaques that suggest myoid differentiation were all appealing (Fig. 2a,b). The fine structure of uniform rounded cells with distinct cell borders corresponded exactly to a glomus line (Fig. 2b).

Within MPC, the intravascular type is a rare histologic variant [10]. To our knowledge, this particular subset has been documented only two (a total of six cases) [9, 10] or three times, if we accept the case of Sajben et al. [14] as the first example. All tumors were located in the subcutis, including elbow, thigh, hand, trunk, and foot; the present lesion arose in the noncutaneous submucosal site, further expanding the list of locations. The differential diagnostic alternatives include a number of other reactive or neoplastic processes that can be intravascular, i.e., *glomus tumor* [1], *papillary endothelial hyperplasia* [6], *pyogenic granuloma* [3], *nodular fasciitis* [12], *leiomyomatosis* [2]. The points of microscopic diagnostic separation were summarized in the previous report [9]. Considering no detectable tumor outside the vessel, none of the intravascular MPC represented a vascular invasion, as occasionally seen in glomus tumors.

The present tumor is referred to as angioleiomyoma-like MPC, depending on the predominant growth pattern [10]. In contrast to classic angioleiomyoma, myoid tumor cells

F. Ide (✉) · K. Obara · H. Yamada · K. Mishima · I. Saito
Department of Pathology,
Tsurumi University School of Dental Medicine,
2-1-3 Tsurumi, Tsurumi-ku,
Yokohama 230-8501, Japan
e-mail: ide-f@tsurumi-u.ac.jp

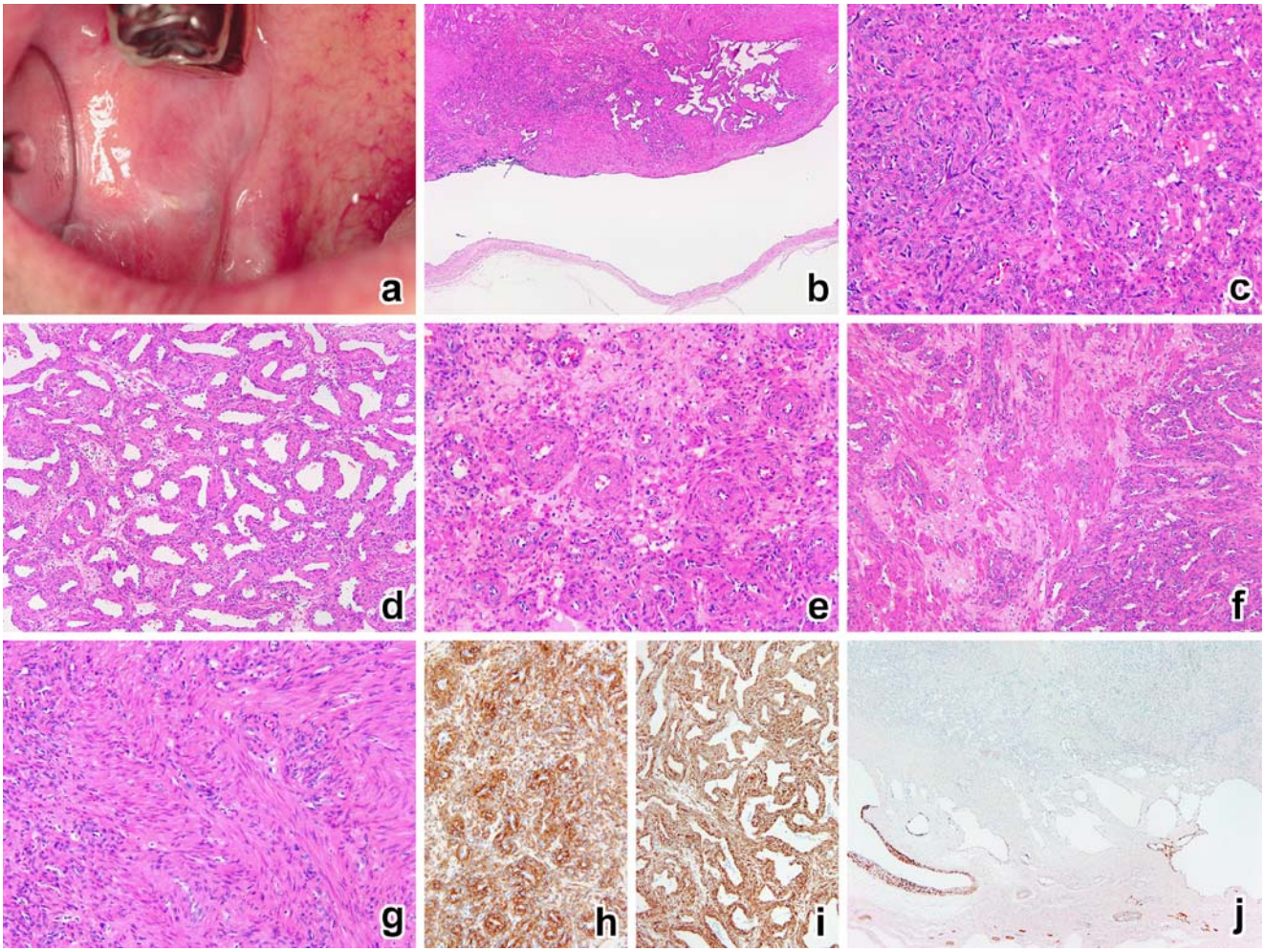

Fig. 1 Morphologic spectrum of intravascular myopericytoma. **a** Submucosal mass in the right buccal tissue. **b** Purely intravenous location, H&E, ×40. **c** and **d** Hemangiopericytoma-like vasculature, H&E, **c**, ×200; **d**, ×100. **e** Concentric "onion skin" pattern, H&E, ×100. **f** Myoid tumor cells with brightly eosinophilic, fibrillar cytoplasm, H&E, ×100. **g** Leiomyoma-like area, H&E, ×200. **h** and **i** Positivity for α-smooth muscle actin (**h**) and h-caldesmon (**i**) accentuates the perivascular arrangement, Immunostain, ×200. **j** Desmin-positive subintimal vascular smooth muscle is carried, via the stalk, a short distance into desmin-negative intraluminal tumor, Immunostain, ×40

directly streaming from medium-sized muscular vessels remained unlabelled for desmin, suggesting a less-differentiated smooth muscle phenotype. Focal areas also shared virtual microscopic and immunophenotypic identity with glomus tumor. Such conjoint or intermediate features codify a single pathologic spectrum of these three tumor types [5, 8, 10]. Based on the ultrastructural attributes [11, 13], the lineage of differentiation pursued by MPC is the perivascular myoid cell/pericyte, named myopericyte [5, 7, 13]. Given the previous case that contained separate tumor nodules within the vein wall [10] and the present findings as well, intramural pericytic precursors native to the venous part of an arteriovenous anastomosis appear to be special candidate cells of origin for intravascular MPC, but we lack concrete proof at present.

The substantial morphological overlap left us querying whether MPC would have been subsumed within the category of myofibroma, hemangiopericytoma, glomus tumor, or angioleiomyoma in the past [4, 5, 7, 10, 13, 14]. Our review of the description and illustrations provided in the relevant literature, however, failed to disclose any of oral lesions histologically identical to our own. Although the involvement of submucosal vein of an adult female's buccal tissue is not surprising, it is hoped that, by presenting this first intraoral case of intravascular MPC, it will aid others in recognizing this rare and unique entity.

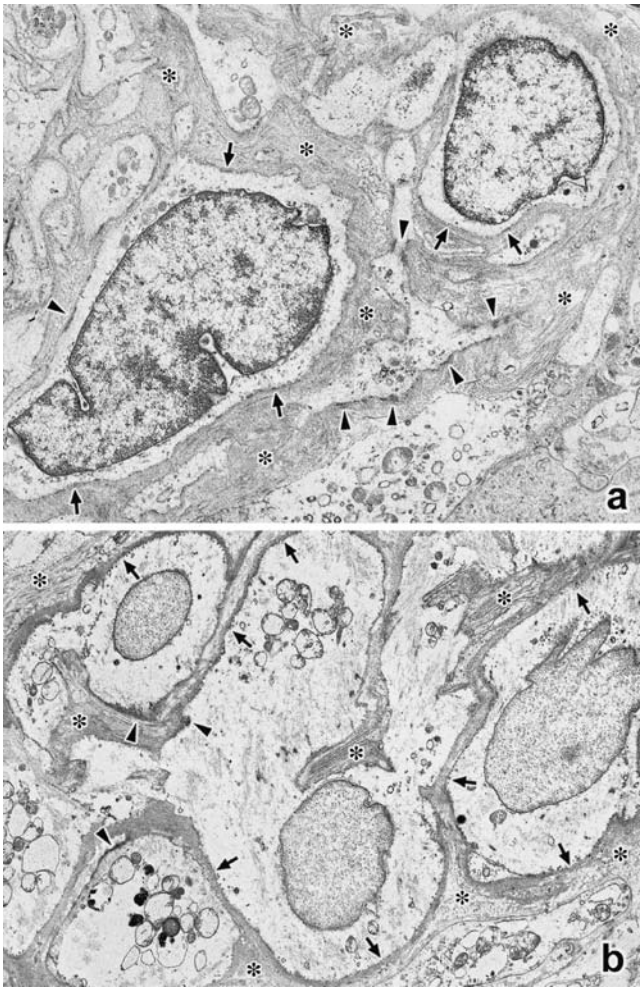

Fig. 2 Ultrastructural characteristics of myopericytoma. **a** Pericytic tumor cells possess paucity of organelles, focal subplasmalemmal densities (*arrow heads*), pinocytotic vesicles (*arrows*), and prominent basal lamina (*asterisks*), ×6,300. **b** Glomoid tumor cells invested by dense basal lamina (*asterisks*) have cytoplasmic thin filaments with occasional dense bodies, pinocytotic vesicles (*arrows*), and attachment plaques (*arrow heads*), suggesting myoid differentiation, ×5,300

References

1. Beham A, Fletcher CDM (1991) Intravascular glomus tumour: a previously undescribed phenomenon. Virchows Arch A Pathol Anat Histopathol 418:175–177
2. Clement PB, Young RH, Scully RE (1988) Intravenous leiomyomatosis of the uterus. A clinicopathological analysis of 16 cases with unusual histologic features. Am J Surg Pathol 12:932–945
3. Cooper PH, McAllister HA, Helwig EB (1979) Intravenous pyogenic granuloma. A study of 18 cases. Am J Surg Pathol 3:221–228
4. Dray MS, McCarthy SW, Palmer AA, Bonar SF, Stalley PD, Marjoniemi V, Millar E, Scolyer RA (2006) Myopericytoma: a unifying term for a spectrum of tumours that show overlapping features with myofibroma. A review of 14 cases. J Clin Pathol 59:67–73
5. Granter SR, Badizadegan K, Fletcher CDM (1998) Myofibromatosis in adults, glomangiopericytoma, and myopericytoma. A spectrum of tumors showing perivascular myoid differentiation. Am J Surg Pathol 22:513–525
6. Hashimoto H, Daimaru Y, Enjoji M (1983) Intravascular papillary endothelial hyperplasia. A clinicopathologic study of 91 cases. Am J Deramtopathol 5:539–546
7. Kutzner H (1998) Perivascular myomas: a new concept for "myofibroblastic" tumors with perivascular myoid differentiation. Verh Dtsch Ges Pathol 82:301–308
8. McMenamin ME (2002) Myopericytoma. In: Fletcher CDM, Unni K, Mertens F (eds) Pathology and genetics of tumours of soft tissue and bone. IARC, Lyon, pp 138–139
9. McMenamin ME, Calonje E (2002) Intravascular myopericytoma. J Cutan Pathol 29:557–561
10. Mentzel T, Dei Tos AP, Sapi Z, Kutzner H (2006) Myopericytoma of skin and soft tissues. Clinicopathologic and immunohistochemical study of 54 cases. Am J Surg Pathol 30:104–113
11. Mikami Y, Shiomi T, Manabe T (2002) Perivascular myoma: case report with immunohistochemical and ultrastructural studies. Pathol Int 52:69–74
12. Patchefsky AS, Enzinger FM (1981) Intravascular fasciitis: a report of 17 cases. Am J Surg Pathol 5:29–36
13. Requena L, Kutzner H, Hugel H, Rutten A, Furio V (1996) Cutaneous adult myofibroma: a vascular neoplasm. J Cutan Pathol 23:445–457
14. Sajben FP, Barnette DJ, Barrett TL (1999) Intravascular angioleiomyoma. J Cutan Pathol 26:165–167

Virchows Arch (2007) 450:479–481
DOI 10.1007/s00428-007-0369-8

LETTER TO THE EDITOR

Intestinal-type adenocarcinoma arising in a congenital sublingual teratoid cyst

Abbas Agaimy · Beate Raab · Viktor Bonkowsky · Peter H. Wünsch

Received: 20 November 2006 / Revised: 27 December 2006 / Accepted: 2 January 2007 / Published online: 7 February 2007
© Springer-Verlag 2007

Dear Editor,

The generic term *dermoid* has been applied to a variety of benign congenital (non-teratomatous) cysts of the head and neck region probably derived from misplaced multipotential ectodermal cells entrapped during midline fusion of the first and second pharyngeal arches [4, 5, 9]. Based on their lining and constituents, head and neck *dermoids* have been traditionally classified into three major subtypes [5, 9]. The simple (epidermoid) cyst represents the most common type and is lined by keratinising squamous epithelium lacking dermal appendages. The compound (dermoid) cyst shows a similar lining but contains, in addition, hairs and skin appendages. The least common type, the complex (teratoid) cyst, reveals an admixture of tissue derivatives from the three germ layers, similar to mature cystic teratoma, from which it takes its name. The lateral third of the eyebrow represents the most common site for head and neck *dermoids* [5, 9]. Approximately 1.6% occur in the floor of the mouth [5, 9], and of them, only 1.8% are teratoid cysts [4, 5, 9]. Head and neck *dermoids* usually present in the early adult life as asymptomatic masses [5, 9], but may present in infancy and childhood with dysphagia, difficult breathing and protrusion of the tongue, depending on the site and size of the lesion [4]. A rapid increase in the size of a congenital cyst may suggest benign complications (bleeding or inflammation), but may rarely herald malignancy.

In the oral cavity, only a single example of squamous cell carcinoma that arose within a sublingual dermoid cyst has been reported so far [3]. We herein report on the first case of intestinal-type adenocarcinoma developing in a congenital sublingual teratoid cyst.

A 41-year-old man with a midline prelaryngeal mass present since birth presented with dysphagia and dyspnoea due to a recent rapid increase in the size of the mass during the last few weeks. The lesion had been aspirated twice previously, but cytology was not performed at that time. A clinical diagnosis of median cervical cyst was suggested by his physician and the patient was referred for surgical removal of the lesion. Clinical examination revealed a 4-cm-submental mass protruding into the left mouth floor. The mass was excised via a combined oral and extra-oral approach. A subsequent ipsilateral neck dissection showed no regional tumour spread. No additional therapy was recommended and the patient remained disease-free 14 months after surgery.

The surgical specimen measured 5×4×2 cm in maximum diameter and showed cystic areas filled with thick, red-brown, dirty secretions interrupted by grey-whitish solid tissue (Fig. 1a). Histologically, it was lined predominantly by ciliated respiratory epithelium and gastric epithelium with intervening small islands of intestinal epithelium and non-keratinising squamous epithelium (Fig. 1b). Lymphoid aggregates were seen beneath respiratory epithelium, as well as lobules of fundic and seromucous glands. The cyst was supported by a peripheral rim of loose connective tissue and disordered smooth muscle fibres. No thyroid tissue, skin appendages, mature cartilage or neuroglial elements were seen. The cyst lining was focally replaced by small foci of villous dysplasia mimick-

A. Agaimy (✉) · P. H. Wünsch
Institute of Pathology, Nuremberg Clinic Center,
Prof.-Ernst-Nathan-Strasse 1,
90419 Nuremberg, Germany
e-mail: abbas.agaimy@klinikum-nuernberg.de

B. Raab · V. Bonkowsky
Department of ENT, Nuremberg Clinic Center,
Nuremberg, Germany

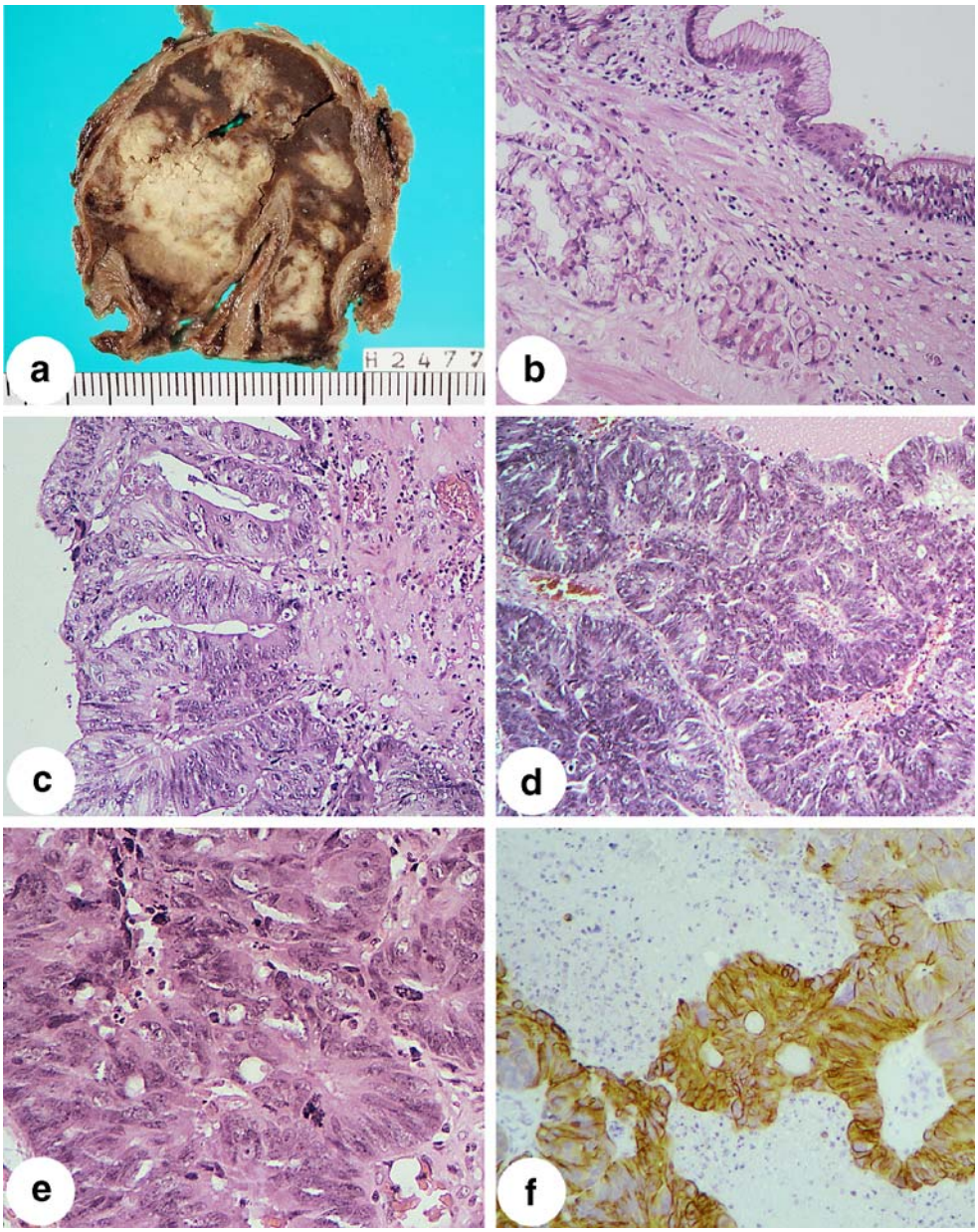

Fig. 1 **a** Gross specimen showing a thick-walled cyst filled with grey-whitish tumour tissue interrupted by dirty secretion. **b** Juxtaposed gastric and respiratory epithelium with intervening small focus of non-keratinising squamous epithelium (note disordered smooth muscle layer and pyloric and fundic glands). **c** Dysplastic villous glands supported by lamina propria. **d** Exophytic intracystic tumour reminiscent of colorectal cancer with high-grade nuclear features (**e**) and strong reactivity for CK20 (**f**)

ing colorectal adenoma (Fig. 1c). The cyst lumen was filled by an exophytic growth of atypical glands showing elongated high-grade nuclei and pale-eosinophilic cytoplasm arranged in tubular, villous and complex gland-in-gland pattern in a background of retained dirty secretions and cell debris (Fig. 1d,e). Lymphovascular invasion was absent. The carcinomatous component was confined entirely within the cyst wall. Immunohistochemistry revealed a strong reactivity for EMA, pan-keratin (AE1/AE3), CK20 (Fig. 1f) and CEA in almost all tumour cells. The tumour cells did not stain for CK7, CK14, S100 and TTF-1.

This unique case demonstrates the occurrence of malignancy as a long-term and rare complication of a congenital teratoid cyst of the oral cavity. Similar to mature teratoma, the teratoid cyst shows tissue elements from all three germ layers. The distinction between the two is rather arbitrary, as lesions with similar histological features are considered mature teratomas (true germ cell neoplasms) in the ovary, but referred to as "teratoid" in the head and neck to indicate their non-teratomatous congenital origin at the latter location from entrapped multipotential (somatic) ectodermal cells [5, 9]. However, subtle differences do exist between the two lesions. Teratoid cysts are usually already present at birth or early childhood, consistent with a congenital origin [5, 9], and may occasionally coexist with other congenital cysts [6, 10]. Histologically, neuroglial elements are fairly common in mature teratoma, but uncommon in teratoid cysts [1, 4, 5, 9]. Teratoid cysts are

sufficiently treated by simple surgical excision or enucleation [1, 4, 6, 10]. Late recurrence is rare [12].

Malignant transformation of congenital cysts could be a source of diagnostic confusion. In this setting, neoplasms with unexpected histology may be encountered at unusual anatomic sites, suggesting an erroneous diagnosis of metastatic carcinoma of unknown primary. Contrasting ovarian dermoid cysts (about 0.7–2% of them may harbour a somatic-type cancer, mainly squamous cell carcinoma) [11], malignant transformation of head and neck *dermoids* is exceptionally rare. Devine et al. described a case of squamous cell carcinoma that arose within a sublingual dermoid cyst [3]. Their patient received post-operative radiotherapy and he remained disease-free 2 years later. However, there are no sufficient data with regard to the appropriate treatment and long-term outcome of this rare type of cancer. In the ovary, somatic-type neoplasms confined to mature teratomas are considered comparable to stage IA ovarian cancer and are treated accordingly [8, 11]. The absence of extra-cystic tumour spread and lymphovascular invasion, as in the current case, suggests a better outcome. Our patient received no adjuvant therapy and he remained disease-free 14 months post-operatively.

The differential diagnosis in the current case was largely facilitated and limited by the confinement of the neoplasm to the cyst lumen and the evidence of its origin from dysplastic intestinal epithelium lining the cyst. However, if similar lesions present in small biopsies or at metastatic sites, they might pose a great diagnostic challenge. Salivary adenocarcinoma of diverse histological types represents the main consideration and can be excluded by appropriate criteria. To our knowledge, enteric-type adenocarcinoma has not been reported as primary salivary gland cancer. Other differential diagnoses include metastatic colorectal adenocarcinoma and intestinal-type pulmonary and sinonasal adenocarcinoma. The latter three types of neoplasms may not be reliably distinguishable from each other in small biopsies by light microscopic and immunohistochemical features alone, and a thorough clinical work-up to exclude an occult primary may be warranted [2, 7].

In summary, this report represents the second documentation of a malignancy developing in a longstanding congenital teratoid cyst of the mouth floor and the first case of adenocarcinoma in this particular setting at this location. Though rare, this type of cancer may be the source of great diagnostic confusion if encountered in small biopsies or at a metastatic site and should be included in the differential of non-salivary adenocarcinoma presenting in the head and neck. A rapid recent increase in the size of a longstanding congenital cyst may herald malignancy, underscoring the necessity for diagnostic intervention.

References

1. Babuccu O, Özen ÖI, Hosnuter M, Kargi E, Babuccu B (2003) The place of fine-needle aspiration in the preoperative diagnosis of the congenital sublingual teratoid cyst. Diagn Cytopathol 29:33–37
2. Cathro HP, Mills SE (2004) Immunophenotypic differences between intestinal-type and low-grade papillary sinonasal adenocarcinomas. An immunohistochemical study of 22 cases utilizing CDX2 and MUC2. Am J Surg Pathol 28:1026–1032
3. Devine JC, Jones DC (2000) Carcinomatous transformation of a sublingual dermoid cyst. A case report. Int J Oral Maxillofac Surg 29:126–127
4. Göl IH, Kiyici H, Yildirim E, Arda IS, Hicsönmez A (2005) Congenital sublingual teratoid cyst: a case report and literature review. J Pediatr Surg 40:E9–E12
5. Gold BD, Sheinkopf DE, Levy B (1974) Dermoid, epidermoid and teratomatous cysts of the tongue and the floor of the mouth. J Oral Surg 32:107–111
6. Ho MWS, Crean SJV (2003) Simultaneous occurrence of sublingual dermoid cyst and oral alimentary tract cyst in an infant: a case report and review of the literature. Int J Paediatr Dent 13:441–446
7. Inamura K, Satoh Y, Okumura S, Nakagawa K, Tsuchiya E, Fukayama M, Ishikawa Y (2005) Pulmonary adenocarcinomas with enteric differentiation. Histologic and immunohistochemical characteristics compared with metastatic colorectal cancers and usual pulmonary adenocarcinomas. Am J Surg Pathol 29:660–665
8. Min KJ, Jee BC, Lee HS, Kim YB (2006) Intestinal adenocarcinoma arising in a mature cystic teratoma of the ovary: a case report. Pathol Res Pract 202:531–535
9. New GB, Erich JB (1937) Dermoid cysts of the head and neck. Surg Gynecol Obstet 65:48–51
10. Obiechina AE, Arotiba JT, Ogunbiya JO (1999) Coexisting sublingual dermoid and bronchogenic cyst. Br J Oral Maxillofac Surg 37:58–60
11. Scully RE, Young RH, Clement PB (1998) Tumors of the ovary, maldeveloped gonads, fallopian tube, and broad ligament. In: Rosai J, Sobin LH (eds) Atlas of tumor pathology, 3rd series, fascicle 23. Armed Forces Institute of Pathology, Washington, D. C., pp 274–284
12. Shigematsu H, Dobashi A, Suzuki S, Kusama K, Sakashita H (2001) Delayed recurrence of teratoid cyst 17 years after enucleation. Oral Surg Oral Med Oral Pathol Oral Radiol Endod 92:539–542

Virchows Arch (2007) 450:483–485
DOI 10.1007/s00428-007-0373-z

LETTER TO THE EDITOR

Myxoid myofibroblastoma of the breast with atypical cells: a potential diagnostic pitfall

Gaetano Magro · Paolo Amico · Alessandra Gurrera

Received: 16 December 2006 / Revised: 11 January 2007 / Accepted: 18 January 2007 / Published online: 15 February 2007
© Springer-Verlag 2007

Keywords Myofibroblastoma · Myxoid variant · Atypical cells · Breast

Sir,

Myofibroblastoma of the breast is an unusual benign mesenchymal tumour that belongs to the family of the so-called benign spindle cell tumours of the mammary stroma [5, 6]. In its classic type, it is typically composed of bland-looking spindle cells exhibiting a variable fibro–myofibroblastic differentiation [5, 6]. In recent years, the morphological spectrum of this tumour has been broadened by the recognition of several variants, including epithelioid, lipomatous, fibromatosis-like, fibrous/collagenized, myxoid ones [4–6].

Recently, we have encountered two cases of mammary myofibroblastoma with atypical cells embedded within a prominent myxoid stroma. To the best of our knowledge, this unusual morphological variant has not hitherto been reported. Two male patients (63 and 56 years) presented with two nodular breast masses, measuring 3 and 3.5 cm in greatest dimension, respectively, which were surgically excised.

Histologically, both surgical samples were represented by unencapsulated mesenchymal tumours with pushing borders, composed of spindle to epithelioid cells, embedded in an abundant myxoid stroma containing isolated thick eosinophilic collagen bands (Figs. 1a and 2a). Myxoid matrix stained positively with Alcian blue at pH 2.5 and negative for periodic acid-Schiff. One tumour was hypocellular (Fig. 1a), while the other one showed alternating hypocellular and moderately cellular areas (Fig. 2a). Neoplastic cells had pale to deeply eosinophilic cytoplasm and round to oval nuclei containing one or two visible nucleoli. In both cases, a significant number of neoplastic cells (50–60%) exhibited a moderate to severe degree of nuclear pleomorphism (Figs. 1a,b and 2a,b). Some cells were bi- or multinucleated (Fig. 2b). A minor mature fatty component was scattered throughout both tumours. Mitoses were absent in the hypocellular tumour, while one mitosis per ten high power fields was observed in the other neoplasm. Necrosis was absent. No epithelial component was identified within both tumours. Immunohistochemically, the cells of both cases had a similar profile: diffuse and strong immunoreactivity to vimentin, α-smooth muscle actin and desmin (Fig. 1c), and a variable staining to CD34, bcl-2 protein, CD99, estrogen (ER), progesterone (PR), and androgen (AR) receptors. No immunoreactivity was obtained for pancytokeratin, epithelial membrane antigen, h-caldesmon, calponin, S-100 protein, and human melanoma black-45 (HMB-45). This immunophenotype was consistent with a fibro-myofibroblastic nature of the neoplastic cells.

We believe that the tumours herein presented fit within the spectrum of breast myofibroblastoma [5, 6], representing an uncommon morphological variant, for which the descriptive term "myxoid myofibroblastoma with atypical cells" is proposed. The following morphological and immunohistochemical features, typically seen in myofibroblastoma [5, 6], support our opinion: (1) Tumours were "pure mesenchymal lesions" lacking any epithelial component; (2) Tumours had pushing borders; (3) The myxoid extracellular matrix contained thick eosinophilic collagen bands; (4) Neoplastic cells resulted to have a fibro-

G. Magro (✉) · P. Amico · A. Gurrera
Dipartimento G.F. Ingrassia, Anatomia Patologica,
Università di Catania,
Via S. Sofia 87,
95123 Catania, Italy
e-mail: g.magro@unict.it

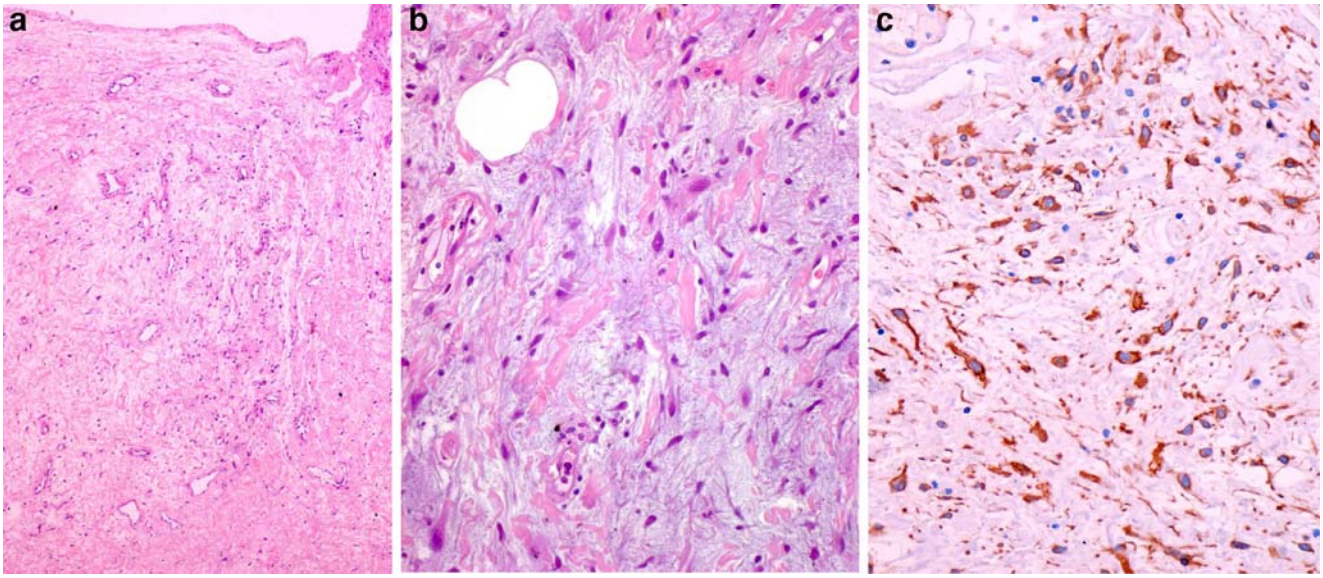

Fig. 1 **a** At low magnification, a hypocellular myxoid tumour with pushing borders can be appreciated. **b** Myxoid hypocellular tumour with atypical spindle-shaped cells. Thick eosinophilic collagen bands are seen. Severe nuclear pleomorphism is evident. **c** Neoplastic cells are immunoreactive to desmin

myofibroblastic profile by means of immunohistochemistry (diffuse immunoreactivity to vimentin, α-smooth muscle actin and desmin); and (5) Neoplastic cells variably expressed CD34, bcl-2, CD99, ER, PR, and AR receptors.

Although the presence of myxoid areas or atypical cells has been documented in some breast myofibroblastomas [1, 3, 5, 6], their association in the same tumour could pose diagnostic problems with some malignant myxoid neoplasms. However, the absence of infiltrative margins, high mitotic activity, atypical mitoses, and necrosis argues against malignancy. In our opinion, cellular pleomorphism in breast myofibroblastoma should be interpreted as a "degenerative phenomenon", similarly to what is observed in the so-called "atypical bizarre leiomyomas, ancient schwannoma", which does not adversely affect the biological behaviour of tumour, accordingly. Differential diagnosis mainly revolved around the myxoid type of spindle cell lipoma and solitary fibrous tumour. Discrimination between myofibroblastoma and spindle cell lipoma/solitary fibrous tumour may be difficult, as they are closely related neoplasms, likely arising from a common mammary stromal stem cell capable to differentiate along several

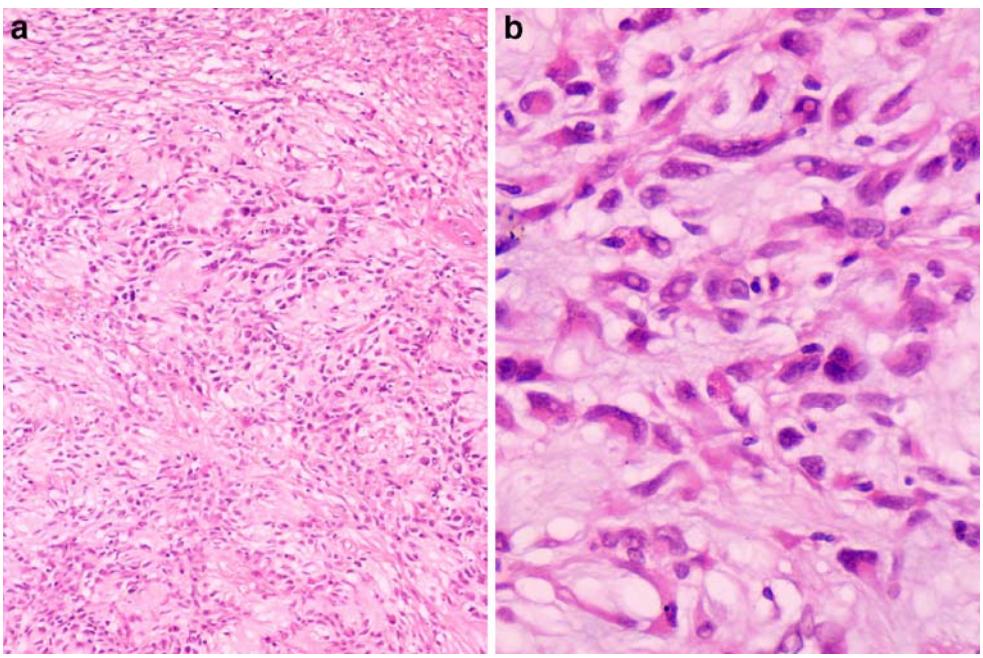

Fig. 2 **a** Myxoid tumour with moderate cellularity. **b** At higher magnification, neoplastic spindle, epithelioid cells with severe nuclear pleomorphism are seen. Some cells are multinucleated

mesenchymal lines, including the fibroblastic, myofibroblastic, and lipomatous ones [4–6]. This hypothesis is supported by the fact that all these tumours share some morphological and immunohistochemical features and by the recognition of hybrid tumours that simultaneously exhibit features of MFB and solitary fibrous tumour or MFB and spindle cell/pleomorphic lipoma [3, 5, 6]. Cytogenetic analyses, revealing that spindle cell lipoma and myofibroblastoma have similar chromosome 13 rearrangements associated with the loss of the 13q14 chromosomal region [2, 7], seem to confirm what we have previously postulated. We admit that immunohistochemistry was crucial for classification of our tumours as "myofibroblastomas", in consonance with the ability of neoplastic cells to differentiate along a myofibroblastic line, as demonstrated by their immunophenotype (α-smooth muscle actin^{+}, desmin^{+}, calponin^{-}, h-caldesmon^{-}).

In conclusion, the present paper, describing two cases of "myxoid myofibroblastoma with atypical cells", contributes to widen the morphological spectrum of this unusual mammary tumour. Although this rare variant exhibits some worrisome morphological features that could alarm a pathologist, the correct diagnosis is confidentially achieved if the well-established morphological and immunohistochemical criteria of myofibroblastoma are applied [5].

References

1. Lazaro-Santander R, Garcia-Prats MD, Nieto S, Andres-Gozalvo C, Cortes, Vizcaino V, Vargas-Holguin S, Vera-Roman JM (1999) Myofibroblastoma of the breast with diverse histological features. Virchows Arch 434:547–550
2. Maggiani F, Debiec-Rychter M, Verbeeck G, Sciot R (2006) Extramammary myofibroblastoma is genetically related to spindle cell lipoma. Virchows Arch 449:244–247
3. Magro G, Fraggetta F, Torrisi A, Emmanuele C, Lanzafame S (1999) Myofibroblastoma of the breast with hemangiopericytoma-like pattern and pleomorphic lipoma-like areas. Report of a case with diagnostic and histogenetic considerations. Pathol Res Pract 195:257–262
4. Magro G, Michal M, Bisceglia M (2000) Lipomatous myofibroblastoma: a potential diagnostic pitfall in the spectrum of the spindle cell lesions of the breast. Virchows Arch 437:540–547
5. Magro G, Michal M, Bisceglia M (2001) Benign spindle cell tumors of the mammary stroma: diagnostic criteria, classification and histogenesis. Review. Pathol Res Pract 197:453–466
6. Magro G, Bisceglia M, Michal M, Eusebi V (2002) Spindle cell lipoma-like tumor, solitary fibrous tumor and myofibroblastoma of the breast: a clinico-pathological analysis of 13 cases in favor of a unifying histogenetic concept. Virchows Arch 440:249–260
7. Pauwels P, Sciot R, Croiset F, Rutten H, Van den Berghe H, Dal Cin P (2000) Myofibroblastoma of the breast: genetic link with spindle cell lipoma. J Pathol 191:282–285

Virchows Arch (2007) 450:487–490
DOI 10.1007/s00428-007-0389-4

LETTER TO THE EDITOR

Multicentric invasive carcinomas derived from intraductal papillary mucinous neoplasm (IPMN) of the pancreas: report of a case

Yoshihisa Naitoh · Shinichi Ban · Chouji Tsuchiya · Yoshiaki Sugiura · Michio Shimizu

Received: 18 December 2006 / Accepted: 12 February 2007 / Published online: 28 February 2007
© Springer-Verlag 2007

Dear Editor,

Although intraductal papillary mucinous neoplasms (IPMNs) of the pancreas are noninvasive lesions, some IPMNs include an invasive carcinoma component. We recently experienced a case of IPMN with multiple foci of invasive carcinoma. To the best of our knowledge, there have been few reports of such cases. Besides, histologic types of invasive carcinoma components of the present IPMN case included both mucinous carcinoma (MC) and tubular carcinoma (TC).

Case report

A 69-year-old Japanese woman was referred to Sakado-chuuou Hospital for abdominal discomfort and an elevated serum value of CA19-9 (112.4 U/l; reference value <37.0 U/l), and a diagnosis of main duct-type IPMN of the pancreas was made based on the imaging studies. Considering the general condition of the patient, distal pancreatectomy with splenectomy was performed. No metastases to the peripancreatic lymph nodes were noted.

The lesion of the resected pancreas consisted of a markedly dilated main pancreatic duct filled with mucin, associated with intraluminal tall and/or short papillary (villous) projections mostly throughout the dilated duct, measuring 75×30×12 mm in size (Fig. 1). Histologically, most of the noninvasive papillary (villous) projections were composed of tall columnar epithelia with eosinophilic or mucinous cytoplasm and pseudostratified hyperchromatic oval to spindle nuclei and were diffusely immunoreactive to MUC5AC and MUC2, being consistent with IPMN of the intestinal type (Figs. 2 and 3a,c) [2]. The histological grade of atypia in the noninvasive papillary (villous) lesion was a borderline to noninvasive carcinoma (Fig. 2b). The noninvasive papillary (villous) lesion was accompanied by some foci of microscopic branch duct spread.

Three invasive carcinomas were seemingly derived from the intestinal-type IPMN. One was a MC (lesion A of Figs. 1 and 3a), and the other was a TC with focal MC (lesion B of Figs. 1 and 3b). The former was immunoreactive to MUC2 (Fig. 3c) and MUC5AC, and the latter was immunoreactive to MUC5AC and MUC1 and non-immunoreactive to MUC2 (Fig. 3d). Another invasive focus of TC with focal MC was observed (lesion C of Figs. 1 and 3e), which was immunoreactive to MUC5AC and MUC1 and partly immunoreactive to MUC2 in the MC area (Fig. 3f). This carcinoma was partly accompanied by noninvasive growth (Fig. 1) in which a small focus of MUC2-positive intestinal-type IPMN was observed, suggesting that the carcinoma outgrew the intestinal-type IPMN. The fourth invasive focus was a small TC immunoreactive to MUC5AC and MUC1 and non-imunoreactive to MUC2 (lesion D of Fig. 1). This lesion was observed in the pancreas parenchyma adjacent to the

Y. Naitoh · S. Ban (✉) · M. Shimizu
Department of Pathology,
Saitama Medical University School of Medicine,
38 Morohongo, Moroyama,
Iruma, Saitama 350-0495, Japan
e-mail: shinba@saitama-med.ac.jp

Y. Naitoh · C. Tsuchiya
Department of Surgery, Sakado-chuuou Hospital,
Saitama, Japan

Y. Sugiura
Department of Surgery,
National Defense Medical College,
Saitama, Japan

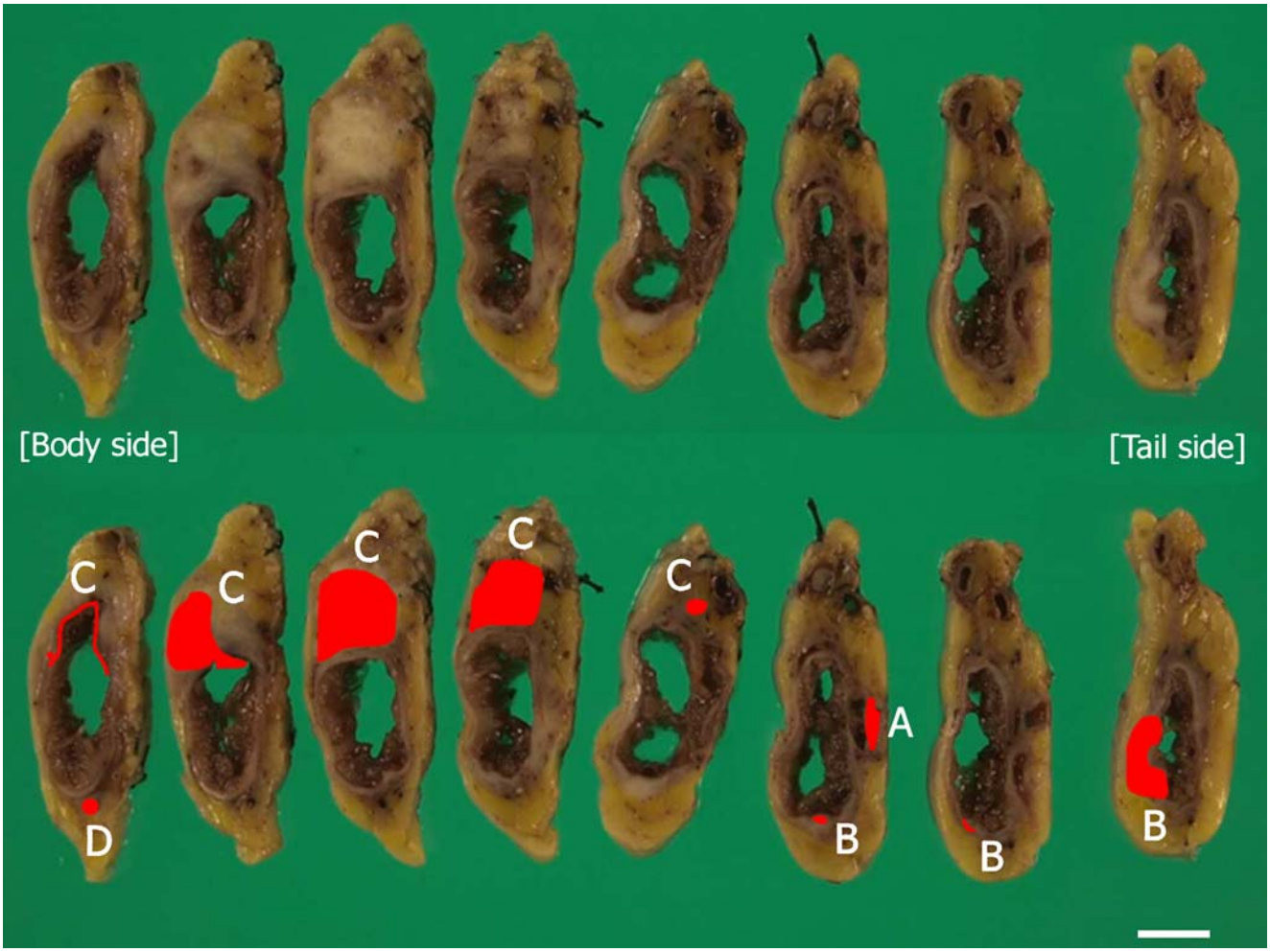

Fig. 1 Macroscopic appearance of the representative part of the distal pancreatectomy specimen cut in round slices. The *upper* and *lower rows* are the same figures. The main pancreatic duct is markedly dilated with intraluminal tall and/or short papillary (villous) projections. The foci of invasive carcinoma are indicated as *red areas* in the *lower* row (lesions *A* to *D*). The *C* lesion is accompanied by noninvasive growth (the *red line* in the leftmost slice). The *white bar* represents a length of 1 cm

intestinal-type IPMN. However, its continuity to the noninvasive intestinal-type IPMN was not proven even after an exhaustive investigation. In the above invasive lesions, MUC1 was immunostained in a linear fashion along the luminal side of the neoplastic epithelia. MUC6 was focally immunoreactive to all the lesions except for lesion A.

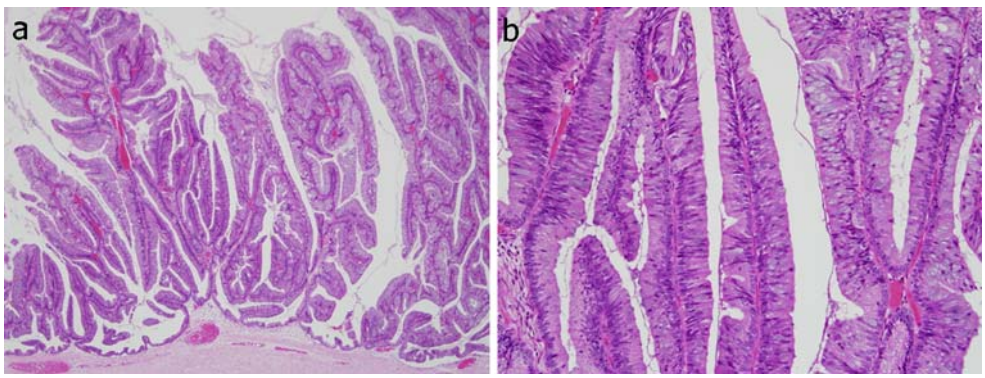

Fig. 2 Histological appearance of the main duct tumor. **a** Low power view shows noninvasive papillary (villous) projections (hematoxylin–eosin, original magnification ×40). **b** In high power view, the projections are composed of tall columnar epithelia with eosinophioic or mucinous cytoplasm and pseudostratified hyperchromatic oval to spindle nuclei, showing the histological grade of borderline to noninvasive carcinoma (hematoxylin–eosin, original magnification ×200)

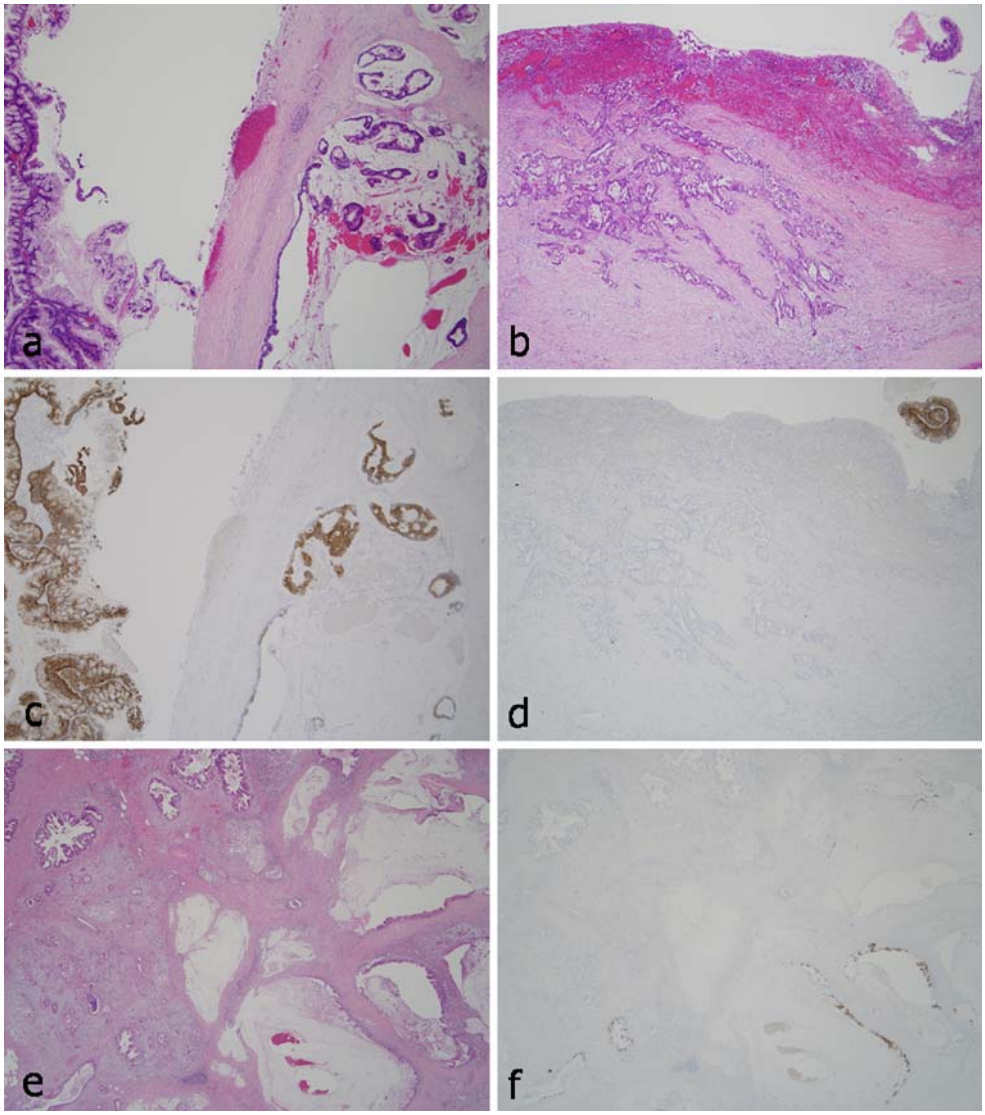

Fig. 3 Histological appearance and mucin immunohistochemistry of foci of the invasive carcinoma derived from the intestinal-type IPMN. **a** Mucinous carcinoma (*right half*, lesion A of Fig. 1) and the intestinal-type IPMN (*left half*; hematoxylin–eosin). **b** Invasive tubular carcinoma (lesion B of Fig. 1) with a small papilla of the intestinal-type IPMN (*upper right*; hematoxylin–eosin). **c** MUC2 immunohistochemistry of the serial section of **a**, in which MUC2 is positive for both the IPMN and the invasive carcinoma. **d** MUC2 immunohistochemistry of the serial section of **b**, in which MUC2 is positive for the IPMN (*upper right*) but negative for the invasive carcinoma. **e** Invasive carcinoma showing a mixed histologic type (lesion C of Fig. 1). Both tubular carcinoma (*upper left*) and mucinous carcinoma (*lower right*) are observed (hematoxylin–eosin). **f** MUC2 immunohistochemistry of the serial section of **e**, in which MUC2 is positive only for part of the mucinous carcinoma (*lower right*; original magnification ×40 for all)

Discussion

IPMNs involving the main pancreatic duct (main duct-type IPMNs) are more frequently accompanied by an invasive carcinoma component than those involving the branch ducts (branch duct-type IPMNs) [4, 5]. Besides, many of the main duct-type IPMNs are reportedly categorized into the intestinal-type IPMN, which represents a histology similar to colorectal villous tumor and is usually positive for MUC2 mucin [1, 2, 4]. The present IPMN case was also a main duct-type IPMN, showing the histology and mucin phenotype of the intestinal-type IPMN [2]. Multicentric foci of invasive carcinoma were observed, although one invasive lesion was not proved to be the main duct lesion origin. This lesion might be derived from a microscopic branch duct spread of the intestinal-type IPMN or an incidental concomitant lesion. IPMNs have been reported to be associated with a concomitant invasive ductal carcinoma [7], which would support the latter speculation. However, considering the presence of microscopic branch duct spread in the present case, we prefer the former speculation.

Some studies have reported that both MC and TC occur from IPMN [3, 4, 6]. In the present IPMN case, both TC and MC were observed partly with a mixed histologic type.

Therefore, the intestinal-type IPMNs would have a potential to yield both TC and MC. However, with regard to the mucin phenotype, the IPMN-derived TCs lost MUC2 expression in contrast to the IPMN-derived MCs, which often preserved MUC2 expression as previously reported [3, 4, 6]. From this standpoint and considering the presence of acellular small mucin pools frequently observed in the stroma surrounding IPMNs, especially the intestinal-type IPMNs [1], the unique histologic type of the invasive carcinomas derived from intestinal-type IPMNs seems to be MC rather than TC. Actually, IPMN-derived MCs seem to be related to the intestinal-type IPMNs in some previous reports [4, 6].

References

1. Ban S, Naitoh Y, Mino-Kenudson M, Sakurai T, Kuroda M, Koyama I, Lauwers GY, Shimizu M (2006) Intraductal papillary mucinous neoplasm (IPMN) of the pancreas: its histopathological difference between two major types. Am J Surg Pathol 30:1561–1569
2. Furukawa T, Klöppel G, Adsay NV, Albores-Saavedra J, Fukushima N, Horii A, Hruban RH, Kato Y, Klimstra DS, Longnecker DS, Lüttges J, Offerhaus GJ, Shimizu M, Sunamura M, Suriawinata A, Takaori K, Yonezawa S (2005) Classification of types of intraductal papillary-mucinous neoplasm of the pancreas: a consensus study. Virchows Arch 447:794–799
3. Lüttges J, Zamboni G, Longnecker D, Klöppel G (2001) The immunohistochemical mucin expression pattern distinguishes different types of intraductal papillary mucinous neoplasms of the pancreas and determines their relationship to mucinous noncystic carcinoma and ductal adenocarcinoma. Am J Surg Pathol 25:942–948
4. Nakamura A, Horinouchi M, Goto M, Nagata K, Sakoda K, Takao S, Imai K, Kim YS, Sato E, Yonezawa S (2002) New classification of pancreatic intraductal papillary-mucinous tumour by mucin expression: its relationship with potential for malignancy. J Pathol 197:201–210
5. Terris B, Ponsot P, Paye F, Hammel P, Sauvanet A, Molas G, Bernades P, Belghiti J, Ruszniewski P, Flejou JF (2000) Intraductal papillary mucinous tumors of the pancreas confined to secondary ducts show less aggressive pathologic features as compared with those involving the main pancreatic duct. Am J Surg Pathol 24:1372–1377
6. Terris B, Dubois S, Buisine MP, Sauvanet A, Ruszniewski P, Aubert JP, Porchet N, Couvelard A, Degott C, Flejou JF (2002) Mucin gene expression in intraductal papillary-mucinous pancreatic tumours and related lesions. J Pathol 197:632–637
7. Yamaguchi K, Ohuchida J, Ohtsuka T, Nakano K, Tanaka M (2002) Intraductal papillary-mucinous tumor of the pancreas concomitant with ductal carcinoma of the pancreas. Pancreatology 2:484–490

Virchows Arch (2007) 450:491–492
DOI 10.1007/s00428-007-0404-9

ANNOUNCEMENTS

Announcements

© Springer-Verlag 2007

14–17 May 2007
Diagnostic Histopathology of Breast Disease
Hammersmith Hospital (Imperial College), London, UK

A four day long course on the Hammersmith Campus designed for pathologists at Consultant and Senior Trainee level and suitable for the final examination for MRCPath. The course will provide a comprehensive coverage of the histopathology of breast disease, with special emphasis on areas which pose diagnostic difficulties. The course is based, historically, on the extensive referral collection of Professor JG Azzopardi, to which has been added new cases from Charing Cross, Nottingham City and Addenbrooke's Hospitals. The course will be slanted to practical diagnostic pathology with a specific session dealing with problems encountered in core biopsies and a special workshop dealing with the interpretation of HER2 immunostaining. The participants will be given ample time to study histological preparations, followed by illustrated discussions of the cases. In addition there will be several daily talks on specific topics, given by eminent breast pathologists and followed by discussions. The topics will include: new issues in the interpretation of breast biopsies, breast immunohistochemistry, problematic breast lesions, dealing with the gross specimen, fibro-epithelial, spindle cell and papillary lesions, proliferative lesions/carcinoma in-situ, sentinel lymph node biopsy and the impact of molecular genetics on diagnostic breast pathology. The faculty will include Anthony Douglas-Jones, Ian Ellis, Bharat Jassani, Andrew Lee, Sarah Pinder, Jorge Reis-Filho and Sami Shousha.

For further information please contact:
Sandra Lock
Department of Histopathology
Hammersmith Hospital
Du Cane Road
London W12 0NN, UK
Tel: +44 (0)20 8383 3292
Fax: +44 (0)20 8740 7417
E-mail: histopathology.shortcourses@imperial.ac.uk

May 18–20, 2007
Postgraduate Course
Molecular Pathology
Graz, Austria

Course Directors
Gerald Höfler, MD, Department of Pathology, Medical University Graz, Austria Falko Fend, MD, Department of Pathology, Technical University Munich, Germany

Course Objectives
This course is designed for pathologists, molecular biologists and technicians with special interest in diagnostic molecular pathology. It features lectures and practical aspects (wet lab course). Topics include DNA/RNA isolation from formalin-fixed paraffin embedded tissue, translocation analysis, clonality analysis (IgH, TCR), microsatellite instability (HNPCC) and quantification of RNA transcripts. The course language will be English.

Course Fee: 400,-€ The course fee includes hands on participation in the wet lab course, a comprehensive handout, coffee breaks, lunch and dinner (Saturday), buffet lunch (Sunday) and guided city walk.

Attendance is limited to 30 participants!

Registration / more information:
To register please use the form on our homepage:
http://pathologie.meduni-graz.at/Pathologie/veranstaltungen.htm
or send your registration to
Edith Kleinferchner
Department of Pathology
Medical University Graz
Auenbruggerplatz 25
8036 Graz, Austria;
Fax 0043-(0)316-385-3432
E-mail: edith.kleinferchner@meduni-graz.at

Since attendance is limited acceptance to the course will be acknowledged and a bill will be mailed.

7–8 June 2007
Thyroid Pathology for the Practising Pathologist
15 rue de l'Ecole de Médecine
Paris, France

A 2-day course will take place in Paris under the auspices of the French Division of the I.A.P. This course will be given in English by Prof. J. Rosai (Milano), Prof. M. Sobrinho-Simoes (Porto) and Prof. R. Heimann (Brussels). It will consist of lectures alternating with slide reviews and a slide seminar over a multiheaded microscope. The cases of the seminar will be sent on CD before the meeting.
The audience will be limited to 30 participants.

Course fees: 410 euros (340 euros for members of any I.A.P. division). The fees include registration, hand-out, CD of the slide seminar and coffee breaks.

For further information, please contact:
Mrs M. Fontanière, Administrative Secretary,
French Division of the I.A.P.
32 Cours Albert Thomas,
69008, Lyon, France
Fax: 33 4 78754311
E-mail: academie.pathologie@wanadoo.fr

24–27 July, 2007
Practical Pulmonary Pathology
London, UK

This course is designed to provide histopathology and cytopathology trainees and consultants with an opportunity to study diagnostic lung pathology in a comprehensive manner. It comprises lectures and practical microscopy sessions, the latter making up roughly half the time and consisting of individual study of a unique collection of cases.

For further information and application forms please contact:
Professor B Corrin,
Brompton Hospital,
London SW3 6NP, UK
Fax +44 20 7351 8293
E-mail: b.corrin@ic.ac.uk

27–31 August 2007 (Part I+II), 29–31 October 2007 (Part III)
Postgraduate Course Lung, Pleural & Mediastinal Diseases,
Department of Pathology,
Medical University, Graz, Austria

Course Director: Helmut Popper, MD (Graz)

Course Objectives:
This three-part course (common and rare lung and pleural, and mediastinal diseases) is designed for trainees as well as for experienced colleagues. Lectures as well as microscopy sessions alternate for each part. Clinical lectures and case studies are also included in selected lung diseases. Each part can be booked separately.

Course fee:
Part I (Common diseases) Aug 27–29, 2007€ 240,00
Part II (Mediastinal diseases) Aug 30–31, 2007€ 240,00
Part III (Rare diseases) Oct 29–31, 2007€ 240,00
Whole 8-day course (Part I + II + III) € 600,00
Two parts (Part I + II or Part I + III or Part II + III) € 450,00

For more information and registration please contact:
Edith Kleinferchner
Department of Pathology, Medical University Graz
Auenbruggerplatz 25
8036 Graz, Austria
Fax: 0043 (0)316 385-3432
e-mail:edith.kleinferchner@meduni-graz.at
http://pathologie.meduni-graz.at/Pathologie/veranstaltungen.htm

September 28th – October1st, 2007
10th International Pituitary Pathology Meeting
Stresa, Italy

A four day long meeting designed for pathologists, endocrinologists, neurosurgeons interested in pituitary pathology.
The course will provide comprehensive coverage of pathogenic and hispathologocal features of pituitary adenomas and an overview on lesions of the parasellar region.

Meeting Organizers: Carlo Capella, Luigi Bartalena, Giustino Tomei.

For further information please contact:
Prof. Carlo Capella
Dept. of Pathology
Ospedale di Circolo
Viale Borri, 57
1-21100 Varese, Italy
Tel: +39 0332 270601
Fax: +39 0332 270600
e-mail: carlo.capella@ospedale.varese.it

Virchows Arch (2007) 450:493–502
DOI 10.1007/s00428-007-0384-9

ORIGINAL ARTICLE

Frequency and diagnostic patterns of lymphomas in liver biopsies with respect to the WHO classification

Christoph Loddenkemper · Thomas Longerich · Michael Hummel · Karen Ernestus · Ioannis Anagnostopoulos · Hans-Peter Dienes · Peter Schirmacher · Harald Stein

Received: 3 November 2006 / Revised: 18 December 2006 / Accepted: 30 December 2006 / Published online: 13 March 2007
© Springer-Verlag 2007

Abstract The recent World Health Organization (WHO) classification of hematopoietic and lymphoid tissue tumors represents the first worldwide consensus classification of these malignancies. However, the applicability of this classification to a representative number of hepatic lymphomas in liver biopsy specimens has not yet been investigated. The frequency and infiltration pattern of a series of 205 liver biopsies with lymphoma manifestations was analyzed with the aid of immunohistochemical and molecular pathological analyses. Diffuse large B-cell lymphoma (DLBCL) was by far the most frequent entity, comprising 45% of the cases analyzed. Using a previously published immunohistochemical algorithm, 35% of 80 DLBCL were assigned to a germinal center B-cell-like (GCB) and 65% to a non-GCB group. Most B-cell lymphoma entities involving the liver revealed a characteristic infiltration pattern. Diagnostically challenging entities were T-cell-rich B-cell lymphomas, anaplastic large cell lymphomas and peripheral T-cell lymphomas, which frequently required additional molecular clonality assessment. Overall, the percentage of T-cell lymphomas in the liver (12%) was higher as compared to other extranodal sites except for the skin and the small intestine. This study provides relevant data on the distribution of hepatic lymphomas and demonstrates the applicability of the WHO classification proposing a diagnostic algorithm for liver biopsies.

Keywords Lymphoma · Liver · Differential diagnosis · Immunohistochemistry · PCR

Christoph Loddenkemper and Thomas Longerich contributed equally to the work.

C. Loddenkemper (✉) · M. Hummel · I. Anagnostopoulos · H. Stein
Institute of Pathology, Consultation and Reference Center for Lymph Node Pathology and Hematopathology, Campus Benjamin Franklin, Charité-University Medicine Berlin, Berlin, Germany
e-mail: christoph.loddenkemper@charite.de

T. Longerich · P. Schirmacher
Department of General Pathology, Institute of Pathology, University of Heidelberg, Heidelberg, Germany

T. Longerich · K. Ernestus · H.-P. Dienes
Institute of Pathology, University of Cologne, Cologne, Germany

Introduction

The liver is most commonly involved in non-Hodgkin lymphomas (NHL) next to lymph nodes, spleen, and bone marrow. In the vast majority of cases hepatic involvement reflects secondary dissemination in advanced disease [15, 18] rather than a primary site according to the definition of Caccamo and coworkers [5]. Histopathological analysis of liver biopsy may be required in patients with an established diagnosis of malignant lymphoma to differentiate lymphoma manifestation from other causes of hepatic dysfunction or to clarify elevated transaminases such as toxic damage because of chemotherapy or other medications. On the other hand, a biopsy may reveal a previously unknown lymphoma during the exploration of a solid hepatic mass or after measuring elevated liver enzyme serology [12]. Occasionally, a malignant lymphoma can be detectable in the setting of other liver diseases such as chronic hepatitis B [20, 22], chronic hepatitis C [2, 3, 7, 21, 25], or primary biliary cirrhosis (PBC) [24].

The goals of the present study were to test the feasibility of lymphoma subtyping according to the World Health Organisation (WHO) classification of tumors of hematopoietic and lymphoid tissues [16] in liver biopsy specimens and to describe the frequencies by which the different entities occur. For this purpose, a series of 205 liver biopsies with a diagnosis of malignant lymphoma were analyzed retrospectively with a specific focus on the histopathology, especially infiltration patterns, which may ultimately allow the use of diagnostic algorithms for subtyping of lymphomas in liver biopsies.

Table 1 Antibodies used in this study

Antibody	Clone	Antigen retrieval	Dilution	Source
ALK1	ALK1	Citrate	1:20	Dako
BCL2	124	Citrate	1:25	Dako
BCL6	594	Citrate	1:25	Dako
CD2	AB75	Citrate	1:50	Novocastra
CD3	F7.2.38	Citrate	1:100	Dako
CD4	1F6	Citrate	1:25	Novocastra
CD5	4C7	Citrate	1:25	Novocastra
CD7	CD7-272	EDTA	1:50	Novocastra
CD8	C8/144B	Citrate	1:100	Dako
CD10	56C6	Citrate	1:25	Novocastra
CD15	C3D1	Citrate	1:20	Dako
CD20	L26	Citrate	1:50	Dako
CD21	1F8	Protease	1:50	Dako
CD23	1B12	Citrate	1:20	Novocastra
CD27	137B4	EDTA	1:100	Novocastra
CD30	BerH2	Citrate	1:50	Dako
CD43	DF-T1	Citrate	1:50	Dako
CD68	PG-M1	Citrate	1:50	Dako
CD79a	JCB117	Citrate	1:100	Dako
CD138	B-B4	Citrate	1:10	Serotec
Cyclin D1	P2D11F11	Citrate	1:50	Novocastra
EBV-LMP	CS1-4	Citrate	1:100	Dako
α-heavychain	Rabbit polyclonal	Citrate	1:40 000	Dako
γ-heavy chain	Rabbit polyclonal	Citrate	1:30 000	Dako
δ-heavy chain	Rabbit polyclonal	Citrate	1:2000	Dako
μ-heavy chain	Rabbit polyclonal	Citrate	1:2000	Dako
Ki-67	MIB-1	Citrate	1:2000	Dako
κ-light chain	Rabbit polyclonal	Citrate	1:100 000	Dako
λ-light chain	HP6054	Citrate	1:16 000	Dako
MUM1/IRF4	MUM1p	Citrate	1:20	Generously provided by Prof. B. Falini, Perugia, Italy
Pax-5	24	Citrate	1:10	Transduction Laboratories
TIA-1	2G9	Citrate	1:500	Coulter

This is an important addition in relation to previous studies, which have mainly described the frequency of liver involvement in autopsy material of patients with leukemia or lymphoma [8, 13, 26, 28, 29] differentiating only between low-grade and high-grade NHL [26] or having performed a categorization according to the outdated Kiel classification [29].

Overall, this study represents the largest series on hepatic lymphomas to date and due to its restriction to bioptic material reflects the primary diagnostic situation.

Materials and methods

All cases of hepatic lymphoma involvement diagnosed by liver biopsy during the years 1994–2003 were retrieved from the archives of the Institute of Pathology, Campus Benjamin Franklin, Charité-University Medicine Berlin and the Institute of Pathology, University of Cologne, Germany. The series comprised a total of 205 cases with 135 cases from Berlin and 70 cases from Cologne. All cases were reevaluated and reclassified independently by three pathologists (C.L., T.L., H.S.) according to the WHO classification [16]. For cases in which the diagnosis was not unanimous, a final consensus diagnosis was reached after further immunophenotyping, molecular analyses, and final consultation. In six cases initially considered "suspicious" for lymphoma, a final diagnosis of lymphoma was made after reevaluation and additional analyses. Nine liver biopsies with insufficient material for additional immunohistochemical or molecular analyses were excluded beforehand, as well as five cases where T-cell receptor (TCR) polymerase chain reaction (PCR) had revealed a polyclonal or oligoclonal rearrangement pattern without a reproducible dominant PCR product.

Overall, 32/205 (16%) cases were reclassified, including eight "low-grade" [5× B-CLL, 2× follicular lymphomas (FL), 1× marginal zone lymphoma (MZL)] and 20 "high-grade" [19× DLBCL, 1× Burkitt lymphoma (BL)] B-cell NHL that were assigned to a specific WHO lymphoma category as well as four cases with a change in the final diagnosis [BL, classical Hodgkin lymphoma (cHL), T-cell-rich B-cell lymphoma (TCRBCL), lymphoplasmacytic lymphoma (LPL) to DLBCL, anaplastic large cell lymphoma (ALCL), peripheral T-cell lymphoma (pTCL) and B-CLL, respectively].

The analyses of the infiltration pattern were based on the assessment of the hepatic architecture. Three main patterns were distinguished: Infiltrates for which an exclusive or predominant association to portal tracts was evident were recorded as portal infiltrates. The second pattern consisted of lymphoma infiltrates which showed a coherent growth pattern thus predominantly resulting in the replacement of the acinar structures. These infiltrates were designated as a nodular growth pattern. Finally, infiltrates that showed

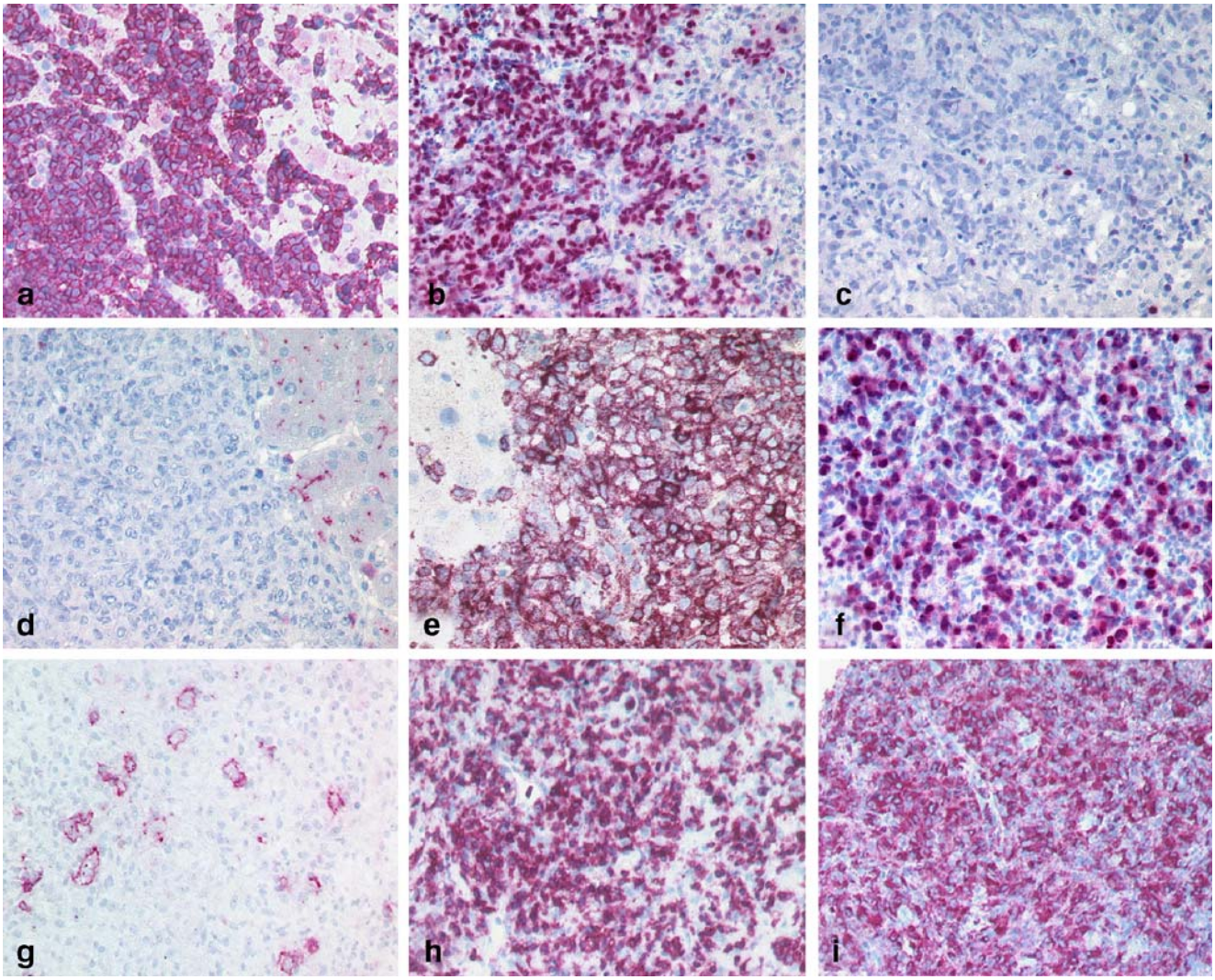

Fig. 1 Nodular pattern: DLBCL of GCB group positive for CD10 (**a**) and BCL6 (**b**) and negative for IRF4/MUM1 (few scattered plasma cells serve as positive intrinsic control; **c**). CD5 positive DLBCL of ABC type negative for CD10 (positive bile canaliculi serve as intrinsic control; **d**), positive for CD5 (**e**) and IRF4/MUM1 (**f**). TCRBCL with less than 10% large CD20 positive neoplastic B-cells (**g**) associated with numerous CD3 positive T-cells (**h**) and CD68 positive histiocytes (**i**)

prominent intrasinusoidal dispersion of the lymphoma cells were recorded as a sinusoidal growth pattern. Additionally, the density of the infiltrate was semiquantitatively assessed. The presence of scattered neoplastic cells in a background rich in reactive bystander cells (e.g., nonneoplastic T-cells and/or macrophages in T-cell rich B-cell lymphoma) was defined as a loose infiltration pattern, whereas the appearance of coherently appearing neoplastic B- or T-cells was referred to as a dense infiltrate.

According to clinical information available, in 76/205 (37%) of the cases the diagnosis of a lymphoma had been previously established from extrahepatic biopsies or peripheral blood indicating secondary involvement of the liver. In four of these cases with known low-grade lymphoma (2× B-CLL, 2× FL) liver biopsy revealed transformation to a high-grade lymphoma (DLBCL). In

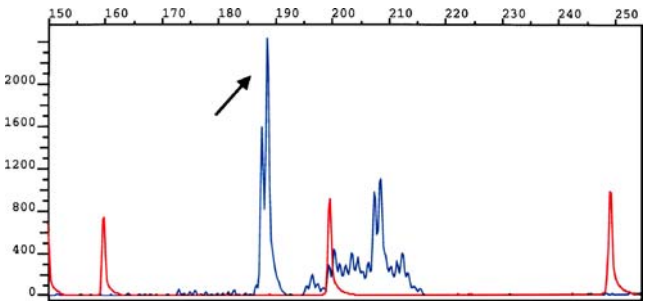

Fig. 2 Size fragment analyses (GeneScan) of the amplificates after TCR-gamma PCR (primer combination JGT1/2). Fluorescence-labelled PCR products (*blue lines*) were separated on capillary electrophoresis system (Applied Biosystems, Model 310A) in parallel to a size standard (*red line*). The dominant PCR product (*arrow*) indicating the presence of a clonal T-cell population was reproducibly detectable in addition to a moderate oligo-/polyclonal T-cell background

Table 2 Frequency, age distribution and pattern of infiltration in the different lymphoma entities presenting in the liver (Berlin/Cologne 1994–2003)

	Berlin	Cologne	Berlin + Cologne, *n* (%)	Age (range)	Age (mean)	Male/female	Pattern			Density of infiltrate	
							Sinusoidal	Portal	Nodular	Dense	Loose
Diffuse large B-cell lymphoma (DLBCL)[a]	52	28	80(39)	16–87	64	50/30	6	19	72	75	5
T-cell rich B-cell lymphoma (TCRBCL)	9	4	13(6)	35–85	59	9/4	0	11	5	0	13
B-cell chronic lymphocytic leukemia (B-CLL)	13	13	26(13)	44–82	66	16/10	7	25	2	25	1
Classical Hodgkin lymphoma (cHL)	10	13	23(11)	21–91	54	14/9	1	21	10	3	20
Follicular lymphoma (FL)	11	3	14(7)	38–83	62	7/7	0	11	4	14	0
Marginal zone lymphoma (MZL)	6	1	7(3)	49–80	70	6/1	2	7	0	6	1
Leukemic Plasmacytoma (PL)	4	2	6(3)	61–88	70	4/2	4	1	2	5	1
Burkitt lymphoma (BL)	5	–	5(2)	30–70	47	3/2	0	0	5	5	0
Mantle cell lymphoma (MCL)	3	–	3(1)	60–66	63	2/1	1	3	1	3	0
B-lymphoblastic leukaemia (B-ALL)	2	–	2(1)	18–28	22	1/1	2	0	0	2	0
Hairy cell leukaemia (HCL)	1	–	1	42	–	0/1	1	0	0	1	0
Peripheral T-cell lymphoma, unspecified (pTCL)	13	5	18(9)	38–84	62	14/4	6	6	8	11	7
Anaplastic large cell lymphoma (ALCL)[b]	5	–	5(2)	24–76	58	5/0	3	3	2	2	3
Hepatosplenic T-cell lymphoma (HSTCL)	1	1	2(1)	38–51	45	2/0	2	0	0	2	0
Total	135	70	205								

[a] Including centroblastic (n=69), immunoblastic (n=3) and anaplastic variant (n=8)
[b] Including one anaplastic large cell lymphoma kinase (ALK) protein positive case

the remaining cases, the biopsy obtained from the liver represented the site of primary diagnosis. In 26 (13%) patients, additional biopsies from extrahepatic sites were available (13 bone marrow biopsies, 10 lymph node biopsies, and three spleen biopsies). Furthermore, in a few cases clinical data regarding a potential predisposing condition for a primary hepatic lymphoma was available: chronic hepatitis C was reported in four patients (3× DLBCL, 1× B-CLL), HIV infection was present in three patients (2× DLBCL, 1× BL), and one marginal zone lymphoma occurred in a patient after liver transplantation.

The frequency of the various lymphoma entities diagnosed in liver biopsy specimen was compared to their frequency and distribution in other extranodal sites (cases from the Consultation and Reference Center for Lymph Node Pathology and Hematopathology, Berlin).

Immunohistochemistry

For immunostaining, 4 μm thick sections were cut, deparaffinized, and subjected to heat-induced epitope retrieval before incubation with antibodies. For this purpose, sections were immersed either in sodium citrate buffer at pH 6.0 or, alternatively, in ethylenediamintetraacetic acid (EDTA) at pH 8.0 and heated in a high-pressure cooker. After cooking, the slides were rinsed in running water, washed with Tris-buffered saline, pH 7.4, and incubated with the respective primary antibodies. All primary antibodies employed are listed in Table 1. With the exception of immunoglobulin detection, in which the streptavidin–biotin peroxidase method was applied [14], labeling was carried out using the alkaline–phosphatase/anti-alkaline–phosphatase complex method [6]. Alkaline phosphatase was developed using Fast Red as the chromogen, whereas peroxidase was visualized with diaminobenzidine chromogen as the substrate.

Molecular pathology analyses

Additional molecular pathology analyses were selectively performed for those cases in which immunoprofiling alone was not sufficient to establish a definite diagnosis of a malignant lymphoma.

For this purpose, DNA was extracted after dewaxing 20-μm-thick paraffin sections with QIAEX (Qiagen, Hilden, Germany) according to the manufacturer's recommendations. TCR-gamma rearrangements were analyzed using four different primer combinations (JGT1/2, JGT3, BioMed-2 Set A and Set B). The primer combinations JGT1/2 und JGT3 suitable to amplify the most frequent

Table 3 Infiltration pattern, differential diagnosis and characteristic immunohistochemical markers

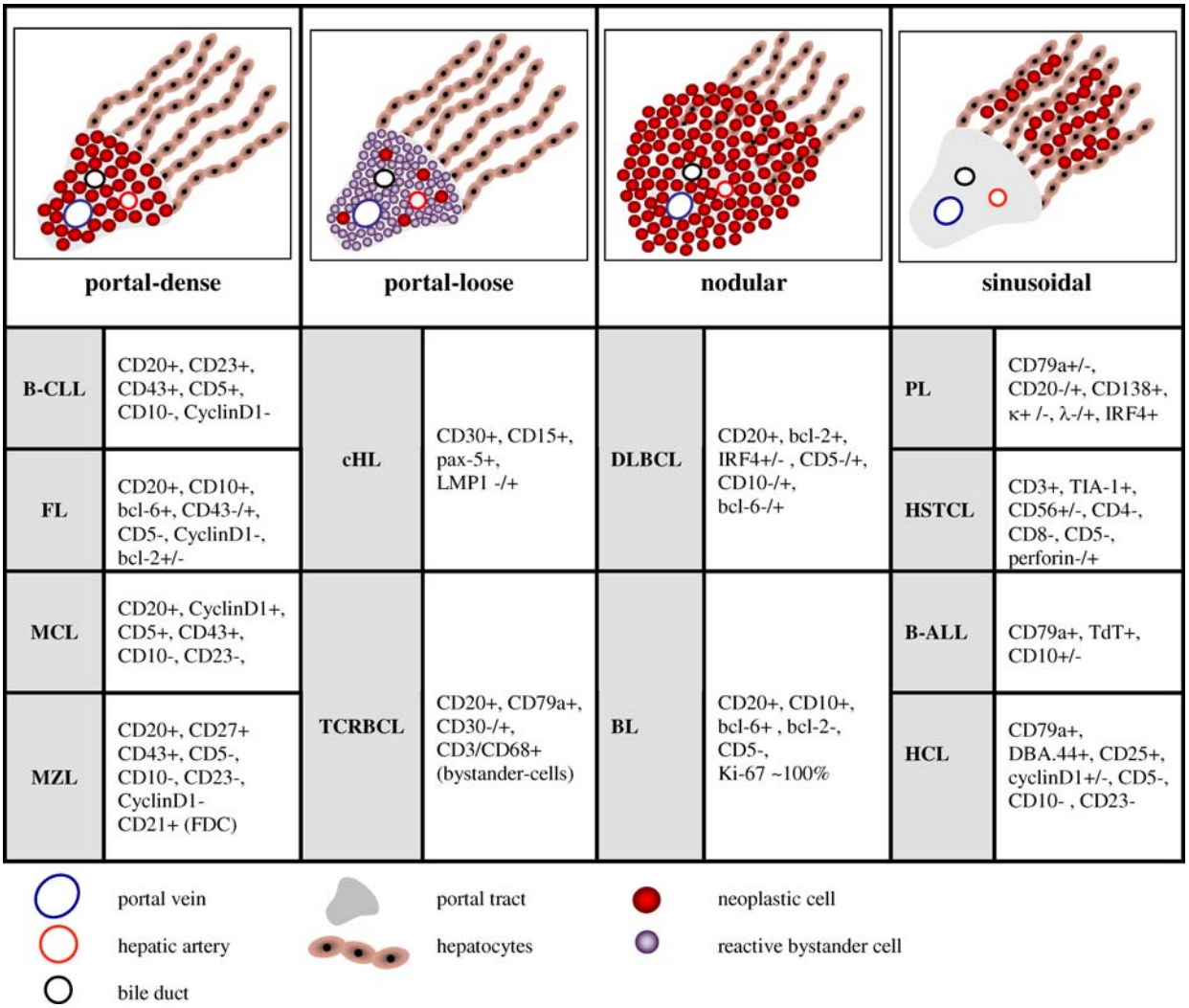

TCR-gamma rearrangements were used in a two-step seminested PCR. The BioMed-2 primer sets A and B able to detect all possible TCR-gamma rearrangements were performed as single round PCRs. The detailed cycling conditions (50 rounds of amplification for BioMed-2 set A and set B; two-time 35 cycles for primer combinations JGT1/2 and JGT3) for all PCRs have been described in detail elsewhere [9, 27].

Amplification of rearranged IgH genes was independently performed at least twice per case employing three different framework primer sets (BioMed-2 FR1, FR2, and FR3) separately in conjunction with a JH primer (JH22). PCR conditions consisted of 50 cycles of denaturation (95°C, 15 s), primer annealing (60°C, 40 s), and elongation (72°C, 45 s), and the reaction mixture contained 1.5 mM MgCl2, 0.8 mM deoxyribonucleotide triphosphates (dNTPs), 70 pmol VH primers, 30 pmol JH22 primer, and 2 U of AmpliTaq Gold polymerase (Applied Biosystems, Weiterstadt, Germany).

Results

Characteristics of hepatic lymphomas

Almost 90% (182/205) of the hepatic lymphomas belonged to the group of NHL, whereas only 23 of the 205 cases were cHL. Regarding NHL, 86% (157/182) were of B-cell and 14% (25/182) of T-cell origin. Overall, diffuse large B-cell lymphoma (DLBCL) was the most common type [51% (93/182) of all B-NHL analyzed] with TCRBCL—a morphologic variant of DLBCL—comprising 14% (13/93) of all DLBCL. According to the algorithm of Hans et al. [11] a predominance of DLBCL of non-GCB (germinal center B-cell-like) type (52/80; 65%) compared to the DLBCL of GCB type (28/80; 35%) was found (Fig. 1a–d,f). Only 4 out of 80 cases (5%) corresponded to the group of CD5-positive DLBCL (Fig. 1e).

In all lymphoma subtypes, men were affected more often, except for FL, which occurred with equal frequencies

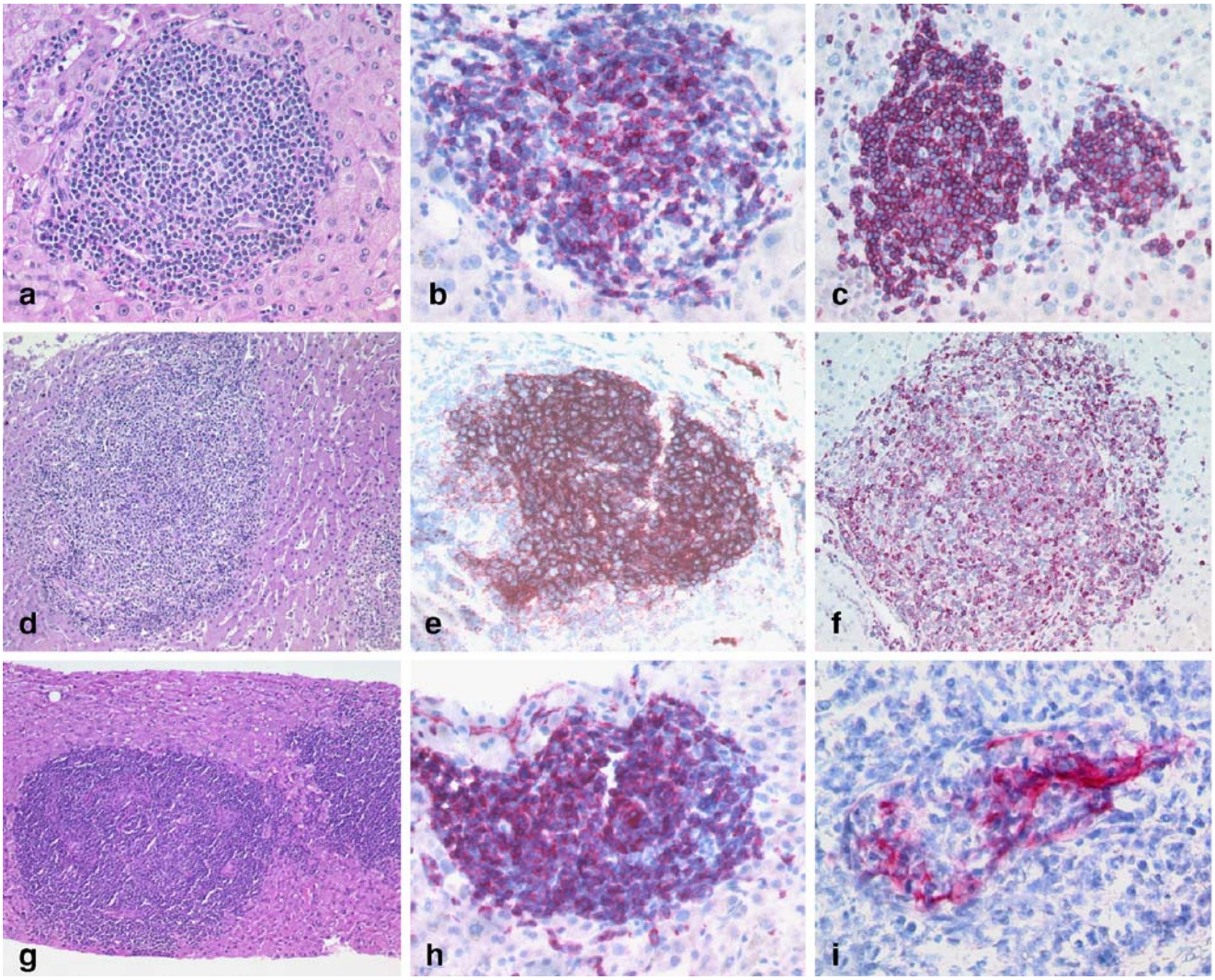

Fig. 3 Portal pattern: chronic lymphocytic leukemia (B-CLL) with a predominantly portal infiltrate of small lymphocytes (**a**) with expression of CD23 (**b**) and CD5 (**c**). FL (**d**) with expression of CD10 (**e**) and BCL2 (**f**). Marginal zone B-cell lymphoma with portal involvement (**g**), expression of memory B-cell marker CD27 (**h**) and a lymphoepithelial lesion of a CK7 positive bile duct (**i**)

in both sexes. The male predominance was most striking in lymphomas of T-cell origin, in which ALCL and hepatosplenic T-cell lymphoma (HSTCL) were encountered exclusively in men. Additional molecular analyses were essential to confirm the suspected diagnosis of a lymphoma in 5 out of 19 T-cell lymphomas (26%) and 3 out of 116 (3%) B-NHLs (Fig. 2).

The relative frequencies of the lymphoma subtypes, the available patient data and the infiltration patterns are summarized in Table 2.

Infiltration patterns of the various lymphoma types

Most of the cases showed the predominance of a certain growth pattern, although some cases exhibited more than one growth pattern. Almost all DLBCL and BL showed a nodular infiltration pattern (91%) composed of a dense infiltrate (94%; Table 3), except for the TCRBCL variant, which was located predominantly within the portal tracts (85%) and exhibited the characteristic scattered infiltrate of fewer than 10% large neoplastic B-cells admixed with many reactive T-cells and histiocytes (Fig. 1g–i). Lymphomas showing a dense portal infiltration pattern were chronic lymphocytic leukemia/small lymphocytic lymphoma (96%; Fig. 3a–c), FL (79%; Fig. 3d–f), MZL (100%; Fig. 3g–i), and mantle cell lymphoma (100%). In contrast, in precursor B lymphoblastic leukemia/lymphoblastic lymphoma (B-ALL/B-LBL; Fig. 4a–c), HSTCL (Fig. 4d–f), leukemic plasmacytoma (Fig. 4g–i), and hairy cell leukemia, a sinusoidal infiltration pattern was observed in the majority of cases. The cHL displayed a predominantly portal infiltration pattern (Fig. 5a–c). Peripheral T-cell

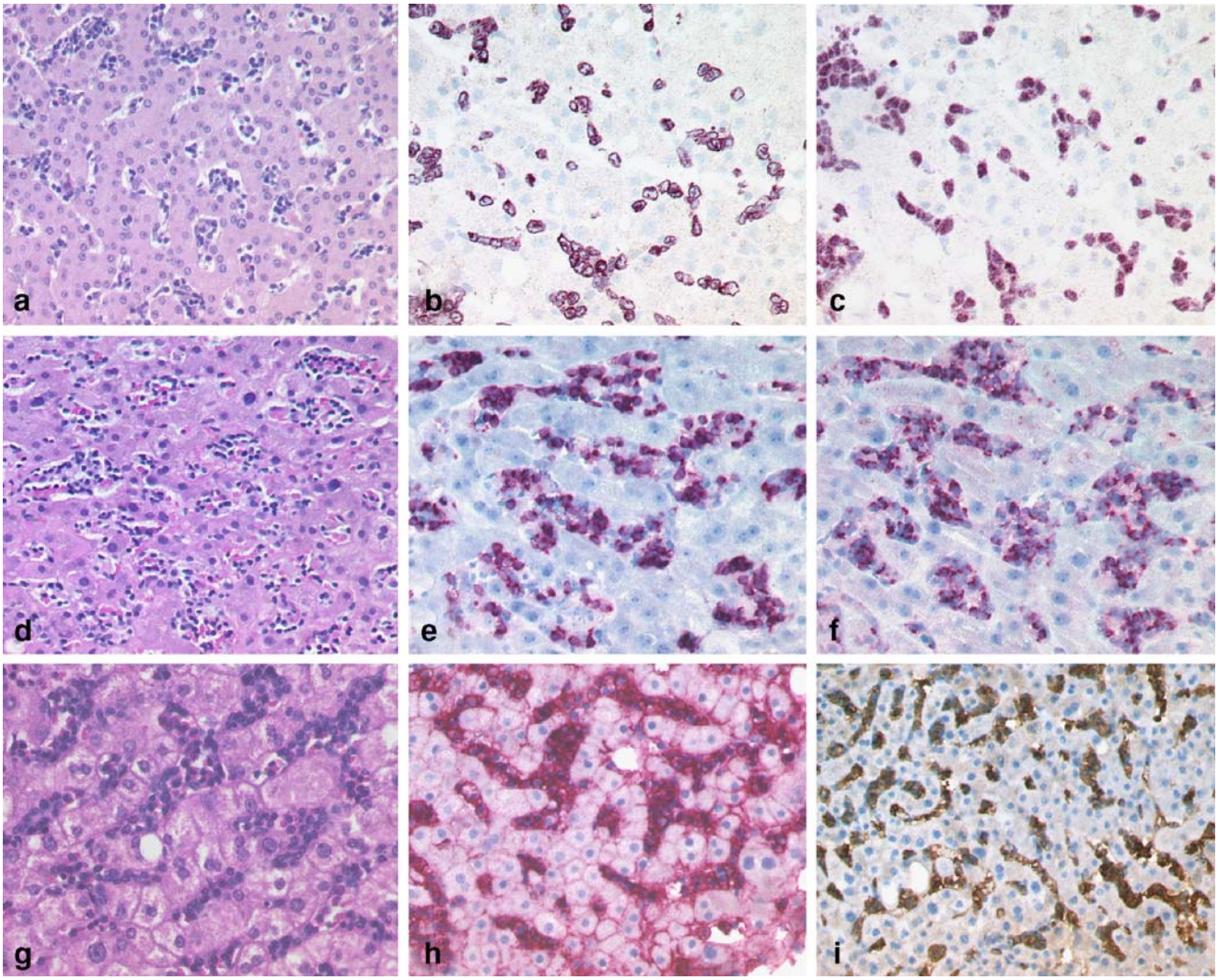

Fig. 4 Sinusoidal pattern: precursor B lymphoblastic lymphoma (B-LBL) with a sinusoidal infiltrate of small blasts (**a**) with cytoplasmic expression of CD79a (**b**) and nuclear expression of terminal deoxynucleotidyl transferase (TdT; **c**). HSTCL with a sinusoidal infiltrate of monotonous neoplastic cells (**d**) with expression of CD3 (**e**) and the cytotoxic granule associated protein TIA-1 (**f**). Peripheral blood involvement (plasma cell leukemia) in a plasmacytoma with a sinusoidal infiltrate of plasma cells (**g**) with expression of CD138 (**h**) and IgG (**i**)

lymphoma and ALCL showed a spectrum of portal, sinusoidal, nodular, or mixed patterns with a varying density of infiltration, and thus did not allow for pattern-based selection of additional analyses (Fig. 5d–f). The infiltration patterns, differential diagnoses, and discriminative immunohistochemical markers are summarized in Table 3.

Comparison of hepatic lymphomas with other extranodal lymphomas

The percentage of T-cell lymphomas was considerably higher in the liver (12%, 25/205) when compared to other extranodal sites (5%, 165/3252) except for the skin (50%, mainly mycosis fungoides/Sézary syndrome) and small intestine (34%, mainly enteropathy-type T-cell lymphomas).

The high proportion of DLBCL in lymphomas of the liver (45%) was only surpassed by the small intestine (64%), the brain (83%), and the testis (97%). Of note, TCRBCL was extremely rare in other extranodal sites (0,3%) with only a few cases occurring in the bone marrow and spleen. Interestingly, one case fulfilled the criteria of TCRBCL in the liver, and an additional lymph node biopsy showed the picture of a typical DLBCL, whereas in another case, both liver and spleen biopsy showed the characteristic features of TCRBCL. The frequencies of other extranodal lymphomas compared to hepatic lymphomas are summarized in Table 4.

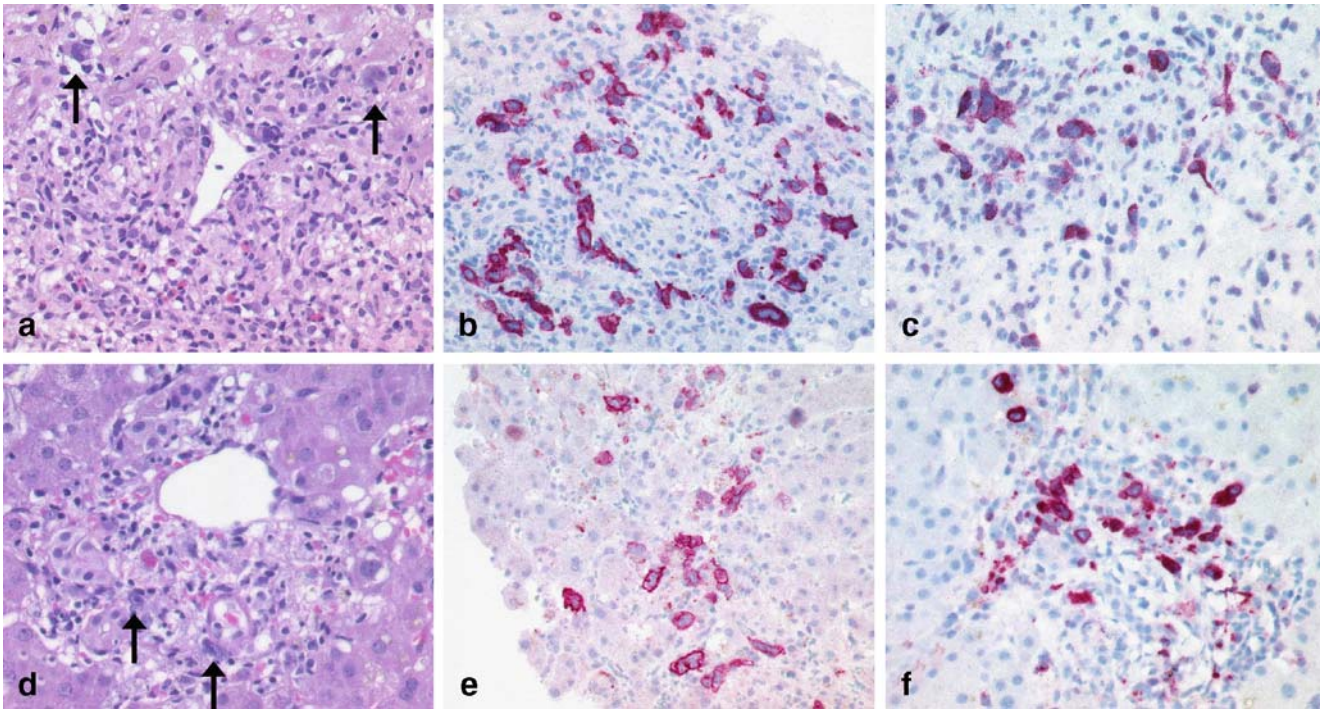

Fig. 5 Classical Hodgkin lymphoma vs. anaplastic large cell lymphoma: cHL with portal infiltrates of Hodgkin and Reed-Sternberg HRS cells (*arrows*) in a background rich in eosinophils (**a**). The HRS cells strongly express CD30 (**b**) and the EBV encoded latent membrane protein 1 (LMP1) (**c**). Anaplastic large cell lymphoma (ALCL) with portal infiltrates of pleomorphic large cells resembling HRS cells (*arrows*) (**d**) and strong positivity for CD30 (**e**) and the cytotoxic molecule perforin (**f**)

Table 4 Frequency of extranodal lymphoma at different sites (Berlin 1994–2003)

	Brain (*n*=31)	Testis (*n*=61)	Lung (*n*=79)	Bone marrow (*n*=1996)	Stomach (*n*=855)	Small intestine (*n*=71)	Large intestine (*n*=102)	Spleen (*n*=128)	Skin (*n*=427)	Liver (*n*=135)
DLBCL	25	57	22	66	238	30	32	21	78	52
TCRBCL	–	–	–	7	–	–	–	3	–	9
FL	1	–	2	168	16	3	3	20	91	11
B-CLL	1	–	2	656	12	–	4	10	7	13
PL	3	–	–	473	–	–	–	1	2	4
MZL	–	–	40	17	577	4	12	18*	12	6
MCL	–	–	3	107	7	7	41	19	6	3
LPL	–	–	3	122	–	–	2	13	5	–
HCL	–	–	–	112	–	–	–	6	–	1
B-ALL	–	1	–	78	–	–	–	1	–	2
BL	–	1	–	4	–	3	2	–	2	5
cHL	–	–	3	52	–	–	–	3	10	10
B-NHL total (%)	30/31 (97%)	59/61 (97%)	75/79 (95%)	1862/1996 (93%)	850/855 (99%)	47/71 (66%)	96/102 (94%)	115/128 (90%)	213/427 (50%)	116/135 (86%)
pTCL	1	–	3	93	4	6	6	12	94	13
NK/T	–	1	–	–	–	2	–	–	2	–
T-ALL	–	1	–	29	–	–	–	–	9	–
ALCL	–	–	1	8	1	6	–	–	26	5
Enteropathy-type TCL	–	–	–	–	–	10	–	–	–	–
HSTCL	–	–	–	5	–	–	–	1	–	1
MF	–	–	–	–	–	–	–	–	83	–
T-NHL total (%)	1/31 (3%)	2/61 (3%)	4/79 (5%)	134/1996 (7%)	5/855 (1%)	24/71 (34%)	6/102 (6%)	13/128 (10%)	214/427 (50%)	19/135 (14%)

*Including nine cases of splenic marginal zone lymphoma (SMZL)

Discussion

To the best of our knowledge, this study represents the largest series focusing on the histopathology of hepatic lymphoma involvement and the first application of the WHO classification of tumors of hematopoietic and lymphoid tissues for this purpose [16]. Our data demonstrate the feasibility of in vivo lymphoma subtyping in liver biopsy with the aid of infiltration pattern analysis, the selection of differentiating immunophenotypic markers and additional molecular methods.

Many B-cell-derived lymphomas involving the liver revealed a characteristic infiltration pattern, which facilitated the use of a restricted panel of immunohistochemical markers to reach a final diagnosis. This approach is critical in those liver biopsies in which a lymphoma diagnosis has previously not been established, as accurate subtyping of lymphomas is fundamental for the initiation of adequate treatment.

Diffuse large B-cell lymphomas (DLBCL) accounted for 51% of all B-NHL cases. DLBCL was recently subdivided into different prognostic groups designated GCB, activated B-cell-like (ABC or non-GCB) and Type 3, according to their gene expression profiles [1]. The GCB group is described to have a better survival than the ABC group and the heterogeneous Type 3 group. Hans et al. [11] have proposed a simple immunohistochemical algorithm to assign cases to a GCB and a non-GCB group. In the present study, the frequency of either group in 80 liver biopsies with DLBCL was investigated, excluding the T-cell/histiocyte rich variant (n= 13). DLBCL of non-GCB type (65%) were more frequent in the liver than the GCB type (35%), whereas these two groups are described in other sites at about equal frequency [23]. As liver involvement with malignant lymphomas occurs secondary in advanced disease [15, 18], this observation may reflect the biological behavior of ABC-group DLBCLs through the selection of more aggressive cases by liver biopsy.

Approximately 10% of the de novo DLBCL express CD5 [4] and may have a poor outcome [31]. They tend to be associated with extranodal sites, especially bone marrow and spleen [19]. In the present series of hepatic lymphoma involvement, the number of CD5 positive DLBCL (4/80 or 5%) was not increased.

The TCRBCL, a variant of DLBCL in which the majority of cells are nonneoplastic T-cells and histiocytes, are often misdiagnosed as a reactive inflammatory condition or as a T-cell lymphoma infiltration of the liver [8, 17]. TCRBCL is relatively rare in lymph node biopsies [(23/976) or 2% of the DLBCL in the Berlin Reference Centre for Lymph Node Pathology from 1994–2003]. However, in the present study, 13/93 (14%) of the DLBCL in the liver were found to fulfill the WHO criteria for TCRBCL thus confirming previous data from Dargent and coworkers in their series of 62 liver specimens [8]. Additionally, one case with TCRBCL characteristics in the liver showed the typical morphology of a conventional DLBCL in an additional lymph node biopsy. This finding indicates that the composition of the reactive coinfiltrate may be influenced by the tissue-specific microenvironment. Therefore, the specific environment of a certain organ may influence the intensity of the T-cell response and subsequently explain the higher frequency of the TCRBCL variant of DLBLC presenting in the liver [10]. Limitations were encountered in the grading of follicular lymphoma and the subtyping of the cHL, which is generally not possible with sufficient certainty in needle biopsies.

In contrast to B-cell lymphomas, T-cell lymphomas infiltrating the liver generally lack a typical infiltration pattern, making their diagnosis more challenging. In particular, ALCL may mimic cHL due to the possible resemblance of Hodgkin and Reed-Sternberg cells and expression of CD30. Thus, additional markers against pan-T and pan-B cell antigens (including pax-5), CD15, ALK-1, cytotoxic molecules, e.g., TIA-1, granzyme B, and perforin) are required when confronted with this differential diagnosis (Fig. 5).

Similarly, the distinction between a T-cell lymphoma and a drug-induced or viral hepatitis (e.g., due to Epstein-Barr virus) can be very difficult in biopsies containing an increased number of sinusoidal T-cells. Therefore, additional clonality analyses by TCR or IgH PCR were necessary in 5 out of 19 (26%) T-cell lymphomas compared to only 3 out of 116 (3%) B-cell lymphomas to establish a diagnosis.

The reason for the relatively high frequency of liver involvement by T-cell lymphomas is not known. As T-cells play an important role in the regulation of the hepatic immune responses, especially in chronic viral and autoimmune hepatitis [30], it is tempting to speculate whether this may influence the relatively high incidence of T-cell lymphomas in the liver compared to other extranodal sites. In the present study, 25 of the 205 (12%) cases were found to represent lymphomas derived from T-cells, whereas lymphomas of the testis, brain, lung, and stomach were B-cell lymphomas in nearly all instances (Table 4).

In summary, the present study demonstrates the feasibility of subtyping lymphoma infiltrates in liver biopsies according to the WHO classification. The large number of 205 cases provides reliable information regarding the relative frequencies of the different lymphoma entities encountered in the liver and demonstrates the usefulness of infiltration pattern analysis for diagnostic purposes.

Acknowledgement We would like to thank Erika Berg, Constanze Cieluch, and Hans-Henning Müller for their excellent technical assistance and Harald Krosch for graphical assistance. This work was supported by grants from the German Cancer Aid.

References

1. Alizadeh AA, Eisen MB, Davis RE, Ma C, Lossos IS, Rosenwald A, Boldrick JC, Sabet H, Tran T, Yu X, Powell JI, Yang L, Marti GE, Moore T, Hudson J Jr, Lu L, Lewis DB, Tibshirani R, Sherlock G, Chan WC, Greiner TC, Weisenburger DD, Armitage JO, Warnke R, Levy R, Wilson W, Grever MR, Byrd JC, Botstein D, Brown PO, Staudt LM (2000) Distinct types of diffuse large B-cell lymphoma identified by gene expression profiling. Nature 403:503–511
2. Ascoli V, Lo Coco F, Artini M, Levrero M, Martelli M, Negro F (1998) Extranodal lymphomas associated with hepatitis C virus infection. Am J Clin Pathol 109:600–609
3. Bronowicki JP, Bineau C, Feugier P, Hermine O, Brousse N, Oberti F, Rousselet MC, Dharancy S, Gaulard P, Flejou JF, Cazals-Hatem D, Labouyrie E (2003) Primary lymphoma of the liver: clinical-pathological features and relationship with HCV infection in French patients. Hepatology 37:781–787
4. Burns BF, Warnke RA, Doggett RS, Rouse RV (1983) Expression of a T-cell antigen (Leu-1) by B-cell lymphomas. Am J Pathol 113:165–171
5. Caccamo D, Pervez NK, Marchevsky A (1986) Primary lymphoma of the liver in the acquired immunodeficiency syndrome. Arch Pathol Lab Med 110:553–555
6. Cordell JL, Falini B, Erber WN, Ghosh AK, Abdulaziz Z, MacDonald S, Pulford KA, Stein H, Mason DY (1984) Immunoenzymatic labeling of monoclonal antibodies using immune complexes of alkaline phosphatase and monoclonal anti-alkaline phosphatase (APAAP complexes). J Histochem Cytochem 32:219–229
7. Dammacco F, Gatti P, Sansonno D (1998) Hepatitis C virus infection, mixed cryoglobulinemia, and non-Hodgkin's lymphoma: an emerging picture. Leuk Lymphoma 31:463–476
8. Dargent JL, De Wolf-Peeters C (1998) Liver involvement by lymphoma: identification of a distinctive pattern of infiltration related to T-cell/histiocyte-rich B-cell lymphoma. Ann Diagn Pathol 2:363–369
9. Dippel E, Assaf C, Hummel M, Schrag HJ, Stein H, Goerdt S, Orfanos CE (1999) Clonal T-cell receptor gamma-chain gene rearrangement by PCR-based GeneScan analysis in advanced cutaneous T-cell lymphoma: a critical evaluation. J Pathol 188:146–154
10. Dogan A, Burke JS, Goteri G, Stitson RN, Wotherspoon AC, Isaacson PG (2003) Micronodular T-cell/histiocyte-rich large B-cell lymphoma of the spleen: histology, immunophenotype, and differential diagnosis. Am J Surg Pathol 27:903–911
11. Hans CP, Weisenburger DD, Greiner TC, Gascoyne RD, Delabie J, Ott G, Muller-Hermelink HK, Campo E, Braziel RM, Jaffe ES, Pan Z, Farinha P, Smith LM, Falini B, Banham AH, Rosenwald A, Staudt LM, Connors JM, Armitage JO, Chan WC (2004) Confirmation of the molecular classification of diffuse large B-cell lymphoma by immunohistochemistry using a tissue microarray. Blood 103:275–282
12. Harris AC, Ben-Ezra JM, Contos MJ, Kornstein MJ (1996) Malignant lymphoma can present as hepatobiliary disease. Cancer 78:2011–2019
13. Harris AC, Kornstein MJ (1993) Malignant lymphoma imitating hepatitis. Cancer 71:2639–2646
14. Hsu SM, Raine L, Fanger H (1981) The use of antiavidin antibody and avidin–biotin–peroxidase complex in immunoperoxidase technics. Am J Clin Pathol 75:816–821
15. Jaffe ES (1987) Malignant lymphomas: pathology of hepatic involvement. Semin Liver Dis 7:257–268
16. Jaffe ES, Harris NL, Stein H, Vardiman JW (eds) (2001) World Health Organisation of Tumours. Pathology World Health Organisation of Tumours. Pathology and genetics of tumours of haematopoietic and lymphoid tissues. IARC, Lyon
17. Khan SM, Cottrell BJ, Millward-Sadler GH, Wright DH (1993) T-cell-rich B-cell lymphoma presenting as liver disease. Histopathology 23:217–224
18. Kim H, Dorfman RF (1974) Morphological studies of 84 untreated patients subjected to laparotomy for the staging of non-Hodgkin's lymphomas. Cancer 33:657–674
19. Kroft SH, Howard MS, Picker LJ, Ansari MQ, Aquino DB, McKenna RW (2000) De novo CD5+diffuse large B-cell lymphomas. A heterogeneous group containing an unusual form of splenic lymphoma. Am J Clin Pathol 114:523–533
20. Matano S, Nakamura S, Annen Y, Hattori N, Kiyohara K, Kakuta K, Kyoda K, Sugimoto T (1998) Primary hepatic lymphoma in a patient with chronic hepatitis B. Am J Gastroenterol 93:2301–2302
21. Mohler M, Gutzler F, Kallinowski B, Goeser T, Stremmel W (1997) Primary hepatic high-grade non-Hodgkin's lymphoma and chronic hepatitis C infection. Dig Dis Sci 42:2241–2245
22. Ozaki S, Ogasahara K, Kosaka M, Inoshita T, Wakatsuki S, Uehara H, Matsumoto T (1998) Hepatosplenic gamma delta T-cell lymphoma associated with hepatitis B virus infection. J Med Investig 44:215–217
23. Poulsen CB, Borup R, Nielsen FC, Borregaard N, Hansen M, Gronbaek K, Moller MB, Ralfkiaer E (2005) Microarray-based classification of diffuse large B-cell lymphoma. Eur J Haematol 74:453–465
24. Prabhu RM, Medeiros LJ, Kumar D, Drachenberg CI, Papadimitriou JC, Appelman HD, Johnson LB, Laurin J, Heyman M, Abruzzo LV (1998) Primary hepatic low-grade B-cell lymphoma of mucosa-associated lymphoid tissue (MALT) associated with primary biliary cirrhosis. Mod Pathol 11:404–410
25. Rubbia-Brandt L, Brundler MA, Kerl K, Negro F, Nador RG, Scherrer A, Kurt AM, Mentha G, Borisch B (1999) Primary hepatic diffuse large B-cell lymphoma in a patient with chronic hepatitis C. Am J Surg Pathol 23:1124–1130
26. Scheimberg IB, Pollock DJ, Collins PW, Doran HM, Newland AC, van der Walt JD (1995) Pathology of the liver in leukaemia and lymphoma. A study of 110 autopsies. Histopathology 26:311–321
27. van Dongen JJ, Langerak AW, Bruggemann M, Evans PA, Hummel M, Lavender FL, Delabesse E, Davi F, Schuuring E, Garcia-Sanz R, van Krieken JH, Droese J, Gonzalez D, Bastard C, White HE, Spaargaren M, Gonzalez M, Parreira A, Smith JL, Morgan GJ, Kneba M, Macintyre EA (2003) Design and standardization of PCR primers and protocols for detection of clonal immunoglobulin and T-cell receptor gene recombinations in suspect lymphoproliferations: report of the BIOMED-2 Concerted Action BMH4-CT98-3936. Leukemia 17:2257–2317
28. Voigt JJ, Vinel JP, Caveriviere P, Pradere B, Chittal S, al Saati T, Cales P, Delsol G. (1989) [Immunochemical diagnosis of hepatic localizations in malignant lymphoid hematologic diseases. Study of 80 cases]. Gastroenterol Clin Biol 13:343–352
29. Walz-Mattmuller R, Horny HP, Ruck P, Kaiserling E (1998) Incidence and pattern of liver involvement in haematological malignancies. Pathol Res Pract 194:781–789
30. Wick MJ, Leithauser F, Reimann J (2002) The hepatic immune system. Crit Rev Immunol 22:47–103
31. Yamaguchi M, Seto M, Okamoto M, Ichinohasama R, Nakamura N, Yoshino T, Suzumiya J, Murase T, Miura I, Akasaka T, Tamaru J, Suzuki R, Kagami Y, Hirano M, Morishima Y, Ueda R, Shiku H, Nakamura S (2002) De novo CD5+ diffuse large B-cell lymphoma: a clinicopathologic study of 109 patients. Blood 99:815–821

Virchows Arch (2007) 450:503–512
DOI 10.1007/s00428-007-0390-y

ORIGINAL ARTICLE

Specific activation of the different fibrogenic cells in rat cultured liver slices mimicking in vivo situations

Christelle Guyot · Chantal Combe · Haude Clouzeau-Girard · Valérie Moronvalle-Halley · Alexis Desmoulière

Received: 12 December 2006 / Revised: 6 February 2007 / Accepted: 12 February 2007 / Published online: 13 March 2007
© Springer-Verlag 2007

Abstract Due to the loss of cell–cell and cell–matrix interactions, cell culture models poorly mimic the in vivo situation. Therefore, we tested the applicability of precision-cut liver slices (PCLS) to study the early activation of the two main liver fibrogenic cell subpopulations: hepatic stellate cells (HSC) and portal fibroblasts (PF). PCLS were treated with thioacetamide or acetaminophen to induce HSC activation. In PCLS culture, both were able to trigger centrolobular lesion and HSC activation as observed in vivo. However, thioacetamide also presented a toxic effect on portal tract cells. In this PCLS model of centrolobular lesion, the antioxidant *N*-acetylcysteine was able to prevent acetaminophen-induced injury. To induce a specific activation of PF, PCLS were treated with epidermal growth factor or β-oestradiol. As in vivo, epidermal growth factor and β-oestradiol induced bile duct epithelial cell proliferation accompanied by PF activation; however, β-oestradiol also triggers sinusoidal cell proliferation. We demonstrated that treatments usually used in vivo to induce liver fibrosis allow, in cultured PCLS, the specific activation of the two main liver fibrogenic cell subpopulations, making this model very useful to study the mechanisms involved in early fibrogenic cell activation.

C. Guyot · C. Combe · H. Clouzeau-Girard · A. Desmoulière
INSERM, E362, Université Victor Segalen Bordeaux 2,
Bordeaux 33076, France

V. Moronvalle-Halley
Sanofi-Aventis,
Alfortville 94140, France

A. Desmoulière (✉)
Département de Physiologie, Faculté de Pharmacie,
Université de Limoges,
Limoges 87025, France
e-mail: alexis.desmouliere@unilim.fr

Keywords Liver slices · Liver fibrosis · Hepatic stellate cell · Portal fibroblast · PDGF receptor-β

Abbreviations

PCLS	precision-cut liver slice
EPO	erythropoietin
LTCM	long-term culture medium
HSC	hepatic stellate cell
PF	portal fibroblast
PDGF	platelet-derived growth factor
FCS	foetal calf serum
HBSS	Hanks' balanced salt solution
MTT	3-(4,5-dimethylthiazol-2-yl)-2,5-diphenyltetrazolium bromide
EGF	epidermal growth factor
BrdU	bromodeoxyuridine

Introduction

Besides in vivo experiments, numerous in vitro models have been developed to decrease the complexity of the experiments and to reduce animal use. Cell culture is widely used and very useful; however, compared with in vivo studies, some disadvantages such as loss of differentiated functions in cultured cells are encountered. The precision cut-liver slice (PCLS) model preserves the normal lobular architecture and allows the maintenance of cell–cell interactions within their original extracellular matrix. Definitively, this model permits to reduce the number of killed animals, as it is possible to test various drugs on the same slice preparation, which also avoids the inter-individual variations. PCLS have been used for metabolic and toxicological studies on various liver cell types [15, 18]. The PCLS culture model has been recently applied to the study of hepatic stellate cell (HSC)

activation [3, 29]; it has also been shown that endothelial cells [21] and Kupffer cells [19, 22] remain viable in PCLS culture. In a recent study, we have used this model to study the effects of bile acids on biliary epithelial cell proliferation and portal fibroblast (PF) activation [6]. We recently applied this model to study HSC and PF behaviour in PCLS derived from fibrotic tissue [11].

We planned to validate the use of this model to study liver fibrosis. Fibrosis is defined as the excessive deposition of extracellular matrix in an organ, and is the main complication of chronic liver damage. The accumulation of extracellular matrix observed is due to the activation of fibrogenic cells, which acquire a myofibroblastic phenotype. Myofibroblasts are absent from normal liver. They derived from the activation of precursor cells, such as HSC or PF [for review, see 10]. According to the etiology of the lesion, different types of fibrosis with different patterns can be observed. In case of lesion caused by toxics or drugs (thioacetamide, acetaminophen, etc.), hepatocyte necrosis is observed around the centrolobular veins, which triggers fibrogenic cell activation and fibrosis if the lesion is chronic. In case of viral hepatitis or bile duct obstruction, the fibrotic lesion grows around the portal tracts. The mechanisms and the fibrogenic cells involved in these two types of fibrosis are different: centrolobular fibrosis implicates HSC [16], whereas portal fibrosis mainly involved PF [28].

The aim of this work was first to define the optimal culture conditions to maintain cell viability without triggering hepatic cell activation or proliferation. Then, we wanted to mimic the in vivo experimental situations treating PCLS with various substances to activate specifically HSC or PF. Our data validate the use of PCLS model to study the early events of fibrogenic cell activation.

Materials and methods

Preparation of rat precision-cut liver slices

Male Wistar rats (Charles Rivers, St Aubin-les-Elbeuf, France) weighing about 400 g were anesthetized with intraperitoneal injection of ketamine (100 mg/kg; Imalgen®, Rhône Mérieux, Lyon, France) and xylazin (10 mg/kg; Rompun®, Bayer Pharma, Puteaux, France). Liver was perfused in situ (20 ml/min) with preoxygenated ice-cold Hanks' balanced salt solution (HBSS; Invitrogen, Cergy Pontoise, France), supplemented with 5 mM glucose and 50 μg/ml gentamycin, via a plastic catheter placed into the portal vein. The vena cava was transected, and the outflow was allowed to drain freely into the abdominal cavity. Then, sus-hepatic vein was transected, and vena cava was clamped. After 5-min perfusion, the liver was excised, and tissue cores were prepared using a motor-driven coring tool (8-mm diameter; Alabama Research and Development Corporation, Munford, AL, USA). PCLS (250-μm thickness) were obtained using a Krumdieck tissue slicer (Alabama Research and Development Corporation). During manipulations, tissue cores and PCLS were maintained in continuously oxygenated ice-cold HBSS.

Culture of rat precision-cut liver slices

Rat PCLS were placed on a stainless-steel insert (Alabama Research and Development Corporation) in an incubation vial containing culture medium. Vials were set on a roller platform and gently agitated in a humidified incubator (Sanyo, Osaka, Japan) at 37°C, with 5% CO_2 and 40% O_2. A central 2-mm diameter hole in the vial caps allowed gas exchanges. PCLS were firstly incubated for 2 h in Williams' E medium (Invitrogen) supplemented with 0.3 μM insulin (Sigma, St Quentin Fallavier, France), 0.1 μM dexamethasone (Sigma) and 5% foetal calf serum (FCS; Dutscher, Issy-les-Moulineaux, France) to promote adherence to the mesh and avoid slice sticking out. After 2 h, the medium was removed, and different culture media and additives were tested: Williams' E medium (supplemented with insulin and dexamethasone) containing 1, 5, 10 or 20% FCS, Williams' E medium (supplemented with insulin and dexamethasone) containing 1% FCS and erythropoietin (EPO 1000 U/ml) or a serum-free long-term culture medium (LTCM) developed to maintain the phenotypical characteristics of human primary hepatocytes in long-term culture [24, 25] (Table 1). PCLS cultured in these different media were processed for histology, and cell viability was checked to optimise culture conditions. This experiment and the following treatments (see below) were performed at least in triplicate, and for each condition, a minimum of six PCLS were used for analysis.

Treatment of rat precision-cut liver slices

After 2 h, rat PCLS were treated for 24 or 48 h with acetaminophen (Sigma) alone or in presence of *N*-acetylcysteine (Fluimucil®, Zambon, France) with thioacetamide (Sigma), *trans*-resveratrol (Sigma), 17β-oestradiol (Sigma) or human recombinant epidermal growth factor (EGF; PeProtech, Rocky Hill, NJ). All these compounds were diluted in Williams' E medium supplemented with insulin, dexamethasone and 1% FCS. In some cases, 1 h before the end of treatment, bromodeoxyuridine (BrdU) (Roche Diagnostics, Meylan, France) was added in the culture medium to detect cell proliferation.

Cytotoxicity assay

After treatment, culture medium was removed, and PCLS were incubated in Williams' E medium containing 2 mg/ml

Table 1 Composition of the long-term culture medium (LTCM)

Products	Final concentrations
Linoleic acid	15.4 μM
Linolenic acid	15.4 μM
Insulin	10 mg/l
Transferrin	5 mg/l
Selenium acid	0.1 μM
Liver growth factor	20 μg/l
CAMP	5 μM
Prolactin	10 IU/l
Ethanolamine	1.25 μM
Glucagon	1 mg/l
Epidermal growth factor	50 μg/l
Glutamine	2 mM
Glucose	2 g/l
Sodium pyruvate	0.25 mM
Dexaméthasone	0.1 μM
Vitamin C	2 mg/l
Penicillin/streptomycin	100 000 IU/l
Fungizone	0.75 mg/l

The long-term culture medium consists of Williams' E medium supplemented with these products.

3-(4,5-dimethylthiazol-2-yl)-2,5-diphenyltetrazolium bromide (MTT). After 2 h at 37°C, PCLS were solubilised with dimethyl sulfoxyde (Merck, Fontenay-sous-Bois, France), and the optical density at 570 nm was measured in a microplate reader (Labsystems, Vantaa, Finland).

Antibodies

For immunohistochemistry, the following antibodies were used: a rabbit polyclonal antibody against platelet-derived growth factor (PDGF) receptor-β (Santa Cruz Biotechnology, Santa Cruz, CA, USA), a rat monoclonal antibody against BrdU (Oxford Biotechnology Immunologicals, Oxford, UK), mouse monoclonal antibodies against active caspase 3 (R&D Systems, Minneapolis, MN, USA) and Ki 67 (DakoCytomation Trappes, France). All these antibodies have been extensively used, and their specificity has been clearly documented.

Histology and immunohistochemistry

After treatment, PCLS were routinely formalin-fixed and paraffin-embedded. Sections (3 μm thick) were stained with hematoxylin–eosin for routine histology or with the periodic acid-Schiff (PAS) to stain glycogen in hepatocytes. Sections were also processed for immunohistochemistry. Briefly, paraffin sections were deparaffinized, hydrated, washed with phosphate buffered saline (PBS) and incubated with 3% H_2O_2 in methanol to inhibit endogenous peroxidase. Non-specific sites were blocked with PBS-3% bovine serum albumin or PBS-20% human serum for 30 min. Sections were incubated with the primary antibody and, after washing, the epitopes were detected with the anti-rabbit or anti-mouse horseradish peroxidase Envision™+ system and revealed with liquid diaminobenzidine (DakoCytomation). Sections were counterstained with hematoxylin. For PDGF receptor-β, Ki 67 and BrdU stainings, sections were subjected to steam heat antigen retrieval in citrate buffer 0.01 M, pH 6.0 for 5 min. For BrdU staining, sections were pre-treated with 2 M HCl for 1 h at 37°C and incubated with rabbit anti-rat immunoglobulins (DakoCytomation) before anti-rabbit Envision™+ system detection. Immunostainings were examined with a Zeiss Axioplan 2 microscope (Carl Zeiss Microscopy, Jena, Germany). Images were acquired with an AxioCam camera (Carl Zeiss Vision, Hallbergmoos, Germany) by means of the AxioVision image processing and analysis system (Carl Zeiss Vision).

Transmission electron microscopy

PCLS fragments were processed for transmission electron microscopy using established procedures. Briefly, small fragments (approximately 1 mm^3) were immersed in 1% osmium tetroxide in 0.1 M cacodylate buffer (pH 7.2) for 2 h, washed, dehydrated in graded ethanols and Epon-embedded. Semi-thin sections were stained with toluidine blue to orientate the tissue. Thin sections were contrasted with uranyl acetate and lead citrate and observed with a Philips CM-120 transmission electron microscope (Philips SA, Zurich, Switzerland).

Results

Optimisation of culture medium

PCLS were cultured for 24, 48 or 72 h in Williams' E medium containing 1% FCS or in LTCM and then processed for histology. Hematoxylin–eosin staining showed a similar well-preserved global histology. However, at a higher magnification, the histological aspect was slightly different: Some cytoplasmic vacuoles were observed in hepatocytes of PCLS cultured in Williams' E medium with a few small necrotic areas, whereas in PCLS cultured in LTCM medium, no vacuoles and rare necrotic cells were observed (Fig. 1a and b). PAS staining was performed to evaluate the glycogen content: In both media, the staining in hepatocyte was intense and homogeneous (data not shown). Few active caspase 3 positive cells were observed, only around necrotic areas, without noteworthy differences between the two media (data not shown). In PCLS cultured in Williams' E medium, immunohistochemistry for PDGF receptor-β revealed a typical staining in vascular structures, particularly in portal tract vessels (Fig. 1c); a slight PDGF receptor-β expression which is early induced in activated

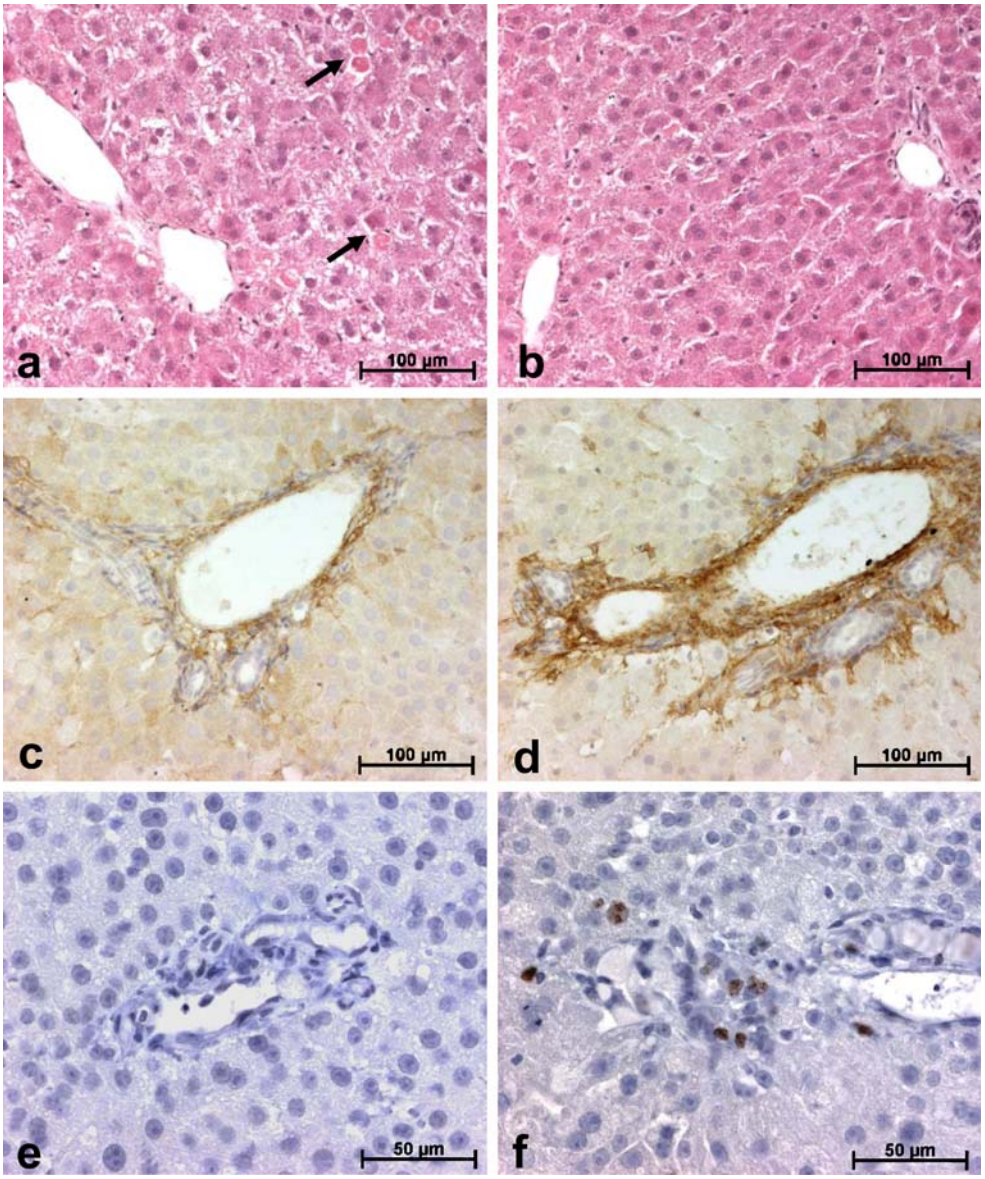

Fig. 1 Hematoxylin–eosin staining (**a**, **b**), PDGF receptor-β (**c**, **d**) and Ki 67 (**e**, **f**) immunostainings in PCLS cultured in Williams' E medium (**a**, **c**, **e**) or LTCM (**b**, **d**, **f**) for 72 h. PCLS cultured in Williams' E medium show rare necrotic areas (*arrows*) and cytoplasmic vacuoles in hepatocytes (**a**); in LTCM, the parenchyma is well preserved with only focal necrotic areas and no cytoplasmic vacuoles (**b**). In PCLS cultured in Williams' E medium (**c**), PDGF receptor-β expression is only observed in vascular structures, whereas in LTCM (**d**), portal fibroblasts also express PDGF receptor-β. Ki 67 immunostaining shows very rare proliferating cells in PCLS cultured in Williams' E medium (**e**), whereas in LTCM, numerous proliferating biliary epithelial cells and portal fibroblasts are observed (**f**)

fibroblasts [26] was also observed in HSC surrounding small lesions where suffering hepatocytes were present (data not shown). In PCLS cultured in LTCM, PDGF receptor-β expression was observed in centrolobular veins and in portal tract vessels but, in addition, numerous cells with fibroblastic appearance expressed PDGF receptor-β in portal areas (Fig. 1d). In PCLS cultured in Williams' E medium, rare proliferating cells expressing Ki 67 were detected in the parenchyma and in a few portal tracts (Fig. 1e). In contrast, in PCLS cultured in LTCM, an important proliferation of biliary epithelial cells and of portal fibroblasts was encountered (Fig. 1f); this proliferation was confirmed with BrdU immunostaining (data not shown). Cell viability evaluated by the MTT test showed no significative differences between the two culture media (Fig. 2). PCLS were processed for transmission electron microscopy to analyse ultrastructural morphology. After 24 or 48 h of culture in Williams' E medium, hepatocytes were generally well preserved with numerous mitochondria (Fig. 3a) and glycogen granules; however, in small ischemic areas, some hepatocytes presented suffering mitochondria (Fig. 3b). In PCLS cultured in LTCM, the tissue aspect was homogeneous, and hepatocyte ultrastructure was well preserved; however, enlarged portal tracts containing numerous portal fibroblasts around bile duct epithelial cells were observed (Fig. 3c and d), confirming the proliferation detected with Ki 67 immunostaining.

Because of the portal proliferation observed in portal tracts of PCLS cultured in the LTCM, Williams' E medium supplemented with insulin and dexamethasone was used for further studies. Different FCS concentrations were tested: With concentrations upper than 5%, a growing enlargement of portal tracts with portal fibroblast activation (PDGF receptor-β positive staining) was observed (data not shown); then, to

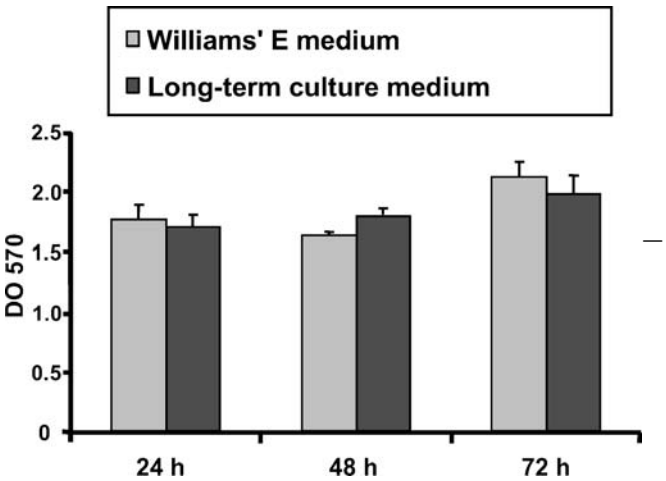

Fig. 2 MTT assay on PCLS cultured in Williams' E medium or LTCM. After 24, 48 or 72 h, the MTT analysis does not show any significative differences (one-way ANOVA) between PCLS cultured in Williams' E medium or PCLS cultured in LTCM

minimise proliferative effects of FCS, PCLS were cultured in 1% FCS; in this condition, fibroblast activation was not detected. Preliminary experiments performed in the presence of EPO were shown to only slightly improve the tissue conservation (data not shown).

Induction of centrolobular cytotoxicity

Thioacetamide is known to induce centrolobular toxicity together with fibrosis [4]. To test if in PCLS, thioacetamide is also able to induce lesions specifically around centrolobular veins, PCLS were treated with thioacetamide for 24 and 48 h. A decrease in viability, evaluated by MTT assay, was observed from 100 mM thioacetamide after 24 h of culture, and this phenomena was accentuated after 48 h of culture (data not shown). In PCLS treated with 80 mM thioacetamide for 48 h, clear circular necrotic lesions limited to hepatocytes located around centrolobular veins were observed (Fig. 4a); in these conditions, the necrosis was accompanied by the activation of HSC as shown by PDGF receptor-β immunostaining (Fig. 4b). Nevertheless, the effect of thioacetamide treatment was not restricted to centrolobular areas; indeed, numerous apoptotic cells expressing active caspase 3 were found in the sinusoids far from the initial lesion (Fig. 4c) and also in the portal tracts (Fig. 4d). After 48 h of culture with 100 mM thioacetamide, tissue lesions in PCLS were obvious: Around centrolobular veins, large circular necrotic areas with apoptotic cells at the periphery of the lesions were observed, and only a few healthy hepatocytes remained at the periphery of portal tracts (data not shown).

Because of the thioacetamide toxicity on sinusoidal and portal cells, we tested another well-known centrolobular toxic: acetaminophen [for review, see 2]. PCLS were cultured in the presence of 2.5 or 5 mM acetaminophen, and cell viability was assessed with MTT test. After 24 h of culture, no significant decrease in cell viability was observed with either 2.5 or 5 mM acetaminophen or after 48 h with 2.5 mM acetaminophen, but a significant decrease was observed after 48 h of treatment with 5 mM acetaminophen (Fig. 5). In PCLS cultured for 48 h with 2.5 mM acetaminophen, even if MTT test did not show a significant decrease in cell viability, suffering hepatocytes with condensed nucleus were observed around centrolobular veins (Fig. 6a); in acetaminophen-treated PCLS, the portal tracts were undamaged. These lesions were accompanied by an important activation of HSC, as shown by the increase of PDGF receptor-β expression in the sinusoids of parenchyma around centrolobular lesions (Fig. 6b). No apoptotic cells were detected outside of the centrolobular lesions, neither in portal tract nor in sinusoidal cells (data not shown). These data demonstrate that, in culture, acetaminophen induced lesions specifically located in centrolobular areas similarly to what was observed in vivo.

Acetaminophen cytotoxicity is prevented by *N*-acetylcysteine

In the case of acute intoxication with acetaminophen, *N*-acetylcysteine treatment is applied. *N*-acetylcysteine can substitute the glutathion, whose pool is insufficient in acute toxicity, and detoxify acetaminophen metabolites. *N*-acetylcysteine was tested to evaluate, in PCLS culture, its ability to prevent acetaminophen toxic effect and, therefore, HSC activation. PCLS were cultured with 2.5 mM *N*-acetylcysteine without or with 2.5 mM acetaminophen, and PCLS histology and HSC activation were analysed. In untreated PCLS (data not shown) or in the presence of *N*-acetylcysteine alone, PCLS histology did not appear modify, and no obvious tissue suffering signs or fibrogenic cell activation were observed (Fig. 6c and d). In the presence of both *N*-acetylcysteine and acetaminophen, hepatocyte lesions were considerably reduced; no necrotic or apoptotic hepatocytes were observed around centrolobular veins even if close to centrolobular veins, and a few vacuolated hepatocytes were observed (Fig. 6e). Together with the reduction of the lesion, a decrease of HSC activation, revealed by a decrease of PDGF receptor-β staining, was observed (Fig. 6f).

To prevent the activation of HSC induced by acetaminophen in cultured PCLS, we have also tested *trans*-resveratrol, a grape-derived polyphenol which has been described to induce deactivation of cultured human liver myofibroblasts [8]. In PCLS culture, treatment with *trans*-resveratrol together with acetaminophen not only was unable to prevent HSC activation but also presented synergic toxic effects, the lesions induced by acetaminophen being increased in the presence of *trans*-resveratrol (data not shown).

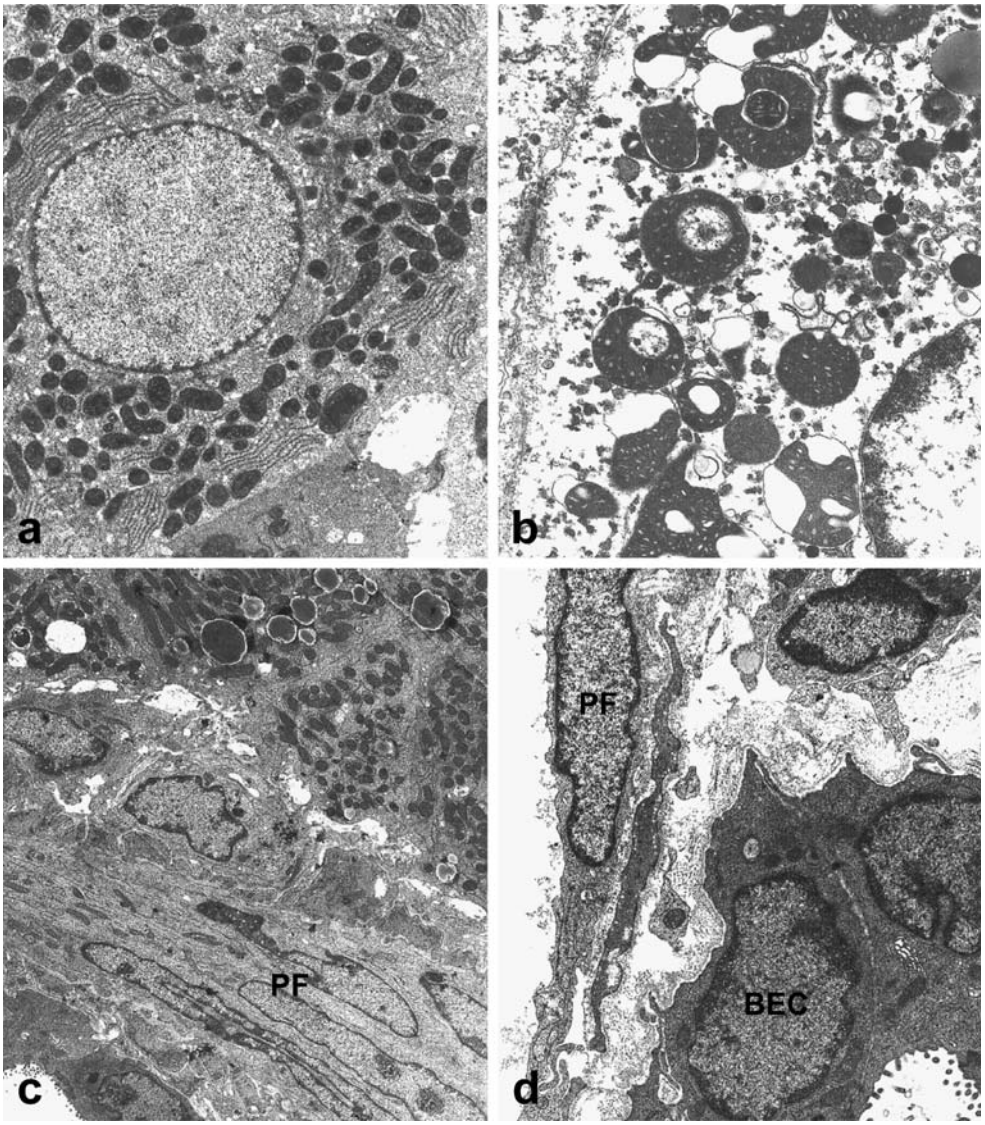

Fig. 3 Transmission electron microscopy of PCLS cultured in Williams' E medium (**a**, **b**) or in LTCM (**c**, **d**) for 48 h. In PCLS cultured in Williams' E medium, normal hepatocyte structures with numerous mitochondria are observed (**a**); in an ischemic area, a necrotic hepatocyte contains suffering mitochondria (**b**). In PCLS cultured in LTCM, numerous layers of portal fibroblasts (*PF*) surrounding bile duct epithelial cells (*BEC*) are observed in well-preserved enlarged portal tracts (**c** and **d**). (magnification: **a** ×5,200; **b** ×8,900; **c** ×2,950; **d** ×6,600)

Induction of early portal fibrogenesis

In human pathology, the development of a portal lesion is supposed to be at least, in part, a consequence of the bile duct epithelial cell proliferation. In this context, the effects of β-oestradiol and of EGF were tested in PCLS culture. In PCLS treated with β-oestradiol (25 nM) or EGF (50 ng/ml) for 24 and 48 h, an obvious enlargement of portal tracts was observed, together with an increase of PDGF receptor-β staining in periportal areas, demonstrating portal fibroblast activation (Fig. 7a and b). Immunostaining against BrdU was performed to localise proliferating cells. In PCLS treated with β-oestradiol, numerous proliferating cells, including biliary epithelial cells and portal myofibroblasts, were present in portal tracts; however, proliferating cells were also observed in the parenchyma (sinusoidal cells and hepatocytes), showing that the effects of β-oestradiol were broader than expected (Fig. 7c). In PCLS treated with EGF, cells incorporating BrdU were restricted to portal tracts (Fig. 7d). These data demonstrated that in cultured PCLS, EGF is efficient to induce specifically the proliferation of biliary epithelial cells and portal fibroblast activation.

Discussion

In this study, we evaluated the applicability of PCLS culture to study the early activation of hepatic fibrogenic cells. Two incubation media were tested for their ability to preserve tissue from injury or basal activation: Williams' E medium supplemented with insulin, dexamethasone and 1% FCS and LTCM, a complex medium which presents the benefit to be serum-free with a well-defined composition [24, 25]. However, an activation of portal fibroblasts together with a proliferation of biliary epithelial cells was observed in PCLS cultured in LTCM. The bile duct

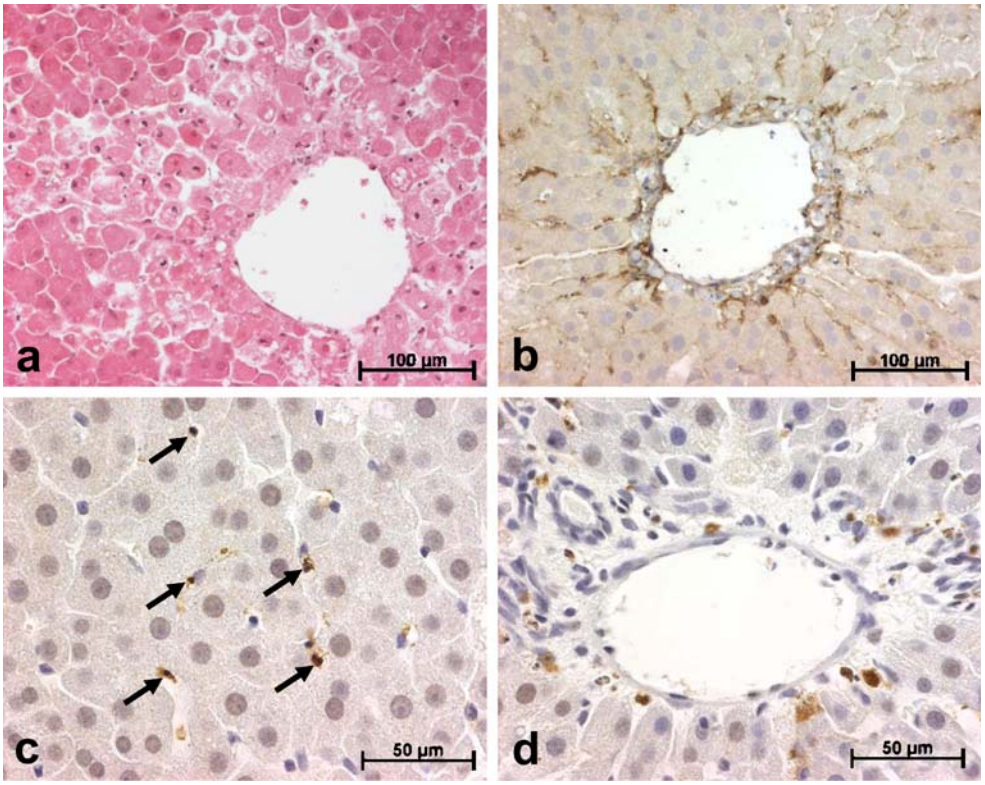

Fig. 4 Hematoxylin–eosin staining (**a**), PDGF receptor-β (**b**) and active caspase 3 (**c**, **d**) immunostainings in PCLS treated with thioacetamide for 48 h. PCLS treated with 80 mM thioacetamide show a circular necrotic lesion involving one or two hepatocyte layer around centrolobular veins (**a**); in these areas, PDGF receptor-β immunostaining shows activated HSC (**b**). Numerous active caspase 3 positive apoptotic cells are present in the sinusoids at a distance from the initial lesion (**c**, *arrows*) and in portal tracts (**d**)

epithelial cell proliferation observed may be due to the presence in this medium of growth factor such as EGF, which was shown to induce DNA synthesis in cultured bile duct cells [17]. To protect the tissue against ischemia, the addition of EPO to the culture medium was tested. Indeed, EPO has been described to show anti-apoptotic and tissue protective effects [7]; moreover, cultured adult rat cardiomyocytes subjected to hypoxia were prevented from apoptosis by EPO [5]. However, in the presence of EPO, the tissue conservation in cultured PCLS was only slightly improved.

In vivo, depending on the etiology of the lesion, different patterns of fibrosis can be observed. However, schematically, fibrosis develops around centrolobular zones inducing centrolobular fibrosis, or in portal tracts leading to portal fibrosis. To validate the PCLS model so as to study liver fibrogenesis and the early steps of fibrogenic cell activation, it was necessary to be able to reproduce the fibrotic process observed in vivo and to induce a specific activation of fibrogenic cells present either in centrolobular areas (i.e. HSC) or in portal tracts (i.e. PF). Numerous toxic compounds are known to induce centrolobular lesions leading to HSC activation. Carbon tetrachloride is one of the most frequently used; however, it is a highly volatile compound, which prevents us to use it in our culture model. We choose to use thioacetamide whose biotransformation by centrolobular hepatocytes induces oxidative liver injury [23] associated with centrolobular lesion and HSC activa-

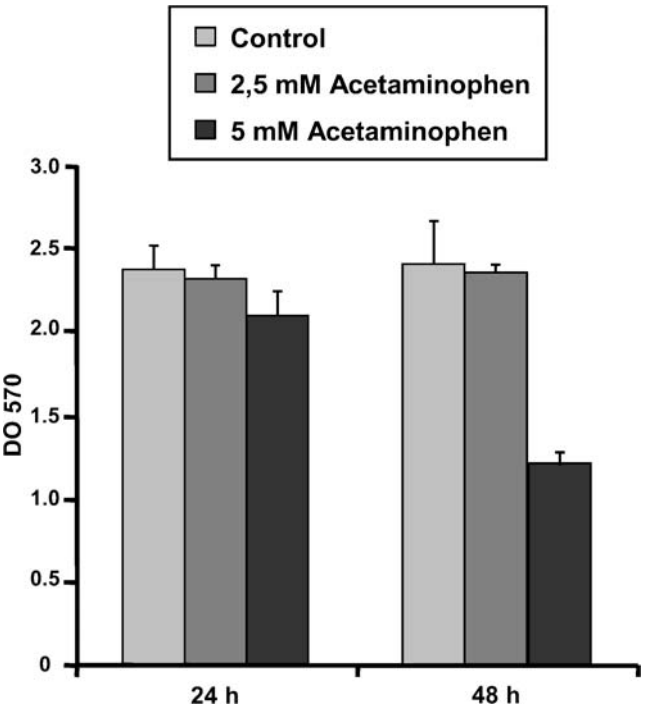

Fig. 5 MTT assay on control or acetaminophen-treated PCLS cultured for 24 h or 48 h. After 24 h of culture, no significant decrease of cell viability is observed in PCLS treated with 2.5 or 5 mM acetaminophen. After 48 h of culture, no difference in cell viability is observed between control and 2.5 mM acetaminophen-treated PCLS, whereas a significant decrease in cell viability is observed in PCLS treated with 5 mM acetaminophen ($P<0.05$; one-way ANOVA)

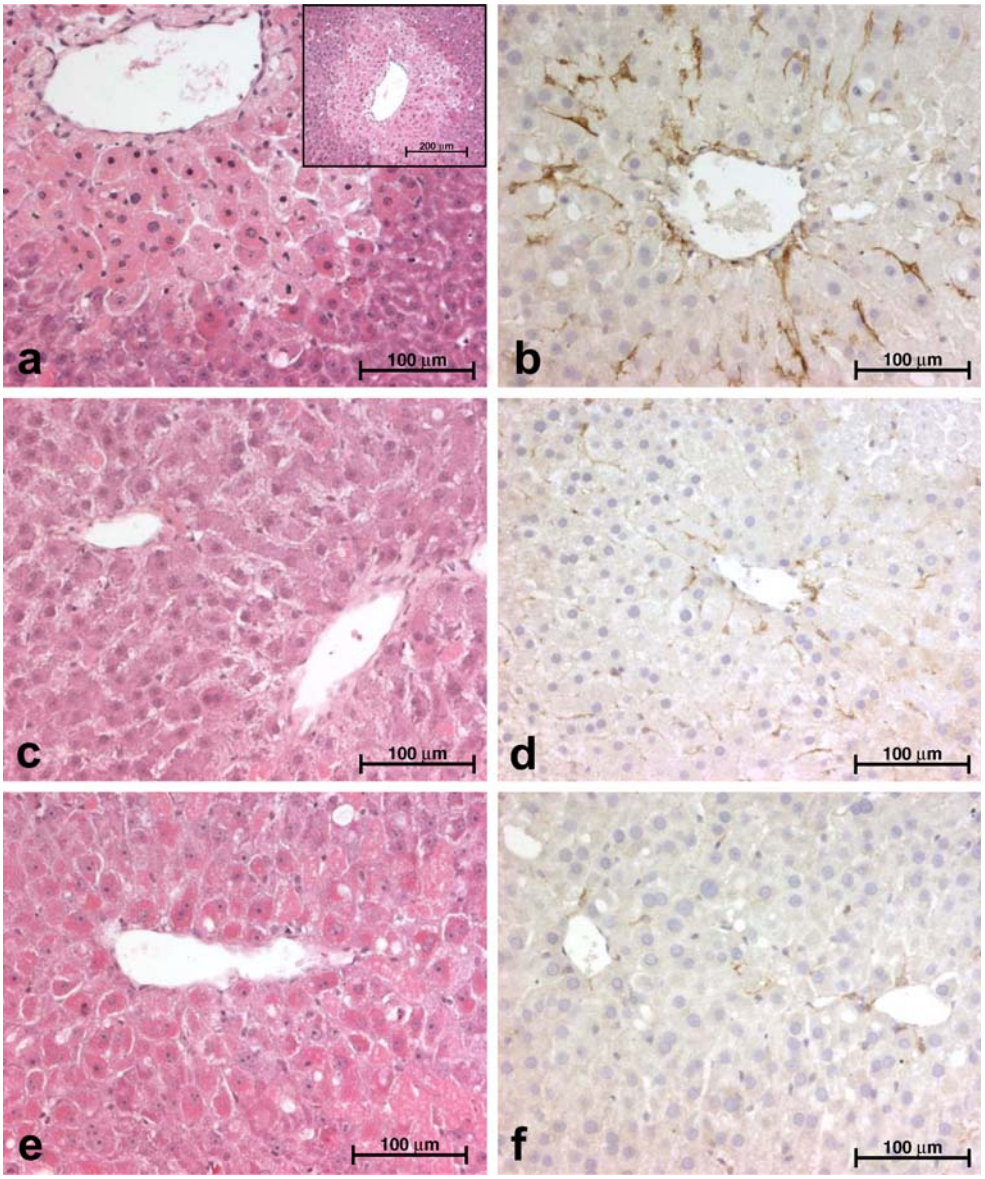

Fig. 6 Hematoxylin–eosin staining (**a**, **c**, **e**) and PDGF receptor-β immunostaining (**b**, **d**, **f**) in PCLS treated with 2.5 mM acetaminophen (**a**, **b**), 2.5 mM *N*-acetylcysteine alone (**c**, **d**) or with acetaminophen (**e**, **f**) cultured for 48 h. In PCLS treated with acetaminophen, suffering hepatocytes are observed around centrolobular veins (**a**) together with HSC activation (**b**). In *N*-acetylcysteine-treated PCLS (**c**, **d**) and in PCLS treated with acetaminophen and *N*-acetylcysteine (**e**, **f**), neither parenchymal lesion around centrolobular veins (**c**, **e**) nor obvious HSC activation (**d**, **f**) is observed

tion [4]. However, in cultured PCLS, we noticed that thioacetamide treatment not only leads to centrolobular lesions with HSC activation but also induces toxic effects on other cells, particularly on portal tract cells. No acute toxicity of thioacetamide on portal tract cells was reported in the literature; however, it was described that long-term thioacetamide treatment is able to induce cholangiocarcinoma in animal models [30], suggesting an effect of thioacetamide on portal tract cells. Anyway, our data show that in vivo observations obtained after thioacetamide treatment are not strictly reproduced in the PCLS model. Then, another well-described hepatotoxic drug, acetaminophen, was tested. Acetaminophen induces a lesion of the hepatocytes in centrolobular areas, but the exact mechanisms of acetaminophen-induced cell injury are still incompletely understood. Recent studies suggest that acetaminophen toxicity is mediated by reactive metabolite formation, glutathion depletion and protein alkylation, which represent the initiating events for the toxicity [12]. Acetaminophen is involved in acute liver failure; however, no studies were reported showing fibrosis induction in chronic treatment. Here, in cultured PCLS, acetaminophen treatment induced specifically centrolobular lesions similarly to in vivo observations; then, acetaminophen treatment of cultured PCLS appears relevant to study the early steps of fibrogenic cell activation. In vivo, to treat patients showing acute liver failure after acetaminophen overdose, the antioxidant *N*-acetylcysteine is used. We performed experiments to know if acetaminophen-induced toxicity could be prevented by *N*-acetylcysteine treatment in PCLS. We observed a suppression of the acetaminophen toxicity under *N*-acetylcysteine addition; these data suggest that HSC activation is a secondary event after hepatocyte injury induced by acetaminophen and underline the relevance of

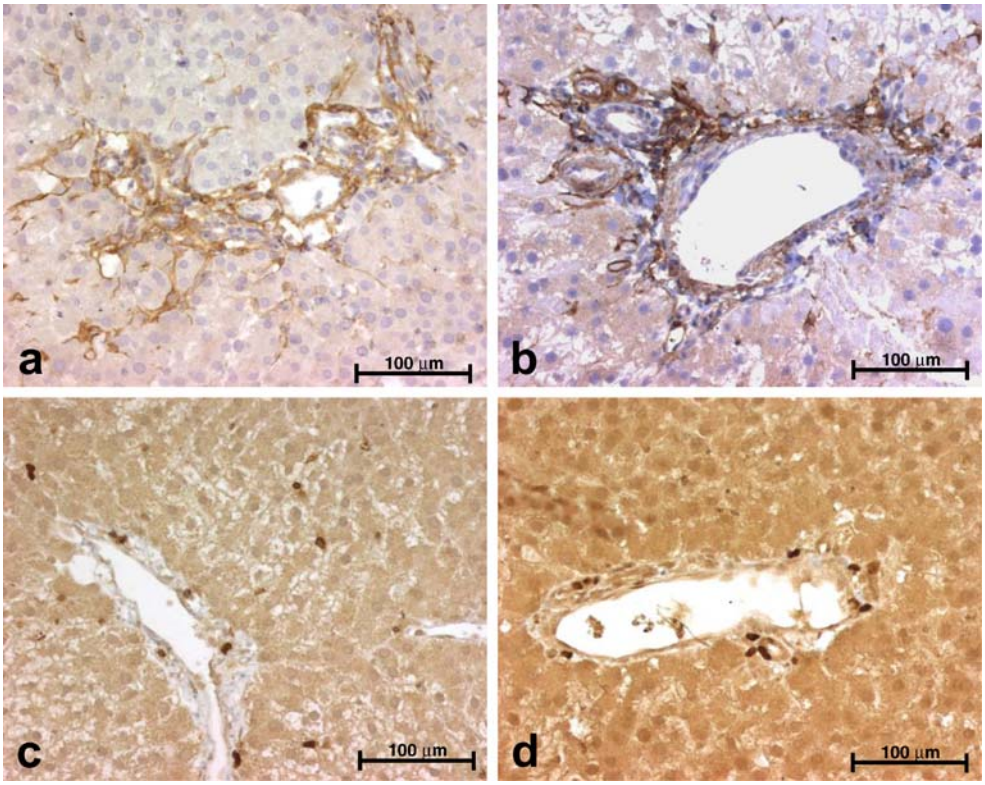

Fig. 7 PDGF receptor-β (**a**, **b**) and BrdU (**c**, **d**) immunostainings in PCLS treated with β-oestradiol (**a**, **c**) or EGF (**b**, **d**) cultured for 48 h. In PCLS treated with β-oestradiol (25 nM) or EGF (50 ng/ml), portal tracts are enlarged, and an important activation of portal fibroblasts is observed (**a**, **b**). In β-oestradiol-treated PCLS, numerous proliferating cells are observed in the portal tract and in the parenchyma (sinusoidal cells and hepatocytes) (**c**). In EGF-treated PCLS, proliferating cells are only observed in the portal tracts (**d**)

the PCLS model to study the early mechanisms involved in HSC activation.

In vivo, early fibrosis developing in portal tracts can result from the activation and proliferation of biliary epithelial cells; this proliferation induces a remodelling of the portal tracts and cytokine production by biliary epithelial cells leading to or accompanied by portal fibroblast activation and proliferation [9, 13, 14, 27]. Some products are known for their ability to trigger specific biliary epithelial cell proliferation. In this context, the effects of β-oestradiol and of EGF, which has been described to stimulate in vitro and in vivo bile duct epithelial cell proliferation [1, 17], were tested in PCLS culture. We show, here in the PCLS model, that the effects of β-oestradiol concern different hepatic cells, and not exclusively biliary epithelial cells. In contrast, we show that EGF is able to induce specifically biliary epithelial cell proliferation and PF activation. Indeed, we suspected EGF to be involved in portal cell proliferation observed in PCLS cultured in LTCM.

In conclusion, in this study, we have defined culture conditions to maintain satisfactory PCLS architecture without significative modifications induced by culture environment. Previous studies comparing different incubation systems reported a better tissue conservation using shaken flask or rocker platform [20]; however, in our hands, for culture duration above 24 h, PCLS culture performed with the roller incubation system showed a better tissue conservation, and PCLS could be maintained in culture for 72 h without obvious alterations. Moreover, even if the global architecture of the liver is well preserved in PCLS culture, it is important to underline that some necrotic hepatocytes are often present, at least at the periphery of the slice; these small injured areas make histological observations absolutely necessary for a faithful interpretation of the data obtained with PCLS culture; in addition, this point is crucial when entire slices are used to extract total RNA or protein samples. However, except these lesions commonly observed at the periphery of the slice, the observations were homogeneous in every layer. In addition, in this study, we demonstrated that it is possible to induce in PCLS hepatic damages which mimic in vivo situation. This model appears especially well suited to the investigation of the mechanisms involved in HSC and PF activation, as it eliminates two confusing factors, hydrostatic pressure and recruitment of circulating inflammatory cells. Therefore, the PCLS culture model represents a good alternative tool to study early events involved in liver fibrogenesis.

Acknowledgements We are very grateful to P. Maurel (INSERM U 632, Montpellier, France) for providing the serum-free long-term culture medium, and we thank the staff of the Service Commun de Microscopie Electronique (SERCOMI, Université Victor Segalen Bordeaux 2, France) for performing transmission electron microscopy sample preparation.

This work was supported in part by Région Aquitaine. C. Guyot was a recipient of a fellowship from Région Aquitaine.

References

1. Alvaro D, Alpini G, Onori P, Perego L, Svegliata Baroni G, Franchitto A, Baiocchi L, Glaser SS, Le Sage G, Folli F, Gaudio E (2000) Estrogens stimulate proliferation of intrahepatic biliary epithelium in rats. Gastroenterology 119:1681–1691
2. Bessems JG, Vermeulen NP (2001) Paracetamol (acetaminophen)-induced toxicity: molecular and biochemical mechanisms, analogues and protective approaches. Crit Rev Toxicol 31:55–138
3. van de Bovenkamp M, Groothuis GM, Draaisma AL, Merema MT, Bezuijen JI, van Gils MJ, Meijer DK, Friedman SL, Olinga P (2005) Precision-cut liver slices as a new model to study toxicity-induced hepatic stellate cell activation in a physiologic milieu. Toxicol Sci 85:632–638
4. Bruck R, Genina O, Aeed H, Alexiev R, Nagler A, Avni Y, Pines M (2001) Halofuginone to prevent and treat thioacetamide-induced liver fibrosis in rats. Hepatology 33:379–386
5. Calvillo L, Latini R, Kajstura J, Leri A, Anversa P, Ghezzi P, Salio M, Cerami A, Brines M (2003) Recombinant human erythropoietin protects the myocardium from ischemia-reperfusion injury and promotes beneficial remodeling. Proc Natl Acad Sci USA 100:4802–4806
6. Clouzeau-Girard H, Guyot C, Combe C, Moronvalle-Halley V, Housset C, Lamireau T, Rosenbaum J, Desmoulière A (2006) Effects of bile acids on biliary epithelial cell proliferation and portal fibroblast activation using rat liver slices. Lab Invest 86:275–285
7. Ghezzi P, Brines M (2004) Erythropoietin as an antiapoptotic, tissue-protective cytokine. Cell Death Differ 11:S37–S44
8. Godichaud S, Krisa S, Couronne B, Dubuisson L, Merillon JM, Desmoulière A, Rosenbaum J (2000) Deactivation of cultured human liver myofibroblasts by trans-resveratrol, a grapevine-derived polyphenol. Hepatology 31:922–931
9. Grappone C, Pinzani M, Parola M, Pellegrini G, Caligiuri A, DeFranco R, Marra F, Herbst H, Alpini G, Milani S (1999) Expression of platelet-derived growth factor in newly formed cholangiocytes during experimental biliary fibrosis in rats. J Hepatol 31:100–109
10. Guyot C, Lepreux S, Combe C, Doudnikoff E, Bioulac-Sage P, Balabaud C, Desmoulière A (2006) Hepatic fibrosis and cirrhosis: the (myo)fibroblastic cell subpopulations involved. Int J Biochem Cell Biol 38:135–151
11. Guyot C, Combe C, Balabaud C, Bioulac-Sage P, Desmouliere A (2007) Fibrogenic cell fate during fibrotic tissue remodelling observed in rat and human cultured liver slices. J Hepatol 46:142–150
12. Jaeschke H, Bajt ML (2006) Intracellular signaling mechanisms of acetaminophen-induced liver cell death. Toxicol Sci 89:31–41
13. Kruglov EA, Nathanson RA, Nguyen T, Dranoff JA (2006) Secretion of MCP-1/CCL2 by bile duct epithelia induces myofibroblastic transdifferentiation of portal fibroblasts. Am J Physiol Gastrointest Liver Physiol 290:765–771
14. Lamireau T, Zoltowska M, Levy E, Yousef I, Rosenbaum J, Tuchweber B, Desmoulière A (2003) Effects of bile acids on biliary epithelial cells: proliferation, cytotoxicity, and cytokine secretion. Life Sci 72:1401–1411
15. Lerche-Langrand C, Toutain HJ (2000) Precision-cut liver slices: characteristics and use for in vitro pharmaco-toxicology. Toxicology 153:221–253
16. Lotersztajn S, Julien B, Teixeira-Clerc F, Grenard P, Mallat A (2005) Hepatic fibrosis: molecular mechanisms and drug targets. Annu Rev Pharmacol Toxicol 45:605–628
17. Mathis GA, Sirica AE (1990) Effects of medium and substratum conditions on the rates of DNA synthesis in primary cultures of bile ductular epithelial cells. In Vitro Cell Dev Biol 26:113–118
18. Moronvalle-Halley V, Sacre-Salem B, Sallez V, Labbe G, Gautier JC (2005) Evaluation of cultured, precision-cut rat liver slices as a model to study drug-induced liver apoptosis. Toxicology 207:203–214
19. Neyrinck AM, Taper HS, Gevers V, Declerck B, Delzenne NM (2002) Inhibition of Kupffer cell activity induces hepatic triglyceride synthesis in fasted rats, independent of lipopolysaccharide challenge. J Hepatol 36:466–473
20. Olinga P, Groen K, Hof IH, De Kanter R, Koster HJ, Leeman WR, Rutten AA, Van Twillert K, Groothuis GM (1997) Comparison of five incubation systems for rat liver slices using functional and viability parameters. J Pharmacol Toxicol Methods 38:59–69
21. Olinga P, Hof IH, Merema MT, Smit M, de Jager MH, Swart PJ, Slooff MJ, Meijer DK, Groothuis GM (2001) The applicability of rat and human liver slices to the study of mechanisms of hepatic drug uptake. J Pharmacol Toxicol Methods 45:55–63
22. Olinga P, Merema MT, de Jager MH, Derks F, Melgert BN, Moshage H, Slooff MJ, Meijer DK, Poelstra K, Groothuis GM (2001) Rat liver slices as a tool to study LPS-induced inflammatory response in the liver. J Hepatol 35:187–194
23. Pallottini V, Martini C, Bassi AM, Romano P, Nanni G, Trentalance A (2006) Rat HMGCoA reductase activation in thioacetamide-induced liver injury is related to an increased reactive oxygen species content. J Hepatol 44:368–374
24. Pichard-Garcia L, Gerbal-Chaloin S, Ferrini JB, Fabre JM, Maurel P (2002) Use of long-term cultures of human hepatocytes to study cytochrome P450 gene expression. Methods Enzymol 357:311–321
25. Pichard L, Raulet E, Fabre G, Ferrini JB, Ourlin JC, Maurel P (2006) Human hepatocyte culture. Methods Mol Biol 320:283–293
26. Pinzani M, Milani S, Grappone C, Weber FL Jr, Gentilini P, Abboud HE (1994) Expression of platelet-derived growth factor in a model of acute liver injury. Hepatology 19:701–707
27. Sedlaczek N, Jia JD, Bauer M, Herbst H, Ruehl M, Hahn EG, Schuppan D (2001) Proliferating bile duct epithelial cells are a major source of connective tissue growth factor in rat biliary fibrosis. Am J Pathol 158:1239–1244
28. Tuchweber B, Desmouliere A, Bochaton-Piallat ML, Rubbia-Brandt L, Gabbiani G (1996) Proliferation and phenotypic modulation of portal fibroblasts in the early stages of cholestatic fibrosis in the rat. Lab Invest 74:265–278
29. Vickers AE, Saulnier M, Cruz E, Merema MT, Rose K, Bentley P, Olinga P (2004) Organ slice viability extended for pathway characterization: an in vitro model to investigate fibrosis. Toxicol Sci 82:534–544
30. Yeh CN, Maitra A, Lee KF, Jan YY, Chen MF (2004) Thioacetamide-induced intestinal-type cholangiocarcinoma in rat: an animal model recapitulating the multi-stage progression of human cholangiocarcinoma. Carcinogenesis 25:631–636

Virchows Arch (2007) 450:513–518
DOI 10.1007/s00428-007-0380-0

ORIGINAL ARTICLE

Tissue preparation for MOHS' frozen sections: a comparison of three techniques

Omid Bakhtar · Abby Close · Terence M. Davidson · Stephen M. Baird

Received: 30 November 2006 / Revised: 26 January 2007 / Accepted: 1 February 2007 / Published online: 4 April 2007
© Springer-Verlag 2007

Abstract Accurate, efficient frozen section analysis is important for tumor control. A few studies address the technical issues. More are needed, especially as new technologies become available. The objective of this study is to compare the efficiency of three techniques of flattening tissue for microscopically oriented histologic surgery (MOHS): conventional frozen sectioning, Cryocup™, and CryoHist™. Conventional chuck/heat sink-frozen section preparation were compared with Cryocup™ and CryoHist™ to determine the most efficient technique to examine 100% of the surgical margin of 4-cm diameter, full thickness, fresh autopsy cylinders of anterior abdominal skin, which were marked on their deep and peripheral margins. The specimens were frozen sectioned at 5 μm until all the marking dye was gone from the deep surface, and 95% of the perimeter epidermis could be seen. The conventional chuck required an average of 304 micrometers to clear the deep margin and four fifths did not contain 95% of the epidermal margin. The Cryocup™ required an average of 284 μm to examine the deep margin and 95% of the epidermal margin. The CryoHist™ required an average of 104 μm to examine the deep margin and 95% of the epidermal border. The new techniques improve the efficiency and presumably the accuracy of tumor margin analysis.

O. Bakhtar · A. Close · T. M. Davidson (✉) · S. M. Baird
University of California, San Diego School of Medicine,
9500 Gilman Drive, Evergreen, MC 0617,
La Jolla, CA 92093-0617, USA
e-mail: tdavidson@ucsd.edu

O. Bakhtar · A. Close · T. M. Davidson · S. M. Baird
VA San Diego Healthcare System,
3350 La Jolla Village Drive,
San Diego, CA 92161, USA

Keywords Histocytologic preparation techniques (MeSH) · Conventional frozen sections (MeSH) · MOHS (MeSH) · Cryocup™ technique · CryoHist™ technique

Introduction

Surgeons send tumor specimens for frozen section analysis to make a diagnosis, to confirm complete resection, or to guide additional tumor extirpation. One approach is to sample a slice of the tissue in an orientation to include tumor and the margin. This provides excellent sampling of the tumor, but limited analysis of the actual margin of the cylindroid-shaped tissue. This sampling technique with 10-μm histology sections is estimated to be about 1:2,000 of the total surgical margin (Fig. 1a); for 5-μm histology sections, it is 1:4,000 of the total surgical margin. An alternate approach, typically called microscopically oriented histologic surgery (MOHS), is to orient and cut the specimen to attempt to examine the entire surgical margin. This approach has been called parallel, MOHS or en face margins. This approach is a technical challenge and requires flattening and orienting the surgical margin to examine it as thoroughly as possible. Different paradigms are practiced. This study compares three different approaches.

Materials and methods

Four- by two-centimeter cylindrical pieces of anterior abdominal skin were harvested at autopsy. A 45° oblique skin incision was used. Each cylinder of skin was cut into four quadrant specimens that were then flattened using one of three methods: "conventional" (heat sink), Cryocup™, or CryoHist™ (Fig. 1b).

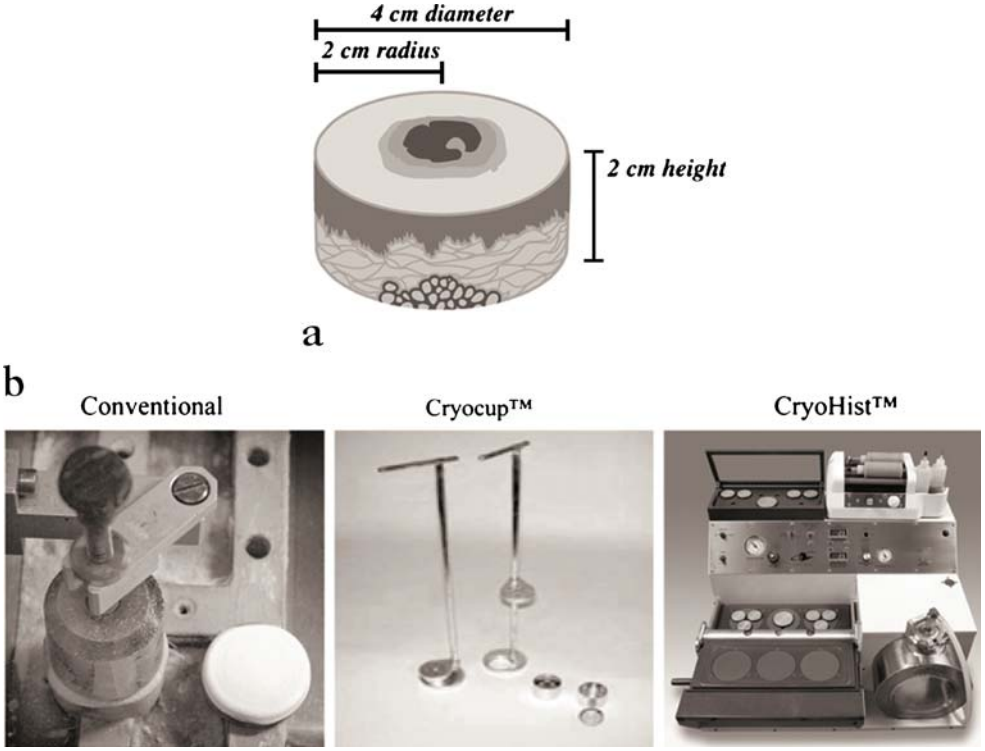

Fig. 1 Sampling techniques. **a** (a) surgical margin surface area (SMSA) of a cylinder (not including the top) is equal to πr^2 (deep margin) + $2\pi rh$ (lateral margin), where r=2 cm and h=2 cm. SMSA = (3.14159) (2 cm)^2 + 2(3.14159)(2 cm) (2 cm)=37.7 cm^2. (b) Microscope slide section surface area is equal to (thickness of section) × (height × 2 + bottom), which is (10 μm) × (8 cm) = 8×10^{-4} cm^2; the surface for 10 sections = 8×10^{-3} cm^2; ratio A/B of 10-μm cuts = approximately 2,000:1; ratio A/B of 5 micron cuts = 4,000:1. **b** Photographs of conventional, Cryocup™, and CryoHist™

Preparation of the specimen before the flattening procedure was identical for the three methods (Fig. 2a–c). The deep and circumferential margins of each cylinder of skin were inked. Different colors were applied to the circumferential and deep margins, respectively. After applying acetone and allowing 3 min of drying time, a relaxing incision was placed in a circular/circumferential manner approximately 0.2 cm from the resection edge (Fig. 2b). The circular cylinders were then divided into equal-sized quadrants and flattened utilizing one of the following three methods:

Conventional

A small quantity of frozen tissue embedding medium commonly called OCT (Optimal Cutting Temperature) was placed onto a cold chuck, and a heat sink was applied to freeze and flatten the OCT base. After freezing the OCT, the color-coded, "relaxed" skin quadrant was placed surgical side up on the center of the OCT surface. Fresh OCT was then applied around and on top of the tissue, and the heat sink (Fig. 1b) was placed on the specimen for a period of 60 s. The resulting frozen tissue, embedded in OCT, was then transferred to the cryostat (OCT, Tissue Tek® embedding medium, Sakura Finetek USA, Torrance, CA 90502, USA).

Cryocup™

Color-coded, "relaxed" tissue was placed surgical side down in the Cryocup™ (Fig. 1b), and a small probe was utilized to gently press the relaxed circumferential margin flat with the deep margin. The electrostatic force between the Cryocup™ and the relaxed circumferential lip of the specimen facilitated their adherence. A small quantity of OCT was added up to the inner ledge of the Cryocup™. A chuck was then placed on top of the tissue, and the Cryocup™/chuck was dipped in liquid nitrogen using the Cryocup™ holder to maintain the post perpendicular to the flattened margin. The holder and enclosed specimen were kept in the liquid nitrogen until temperature equilibrium was reached (approximately 20–40 s). The Cryocup™ was removed from the holder and warmed by immersion into tap water for 10–20 s. With the resulting chuck mounted, the OCT-embedded tissue was then transferred to the cryostat (Bradley Products, P.O. Box 201405, Bloomington, MN 55420, USA).

CryoHist™

Color coded, "relaxed" tissue was placed surgical side down on the freezing platform of the CryoHist™ (Fig. 1b). A membrane was utilized to create a suction vacuum that flattened the specimen. The specimen was then snap frozen through cooling of the platform with liquid nitrogen. The membrane was removed, and OCT was applied to the frozen specimen. Flipping the stage brought the specimen, OCT, and chuck into contact. Further freezing down to −20°C resulted in an OCT- embedded and flattened specimen that was then transferred to the cryostat (Cryo Histology, P.O. Box 3826, Shawnee, KS 66203, USA).

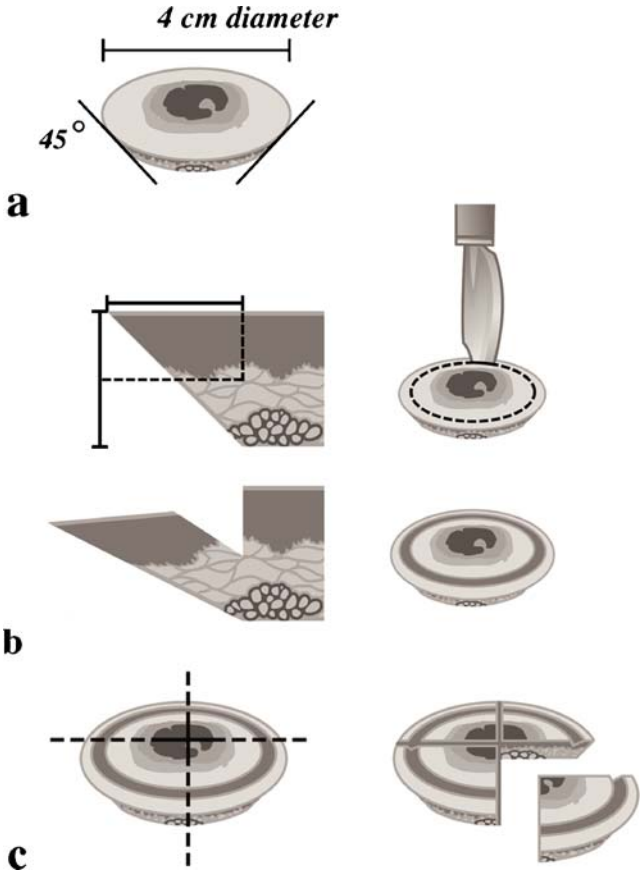

Fig. 2 Harvesting and preparing abdominal cadaver skin. **a** The cylinder is cut into 4×2 cm diameter with a 45° oblique edge. **b** A partial thickness circumferential relaxing incision is made 2 mm from the perimeter. **c** The specimen is cut in quarters

The embedded tissue from each method was mounted for cutting in a cryostat. The head of the cryostat was non-adjustable and was preset at an angle identical to that of the cutting blade. The specimen was cut until ink was grossly visible in the OCT section. This cut represented the "start" of the tissue block. The block was then cut at 5-μm sections, and the serial sections were counted and maintained for H & E staining followed by microscopic analysis. The sections were reviewed until all the marking dye was gone from the deep surface, and 95% of the perimeter epidermis could be seen. This was the end point. Examples of complete and incomplete margins in the histologic sections are shown in Fig. 3a and b.

Results

There were a total of 15 pieces of skin frozen, embedded, and sectioned in the study. Each of the three methods of freezing (conventional, CryoHist™, and Cryocup™) was repeated five times. The number of 5-μm sections it took for 95% of the skin margin to be visualized on one section was recorded. These results are displayed in Table 1. The CryoHist™ and Cryocup™ techniques consistently provided sections demonstrating >95% of the skin margin. However, using the conventional method, it was very difficult to get a section demonstrating >95% of the skin edge. With the conventional method, four of the five samples were not flat enough to obtain a slide with >95% of the skin margin. A majority of the time, the tissue would "chunk out" of the block before the goal of near-complete margins was obtained. This problem only occurred with the conventional method.

Discussion

Both the CryoHist™ and the Cryocup™ methods allowed for visualization of >95% of the margin. On average, it took

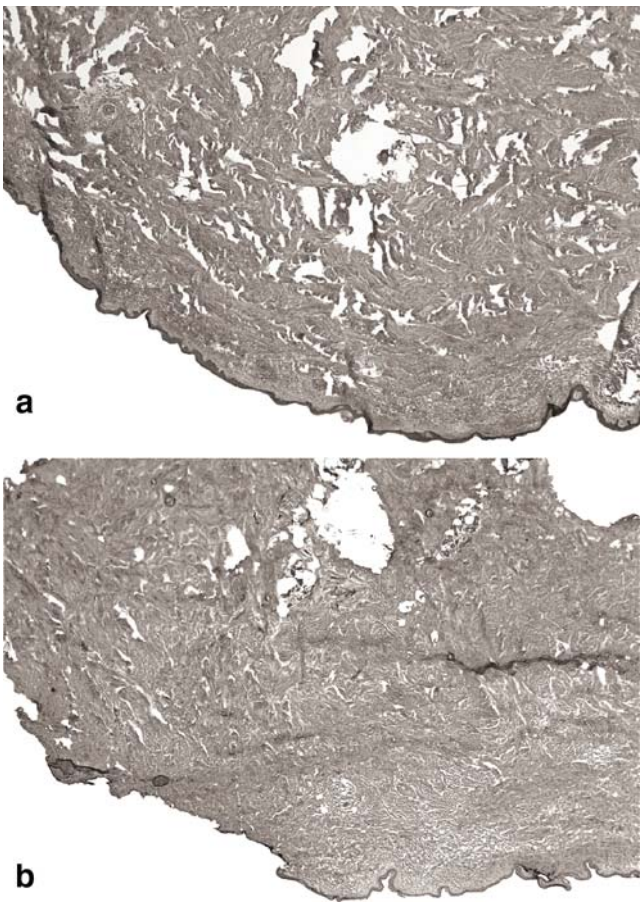

Fig. 3 Complete and incomplete margin. **a** The complete margin can be identified in this section. The periphery of the tissue demonstrates a thin rim of flattened epidermis (circumferential margin), while the central portion of the tissue demonstrates the deep margin. **b** An incomplete peripheral margin is present in this section. The thin rim of epidermis only extends halfway around the circumference. To complete the tissue microarray (TMA), additional deeper cuts must be performed

Table 1 Comparison of three methods of freezing

Methods	First	Second	Third	Fourth	Fifth
CyroHist™	100	100	100	140	80
Cryocup™	200	240	220	420	340
Conventional	380[a]	280[b]	320	300[b]	240[b]

[a] Number of sections to section through the tissue completely without ever obtaining a slide with >95% margins.
[b] Number of sections when the sample "chunked out," not able to obtain a section with near complete margins.

104 sections using the CryoHist™ and 284 sections using the Cryocup™ to obtain a section with near-complete margins. This difference is attributable directly to the flattening power of the respective methods. The conventional method proved significantly less than ideal, which was demonstrated by the number of cuts required to approach clearing the margins. The "chunking out" of tissue was a direct consequence of the inability to align the epidermis with the deep margin and to orient the deep margin perpendicular to the chuck post.

Given that the Cryocup™ and the CryoHist™ are more efficient in flattening the specimens, how is this achieved? Conventional flattening and orientation are entirely dependent on the technical skills of the histologist. The Cryocup™ relies on the adhesion between the tissue and the aluminum cup to flatten the surgical surface and then achieves perpendicular orientation by aligning the chuck post with the Cryocup™ stand. This does well with soft and flattened tissues up to a diameter of 2.4 cm. The CryoHist™ flattens the tissue by placing the tissue face down, covering it with cellophane, and then applying a vacuum to the cellophane, which flattens the tissue against a cold metal platform. The platform and tissue are frozen, the cellophane is removed, and the chuck, held perpendicular to the tissue surface platform, is attached to the specimen with additional OCT. This makes a very flat surface perpendicular to the surgical margin. The flatter the frozen surgical margin and the better the perpendicular orientation, the more efficient and accurate is the histologic sectioning.

It is important that the peripheral margins be pulled into the same plane as the remainder of the specimen. For many tissues, the surgical margin surface is not naturally flat. Tissue contraction and deformation leave this surface somewhat irregular. Flattening insures that 100% of the true surgical margin is on the first cryostat cut. This is the ideal. The better the technique, the more likely the first cut is a true representation of the entire surgical margin.

This becomes a clinical issue in the following scenario. Histology technicians are taught to take the first slices off the cryostat for these represent the true surgical margin. Permanent sections are taken from deeper in the tissue. A clinical problem arises when the frozen section margin is interpreted as clear, but the permanent section margin is interpreted as positive. One must then look at both sections and determine whether the site of the positive permanent section margin is present in the frozen section. If it is present in the frozen section and there is in fact no tumor, then the margin is clear. However, if the frozen section does not include the area of concern, one must assume the permanent section is the true margin, and the margin is, therefore, positive. Reoperation must now be performed.

The aforementioned data demonstrate the inadequacy of the conventional method for MOHS as well as the benefits gained by utilizing specialized systems for tissue flattening. Both the Cryocup™ and the CryoHist™ systems are capable of flattening the skin sections to a degree that

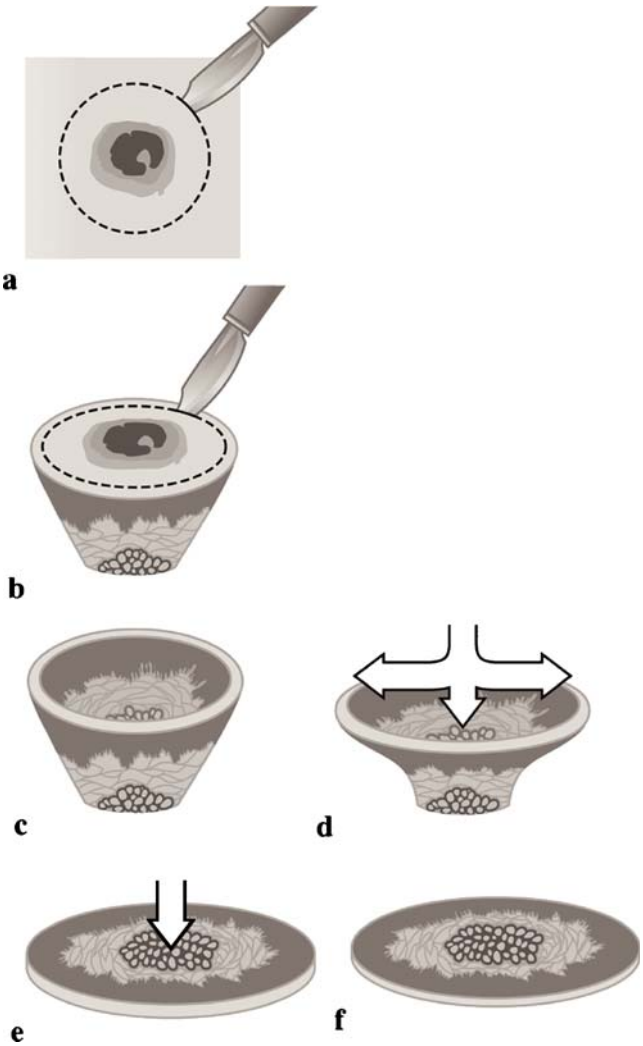

Fig. 4 Excision of skin tumor for TMA. **a** The tumor is excised with an oblique incision. **b** A circumferential relaxing incision is made, 2–3 mm in from the perimeter. **c** The central core tissue is removed with curette, scalpel, or scissors. **d** The peripheral margins are pressed outwards. **e** The base is pressed flat. **f** The total margin is now flat and is ready for freezing and histological sectioning

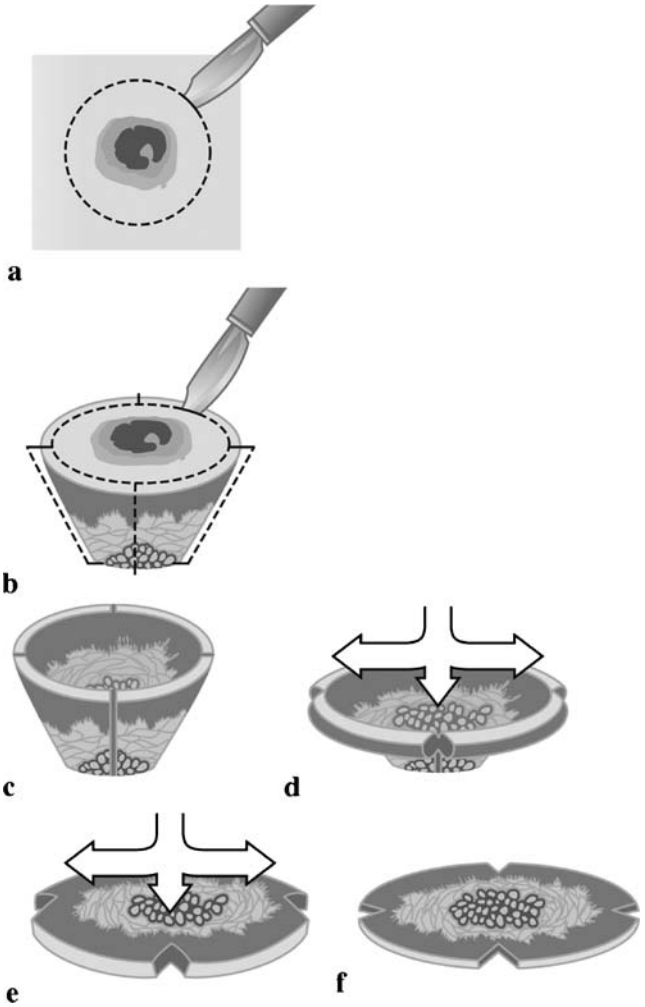

Fig. 5 Excision of intermediate thick, stiff skin for TMA. **a** The tumor is excised with an oblique incision. **b** A circumferential relaxing incision is made and radial cuts are made; 2, 3, 4, 5, or 6 cuts can be made. Incisions rose-petal the specimen so that the margins fall flat. **c** The central core is excised. **d** The periphery is pressed flat. **e** The base is pressed flat. **f** The total margin is now flat and is ready for freezing and histological sectioning

improves the efficiency and accuracy, albeit not measured, of the margin analysis. The CryoHist™ outperforms the Cryocup™ system in the degree of flattening and the subsequent number of sections required to clear the deep and circumferential margins. Both are substantially superior to conventional free-hand techniques.

A review of the literature demonstrates publications describing various methods of flattening for frozen section analysis. A popular method for flattening uses a glass slide for the compression of the tissue [1–4]. There are also several papers describing less commonly used methods such as the cryomold [5], Miami special [6], special discs [7], and gradual freezing with liquid nitrogen [8]. Motley and Holt [9] published results from a survey of the members of the American College of MOHS Micrographic Surgery and Cutaneous Oncology, with data on the methods used for freezing tissue. Their survey found that 30% uses a heat extractor, 20% a glass slide, 16% a Bard Parker scalpel handle, 11% a Miami special, and 5% a cryomold. None of these publications have compared multiple methods of flattening in a controlled prospective study with quantitative data, as is done in this study.

There are multiple approaches to tissue preparation for MOHS. Most of the techniques focus on reducing the tension intrinsic to the skin to minimize cryocontraction of the dermis, which pulls up the epidermis if not incisionally released [10]. Ideally, if the specimen's size permits,

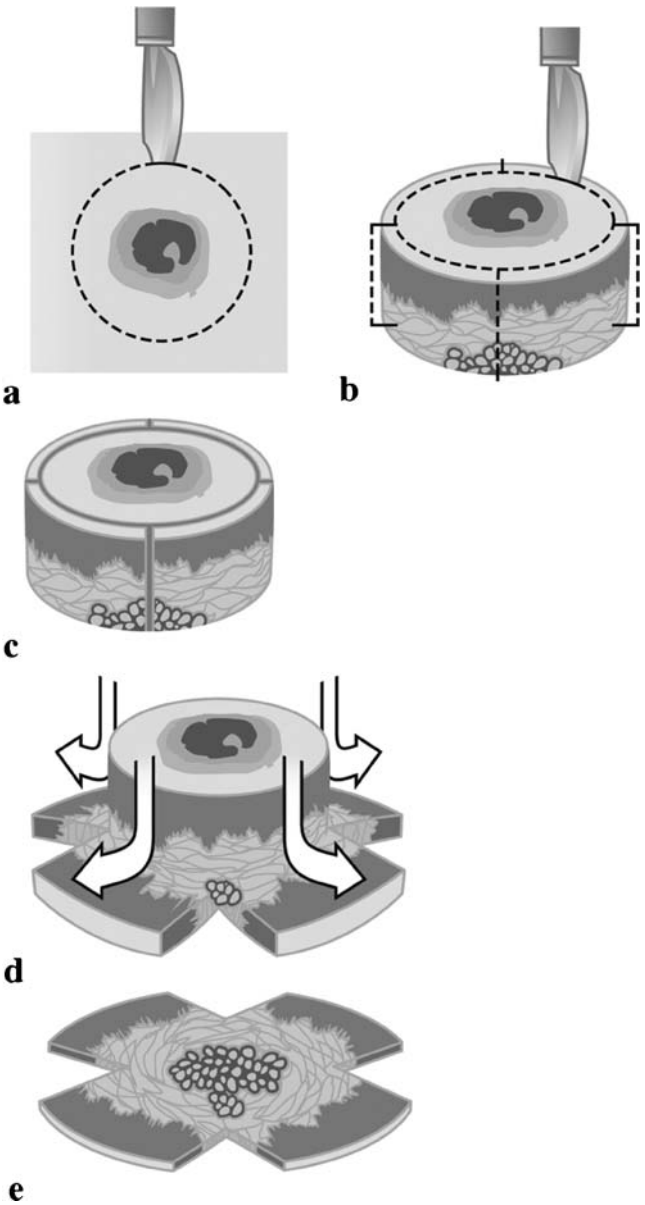

Fig. 6 Excision of extreme, thick, stiff skin for TMA. **a** The tumor is excised with a 90°, or perpendicular, incision. **b** A total or near-total thickness circumferential relaxing incision is made. **c** The lateral margin is rose-petaled. **d** The surgical margin is flattened. **e** The central core of the tissue is resected to facilitate the flattening for histological sectioning

relaxing incisions should be cut through the dermis to form a "subcutaneous hinge" so that the epidermis drops into the same plane as the deep margin. To do so, the various techniques require either scoring of the tissue with or without removal of the central portion of the tissue. The technique chosen may depend on the practitioner's personal preference or may depend on the size and quality of the tissue being cut.

Small and thin fragments of skin can be easily flattened by placing relaxing incisions along the superficial epidermis. Thicker excisions may require scooping of the central tumor from the tissue and/or relaxing incisions. The most basic approach to deep sections is the removal of the center of the lesion by making an incision circumferentially and scooping out the center-most epidermis and dermis. This technique, as well as all other MOHS approaches, requires that the deep margin be left intact. The remaining shell can then be more easily flattened. This approach is illustrated in Fig. 4a–f.

More fibrotic (or larger) fragments of skin may require that the aforementioned scoop approach as well as the peripheral relaxing incisions be made in a radial fashion. This technique called the rose petal technique is demonstrated in Fig. 5a–f.

A third approach works well with thicker, stiffer (such as from the nape of the neck) tissue. This technique requires a full-thickness or near-full-thickness circumferential incision just inside the outer rim of tissue. Additional radial, relaxing incisions are made, as they required to allow the unfolding of the circumferential walls (see Fig. 6a–e). Once this is accomplished, the central core of the lesion can be removed or left intact. If the conventional approach is utilized, the tumor core must be removed to allow for pressure on the flattened walls. Specialized systems such as the Cryocup™ or CryoHist™ may require that the central core be removed.

The data and procedures presented in this paper demonstrate a few techniques that can be utilized in MOHS frozen sections. Like all medical techniques, these frozen section systems require practice before efficiency is achieved. However, once mastered, the refined Cryocup™ and CryoHist™ techniques, coupled with the appropriate tissue preparation, are vastly superior to conventional, free-hand methods of frozen section preparation and analysis.

References

1. Carter D (1996) Evaluation of breast lesions by biopsy, 3rd edn. Interpretation of breast biopsies. Lippincott Williams & Wilkins, USA, pp 57–59
2. Carter VH (1985) A new method for preparing tissue blocks for cryostat sectioning. J Dermatol Surg Oncol 11(7):687–689
3. Dogan MM, Snow SN, Lo J (1991) Rapid skin edge elevation using the OCT compound droplet technique to obtain horizontal microsections in MOHS micrographic surgery. J Dermatol Surg Oncol 17(11):857–860
4. Hanke CW, Lee MW (1989) Cryostat use and tissue processing in MOHS micrographic surgery. J Dermatol Surg Oncol 15(1):29–32
5. Hanke CW, Menn H, O'Brian JJ (1983) Chemosurgical reports: frozen-section processing with the Miami special. J Dermatol Surg Oncol 9(4):260–262
6. Honda NS, Friedman DH (1989) A simple method of tissue embedding for MOHS micrographic surgery. J Dermatol Surg Oncol 15(5):502–504
7. Koehn GG (1992) A new modification for preparing tissue blocks for cryostat sectioning. J Dermatol Surg Oncol 18 (6):485–486
8. Leshin B, Cook SR, Frye DW (1991) Cryomold: a device for tissue embedding in MOHS micrographic surgery. J Dermatol Surg Oncol 17(3):234–236
9. Motley RJ, Holt PJ (1992) A simple device for optimal tissue preparation for MOHS micrographic surgery. Br J Dermatol 126(1): 57–59
10. Weber PJ, Moody BR, Dryden RM, Foster JA (2000) MOHS surgery and processing: novel optimizations and enhancements. Dermatol Surg 26(10):909–914

Virchows Arch (2007) 450:519–527
DOI 10.1007/s00428-007-0396-5

ORIGINAL ARTICLE

Expression of nuclear factor κB in human gastric carcinoma: relationship with IκBa and prognostic significance

Georgia Levidou · Penelope Korkolopoulou · Nikolaos Nikiteas · Nikolaos Tzanakis · Irene Thymara · Angelica A. Saetta · Christos Tsigris · George Rallis · Konstantin Vlasis · Efstratios Patsouris

Received: 13 December 2006 / Revised: 13 February 2007 / Accepted: 1 March 2007 / Published online: 12 April 2007
© Springer-Verlag 2007

Abstract Nuclear factor (NF)-κB is a transcription factor constitutively activated in various neoplasms, including gastric carcinoma. However, its clinical significance in the latter remains an unresolved issue, as published information is limited and controversial. Furthermore, no data is available about the interaction of NFκB with its inhibitory protein IκBa in gastric carcinoma cases. In this study, the expression of NFκB1/p50 and pIκBa protein was evaluated immunohistochemically in paraffin-embedded tissues from 93 patients. The effect of NFκB1/p50 and pIκBa on clinical outcome was assessed. Positive immunostaining was detected for nuclear NFκB1/p50, cytoplasmic NFκB1/p50 and pIκBa in 91, 68 and 85.7% of cases, respectively. A positive correlation emerged between nuclear NFκB1/p50 and pIκBa ($p<0.0001$) and a negative one between cytoplasmic NFκB1/p50 and pIκBa ($p=0.0033$). Nuclear NFκB1/p50 was associated with stage ($p=0.0388$), the depth of invasion ($p=0.0382$), World Health Organization (WHO; $p=0.0326$) and Lauren's histological classification ($p=0.0046$). NFκB1/p50 nuclear expression adversely affected survival in both univariate and multivariate analysis ($p<0.0001$ and $p=0.02$, respectively). Our results suggest that NFκB1/p50 nuclear expression and therefore activation is regulated by its interaction with IκBa and that the former may serve as a useful independent molecular marker for stratifying patients with gastric carcinoma in terms of prognosis.

Keywords NF-κB · IκBa · Gastric carcinoma · Immunohistochemistry

Introduction

Gastric cancer remains one of the most common malignancies worldwide and a major cause of cancer-related death in Asia, having a global burden substantially varying between the developed and the developing countries [26]. Despite the worldwide decline in the incidence rates and the significant advances in diagnosis and treatment, a cure remains elusive for as many as 80% of the patients who will succumb to their disease during the first 5 years [32]. Gaining insight into the underlying molecular mechanisms of initiation and progression of gastric cancer is imperative to identify groups of patients with a particularly poor prognosis. Recent evidence suggests that perturbations in apoptosis and accelerated proliferation constitute the major steps in the development and evolution of gastric cancer [17, 32]. Therefore, contemporary research has been directed towards the identification of genetic alterations of genes interfering with apoptotic process and facilitating cell proliferation [41] to understand the clinical behaviour in individual cases.

Nuclear factor (NF)-κB is a family of dimeric transcription molecules that regulate the expression of immune and inflammatory genes and therefore are involved in cell

G. Levidou, P. Korkolopoulou and N. Nikiteas have equally contributed to this manuscript.

G. Levidou (✉) · P. Korkolopoulou · I. Thymara · A. A. Saetta · E. Patsouris
Department of Pathology, Medical School,
National and Kapodistrian University of Athens,
75 Mikras Asias Street,
Athens 11517, Greece
e-mail: glevidou@yahoo.gr

N. Nikiteas · N. Tzanakis · C. Tsigris · G. Rallis · K. Vlasis
2nd Propedeutic Department of Surgery, Medical School,
National and Kapodistrian University of Athens,
Athens 11517, Greece

apoptosis, differentiation, adhesion and survival [7, 19]. The Rel/NFκB family comprises NFκB1 (p50), NFκB2 (p52) and Rel proteins RelA (p65), RelB and c-Rel [10]. NFκB commonly refers to a p50-RelA heterodimer, which is one of the most avidly forming dimers and the major Rel complex in most cells [7, 10]. NF-κB function is tightly regulated by its interaction with IκB inhibitory proteins through a highly conserved N-terminal homology domain, which apart from the association with IκB proteins is responsible for binding to intronic enhancers of target genes for the induction of gene transcription [10].

IκB gene family contains six mammalian members (IκBa, IκBβ, IκBε, Bcl-3, p100 and p105) characterised by their six to seven repetitive sequences, which are named ankyrin repeats because of their similarity with the human protein ankyrin [28]. The ankyrin domain of these proteins, with the exception of Bcl-3, covers the nuclear localisation signal of NFκB proteins and is responsible for their sequestration in the cytoplasm of normal cells [6, 10, 15]. A variety of stimuli can liberate NFκB from its inhibitor molecule and thus allow its nuclear translocation [11, 18]. The best studied Rel-IκB interaction is that of IκBa with NFκB [7, 11]. The two molecules are known to interact through multiple contacts [5]. The disruption of the cytoplasmic NFκB/IκBa complex entails the phosphorylation of IκBa, which targets IκBa for ubiquitination and proteasomal degradation [18].

Several investigators have reported constitutive activation of NFκB in various human tumour cell lines, including those of lymphoid origin [3, 8, 12] as well as those of ovarian [4], lung [23], breast [24], pancreatic [34, 35], hepatocellular [33], thyroid carcinomas [34] and melanoma [30]. Furthermore, NFκB immunoexpression has been regarded as a marker of poor prognosis in human lung [41], esophageal [16] and tonsillar squamous carcinoma [40] as well as adenoid cystic carcinoma of salivary glands [39]. Recent studies using the anti-RelA/p65 immunostaining indicated that NFκB is constitutively activated in gastric carcinoma [20, 29], whereas others have shown its relationship with *Helicobacter pylori* infection for tumourigenesis [31, 37]. However, these investigations have reported conflicting data concerning the relationship of NFκB protein with patients' survival [20, 29, 38]. This fact prompted us to undertake this study focusing on the expression of the least investigated p50 subunit of the NFκB heterodimer. In addition, as little information is available about the role of IκBa phosphorylation in relation to NFκB activation in gastric adenocarcinomas, the present study also aimed to clarify the role of NFκB1/p50 in prognosis, to determine its association with a phosphorylated member of IκB family-pIκBa, as well as to define the impact of this interaction in tumour evolution and clinical behaviour in gastric carcinomas.

Materials and methods

Patients

Ninety-three patients with histologically diagnosed gastric carcinomas, for whom archival tumour material was available from gastrectomy specimens (partial 49, total 44), were enrolled in the present investigation. Informed consent was obtained from all patients before this study was undertaken. None of the patients had received chemotherapy or radiation before surgery. The mean age of patients was 65.48±11.90 ranging from 29 to 89 years, whereas the male to female ratio was 53:40. According to the pTNM classification, 17 cases were in stage I, 11 in stage II, 38 in stage III and 25 in stage IV. All cases were reviewed and assigned a histologic grade according to the latest World Health Organization (WHO) classification [13] of gastric carcinomas: There were 5 grade 1, 22 grade 2 and 66 grade 3 carcinomas. Histologic type was determined according to Lauren's (47 intestinal/46 diffuse) and WHO classification (4 papillary/43 tubular/3 mucinous/43 signet ring) [13]. Follow-up period ranged from 3 to 101 months (median, 20 months). During this period, 66 disease-specific deaths were recorded. The clinicopathological characteristics of our patients are shown in Table 1.

Immunohistochemical staining

Four micrometers serial sections were cut from each specimen on Superfrost plus glass slides and left to dry overnight at 37°C. After deparaffinisation, immunostaining was performed by using rabbit polyclonal anti-NFκB p50 antibody (sc-114, Santa Cruz Biotechnology) and mouse monoclonal anti-pIκBa antibody (sc-8404, Santa Cruz Biotechnology). The latter recognises Ser 32 phosphorylated pIκBa at Ser 32. The NFκB p50 antibody was diluted 1:40 and the IκB antibody 1:50. Both antibodies were incubated overnight at 37°C. For p50 and pIκBa detection, antigen retrieval with microwaving for 15 min at 750 W in citrate buffer, pH 6.0 was required. The two-step peroxidase technique was used with a peroxidase-conjugated polymer (DAKO Envision kit, DAKO, Carpinteria, CA, USA). Known positive controls (i.e. breast carcinoma cells) as well as negative controls (sections in which p50 and pIκBa antibodies were substituted by non-specific rabbit and mouse serum, respectively) were also stained in each run. In addition, the specificity of staining was tested in gastric carcinomas sections in which NFκB and pIκBa primary antibodies were pre-absorbed with an equal amount of the corresponding peptides (sc-114P and sc-8404P, respectively, Santa Cruz Biotechnology) and incubated.

Light microscopic evaluation of immunostained slides was performed independently by two pathologists without knowledge of the clinical information. If a discrepancy

Table 1 Relationship between nuclear NFκB1/p50 expression and clinicopathological parameters in 93 patients with gastric carcinoma

	NFkB nuclear expression			
	Number of patients	Median	Range	*p* value
Lauren classification				
Intestinal	47	5	0–80	0.0046
Diffuse	46	25	9–90	
WHO classification				
Papillary	4	10	5–30	0.0326
Tubular	43	5	0–80	
Mucinous	3	5	0–10	
Signet-ring	43	30	0–90	
Grade				
1	5	20	0–80	0.2820
2	22	5	0–60	
3	66	15	0–90	
Stage				
I	17	5	0–40	0.0388
II,III,IV	74	15	0–90	
Tumour location				
Upper	13	10	0–90	0.0693
Middle	32	20	2–80	
Lower	48	7.5	0–80	
Tumour T status				
T1	24	5	0–80	
T2/T3/T4	69	15	0–90	0.0382
Lymph node metastases				
No	21	5	0–60	
Yes	70	12.5	0–90	0.2618
Distant metastases				
No	73	10	0–90	
Yes	18	20	0–80	0.3761
Borrman's classification				
Polypoid protrusion	9	20	0–80	
Circumscribed excavation	3	5	5–20	0.0130
Induration with ulceration	67	10	0–90	
Diffuse thickening	5	50	5–80	

occurred between the two assessments, the slides were reassessed jointly without information of the previous scores. In each case, 1,000–1,500 neoplastic cells throughout the section were counted at high-power magnification. Nuclear and cytoplasmic NFκB1/p50 expression was evaluated separately. Nuclear NFκB1/p50 labelling index (LI) was defined as the percentage of neoplastic cells with nuclear immunoreactivity out of the total number of neoplastic cells counted. Cytoplasmic NFκB1/p50 and pIκBa expression were categorised in four levels according to the percentage of neoplastic cells with cytoplasmic staining as follows: absent (0, no positive cell cytoplasm), low (1, in staining 1–20% neoplastic cells with cytoplasmic staining), moderate (2, 21–50% of neoplastic cells with cytoplasmic staining) and extensive (3, more than 50% of neoplastic cells with cytoplasmic staining) immunostaining.

Statistical methods

In the basic statistical analysis, NFκB1/p50 nuclear expression was treated as continuous variable, whereas pIκBa and cytoplasmic NFκB1/p50 expression as ordinal. Correlation between pIκBa and nuclear NFκB1/p50 expression was tested with Kruskal–Wallis analysis of variance (ANOVA) along with Kendall's rank correlation coefficient. The respective association between cytoplasmic NFκB1/p50 and pIκBa expression was tested with Fisher's exact test. Associations of NFκB1/p50 nuclear expression with other clinicopathological parameters, such as grade, stage, tumour location, WHO and Lauren histological classification were tested with Kruskal–Wallis ANOVA and Mann–Whitney *U* test, whereas the corresponding associations of pIκBa and cytoplasmic NFκB1/p50 expression were tested with Fisher's exact test.

The survival analysis was performed using death of disease as end-point. The effect of various parameters (age, sex, tumour location, stage, grade and NFκB1/p50 nuclear and cytoplasmic expression and pIκBa) on clinical outcome was assessed by plotting survival curves according to the Kaplan–Meier method and comparing groups using the log-rank test, as well as by using multivariate analysis (Cox's model). In survival analysis NFκB1/p50 nuclear expression was categorised on the basis of the median value (10%). Statistical calculations were performed using the statistical package Stata 9.0/SE for Windows. All results with a two-sided p level ≤ 0.05 were considered significant.

Results

Expression of NFκB1/p50 and pIκBa in gastric carcinomas

The immunostaining pattern for NFκB1/p50 was nuclear and cytoplasmic, whereas pIκBa displayed a predominantly cytoplasmic staining pattern. Both staining patterns for NFκB1/p50 were abolished in sections were the primary antibody was pre-absorbed with its corresponding peptide, as well as in negative control sections. Nuclear immunoreactivity for NFκB1/p50 was detected in 91% (85/93) of cases, whereas cytoplasmic immunoreactivity was detected in 67.7% of cases (63/93). In 58 cases (62%), concurrent cytoplasmic and nuclear positivity was recorded. pIκBa expression was found in 85.7% (78/91) of cases and was predominantly cytoplasmic. In 83.3% (66/78), positive cases with some scattered positive nuclei were also seen. Seventy-seven cases displayed both pIκBa and nuclear NFκB1/p50 immunoexpression (chi-square, $p=0.002$). Normal gastric mucosa displayed a scattered nuclear NFκB1/p50 expression mainly observed in the regenerative zone of gastric glands, whereas normal gastric mucosa was

negative for pIκBa with some scattered positive cells, mainly located in the neck region of gastric glands.

Nuclear expression of NFκB1/p50 increased with increasing levels of pIκBa expression (Kruskal–Wallis ANOVA, p=0.0001; Fig. 1). This positive correlation was confirmed with the calculation of Kendall's rank correlation coefficient (tau-b=0.6740, p<0.0001). Importantly, NFκB1/p50 cytoplasmic expression decreased with increasing levels of pIκBa expression (Fisher's exact test, p<0.0001), reflecting the significant negative correlation between cytoplasmic NFκB1/p50 and pIκBa immunoreactivity (tau-b=−0.2726, p=0.0033).

Associations between NFκB1/p50 or IκBa and clinicopathological features

The NFκB1/p50 nuclear LI was related to Lauren's and WHO histological classification (p=0.0046 and p=0.0326, respectively; Figs. 2a and 3a,b), stage (I vs II/III/IV, p=0.0388; Fig. 2b), tumour T category (p=0.0382) and Borrmann's macroscopic classification (p=0.0141) but was unrelated to tumour grade and the presence of lymph node or distant metastasis (p>0.10). Thus, diffuse or signet-ring type histology, Borrmann's type macroscopic type IV and advanced (II or higher) stage or T category (advanced vs early gastric carcinoma) tended to display higher NFκB1/p50 nuclear immunoreactivity levels. A marginal association also emerged between tumour location and NFκB1/p50 nuclear expression levels (p=0.0693), suggesting higher expression in tumours located in the stomach body. On the contrary, the NFκB1/p50 cytoplasmic expression was significantly higher in intestinal (p<0.0001), as well as in papillary and tubular carcinomas (p<0.0001, Table 2, Fig. 3). Accordingly, cytoplasmic NFκB1/p50 reactivity marginally decreased with increasing tumour grade (p=0.055; Table 2). The expression of pIκBa was not associated with any of the studied clinicopathological parameters (p>0.10; Table 2).

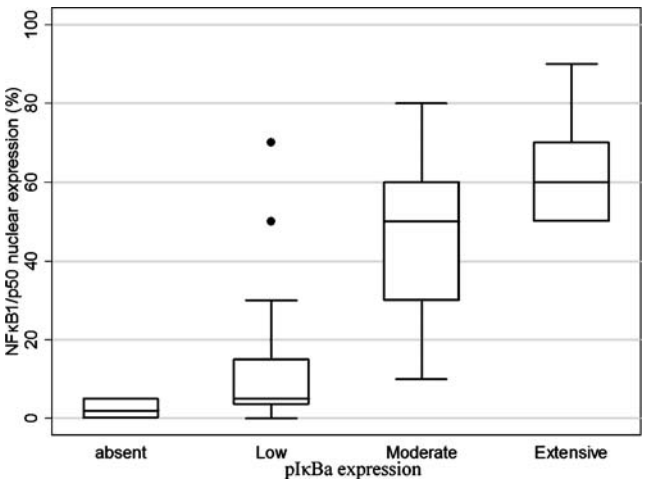

Fig. 1 Schematic representation of the association of NFκB1/p50 nuclear expression with pIκBa expression. NFκB1/p50 increases parallel with pIκBa

Survival analysis

In univariate analysis, higher NFκB1/p50 nuclear expression levels (HR=2.64, 95% CI of 1.53 to 4.55, p<0.0001, Fig. 4a), increased pIκBa expression (0/1/2/3; HR=1.56, 95% CI of 1.16 to 2.10, p=0.003, Fig. 4b), the presence of residual tumour after primary surgery (no residual vs macroscopic/microscopic residual; HR=3.19, 95% CI of 1.78 to 5.72, p<0.0001), advanced tumour stage (2/3/4 vs 1; HR=13.77, 95% CI of 3.34 to 56.78, p<0.0001), advanced T category (T2/T3/T4 vs T1; HR=7.05, 95% CI of 2.79 to 17.79, p<0.0001), the presence of lymph node metastasis (0 vs 1; HR=14.17, 95% CI of 3.44 to 58.43, p<0.0001) and the presence of distant metastasis (0 vs 1; HR=5.30, 95% CI of 2.79 to 10.08, p<0.001) were associated with worse prognosis. The median survival time for patients whose tumours over-expressed NFκB1/p50 was 12 months compared with 40 months for those who did not. The corresponding value for patients whose tumours did not express pIκBa was 40 months compared with 9 months for those who displayed extensive pIκBa expression.

In multivariate analysis, higher NFκB1/p50 nuclear expression, advanced tumour stage and the presence of residual tumour maintained their statistical significance and turned out to be independent prognostic factors (Table 3A). In addition, multivariate survival analysis showed that not only NFκB1/p50 nuclear expression was a significant prognostic factor but also that its role is independent of detailed traditional parameters including tumour invasiveness, lymph node and distant metastasis (Table 3B).

Discussion

A wide spectrum of molecular markers, especially those involved in the regulation of cell apoptosis, has been tested as potentially useful parameters to predict clinical outcome in gastric cancer [32, 42]. These include interleukin 1β, interleukin 8, tumour necrosis factor alpha [21] and COX-2 [22]. Although changes in expression levels of several cell apoptosis regulatory proteins are frequently reported, their suggested role in the pathogenesis and progression of gastric carcinomas remains controversial. The results of such studies may be confounded by several factors, including small patient sample size and the variable therapeutic protocols that may potentially affect patient outcome.

In a recent study, the expression of NFκB in human gastric adenocarcinoma tissues was assessed by immunohistochemistry using an anti-p65 (RelA) antibody. The immunostaining

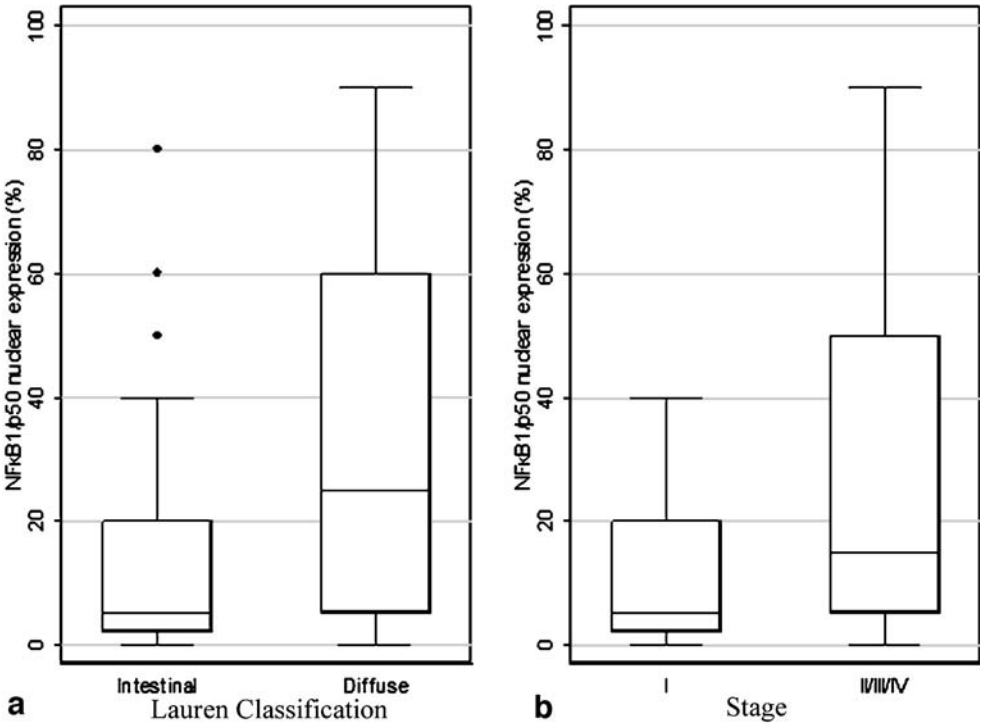

Fig. 2 Schematic representation of the association of NFκB1/p50 expression with **a** Lauren histological classification and **b** tumour stage. NFκB1/p50 is higher in diffuse type gastric adenocarcinomas (Mann–?Whitney *U* test, $p=0.0046$) and increases with increasing stage (Mann–Whitney *U* test, $p=0.0388$)

pattern was nuclear with or without cytoplasmic staining and was found to be associated with a better disease outcome [20]. In two other studies using the same antibody, researchers yielded a completely opposite result, namely, that NFκB/p65 overexpression was inversely linked with tumour grade and patients' prognosis [29, 38]. In the present study, we used for the first time an anti-p50 antibody, and we found that immunoreactivity was either nuclear and/or cytoplasmic, in alignment with the staining pattern of p65 [20, 29, 38]. Nuclear immunoreactivity is considered a surrogate marker of NFκB activation, whereas cytoplasmic immunolocalisation is thought to correspond to the inactive form of NFκB [2]. As expected, in the non-neoplastic mucosa, nuclear NFκB1/p50 expression was mainly observed in the proliferative zone of normal gastric glands, strengthening the initial idea that this is the activated form of NFκB protein and advocating that this activation parallels cell proliferation [20, 29, 38]. Accordingly, normal gastric mucosa is negative for pIκBa except for some scattered positive cells, mainly located in the neck region of gastric glands. Diffuse type gastric carcinoma displayed a predominantly nuclear NFκB immunoreactivity as compared to that of intestinal type carcinomas. Cytoplasmic NFκB1/p50 expression prevailed in intestinal type adenocarcinomas, in agreement with previous studies [20], probably illustrating the distinct molecular pathways underlying the tumourigenesis of these two histologic types.

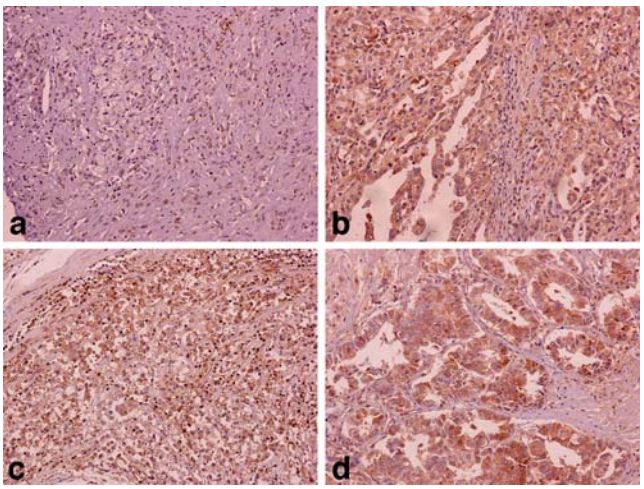

Fig. 3 **a**, **b**. Immunohistochemical expression of NFκB1/p50 in diffuse (**a**) and intestinal type gastric adenocarcinomas (**b**) (magnification ×40). Nuclear NFκB1/p50 expression prevails in diffuse-type carcinomas in contrast to diffuse-type carcinomas that display a predominantly cytoplasmic immunoreactivity. **c**, **d** Extensive and moderate immunohistochemical expression of pIκBa in diffuse (**c**) and intestinal (**d**) type gastric adenocarcinomas. The tumour cells also display some nuclear positivity (magnification ×40)

This appears to be the first report describing the expression of pIκBa in gastric cancer and the first attempt to link NFκB and IκBa in this neoplasm. pIκBa staining in tumour cells was predominantly cytoplasmic with some nuclear localisation in most cases. The staining pattern of activated IκBa is compatible with this molecule's function. IκBa activation depends on phosphorylation of two conserved serines (S32 and S36) in the N-terminal regulatory domain by a serine specific kinase [18]. This phosphorylation targets IκBa for ubiquitination and degradation by the proteasome 26S with consequent liberation of

Table 2 Associations of cytoplasmic NFκB1/p50 and pIκBa expression with clinicopathological parameters in 93 patients with gastric carcinoma (results of Fisher's exact test)

	Cytoplasmic NFκB1/p50				pIκBa				
	Absent/low	Medium	Excessive	*p* value	Absent	Low	Medium	Excessive	*p* value
Lauren									
Diffuse	27	15	4	<0.0001	9	27	6	4	>0.10
Intestinal	3	20	24		4	21	11	9	
WHO									
Papillary	0	2	2	<0.0001	1	2	1	0	>0.10
Tubular	4	17	22		8	25	5	4	
Mucinous	1	2	0		1	2	0	0	
Signet-ring	25	14	4		3	19	11	9	
Grade									
1	1	1	3	0.077	0	3	1	1	>0.10
2	3	9	10		6	8	6	1	
3	26	25	15		7	37	10	11	
Stage									
I	5	5	7	>0.10	2	12	3	0	>0.10
II	1	7	3		2	5	1	3	
III	14	16	8		6	15	10	5	
IV	9	7	9		3	15	3	4	
T category									
T1	6	10	8	>0.10	3	16	3	2	>0.10
T2/T3/T4	24	25	20		10	32	14	11	
Lymph node metastasis									
No	4	9	8		3	12	4	2	>0.10
Yes	25	26	19	>0.10	10	35	13	10	
Distant metastasis									
No	22	30	21		11	36	14	10	>0.10
Yes	7	5	6		2	11	3	2	
Borrmann's classification									
Polypoid protrusion	2	4	3	>0.10	4	3	1	1	>0.10
Circumscribed excavation	0	1	2		0	3	0	0	
Induration with ulceration	22	26	19		8	35	13	9	
Diffuse thickening	4	1	2		0	3	3	1	

NFκB from the NFκB/IκBa complex and its translocation into the nucleus. Activated IκBa is essentially detected in the cell cytoplasm [9, 33] before being degraded by its proteasome. A small percentage of pIκBa may also enter the cell nucleus [33] being responsible for the positive nuclear signal recorded in our cases, although the biological significance of this nuclear pIκBa is not clear.

The expression of NFκB1/p50, either nuclear or cytoplasmic, was correlated with the expression of activated IκBa, attesting at the tissue level to the intimate liaison between these two molecules. The inverse relationship between cytoplasmic NFκB1/p50 and pIκBa expression may be largely attributed to the fact that NFκB dimeric protein is sequestered in the cytoplasm of most cells though interaction with non-phosphorylated inhibitory proteins that preclude NFκB from entering the nucleus. On the contrary, the positive correlation of NFκB1/p50 nuclear expression with pIκBa, obviously reflect the necessity of IκBa activation via phoshorylation for the liberation of NFκB and its translocation into the cell nucleus.

In our study, NFκB/p50 nuclear expression was positively associated with the depth of infiltration confirming the findings of Sasaki et al. [29]. Relevant to this finding is the notion that the accumulation of the active form of NFκB stimulates cell proliferation and thereby combined with tumour aggressiveness. Furthermore, in accordance with previous studies [29, 36], our investigation revealed a significant positive correlation between nuclear NFκB1/p50 staining and clinical stage, lending further support to the observed association of NFκB activation with tumour's invasive potential. In agreement with Yamanaka et al. [38], we failed to elicit a significant relationship between NFκB activation and lymph node metastasis, possibly because the metastatic process depends on more complex interactions of various molecules.

An important finding emerging from our investigation is that nuclear NFκB1/p50 overexpression by tumour cells

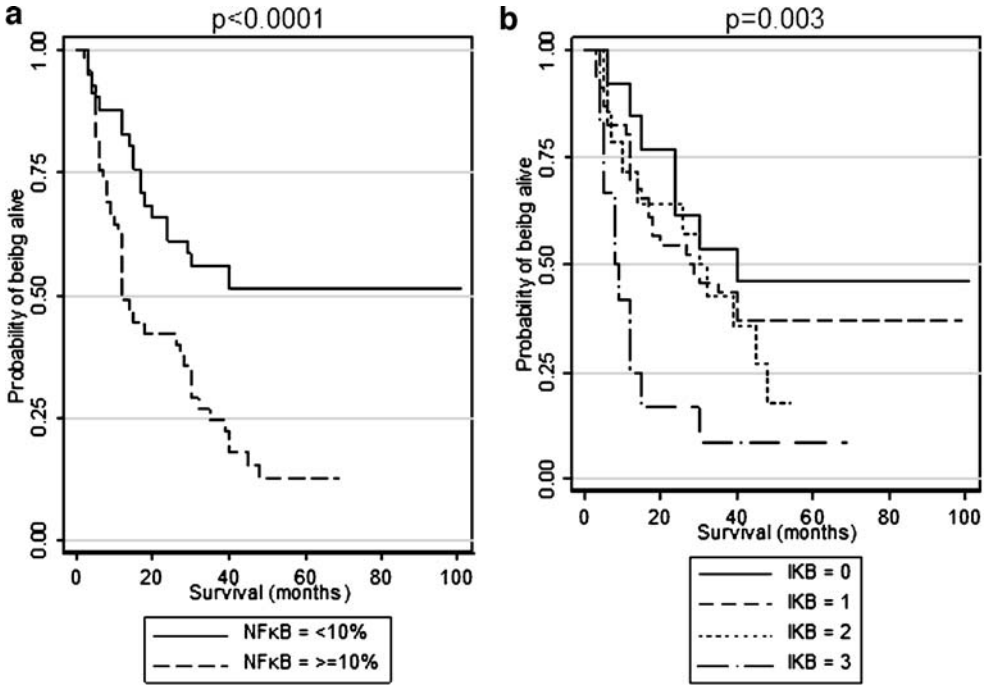

Fig. 4 Kaplan Meier survival curves according to **a** NFκB1/p50 expression and **b** pIκBa expression in 93 patients with gastric carcinoma

connotes a poor survival probability and that in combination with tumour stage and the presence of residual tumour after surgery, remains a prognostic factor in multivariate analysis. pIκBa expression does not seem to be informative in this regard. A plausible explanation for this finding is that the relationship between pIκBa and survival that was elicited in univariate survival analysis largely resides in its relationship with nuclear IFκB1/p50, the latter molecule thus acting as a confounding factor. In addition, cytoplasmic NFκB1/p50 expression did not seem to convey any important prognostic information. A caveat of the previous studies dealing with the prognostic utility of NFκB in gastric cancer is that a clear distinction between nuclear and cytoplasmic expression was not made. For example, Sasaki et al. [29] separated cases with only nuclear staining from those in which nuclear staining was accompanied by cytoplasmic staining. Yamanaka et al. [38] dichotomised NFκB staining according to the presence or absence of nuclear positivity, without taking into consideration that even normal gastric mucosa displays some scattered positive nuclei. Furthermore, Lee et al. [20], although they had a large cohort of patients with gastric adenocarcinoma, in survival analysis compared tumours with nuclear staining regardless of cytoplasmic staining with those displaying only cytoplasmic staining, without any quantification of either the nuclear or the cytoplasmic positivity. On the basis of our findings, one may speculate that the absence of clear-cut criteria in the evaluation of NFκB immunoexpression might be the major reason accounting for the conflicting previously published data regarding the prognostic impact of this molecule in gastric cancer.

The results of multivariate survival analysis recapitulate many of the traditional parameters that have been proposed as important determinants of clinical outcome in gastric cancer, namely, the depth of infiltration and the presence of lymph node or distant metastasis [20], supporting the

Table 3 Multivariate Cox survival analysis addressing the association between NKκB/p50 and pIκBa expression and survival time after tumour removal

Predictor variable	Multivariate (HR and 95% CI)
A	
NFκB nuclear expression (>=10% vs <10%)	2.40 (1.06–3.93); p=0.020
pIκBa expression (0 vs 1 vs 2 vs 3)	0.98 (1.14–5.03); p=0.997
Stage (I vs II/III/IV)	10.76 (2.58–44.91); p=0.001
Presence of residual tumour (0:no 1:yes)	2.22 (1.21–4.07); p=0.010
B	
NFκB nuclear expression (>=10% vs <10%)	2.11 (1.01–4.39); p=0.046
pIκBa expression (0 vs 1 vs 2 vs 3)	1.03 (0.69–1.55); p=0.852
Tumour invasiveness (T1 vs T2/T3/T4)	4.49 (1.70–11.86); p=0.002
Lymph node metastasis (0:no 1:yes)	5.20 (1.59–34.21); p=0.029
Distant metastasis (0:no 1:yes)	3.50 (1.18–22.86); p<0.001
Presence of residual tumour	1.97 (1.04–3.73); p=0.035

validity of statistical analysis and denoting that our cohort, although with a relatively short follow-up, is representative. Of these parameters, lymph node metastasis followed by distant metastasis seemed to be among the more important risk factors for predicting overall survival in gastric carcinoma patients. However, there was no significant correlation between lymph node or distant metastasis and NFκB1/p50 activation, further indicating the independence of NFκB1/p50 for predicting patient's outcome from lymph node metastasis. It could be argued that the prognostic significance assigned to nuclear NFκB1/p50 over expression may partly reflect its relationship with the depth of tumour invasion. The fact, however, that both parameters remained in multivariate analysis denotes that there should be additional reasons accounting for this finding. An alternative candidate could be the inhibition of apoptotic response caused by NFκB activation. In this context, inhibition of NFκB restores apoptosis sensitising tumour cells to cytotoxic drug-induced cell death, whereas activation of NFκB enhances chemoresistance and radioresistance [1, 18]. Furthermore, NFκB induces the expression of various molecules promoting cell proliferation and cell cycle progression such as c-myc and cyclin D1 [7, 27]. However, high level expression of NFκB in cell culture systems and transgenic epithelial tissue have been reported to cause a G1/S arrest of the cell cycle [27].

In conclusion, we demonstrated that NFκB1/p50 nuclear expression is positively related to pIκβa expression in tumour cells reinforcing the concept that NFκB1/p50 activation is largely dictated by its interaction with IκBa. Additionally, NFκB1/p50 nuclear expression parallels tumour stage and depth of invasion, a result that suggests its contribution to the acquisition of an aggressive phenotype. Finally, although both NFκB1/p50 nuclear over-expression and pIκBa implied a poor prognosis in univariate analysis, only NFκB1/p50 retained its significance in multivariate analysis, along with stage and the presence of residual tumour. Thus, NFκB1/p50 expression could be included in the armamentarium of molecular markers in gastric carcinoma to refine the prognostic information gained by standard parameters. More importantly, our results encourage further investigations into the use of NFκB inhibitors as an adjunct to the currently available treatment option in gastric cancer, as proposed in other tumour cells [14, 25]. Analysis of the potential role of such molecules in human gastric cancer cell lines are needed to extend our observations and to provide more insight into their function in gastric cancer.

References

1. Abdel-Latif MM, O'Riodan J, Windle HJ, Carton E, Ravi N, Kelleher D, Reynolds JV (2004) NF-κB activation in esophageal adenocarcinoma. Relationship to Barrett's metaplasia, survival, and response to neoadjuvant chemoradiotherapy. Ann Surg 239:491–499
2. Baldwin AS (1996) The NF-κB and IκB proteins: new discoveries and insights. Annu Rev Immunol 14:649–683
3. Bargou RC, Leng C, Krappmann D, Emmerich F, Mapara MY, Bommert K, Royer HD, Scheidereit C, Dorken B (1996) High-level nuclear NF-κB and Oct-2 is a common feature of cultured Hodgkin/Reed-Sternberg cells. Blood 87:4340–4347
4. Bours V, Dejardin E, Goujon-Letawe F, Merville MP, Castronovo V (1994) The NF-κB transcription factor and cancer: high expression of NF-κB and IκB-related proteins in tumour cell lines. Biochem Pharmacol 47:145–149
5. Chen FE, Ghosh G (1999) Regulation of DNA binding by Rel/NFκB transcription factors: structural reviews. Oncogene 18:6845–6852
6. Dejardin E, Deregowski V, Chapelier M, Jacobs N, Gielen J, Merville MP, Bours V (1999) Regulation of NF kappa B activity by I kappaB-related proteins in adenocarcinoma cells. Oncogene 18:2567–2577
7. Dolcet X, Llobet D, Pallares J, Matias-Guiu X (2005) NF-kappaB in development and progression of human cancer. Virchows Arch 5:475–482
8. Feinman R, Koury J, Thames M, Barlogie B, Epstein J, Siegel DS (1999) Role of NF-kappaB in the rescue of multiple myeloma cells from glucocorticoid-induced apoptosis by bcl-2. Blood 93:3044–3052
9. Ghiorzo P, Mantelli M, Gargiulo S, Gramigni C, Pastorino L, Banelli B, Villaggio B, Coccia MC, Sementa AR, Garre C, Bianchi-Scarra G (2004) Inverse correlation between p16INK4A expression and NF-κB activation in melanoma progression. Hum Path 35:1029–1037
10. Ghosh S, May M, Kopp EB (1998) NFκB and Rel proteins: evolutionary conserved mediators of immune responses. Annu Rev Immunol 16:225–260
11. Gilmore TD (1999) The Rel/NFκB signal transduction pathway: introduction. Oncogene 18:6842–6844
12. Giri DK, Aggarwal BB (1998) Constitutive activation of NF-B causes resistance to apoptosis in human cutaneous T cell lymphoma HuT-78 cells. Autocrine role of tumour necrosis factor and reactive oxygen intermediates. J Biol Chem 273:14008–14014
13. Hamilton SR, Aaltonen LA (2000) World Health Organization classification of tumours-pathology and genetics of the digestive system, pp 38, 43–46
14. Horiguchi Y, Kuroda K, Nakashima J, Murai M, Umezawa K (2003) Antitumour effect of a novel nuclear factor-kappa B activation inhibitor in bladder cancer cells. Expert Rev Anticancer Ther 6:793–798
15. Ito CY, Adey N, Bautch VL, Baldwin AS Jr (1995) Structure and elocution of the human IκBA gene. Genomics 29:490–495
16. Izzo JG, Malhotra U, Wu TT, Ensor J, Luthra R, Lee JH, Swisher SG, Liao Z, Chao KS, Hittelman WN, Aggarwal BB, Ajani JA (2006) Association of activated transcription factor nuclear factor kappab with chemoradiation resistance and poor outcome in esophageal carcinoma. J Clin Oncol 5:748–754
17. Jackel MC (1998) Genetic control of programmed cell death (apoptosis). Prospects for biological tumour staging? HNO 46:614–625
18. Karin M (1999) How NFκB is activated: the role of IκB kinase (IKK) complex. Oncogene 18:6867–6874
19. Karin M, Cao Y, Greten FR, Li AW (2002) NFκB in cancer: from innocent bystander to major culprit. Nat Rev Cancer 2:301–310
20. Lee BL, Lee HS, Jung J, Cho SJ, Chung HY, Kim WH, Jin YW, Kim CS, Nam SY (2005) Nuclear factor-kappaB activation correlates with better prognosis and Akt activation in human gastric cancer. Clin Cancer Res 7:2518–2525
21. Macri A, Versaci A, Loddo S, Scuderi G, Travagliante M, Trimarchi G, Teti D, Famulari C (2006) Serum levels of

interleukin 1beta, interleukin 8 and tumour necrosis factor alpha as markers of gastric cancer. Biomarkers 2:184–193
22. Mrena J, Wiksten JP, Nordling S, Kokkola A, Ristimaki A, Haglund C (2006) MMP-2 but not MMP-9 associated with COX-2 and survival in gastric cancer. J Clin Pathol 59(6):618–623
23. Mukhopadhyay T, Roth JA, Maxwell SA (1995) Altered expression of the p50 subunit of the NF-kappaB transcription factor complex in non-small cell lung carcinoma. Oncogene 11:999–1003
24. Nakshatri H, Bhat-Nakshatri P, Martin DA, Goulet RJ, Sledge GW (1997) Constitutive activation of NF-kappaB during progression of breast cancer to hormone-independent growth. Mol Cell Biol 17:3629–3639
25. Orlowski JR, Baldwin AS (2002) NFκB as a therapeutic target in cancer. Trends Mol Med 8:385–389
26. Parkin DM (2001) Global cancer statistics in the year 2000. Lancet Oncol 2:533–543
27. Rayet B, Gelinas C (1999) Aberrant rel/nfkb genes and activity in human cancer. Oncogene 18:6938–6947
28. Ross JS, Kallakury BV, Sheehan CE, Fisher HA, Kaufman RP Jr, Kaur P, Gray K, Stringer B (2004) Expression of nuclear factor-κB and IκB proteins in prostatic adenocarcinomas: correlation of nuclear factor-κB immunoreactivity with disease recurrence. Clin Cancer Res 10:2466–2472
29. Sasaki N, Morisaki T, Hashizume K, Yao T, Tsuneyoshi M, Noshiro H, Nakamura K, Yamanaka T, Uchinaya A, Tabaka M, Katano M (2001) Nuclear factor-κB (RelA) trascription factor is constitutively activated in human gastric carcinoma tissue. Clin Cancer Res 7:4136–4142
30. Shattuck-Brandt RL, Richmond A (1997) Enhanced degradation of IκB contributes to endogenous activation of NF-B in Hs294T melanoma cells. Cancer Res 57:3032–3039
31. Shibata W, Hirata Y, Yoshida H, Otsuka M, Hoshida Y, Ogura K, Maeda S, Ohmae T, Yanai A, Mitsuno Y, Seki N, Kawabe T, Omata M (2005) NF-kappaB and ERK-signaling pathways contribute to the gene expression induced by cag PAI-positive-Helicobacter pylori infection. World J Gastroenterol 39:6134–6143
32. Smith MG, Hold GL, Tahara E, El-Omar EM (2006) Cellular and molecular aspects of gastric cancer. World J Gastroenterol 12 (19):2979–2990
33. Tai DI, Tsai SL, Chang YH, Huang SN, Chen TC, Chang KS, Liaw YF (2000) Constitutive activation of nuclear factor kappaB in hepatocellular carcinoma. Cancer 89(11):2274–2281
34. Visconti R, Cerutti J, Battista S, Fedele M, Trapasso F, Zeki K, Miano MP, Nigris F, Casalino L, Curcio F, Santoro M, Fusco A (1997) Expression of the neoplastic phenotype by human thyroid carcinoma cell lines requires NF-κB p65 protein expression. Oncogene 15:1987–1994
35. Wang W, Abbruzzese JL, Evans DB, Larry L, Cleary KR, Chiao PJ (1999) The nuclear factor-κB/RelA transcription factor is constitutively activated in human pancreatic adenocarcinoma cells. Clin Cancer Res 5:119–127
36. Wang W, Luo HS, Yu BP (2004) Expression of NFκB and human telomerase reverse transcriptase in gastric cancer and precancerous lesions. World J Gastroenterol 2:177–181
37. Wu CY, Wang CJ, Tseng CC, Chen HP, Wu MS, Lin JT, Inoue H, Chen GH (2005) Helicobacter pylori promote gastric cancer cells invasion through a NF-kappaB and COX-2-mediated pathway. World J Gastroenterol 21:3197–3203
38. Yamanaka N, Sasaki N, Tasaki A, Nakashima H, Kubo M, Morisaki T, Noshiro H, Yao T, Tsuneyoshi M, Tanaka M, Katano M (2004) Nuclear factor-kappaB p65 is a prognostic indicator in gastric carcinoma. Anticancer Res 24:1071–1075
39. Zhang J, Peng B, Chen X (2005) Expressions of nuclear factor kappaB, inducible nitric oxide synthase, and vascular endothelial growth factor in adenoid cystic carcinoma of salivary glands: correlations with the angiogenesis and clinical outcome. Clin Cancer Res 20:7334–7343
40. Zhang PL, Pellitteri PK, Law A, Gilroy PA, Wood GC, Kennedy TL, Blasick TM, Lun M, Schuerch C 3rd, Brown RE (2005) Overexpression of phosphorylated nuclear factor-kappa B in tonsillar squamous cell carcinoma and high-grade dysplasia is associated with poor prognosis. Mod Pathol 7:924–932
41. Zhang Z, Ma J, Li N, Sun N, Wang C (2006) Expression of nuclear factor-kappaB and its clinical significance in non small-cell lung cancer. Ann Thorac Surg 1:243–248
42. Zhao XH, Gu SZ, Tian HG, Quan P, Pan BR (2005) Clinical significance of expression of apoptotic signal proteins in gastric carcinoma tissue. World J Gastroenterol 25:3846–3849

Virchows Arch (2007) 450:529–537
DOI 10.1007/s00428-007-0398-3

ORIGINAL ARTICLE

CpG island methylation, response to combination chemotherapy, and patient survival in advanced microsatellite stable colorectal carcinoma

Shuji Ogino · Jeffrey A. Meyerhardt · Takako Kawasaki · Jeffrey W. Clark · David P. Ryan · Matthew H. Kulke · Peter C. Enzinger · Brian M. Wolpin · Massimo Loda · Charles S. Fuchs

Received: 14 December 2006 / Revised: 30 January 2007 / Accepted: 2 March 2007 / Published online: 20 March 2007
© Springer-Verlag 2007

Abstract The CpG island methylator phenotype (CIMP) is a distinct epigenetic phenotype in colorectal carcinoma with concordant methylation in multiple promoter CpG islands. The relationship between CpG island methylation and clinical outcomes among colorectal cancer patients treated with chemotherapy has been a controversial subject. Utilizing real-time polymerase chain reaction (PCR; MethyLight technology), we quantified DNA methylation in 13 CpG island loci (*CACNA1G*, *CDKN2A*, *CRABP1*, *IGF2*, *MLH1*, *NEUROG1*, *RUNX3*, *SOCS1*, *MINT1*, *MINT31*, *IGFBP3*, *MGMT*, and *WRN*) in 30 metastatic microsatellite stable colorectal carcinomas in phase I/II clinical trials of combination chemotherapy (5-fluorouracil, irinotecan, leucovorin, and gefitinib). Tumor response was assessed by CT scans performed at baseline and every 6 weeks thereafter. Overall CIMP-high status (either ≥9/13 or ≥7/13 methylated markers; identifying 3 or 5 CIMP-high tumors, respectively) and methylation in *CACNA1G*, *IGF2*, *MLH1*, *NEUROG1*, *RUNX3*, *MINT31*, and *WRN* were associated with worse survival (all $p<0.01$). Although not statistically significant, there was a trend toward resistance to chemotherapy among tumors with CpG island methylation. In conclusion, CpG island methylation may predict poor survival in metastatic microsatellite stable colorectal carcinoma treated with chemotherapy. Additional studies are necessary to examine the role of DNA methylation in treatment efficacy.

Keywords Colon cancer · CIMP · DNA methylation · Epigenetics · Chemotherapy

S. Ogino (✉) · M. Loda
Department of Pathology, Brigham and Women's Hospital,
Harvard Medical School,
75 Francis Street,
Boston, MA 02115, USA
e-mail: shuji_ogino@dfci.harvard.edu

S. Ogino · M. Loda
Department of Pathology, Harvard Medical School,
Boston, MA, USA

S. Ogino · J. A. Meyerhardt · T. Kawasaki · M. H. Kulke · P. C. Enzinger · B. M. Wolpin · M. Loda · C. S. Fuchs
Department of Medical Oncology, Dana-Farber Cancer Institute,
Boston, MA, USA

J. A. Meyerhardt · M. H. Kulke · P. C. Enzinger · B. M. Wolpin · C. S. Fuchs
Department of Medicine, Brigham and Women's Hospital,
Boston, MA, USA

J. A. Meyerhardt · J. W. Clark · D. P. Ryan · M. H. Kulke · P. C. Enzinger · B. M. Wolpin · C. S. Fuchs
Department of Medicine, Harvard Medical School,
Boston, MA, USA

J. W. Clark · D. P. Ryan
Department of Medicine, Massachusetts General Hospital,
Boston, MA, USA

Abbreviations and HUGO Gene Nomenclature Committee (HGNC)-approved official gene symbols

CACNA1G	calcium channel, voltage-dependent, T-type alpha-1G subunit
CDKN2A	cyclin-dependent kinase inhibitor 2A (p16/INK4A)
CIMP	CpG island methylator phenotype
CRABP1	cellular retinoic acid binding protein 1
5-FU	5-fluorouracil
IGF2	insulin-like growth factor 2
IGFBP3	insulin-like growth factor binding protein 3
MGMT	*O*-6-methylguanine-DNA methyltransferase

MINT1	methylated in tumor 1
MINT31	methylated in tumor 31
MSI	microsatellite instability
MSS	microsatellite stable
NEUROG1	neurogenin 1
PMR	percentage of methylated reference (degree of DNA methylation)
RUNX3	runt-related transcription factor 3
SOCS1	suppressor of cytokine signaling 1
WRN	Werner syndrome gene

Introduction

Transcriptional inactivation by cytosine methylation at promoter CpG islands of tumor suppressor genes is thought to be an important mechanism in human carcinogenesis [7, 11]. A number of tumor suppressor genes are silenced by promoter methylation in colorectal carcinoma [7, 11], and promoter CpG island methylation has been shown to occur early in colorectal carcinogenesis [8]. A subset of colorectal cancers exhibit promoter methylation in multiple genes, referred to as the CpG island methylator phenotype (CIMP) [7, 27]. CIMP-high colorectal carcinomas appear to have a distinct clinical, pathologic, and molecular profile, including associations with female sex, proximal tumor location, mucinous and poor differentiations, microsatellite instability (MSI), and *BRAF* mutations [9, 12, 17, 23, 28, 31].

The relationship between epigenetic alterations in tumor and prognosis of colorectal cancer patients who receive chemotherapy has been investigated. CIMP positivity appeared to confer an improved survival among patients who received 5-fluorouracil (5-FU)-based adjuvant chemotherapy for stage III colorectal cancers [29]. In contrast, another study showed that CIMP positivity did not appear to be a significant prognostic factor in stages II and III colorectal cancers treated with adjuvant chemotherapy [30]. As an individual methylation marker, *MGMT* methylation may be a predictor for a low risk of recurrence in colorectal cancer patients receiving adjuvant chemotherapy [13]. Another study has shown that *WRN* (the Werner syndrome gene) promoter methylation may predict longer survival among colorectal cancer patients receiving irinotecan-based chemotherapy [1]. Almost all studies on patient outcomes utilized non-quantitative methylation-specific polymerase chain reaction (PCR). To date, no study on outcomes of colorectal cancer patients has utilized quantitative DNA methylation analysis.

Regarding epigenetic alterations in tumor and response to chemotherapy, microsatellite unstable colorectal cancer cell lines with *MLH1* promoter methylation have been shown to be resistant to 5-FU [2], and resistance of *MLH1*-deficient tumors to 5-FU may be due to the overexpression of thymidylate synthase and functional p53 [21]. However, no study has examined objective tumor response to chemotherapy in relation to overall CIMP status and DNA methylation in multiple individual CpG islands in colorectal cancer.

In this study, we have correlated CpG island methylation in multiple loci with the treatment response and survival among patients who were enrolled in phase I/II trials of combination chemotherapy (irinotecan, 5-FU, leucovorin, and gefitinib) for previously untreated metastatic colorectal carcinoma. CIMP status in this study was determined by 13 CpG island loci, including 8 CIMP-specific promoters (*CACNA1G*, *CDKN2A*, *CRABP1*, *IGF2*, *MLH1*, *NEUROG1*, *RUNX3*, and *SOCS1*, all of which were selected from a screening of 195 loci throughout the human genome [17, 31]) as well as MINT1, MINT31, *IGFBP3*, *MGMT*, and *WRN*. MethyLight assays were used for quantitative DNA methylation analysis because evidence suggest that low levels of DNA methylation do not generally silence gene expression [18, 26].

Materials and methods

Patient selection and treatment

Patients for this analysis were enrolled into one of two phase I/II trials that used intravenous irinotecan, leucovorin, and 5-FU in combination with daily oral gefitinib for previously untreated metastatic colorectal cancer [15]. The study has been approved by the Dana–Farber Cancer Institute Institutional Review Board. All patients provided written informed consent, permitting us to perform genomic/genetic analysis on their samples, before participation in the clinical trials. In both trials, the patients had histologically confirmed metastatic colorectal cancer. Prior therapy for metastatic disease was not permitted, and all patients had measurable disease based on the response evaluation criteria in solid tumors (RECIST) criteria [25]. The eligibility criteria also included the following: age, ≥18; Eastern Cooperative Oncology Group (ECOG) performance status of 0–2; life expectancy, ≥12 weeks; adequate hematopoietic function (absolute neutrophil count, ≥1,500/mm^3; platelets, ≥100,000/mm^3); and adequate renal (serum creatinine, ≤1.5 mg/dl) and hepatic function (serum bilirubin, ≤1.5 mg/dl). A total of 35 patients were initially included.

The patients in the first trial (bolus IFL plus gefitinib) received irinotecan 100 (or 125) mg/m^2, leucovorin 20 mg/m^2, and 5-FU 400 (or 500) mg/m^2 delivered intravenously weekly for two consecutive weeks followed by 1-week rest, in combination with daily oral gefitinib. Enrollment in this trial was between September 2001 and August 2002. In the second trial (FOLFIRI plus gefitinib), the patients received irinotecan 180 mg/m^2 IV bolus, leucovorin 200 mg/m^2 IV bolus, 5-FU

400 mg/m^2 IV bolus, followed by 5-FU 2400 mg/m^2 via continuous infusion over 46 h, in combination with daily oral gefitinib; chemotherapy was repeated every 2 weeks. Enrollment in this latter trial was between April 2003 and April 2004. Therapy was continued until disease progression, unacceptable toxicity, or withdrawal of patient consent.

Assessment of objective tumor response

In each trial, computed axial tomographic scans were performed at baseline and every 6 weeks thereafter. The response evaluation was assessed according to the RECIST criteria [25].

Tumor tissue samples, genomic DNA extraction, and whole genome amplification

Of the 35 patients enrolled in the two trials, both tumor response data and adequate primary tumor specimens for DNA methylation analysis were available from 30 patients (Table 1). One patient presented uncertain response data despite the presence of adequate tumor tissue. Paraffin-embedded tissue blocks were obtained at the time of resection of the primary tumor. Tumor tissue sections obtained from paraffin blocks were reviewed, and genomic DNA was extracted using QIAmp DNA mini-kit (Qiagen, Valencia, CA, USA) by manual dissection as previously

Table 1 CpG island methylation status and response to combination chemotherapy in advanced microsatellite stable colorectal cancer

Case no.	Age/sex	Tumor location	Therapy regimen	Best response	No. of methylated markers	CIMP status[a]
1	67F	Sigmoid	IFL[b]	PR	4	Low
2	52F	Sigmoid	IFL[c]	S	2	Low
3	39M	Rectum	IFL[c]	S	2	Low
4	66F	Sigmoid	IFL[c]	PR	1	Low
5	51M	Sigmoid	IFL[c]	PR	6	Low
6	59M	–	IFL[c]	–	5	Low
7	57M	Cecum	IFL[c]	S	4	Low
8	68M	Sigmoid	IFL[c]	PR	1	Low
9	56M	Sigmoid	IFL[c]	PR	1	Low
10	49M	Sigmoid	IFL[c]	S	9	High
11	58M	Sigmoid	IFL[c]	PR	4	Low
12	45M	Sigmoid	IFL[c]	PR	1	Low
13	46M	Rectum	IFL[c]	PR	0	0
14	64M	Sigmoid	IFL[c]	S	0	0
15	62F	Sigmoid	FOL[d]	S	7	Low
16	31M	Sigmoid	FOL[d]	S	1	Low
17	41M	Rectum	FOL[d]	S	1	Low
18	38M	Sigmoid	FOL[d]	PR	0	0
19	46M	Sigmoid	FOL[d]	S	1	Low
20	83M	Cecum	FOL[d]	S	4	Low
21	63M	Cecum	FOL[d]	PR	3	Low
22	41M	Rectum	FOL[d]	S	1	Low
23	67M	Cecum	IFL[b]	S	3	Low
24	57F	Cecum	FOL[d]	S	7	Low
25	60M	Rectum	FOL[d]	PR	0	0
26	66F	Sigmoid	FOL[d]	S	2	Low
27	38F	Sigmoid	FOL[d]	S	0	0
28	43F	Sigmoid	IFL[c]	S	1	Low
29	59M	Ascending	FOL[d]	PD	11	High
30	51M	Ascending	FOL[d]	PR	1	Low
31	79F	Right	FOL[d]	S	11	High

The case numbers match with those in our previous report [20] that describes other molecular alterations in tumor. The hyphen indicates no result.
F Female; *FOL* infusional 5-fluorouracil (5-FU), leucovorin, and irinotecan; *IFL* bolus 5-FU, leucovorin, and irinotecan; *M* male, *PD* progressive disease; *PR* partial response; *S* stable disease; *5-FU* 5-fluorouracil

[a] CIMP-high was defined as the presence of =9/13 methylated promoters, CIMP-low as 1/13 to 8/13 methylated promoters, and CIMP-0 as the absence of methylated promoters.

[b] 5-FU 500 mg/m^2, leucovorin 20 mg/m^2, irinotecan 125 mg/m^2; days 1 and 8 of the 21-day cycle.

[c] 5-FU 400 mg/m^2, leucovorin 20 mg/m^2, irinotecan 100 mg/m^2; days 1 and 8 of the 21-day cycle.

[d] 5-FU bolus 400 mg/m^2, leucovorin 200 mg/m^2, irinotecan 180 mg/m^2, and infusional 5-FU 2.4 g/m^2 over 46 h, repeated every 2 weeks.

described [15]. Tumor cell content was 50% or more in all cases. Whole genome amplification was performed for MSI analysis, using PCR with random 15-mer primers as previously described [5, 14].

MSI analysis

We analyzed BAT25, BAT26, and BAT40 mononucleotide repeats for the determination of MSI status as previously described [16]. BAT25 and BAT26 were the most predictive markers among the five markers in the US National Cancer Institute (NCI) consensus panel [3].

Quantitative real-time PCR for DNA methylation (MethyLight)

Sodium bisulfite treatment on genomic DNA was performed as previously described [18]. Real-time PCR to measure DNA methylation (MethyLight) was performed as previously described [6, 32]. We used ABI 7300 (Applied Biosystems, Foster City, CA, USA) for quantitative real-time PCR on eight CIMP-specific promoters (*CACNA1G*, *CDKN2A* (*p16*), *CRABP1*, *IGF2*, *MLH1*, *NEUROG1*, *RUNX3*, and *SOCS1*) [17, 31], as well as MINT1, MINT31, *IGFBP3*, *MGMT*, and *WRN*. All of the first eight markers have been shown to be sensitive and specific markers for CIMP-high using a large number of samples [20]. All but two makers (*IGFBP3* and *WRN*) previously showed cancer-specific methylation patterns by MethyLight analysis [31]. *COL2A1* (the collagen 2A1 gene) was used to normalize for the amount of input bisulfite-converted DNA [18, 32]. PCR amplification primers for WRN and IGFBP3 were (bisulfite-converted nucleotides are highlighted by boldface and italics) WRN-F, 5′-G***T***A TCG ***TT***C GCG GCG ***TTT*** A***T***-3′ (GenBank no. AY442327, nucleotide nos. 1827–1846); WRN-R, 5′-***A***CG ***AAA*** CCG ATA TCC GAA ATC A-3′ (GenBank no. AY442327, nucleotide nos. 1887–1908); WRN-probe, 6FAM-5′-***TTT*** TTT TTG CGG TCG TTG CGG G-3′-BHQ-1 (GenBank no. AY442327, nucleotides 1855–1876); IGFBP3-F, 5′-G***T***T TCG GGC GTG AG***T*** ACG A-3′ (GenBank no. M35878, nucleotides 1692–1710); IGFBP3-R, 5′-G***AA*** TCG ACG CA***A*** ACA CG***A*** CT***A*** C-3′ (GenBank no. M35878, nucleotides 1789–1810); and IGFBP3-probe, 6FAM-5′-***T***CG G***T***T G***T***T TAG GGC GAA GTA CGG G-3′-BHQ-1 (GenBank no. M35878, nucleotides 1760–1784). For *IGFBP3* and *WRN*, the analyzed CpG islands were exactly the same as those examined by Wiley et al. [33] and by Agrelo et al. [1], respectively. Other primers and probes were previously described [31, 32]. PCR conditions were exactly the same for all of the reactions: 95°C for 10 min, followed by 45 cycles of 95°C for 15 s and 60°C for 1 min. The percentage of methylated reference (PMR, i.e., degree of methylation) at each locus was calculated as previously described [6], and methylation positivity was defined as PMR>4 (PMR>6 for *CRABP1* based on distributions of PMR values) [17, 18]. The precision and performance characteristics of bisulfite conversion and subsequent MethyLight assays have been previously evaluated, and the assays have been validated [18].

Criteria for CIMP status

Using the 13 methylation markers (*CACNA1G*, *IGF2*, *NEUROG1*, *RUNX3*, *SOCS1*, *CDKN2A*, *CRABP1*, *MLH1*, *MINT1*, *MINT31*, *IGFBP3*, *MGMT*, and *WRN*), CIMP-high was defined as ≥9 methylated markers, CIMP-low as 1 to 8 methylated markers, and CIMP-0 as the absence of methylated markers. When we used a CIMP marker panel including only the first eight markers (*CACNA1G*, *IGF2*, *NEUROG1*, *RUNX3*, *SOCS1*, *CDKN2A*, *CRABP1*, and *MLH1*) [17, 31], or a CIMP maker panel including the first five markers (*CACNA1G*, *IGF2*, *NERUOG1*, *RUNX3*, and *SOCS1*) [31], CIMP-high tumors were exactly the same as those by the 13-marker CIMP panel. We have shown that good concordance between CIMP diagnosis by the first eight markers and the first five markers, with only 1.4% discordance rate among 920 tumors [20]. Our criteria for CIMP-high was based on our previous data that showed associations of CIMP-high and CIMP-low with *BRAF* mutations and *KRAS* mutations, respectively [19]. However, because previous studies by other investigators have used less stringent criteria for CIMP-high (typically ≥50% methylated markers), analysis was also performed with less stringent criteria for CIMP-high tumors with ≥7/13 methylated markers.

Statistical analysis

Survival and time-to-event probabilities were estimated using the methods of Kaplan and Meier [10], and differences were assessed by the log-rank test. Fisher's exact test was utilized for categorical response data. All statistical analyses were performed using the SAS program (version 9.1, SAS Institute, Cary, NC, USA). Statistical significance was set at $p \leq 0.05$. All p values are two sided.

Results

Clinical characteristics

Both tumor response data and adequate tumor samples for DNA methylation analysis were available in 30 cases,

enrolled in two trials assessing the efficacy and safety of a combination of irinotecan, 5-FU, leucovorin, and gefitinib in previously untreated metastatic colorectal carcinoma [15]. The clinical characteristics of these patients are listed in Table 1, in which the case identification numbers match with those in our previous report [15]. Forty three percent and 57% of the patients had ECOG performance status of 0 and 1, respectively, and the ECOG performance status was not a predictor of chemo-responsiveness [15]. All 30 patients had measurable disease by RECIST criteria; 12 patients (40%) experienced a partial response as their best response; 17 patients (57%) experienced stable disease, and 1 patient (3%) experienced progressive disease. At the time of this analysis, 74% of the patients had died, and the median follow-up of the patients who were alive was 2.8 years. No patient was lost from follow-up.

MSI status

All of the 30 tumors with available outcome data were confirmed to be microsatellite stable (MSS) by BAT25, BAT26, and BAT40 microsatellite markers.

CpG island methylation and patient survival

Utilizing MethyLight technology, we determined the CpG island methylation status in 13 CpG island loci, including *CACNA1G*, *CDKN2A* (p16), *CRABP1*, *IGF2*, *MLH1*, *NEUROG1*, *RUNX3*, *SOCS1* [17, 31], as well as MINT1, MINT31 [27], *IGFBP3* [4, 33], *MGMT* [13], and *WRN* [1]. CIMP status was determined in the 30 tumors with available tumor response and patient survival data. Three tumors were CIMP-high with ≥9/13 methylated markers. Among patients with CIMP-high tumors, the median survival was only 0.93 years and 1 year survival rate was 33%, compared to the median survival of 1.9 years and 85% 1 year survival among patients with CIMP-low or CIMP-0 tumors ($p=0.0004$; Table 2; Fig. 1). Because less stringent criteria for CIMP-high (typically ≥50% of markers methylated) have been used in the literature [23, 29, 30], we also used a lower cutoff for CIMP-high (≥7/13 methylated markers). By this less stringent criteria, five tumors were diagnosed as CIMP-high and were significantly associated with worse survival compared to CIMP-low or CIMP-0 tumors ($p=0.0007$; Table 2; Fig. 1).

With regard to individual methylation markers, survival among patients with methylated tumors was significantly worse than survival with unmethylated tumors, in *CACNA1G* ($p<0.0001$), *IGF2* ($p=0.0004$), *MLH1* ($p<0.0001$), *NEUROG1* ($p=0.006$), *RUNX3* ($p=0.001$), *MINT31* ($p=0.009$), or *WRN* ($p=0.001$; Table 2).

CpG island methylation and tumor response to chemotherapy

The three CIMP-high tumors were resistant to chemotherapy (0% response rate). Among the other 27 CIMP-low or CIMP-0 tumors, 12 tumors (44%) showed partial response (Table 2). However, the difference in the response rates did not reach statistical significance. Using the less stringent criteria for CIMP-high (≥7/13 methylated markers), all five CIMP-high tumors were resistant to chemotherapy (0% response rate), and CIMP-low or CIMP-0 tumors appeared to show a trend toward a better response rate (48%, $p=0.07$).

None of the 13 individual methylation markers was a significant predictor for tumor response to combination chemotherapy (Table 2). However, there was a trend toward lower response rates among methylated tumors for most of the 13 individual methylation markers except for *CRABP1* and *IGFBP3*.

Discussion

We sought to examine whether CpG island methylation can predict survival or tumor response among patients with advanced microsatellite stable (MSS) colorectal carcinoma treated with 5-FU and irinotecan-based combination chemotherapy. We utilized quantitative DNA methylation analyses (MethyLight technology) to measure the DNA methylation in 13 markers, including 8 promoters (*CACNA1G*, *CDKN2A*, *CRABP1*, *IGF2*, *MLH1*, *NEUROG1*, *RUNX3*, and *SOCS1*), which have been selected from a screening of 195 loci throughout the human genome and specific for CIMP in colorectal carcinoma [17, 31]. All of these eight markers have been shown to be sensitive and specific markers for diagnosis of CIMP-high using 920 colorectal cancers [20]. In addition, we also analyzed the DNA methylation in *MINT1*, *MINT31* [27], *IGFBP3* [4, 33], *MGMT* [13], and *WRN* [1].

We have shown that overall CIMP-high status and methylation in *CACNA1G*, *IGF2*, *MLH1*, *NEUROG1*, *RUNX3*, *MINT31*, and *WRN* predict worse survival among patients with advanced MSS colorectal cancer treated with combination chemotherapy. Our results may suggest that CIMP-high is a biologically different phenotype from CIMP-low/0 among MSS tumors. However, our results are limited by a small sample size. Additional studies are necessary to examine a predictive value of the methylation markers for survival among patients with colorectal cancers in other stages, or colorectal cancers treated with only surgical resection. Because CIMP-high is associated with methylation in individual markers, a larger number of cases are also necessary to analyze the interrelationship between CIMP status, methylation in individual markers, and survival. In

Table 2 CpG island methylation, response to chemotherapy, and patient survival in advanced microsatellite stable colorectal cancer

Marker	Result	*N*	Response rate (%)	*P* value	Median survival (year)	One year survival (%)	*P* value
CIMP	High (≥9/13)	3	0	0.25	0.9	33	0.0004
	Low/0 (≤8/13)	27	44		1.9	85	
CIMP (less stringent criteria for CIMP-high)[a]	High (≥7/13)	5	0	0.07	0.9	40	0.0007
	Low/0 (≤6/13)	25	48		1.9	88	
CACNA1G	Methylated	3	0	0.25	0.6	0	<0.0001
	Unmethylated	27	44		1.9	89	
CDKN2A	Methylated	10	30	0.69	1.3	70	0.10
	Unmethylated	20	45		1.9	85	
CRABP1	Methylated	9	44	1.0	1.5	67	0.47
	Unmethylated	21	38		1.9	85	
IGF2	Methylated	3	0	0.25	0.9	33	0.0004
	Unmethylated	27	44		1.9	85	
MLH1	Methylated	1	0	1.0	0.1	0	<0.0001
	Unmethylated	29	41		1.8	82	
NEUROG1	Methylated	7	14	0.19	1.1	57	0.006
	Unmethylated	23	48		1.9	87	
RUNX3	Methylated	6	17	0.36	0.8	33	0.001
	Unmethylated	24	46		1.9	91	
SOCS1	Methylated	4	25	0.63	NR	100	0.56
	Unmethylated	26	42		1.8	77	
MINT1	Methylated	7	14	0.19	1.1	57	0.53
	Unmethylated	23	48		1.8	87	
MINT31	Methylated	7	14	0.19	1.0	57	0.009
	Unmethylated	23	48		1.9	87	
IGFBP3	Methylated	10	40	1.0	1.6	80	0.94
	Unmethylated	20	40		1.9	79	
MGMT	Methylated	10	30	0.69	1.5	70	0.19
	Unmethylated	20	45		1.9	85	
WRN	Methylated	11	27	0.32	1.1	64	0.001
	Unmethylated	19	47		2.6	89	

[a] Results by less stringent criteria (≥7/13 methylated markers) for CIMP-high
NR Not reached

addition, randomized controlled trials are necessary to assess whether a survival benefit by chemotherapy is different according to the methylation status in tumor.

The relationship between epigenetic alterations in tumors and prognosis of colorectal cancer patients treated with chemotherapy has been investigated. CIMP positivity determined by methylation-specific PCR on the *CDKN2A* (p16), MINT2, and *MDR1* loci appeared to confer an improved survival among patients who received 5-FU-based adjuvant chemotherapy for stage III colorectal cancers [29]. In that study [29], however, only three markers were analyzed for the determination of CIMP status, and the criteria for CIMP was ≥ 2/3 methylated loci, resulting in a high frequency of CIMP positivity (33%). Large population-based studies have shown that the frequency of CIMP is within the range of 15 to 25% [17, 23]. In contrast, another study showed that CIMP positivity [≥3/5 methylated loci among *CDKN2A* (p16), MINT1, MINT2, MINT12, and MINT31] did not appear to be a significant prognostic factor in stages II and III colorectal cancers treated with adjuvant chemotherapy [30]. In the same study [30], CIMP-high predicted worse survival among patients with MSS tumors, but not among patients with MSI-high tumors. A large population-based study has shown that *BRAF* mutation is significantly associated with poor survival in MSS tumors, but CIMP-high status defined by different markers and criteria is not associated with worse outcomes [24]. Our current study utilizing methods of quantitative DNA methylation analysis for the 13 methylation markers suggest the association of CIMP-high in MSS colorectal cancer with worse survival and possibly with resistance to chemotherapy as well. However, further studies are necessary to draw definitive conclusions on a predictive value of CIMP for survival and response to chemotherapy.

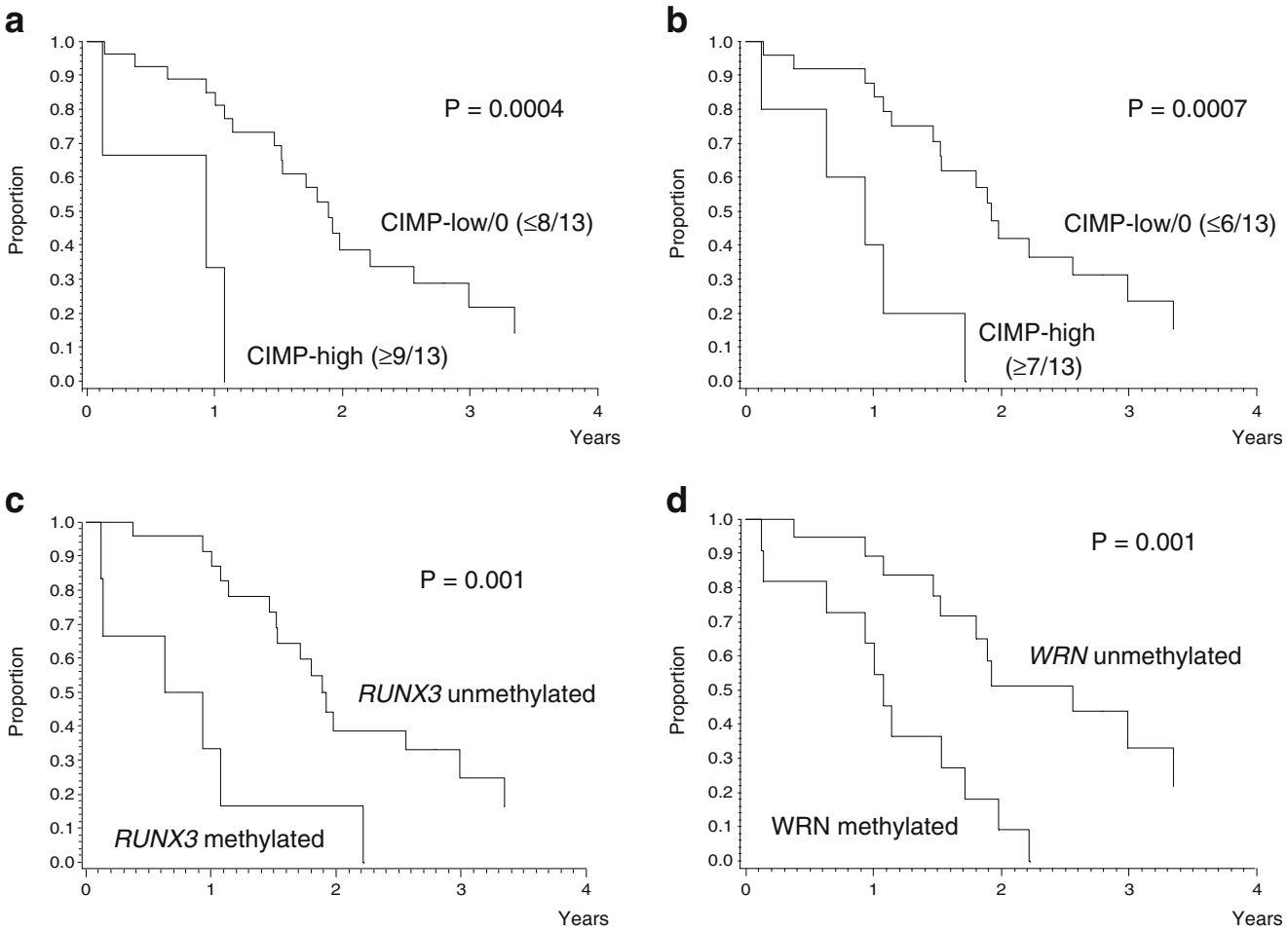

Fig. 1 Kaplan–Meier survival curves of patients with metastatic microsatellite stable colorectal cancer. **a** CIMP-high (≥9/13 methylated markers) vs CIMP-low/0 (≤8/13 methylated markers) by the stringent criteria for CIMP-high. **b** CIMP-high (≥7/13 methylated markers) vs CIMP-low/0 (≤6/13 methylated markers) by less stringent criteria for CIMP-high. **c** *RUNX3* methylated vs *RUNX3* unmethylated. **d** *WRN* methylated vs *WRN* unmethylated

As an individual methylation marker, Nagasaka et al. [13] examined *MGMT* methylation by methylation-specific PCR and suggested that *MGMT* methylation might predict a low risk of recurrence among colorectal cancer patients receiving adjuvant chemotherapy. However, it remains a possibility that clinical outcomes may be directly linked to CIMP rather than *MGMT* methylation. The CIMP status reflects the global epigenomic status in tumor cell, and it is conceivable that another unidentified factor related to CIMP may primarily affect the outcomes of colorectal cancer patients receiving chemotherapy. Thus, it is important to examine overall CIMP status when one evaluates DNA methylation in a single methylation marker in relation to patient outcomes.

Another study has suggested that *WRN* promoter methylation may predict significantly longer survival among colorectal cancer patients treated with irinotecan-based chemotherapy [1], which contradicts our observations (i.e., worse survival of patients with *WRN*-methylated tumors). These conflicting results could be due to differences in patient populations and treatment regimens. However, characteristics of the patients in the study by Agrelo et al. [1] have not been described in detail in their cited reference [22], precluding further evaluation of their study.

In conclusion, our results suggest that CpG island methylation may predict worse survival among colorectal cancer patients who receive 5-FU and irinotecan-based chemotherapy. We did not confirm earlier observations that *MGMT* or *WRN* promoter methylation might predict better outcomes in colorectal cancer patients who receive 5-FU-based or irinotecan-based chemotherapy, respectively. Further studies should examine the role of DNA methylation in treatment efficacy.

Acknowledgment This work was partly supported by the United States National Institute of Health (NIH) grants P01 CA87969-03 and P01 CA55075-13. We deeply thank the patients who participated in the clinical trials, and Ann L. Michelini and Kate Kinsella for their assistance in the management of the clinical trials. This study complied with the current laws of the USA.

References

1. Agrelo R, Cheng WH, Setien F, Ropero S, Espada J, Fraga MF, Herranz M, Paz MF, Sanchez-Cespedes M, Artiga MJ, Guerrero D, Castells A, von Kobbe C, Bohr VA, Esteller M (2006) Epigenetic inactivation of the premature aging Werner syndrome gene in human cancer. Proc Natl Acad Sci U S A 103:8822–8827
2. Arnold CN, Goel A, Boland CR (2003) Role of hMLH1 promoter hypermethylation in drug resistance to 5-fluorouracil in colorectal cancer cell lines. Int J Cancer 106:66–73
3. Bacher JW, Flanagan LA, Smalley RL, Nassif NA, Burgart LJ, Halberg RB, Megid WM, Thibodeau SN (2004) Development of a fluorescent multiplex assay for detection of MSI-high tumors. Dis Markers 20:237–250
4. Chang YS, Wang L, Liu D, Mao L, Hong WK, Khuri FR, Lee HY (2002) Correlation between insulin-like growth factor-binding protein-3 promoter methylation and prognosis of patients with stage I non-small cell lung cancer. Clin Cancer Res 8:3669–3675
5. Dietmaier W, Hartmann A, Wallinger S, Heinmoller E, Kerner T, Endl E, Jauch KW, Hofstadter F, Ruschoff J (1999) Multiple mutation analyses in single tumor cells with improved whole genome amplification. Am J Pathol 154:83–95
6. Eads CA, Danenberg KD, Kawakami K, Saltz LB, Blake C, Shibata D, Danenberg PV, Laird PW (2000) MethyLight: a high-throughput assay to measure DNA methylation. Nucleic Acids Res 28:E32
7. Issa JP (2004) CpG island methylator phenotype in cancer. Nat Rev Cancer 4:988–993
8. Jass JR (2005) Serrated adenoma of the colorectum and the DNA-methylator phenotype. Nat Clin Pract Oncol 2:398–405
9. Kambara T, Simms LA, Whitehall VLJ, Spring KJ, Wynter CVA, Walsh MD, Barker MA, Arnold S, McGivern A, Matsubara N, Tanaka N, Higuchi T, Young J, Jass JR, Leggett BA (2004) BRAF mutation is associated with DNA methylation in serrated polyps and cancers of the colorectum. Gut 53:1137–1144
10. Kaplan E, Meier P (1958) Nonparametric estimation from incomplete observations. J Am Stat Assoc 53:457–481
11. Laird PW (2005) Cancer epigenetics. Hum Mol Genet 14(Spec no. 1):R65–R76
12. Nagasaka T, Sasamoto H, Notohara K, Cullings HM, Takeda M, Kimura K, Kambara T, MacPhee DG, Young J, Leggett BA, Jass JR, Tanaka N, Matsubara N (2004) Colorectal cancer with mutation in BRAF, KRAS, and wild-type with respect to both oncogenes showing different patterns of DNA methylation. J Clin Oncol 22:4584–4594
13. Nagasaka T, Sharp GB, Notohara K, Kambara T, Sasamoto H, Isozaki H, MacPhee DG, Jass JR, Tanaka N, Matsubara N (2003) Hypermethylation of O6-methylguanine-DNA methyltransferase promoter may predict nonrecurrence after chemotherapy in colorectal cancer cases. Clin Cancer Res 9:5306–5312
14. Ogino S, Kawasaki T, Brahmandam M, Yan L, Cantor M, Namgyal C, Mino-Kenudson M, Lauwers GY, Loda M, Fuchs CS (2005) Sensitive sequencing method for KRAS mutation detection by pyrosequencing. J Mol Diagnostics 7:413–421
15. Ogino S, Meyerhardt JA, Cantor M, Brahmandam M, Clark JW, Namgyal C, Kawasaki T, Kinsella K, Michelini AL, Enzinger PC, Kulke MH, Ryan DP, Loda M, Fuchs CS (2005) Molecular alterations in tumors and response to combination chemotherapy with gefitinib for advanced colorectal cancer. Clin Cancer Res 11:6650–6656
16. Ogino S, Brahmandam M, Cantor M, Namgyal C, Kawasaki T, Kirkner G, Meyerhardt JA, Loda M, Fuchs CS (2006) Distinct molecular features of colorectal carcinoma with signet ring cell component and colorectal carcinoma with mucinous component. Mod Pathol 19:59–68
17. Ogino S, Cantor M, Kawasaki T, Brahmandam M, Kirkner G, Weisenberger DJ, Campan M, Laird PW, Loda M, Fuchs CS (2006) CpG island methylator phenotype (CIMP) of colorectal cancer is best characterised by quantitative DNA methylation analysis and prospective cohort studies. Gut 55:1000–1006
18. Ogino S, Kawasaki T, Brahmandam M, Cantor M, Kirkner GJ, Spiegelman D, Makrigiorgos GM, Weisenberger DJ, Laird PW, Loda M, Fuchs CS (2006) Precision and performance characteristics of bisulfite conversion and real-time PCR (MethyLight) for quantitative DNA methylation analysis. J Mol Diagnostics 8:209–217
19. Ogino S, Kawasaki T, Kirkner GJ, Loda M, Fuchs CS (2006) CpG island methylator phenotype-low (CIMP-low) in colorectal cancer: possible associations with male sex and KRAS mutations. J Mol Diagnostics 8:582–588
20. Ogino S, Kawasaki T, Kirkner GJ, Kraft P, Loda M, Fuchs CS (2007) Evaluation of markers for CpG island methylator phenotype (CIMP) in colorectal cancer using a large population-based sample. J Mol Diagnostics (in press)
21. Ricciardiello L, Ceccarelli C, Angiolini G, Pariali M, Chieco P, Paterini P, Biasco G, Martinelli GN, Roda E, Bazzoli F (2005) High thymidylate synthase expression in colorectal cancer with microsatellite instability: implications for chemotherapeutic strategies. Clin Cancer Res 11:4234–4240
22. Ropero S, Setien F, Espada J, Fraga MF, Herranz M, Asp J, Benassi MS, Franchi A, Patino A, Ward LS, Bovee J, Cigudosa JC, Wim W, Esteller M (2004) Epigenetic loss of the familial tumor-suppressor gene exostosin-1 (EXT1) disrupts heparan sulfate synthesis in cancer cells. Hum Mol Genet 13:2753–2765
23. Samowitz W, Albertsen H, Herrick J, Levin TR, Sweeney C, Murtaugh MA, Wolff RK, Slattery ML (2005) Evaluation of a large, population-based sample supports a CpG island methylator phenotype in colon cancer. Gastroenterology 129:837–845
24. Samowitz WS, Sweeney C, Herrick J, Albertsen H, Levin TR, Murtaugh MA, Wolff RK, Slattery ML (2005) Poor survival associated with the BRAF V600E mutation in microsatellite-stable colon cancers. Cancer Res 65:6063–6069
25. Therasse P, Arbuck SG, Eisenhauer EA, Wanders J, Kaplan RS, Rubinstein L, Verweij J, Van Glabbeke M, van Oosterom AT, Christian MC, Gwyther SG (2000) New guidelines to evaluate the response to treatment in solid tumors. European Organization for Research and Treatment of Cancer, National Cancer Institute of the United States, National Cancer Institute of Canada. J Natl Cancer Inst 92:205–216
26. Toyooka KO, Toyooka S, Maitra A, Feng Q, Kiviat NC, Smith A, Minna JD, Ashfaq R, Gazdar AF (2002) Establishment and validation of real-time polymerase chain reaction method for CDH1 promoter methylation. Am J Pathol 161:629–634
27. Toyota M, Ahuja N, Ohe-Toyota M, Herman JG, Baylin SB, Issa JP (1999) CpG island methylator phenotype in colorectal cancer. Proc Natl Acad Sci U S A 96:8681–8686
28. Toyota M, Ohe-Toyota M, Ahuja N, Issa JP (2000) Distinct genetic profiles in colorectal tumors with or without the CpG island methylator phenotype. Proc Natl Acad Sci U S A 97:710–715

29. Van Rijnsoever M, Elsaleh H, Joseph D, McCaul K, Iacopetta B (2003) CpG island methylator phenotype is an independent predictor of survival benefit from 5-fluorouracil in stage III colorectal cancer. Clin Cancer Res 9:2898–2903
30. Ward RL, Cheong K, Ku SL, Meagher A, O'Connor T, Hawkins NJ (2003) Adverse prognostic effect of methylation in colorectal cancer is reversed by microsatellite instability. J Clin Oncol 21:3729–3736
31. Weisenberger DJ, Siegmund KD, Campan M, Young J, Long TI, Faasse MA, Kang GH, Widschwendter M, Weener D, Buchanan D, Koh H, Simms L, Barker M, Leggett B, Levine J, Kim M, French AJ, Thibodeau SN, Jass J, Haile R, Laird PW (2006) CpG island methylator phenotype underlies sporadic microsatellite instability and is tightly associated with BRAF mutation in colorectal cancer. Nat Genet 38:787–793
32. Widschwendter M, Siegmund KD, Muller HM, Fiegl H, Marth C, Muller-Holzner E, Jones PA, Laird PW (2004) Association of breast cancer DNA methylation profiles with hormone receptor status and response to tamoxifen. Cancer Res 64: 3807–3813
33. Wiley A, Katsaros D, Fracchioli S, Yu H (2006) Methylation of the insulin-like growth factor binding protein-3 gene and prognosis of epithelial ovarian cancer. Int J Gynecol Cancer 16:210–218

Virchows Arch (2007) 450:539–547
DOI 10.1007/s00428-007-0402-y

ORIGINAL ARTICLE

Myoepithelial cells in solid variant of intraductal papillary carcinoma of the breast: a potential diagnostic pitfall and a proposal of an immunohistochemical panel in the differential diagnosis with intraductal papilloma with usual ductal hyperplasia

Suzuko Moritani · Shu Ichihara · Ryoji Kushima · Hidetoshi Okabe · Masamichi Bamba · Tadao K. Kobayashi · Takanori Hattori

Received: 13 November 2006 / Revised: 28 February 2007 / Accepted: 3 March 2007 / Published online: 22 March 2007
© Springer-Verlag 2007

Abstract We examined myoepithelial status in intraductal papillary carcinoma (IPC) along with the expression of high-molecular weight cytokeratin (HMWK) and neuroendocrine markers, with special reference to the differential diagnosis of solid intraductal papillary carcinoma(SIPC) and intraductal papilloma with usual ductal hyperplasia (IP-UDH). Twenty-six (93%) of the twenty-eight intraductal papillomas (IP) had myoepithelial cells in >70% of the epithelial–stromal interface of the intraluminal proliferating component. Six (29%) of twenty-one SIPC had almost complete myoepithelial layer like IP-UDH at the epithelial–stromal interface. HMWK (34βE-12) was diffusely positive in 14 (93%) of 15 IP-UDH, but 16 (76%) of 21 SIPC were completely negative for HMWK. Neuroendocrine markers were positive in 14 (67%) of SIPC, but all 28 IPs were completely negative. If only the presence of myoepithelial cells is emphasized as a benign hallmark, about 30% of SIPCs may be underdiagnosed as IP-UDH. However, by using a combination of myoepithelial markers, HMWK, and neuroendocrine markers, all of the 36 solid intraductal papillary lesions were properly classified as benign and malignant. Solid intraductal papillary lesions meeting at least two of the following criteria are highly likely to be malignant: (1) absence of myoepithelial cells (<10% of epithelial–stromal interface of intraluminal proliferating component), (2) negative HMWK(<10%), (3) positive neuroendocrine markers (>10%).

Keywords Solid intraductal papillary carcinoma · Intraductal papilloma · Usual ductal hyperplasia · Myoepithelial cell · Neuroendocrine differentiation

S. Moritani (✉) · S. Ichihara
Department of Pathology and Clinical Laboratories,
Nagoya Medical Center,
4-1-1, Sannomaru, Naka-ku, Nagoya, Aichi, 460-0001, Japan
e-mail: moritani@nnh.hosp.go.jp

R. Kushima · H. Okabe
Department of Diagnostic Pathology,
Shiga University of Medical Science,
Setatsukinowa-cho, Ohtsu, Shiga, Japan

M. Bamba · T. K. Kobayashi
Department of Pathology, Saiseikai Shiga Hospital,
Imperial Gift Foundation Inc,
2-4-1, Ohashi, Ritto, Shiga, Japan

T. Hattori
Department of Pathology, Shiga University of Medical Science,
Setatsukinowa-cho, Ohtsu, Shiga, Japan

Introduction

Among the histopathological criteria for differentiating benign from malignant intraductal papillary lesions, the most emphasized histological hallmark of benignity is the preservation of myoepithelial cells along the epithelial–stromal interface of the papillary fronds [22]. However, distinction between benign and malignant intraductal papillary lesions is not always straightforward. The architectural variety accompanying occasional intraductal papillomas (IPs) attributes to this difficulty [21]. There are two worrisome architectural patterns in IPs that cause over-

diagnosis. One pattern is compact tubulopapillary proliferation that sometimes obscures the myoepithelial cells in routine hematoxylin and eosin sections. Pseudo-invasion at the periphery may lead to an overdiagnosis of an invasive ductal carcinoma. The other pattern is coexistent usual ductal hyperplasia (UDH). It can be so florid as to obliterate the entire lumen of the original duct, resulting in islands of connective tissue stalks surrounded by solid and fenestrated epithelial proliferation, which resemble cribriform and solid ductal carcinoma in situ (DCIS).

Immunohistochemical staining for myoepithelial markers are useful in the former situation. Myoepithelial cells are uniformly decorated along the epithelial–stromal interface of tightly proliferating tubular or papillary structures in IPs. Absent or markedly reduced myoepithelial cells indicates intraductal papillary carcinoma (IPC) [8, 17, 20]. Among the various immunohistochemical markers, p63, CD10 and calponin are relatively sensitive and specific markers of breast myoepithelial cells [5, 15].

As for the differential diagnosis of UDH and low-grade DCIS, cellular monotony and polarized nuclear arrangement favor malignancy. Immunohistochemical studies have demonstrated a uniform lack of high-molecular weight cytokeratin (HMWK) in low-grade DCIS, whereas UDH showed an intense mosaic distribution of HMWK throughout the lesion [4, 6, 10]. This pattern of HMWK expression reflects the participation of basal cells as well as luminal epithelial cells in UDH, which indicates polyclonal proliferation. The usefulness of HMWK immunohistochemistry in the differential diagnosis of intraductal proliferative lesions was confirmed by comparative genomic hybridization [2].

Tse et al. [23] recently showed that a combination of immunohistochemistry for HMWK and myoepithelial markers is useful in assessing difficult papillary lesions of the breast. Our group also showed similar results using double-immunostaining with p63 and HMWK (34βE-12) [9].

Solid intraductal papillary carcinoma (SIPC) is a variant of IPC characterized by a predominant solid proliferation of neoplastic cells. Scattered fibrovascular stromal cores within the solid epithelial proliferation are clues to recognize the background papillary architecture [13, 16]. The neoplastic epithelial cells tend to have monotonous nuclear appearance and show a palisading arrangement at the stromal interface. The tumor frequently shows neuroendocrine features such as plasmacytoid appearance, eosinophilic granular cytoplasm, and nuclei with fine chromatin pattern. Neuroendocrine markers such as chromogranin A and Grimerius staining are positive in around 60% of the cases [13]. Focal mucin production and a relationship to certain mucinous carcinomas have also been reported [3, 13, 16].Tumor cells are occasionally spindle shaped and give a biphasic appearance, resulting in an underdiagnosis of benign lesions [14]. The distinction of SIPC from intraductal papilloma with UDH (IP-UDH) is one of the most challenging differential diagnosis in breast pathology. There have been only a few immunohistochemical studies on this issue that have used a large number of cases, with the exception of one recent study by Rabban et al. [19]. They showed that HMWK (cytokeratin5/6) expression was characteristic to IP-UDH. However, the degree of myoepithelial preservation in SIPC has not been examined in detail so far. In the present study, we focused on intraductal papillary lesions with predominant solid epithelial growth. Using immunohistochemistry of myoepithelial markers, HMWK, and neuroendocrine markers, we identified a diagnostic pitfall as well as a useful panel of immunohistochemical markers for the differential diagnosis of solid intraductal proliferative lesions.

Materials and methods

Surgically resected IPs and IPCs were retrieved from the surgical pathology files of Nagoya Medical Center, Shiga University of Medical Science, and Saiseikai Shiga Hospital. The surgeries were performed during a 5-year period from 2000 to 2005. We excluded the cases in which pathological diagnosis on hematoxyline and eosin (H&E) sections were equivocal or those which fall into a borderline category. The latter includes the lesions in which monotonous epithelial proliferation resembling low-grade DCIS involves less than one third of the papilloma's entire transections. At least three pathologists, including two with a subspecialty in breast pathology (SM and SI), agreed upon the diagnosis for each lesion. A total of 22 IPs and 37 IPCs were included in the study.

The architectural pattern of each lesion was classified into solid and nonsolid types. Solid type of IP was defined as IP-UDH in which UDH component predominates. In this study, as we especially focused on the architectural pattern, any areas of different architectural patterns inside the same case were evaluated separately (Fig. 1). If solid and nonsolid parts were coexistent in one lesion (Fig. 1a,b), each part was evaluated separately. If a fused tubular or cribriform pattern in addition to a papillary pattern in nonsolid IPCs, the area with each pattern was evaluated separately (Fig. 1c).

Four-micrometer-thick serial sections were cut from a representative tissue block of each case. Immunohistochemistry was performed by the avidin–biotin-peroxidase method using LSAB2/HRP (DakoCytomation, Carpinteria, CA) and the following antibodies: as myoepithelial markers, p63 (clone:4A4, 1:50, DakoCytomation, Glostrup, Denmark), calponin (clone: CALP, 1:100, DakoCytomation, Carpinteria, CA), and CD10 (clone:56C6, 1:50, Novocastra, Newcastle upon Tyne, UK), as neuroendocrine

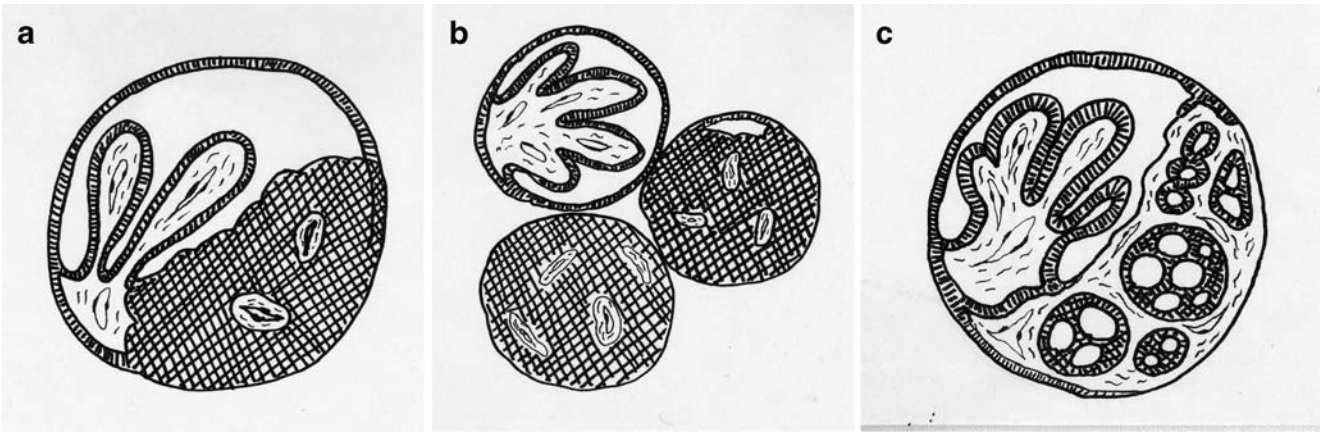

Fig. 1 Schema of the mixed architectural pattern within one case. **a** Solitary papilloma with both solid and nonsolid pattern. **b** Multiple papilloma with both solid and nonsolid pattern. **c** Nonsolid intraductal papillary carcinoma which has fused tubular and cribriform patterns in addition to the papillary pattern

markers, chromogranin A (polyclonal, 1:100, DakoCytomation, Glostrup, Denmark), and synaptophysin (polyclonal, 1:100, Glostrup, Denmark), and a HMWK (clone: 34βE-12, 1:100, DakoCytomation, Carpinteria, CA). The slides for p63, CD10, and synaptophysin were pretreated in citrate buffer (pH6.0) at 121°C for 15 min using an autoclave. Slides for calponin and HMWK were pretreated by proteinase K at room temperature for 5 min. As a positive control of neuroendocrine markers, we used a case of breast endocrine DCIS. For myoepithelial markers and HMWK, normal breast lobules were used as internal positive controls.

Degree of immunohistochemical staining for *HMWK and neuroendocrine markers* were scored as follows: 0, no positive cells; 1, less than 10%; 2, more than 10% and less than 50%; 3, more than 50% and less than 70%; 4, more than 70% of the *intraluminal proliferating cells* were positive. For the evaluation of myoepithelial markers, we focused only on the epithelial–stromal interface of intraluminal proliferating component; we did not evaluate myoepithelial cells at the periphery of the original ducts. The immunostaining score for myoepithelial markers was determined by the percentage of the epithelial–stromal interface that was accompanied by myoepithelial cells. A score of 4 was given for almost continuous myoepithelial staining as seen in normal breast tissue. If a focal loss of myoepithelial cells was identified, the percentage of remaining myoepithelial cells in all epithelial–stromal interface was evaluated *and scored in the same way as in HMWK and neuroendocrine markers*. If the scores were different among the same markers, the highest score was regarded as the proper score for the lesion. However, when the stromal cores were too narrow and blood vessels were closely apposed to the epithelial cells, the presence of myoepithelial cells was confirmed only by CD10 and p63 because calponin usually decorates the vascular walls.

The chi-square test was used for the statistical analyses. p values less than 0.05 were considered statistically significant.

Results

Cinicopathological findings

The mean ages of the patients with 22 IP and 37 IPC were 46.7 (range, 28–72), and 67.0 years (range, 31–90), respectively. The patients with IPC were significantly older than those with IP ($p<0.01$). The mean diameters of IP lesions and IPC lesions were 7.6 mm (range, 2–21 mm) and 12.2 mm (range, 3–40 mm), respectively. The mean tumor size of IPC was significantly larger than that of IP ($p=0.02$).

Histological features of IPs were shown in Table 1. In the 22 IPs, six cases had both solid and nonsolid components in the same lesion. Fifteen cases were solitary and seven were multiple papillomas. Three of the latter contained solid and nonsolid components in different duct transections. Thirteen nonsolid (Fig. 2a) and 15 solid-type (Fig. 2b) lesions were identified in the 22 IPs. The nuclear features of solid IP were ovoid or spindle shaped. The proliferating epithelial cells were arranged haphazardly with occasional streaming. Nuclear overlapping was not infrequent. Secondary lumens were, if any, predominantly located peripherally and were irregularly shaped without polarization of the surrounding cells.

Histological features of IPCs were shown in Table 2. In the 37 IPCs, four cases had both solid and nonsolid components in the same lesion. Four nonsolid lesions had cribriform and papillary patterns in the same lesions. A total of 24 nonsolid (Fig. 3a) and 21 solid type lesions (Fig. 3b) were identified in the 37 IPCs. The cellular appearance of

Table 1 Histological and immunohistochemical features of the intraductal papillomas

No.	Pattern	CD10	p63	Calp	CgA	Syn	34β	
1	nonsolid	4	4	4	0	0	0	Multiple
2	nonsolid	4	4	4	0	0	0	
3	nonsolid	4	2	4	0	0	0	
4	nonsolid	4	3	4	0	0	4	Multiple
5	nonsolid	4	4	4	0	0	0	
6	nonsolid	1	3	4	0	0	3	Multiple
7	nonsolid	2	2	4	0	0	0	
8	nonsolid	4	4	4	0	0	0	
9	nonsolid	4	4	4	0	0	0	Multiple
10	nonsolid	4	4	4	0	0	0	
11	nonsolid	1	1	2	0	0	0	
12	nonsolid	4	4	4	0	0	0	
13	nonsolid	4	4	4	0	0	0	Multiple
14	solid	4	4	4	0	0	4	
15	solid	0	4	4	0	0	4	
16	solid	4	4	4	0	0	4	
17	solid	4	4	4	0	0	4	Multiple
18	solid	1	4	4	0	0	4	
19	solid	3	4	4	0	0	4	
20	solid	3	4	4	0	0	4	
21	solid	4	4	4	0	0	4	
22	solid	4	4	4	0	0	4	Multiple
23(=2)	solid	4	4	4	0	0	4	
24(=3)	solid	4	2	4	0	0	4	
25(=4)	solid	4	3	4	0	0	3	Multiple
26(=8)	solid	4	4	4	0	0	4	Multiple
27(=9)	solid	4	4	4	0	0	4	Multiple
28(=11)	solid	1	1	2	0	0	4	

If the lesion was from the same case, the no. of the lesion was indicated in the parentheses.
Calp, calponin; *CgA*, chromogranin A; *Syn*, synaptophysin; *34β*, HMWK (34βE-12); *Multiple*, multiple papilloma

SIPC was more monotonous than that of the solid IP, and nuclear overlapping was rare. However, nuclear spindling was frequent. Focal mucin production was seen in 3 (14%) of 21 lesions. Twenty-one IPC cases had a nuclear grade of 1, and 16 cases had nuclear grade of 2. None of the tumors were grade 3. In the eight cases with different architectural patterns in the same lesion, the nuclear grade was the same throughout the lesion. The nuclei were monotonous and uniformly showed a fine chromatin pattern. Benign peripheral papilloma was seen in the same slides in 10 (28%) of 37 cases, four of which were nonsolid type, four of which were solid type, and two of which were mixed nonsolid and solid type IPCs. In all these lesions, the papillomas were close proximity to the cancerous foci. Five of the six nonsolid-type lesions that had peripheral papillomas showed fused tubular and cribriform patterns between the fibrovascular stromal cores (Fig. 3c). Ducts having a spectrum of benign, atypical, and malignant lesions were seen in one of these five lesions.

Immunohistochemistry

The detailed immunohistochemical results of IP and IPC are shown in Tables 1 and 2, respectively. The staining patterns of myoepithelial markers were significantly different between IPs and IPCs in both nonsolid and solid lesions (Table 3; $p<0.01$). Myoepithelial cells were present at the epithelial–stromal interface of intraluminal proliferating area of all IP lesions (Fig. 2c,d). Twelve (92%) of 13 nonsolid and 14 (93%) of 15 solid IPs were score 4 (more than 70% of epithelial–stromal interface was accompanied by intact myoepithelial layer.). One nonsolid IP lesion and one solid IP lesion had a myoepithelial score of 2. The two lesions were from the same case. The areas lacking myoepithelial cells showed apocrine metaplasia without atypia. Myoepithelial cells were present in 15 (33%) of 45 lesions of IPC. Six (25%) of nonsolid and six (29%) of solid IPC were score 4 (Fig. 3d,e). Five (83%) of the six nonsolid IPCs and three (50%) of the solid IPCs with score

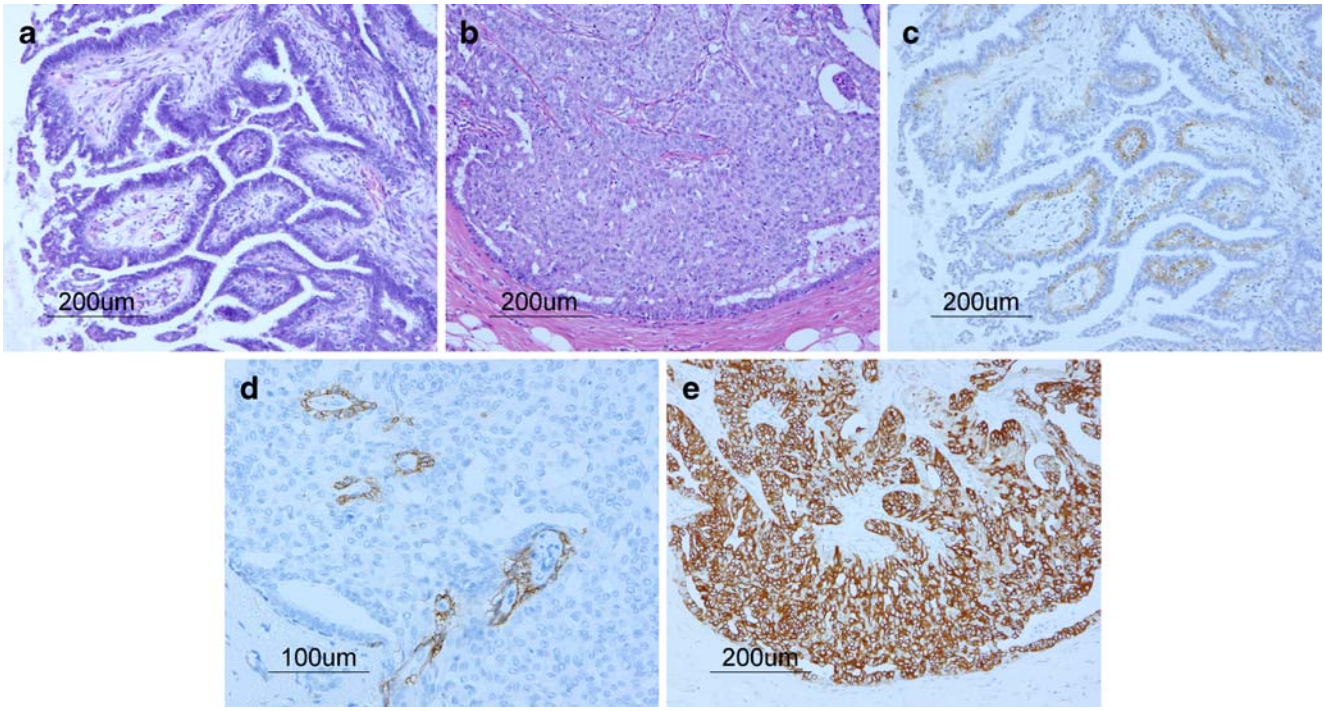

Fig. 2 Intraductal papilloma. **a** Nonsolid type. **b** Solid type intraductal papilloma with usual ductal hyperplasia. **c** Myoepithelial marker (calponin) in nonsolid intraductal papilloma. Myoepithelial cells were present in more than 70% of epithelial–stromal interface. **d** Myoepithelial marker (CD10) in solid intraductal papilloma. Myoepithelial cells were present in more than 70% of epithelial stromal interface. **e** High molecular weight cytokeratin (34βE-12) expression in solid intraductal papilloma

4 contained benign papillomas in the same slides. One SIPC with score 3 also had benign papilloma. All six of the score 4 nonsolid IPCs showed fused tubular and cribriform patterns between the fibrovascular stromal cores (Fig. 3c).

The staining patterns of HMWK are shown in Table 4. Eleven (85%) of the 13 nonsolid IPs, 21 (87.5%) of the 24 nonsolid IPCs, and 16 (76%) of the 21 SIPCs were score 0. Fourteen (93%) of the 15 solid IPs were score 4 (Fig. 2e). The remaining solid IP was score 3. In the positive areas, the signals were strong and diffuse with a few scattered negative cells. There was a significant difference in the staining pattern of HMWK between solid IPs and SIPCs ($p<0.01$). However, no difference was seen between nonsolid IPs and nonsolid IPCs ($p=0.811$). Six lesions of IPC (three nonsolid and three solid type) had a small number of HMWK-positive flat cells at the luminal surface. Three of such cases had the myoepithelial score 4, and the other three cases had score 0.

The staining patterns of neuroendocrine markers are shown in Table 5. All cases of IP were score 0. Twenty (83%) of 24 nonsolid IPCs were also score 0. Fourteen (67%) of SIPCs and two (8%) of nonsolid IPCs were score 4 (Fig. 3f). There was a significant difference in the staining pattern of neuroendocrine markers between solid IPs and SIPCs ($p<0.01$).

Discussion

Although a lack of myoepithelial cells in papillary lesions usually indicates malignancy, the presence of myoepithelial cells in a small number of IPCs was reported in several studies [17, 19, 20]. In most of these cases, the myoepithelial cells were less than 10% of epithelial–stromal interface. Tse et al. [23] recently reported that 53% of papillary carcinomas (including invasive carcinomas) showed staining of myoepithelial markers using p63 and CD10. The myoepithelial cells in their cases were also very scanty and discontinuous. However there has not been enough data concerning how many IPCs retain myoepithelial cells. The histological features of IPCs that have an intact myoepithelial layer have not been clarified. Lefkowitz et al. [11] described a histological variety occurring in intracystic papillary lesions. A spectrum of epithelial proliferation can accompany both benign and malignant papillary lesions [21]. However, the relationship between architectural variety and degree of myoepithelial preservation in intraductal papillary lesions has not been clarified. One reason for this lack of clarity seems to be the diagnostic difficulty of such lesions. When myoepithelial cells are present, but at less than 30%, the possibility of DCIS arising in papilloma comes into the differential diagnosis of pure IPC. When

Table 2 Summary of the histological and immunohistochemical features in carcinomas

No.	Pattern	CD10	p63	Calp	CgA	Syn	34β	Papilloma
1	nonsolid (f/c)	0	0	0	0	0	1	(−)
2	nonsolid (f/c)	0	0	0	0	0	0	(−)
3	nonsolid (f/c)	0	0	0	0	0	0	(−)
4	nonsolid (f/c)	3	0	4	0	0	0	(+)
5	nonsolid (f/c)	0	0	4	2	0	0	(+)
6	nonsolid (f/c)	4	2	1	0	0	0	(+)
7	nonsolid (f/c)	0	0	0	0	0	0	(−)
8	nonsolid (f/c)	0	0	0	4	1	0	(−)
9	nonsolid (f/c)	1	0	0	4	4	0	(−)
10	nonsolid (f/c)	0	0	0	0	0	0	(−)
11	nonsolid (f/c)	4	4	N.E.	0	0	0	(+)
12	nonsolid (f/c)	0	0	0	0	0	0	(−)
13	nonsolid (f/c)	0	0	0	0	0	0	(−)
14	nonsolid (f/c)	4	0	0	0	0	0	(−)
15	nonsolid (f/c)	0	0	0	0	0	0	(−)
16	nonsolid (f/c)	4	4	4	0	1	0	(+)
17	nonsolid (pap)	0	0	0	0	0	0	(−)
18(=1)	nonsolid (pap)	0	0	0	0	0	2	(−)
19	nonsolid (pap)	0	0	0	0	0	2	(−)
20(=3)	nonsolid (pap)	0	0	0	0	0	0	(−)
21(=13)	nonsolid (pap)	0	0	0	0	0	0	(−)
22	nonsolid (pap)	0	0	0	0	0	0	(+)
23(=8)	nonsolid (pap)	0	0	0	0	0	0	(−)
24	nonsolid (pap)	0	0	0	0	0	0	(−)
25	solid	0	0	0	4	2	4	(−)
26	solid	0	0	0	4	0	0	(−)
27	solid	0	3	0	4	4	0	(−)
28	solid	0	0	0	1	0	0	(−)
29	solid	0	0	0	0	0	0	(−)
30	solid	0	0	0	4	1	1	(−)
31	solid	0	0	0	0	0	0	(−)
32	solid	1	2	4	4	4	0	(−)
33	solid	4	4	1	4	4	0	(+)
34	solid	4	4	4	4	4	0	(−)
35	solid	0	0	0	0	2	4	(+)
36	solid	3	0	4	2	4	0	(+)
37	solid	3	0	3	2	4	0	(+)
38	solid	4	4	4	3	4	0	(−)
39	solid	0	0	0	4	3	4	(−)
40	solid	0	0	0	4	4	0	(−)
41	solid	0	0	0	0	0	1	(−)
42(=5)	solid	4	1	4	3	4	0	(+)
43(=12)	solid	0	0	0	4	0	0	(−)
44(=15)	solid	0	0	0	0	0	0	(−)
45(=23)	solid	0	0	0	0	0	0	(+)

Calp, calponin; *CgA*, chromogranin A; *Syn*, synaptophysin; *34β*, HMWK (34βE-12); *N.E.*, not evaluated because the fibrovascular stromal core was too narrow and distinction between vessels and myoepithelial cells was difficult; *f/c*, fused tubular and cribriform pattern; *pap*, pure papillary pattern; *papilloma*, presence or absence of an associated papilloma; (+),papilloma was present in the same slide of IPC; (−) papilloma was absent.

myoepithelial cells are present at 30% or more, atypical papilloma comes into the differential diagnosis of pure IPC [12, 18, 21]. Because the histological features of proliferating epithelial cells must also be taken into consideration in such differential diagnosis, histopathological diagnosis of DCIS arising in papilloma and atypical papilloma by routine H&E sections is often subjective and confusing.

In this study, we used only the cases in which the histological diagnosis was straightforward without immunohistochemistry and was agreed to by at least three

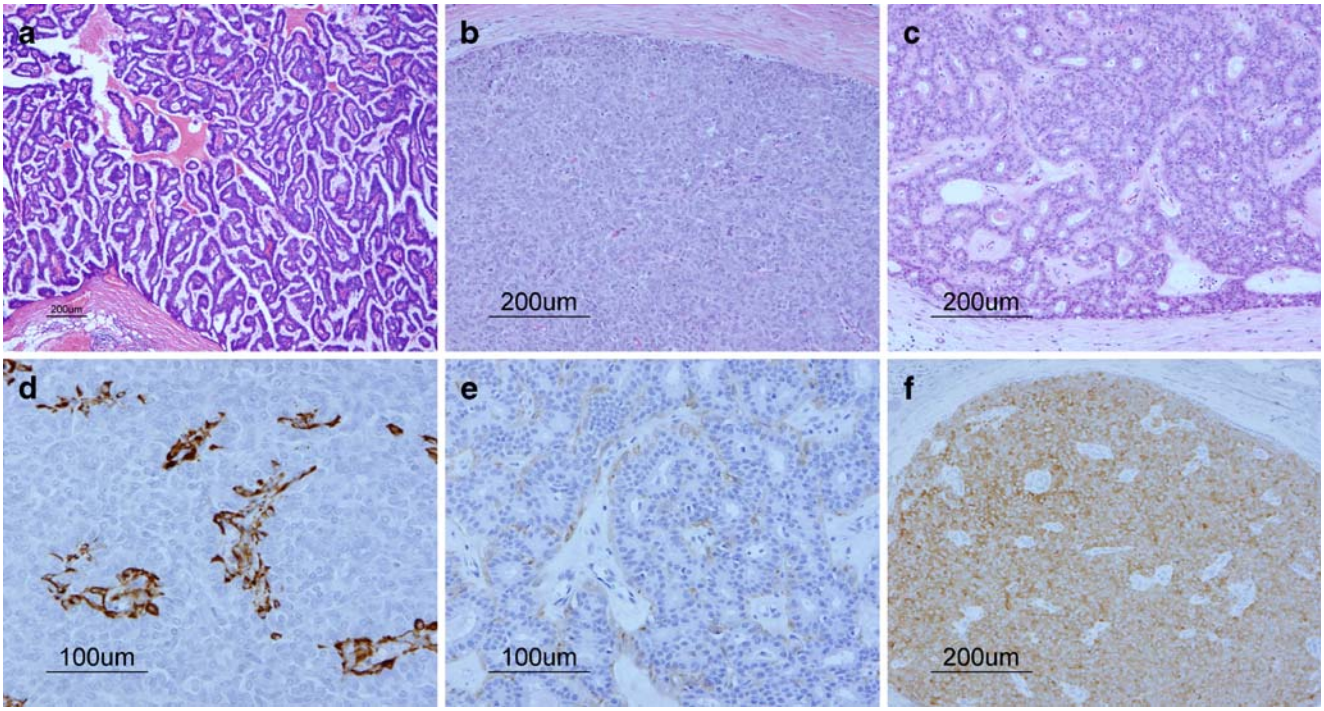

Fig. 3 Intraductal papillary carcinoma. **a** Nonsolid type. **b** Solid intraductal papillary carcinoma. **c** Nonsolid intraductal papillary carcinoma showing fused tubular and cribriform patterns. **d** Myoepithelial marker (calponin) in solid intraductal papillary carcinoma. More than 70% of epithelial–stromal interface is positive. **e** Myoepithelial marker (CD10) in intraductal papillary carcinoma of nonsolid type. Cancer cells are arranged in fused tubular and cribriform patterns. More than 70% of epithelial–stromal interface is positive. **f** Neuroendocrine marker (synaptophysin) expression in solid intraductal papillary carcinoma

pathologists, including two breast subspecialists. We paid great attention to the architectural variety of intraductal papillary lesions to clarify the relationships between a certain architectural pattern and the degree of myoepithelial preservation. Although the myoepithelial marker score was significantly higher in IPs than in IPCs, it should be noted that 6 (25%) of 24 nonsolid IPCs and 6 (29%) of 21 SIPCs retained the intact myoepithelial layer to the same degree as that of IPs. All six cases of the nonsolid IPC with intact myoepithelial layer showed fused tubular and cribriform pattern between the fibrovascular cores. This finding indicates a potential pitfall in the differential diagnosis of intraductal papillary lesions. If only the presence of myoepithelial cells is emphasized as a hallmark of benignity, around 30% of IPCs may be underdiagnosed as benign. The diagnostic difficulty of intraductal papillary lesions because of the architectural complexity seems to be further increased by this paradoxical myoepithelial staining patterns.

SIPC tends to be underdiagnosed as benign because of the low nuclear grade and less monotony of the tumor cells compared to those of other types of DCIS [19]. Special care should be taken when assessing solid intraductal papillary lesions, because the presence of a complete myoepithelial layer is not sufficient to make a benign diagnosis. Although neuroendocrine markers are useful in differentiating SIPC from IP-UDH, 5 (24%) of 21 SIPCs were negative for these markers.

To overcome this diagnostic pitfall, we propose an immunohistochemical panel for the differential diagnosis of solid intraductal papillary lesions. According to the results of the three immunohistochemistry, the following

Table 3 Myoepithelial markers in intraductal papillomas and intraductal papillary carcinomas

Score	0	1	2	3	4	Total number
Nonsolid IP	0	0	1	0	12	13
Solid IP	0	0	1	0	14	15
Nonsolid IPC	17	1	0	0	6	24
Solid IPC	13	0	0	2	6	21

IP, intraductal papilloma; *IPC*, intraductal papillary carcinoma

Table 4 High-molecular-weight cytokeratin in intraductal papillomas and intraductal papillary carcinomas

Score	0	1	2	3	4	Total number
Nonsolid IP	11	0	0	1	1	13
Solid IP	0	0	0	1	14	15
Nonsolid IPC	21	1	2	0	0	24
Solid IPC	16	2	0	0	3	21

IP, intraductal papilloma; *IPC*, intraductal papillary carcinoma

Table 5 Neuroendocrine markers in intraductal papillomas and intraductal papillary carcinomas

Score	0	1	2	3	4	Total number
Nonsolid IP	13	0	0	0	0	13
Solid IP	15	0	0	0	0	15
Nonsolid IPC	20	1	1	0	2	24
Solid IPC	5	1	1	0	14	21

IP, intraductal papilloma; *IPC*, intraductal papillary carcinoma

Table 7 Number of the fulfilled conditions out of the three proposed criteria[a] of malignancy

	0 or 1	2 or 3	Total number
Solid IP	15	0	15
Solid IPC	0	21	21

IP, intraductal papilloma; *IPC*, intraductal papillary carcinoma
[a] Absent myoepithelial cells, negative for high molecular weight cytokeratin, and positive for neuroendocrine marker.

conditions were seen significantly more frequently in SIPCs than in solid IPs: (1) absent myoepithelial cells, (2) negative for HMWK, and (3) positive for neuroendocrine marker. Based on these results, we set a tentative cut-off index to score 1 (10%) for each marker. With this cut-off index, we classified each staining result as negative or positive. The combination of the three staining patterns of solid IPs and SIPC are shown in Table 6. All 21 SIPCs fulfilled at least two of the three conditions mentioned above. On the other hand, the 15 solid IPs lacked all three conditions (Table 7). Based upon the combination of staining patterns of three markers, we propose provisional criteria for the likelihood of malignancy. If a solid intraductal papillary lesion fulfills at least two of the following three criteria, the lesion is considered SIPC: (1) Myoepithelial cells are less than 10% of the epithelial–stromal interface of intraluminal proliferating component; (2) HMWK is negative (<10%); and (3) the neuroendocrine marker is positive(>10%). Using these criteria, all 36 solid intraductal papillary lesions were properly classified as benign or malignant. Thus, the combination of myoepithelial marker, HMWK, and neuroendocrine markers is a useful immunohistochemical panel for diagnosing solid intraductal papillary lesions. To minimize the possibility of false negative results, it is reasonable to use several different antibodies for one marker.

This immunohistochemical panel was not always contributory to the diagnosis of nonsolid intraductal papillary lesions. In pure papillary type lesions, the presence of myoepithelial layer alone could be a good hallmark of benignity. However, in IPCs with fused tubular and cribriform pattern, myoepithelial cells could not always be a hallmark of benignity. Six (35%) of nonsolid IPCs with fused tubular and cribriform pattern had almost complete myoepithelial layer. Because both HMWK and neuroendocrine markers were negative in most of the nonsolid IPs and the nonsolid IPCs, immunohistochemistry seems to play little role in the differential diagnosis of this kind of nonsolid intraductal papillary lesions. It is interesting that five (83%) of six nonsolid IPCs with complete myoepithelial layers were accompanied by benign peripheral papilloma. In one of these five lesions, ducts having a spectrum of benign, atypical and malignant lesions were identified. At least some of this type of IPC may arise within or have a close association with preexistent benign peripheral papilloma. This speculation was also discussed by Ali-Fehmi et al. [1]. The presence of complete myoepithelial layer in DCIS arising within preexistent papilloma resembles the common presence of myoepithelial layer at the periphery of the duct and lobules involved by usual DCIS [6].

Six (24%) of twenty-one solid IPCs also had benign papilloma in the same slide, and 4(67%) of these showed positive myoepithelial and neuroendocrine markers. Therefore, some cases of SIPC may also arise within or have a close association with benign peripheral papilloma, although the frequency is less than that of nonsolid IPC. The presence of myoepithelial layer in SIPC may be explained by another mechanism. The neoplastic cells of SIPC may have the ability to induce non-neoplastic myoepithelial cells (like putting up scaffolding) around the epithelial–stromal interface. In nude mice, breast cancer cell line that can produce myoepithelial cells at the stromal–epithelial junction was established [7]. The cancer-derived myoepithelial cells had morphological and immunohistochemical similar-

Table 6 High-molecular-weight cytokeratin, neuroendocrine markers, and myoepithelial markers in intraductal papillomas with solid ductal hyperplasia and solid intraductal papillary carcinomas

	H+E−M+	H+E−M−	H−E+M+	H−E+M−	H−E−M−	H−E−M+	H+E+M−	H+E+M+	Total number
Solid IP	15	0	0	0	0	0	0	0	15
Solid IPC	0	0	8	4	6	0	3	0	21

IP, intraductal papilloma; *IPC*, intraductal papillary carcinoma; *H*, high-molecular-weight cytokeratin (34βE-12); *E*, neuroendocrine marker; *M*, myoepithelial marker; + indicates a score of at least 2; − indicates a score of 1 or 0.

ities to normal myoepithelial cells, but they lacked the ability to interact with luminal epithelial cells for polarity and deposition of certain basement membrane material [7]. The myoepithelial cells seen in the SIPCs in our study might be cancer-derived myoepithelial cells which are morphologically normal but functionally abnormal.

Acknowledgements This study was supported by a Grant-in-Aid for Cancer Research from the Ministry of Health, Labor and Welfare, Japan and a Grant-in-Aid for Clinical Research from the National Hospital Organization.

References

1. Ali-Fehmi R, Carolin K, Wallis T, Visscher DW (2003) Clinicopathologic analysis of breast lesions associated with multiple papillomas. Human Pathol 34:234–239
2. Boecker W, Buerger H, Schmitz K, Ellis IA, van Diest PJ, Sinn HP, Geradts J, Diallo R, Poremba C, Herbs H (2001) Ductal epithelial proliferations of the breast: biological continuum? Comparative genomic hybridization and high-molecular-weight cytokeratin expression patterns. J Pathol 195:415–421
3. Capella C, Eusebi V, Mann B, Azzopardi JG (1980) Endocrine differentiation in mucoid carcinoma of the breast. Histopathology 4:613–630
4. Diallo R, Schaefer H, Poremba C, Shivazi N, Willmann V, Buerger H, Dockhorn-Dworniczak B, Boecker W (2001) Monoclonality in normal epithelium and in hyperplastic and neoplastic lesions of the breast. J Pathol 193:27–32
5. Douglas-Jones A, Shah V, Morgan J, Dallimore N, Rashid M (2005) Observer variability in the histopathological reporting of core biopsies of papillary breast lesions is reduced by the use of immunohistochemistry for CK5/6, calponin and p63. Histopathology 47: 202–208
6. Going JJ (2003) Stages on the way to breast cancer. J Pathol 199:1–3
7. Gudjonsson T, Rønnov-Jessen L, Villadsen R, Rank F, Bissell MJ, Petersen OW (2002) Normal and tumor-derived myoepithelial cells differ in their ability to interact with luminal breast epithelial cells for polarity and basement membrane deposition. J Cell Sci 115:39–50
8. Hill CB, Yeh IT (2005) Myoepithelial cell staining patterns of papillary breast lesions. From intraductal papillomas to invasive papillary carcinomas. Am J Clin Pathol 123:36–44
9. Ichihara S, Fujimoto T, Hashimoto K, Moritani S, Hasegawa M, Yokoi T (2007) Double immunostaining with p63 and high-molecular-weight cytokeratins distinguishes borderline papillary lesions of the breast. Pathol Int 57:126–132
10. Jarasch ED, Nagle RB, Kaufmann M, Maurer C, Böcker W (1988) Differential diagnosis of benign epithelial proliferations and carcinomas of the breast using antibodies to cytokeratins. Human Pathol 19:276–289
11. Lefkowitz M, Usar CM, Lefkowitz W, Wargotz ES (1994) Intraductal(intracystic) papillary carcinoma of the breast and its variants: a clinicopathological study of 77 cases. Human Pathol 25:802–809
12. MacGrogan G, Tavassoli FA (2003) Central atypical papillomas of the breast: a clinicopathological study of 119 cases. Virchows Arch 443:609–617
13. Maluf HM, Koerner FC (1995) Solid papillary carcinoma of the breast. A form of intraductal carcinoma with endocrine differentiation frequently associated with mucinous carcinoma. Am J Surg Pathol 19:1237–1244
14. Maluf HM, Zukerberg LR, Dickersin GR, Koerner FC (1991) Spindle-cell argyrophilic mucin-producing carcinoma of the breast. Histological, ultrastructural, and immunohistochemical studies of two cases. Am J Surg Pathol 15:677–686
15. Moritani S, Kushima R, Sugihara H, Bamba M, Kobayashi TK, Hattori T (2002) Availability of CD10 immunohistochemistry as a marker of breast myoepithelial cells on paraffin sections. Mod Pathol 15:397–405
16. Nassar H, Qureshi H, VolkanAdsay N, Visscher D (2006) Clinicopathologic analysis of solid papillary carcinoma of the breast and associated invasive carcinomas. Am J Surg Pathol 30:501–507
17. Papotti M, Gugliotta P, Eusebi V, Bussolati G (1983) Immunohistochemical analysis of benign and malignant papillary lesions of the breast. Am J Surg Pathol 7:451–461
18. Purcell CA, Norris HJ (1998) Intraductal proliferations of the breast: a review of histologic criteria for atypical intraductal hyperplasia and ductal carcinoma in situ, including apocrine and papillary lesions. Ann Diagn Pathol 2:135–145
19. Rabban JT, Koerner FC, Lerwill ME (2006) Solid papillary carcinoma in situ versus usual ductal hyperplasia in the breast: a potentially difficult distinction resolved by cytokeratin5/6. Human Pathol 37:787–793
20. Raju UB, Zarbo RJ, Crissman JD (1989) Papillary neoplasm of the breast: Immunohistochemically defined myoepithelial cells in the diagnosis of benign and malignant papillary breast neoplasms. Mod Pathol 2:569–576
21. Tavassoli FA (1999) Papillary lesions. In: Pathology of the breast, 2nd edn. McGraw-Hill, New York, NY, pp 325–371
22. Tavassoli FA, Devilee P (eds) (2003) World Health Organization Classification of Tumours. Pathology and genetics of tumours of the breast and female genital organs. IARC, Lyon, pp 76–80
23. Tse GM, Tan PH, Lui PCW, Gilks B, Poon CSP, Ma TKF, Law BKB, Lam WWM (2006) The role of immunohistochemistry for smooth muscle actin, p63, CD10 and CK14 in the differential diagnosis of papillary lesions of the breast. J Clin Pathol 12:(Epub ahead of print)

Virchows Arch (2007) 450:549–557
DOI 10.1007/s00428-007-0406-7

ORIGINAL ARTICLE

Claudin expression in pancreatic endocrine tumors as compared with ductal adenocarcinomas

Katalin Borka · Péter Kaliszky · Erzsébet Szabó · Gábor Lotz · Péter Kupcsulik · Zsuzsa Schaff · András Kiss

Received: 17 October 2006 / Revised: 12 March 2007 / Accepted: 13 March 2007 / Published online: 12 April 2007
© Springer-Verlag 2007

Abstract Altered expression of recently described claudins (CLDNs) as members of tight junction (TJ) transmembrane proteins was noted in several malignancies. We aimed to analyze protein and messenger RNA (mRNA) expressions of different CLDNs in human pancreatic endocrine tumors (PET) and ductal adenocarcinomas. A total of 45 formalin-fixed, paraffin-embedded samples were studied. Immunohistochemistry and real-time reverse transcriptase polymerase chain reaction analysis were carried out for quantification of CLDN 1, -2, -3, -4, and -7 expressions. Normal acini and ducts showed strong CLDNs 1, -3, -4, and -7 and scattered CLDN 2 protein expressions, while Langerhans islands revealed only CLDN 3 and -7 expressions. CLDN 2 expression was found in the half of ductal adenocarcinomas, while the vast majority of endocrine tumors were negative. CLDN 1, -4, and -7 immunohistochemistry was positive in all adenocarcinomas, whereas endocrine tumors were completely negative for CLDNs 1 and -4. CLDN 3 and -7 proteins were detected in all endocrine tumors, while CLDN 3 in ductal adenocarcinomas was negative. The mRNA expression of CLDNs showed differences between endocrine tumors and ductal adenocarcinomas, similar as found for protein expression. Our findings support that PET and ductal carcinomas are specifically characterized by different expression pattern of CLDNs. High expressions of CLDN 3 in endocrine tumors and CLDN 4 in ductal carcinomas might attract them as targets for adjuvant therapy.

Keywords Endocrine pancreatic tumor · Pancreatic adenocarcinoma · Claudin · Tight junction · Immunohistochemistry

Schaff and Kiss have equally contributed to this study.

K. Borka · E. Szabó · G. Lotz · Z. Schaff (✉) · A. Kiss
2nd Department of Pathology, Semmelweis University,
Üllői út 93,
1091 Budapest, Hungary
e-mail: schaff@korb2.sote.hu

P. Kaliszky · P. Kupcsulik
1st Department of Surgery, Semmelweis University,
Üllői út 78,
1082 Budapest, Hungary

Introduction

Claudins (CLDNs) are recently identified structural and functional components of the tight junction (TJ) barrier and are responsible for maintaining cell polarity, cellular arrangement, adhesion, and paracellular fluid transport. At least two transmembrane CLDN molecules (generally more) characterize each cell and tissue type. The heterogenous CLDN types are copolymerized to form individual TJs [7]. Members of the CLDN family are involved during carcinogenesis and may play an important role in influencing tumor progression and invasion. Several studies have described changes in expression of these molecules during carcinogenesis, as in breast [17, 41], prostate [20], ovarian [29], gastric [2, 18, 38], biliary tract cancers [19], and several other tumors [8, 9, 34–36]. Beneath chemotherapy and radiotherapy clinical trials using molecular-targeted therapy at the molecular level (epidermal growth factor receptor, vascular endothelial growth factor, and platelet-derived growth factor inhibitors) are new strategies in adenocarcinoma patients [3, 11, 14, 24]. However, few information are available on endocrine neoplasms about cell adhesion molecules [6, 15]. Out of the 24 types, CLDNs 3 and -4 have been described as receptors for the cytotoxic Clostridium perfringens enterotoxin (CPE) [39]. The cytotoxic effect of CPE has been observed in pancreatic

cancer cells, supporting the use of CLDN 4 as target for novel therapy for pancreatic cancers [21] and CLDNs 3 and -4 for prostate cancer [20]. Based on the data that target-oriented therapy on tumors overexpressing CLDN 4 might be a possibility in the future, the question arises as to how it would affect the endocrine component of the pancreas and/or PET. It is expected that the cell adhesion properties including CLDN expression of the exocrine and endocrine pancreatic tumors differ from each other.

Contrary to the high expression of CLDN 4 in pancreatic adenocarcinomas, no data are available on the expression of CLDNs in pancreatic endocrine neoplasms, which represent 1 to 2% of all pancreatic tumors. Aside from insulinomas, which metastasize in only 10% of cases, the majority of endocrine tumors (gastrinomas, glucagonomas, vasoactive intestinal peptide tumors, somatostatinomas, or nonfunctioning tumors) are malignant [1, 13, 16, 30, 46].

A different CLDN pattern might be detected in the tumors of different biological behavior, some of them might be used as a therapeutic target [20, 21].

Data on the expression of different CLDNs in pancreatic endocrine tumors (PET) are not available contrary to ductal adenocarcinomas, where CLDNs 1, -3, -4 have been already studied [21, 22, 24]. However, tissue localization of other types of CLDN, as of CLDNs 2 and -7, in ductal carcinomas has not been described yet. The lack of data initiated the present study to examine the CLDN expression in PET and compare the pattern to adenocarcinomas. On the other hand, the question has been raised whether the CLDN pattern changes during tumor formation and with increasing malignancy.

The aim of this study was to examine the tissue localization and messenger RNA (mRNA) expression pattern of CLDNs in endocrine pancreatic cells, to compare these with the expression panel of the PET and CLDN expression between PET and pancreatic ductal adenocarcinomas.

Materials and methods

Samples

Retrospective series of formalin-fixed, paraffin-embedded blocks were obtained from the archive of our department with the permission of the Regional Ethical Committee of the Semmelweis University of Budapest (#172/2003).

Samples from five normal pancreas were studied to analyze the expression pattern of different CLDNs in nontumorous tissue. Pancreatic adenocarcinoma tissue samples were obtained from 20 patients who underwent surgery for surgically resectable disease. The mean age of the adenocarcinoma patients was 60, with a range of 31 to 84 years (13 men, 7 women). Eighteen adenocarcinoma cases were localized in the head of the pancreas, while two tumors were identified in the tail. The tumor samples were classified according to the pathological tumor–node–metastasis classification of pancreatic tumors. The majority of adenocarcinomas infiltrated the duodenal wall (pT3: 11), while eight did not (pT1: 2, pT2: 6). One of the 20 tumors was found to be extended to the spleen (pT4). Sixty-five percent of the patients had lymph node metastases (13/20) with no organ metastases present at the time of diagnosis. Seventy-five percent (15/20) of the tumors were moderately differentiated (Grade II); however, two tumors were well- (Grade I) and the remaining three poorly (Grade III) differentiated, respectively.

Twenty endocrine tumors were studied, which were localized as follows: head: 8, body: 4, tail: 8. The mean age of these patients was 55 (range from 28 to 78), with 6 men and 14 women comprising the group. According to the WHO classification, 4 endocrine tumors were benign, 11 proved to be borderline, and 5 were malignant tumors. Two benign tumors and three borderline tumors were functional, producing insulin. The others were nonfunctioning tumors. Immunohistochemically, one of the malignant tumors showed positivity with somatostatin and glucagon.

Histology, immunohistochemistry

The pancreatic and tumor tissues were fixed in 10% neutral buffered formalin for 24 h, followed by paraffin embedding, then cut and stained with hematoxylin eosin to establish the diagnosis.

Paraffin-embedded, 3- to 4-μm thick sections were used for immunohistochemistry. The slides were treated for 30 min with target retrieval solution (DAKO, Glostrup, Denmark) in a microwave oven, followed by incubation with the primary antibodies (Zymed, San Francisco, CA, USA) in 1:80 dilution at room temperature for 1 h. CLDNs 2 and -4 antibodies were monoclonals, CLDNs 1, -3, and -7 were polyclonal antibodies purified from rabbit antiserum. Avidin–biotin–peroxidase technique (ABC system, DAKO) with diaminobenzidin was used for visualization and counterstained with hematoxylin. For negative controls, the appropriate antibody was omitted, and either the antibody diluent alone or isotype-matched IgG serum was used. The reactions were processed and revealed no signal. Positive controls recommended by the manufacturer (Zymed) were used to confirm correct immunohistochemical staining for CLDNs, that is, normal skin epithelium for CLDN 1, normal colon mucosa for CLDNs 2, -3, and -4, and normal ductal cells in breast for CLDN 7.

Scoring for semiquantitative analysis was independently evaluated by three pathologists (KB, ZS, AK), and discrepancies were resolved by consensus. Ten randomly selected areas of each slide were analyzed using high-power field

objective (×40) with 100 cells counted per field. Reactions were scored positive where linear membrane staining was seen, except for CLDN 2, where cytoplasmic reaction was detected. Immunoreaction was evaluated by the percentage of cells staining positively. The following values were given for semiquantitative evaluation: 0 (0–5% positivity), 1 (6–20% positivity), 2 (21–40% positivity), 3 (41–60% positivity), 4 (61–80% positivity), and 5 (81–100% positivity). The tumors scored by 1–5 were regarded as positive, while 0 scores were handled as negative.

Ductal adenocarcinomas and endocrine pancreatic tumors were compared regarding CLDN expression. Further, CLDN scores characterizing different grades in ductal carcinomas and benign, borderline, and malignant endocrine tumors were statistically evaluated as well. Statistical analysis of the immunohistochemical scores was achieved by the Mann–Whitney *U* test. Probability values of $p<0.05$ were accepted as being significant.

Real-time reverse transcriptase polymerase chain reaction

RNA isolation

Total RNA from eight exocrine and eight endocrine formalin-fixed, paraffin-embedded tumor tissues was isolated with High Pure RNA Paraffin Kit (Roche, Indianapolis, IN, USA). Samples were microdissected to select the areas containing purely exocrine or endocrine pancreatic tumors. Depending on the size of the dissected area, two to eight 5-μm-thick sections were cut from each tissue block. Proteinase K digestion time was 16 h for each sample. All purification were performed in accordance with the manufacturer's protocol. After total RNA isolation, samples were kept at -80°C until use. Total RNA integrity was verified as described previously [8, 26].

Reverse transcription of RNA

Total RNA (500 ng) was reverse transcribed for 50 min at 42°C in 30 μl with MulV reverse transcriptase (Applied Biosystems, Foster City, CA, USA) in the presence of RNAse inhibitor (Applied Biosystems) using random hexamers (Applied Biosystems).

Real-time quantitative RT-PCR

Real-time polymerase chain reaction (PCR) reaction was performed with 2 μl complementary DNA (cDNA) template in a total volume of 25 μl, using the ABI Prism 7000 Sequence Detection System (Applied Biosystems). Each PCR was conducted in 25 μl volume of SYBR Green Supermix (Bio-Rad, Hercules, CA, USA, 1708851). The primer sequences used to detect members of the CLDN family were the following: CLDN 1 (GI: 9966780), forward 5′-GCG CGA TAT TTC TTC TTG CAG G-3′, (378–399), reverse 5′-TTC GTA CCT GGC ATT GAC TGG-3′ (470–490); CLDN 2 (GI: 9966780), forward 5′-CTC CCT GGC CTG CAT TAT CTC-3′ (273–293), reverse 5′-ACC TGC TAC CGC CAC TCT GT-3′ (344–363); CLDN 3 (GI: 21536298), forward 5′-CTG CTC TGC TGC TCG TGT CC-3′ (732–751), reverse 5′-TTA GAC GTA GTC CTT GCG GTC GTA G-3′ (836–860); CLDN 4 (GI: 14790131), forward 5′-GGC TGC TTT GCT GCA ACT GTC-3′ (741–761), reverse 5′-GAG CCG TGG CAC CTT ACA CG-3′

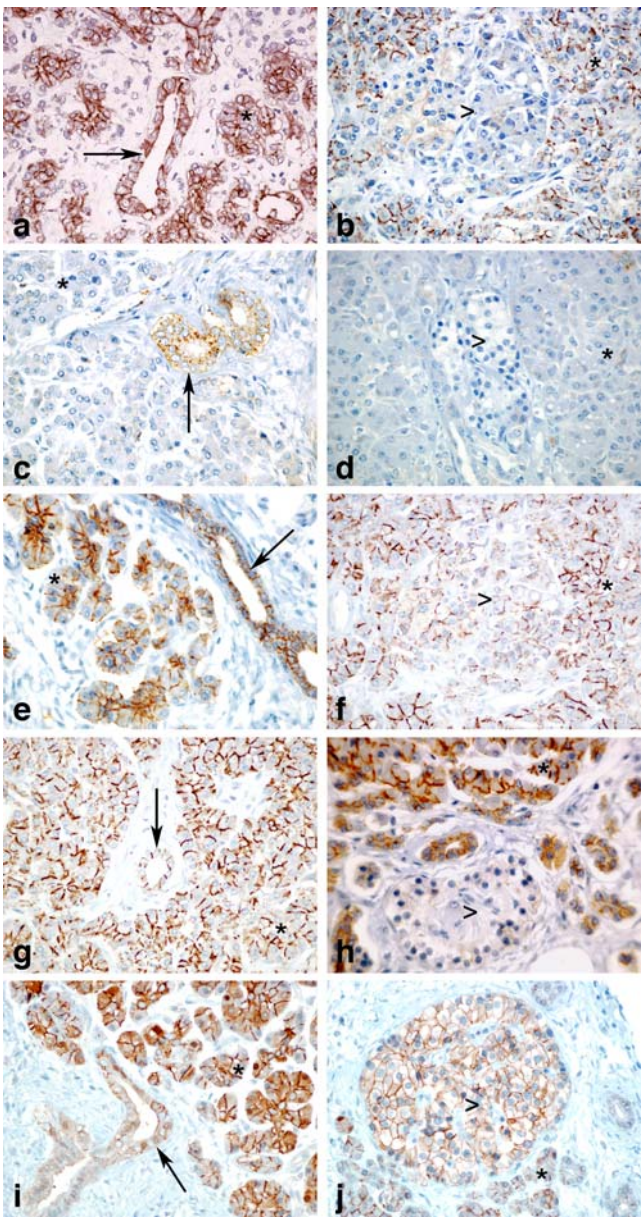

Fig. 1 Immunohistochemical staining for CLDNs in normal ducts, exocrine acini, and Langerhans islands of pancreas. Panels **a** and **b** show CLDN 1 staining, panels **c**–**j** indicate CLDN 2, -3, -4 and -7 stainings, respectively. *Asterisk* marks the acini; *arrowhead* indicates endocrine islands; *arrow* shows the exocrine ducts. (×600)

(741–761); CLDN 7 (GI: 24496764), forward 5′-CAT CGT GGC AGG TCT TGC C-3′ (813–831), reverse 5′-GAT GGC AGG GCC AAA CTC ATA C-3′ (909–930); GAPDH (GI: 7669491), forward 5′-CAT GGG TGT GAA CCA TGA GAA GT-3′ (590–611), reverse 5′-TGG ACT GTG GTC ATG AGT CCT T-3′ (471–493).

Real-time PCR reaction was performed in duplicates in 96 well plates, for 2 min at 95°C for initial denaturing, then 40 cycles at 95°C for 20 s, at 63°C for 30 s, and at 72°C for 1 min.

Data analysis and statistical evaluation were performed by REST (expression software tool, http://www.wzw.tum.de/gene-quantification) [27], using the average of GAPDH as reference gene for relative quantification.

Results

Immunohistochemistry

Normal pancreatic tissue CLDN immunoreaction was predominantly localized to the cell membrane as linear staining except for CLDN 2, which showed granular cytoplasmic reaction. CLDN 1 protein was found in normal acini and pancreatic ducts; however, the endocrine islands were negative (Fig. 1a,b). CLDN 2 reaction was scattered positive in the ducts, on the other hand, acini and Langerhans islands were negative (Fig. 1c,d). CLDN 3 protein was detected in the exocrine glands, ducts, and endocrine cells as well (Fig. 1e,f). CLDN 4 protein was expressed in pancreatic ducts as well as in the acini; however, endocrine islands were negative (Fig. 1g,h). CLDN 7 reaction gave positivity in the pancreatic ducts, the acini, and the Langerhans islands, too (Fig. 1i,j). In summary, CLDN 1, -2, -3, -4, and -7 proteins were detected in ductal cells, the endocrine cells expressed CLDNs 3 and -7 only, whereas acinar cells revealed positivity for CLDNs 1, -3, -4, and -7 (Table 1).

Exocrine pancreatic adenocarcinoma The intratumoral distribution of positive cells did not show major variation within one tumor. CLDNs 1 and -4 definitely showed high, diffuse expression in all adenocarcinomas (Fig. 2a,g). Intracellular granular staining was noted for CLDN 2 in 45% of ductal adenocarcinomas (9/20; Fig. 2c). No CLDN 3 was detected (Fig. 2e). CLDN 7 was positive in all cases with focal, variable positivity (Fig. 2i). CLDN 4 had the highest expression in these tumors. CLDN expression scores representing different grades of ductal adenocarcinomas were compared. There was no statistically significant difference between Grade I, II, and III tumors in CLDN expression (p values range 0.0578–0.8805).

Table 1 The expression pattern of different claudins in pancreatic tissue

Claudins	Exocrine cells		Endocrine cells
	Acinus	Ductus	
CLDN 1	Positive	Positive	Negative
CLDN 2	Negative	Positive	Negative
CLDN 3	Positive	Positive	Positive
CLDN 4	Positive	Positive	Negative
CLDN 7	Positive	Positive	Positive

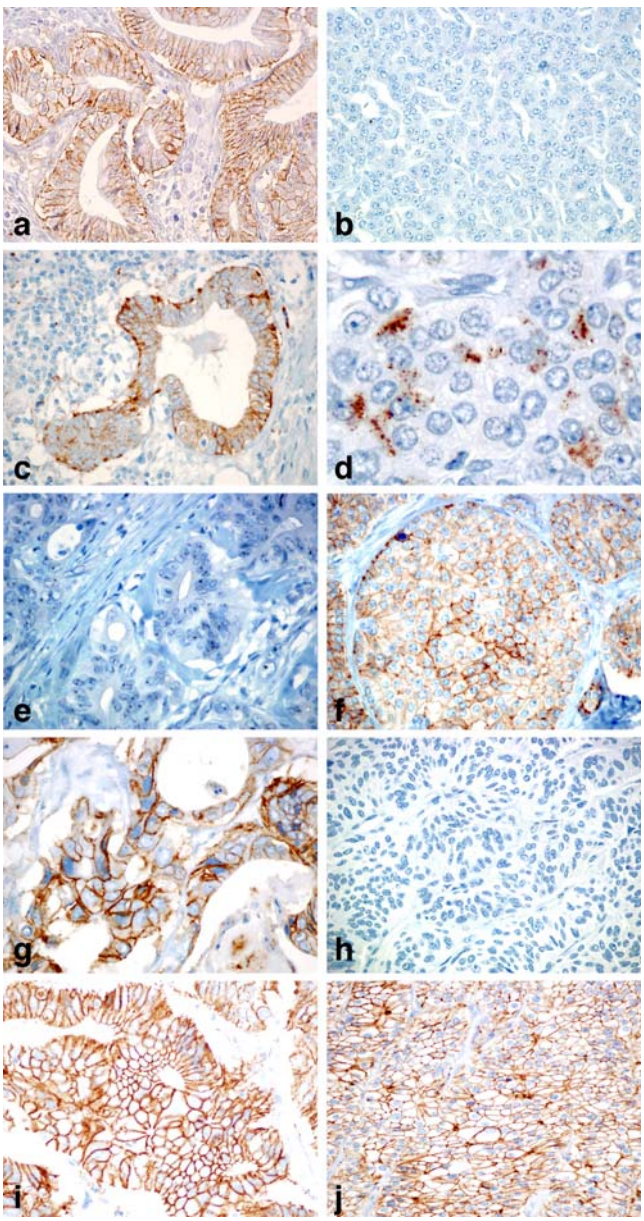

Fig. 2 Immunohistochemical staining for CLDNs in endocrine tumors and in exocrine adenocarcinomas of the pancreas. Panels **a** and **b** show staining for CLDN 1, panels **c** and **d** for CLDN 2, panels **e** and **f** for CLDN 3, panels **g** and **h** for CLDN 4, and panels **i** and **j** for CLDN 7, respectively. (**a**–**c**, **e**–**j** ×600; **d** ×1,000)

Endocrine tumors Similarly to ductal adenocarcinomas, the intratumoral distribution of positive cells did not show major variation within one tumor. CLDN 1 and -4 immunoreactions proved to be negative in all endocrine tumors (Fig. 2b,h); however, only one endocrine tumor (1/20) was positive for CLDN 2 (Fig. 2d). On the other hand, high CLDN 3 and -7 expressions were detected in all endocrine tumors (Fig. 2f,j). No statistically significant differences were detected between benign, borderline, and malignant endocrine tumors. However, the mean and ±SEM of CLDN 3 and -7 scores were increasing with malignant degree.

The distribution of individual immunohistochemistry scores for CLDNs 1, -2, -3, -4, and -7 in pancreatic ductal adenocarcinomas and endocrine tumors is illustrated in Fig. 3. CLDNs 1 and -4 showed the highest reaction in pancreatic ductal adenocarcinomas, while positivity for CLDNs 2 and -7 was less frequent. The scores evaluating the expression of CLDN 7 in endocrine tumors was higher, compared with CLDN 3. The reaction for CLDN 7 in endocrine tumors was higher as compared with adenocarcinomas.

The scores for immunohistochemistry regarding CLDN expressions in ductal adenocarcinomas vs endocrine tumors were compared by using the Mann–Whitney *U* test (Table 2). A significantly higher percentage of endocrine tumor cells expressed CLDNs 3 and -7, while a considerably higher percentage of adenocarcinomas expressed CLDNs 1, -2, and -4 (Fig. 4).

mRNA expression of CLDNs 1, -2, -3, -4, and 7 detected by real-time RT-PCR

Upon comparing ductal adenocarcinomas and endocrine carcinomas, mRNA expression analysis of representative and dissected samples revealed the mRNA expression of individual CLDNs to reflect changes parallel with the protein expression of these tumors. GAPDH as reference gene was used for relative quantification to analyze CLDN expression in the tumors (Fig. 5). Real-time PCR analysis revealed that CLDN 1, -2, and -4 mRNA expressions were higher in the ductal adenocarcinomas compared with the endocrine ones. The increased CLDN 1, -2, and -4 mRNA expressions in exocrine tumors were found to be parallel with the positive immunohistochemical staining. Coinciding with the immunohistochemical results, endocrine tumors showed increased CLDN 3 (2.75×) and -7 mRNA (3,678×) expressions compared with adenocarcinomas. CLDN 4 mRNA expression was higher in ductal adenocarcinomas upon comparison with endocrine tumors (2,796×), which is in agreement with the immunohistochemical results.

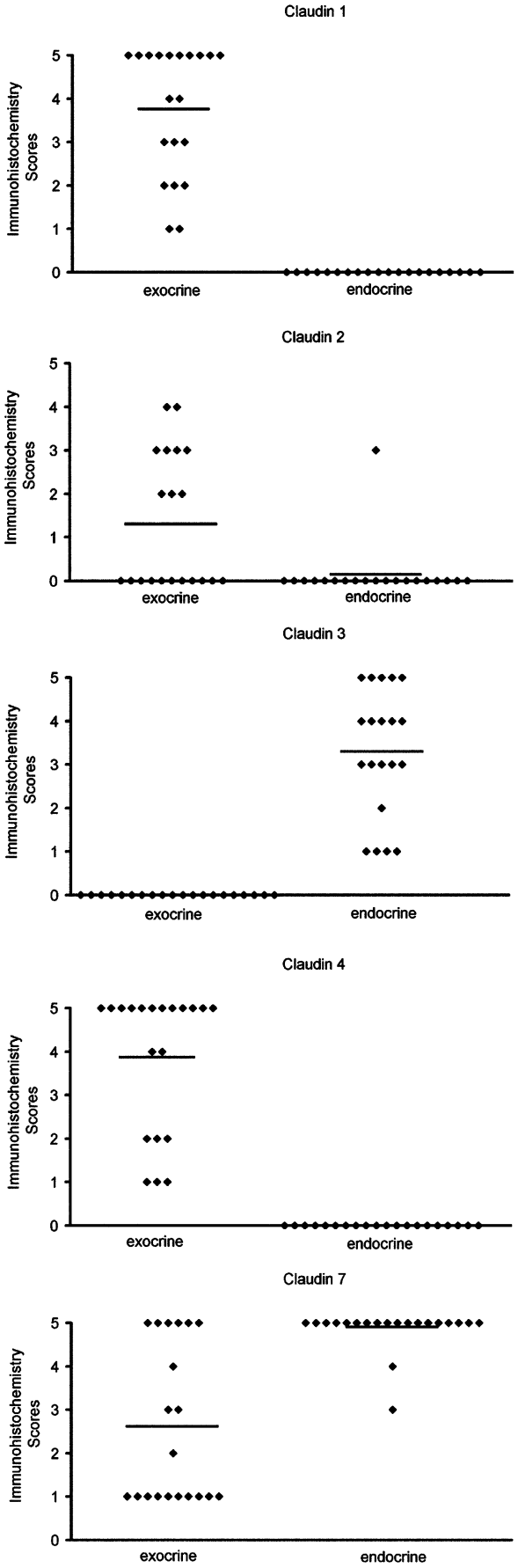

Fig. 3 Comparison of CLDN expressions by immunohistochemistry in exocrine and endocrine pancreatic tumors. *Right lines* indicate the mean value of the group

Table 2 Semiquantitative analysis of immunohistochemical stainings in exocrine adenocarcinomas and endocrine pancreas tumors

	Exocrine	Endocrine	*p* values of comparison
CLDN 1	3.8±0.3	0.0±0.0	<0.0001
CLDN 2	1.3±0.4	0.2±0.2	0.0268
CLDN 3	0.0±0.0	3.3±0.3	<0.0001
CLDN 4	3.9±0.4	0.0±0.0	<0.0001
CLDN 7	2.6±0.4	4.9±0.1	0.0003

Values expressed as mean±SE of CLDN scores. Pairwise comparison made by Mann–Whitney *U* test.
CLDN Claudin; *p* significance
$p<0.05$

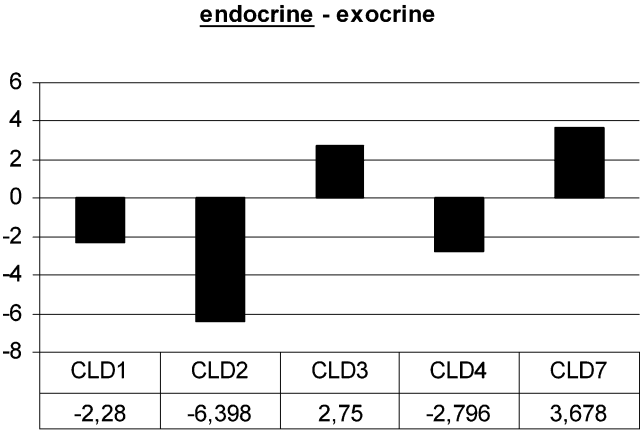

Fig. 5 mRNA expression analysis of exocrine and endocrine tumors. Data indicate the fold change differences in CLDN expressions in the underlined group as compared with the other group (endocrine tumors are compared with exocrine tumors). Relative quantification was carried out using the mean of GAPDH as reference genes (example: CLDN 1 is upregulated in the adenocarcinomas as compared with the endocrine tumors 2.28 times). *Underline* means downregulated, *p* values: CLDN 1: 0.158, CLDN 2: 0.116, CLDN 3: 0.343, CLDN 4: 0.107, CLDN 7: 0.7

Discussion

Pancreatic adenocarcinoma is listed among the most fatal types of cancers owing to the missing early symptoms, which therefore result in late diagnosis and the lack of effective therapies. On the other hand, endocrine pancreatic tumors possess uncertain clinical behavior regarding local infiltration and metastasis. Comprehensive studies are needed for better understanding and addressing of the cellular mechanisms and pathway of tumorigenesis in these two tumor types of the pancreas.

Cell adhesion molecules, including intercellular junctional complexes, are critical for the maintenance of cellular integrity, polarity, and even signal transduction. Disturbance of maintenance of cellular adhesion might play role in carcinogenesis by loss of cell–cell interaction, leading to increased cell motility [45].

Overexpression may be an attempt of tumor cells to overcompensate the loss of cell adhesion due to other adhesion molecules; however, another function in carcinogenesis unrelated to cell adhesion cannot be ruled out [10].

The cell–cell junctional complexes, including TJs, are composed of different molecules belonging to distinct protein families [23]. A new family of transmembrane TJ proteins called CLDNs was discovered in 1998 [7, 43]. To date, 24 different CLDNs have been identified. Altered

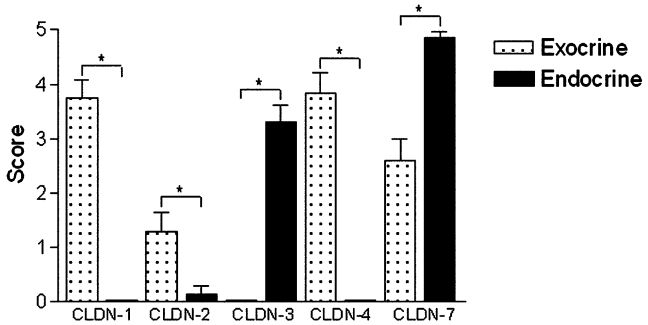

Fig. 4 Bar diagrams illustrating the differences in CLDN expressions detected by immunohistochemistry and evaluated by semiquantitative scoring. *Asterisk* significant difference

expression might change CLDN cellular attachment and cell surface architecture, resulting in aberrant cell–cell interactions that represent a reproducible characteristic of cancer cells, modulated in tumorigenesis by means of unrestricted growth and invasion [32, 44]. In the present study, the expression of different CLDNs in normal pancreas and altered expression pattern in pancreatic adenocarcinomas as well as endocrine tumors were identified.

In human tumor-free pancreas, CLDNs 1, -3, -4, and -7 were expressed in the main and branching ducts, terminal ductules, and acinar cells, whereas CLDN 2 was found only in the ductular components. Others detected CLDN 2 only in junctions of ductal cells and CLDNs 3 and -4 in both ductal and acinar cells in normal rat pancreas [28]. Strong expression of CLDN 1 [33, 42] and CLDN 4 [42] was found in the main and branching ducts, terminal ductules, and acinic cells, but not in endocrine cells.

In pancreatic intraepithelial neoplasia (PanIN), 91% positivity was described for CLDN 4 [22]. In another study, CLDN 1 was observed in the PanIN lesions, but the reaction for CLDN 4 was negative [42]. In adenomas, borderline, noninvasive, and invasive intraductal papillary mucinous neoplasias (IPMNs), a linear increase in the expression of CLDN 4 was detected [31, 42]. On the other hand, higher CLDN 1 expression was seen in adenomas in contrast to the borderline, noninvasive, and invasive tumors, showing negative correlation with histological grade [42]. These results suggest that CLDNs 1 and -4 could be used in the preoperative setting to differentiate between invasive and noninvasive IPMNs and other types of pancreatic carcinomas. Using a cDNA microarray, the

CLDN 4 gene was upregulated in IPMNs such as in "classical" pancreatic carcinomas, similarly as found in our study [40].

CLDNs 3 and -4 are receptors of the CPE, which has cytotoxic effect on pancreatic tumor cells [39]. Binding of CPE to these cancer cells might be a way for antibody-based therapies. There are data indicating that CLDN 3 and -4 protein expressions have important role in metastatic progression. CLDN 4 overexpression was reported in tumors of different histological origin, in prostate cancer [20], intraductal papillary-mucinous tumors of the pancreas [31, 40, 42], ovarian carcinomas [29], breast cancers [41], gastric carcinomas [18, 38], endometrial [34], colon, kidney, lung, thyroid cancers [37], in esophageal adenocarcinomas [8], cervical carcinomas [36], biliary tract cancers [19], as well as in primary and metastatic pancreatic adenocarcinomas [21, 22]. These findings suggest CLDN 4 to be a novel target for adjuvant therapy in pancreatic cancers. In human pancreatic cancer cell lines, CLDN 4 expression was stronger in well-differentiated tumors as compared with poorly differentiated ones. Based on this observation, some authors hypothesized that expression of CLDN 4 could be inversely correlated and might modulate invasion [21].

In another study, CLDNs 1, -3, -4, and -7 were expressed in all investigated pancreatic cancer cell lines by PCR reaction, but CLDN 8 was confined only to one cell line [24]. Hewitt et al. [12] showed high CLDN 3, -4, and -7 expressions by RT-PCR in normal pancreatic tissue and in exocrine tumors of the pancreas, too.

mRNA expression analysis of representative and dissected samples comparing ductal adenocarcinomas and endocrine carcinomas revealed the mRNA expression of certain CLDNs to reflect parallel changes with protein expression of these tumors. CLDN 1, -2, and -4 expressions were higher in exocrine than in endocrine tumors, which differences were detected by immunohistochemical reaction, too.

In correspondence with the literature, all the ductal carcinomas showed membrane positivity with CLDNs 1, -4, and -7, opposite to the endocrine tumors in the present study. In contrast, the endocrine tumors showed high expression of CLDNs 3 and -7. The expression of CLDN 7 was higher in comparison with that of CLDN 3. There are data implying that in neuroendocrine tumors, cell adhesion molecules are implicated in modulating cell growth, and disruption of these adhesive forces might contribute to the tumorigenic process, as in other tumors of different tissue origin [6]. To our knowledge, this is the first report to describe CLDN 3 expression in endocrine pancreatic tumors. The presented results suggest that approaches targeting CLDN 3 might mean new possibilities for future therapy.

Analyzing CLDN expression in tumors representing different grades of ductal adenocarcinomas did not reveal a statistically significant difference between Grade I, II, and III tumors. This set of data indicates that changes in CLDN expression are not associated with pancreatic ductal tumor differentiation. Sato et al. [31], on the other hand, described decreased CLDN 4 expression in noninvasive IPMN in comparison to invasive IPMNs. Poor tumor differentiation is generally related to increased tumor invasiveness and associated with decreased TJs. However, many data suggest that altered CLDN expression in tumor progression often involves increased, overexpressed amount of certain CLDNs, such as CLDN 1 [36], CLDN 4 [19], and CLDN 1 in colon cancer [5]. Statistical analysis did not detect significant differences between benign, borderline, and malignant endocrine tumors either.

The biological role of TJs in Langerhans islet cells is not described yet. Orci et al. [25] has described the presence of TJ in human islet cells. Upregulation of occluding and ZO-1 has been shown during the maturation of neonatal pancreatic islet cells in vitro. Gap junctions have been involved in regulation of insulin secretion [4]. However, besides being involved in normal islet intercellular communication, it is likely that TJs also provide adaptive mechanisms intended to seal and protect islet microdomains against sudden perturbations in extracellular environment. The discovery of exact biological role of CLDNs in pancreatic endocrine and exocrine cells will be the next challenge of the cell adhesion research.

Our findings are supportive of the fact that the combined expression pattern of CLDNs 3, -4, and -7 characterizes and differentiates the two groups of endocrine pancreatic tumors and ductal adenocarcinomas of the pancreas. Further studies are necessary to assess the biological role of these proteins in pancreatic carcinogenesis and tumor progression. High expression levels of CLDN 3 in endocrine tumors—the first time presented in our study—and CLDN 4 in ductal adenocarcinomas already published by others might even make them attractive for future adjuvant target-oriented therapy.

Acknowledgements This work was supported by grants NKFP-1A/002/2004 from the Hungarian Ministry of Health, National Research Development Projects, OTKA T049559 from the National Science Research Foundation, ETT 49/2006 and ETT 156/2006 from the Committee of Health Sciences.

References

1. Arnold R, Rinke A, Schmidt Ch, Hofbauer L (2005) Endocrine tumours of the gastrointestinal tract: chemotherapy. Best Pract Res Clin Gastroenterol 19:649–656
2. Aung PP, Mitani Y, Sanada Y, Nakayama H, Matsusaki K, Yasui W (2006) Differential expression of claudin-2 in normal human tissues and gastrointestinal carcinomas. Virchows Arch 448:428–434

3. Cardenes HR, Chiorean EG, Dewitt J, Schmidt M, Loehrer P (2006) Locally advanced pancreatic cancer: current therapeutic approach. Oncologist 11:612–623
4. Collares-Buzato CB, Carvalho CPF, Furtado AG, Boschero AC (2004) Upregulation of the expression of tight and adherens junction-associated proteins during maturation of neonatal pancreatic islets in vitro. J Mol Histol 35:811–822
5. Dhawan P, Singh AB, Deane NG et al (2005) Claudin-1 regulates cellular transformation and metastatic behavior in colon cancer. J Clin Invest 115:1765–1776
6. Ezzat S, Asa SL (2005) The molecular pathogenetic role of cell adhesion in endocrine neoplasia. J Clin Pathol 58:1121–1125
7. Furuse M, Fujita K, Hiiragi T, Fujimoto K, Tsukita S (1998) Claudin-1 and -2: novel integral membrane proteins localizing at tight junctions with no sequence similarity to occludin. J Cell Biol 141:1539–1550
8. Győrffy H, Holczbauer Á, Nagy P, Szabó Z, Kupcsulik P, Páska C, Papp J, Schaff Z, Kiss A (2005) Claudin expression in Barrett's esophagus and adenocarcinoma. Virchows Arch 447:961–968
9. Halász J, Holczbauer Á, Páska C, Kovács M, Benyó G, Verebély T, Schaff Z, Kiss A (2006) Claudin-1 and claudin-2 differentiate fetal and embryonal components in human hepatoblastoma. Hum Pathol 37:555–561
10. Heinzelmann-Schwarz VA, Gardiner-Garden M, Henshall SM, Scurry J, Scolyer RA, Davies MJ, Heinzelmann M, Kalish LH, Bali A, Kench JG, Edwards LS, Van den Bergh PM, Hacker NF, Sutherland RL, O'Brien PM (2004) Overexpression of the cell adhesion molecules DDR1, claudin 3, and Ep-CAM in metaplastic ovarian epithelium and ovarian cancer. Clin Cancer Res 10:4427–4436
11. Henne-Bruns D, Vogel I, Luttges J, Kloppel G, Kremer B (1998) Ductal adenocarcinoma of the pancreas head: survival after regional versus extended lymphadenectomy. Hepatogastroenterology 45:855–866
12. Hewitt KJ, Agarwal R, Morin PJ (2006) The claudin gene family: expression in normal and neoplastic tissues. BMC Cancer 6:186
13. House MG, Schulick RD (2006) Endocrine tumors of the pancreas. Curr Opin Oncol 18:23–29
14. Jacobs AD (2002) Gemcitabine-based therapy in pancreas cancer: gemcitabine–docetaxel and other novel combinations. Cancer 95 (Suppl):923–927
15. Kaifi JT, Heidtmann S, Schurr PG, Reichelt U, Mann O, Yekebas EF, Wachowiak R, Strate T, Schachner M, Izbiczki JR (2006) Absence of L1 in pancreatic masses distinguishes adenocarcinomas from poorly differentiated neuroendocrine carcinomas. Anticancer Res 26:1167–1170
16. Kloppel G (2003) Tumors of the endocrine pancreas. Pathologe 24:265–271
17. Kominsky SL, Argani P, Korz D, Evron E, Raman V, Garrett E, Rein A, Sauter G, Kallioniemi OP, Sukumar S (2003) Loss of the tight junction protein claudin-7 correlates with histological grade in both ductal carcinoma in situ and invasive ductal carcinoma of the breast. Oncogene 22:2021–2033
18. Lee SK, Moon J, Park SW, Song SY, Chung JB, Kang JK (2005) Loss of the tight junction protein claudin 4 correlates with histological growth-pattern and differentiation in advanced gastric adenocarcinoma. Oncol Rep 3:193–199
19. Lodi Cs, Szabo E, Holczbauer Á, Batmunkh E, Szijarto A, Kupcsulik P, Kovalszky I, Paku S, lllyés G, Kiss A, Schaff Zs (2006) Claudin-4 differentiates biliary tract cancers from hepatocellular carcinomas. Mod Path 19:460–469
20. Long H, Crean CD, Lee WH, Cummings OW, Gabig TG (2001) Expression of Clostridium perfringens enterotoxin receptors claudin-3 and claudin-4 in prostate cancer epithelium. Cancer Res 61:7878–7881
21. Michl P, Barth C, Buchholz M, Lerch MM, Rolke M, Holzmann KH, Menke A, Fensterer H, Giehl K, Lohr M, Leder G, Iwamura T, Adler G, Gress TM (2003) Claudin-4 expression decreases invasiveness and metastatic potential of pancreatic cancer. Cancer Res 63:6265–6271
22. Nichols LS, Ashfaq R, Iacobuzio-Donahue CA (2004) Claudin 4 protein expression in primary and metastatic pancreatic cancer: support for use as a therapeutic target. Am J Clin Pathol 121:226–230
23. Nishimura M, Kaltizaki M, Ono Y, Morimoto K, Takeuchi M, Inoue Y, Imai T, Takayi Y (2001) JEAP, a novel component of tight junctions in exocrine cells. J Biol Chem 277:5583–5587
24. Offner S, Hekele A, Teichmann U, Weinberger S, Gross S, Kufer P, Itin C, Baeuerle PA, Kohleisen B (2005) Epithelial tight junction proteins as potential antibody targets for pancarcinoma therapy. Cancer Immunol Immunotheras 54:431–445
25. Orci L, Malaisse-Lagae F, Amherdt M, Ravazzola M, Weisswange A, Dobbs R, Perrelet A, Unger R (1975) Cell contacts in human islets of Langerhans. J Clin Endocrinol Metab 41(5):841–844 (Nov)
26. Páska C, Bögi K, Szilák L, Tőkés AM, Szabó E, Sziller I, Rigó J Jr, Sobel G, Szabó I, Kaposi-Novák P, Kiss A, Schaff Z (2004) Effect of formalin, acetone, and RNAlater fixatives on tissue preservation and different size amplicons by real-time PCR from paraffin-embedded tissue. Diagn Mol Pathol 13:234–240
27. Pfaffl MW, Horgan GW, Dempfle L (2002) Relative expression software tool (REST) for group-wise comparison and statistical analysis of relative expression results in real-time PCR. Nucleic Acids Res 30:e36
28. Rahner C, Mitic LL, Anderson JM (2001) Heterogeneity in expression and subcellular localization of claudins 2, 3, 4, and 5 in the rat liver, pancreas, and gut. Gastroenterology 120:411–422
29. Rangel LB, Agarwal R, D'Souza T, Pizer ES, Alo PL, Lancaster WD, Gregoire L, Schwartz DR, Cho KR, Morin PJ (2003) Tight junction proteins claudin-3 and claudin-4 are frequently overexpressed in ovarian cancer but not in ovarian cystadenomas. Clin Cancer Res 9:2567–2575
30. Rindi G, Kloppel G (2004) Endocrine tumors of the gut and pancreas tumor biology and classification. Neuroendocrinology 80 (Suppl 1):12–15
31. Sato N, Fukushima N, Maitra A, Iacobuzio-Donahue CA, van Heek NT, Cameron JL, Yeo CJ, Hruban RH, Goggins M (2004) Gene expression profiling identifies genes associated with invasive intraductal papillary mucinous neoplasms of the pancreas. Am J Pathol 164:903–914
32. Sawada N, Murata M, Kikuchi K, Osanai M, Tobioka H, Kojima T, Chiba H (2003) Tight junctions and human diseases. Med Electron Microsc 36:147–156
33. Schmitt M, Klonowski-Stumpe H, Eckert M, Luthen R, Haussinger D (2004) Disruption of paracellular sealing is an early event in acute caerulein-pancreatitis. Pancreas 28:181–190
34. Sobel G, Páska C, Szabó I, Kiss A, Kádár A, Schaff Z (2005) Increased expression of claudins in cervical squamous intraepithelial neoplasia and invasive carcinoma. Hum Pathol 36:162–169
35. Sobel G, Németh J, Kiss A, Lotz G, Szabó I, Udvarhelyi N, Schaff Z, Páska C (2006) Claudin 1 differentiates endometrioid and serous papillary endometrial adenocarcinoma. Gynecol Oncol 103:591–598
36. Sobel G, Szabó I, Páska C, Kiss A, Kovalszky I, Kádár A, Paulin F, Schaff Z (2005) Changes of cell adhesion and extracellular matrix (ECM) components in cervical intraepithelial neoplasia. Pathol Oncol Res 11:26–31
37. Soini Y (2005) Expression of claudins 1, 2, 3, 4, 5 and 7 in various types of tumours. Histopathology 46:551–560
38. Soini Y, Tommola S, Helin H, Martikainen P (2006) Claudins 1, 3, 4 and 5 in gastric carcinoma, loss of claudin expression associates with the diffuse subtype. Virchows Arch 448:52–58
39. Sonoda N, Furuse M, Sasaki H, Yonemura S, Katahira J, Horiguchi Y, Tsukita S (1999) Clostridium perfringens enterotoxin fragment removes specific claudins from tight junction strands:

evidence for direct involvement of claudins in tight junction barrier. J Cell Biol 147:195–204
40. Terris B, Blaveri E, Crnogorac-Jurcevic T, Jones M, Missiaglia E, Ruszniewski P, Sauvanet A, Lemoine NR (2002) Characterization of gene expression profiles in intraductal papillary-mucinous tumors of the pancreas. Am J Pathol 160:1745–1754
41. Tőkés AM, Kulka J, Paku S, Szik A, Páska C, Novák PK, Szilák L, Kiss A, Bögi K, Schaff Zs (2005) Claudin-1, -3 and -4 proteins and mRNA expression in benign and malignant breast lesions: a research study. Breast Cancer Res 7:R296–R305
42. Tsukahara M, Nagai H, Kamiakito T, Kawata H, Takayashiki N, Saito K, Tanaka A (2005) Distinct expression patterns of claudin-1 and claudin-4 in intraductal papillary-mucinous tumors of the pancreas. Pathol Int 55:63–69
43. Tsukita S, Furuse M (1998) Overcoming barriers in the study of tight junction functions: from occludin to claudin. Genes Cells 3:569–573
44. Turksen K, Troy TC (2004) Barriers built on claudins. J Cell Sci 117:2435–2447
45. Van Grevenstein WM, Hofland LJ, Jeekel J, van Eijck CH (2006) The expression of adhesion molecules and the influence of inflammatory cytokines on the adhesion of human pancreatic carcinoma cells to mesothelial monolayers. Pancreas 32:396–402
46. Viola KV, Sosa JA (2005) Current advances in the diagnosis and treatment of pancreatic endocrine tumors. Curr Opin Oncol 17:24–27

Virchows Arch (2007) 450:559–565
DOI 10.1007/s00428-007-0407-6

ORIGINAL ARTICLE

Molecular cytogenetic characterization of t(14;19)(q32;p13), a new recurrent translocation in B cell malignancies

Francesca Micci · Ioannis Panagopoulos · Geir E. Tjønnfjord · Arne Kolstad · Jan Delabie · Klaus Beiske · Sverre Heim

Received: 30 November 2006 / Revised: 14 March 2007 / Accepted: 15 March 2007 / Published online: 4 April 2007
© Springer-Verlag 2007

Abstract Translocations involving an immunoglobulin (*IG*) locus are a recurring theme in B cell neoplasia. The rearrangements lead to the joining of an *IG* gene with a (proto)oncogene, whereby the latter comes under the influence of transcription-stimulating sequences in the constitutively active *IG* locus resulting in deregulation of the oncogene and neoplastic growth. We present here three cases of B cell neoplasia that showed a t(14;19)(q32;p13) by karyotypic analysis. Detailed molecular cytogenetic characterization of the breakpoints on chromosomes 14 and 19 in the two cases from which extra material was available, demonstrated the involvement of the immunoglobulin heavy-chain (*IGH@*)-variable region on chromosome 14 in both and, in one case, that the breakpoint was within the *BRD4* gene on chromosome 19. Against the background of what one knows about *IGH@* involvement in lymphatic malignancies, it is difficult to envisage a fusion gene with qualitatively altered protein product as the crucial pathogenetic outcome of the translocation. In spite of the fact that we found *BRD4* split by the t(14;19)(q32;p13) in one of the two informative cases, we cannot be sure that this was the pathogenetically relevant target gene. Other pathogenetic possibilities could be deregulation of the neighboring *NOTCH3* and/or *ABHD9* genes, located distal to *BRD4* in 19p13.

Keywords ALL · Large B cell lymphoma · Cytogenetics · t(14;19)(q32;p13) · *BRD4*

F. Micci (✉) · S. Heim
Department of Medical Genetics,
Rikshospitalet-Radiumhospitalet Medical Centre (Montebello),
0310 Oslo, Norway
e-mail: francesca.micci@labmed.uio.no

I. Panagopoulos
Department of Clinical Genetics, University Hospital,
Lund, Sweden

G. E. Tjønnfjord
Medical Department, Division of Hematology,
Rikshospitalet-Radiumhospitalet Medical Centre (Gaustad),
Oslo, Norway

A. Kolstad
Department of Oncology,
Rikshospitalet-Radiumhospitalet Medical Centre (Montebello),
Oslo, Norway

J. Delabie · K. Beiske
Department of Pathology,
Rikshospitalet-Radiumhospitalet Medical Centre (Montebello),
Oslo, Norway

G. E. Tjønnfjord · S. Heim
Faculty of Medicine, University of Oslo,
Oslo, Norway

Introduction

Translocations involving an immunoglobulin (*IG*) locus are a recurring theme in B cell oncogenesis. The rearrangements lead to the joining of the *IG* gene with a (proto) oncogene [6]. Prime examples are the t(8;14) and its variants t(2;8) and t(8;22), which are associated with Burkitt lymphoma/Burkitt-like leukemia. The crucial event in the three translocations is the juxtapositioning of the oncogene *MYC* (located in 8q24) and either the immunoglobulin heavy-chain (*IGH@*) locus (in 14q32), the *IGK@* light-chain locus (in 2p12), or the *IGL@* light-chain locus (in 22q11). Through either of these rearrangements, *MYC* comes under the influence of transcription-stimulating

sequences in the constitutively active *IG* locus. This, in turn, leads to deregulation of the oncogene, increased transcription, and ultimately to neoplastic growth [1, 24]. In addition to the classic Burkitt-associated rearrangements that target *MYC*, many other translocations recombine an *IG* locus with other genes. Among them is also the t(14;19)(q32;q13) in chronic lymphocytic leukemia which recombines *IGH@* with the *BCL3* (B cell CLL/lymphoma 3) gene in 19q13 [21].

We present here three cases of B cell neoplasia, two acute lymphocytic leukemia (ALL), and one mediastinal large B cell lymphoma (Med-DLBCL), which showed a t(14;19)(q32;p13) by karyotypic analysis. Detailed molecular cytogenetic characterization of the breakpoint position on chromosomes 14 and 19 in the two cases from which extra material was available, demonstrated the involvement of the *IGH@*-variable region on chromosome 14 in both and, in one case, splitting of the *BRD4* (bromodomain-containing 4 isoform long) gene on chromosome 19.

Materials and methods

Case history

Case 1 A 16-year-old man was, in March 2004, admitted to our hospital with progressive pancytopenia and was diagnosed with common B-ALL [5]. The leukemic blasts displayed the following immunophenotype: $CD10^{+}$ $CD19^{+}CD20^{+}CD22^{+}CD34^{+}CD79\alpha^{+}\mu^{-}$. The patient was treated according to our institutional treatment protocol [10] and achieved a complete remission. He remains in remission 27 months after diagnosis while receiving maintenance therapy.

Case 2 A 36-year-old woman was, in September 1996, admitted to our hospital with pharyngitis and progressive anemia. Common B-ALL was diagnosed with coexpression of myeloid markers [5]. The leukemic blasts were of the following immunophenotype: $CD10^{+}CD19^{+}CD20^{+}CD22^{+}$ $CD33^{+}CD34^{+}CD79\alpha^{+}\mu^{-}$. A complete remission was achieved following induction therapy [10]. Twelve months later, during maintenance therapy, she was diagnosed with a bone marrow relapse. Following reinduction therapy, she experienced a short second remission. However, she died from progressive leukemia 18 months after diagnosis.

Case 3 A 20-year-old man was, in May 1998, admitted to our hospital because of a 5-cm tumor in the right supraclavicular region. Apart from being treated for a pyelonephritis 2 years earlier, he had had no health problem before this and no family history of cancer. Biopsy of the tumor showed a lymphoma composed of sheets of large atypical cells with often polylobulated nuclei against a background of abundant fibrous tissue. Immunohistochemistry showed that the lymphoma cells expressed CD45, CD20, MUM1, and Ki-67 (40%), but not CD10, Bcl-6, CD5, CD23, cyclin D1, CD15, CD30, CD3, or TdT. Staging was performed with computed tomography scans and bone marrow biopsy. The lymphoma extended from the neck and down into the upper anterior mediastinum. It was finally diagnosed as a primary Med-DLBCL, stage IIA. Standard therapy at our institution for this age group and diagnosis was the BFM-93 regimen, and the patient received Vorphase and two cycles (A and B). He developed transient kidney failure and delayed methotrexate excretion after the second cycle, and the treatment was, therefore, changed to four cycles of standard cyclophosphamide+doxorubicin+vincristine+prednisolone (CHOP-21). He completed the chemotherapy with no further problem and achieved a complete remission. There was a complete normalization of kidney function. Radiotherapy was given to the supra/infra-clavicular and upper mediastinal regions (36 Gy). The treatment was completed in November 1999. At follow-up visits (last time in December 2004), no signs of relapse or late complications have been noticed.

G-banding analysis

The initial G-banding cytogenetic analysis was performed as part of our clinical diagnostic service using standard techniques [7]. The chromosome preparations were from short-term cultured bone marrow cells in cases 1 and 2 and from a lymph node biopsy in case 3. G-banding was obtained with trypsin (DIFCO Laboratories, Detroit, MI, USA) and Leishman stain (BDH, Poole, England). The karyotype interpretations based on the ISCN [17] are presented in Table 1.

Table 1 Karyotypic data on the B cell neoplasms

Case	Tumor type	Karyotype
1	Common ALL	46,XY,t(14;19)(q32;p13)[15]/46,XY[1]
2A Diagnosis	Common ALL	46,XX,t(14;19)(q32;p13)[6]/46,XX[20]
2B Relapse		46,XX,t(14;19)(q32;p13),add(14)(q11)[7]/46,XX[18]
3	Med-DLBCL	50,XY,+X,+add(8)(p11),t(14;19)(q32;p13),+2mar[3]/50,idem,t(1;12)(p36;q24)[12]

FISH analysis

Fluorescence in situ hybridization (FISH) was performed on fresh metaphase chromosomes and interphase nuclei preparations from cases 1 and 2. Locus-specific probes derived from bacterial artificial chromosomes (BAC), bacteriophage P1 artificial chromosomes (PAC), and fosmid clones were prepared and hybridized to detect the exact breakpoint of the 14;19 translocation. The BAC clones were retrieved from the RPCI-11 Human BAC library and CalTech human BAC library D, the PAC clones were from the RPCI-5 Human PAC library, and the fosmid clones were retrieved from the LLNL Human Chromosome 19 fosmid library (P. de Jong libraries, http://bacpac.chori.org/home.htm). All clones were selected according to the physical and genetic mapping data on chromosomes 14 and 19 reported in the Human Genome Browser at the University of California Santa Cruz Web site (May 2005, http://genome.ucsc.edu/). In addition, FISH mapping of the clones on normal controls was performed to confirm their chromosomal location (Fig. 1). The clones used to detect the breakpoint position of the 14;19 translocation were RP5-998D24, RP11-1145H5, CTD-2366K3, and RP11-47P23 mapping to 14q32 (from centromere to telomere) and RP11-737I1, RP11-645H15, RP11-207I16, RP11-74L8, RP11-637P24, RP11-959O6, RP11-347E20, RP11-876D1, RP11-615O9, RP11-846C18, RP5-1116F22, and RP11-75H6 mapping to 19p13 (from centromere to telomere). Additional FISH analyses with clone RP11-84C16 were performed to check specifically for possible involvement of the *BCL3* gene in 19q13. Furthermore, fosmid clones G248P84243B7 and G248P8276B1, covering the *BRD4* locus, and G248P88694F12 and G248P86072D3, covering the *AKAP8* (A-kinase anchor protein 8) locus, were used in case 1 to identify or rule out the possible involvement of these two genes with certainty. The clones were grown in selective media, and DNA was extracted according to standard methods [26]. DNA probes were directly labeled with a combination of fluorescein isothiocyanate (FITC)-12-deoxycytidine triphosphate (dCTP) and FITC-12-2′-deoxyuridine 5′-triphosphate (dUTP), Texas Red-6-dCTP and Texas Red-6-dUTP (New England Nuclear, Boston, MA, USA), or indirectly with Biotin-dUTP (Molecular Probes, Invitrogen, Carlsbad, CA, USA) by nick translation and detected with streptavidin–diethylaminocoumarin (DEAC; Invitrogen). The subsequent hybridization conditions as well as the detection procedure were according to standard protocols [18]. The hybridizations were analyzed using a CytoVision system (Applied Imaging, Newcastle, UK).

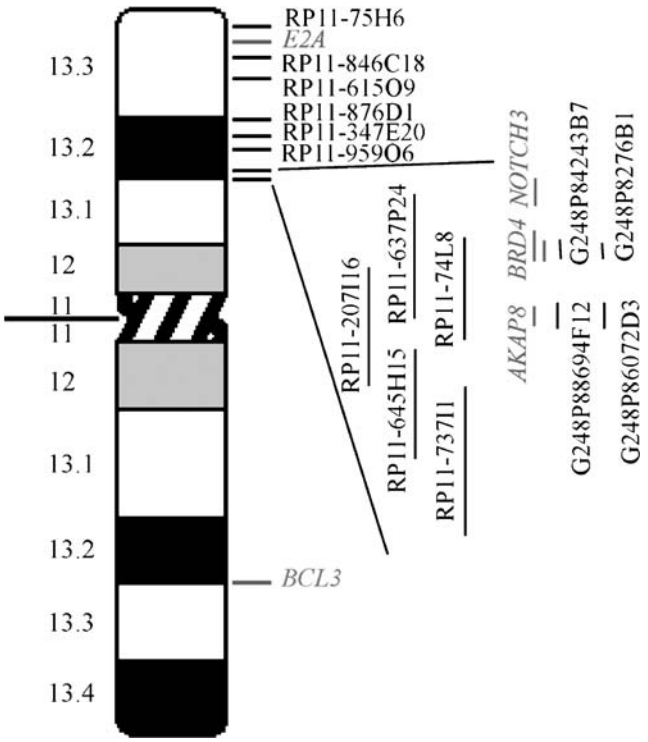

Fig. 1 Ideogram of chromosome 19 showing the localization of the BAC, PAC, and fosmid clones used to localize the breakpoint positions. The clones are represented *in black*, whereas relevant genes are represented *in gray*. The clones used for *TCF3* and *BCL3* testing were RP5-1116F22 and RP11-84C16, respectively

Results

The three cases were selected because they all showed a t(14;19)(q32;p13) by G-banding analysis (Fig. 2). In cases 1 and 2, the translocation was the sole karyotypic abnormality, whereas in case 3, it was one of several rearrangements (Table 1). It is noteworthy that, in case 2, the t(14;19) was the sole aberration in sample 2A, taken at disease debut, whereas an additional abnormality could be identified in the relapse sample 2B, indicative of disease progression.

Leftover suspension of fixed cells was available for FISH experiments in cases 1 and 2, and BAC clones were selected and hybridized to the metaphase plates to map the exact translocation breakpoint positions on chromosomes 14 and 19. Not surprisingly, on chromosome 14, we could identify the breakpoint to the variable region of *IGH@* in both analyzed cases. The signal from clone RP5-998D24 mapping to the *IGH@* constant region was retained on the der(14), whereas clones RP11-1145H5 and RP11-47P23, specific for the distal region of the *IGH@* variable cluster, hybridized on the der(14) and the der(19), respectively, indicating that the breakpoint lay between the two clones. On chromosome 19, however, the breakpoint position varied between the two cases. In case 1, the FISH analysis pinpointed the breakpoint to inside the genomic region covered by BAC clone RP11-74L8 because on metaphase

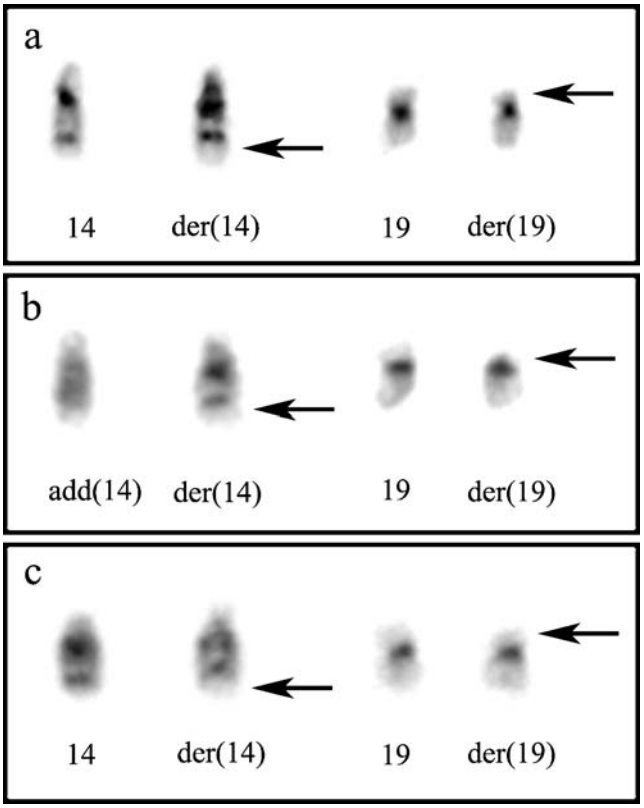

Fig. 2 Partial G-band karyograms illustrating the t(14;19)(q32;p13) seen in case 1(ALL; **a**), case 2 (ALL; **b**), and case 3 (Med-DLBCL; **c**). Normal homologous chromosomes are included to facilitate comparison. *Arrows* indicate breakpoint positions

spreads, one saw three fluorescent signals, i.e., on the normal chromosome 19, on the der(19), and on the der(14). As the RP11-74L8 clone contains sequences of two different genes mapping to 19p13, *BRD4* and *AKAP8*, additional FISH experiments were planned to discriminate between the possible involvement of these two genes. Fosmid clones spanning *BRD4* and *AKAP8* were selected. Hybridization with the clones G248P84243B7 and G248P8276B1, which contain sequences from the *BRD4* gene, gave three signals: on the normal chromosome 19, on the der(19), and on the der(14) (Fig. 3a); this demonstrates that *BRD4* was split by the translocation. Attempts to identify the breakpoint at the molecular level using long distance inverse polymerase chain reaction, as described by Willis et al. [29] and Sonoki et al. [28], failed.

In case 2, the breakpoint on chromosome 19 was found to lie between BAC clones RP11-347E20 and RP11-959O6, as the fluorescent signal from the former was seen on der(14), whereas the signal from the latter clone was seen on the der(19). After a few hybridizations, however, there was no material left to increase the resolution of our investigation, which mapped the breakpoint to a genomic region of 2 Mb. When the clone containing the sequence for the *BRD4* gene was hybridized to metaphase plates from this case, the sequences with which the probe hybridized were shown to be retained on the der(19), showing a more distal (about 2 Mb) breakpoint position than in case 1. In addition, in both cases, the involvement of the two oncogenes *TCF3* (transcription factor 3, also known as *E2A*), located on 19p13, and *BCL3* (B cell CLL/lymphoma 3), which maps to 19q13, was specifically tested for. We could exclude the involvement of these two genes in the present cases because *TCF3* moved to the der(14) and, hence, lay distal to the breakpoint, whereas *BCL3* showed a fluorescence signal on the long (i.e., opposite of the arm involved) arm of chromosome 19 both on the normal and on the derivative chromosome.

No fixed cell suspension from case 3 was available for molecular cytogenetic investigation. We tried FISH experiments on previously G-banded slides archived since 1998 using clones RP11-47P23, RP11-74L8, and RP11-637P24, but the hybridization gave no informative results.

Discussion

The involvement of the *IGH@* locus in B-lineage ALL and Med-DLBCL with different translocation partners is well documented in the cancer cytogenetic literature [16]. We report here a hitherto unrecognized, recurrent 14;19 translocation with breakpoints in 14q32 and 19p13 in three B cell malignancies. The Mitelman Database of Chromosome Aberrations in Cancer lists 49 cases of leukemia or lymphoma with translocations between chromosomes 14 and 19 [22] (update April 2006). However, only four of these cases were reported to show rearrangement of 19p [9, 11, 19, 27]; the breakpoint position of all the others allegedly was on the long arm on chromosome 19, possibly with involvement of the *BCL3* gene. Only 25 of these cases had been tested by cytogenetic and/or molecular techniques for actual involvement of this gene [2, 21, 23, 25], however, providing indisputable evidence that the breakpoint really was on 19q. It is well known in cancer cytogenetics that breakpoints on chromosome 19 are notoriously difficult to locate, as by G-banding analysis, both arms look fairly similar. In addition, the chromosomal preparations of acute leukemia and malignant lymphoma are not always of optimal quality, something that can contribute to misinterpretation of the breakpoint position. It is, therefore, possible that some of the reported 19q breakpoints could have been 19p breakpoints and that the involvement of 19p in B cell neoplasia thus may be more frequent than it currently appears.

In two of our cases, a detailed molecular cytogenetic characterization of the breakpoints was possible. In the *IGH@* locus on 14q32, the break occurred in the variable region in both. In case 1, a gene was identified in 19p13

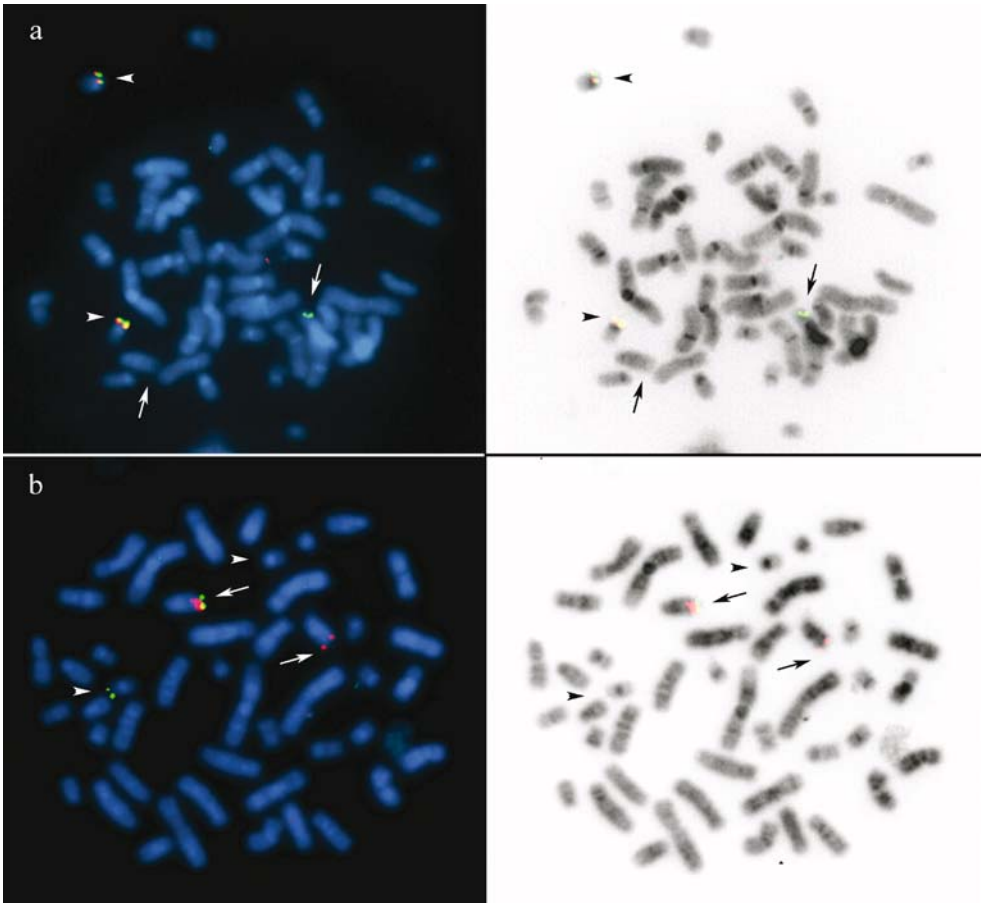

Fig. 3 **a** Metaphase spread from case 1 showing hybridization with fosmid clones G248P88694F12 and G248P86072D3 (*labeled in red*) and G248P84243B7 and G248P8276B1 (*labeled in green*), containing sequences of *AKAP8* and *BRD4*, respectively. The probe specific for BRD4 splitting gave three signals, i.e., on the normal 19, on the der(19), and on the der(14). **b** Metaphase spread from case 1 showing hybridization with BAC clones RP5-998D24 (*labeled in red*) and RP5-1116F22 (*labeled in green*), specific for *IgH@* and *TCF3*, respectively. In all metaphases, *arrows* point to chromosomes 14 (normal and derivative), whereas *arrowheads* point to chromosomes 19 (normal and derivative). The inverted 4′,6-diamidino-2-phenylindole (DAPI) image is presented on the *right side* of each metaphase to facilitate identification of chromosomes

that was split by the translocation, namely, *BRD4*. The same gene has also been found to be rearranged in the rare and aggressive midline carcinomas of young people [12–14] as well as in a cell line from an aggressive lung carcinoma [15]. In both situations, a t(15;19)(q32;p13) was identified leading to a *BRD4/NUT* fusion. The *BRD4* gene is expressed normally as two alternative transcripts with identical 5′ ends, the coding sequence of the longer *BRD4* transcript being approximately twice the length of the shorter transcript. Both *BRD4* transcripts encode NH2-terminal bromodomains, but the longer transcript also encodes COOH-terminal lysine-rich regions that are not encoded by the shorter *BRD4* transcript. It is noteworthy that the 15;19 translocation breakpoint transects the coding sequence of the longer *BRD4* gene, whereas the shorter form remains unperturbed [13, 14]. The BRD4 protein product belongs to the BET family of nuclear proteins that interact with acetylated chromatin, and overexpression of *BRD4* has been reported to inhibit cell cycle progression from the G1 to S phase [20]. The exact mechanism by which t(15;19) contributes to tumorigenesis remains unclear, however. It has been suggested that the BRD4 short and long isoforms might have qualitatively different, and even opposing, functions in cell cycle regulation [14]. Possibly, the t(15;19) abrogates the BRD4 long isoform function in which case it is significant that the BRD4 component in the BRD4/NUT fusion protein comprises virtually all the predicted BRD4 short isoform. The BRD4/NUT oncoprotein could then function as a dominant negative in relation to the BRD4 long isoform and might also contribute to a gain-of-function equivalent of the BRD4 short isoform [14]. The BRD4 isoforms are expected to compete for binding to chromatin, given that their bromodomain-containing NH2-terminal regions are identical.

In our case 1, the *BRD4* gene was recombined with *IGH@* by means of a t(14;19). It is well known that rearrangements involving one of the *IG* loci in B cell malignancies always lead to deregulation, usually overexpression, of an oncogene in one of the breakpoints (quantitative oncogene activation). Can this mechanism be reconciled with the fact that the breakpoint was actually located inside the *BRD4* gene sequence in case 1? It is difficult to envisage a fusion gene as the crucial pathogenetic outcome of the translocation leading to a hybrid gene product when one of the partners is the *IGH@*, deregulation of one or both isoforms of BRD4 intuitively seems the more likely result. If in case 1 the most likely pathogenetically important gene is *BRD4*, as it was found directly

rearranged, in case 2, no splitting of this gene was identified. More specifically, the breakpoint on chromosome 19 was in case 2 found in a 2.1-Mb region in 19p13.13~19p13.2 at a distance of 3~5 Mb from *BRD4* and distally (i.e., towards the telomere) from it, as the probe containing *BRD4* sequence was retained on the der(19). For both cases, it is possible to hypothesize a position effect on pathogenetically important gene(s) brought about by the t(14;19); are there any candidates known for such a role? It may be relevant that another gene already known for its involvement in human neoplasia is located only 45 kb upstream from *BRD4*, namely, *NOTCH3* (Notch homolog 3). This gene was found highly expressed in the lung cancer cell line reported by Hakuri et al. [15] in which the t(15;19) with rearrangement of *BRD4* was also identified and also in a panel of lung cancer cell lines showing translocation of chromosome 19 with different partner chromosomes [8]. The *NOTCH* genes encode large, single-pass, type I transmembrane receptors whose role in tumorigenesis has been demonstrated [3]. High-level expression of *NOTCH1* and *NOTCH3* is found in almost all T cell T-ALL [4] and also in cervical and colon carcinomas [30]. Finally, also the putative gene *ABHD9* (abhydrolase domain containing 9) is located very close to the breakpoint in 19p (Human Genome Browser at the University of California Santa Cruz, at http://genome.ucsc.edu/). However, no information is yet available regarding its function in humans that may hint to a role in neoplasia.

It is worthy of note that the t(14;19)(q32;p13) was found in two different, albeit related, malignancies, namely, ALL (cases 1 and 2) and Med-DLBCL (case 3). As the same lymphoid cells are capable of both disseminated bone marrow proliferation with spillover into peripheral blood (leukemia) and localized tumor growth (lymphoma), one can hypothesize that the t(14;19) is an early event that may lead to both types of neoplastic differentiation. Lack of spare material prevented us from better characterizing the breakpoint in the Med-DLBCL; hence, we do not know which gene was directly involved in the rearrangement in that case. The presence of such disease heterogeneity is, nevertheless, clearly compatible with the presence of functionally equivalent rearrangements and/or alteration of the same pathway, as exemplified by the presence of identical t(8;14), t(8;22), and t(2;8) in both Burkitt lymphoma and Burkitt-like leukemia. On the other hand, molecular and, hence, pathogenetic differences between case 3 (Med-DLBCL) and cases 1 and 2 (ALL) remain a possibility. Pending further evidence, however, we deem it more likely that all these cases exemplify a new and yet partly unknown pathogenetic mechanism in B-lineage malignancy and that other factors than the molecular details of the t(14;19)(q32;q13) determine the phenotypic disease heterogeneity.

Acknowledgments This work was supported by grants from the Norwegian Cancer Society, COST Action B-19—Molecular cytogenetics of solid tumors—Short-term Scientific Mission programme, the Gunnar Nilsson's Cancer Foundation, and The Swedish Children's Cancer Foundation.

References

1. Adhikary S, Eilers M (2005) Transcriptional regulation and transformation by Myc proteins. Nat Rev Mol Cell Biol 6:635–645
2. Au WY, Horsman DE, Ohno H, Klasa RJ, Gascoyne RD (2002) Bcl-3/IgH translocation (14;19)(q32;q13) in non-Hodgkin's lymphomas. Leuk Lymphoma 43:813–816
3. Axelson H (2004) Notch signaling and cancer: emerging complexity. Semin Cancer Biol 14:317–319
4. Bellavia D, Campese AF, Checquolo S, Balestri A, Biondi A, Cazzaniga G, Lendahl U, Fehling HJ, Hayday AC, Frati L, von Boehmer H, Gulino A, Screpanti I (2002) Combined expression of pTalpha and Notch3 in T cell leukemia identifies the requirement of preTCR for leukemogenesis. Proc Natl Acad Sci USA 99:3788–3793
5. Bene MC, Castoldi G, Knapp W, Ludwig WD, Matutes E, Orfao A, van't Veer MB (1995) Proposals for the immunological classification of acute leukemias. European Group for the Immunological Characterization of Leukemias (EGIL). Leukemia 9:1783–1786
6. Campbell LJ (2005) Cytogenetics of lymphomas. Pathology 37:493–507
7. Czepulkowski B, Gibbons B (2001) Cytogenetics in acute lymphoblastic leukemia. In: Rooney DE (ed) Human cytogenetics: malignancy and acquired abnormalities. Oxford University Press, Oxford, pp 57–85
8. Dang TP, Gazdar AF, Virmani AK, Sepetavec T, Hande KR, Minna JD, Roberts JR, Carbone DP (2000) Chromosome 19 translocation, overexpression of Notch3, and human lung cancer. J Natl Cancer Inst 92:1355–1357
9. Douet-Guilbert N, Morel F, Le Bris MJ, Herry A, Le Calvez G, Marion V, Abgrall JF, Berthou C, De Braekeleer M (2004) Cytogenetic studies in T-cell acute lymphoblastic leukemia (1981–2002). Leuk Lymphoma 45:287–290
10. Evensen SA, Brinch L, Tjonnfjord G, Stavem P, Wisloff F (1994) Estimated 8-year survival of more than 40% in a population-based study of 79 adult patients with acute lymphoblastic leukaemia. Br J Haematol 88:88–93
11. Finn WG, Thangavelu M, Yelavarthi KK, Goolsby CL, Tallman MS, Traynor A, Peterson LC (1996) Karyotype correlates with peripheral blood morphology and immunophenotype in chronic lymphocytic leukemia. Am J Clin Pathol 105:458–467
12. French CA, Kutok JL, Faquin WC, Toretsky JA, Antonescu CR, Griffin CA, Nose V, Vargas SO, Moschovi M, Tzortzatou-Stathopoulou F, Miyoshi I, Perez-Atayde AR, Aster JC, Fletcher JA (2004) Midline carcinoma of children and young adults with NUT rearrangement. J Clin Oncol 22:4135–4139
13. French CA, Miyoshi I, Aster JC, Kubonishi I, Kroll TG, Dal Cin P, Vargas SO, Perez-Atayde AR, Fletcher JA (2001) BRD4 bromodomain gene rearrangement in aggressive carcinoma with translocation t(15;19). Am J Pathol 159:1987–1992
14. French CA, Miyoshi I, Kubonishi I, Grier HE, Perez-Atayde AR, Fletcher JA (2003) BRD4–NUT fusion oncogene: a novel mechanism in aggressive carcinoma. Cancer Res 63:304–307
15. Haruki N, Kawaguchi KS, Eichenberger S, Massion PP, Gonzalez A, Gazdar AF, Minna JD, Carbone DP, Dang TP (2005) Cloned fusion product from a rare t(15;19)(q13.2;p13.1) inhibit S phase in vitro. J Med Genet 42:558–564

16. Heim S, Mitelman F (eds) (1995) Cancer cytogenetics. Wiley-Liss, New York
17. Shaffer LG, Tommerup N (eds) (2005) ISCN 2005: an international system for human cytogenetic nomenclature. S Karger, Basel
18. Kearny L, Hammomd DW (2001) Molecular cytogenetic technologies. In: Rooney DE (ed) Human cytogenetics—malignancy and acquired abnormalities. Oxford University Press, Oxford, pp 129–163
19. Martinez-Climent JA, Sanchez-Izquierdo D, Sarsotti E, Blesa D, Benet I, Climent J, Vizcarra E, Marugan I, Terol MJ, Sole F, Cigudosad JC, Siebert R, Dyer MJ, Garcia-Conde J (2003) Genomic abnormalities acquired in the blastic transformation of splenic marginal zone B-cell lymphoma. Leuk Lymphoma 44:459–464
20. Maruyama T, Farina A, Dey A, Cheong J, Bermudez VP, Tamura T, Sciortino S, Shuman J, Hurwitz J, Ozato K (2002) A Mammalian bromodomain protein, brd4, interacts with replication factor C and inhibits progression to S phase. Mol Cell Biol 22:6509–6520
21. McKeithan TW, Takimoto GS, Ohno H, Bjorling VS, Morgan R, Hecht BK, Dube I, Sandberg AA, Rowley JD (1997) BCL3 rearrangements and t(14;19) in chronic lymphocytic leukemia and other B-cell malignancies: a molecular and cytogenetic study. Genes Chromosomes Cancer 20:64–72
22. Mitelman, F., Johansson, B., Mertens, F. (2006) Mitelman database of chromosome aberrations in cancer. http://cgap.nci.nih.gov/Chromosomes/Mitelman
23. Ohno H, Doi S, Yabumoto K, Fukuhara S, McKeithan TW (1993) Molecular characterization of the t(14;19)(q32;q13) translocation in chronic lymphocytic leukemia. Leukemia 7:2057–2063
24. Popescu NC, Zimonjic DB (2002) Chromosome-mediated alterations of the *MYC* gene in human cancer. J Cell Mol Med 6:151–159
25. Robinson HM, Taylor KE, Jalali GR, Cheung KL, Harrison CJ, Moorman AV (2004) t(14;19)(q32;q13): a recurrent translocation in B-cell precursor acute lymphoblastic leukemia. Genes Chromosomes Cancer 39:88–92
26. Sambrook J, Fritsch EF, Maniatis T (1989) Molecular cloning: a laboratory manual. Cold Spring Harbor Laboratory Press, Cold Spring Harbor
27. Schlegelberger B, Weber-Matthiesen K, Himmler A, Bartels H, Sonnen R, Kuse R, Feller AC, Grote W (1994) Cytogenetic findings and results of combined immunophenotyping and karyotyping in Hodgkin's disease. Leukemia 8:72–80
28. Sonoki T, Willis TG, Oscier DG, Karran EL, Siebert R, Dyer MJ (2004) Rapid amplification of immunoglobulin heavy chain switch (IGHS) translocation breakpoints using long-distance inverse PCR. Leukemia 18:2026–2031
29. Willis TG, Jadayel DM, Coignet LJ, Abdul-Rauf M, Treleaven JG, Catovsky D, Dyer MJ (1997) Rapid molecular cloning of rearrangements of the IGHJ locus using long-distance inverse polymerase chain reaction. Blood 90:2456–2464
30. Zagouras P, Stifani S, Blaumueller CM, Carcangiu ML, Artavanis-Tsakonas S (1995) Alterations in Notch signaling in neoplastic lesions of the human cervix. Proc Natl Acad Sci USA 92:6414–6418

Virchows Arch (2007) 450:567–574
DOI 10.1007/s00428-007-0391-x

ORIGINAL ARTICLE

Skp2 expression is associated with down-regulation of p27 protein and cell proliferation in salivary adenoid cystic carcinoma

Mohammad Reza Keikhaee · Yasusei Kudo · Samadarani Siriwardena · Lanyan Wu · Ikuko Ogawa · Takashi Takata

Received: 5 December 2006 / Revised: 14 February 2007 / Accepted: 14 February 2007 / Published online: 13 March 2007
© Springer-Verlag 2007

Abstract Adenoid cystic carcinoma (ACC) is a malignant salivary gland tumor, which shows frequent recurrence and metastasis, ultimately with a poor outcome. We previously demonstrated that p27 down-regulation is frequently found and is due to an enhancement of its degradation in ACC. In this study, we transfected nondegradable p27 mutant (T187A) and wild-type gene into ACC cell line. Transfection of T187A mutant gene was more effective on inhibition of cell growth of ACC cells, suggesting that aberration of p27 degradation may be present in ACC. As F-box protein S-phase kinase-associated protein 2 (Skp2), which is necessary for ubiquitin-mediated degradation of p27, is involved in p27 down-regulation in various cancers, we examined the Skp2 expression and its association with p27 expression in 50 ACC cases. We found Skp2 expression in 36% of ACC cases and inverse association between the expression of Skp2 and p27. Moreover, Skp2 small interfering ribonucleic acid (siRNA) transfection decreased Skp2 protein and accumulation of p27 protein and inhibited the cell growth of ACC cells in vitro. These findings, overall, suggest that Skp2 may play an important role in ACC development through the down-regulation of p27 and that Skp2 siRNA can be a novel modality of cancer gene therapy for suppression of p27 down-regulation in ACC.

Keywords Adenoid cystic carcinoma · Skp2 · p27 · Proliferation · Salivary gland

Abbreviations

ACC	adenoid cystic carcinoma
Skp2	S-phase kinase-associated protein 2
TGF-β	transforming growth factor-beta
siRNA	small interfering RNA
Cul1	cullin1
PCNA	proliferating cell nuclear antigen
Jab1	Jun activation domain-binding protein-1
KPC	Kip1 ubiquitination-promoting complex

Introduction

Adenoid cystic carcinoma (ACC) is one of the most common malignant tumors of major and minor salivary glands [4, 23, 31, 33, 36]. Although ACC tends to grow slowly, this neoplasm has a poor prognosis in comparison with the majority of other malignant salivary gland tumors [23, 31]. ACC shows various histological patterns such as cribriform, tubular, and solid. It is generally regarded that tubular or cribriform pattern dominant subtypes have much better prognosis than those with predominantly solid patterns [5–7].

M. R. Keikhaee · Y. Kudo (✉) · S. Siriwardena · T. Takata (✉)
Department of Oral and Maxillofacial Pathobiology,
Division of Frontier Medical Science,
Graduate School of Biomedical Sciences, Hiroshima University,
1-2-3 Kasumi, Minami-ku,
Hiroshima 734-8553, Japan
e-mail: ykudo@hiroshima-u.ac.jp
e-mail: ttakata@hiroshima-u.ac.jp

I. Ogawa
Center of Oral Clinical Examination,
Hiroshima University Hospital,
Hiroshima, Japan

L. Wu
Department of Oral Pathology, HuaXi Stomatology Hospital,
Sichuan University,
Chengdu, Sichuan 610041, People's Republic of China

However, it is often difficult to predict the prognosis of ACC by histological findings alone, especially when dealing with inadequate biopsy material [23, 41]. Thus, there is a need to explore additional parameters for predicting the prognosis of ACC. Our previous study demonstrated that cyclin-dependent kinase inhibitor, p27, was frequently down-regulated and well correlated with its malignant behavior in ACC [34]. p27 mediates G1 arrest induced by TGF-β, contact inhibition, or serum deprivation in epithelial cell lines [25, 38]. The increase in the cellular abundance of p27 upon induction of cell quiescence is primarily due to a decrease in the rate of its degradation [22]. p27 is poly-ubiquitinated both in vivo and in vitro and a lower amount of p27 ubiquitinating activity is present in proliferating cells compared to quiescent cells [22]. Furthermore, p27 ubiquitination requires its phosphorylation on threonine 187 (T187) [19]. Down-regulation of p27 was frequently found in various cancers, and the lack of p27 is suggested to be due to an enhancement of its degradation [30]. Aggressive human cancers express low levels of p27 because of its decreased stability [30]. Importantly, reduced p27 levels represent a powerful prognostic marker for poor survival in cancer patients [15, 30].

S-phase kinase-associated protein 2 (Skp2) was originally identified as a protein that interacts with cyclin A [43]. It has been reported that p27 is specifically recognized and targeted for ubiquitination by Skp2 [1, 32, 39]. Skp2 is required for the ubiquitination and consequent degradation of p27 both in vivo and in vitro [1, 32, 39]. Skp2 is a rate-limiting component of the machinery that ubiquitinates and degrades phosphorylated p27 [1]. Skp2 is frequently over-expressed in tumor cell lines, and forced expression of Skp2 in quiescent fibroblasts induces deoxyribonucleic acid (DNA) synthesis [32, 43]. Recently, it has been revealed that Skp2 overexpression is frequently found and is well correlated with down-regulation of p27 protein in various types of cancer [15, 39].

In the present study, we transfected nondegradable mutant and wild-type (WT) p27 into ACC cell line. Moreover, we examined the immunohistochemical expression of Skp2 and its association with p27 expression. Finally, we examined if small interfering RNA (siRNA)-mediated gene silencing of Skp2 can be employed to inhibit p27 down-regulation in ACC.

Materials and methods

All procedures of the present studies were performed in compliance with regulations administered by the Hiroshima University.

Cell culture

We used ACCh cell line that was established in the Department of Oral Maxillofacial Surgery, Hiroshima University School of Dentistry (kindly provided by T. Okamoto) and was maintained in 5% CO_2, 95% air at 37°C. ACCh cells were maintained in serum-free RD153 medium (Roswell Park Memorial Institute cell culture medium 1640/Dulbecco's modified Eagle's medium/molecular, cellular, and developmental biology medium 153; 1:1:2, *v*/*v*/*v*) containing 10 mg/ml insulin, 10 mM 2-mercaptoethanol, 10 mM 2-aminoethanol, and 10 nM selenite [20, 26, 28]. For experiments, these cells were grown to sub-confluence in each medium.

Generation of stable clones expressing inducible p27

For stably expressing p27 WT and mutant in an inducible way, we used an ecdysone-inducible mammalian expression system (Invitrogen, Carlsbad, CA) as we described previously [14]. To construct pIND-p27 WT or pIND-p27 (threonine-to-alanine p27 mutant; T187A), a *Bam*HI/*Eco*RI fragment was isolated from pcDNA3-p27 WT or pcDNA3-p27 T187A (kindly provided by M. Pagano) and cloned into pIND ecdysone-inducible expression vector (Invitrogen) digested with *Bam*HI/*Eco*RI. Transfection was performed in 60-mm plates using 2 μg of expression vector by using Fugene 6 (Roche). ACCh cells stably expressing ecdysone receptor (EcR) were first isolated with Zeocin (Invitrogen) as a selective marker. The EcR cells were then used to generate clones that incorporated ecdysone response elements followed by WT and T187A mutant p27 with G418 (Life Technologies) as a selective marker. Cells were treated with ponasterone A (5 μM) for 24, 48, and 72 h for induction of p27 expression. For cell growth, cells were cultured in the medium containing ponasterone A (5 μM), and then, trypsinized cells were counted by cell counter (Coulter Z1, Coulter) at 0, 2, 4, and 6 days.

Western blot analysis

We examined the expression of p27, Skp2, and cullin1 (Cul1) proteins in ACC cell lines by Western blot analysis. Western blotting was carried out as we described previously [13]. We used an anti-p27 mouse monoclonal antibody (K25020, Transduction Laboratories, Lexington, KY), anti-Skp2 monoclonal antibody (clone 8D9, Zymed Laboratories, San Francisco, CA), and an anti-Cul1 polyclonal antibody (cat. no. 71-8700, Zymed Laboratories). Cul1 is one of a component of Skp, Cullin, F-box containing complex (SCF complex) and is used as a loading control. Thirty micrograms of protein was subjected to 10% polyacrylamide gel electrophoresis followed by electroblotting onto a nitrocellulose filter. For detection of the immunocomplex, the ECL Western blotting detection system (Amersham, Aylesbury, UK) was used.

Tissue samples

Fifty ACCs including seven cases with metastasis were retrieved from the pathological files of Hiroshima University Hospital (Japan), Peradeniya University (Sri Lanka), and Sichuan University (China). Clinical data of the patients are summarized in Table 1. Among the 50 ACC patients, 20 were men and 30 were women. At the time of diagnosis, their age ranged from 30 to 84 years (average; 59.7±15.1). For the present analysis, only primary tumors were used for immunohistochemistry. The tumors were subclassified according to the histological grading of Szanto et al. [33] as follows: Grade I, tumors with cribriform and/or tubular structures without a solid component; Grade II, tumors composed of cribriform and/or tubular structures with less than 30% of solid areas; and Grade III, tumors with more than 30% of solid areas.

Immunohistochemistry

Immunohistochemical detection of Skp2, p27, and proliferating cell nuclear antigen (PCNA) was performed using a streptavidin–biotin–peroxidase technique as described previously [13, 34]. PCNA is a marker for cells in early G1 phase and S phase of the cell cycle and is well known as a proliferation marker. An antihuman Skp2 mouse monoclonal antibody (clone 8D9, dilution 1:100, Zymed Laboratories), an antihuman p27 mouse monoclonal antibody (K25020, dilution 1:100, Transduction Laboratories), and an antihuman PCNA antibody (PC-10, dilution 1:100, Dako, Denmark) were used. Nuclear staining of Skp2, p27, and PCNA was scored on a semiquantitative scale (see below) by evaluating the percentage within representative areas of each tumor. For small carcinomas, stained sections were observed throughout the lesion. For advanced large

Table 1 Clinical data of ACC patients and immunohistochemical results

Case no.	Age	Sex	Site	Grading[a]	Metastasis	Skp2 expression[b]	p27 expression[c]	PCNA score[d]
1	40	M	Palate	II	−	−	−	I
2	76	M	Lower lip	II	−	−	−	II
3	60	F	SM	I	−	−	−	II
4	55	F	SM	I	−	−	+	I
5	78	F	FOM	I	−	−	+	I
6	65	F	FOM	I	−	−	+	I
7	81	F	FOM	I	−	−	+	I
8	74	F	Palate	III	+	−	+	I
9	64	F	SLG	I	+	−	+	I
10	75	M	Palate	I	−	−	+	I
11	57	F	Parotid	II	−	−	+	II
12	49	F	Maxilla	III	−	−	+	II
13	48	F	Retromoral	II	+	−	+	II
14	37	F	FOM	III	+	−	+	III
15	77	F	Tongue	II	−	−	++	I
16	79	M	Palate	II	−	−	++	I
17	76	M	Palate	I	−	−	++	I
18	84	F	FOM	II	−	−	++	I
19	74	F	SM	I	−	−	++	I
20	49	F	SM	I	−	−	++	I
21	79	F	SM	II	−	−	++	I
22	74	M	FOM	I	−	−	++	I
23	46	F	FOM	I	−	−	++	II
24	79	M	Palate	III	−	−	++	II
25	40	M	Palate	II	−	−	++	II
26	78	M	Tongue	I	−	−	++	II
27	65	M	SM	III	−	−	++	II

SM Submandibular gland, *FOM* floor of mouth, *SLG* sublingual gland

[a] The tumors were subclassified according to the histological grading of Szanto et al. [33] as follows: Grade I, tumors with cribriform and/or tubular structures without a solid component; Grade II, tumors composed of cribriform and/or tubular structures with less than 30% of solid areas; and Grade III, tumors with more than 30% of solid areas.

[b] Skp2 expression was graded as + (more than 5% of tumor cells showed strong or diffuse immunopositivity) and − (less than 5% of the tumor cells showed weak or focal immunopositivity or no staining).

[c] p27 expression was graded as described previously [34].

[d] PCNA labeling index was graded as I (less than 25% of cells are positive), II (25–50% of cells are positive), and III (more than 50% of cells are positive).

tumors, at least ten fields (including peripheral and central areas) were observed, and the number of cells and intensity were evaluated. In each field, we counted at least more than 300 cells using an eyepiece graticule to prevent recounting. Although qualitative differences in staining intensity were observed with considerable intratumoral heterogeneity, all positive cases showed obvious nuclear staining, at least focally. In the nontumorous salivary glands, the nuclei of acini and ducts showed frequent positivity for p27 and rare for PCNA. Lymphocytes are also positive for p27, which is the internal positive control. On the other hand, as Skp2 is usually negative in normal salivary gland, we used tissue section of squamous cell carcinoma case, which was confirmed to express this protein by Western blot as positive control of immunostaining. The expression of Skp2 was graded as + (more than 5% of tumor cells showed strong or diffuse immunopositivity) and − (less than 5% of the tumor cells showed weak or focal immunopositivity or no staining). The expression of p27 was graded as described previously [34]. A labeling index of PCNA was determined by the examination of at least 500 cells in three representative and intensely stained areas. PCNA labeling index was graded as I (less than 25% of cells are positive), II (25–50% of cells are positive), and III (more than 50% of cells are positive). Three observers (I. O., Y. K., and S. S.) made independent assessments of the immunohistochemical grading of Skp2, p27, and PCNA, and where the gradings were divergent, an agreement was reached after discussion.

Statistical analysis

Possible association between variables of the analyzed tumor samples was confirmed by the chi-square test. A p value<0.05 was required for significance.

Plasmids and synthetic siRNA

Vector pSuppressorNeo generates biologically active siRNAs from the U6 promoter (Imgenex, San Diego, CA). Two synthetic oligonucleotide primers (5′-tcgaGGGAGU GACAAAGACUUUGgaguacugCAAAGUCUUUGUCAC UCCCUUUUU-3′ and 5′-ctagAAAAAGGGAGUGA CAAAGACUUUGcaguacucCAAAGUCUUUGUCA CUCCC-3′) containing *Xho*I and *Xba*I overhangs were annealed and then were introduced into pSuppressorNeo vector. Oligonucleotide sequences correspond to a 19-nt sequence from Skp2 (nucleotide 114–133), which are separated by an 8-nt linker (lower case letters) from the reverse complement of the same 19-nt sequence. We also added transcriptional termination (UUUUU) to the end of the oligonucleotide. We used circular control plasmid, which contains a scrambled sequence (5′-TCGATCAGT CACGTTAATGGTCGTTttcaagagaAACGACCAT TAACGTGACTGATTTTT-3′ and 5′-CTAGAAAAATC AGTCACGTTAATGGTCGTTtctcttgaaAACGACCAT TAACGTGACTGA-3′) that does not show significant homology to rat, mouse, or human gene sequences, as a negative control. Transfection was performed in 60-mm plates using 2 μg of vector and 10 μl of Fugene 6 reagent (Roche). After 48 h of transfection, cells were treated with G418 (Gibco) for 2 weeks as a selective marker. After G418 treatment, we obtained stably transfectant cells.

Results

Nondegradable p27 mutant more effectively inhibits cell growth of ACC cells in comparison with WT

In our previous study, frequent reduced expression of p27 was observed and well correlated with its malignant behavior in ACC [34]. We also found a high p27 degradation activity in ACCh cells, which did not express p27 protein [34]. Therefore, in the present study, we transfected ACCh cells with p27 T187A mutant gene, which is not influenced by ubiquitin-mediated degradation, and p27 WT gene in an inducible way. These cells were first transfected with a *Drosophila* EcR, then with the p27 WT or T187A mutant gene that was placed under the control of the ecdysone-inducible promoter element such that expression of the p27 transgenes could be regulated with the ecdysone analog ponasterone A. Ponasterone A induced overexpression p27 WT and T187A mutant proteins at 72 and 24 h, respectively (Fig. 1a and b). We next determined the effects of p27 transfection on cell growth. The induction of T187A mutant protein by ponasterone A inhibited cell growth in ACCh cells (Fig. 1a and b). The growth inhibitory effect in WT induction was lower than that in T187A mutant. Our previous study showed that WT p27 was more stable than T187A mutant [14]. Therefore, we think that exogenous WT was induced later than T187A. Similarly to other types of cancer, aberrant regulation of p27 protein degradation may play an important role for down-regulation of p27 protein in ACC.

Immunohistochemical expression of Skp2 and p27 in ACC

p27 is specifically recognized and targeted for ubiquitination by Skp2 [1, 32, 39]. It has been reported that Skp2 overexpression is found and is well correlated with p27 down-regulation in various types of malignant tumors [3, 8, 9, 13, 16, 18, 29, 42]. In this study, therefore, we examined the expression of Skp2 and its association with p27 expression in 50 ACC cases. Table 1 summarizes the

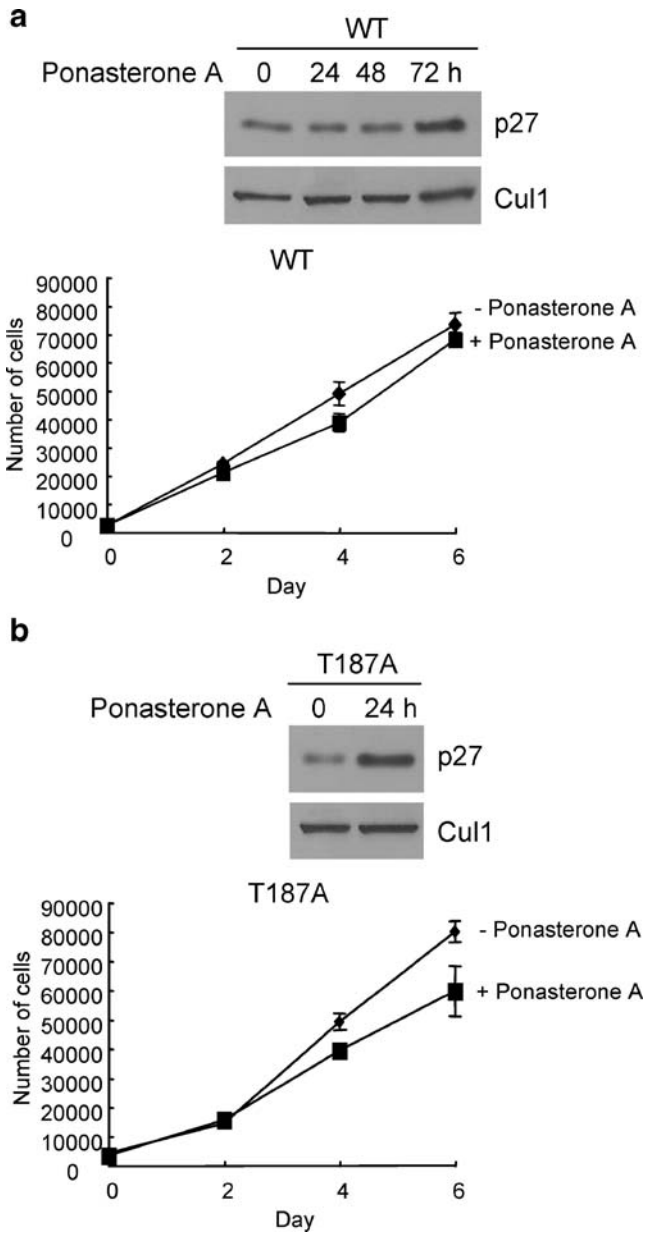

Fig. 1 Transfection of p27 WT gene and T187A mutant gene into ACCh cells. For stably expressing p27 WT and mutant in an inducible way, we used ecdysone-inducible mammalian expression system. Expression of WT and mutant p27 was induced by ponasterone A (5 μM) for 24, 48, and 72 h followed by Western blot analysis. **a** Induction of p27 WT protein was observed at 72 h in ACCh cells (*upper panel*). Cell growth in WT p27 transfectant ACCh cells with or without ponasterone A (*lower panel*). Each cell was cultured in the medium containing ponasterone A (5 μM), and then, trypsinized cells were counted by Cell Counter at 0, 2, 4, and 6 days. *Bars*, SD. **b** Induction of p27 T187A mutant protein was observed at 24 h in ACCh cells (*upper panel*). Cell growth in T187A mutant p27 transfectant ACCh cells with or without ponasterone A (*lower panel*). Each cell was cultured in the medium containing ponasterone A (5 μM), and then, trypsinized cells were counted by Cell Counter at 0, 2, 4, and 6 days. *Bars*, SD

clinical and immunohistochemical results of 50 patients. In brief, there were 30 female and 20 male patients, and the age ranges from 30–84 years. Palate was the commonest site. Out of 50 cases, Skp2 expression was found in 18 (36%) cases. Then, Skp2 expression was compared with p27 expression, PCNA labeling index, and clinicopathological parameters including histology and metastasis as summarized in Table 2. Reduced expression of p27 was found in 38 (76%) cases similar to our previous report [34]. Interestingly, Skp2 expression was inversely correlated with p27 expression (p=0.005; Fig 2a–d and Table 2). Furthermore, Skp2 expression was statistically correlated with high proliferative activity (PCNA index; p=0.0003; Table 2). However, Skp2 expression was not associated with histological grading and lymph node metastasis (Table 2).

Skp2 siRNA induced p27 accumulation and inhibited the cell proliferation in ACC cells

Next, to suppress the ubiquitin-mediated degradation of p27, which is frequently shown in ACC, we inhibited Skp2 expression by siRNA in ACCh cells. ACCh cells showed

Table 2 Summary of Skp2 expression in ACC

		Total	Skip2 expression[a]		p value[b]
			−	+	
p27[c] expression	−	23	18	5	0.005
	+	15	11	4	
	++	12	3	9	
PCNA[d] grading	I	17	16	1	0.0003
	II	20	13	7	
	III	13	3	10	
Histological grading[e]	I	20	14	6	0.37
	II	14	10	4	
	III	16	8	8	
Lymph node metastasis	−	43	27	16	0.66
	+	7	5	2	
Total	50	32	18		

[a] Skp2 expression was graded as + (more than 5% of tumor cells showed strong or diffuse immunopositivity) and − (less than 5% of the tumor cells showed weak or focal immunopositivity or no staining).

[b] Possible correlation association between variables of the analyzed tumor samples was confirmed by the chi-square test. A p value<0.05 was required for significance.

[c] p27 expression was graded as described previously [34].

[d] PCNA labeling index was graded as I (less than 25% of cells are positive), II (25–50% of cells are positive), and III (more than 50% of cells are positive).

[e] The tumors were subclassified according to the histological grading of Szanto et al. [33] as follows: Grade I, tumors with cribriform and/or tubular structures without a solid component; Grade II, tumors composed of cribriform and/or tubular structures with less than 30% of solid areas; and Grade III, tumors with more than 30% of solid areas.

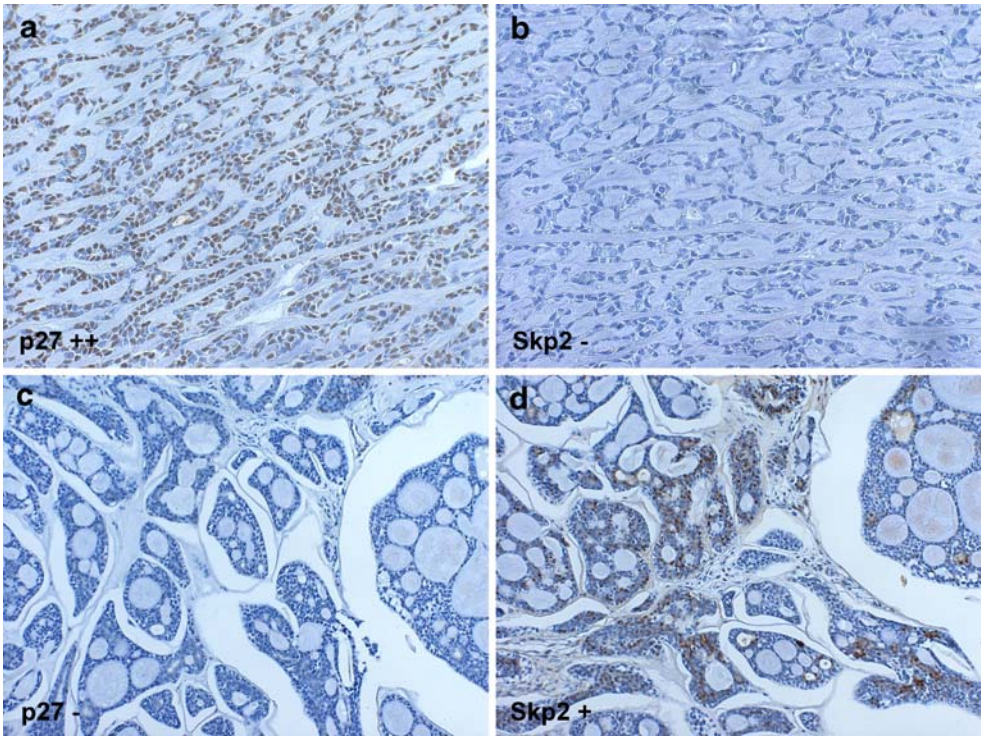

Fig. 2 Immunohistochemical expression of Skp2 and p27 in ACC. Representative case with high p27 expression (**a**) and low Skp2 expression (**b**) and case with low p27 expression (**c**) and high Skp2 expression (**d**) are shown

high expression of Skp2 and down-regulation of p27 (Fig. 3a). To block Skp2 expression selectively by siRNA, 19-nt target sequence, separated by an 8-nt spacer from its reverse complement sequence, was introduced into the siRNA generating pSuppressorNeo vector system. Skp2 siRNA was transfected into ACCh cells. After selection using G418, we could get stable clones of Skp2 siRNA. Skp2 siRNA transfection induced the down-regulation of Skp2 protein (Fig. 3a). As we expected, accumulation of p27 protein was observed in Skp2 siRNA transfectant cells. Next, we examined the effect of Skp2 siRNA transfection on cell proliferation. Skp2 siRNA transfectant cells grew in vitro slower than control siRNA transfectant cells (Fig. 3b).

Discussion

ACC, which is one of the most common malignant tumors of major and minor salivary glands, typically presents an indolent and slow growth associated to frequent late distant metastases, which are together with local recurrences, the reasons for the low long-term survival rate [4, 23, 31, 33, 36, 40]. Standard treatment has not yet been established, although many series of ACC have been described. Several studies showed that advanced clinical stage and solid histological subtype are relevant prognostic factors associated with survival of the patients [12, 21]. However, it is often difficult to predict the prognosis of ACC by

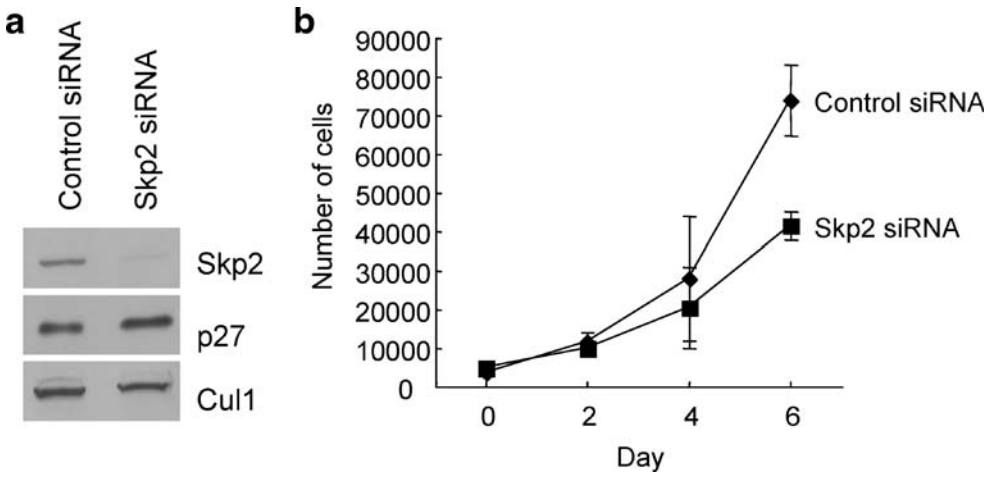

Fig. 3 Skp2 knockdown inhibits cell growth in ACC cells. **a** Expression of p27 and Skp2 protein in control ACCh cells and Skp2 siRNA transfectant ACCh cells. Cul1 expression is used as a loading control. **b** Cell proliferation of control ACCh cells and Skp2 siRNA transfectant ACCh cells. 5×10^3 Cells were plated in 24 well plates, and cells were counted at 0, 2, 4, and 6 days by using cell counter

histological findings alone, especially when dealing with inadequate biopsy material [23, 41]. Thus, there is a need to explore additional parameters for predicting the prognosis of ACC.

The proliferation and progression of cancer cells may be caused by abnormalities of various positive and negative cell cycle regulators [10, 27]. Recently, reduced expression of p27 was found in various cancers and was correlated to their malignancy and poor prognosis [13]. Our previous study showed that down-regulation of p27 was observed in 83% of ACCs and was well correlated with metastasis [34]. These findings suggest that the down-regulation of p27 protein may be involved in the development of ACC and might be a prognostic marker for ACC patients. Moreover, we found that p27 protein was induced by proteasome inhibitor treatment in ACC cell line, ACCh cells that showed reduced expression of p27 protein [34]. In addition, here, we demonstrated that exogenous nondegradable p27 mutant was more rapidly induced and more effective for inhibition of cell growth in comparison with WT p27 by using an inducible way in ACC cells (Fig. 1). Therefore, we strongly suggest that p27 down-regulation found in ACC might be caused by increased degradation of p27 protein. This hypothesis is supported by previous findings that aggressive human cancers such as colon cancers, lymphomas, and astrocytic brain tumors express low levels of p27 because of its decreased stability [2, 17, 24, 35].

Recently, SCF^{Skp2} was identified as the E3 ubiquitin ligase that targets p27 for ubiquitination [1, 32, 39]. Importantly, Skp2 is frequently over-expressed in tumor cell lines, and forced expression of Skp2 in quiescent fibroblasts induces DNA synthesis [43]. It has been reported that Skp2 overexpression is found in other types of malignant tumor including lymphomas, oral cancers, breast cancers, colon cancers, lung cancers, and gastric cancers [3, 8, 9, 13, 16, 18, 29, 42]. In fact, here we found that Skp2 expression was inversely associated with p27 expression in ACC cases. Therefore, we suggest that p27 down-regulation mediated by Skp2 overexpression may be a common event in various salivary gland cancers. This is the first report on Skp2 expression in ACC. Previously, we reported that down-regulation of p27 was well correlated with metastasis in ACC [34]. In the present study, we also found similar relationship; 5 of 7 (71%) cases with metastasis showed low expression of p27, while 22 of 43 (51%) cases without metastasis showed low expression of p27 (data not shown). However, we could not find possible association between Skp2 expression and metastasis. This discrepancy may be accounted for by other pathways of p27 degradation such as Jab1, KPC, and so on [11, 37]. To clarify the detailed mechanism of p27 degradation in cancer, further studies are required. Although it is generally regarded that subtypes of dominant tubular or cribriform pattern have much better prognosis than those with predominantly solid patterns [5–7], we could not find the association between Skp2 expression and histological grading. Interestingly, Skp2 expression was well correlated with PCNA. These data were confirmed by the finding that Skp2 knockdown by using siRNA transfection inhibited cell growth through accumulation of p27 protein in ACC cells (Fig. 3). We suggest that Skp2 overexpression may be involved in growth of ACC cells through p27 protein degradation and that Skp2 siRNA can be a therapeutic target for ACC patients.

In conclusion, we showed that Skp2 expression is strongly correlated with p27 down-regulation and cell proliferation in ACC. Our findings are in agreement with those reported previously and provide evidence for the p27 degradative function of Skp2 in ACC.

Acknowledgments This work is supported in part by grants-in-aid from the Ministry of Education, Science and Culture of Japan to YK, IO, and TT.

References

1. Carrano AC, Eytan E, Hershko A, Pagano M (1999) SKP2 is required for ubiquitin-mediated degradation of the CDK inhibitor p27. Nat Cell Biol 1:193–199
2. Chiarle R, Budel LM, Skolnik J, Frizzera G, Chilosi M, Corato A, Pizzolo G, Magidson J, Montagnoli A, Pagano M, Maes B, De Wolf-Peeters C, Inghirami G (2000) Increased proteasome degradation of cyclin-dependent kinase inhibitor p27 is associated with a decreased overall survival in mantle cell lymphoma. Blood 95:619–626
3. Chiarle R, Fan Y, Piva R, Boggino H, Skolnik J, Novero D, Palestro G, De Wolf-Peeters C, Chilosi M, Pagano M, Inghirami G (2002) S-phase kinase-associated protein 2 expression in non-Hodgkin's lymphoma inversely correlates with p27 expression and defines cells in S phase. Am J Pathol 160:1457–1466
4. Chilla R, Schroth R, Eysholdt V, Droese M (1980) Adenoid cystic carcinoma of the head and neck: Controllable and uncontrollable factors in treatment and prognosis. ORL J Otorhinolaryngol Relat Spec 42:346–367
5. Chomette G, Auriol M, Tranbaloc P, Vaillant JM (1982) Adenoid cystic carcinoma of minor salivary glands: Analysis of 86 cases. Clinico-pathological, histoenzymological and ultrastructual studies. Virchows Arch 395:289–301
6. Gates GA (1982) Malignant neoplasm of the minor salivary glands. N Engl J Med 306:718–722
7. Goepfert H, Luna MA, Lindberg RD, White AK (1983) Malignant salivary gland tumors of the paranasal sinuses and nasal cavity. Arch Otolaryngol 109:662–668
8. Gstaiger M, Jordan R, Lim M, Catzavelos C, Mestan J, Slingerland J, Krek W (2001) Skp2 is oncogenic and overexpressed in human cancers. Proc Natl Acad Sci USA 98:5043–5048
9. Hershko D, Bornstein G, Ben-Izhak O, Carrano A, Pagano M, Krausz MM, Hershko A (2001) Inverse relation between levels of $p27^{Kip1}$ and of its ubiquitin ligase subunit Skp2 in colorectal carcinomas. Cancer 91:1745–1751
10. Hunter T, Pines J (1994) Cyclins and cancer II: cyclin D and CDK inhibitors come of age. Cell 79:573–582

11. Kamura T, Hara T, Matsumoto M, Ishida N, Okumura F, Hatakeyama S, Yoshida M, Nakayama K, Nakayama KI (2004) Cytoplasmic ubiquitin ligase KPC regulates proteolysis of $p27^{Kip1}$ at G1 phase. Nat Cell Biol 6:1229–1235
12. Khan AJ, DiGiovanna MP, Ross DA, Sasaki CT, Carter D, Son YH, Haffty BG (2001) Adenoid cystic carcinoma: a retrospective clinical review. Int J Cancer 96:149–158
13. Kudo Y, Kitajima S, Ogawa I, Sato S, Miyauchi M, Takata T (2001) High expression of Skp2, human F-box protein, correlates with poor prognosis in oral squamous cell carcinomas. Cancer Res 61:7044–7047
14. Kudo Y, Kitajima S, Sato S, Ogawa I, Miyauchi M, Takata T (2002) Transfection of $p27^{Kip1}$ threonine residue 187 mutant type gene, which is not influenced by ubiquitin-mediated degradation, induces cell cycle arrest in oral squamous cell carcinoma cells. Oncology 63:398–404
15. Kudo Y, Kitajima S, Ogawa I, Miyauchi M, Takata T (2005) Down-regulation of Cdk inhibitor p27 in oral squamous cell carcinoma. Oral Oncol 41:105–116
16. Latres E, Chiarle R, Schulman BA, Pavletich NP, Pellicer A, Inghirami G, Pagano M (2001) Role of the F-box protein Skp2 in lymphomagenesis. Proc Natl Acad Sci USA 98:2515–2520
17. Loda M, Cukor B, Tam S, Lavin P, Fiorentino M, Draetta GF, Jessup JM, Pagano M (1997) Increased proteasome-dependent degradation of the cyclin-dependent kinase inhibitor p27 in aggressive colorectal carcinomas. Nat Med 3:231–234
18. Masuda TA, Inoue H, Sonoda H, Mine S, Yoshikawa Y, Nakayama K, Nakayama K, Mori M (2000) Clinical and biological significance of S-phase kinase-associated protein 2 (Skp2) gene expression in gastric carcinoma: modulation of malignant phenotype by Skp2 overexpression, possibly via p27 proteolysis. Cancer Res 62:3819–3825
19. Montagnoli A, Fiore F, Eytan E, Carrano AC, Draetta GF, Hershko A, Pagano M (1999) Ubiquitination of p27 is regulated by Cdk-dependent phosphorylation and trimeric complex formation. Genes Dev 13:1181–1189
20. Moore GE, Gerner RE, Franklin HA (1967) Culture of normal human leukocytes. JAMA 199:519–524
21. Nascimento AG, Amaral AL, Prado LA, Kligerman J, Silveira TR (1986) Adenoid cystic carcinoma of the salivary glands. A study of 61 cases with clinicopathologic correlation. Cancer 57:312–319
22. Pagano M, Tam SW, Theodoras AM, Beer-Romero P, Del Sal G, Chau V, Yew PR, Draetta GF, Rolfe M (1995) Role of the ubiquitin proteasome pathway in regulating abundance of the cyclin-dependent kinase inhibitor p27. Science 269:682–685
23. Peel RL, Gnepp DR (1985) Disease of the salivary glands. In: Barnes L (ed) Surgical pathology of the head and neck. Dekker, New York, pp 533–545
24. Piva R, Cancelli I, Cavalla P, Bortolotto S, Dominguez J, Draetta GF, Schiffer D (1999) Proteasome-dependent degradation of p27/kip1 in gliomas. J Neuropathol Exp Neurol 58:691–696
25. Polyak K, Lee MH, Erdjument-Bromage H, Koff A, Roberts JM, Tempst P, Massague J (1994) Cloning of $p27^{Kip1}$, a cyclin-dependent kinase inhibitor and a potential mediator of extracellular antimitogenic signals. Cell 78:59–66
26. Sato JD, Kawamoto T, Okamoto T (1987) Cholesterol requirement of P3-X63-Ag8 and X63-Ag8.653 mouse myeloma cells for growth in vitro. J Exp Med 165:1761–1766
27. Sherr CJ (1994) G1 phase progression: cycling on cue. Cell 79:515–555
28. Shipley GD, Pittelkow MR (1987) Control of growth and differentiation in vitro of human prokeratinocytes cultured in serum-free medium. Arch Dermatol 123:1541–1544
29. Signoretti S, Di Marcotullio L, Richardson A, Ramaswamy S, Isaac B, Rue M, Monti F, Loda M, Pagano M (2002) Oncogenic role of the ubiquitin ligase subunit Skp2 in human breast cancer. J Clin Invest 110:633–641
30. Slingerland JM, Pagano M (2000) Regulation of the cdk inhibitor p27 and its deregulation in cancer. J Cell Physiol 183:10–17
31. Spiro RH, Huvos AG, Strong EW (1974) Adenoid cystic carcinoma of salivary origin: a clinicopathologic study of 242 cases. Am J Surg 128:512–520
32. Sutterluty H, Chatelain E, Marti A, Wirbelauer C, Senften M, Muller U, Krek W (1999) p45SKP2 promotes $p27^{Kip1}$ degradation and induces S phase in quiescent cells. Nat Cell Biol 1:207–214
33. Szanto PA, Luna MA, Tortoledo E, White RA (1984) Histologic grading of adenoid cystic carcinoma of the salivary glands. Cancer 54:1062–1069
34. Takata T, Kudo Y, Zhao M, Ogawa I, Miyauchi M, Sato S, Cheng J, Nikai H (1999) Reduced expression of $p27^{Kip1}$ protein in relation to metastasis in salivary adenoid cystic carcinoma. Cancer 86:928–935
35. Tan P, Cady B, Wanner M, Worland P, Cukor B, Magi-Galluzzi C, Lavin P, Draetta G, Pagano M, Loda M (1997) The cell cycle inhibitor p27 is an independent prognostic marker in small (T1a, b) invasive breast carcinomas. Cancer Res 57:1259–1263
36. Tomich CE (1991) Adenoid cystic carcinoma. In: Ellis GE, Auclair PL, Gnepp DR (eds) Surgical Pathology of the salivary glands. Saunders, Philadelphia, pp 333–349
37. Tomoda K, Kubota Y, Kato JY (1999) Deregulation of the cyclin-dependent-kinase inhibitor $p27^{Kip1}$ is instigated by Jab1. Nature 398:160–165
38. Toyoshima H, Hunter T (1994) p27, a novel inhibitor of G1 cyclin–Cdk protein kinase activity, is related to p21. Cell 78:67–74
39. Tsvetkov LM, Yeh KH, Lee S, Sun H, Zhang H (1999) $p27^{Kip1}$ ubiquitination and degradation is regulated by the SCF^{Skp2} complex through phosphorylated Thr187 in p27. Curr Biol 9:661–664
40. van der Wal JE, Becking AG, Snow GB, van der Waal I (2002) Distant metastases of adenoid cystic carcinoma of the salivary glands and the value of diagnostic examinations during follow-up. Head Neck 24:779–783
41. Vuhahula EA, Nikai H, Ogawa I, Miyauchi M, Takata T, Ito H, Ito R (1995) Correlation between argyrophilic nucleolar organizer region (AgNOR) counts and histologic grades with respect to biologic behavior of salivary adenoid cystic carcinoma. J Oral Pathol Med 24:437–442
42. Yokoi S, Yasui K, Saito-Ohara F, Koshikawa K, Iizasa T, Fujisawa T, Terasaki T, Horii A, Takahashi T, Hirohashi S, Inazawa J (2002) A novel target gene, SKP2, within the 5p13 amplicon that is frequently detected in small cell lung cancers. Am J Pathol 161:207–216
43. Zhang H, Kobayashi R, Galaktionov K, Beach D (1995) p19Skp-1 and p45Skp-2 are essential elements of the cyclin A-Cdk2 S phase kinase. Cell 82:915–925

Virchows Arch (2007) 450:575–584
DOI 10.1007/s00428-007-0394-7

ORIGINAL ARTICLE

Predominant expression of OLIG2 over ID2 in oligodendroglial tumors

Shuji Mikami · Yuichi Hirose · Kazunari Yoshida · Takeshi Kawase · Akiko Ohnishi · Kazuo Nagashima · Makio Mukai · Yasunori Okada · Eiji Ikeda

Received: 25 October 2006 / Revised: 23 January 2007 / Accepted: 21 February 2007 / Published online: 13 March 2007
© Springer-Verlag 2007

Abstract OLIG2 is a basic helix–loop–helix transcription factor regulating the generation of oligodendrocytes from neural progenitor cells, and the function of OLIG2 is inhibited posttranslationally through the interaction with ID2. This study aims to examine if the analysis of OLIG2 and ID2 expression in glioma tissues helps the differential diagnosis of chemosensitive oligodendroglial tumors from astrocytic tumors. Expression levels of OLIG2 and ID2 in 11 oligodendroglial and 27 astrocytic tumors were analyzed by reverse transcription-polymerase chain reaction (RT-PCR), real-time quantitative PCR, and immunohistochemistry. The mean expression level of OLIG2 was higher in oligodendroglial tumors than astrocytic tumors, but some astrocytic tumors showed high OLIG2 expression, indicating that OLIG2 cannot be an independent marker of oligodendroglial tumors. No significant difference was observed between ID2 expression in oligodendroglial tumors and astrocytic tumors. It was notable that OLIG2 expression was predominant over ID2 expression in oligodendroglial tumors, while ID2 expression was predominant over OLIG2 expression in astrocytic tumors. Comparative genomic hybridization revealed that gliomas with loss on chromosome 1p, which is closely associated with chemosensitivity, also showed the predominant expression of OLIG2 over ID2. These results indicate that the immunohistochemical study on the relative expression level of OLIG2 to ID2 can be a useful screening for oligodendroglial tumors.

Keywords OLIG2 · ID2 · Oligodendroglioma · CGH · 1p

S. Mikami · Y. Okada · E. Ikeda (✉)
Department of Pathology, School of Medicine, Keio University,
35 Shinanomachi, Shinjuku-ku, Tokyo 160-8582, Japan
e-mail: eikeda@sc.itc.keio.ac.jp

S. Mikami · M. Mukai
Division of Diagnostic Pathology, Keio University Hospital,
35 Shinanomachi, Shinjuku-ku, Tokyo 160-8582, Japan

Y. Hirose · K. Yoshida · T. Kawase
Department of Neurosurgery, School of Medicine, Keio University,
35 Shinanomachi, Shinjuku-ku, Tokyo 160-8582, Japan

A. Ohnishi · K. Nagashima
Laboratory of Molecular and Cellular Pathology,
Hokkaido University Graduate School of Medicine,
Kita 15, Nishi 7, Kita-ku, Sapporo 060-8638, Japan

Present address:
A. Ohnishi
Neurosurgery Division, National Cancer Center Hospital,
5-1-1, Tsukiji, Chuo-ku, Tokyo 104-0045, Japan

Introduction

Gliomas are the most common primary tumors originating in the cranium [9]. A certain group of oligodendroglial tumors are of favorable prognosis with increased sensitivity to chemotherapy with procarbazine, lomustine, and vincristine which is termed PCV therapy [4, 6], while astrocytic tumors are generally refractory to treatments including surgery, radiation, and chemotherapy [19]. Furthermore, recent studies have demonstrated that losses on chromosomes 1p and 19q are frequently found in oligodendroglial tumors and that especially the loss on 1p is correlated with the longer recurrence-free survival with increased chemosensitivity to PCV therapy [4, 6, 20]. Although the accurate diagnosis of gliomas is crucial to provide the appropriate treatment, there are problems regarding the interpretation of histological criteria for the classification of gliomas, which are most apparent with respect to differentiating oligodendroglial tumors from astrocytic tumors [5].

OLIG1 and OLIG2 were identified as the basic helix–loop–helix factors (bHLHs) which are expressed in cells of oligodendrocyte lineage, and OLIG2 is thought to be an earliest marker of developing oligodendrocyte [11, 24]. However, the expression of OLIG2 is detected not only in oligodendroglial tumors but also in astrocytic tumors [2, 10, 14, 16, 23]. Therefore, the expression of OLIG2 in tumor cells does not necessarily mean their biological commitment to the oligodendrocyte lineage. Inhibitor of differentiation (ID) proteins, ID1, ID2, ID3, and ID4, are the factors which are structurally similar to bHLH factors except for their lacking of the basic DNA binding sequence [17]. IDs inhibit as dominant negative regulators the functions of bHLH factors including OLIG2 by blocking their heterodimerization and subsequent binding to DNA sequences [1, 18]. An in vitro study showed that overexpression of ID2 inhibits the oligodendrocyte differentiation, while absence of ID2 led to the differentiation of premature oligodendrocyte [22]. Inhibitory effects of bone morphogenetic protein 4 (BMP4) on the generation of oligodendrocytes by neural progenitor cells was shown to be mediated by the suppressed heterodimerization of OLIG proteins through induction of ID2 and/or ID4 [18]. These data indicate that the interaction between OLIGs and IDs plays a role in the glial cell development. Therefore, it is possible that the interaction between these two molecules is also involved in the cell lineage commitment of glioma cells. In fact, IDs1-3 expression level was reported to be significantly higher in astrocytomas compared to that in oligodendroglial tumors [21]. Among IDs1-3, ID2 was shown to inhibit the oligodendroglial differentiation through the interaction with OLIG2 [18]. To our knowledge, studies on the interaction between OLIG2 and ID2 protein in glioma cells and its association with histological subtypes have not been performed. Here, we have demonstrated that the data showing that the expression of OLIG2 is exclusively predominant over that of ID2 in oligodendroglial tumors, and therefore the immunohistochemical analyses of OLIG2 and ID2 in glioma cells can be a useful screening of oligodendroglial tumors.

Materials and methods

Glioma samples

Glioma tissues were surgically resected from 38 patients and immersion fixed in 10% neutral buffered formalin solution and embedded in paraffin for histological examination and comparative genomic hybridization (CGH). The clinicopathological parameters of glioma tissues investigated in this study were summarized in Table 1. Two non-neoplastic brain tissues, which had surrounded the removed metastatic brain tumor, were also used for immunostaining of OLIG2 and ID2. As for ten samples (patients' no. 1, 7, 8, 9, 10, 11, 13, 17, 22, and 27 in Table 1), small pieces of tumor tissues were frozen in liquid nitrogen to determine the mRNA expression levels of OLIG2 and ID2.

Hematoxylin and eosin (HE)-stained sections were reviewed independently by two certified pathologists (S. M. and E. I.) and classified in principle based on the World Health Organization (WHO) Classification of Tumors of the Nervous System [9]. Diagnostic discrepancy was found in six samples between two pathologists after the first review, and their consensus diagnoses were made by mutual agreement through sufficient discussion (Table 2). Finally, the gliomas used in this study (38 gliomas) were 11 oligodendroglial tumors [6 oligodendroglioma (WHO grade II) and 5 anaplastic oligodendrogliomas (WHO grade III)], 27 astrocytic tumors [11 diffuse astrocytomas (WHO grade II), 8 anaplastic astrocytomas (WHO grade III)] and 8 glioblastomas (WHO grade IV) (Table 1). For the experimental use of the surgical specimens, informed consent was obtained from the patients according to the hospital ethical guidelines with the Helsinki declaration.

RT-PCR and real-time quantitative PCR

Total RNA were extracted from ten tumor samples using ISOGEN (Nippon Gene, Toyama, Japan) according to the manufacturer's instruction, and the quality of RNA was evaluated with Agilent 2100 Bioanalyzer (Agilent Technologies, Palo Alto, CA). One microgram of total RNA was reverse transcribed with ReveTra Ace Reverse Transcriptase (TOYOBO, Tokyo, Japan) in a 20-μl reaction volume containing Oligo $(dT)_{12–18}$ primers. One microliter of reaction mixture was then subjected to 30 cycles of polymerase chain reaction (PCR) for amplification of cDNAs for OLIG2, ID2, and β-actin. PCR was performed in a 50-μl reaction volume containing 200 nM of each primer, 200 nM of dNTPs, and 2.5 U *Taq* DNA polymerase (Takara Bio., Shiga, Japan) with a thermal controller (MiniCycler; MJ Research, Watertown, MA). The thermal cycle was 1 min at 94°C, 1 min at 60°C (for OLIG2 and ID2), or 67°C (for β-actin), and 1 min at 72°C, followed by final extension for 10 min at 72°C. Primer sequences were 5′-CCCTGAGGCTTTTCGGAGCG-3′ (forward) and 5′-GCGGCTGTTGATCTTGAGACGC-3′ (reverse) for OLIG2; 5′-CTGGACTCGCATCCCACTAT-3′ (forward) and 5′-AGATTGGGCAATTCCTTGTG-3′ (reverse) for ID2; 5′-TGACGGGGTCACCCA CACTGTGCCCATGTA-3′ (forward) and 5′-CTAGAAG CATTTGCGGTGGAC GATGGAGGG-3′ (reverse) for β-actin. Expected sizes of amplified cDNAs for OLIG2, ID2, and β-actin are 452, 491, and 661 bp, respectively. Five microliters of each PCR product was electrophoresed on a 2% agarose gel and then stained with ethidium bromide.

Table 1 Summary of the clinicopathological parameters, the OLIG2 and ID2 expression and the chromosomal aberration in gliomas

Patients' number	WHO grade	Age/ gender	ID2 IR score	OLIG2 IR score	Gain	Chromosomal aberration loss
1	OII	53/M	0.30	0.44		1p, 13q, 19q
2	OII	41/M	0.90	1.30	17q	1p, 19q
3	OII	59/M	0.09	1.26	7p, 8q21.1-ter, 10p	13q14–32, 16q, 19q
4	OII	28/M	0.25	0.41	10	1p, 18, 19q, X
5	OII	47/F	0.30	1.16	7q31.3-ter, 10, 20	1p, 19q
6	OII	6/F	0.15	1.32	7q22-ter, 8q, 10p	X
7	OIII	77/F	2.70	2.79	1q, 3q, 7, 11, 16, 20,	4, 9, 12, 14q, 15q, 18, 19q
8	OIII	39/M	1.60	1.66		1p, 4, 19q
9	OIII	31/M	0.13	2.25	15q24-ter	1p, 13q, 19q
10	OIII	50/F	0.70	1.98	7q, 8q, 15q24–25	10q23-ter, 13q14–21,
11	OIII	37/F	0.70	2.97	1q21-24, 7q, 16, 17, 19p, 20, 21q	1p, 4q23–27, 14q, 19q,
12	AII	22/M	0.97	0.27	8q22-ter, 10pter-q23,	10q25-ter, X
13	AII	30/M	1.96	0.12	17q, 19p	10, 17p,
14	AII	63/F	0.65	0.90	1q, 2q24–31, 4q12-28, 7, 9	1p. 4q31-ter, 6q, 10 13q12-21, 14q, 17p, 19q
15	AII	9/F	1.46	0.41	6q16–24, 9p22–12, 22q	
16	AII	10/M	0.05	0.10	7q11.2–22, 9q31-ter, 11q	12q21–24.2, 20p
17	AII	45/M	1.70	0.50	7q11.2–22, 19,	11q23-ter
18	AII	47/F	0.15	0.10	7q33-ter, 10q	X
19	AII	38/M	0.57	0.01	7q32-ter	10q23-ter, 14q24-ter
20	AII	36/M	1.54	0.45	7q22-ter, 8q, 10pter-q24,	9p, X
21	AII	29/M	0.45	0.03	7q31.3-ter, 10p, 19	X
22	AII	27/M	2.64	0.02	7q31.3-ter, 10, 20	
23	AII	38/M	0.10	0.80	7q32-ter, 10p	9p, 13q22–32, 22q
24	AIII	27/M	1.80	0.85	7, 19, X	12q22-ter
25	AIII	27/F	1.34	0	5p, 7pter-21, 8, 10pter-13, 12p	3, 4q28-ter, 10q, 13q14–31
26	AIII	26/M	1.10	0	7p, 9q22–33, 15q22–24	
27	AIII	27/M	1.98	1.20	7p, 8q, 10p, 14q24.3ter	3p21–13, 13q, 16q, 19q, X
28	AIII	62/M	0.47	0.05	2pter-23, 7p, 15q21-ter	9p, 10, 11p, 13q21-ter, 14q13-ter
29	AIII	76/F	2.97	2.94	7q, 8q, 9, 17q	8p, 14q, 17p, 19q
30	AIII	39/F	2.55	0.35	1q21–31, 2p16-11.2, 7q, 8q23-ter, 17q	1q32.2-ter, 5q, 6q, 9q22-33 10p, 19q, Xp
31	AIV	25/F	1.24	1.58	2p, 9q22–33, 14q, 17q22-23, 20q	2q24-ter, 10q, 13q, 16, 19q, Xq
32	AIV	61/F	1.04	0.20	7p13-qter, 10q21.2–22.1, 14q, 19	9p22–12, 10p13–12, 10q25–26.1, 21q
33	AIV	14/M	2.94	0.97	1q, 2p21–11, 5p, 7p, 9q13-33	2q11.2–22, 11p, 19q
34	AIV	68/M	0.40	1.10	7q31–32	
35	AIV	77/F	0.42	0.27	15q, 10q	2p24–14, 6q13–24, 13q21-ter, X
36	AIV	66/F	0.03	1.29	+3q, +7	1q31-ter, 5q, 6q13–24, 10q23-ter 11q14–22, 12q13–15, 13q21.3–31, 19q
37	AIV	60/M	0	1.60	7q32-ter, 10q, 20	X
38	AIV	29/M	0.10	0.76	1q21–32, 7, 8q, 9q, 10p, 18	9p, 13q13–21, 14q22–24, X

OII oligodendroglioma, grade II, *OIII* anaplastic oligodendroglioma, *AII* diffuse astrocytoma, *AIII* anaplastic astrocytoma, *AIV* glioblastoma

For quantitative analysis of OLIG2 and ID2 mRNA expression, cDNA was used as template in a TaqMan real-time PCR assay (ABI Prism 7000 Sequence Detection System, Applied Biosystems, Foster City, CA), as described previously [13]. Cycling conditions were 50°C for 10 min, 95°C for 10 min, and then 40 cycles at 95°C for 15 s and 60°C for 1 min. The primers and TaqMan probes sets (TaqMan Gene Expression Assays, Inventoried) for OLIG2 (Hs00300164_s1), ID2 (Hs00747379_m1) and human β-actin endogenous control (4310881E) were purchased from Applied Biosystems, CA (sequences not disclosed). Data were normalized to β-actin, and the OLIG2/ID2 mRNA ratio was calculated for each sample.

Immunohistochemistry

Paraffin sections (4 μm thick) were mounted on 3-aminopropyl triethoxysilane-coated glasses. After deparaffinization, the slides were treated for 20 min with microwave in 10 mM citrate buffer (pH 6.0) for antigen retrieval. They were incubated with methanol containing 0.3% hydrogen peroxide for 15 min at room temperature and subsequently

Table 2 Diagnostic concordance rates (%) for histological diagnosis of gliomas

Consensus diagnosis	Diagnostic concordance rates (%)	Patients' number of the cases showing diagnostic discrepancies
OII (n=6)	83	4
OIII (n=5)	60	8, 10
AII (n=12)	75	20, 22, 23
AIII (n=7)	100	
AIV (n=8)	100	
Total (n=38)	84	

OII Oligodendroglioma, grade II, *OIII* anaplastic oligodendroglioma, *AII* diffuse astrocytoma, *AIII* anaplastic astrocytoma, *AVI* glioblastoma

with 10% normal goat serum for 15 min at room temperature. Then, the sections were incubated with rabbit polyclonal antibodies against OLIG2 (1/500 dilution; generated by Nagashima K) [16] or ID2 (1/100 dilution; sc-489, Santa Cruz Biotechnology) for 60 min at room temperature. After being washed in phosphate-buffered saline (PBS), they were incubated with goat antibodies against rabbit immunoglobulins conjugated to a peroxidase-labeled dextran polymer (En Vision+rabbit; DAKO JAPAN, Tokyo, Japan) for 30 min at room temperature. As the negative control, the primary antibodies were replaced with nonimmune rabbit immunoglobulins (DakoCytomation Denmark A/S). Color was developed with 3,3′-diaminobenzidine tetrahydrochloride (0.2 mg/ml; Dojindo Laboratories) in 0.05 M Tris–HCl (pH 7.6) containing 0.003% H_2O_2, and the sections were counterstained with hematoxylin.

Double staining of OLIG2 and ID2 was performed to examine their co-expression in a glioma cell. Deparaffinized sections were microwaved in 10 mM citrate buffer (pH 6.0), followed by incubation with methanol containing 0.3% hydrogen peroxide for 15 min, 10% normal goat serum for 15 min, rabbit polyclonal antibodies against ID2 (1/100 dilution; sc-489, Santa Cruz Biotechnology) for 60 min. After being washed in PBS, they were incubated with goat antibodies against rabbit immunoglobulins conjugated to a peroxidase-labeled dextran polymer (Histofine® Simple Stain MAX PO; Nichirei, Tokyo, JAPAN) for 30 min. Color was developed with 3,3′-diaminobenzidine tetrahydrochloride (0.2 mg/ml; Dojindo Laboratories) in 0.05 M Tris–HCl (pH 7.6) containing 0.003% H_2O_2. The sections were heated in 10 mM citrate buffer (pH 6.0) at 120°C for 15 min to exclude the possibility of a cross-reaction and then sequentially incubated with 10% normal goat serum for 15 min, rabbit polyclonal antibodies against OLIG2 (1/500 dilution; generated by Nagashima K) [16] for 60 min, goat antibodies against rabbit immunoglobulins conjugated to a peroxidase-labeled dextran polymer (ImmPress Reagent; Vector Laboratories, Burlingame, CA) for 30 min. Color was developed with Vector® SG substrate kit (Vector Laboratories), according to the manufacturer's instruction.

Semiquantification of OLIG2 and ID2 expression in glioma tissues

The degree of OLIG2 and ID2 expression in each glioma was semiquantified as the immunoreactivity score (IR score) according to the previously reported method [21] with modification. In brief, for the intensity score, signal intensity was stratified into four categories; 0, no signals; 1, weak intensity; 2, moderate intensity; 3, strong intensity. The proportion score was determined, by counting at least 1,000 cells in randomly selected fields, as the ratio of positively stained cells to the whole cells; 0 (0%) to 1.0 (100%). Finally, the indices of representation (IR) score was calculated by multiplying the intensity score and the proportion score together and used as the degree of OLIG2 or ID2 expression.

Comparative genomic hybridization (CGH)

The CGH analysis was performed according to a protocol described elsewhere [7, 8] with slight modification. Briefly, tumor DNA was extracted from a microdissected piece of

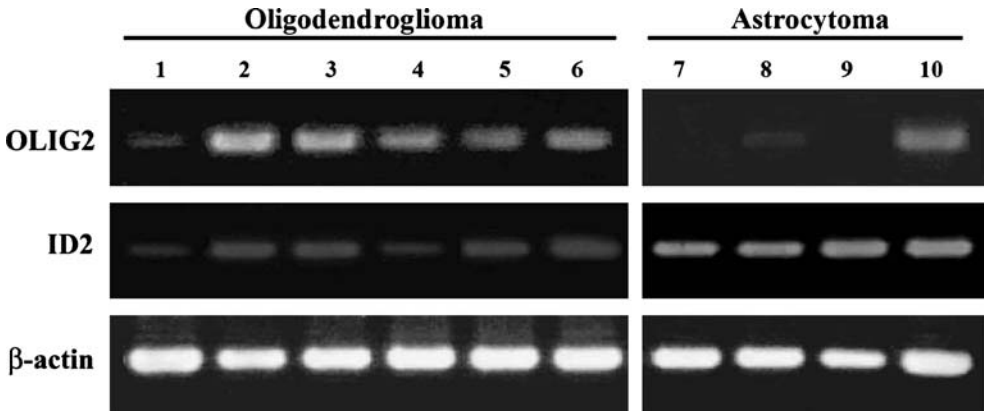

Fig. 1 Expression of OLIG2 and ID2 mRNAs in oligodendroglial tumors and astrocytic tumors. By RT-PCR, the OLIG2 mRNA is detected in all the oligodendroglial tumors (*lanes 1–6*) (100%) and two out of four astrocytic tumors (*lanes 7–10*) (50%), while the ID2 mRNA is expressed in all the oligodendroglial tumors (100%) and astrocytic tumors (100%)

Table 3 Summary of the clinicopathological parameters and the relative OLIG2 to ID2 mRNA ratio determined by real-time quantitative PCR

Lane number in Fig. 1 (patients' number in Table 1)	WHO grade	Age/ gender	OLIG2/ β-actin	ID2/ β-actin	OLIG2/ ID2
1 (1)	OII	53/M	0.4	0.1	3.1
2 (7)	OIII	77/F	3.2	0.6	4.9
3 (8)	OIII	39/M	3.4	0.4	7.7
4 (9)	OIII	31/M	3.6	0.1	32
5 (10)	OIII	50/F	2.9	0.7	4.4
6 (11)	OIII	37/F	6.2	1.2	5.1
7 (13)	AII	30/M	0.04	0.8	0.05
8 (17)	AII	45/M	0.3	0.9	0.3
9 (22)	AII	27/M	0.04	1.2	0.04
10 (27)	AIII	27/M	3.6	1.1	3.4

OII Oligodendroglioma, grade II, *OIII* anaplastic oligodendroglioma, *AII* diffuse astrocytoma, *AIII* anaplastic astrocytoma

formalin-fixed and paraffin-embedded tissue section (5 μm thick) and amplified by degenerate oligonucleotide-primed polymerase chain reaction (DOP-PCR). Tissue microdissection was performed referring to the pathological findings of consecutive sections that were stained with HE to select the region of truly neoplastic tissue. DNA was labeled with another DOP-PCR reaction using digoxygenin (DIG)-11-dUTP (Roche, Indianapolis, IN), and the reference DNA was amplified from 50 ng normal male DNA and labeled as described above except that rhodamine-dUTP (Roche) was used instead of DIG-dUTP. The probe mixture was denatured and hybridized to normal metaphase spreads (Vysis, Downers Grove, IL). After unhybridized probes were washed, the metaphase spread was incubated with fluorescent isothiocyanate-conjugated anti-DIG-antibody (Roche). The preparations were washed and counterstained with 4,6-diamino-2-phenylinodole in antifade solution. Red, green, and blue images were acquired, and the ratios of fluorescence intensity along the chromosomes were quantitated using the CytoVision analysis system (Applied Imaging, San Jose, CA).

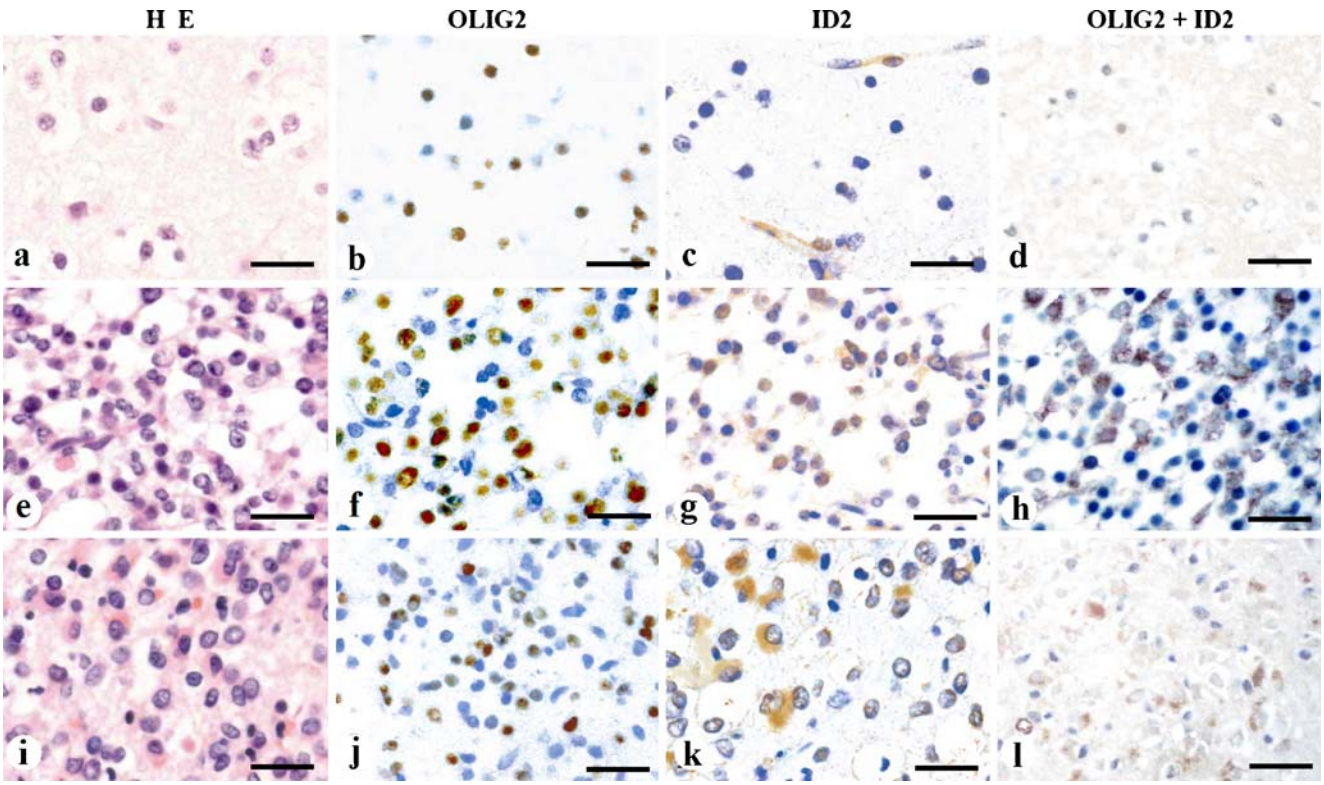

Fig. 2 OLIG2 and ID2 expression in oligodendroglial tumors. Expression of OLIG2 and ID2 in oligodendroglioma (**a**–**d**, **i**–**l**) and anaplastic oligodendroglioma (**e**–**h**) was examined by immunohistochemistry. Oligodendroglioma shows diffuse and moderate OLIG2 staining (**b**), while there is no apparent ID2 staining in tumor cells (**c**). Anaplastic oligodendroglioma shows diffuse and strong OLIG2 staining (**f**) with diffuse and weak ID2 staining (**g**). In oligodendroglioma containing minigemistocytes (**i**), not only the same diffuse and moderate OLIG2 staining (**j**) but also the ID2 signal in tumor cells with eosinophilic cytoplasm are noted (**k**). Double immunostaining of OLIG2 (*blue*) and ID2 (*brown*) revealed that the relative expression of OLIG2 to ID2 was closely associated with glioma cell type, even in the same cases (**d**, **h**, **l**). *Bars*, 50 μm. Nuclei were counterstained with hematoxylin in single immunostaining (**b**, **c**, **f**, **g**, **i**, **k**), while no counterstaining was performed in double staining (**d**, **h**, **l**)

Statistical analysis

Statistical analyses were performed using the Mann–Whitney *U* test and chi-square test. *P* values less than 0.05 were considered statistically significant.

Results

Expression of OLIG2 and ID2 in glioma tissues

OLIG2 mRNA expression was observed in all oligodendroglial tumors and two out of four astrocytic tumors, while the ID2 mRNA was expressed in all the oligodendroglial tumors (6/6 tumors) and astrocytic tumors (4/4 tumors) (Fig. 1). Real-time quantitative PCR revealed that the OLIG2/ID2 mRNA ratio in oligodendroglial tumors was higher than that in astrocytic tumors (Table 3).

Immunohistologically, in non-neoplastic brain tissues, weak nuclear OLIG2-staining was observed in round to oval nuclei of oligodendrocytes, and only weak ID2 staining was observed in astrocytes (data not shown).

In oligodendroglial tumors, OLIG2 expression was almost diffusely detected in nuclei of tumor cells, and the signal intensity of OLIG2 was higher in anaplastic oligodendrogliomas than oligodendrogliomas (Fig. 2a,b,e,f). ID2 expression was very weak or negligible in oligodendrogliomas, but moderate ID2 expression seen in anaplastic oligodendrogliomas (Fig. 2a,c,e,g). In oligodendroglial tumors containing minigemistocytes, the staining of OLIG2 was diffuse with no significant difference from that of oligodendroglial tumors composed of only tumor cells with clear cytoplasm (Fig. 2i,j). In contrast, positive staining for ID2 was obtained in minigemistocytes (Fig. 2i,k). Microvessels within tumors were also positive for ID2 (Fig. 2c). Predominant expression of OLIG2 over that of ID2 in oligodendroglial tumor cells with clear cytoplasm was confirmed by double immunostaining (Fig. 2d,h). On the other hand, tumor cells with eosinophilic cytoplasm, such as minigemistocytes, showed higher expression of ID2 than tumor cells with clear cytoplasm (Fig. 2l).

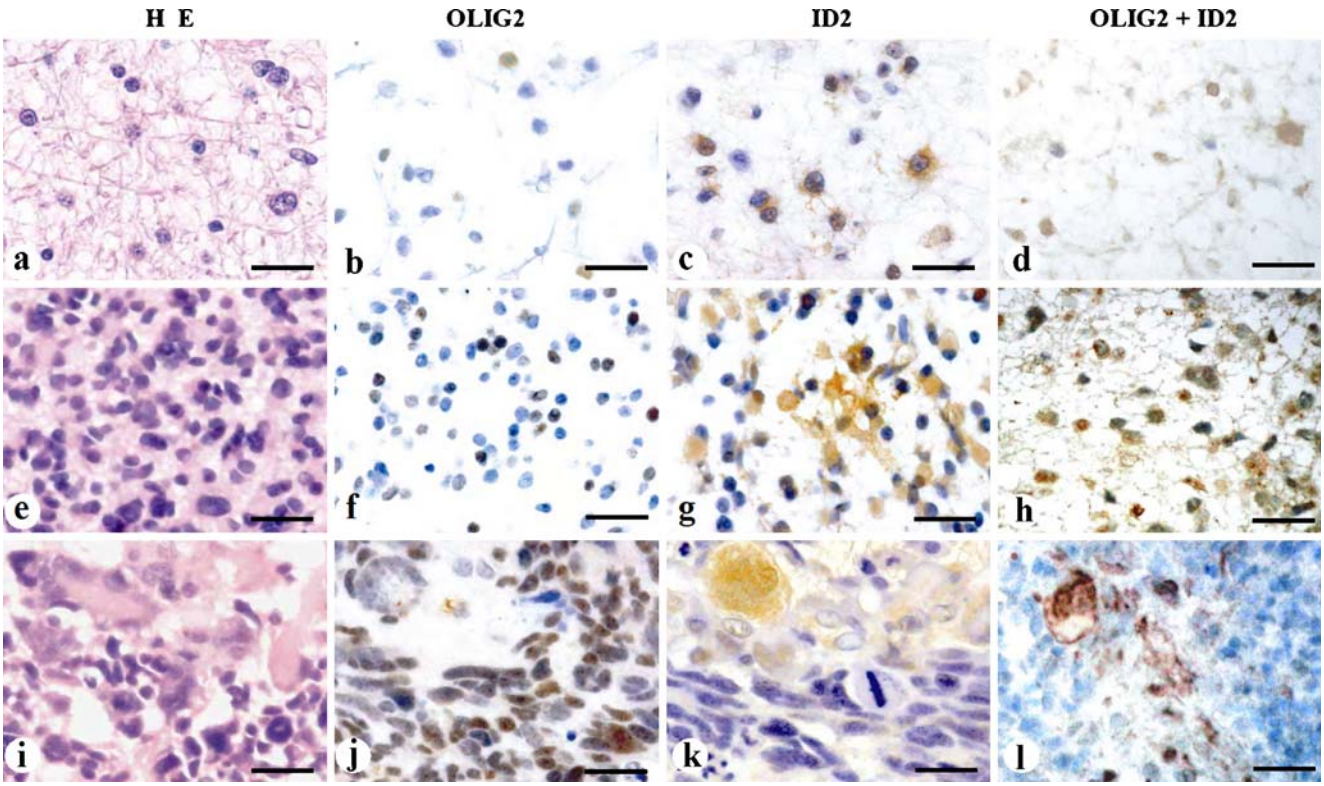

Fig. 3 OLIG2 and ID2 expression in astrocytic tumors. Expression of OLIG2 and ID2 in diffuse astrocytoma (**a**–**d**) and anaplastic astrocytoma (**e**–**h**), and glioblastoma (**i**–**l**) was examined by immunohistochemistry. In diffuse astrocytoma, only a small number of tumor cells are weakly positive for OLIG2 (**b**), whereas the diffuse and moderate staining for ID2 is observed in tumor cells (**c**). In anaplastic astrocytoma, the weak to moderate OLIG2 signal is observed in about half of tumor cells (**f**), and the strong ID2 staining is detected in almost all of the tumor cells (**g**). Glioblastoma contains tumor cells of various morphologies (**i**). Small round tumor cells show moderate staining for OLIG2, but giant cells with plump cytoplasm are negative for OLIG2 (**j**). On the contrary, giant tumor cells are moderately positive for ID2 and small round cells show no apparent ID2 expression (**k**). Double immunostaining of OLIG2 (*blue*) and ID2 (*brown*) revealed that the relative expression of OLIG2 to ID2 was closely associated with glioma cell type, even in the same cases (**d**, **h**, **l**). *Bars*, 50 μm. Nuclei were counterstained with hematoxylin in single immunostaining (**b**, **c**, **f**, **g**, **i**, **k**), while no counterstaining was performed in double staining (**d**, **h**, **l**)

Compared to the distinct signals of OLIG2 in oligodendroglial tumors, its staining in astrocytic tumors was weak and sparse, although the proportion of OLIG2-positive tumor cells and the signal intensity tended to increase as the grade of astrocytic tumors became higher (Fig. 3a,b,e,f,i,j). ID2 was immunolocalized to nuclei and cytoplasms of astrocytic tumor cells (Fig. 3a,c,e,g,i,k), and staining intensity of ID2 was higher in anaplastic astrocytomas than diffuse astrocytomas and glioblastomas (Fig. 3a,c,e,g,i,k). In glioblastomas, small round tumor cells were moderately positive for OLIG2, but giant cells with plump cytoplasm showed no apparent OLIG2 expression (Fig. 3j). On the contrary, giant tumor cells were moderately positive for ID2 and small round tumor cells showed no apparent ID2 expression (Fig. 3k). Double immunostaining revealed that ID2 expression was predominant over OLIG2 expression in tumor cells with rich eosinophilic cytoplasm (Fig. 3d,g,l).

Relationship between the OLIG2 and/or ID2 IR scores of gliomas and the glioma cell lineages

Mean OLIG2 and ID2 IR scores in each histological subtype were summarized in Table 4. Anaplastic oligodendroglioma showed the highest OLIG2 IR score (2.3±0.5), and it was significantly higher than those in the other gliomas; oligodendroglioma, (1.0±0.4, $P<0.01$), diffuse astrocytoma (0.3±0.3, $P<0.001$) and anaplastic astrocytoma (0.8±1.1, $P<0.05$), and glioblastoma (1.0±0.5, $P<0.005$). OLIG2 IR score of diffuse astrocytoma was low compared to those of oligodendrogliomas ($P<0.01$) and anaplastic oligodendroglioma ($P<0.001$), and glioblastoma ($P<0.01$). Anaplastic astrocytoma showed the highest ID2 IR score (1.7±0.9), which was significantly higher than that of oligodendroglioma (0.3±0.3, $P<0.005$).

Correlations between the OLIG2 and/or ID2 IR scores and the histological classification were analyzed, in reference to their availability as the markers for the diagnosis of oligodendroglial tumors. Although the mean OLIG2 IR score of oligodendroglial tumors was significantly high compared to that of astrocytic tumors (Fig. 4a), some oligodendroglial tumors had low OLIG2 IR scores and some astrocytic tumors showed high OLIG2 IR scores. These indicated that OLIG2 expression was not merely restricted to oligodendroglial tumors. There was no significant correlation between ID2 expression and the histological types (Fig. 4b).

Because ID2 inhibits the function of OLIG2 during oligodendrocyte differentiation in vitro [1, 18, 22], the relative OLIG2 IR score to ID2 IR score was evaluated in this study. As shown in Fig. 5a, the ratio of OLIG2 IR score to ID2 IR score of all the oligodendroglial tumors was

Table 4 OLIG2 and ID2 IR score in gliomas

Pathological diagnosis	OLIG2 IR score Mean±SD	ID2 IR score Mean±SD
Oligodendroglial tumor		
Oligodendroglioma (n=6)	1.0±0.4	0.3±0.3
Anaplastic oligodendroglioma (n=5)	2.3±0.5	1.2±1.0
Total (n=11)	1.6±0.8	0.7±0.8
Astrocytic tumor		
Diffuse astrocytoma (n=12)	0.3±0.3	1.0±0.8
Anaplastic astrocytoma (n=7)	0.8±1.1	1.7±0.9
Glioblastoma (n=8)	1.0±0.5	0.8±1.0
Total (n=27)	0.6±0.7	1.1±0.9

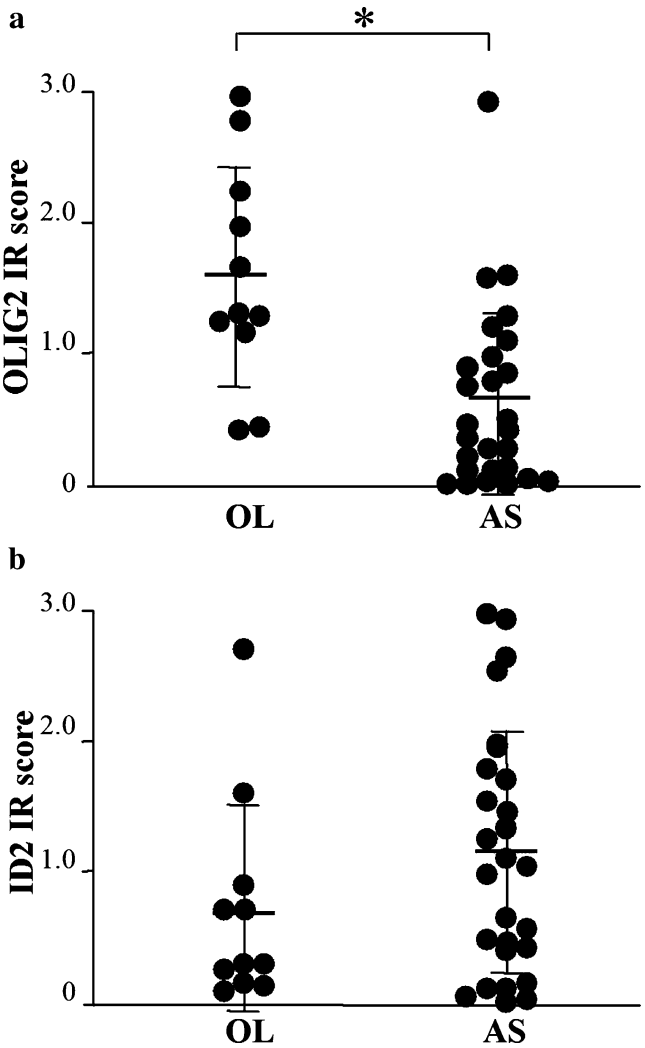

Fig. 4 Correlation between the OLIG2 or ID2 expression and the cell lineage commitment of glioma cells. **a** Oligodendroglial tumors show the higher mean value of OLIG2 IR score than that in astrocytic tumors, and it is statistically significant. However, it is noteworthy that there are oligodendroglial tumors with the OLIG2 scores equal to or lower than those of some astrocytic tumors. **b** No significant correlation is found between the ID2 IR score and the tumor cell lineages. *OL* oligodendroglial tumors, *AS* astrocytic tumors. *$P<$ 0.001, Mann–Whitney U test

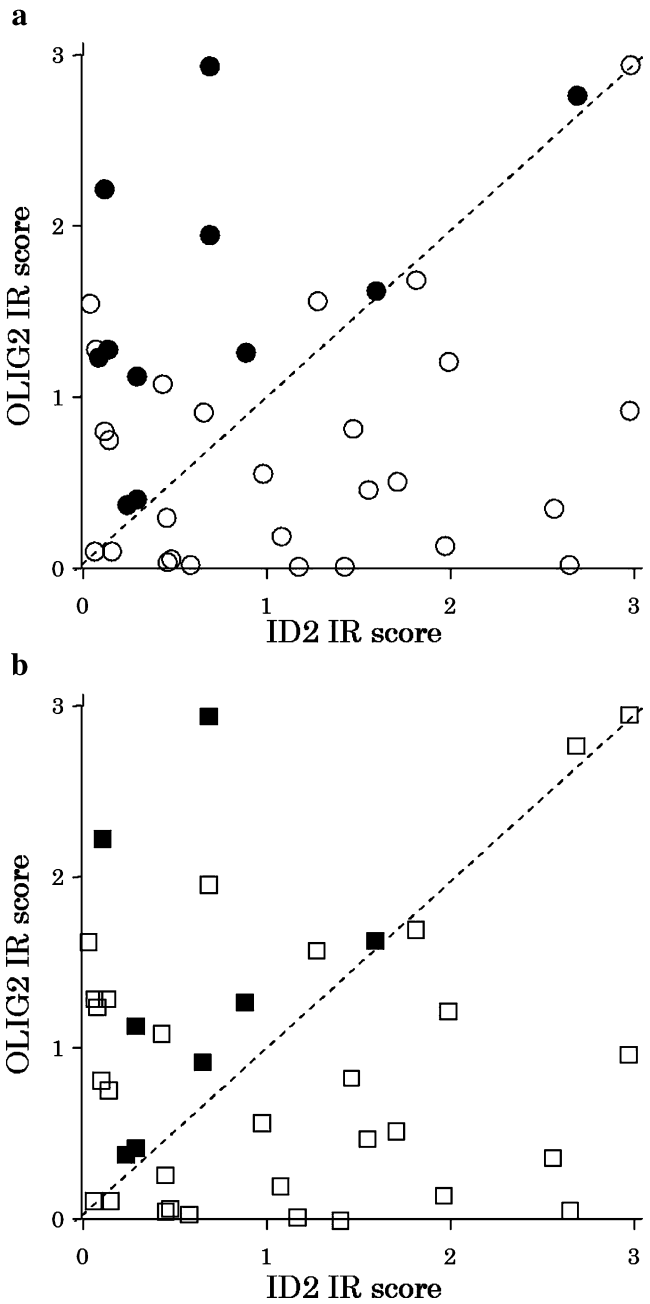

Fig. 5 Relative expression level of OLIG2 to ID2 in gliomas and their correlation with the tumor cell lineage and the loss on chromosome 1p. **a** OLIG2 and ID2 IR scores of gliomas are plotted as scattergrams, and their correlation with the tumor cell lineage is presented. Note that the ratio of OLIG2 IR score to ID2 IR score of all oligodendroglial tumors (*black circles*) are more than 1.0, and 19 of 27 astrocytic tumors (*white circles*) show the ratio equal or less than 1.0. *Black circles* oligodendroglial tumors, *white circles* astrocytic tumors. **b** OLIG2 and ID2 IR scores of gliomas are plotted as scattergrams, in reference to the loss on chromosome 1p. Gliomas with loss on 1p (*black squares*), which are the candidates for chemosensitive gliomas, show the ratio of OLIG2 IR score to ID2 IR score more than 1.0. *Black square* glioma with loss on 1p, *white square* glioma without loss on 1p

Table 5 OLIG2/ID2 IR score ratio and histological classification

Pathological diagnosis	OLIG2/ID2 IR score>1	OLIG2/ID2 IR score<1	Chi-square test
Oligodendroglial tumor (n=11)	100% (n=11)	0% (n=0)	P<0.0005
Astrocytic tumors (n=27)	30% (n=8)	70% (n=19)	

exclusively more than 1.0, while that of astrocytic tumors was equal or less than 1.0 in 19 of 27 cases (70%). There was a statistically significant correlation between the ratio and histological classification (Table 5, P<0.0005, Chi-square test).

Chromosomal aberration of gliomas and its correlation with OLIG2 and/or ID2 IR scores

Chromosomal aberrations of 38 gliomas are summarized in Table 1. This study was focused on the loss on 1p because it is frequently found in oligodendroglial tumors with increased chemosensitivity. In this study, the loss on 1p was detected in 4 of 6 oligodendrogliomas (67%), 3 of 5 anaplastic oligodendrogliomas (60%), 1 of 12 diffuse astrocytomas (8%), 0 of 7 anaplastic astrocytomas (0%) and 0 of 8 glioblastomas (0%). Loss on 1p was always accompanied with loss on 19q. Relationship between the loss on 1p and the OLIG2 and/or ID2 scores is presented in Fig. 5b. It is noteworthy that the ratio of OLIG2 IR score to ID2 IR score of all the gliomas with the loss on 1p was exclusively more than 1.0, while that of gliomas without loss on 1p was less than 1.0 in 19 of 30 cases (63%) (P< 0.005). There was a statistically significant correlation between the ratio and loss on 1p (Table 6, P<0.0005, Chi-square test).

Discussion

Accurate diagnosis is essential for the application of appropriate therapeutic strategies to patients with gliomas [12]. As there are gliomas of similar histological figures

Table 6 OLIG2/ID2 IR score ratio and loss on chromosome 1p

Pathological diagnosis	OLIG2/ID2 IR score>1	OLIG2/ID2 IR score<1	Chi-square test
Glioma with 1p loss (+) (n=8)	100% (n=8)	0% (n=0)	P<0.005
Glioma with 1p loss (−) (n=30)	37% (n=11)	63% (n=19)	

with distinct prognosis, the morphological examination alone cannot provide the sufficient information about biological properties of tumors such as the tumor cell lineage commitment, oligodendroglial, or astrocytic, and the sensitivity to therapies [3]. In this study, we showed for the first time that all oligodendroglial tumors and gliomas with loss on 1p showed predominant expression of OLIG2 over ID2, indicating that the immunohistochemical analysis of these markers is a useful screening for chemosensitive oligodendrogliomas.

OLIG2 was identified as an oligodendrocyte lineage-specific bHLH factor and shown to be an earliest known marker of developing oligodendrocytes [11, 24]. According to our data, OLIG2 was expressed not only in oligodendroglial tumors but also in astrocytic tumors. It is true that the degree of OLIG2 expression was generally high in oligodendroglial tumors compared to astrocytic tumors, but some astrocytic tumors showed high OLIG2 expression, indicating that OLIG2 could not be an independent marker for oligodendroglial tumors. Our data are consistent with the previous reports [16, 23], which imply that OLIG2 cannot be a specific marker of oligodendroglial tumors. In vitro studies have demonstrated that OLIG2 promotes the generation of oligodendrocytes by neural progenitor cells [11, 15, 24] and that ID2 inhibits the oligodendrocyte differentiation as a dominant negative regulator by blocking the heterodimerization of OLIG2 with E2A proteins [18, 22]. Thus, the functions of OLIG2 during neural development are modified by ID2, and it is possible that the cell lineage commitment of glioma cells is also influenced by the interaction between OLIG2 and ID2. Therefore, the relative expression of OLIG2 to ID2 in glioma cells was evaluated in this study. We obtained the data that all the oligodendroglial tumors examined in this study showed that the ratio of OLIG2 to ID2 IR scores was more than 1.0, while the ratio was equal or less than 1.0 in 19 of 27 astrocytic tumors (70%). These results suggest that the interaction between OLIG2 and ID2 in gliomas cells affects, at least in part, the cell lineage to which tumor cells are committed.

Minigemistocytes in the oligodendroglial tumors with diffuse OLIG2 staining were positive for ID2, although tumor cells with clear cytoplasm were ID2-negative. Furthermore, in glioblastomas, small round tumor cells were OLIG2-positive and ID2-negative, whereas giant tumor cells with abundant eosinophilic cytoplasm were OLIG2-negative and ID2-positive. These findings may suggest that the balance between ID2 and OLIG2 influences the glioma cell type with the same genetic background. It is possible that the expression of ID2 masks the oligodendrocytic biological property with astrocytic morphology.

Precise diagnosis of gliomas aims to differentiate the chemosensitive tumors from chemoresistant tumors. Chromosomal analyses have revealed the loss on 1p to be found frequently in chemosensitive oligodendroglial tumors [4, 6]. Accordingly, we analyzed the chromosomal aberration of the gliomas by CGH and compared it with the expression levels of OLIG2 and/or ID2. It is of note that all of the gliomas with loss on 1p showed the ratio of OLIG2 to ID2 IR scores to be more than 1.0. A case of diffuse astrocytoma with the ratio more than 1.0, which should be morphologically classified into astrocytic tumors, was found to be accompanied with the loss on 1p. It was reported that there were gliomas with loss on 1p, which were histologically diagnosed as diffuse astrocytomas [8]. These data support our hypothesis that the immunohistochemistry to investigate the relative expression level of OLIG2 to ID2 can be used as index for screening the chemosensitive gliomas with loss on 1p.

In summary, it is suggested that the cell lineage commitment of glioma cells, especially oligodendrocytic or astrocytic, is under the influence of OLIG2 and ID2 expression, and the immunohistochemistry for the relative expression levels of these molecules can be a useful screening for chemosensitive oligodendroglial tumors from astrocytic tumors.

Acknowledgements We thank Mr. Hitoshi Abe, Department of Pathology, School of Medicine, Keio University, for the excellent technical assistance.

This study was supported in part by the Grant-in-Aid for Young Scientists (B), from the Ministry of Education, Culture, Sports, Science and Technology of Japan (no. 16790216).

References

1. Benezra R, Davis RL, Lockshon D, Turner DL, Weintraub H (1990) The protein Id: a negative regulator of helix–loop–helix DNA binding proteins. Cell 61:49–59
2. Bouvier C, Bartoli C, Aguirre-Cruz L, Virard I, Colin C, Fernandez C, Gouvernet J, Figarella-Branger D (2003) Shared oligodendrocyte lineage gene expression in gliomas and oligodendrocyte progenitor cells. J Neurosurg 99:344–350
3. Burton EC, Prados MD (2000) Malignant gliomas. Curr Treat Options Oncol 1:459–468
4. Cairncross JG, Ueki K, Zlatescu MC, Lisle DK, Finkelstein DM, Hammond RR, Silver JS, Stark PC, Macdonald DR, Ino Y, Ramsay DA, Louis DN (1998) Specific genetic predictors of chemotherapeutic response and survival in patients with anaplastic oligodendrogliomas. J Natl Cancer Inst 90:1473–1479
5. Coons SW, Johnson PC, Scheithauer BW, Yates AJ, Pearl DK (1997) Improving diagnostic accuracy and interobserver concordance in the classification and grading of primary gliomas. Cancer 79:1381–1393
6. Fortin D, Cairncross GJ, Hammond RR (1999) Oligodendroglioma: an appraisal of recent data pertaining to diagnosis and treatment. Neurosurgery 45:1279–1291
7. Hirose Y, Aldape K, Takahashi M, Berger MS, Feuerstein BG (2001) Tissue microdissection and degenerate oligonucleotide primed-polymerase chain reaction (DOP-PCR) is an effective method to analyze genetic aberrations in invasive tumors. J Mol Diagnostics 3:62–67

8. Hirose Y, Aldape KD, Chang S, Lamborn K, Berger MS, Feuerstein BG (2003) Grade II astrocytomas are subgrouped by chromosome aberrations. Cancer Genet Cytogenet 142:1–7
9. Kleihues P, Burger P, Collins V, Newcomb E, Ohgaki H, Cavenee W (2000) World Health Organization Classification of Tumours of the Central Nervous System. International Agency for Research on Cancer (IARC)/World Health Organization (WHO)
10. Lu QR, Park JK, Noll E, Chan JA, Alberta J, Yuk D, Alzamora MG, Louis DN, Stiles CD, Rowitch DH, Black PM (2001) Oligodendrocyte lineage genes (OLIG) as molecular markers for human glial brain tumors. Proc Natl Acad Sci U S A 98:10851–10856
11. Lu QR, Yuk D, Alberta JA, Zhu Z, Pawlitzky I, Chan J, McMahon AP, Stiles CD, Rowitch DH (2000) Sonic hedgehog-regulated oligodendrocyte lineage genes encoding bHLH proteins in the mammalian central nervous system. Neuron 25:317–329
12. Mason WP (2005) Oligodendroglioma. Curr Treat Options Neurol 7:305–314
13. Mitsui Y, Mochizuki S, Kodama T, Shimoda M, Ohtsuka T, Shiomi T, Chijiiwa M, Ikeda T, Kitajima M, Okada Y (2006) ADAM28 is overexpressed in human breast carcinomas: implications for carcinoma cell proliferation through cleavage of insulin-like growth factor binding protein-3. Cancer Res 66:9913–9920
14. Mokhtari K, Paris S, Aguirre-Cruz L, Privat N, Criniere E, Marie Y, Hauw JJ, Kujas M, Rowitch D, Hoang-Xuan K, Delattre JY, Sanson M (2005) Olig2 expression, GFAP, p53 and 1p loss analysis contribute to glioma subclassification. Neuropathol Appl Neurobiol 31:62–69
15. Oh S, Huang X, Chiang C (2005) Specific requirements of sonic hedgehog signaling during oligodendrocyte development. Dev Dyn 234:489–496
16. Ohnishi A, Sawa H, Tsuda M, Sawamura Y, Itoh T, Iwasaki Y, Nagashima K (2003) Expression of the oligodendroglial lineage-associated markers Olig1 and Olig2 in different types of human gliomas. J Neuropathol Exp Neurol 62:1052–1059
17. Ruzinova MB, Benezra R (2003) Id proteins in development, cell cycle and cancer. Trends Cell Biol 13:410–418
18. Samanta J, Kessler JA (2004) Interactions between ID and OLIG proteins mediate the inhibitory effects of BMP4 on oligodendroglial differentiation. Development 131:4131–4142
19. See SJ, Gilbert MR (2004) Anaplastic astrocytoma: diagnosis, prognosis, and management. Semin Oncol 31:618–634
20. Stege EM, Kros JM, de Bruin HG, Enting RH, van Heuvel I, Looijenga LH, van der Rijt CD, Smitt PA, van den Bent MJ (2005) Successful treatment of low-grade oligodendroglial tumors with a chemotherapy regimen of procarbazine, lomustine, and vincristine. Cancer 103:802–809
21. Vandeputte DA, Troost D, Leenstra S, Ijlst-Keizers H, Ramkema M, Bosch DA, Baas F, Das NK, Aronica E (2002) Expression and distribution of id helix–loop–helix proteins in human astrocytic tumors. Glia 38:329–338
22. Wang S, Sdrulla A, Johnson JE, Yokota Y, Barres BA (2001) A role for the helix–loop–helix protein Id2 in the control of oligodendrocyte development. Neuron 29:603–614
23. Yokoo H, Nobusawa S, Takebayashi H, Ikenaka K, Isoda K, Kamiya M, Sasaki A, Hirato J, Nakazato Y (2004) Anti-human Olig2 antibody as a useful immunohistochemical marker of normal oligodendrocytes and gliomas. Am J Pathol 164:1717–1725
24. Zhou Q, Wang S, Anderson DJ (2000) Identification of a novel family of oligodendrocyte lineage-specific basic helix–loop–helix transcription factors. Neuron 25:331–343

Virchows Arch (2007) 450:585–590
DOI 10.1007/s00428-007-0395-6

ORIGINAL ARTICLE

Pulmonary "inflammatory myofibroblastic" tumors: a critical examination of the diagnostic category based on quantitative immunohistochemical analysis

A. B. Farris III · E. J. Mark · R. L. Kradin

Received: 18 December 2006 / Revised: 22 February 2007 / Accepted: 23 February 2007 / Published online: 20 March 2007
© Springer-Verlag 2007

Abstract The World Health Organization classification applies the term "pulmonary inflammatory myofibroblastic tumor" to a histologically variegate set of pulmonary inflammatory pseudotumors. However, often these lesions bear little resemblance to tumors of myofibroblastic origin. To elucidate histogenesis, we examined 18 cases from our institution files. The cases were stained with antibodies to smooth muscle actin (SMA), Factor XIIIa, CD3, CD20, CD68, S-100, anaplastic lymphoma kinase (ALK-1), and human herpevirus-8 (HHV-8). The percentage of positive-staining cells within a defined tumor area (400,000 μm^2) was determined by light microscopy and morphometric analysis. Ten cases (56%) showed myofibroblastic differentiation, as judged by positive SMA staining of spindle cells. All cases showed substantial numbers of CD68+, Factor XIIIa+, and S-100+ monocytoid cells. Fifty percent were ALK-1+, and one was HHV-8+. We conclude that the term "inflammatory myofibroblastic tumor" is a misnomer, as nearly half of cases show no myofibroblastic differentiation. Instead, the results suggest that these lesions are composed predominantly of cells of macrophage-dendritic cell lineage. Although the multiplicity of terms previously applied to these lesions is cumbersome, retaining a descriptive phenomenological terminology may ultimately promote accurate elucidation of pathogenesis.

A. B. Farris III · E. J. Mark
Department of Pathology, Massachusetts General Hospital,
Boston, MA 02114, USA

R. L. Kradin (✉)
Departments of Pathology and Medicine,
Massachusetts General Hospital,
Boston, MA 02114, USA
e-mail: rkradin@partners.org

Keywords Pulmonary inflammatory myofibroblastic tumor · Pseudotumor · Factor XIIIa

The current World Health Organization (WHO) criteria adopts the term "inflammatory myofibroblastic tumor" (IMT) to refer to pulmonary tumors that previously were referred to as inflammatory pseudotumor, fibroxanthoma, fibrous histiocytoma, pseudosarcomatous myofibroblastic tumor, invasive fibrous tumor of the tracheobronchial tree, xanthogranuloma, plasma cell granuloma, and plasma cell granuloma–histiocytoma complex [22]. As evidenced by the number of diagnostic entities that are currently included within the WHO rubric of IMT, these lesions have a wide variety of presentations and morphologic manifestations. IMT was first described by Brunn [2] in 1939 as tumors in the lung of two patients. Pettinato et al. [16] was the first to adopt the term "inflammatory myofibroblastic tumor". Although under the current classification IMTs are thought to be myofibroblastic, smooth muscle actin (SMA) positivity and other markers of myofibroblastic differentiation cannot always be demonstrated. In addition, it has been suggested that these lesions are neoplasms of other cell types [15]. Therefore, a precise understanding of their etiology and histogenesis has eluded classification.

Materials and methods

Sections of the tumor were fixed in 10% phosphate-buffered formalin, embedded in paraffin, sectioned at 5 μm, and stained with hematoxylin and eosin (H&E). Immunohistochemical studies were performed on the paraffin-embedded sections. Primary antibodies included CD1a, CD21, CD68, anaplastic lymphoma kinase (ALK-1), S100,

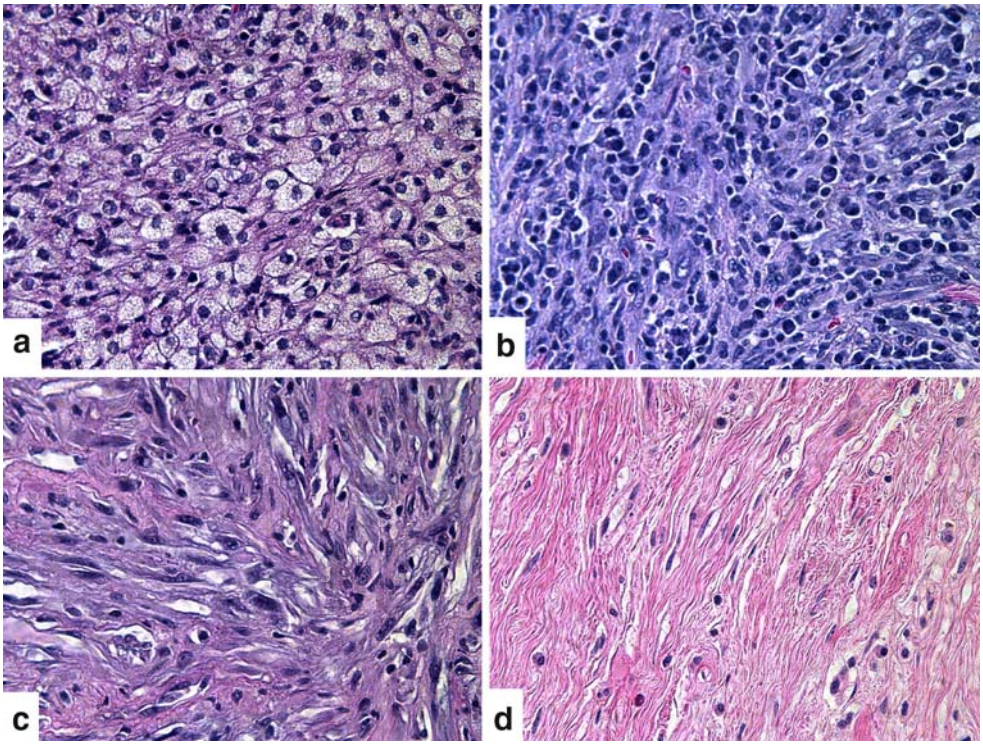

Fig. 1 Subtypes of lesions based on morphologic patterns: **a** xanthogranulomatous, **b** plasma cell granuloma, **c** fibrohistiocytic, and **d** hypocellular fibrous (H&E; original magnification, ×400)

Factor XIIIa, human herpes virus 8 (HHV-8), SMA, vimentin (all from Ventana, Tucson, AZ), and fascin (DAKO, Carpinteria, CA). Expression of Epstein-Barr virus (EBV)-encoded RNA (EBER) was evaluated by in situ hybridization (ISH) using the INFORM EBER probe (Ventana).

Results

Eighteen cases with diagnoses that currently fall under the rubric of pulmonary IMT were identified in our institution files from 1989–2006. The cases were evenly distributed between men (n=9) and women (n=9). The average patient age ranged from 6–77 years old with an average age of 50± 9.2 years (95% confidence interval). All cases showed various numbers of spindle cells, plasma cells, eosinophils, macrophages, and lymphocytes. They were reclassified into non-WHO categories based on their histologic appearance in H&E sections according to previously published criteria (Table 3) [4, 20]. The cases were reclassified as follows: fibrohistiocytic (eight cases), plasma cell granuloma (four cases), hypocellular fibrous (three cases), and xanthogranulomatous (three cases; Fig. 1).

Tumor cells stained for CD68, Factor XIIIa, and S100 in ≥90% of cases and accounted for 22 (range 1–59%), 21 (range 1–80%), and 5% of the tumor area (1–16%), respectively (Fig. 2 and Table 1). Only 10/18 (56%) showed myofibroblastic differentiation, as judged by positive SMA staining, with SMA+ cells accounting for 22% of the tumor area (range 3–34%; Fig. 3). The plasma

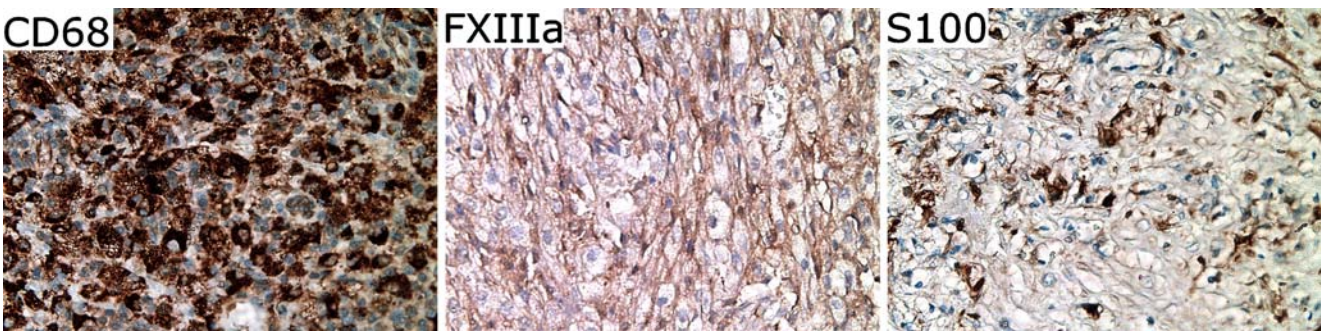

Fig. 2 Lesions showing high levels of positive staining for CD68, Factor XIIIa, and S100 (peroxidase; original magnification, ×400)

Table 1 Quantitation of immunohistochemical staining

	SMA	CD68	FXIIIa	S100	ALK-1
Number (%) positive	10 (56%)	18 (100%)	17 (94%)	18 (100%)	9 (50%)
Percent cases positive 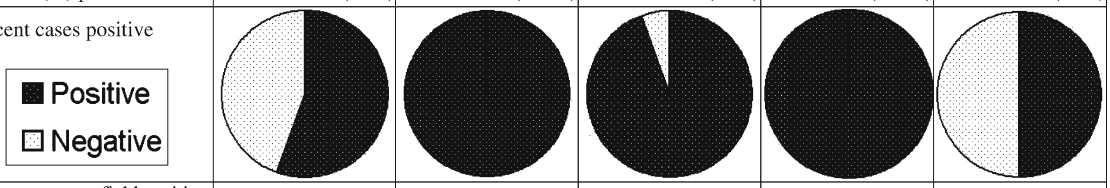					
Average percent field positive (SD)	21.7 (9.6)	22.3 (14.6)	20.5 (17.1)	5.3 (4.9)	10.1 (9.9)
Range (percent field positive)	3.5- 34.5	1.1-59.3	6.15-79.9	0.3-16.0	0.07-24

cell granuloma subtype had the highest proportion of cases with SMA staining (75% of cases), followed by the hypocellular fibrous type (67%), the fibrohistiocytic type (50%), and the xanthogranulomatous type (33%; Fig. 3 and Table 3). Fifty percent of cases showed ALK-1+, cells; in a previously reported case with xanthomatous features, tumor cells were virtually all HHV-8 positive [7]. All cases showed infiltrates composed of CD3+ T-lymphocytes, and the majority of cases showed CD20+ B-cell lymphoid aggregates and/or follicles (Fig. 4 and Table 2). Tumors with xanthogranulomatous features showed SMA positivity in one-third of cases, the lowest percentage for any subtype. Xanthogranulomatous tumors showed the highest positivity for CD68, Factor XIIIa, and ALK-1 (Table 3); HHV-8 positivity was limited to a single case with xanthomatous features.

Discussion

In our study, only 10 of 18 cases (56%) showed myofibroblastic differentiation, as judged by positive SMA staining, whereas all cases showed substantial numbers of CD68+, Factor XIIIa+, and S-100+ monocytoid cells. All cases showed inflammatory infiltrates composed of T- and B-lymphocytes. These findings lead us to conclude that a myofibroblastic differentiation is not a necessary feature of these inflammatory lesions.

IMT is thought to represent either a low grade mesenchymal malignancy or a reactive inflammatory lesion [12, 20]. Patients with pulmonary IMTs are on average 30 years old with 60% younger than 40 years, somewhat

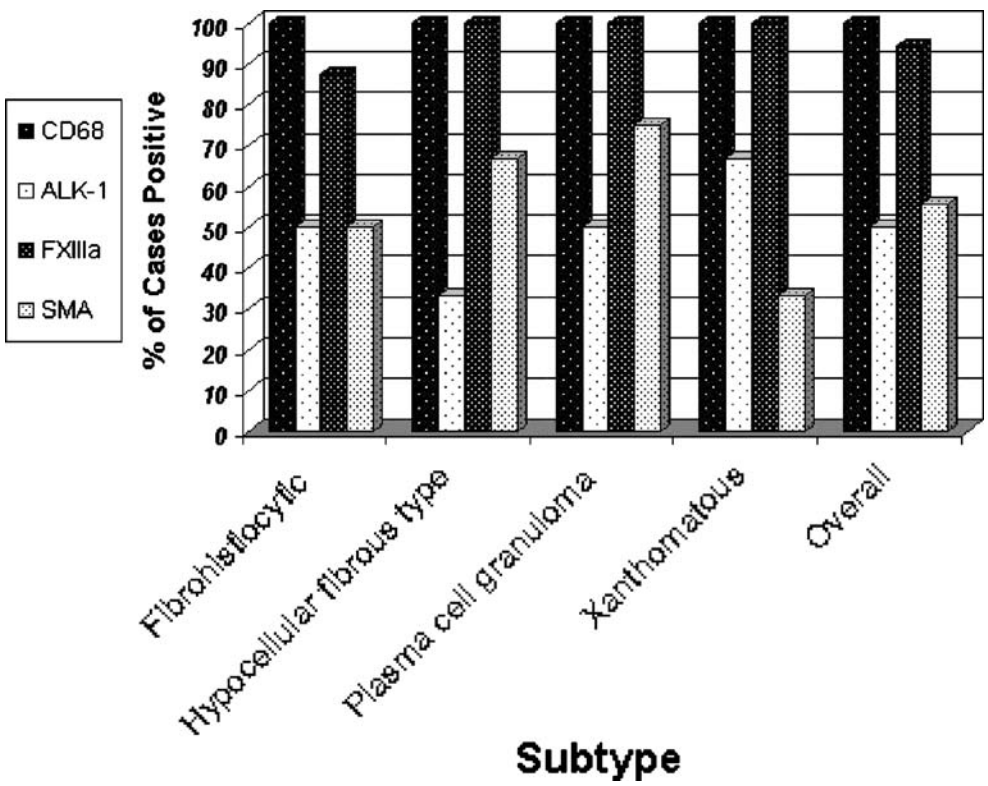

Fig. 3 Distribution of antibody expression based on subtypes

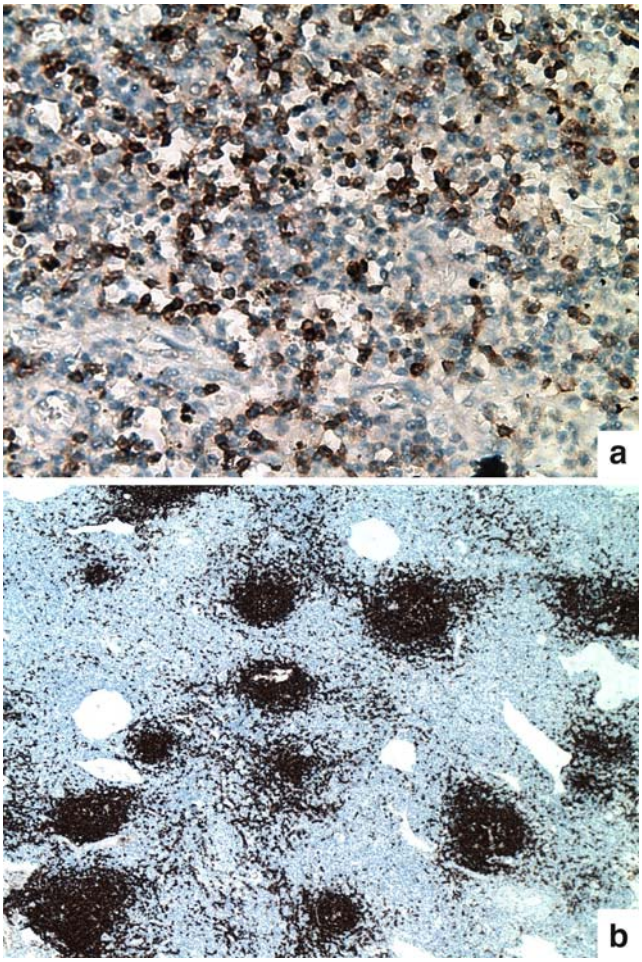

Fig. 4 **a** CD3+ lymphocytes were present in all cases (peroxidase; original magnification, ×400). **b** Follicular aggregates of CD20+ lymphocytes seen in most cases (peroxidase; original magnification, ×50)

younger than in the present series [22]. As in the present series, Travis et al. [20] noted an equal sex predilection.

The clinical presentation of IMT can vary from asymptomatic to cough, fever, chest pain, and hemoptysis. Radiographically, they are usually well-defined lobulated solitary peripheral pulmonary nodules [22].

Table 2 Characterization and quantitation of the lymphoid infiltrate using immunohistochemical markers

	CD3	CD20
Number of cases showing positively antigen (%)	18 (100%)	16 (89%)
Average (percent field positive) (standard deviation)[a]	13.2 (10.5)	22.6 (15.4)
Range (percent field positive)	0.4–36.0	1–58.0

[a] The values for CD3 are expressed as the percent of the field positive, and the values for CD20 are expressed as the number of lymphoid aggregates in ten 10× objective microscope fields

The lesions are generally diagnosed at the time of total excision with a low incidence of recurrence, and with extrapulmonary invasion, or metastases reported in approximately 5% of cases [20, 22].

Grossly, the tumor lesions are well circumscribed, solitary, and round to ovoid. They may be as large as 36 cm but are most often 1–6 cm. Direct penetration into the pleura, mediastinum or chest wall is seen in 5–10% of cases, and polypoid endobronchial lesions account for 12% of cases [22].

Histologically, there is a predominance of spindle cells in a storiform or fascicular pattern. The matrix may be myxoid or fibroxanthomatous. The nuclei of the spindle cells are oval with fine chromatin, and the cytoplasm is usually eosinophilic. Mitoses are rare. Inflammatory cells, including lymphocytes, plasma cells, eosinophils, histiocytes, and Touton giant cells can predominate. Dystrophic calcifications and osseous metaplasia have been reported. Vascular invasion is rarely seen [20, 22].

Flow cytometry studies have found aneuploid (hyperdiploid) indices in IMT, leading to the suggestion that it is a neoplasm [1, 3, 11]. Cytogenetic studies have found multiple chromosomal abnormalities in IMT, most notably the translocation of the ALK gene on chromosome 2p23 to chromosome 5 to create ALK fusion gene products [19, 20]. The expression of ALK1 and p80 are noted in IMT in approximately 40% of cases [14, 20]. Reactivity with p53 is rare but has been associated with recurrence and malignant transformation [22].

IMT-like lesions have been associated with infectious etiologies such as *Campylobacter jejuni*, *Actinomyces*, mycobacteria, *Histoplasma*, EBV, and human herpesvirus-8 (HHV-8) [7, 14, 22]. Gomez-Roman et al. found HHV-8 molecular transcripts using PCR and ISH in IMTs. The proteins encoded by these transcripts included human homologous oncoproteins (viral cyclin-D), inflammatory cytokines (viral IL-6), and inhibitors of apoptotic pathways (viral FLIP and viral Bcl-2), mostly expressed in a latent viral replicative stage. Viral-induced changes brought about by these transcripts could explain the resulting histopathologic changes in IMT in some cases [6, 8, 9]. An association with Histoplasma capsulatum has been observed in patients with acquired immunodeficiency syndrome (AIDS) [21]. Studies have found an association with IMT and local cytokine dysregulation, including production of interleukins (IL) and monocyte chemoattractant protein (MCP)-1 [22].

The current WHO nomenclature implies that the spindle cells in IMT are of myofibroblastic differentiation [22]. Past literature has demonstrated that the lesional spindle cells react immunohistochemically with vimentin and SMA but are usually negative for desmin. The tumors are generally negative for myogenin, myoglobin, CD117 (c-kit), and

Table 3 Comparison of immunohistochemical staining among subtypes

Subtype	Cases (number)	CD68		ALK-1		FXIIIa		SMA	
		Number of cases + (%)	Percent field +	Number of cases + (%)	Percent field +	Number of cases + (%)	Percent field +	Number of cases + (%)	Percent field +
Fibrohistiocytic	8	8 (100%)	22	4 (50%)	12	7 (88%)	18	4 (50%)	26
Hypocellular fibrous type	3	3 (100%)	13	1 (33%)	0.82	3 (100%)	18	2 (67%)	14
Plasma cell granuloma	4	4 (100%)	20	2 (50%)	1.9	4 (100%)	15	3 (75%)	20
Xanthogranulomatous	3	3 (100%)	34	2 (67%)	20	3 (100%)	35	1 (33%)	25

The subtypes were defined as [20] fibrohistiocytic: spindled cells in a storiform pattern; hypocellular fibrous type: dense collagen with sparse spindle cells; plasma cell granuloma: spindled cells in a fascicular pattern with plasma cells and lymphocytes; and xanthogranulomatous: nearly pure infiltrates of xanthomatous cells.

S100 protein and may be focally positive for keratin [20]. However, as demonstrated in both the present series and by others [15], it is not always possible to identify SMA positivity or positivity for other markers of myofibroblastic differentiation.

Pileri et al. [17] have reported that dendritic cell neoplasms and Langerhans' cell tumors express CD68, CD1a, and S100, comparable to the cells seen in the present as series. Rosai et al. have suggested that IMT may be proliferative disorder of the "accessory immune system." The latter includes T- and B-cell related dendritic cells, as well as fibroblastic reticulum cells, myoid cells, and dictyocytes [15]. It is possible that distinguishing subsets of accessory cells by virtue of their antigenic markers, e.g., CD23, fascin, Langerin, etc., may help to determine the participation of specific monocytoid cells in these lesions. Others have suggested that clusterin may be a useful marker for dendritic cell tumors [10]. Dendritic cell-specific intercellular adhesion molecule 3 (ICAM-3)-grabbing non-integrin (DC-SIGN) expressed by dendritic cells and macrophages is a recognized receptor for HHV-8, which has been linked to IMT in some cases [18].

Factor XIIIa, a plasma transglutaminase that plays a critical role in the cross-linking of the fibrin clot, is expressed in a number of normal, benign, and reactive conditions. Factor XIIIa is produced by human pulmonary macrophages, dermal dendrocytes, and interstitial macrophages. Factor XIIIa labels the cells of a variety of benign or reactive tumors, including xanthogranulomas, xanthoma disseminatum, and dermatofibroma. The consistent presence of Factor XIIIa+ cells in the present case supports either a dendritic or xanthogranulomatous lineage for the lesion in these cases [5, 13].

We conclude that the term IMT is a misnomer in approximately 50% of cases. We suggest that these lesions be separated into two major subsets, one for lesions showing myofibroblastic differentiation and the other for those showing differentiation along macrophage-dendritic cell lines. Although, the multiplicity of terms previously applied to these lesions is admittedly cumbersome, retaining descriptive terminology may ultimately promote the accurate elucidation of pathogenesis.

References

1. Biselli R, Ferlini C, Fattorossi A, Boldrini R, Bosman C (1996) Inflammatory myofibroblastic tumor (inflammatory pseudotumor): DNA flow cytometric analysis of nine pediatric cases. Cancer 77:778–784
2. Brunn H (1939) Two interesting benign lung tumors of contradictory histopathology. J Thorac Surg 9:119–131
3. Cessna MH, Zhou H, Sanger WG, Perkins SL, Tripp S, Pickering D, Daines C, Coffin CM (2002) Expression of ALK1 and p80 in inflammatory myofibroblastic tumor and its mesenchymal mimics: a study of 135 cases. Mod Pathol 15:931–938
4. Coffin CM, Humphrey PA, Dehner LP (1998) Extrapulmonary inflammatory myofibroblastic tumor: a clinical and pathological survey. Semin Diagn Pathol 15:85–101
5. Helm, KF (2002) Immunohistochemistry of skin tumors. In: Dabbs DJ (ed) Diagnostic immunohistochemistry. Churchill Livingstone, New York, p 318
6. Ding Y, Saylors RL, Brown H, Parham DM (2002) Pulmonary inflammatory pseudotumor with HHV-8. Am J Surg Pathol 26:1089–1091
7. Farris AB 3rd, Kradin RL (2006) Follicular localization of dendritic cells in a xanthomatous inflammatory tumor of lung associated with human herpes virus-8 infection. Virchows Arch 449:726–729
8. Gomez-Roman JJ, Sanchez-Velasco P, Ocejo-Vinyals G, Hernandez-Nieto E, Leyva-Cobian F, Val-Bernal JF (2001) Human herpesvirus-8 genes are expressed in pulmonary inflammatory myofibroblastic tumor (inflammatory pseudotumor). Am J Surg Pathol 25:624–629
9. Gomez-Roman JJ, Ocejo-Vinyals G, Sanchez-Velasco P, Nieto EH, Leyva-Cobian F, Val-Bernal JF (2000) Presence of human herpesvirus-8 DNA sequences and overexpression of human IL-6 and cyclin D1 in inflammatory myofibroblastic tumor (inflammatory pseudotumor). Lab Invest 80:1121–1126
10. Grogg KL, Macon WR, Kurtin PJ, Nascimento AG (2005) A survey of clusterin and fascin expression in sarcomas and spindle cell neoplasms: strong clusterin immunostaining is highly specific for follicular dendritic cell tumor. Mod Pathol 18:260–266

11. Hussong JW, Brown M, Perkins SL, Dehner L, Coffin C (1999) Comparison of DNA ploidy, histologic, and immunohistochemical findings with clinical outcome in inflammatory myofibroblastic tumors. Mod Pathol 12:279–286
12. Kovach SJ, Fischer AC, Katzman PJ, Salloum RM, Ettinghausen SE, Madeb R, Koniaris LG (2006) Inflammatory myofibroblastic tumors. J Surg Oncol 94:385–391
13. Kradin RL, Lynch GW, Kurnick JT, Erikson M, Colvin RB, McDonagh J (1987) Factor XIII A is synthesized and expressed on the surface of U937 cells and alveolar macrophages. Blood 69:778–785
14. Mergan F, Jaubert F, Sauvat F, Hartmann O, Lortat-Jacob S, Revillon Y, Nihoul-Fekete C, Sarnacki S (2005) Inflammatory myofibroblastic tumor in children: clinical review with anaplastic lymphoma kinase, Epstein-Barr virus, and human herpesvirus 8 detection analysis. J Pediatr Surg 40:1581–1586
15. Nonaka D, Birbe R, Rosai J (2005) So-called inflammatory myofibroblastic tumor: a proliferative lesion of fibroblastic reticulum cells? Histopathology 46:604–613
16. Pettinato G, Manivel J, DeRosa N, Dehner L (1990) Inflammatory myofibroblastic tumor (plasma cell granuloma): clinicopathologic study of 20 cases with immunohistochemical and ultrastructural observations. Am J Clin Pathol 94:538–546
17. Pileri SA, Grogan TM, Harris NL, Banks P, Campo E, Chan JK, Favera RD, Delsol G, De Wolf-Peeters C, Falini B, Gascoyne RD, Gaulard P, Gatter KC, Isaacson PG, Jaffe ES, Kluin P, Knowles DM, Mason DY, Mori S, Muller-Hermelink HK, Piris MA, Ralfkiaer E, Stein H, Su IJ, Warnke RA, Weiss LM (2002) Tumours of histiocytes and accessory dendritic cells: an immunohistochemical approach to classification from the International Lymphoma Study Group based on 61 cases. Histopathology 41:1–29
18. Rappocciolo G, Jenkins FJ, Hensler HR, Piazza P, Jais M, Borowski L, Watkins SC, Rinaldo CR Jr (2006) DC-SIGN is a receptor for human herpesvirus 8 on dendritic cells and macrophages. J Immunol 176:1741–1749
19. Snyder CS, Dell'Aquila MD, Haghighi P, Baergen RN, Suh YK, Yi ES (1995) Clonal changes in inflammatory pseudotumor of the lung: a case report. Cancer 76:1545–1549
20. Travis WD, Colby TV, Koss MN, Rosado-de-Christenson ML, Muller NL, Talmadge E. King J (2002) Miscellaneous diseases of uncertain etiology: inflammatory myofibroblastic tumor (inflammatory pseudotumor). In: King DW (ed) Atlas of nontumor pathology: non-neoplastic disorders of the lower respiratory tract. Armed Forces Institute of Pathology, Bethesda, MD, pp 857–867
21. Umlas J, Federman M, Crawford C, O'Hara CJ, Fitzgibbon JS, Modeste A (1991) Spindle cell pseudotumor due to Mycobacterium avium-intracellulare in patients with acquired immunodeficiency syndrome (AIDS). Positive staining of mycobacteria for cytoskeleton filaments. Am J Surg Pathol 15:1181–1187
22. Yousem SA, Tazelaar HD, Manabe T, Dehner LP (2004) Inflammatory myofibroblastic tumor. In: Travis WD, Brambilla E, Muller-Hermelink HK, Harris CC (eds) Pathology and genetics of tumours of the lung, pleura, thymus and heart. IARC, Lyon, pp 105–106

Virchows Arch (2007) 450:591–594
DOI 10.1007/s00428-007-0392-9

CASE REPORT

"Benign" metastatic meningioma: clinico-pathological analysis of one case metastasising to the lung and overview on the concepts of either primitive or metastatic meningiomas of the lung

Sofia Asioli · Rebecca Senetta · Elena Maldi · Enrico D'Ambrosio · Maria Antonietta Satolli · Gianni Bussolati · Paola Cassoni

Received: 8 February 2007 / Revised: 15 February 2007 / Accepted: 18 February 2007 / Published online: 13 March 2007
© Springer-Verlag 2007

Abstract Lung "metastases" of benign meningiomas are rarely described events of biological and clinical interest. We, here, report of a 70-year-old healthy woman found by CT scan to have multiple lesions, the two largest in the right lung on routine examination. Anamnesis revealed that the patient underwent a surgical resection of cerebral meningioma 12 years before. The larger lung lesion was a 3-cm node located in the right lung and was removed by wedge resection. Macroscopically, it showed well-defined borders, whitish colour and firm consistency; histologically, it was uniformly composed by spindle meningothelial cells arranged in fascicules including psammoma bodies. The morphological and immunohistochemical features of this lesion, together with the similarity with the original cerebral tumour and its indolent evolution, led to a final diagnosis of "benign" meningioma metastatic to the lung. Lung metastatic meningiomas may be a diagnostic challenge because of their unusual site of presentation and the possible confusion with primitive lung meningiomas or primary mesenchymal lung lesions. They represent a typical example of "benign" tumours that may implant to the lung similar to other tumours, definitely considered benign but reported to rarely present unusual secondary localization.

S. Asioli (✉) · R. Senetta · E. Maldi · M. A. Satolli · G. Bussolati · P. Cassoni
Department of Biomedical Sciences and Human Oncology
Molinette Hospital, University of Turin,
Via Santena 7,
10100 Turin, Italy
e-mail: sofia.asioli@unito.it

E. D'Ambrosio
Department of Pathology, Vito Fazzi Hospital,
Lecce, Italy

Keywords Meningioma · Metastasis · Lung · Benign metastatic tumours

Introduction

Meningiomas arise from the intracranial and spinal meninges and constitute 13–26% of all central nervous system (CNS) tumours. Low-grade meningiomas (grade I, World Health Organization [WHO]) are considered benign lesions as they generally are not locally invasive and are usually cured by surgical resection [14]. However, they have a potential to become, with time, more aggressive (grade II and III) and to invade the brain and/or to metastasise outside the CNS [2]. The local recurrence rates even after complete resection vary from 9 to 32% and, although some histological and immunophenotypical parameters predictably identify grade II and III meningiomas of higher biological aggressiveness, no definite criteria are available to establish evolution. Metastases outside the CNS are known to rarely occur even from meningiomas that at first diagnosis are considered grade I tumours. In view of the slow-growing nature of these metastases and their good prognosis after resection, surgery is the treatment of choice [14].

Clinical history

A 58-year-old healthy woman underwent neurosurgery for the resection of intracranial meningioma. Twelve years later, she was found to have multiple lesions, the two largest in the right lung on radiological routine examina-

tion. CT scan confirmed the presence of the lesions: the larger node was 2.6 cm in diameter (Fig. 1a). The patient underwent wedge resection of two lesions in the right lobe.

Materials and methods

Tissues were fixed in buffered formalin, paraffin embedded and routinely processed for histological diagnosis. For immunohistochemistry, the avidinbiotin peroxidase complex method was used. The antisera employed are listed in Table 1, together with their source, dilution and antigen retrieval method.

Results

Macroscopically, the two lesions in the right lobe had well-defined borders, whitish colour and firm consistency. Histopathology showed spindle meningothelial cells arranged in fascicules with psammoma bodies infiltrating the lung (Fig. 1b,c). The tumour was intensively immunoreactive for vimentin and weakly positive for epithelial membrane antigen, whereas it was negative for smooth muscle actin, cytocheratin 7, thyroid transcript factor 1, CD34, desmin, chromogranin A as well as oestrogen receptor. Ki-67/MIB1 showed occasional scattered positive cells (2%; Fig. 1d). No mitotic figures were found. Moreover, progesterone receptor showed focal positivity in 10% of the neoplastic cells. These immuno-morphological data, together with the clinical history of a previous intracranial meningioma, were suggestive of metastatic meningioma. All the cut margins of the resection were free. The patient was not given any postoperative therapy.

We reviewed the primitive neoplasm resected 12 years before and, on histology, the neoplasm showed spindle meningothelial cells arranged in fascicules with psammoma bodies sharing the feature of the lung lesions (Fig. 1e,f). Immunohistochemical parameters matched those of the lung lesions, including the focal positivity for progesterone receptors. No mitotic figures were found and ki-67/MIB 1 was about 3% (Fig. 1d).

Patient is now asymptomatic 18 months after surgery, and the remaining pulmonary nodules are stable in size.

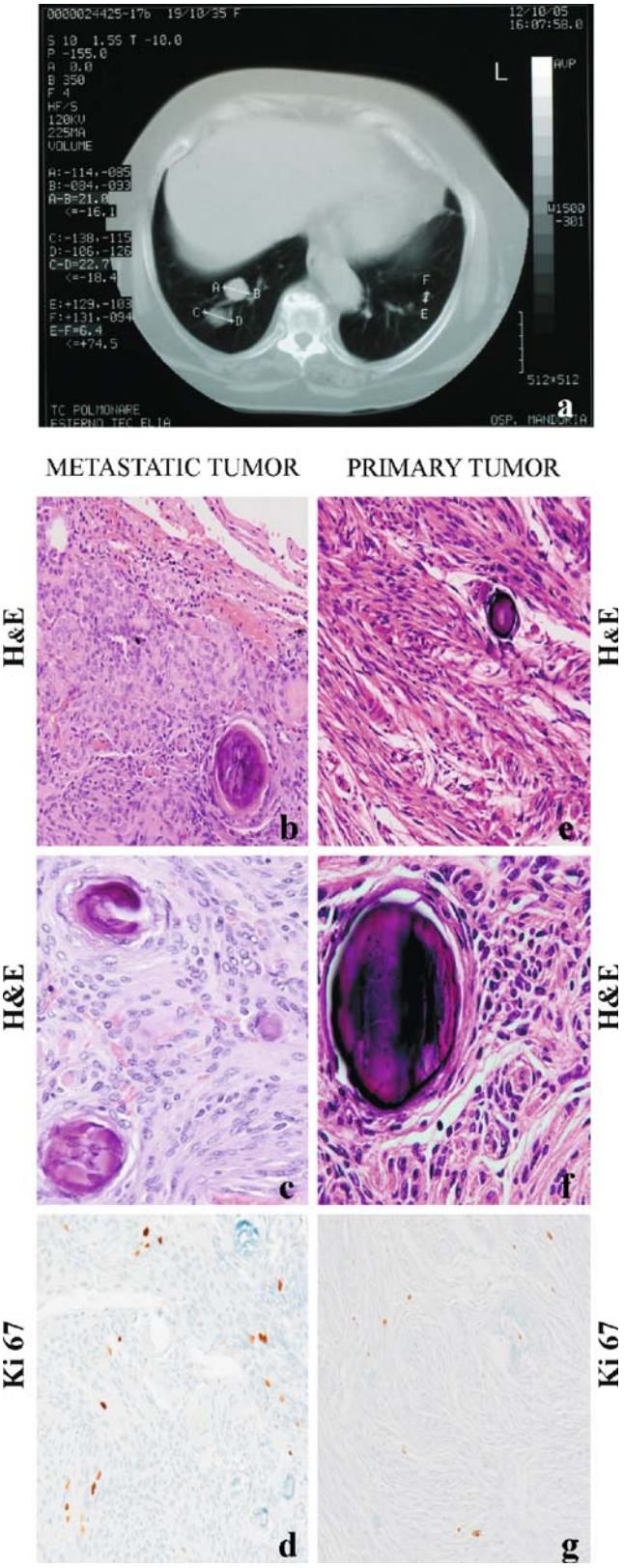

Fig. 1 Lung metastatic meningioma and primary intracranial lesion. ▶ CT scan of the multiple pulmonary nodes, the two largest located in the right lobe underwent surgical resection (**a**). Metastatic lung lesion; at *H&E*, the lesion is composed of meningothelial cells arranged in whirls and includes various psamomma bodies (**b** 10× and **c** 40×). At immunohistochemistry, the lesion showed low ki-67/MIB1, <3% (**d**). Primitive intracranial meningioma; at *H&E*, the lesion showed spindle meningothelial cells arranged in fascicules and psammoma bodies (**e** 10× and **f** 40×). (*E*) The proliferation index determined by ki-67/MIB1 was lower than 2% (**g**)

Table 1 Antibodies employed for immunohistochemistry

Antibody	Clone, source	Dilution	Antigen retrieval
Vimentin	V9, Ventana	–	–
EMA	E29, DAKO	1:100	–
SMA	1A4, DAKO	1:20	–
CK 7	CV-TG-12/30 DAKO	1:25	Citrate 40′
TTF1	8G7G3/1, VENTANA	–	–
CD34	QBEnd/10, VENTANA	–	–
Desmin	D33, DAKO	1:50	Citrate 10′
CGA	LK2H10, VENTANA	–	–
ER	6F11, VENTANA	–	–
PR	1E2, VENTANA	–	–
Ki-67	MIB1, DAKO	1:100	Edta 40′

CK 7 Cytokeratin 7; *SMA* smooth muscle actin; *TTF-1* thyroid transcriptor factor-1; *EMA* epithelial membrane antigen; *CGA* chromogranin A; *ER* oestrogen receptor; *PR* progesterone receptor
DAKO, Glostrup, Denmark; VENTANA-DIAPATH, Tucson, AZ

Discussion

Meningiomas (except grade II and III, WHO) are usually non-invasive tumours, do not metastasise and hence are perceived as benign tumours for which radical surgery is the treatment of choice [1, 14]. However, even "histologically benign" meningiomas (such as grade I meningiomas) may seed outside the brain despite their benign appearance. Extra-cranial metastases in cases of meningioma grade I (WHO) are rare and only ten such cases have been described in literature. In order of occurrence, the most common sites of metastases are lung, liver, lymph nodes and bone [6, 7, 11, 16, 18, 27]. Moreover, most of such reports are clinical or radiological, without evidence of pathological data.

The differential diagnosis of "benign" metastasizing meningioma with primary pulmonary meningothelial-like lesions is difficult. In general, the interpretation of lesions with typical "meningiomatous" features in the lung should be made taking into consideration two main crucial points: the previous occurrence of a meningioma in the CNS and the possible occurrence of a primary lung meningioma or minute pulmonary meningothelial-like nodules (MPMNs). Primary meningiomas of the lung are uncommon and histologically are identical to CNS meningiomas. The histogenesis of such ectopic meningiomas is controversial; some authors suggested that they might arise from minute solitary meningothelial-like nodules (MPMN) of the lung [25], but genetic evidence recently reported seem to be against such hypothesis [10, 22]. In addition, MPMNs are usually smaller than 0.3 cm in size and radiologically undetectable; larger lesions in the setting of multiple nodules radiologically evident address the diagnosis towards metastatic meningiomas from the CNS [8, 17, 24]. This opens an additional controversial point on lung meningothelial lesions; in fact, whereas the relationship between MPMN and primary pulmonary meningiomas remains to be fully clarified, it is important to separate metastatic meningiomas from both MPMN and primary meningiomas.

Metastatic meningiomas are usually grade II–III lesions, displaying histologic clues of help in addressing the diagnosis, including their usual multicentricity and the presence of lymphangitic involvement at distance from the larger nodules, frequently involving the broncho-vascular bundles. Such pattern virtually excludes MPMN because pulmonary meningotelial-like nodules are nearly always associated with pulmonary vein and not associated with airways.

In the case here reported, as well as in few other cases reported in the literature [3, 4, 19, 21, 23, 26], the metastatic meningioma shares the identical, benign phenotype of the primary lesion. Similarly, exceptional cases of benign tumours metastatic to the lung have been reported (resumed in Table 2) and should be remembered.

Finally, despite the "conceptual" concern on the different origin of lung meningiomatous lesions, a practical approach to the problem requires to consider that, in addition to the more aggressive grade II and III meningiomas, even "benign" grade I meningiomas, which are not expected to metastasise, could present distant lesions with an indolent behaviour that mimics that of the primary original intracranial lesion and whose choice treatment is surgery. In the presence of such lesions, the alternative diagnosis of primary "meningothelial-like" lesions, including primary

Table 2 "Benign" tumours metastatic to the lung described in the literature

Type	Site of origin	Metastasis	References
Leyomioma	Uterus	Lung	[28]
Meningioma	CNS	Lung	[4, 12, 15, 16, 19–21, 23, 26, 28]
Giant cell tumours of bone	Bone	Lung	[2]
Thymoma	Thymus	Lung	[28]
Acanthomatous ameloblastoma	Maxilla	Lung	[9]
Digital papillary adenoma	Skin	Lung	[13]
Dematofibroma	Skin	Lung	[5]
Glomous tumours	Skin	Lung	[28]
Mixed tumour	Parotid gland	Lung	[29]

lung meningiomas, should be considered, but would definitely not modify the therapeutic approach. In conclusion, different entities with meningiomatous features can be found in the lung. Morphological and clinical data (in our case, similarity with the CNS lesion removed 12 years before) address to the correct diagnosis.

Acknowledgements This paper was supported by grants from AIRC (Associazione Italiana per la Ricerca sul Cancro), MIUR and Compagnia di San Paolo "Special Project Oncology".

References

1. Alvarez F, Roda JM, Perez Romero M, Morales C, Sarmiento MA, Blazquez MG (1987) Malignant and atypical meningiomas: a reappraisal of clinical, histological and computed tomographic features. Neurosurgery 20:688–694
2. Bertoni F, Present D, Sudanese A, Baldini N, Bacchini P, Campanacci M (1988) Giant cell tumor of bone with pulmonary metastases. Six case reports and a review of literature. Clin Orthop 237:275–285
3. Celli P, Palma L, Domenicucci M, Scarpinati M (1992) Histologically benign reccurent meningioma metastasizing to the parotid gland: case report and review of the literature. Neurosurgery 31 (6):1113–1116
4. Cerda-Nicholas M, Lopez-Gines C, Perez-Bacete M, Roldan P, Talamantes F, Barbera J (2003) Histologically benign metastatic meningioma: morphological and cytogenetic study. Case report. J Neurosurg 98(1):194–198
5. Colby TV (1997) Metastasizing dermatofibroma. Am J Surg Pathol 21(8):976
6. Falleni M, Roz E, dessy E, Del Curto B, Braidotti P, Giannelli U, Pietra GG (2001) Primary intrathoracic meningioma: histopathological, immunohistochemical and ultrastructural study of two cases. Virchows Arch 439(2):196–200
7. Flynn SD, Yousem SA (1991) Pulmonary meningiomas: a report of two cases. Hum Pathol 22(5):469–474
8. Gaffey MJ, Mills SE, Askin FB (1988) Minute pulmonary meningothelial-like nodules. A clinicopathologic study of so-called minute pulmonary chemodectoma. Am J Surg Pathol 12 (3):167–175
9. Henderson JM, Sonnet JR, Schlesinger C, Ord RA (1999) Pulmonary metastasis of ameloblastoma: case report and review of the literature. Oral Surg Oral Med Oral Pathol Oral Radiol Endod 88(2):170–176
10. Ionescu DN, Sasatomi E, Aldeeb D, Omalu BI, Finkelstein SD, Swalsky PA, Yousem SA (2004) Pulmonary meningothelial-like nodules: a genotypic comparison with meningiomas. Am J Surg Pathol 28(2):207–214
11. Kaleem Z, Fitzpatrick MM, Ritter JH (1997) Primary pulmonary meningioma. Report of a case and review of the literature. Arch Pathol Lab Med 121(6):631–636
12. Kaminski JM, Movsas B, King E, Yang C, kronz JD, Alli PM, Williams J, Brem H (2001) Metastatic meningioma to the lung with multiple pleural metastases. Am J Clinc Oncol 24(6):579–582
13. Kao GF, Helwig EB, Graham JH (1987) Aggressive digital papillary adenoma and adenocarcinoma. A clinicopathological study of 57 patients, with histochemical, immunopathological, and ultrastructural observations. J Cutan Pathol 14(3):129–146
14. Kleihues P, Carehee WK (2000) Pathology and genetics of tumors of the nervous system. World Hearth Organization. IARC, Lyon
15. Knoop M, Sola S, Hebecker R, Mann S, Bauer HG, Schmidt W (2004) Rare pulmonary manifestation of an intracranial meningothelial meningioma. Dtsch Med Wochenschr 129(36):1854–1857
16. Kodama K, Dol O, Higashiyama M, Horai T, Tateishi R, Nakagawa H (1991) Primary and metastatic pulmonary meningioma. Cancer 67(5):1412–1417
17. Kuroki M, Nakata H, Masuda T, Hashiguchi N, Tamura S, Nabeshima K, Matsuzaki Y, Onitsuka T (2002) Minute pulmonary meningothelial-like nodules: high-resolution computed tomography and pathologic correlations. J Thorac Imaging 17(3):227–229
18. Lockett L, Chiang V, Scully N (1997) Primary pulmonary meningioma: report of a case and review of the literature. Am J Surg Pathol 21(4):453–460
19. Miller DC, Ojemann RG, Proppe KH, McGinnis BD, Grillo HC (1985) Benign metastasizing meningioma. Case report. J Neurosurg 62(5):763–766
20. Murrah CP, Ferguson ER, Jennelle Rl, Guthrie BL, Holman WL (1996) Resection of multiple pulmonary metastases from a recurrent intracranial meningioma. Ann Thorac Surg 61 (6):1823–1824
21. Ng TH, Wong MP, Chan KW (1990) Benign matastasizing meningioma. Clin Neurol Neurosurg 92(2):152–154
22. Niho S, Yokose T, Nishiwaki Y, Mukai K (1999) Immunohistochemical and clonal analysis of minute pulmonary meningothelial-like nodules. Hum Pathol 30(4):425–429
23. Pramesh CS, Saklani AP, Pantvaidya GH, Heroor AA, Naresh KN, Sharma S, Deshpande RK (2003) Benign metastasizing meningioma. Jpn J Clin Oncol 33(2):86–88
24. Sellami D, Gotway MB, Hanks DK, Webb WR (2001) Minute meningothelial-like nodules: thin-section CT appearance. J Comput Assit Tomogr 25(2):311–313
25. Spinelli M, Claren R, Colombi R, Sironi M (2000) Primary pulmonary meningioma may arise from meningothelial-like nodules. Adv Clin Path 4(1):35–39
26. Som PM, sacher M, Strenger SW, Biller HF, Malls LI (1987) "Benign" metastasizing meningiomas. AJNR Am J Neuroradiol 8 (1):127–130
27. Strimlan CV, Golembiewski RS, Celko DA, Fino GJ (1988) Primary pulmonary meningioma. Surg Neurol 29(5):410–413
28. Suster S, Moran CA (1995) Unusual manifestations of metastatic tumors to the lungs. Semin Diagn Pathol 12 (2):193–206
29. Yoshizaki T, Kinsen H, Minato H, Kita T, Furukawa M (2004) Metastasizing mixed tumour of the parotid gland presenting as multiple lung metastases. J Laryngol Otol 118(9):724–726

Virchows Arch (2007) 450:595–599
DOI 10.1007/s00428-007-0393-8

CASE REPORT

Non-sebaceous lymphadenoma of the salivary gland: case report with immunohistochemical investigation

Shaodong Yang · Xinming Chen · Li Wang · Jiali Zhang

Received: 3 January 2007 / Revised: 9 February 2007 / Accepted: 21 February 2007 / Published online: 13 March 2007
© Springer-Verlag 2007

Abstract Non-sebaceous lymphadenoma (NSL) is a rare, recently described, benign salivary gland tumor characterized by a dense lymphoid infiltrate and absence of sebaceous differentiation. To our knowledge, only seven previous cases have been reported. In this paper, we describe an additional example of NSL along with an extensive analysis of its keratin (CK) profile. The patient was a 50-year-old woman presenting with a slowly growing painless mass in the right parotid gland. The tumor was encapsulated and measured 3×2×2 cm. Microscopically, the tumor comprised islands of epithelial cells with centrally located duct-like structures within a dense lymphoid stroma. Immunohistochemically, the tumor regularly expressed CKs 7, 8/18, and 19, which are typical for columnar differentiation and CKs 17 and 5/6, which are most typically expressed in basal cells of complex epithelia. CK14 was only expressed in rare scattered cells and eventually in groups of cells. The expression of CK10/13, which correlates with squamous differentiation, was negative. Additionally, immunostaining for smooth muscle actin, vimentin, and S-100 was also performed. The immunohistochemical findings in the neoplastic epithelial component of our case suggest a differentiation of "intercalated duct phenotype" without myoepithelial cell participation.

S. Yang · J. Zhang
Key Laboratory for Oral Biomedical
Engineering of Ministry of Education,
School and Hospital of Stomatology, Wuhan University,
Wuhan, Hubei, China

X. Chen (✉) · L. Wang
Department of Pathology,
School and Hospital of Stomatology, Wuhan University,
Wuhan 430079 Hubei, China
e-mail: xmchen301@yahoo.com.cn

Keywords Salivary gland tumor · Non-sebaceous lymphadenoma · Lymphadenoma · Immunohistochemistry

Introduction

Non-sebaceous lymphadenoma (NSL) is a rare, recently described, benign salivary gland tumor [7]. In 1991, Auclair et al. [5] first described some cases of cystadenoma with a prominent lymphoid element that were named cystic lymphadenoma. Then, in a review paper, they used the term lymphadenoma to describe some salivary gland adenomas accompanied by a prominent lymphoid component that lacked characteristic features of specific adenoma types [6]. Subsequently, this entity was included by the same authors as a variant of sebaceous lymphadenoma ("lymphadenoma that lacks sebaceous differentiation") in the 1996 Armed Forces Institute of Pathology fascicle on salivary gland tumors [12]. To the best of our knowledge, thereafter, only seven cases of NSL have been reported in the medical literature [8, 9, 15, 17, 20]. In the 2005 World Health Organization histological classification of salivary gland tumors, NSL is classified as a lymphadenoma, together with sebaceous lymphadenoma [7]. Herein, we report a case of NSL arising from the parotid gland along with an extensive analysis of its keratin (CK) profile because previous immunophenotypic studies of NSL have been rather limited in scope.

Clinical history

The patient, a 50-year-old woman, had a slowly growing painless mass in her right infra-auricular area of 1 month's duration. She was otherwise well with no significant past

medical history. The tumor was surgically excised with the safe margins of the adjacent non-tumorous tissues. There were no signs of recurrence 11 months after surgery.

Materials and methods

The surgical specimen was fixed in formalin, routinely processed, with representative tissue sections being embedded in paraffin and stained with hematoxylin and eosin (H and E). Immunohistochemical stains were performed in selected blocks. Staining using a standard streptavidinbiotin method was performed for keratin 7 (CK7, Dako, 1:100), keratin 8/18 (CK8/18, Dako, 1:160), keratin 19 (CK19, Dako, 1:50), keratin 5/6 (CK5/6, Dako, 1:50), keratin 14 (CK14, Dako, 1:100), keratin 10/13 (CK10/13, Dako, 1:50), S-100 (Dako, polyclonal, 1:200), smooth muscle actin (SMA, Dako, 1:400), and vimentin (Neomarker, 1:100). Appropriate positive and negative controls were included.

Results

The tumor was 3×2×2 cm in size, well-circumscribed without signs of necrosis or hemorrhage. It had a soft consistency and was white to gray in color on cut section. Microscopically, the tumor was composed of islands of epithelial cells in which centrally located duct-like structures with eosinophilic secretions were frequently seen, accompanied by a dense lymphoid stroma (Fig. 1). No sebaceous glands were identified. There was no evidence of cytological atypia or abnormal mitotic activity. The lymphoid stroma showed follicle formation with germinal centers, but no subcapsular sinus was seen.

Immunohistochemically, CK7 and CK8/18 were expressed in almost all tumor cells with stronger immunoreactivity in inner cells compared with outer cells (Fig. 2a,b). CK19 was mainly found in luminal cells (Fig. 2c). CK17 was positive in most of the tumor cells, but negative in some luminal cells (Fig. 2d). CK5/6 was present in the periphery of epithelial component (Fig. 3a), and CK14 was found in rare scattered cells and eventually in groups of cells (Fig. 3b). Anti-S100 protein antibodies revealed weak staining of the luminal cells of epithelial component and strong positivity in the cells with elongated projections irregularly distributed throughout both the neoplastic epithelial component and the lymphoid stroma (Fig. 3c). Only a few tumor cells scattered among the neoplastic epithelial component were positive to vimentin, whereas the stromal cells showed diffuse immunoreactivity (Fig. 3). CK10/13 and SMA were negative in all tumor cells.

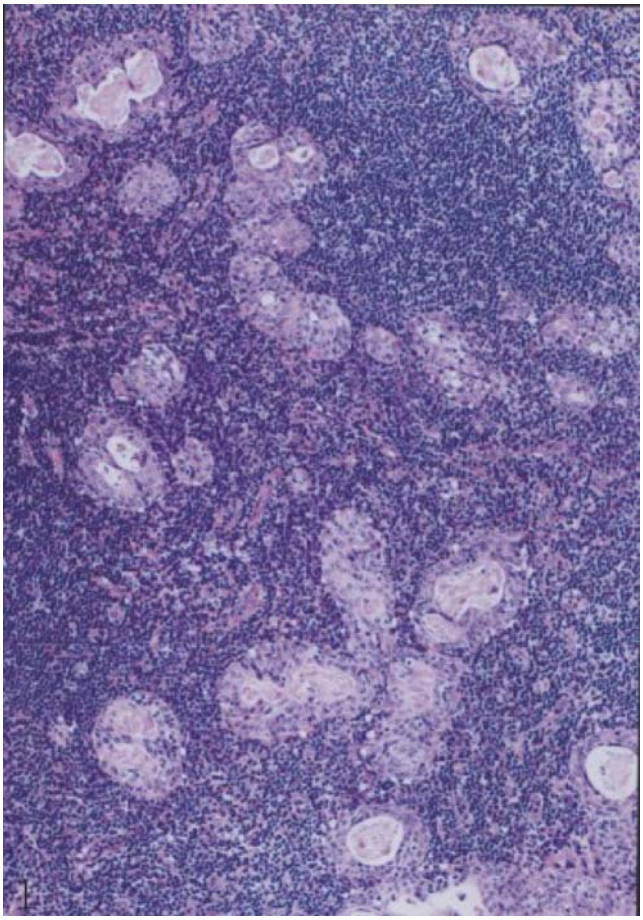

Fig. 1 Islands of epithelial cells with frequent centrally located duct-like structures formation accompanied by a prominent lymphoid stroma (H and E; original magnification ×100)

Discussion

NSL is a rare benign tumor of salivary gland origin. To the best of our knowledge, only eight cases, including the present case, have been reported in the medical literature [8, 9, 15, 17, 20]. All cases have exclusively occurred in the parotid gland with male predilection. Patients typically present with a painless mass, and these tumors rarely recur. The tumor, which is well circumscribed and encapsulated, was composed of epithelial component within a background of lymphocytes and lymphoid follicles, which is similar to sebaceous lymphadenoma but lacks sebaceous differentiation. The epithelial component can take the form of anastomosing trabeculae or solid tubules surrounded by basement membrane-like material or cystically dilated glands filled with proteinaceous materials [7, 17]. The current case is similar to previous observations, and it is the second case reported occurring in woman.

A prominent lymphoid element that accompanies epithelial neoplasms of the salivary glands is not infrequent and can occur among a variety of salivary gland tumors,

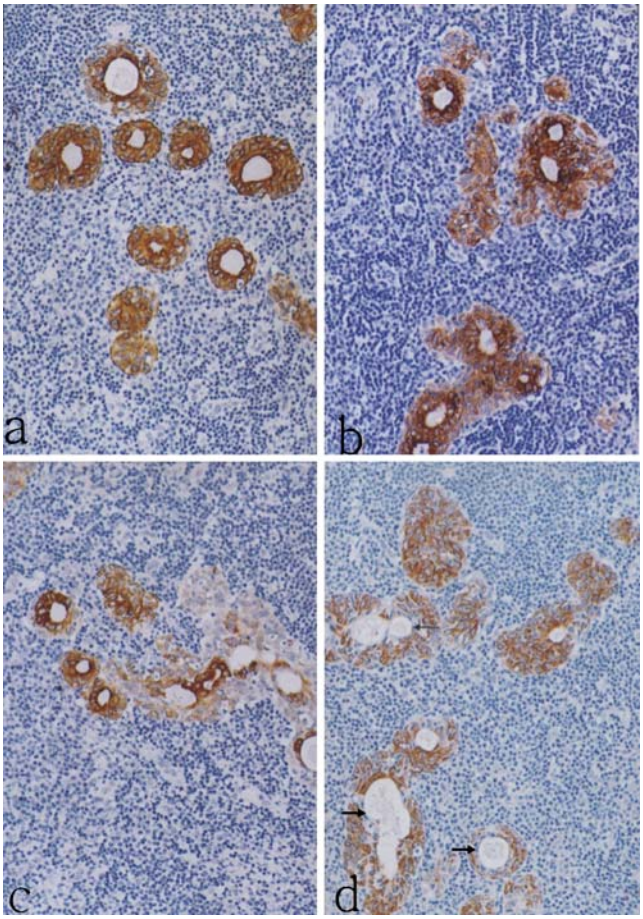

Fig. 2 **a** Intense expression of CK7 by the tumor cells (Strep.; original magnification ×200). **b** CK8/18 staining with strong expression in the tumor cells (Strep.; original magnification ×200). **c** Internal cells showing strong positive to CK19 compared with outer cells of the epithelial component (Strep.; original magnification ×200). **d** Tumoral islands showing diffuse positivity to CK17. Note non-immunoreactivity in some luminal cells (*arrows*; Strep.; original magnification ×200)

such as Warthin's tumor, sebaceous lymphadenoma, NSL, lymphoepithelial carcinoma, acinic cell carcinoma, mucoepidermoid carcinoma, etc [6]. The lymphoid element in such lesions often should be regarded as a required element in diagnosis. However, this feature may result in the misinterpretation of malignant tumors of the parotid as benign neoplastic or non-neoplastic lesions and of primary benign and malignant tumors as carcinomas that have metastasized to intra-glandular lymph nodes. The most important differential diagnosis of the present case is lymphoepithelial carcinoma. Lack of mitotic activity, lack of invasive growth with desmoplastic stroma, and presence of overt ductal differentiation in lymphadenoma can set it apart from lymphoepithelial carcinoma. In addition, metastatic carcinoma and malignant lymphoma should be considered [6, 17].

The lymphoid component in NSL is generally considered to represent tumor-associated lymphoid proliferation [5, 7, 17], but the histogenesis of the neoplastic epithelial component is unclear. Immunohistochemical labeling with antibodies for various antibodies such as cytokeratin subtypes, S-100, vimentin, or SMA is an important technique used to better understand the histogenesis of normal and pathological epithelial tissues and has helped to characterize different salivary gland tumors [1–4, 11, 13, 14, 16, 18, 19, 21, 25–29]. The expression of CKs 7, 8, 18, and 19 is typical for columnar differentiation of epithelia [10, 25]. In the current study, CKs 7 and 8/18 were positive in almost all epithelial neoplastic cells, while the staining intensities were higher in inner cells compared with outer cells. CK19 mainly expressed in luminal cells. On the other hand, immunoreactivity with antibodies to CKs 5/6 and 17,

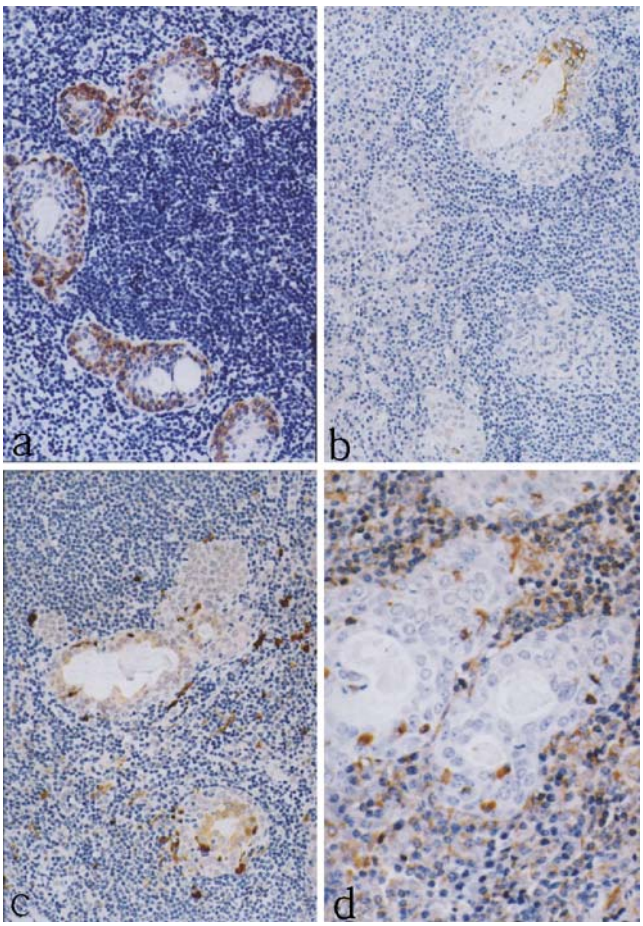

Fig. 3 **a** Tumoral islands showing positivity of the peripheral cells to CK5/6 (Strep.; original magnification ×200). **b** CK14 is expressed by a few cells (Strep.; original magnification ×200). **c** S-100 staining of the luminal cells of epithelial component and cells with elongated projections throughout both the neoplastic epithelial component and the lymphoid stroma (Strep.; original magnification ×200). **d** Only scattered epithelial cells showing positivity to anti-vimentin antibody, while the stroma demonstrating diffuse immunoreactivity (Strep.; original magnification ×400)

which are most typically expressed in basal cells of complex epithelia [10, 25], was present mainly in the outer cells. Negative staining results were obtained with antibody to CK10/13, the expression of which correlates with squamous differentiation of epithelia [10, 16, 25, 27]. CK14, which is an indicator of the basal cells in the keratinized epithelium and also has been identified in basal cells of the excretory ducts [3, 4, 10, 13, 18], stained only rare tumor cells in the present case. This expression pattern for keratin in our case indicates the presence of dual luminal cell and abluminal cell differentiation and suggests that this tumor mirrors what might be expected of a tumor with differentiation toward that of an intercalated duct [3, 4, 13, 14, 18, 28]. Ma et al. [17] reported three cases of NSL and the immunohistochemical reactivities of these cases, in which abluminal cells were usually predominant. Bos et al. [8] described a case of NSL with CK5/6, CK10/13, and CK14 expression in most tumor cells and mild expression of columnar type cytokeratins. The expression of cytokeratin profile in our case is different from that in previous studies because of its obvious columnar cell differentiation, which may be due to the different degrees of differentiation of the tumor cells.

Immunohistochemical profile of neoplastic myoepithelial cells is a perplexing issue [24]. The expression of SMA, which is an indicator of myoepithelial cell differentiation [2, 4, 18, 24], was not detected in our case. Vimentin and S-100, although nonspecific, in conjunction with cytokeratins, have been demonstrated to be sensitive markers of neoplastic myoepithelial cells [1, 4, 24]. However, immunoreactivity for vimentin was seen in single scattered tumor cells in our case, which probably reflects the loss of cellular adhesion under inflammatory conditions [18, 19]. Previous studies have demonstrated S-100 protein is not a specific marker for myoepithelial cells [21]. Our study revealed that S-100 weakly expressed in luminal cells. We assumed that this reactivity is related to the intercalated duct origin of tumor cells and the S-100 positive cells with elongated projections in the epithelial element belong to the Langerhans cells just as that in the lymphoid stoma, similar to previous study in basal cell adenoma and Warthin's tumor [21, 26, 29]. These findings point to the absence of myoepithelial cell participation within this neoplasm and are in agreement with previous study by Ma et al. [17].

Although NSL has been considered to be a distinctive entity, the exact morphologic and nosologic relationships to other salivary gland tumors are not clearly established. Without lymphoid stroma, the hitherto reported cases of NSL would be easily recognized as basal cell adenoma or cystadenoma [17]. Given that sebaceous differentiation is a rather common finding in normal salivary gland and can be seen in many known benign and malignant salivary gland tumors, a relationship between sebaceous lymphadenoma and NSL is suggested [15]. Sebaceous lymphadenoma is thought to be related to Warthin's tumor, as both can have overlapping histological features, both are purported to arise from parotid lymph node salivary duct inclusions with concomitant oncocytic and sebaceous metaplasia, both can present with or without associated lymph node architecture, and synchronous presentation of both was reported in literature [23]. Similarities between NSL and Warthin's tumor have been shown in previous studies [5, 15, 17]. The present case reveals a similar cytokeratin profile to Warthin's tumor [25], which is also devoid of myoepithelial cell differentiation [22, 24]. Therefore, further studies would be necessary to elucidate the pathogenesis of prominent lymphoid proliferation in salivary gland adenomas and the relationships among those adenomas with prominent lymphoid proliferation.

In conclusion, the authors presented a case of NSL with immunohistochemical investigation. The immunohistochemical findings in the neoplastic epithelial component of our case suggest a differentiation of "intercalated duct phenotype" without myoepithelial cell participation. More cases are required to better understand this entity.

Acknowledgements The authors thank Mrs. Li Yuan and Mr. Xiong Shichun for their skilled technical assistance.

References

1. Araújo VC, Araújo NS (1990) Vimentin as a marker of myoepithelial dells in salivary gland tumors. Eur Arch Otorhinolaryngol 247:252–255
2. Araújo VC, Carvalho YR, Araújo NS (1994) Actin versus vimentin in myoepithelial cells of salivary gland tumors. A comparative study. Oral Surg Oral Med Oral Pathol 77:387–391
3. Araújo VC, Sousa SOM (1996) Expression of different keratins in salivary gland tumours. Oral Oncol Eur J Cancer 32B:14–18
4. Araújo VC, Souza SOM, Carvalho YR, Araújo NS (2000) Application of immunohistochemistry to the diagnosis of salivary gland tumors. Appl Immunohistochem Mol Morphol 8:195–202
5. Auclair PL, Ellis GL, Gnepp DR (1991) Other benign epithelial neoplasms. In: Ellis GL, Auclair PL, Gnepp DR (eds) Surgical pathology of the salivary glands. Saunders, Philadelphia, pp 252–268
6. Auclair PL (1994) Tumor-associated lymphoid proliferation in the parotid gland. A potential diagnostic pitfall. Oral Surg Oral Med Oral Pathol 77:19–26
7. Barnes L, Eveson JW, Reichart P, Sidransky D (2005) Tumors of the salivary glands. World Health Organization classification of tumors. Pathology and genetics of head and neck. IARC, Lyon, p 269
8. Bos I, Meyer S, Merz H (2004) Lymphadenoma of the parotid gland without sebaceous differentiation. Immunohistochemical investigations. Pathologe 25:73–78
9. Chang JY, Hsiao CH (2004) Lymphadenoma lacking sebaceous differentiation in the parotid gland. J Formos Med Assoc 103:459–462
10. Chu PG, Weiss LM (2002) Keratin expression in human tissues and neoplasms. Histopathology 40:403–439

11. Crivelini MM, Souza SOM, Araújo VC (1997) Immunohistochemical study of acinic cell carcinoma of minor salivary gland. Oral Oncol 33:204–225
12. Ellis GL, Auclair PL (1996) Benign epithelial neoplasms. In: Rosai J, Sobin LH (eds) Tumors of the salivary glands. Atlas of tumor pathology, third series. Armed Forces Institute of Pathology, Washington, DC, pp 135–136
13. Foschini MP, Marucci G, Eusebi V (2002) Low-grade mucoepidermoid carcinoma of salivary glands: characteristic immunohistochemical profile and evidence of striated duct differentiation. Virchows Arch 440(5):536–542
14. Gustafsson H, Kjorell U, Eriksson A, Virtanen I, Thornell L-E (1988) Distribution of intermediate filament proteins in developing and adult salivary glands in man. Anat Embryol 178: 243–251
15. Kwon GY, Kim EJ, Go JH (2002) Lymphadenoma arising in the parotid gland: a case report. Yonsei Med J 43:536–538
16. Loyola AM, Souza SOM, Araújo NS, Araújo VC (1998) Study of minor salivary gland mucoepidermoid carcinoma differentiation based on immunohistochemical expression of cytokeratins, vimentin, and muscle-specific actin. Oral Oncol 34:112–118
17. Ma J, Chan JKC, Chow CW, Orell SR (2002) Lymphadenoma: a report of three cases of an uncommon salivary gland neoplasm. Histopathology 41:342–350
18. Martins MD, Cavalcanti de Araújo V, Raitz R, Soares de Araújo N (2002) Expression of cytoskeletal proteins in developing human minor salivary glands. Eur J Oral Sci 110:316–321
19. Morinaga S, Nakajima T, Shimosato Y (1987) Normal and neoplastic myoepithelial cells in salivary glands: an immunohistochemical study. Hum Pathol 18:1218–1226
20. Musthyala NB, Low SE, Seneviratne RH (2004) Lymphadenoma of the salivary gland: a rare tumour. J Clin Pathol 57:1007
21. Ogawa I, Nikai H, Takata T, Miyauchi M, Ito H, Ijuhin N (1990) The cellular composition of basal cell adenoma of the parotid gland: an immunohistochemical analysis. Oral Surg Oral Med Oral Pathol 70(5):619–626
22. Prasad AR, Savera AT, Gown AM, Zarbo RJ (1999) The myoepithelial immunophenotype in 135 benign and malignant salivary gland tumors other than pleomorphic adenoma. Arch Pathol Lab Med 123(9):801–806
23. Rund CR, Spies JA (2005) A neck mass in a 57-year-old man. Arch Pathol Lab Med 129(7):e171–e172
24. Savera AT, Zarbo RJ (2004) Defining the role of myoepithelium in salivary gland neoplasia. Adv Anat Pathol 11:69–85
25. Schwerer MJ, Kraft K, Baczako K, Maier H (2001) Cytokeratin expression and epithelial differentiation in Warthin's tumour and its metaplastic (infarcted) variant. Histopathology 39:347–352
26. Segami N, Fukuda M, Manabe T (1989) Immunohistological study of the epithelial components of Warthin's tumor. Int J Oral Maxillofac Surg 18:133–137
27. Sobral AP, Loducca SV, Kowalski LP, Santos IR, Almeida OP, Araújo NS, Araújo VC (2002) Immunohistochemical distinction of high-grade mucoepidermoid carcinoma and epidermoid carcinoma of the parotid region. Oral Oncol 38(5):437–440
28. Su L, Morgan P, Harrison DL, Waseem A, Lanes B (1993) Expression of keratin mRNAs and proteins in normal salivary epithelia and pleomorphic adenomas. J Pathol 171:173–181
29. Takahashi H, Tsuda N, Tezuka F, Okabe H (1986) An immunoperoxidase investigation of S-100 protein in the epithelial component of Warthin's tumor. Oral Surg Oral Med Oral Pathol 62(1):57–62

Virchows Arch (2007) 450:601–602
DOI 10.1007/s00428-007-0397-4

LETTER TO THE EDITOR

How often does cervical involvement upstage patients with non-myoinvasive (otherwise stage 1A) endometrioid adenocarcinoma of the endometrium?

Oluwole Fadare · Laurephile Desrosiers · Zhefu F. Xiao · Sa A. Wang

Received: 31 December 2006 / Accepted: 1 March 2007 / Published online: 4 April 2007
© Springer-Verlag 2007

Dear Editor,

With an estimated 40,880 new cases diagnosed annually, cancers of the uterine corpus represent the most common malignancy of the gynecologic tract in the United States [5]. More than 80% of these cases are endometrioid carcinomas of the endometrium (EEC); a variant, which has a relatively favorable prognostic profile and a 5-year overall survival of approximately 81.2% [2]. In the current staging system of endometrial cancers endorsed by the International federation of Gynecology and Obstetrics (FIGO) and the American Joint Committee on Cancer [2, 4], endometrial cancers that do not invade the myometrium are classified as stage 1A. Any cervical involvement of a tumor that is confined to the corpus irrespective of the depth of myometrial invasion upstages a patient to stage 2 [2, 4]. Among 8,790 patients reported to the FIGO as outlined in a recent report, 5,884 were stage 1 and 984 were stage 2 [2]. The aforementioned staging schemes are based on multiple studies of independent datasets that have shown that cervical involvement (especially stromal invasion) increases the probability of either local relapse, metastases or death from disease in patients with cancers that would otherwise be classified as stage 1 [1–3, 7, 8]. However, the independent prognostic power of cervical involvement has been relatively controversial because cervical involvement significantly covaries with depth of myometrial invasion and histologic grade. Morrow et al. [8] noted that "it is unclear that cervix invasion per se diminishes survival, because it is more often associated with poor tumor differentiation and deep myoinvasion than cases without cervix invasion". Similarly, Lee et al. [7] found that while cervical stromal invasion was associated with increased risk of recurrence, this finding was not independent of the grade and depth of myometrial invasion. Opinions are relatively diverse on the optimal adjuvant management of patients with corpus-confined EEC [6] and cervical involvement in non-myoinvasive (otherwise stage 1A) EEC represents a potential decision point (at which some oncologists apply adjuvant vaginal cuff brachytherapy in patients that otherwise would only be observed postoperatively). Therefore, we sought to investigate the precise *frequency* with which this finding—cervical involvement in non-myoinvasive EEC—occurs in routine practice. We also compared broad clinicopathologic factors between patients with stage 1A EEC and patients with stage 2 EEC but who were upstaged solely due to cervical involvement of their non-myoinvasive EEC. After approval from our institutional review board, we retrieved and reviewed pathologic reports for all stage 1 and stage 2 EEC diagnosed between 1997 and 2005 at the Department of Pathology, University of Massachusetts Medical Center, (Worcester, MA, USA). The frequency with which patients with non-myoinvasive (stage 1A) EEC were

This study was presented in part at the 96th annual meeting of the United States and Canadian Academy of Pathologists, San Diego, CA, March 24, 2007.

O. Fadare (✉)
Department of Pathology,
Wilford Hall Medical Center,
2200 Bergquist Dr., Ste 1,
Lackland AFB, TX 78236, USA
e-mail: oluwolefadare@yahoo.com

O. Fadare
Department of Pathology,
University of Texas Health Science Center at San Antonio,
San Antonio, TX, USA

L. Desrosiers · Z. F. Xiao · S. A. Wang
Department of Pathology,
University of Massachusetts Medical Center,
Worcester, MA, USA

upstaged to stage 2 solely due to cervical involvement was determined (group 1). The latter patients were then compared with patients with corpus-confined, non-myoinvasive (stage 1A) EEC (group 2). Follow-up information was obtained from the patients' medical records. Fisher's exact and *t*-tests were used for statistical comparisons with $p<0.05$ considered as significant. Of 345 stage 1 EEC diagnosed during this period, 121 were staged 1A, of which 109 were sufficiently documented for the purpose of this analysis. Only 4 patients were upstaged solely due to cervical involvement (stage 2a $n=2$, stage 2b $n=2$) for an overall incidence of 4 (3.5%) of 113 non-myoinvasive cancers. One (25%) of 4 and 65 (57.5%) of 113 patients in groups 1 and 2 were completely staged, respectively. The latter included pelvic and/or paraaortic lymph node sampling, in addition to the hysterectomy and bilateral salpingo-oophorectomy, which all patients in the cohort received. Neither group had any case with positive lymph nodes. Lymphovascular invasion was present in 1 (25%) of 4 patients in group 1 and 0 (0%) of 109 patients in group 2. Three (75%) of the 4 group 1 patients had tumors with FIGO architectural grade 3, whereas the fourth patients had grade 1 (3-tiered scale). In contrast, the distribution of architectural grades in the group 2 patients was as follows: grade 1 (90/109, 82.5%), grade 2 (17/109, 15.6%), grade 3 (2/109, 1.8%). Because 75% of the group 1 patients had grade 3 cancers, our findings suggest that architectural grade is a dominant variable in this context. The median follow-up for the whole cohort was 80 months (mean 46 months). At a mean follow-up of 3.7 and 5.3 years, there were 0 and 2 vaginal relapses in groups 1 and 2, respectively. No extrapelvic or distant relapses were identified in either group. No significant differences were noted between groups 1 and 2 patients with respect to the mean body mass index (35.9 vs 35.3, respectively, $p=0.9$) or patient age (55.2 years vs 57.9 years, respectively, $p=0.8$).

We conclude that cervical involvement in non-myoinvasive EEC is a very rare finding (4/113, 3.5%). Larger prospectively collected datasets of patients with standardized therapeutic modalities are required to conclusively define the significance of this finding. In this preliminary study, however, patients upstaged solely due to cervical involvement did not have higher relapse rates than patients with FIGO stage 1A disease. Three of the four patients so upstaged had architectural grade 3 cancers. Furthermore, no distinctive clinical differences were noted between these two groups. If confirmed, our findings suggest that when there is cervical involvement in the setting of non-myoinvasion, other clinicopathologic factors (e.g. tumor grade or lymphovascular invasion) should determine the decision to administer adjuvant therapy, rather than cervical involvement in itself.

References

1. Boronow RC, Morrow CP, Creasman WT, Disaia PJ, Silverberg SG, Miller A, Blessing JA (1984) Surgical staging in endometrial cancer: clinical-pathologic findings of a prospective study. Obstet Gynecol 63:825–832
2. Creasman WT, Odicino F, Maisonneuve P, Beller U, Benedet JL, Heintz AP, Ngan HY, Pecorelli S (2003) Carcinoma of the corpus uteri. Int J Gynaecol Obstet 83(Suppl 1):79–118
3. Fanning J, Alvarez PM, Tsukada Y, Piver MS (1991) Prognostic significance of the extent of cervical involvement by endometrial cancer. Gynecol Oncol 40:46–47
4. Greene FL, Page DL, Fleming ID, Fritz A, Balch CM, Haller DG, Morrow M (eds) (2002) AJCC cancer staging handbook, 6th edn. Springer, Berlin Heidelberg New York
5. Jemal A, Murray T, Ward E, Samuels A, Tiwari RC, Ghafoor A, Feuer EJ, Thun MJ (2005) Cancer statistics, 2005. CA Cancer J Clin 55:10–30
6. Koh WJ, Tran AB, Douglas JG, Stelzer KJ (2001) Radiation therapy in endometrial cancer. Best Pract Res Clin Obstet Gynaecol 15:417–432
7. Lee KR, Vacek PM, Belinson JL (1994) Traditional and nontraditional histopathologic predictors of recurrence in uterine endometrioid adenocarcinoma. Gynecol Oncol 54:10–18
8. Morrow CP, Bundy BN, Kurman RJ, Creasman WT, Heller P, Homesley HD, Graham JE (1991) Relationship between surgical–pathological risk factors and outcome in clinical stage I and II carcinoma of the endometrium: a Gynecologic Oncology Group study. Gynecol Oncol 40:55–65

Virchows Arch (2007) 450:603–605
DOI 10.1007/s00428-007-0399-2

LETTER TO THE EDITOR

Epithelial misplacement in the muscularis propria after biopsy of a colonic adenoma

Gaetano Magro · Giuseppe Aprile · Giuseppe Vallone · Paolo Greco

Received: 18 January 2007 / Revised: 9 February 2007 / Accepted: 1 March 2007 / Published online: 20 March 2007
© Springer-Verlag 2007

Sir,

Hyper-plastic and hamartomatous colonic polyps may show misplaced epithelium (pseudo-invasion) within the sub-mucosa or more rarely even extending into the muscular wall and/or serosa, potentially simulating an invasion by a well-differentiated adenocarcinoma [2, 4]. The pathogenesis of this condition is referred to as the passage of the mucosal glands through the anatomical defects in the muscularis mucosae due to tissue damage from torsion, or twisting, of the polyp [2, 4]. It is likely that even minor trauma, resulting from vigorous peristalsis or bulky intraluminal material, may be responsible of epithelial misplacement, especially in sessile polyp [4]. Pseudo-invasion can also commonly occur in peduncolated adenomatous polyps, especially in the form of herniated mucosal glands through natural spaces in the muscularis mucosae, into the sub-mucosa of the polyp stalk [3].

Although it is known that transient epithelial misplacement in the sub-mucosa can occur in colonic adenomas within a short period after biopsy [1], to the best of our knowledge, an extension into the muscularis propria has not been reported to date. We first report an epithelial misplacement (pseudo-invasion) in the muscularis propria after an endoscopic biopsy of a sessile colonic adenoma.

An 86-year-old man underwent colonoscopy for rectal bleeding. A large broad-based polypoid mass was found in the sigmoid colon, and bioptic material was obtained for histological examination. Histologically, the removed fragments were consistent with an adenoma with low-grade dysplasia. Because of the large dimension of the tumour, surgical resection (sigmoid colon and upper rectum) was performed after 12 days from biopsy. Grossly, a broad-based polypoid mass, measuring 4.5 cm in diameter, was observed in the sigmoid colon. The tumour was entirely sampled and processed for microscopic examination. Histologically, the tumour was a tubulovillous adenoma with low-grade dysplasia. At the base of the tumour, mucosal ulceration covered by a mixture of mucus lakes and suppurative exudate with isolated free-lying glands could be noted (Fig. 1a). It is surprising to note that isolated atypical glands were found in the underlying muscularis propria (Fig. 1b). Cytologically, the glandular epithelium was composed of atypical mucin-depleted cells with enlarged, vesicular, oval to round nuclei containing small nucleoli. These glands were completely enveloped by granulation tissue containing inflammatory cells, newly formed capillaries and a minor amount of fibroblasts (Fig. 1b). Despite additional histological sections prepared from deeper levels of the tissue blocks, foci of malignant transformation were not identified. It was possible to identify a continuous rim of granulation tissue in only one section, extending from the mucosal ulceration at the base of the tumour into the sub-mucosa and muscularis propria. Isolated atypical glands, cytologically similar to those formerly observed, were entrapped at different levels (from mucosa to muscularis propria) within the abovementioned granulation

G. Magro (✉) · P. Greco
Department G.F.Ingrassia, Anatomia Patologica,
Azienda Ospedaliero-Universitaria Policlinico di Catania,
Via S. Sofia 87,
95123 Catania, Italy
e-mail: g.magro@unict.it

G. Aprile
Servizio di Chirurgia Endoscopica,
Azienda Ospedaliero-Universitaria Policlinico di Catania,
Via S. Sofia 87,
95123 Catania, Italy

G. Vallone
Servizio Anatomia Patologica, Ospedale di Enna,
Enna, Italy

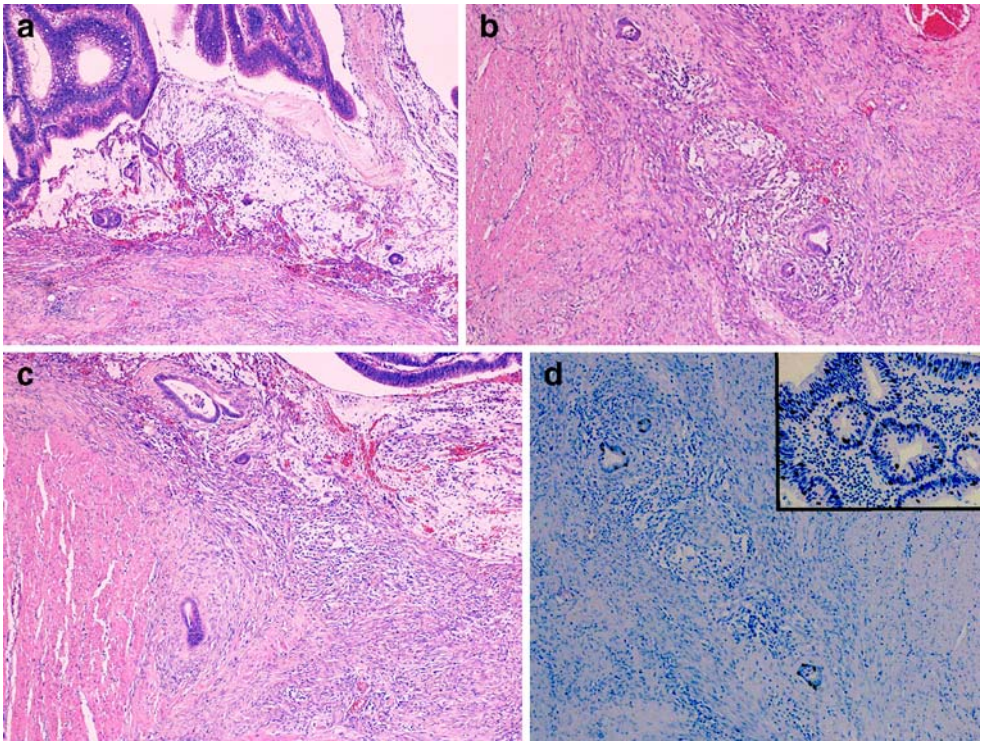

Fig. 1 **a** Ulceration at the base of the tumour: glands within mucus and exudate. **b** Muscularis propria: isolated atypical glands enveloped by granulation tissue. **c** Isolated atypical glands are seen within granulation tissue extending from mucosal ulceration to muscularis propria. **d** Scattered p53 positive nuclei are seen both in glands of mucosal adenoma (*inset*) and in misplaced glands within the muscularis propria

tissue (Fig. 1c). Because some immunohistochemical analyses, including p53 staining, may have utility in the differential diagnosis of adenomas with pseudo-invasion vs adenomas with invasive adenocarcinoma, we tested our case with p53 immunostaining. As expected, immunoreactivity with a similar staining intensity (low to moderate) for p53 was focally present in the scattered nuclei of the intramucosal component of the adenoma and in the misplaced glandular epithelium (Fig. 1d). Accordingly, our final diagnosis was adenoma with low-grade dysplasia with associated sub-mucosal and muscularis propria pseudo-invasion due to biopsy-induced trauma. Surgical resection margins and 19 lymph nodes retrieved were normal. Patient is well after 8 months follow-up period.

The presence of atypical glands in the sub-mucosa with extension into the muscularis propria may mimic an invasive adenocarcinoma. The distinction of a true invasion from a pseudo-invasion may be difficult, especially in cases of adenomas with high-grade dysplasia showing glandular misplacement throughout the bowel wall. A careful evaluation of the following morphological and immunohistochemical features can help in ruling out a true invasion: (1) absence of malignant foci within the adenoma (intramucosal adenocarcinoma); (2) demonstration of anatomical continuity (by histological serial sections) between mucosal adenoma and misplaced epithelium and (3) similar degree of p53 staining in misplaced epithelium when compared with mucosal portion of adenoma [5]. In our case, all these features were present. The absence of high-grade dysplasia/intra-mucosal adenocarcinoma within the adenoma was the most important parameter against a true invasion. The evidence that misplaced glands were entrapped within granulation tissue covering an anatomical defect, extending from a superficial ulceration to the muscularis propria, was an additional morphological finding strongly in favour of pseudo-invasion. Finally, even immunohistochemical analysis for p53 was consistent with pseudo-invasion as invasive adenocarcinoma usually exhibits numerous strongly positive p53 nuclei [5].

The occurrence of an ulceration extending from the mucosal surface into the muscularis propria, identified in the surgically removed sample, lead us to think that pseudo-invasion in our case was closely related to a biopsy-induced tissue trauma. It is likely hypothesised that an avulsion of the mucosal glands with an associated underlying fissured ulcer of the sub-mucosa, partially extending into the muscularis propria, developed at the site of biopsy. Subsequently, isolated mucosal glands were first entrapped within the superficial ulcerated tissue, which later passed through the anatomical defect into the sub-mucosa and muscularis propria, wherein they were completely surrounded by granulation tissue healing the biopsy-induced deep ulceration.

In conclusion, the present paper provides evidence that misplaced epithelium in the muscularis propria may rarely occur after endoscopic biopsy of a sessile colonic adenomatous polyp. Pathologists should be aware of this possibility to avoid an over-diagnosis of invasive adenocarcinoma.

References

1. Dirschmid K, Kiesler J, Mathis G, Beller S, Stoss F, Schobel B (1993) Epithelial misplacement after biopsy of colorectal adenomas. Am J Surg Pathol 17:1262–1265
2. Petersen VC, Sheehan AL, Bryan RL, Armstrong CP, Shepherd NA (2000) Misplacement of dysplastic epithelium in Peutz–Jeghers polyps: the ultimate diagnostic pitfall? Am J Surg Pathol 24:34–39
3. Qizilbash AH, Meghji M, Castelli M (1980) Pseudocarcinomatous invasion of the colon and rectum. Dis Colon Rectum 23:529–535
4. Yantiss RK, Goldman H, Odze RD (2001) Hyperplastic polyp with epithelial misplacement (inverted hyperplastic polyp): a clinicopathologic and immunohistochemical study of 19 cases. Mod Pathol 14:869–875
5. Yantiss RK, Bosenberg MW, Antonioli DA, Odze RD (2002) Utility of MMP-1, p53, E-cadherin, an collagen IV immunohistochemical stains in the differential diagnosis of adenomas with misplaced epihtelium versus adenoma with invasive adenocarcinoma. Am J Surg Pathol 26:206–215

Virchows Arch (2007) 450:607–609
DOI 10.1007/s00428-007-0403-x

LETTER TO THE EDITOR

A novel myoepithelial/progenitor cell marker in the breast?

Zdenek Kolar · Jiri Ehrmann Jr · Gulisa Turashvili · Jan Bouchal · Jaroslav Mokry

Received: 31 January 2007 / Revised: 8 March 2007 / Accepted: 9 March 2007 / Published online: 12 April 2007
© Springer-Verlag 2007

Dear Editor,

Neuroepithelial stem cell protein (Nestin) is an intermediate filament (IF) protein considered to be a marker of neural stem cells. Nestin expression has been confirmed in stem/progenitor cells of the dermis, hair follicles, intestine, pancreas, bone marrow as well as in neural, muscle and other tissues (reviewed in [7]). Its expression is down regulated in the course of differentiation and subsequently replaced by another type of IF [3, 10]. Nestin expression has also been detected in the endothelium [11, 12], and we have noted the activation of nestin expression in newly formed human blood vessels [7]. The human nestin molecule has a homology with rodent nestin confirming its highly conserved nature (Fig. 2c) [5].

The myoepithelial cells of the breast form an outer layer of the terminal duct lobular unit. They play an active part in mammary gland branching morphogenesis [6], and their correct recognition and detection is crucial in the diagnosis of a number of pathological breast lesions [4, 8]. Several markers have been reported for the immunohistochemical detection of breast myoepithelial cells such as α-smooth muscle actin, smooth muscle myosin heavy chain, calponin, h-caldesmon, S100 protein, p63, CD10, maspin and specific cytokeratins 5, 7, 15 and 17 (reviewed in [2, 8]). However, the specificity and sensitivity of these markers vary widely. Of these, maspin [9] and p63 [1, 2, 13] are generally considered the most promising. In histopathological practice it is very often necessary to confirm a diagnosis using a wide battery of immunohistological stainings. Undoubtedly, the identification of new markers is desirable.

We analysed the expression of nestin by an indirect immunohistochemical method (primary monoclonal anti-nestin antibody, clone 10C2, cat. no. MAB5326, Chemicon International, diluted 1:200; secondary staining system EnVision, Dako; antigen retrieval by microwave generator in citrate buffer pH 7.0; diaminobenzidine as chromogen) in 300 archival formalin-fixed and paraffin-embedded tissue samples of breast cancer and surrounding mammary tissue as well as in tissue microarrays consisting of 109 cases of breast cancer, developed for another project.

Nestin expression of various intensities was seen in the cytoplasm of myoepithelial cells of almost all normal ducts and lobular acini found in the vicinity of tumours (Fig. 1a and b). The intensity of expression varied from strong/marked (32 cases, ~10%), to moderate/clearly visible (91 cases, ~29%) to low/visible (113 cases, ~38%) and to very low/visible in less than 50% cells only (64 cases, ~21%). In our opinion, the reasons for the lower positive intensity in some cases can be explained by the fixation conditions. The specimens obtained by excision were generally more positive than specimens from the centre of the mastectomy. Pathological lesions like adenosis with atypical hyperplasia and in situ carcinoma exhibited very strong positivity (Fig. 1c and d), and the detection of nestin could also be used for the diagnosis of pseudo-invasion in some controversial cases (Fig. 1e). In invasive carcinomas, we found nestin positivity in a portion of epithelial cells in a minority (~1/3) of cases. The positivity in the epithelial component was confirmed by simultaneous AE1/AE3

Z. Kolar (✉) · J. Ehrmann Jr · G. Turashvili · J. Bouchal
Department of Pathology and Laboratory of Molecular Pathology,
Faculty of Medicine and Dentistry,
Palacky University,
Hnevotinska 3,
77515 Olomouc, Czech Republic
e-mail: kolarz@tunw.upol.cz

J. Mokry
Department of Histology and Embryology,
Faculty of Medicine, Charles University,
50038 Hradec Kralove, Czech Republic

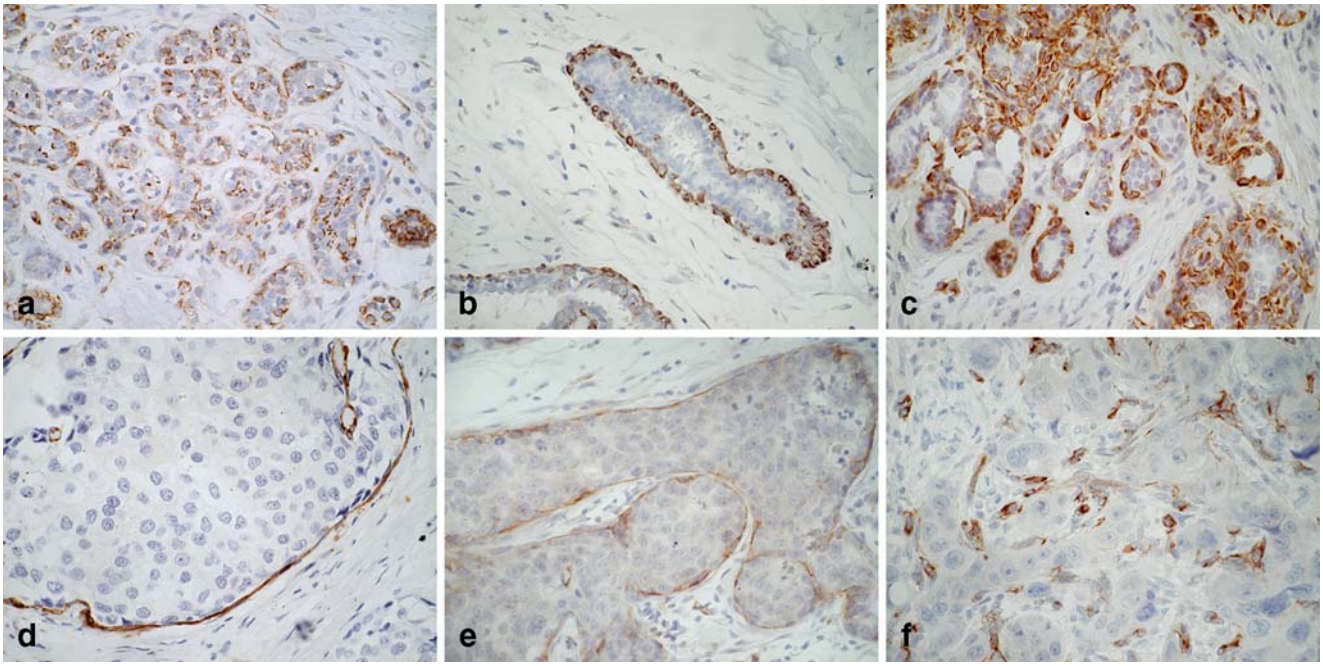

Fig. 1 **a** Nestin expression in myoepithelial cells of mammary gland acinus. **b** Nestin expression in myoepithelial cells of small mammary gland ductus. **c** Nestin expression in myoepithelial cells of lesion exhibiting the features of atypical adenosis (hyperplasia). **d** Nestin expression in myoepithelial cells surrounding ductal carcinoma in situ. **e** Nestin expression in the area of pseudo-invasion. **f** Nestin expression in stromal, endothelial and some epithelial cells of ductal invasive carcinoma G3

cytokeratin immunostaining and was significantly higher in hormone receptor and c-erbB-2/HER2/neu negative cases, which likely corresponded to basal cell phenotype cancer ($p \leq 0.003$). Apart from the epithelial component, nestin positivity in carcinomatous samples was also confirmed in some stromal elements and endothelium of the capillary network (confirmed by simultaneous CD34 immunostaining; Fig. 1f). In another ongoing study, we are examining whether these positivities are related to the presence of tumour stem/progenitor cells (in the case of cells with epithelial/myoepithelial phenotype) and to neoangiogenesis (in the case of cells with endothelial/mesenchymal phenotype) and whether this has any prognostic or predictive value.

Embryological studies consider the mammary gland to be derived from skin adnexa related to sweat glands. In this light, we compared nestin expression in mammary and sweat glands. Interestingly, we found nestin positivity in sweat glands, not in myoepithelium but in luminal cells (Fig. 2a,b). We observed no nestin expression in the epidermis or squamous epithelial mucosa. This result confirms the complexity and tissue-specific uniqueness of the differentiation and developmental pathways.

In summary, we have described the potential utility of nestin immunostaining in breast pathology for the detection of myoepithelial/progenitor cells and suggest its potential involvement in the processes of tumour development and neoangiogenesis.

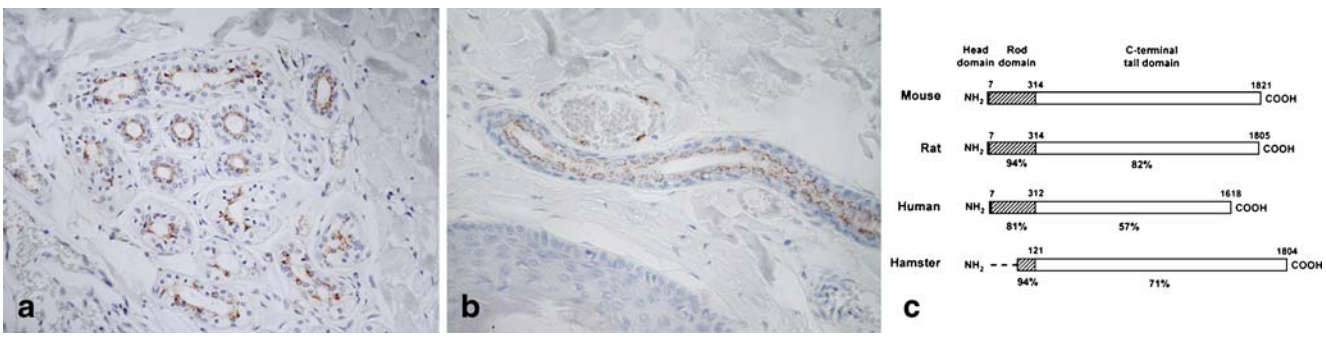

Fig. 2 **a** Nestin expression in luminal cells of sweat gland. **b** Nestin expression in luminal cells of sweat gland ductus. **c** Homology of nestin protein sequences in different animal species (adapted according to [5])

Acknowledgement This work was supported in part by grants MSM 6198959216, MSM 0021620820 and IGA MH NR 7844.

References

1. Barbareschi M, Pecciarini L, Cangi MG, Macri E, Riyyo A, Viale G, Doglioni C (2001) p63, a p53 homologue, is a selective nuclear marker of myoepithelial cells of the human breast. Am J Surg Pathol 25:1054–1060
2. Batistatou A, Stefanou D, Arkoumani E, Agnantis NJ (2003) The usefulness of p63 as a marker of breast myoepithelial cells. Invivo 17:573–576
3. Cattaneo E, McKay R (1990) Proliferation and differentiation of neuronal stem cells regulated by nerve growth factor. Nature 347:762–765
4. Clarke C, Sandle J, Lakhani SR (2005) Myoepithelial cells: pathology, cell separation and markers of myoepithelial differentiation. J Mammary Gland Biol Neoplasia 10:273–280
5. Dahlstrand J, Zimmerman LB, McKay RDG, Lendahl U (1992) Characterization of the human nestin gene reveals a close evolutionary relationship to neurofilaments. J Cell Sci 103:589–597
6. Gudjonsson T, Adriance MC, Sternlicht MD, Petersen OW, Bissell MJ (2005) Myoepithelial cells: their origin and function in breast morphogenesis and neoplasia. J Mammary Gland Biol Neoplasia 10:261–272
7. Mokry J, Cizkova D, Filip S, Ehrmann J, Osterreicher J, Kolar Z, English D (2004) Nestin expression by newly formed human blood vessels. Stem Cells Dev 13:658–664
8. Moriya T, Kasajima A, Ishida K, Kariya Y, Akahira J, Endoh M, Watanabe M, Sasano H (2006) New trends of immunohistochemistry for making differential diagnosis of breast lesions. Med Mol Morphol 39:8–13
9. Reis-Filho JS, Milanezi F, Paredes J, Silva P, Pereira EM, Maeda SA, de Carvalho LV, Schmitt FC (2003) Novel and classic myoepithelial/stem cell markers in metaplastic carcinomas of the breast. Appl Immunohistochem Mol Morphol 11:1–8
10. Sjöberg G, Jiang W-Q, Ringertz NR, Lendahl U, Sejersen T (1994) Colocalization of nestin and vimentin/desmin in skeletal muscle cells demonstrated by three-dimensional fluorescence digital imaging microscopy. Exp Cell Res 214:447–458
11. Sugawara K, Kurihara H, Negishi M, Saito N, Nakazato Y, Sasaki T, Takeuchi T (2002) Nestin as a marker for proliferative endothelium in gliomas. Lab Invest 82:345–351
12. Tohyama T, Lee VMY, Rorke LB, Marvin M, McKay RDG, Trojanowski JQ (1992) Nestin expression in embryonic human neuroepithelium and in human neuroepithelial tumor cells. Lab Invest 66:303–313
13. Westfall MD, Pietenpol JA (2004) p63: molecular complexity in development and cancer. Carcinogenesis 25:857–864

Virchows Arch (2007) 450:611–612
DOI 10.1007/s00428-007-0419-2

ANNOUNCEMENTS

Announcements

© Springer-Verlag 2007

7–8 June 2007
Thyroid Pathology for the Practising Pathologist
15 rue de l'Ecole de Médecine
Paris, France

A 2-day course will take place in Paris under the auspices of the French Division of the I.A.P. This course will be given in English by Prof. J. Rosai (Milano), Prof. M. Sobrinho-Simoes (Porto) and Prof. R. Heimann (Brussels). It will consist of lectures alternating with slide reviews and a slide seminar over a multiheaded microscope. The cases of the seminar will be sent on CD before the meeting. The audience will be limited to 30 participants.

Course fees: 410 euros (340 euros for members of any I.A.P. division). The fees include registration, hand-out, CD of the slide seminar and coffee breaks.

For further information, please contact:
Mrs M. Fontanière, Administrative Secretary,
French Division of the I.A.P.
32 Cours Albert Thomas,
69008, Lyon, France
Fax: 33 4 78754311
E-mail: academie.pathologie@wanadoo.fr

24–27 July, 2007
Practical Pulmonary Pathology
London, UK

This course is designed to provide histopathology and cytopathology trainees and consultants with an opportunity to study diagnostic lung pathology in a comprehensive manner. It comprises lectures and practical microscopy sessions, the latter making up roughly half the time and consisting of individual study of a unique collection of cases.

For further information and application forms please contact:
Professor B Corrin,
Brompton Hospital,
London SW3 6NP, UK
Fax +44 20 7351 8293
E-mail: b.corrin@ic.ac.uk

27–31 August 2007 (Part I+II), 29–31 October 2007 (Part III)
Postgraduate Course Lung, Pleural & Mediastinal Diseases,
Department of Pathology,
Medical University, Graz, Austria

Course Director: Helmut Popper, MD (Graz)

Course Objectives:
This three-part course (common and rare lung and pleural, and mediastinal diseases) is designed for trainees as well as for experienced colleagues. Lectures as well as microscopy sessions alternate for each part. Clinical lectures and case studies are also included in selected lung diseases. Each part can be booked separately.

Course fee:
Part I (Common diseases) Aug 27–29, 2007€ 240,00
Part II (Mediastinal diseases) Aug 30–31, 2007€ 240,00
Part III (Rare diseases) Oct 29–31, 2007€ 240,00
Whole 8-day course (Part I + II + III) € 600,00
Two parts (Part I + II or Part I + III or Part II + III) € 450,00

For more information and registration please contact:
Edith Kleinferchner
Department of Pathology, Medical University Graz
Auenbruggerplatz 25
8036 Graz, Austria
Fax: 0043 (0)316 385-3432
e-mail:edith.kleinferchner@meduni-graz.at
http://pathologie.meduni-graz.at/Pathologie/veranstaltungen.htm

September 28th – October 1st, 2007
10th International Pituitary Pathology Meeting
Stresa, Italy

A four day long meeting designed for pathologists, endocrinologists, neurosurgeons interested in pituitary pathology. The course will provide comprehensive coverage of pathogenic and hispathologocal features of pituitary adenomas and an overview on lesions of the parasellar region.

Meeting Organizers: Carlo Capella, Luigi Bartalena, Giustino Tomei.

For further information please contact:
Prof. Carlo Capella
Dept. of Pathology
Ospedale di Circolo
Viale Borri, 57
1-21100 Varese, Italy
Tel: +39 0332 270601
Fax: +39 0332 270600
e-mail: carlo.capella@ospedale.varese.it

8 December 2007
International Board Certification in Dermatopathology
Frankfurt/Main, Germany

The European Union of Medical Specialists (Union Européenne des Médecins Spécialistes=UEMS)/Section of Dermato-Venereology and Section of Pathology will organize under the auspices of the International Committee for Dermatopathology the **5th International Board Certifying Examination in Dermatopathology (Diploma in Dermatopathology).**

For further information and application forms, please contact:
Lorenzo Cerroni, M.D.
Department of Dermatology
Medical University of Graz
Auenbruggerplatz 8
A-8036 Graz/Austria
Ph.: +43-316-3852423
Fax: +43-316-3852466
e-mail:lorenzo.cerroni@meduni-graz.at
http://www.icdermpath.org

Virchows Arch (2007) 450:613–618
DOI 10.1007/s00428-007-0413-8

ORIGINAL ARTICLE

Serrated polyps of the colorectum: is sessile serrated adenoma distinguishable from hyperplastic polyp in a daily practice?

Dominique Sandmeier · Walter Seelentag · Hanifa Bouzourene

Received: 26 January 2007 / Revised: 26 March 2007 / Accepted: 28 March 2007 / Published online: 21 April 2007
© Springer-Verlag 2007

Abstract The distinction between serrated polyps of the colon is complex, particularly between hyperplastic polyps (HP) and sessile serrated adenomas (SSA). Recent data show that SSA might be the precursors of serrated colonic cancers, underlining the necessity of identifying them. We characterized the demographic and pathologic characteristics of 102 serrated lesions among 321 polyps of the colorectum and determined if SSA can be microscopically distinguished from HP in biopsy material of a daily practice. There were 81 HP (79%) and 7 SSA (7%) of which one displayed low-grade dysplasia. Only six serrated polyps (6%) could not be correctly classified. The main architectural criteria for distinguishing SSA from HP is the serrated feature along the crypt axis and the rarity of undifferentiated cells in the lower third of the crypts. SSA was significantly more often located in the right colon and larger (median, 11 vs 4 mm) than HP. SSA are rare serrated polyps that can be distinguished from HP based on their morphology, location in the right colon, and larger size. One SSA of our series showed low-grade dysplasia supporting the concept that this lesion might be a precursor of serrated adenocarcinoma.

Keywords Serrated polyp · Hyperplastic polyp · Sessile serrated adenoma

Introduction

Until recently, serrated non-adenomatous polyps of the colon were diagnosed as hyperplastic polyps (HP) and considered as innocuous and benign lesions without playing a significant role in carcinogenesis [12, 13, 27]. However, over the past several years, serrated polyps have been the focus of morphologic and critical reappraisal.

In 1996, Torlakovic and Snover [25] published a reappraisal of HP occurring in the context of hyperplastic polyposis and proposed that these polyps should be classified as sessile serrated adenomas (SSA). Some authors considered SSA as "aggressive" HP and precursors of serrated colonic cancer [5, 8, 14]. Recently, Snover et al. [23] reported a detailed morphologic and molecular review about serrated polyps of the large intestine and defined morphologic criteria to distinguish HP from SSA. A nomenclature has been proposed by this group but to date there is no consensus for the adoption of an unanimous terminology and classification of SP.

The aim of the current study was to characterize morphologically and demographically a series of serrated polyps focusing particularly on the distinction between SSA and HP. We tested the reproducibility of Snover's histological criteria of serrated polyps and their applicability in a daily practice, particularly when dealing with SSA, a serrated lesion that should be recognized because of its potential implication in the "serrated neoplasia pathway" [1, 9, 11].

Material and methods

Samples

The biopsy specimens of polyps collected consecutively from November 2005 to January 2006 were provided from the Department of Pathology archives in Lausanne, Switzerland. All the polyps obtained by colonoscopic polypectomy were included in the initial assessment. We retrospectively

D. Sandmeier · W. Seelentag · H. Bouzourene (✉)
Institute of Pathology, Centre Hospitalier Universitaire Vaudois,
Bugnon 25,
CH 1011 Lausanne, Switzerland
e-mail: Hanifa.Bouzourene@chuv.ch

examined 321 polyps of the large intestine from 200 patients, and 102 serrated polyps were selected from this series. For morphological analysis, all the polyps were sectioned in an identical way, and three levels were routinely examined. All the polyps were examined, including the superficially and tangentially oriented specimen, to have an overview about the reality of a routine and daily practice. The resection of the polyp in one-piece (polypectomy) vs in multiple biopsies was recorded. Microscopic characteristics of the polyps were assessed in a double-headed microscope by two observers involved in the gastrointestinal (GI) tract (D.S. and H.B.). The observers were blinded as to the location of the biopsies because knowledge of the site of the polyp might lead to a bias in the interpretation of the histopathologic findings. When there were disagreements between the two observers as to the interpretation of some histologic characteristics and/or classification of a polyp, the case was re-examined and a consensus was obtained. The location, number, and size of the serrated polyps, and the number of samples for each serrated polyp were recorded. The location of colorectal serrated polyps was divided into two groups: right colon (including the splenic flexure) and left colon (descending colon, sigmoid and rectum). The size of the polyps was obtained either from the endoscopist's measurements or from the macroscopic size of the specimen when the clinician did not mention the measure.

Morphologic classification of polyps

The diagnosis of traditional serrated adenoma (TSA) was based on the criteria established by Longagre and Fenoglio-Preiser [5], combining the serrated glandular pattern of an HP and dysplasia. The Snover's criteria were used to separate HP from SSA and to subdivide HP into three types according to their amount of mucin (i.e., microvesicular, goblet-cell-rich, and mucin-poor). The diagnosis of mixed serrated polyp was considered if there was an admixture of an adenoma and a serrated polyp. For all serrated polyps, the following histological features were evaluated: location of the serrated appearance (limited to the superficial half of the crypts vs the complete length of the crypts), branching, horizontalization of the crypts (L shaped), dilatation or narrowing of the base of the crypts, and crypt herniation through the muscularis mucosae. Presence of epithelial tufts, foci of pseudostratification of the surface epithelium, cytoplasmic eosinophilia, and dysplasia were also recorded. The different types of crypt cells were assessed (i.e., goblet cells, gastric foveolar, and undifferentiated cells) and scored semi-quantitatively as follows: + if the number was ≤30%, ++ if the number was >30 and ≤60%, and +++ if the number was >60%.

For the second assessment of the serrated polyps, we required, as minimal criteria for the diagnosis of SSA, a serrated pattern throughout the entire length of the crypts and the absence or rarity of undifferentiated cells in the lower third of the crypts. Dilatation of crypts was considered as a minor criterion for the diagnosis of SSA, particularly in tangential or superficial samples, because it was often found in the upper part of the crypts in HP. In poorly orientated or superficial samples, criteria such as branching, herniation, or horizontalization of the crypts could frequently not be assessed. Therefore, we decided to classify a serrated polyp containing more than 30% of undifferentiated cells as HP. If the above-described minimal criteria for diagnosis of SSA could not be assessed in a serrated polyp and if it contained less than 30% undifferentiated cells, then it remained classified as HP vs SSA.

Statistical analysis

Correlations between HP and SSA were assessed using the Fisher's exact test for categorical variables (sex, site, pseudostratification) and the Mann–Whitney test for continuous variables (age and size). All statistical significance tests were two-tailed, and significance was set at $p<0.05$.

Statistical analyses were carried out by means of the software Statistical Package for the Social Sciences (SPSS) version 14 for PC (SPSS, Chicago, IL, USA).

Results

One hundred two (32%) serrated polyps were selected from a series of 321 polyps obtained from 200 patients. Thirty-six biopsies (35%) were superficial (i.e., above the muscularis mucosae) or tangentially oriented, whereas 66 (65%) biopsies were well oriented. Nine polyps were resected in one piece (polypectomy) and 93 polyps in multiple fragments. During the first histologic assessment, the 102 serrated polyps were classified as follows: 58 HP (Fig. 1a,b); 7 SSA (Fig. 2a–d), of which one presented small foci of low-grade dysplasia (Fig. 3); 5 TSA, and 3 mixed polyps (i.e., HP and tubular adenoma). Twenty-nine remaining polyps (28%) were serrated lesions but a more precise diagnosis could not be made on the first histologic review because the biopsy specimens were either small (all measured less than 5 mm) or superficial or tangentially oriented. Moreover, all of them were resected in multiple fragments (between 3–5), rendering the morphologic analysis more difficult. In these cases, the architectural features of either HP or SSA were difficult to be assessed.

After a second review of the 29 not-otherwise-specified serrated lesions (HP vs SSA), 23 serrated polyps were reclassified as HP because the proliferative zone lined by more than 30% of undifferentiated cells was recognizable, even on poorly oriented biopsies. The differential diagnosis between HP and SSA remained unsolved in six cases (6%).

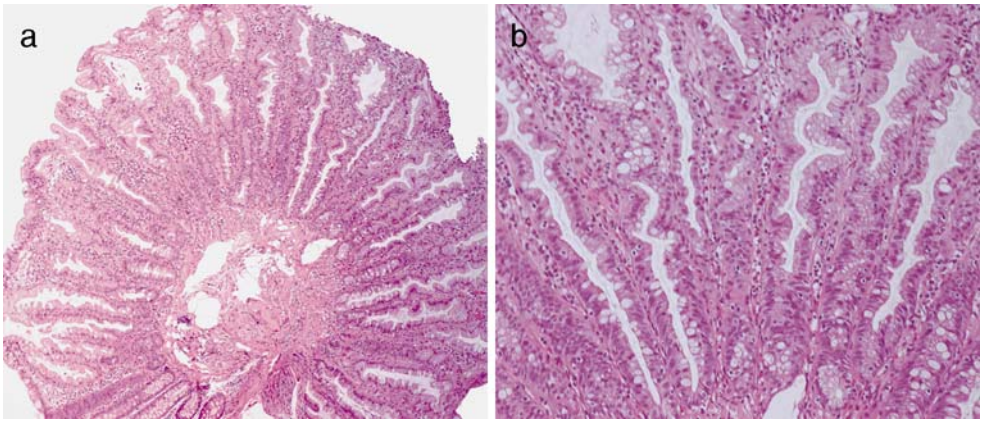

Fig. 1 **a**, **b** Low and high power view of a hyperplastic polyp. The crypts are serrated only at the surface (**a**), and the base of the crypts is narrow, lined predominantly with undifferentiated cells (**b**)

The seven SSA were all resected in one piece, which facilitated the diagnosis, and their morphologic characteristics are detailed in Table 1. In all of them, the crypts were mainly composed of goblet-cell-rich cells with rare or absence of undifferentiated cells. Dilatation, horizontalization, branchment of the crypts, and herniation of the crypts through the muscularis mucosae were often combined in the same lesion in the majority of SSA. Crypt herniation was less frequently seen than branchment or horizontalization. In three SSA, we found that some areas of the polyps were reminiscent of HP, but we did not consider these polyps as mixed serrated polyps because the foci of HP were too small.

Morphological differences between HP and SSA are summarized in Table 2. Branching, L-shaped, and herniation of the crypts are the most useful criteria to distinguish HP from SSA.

There was a statistically significant difference in site and size between HP and SSA (Table 3). HP were preferentially located in the left colon and rectum (n=60, 74%), whereas most SSA (n=5, 71%) were located in the right colon (p=

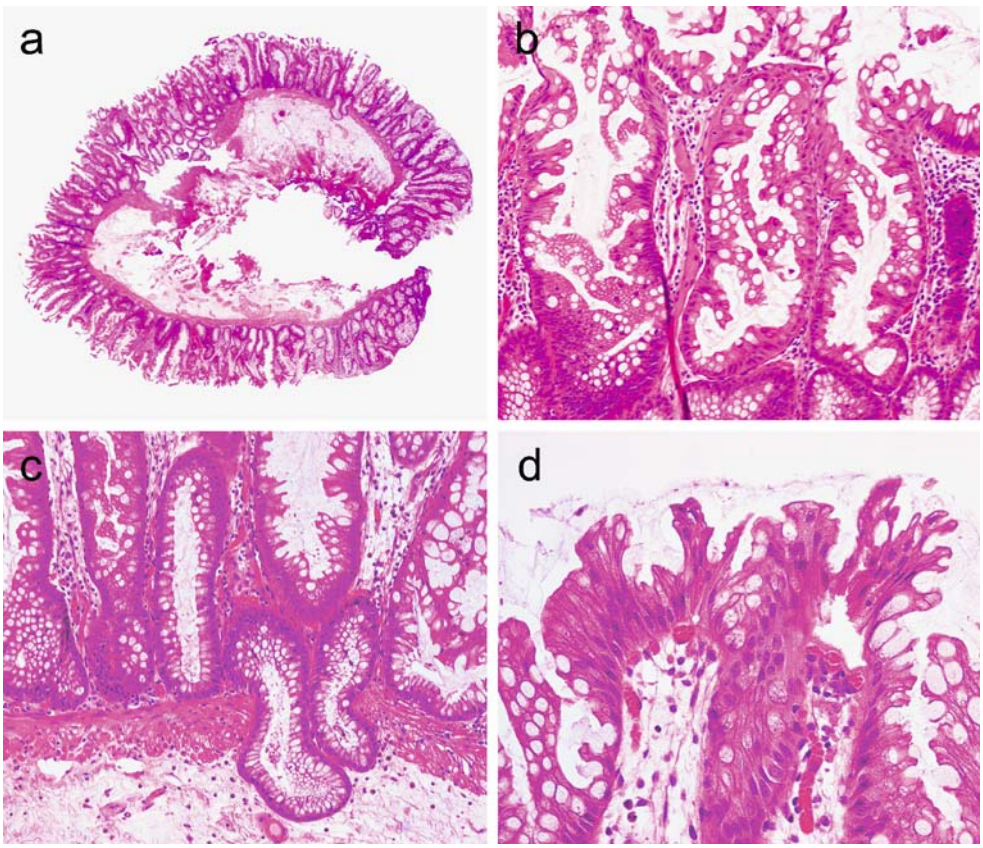

Fig. 2 **a**–**d** Low and high power view of a SSA. Crypts are serrated from their base to the surface (**a**), are branched (**b**), and present herniation through the muscularis mucosae (**c**). Some of the surface of SSA is lined with tufted surface, and cells might be eosinophilic with pseudostratified nuclei (**d**)

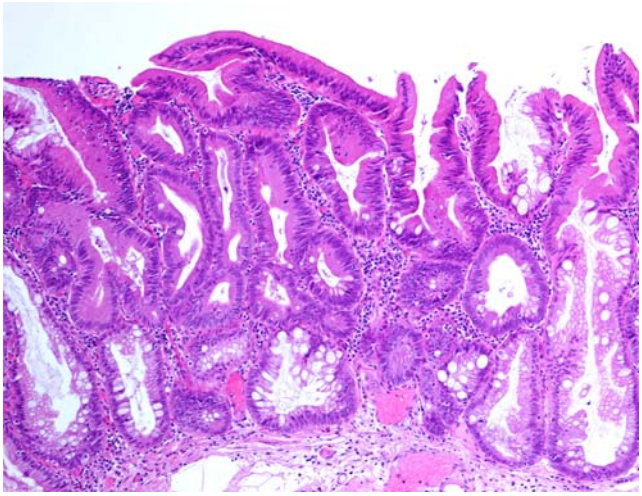

Fig. 3 SSA with dysplastic foci

0.002, Fisher exact test). HP were smaller (median, 4 mm) than SSA (median, 11 mm) in a highly significant manner ($p<0.001$, Mann–Whitney test). Interestingly, the polyps in the category of indefinite diagnosis (HP/SSA) had the smallest median size (−2.5 mm). There was no significant difference between HP and SSA with regard to age (median, 61 vs 57 years, $p=0.2$). The sex ratio was also not statistically different between HP and SSA (p=0.4).

Discussion

Traditionally, the two principal categories of colorectal polyps have been adenomas and HP. Conventional adenomas are well-identified precursor lesions of the tumor suppressor pathway first proposed by Vogelstein et al. [26]. In contrast, HP have been considered as benign and innocent mucosal lesions for many years, with no involvement in colonic carcinogenesis [12, 13, 27]. However, reassessment of the HP through clinical and epidemiological reports combined with the genetic alterations has led to a reinterpretation of its significance in colorectal carcinogenesis [13, 15]. The serrated polyps demonstrate a "saw-toothed" infolding of the crypt epithelium, probably as a consequence of inhibition of programmed cellular apoptosis of the surface mucosa or more precisely of anoïkis, which is the inhibition of programmed cell exfoliation, leading to prolonged cell life [15]. But to date, no consensus has been established about what classification or nomenclature to use when dealing with serrated polyps. SSA has been described by Torlakovic and Snover in 1996 [25] but has been ignored for several years and designated with different names, rendering this entity quite confusing. Recently, Snover et al. [23] reported an excellent morphologic and molecular review about serrated polyps of the large intestine.

In the present study, we tested the ease of use of this classification on the basis of the described morphological aspects and tried to apply them to the daily practice. We found that the incidence of SSA is very low, as they represent 7% of the serrated polyps and only 2% of all colonic polyps of our series, which is in the range of previously published data [10]. The distinction between HP and SSA was based mainly on architectural features, which seem to be due to abnormal proliferation and probably also decreased apoptosis [24]. These architectural features can be better recognized when a well-oriented polypectomy has been performed. We found that the diagnostic was more difficult when the biopsy specimens were superficial and tangentially cut, when the polyp was addressed fragmented, and when the polyp was small. However, even if the orientation of the biopsy was not optimal, we could distinguish between HP and SSA in the majority of the cases (94%) mainly due to the presence of a great number of undifferentiated cells in the lower third of HP crypts, contrasting with the predominance of goblet or gastric foveolar cells in SSA. Only in six polyps, the differential diagnosis between HP and SSA could not be resolved due

Table 1 Morphologic characteristics of SSA of the colon

SSA cases	Crypt serration	Crypt branching	L-shaped crypt	Crypt dilatation	Crypt herniation	Nuclear pseudo-stratification	Cell eosinphilia	Dysplasia	Goblet cells	Gastrin cells	Undifferentiated cells
1	1	1	1	1	1	1	0	0	+++	+	0
2	1	1	1	1	1	1	1	0	+++	++	+
3	1	0	1	1	0	0	0	0	+++	+	0
4	1	1	1	1	0	0	0	1	+++	++	+
5	1	1	1	1	1	1	0	0	+++	++	+
6	1	0	0	1	0	0	0	0	+++	++	0
7	1	1	0	1	0	0	0	0	+++	++	+

SSA Sessile serrated adenoma, *0* absent, *1* present, + < than 30% of the cells, ++ < than 60% of the cells, +++ > than 60% of the cells

Table 2 Morphologic differences between 81 hyperplastic polyps and 7 SSA

	Crypt branching (%)	L-shaped crypt (%)	Crypt dilatation (%)	Crypt herniation (%)	Epithelial tufts (%)	Nuclear pseudo-stratification (%)	Cytoplasmic eosinophilia (%)
SSA	71	71	100	43	43	43	14
HP	5	0	27	0	17	14	4

SSA Sessile serrated adenoma, *HP* hyperplastic polyps

to the above-mentioned reasons. The fact that the polyps in the category of indefinite diagnosis (HP/SSA) had the smallest median size (−2.5 vs 4 and 11 mm for the HP and SSA, respectively) appears to indicate that the size of the polyp is an important factor in the distinction of SSA from HP. The smaller the lesion, the more SSA and HP histologically overlap. Intermingling features of HP and SSA in a same serrated polyp, which was observed in three out of seven SSA, might add more difficulty to the distinction between both types of lesions. These findings support the idea that serrated polyps might constitute a continuous spectrum of lesions.

We found that the absence or presence of undifferentiated cells, location of the serration, branchment, horizontalization, and herniation of the crypts appeared to be good discriminators between HP and SSA.

Beside size and morphological features, other parameters seem to be discriminators between HP and SSA. HP are reported to be more frequently located in the distal colon and rectum [3, 6, 10]. Our results are in agreement with these data because we found that the majority of HP were left sided, whereas most SSA were right sided.

For Snover et al. [23], cytological dysplasia is not needed for the diagnosis of SSA, which is in contradiction with the generally accepted consensus about diagnostic criteria in gastrointestinal adenomas. Therefore, some authors do not fully agree with this concept and prefer to label SSA as "atypical HP" or "sessile serrated polyp" [2]. However, in our series, we found one case of SSA showing a low-grade dysplasia, and recently, Goldstein [5] reported eight cases of SSA with incidental high-grade dysplasia or invasive adenocarcinoma. This supports that dysplasia may emerge in SSA and that they are probably precursors of the serrated adenocarcinoma [21]. Molecular studies will probably be able to elucidate the link between morphologic features and molecular changes. Serrated mucosal lesions of the colorectum have emerged as an important concept supporting the existence of an alternate polyp–neoplasia pathway in addition to the classical adenoma–carcinoma sequence [1, 7, 9, 11, 26]. The most common genetic changes seem to be BRAF-activating mutation and CpG island mutation [1, 4, 10, 17, 18, 20, 22]. However, most of the molecular results already published have to be interpreted with caution because the serrated polyps studied were heterogeneous and the diagnostic criteria were poorly defined [4, 6, 17, 19]. To our knowledge, only one recent study analyzed the molecular features of morphologically well-defined serrated polyps of the colorectum [16]. However, molecular studies will be helpful only when a consensual classification will be established to be sure to study specific morphologic subtypes of SP and not a broad range of lesions.

In summary, SSA has clinic and morphologic features distinctive from that of HP. In our view, correct morphologic identification of SSA is essential to enable further studies that are required to assess molecular basis and clinical impact of these lesions.

Table 3 Clinical characteristics of hyperplastic polyps and SSA out of 102 serrated polyps of the colon

		HP	SSA	*p* value
Total number of polyps		81	7	
Percent of all polyps		79	7	
Age (years)	Median	61	57	0.2
	25th percentile	56	46	
	75th percentile	65	62	
Sex (*n*, %)	Male	41 (51%)	2 (29%)	0.4
	Female	40 (49%)	5 (71%)	
Site (*n*, %)	Right colon	19 (24%)	5 (71%)	0.002
	Left colon	27 (33%)	2 (29%)	
	Rectum	33 (41%)	0	
	Unknown	2 (2%)	0	
Size (mm)	Median	4	11	<0.001
	25th percentile	2	8	
	75th percentile	5.2	12	

Numbers in parentheses are percentages within the same diagnostic category.
HP Hyperplastic polyp, *SSA* sessile serrated adenoma, *n* number of polyps

References

1. Chan TL, Zhao W, Leung SY, Yuen ST (2003) BRAF and KRAS mutations in colorectal hyperplastic polyps and serrated adenomas. Cancer Res 63:4878–4881
2. Cunningham KS, Riddell RH (2006) Serrated mucosal lesions of the colorectum. Curr Opin Gastroenterol 22:48–53
3. Di Sario JA, Foutch PG, Mai HD (1991) Prevalence and malignant potential of colorectal polyps in asymptomatic, average-risk men. A. J Gastroenterol 86:941–945
4. Dong SM, Lee EJ, Jeon ES, Park CK, Kim KM (2005) Progressive methylation during the serrated neoplasia pathway of the colorectum. Mod Pathol 18:170–178
5. Goldstein NS (2006) Small colonic microsatellite unstable adenocarcinomas and high grade epithelial dysplasias in sessile serrated adenoma polypectomy specimen. A study of eight cases. Am J Clin Pathol 1:132–145
6. Goldstein NS, Bhanot P, Odish E, Hunter S (2003) Hyperplastic-like colon polyps that preceded microsatellite unstable adenocarcinomas. Am J Clin Pathol 119:778–796
7. Golstein NS (2006) Serrated pathway and APC (conventional)-type colorectal polyps: molecular-morphologic correlations, genetic pathways, and implications for classification. Am J Clin Pathol 1:146–153
8. Hamilton SR (2001) Origin of colorectal cancers in hyperplastic polyps and serrated adenomas: another truism bites the dust. J Natl Cancer Inst 5:93.1282–93.1283
9. Hawkins NJ, Bariol C, Ward RL (2002) The serrated neoplasia pathway. Pathology 34:548–555
10. Higuchi T, Sugihara K, Jass JR (2005) Demographic and pathological characteristics of serrated polyps of colorectum. Histopathology 47:32–40
11. Huang CS, O'Brien MJ, Yang S, Farraye FA (2004) Hyperplastic polyps, serrated adenomas and the serrated polyp neoplasia pathway. Am J Gastroenterol 99:2242–2255
12. Jass JR (2001) Hyperplastic polyps of the colorectum—innocent or guilty? Dis Colon Rectum 44:163–166
13. Jass JR, Whitehall VL, Young J, Leggett BA (2002) Emerging concepts in colorectal neoplasia. Gastroenterology 123:862–876
14. Jass JR (2003) Serrated adenoma of the colorectum. A lesion with teeth. Am J Pathol 162:705–708
15. Jass JR (2002) Pathogenesis of colorectal cancer. Surg Clin North Am 82:891–904
16. Jass JR, Baker K, Zlobec I, Higuchi T, Barker M, Buchanan D, Young J (2006) Advanced colorectal polyps with the molecular and morphological features of serrated polyps and adenomas: concept of a "fusion" pathway to colorectal cancer. Histopathology 49:121–131
17. Kambara T, Simms LA, Whitehall VLJ, Spring KJ, Wynter CVA, Walsh MD, Barker MA, Arnold S, McGivern A, Matsubara N, Tanaka N, Higuchi T, Young, Jass JR, Leggett BA (2004) BRAF mutation is associated with DNA methylation in serrated polyps and cancers of the colorectum. Gut 53:1137–1144
18. Konishi K, Yamochi T, Makino R, Kaneko K, Yamamoto T, Nozawa H, Katagiri A, Ito H, Nakayama K, Ota H, Mitamura K, Imawari M (2004) Molecular differences between sporadic serrated and conventional colorectal adenomas. Clin Cancer Res 10:3082–3090
19. Lazarus R, Junttila OE, Karttunen TJ, Mäkinen MJ (2005) The risk of metachronous neoplasia in patients with serrated adenoma. Am J Clin Pathol 123:349–359
20. Lee EJ, Choi C, Park CK, Maeng L, Lee J, Lee A, Kim KM (2005) Tracing origin of serrated adenomas with BRAF and KRAS mutations. Virchows Arch 3:597–602
21. O'Brien MJ, Yang S, Clebanoff JL, Mulcahy E, Farraye FA, Amorosino M, Swan N (2004) Hyperplastic (serrated) polyps of the colorectum: relationship of CpG island methylator phenotype and K-ras mutation to location and histologic subtype. Am J Surg Pathol 28:423–434
22. Park SJ, Rashid A, Lee JH, Kim SG, Hamilton SR, Wu TT (2003) Frequent CpG island methylation in serrated adenomas of the colorectum. Am J Pathol 162:815–822
23. Snover DC, Jass JR, Fenoglio-Preiser C, Batts KP (2005) Serrated polyps of the large intestine. A morphologic and molecular review of an evolving concept. Am J Clin Pathol 124:380–391
24. Tateyama H, Li W, Takahashi E, Miura Y, Sugiura H, Eimoto T (2002) Apoptosis index and apoptosis—related antigen expression in serrated adenoma of the colorectum0: the saw-toothed structure may be related to inhibition of apoptosis. Am J Surg Pathol 26:249–256
25. Torlakovic E, Snover DC (1996) Serrated adenomatous polyposis in humans. Gastroenterology 110:748–755
26. Vogelstein B, Fearon ER, Hamilton SR, Kern SE, Preisinger AC, Leppert M, Nakamura Y, White R, Smits AM, Bos JL (1988) Genetic alterations during colorectal tumor development. N Engl J Med 319:525–532
27. Wynter CVA, Walsh MD, Higuchi T, Leggett BA, Young J, Jass JR (2004) Methylation patterns define two types of hyperplastic polyp associated with colorectal cancer. Gut 3:573–580

Virchows Arch (2007) 450:619–626
DOI 10.1007/s00428-007-0420-9

ORIGINAL ARTICLE

A subset of colorectal carcinomas express c-KIT protein independently of *BRAF* and/or *KRAS* activation

Ana Preto · Cátia Moutinho · Sérgia Velho · Carla Oliveira · Ana Paula Rebocho · Joana Figueiredo · Paula Soares · José Manuel Lopes · Raquel Seruca

Received: 22 February 2007 / Revised: 28 March 2007 / Accepted: 5 April 2007 / Published online: 9 May 2007
© Springer-Verlag 2007

Abstract c-KIT is a tyrosine kinase receptor found to be overexpressed in several tumours, namely, GISTs, breast, lung, prostate, ovarian and colorectal carcinomas (CRC). We aimed at determining the frequency of c-KIT expression and mutations in a series of 109 CRC cases (73 primary tumours and 36 lymph node metastases) characterised for *KRAS* and *BRAF* mutations. We also aimed at analysing the cellular effects of STI571/Gleevec in CRC-derived cell lines displaying c-KIT expression and *KRAS* or *BRAF* mutations. By immunohistochemistry, we found c-KIT overexpression in 15% (11/73) of primary tumours and in 14% (5/36) of metastasis; however, cases showing overexpression did not show *c-kit* mutations in *hotspot* regions. The majority (64%) of primary tumours with c-KIT overexpression had mutations at *KRAS–BRAF* genes. The same was true for 60% of the metastases. We treated CRC cell lines with STI571/Gleevec and verified that it inhibits proliferation and induces apoptosis in all cell lines. In conclusion, overexpression of c-KIT is observed in a subset of primary and CRC metastases in the absence of *c-kit* mutations. STI571/Gleevec increases apoptosis in CRC cell lines independently of its genetic profile, suggesting that STI571/Gleevec is likely to be an alternative drug for the clinical trials of CRC.

Keywords Colorectal carcinoma · c-KIT · STI571/Gleevec · *BRAF* · *KRAS*

A. Preto (✉) · C. Moutinho · S. Velho · C. Oliveira · A. P. Rebocho · J. Figueiredo · P. Soares · J. M. Lopes · R. Seruca
Institute of Molecular Pathology and Immunology of the University of Porto (IPATIMUP), Rua Dr Roberto Frias s/n, 4200-465 Porto, Portugal
e-mail: apreto@ipatimup.pt

P. Soares · J. M. Lopes · R. Seruca
Medical Faculty, University of Porto, 4200-465 Porto, Portugal

J. M. Lopes
Department of Pathology, Hospital São João, 4200-465 Porto, Portugal

Introduction

The proto-oncogene *c-kit* encodes a tyrosine kinase receptor normally expressed in a variety of human tissues including hematopoietic stem cells, melanocytes, mast cells, germ cells and the interstitial cells of Cajal [1]. The ligand for c-KIT is the stem cell factor (SCF) that activates c-KIT tyrosine kinase via homodimerisation and autophosphorylation of the receptor at specific tyrosine residues in the intracellular domain of the receptor [28, 40]. c-KIT activates several signal transduction pathways implicated in cell survival, proliferation, differentiation, adhesion and migration [4, 6].

Aberrant expression of c-KIT has been reported in several tumours, namely, gastrointestinal stromal tumours (GISTs), breast, lung, neural, prostate and ovarian tumours [11, 14, 28, 35]. Gain-of-function mutations of the *c-kit* gene and overexpression of c-KIT have been reported in mast cell tumours [12, 19], GISTs [15, 16, 39], germ cell tumours (GCTs) [32, 36] and melanomas [37, 38]. The five mutational hotspots at the *c-kit* gene have been identified in exons 9, 10, 11, 13 and 17 [27, 31].

In colorectal cancer (CRC), data concerning expression of c-KIT is controversial. Some authors have demonstrated

overexpression of both c-KIT transcripts and protein in CRC [6, 28], while others have failed to detect the c-KIT protein in the majority of CRC examined [20, 26]. In CRC, oncogenic mutations in *KRAS* mutations are well known to occur in the first steps of carcinogenesis both in MSI and MSS settings [22, 23, 25]. In sporadic CRC, oncogenic *BRAF* mutations are found in about 12% of the tumours analysed, mainly in MSI cases (31–45%) [9, 10, 22, 25]. *BRAF* mutations are also very frequent in melanomas [9]. Recently, a subset of melanomas was described to harbour *c-kit* activating mutations associated to c-KIT expression. Moreover, *c-kit*-activating mutations were shown to be alternative to *BRAF* mutations [8, 37, 38]. Further, similarly to *KRAS* and *BRAF*, it has been demonstrated that activated c-KIT signals through the MAPK pathway [9, 29, 33]. The lack of such knowledge in CRC leads us to hypothesise that c-KIT expression/mutation may be alternative to *KRAS* and *BRAF*-activating mutations.

Having available CRC-derived cell lines displaying different genetic background: HCT116 expresses c-KIT and harbours a RAS^{G13D} mutation, CO115 harbours a $BRAF^{V600E}$ mutation and HCT15 harbours a RAS^{G13D} mutation, we study the cellular effects of an inhibitor of c-KIT receptor tyrosine kinase (STI571/ Gleevec). Imatinib mesilate (STI571/Gleevec), an inhibitor of Bcr-Abl and c-Abl tyrosine kinase, primarily designed to treat chronic myeloid leukaemia (Philadelphia chromosome-positive), is also an inhibitor of c-KIT receptor tyrosine kinase and platelet-derived growth factor (PDGF) receptor. This drug is currently the therapeutic choice for metastatic GISTs known to express c-KIT and PDGFR [13, 17, 34]. We studied the cellular effects (proliferation and apoptosis) of STI571/Gleevec in CRC cell lines in an attempt to clarify whether STI571/Gleevec may be useful for treating CRC patients harbouring different genetic alterations.

Materials and methods

Tumour specimens

A total of 109 formalin-fixed paraffin-embedded samples (73 primary sporadic colorectal carcinomas, 36 of which with a corresponding lymph node metastasis) were obtained from S. João Hospital, Porto, Portugal. Age of the patients, location of the tumour, histological classification, presence or absence of lymph nodes metastasis, Dukes classification and TNM tumour staging were available from every case.

Immunohistochemical study

Immunohistochemistry was performed using the avidin-biotin-peroxidase method. Briefly, endogenous peroxidase activity and non-specific binding were blocked by hydrogen peroxide and a blocking reagent in the LSAB2 kit (Dako), respectively. The slides were incubated overnight at 4°C using a dilution of 1/500 with the primary antibody and then incubated sequentially at room temperature with a biotinylated secondary antibody for 30 min, streptavidin peroxidase for 15 min and Dako DAB for 10 min. The slides were then counterstained with Mayer's hematoxylin and amoniacal water. We used as primary antibodies rabbit polyclonal antibody raised against human c-KIT (CD117, Dako) and as a negative control, a rabbit polyclonal antibody to single-stranded DNA (ssDNA; Dako, Glostrup, Denmark). We used as a positive control a case of GIST with *c-KIT* expression and as internal positive control, interstitial cells of Cajal [30]. Membrane and/or cytoplasmic immunoreactivity for CD117 was considered positive.

Genomic DNA extraction and mutational analysis of *c-kit*

c-kit mutation screening was restricted to cases displaying c-KIT immunoexpression. Genomic DNA was extracted from dissected paraffin-embedded material using phenol-chloroform according to standard procedures. The fragment encompassing exon 9, 10, 11, 13 and 17 was amplified by polymerase chain reaction (PCR) in all carcinoma samples. Genomic DNA (25–100 ng) was amplified by PCR using the following cycling conditions: 30 s at 94°C, 30 s at 58°C and 45 s at 72°C for 40 cycles. All PCR products were purified and directed sequenced on an ABI Prism 377 Automatic sequencer (Perkin-Elmer, Foster City, CA) using the ABI Prism Dye Terminator Cycle Sequencing Kit (Perkin-Elmer). All sequencing reactions were performed in both forward and reverse directions, and all mutations were confirmed by an independent PCR amplification. For amplification of exon 9, 10, 11, 13 and 17 of *c-kit* gene, the following primers were used: Ex9F: 5′-GAT GCT CTG CTT CTG TAC TG-3′; Ex9R: 5′-AAG GGG ATG TTT AGG CTC TG-3′); Ex10F: 5′-TCC TGC CAA AGT TTG TGA TTC-3′; Ex10R: 5′-CCA GAG TGC TCT AAT GAC TG-3′); Ex11F: 5′-CCA GAG TGC TCT AAT GAC TG-3′; Ex11R: 5′-TGG TCA GTA TGA AAC AGG GG-3′); Ex13F: 5′-CAT CAG TTT GCC AGT TGT GC-3′; Ex13R: 5′-CGT GTC CAA GCT GCC TTT TA-3′); Ex17F: 5′-CTT TTC TCC TCC AAC CTA ATA G-3′; Ex17R: 5′-CCC ATT CTC TGC TTG ACA GT-3′).

KRAS and *BRAF* and mutation screening

KRAS and *BRAF* mutations were screened in all 109 CRC cases (primary tumours and metastases). In all cases, we analysed the mutation status of *KRAS* by direct sequencing. Mutational analysis of *BRAF* was performed by single-

stranded conformation polymorphism and heteroduplex analysis (SSCP/HA) [23].

CRC Cell lines, culture conditions and drug treatment

Three CRC cancer cell lines were analysed (CO115, HCT116 and HCT15). HCT116 express c-kit and harbours a $KRAS^{G13D}$ mutation, CO115 harbours a $BRAF^{V600E}$ mutation and HCT15 harbours a $KRAS^{G13D}$ mutation. The human colon carcinoma-derived cell lines CO115, HCT116 and HCT15 were grown in RPMI 160 medium (with L-glutamine and HEPES—Gibco, Invitrogen) supplemented with 10% fetal bovine serum (FBS; Gibco, Invitrogen) and 100 units/ml penicillin-streptomycin (Gibco, Invitrogen). All cells were grown in a humidified incubator with 5% CO_2 at 37°C. Gleevec was kindly provided by Novartis Pharma AG (Basel, Switzerland). Gleevec stock solution was made at a concentration of 30 mM in DMSO, and aliquots were kept at −20°C. The day after plating, cells were cultured in serum-free medium with 20 and 30 μM of Gleevec or DMSO vehicle, incubated for 48 h and then analysed for TUNEL and bromodeoxyuridine (BrdU).

Assessment of DNA synthesis by BrdU incorporation and apoptosis assay

For the proliferation (BrdU) and apoptosis (TdT mediated dUTP Nick End Labelling, TUNEL) analysis, cells were plated in six well dishes in 10% FBS at a cell density of 2×10^5 (HCT15, HCT116) and $2{,}6\times10^5$ (Co115). For proliferation analyses, cells were labelled by incubation in 10 μM of BrdU for 1 h, fixed with 4% paraformaldehyde, and nuclear incorporation was detected by immunofluoresce assay using an anti-BrdU antibody (Dako®). The proportion of positive nuclei (BrdU index) was determined from a count of >500 cells per datum point. For apoptosis analyses, cytospin preparations of both floating and attached cells were collected from each sample and fixed with 4% paraformaldehyde (15 min) at room temperature. Cells were washed in PBS and permeabilised with 0.1% Triton X-100 in 0.1% sodium citrate (2 min) on ice. TUNEL analysis was performed using the "In situ cell death detection kit, fluorescein" from Roche®, following the manufacturer's instructions.

Results

Immunoexpression and mutational analysis of c-KIT in CRC

We found immunoreactivity in 11 of 73 (15%) primary CRCs. These 11 tumours displayed cytoplasmic and/or membrane c-KIT expression in 5–30% of the neoplastic cells (Fig. 1).

Thirty six lymph node metastases were also analysed for c-KIT expression, and 5 of 36 (14%) were positive (Fig. 2). In one metastasis, c-KIT expression was also found in the primary tumour. In the remaining four positive metastases,

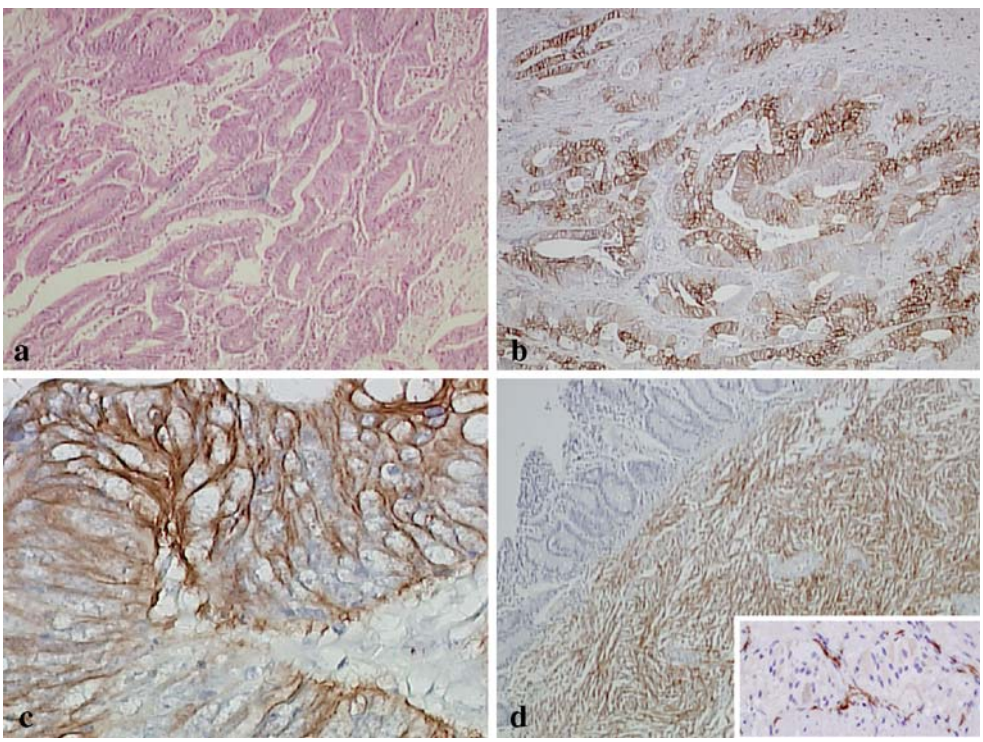

Fig. 1 Expression of c-KIT (CD117) in colorectal carcinomas (**a**, glandular features) showing cytoplasmic/membrane (**b**) and predominantly membrane (**c**) location. Note internal (positive mast cells in the upright stroma of **b**) and external positive controls [enteric GIST (**d**) and interstitial cells of Cajal (**d** inset)]. **a** H&E×5; **b**, **d** ABC×5 and **c** ABC×40

the corresponding primary tumours were negative for c-KIT immunoexpression.

We performed statistical analysis comparing c-KIT positive tumours with age, location, stage and Dukes classification, and no statistical significant correlation was found.

All primary tumours and metastases showing c-KIT immunoreactivity were screened for mutations in the *c-kit* gene. The mutation screening was restricted to the hotspot regions of the gene (exons 9, 10, 11, 13 and 17) by direct sequencing. None of the cases showing immunoreactivity for c-KIT displayed mutations in the hotspot regions of the *c-kit* gene (Fig. 2).

KRAS and *BRAF* mutational analysis, correlation with c-KIT expression

KRAS and *BRAF* genes were screened for mutations in all 73 primary CRCs analysed for c-KIT expression. We found *KRAS* mutations in 41/73 (56%) and *BRAF* mutations in 17/73 (23%) of the cases. Seven of eleven (64%) primary CRC displaying c-KIT expression had mutations at *KRAS* and/or *BRAF*, three CRC had mutations at *KRAS* only and four had mutations both in *KRAS* and *BRAF*. Four of the 11 cases with c-KIT expression did not show *KRAS* or *BRAF* genes.

KRAS and *BRAF* mutations were also screened in 36 lymph node metastases analysed for c-KIT expression, five of which with c-KIT imunoexpression. From these five c-KIT positive metastasis, three (60%) had mutations at *KRAS* and/or *BRAF*—two at *KRAS* only and one both at *KRAS* and *BRAF*.

Cellular effect of STI571/Gleevec in CRC-derived cell lines displaying different genetic profiles

To investigate the cellular effects of STI571/Gleevec in CRC, we selected three CRC-derived cell lines harbouring different genetic alterations: HCT116 harbours a $KRAS^{G13D}$ mutation and expresses c-KIT, CO115 harbours a $BRAF^{V600E}$ mutation and does not express c-KIT and HCT15 harbours a $KRAS^{G13D}$ mutation and does not express c-KIT ([22]; data not shown). We treated the three CRC cell lines with 20 and 30 μM of STI571/Gleevec for 48 h and studied cell proliferation by BrdU incorporation analysis and apoptosis by TUNEL analysis. Our results showed that STI571/Gleevec leads to a significant inhibition of BrdU incorporation in all the cell lines analysed ($p<0.05$). The inhibition was more effective using a dose of 30 μM (Fig. 3). Concerning apoptosis analyses, our results showed that STI571/Gleevec was able to induce apoptosis in all the cell lines, reaching statistical significance at a dose of 30 μM ($p<0.05$; Fig. 4).

Discussion

Several reports described the expression of c-KIT tyrosine kinase receptor in CRCs. While some authors argue that c-KIT expression is a rare event in CRC [26, 40], more recently, several authors detected c-KIT-positive staining in CRC ranging from 10 to 25% [6, 7, 28]. In the present study, we analysed a large series of primary CRC and

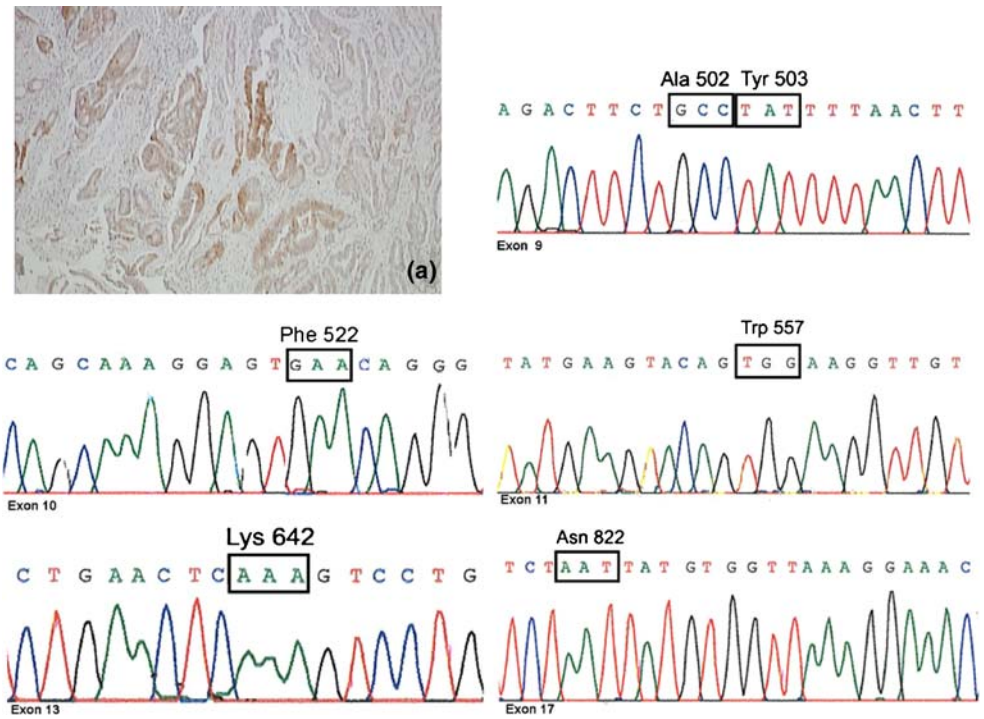

Fig. 2 Expression of c-KIT in a lymph node metastasis (**a**) and corresponding representative fragments of the sequencing analysis of *c-kit* exons 9, 10, 11, 13 and 17. Examples of commonly mutated codons in those exons are *highlighted*.
a ABC×5

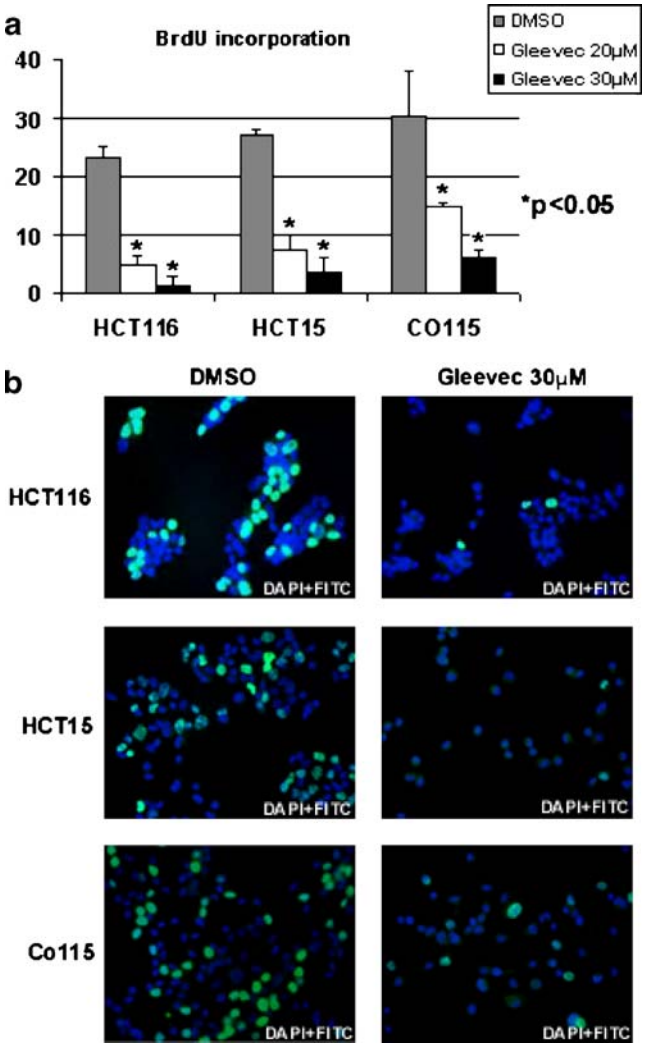

Fig. 3 **a** Representative proliferation graphs of bromodeoxy uridine (BrdU) analysis in HCT116, HCT15 and CO115 colorectal carcinoma-derived cell lines. Cells were treated with the vehicle control (DMSO) and different doses of Gleevec (20 and 30 μM) for 48 h. Significative inhibition of proliferation was observed in all the cell lines analysed with both doses ($p<0.05$, Gleevec 20 μM: $p=0.002$ for HCT116, $p=0.003$ for HCT15 and $p=0.007$ for CO115; Gleevec 30 μM: $p<0.0001$ for HCT116, $p=0.003$ for HCT15 and $p=0.003$ for CO115). **b** Representative photomicrographs of BrdU incorporation (positivity is shown by FITC-stained cells). Nuclei of the cells are counterstained with DAPI (magnification ×40)

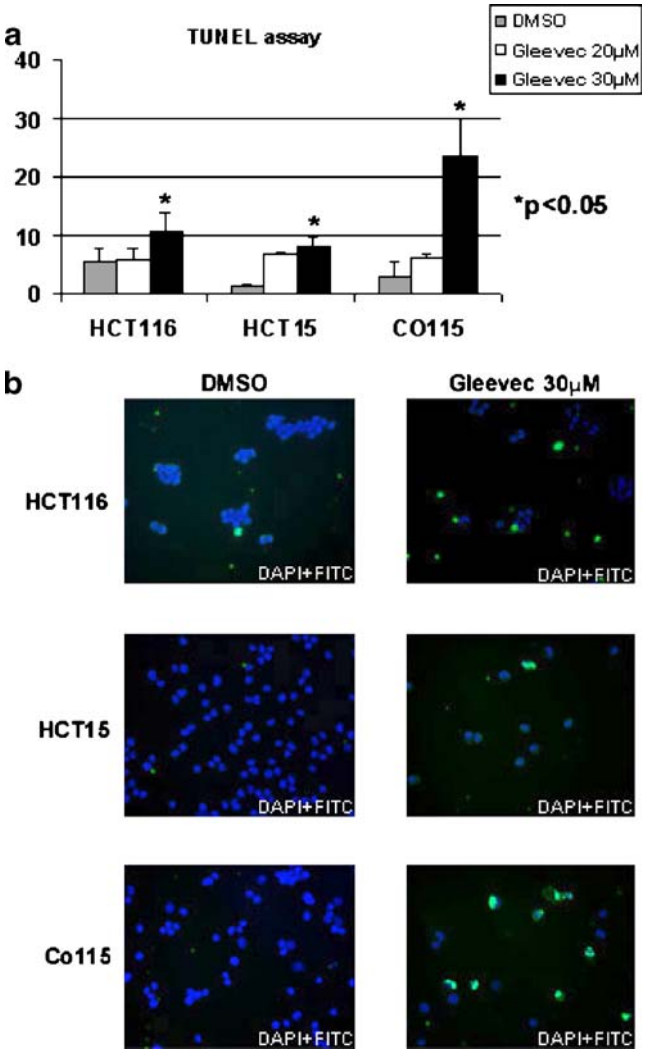

Fig. 4 **a** Apoptosis analysis by TUNEL assay in HCT116, HCT15 and CO115 colorectal carcinoma-derived cell lines representative graphs. Gleevec induced significative apoptosis in all the cell lines analysed at a dose of 30 μM after 48 h of treatment ($p<0.05$, Gleevec 30 μM: $p=0.03$ for HCT116, $p=0.02$ for HCT15 and $p=0.006$ for CO115). **b** Representative photomicrographs of TUNEL analysis in HCT116, HCT15 and CO115 treated with DMSO or Gleevec 30 μM. DAPI: counterstained to detect nuclei in FITC-stained cells in TUNEL assay (magnification ×40)

respective metastases and found c-KIT immunoreactivity in 15% of primary CRC and in 14% of CRC metastases. Our results are similar to the ones published in the latest reports. This similarity is reinforced by the fact that the same antibody, which is recommended for GIST diagnosis, was used [6, 7, 28]. To the best of our knowledge, this is the first report describing c-KIT expression in CRC metastases.

The biological role of c-KIT activation was investigated in CRC cell lines, and it was shown that it stimulates growth [6], protects colon carcinoma cells from apoptosis and enhances their migration and invasive potential [4]. Moreover, it was demonstrated that inhibition of c-KIT by STI571/Gleevec in c-KIT expressing CRC cell lines blocked cellular invasion [2, 5, 41]. Altogether, these results suggest a possible role for c-KIT in the invasive potential of the cells. In the present study, we observed that five metastases displayed c-KIT immunoexpression, four (80%) of which showed “de novo” expression of c-KIT protein that was not observed in the corresponding primary tumours. This observation suggests that c-KIT expression may have been acquired during metastization and is in accordance with its putative role in cell invasion.

Activating mutations in the *c-kit* gene were found associated with overexpression of c-KIT protein, namely, in GISTs [18, 21]. Nevertheless, it was already reported that in ovarian cancers, c-KIT expression by immunohistochemistry is not associated with mutations in the *c-kit* gene [35]. None of the previous reports on c-KIT expression in CRC performed mutation analysis of the *c-kit* proto-oncogene. We screened specifically *c-kit* exons previously appointed to be *hotspots* for mutations in tumour models as melanoma, intracranial germinomas and GISTS [8, 21, 27, 31, 37, 38]. To the best of our knowledge, somatic mutations in *c-kit* were never described outside of these *hotspot* exons in any cancer model, even in studies where all exons were screened.

Herein, we showed that c-KIT immunopositive CRC cases do not harbour mutations in the hotspot regions of *c-kit* gene. The mechanism by which c-KIT is overexpressed in CRCs remains to be clarified. Recently, *c-kit* amplification was described in gliomas as one of the underlying mechanisms leading to c-KIT overexpression [24]. Moreover, Bellone et al. [7] showed that the c-KIT ligand, SCF, was co-expressed in the majority of c-KIT-positive CRC, suggesting the possibility of c-KIT expression by an autocrine stimulation mechanism. In the present study, we did not analyse *c-kit* amplification nor SCF expression; thus, we cannot rule out these mechanisms as promoters of c-KIT overexpression in our CRC cases.

Others and our group described the presence of *KRAS* and *BRAF* mutations in a subset of CRC [9, 10, 22, 23]. Sixty four percent of the cases with c-KIT expression had *KRAS* or *BRAF* mutations. Our results suggest that c-KIT positive expression may co-exist with other oncogenic activation events, namely, *BRAF* and *KRAS*, in contrast to what was described for melanomas in which *BRAF* kinase-activating mutations are alternative to *c-kit* activating mutations [37, 38]. We would expect that in some cases of CRC, *c-kit* gene alterations could play a role in alternative to *BRAF* and *KRAS* as it was described that c-KIT pathway also signals to MAPK pathway. However, the results obtained did not support our initial hypothesis. In CRC, c-KIT expression seems to be independent of the activation of both *BRAF* and *KRAS* oncogenes.

STI571/Gleevec is a tyrosine kinase inhibitor. Several studies have already shown that STI571/Gleevec is able to inhibit proliferation, induce apoptosis and inhibit invasion in CRC cell lines [2, 5, 41]. In our study, we aimed to study the effect of STI571/Gleevec in cell lines with different genetic profiles. Our results showed that STI571/Gleevec was able to inhibit proliferation and induce apoptosis in all cell lines analysed independently of expressing c-KIT or harbouring mutations at *KRAS* or *BRAF* genes. As it has been shown that STI571/Gleevec inhibit other tyrosine kinase receptors as PDGFR [3, 17], we hypothesise that in two cell lines lacking c-KIT expression, PDGFR overexpression could be a possible mechanism by which STI571/Gleevec would act on those cell lines. However, the analysis of this gene by reverse transcriptase-PCR showed no PDGFR expression in both cell lines lacking c-KIT (data not shown). Accordingly, we hypothesise that STI571/Gleevec might interact with other signalling pathways involved in CRC cell survival. The mechanism by which STI571/Gleevec induces apoptosis in these cell lines needs to be further clarified. Moreover, our results show that c-KIT expression is not a predictor of STI571/Gleevec sensitivity in CRCs.

In conclusion, our results show that a subset of primary colorectal tumours and metastases express c-KIT in the absence of *c-kit*-activating mutations in *hotspot* regions, and this expression is not alternative to *BRAF* and/or *KRAS* activation. Moreover, our results suggest that STI571/Gleevec may be considered as another potential drug for CRC treatment because of its capacity to inhibit cell proliferation and promote apoptosis of tumour cells, regardless of the genetic background and by a still unknown mechanism.

Acknowledgement This work was supported by the Foundation for Science and Technology (FCT). We are grateful to the FCT for the grant support to Ana Preto (SFRH/BPD/14882/2003) and for funding the project POCTI/SAU-OBS/56921/2004. We thank Novartis Oncology for funding and for providing us the STI571/Gleevec.

References

1. Ashman LK (1999) The biology of stem cell factor and its receptor C-kit. Int J Biochem Cell Biol 31:1037–1051
2. Attoub S, Rivat C, Rodrigues S, Van Bocxlaer S, Bedin M, Bruyneel E, Louvet C, Kornprobst M, Andre T, Mareel M, Mester J, Gespach C (2002) The c-kit tyrosine kinase inhibitor STI571 for colorectal cancer therapy. Cancer Res 62:4879–4883
3. Baranowska-Kortylewicz J, Abe M, Pietras K, Kortylewicz ZP, Kurizaki T, Nearman J, Paulsson J, Mosley RL, Enke CA, Ostman A (2005) Effect of platelet-derived growth factor receptor-beta inhibition with STI571 on radioimmunotherapy. Cancer Res 65:7824–7831
4. Bellone G, Carbone A, Sibona N, Bosco O, Tibaudi D, Smirne C, Martone T, Gramigni C, Camandona M, Emanuelli G, Rodeck U (2001) Aberrant activation of c-kit protects colon carcinoma cells against apoptosis and enhances their invasive potential. Cancer Res 61:2200–2206
5. Bellone G, Ferrero D, Carbone A, De Quadros MR, Gramigni C, Prati A, Davidson W, Mioli P, Dughera L, Emanuelli G, Rodeck U (2004) Inhibition of cell survival and invasive potential of colorectal carcinoma cells by the tyrosine kinase inhibitor STI571. Cancer Biother 3:385–392
6. Bellone G, Silvestri S, Artusio E, Tibaudi D, Turletti A, Geuna M, Giachino C, Valente G, Emanuelli G, Rodeck U (1997) Growth stimulation of colorectal carcinoma cells via the c-kit receptor is inhibited by TGF-beta 1. J Cell Physiol 172:1–11
7. Bellone G, Smirne C, Carbone A, Buffolino A, Scirelli T, Prati A, Solerio D, Pirisi M, Valente G, Nano M, Emanuelli G (2006) KIT/

stem cell factor expression in premalignant and malignant lesions of the colon mucosa in relationship to disease progression and outcomes. Int J Oncol 29:851–859

8. Curtin JA, Busam K, Pinkel D, Bastian BC (2006) Somatic activation of KIT in distinct subtypes of melanoma. J Clin Oncol 24:4340–4346
9. Davies H, Bignell GR, Cox C, Stephens P, Edkins S, Clegg S, Teague J, Woffendin H, Garnett MJ, Bottomley W, Davis N, Dicks E, Ewing R, Floyd Y, Gray K, Hall S, Hawes R, Hughes J, Kosmidou V, Menzies A, Mould C, Parker A, Stevens C, Watt S, Hooper S, Wilson R, Jayatilake H, Gusterson BA, Cooper C, Shipley J, Hargrave D, Pritchard-Jones K, Maitland N, Chenevix-Trench G, Riggins GJ, Bigner DD, Palmieri G, Cossu A, Flanagan A, Nicholson A, Ho JW, Leung SY, Yuen ST, Weber BL, Seigler HF, Darrow TL, Paterson H, Marais R, Marshall CJ, Wooster R, Stratton MR, Futreal PA (2002) Mutations of the *BRAF* gene in human cancer. Nature 417:949–954
10. Domingo E, Espin E, Armengol M, Oliveira C, Pinto M, Duval A, Brennetot C, Seruca R, Hamelin R, Yamamoto H, Schwartz S Jr (2004) Activated *BRAF* targets proximal colon tumors with mismatch repair deficiency and MLH1 inactivation. Genes Chromosomes Cancer 39:138–142
11. Fletcher JA, Fletcher CD, Rubin BP, Ashman LK, Corless CL, Heinrich MC (2002) KIT gene mutations in gastrointestinal stromal tumors: more complex than previously recognized? Am J Pathol 161:737–738; author reply 738–739
12. Furitsu T, Tsujimura T, Tono T, Ikeda H, Kitayama H, Koshimizu U, Sugahara H, Butterfield JH, Ashman LK, Kanayama Y et al (1993) Identification of mutations in the coding sequence of the proto-oncogene c-kit in a human mast cell leukemia cell line causing ligand-independent activation of c-kit product. J Clin Invest 92:1736–1744
13. Hassan I, You YN, Dozois EJ, Shayyan R, Smyrk TC, Okuno SH, Donohue JH (2006) Clinical, pathologic, and immunohistochemical characteristics of gastrointestinal stromal tumors of the colon and rectum: implications for surgical management and adjuvant therapies. Dis Colon Rectum 49:609–615
14. Heinrich MC, Blanke CD, Druker BJ, Corless CL (2002) Inhibition of KIT tyrosine kinase activity: a novel molecular approach to the treatment of KIT-positive malignancies. J Clin Oncol 20:1692–1703
15. Hirota S, Isozaki K, Moriyama Y, Hashimoto K, Nishida T, Ishiguro S, Kawano K, Hanada M, Kurata A, Takeda M, Muhammad Tunio G, Matsuzawa Y, Kanakura Y, Shinomura Y, Kitamura Y (1998) Gain-of-function mutations of c-kit in human gastrointestinal stromal tumors. Science 279:577–580
16. Hirota S, Nishida T, Isozaki K, Taniguchi M, Nakamura J, Okazaki T, Kitamura Y (2001) Gain-of-function mutation at the extracellular domain of KIT in gastrointestinal stromal tumours. J Pathol 193:505–510
17. Holdhoff M, Kreuzer KA, Appelt C, Scholz R, Na IK, Hildebrandt B, Riess H, Jordan A, Schmidt CA, Van Etten RA, Dorken B, le Coutre P (2005) Imatinib mesylate radiosensitizes human glioblastoma cells through inhibition of platelet-derived growth factor receptor. Blood Cells Mol Diseases 34:181–185
18. Kang HJ, Nam SW, Kim H, Rhee H, Kim NG, Hyung WJ, Noh SH, Kim JH, Yun CO, Liu ET (2005) Correlation of KIT and platelet-derived growth factor receptor alpha mutations with gene activation and expression profiles in gastrointestinal stromal tumors. Oncogene 24:1066–1074
19. Longley BJ Jr, Metcalfe DD, Tharp M, Wang X, Tyrrell L, Lu SZ, Heitjan D, Ma Y (1999) Activating and dominant inactivating c-KIT catalytic domain mutations in distinct clinical forms of human mastocytosis. Proc Natl Acad Sci USA 96:1609–1614
20. Matsuda R, Takahashi T, Nakamura S, Sekido Y, Nishida K, Seto M, Seito T, Sugiura T, Ariyoshi Y et al (1993) Expression of the c-kit protein in human solid tumors and in corresponding fetal and adult normal tissues. Am J Pathol 142:339–346
21. Miettinen M, Sarlomo-Rikala M, Sobin LH, Lasota J (2000) Gastrointestinal stromal tumors and leiomyosarcomas in the colon: a clinicopathologic, immunohistochemical, and molecular genetic study of 44 cases. Am J Surg Pathol 24:1339–1352
22. Oliveira C, Pinto M, Duval A, Brennetot C, Domingo E, Espin E, Armengol M, Yamamoto H, Hamelin R, Seruca R, Schwartz S Jr (2003) BRAF mutations characterize colon but not gastric cancer with mismatch repair deficiency. Oncogene 22:9192–9196
23. Oliveira C, Velho S, Moutinho C, Ferreira A, Preto A, Domingo E, Capelinha AF, Duval A, Hamelin R, Machado JC, Schwartz S Jr, Carneiro F, Seruca R (2007) *KRAS* and *BRAF* oncogenic mutations in MSS colorectal carcinoma progression. Oncogene 26:158–163
24. Puputti M, Tynninen O, Sihto H, Blom T, Maenpaa H, Isola J, Paetau A, Joensuu H, Nupponen NN (2006) Amplification of KIT, PDGFRA, VEGFR2, and EGFR in gliomas. Mol Cancer Res 4:927–934
25. Rajagopalan H, Bardelli A, Lengauer C, Kinzler KW, Vogelstein B, Velculescu VE (2002) Tumorigenesis: RAF/RAS oncogenes and mismatch-repair status. Nature 418:934
26. Reed J, Ouban A, Schickor FK, Muraca P, Yeatman T, Coppola D (2002) Immunohistochemical staining for c-Kit (CD117) is a rare event in human colorectal carcinoma. Clin Colorectal Cancer 2:119–122
27. Sakuma Y, Sakurai S, Oguni S, Satoh M, Hironaka M, Saito K (2004) *c-kit* gene mutations in intracranial germinomas. Cancer Sci 95:716–720
28. Sammarco I, Capurso G, Coppola L, Bonifazi AP, Cassetta S, Delle Fave G, Carrara A, Grassi GB, Rossi P, Sette C, Geremia R (2004) Expression of the proto-oncogene c-KIT in normal and tumor tissues from colorectal carcinoma patients. Int J Colorectal Dis 19:545–553
29. Schmidt EK, Fichelson S, Feller SM (2004) PI3 kinase is important for Ras, MEK and Erk activation of Epo-stimulated human erythroid progenitors. BMC Biol 2:7
30. Shafik A, El-Sibai O, Ahmed I, Shafik AA (2004) Identification of interstitial cells of Cajal in the human rectum. Front Biosci 9:2848–2851
31. Sheng ZM, Przygodzki RM, O'Leary TJ (2001) Rapid screening for KIT mutations by capillary electrophoresis. Clin Chem 47:1325–1326
32. Tian Q, Frierson HF Jr, Krystal GW, Moskaluk CA (1999) Activating *c-kit* gene mutations in human germ cell tumors. Am J Pathol 154:1643–1647
33. Wandzioch E, Edling CE, Palmer RH, Carlsson L, Hallberg B (2004) Activation of the MAP kinase pathway by c-Kit is PI-3 kinase dependent in hematopoietic progenitor/stem cell lines. Blood 104:51–57
34. Wiedmann MW, Caca K (2005) Molecularly targeted therapy for gastrointestinal cancer. Curr Cancer Drug Targets 5:171–193
35. Wilczynski SP, Chen YY, Chen W, Howell SB, Shively JE, Alberts DS (2005) Expression and mutational analysis of tyrosine kinase receptors c-kit, PDGFRalpha, and PDGFRbeta in ovarian cancers. Human Pathol 36:242–249
36. Willmore-Payne C, Holden JA, Chadwick BE, Layfield LJ (2006) Detection of c-kit exons 11- and 17-activating mutations in testicular seminomas by high-resolution melting amplicon analysis. Mod Path 19:1164–1169
37. Willmore-Payne C, Holden JA, Hirschowitz S, Layfield LJ (2006) *BRAF* and *c-kit* gene copy number in mutation-positive malignant melanoma. Human Pathol 37:520–527

38. Willmore-Payne C, Holden JA, Tripp S, Layfield LJ (2005) Human malignant melanoma: detection of *BRAF*- and *c-kit*-activating mutations by high-resolution amplicon melting analysis. Human Pathol 36:486–493
39. Willmore-Payne C, Layfield LJ, Holden JA (2005) *c-KIT* mutation analysis for diagnosis of gastrointestinal stromal tumors in fine needle aspiration specimens. Cancer 105:165–170
40. Yorke R, Chirala M, Younes M (2003) c-kit proto-oncogene product is rarely detected in colorectal adenocarcinoma. J Clin Oncol 21:3885–3886; discussion 3886–3887
41. Zhou L, An N, Haydon RC, Zhou Q, Cheng H, Peng Y, Jiang W, Luu HH, Vanichakarn P, Szatkowski JP, Park JY, Breyer B, He TC (2003) Tyrosine kinase inhibitor STI-571/Gleevec down-regulates the beta-catenin signaling activity. Cancer Lett 193:161–170

Virchows Arch (2007) 450:627–636
DOI 10.1007/s00428-007-0400-0

ORIGINAL ARTICLE

Grading invasive ductal carcinoma of the breast: advantages of using automated proliferation index instead of mitotic count

Ossama Tawfik · Bruce F. Kimler · Marilyn Davis · Christopher Stasik · Sue-Min Lai · Matthew S. Mayo · Fang Fan · John K. Donahue · Ivan Damjanov · Patricia Thomas · Carol Connor · William R. Jewell · Holly Smith · Carol J. Fabian

Received: 12 January 2007 / Revised: 1 March 2007 / Accepted: 2 March 2007 / Published online: 26 April 2007
© Springer-Verlag 2007

Abstract Breast carcinomas are graded according to the "Nottingham modification of the Bloom–Richardson system" (SBR). The system is hindered, however, by lack of precision in assessing all three parameters including nuclear grade, mitosis, and tubular formation, leading to an element of subjectivity. Our objective was to evaluate a new grading system [the nuclear grade plus proliferation (N+P) system] for subjectivity, ease, and better representation of tumor biology. Its components are nuclear grade and automated proliferation index. Invasive ductal carcinomas, consisting of 137 SBR grade I, 247 grade II, and 266 grade III, were re-evaluated by the N+P system. The two systems were compared with each other and correlated with patients' overall survival, tumor size, angiolymphatic invasion, lymph node status, and biomarker status including estrogen receptor, progesterone receptor, p53, epidermal growth factor receptor, BCL-2, and Her-2. Although there was an agreement between the two systems with histologic and prognostic parameters studied, there was 37% disagreement when grading individual tumors. Fifty-three percent of SBR grade II tumors were "down-graded" to N+P grade I, and 7% were "up-graded" to N+P grade III. Distinction among the different histologic grades for overall survival curves was better indicated by the N+P than the SBR system.

Keywords Invasive breast carcinoma grading · MIB-1 (Ki-67) Immunohistochemistry · Automation · Image analysis · Survival

O. Tawfik (✉) · M. Davis · C. Stasik · F. Fan · J. K. Donahue · I. Damjanov · P. Thomas
Department of Pathology and Laboratory Medicine,
Kansas University Medical Center,
3901 Rainbow Boulevard,
Kansas City, KS 66160, USA
e-mail: otawfik@kumc.edu

B. F. Kimler
Department of Radiation Oncology,
Kansas University Medical Center,
Kansas City, KS 66160, USA

S.-M. Lai · M. S. Mayo
Department of Preventive Medicine and Public Health,
Kansas University Medical Center,
Kansas City, KS 66160, USA

C. Connor · W. R. Jewell
Department of Surgery, Kansas University Medical Center,
Kansas City, KS 66160, USA

M. S. Mayo · H. Smith
Center for Biostatistics and Advanced Informatics,
Kansas University Medical Center,
Kansas City, KS 66160, USA

C. J. Fabian
Department of Medicine, Oncology Division,
Kansas University Medical Center,
Kansas City, KS 66160, USA

Introduction

In the late nineteenth century, Von Hansemann [57] proposed that the nuclear morphology of tumor cells might foretell their ultimate biological behavior. This concept laid the foundation for a multitude of grading schemes that are in use today. A relationship between breast cancer histologic grade and survival was first documented in the

1920s by Greenhough et al. [21]. They assessed eight morphological factors including gland formation, secretory vacuoles, cell size, nuclear size, pleomorphism, degree of hyperchromasia, and number of mitoses. Later on, additional studies by Patey, Scarff, and Haagensen confirmed the relationship between histologic grade and patient survival. Patey and Scarff [39] highlighted the importance of tubular formation, variation in nuclear size, and hyperchromatism in histologic grading, whereas Haagensen [22] evaluated 15 histological features categorized under growth pattern, cell morphology, and the reaction of the surrounding stroma. In 1950, Bloom divided tumors into low, moderate, or high-grade malignancies according to the degree of tubule formation, nuclear features, hyperchromasia, and mitotic activity, and recognized a correlation between tumor grade and survival. Seven years later, Bloom and Richardson [3] proposed a numerical scoring system to facilitate the grading effort. Each of the above three features was examined and given a score of 1, 2, or 3 for a total possible score ranging from 3 to 9. Meanwhile, Black et al. [2] concluded that nuclear morphology was the most significant prognostic factor. They proposed a five-tier nuclear grading system that was later reduced to three tiers by Fisher et al. [18]. In the early 1990s, Elston and Ellis [16] re-examined and modified the grading system by combining Bloom and Richardson's and Black's approaches. They deleted "nuclear hyperchromasia" and refined the numerical method in assessing mitotic count. This system, also referred to as the "Nottingham modification of the Bloom–Richardson system", has become a popular and widely used grading scheme with proven prognostic significance. It is currently recommended by the WHO to include this tumor grading for all invasive breast cancers [52]. Although the Scarff–Bloom–Richardson (SBR) system correlates well with prognosis, the literature regarding its routine use is divided. It has been criticized for being imprecise in the assessment of all three parameters, most notably mitotic frequency, causing an element of subjectivity to influence tumor grade [4, 13, 24, 29]. Elsewhere, it has been shown to be acceptably reproducible when strict criteria are defined [10, 11, 19, 48, 54]. Ductoglandular differentiation has been shown to be the least predictive component of the SBR system, whereas nuclear pleomorphism and mitotic activity are the most useful [31].

Cell proliferation or mitotic activity as a predictor of tumor behavior has received increasing attention in recent years. The Ki-67 antigen, first described in 1983, is a non-histone protein [20]. The protein is expressed in cycling cells in the G1 phase, S phase, G2 phase, and during mitosis, which provides an accurate interpretation of the growth fraction of the tumor. The MIB-1, an anti-Ki-67, antibody has proven to be superior to other antibodies for assessing cells, which have been triggered into the cell cycle [7]. Several studies have proven the prognostic significance of data obtained with this antibody in breast cancer and its positive relationship with histologic grade, tumor size, mitotic activity, hormonal and Her-2 status, and disease-free survival [5, 9, 27, 28, 33, 34, 37, 40–42, 46, 50, 56, 58]. Problems did exist, however, with inter-laboratory and inter-observer reproducibility of immunohistochemical (IHC) analysis of MIB-1 (Ki-67) labeling in breast cancer, leading some authors to question its utility as an independent prognostic factor [23, 32, 35, 37].

In the current study, our objective was to develop a new grading system [the nuclear grade plus proliferation (N+P) system] which is comparable to the SBR system in terms of defining prognostically relevant groups. The N+P system demonstrated at least equivalent correlation between histologic grade and overall survival as the SBR system. Our system relies on automated methods that, while not immune to the influence of subjective bias, may (given time and further study) prove to increase the objectivity and reproducibility of breast cancer grading.

Materials and methods

Patient cohort

A total of 650 primary breast carcinomas, ductal type, consisting of 137 SBR grade I, 247 grade II, and 266 grade III tumors were examined. The retrospective study was approved by the Institutional Research Committee at the Kansas University Medical Center. Histologic tumor samples were obtained from lumpectomy or mastectomy specimens as well as core needle biopsies. The samples were taken from 542 lumpectomy/mastectomy specimens and 108 core biopsies from patients ranging in age from 24 to 95 years with a median age of 55 years. Histopathologic parameters, including histologic grade, type, nuclear grade, and angiolymphatic invasion, were recorded for all patients. All tumors were graded using the modified "Nottingham" criteria of Bloom and Richardson [16]. Additional parameters including tumor size and lymph node metastasis were also recorded for lumpectomy/mastectomy specimens.

Patient outcome data were obtained from the Kansas Tumor Registry. Specifically, the date of death was recorded and used to calculate overall survival. Overall (rather than disease-specific) survival was reported because discrepancies and/or incomplete cause of death data were not uncommon.

Criteria for the newly proposed N+P grading system

The goal of this study was to develop a valid, reproducible, and user-friendly system for grading invasive breast cancers. The N+P grading system is a three-tiered system that evaluates two features: nuclear pleomorphism and the

automated MIB-1 count. Tubule formation and the manual mitotic count were eliminated. The nuclear grade was scored conventionally from 1 to 3 using the SBR system. Specifically, nuclear grade 1 is characterized by small regular uniform nuclei with little variation in size and shape; nuclear grade 2 by moderate nuclear variation in size and shape; and nuclear grade 3 by marked variation in size and shape, including bizarre nuclei.

The automated MIB-1 count was likewise classified into three categories: ≤9%, 10–25%, and >25%. These cutoffs (9 and 25%) were selected initially based on tertiles to produce three equal groups, but then shifted slightly to avoid placing a cut-point at a value with a large number of cases (Table 1).

Next, the information from nuclear pleomorphism and MIB-1 was combined to yield a new N+P grading system based on the number of bad prognostic factors present in the tumor, i.e., whether the tumor was nuclear grade 3 (Fig. 1) and/or whether MIB-1 expression was >25% (Fig. 2). Thus, N+P grade I was defined as a tumor having nuclear grade 1 or 2 and MIB-1 ≤25%; N+P grade II describes a tumor having either nuclear grade 3 and a MIB-1 >25% or nuclear grade 1 or 2 with a MIB-1 >25%. N+P grade III was a tumor having both nuclear grade 3 and MIB-1 >25% (Tables 1 and 2).

Immunohistochemical studies

Tissue blocks containing the most representative and well-preserved tumor areas were selected for IHC. Immunohistochemical analysis was performed on tissue fixed with 10% neutral buffered formalin. MIB-1, p53, epidermal growth factor receptor (EGFR), Bcl-2, and Her-2 IHC analyses were performed on all specimens using a Dako Autostainer (DAKO, Carpinteria, CA). The paraffin-embedded tissue blocks were cut to 5-μm sections, deparaffinized and heat-treated for antigen retrieval. Her-2 antibody was detected using the HercepTest (DAKO) per manufacture protocol. For individual antibodies, the vendor, clone, titration titer, time of titration, epitope retrieval method, and method of detection, please refer to Table 3. Hematoxylin was used as a counterstain. Appropriate positive and negative controls were included. Positive controls for the markers were selected from surgical specimens received in the surgical pathology laboratory and confirmed to be positive when compared with other samples. Negative controls included samples run without the primary antibody or with non-immune serum. Positive and negative controls supplied in the HercepTest kit were used for the evaluation of the Her-2 stains. Nuclear morphology, tubular formation, and MIB-1 labeling index were then analyzed and assigned scores.

Table 1 N+P scheme for grading invasive ductal carcinoma of the breast

Feature	Score
Nuclear grade	
Small regular uniform nuclei with little variation	1
Moderate nuclear variation	2
Marked variation in size and shape	3
MIB-1 count (%)	
≤9	1
10–25	2
>25	3
N+P grading	
Grade 1: nuclear grade 1 or 2 and MIB-1 count 1 or 2	
Grade 2: nuclear grade 3 and MIB-1 count 1 or 2 or MIB-1 count 3 and nuclear grade 1 or 2	
Grade 3: both nuclear grade 3 and MIB-1 count 3	

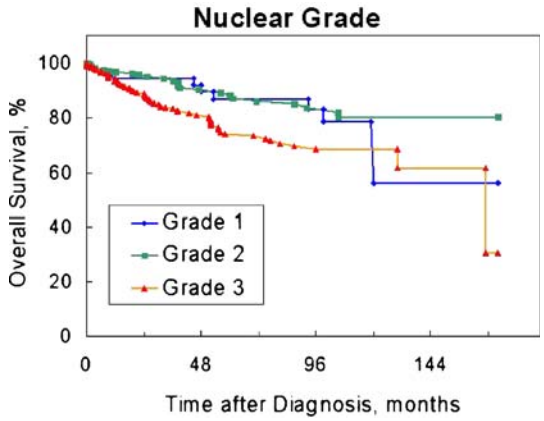

Fig. 1 Overall survival of patients with invasive ductal carcinoma classified by nuclear grade. Survival curves of patients with nuclear grade 3 are statistically significantly different those of nuclear grades 1 and 2 (p=0.0004; log-rank test)

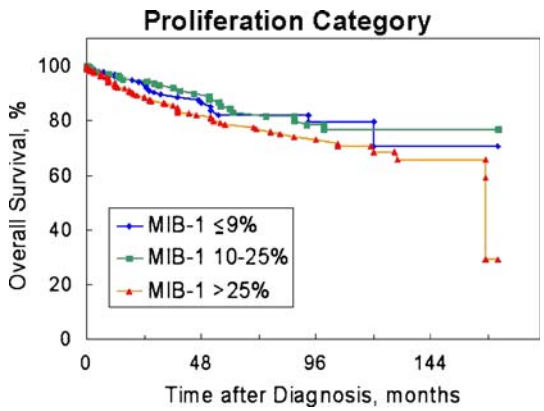

Fig. 2 Overall survival of patients with invasive ductal carcinoma classified by level of immunohistochemical expression of MIB-1. The three survival curves are NOT statistically significantly different (p= 0.068; log-rank test)

Table 2 Classification of invasive ductal carcinomas graded according to the proposed N+P grading system

MIB-1 category (count)	*N*	Nuclear grade		
		1 *N*=57	2 *N*=265	3 *N*=328
1 (≤9%)	194	43 (7%)	114 (18%)	37 (6%)
2 (10 to 25%)	186	8 (1%)	94 (15%)	84 (13%)
3 (>25%)	270	6 (1%)	57 (9%)	207 (32%)
Total	650	259 (40%) N+P (I)	184 (28%) N+P (II)	207 (32%) N+P (III)

Quantification of immunohistochemistry

Positive IHC reactions were defined as a dark brown circumferential reaction on the cell membrane for Her-2 and EGFR, distinct nuclear staining for MIB-1, ER, PR, and p53, and intense cytoplasmic staining for Bcl-2. Staining parameters were evaluated at 100×, and areas of high-density immunostaining were chosen for image analysis or manual scoring. For proliferation index (PI) of MIB-1, the percentage of nuclei with immunopositivity was determined using the PI program of either the cell analysis system (CAS) 200 image analyzer (Bacus Laboratory, Chicago, IL) for the period between 1991 to 2001 or (later) with the Clarient automated cellular imaging system (ACIS™; San Juan Capistrano, CA). Five to ten areas with the highest staining intensity were selected for quantitation from each specific lesion (Fig. 3). An average score for all selected areas was then calculated. For ER, PR and p53, both the CAS-200 and ACIS™ systems were used for automated counts. Manual microscopy was utilized to score tumor staining with antibodies to EGFR and Bcl-2. Her-2 staining was quantified using a score of 0 or 1+ to indicate "negative" results, and 2+ or 3+ to represent "positive" results, per the scoring instructions included in the HercepTest kit. Results were validated using the Her-2 scoring system of the ACIS machine. Using both manual and automated microscopy, up to ten high power fields were evaluated with each marker to provide the final score. A staining of 10% or more of the tumor cells with the antibody to EGFR or Bcl-2 was considered positive, whereas for p53, any counts greater than or equal to 5% were considered positive.

Statistical analysis

Overall frequencies and percentages were summarized for tumor grade, via both the N+P and SBR system, ER, PR, p53, EGFR, Bcl-2, Her-2, vascular invasion, and node positivity. The frequencies of each variable stratified by the grading system were calculated, and their relationships to each grading system were evaluating using the chi square test. Summaries of biomarker expression by N+P system stratified by SBR system are also given. The log-rank test was used to compare overall survival across the three grades for the N+P and SBR systems independently.

Results

Nuclear grade alone provided reasonable prognostic prediction for overall survival (p=0.0017; log-rank test), with obvious separation of high grade versus low and intermediate grades (p=0.0004; Fig. 1). The segregation of MIB-1 quantification into three categories resulted in a fairly even distribution between grades I, II, and III (194, 186, 270, respectively) and was prognostic for overall survival (p=0.068; log-rank test). The highest level of MIB-1 expression significantly differed from the low and intermediate levels of expression (p=0.022; log-rank test; Fig. 2). We evaluated whether shifting the cut-points by a few percentage points either way would alter the prognostic ability, but there was no improvement in the separation of the curves.

The nuclear grade and automated MIB-1 count was combined as previously described into a three-tier grading system (the N+P grading system.) This classification system was prognostic for overall survival (p=0.0013;

Table 3 Protocols for immunohistochemistry

Antibody	Vendor	Clone	Titer	Time (min)	Epitope retrieval	Method of detection
ER 07	BioCare	Labvision (RM) SP1	1:1000	30	BioCare nuclear decloaker	Envision + LP, mouse (Dako)
P53	Biogenex	Biogenex 1801	1:60	30	Citrate, pH 6	Envision + LP, mouse (Dako)
PR	Dako	Dako PR 1294	1:5,000	30	Citrate, pH 6	Envision + LP, mouse (Dako)
EGFR	Zymed	Zymed 31G7	1:20	30	Proteinase K, 10′	LSAB + (Dako)
Bcl-2	Dako	Dako 124	1:100	30	BioCare reveal	Envision + LP, mouse (Dako)
MIB-1	Dako	Dako MIB-1	1:200	30	BioCare reveal	Envision + LP, mouse (Dako)
HercepTest	Dako	Dako HercepTest®	P.D. Her2/neu	30	Per kit instructions	Kit components (K5204, Dako)

All stains were performed using the Dako Autostainer per manufacturer procedures. Buffer used was Tris–buffered saline with Tween; visualization with Dab + (Dako)

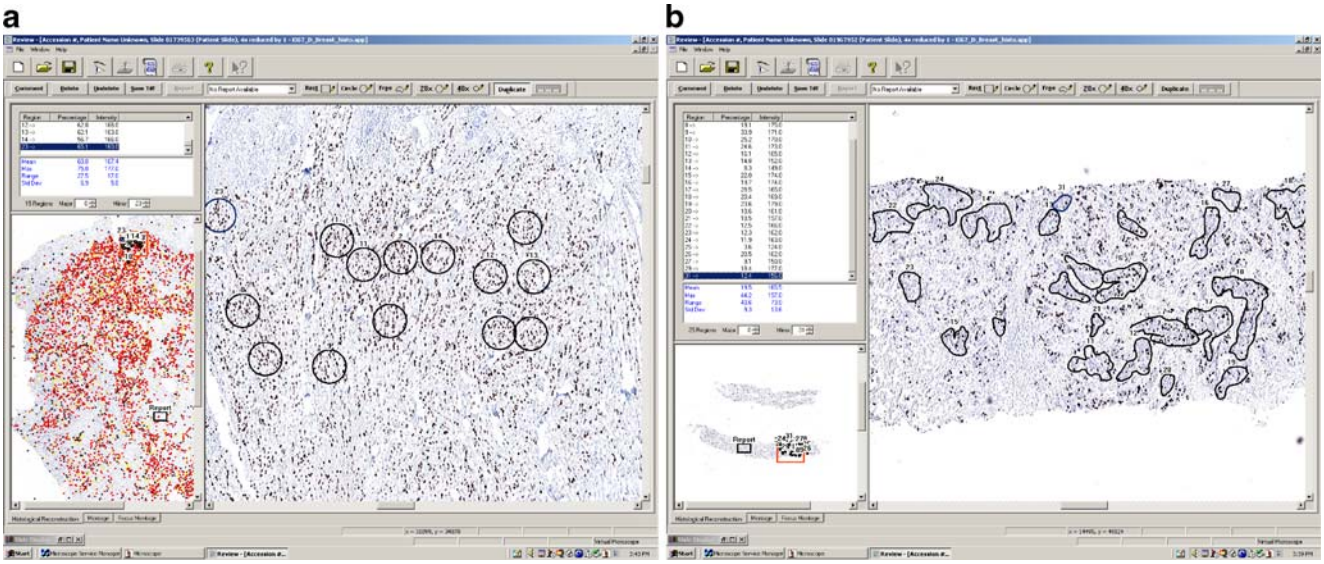

Fig. 3 Screen images from the ACIS™ program depicting the process of selecting tissue areas to be evaluated for MIB-1 expression. **a** A representative tumor resection specimen. The exclusive "hot spots" feature identifies areas with the most intense staining (*left lower corner*). Quick identification of the relevant regions is then possible. Circular areas of representative tumor are then automatically selected, and positive MIB-1 staining is calculated and expressed as a percentage of the total tumor cells (*right image*). **b** Highlights two additional valuable features of the ACIS™ system. It shows an image of a representative core biopsy specimen (*left image*), as well as the use of the manual mapping feature of irregular areas involved by tumor for calculation of percent of cells stained with MIB-1 (*right image*)

log-rank test), with greatest separation of grades II and III versus grade I (Fig. 4). Comparing individual grades, grade I was statistically significantly different from both grade II ($p=0.0025$) and grade III ($p=0.0004$). There was a suggestion of separation between N+P grade II and N+P grade III for times less than 4 years, but this was of marginal statistical significance ($p=0.078$; log-rank test).

The N+P grading system was compared to the standard SBR grading system. The SBR system was overall prognostic ($p=0.0032$; log-rank test) and identified a cohort of patients with bad prognosis (grade III), but there was no clear separation between grades I and II (Fig. 5). Comparing individual grades, grade III was statistically significantly different from both grade I ($p=0.0096$) and grade II ($p=0.0043$).

Of more clinical relevance, if one simply takes SBR grade II patients, who have survival data indistinguishable from SBR grade I patients, and compares them on the basis of being N+P grade I versus N+P grade II, there is an obvious and statistically significant ($p=0.025$) separation (Fig. 6). In other words, roughly one third of the patients would be identified who have an increased risk of death. Using SBR grading alone, these patients would have been given a moderately good prognosis.

Comparison of the N+P grading system to the SBR system

The two histologic grading systems (the SBR and N+P systems), in general, demonstrated similar frequencies for the different histologic grades (Table 4). More importantly, the greatest difference between the two systems was observed for those tumors initially classified as grade II by SBR. Whereas 91% of tumors initially classified as SBR I remained as N+P I and 70% of tumors initially classified as SBR III remained as N+P III, only 39% of tumors initially classified as SBR II remained as N+P II. The majority (53%) of the tumors initially classified as SBR II were "down-graded" to N+P I. As shown above, this shift provided definite prognostic value.

The two grading systems also demonstrated similar frequencies, grade for grade, for expression of other clinical and immunohistochemical prognostic factors studied (Table 5).

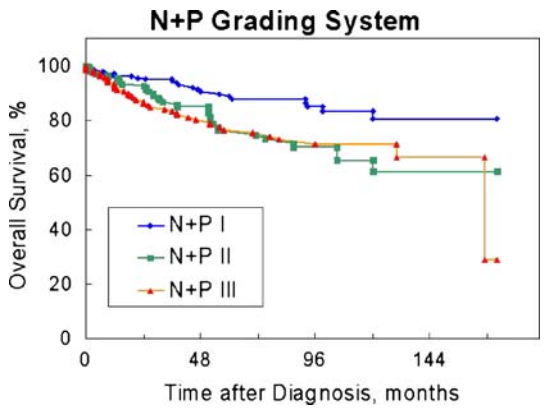

Fig. 4 Overall survival of patients with invasive ductal carcinoma classified by the N+P grading system. The three survival curves are statistically significantly different ($p=0.0013$; log-rank test)

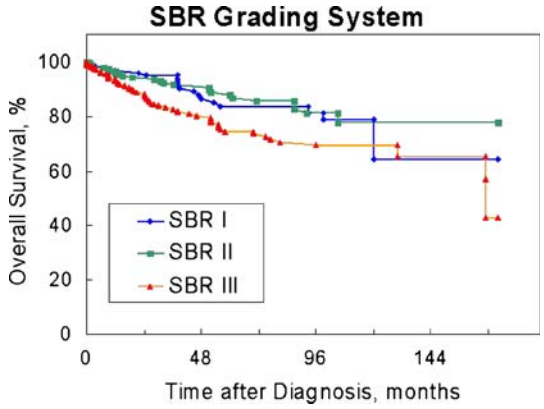

Fig. 5 Overall survival of patients with invasive ductal carcinoma classified by the SBR grading system. The three survival curves are statistically significantly different (p=0.0032; log-rank test)

At surgery, low-grade tumors were smaller in size (median diameter of 1.3 and 1.5 cm for SBR and N+P grade I, respectively, to 2.2 and 2.3 cm for SBR and N+P grade III, respectively) and less likely to be associated with angiolymphatic invasion or nodal metastasis. The majority of low-grade tumors were ER, PR, and Bcl-2 positive and negative for p53, EGFR, and Her-2. In contrast, the majority of the high-grade tumors were ER, PR, and Bcl-2 negative. In addition, more high-grade tumors showed increased expression of p53, EGFR, and Her-2, consistent with the biological aggressiveness of these tumors. Moderately differentiated tumors were, as expected, somewhere in the middle between well and poorly differentiated tumors.

The available demographic, clinical, and pathologic data were subjected to Cox regression analysis to identify predictors of overall survival. Variables included were age at diagnosis, evidence of vascular invasion, type of specimen (biopsy or surgical), MIB-1 percent positive cells, nuclear grade, and both the SBR and N+P grades. Lymph node status and tumor size were excluded, as information was not available on 280 and 108 subjects, respectively. Similarly, immunohistochemical expression of the other molecular markers was also excluded because of incomplete data. The first variable to enter the model was the N+P grade (p=0.001), followed by vascular invasion (p=0.017).

Discussion

In this study, we described a new three-tier grading system, the N+P system, which eliminates the ductoglandular differentiation component of the SBR system and replaces the manual counting of mitotic figures with an automated MIB-1 count. Our results demonstrate that the N+P system correlates well with a variety of tumor biomarkers and clinicopathologic parameters which have well-known prognostic value, including vascular invasion and lymph node status. The N+P system is at least comparable to the SBR system in terms of predicting overall survival and correlates similarly with prognostic biomarkers. Additionally, one potential advantage of the new system was highlighted by its ability to discriminate a group of intermediate risk patients not identified by the SBR system. About one third of the patients classified as SBR grade II exhibited a survival indistinguishable from SBR grade I. When graded by the N+P system, these patients were shown to have a statistically significantly worse overall survival than would be predicted by the SBR system.

For decades, investigators have known that data collected from routine pathologic evaluation of breast tumors can be used to provide important prognostic information. Histologic grade [8, 15, 26, 41], tumor type [15], tumor size [6, 26, 47], angiolymphatic invasion [12] and lymph node status [14, 17, 26, 43] have all been shown to yield clinically valuable information. As medical understanding of tumor biology has expanded, breast cancer grading has evolved through many stages. The Elston modification of the SBR grading system is currently the most widely used system in North America and Europe [38] and is currently recommended by the WHO [52]. It provides criteria for the assignment of a histological grade which reflects both tumor morphology and biological behavior. Although defined cutoffs exist within the SBR system, the determination of these factors is arguably based on subjective judgments, leading to potential problems with intra- and inter-observer reproducibility. In fact, the latest Breast Task Force of the American Joint Committee on Cancer did not include histologic grading in its staging criteria due to "insurmountable inconsistencies" between institutions and pathologists.

The literature is divided. Some studies demonstrate a lack of precision in assessing all three parameters of the

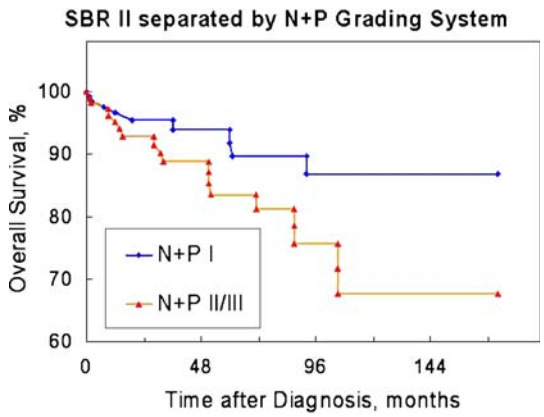

Fig. 6 Overall survival for patients classified as SBR grade II, plotted as a function of the N+P grades I vs II. The two survival curves are statistically significantly different (p=0.025; log-rank test)

Table 4 Comparison of the SBR to the N+P grading systems for invasive ductal carcinoma

N+P grading system	*N*	SBR grading system		
		I	II	III
0 Risk (I)	259	124 (19%)	131 (20%)	4 (0.6%)
1 Risk (II)	184	13 (2%)	97 (15%)	74 (11%)
2 Risk (III)	207	0 (0%)	19 (3%)	188 (29%)
Total	650	137	247	266
	209 (32%)	"Down-graded" from SBR to N+P system		
	409 (63%)	No change from SBR to N+P system		
	32 (5%)	"Up-graded" from SBR to N+P system		

SBR system, specifically mitotic frequency [4, 13, 24, 29, 30, 36, 44, 45, 51]. Elsewhere, it has been shown that with experienced pathologists and strictly defined criteria, the SBR system is quite reproducible [51, 10, 11, 19, 48, 54]. Agreement ranges from poor (35%) to acceptable (75%) among pathologists using the SBR grading system, and there exists a low predictive value of prognosis for individual patients [4, 13, 24, 30, 31, 36, 44, 45, 51]. The source of most pathologist disagreement is within the SBR grade II group. There also exists doubt about the utility of the SBR system when grading small lesions [55].

An important feature common to both the N+P and SBR grading systems is the evaluation of tumor proliferative activity. Performing a manual mitotic count is time-consuming and somewhat subjective. Experience, interest, and diligence in counting mitosis can vary between individuals. It is also known that tissue fixation and slide quality has a negative effect on one's ability to perform an accurate mitotic count. Furthermore, specimens containing limited tumor material (i.e., core needle biopsies or residual tumor after neoadjuvant chemotherapy) could further limit the accuracy of the count. These factors may impact tumor grade and, consequently, clinical management. The use of an automated MIB-1 count removes some of the subjectivity from the assessment of mitotic activity within a given tumor; however, biologic variability and examiner individuality can never be totally eliminated. While it is our belief that the automatic MIB-1 count is less susceptible to these factors, the inherent proliferative variability within any given tumor, combined with the reliance of our system on accurately choosing the best "hot spots" to be analyzed, prevents the elimination of all sources of potential subjectivity. Newer systems have programs capable of extensively sampling an entire tumor on a slide, further reducing the potential for sampling error. It is our opinion that the N+P system represents a move toward a more objective approach to breast cancer grading; however, further studies need to be carried out to demonstrate the reproducibility of these methods.

The grading of special types of breast carcinoma, as well as invasive lobular carcinoma, is of particular interest. The SBR system is strongest when grading unselected cases of ductal carcinoma; however, investigations have also focused on its utility in invasive lobular carcinoma [1, 49]. In clinical practice, an SBR grade is often reported for lobular carcinoma; however, the impact of using predefined grades (i.e., SBR grade 2 for lobular carcinoma, grade 1 for tubular carcinoma, and grade 3 for medullary carcinoma) on the ability of the SBR to prognosticate these malignancies remains unknown [52]. No universally accepted grading system for non-ductal carcinomas currently exists. In developing the N+P system, it was our goal to not only show equivalence with the SBR system for grading ductal carcinoma but also to identify a single system which may potentially be used for grading other types of invasive breast carcinoma. It is our hypothesis that the N+P system will ultimately prove to be a viable means for grading all types of breast carcinoma. Our preliminary data analyzing ductal carcinoma in situ [53] and lobular carcinoma (unpublished) is promising.

Table 5 Frequency (%) of expression of various biomarkers and clinicopathologic parameters for tumors classified by SBR and N+P grading systems for invasive ductal carcinoma

Grade	*N*		Vascular invasion	Lymph node positive	ER	PR	p53	EFGR	Bcl-2	Her-2
I	SBR	137	1	8	91	71	8	4	91	3
	N+P	259	2	9	89	68	9	7	85	10
II	SBR	247	34	22	76	56	25	18	71	21
	N+P	184	47	31	64	46	38	28	57	25
III	SBR	266	51	37	32	21	54	45	38	28
	N+P	207	44	34	23	15	59	51	35	28
All		650	36	27	61	45	34	27	61	20

Replacing the manual mitotic count with an automated MIB-1 count has been shown to be beneficial, providing both standardization and precision [25]. Our results demonstrate a positive correlation between the N+P grade and the MIB-1 status of these breast tumors. When nuclear grade and MIB-1 status are combined to arrive at an N+P grade, the results are comparable to the SBR system in terms of overall survival and prognostic biomarkers. In addition, the N+P system is able to accurately grade tumors in needle core biopsy specimens. Tumors graded in these limited tissue samples positively correlated with the different histologic and prognostic parameters studied, as well as with their paired excision specimens.

As stated previously, our goals were to introduce a method of breast cancer grading which is applicable to all forms of invasive and in situ carcinoma and reduces, as much as possible, the subjectivity inherent in many current grading schemes, specifically the Scarff–Bloom–Richardson system. Our results demonstrate the feasibility of the N+P system as a viable alternative to SBR grading; however, our findings need to be interpreted with caution. Two main shortcomings limit our conclusions. First, we evaluated both the SBR and the N+P grading systems by comparing overall survival rather than disease-free survival. Second, we lacked data regarding lymph node status or tumor size on a considerable number of specimens (280 and 108, respectively.) Drawing conclusions regarding potential outcome without fully taking into account the impact of these well-established prognostic factors should be done with caution. Future study may be directed at further assessing the reproducibility of our methods or assessing the ability of the N+P system to prognosticate patients based on disease-free survival. Another potential avenue for investigation would involve attempting to modify the N+P system to segregate tumors into a two-tier system (low- or high-grade) as has been done for urothelial carcinoma.

In conclusion, we have demonstrated that the N+P system is at least equivalent to the SBR system for predicting overall survival and prognostic biomarker expression in invasive ductal carcinoma. Future research is needed (and encouraged) to assess the reproducibility of these methods. The applicability of the N+P system to the grading of other forms of breast carcinoma such as mucinous carcinoma, lobular carcinoma, or even ductal and lobular carcinoma in situ is currently under investigation.

References

1. Bane AL, Tjan S, Parkes RK, Andrulis I, O'Malley FP (2005) Invasive lobular carcinoma: to grade or not to grade. Mod Pathol 18:621–628
2. Black MM, Barclay THC, Hankey BF (1975) Prognosis in breast cancer utilizing histologic characteristics of the primary tumor. Cancer 36:2048–2055
3. Bloom HJG, Richardson WW (1957) Histologic grading in breast cancer: a study of 1,409 cases of which 359 have been followed for 15 years. Br J Cancer 11:359–377
4. Boiesen P, Bendahl PO, Anagnostaki L, Domanski H, Holm E, Idvall I, Johansson S, Ljungberg O, Ringberg A, Ostberg G, Ferno M (2000) Histologic grading in breast cancer—reproducibility between seven pathologic departments. South Sweden Breast Cancer Group. Acta Oncol 39:41–45
5. Brown RW, Allred CD, Clark GM, Osborne CK, Hilsenbeck SG (1996) Prognostic value of Ki-67 compared to S-phase fraction in axillary node-negative breast cancer. Clin Cancer Res 2:585–592
6. Cady B, Stone MD, Schuler JG, Thakur R, Wanner MA, Lavin PT (1996) The new era in breast cancer. Invasion, size and nodal involvement dramatically decreasing as a result of mammography screening. Arch Surg 131:301–308
7. Cattoretti G, Becker MH, Key G, Duchrow M, Schluter C, Galle J, Gerdes J (1992) Monoclonal antibodies against recombinant parts of the Ki-67 antigen (MIB-1 and MIB-3) detect proliferating cells in microwave-processed formalin-fixed paraffin sections. J Pathol 168:357–363
8. Chia SK, Speers CH, Bryce CJ, Hayes MM, Olivotto IA (2004) Ten-year outcomes in a population-based cohort of node-negative, lymphatic, and vascular invasion-negative early breast cancers without adjuvant systemic therapies. J Clin Oncol 22:1630–1637
9. Clahsen PC, van de Velde CJ, Duval C, Pallud C, Mandard AM, Delobelle-Deroide A, van den Broek L, van de Vijver MJ (1999) The utility of mitotic index, oestrogen receptor and Ki-67 measurements in the creation of novel prognostic indices for node-negative breast cancer. Eur J Surg Oncol 25:356–363
10. Dalton LW, Page DL, Dupont WD (1994) Histologic grading of breast carcinoma. A reproducibility study. Cancer 73:2765–2770
11. Dalton LW, Pinder SE, Elston CE, Page DL, Dupont WD, Blamey RW (2000) Histologic grading of breast cancer: linkage of patient outcome with level of pathologist agreement. Mod Pathol 13:730–735
12. Davis BW, Gelber R, Goldhirsch A, Hartmann WH, Hollaway L, Russell I, Rudenstam CM (1985) Prognostic significance of peritumoral vessel invasion in clinical trials of adjuvant therapy for breast cancer with axillary lymph node metastasis. Human Pathol 16:1212–1218
13. Delides GS, Garas G, Georgouli G, Jiortziotis D, Lecca J, Liva T, Elemenoglou J (1982) Intralaboratory variations in the grading of breast carcinoma. Arch Pathol Lab Med 106:126–128
14. Eisen T, Smith IE, Johnston S, Ellis PA, Prendiville J, Seymour MT, Walsh G, Ashley S (1998) Randomized phase II trial of infusional fluorouracil, epirubicin and cyclophosphamide versus infusional fluorouracil, epirubicin and cisplatin in patients with advanced breast cancer. J Clin Oncol 16:1350–1357
15. Ellis IO, Galea M, Broughton N, Locker A, Blamey RW, Elston CW (1992) Pathological prognostic factors in breast cancer. II. Histological type. Relationship with survival in a large study with long-term follow up. Histopathology 20:479–489
16. Elston CW, Ellis IO (1991) Pathological prognostic factors in breast cancer. I. The value of histological grade in breast cancer: experience from a large study with long-term follow up. Histopathology 19:403–410
17. Fisher B, Bryant J, Wolmark N, Mamounas E, Brown A, Fisher ER, Wickerham DL, Begovic M, DeCillis A, Robidoux A, Margolese RG, Cruz AB Jr, Hoehn JL, Lees AW, Dimitrov NV, Bear HD (1998) Effect of preoperative chemotherapy on the outcome of women with operable breast cancer. J Clin Oncol 16:2672–2685
18. Fisher ER, Redmond C, Fisher B (1980) Histologic grading of breast cancer. Pathol Annu 15:239–251

19. Frierson HF Jr, Wolber RA, Berean KW, Franquemont DW, Gaffey MJ, Boyd JC, Wilbur DC (1995) Interobserver reproducibility of the Nottingham modification of the Bloom and Richardson histologic grading scheme for infiltrating ductal carcinoma. Am J Clin Pathol 103:195–198
20. Gerdes J, Lemke H, Baisch H, Wacker H-H, Schwab U, Stein H (1984) Cell cycle analysis of a cell proliferation-associated human nuclear antigen defined by the monoclonal antibody Ki-67. J Immunol 133:1710–1715
21. Greenhough RB (1925) Varying degree of malignancy in cancer of the breast. J Cancer Res 9:453–463
22. Haagensen CD (1933) The basis for histologic grading of the breast. Am J Cancer 1:285–327
23. Haerslev T, Jacobsen GK, Zedeler K (1996) Correlation of growth fraction by Ki-67 and proliferating cell nuclear antigen (PCNA) immunohistochemistry with histopathological parameters and prognosis in primary breast carcinomas. Breast Cancer Res Treat 37:101-113
24. Harvey JM, de Klerk NH, Sterrett GF (1992) Histological grading in breast cancer. Interobserver agreement and relation to other prognostic factors including ploidy. Pathology 24:63–68
25. Hilbe W, Gachter A, Duba HC, Dirnhofer S, Eisterer W, Schmid T, Mildner A, Bodner J, Woll E (2003) Comparison of automated cellular imaging system and manual microscopy for immunohistochemically stained cryostat sections of lung cancer specimens applying p53, Ki-67 and p120. Oncol Rep 10:15–20
26. Hlupic L, Jakic-Razumovic J, Bozikov J, Coric M, Belev B, Vrbanec D (2004) Prognostic values of different factors in breast carcinoma. Tumori 90:112–119
27. Jansen RL, Hupperets PS, Arends JW, Joosten-Achjanie SR, Volovics A, Schouten HC, Hillen HF (1998) MIB-1 labeling index is an independent prognostic marker in primary breast cancer. Br J Cancer 78:460–465
28. Keshgegian AA, Cnaan A (1995) Proliferation markers in breast carcinoma. Mitotic figure count, S-phase fraction, proliferating cell nuclear antigen, Ki-67 and MIB-1. Am J Clin Pathol 104:42–49
29. Kronqvist P, Montironi R, Kuopio T, Collan YU (1997) Subjective breast cancer grading. Analyses of reproducibility after application of Bayesian belief networks. Anal Quant Cytol Histol 19:423–429
30. Lakhani SR, Jacquemier J, Sloane JP, Gusterson BA, Anderson TJ, van de Vijver MJ, Farid LM, Venter D, Antoniou A, Storfer-Isser A, Smyth E, Steel CM, Haites N, Scott RJ, Goldgar D, Neuhausen S, Daly PA, Ormiston W, McManus R, Scherneck S, Ponder BA, Ford D, Peto J, Stoppa-Lyonnet D, Bignon YJ, Struewing JP, Spurr NK, Bishop DT, Klijn JG, Devilee P, Cornelisse CJ, Lasset C, Lenoir G, Barkardottir RB, Egilsson V, Hamann U, Chang-Claude J, Sobol H, Weber B, Stratton MR, Easton DF (1998) Multifactorial analysis of differences between sporadic breast cancer and cancers involving BRCA1 and BRCA2 mutations. J Natl Cancer Inst 90:1138–1145
31. Le Doussal V, Tubiana-Hulin M, Friedman S, Hacene K, Spyratos F, Brunet M (1989) Prognostic value of histologic grade nuclear components of Scarff–Bloom–Richardson (SBR). An improved score modification based on a multivariate analysis of 1262 invasive ductal breast carcinomas. Cancer 64:1914–1921
32. Lehr HA, Hansen DA, Kussick S, Li M, Hwang H, Krummenauer F, Trouet S, Gown AM (1999) Assessment of proliferative activity in breast cancer: MIB-1 immunohistochemistry versus mitotic figure count. Human Pathol 30:1314–1320
33. Leonardi E, Girlando S, Serio G, Mauri FA, Perrone G, Scampini S, Dalla Palma P, Barbareschi M (1992) PCNA and Ki67 expression in breast carcinoma: correlations with clinical and biological variables. J Clin Pathol 45:416–419
34. Marchetti E, Querzoli P, Marzola A, Bagni A, Ferretti S, Fabris G, Nenci I (1990) Assessment of proliferative rate of breast cancer by Ki-67 monoclonal antibody. Mod Pathol 3:31–35
35. Mengel M, von Wasielewski R, Wiese B, Rudiger T, Muller-Hermelink HK, Kreipe H (2002) Inter-laboratory and inter-observer reproducibility of immunohistochemical assessment of the Ki-67 labeling index in large multi-centre trial. J Pathol 198:292–299
36. Meyer JS, Alvarez C, Milikowski C, Olson N, Russo I, Russo J, Glass A, Zehnbauer BA, Lister K, Parwaresch R, Cooperative Breast Cancer Tissue Resource (2005) Breast carcinoma malignancy grading by Bloom–Richardson system vs. proliferation index: reproducibility of grade and advantages of proliferation index. Mod Pathol 18:1067–1078
37. Offersen BV, Sorensen FB, Knoop A, Overgaard J, Danish Breast Cancer Cooperative Tumour Biology Committee (2003) The prognostic relevance of estimates of proliferative activity in early breast cancer. Histopathology 43:573–582
38. Page DL, Ellis IO, Elston CW (1995) Histologic grading of breast cancer. Let's do it. Am J Clin Pathol 103:123–124
39. Patey DH, Scarff RW (1928) The position of histology in the prognosis of the breast. Lancet 1:801–804
40. Petit T, Wilt M, Velten M, Millon R, Rodier JF, Borel C, Mors R, Haegele P, Eber M, Ghnassia JP (2004) Comparative value of tumour grade, hormonal receptors, Ki-67, HER-2 and topoisomerase II alpha status as predictive markers in breast cancer patients with neoadjuvant anthracycline based chemotherapy. Eur J Cancer 40:205–211
41. Pinder SE, Murray S, Ellis IO, Trihia H, Elston CW, Gelber RD, Goldhirsch A, Lindtner J, Cortes-Funes H, Simoncini E, Byrne MJ, Golouh R, Rudenstam CM, Castiglione-Gertsch M, Gusterson BA (1998) The importance of histologic grade in invasive breast carcinoma and response to chemotherapy. Cancer 83:1529–1539
42. Pinder SE, Wencyk P, Sibbering DM, Bell JA, Elston CW, Nicholson R, Robertson JF, Blamey RW, Ellis IO (1995) Assessment of the new proliferation marker MIB-1 in breast carcinoma using image analysis: associations with other prognostic factors and survival. Br J Cancer 71:146–149
43. Powles TJ, Hickish TF, Makris A, Ashley SE, O'Brien ME, Tidy VA, Casey S, Nash AG, Sacks N, Cosgrove D et al (1995) Randomized trial of chemoendocrine therapy started before and after surgery for treatment of primary breast cancer. J Clin Oncol 13:547–552
44. Raabe NK, Schistad O, Sauer T, Bofin A, Kaaresen R, Fossaa SD (1997) Prognosis of radically operated breast carcinoma patients. A retrospective study of 167 consecutive patients with emphasis on histopathological grading, reproducibility and mean nuclear area. Acta Pathol Microbiol Immunol Scand APMIS 105:363–370
45. Robbins P, Pinder S, de Klerk N, Dawkins H, Harvey J, Sterrett G, Ellis I, Elston C (1995) Histological grading of breast carcinomas: a study of interobserver agreement. Human Pathol 26:873–879
46. Rudolph P, MacGrogan G, Bonichon F, Frahm SO, de Mascarel I, Trojani M, Durand M, Avril A, Coindre JM, Parwaresch R (1999) Prognostic significance of Ki-67 and topoisomerase II alpha expression in infiltrating ductal carcinoma of the breast. Breast Cancer Res Treat 55:61–71
47. Sediman JD, Schnaper LA, Aisner SC (1995) Relationship of the size of the invasive component of the primary breast carcinoma to axillary lymph node metastasis. Cancer 75:65–71
48. Sikka M, Agarwal S, Bhatia A (1999) Interobserver agreement of the Nottingham histologic grading scheme for infiltrating duct carcinoma breast. Indian J Cancer 36:149–153
49. Sinha PS, Bendall S, Bates T (2000) Does routine grading of invasive lobular cancer of the breast have the same prognostic significance as for ductal cancers? Eur J Surg Oncol 26:733–737

50. Spyratos F, Ferrero-Pous M, Trassard M, Hacene K, Phillips E, Tubiana-Hulin M, Le Doussal V (2002) Correlation between MIB-1 and other proliferation markers: clinical implications of the MIB-1 cutoff value. Cancer 94:2151–2159
51. Stenkvist B, Bengtsson E, Eriksson O, Jarkrans T, Nordin B, Westman-Naeser S (1982) Histopathological systems of breast classification: reproducibility and clinical significance. J Clin Pathol 36:392–398
52. Tavassoli FA, Devilee P (eds) (2003) World Health Organization classification of tumours. Pathology and genetics. Tumours of the breast and female genital organs. Chapter 1. IARC, Lyon, France, pp 9–112
53. Tawfik O, Davis MK, Clark J, Fan F, Damjanov I, Namiq A, Thomas P, Kimler BF (2006) A newly proposed semi-automated method of grading ductal carcinoma in situ of the breast. 19 (Suppl):43A (abstract 187)
54. Theissig F, Kunze KD, Haroske G, Meyer W (1990) Histological grading of breast cancer. Interobserver, reproducibility and prognostic significance. Pathol Res Pract 186:732–736
55. Tot T (2006) The limited prognostic value of measuring and grading small invasive breast carcinomas: the whole sick lobe versus the details within it. Med Sci Monit 12:RA170–RA175
56. Trihia H, Murray S, Price K, Gelber RD, Golouh R, Goldhirsch A, Coates AS, Collins J, Castiglione-Gertsch M, Gusterson BA, International Breast Cancer Study Group (2003) Ki-67 expression in breast carcinoma. Its association with grading systems, clinical parameters, and other prognostic factors—a surrogate marker? Cancer 97:1321–1331
57. Von Hansemann D (1892) Ueber die Anaplasie der Geschwulstzellen und die asymmetrische mitose. Virchows Arch Pathol Anat 129:436–449
58. Warnberg F, Nordgren H, Bergkvist L, Holmberg L (2001) Tumour markers in breast carcinoma correlate with grade rather than with invasiveness. Br J Cancer 85:869–874

Virchows Arch (2007) 450:637–642
DOI 10.1007/s00428-007-0421-8

ORIGINAL ARTICLE

GSTP1 promoter hypermethylation is an early event in breast carcinogenesis

Ji Shin Lee

Received: 24 January 2007 / Revised: 21 March 2007 / Accepted: 12 April 2007 / Published online: 4 May 2007
© Springer-Verlag 2007

Abstract Promoter hypermethylation in precursor lesions of the breast cancer may be biomarkers of cancer risk and targets for cancer chemoprevention. Pi-class glutathione-*S*-transferases (GSTP1) is inactivated by promoter hypermethylation in invasive breast cancers. However, little is known about epigenetic silencing of GSTP1 gene by promoter hypermethylation in precursor lesions. To determine the significance of GSTP1 promoter hypermethylation in breast carcinogenesis, methylation status of GSTP1 gene was studied by nested methylation-specific polymerase chain reaction, and GSTP1 expression was studied by immunohistochemistry in invasive ductal carcinoma (IDC), ductal carcinoma in situ (DCIS), usual ductal hyperplasia (UDH), and normal breast tissue. GSTP1 promoter hypermethylation was detected in 4/24 (16.7%) of UDH, 18/49 (36.7%) of DCIS, and 14/36 (38.9%) of IDC. No hypermethylation was detected in normal breast tissues. GSTP1 promoter hypermethylation was found to be progressively elevated during breast carcinogenesis ($p<0.01$). GSTP1 promoter hypermethylation was associated with loss of GSTP1 expression ($p<0.01$ for UDH, $p<0.001$ for DCIS and IDC). Our results suggest that GSTP1 promoter hypermethylation is an early event in breast carcinogenesis and appears to functionally silence GSTP1 expression. GSTP1 promoter hypermethylation in the precursor lesions of breast cancer may be used as a target for cancer chemoprevention.

Keywords Breast · Carcinogenesis · Methylation · GSTP1

Introduction

The currently favored working hypothesis of breast cancer evolves in a linear progression through sequential stages of hyperplastic benign breast lesions with or without cellular atypia, carcinoma in situ, and ultimately, invasive cancer [2, 7]. Molecular studies have shown that numerous genetic alterations found in invasive cancer are also found with increased frequency during progression in this proposed continuum [5, 16, 25]. Inactivation of tumor suppressor genes by promoter hypermethylation has been considered as a potentially important mechanism involved in the development of breast cancer. It is generally assumed that breast cancer develops in a stepwise manner from normal breast epithelium towards cancer by the accumulation of epigenetic alterations [24].

Glutathione-*S*-transferases (GST) are an enzyme family that can detoxify reactive chemical species by catalyzing their conjugation to reduced glutathione [6]. Among the isoenzymes, the role of pi-class GST (GSTP1) is involved in the metabolism, detoxification, and elimination of potentially genotoxic foreign compounds and, thus, acts to protect cells from DNA damage and cancer initiation [13]. Previous studies have shown that the CpG-rich promoter regions are methylated in several types of human cancers [4, 23, 26]. GSTP1 promoter hypermethylation is also associated with loss of GSTP1 expression, as measured by immunohistochemistry [4, 26]. Previous studies have

J. S. Lee
Department of Pathology, Chonnam National University Medical School and Research Institute of Medical Sciences, Gwangju 501-746, South Korea

J. S. Lee (✉)
Department of Pathology,
Chonnam National University Hwasun Hospital,
160, IIsim-ri, Hwasun-eup, Hwasun-gun,
Jeollanam-do 519-809, South Korea
e-mail: jshinlee@hanmail.net

already investigated the methylation status of GSTP1 in invasive breast cancer [1, 8, 11, 19, 21]. Promoter hypermethylation of GSTP1 is associated with a poor prognosis of breast cancer [1]. However, little is known about epigenetic silencing of GSTP1 gene by promoter hypermethylation in the precursors of breast cancer. Consequently, the significance of alterations in GSTP1 promoter hypermethylation status during multistage carcinogenesis of the breast is not fully understood. Cancer chemoprevention can be defined as the prevention of cancer or treatment of identifiable precursors [22]. If GSTP1 promoter hypermethylation occurs in precursor lesions, then this opens new avenues for cancer chemoprevention based on the inhibition or reversal of epigenetic alterations before the onset of invasive breast cancer. Moreover, the detection of promoter hypermethylation in precursor lesions at risk for progression to invasive cancer paves the way for the use of DNA methylation markers in risk assessment.

To elucidate the role of GSTP1 in breast carcinogenesis, we have investigated the promoter methylation status of GSTP1 in normal breast tissues, usual ductal hyperplasia (UDH), ductal carcinoma in situ (DCIS), and invasive ductal carcinoma (IDC). We have also studied the expression of GSTP1 protein by immunohistochemistry and compared its expression with GSTP1 methylation status.

Materials and method

Tissues

A total of 124 breast specimens, representing 15 normal breast tissues, 24 UDH, 49 DCIS, and 36 IDC, not otherwise specified, were selected from the files of the Department of Pathology, Chonnam National University Hospital, Gwangju, South Korea. We only selected stage I IDC to rule out complex genetic alterations relating to metastasis.

Nested methylation-specific PCR

For DNA extraction, one 5-μm tissue section was deparaffinized with xylene. On a mirror-imaged hematoxylin–eosin stained slide, the region of interest was manually scraped off to ensure a specific cell population of more than 80% in the preparation. The scraped tissue extracted in 27 μl TNES (10 mM Tris, pH 8.0, 150 mM NaCl, 2 mM EDTA, 1% SDS) containing 3 μl proteinase K for 4 h at 52°C. The tissue extract was heat inactivated at 99°C for 10 min and clarified by centrifugation at 13,000 rpm for 30 s. Supernatant (13.5 μl) was used directly as a source of DNA for sodium bisulfite treatment. DNA was heated 10 min to 99°C, quick chilled, and incubated with 1.5 μl of 2 mol/l NaOH for 30 min at 42°C. Freshly prepared 3.6 mol/l sodium bisulfite containing 1 mmol/l hydroquinone was mixed with DNA, then overlaid with oil, and incubated at 55°C for 5 h in the dark. The sample was desalted using ion exchange columns (Amersham, Piscataway, NJ, USA). DNA was precipitated with 200-μl absolute alcohol, washed with 70% ethanol, air dried, and resuspended in water (20 μl). Samples were stored at −80°C until use.

To facilitate methylation-specific PCR (MSP) analysis on DNA retrieved from formalin-fixed, paraffin-embedded tissue, the methylation status of GSTP1 was analyzed by a nested, two-step PCR approach, as described previously, with slight modifications [18]. Step 1 of the nested MSP was performed to amplify a 303-bp fragment of the GSTP1 gene with primer sets flanking the CpG-rich promoter region. Hence, these primers did not discriminate between methylated and unmethylated nucleotides after bisulfite treatment. The primer sequences for step 1 were 5′-ATT TGG GAA AGA GGG AAA GGT-3′ as the forward and 5′-ACT AAA AAC TCT AAA CCC CAT C-3′ as the reverse. Reactions were carried out using the following conditions: 95°C for 5 min; then 36 cycles at 95°C for 30 s, 56°C for 30 s, and 72°C for 40 s; and a final extension step at 72°C for 5 min. A negative control for the assay (water only) and unmethylated (human sperm DNA) and methylated controls (MDA-MB-231 cells) were included in step 1 reactions.

PCR products from step 1 reactions were diluted 1:5 in water and subjected to the second step of MSP, which incorporated one set of primers (labeled as unmethylated or methylated) that were designed to recognize bisulfite-induced modifications of unmethylated cytosines. The sense and antisense primers for the methylated GSTP1 sequence were 5′-TTC GGG GTG TAG CGG TCG TC-3′ and 5′-GCC CCA ATA CTA AAT CAC GAC G-3′, respectively. The sense and antisense primers for the unmethylated sequence were 5′-GAT GTT TGG GGT GTA GTG GTT GTT-3′and 5′-CCA CCC CAA TAC TAA ATC ACA ACA-3′, respectively. The PCR amplification protocol for step 2 was as follows: 95°C for 5 min, then denature at 95°C for 30 s, anneal at 60°C for 30 s, extension at 72°C for 40 s for 30 cycles followed by a 5-min final extension. Primer sequences used in the step 2 amplification were previously described [8].

The PCR products were resolved by electrophoresis in a 2% agarose gel, and the ethidium bromide-stained PCR products were imaged with the Eagle Eye II Video System (Stratagene, La Jolla, CA, USA). Any tumor sample that reliably yielded a PCR product in the methylated reaction visible by ethidium bromide staining was considered positive for promoter hypermethylation.

Immunohistochemistry

Immunohistochemical analysis of GSTP1 protein expression in matching tissue sections was performed by applying the avidin–biotin–peroxidase complex method. Sections were deparaffinized and then were placed in a microwave oven with a 2.1% citric acid buffer solution (pH 6.0) for 10 min to retrieve the antigens. After microwave processing, the sections were incubated overnight at 4°C with primary anti-GSTP1 antibody (1:100 dilution, clone GSTpi, Novocastra, Burlingame, CA, USA). The streptavidin–horseradish peroxidase (Research Genetics, Huntsville, AL, USA) detection system was then applied, followed by 30 min of incubation at room temperature. After washing, the tissue sections were developed with a peroxidase substrate solution (3,3-diaminobenzidine tetrahydrochloride). The sections were counterstained with hematoxylin, dehydrated, and mounted. For negative controls, sections were treated similarly with the exception of the primary antibody.

GSTP1 expression was considered to be positive when >10% of cells exhibited cytoplasmic or nuclear staining [12].

Statistical analysis

The χ^2 test was used for group comparison. For the statistical analysis, a two-sided value of $p<0.05$ was considered to indicate statistical significance. Data were analyzed using the SPSS software 11.5 for windows.

Results

Frequency of GSTP1 promoter hypermethylation

GSTP1 promoter hypermethylation was detected in 16.7% (4 of 24) of UDH, 36.7% (18 of 49) of DCIS, and 38.9% (14 of 36) of IDC samples. No hypermethylation was detected in normal breast tissues. Representative results of MSP assay are shown in Fig. 1. The frequency of GSTP1 promoter hypermethylation was found to be progressively increased along the continuum from normal breast tissue to IDC ($p<0.01$). DCIS and IDC showed statistically higher frequency of GSTP1 promoter methylation compared to normal breast tissues ($p<0.01$ and $p<0.01$, respectively). Although not statistically significant, the incidence of GSTP1 promoter hypermethylation was higher in high nuclear grade DCIS: 18.2% (2 of 11) for grade 1, 35.3% (6 of 17) for grade 2, and 47.6% (10 of 21) for grade 3.

We also determined the association of risk factors, such as age, tumor grade, and estrogen receptor status with GSTP1 promoter hypermethylation in IDC. None of the risk factors showed significant association with promoter hypermethylation of GSTP1 (data not shown).

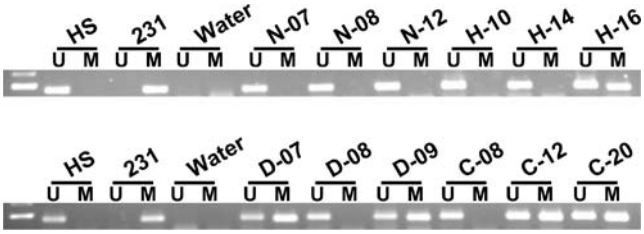

Fig. 1 Representative results of nested methylation-specific PCR analysis for GSTP1 in breast carcinogenesis. *Lanes U and M* correspond to unmethylated and methylated DNA, respectively. DNA from human sperm (*HS*) and MDA-MB-231 (*231*) breast cancer cell line served as negative and positive controls for methylated genes, respectively. Water served as negative control for both unmethylated and methylated genes. *N* normal breast case; *H* usual ductal hyperplasia case; *D* ductal carcinoma in situ case; *C* invasive ductal carcinoma case

Immunohistochemical analysis of GSTP1

To determine whether the GSTP1 promoter hypermethylation was correlated with the loss of GSTP1 expression, immunohistochemical staining using an anti-GSTP1 antibody was carried out on all samples that were subjected to methylation analysis in this study. Representative results of GSTP1 immunohistochemistry are shown in Fig. 2. In all of the 15 normal breast tissues, mammary epithelium including myoepithelial cells showed both nuclear and cytoplasmic immunoreactivity for GSTP1. GSTP1 was also detected in non-epithelial cells (e.g., stromal cells and inflammatory cells). Loss of GSTP1 expression (negative) was observed in 8.3% of UDH, 49.0% of DCIS, and 41.7% of IDC. Strong staining was found in non-neoplastic breast tissues of all samples with UDH, DCIS, and IDC. When the GSTP1 expression was compared against the methylation status of GSTP1, GSTP1 expression was more frequently lost in breast tissues with methylation ($p<0.01$ for UDH, $p<0.001$ for DCIS and IDC; Table 1).

Discussion

GSTP1 is known to play a role in detoxification of potential carcinogens [13]. Breast epithelial cells with lack the expression of GSTP1 is supposed to suffer from DNA damage more easily upon exposure to carcinogens. Loss of GSTP1 expression is observed in approximately two thirds of breast cancers, which indicates its potential role in breast carcinogenesis [1]. GSTP1 promoter hypermethylation appears likely to be responsible for absence of GSTP1 expression [4, 26]. Previous studies have described the significance of GSTP1 promoter hypermethylation in invasive breast cancer [1, 8, 11, 19, 21]. To determine when, in the breast carcinogenesis, promoter hypermethylation of the GSTP1 gene begins to play a role, we analyzed the

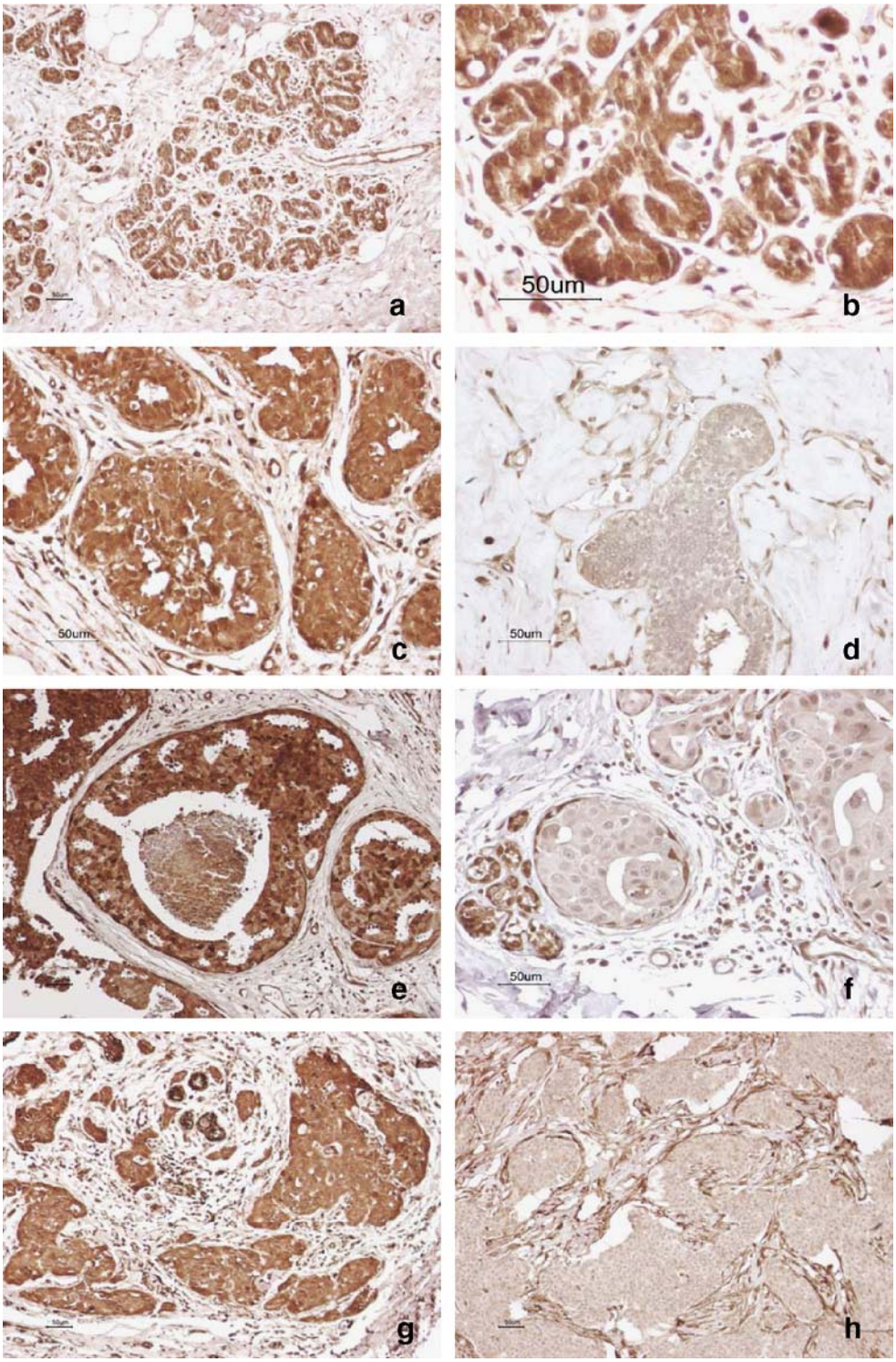

Fig. 2 Positive and negative immunohistochemical staining of GSTP1 in normal breast tissue, UDH, DCIS, and IDC. Normal breast tissues show strong, diffuse nuclear and cytoplasmic staining representing a positive expression of GSTP1 (**a** and **b**). UDH (**c**), DCIS (**e**), and IDC (**g**) show strong positivity in unmethylated cases. In methylated UDH (**d**), DCIS (**f**), and IDC (**h**), loss of GSTP1 expression is observed. Adjacent non-neoplastic breast tissues show strong GSTP1 expression

promoter hypermethylation of GSTP1 in invasive breast cancer as well as its precursor lesions. We found out that GSTP1 promoter hypermethylation is an early event in breast carcinogenesis.

The frequency of GSTP1 promoter hypermethylation in IDC (38.9%) was found to be higher than reported previously. The frequency given in other studies of breast cancer varied between 13 and 30% [1, 8, 11, 19, 21]. The higher detection rate in our study might be due to the nested MSP. A PCR-based approach called MSP can detect 1 copy of methylated DNA in 1,000 unmethylated copies of genomic DNA [10]. We used nested MSP. This method is very sensitive and can detect 1 methylated allele in >50,000 unmethylated alleles [18].

Table 1 GSTP1 expression in usual ductal hyperplasia, ductal carcinoma in situ, and invasive ductal carcinoma according to GSTP1 promoter hypermethylation

	Usual ductal hyperplasia			Ductal carcinoma in situ			Invasive ductal carcinoma		
	GSTP1 negative	GSTP1 positive	*p* value	GSTP1 negative	GSTP1 positive	*p* value	GSTP1 negative	GSTP1 positive	*p* value
GSTP1 unmethylated	0 (0%)	20 (100%)	<0.01	9 (29.0%)	22 (71.0%)	<0.001	4 (18.2%)	18 (81.8%)	<0.001
GSTP1 methylated	2 (50%)	2 (50%)		15 (83.3%)	3 (16.7%)		11 (78.6%)	3 (21.4%)	

Previous studies reported that GSTP1 promoter hypermethylation is associated with loss of GSTP1 protein expression, as measured by immunohistochemistry [1, 4, 26]. In this study, we have demonstrated a significant correlation between the promoter hypermethylation of GSTP1 and the data obtained from immunohistochemical analyses. Promoter hypermethylation of GSTP1 resulted in loss of GSTP1 protein expression in samples with methylation. These data provide evidence that GSTP1 promoter hypermethylation is a major mechanism involved in GSTP1 gene inactivation, resulting in impaired GSTP1 function during breast cancer development. While GSTP1 promoter hypermethylation status correlated well with GSTP1 expression, 21 cases of IDC and its precursors gave discordant data. The inconsistency between GSTP1 promoter hypermethylation and protein expression has been reported previously [1, 4, 8, 26]. Twenty-one cases can be divided into two groups: methylated and positive group (8 cases) and unmethylated and negative group (13 cases). The finding of GSTP1 hypermethylation in the fraction of IDC and its precursors that retained GSTP1 expression could be due to incomplete or low methylation. We used nested MSP. This is a very sensitive method, but it cannot distinguish high from low levels of promoter methylation. Using quantitative methylation analysis, Ogino et al. [17] found that tumors that show low levels of methylation in the gene promoters do not silence protein expression. GSTP1 unmethylated and negative group might be caused by mechanisms other than hypermethylation of GSTP1 promoter region. We concluded that GSTP1 is inactivated not only by promoter hypermethylation but also by other factors or mechanisms.

The potential reversibility of epigenetic states offers exciting opportunities for novel cancer drugs that can reactivate epigenetically silenced tumor suppressor genes. If epigenetic changes occur in precursor lesions of cancer, these changes may be targets for chemoprevention. GSTP1 detoxify carcinogens by conjugating them with glutathione. It is suggested that GSTP1 plays an important role in the prevention of the development of cancer upon exposure to carcinogens [13]. GSTP1 is a good candidate for cancer chemoprevention. To date, almost all of the studies on GSTP1 promoter hypermethylation have been analyzed in invasive breast cancer. To our knowledge, there are no data available about GSTP1 promoter hypermethylation in precursor lesions of breast cancer. In this study, promoter region of GSTP1 gene was methylated in 36.7% of DCIS and in 16.7% of UDH. However, GSTP1 promoter hypermethylation was not detected in normal breast tissues. Although not statistically significant, the incidence of GSTP1 promoter hypermethylation was higher in high nuclear grade DCIS. Loss of GSTP1 expression was observed in 49.0% of DCIS and in 17.7% of UDH. The data of GSTP1 immunohistochemistry in DCIS are consistent with previous report [3]. Promoter hypermethylation and loss of GSTP1 expression in DCIS and UDH provide opportunities for breast cancer prevention strategies including restoration of GSTP1 function via treatment with inhibition of promoter methylation.

Consistent with our results, previous studies reported the detection of promoter hypermethylation for other genes in tissue samples from precursor lesions of breast cancer [9, 14, 15]. The histologic appearance of precursor lesions is similar regardless of whether they progress or stabilize, suggesting that there may be morphologically silent molecular differences that result in progression, regression, or stabilization of these precursor lesions [2]. Promoter hypermethylation in precursor lesions can be used as a cancer risk marker. Promoter hypermethylation of p16, RUNX3, and HPP1 in Barrett's esophagus or low-grade dysplasia was independently associated with an increased risk of progression of Barrett's esophagus to high-grade dysplasia or esophageal adenocarcinoma [20]. It is presently unknown whether precursor lesions with GSTP1 promoter hypermethylation harbor an increased risk of malignant transformation. It would be interest to test in retrospective studies whether precursor lesions with and without promoter hypermethylation of GSTP1 may differ for the risk of developing invasive breast cancer.

In conclusion, we have shown that GSTP1 promoter hypermethylation occurred almost exclusively in IDC and its precursor lesions. GSTP1 promoter hypermethylation was found to be progressively elevated along the continuum from normal breast tissue to invasive breast cancer. GSTP1 promoter hypermethylation was associated with loss of

GSTP1 expression. Our results suggest that GSTP1 promoter hypermethylation is an early event in breast carcinogenesis and appears to functionally silence GSTP1 expression. GSTP1 promoter hypermethylation in the precursor lesions of breast cancer may be used as a target for cancer chemoprevention and a cancer risk marker.

References

1. Arai T, Miyoshi Y, Kim SJ, Taguchi T, Tamaki Y, Noguchi S (2006) Association of GSTP1 CpG islands hypermethylation with poor prognosis in human breast cancers. Breast Cancer Res Treat 100:169–176
2. Arpino G, Laucirica R, Elledge RM (2005) Premalignant and in situ breast disease: biology and clinical implications. Ann Intern Med 43:446–457
3. Bellamy CO, Harrison DJ (1994) Evaluation of glutathione *S*-transferase pi in non-invasive ductal carcinoma of breast. Br J Cancer 69:183–185
4. Chan QK, Khoo US, Chan KY, Ngan HY, Li SS, Chiu PM, Man LS, Ip PP, Xue WC, Cheung AN (2005) Promoter methylation and differential expression of pi-class glutathione *S*-transferase in endometrial carcinoma. J Mol Diagn 7:8–16
5. Cho MH, Yoon JH, Jaegal YJ, Choi YD, Lee JS, Lee JH, Nam JH, Choi C, Lee MC, Park CS, Juhng SW, Min KW (2006) Expression of cyclooxygenase-2 in breast carcinogenesis and its relation to HER-2/neu and p53 protein expression in invasive ductal carcinoma. Breast 15:390–398
6. Coles BF, Kadlubar FF (2003) Detoxification of electrophilic compounds by glutathione *S*-transferase catalysis: determinants of individual response to chemical carcinogens and chemotherapeutic drugs? Biofactors 17:115–130
7. Dupont WD, Page DL (1985) Risk factors for breast cancer in women with proliferative breast disease. N Engl J Med 312:146–151
8. Esteller M, Corn PG, Urena JM, Gabrielson E, Baylin SB, Herman JG (1998) Inactivation of glutathione *S*-transferase P1 gene by promoter hypermethylation in human neoplasia. Cancer Res 58:4515–4518
9. Fackler MJ, McVeigh M, Evron E, Garrett E, Mehrotra J, Polyak K, Sukumar S, Argani P (2003) DNA methylation of RASSF1A, HIN-1, RAR-beta, cyclin D2 and twist in in situ and invasive lobular breast carcinoma. Int J Cancer 107:970–975
10. Herman JG, Graff JR, Myohanen S, Nelkin BD, Baylin SB (1996) Methylation-specific PCR: a novel PCR assay for methylation status of CpG islands. Proc Natl Acad Sci USA 93:9821–9826
11. Hoque MO, Feng Q, Toure P, Dem A, Critchlow CW, Hawes SE, Wood T, Jeronimo C, Rosenbaum E, Stern J, Yu M, Trink B, Kiviat NB, Sidransky D (2006) Detection of aberrant methylation of four genes in plasma DNA for the detection of breast cancer. J Clin Oncol 24:4262–4269
12. Huang J, Tan PH, Thiyagarajan J, Bay BH (2003) Prognostic significance of glutathione *S*-transferase-pi in invasive breast cancer. Mod Path 16:558–565
13. Lee WH, Morton RA, Epstein JI, Brooks JD, Campbell PA, Bova GS, Hsieh WS, Isaacs WB, Nelson WG (1994) Cytidine methylation of regulatory sequences near the pi-class glutathione *S*-transferase gene accompanies human prostatic carcinogenesis. Proc Natl Acad Sci USA 91:11733–11737
14. Lehmann U, Langer F, Feist H, Glockner S, Hasemeier B, Kreipe H (2002) Quantitative assessment of promoter hypermethylation during breast cancer development. Am J Pathol 160:605–612
15. Lo PK, Mehrotra J, D'Costa A, Fackler MJ, Garrett-Mayer E, Argani P, Sukumar S (2006) Epigenetic suppression of secreted frizzled related protein 1 (SFRP1) expression in human breast cancer. Cancer Biol Ther 5:281–286
16. O'Connell P, Pekkel V, Fuqua SA, Osborne CK, Clark GM, Allred DC (1998) Analysis of loss of heterozygosity in 399 premalignant breast lesions at 15 genetic loci. J Natl Cancer Inst 90:697–703
17. Ogino S, Kawasaki T, Brahmandam M, Cantor M, Kirkner GJ, Spiegelman D, Makrigiorgos GM, Weisenberger DJ, Laird PW, Loda M, Fuchs CS (2006) Precision and performance characteristics of bisulfite conversion and real-time PCR (MethyLight) for quantitative DNA methylation analysis. J Mol Diagn 8:209–217
18. Palmisano WA, Divine KK, Saccomanno G, Gilliland FD, Baylin SB, Herman JG, Belinsky SA (2000) Predicting lung cancer by detecting aberrant promoter methylation in sputum. Cancer Res 60:5954–5958
19. Parrella P, Poeta ML, Gallo AP, Prencipe M, Scintu M, Apicella A, Rossiello R, Liguoro G, Seripa D, Gravina C, Rabitti C, Rinaldi M, Nicol T, Tommasi S, Paradiso A, Schittulli F, Altomare V, Fazio VM (2004) Nonrandom distribution of aberrant promoter methylation of cancer-related genes in sporadic breast tumors. Clin Cancer Res 10:5349–5354
20. Schulmann K, Sterian A, Berki A, Yin J, Sato F, Xu Y, Olaru A, Wang S, Mori Y, Deacu E, Hamilton J, Kan T, Krasna MJ, Beer DG, Pepe MS, Abraham JM, Feng Z, Schmiegel W, Greenwald BD, Meltzer SJ (2005) Inactivation of p16, RUNX3, and HPP1 occurs early in Barrett's-associated neoplastic progression and predicts progression risk. Oncogene 24:4138–4148
21. Shinozaki M, Hoon DS, Giuliano AE, Hansen NM, Wang HJ, Turner R, Taback B (2005) Distinct hypermethylation profile of primary breast cancer is associated with sentinel lymph node metastasis. Clin Cancer Res 11:2156–2162
22. Steele VE, Kelloff GJ (2005) Development of cancer chemopreventive drugs based on mechanistic approaches. Mutat Res 591:16–23
23. Tokumaru Y, Harden SV, Sun DI, Yamashita K, Epstein JI, Sidransky D (2004) Optimal use of a panel of methylation markers with GSTP1 hypermethylation in the diagnosis of prostate adenocarcinoma. Clin Cancer Res 10:5518–5522
24. Widschwendter M, Jones PA (2002) DNA methylation and breast carcinogenesis. Oncogene 21:5462–5482
25. Yang C, Trent S, Ionescu-Tiba V, Lan L, Shioda T, Sgroi D, Schmidt EV (2006) Identification of cyclin D1- and estrogen-regulated genes contributing to breast carcinogenesis and progression. Cancer Res 66:11649–11658
26. Zhong S, Tang MW, Yeo W, Liu C, Lo YM, Johnson PJ (2002) Silencing of GSTP1 gene by CpG island DNA hypermethylation in HBV-associated hepatocellular carcinomas. Clin Cancer Res 8:1087–1092

Virchows Arch (2007) 450:643–652
DOI 10.1007/s00428-007-0414-7

ORIGINAL ARTICLE

Pulmonary vascular changes in piglets with increased pulmonary blood flow and pressure

Matthias Gorenflo · Esther Herpel · Michael V. Ullmann · Karoline Röhlig · Sueha Demirakca · Homa Klimpel · Siegfried Hagl · Martha Maria Gebhard · Philipp A. Schnabel

Received: 2 October 2006 / Revised: 26 February 2007 / Accepted: 26 March 2007 / Published online: 21 April 2007
© Springer-Verlag 2007

Abstract In this model of pulmonary vascular disease, high pulmonary blood flow was created by an anastomosis between the left subclavian artery and the main pulmonary artery [Blalock–Taussig (BT) shunt] in 4-week-old piglets (n=6). Additional ligation of the left pulmonary artery (LPA) was used to increase pulmonary artery pressure (n=6). Seven piglets were sham-operated. After 3 months, mean pulmonary artery pressure was higher in animals with BT shunt and LPA ligation (22±5; mean±SD) compared to sham-operated animals (15±2). In addition, thickening of the medial coat (20.1±2.8% versus 13.6±3.1% wall thickness) and increased immunostaining for vascular endothelial growth factor A (VEGF-A) were observed. Relative gene expression for endothelin-converting enzyme-1 (ECE-1) mRNA was 1.8 times higher, and VEGF-A mRNA was 2.5 times higher in pigs with BT shunt and LPA ligation compared with sham-operated animals. VEGF receptor-1 and VEGF receptor-2 mRNA was lower in shunted animals and in animals with additional ligation of LPA. Upregulation of ECE-1 and VEGF-A, as well as changes in VEGFR expression in the pulmonary hypertensive lung, may contribute to pulmonary vascular changes.

Keywords Lung · Hypertension · Pulmonary · Morphology

M. Gorenflo and E. Herpel equally contributed to this work and are both first authors of this manuscript.

M. Gorenflo (✉) · K. Röhlig · H. Klimpel
Department of Pediatric Cardiology, University Medical Centre,
University of Heidelberg,
Im Neuenheimer Feld 153,
69120 Heidelberg, Germany
e-mail: Matthias.Gorenflo@med.uni-heidelberg.de

E. Herpel · P. A. Schnabel
Department of Pathology, University Medical Center,
University of Heidelberg,
Im Neuenheimer Feld 220,
69120 Heidelberg, Germany

M. V. Ullmann · S. Hagl
Department of Cardiac Surgery, University Medical Center,
University of Heidelberg,
Im Neuenheimer Feld 110,
69120 Heidelberg, Germany

S. Demirakca
Pediatric Intensive Care and Pediatric Pulmonology,
University Children's Hospital,
Theodor-Kutzer Ufer 1–3,
68167 Mannheim, Germany

M. M. Gebhard
Department of Experimental Surgery, University Medical Center,
University of Heidelberg,
Im Neuenheimer Feld 365,
69120 Heidelberg, Germany

Introduction

Pulmonary hypertension associated with left-to-right shunt in congenital heart disease is associated with functional and morphological alterations of the pulmonary vasculature [4, 16]. The pathological changes in humans are characterized by medial hypertrophy and intimal proliferation finally leading to plexiform lesions and obliterative intimal fibrosis [14]. Both impaired endogenous nitric oxide synthesis [4] and an increase in pulmonary endothelin-1 (ET-1) [11] have been associated with pulmonary vascular changes in humans. Vascular endothelial growth factor A (VEGF-A) was the first known member of a family of VEGFs, including VEGF-B, -C and -D. VEGF-A acts as a growth factor for endothelial cells [34]. VEGF-A binds to VEGF receptor 1 (VEGFR-1) and 2 (VEGFR-2). In endothelial

cells, VEGF-A ligand binding to VEGFR-2 leads to upregulated expression of endothelial nitric oxide synthase (eNOS) and to increased prostacyclin production. VEGFR-1 enhances VEGF-induced VEGFR-2 signaling in several pathological conditions [3]. VEGF-A is strongly expressed in angioproliferative lesions from patients with severe primary idiopathic and secondary forms of pulmonary hypertension [10, 17]. VEGF-C and VEGF-D have been identified as lymphangiogenic growth factors [22]. During development, VEGF-C and its receptor VEGFR-3 are localized primarily to regions of lymphatic vessels, and recent data from human preterm infants showed that VEGF-C and VEGFR-3 play an important role in the physiologic development of the lymphatic system of the lung [21].

Animal models with left-to-right shunt have been established in lambs [1] and piglets [9, 27]. Experimental data suggest that high pulmonary blood pressure, but not high pulmonary blood flow, is responsible for an increase in pulmonary ET-1 synthesis [6]. The data concerning the effect of high pulmonary blood flow on pulmonary nitric oxide production in the human are controversial [20, 32]. We therefore modified our animal model of high pulmonary blood flow [33] consisting of an anastomosis between the left subclavian artery and the main pulmonary artery (left-sided Blalock–Taussig (3T) shunt) by additional ligation of the left pulmonary artery to induce high pulmonary arterial blood pressure. We aimed to study the effect of high pulmonary blood flow and pressure on morphology of pulmonary blood vessels by histomorphometry and immunostaining for eNOS, ET-1 and VEGF-A, VEGF-C and VEGFR-1, and VEGFR-2. In addition, we analyzed the expression of VEGF-A and VEGFR-1 and VEGFR-2 mRNA in lung tissue. We further asked whether high pulmonary blood flow and pressure would lead to alterations in lung lymphatic vessels assessed by immunostaining for podoplanin, VEGF-C, and VEGFR-3.

Materials and methods

The investigation conforms to the "Guide for the Care and Use of Laboratory Animals" published by the US National Institutes of Health (NIH Publication No. 85-23, revised 1996) and was approved by the local authorities (Regierungspräsidium Karlsruhe, approval no. 35-9185.81/G-5/03, 04-02-2003).

Surgical procedure

Nineteen domestic farm piglets (German Landrace) 4 weeks of age and with a body weight of 12 kg [10–16] [median (range)] were used. The piglets were intubated and ventilated with a respirator (Servo Ventilator 900C, Siemens-Elema, Umea, Sweden) using tidal volumes of 10 to 15 ml/kg and a respiratory rate of 12 to 15 breaths per minute. General anesthesia was induced and maintained with isoflurane 1%. After left thoracotomy, the left subclavian artery was connected to the main pulmonary artery [Blalock–Taussig (BT) shunt]. The animals were then randomized to three groups:

- Sham operation ($n=7$) with immediate ligation of the shunt
- BT shunt ($n=6$)
- BT shunt with additional ligation of the left pulmonary artery (LPA; $n=6$).

Shunt flow was determined by transit time ultrasound measurement using perivascular flow probes of 4 mm in size, with a flow accuracy of ±2%, resolution of 0.2 ml/min, and a frequency of 2.4 MHz (Transonic Flowprobes R-Serie, Transonic Systems, Ithaca, NY, USA).

Hemodynamic evaluation

At the initial operation the right and left atrium, the main pulmonary artery and the descending aorta were cannulated for measurement of blood pressure and oxygen saturation. Pulmonary and systemic blood flow was determined according to the Fick principle with oxymetry and measured oxygen uptake (Deltatrac II, Datex Ohmeda, Düsseldorf, Germany). Pulmonary (PVR) and systemic (SVR) vascular resistance were calculated according to standard formula [35].

After 3 months, the animals underwent cardiac catheterization using the same protocol for anesthesia as mentioned above. Blood specimens were drawn for repeat measurements of plasma ET-1, guanosine-3′,5′-cyclic monophosphate (cGMP), and nitrite/nitrate. Quantification of left-to-right shunt was determined by oxymetry using standard formula [35]. Aortic angiography was performed in each case to ascertain patency or ligation of the shunt. Animals were killed thereafter. Tissue specimens of right lung were snap-frozen for biochemical measurements. In addition, lung tissue was fixed in 4% formalin for histological, immunohistochemical, and histomorphometric analyses.

Histomorphometry

Pulmonary arteries were measured planimetrically. The accompanying airway, the diameter of pulmonary arteries, and the percent medial thickness were determined as previously described [13]. Several slides were examined from the right upper and lower lung lobe. For each animal, more than 100 arteries between 50 and 150 μm thus could be obtained.

Immunohistochemistry

For immunohistochemical staining, the streptavidin-biotin peroxidase method was used [5]. Paraffin-embedded sections were cut on a microtome at 3-μm thickness. Sections of left and right lung were collected on the same slide. Slides were deparaffinized in a graded series of ethanol (100, 90, 70%) and preincubated with a citrate buffer pH=6 (Target Retrieval Solution, DAKO, Glostrup, Denmark), for 30 min at 96°C and afterwards washed with Tris-buffered saline (TBS). After preincubation, the mouse anti-eNOS monoclonal antibody (dilution=1:100; Transduction Laboratories, Lexington, KY, USA) in antibody diluent (DAKO) was added and incubated for 30 min at room temperature. Likewise, anti-ET-1 (1:100; SM5063 TRET 48.5, Acris Antibodies, Hamburg, Germany), anti-VEGF-A (1:100; A-20 sc-152, Santa Cruz Biotechnology, Santa Cruz, CA, USA), anti-VEGF-C (1:100; sc-25783, Santa Cruz Biotechnology), anti VEGFR-1 (1:100, sc-316, Santa Cruz Biotechnology), anti VEGFR-2 (1:50, sc-504, Santa Cruz Biotechnology), anti-VEGFR-3 (1:100, DP135, Acris Antibodies), and anti-podoplanin (1:50, 18H5, Acris Antibodies) were added. To detect bound antibodies, the slides were washed in TBS and then incubated for 30 min with the secondary antibody, (DAKO, ChemMate detection kit AB2), and afterwards washed in TBS. Next, streptavidin conjugated to horseradish peroxidase in a protein-buffered solution was applied (ChemMate streptavidin peroxidase HRP, DAKO). After this, the endogenous peroxidase was blocked using ChemMate peroxidase-blocking solution (DAKO). After blocking and washing in TBS, the peroxidase/AEC reactivity was developed using the ChemMate AEC/H_2O_2 (DAKO) substrate solution. Finally, the slides were washed in aqua destillata, counterstained with hematoxylin (DAKO), and coverslipped with Aquatex (Merck, Darmstadt, Germany). As negative control, the isotype negative control from DAKO was used. For rabbit polyclonal antibodies, we used preimmune rabbit serum as negative control.

Pulmonary arteries staining with eNOS, ET-1, and VEGF were rated upon the following grading criteria: grade 0, no staining; grade 1, weak staining in <50% of cells; grade 2, weak staining in >50% of cells or strong staining in <10% of cells; grade 3, strong staining in 10–50% of cells; grade 4, strong staining in >50% of cells; grade 5, strong staining in 100% of cells [23].

Real-time RT-PCR

Real-time reverse transcriptase polymerase chain reaction (RT-RT-PCR) for quantification of ET-1, endothelin-converting enzyme-1 (ECE-1), endothelin A (ET_A), and endothelin B (ET_B) receptor, eNOS and VEGF mRNA in pig lung tissue was performed as previously described [19]. We verified that quantitative mRNA for ET-1 and VEGF-A did not differ between right upper and lower lung lobe (Gorenflo M, unpublished data), and therefore, RT-RT-PCR was performed using tissue from the right upper lobe: RNA was isolated using Tri Reagent (Sigma, Munich, Germany), checked for integrity on an agarose gel, and quantified photometrically. One microgram of total RNA was reverse-transcribed using oligo(dT)/random hexamer primers (10:1). RT-RT-PCR was performed using the Abi Prism 7000 Real Time PCR system (Applied Biosystems, Darmstadt, Germany) with specific primers for 18S (see Table 1) and Universal Mastermix (also Applied Biosystems) with SYBR green to detect PCR products at the end of each amplification step. Serial dilutions of an arbitrary cDNA pool were used to establish a standard curve. Relative quantities of RNA levels were determined, accounting for amplification efficacy using the software provided with the PCR system. mRNA levels were normalized to corresponding 18S quantities determined within the same run. (RT-) RNA controls, in which the cDNA synthesis step was omitted, and controls without template did not show a detectable amplification product.

Determination of plasma L-arginine, cGMP, nitrite/nitrate, and ET-1

Blood samples from the aorta were taken at baseline and collected in cooled Na+ and ethylenediamine tetraacetic acid (for cGMP and ET-1) and Li-Heparin—tubes (for nitrite/nitrate) which were immediately placed on ice and centrifuged at 2,000×*g* (15 min, +4°C). The plasma was separated and stored at −80°C.

Plasma cGMP was measured by radioimmunoassay using a kit from Immunotech SA (Marseille, France) as previously described [15]. Plasma ET-1 was determined by radioimmunoassay using a kit purchased from GE Health Sciences (Freiburg, Germany). Plasma nitrite/nitrate was measured with a modified Griess reaction using a kit from Assay Design (Ann Arbor, MI, USA) as previously described [15].

Statistics

Specific software (Sigmastat for Windows®, Version 3.00, SPSS, Chicago, USA) was used for statistical analysis. Data are given as mean±SD. One-way analysis of variance with subsequent pairwise multiple comparison procedures (Holm's Sidak) were used to analyze whether morphometric, immunohistochemical, hemodynamic, and biochemical measurements were different between groups. Probability (*P*) of <0.05 was considered statistically significant.

Table 1 Primers fo RT-RT-PCR

Gene	
HPRT pig forward	5′-TCA GGC AGT ATA ATC CAA AGA TGG T-3′
HPRT pig reverse	5′-AGT CTG GCT TAT ATC CAA CAC TTC G-3′
ECE-1 pig forward	5′-TGG GGG ACC TTC AGC AAC CT–3′
ECE-1 pig reverse	5′-GGG TGT CCT GGA AGT TGT CCT TG-3′
VEGF-A pig forward	5′-TAC CTC CAC CAT GCA AGT GG-3′
VEGF-A pig reverse	5′-GTA GCT GCG CTG GTA GAC GTC-3′
VEGFR-1 pig forward	5′-CCG GAA ATC TAT CAG ATC ATG TTG-3′
VEGFR-1 pig reverse	5′-TTG CCG TCC TGT TGT ACA TTG-3
VEGFR-2 pig forward	5′-ACA TGG AGT CGT GTA CAT CAC TGA-3′
VEGFR-2 pig reverse	5′-TCT GGA TAC CTC GCA CAA AGG-3′
ET-1 pig forward	5′-TGC TCC TGC TCT TCC CTG AT-3′
ET-1 pig reverse	5′-TTC CAA GTC CGT ATG GGA CAA T-3′
Endothelin A receptor pig forward	5′-TTT ATC CTG GCC ATC CCT GA-3′
Endothelin A receptor pig reverse	5′-GCT CTT CGC CCT TGT ATT CAA-3′
Endothelin B receptor pig forward	5′-CCC CTT CAT CTC AGC AGG ATT-3′
Endothelin B receptor pig reverse	5′-GCA CCA GCA GCA TAA GCA TG-3′
eNOS pig forward	5′-CTC TCC TGT TGG CCT GAC CA-3′
eNOS pig reverse	5′-CCG GTT ACT CAG ACC CAA GG-3′
18S pig forward	5′-CGC CGC TAG AGG TGA AAT TC-3′
18S pig reverse	5′-CGA ACC TCC GAC TTT CGT TCT-3′

Results

Hemodynamic evaluation

At baseline, hemodynamic parameters did not differ between groups (Table 2). The flow across the BT shunt was highest in animals with BT shunt alone. Additional ligation of the LPA resulted in a decrease in flow across the BT shunt, but the difference did not reach statistical significance ($p = 0.07$; Fig. 1). In sham-operated animals, we could rule out residual flow across the ligated BT shunt.

At cardiac catheterization after 3 months, mean PAP and PVR were significantly higher in pigs with BT shunt and LPA ligation (Table 3). The ratio of pulmonary to systemic blood pressure (Pp/Ps) was significantly higher in animals with BT shunt ($p = 0.025$) and in animals with BT shunt and additional LPA ligation ($p = 0.017$) compared with sham-operated animals. The ratio of pulmonary to systemic blood flow (Qp/Qs) was slightly but not significantly higher in the animals with BT shunt alone compared to the group of animals with BT shunt and LPA ligation ($p = 0.64$; Table 3). Cardiac index was lower in the animals with BT shunt and LPA ligation compared to animals with BT shunt alone, but this difference did not reach statistical significance ($p = 0.422$; Table 3).

Morphometry

In shunted animals, we observed pulmonary vascular changes with thickening of the medial coat. We did not observe advanced vascular lesions such as intimal fibrosis or plexiform lesions in this series. Wall thickness of pulmonary arteries with a diameter of 50–150 μm was higher in the group with BT shunt than in sham-operated animals ($p = 0.026$), but highest values were measured in the group of animals with additional ligation of the LPA ($p = 0.003$ versus sham; Fig. 2).

Table 2 Hemodynamic variables at baseline (mean±SD)

Hemodynamic variable	Sham (n=7)	BT shunt (n=6)	BT shunt + LPA ligation (n=6)	p value versus sham
Mean PAP (mmHg)	15±2	16±3	15±2	0.28
Mean SAP (mmHg)	64±12	59±14	57±8	0.44
PVR [(dyne × s × cm^{-5}) × m^2]	130±30	135±33	141±31	0.78
SVR [(dyne × s × cm^{-5}) × m^2]	984±191	800±164	841±81	0.09
Cardiac index [l/(min × m^2)]	5.0±0.5	5.4±0.7	4.9±0.9	0.47

PAP Pulmonary arterial pressure, *SAP* systemic arterial pressure, *PVR* pulmonary vascular resistance, *SVR* systemic vascular resistance

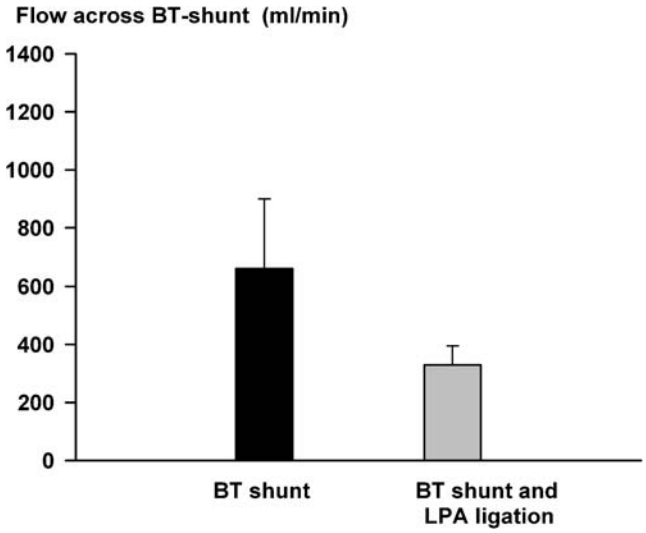

Fig. 1 Flow across the BT shunt (ml/min) in the group with BT shunt alone versus the group with BT shunt and additional ligation of the LPA (p=0.07)

Immunohistochemistry

Semi-quantitative grading of ET-1 protein expression (by immunostaining) in pulmonary arteries was not different between groups (Fig. 3). Protein expression of eNOS was higher in animals with BT shunt (p=0.048) and in animals with BT shunt and additional ligation of the LPA (0.013) compared with sham-operated animals (Fig. 3).

Animals with BT shunt alone (p=0.014) and animals with BT shunt and additional LPA ligation (p=0.014) showed higher protein expression for VEGF-A compared with sham-operated animals (Figs. 3 and 4). The VEGFR-1 protein expression was weak and did not differ between groups (Fig. 5). VEGFR-2 protein expression was slightly higher in animals with BT shunt, but this difference did not reach statistical significance. Protein expression for VEGFR-3 and VEGF-C was weak and did not differ between groups.

Pulmonary lymphatic vessels could be immunostained with podoplanin antibody. However, protein expression was scarce both in the controls as in the shunted animals. In addition, there was no indication for a significant morphological change in lymphatic vessel diameter (Figs. 3 and 6).

Metabolites of the L-arginine NO pathway and ET-1

There were no significant changes for plasma ET-1 and cGMP between groups (Table 4). Plasma nitrite/nitrate was significantly higher in animals with BT shunt compared with sham-operated animals (p=0.025). Plasma nitrite/nitrate was significantly higher in animals with BT shunt and ligation of the LPA compared with animals with BT shunt alone (p=0.01).

Real-time RT-PCR

In lung tissue from the right upper lobe, quantitative mRNA for ET-1 was highest in shunted piglets, but this difference did not reach statistical significance (p=0.087). Quantitative mRNA for ET_A-receptor and ET_B-receptor and eNOS did not differ significantly between groups (Fig. 7). Quantitative mRNA content for ECE-1 was significantly higher in piglets with BT shunt and ligation of LPA compared with sham-operated animals (p=0.011; Fig. 7). VEGF-A mRNA was higher in animals with BT shunt alone compared to sham-operated animals, but in multiple comparisons, this difference did not reach statistical significance (p=0.05). Quantitative mRNA content for VEGF-A was significantly higher in piglets with BT shunt and ligation of LPA compared with animals with BT shunt alone (p=0.017) and sham-operated animals (p<0.001; Fig. 7). VEGFR-1 mRNA was lower both in animals with BT shunt and in animals with BT shunt and additional ligation of LPA. VEGFR-2 mRNA was considerably lower in animals with

Table 3 Hemodynamic findings after 3 months at cardiac catheterization (mean±SD)

Hemodynamic variable	Sham (n=7)	Shunt	
		BT shunt (n=6)	BT shunt + LPA ligation (n=6)
Mean PAP (mmHg)	15±2	18±2	22±5***·**
Mean SAP (mmHg)	64±5	58±12	59±6
Pp/Ps	0.24±0.03	0.33±0.07*	0.38±0.08**
Qp/Qs	1.0	1.9±0.8*	1.8±0.7**
PVR [(dyne × s × cm^{-5}) × m^2]	121±45	116±41	191±51**
Rp/Rs	0.18±0.04	0.16±0.08	0.21±0.05
Cardiac index [l/(min × m^2)]	5.8±0.6	5.6±1.0	5.1±1.4

*p<0.05 sham versus BT shunt
**p<0.05 sham versus BT shunt + LPA ligation
***p<0.05 BT shunt versus BT shunt + LPA ligation
PAP Pulmonary arterial pressure, *SAP* systemic arterial pressure, *Pp/Ps* ratio of pulmonary to systemic arterial pressure, *PVR* pulmonary vascular resistance, *Rp/Rs* ratio of pulmonary to systemic vascular resistance

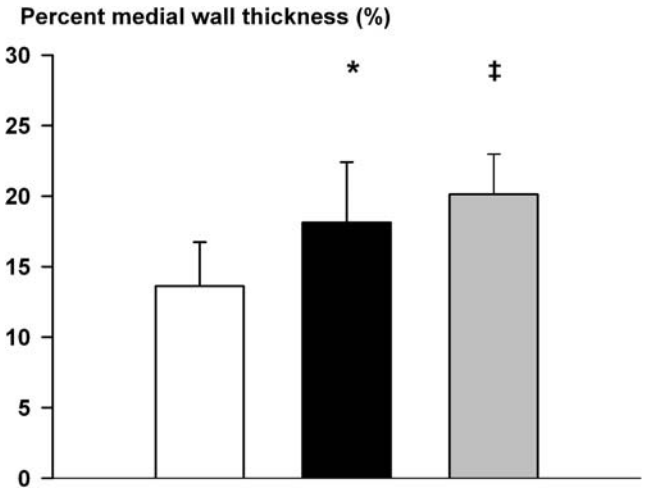

Fig. 2 Percent medial wall thickness of pulmonary arteries (*D*, 50–150 μm) as measured planimetrically (mean±SD). *$p<0.05$ sham versus BT Shunt; ‡$p<0.05$ sham versus BT shunt + LPA ligation

BT shunt (relative gene expression, 0.11±0.05) compared with sham-operated animals. VEGFR-2 mRNA was virtually absent in animals with BT shunt and ligation of LPA (relative gene expression, 0.04±0.01) compared with sham-operated animals ($p<0.001$).

Discussion

This study demonstrates that increases in pulmonary blood flow and pulmonary arterial pressure exert different effects on morphology of pulmonary vasculature and on metabolites and mRNA of the pulmonary nitric oxide and ET-1 synthesis.

In this study, pig lung tissue was examined at 4 months of age after 3 months of chronic pulmonary hyperperfusion. At this age, there was no indication for an upregulation of eNOS gene expression in piglets with increased pulmonary blood flow and pulmonary hypertension, which is consistent with others [7, 28]. eNOS protein expression was increased in shunted animals in this series, but this was not related to an increase in eNOS gene expression. Others have shown that eNOS protein does not differ in shunted piglets compared to controls [9, 27]. The discrepancy may be explained by differences in age of the animals at the operation for BT shunt, as in other species, eNOS gene expression, eNOS protein, and eNOS activity have been shown to be time-dependent [1, 2]. The additional increase in pulmonary arterial pressure by ligation of the left pulmonary artery did not influence gene expression and protein expression for eNOS compared with shunted animals alone in this series. However, the increase in final NO products (nitrate/nitrite) in plasma in this group cannot be interpreted as the result of an increased NO production by the pulmonary vasculature. Fernandez-Mondéjar et al. [8] have shown that exhaled NO increases considerably from lung regions with occluded vessels. Therefore, the increase in stable end products of NO in plasma in shunted animals with additional ligation of the left pulmonary artery are rather an effect of chronic ligation of the left pulmonary

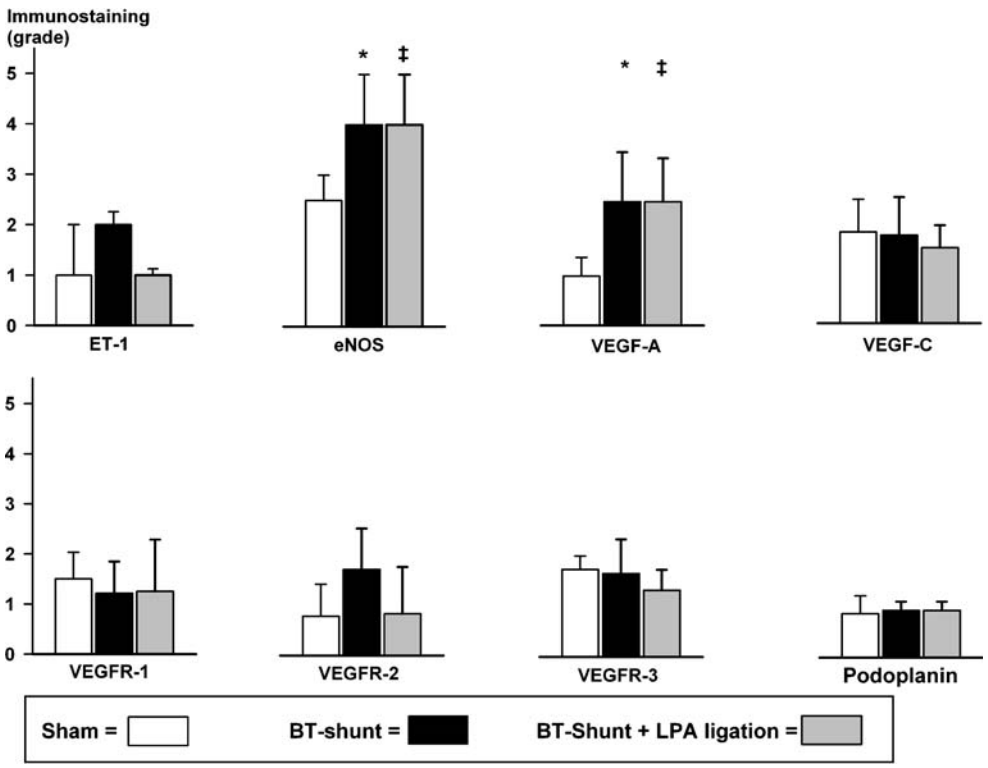

Fig. 3 Semiquantitative immunostaining for ET-1, eNOS, VEGF-A, VEGF-C, VEGFR-1, -2 and -3 and podoplanin (mean±SD). *$p<0.05$ sham versus BT shunt; ‡$p<0.05$ sham versus BT shunt + LPA ligation

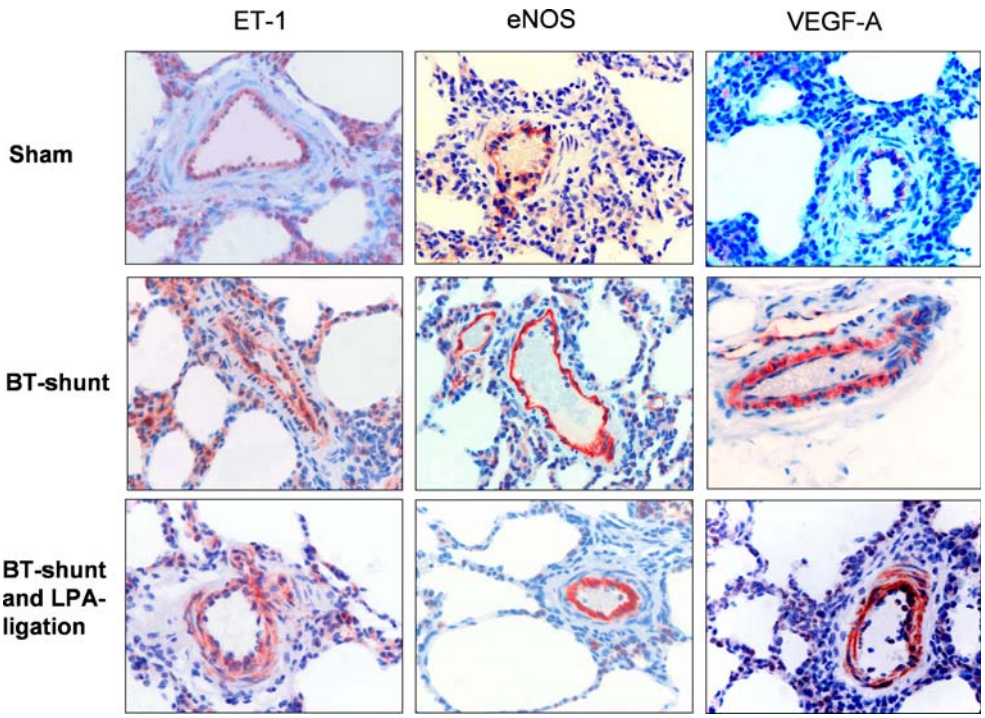

Fig. 4 Immunostaining for ET-1, eNOS, and VEGF-A in lung tissue (×40)

artery than of increased pulmonary blood flow and pressure to the right lung. The fact that neither eNOS mRNA nor immunohistochemical expression of eNOS changed significantly in the right lung of piglets after BT shunt and ligation of the LPA (compared to BT shunt alone) supports this view.

The pulmonary ET system was affected differently by high pulmonary blood flow and high pulmonary arterial blood pressure in this series. Plasma levels of ET-1 were not different in both groups compared with sham-operated animals in this series. Stenbøg et al. [30] did not find a difference in plasma ET-1 in piglets with aorto-pulmonary shunt alone, which is consistent with our data. ET-1 protein expression and ET-1 gene expression were higher in piglets with increased pulmonary blood flow, but the difference did not reach statistical significance. More important, an increase in pulmonary arterial blood pressure to the level obtained in this series was not associated with increased ET-1 protein expression or ET-1 gene expression. Other groups [28] have found an increased ET-1 protein expression and lung tissue mRNA in shunted piglets. The discrepancy to our findings may be explained by higher pulmonary arterial as well as systemic arterial blood pressure levels in their series compared to our data. In this series, ECE-1 mRNA was higher in pigs with high pulmonary arterial pressure only. This finding is consistent with observations made in human pulmonary arteries of patients with pulmonary hypertension where ECE-1 protein expression has been found to be increased [12].

VEGF-A protein expression was higher in piglets with increased pulmonary blood flow and in the group of piglets with both increased pulmonary blood flow and pressure.

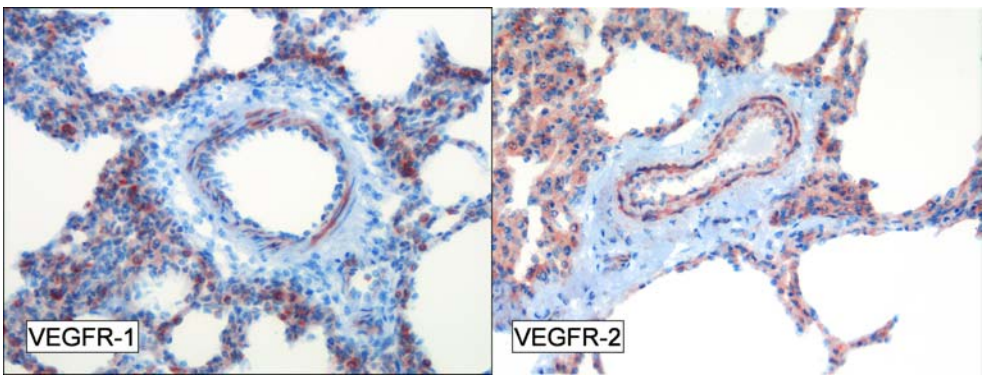

Fig. 5 Immunostaining for VEGFR-1 and VEGFR-2 in lung tissue of shunted piglets (×40)

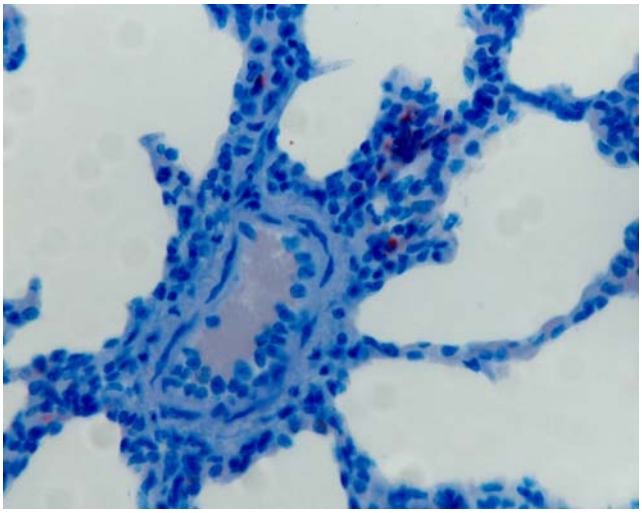

Fig. 6 Immunostaining for podoplanin in lung tissue of piglets with BT shunt and additional ligation of LPA (×40)

VEGF-A mRNA was highest in piglets with increased pulmonary arterial pressure. Increased pulmonary blood flow has been associated with upregulation of expression of VEGF-A and its receptors also in shunted lambs in vitro [25] and in vivo [24]. VEGF-A expression has been associated with the formation of plexiform lesions in the human with congenital heart disease and pulmonary hypertension [10, 17]. Enhanced expression of VEGF-A has been observed also in neonates with congenital diaphragmatic hernia and pulmonary hypertension [29].

Table 4 Biochemical determinations after 3 months (mean±SD)

Variable	Sham (n=7)	Shunt	
		BT shunt (n=6)	BT shunt + LPA ligation (n=6)
Plasma ET-1 (pg/ml)	6.3±0.9	6.6±3.2	7.6±1.8
Plasma cGMP (nmol/l)	12.2±7.4	27.3±21	23.6±15
Plasma nitrite/ nitrate (μmol/l)	96±60	209±92*	350±105**,***

*p<0.05 sham versus BT shunt
**p<0.05 sham versus BT shunt + LPA ligation
***p<0.05 BT shunt versus BT shunt + LPA ligation

The precise role of the interaction of VEGF-A with VEGFR signaling in pulmonary hypertension currently is incompletely understood: Lack of VEGFR signals impairs vascularization [31], but hyperactive VEGFR signaling causes angioproliferation [18]. Others showed that VEGF-induced prostacyclin synthesis by endothelial cells requires a VEGFR-1/VEGFR-2 heterodimer [26]. Although protein expression for VEGFR-1 and -2 did not differ between groups in this series, the lower VEGFR-1 and VEGFR-2 mRNA content might impair the VEGF-A induced NO and prostacyclin upregulation [34] in the pulmonary hypertensive lung.

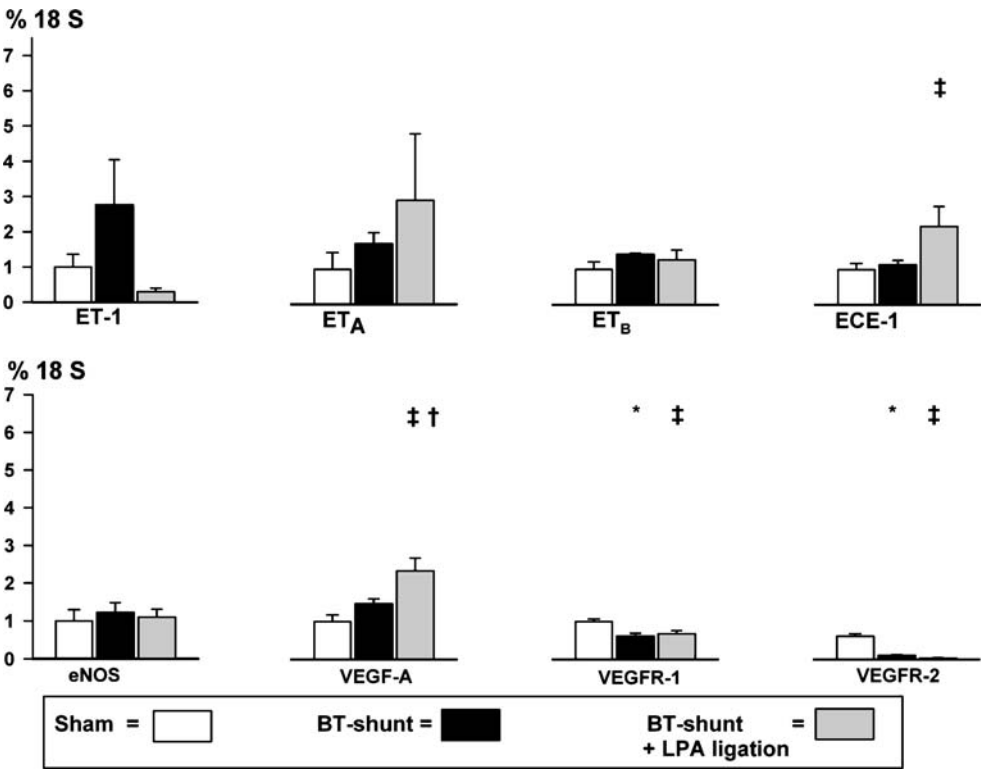

Fig. 7 Quantitative mRNA content in lung tissue for ET-1, ET_A, and ET_B receptor, ECE-1, eNOS, VEGF-A and VEGFR-1 and -2 (mean±SD). *p<0.05 sham versus BT Shunt; ‡p<0.05 sham versus BT shunt + LPA ligation; †p<0.05 BT shunt versus BT shunt + LPA ligation

Limitations

In situ hybridization techniques for localization of mRNA were not performed in this study. We therefore cannot report the proportion of mRNA in lung parenchyma versus lung vessels.

In summary, we demonstrate that in piglets, high pulmonary blood flow and pressure is not associated with changes in eNOS protein expression and eNOS mRNA in lung tissue. Medial thickening was highest in piglets with high pulmonary arterial pressure, and this was associated with upregulation of ECE-1 and VEGF-A. Both high pulmonary blood flow and high pulmonary blood pressure are associated with a reduced expression of VEGFR-1 and VEGFR-2. These alterations might contribute to pulmonary vascular changes observed in the human with left-to-right shunt and pulmonary arterial hypertension.

Acknowledgement We are grateful to Dr. Meike Hömme for perfect technical assistance with the real-time PCR analysis. This study was supported by a grant of the German Heart Foundation, Frankfurt/Main, Germany (grant no. F02/02).

References

1. Black SM, Fineman JR, Steinhorn RH, Bristow J, Soifer SJ (1998) Increased endothelial NOS in lambs with increased pulmonary blood flow and pulmonary hypertension. Am J Physiol 275:H1643–H1651
2. Black SM, BekkerJM, McMullan M, Parry AJ, Ovadia B, Reinhartz O, Lakshminrushimha S, Mata-Greenwood E, Steinhorn RH, Fineman JR (2002) Alterations in nitric oxide production in 8-week-old lambs with increased pulmonary blood flow. Pediatr Res 52:233–244
3. Carmeliet P, Moons L, Luttun A, Vincenti V, Compermolle V, De MM, Wu Y, Bono F, Devy L, Beck H, Scholz D, Acker T, DiPalma T, Dewerchin M, Noel A, Stalmans I, Barra A, Blacher S, Vandendrissche T, Ponten A, Eriksson U, Plate KH, Foidart JM, Schaper W, Charnock-Jones DS, Hicklin DJ, Herbert JM, Collen D, Persico MG (2001) Synergism between vascular endothelial growth factor and placental growth factor contributes to angiogenesis and plasma extravasation in pathological conditions. Nat Med 7:575–583
4. Celermajer DS, Cullen S, Deanfield JE (1993) Impairment of endothelium-dependent pulmonary artery relaxation in children with congenital heart disease and abnormal pulmonary hemodynamics. Circulation 87:440–446
5. Coers W, Temens W, Kempinga C, Klok PA, Moshage H (1998) Specificity of antibodies to nitric oxide synthase isoforms in human, guinea pig, rat, and mouse tissue. J Histochem Cytochem 46:1385–1391
6. Dschietzig T, Richter C, Bartsch C, Böhme C, Heinze D, Ott F, Zartnack F, Baumann G, Stangl K (2001) Flow induced pressure differentially regulates endothelin-1, urotensin II, adrenomedullin, and relaxin in pulmonary vascular endothelium. Biochem Biophys Res Commun 289:245–251
7. Everett AD, Le Cras TD, Xue TD, Johns RA (1998) eNOS expression is not altered in pulmonary vascular remodeling due to increased pulmonary blood flow. Am J Physiol 274:L1058–L1065
8. Fernandez-Mondéjar E, Hambraeus-Jonzon K, Ronéus A, Hedenstierna G (2003) Nitric oxide indreases dramatically in air exhaled from lung regions with occluded vessels. Acta Anaesthesiol Scand 47:312–318
9. Fike CD, Kaplowitz MR, Bousamra II M (2001) eNOS and prostanoid enzymes in lungs of newborn piglets with chronic aortopulmonary shunts. Am J Physiol 281:L475–L482
10. Geiger R, Berger RMF, Hess J, Bogers AJJC, Sharma HS, Mooi WJ (2000) Enhanced expression of vascular endothelial growth factor in pulmonary plexogenic due to congenital heart disease. J Pathol 191:202–207
11. Giaid A, Yanagisawa M, Langleben D, Michel, RP, Levy R, Shennib, H, Kimura S, Masaki T, Duguid WP, Stewart DJ (1993) Expression of endothelin-1 in the lungs of patients with pulmonary hypertension. N Engl J Med 328:1732–1739
12. Giaid A (1998) Nitric oxide and endothelin-1 in pulmonary hypertension. Chest 114(Suppl 3):208S–212S
13. Gorenflo M, Vogel M, Hetzer R, Schmitz L, Berger F, Bein G, Alexi V, Lange PE (1996) Morphometric techniques in the evaluation of pulmonary vascular changes due to congenital heart disease. Pathol Res Pract 192:107–116
14. Gorenflo M, Ullmann M, Sebening Ch, Brockmeier K, Hagl S, Ulmer HE, Otto HF, Schnabel Ph A (2002) The index of pulmonary vascular disease in children with congenital heart disease: Relation to clinical and haemodynamic findings. Virchows Arch 441: 264–270
15. Gorenflo M, Ullmann MV, Eitel K, Gross J, Fiehn W, Hagl S, Dreyhaupt J (2005) Plasma L-arginine and metabolites of nitric oxide synthase in patients with left-to-right shunt after intracardiac repair. Chest 127:1184–1189
16. Haworth SG (1993) Pulmonary hypertension in childhood. Eur Respir J 6:1037–1043
17. Hirose S, Hosoda Y, Furuya S, Otsuki T, Ikeda E (2000) Expression of vascular endothelial growth factor and its receptors correlates closely with formation of the plexiform lesion in human pulmonary hypertension. Pathol Int 50:472–479
18. Hoeben A, Landuyt B, Highey MS, Wildiers H, Van Oosterom AT, De Bruijn EA (2004) Vascular endothelial growth factor and angiogenesis. Pharmacol Rev 56:549–580
19. Hömme M, Schmitt CP, Mehls O, Schäfer F (2004) Mechanisms of mitogen-activated protein kinase inhibition by parathyroid hormone in osteoblast-like cells. J Am Soc Nephrol 15:2844–2850
20. Humpl T, Campbell R, Stephens D, van Arsdell G, Benson LN, Holtby HM, Slutsky AS, Adatia I (2002) Levels of exhaled nitric oxide before and after surgical and transcatheter device closure of atrial septal defects in children. J Thorac Cardiovasc Surg 124:806–810
21. Janér J, Lassus P, Haglund C, Paavonen K, Alitalo K, Andersson (2006) Pulmonary vascular endothelial growth factor-C in development and lung injury in preterm infants. Am J Respir Crit Care Med 174:326–330
22. Jeltsch M, Kaipanen A, Joukov V, Meng X, Lakso M, Rauvala H, Swartz M, Fukumura D, Jain RK, Alitalo K (1997) Hyperplasia of lymphatic vessels in VEGF-C transgenic mice. Science 276:1423–1425
23. Laufs U, Endres M, Stagliano N, Amin-Hanjani S, Chui DS, Yang SX, Simoncini T, Yamada M, Rabkin E, Allen PG, Huang PL, Böhm M, Schoen FJ, Moskowitz MA, Liao JK (2000) Neuroprotection mediated by changes in the endothelial actin cytoskeleton. J Clin Invest 106:15–24
24. Mata-Greenwood E, Meyrick B, Soifer SJ, Fineman JR, Black SM (2003) Expression of VEGF and its receptors Flt-1 and Flk-1/KDR is altered in lambs with increased pulmonary blood flow and pulmonary hypertension. Am J Physiol Lung Cell Mol Physiol 285:L222–L231
25. Mata-Greenwood E, Grobe A, Kumar S, Noskina Y, Black SM (2005) Cyclic stretch increases VEGF expression in pulmonary

arterial smooth muscle cells via TGF-β1 and reactive oxygen species: a requirement for NAD(P)H oxidase. Am J Physiol Lung Cell Mol Physiol 289:L288–L298
26. Neagoe PE, Lemieux C, Sirois MG (2005) Vascular endothelial growth factor (VEGF)-A165 induced prostacyclin synthesis requires the activation of VEGF receptor-1 and -2 heterodimer. J Biol Chem 280:9904–9912
27. Parviz M, Bousamra II M, Chammas JH, Birks EK, Presberg KW, Jacobs ER, Nelin LD (1999) Effects of chronic pulmonary overcirculation on pulmonary vascular tone. Ann Thorac Surg 67:522–527
28. Rondelet B, Kerbaul F, Motte S, Beneden R, Remmelink M, Brimioulle S, McEntee K, Wauthy P, Salmon I, Ketelsleger J-M, Naeije R (2003) Bosentan for the prevention of overcirculation-induced experimental pulmonary arterial hypertension. Circulation 107:1329–1335
29. Shehata SM, Mooi WJ, Okazaki T (1999) Enhanced expression of vascular endothelial growth factor in lungs of newborn infants with congenital diaphragmatic hernia and pulmonary hypertension. Thorax 54:427–431
30. Stenbøg EV, Steinbrüchel DA, Thomsen AB, Baandrup U, Heickendorff L, Ingerslev J, Andersen NT, Emmertsen K (2001) The pulmonary vasculature in a neonatal porcine model with increased pulmonary blood flow and pressure. Cardiol Young 11:420–430
31. Tang K, Breen EC, Gerber HC, Ferrara NM, Wagner PD (2004) Capillary regression in vascular endothelial growth factor - deficient skeletal muscle. Physiol Genomics 18:63–69
32. Tworetzky W, Moore P, Bekker JM, Bristow J, Black SM, Fineman JR (2000) Pulmonary blood flow alters nitric oxide production in patients undergoing device closure of atrial septal defects. J Am Coll Cardiol 35:463–467
33. Ullmann MV, Tran T, Gebhard MM, Fiehn W, Schnabel PA, Ulmer HE, Hagl S, Gorenflo M (2003) Chronic Blalock–Taussig shunts in piglets: a model of pulmonary vascular disease by high pulmonary blood flow. Cardiol Young 13(Suppl 1):65 (abstract)
34. Voelkel NF, Vandivier RW, Tuder RM (2006) Vascular endothelial growth factor in the lung. Am J Physiol Lung Cell Mol Physiol 290:L209–L221
35. Wilkinson JL (2001) Haemodynamic calculations in the catheter laboratory. Heart 85:113–120

Virchows Arch (2007) 450:653–657
DOI 10.1007/s00428-007-0430-7

ORIGINAL ARTICLE

Bone formation in cardiac valves: a histopathological study of 128 cases

Ivo Steiner · Petra Kašparová · Aleš Kohout · Jan Dominik

Received: 14 February 2007 / Revised: 23 April 2007 / Accepted: 30 April 2007 / Published online: 24 May 2007
© Springer-Verlag 2007

Abstract In a series of 1,177 patients with surgical valve resection, there were 128 (10.9%) patients with the histological finding of bone and/or cartilage formation (bony metaplasia; heterotopic ossification) in the excised valve (119 aortic, 9 mitral). The incidence was higher in men (12.8%) than in women (8.5%). The bony metaplasia was always associated with valvular calcification. The metaplastic changes were encountered in all types of calcific aortic valve disease (senile, bicuspid valve, post-rheumatic). The marrow of the heterotopic lamellar bone was mostly composed of adipose tissue. Frequently, it showed chronic inflammation with polyclonal plasmocytic infiltration. Complete haematopoiesis was present only rarely.

Keywords Bony metaplasia · Cardiac valves · Calcific aortic stenosis · Bone marrow

Dystrophic calcification is the most common pathological finding in operatively excised cardiac valves. Several reports describe bone in calcified cardiac valves and recent studies have identified bone proteins in such valves [10, 12, 13, 15, 17, 18]. The goal of this article is to show the frequency of bone formation (heterotopic ossification, bony metaplasia) in a large series of surgically excised cardiac valves (mostly aortic) and to describe its histopathological features with particular aim at the bone marrow pattern.

I. Steiner (✉) · P. Kašparová · A. Kohout
The Fingerland Department of Pathology, Charles University Faculty of Medicine and Faculty Hospital,
500 05 Hradec Králové, Czech Republic
e-mail: steiner@lfhk.cuni.cz

J. Dominik
Department of Cardiosurgery, Charles University Faculty of Medicine and Faculty Hospital,
Hradec Králové, Czech Republic

Materials and methods

From January 1999 to June 2006, every cardiac valve operatively excised at the Department of Cardiac Surgery, Charles University Faculty Hospital, Hradec Kralove (Czech Republic) and submitted to the Fingerland Department of Pathology was examined personally by one of the authors (I.S.). A total of 1,492 patients had valve replacements during this time and, after exclusion of 225 patients with myxoid degeneration and 90 with infective endocarditis, there remained 1,177 whose excised valves formed the basis of this study. Among them, there were 128 patients with the histological finding of bone and/or cartilage formation in their valves. Practically none of them had undergone prior balloon valvuloplasty [4].

After gross examination and description, at least one tissue block was taken from each valve leaflet near its centre. The formalin-fixed specimen was de-mineralised with the Sakura TDE 30 solution in an automatic decalcifier, processed, embedded in paraffin wax, sectioned and stained with haematoxylin and eosin. In selected 18 cases with intensive round cell infiltration of the metaplastic bone's marrow, appropriate immunohistochemistry was performed using antibodies (Dako Cytomation) to the CD 138, CD 20 and CD 3 antigens and to the kappa and lambda light chains.

Results

Of the total of 1,177 patients included in the study, there were 1,049 (89.1%) *without* the histological finding of bony metaplasia in their excised valves. These comprised of 567 men (average age 63.2 years) and of 482 women (average age 65.7 years); the collective average age was 64.3 years.

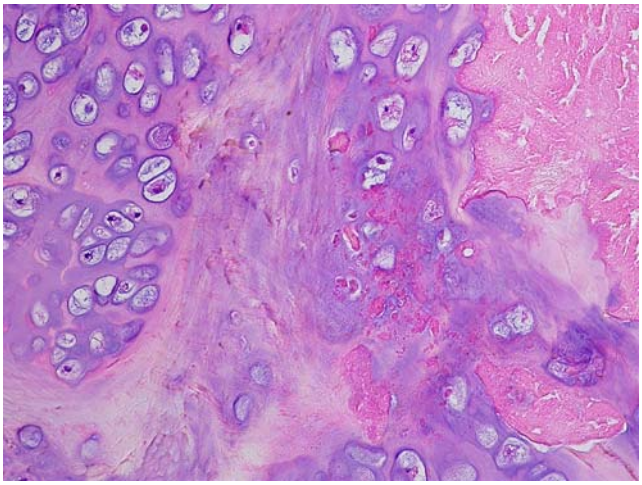

Fig. 1 Cartilaginous nodule in the vicinity of necrotic lipid deposits (in the *upper right corner*). Aortic valve, male, 58 years. H & E, ×250

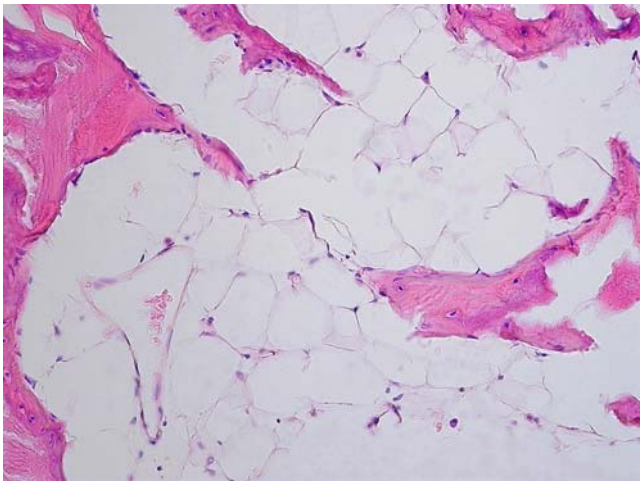

Fig. 3 Lamellar bone with fatty marrow. Aortic valve, male, 72 years. H & E, ×125

The remaining 128 (10.9%) patients had metaplastic bone and/or cartilage in their excised valve. There were 83 men (median age 64 years; average age 62.5±10.99 years) and 45 women (median age 69 years; average age 66.9± 9.4 years); the collective average age was 64.1 years. The incidence of metaplasia in men (12.8%) was significantly higher than that in women (8.5%) (Fisher's exact test; *P* value=0.0236). The age was significantly lower in men than in women (Mann–Whitney's non-parametric test; *P* value=0.0174). The 128 valves with metaplasia comprised of 119 aortic and 9 mitral. All of these valves were calcified, 75 were to a severe degree.

The 9 *mitral* valves, most post-rheumatic, came from 7 women and 2 men (average age 63.1 years). The metaplastic bone was present in the valve itself in five patients and in its calcified annulus (annular calcification) in four patients.

The 119 *aortic* valves, replaced for aortic stenosis with or without associated aortic regurgitation, came from 81 men (average age 62.3 years) and 38 women (average age 68.1 years). As assessed by gross examination, the aortic valvular lesion was senile in origin in 57 patients (36 men, 21 women; average age 68.4 years); complicated malformed, mostly bicuspid, valves in 38 (27 men, 11 women; average age 62.1 years); post-rheumatic in 7 (6 men, 1 woman; average age 60.4 years) and of un-determined type in 17 patients (12 men, 5 women; average age 55.8 years).

The metaplastic tissue in the valves comprised of only bone in 84 cases, of only cartilage in 25 (Fig. 1) and of both bone and cartilage in 19. Metaplastic ossification in the valve commenced as thin rims of lamellar bone lining calcified lipid deposits. At a more advanced stage, there were large areas of bone with small remnants of necrotic tissue at their centre. The process of endochondral ossification was observed in some cases; through a zone of provisional calcification, the cartilage was transformed into lamellar bone (Fig. 2). The foci of metaplastic bone and/or cartilage measured usually less than 1 mm, but in 15

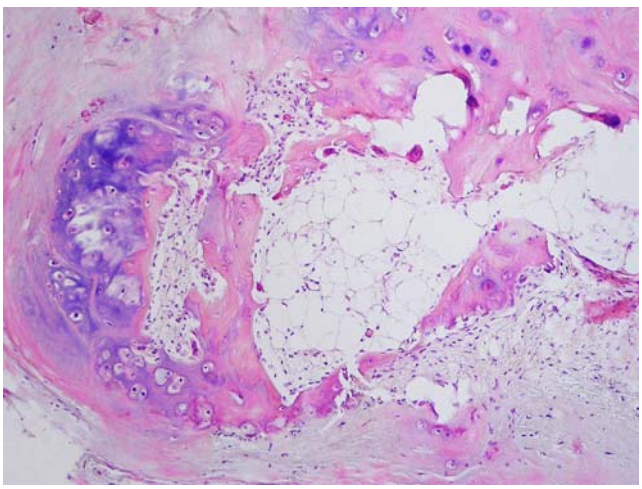

Fig. 2 Area of endochondral ossification with fatty marrow. Aortic valve, male, 76 years. H & E, ×125

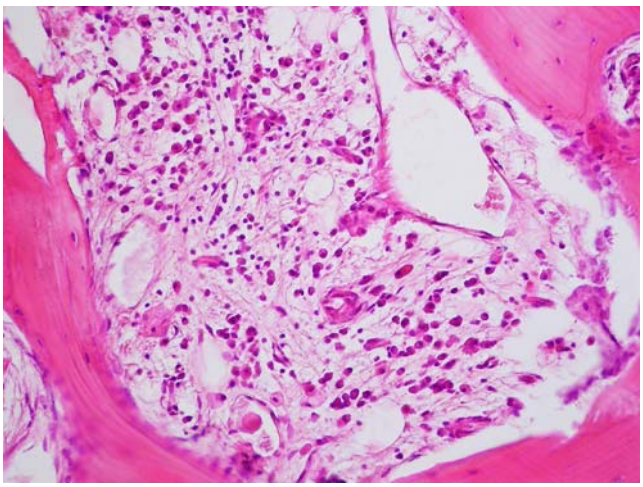

Fig. 4 Lamellar bone with fatty marrow showing plasma cells, lymphocytes, mast cells and thin-walled vessels. Aortic valve, male, 68 years. H & E, ×125

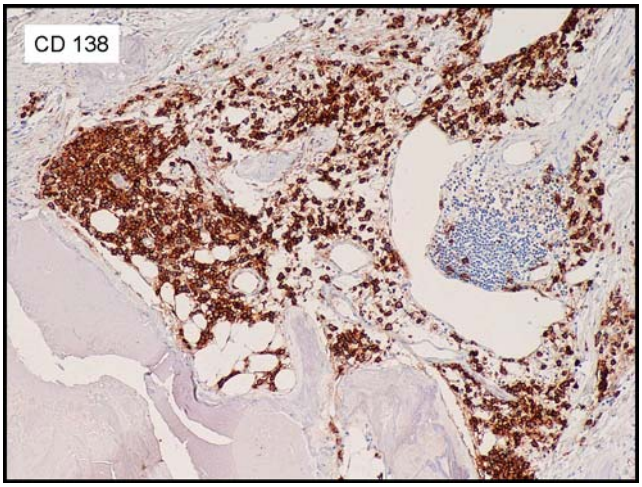

Fig. 5 Plasma cell infiltrate. Immunohistochemistry (CD 138), ×100

cases, they were larger than 2 mm. The largest lesion encountered measuring 13 mm in diameter.

In most cases, the metaplastic bone marrow was atrophic and fatty (Fig. 3) and infiltrated by plasma cells, sometimes quite heavily with the presence of Russell bodies (Figs. 4 and 5). Invariably, this infiltrate was a mixture of kappa-secreting and lambda-secreting cells. Lymphocytic nodules (B+T cells) (Fig. 6), mast cells and occasional neutrophils were also present in some cases. Not infrequently, the marrow was focally fibrosed (Fig. 7). In rare instances, normal haematopoietic marrow was present with normally maturating erythroid, myeloid and megakaryocytic elements (Fig. 8).

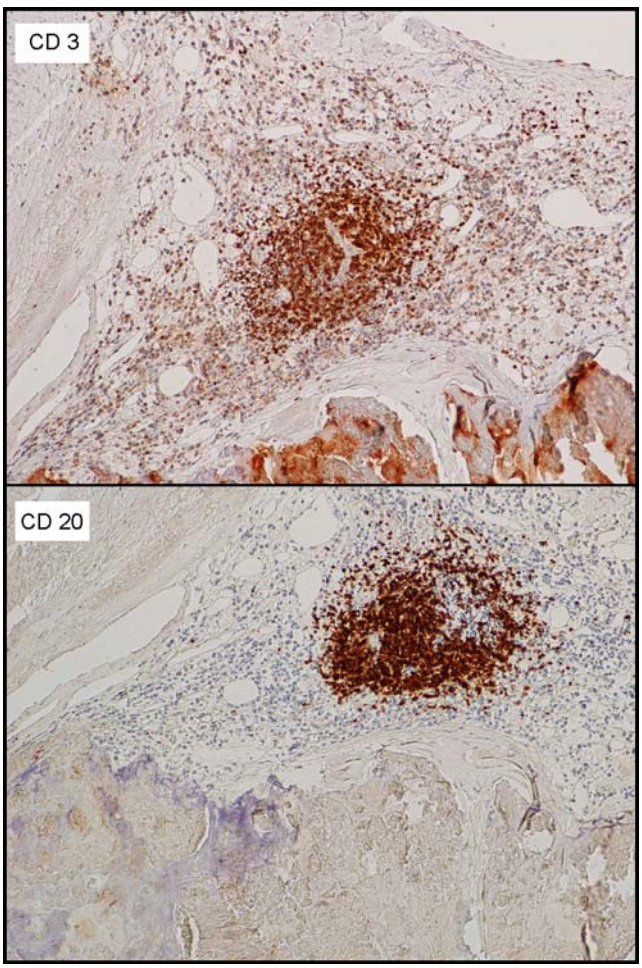

Fig. 6 Lymphocytic nodule (B+T cells). Immunohistochemistry (CD 3, CD 20), both ×100

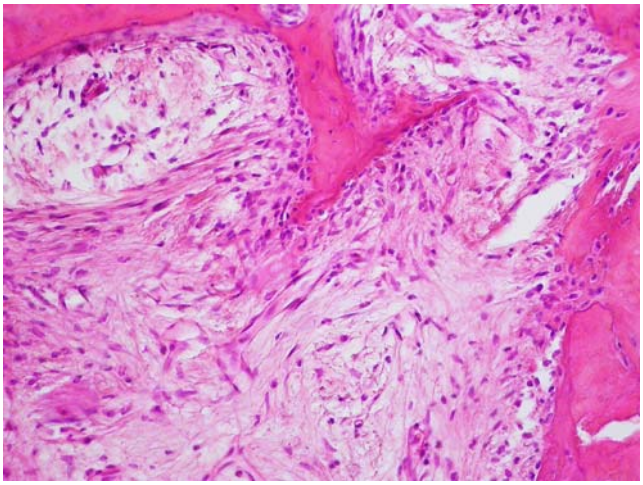

Fig. 7 Lamellar bone with fibrosed marrow. Aortic valve, male, 68 years. H & E, ×125

Discussion

The topic of bone formation in cardiac valves appears infrequently in the literature and usually as small series or single case reports [2, 4, 5, 11], perhaps because surgically resected, calcified valves are not routinely examined histologically. It has been shown that heterotopic bone formation is closely related to the process of calcification, such that its

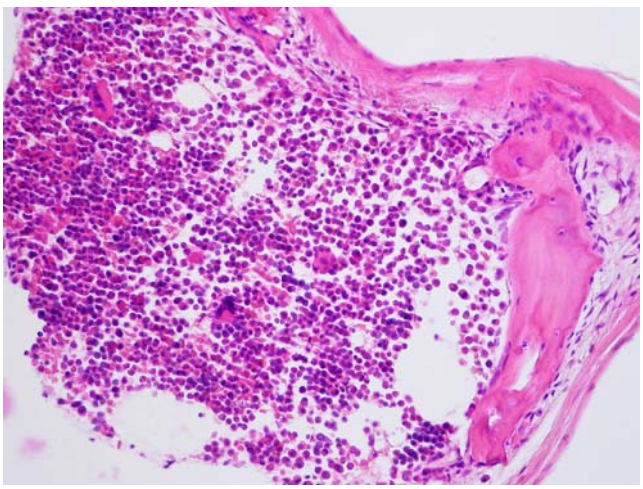

Fig. 8 Complete haematopoiesis in the bone marrow. Mitral valve, female, 63 years. H & E, ×125

presence has been described particularly in the aortic valve, in the calcified annulus of the mitral valve (annular calcification) and, rarely, in arterial atherosclerotic plaques [3, 8, 9].

Bone formation in cardiac valves is closely associated with the process of calcific aortic disease [17]. In the past, this process was thought to be due to 'degenerative', time-dependent, wear-and-tear of the leaflets with passive dystrophic calcium deposition. Now, there is compelling histopathological and clinical data to suggest that calcific aortic disease is an active disease process similar to atherosclerosis, involving endothelial injury, lipoprotein deposition, neovascularisation, chronic inflammation and leaflet calcification, and associated with similar risk factors [1, 6, 10, 12, 13, 16, 18, 19]. This notion applies to the two commonest types of calcific aortic stenosis that occur in a normal trileaflet valve ('senile stenosis') and develop in a congenitally bicuspid aortic valve.

A crucial role in the process of calcific aortic stenosis is played by valvular interstitial fibroblasts that, under various stimuli, become activated to myofibroblasts. A sub-set of valvular myofibroblasts may differentiate into an osteoblastic phenotype capable of promoting the formation of nodules of calcium and bone. In addition, previous studies have reported the presence of bone proteins such as osteopontin, osteocalcin and osteonectin in calcified valves [12, 14]. Cartilage in calcified valves indicates that endochondral ossification, similar to that seen in bone fracture healing, is operative [7, 13].

There are no data available in the relevant literature regarding the clinical and pathophysiological features of valvular bony metaplasia. We assume that the valve function is impaired mostly by the process of calcification whilst the additional presence of bone has no functional role. We also assume that whilst degenerative valvular calcification is related to cardiovascular risk factors, the bone formation is just a local phenomenon secondary to the process of calcification. The polyclonal plasma cell and lymphocytic infiltrate in the bone marrow seems to be reactive with no relation to the bone formation.

This study has several limitations, including that it is a retrospective histopathological analysis and the clinical diagnostic work-up of each individual was not critically reviewed.

We are aware of only 1 study that describes the incidence of valvular ossification. In an evaluation of 347 surgically removed valves (256 aortic and 91 mitral) Mohler et al. [12] identified mature lamellar bone in 37 (34 aortic and 3 mitral), i.e. in 10.7%.

The findings of our study of 1,177 patients undergoing resection of cardiac valves can be summarised as follows:

- In a series of 1,177 patients with valve resection, there were 128 (10.9%) patients with bone and/or cartilage formation (metaplasia) in the excised valve (119 aortic, 9 mitral). The incidence was significantly higher in men (12.8%) than in women (8.5%). Because of the limited extent of valvular examination (only one sample from each valve leaflet), the true incidence is very probably higher.
- The average age was significantly higher in women (66.9 years) than in men (62.5 years).
- Bony metaplasia was always associated with valvular calcification.
- The average age of patients with metaplasia (64.1 years) did not differ from the average age of those without it (64.3 years). This implies that bony metaplasia does not appear to be a late stage in the process of valvular calcification, but rather develops in parallel with it.
- Metaplastic changes were encountered in all types of calcific aortic valve disease (senile, bicuspid valve, post-rheumatic).
- The marrow of the heterotopic mature lamellar bone was usually formed by adipose tissue. There was often non-specific chronic inflammation with an infiltrate composed predominantly of polyclonal plasma cells. Rarely, complete haematopoiesis was present.

Acknowledgments The authors are grateful to Dr. J. Gosney for the English edition. The study was supported by the Research Project MZO (Grant 00179906).

References

1. Agmon Y, Khandheria BK, Meissner I, Sicks JRD, O'Fallon WM, Wiebers DO, Whisnant JP, Seward JB, Tajik AJ (2001) Aortic valve sclerosis and aortic atherosclerosis: different manifestations of the same disease? J Am Coll Cardiol 38:827–834
2. Charokopos NA, Antonitsis P, Rouska E, Kostopoulos I, Charaf A, Spanos PK (2006) Cartilaginous and osseous metaplasia with bone marrow formation in the aortic valve of a patient with giant cell aortitis. Ann Thorac Surg 81:1877–1879
3. Doherty TM, Asotra K, Fitzpatrick LA, Qiao JH, Wilkin DJ, Detrano RC, Dunstan CR, Shah PK, Rajavashisth TB (2003) Calcification in atherosclerosis: bone biology and chronic inflammation at the arterial crossroads. Proc Natl Acad Sci USA 10:11201–11206
4. Feldman T, Glagov S, Carroll JD (1993) Restenosis following successful balloon valvuloplasty: bone formation in aortic valve leaflets. Catheter Cardiovasc Diagn 29:1–7
5. Fernández Gonzáles AL, Montero JA, Martinez Monzonís A, Gil O, Alemany P (1997) Osseous metaplasia and hematopoietic bone marrow in a calcified aortic valve. Texas Heart Inst J 24:232
6. Freeman RV, Otto CM (2005) Spectrum of calcific aortic valve disease. Pathogenesis, disease progression, and treatment strategies. Circulation 111:3316–3326
7. Groom DA, Starke WR (1990) Cartilaginous metaplasia in calcific aortic valve disease. Am J Clin Pathol 93:809–812
8. Hunt JL, Fairman R, Mitchell ME, Carpenter JP, Golden M, Khalapyan T, Wolfe M, Neschis D, Milner R, Scoll B, Cusack A, Mohler ER (2002) Bone formation in carotid plaques: a clinicopathological study. Stroke 33:1214–1219
9. Jeziorska M, McCollum C, Woolley DE (1998) Observations on bone formation and remodelling in advanced atherosclerotic lesions of human carotid arteries. Virchows Arch 433:559–565

10. Mazzone A, Epistolato MC, Gianetti J, Castagnini M, Sassi C, Ceravolo R, Bevilacqua S, Gevilacqua S, Glauber M, Biagini A, Tanganelli P (2006) Biologic features (inflammation and neo-angiogenesis) and atherosclerotic risk factors in carotid plaques and calcified aortic valve stenosis. Two different sites of the same disease? Am J Clin Pathol 126:494–502
11. Mirzaie M, Schultz M, Schwartz P, Coulibaly M, Schöndube F (2003) Evidence of woven bone formation in heart valve disease. Ann Thorac Cardiovasc Surg 9:163–169
12. Mohler ER, Gannon F, Reynolds C, Zimmerman R, Keane MG, Kaplan FS (2001) Bone formation and inflammation in cardiac valves. Circulation 103:1522–1528
13. Mohler ER (2004) Mechanisms of aortic valve calcification. Am J Cardiol 94:1396–1402
14. O'Brien KD, Kuusisto J, Reichenbach DD, Ferguson M, Giachelli C, Alpers CE, Otto CM (1995) Osteopontin is expressed in human aortic valvular lesions. Circulation 92:2163–2168
15. Rajamannan NM, Subramaniam M, Rickard D, Stock SR, Donovan J, Springett M, Orszulak T, Fullerton DA, Tajik AJ, Bonow RO, Spelsberg T (2003) Human aortic valve calcification is associated with an osteoblast phenotype. Circulation 107:2181–2184
16. Ross R (1999) Atherosclerosis—an inflammatory disease. N Engl J Med 340:115–126
17. Schoen FJ (2005) Cardiac valves and valvular pathology. Update on function, disease, repair, and replacement. Cardiovasc Pathol 14:189–194
18. Schoen FJ (2006) New frontiers in the pathology and therapy of heart valve disease: 2006 Society for Cardiovascular Pathology, Distinguished Achievement Award Lecture, United States–Canadian Academy of Pathology, Atlanta, GA, February 12, 2006. Cardiovasc Pathol 15:271–279
19. Soini Y, Salo T, Satta J (2003) Angiogenesis is involved in the pathogenesis of nonrheumatic aortic valve stenosis. Hum Pathol 34:756–763

Virchows Arch (2007) 450:659–664
DOI 10.1007/s00428-007-0409-4

ORIGINAL ARTICLE

Expression and prognostic significance of Tetranectin in invasive and non-invasive bladder cancer

A. Brunner · C. Ensinger · M. Christiansen · S. Heiss · I. Verdorfer · G. Mikuz · A. Tzankov

Received: 2 January 2007 / Revised: 16 March 2007 / Accepted: 16 March 2007 / Published online: 13 April 2007
© Springer-Verlag 2007

Abstract Tetranectin (TN) is a plasminogen kringle-4 binding protein that can be detected in the plasma and the extracellular matrix. In malignancies, TN is thought to enhance proteolytic processes enabling tumor cells to invade and metastasize. So far, TN expression has not been described in transitional cell bladder cancer (TCC), and there is no information on the prognostic significance of its in situ expression. TN expression was studied in 99 TCC patients diagnosed between 1994 and 1997. Immunohistochemistry was performed on a tissue microarray using a monoclonal antibody against TN (clone 11F1). Within the mean follow-up period of 60 months, pTa and pT2-4 TCC patients with stainable TN in the tumor stroma had a significant shorter recurrence-free survival and higher risk of recurrence compared to those without stainable TN (p=0.0002 for both). TN expression in the tumor cells did not influence recurrence-free survival. In conclusion, TN is expressed in a subgroup of bladder cancer patients with a higher risk of recurrence who may take benefit from a closer follow-up.

Keywords Tetranectin · Transitional cell carcinoma · Prognosis

A. Brunner (✉) · C. Ensinger · S. Heiss · I. Verdorfer · G. Mikuz
Institute of Pathology, Medical University of Innsbruck,
Muellerstrasse 44,
6020 Innsbruck, Austria
e-mail: andrea.brunner@i-med.ac.at

M. Christiansen
Department of Clinical Biochemistry, Statens Serum Institut,
Copenhagen, Denmark

A. Tzankov
Institute of Pathology, University of Basel,
Basel, Switzerland

Introduction

Tetranectin (TN) is a plasminogen-binding protein which can be encountered in the plasma and in the extracellular matrix (ECM) [4, 9]. Beside its plasminogen-binding properties, TN can bind to heparin, apolipoprotein (a), tissue plasminogen activator (tPA), hepatocyte growth factor, and angiostatin (AST^{K1-4}) [3, 15, 17, 18, 24]. TN expression has been detected in various endocrine tissues, in epithelial and mesenchymal cells including fibroblasts, monocytes, and neutrophils [2, 5, 7, 8, 20]. It is also a crucial component of the ECM in osteogenesis, muscle development, and regeneration, suggesting an important physiological role in tissue remodeling [26, 27]. Plasma TN is decreased after trauma, acute myocardial infarction, during pregnancy, in patients with liver cirrhosis, rheumatoid arthritis, and malignant tumors [4, 12–14, 16].

In malignancies, TN has been detected in the stroma and in tumor cells of different tumor types with varying distribution patterns [1, 6, 10, 11, 21, 23, 25]. In breast cancer, mainly cytoplasmic staining was found [6, 21], while in other tumors, TN expression was predominantly or even completely restricted to the tumor stroma [1, 10, 11, 23, 25]. TN is thought to enhance proteolytic processes through activation of the plasminogen-cascade, enabling tumor cells invasion and metastasizing [10, 23, 25]. Thus, for example, TN expression is associated with poor disease-free and overall survival (OS) in ovarian and breast cancer [11, 21].

To assess the expression and the prognostic value of in situ TN expression in transitional cell bladder cancer (TCC), we performed a retrospective study on 99 paraffin-embedded tissue samples from newly diagnosed TCC which were brought into a tissue microarray format.

Materials and methods

Samples

Ninety-nine TCC cases, diagnosed between January 1994 and December 1997, were selected from the files of the Institute of Pathology at the Medical University of Innsbruck based on tissue preservation and availability of clinical data. All specimens were obtained by means of transurethral resection and included solely primary diagnoses without any previous surgical or neoadjuvant therapy. Disease recurrence was defined as detection of a newly developed local tumor more than 1 month after primary resection. Recurrence after cystectomy was defined as development of a tumor at the operation site, including the anastomoses of the distal ureter with the newly formed bladder. Disease progression was defined as an increase of stage and/or grade in a recurrent tumor. As most patients died at home, making it difficult to verify if death was caused by progressive bladder cancer or occurred while suffering on bladder cancer, overall, but not disease-specific, survival was considered.

Tissue microarray construction

All samples were brought into a tissue microarray format as previously described [22]. Three tissue cores (0.6 mm) from the superficial and the invasive portion of the tumor including the adjacent tumor stroma were taken where possible; in non-invasive tumors, only cores from the superficial portion could be taken with at least one core containing tumor stroma. In small specimens, one to three cores were obtained based on tissue amount.

Immunohistochemistry

Immunohistochemistry was performed by an automated immunostainer (Nexes, Ventana, USA) applying the streptavidin–biotin peroxidase technique with diaminobenzidine as chromogen. The monoclonal antibody against TN (clone 11F1, NeoMarkers) was used at a dilution of 1:100. Heat-induced antigen retrieval was performed (citrate buffer pH 6, microwave oven 750 W, 15 min). For positive control experiments, a breast cancer tissue was used, and for negative control experiments, non-relevant IgG was applied instead of the primary antibody. Slides from normal urothelium were used to assess physiological TN expression in the bladder. TN staining was scored semi-quantitatively, taking into consideration weak, moderate, and strong staining intensity. Stromal staining and cytoplasmic staining in non-invasive and invasive tumor cells were evaluated separately.

Statistics

For statistical analysis, the Statistical Package of Social Sciences (SPSS 12.0 for Windows) was used. Recurrence-free survival (RFS) and OS were analyzed by the Kaplan–Meier method and compared by the log rank test, except for continuous variables such as age and number of recurrences where a Cox regression model was applied. The Spearman rank test was used to test correlations between TN expression and number of recurrences as well as tumor grade and stage. Multivariate analysis was performed to identify independent prognostic markers for RFS using a Cox multistep regression model; continuous variables were not dichotomized for multivariate analysis. A value of $p < 0.05$ was considered significant.

Results

Patients, samples, reclassification

Our study group included 69 (70%) male and 30 (30%) female patients. The mean patients' age was 72 years (range 42–98). Histopathologically, there were 27 pTa, 33 pT1, 34 pT2-4 tumors, including 29 pT2, three pT3, and two pT4 tumors and five carcinomata in situ (CIS). All specimens were reclassified according to the current WHO classification (Table 1) [19].

Cystectomy was performed in 17 patients (eight immediately and nine later on). Of the eight patients who were

Table 1 Tumor grade, stage, number of cystectomies, recurrence, and progression rates of cases included in the study

Stage	N[a]	Grade (WHO 2004)		Cystectomies	Recurrences	Progresses at relapse
		Low	High			
pTis (CIS)	5	0	5	2 (40%)	4 (80%)	4 (80%)
pTa	27	22	5	0	15 (56%)	3 (11%)
pT1	33	2	31	6 (18%)	18 (55%)	8 (24%)
pT2-4[b]	34	0	34	9 (26%)	15 (44%)	2 (6%)

[a] *N* Total number of cases
[b] 29 pT2, 3 pT3, 2 pT4

Table 2 Number of TCC according to TN staining intensity in superficial tumor, invasive tumor, and tumor stroma

TN staining	N[a]	Staining intensity			
		No staining	Weak	Moderate	Strong
Tumor stroma	97	79 (82%)	15 (15%)	3 (3%)	0
Superficial tumor	70	49 (70%)	18 (26%)	2 (3%)	1 (1%)
Invasive tumor	55	36 (65%)	15 (27%)	3 (5%)	1 (2%)

[a] *N* Total number of cases

immediately cystectomized, none was recorded to have had local recurrence. The nine patients underwent later on cystectomy due to tumor progression or after several recurrences.

In 52 patients (52%), TCC relapsed during the follow-up, with a mean number of two sequential recurrences (median two recurrences, range 1–10). Recurrence and recurrent disease with progression rates are shown in Table 1. Twelve patients (12%) had tumor-associated CIS at initial presentation. Within the mean follow-up of 60 months (range 0–142 months), there were 39 deaths with/on disease; 16 patients died from a secondary neoplasm, 11 from cardiovascular disease, and five from other causes including pulmonary disease and trauma.

Tissue microarray quality

The maximum of three tissue cores/case was arrayed in 90 cases, whereas only two and one core could be obtained in six and three cases, respectively, due to sparse material, resulting in a total number of 285 tissue microarray cores. After immunohistochemistry, 240 cores (84%) and 97 cases (98%), respectively, could be evaluated.

TN expression

In bladder specimens, TN was expressed in inflammatory cells, endothelial cells, in smooth muscle cells of the bladder wall, as well as in superficial cells of the normal urothelium. Stromal staining was absent. Positive cells revealed a diffuse and weak cytoplasmic staining pattern.

TN staining results in tumor stroma was conclusive in all 97 specimens. Staining in the superficial proportion of the tumor could be assessed in 70 cases as, particularly in pT2-T4 tumors, the superficial proportion could not be clearly identified (Tables 2 and 3). Staining in invasive tumor cells could be evaluated in 55 cases in which the invasive proportion was well preserved and available on the tissue microarray slides (Tables 2 and 3; Fig. 1).

Correlations

Stainable stromal TN did not correlate with age, grade, stage, or cytoplasmic staining in tumor cells. Cytoplasmic staining in invasive tumor cells showed a negative correlation with the number of recurrences ($r=-0.407$; $p=0.031$).

Survival analysis

Patients expressing TN in tumor stroma had a significantly higher risk of recurrence and shorter interval to recurrence (13 recurrences out of 17 patients; mean RFS 14 months) compared to those without stainable TN (38 out of 78 patients, mean RFS 69 months; $p<0.0001$; Fig. 2). Survival analysis stratified by stage showed that patients with pTa TCC and stromal TN expression had a significantly higher risk of recurrence and shorter interval to recurrence (four recurrences in four patients; mean RFS 8 months) compared to those without stainable stromal TN (11 recurrences in 23 patients; mean RFS 69 months; $p=0.0002$; Fig. 3). Patients with pT2-4 TCC and stromal TN expression showed also a higher risk of recurrence and a significantly shorter RFS (six recurrences in eight patients, mean RFS 4 months) than those without stainable stromal TN (9 recurrences in 25 patients, mean RFS 81 months; $p=0.0002$; Fig. 4). In pT1 tumors, TN expression in the stroma did not correlate with RFS.

Table 3 Number of TCC with and without TN staining in superficial tumor, invasive tumor, and tumor stroma according to stage

Stage	N[a]	TN staining					
		Tumor stroma		Superficial tumor		Invasive tumor	
		Positive/evaluable	Percentage	Positive/evaluable	Percentage	Positive/evaluable	Percentage
pTis	4	0/4	–	1/4	25	–	–
pTa	27	4/27	15	8/26	31	–	–
pT1	32	6/32	19	8/25	32	6/22	27
pT2-4[b]	34	8/34	24	4/15	27	13/33	39

[a] *N* Total number of informative cases
[b] 29 pT2, 3 pT3, 2 pT4

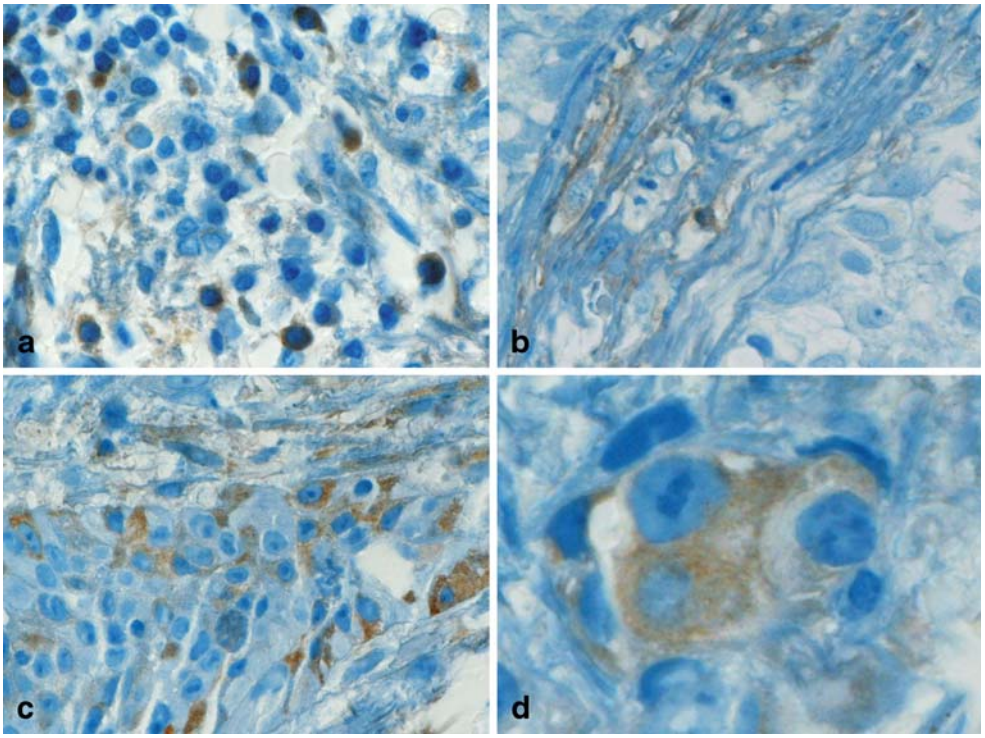

Fig. 1 High power view of tetranectin staining in inflammatory cells (**a**) (400×), in the papillary cores (**b**) (400×), and in the cells of invasive bladder cancer (**c** and **d**) (400× and 600×)

Patients with disease progression at relapse had a significantly shorter RFS than those with out disease progression (11 months versus 41 months, $p=0.01$). Besides TN in tumor stroma and progression, neither age, grade, stage nor associated CIS significantly contributed to RFS. In a multivariate analysis, both stainable TN in tumor stroma and progressive disease were independent prognostic factors considering RFS (Table 4).

Cytoplasmic staining in superficial, as well as in the invasive tumor cells, did not influence RFS. TN expression in the stroma or in the tumor cells did not influence OS. The factors significantly contributing to OS were, as expected, tumor stage ($p=0.0002$), tumor grade ($p=0.009$), age ($p<0.001$), and number of recurrences ($p=0.014$). Multivariate analysis revealed only age, grade, and number of recurrences as independent prognostic factors considering OS (Table 5).

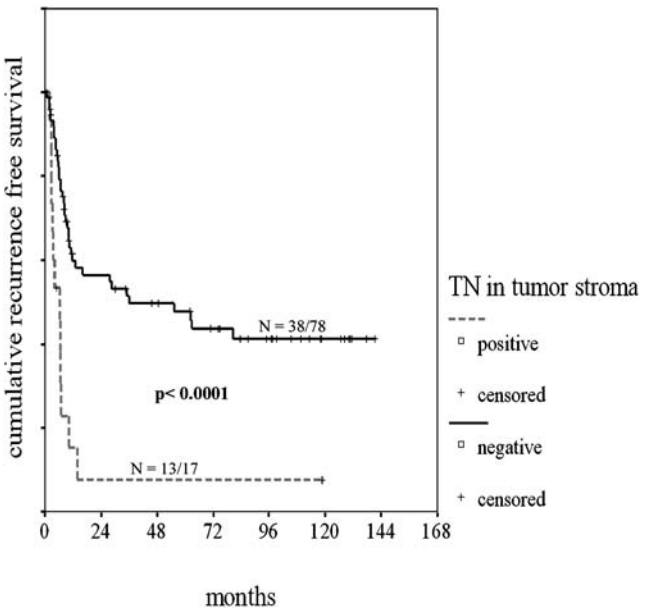

Fig. 2 RFS of TCC patients with stainable TN in tumor stroma TN positive versus TN-negative cases compared by the log-rank test. *N* Number of recurrences/number of cases

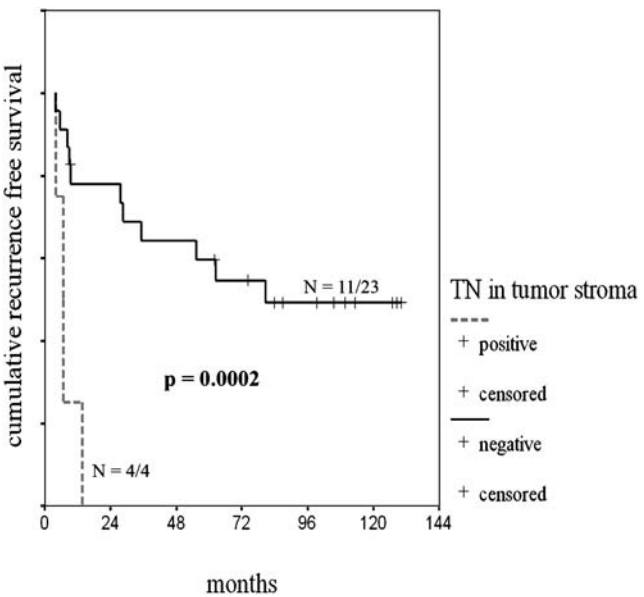

Fig. 3 RFS of pTa TCC patients with stainable TN in tumor stroma. TN positive versus TN-negative cases compared by the log-rank test. *N* Number of recurrences/number of cases in each subgroup

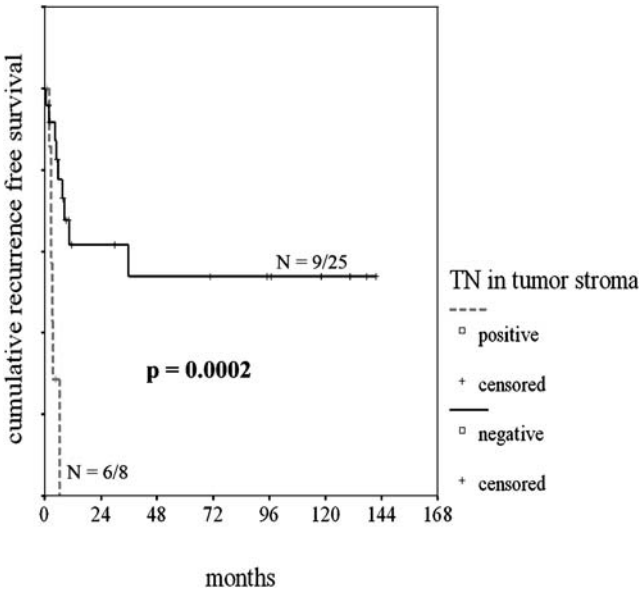

Fig. 4 RFS of pT2-4 TCC patients with TN staining in tumor stroma. TN-positive versus TN-negative cases compared by the log-rank test. *N* Number of recurrences/number of cases in each subgroup

Discussion

In this study, we report for the first time the expression pattern and prognostic significance of TN in TCC. While TN was only focally expressed in superficial cells of normal urothelium, cytoplasmic tumor cell, as well as stromal expression of TN, was detected in a subgroup of TCC.

Only a few data are available on the prognostic significance of TN expression in malignant tumors, and results are conflicting [11, 21]. In most tumors, TN expression correlated with prognostic parameters including grade of differentiation or histological subtypes [1, 21]. In breast cancer, only high TN expression in tumor cells was relevant for inferior OS, whereas in ovarian cancer, stromal TN staining could predict poor prognosis [11, 21]. In our study, TN expression by TCC cells and in surrounding stroma had no prognostic value considering OS. Stromal TN expression was associated with poorer RFS in pTa and pT2-4, but not in pT1 TCC. We therefore speculate that TN could probably play a minor role during invasion of the lamina propria, but is important in the degradation of the ECM during muscle invasion. The biological background for the important prognostic significance of stromal TN expression in pTa TCC remains unclear, but indicates that abnormal stromal components could play an important role in the development of tumor recurrences, which is probably not affected by current treatment. Indeed, low plasma TN levels have been found together with an increased TN staining in tumor stroma and have been linked to chemoresponsiveness in other tumors [11, 12, 21].

Table 4 Multivariate analysis for the independent prognostic value of factors influencing RFS

Factor	Relative risk	*p* value
TN in tumor stroma	9.94	0.002
Progressive disease	7.26	0.007

Table 5 Multivariate analysis for the independent prognostic value of factors influencing OS

Factor	Relative risk	*p* value
Age	6.55	0.01
Grade	5.09	0.024
Number of recurrences	3.93	0.047
Stage	1.37	0.24

Cell culture experiments showed that stromal cells are the main source of TN in normal tissue [8]. In malignant tumors, stromal staining has been observed in the absence of tumor TN expression, and mRNA in situ hybridization showed mainly stromal cells rather than tumor cells to produce TN [1, 25]. Stromal TN is thought to be involved in proteolytic processes via binding to plasminogen [10, 25]. Several other ligands have been identified, suggesting that TN might have a complex regulatory function during tissue remodeling and even angiogenesis [18, 24]. Importantly, degradation of ECM and angiogenesis are two key mechanisms supporting tumor growth, invasion, and metastasis [18, 24]. Our results indicate that in TCC TN in the stroma indicates a more aggressive behavior. This finding is in line with observations considering stainable stromal TN in other tumor types [1, 11].

The value of cytoplasmic tumor cell expression of TN remains questionable. In breast cancer, cytoplasmic expression was reported to be an important prognostic factor [21]. In our study, cytoplasmic TN staining in invasive tumor cells showed a weak negative correlation with the absolute number of recurrences, although it was mostly found in high-grade pT2-4 tumors. As we could not show any correlation between stromal and cytoplasmic TN expression, we speculate that TN, produced in different tissue compartments, results in diverse functions considering tumor behavior at least in some high-grade tumors. Indeed, in other tumor types, cytoplasmic staining did not correlate with stromal TN expression or any other prognostic parameter as well [1, 11, 23, 25].

In conclusion, our study showed that TN is expressed in a subgroup of TCC with distinct prognostic relevance, dependent on its stainability in different compartments. Patients with stromal TN expression are at higher risk of recurrence and of a shorter RFS, suggesting that these patients might benefit from a closer follow-up.

Acknowledgments We thank H. Muehlboeck from the Cancer Registry of Tyrol/Austria, Institute for Epidemiology for providing epidemiologic data and S. Jöbstl for excellent technical assistance.

References

1. Arvanitis DL, Kamper EF, Kopeikina L, Stavridou A, Sgantzos MN, Kallioras V, Athanasiou E, Kanavaros P (2002) Tetranectin expression in gastric adenocarcinomas. Histol Histopathol 17:471–475
2. Borregaard N, Christensen L, Bejerrum OW, Birgens HS, Clemmensen I (1990) Identification of a highly mobilizable subset of human neutrophil intracellular vesicles that contains tetranectin and latent alkaline phosphatase. J Clin Invest 85:408–416
3. Caterer NR, Graversen JH, Jacobsen C, Moestrup SK, Sigurskjold BW, Etzerodt M, Thogersen HC (2002) Specificity determinants in the interaction of apolipoprotein(a) kringles with tetranectin and LDL. Biol Chem 383:1743–1750
4. Christensen L (1992) The distribution of fibronectin, laminin and tetranectin in human breast cancer with special attention to the extracellular matrix. APMIS Suppl 26:1–39
5. Christensen L, Clemmensen I (1989) Tetranectin immunoreactivity in normal human tissues. An immunohistochemical study of exocrine epithelia and mesenchyme. Histochemistry 92:29–35
6. Christensen L, Clemmensen I (1991) Differences in tetranectin immunoreactivity between benign and malignant breast tissue. Histochemistry 95:427–433
7. Christensen L, Johansen N, Jensen BA, Clemmensen I (1987) Immunohistochemical localization of a novel, human plasma protein, tetranectin, in human endocrine tissues. Histochemistry 87:195–199
8. Clemmensen I, Lund LR, Christensen L, Andreasen PA (1991) A tetranectin-related protein is produced and deposited in extracellular matrix by human embryonal fibroblasts. Eur J Biochem 195:735–741
9. Clemmensen I, Petersen LC, Kluft C (1986) Purification and characterization of a novel, oligomeric, plasminogen kringle 4 binding protein from human plasma: tetranectin. Eur J Biochem 156:327–333
10. De Vries TJ, De Wit PE, Clemmensen I, Verspaget HW, Weidele UH, Bröcker EB, Ruiter DJ, Van Muijen GNP (1996) Tetranectin and plasmin/plasminogen are similarly distributed at the invasive front of cutaneous melanoma lesions. J Pathol 179:260–265
11. Hogdall CK, Christensen L, Clemmensen I (1993) The prognostic value of tetranectin immunoreactivity and plasma tetranectin in patients with ovarian cancer. Cancer 72:2415–2422
12. Hogdall CK, Christiansen M, Nogaard B, Bentzen SM, Kronenberg O, Clemmensen I (1995) Plasma tetranectin and colorectal cancer. Eur J Cancer 31:888–894
13. Hogdall CK, Hogdall EV, Hording U, Daugaard S, Clemmensen I, Norgaard-Pedersen B, Toftager-Larsen K (1991) Plasma tetranectin and ovarian neoplasms. Gynecol Oncol 43:103–107
14. Kamper EF, Kopeikina LT, Trontzas P Kyrazis NC, Vaiopoulos G, Stavridis J (1998) Comparative study of tetranectin levels in serum and synovial fluid of patients with rheumatoid arthritis, seronegative spondylarthritis and osteoarthritis. Clin Rheumatol 17:318–324
15. Kluft C, Jie AF, Los P, de Wit E, Havekes L (1989) Functional analogy between lipoprotein(a) and plasminogen in the binding to the kringle 4 binding protein, tetranectin. Biochem Biophys Res Commun 15(161):427–433
16. Kluft C, Los P, Clemmensen I, Brommer EJP, Leuven JAG, Bogs AL, Vellenga E (1989) Quantitation of plasma levels of tetranectin —effects of oral contraceptives, pregnancy, treatment with L-asparaginase and liver cirrhosis. Thromb Haemost 62:792–796
17. Lorentsen RH, Graversen JH, Caterer NR, Thogersen HC, Etzerodt M (2000) The heparin-binding site in tetranectin is located in the N-terminal region and binding does not involve the carbohydrate recognition domain. Biochem J 347(Pt 1):83–87
18. Mogues T, Etzerodt M, Hall C, Engelich G, Graversen JH, Hartshorn KL (2004) Tetranectin binds to the kringle 1–4 form of angiostatin and modifies its functional activity. J Biomed Biotechnol 2:73–78
19. Montironi R, Lopez-Beltran A (2005) The 2004 WHO classification of bladder tumors: a summary and commentary. Int J Surg Pathol 13:143–153
20. Nielsen H, Clemmensen I, Kharazmi A (1993) Tetranectin: a novel secretory protein from human monocytes. Scand J Immunol 37:39–42
21. Obrist P, Spizzo G, Ensinger C, Fong D, Brunhuber T, Schäfer G, Varga M, Margreiter R, Amberger A, Gastl G, Christiansen M (2004) Aberrant tetranectin expression in human breast carcinomas as a predictor of survival. J Clin Pathol 57:417–421
22. Tzankov A, Went P, Zimpfer A, Dirnhofer S (2005) Tissue microarray technology: principles, pitfalls and perspectives—lessons learned from hematological malignancies. Exp Gerontol 40:737–744
23. Verspaget HW, Clemmensen I, Ganesh S, Christensen L, Sier CFM, Griffioen G, Lamers CBHW (1995) Tetranectin expression in human colonic neoplasia. Histopathology 25:463–746
24. Westergaard UB, Andersen MH, Heegaard CW Fedosov SN, Petersen TE (2003) Tetranectin binds hepatocyte growth factor and tissue-type plasminogen activator. Eur J Biochem 270:1850–1854
25. Wewer UM, Albrechtsen R (1992) Tetranectin, a plasminogen kringle 4-binding protein. Cloning and gene expression pattern in human colon cancer. Lab Invest 67:253–26
26. Wewer UM, Iba K, Durkin ME, Nielsen FC, Loechel F, Gilpin BJ, Kuang W, Engvall E, Albrechtsen R (1998) Tetranectin is a novel marker for myogenesis during embryonic development, muscle regeneration, and muscle cell differentiation in vitro. Dev Biol 200:247–259
27. Wewer UM, Ibaraki K, Schjorring P, Durkin ME, Young MF, Albrechtsen R (1994) A potential role for tetranectin in mineralization during osteogenesis. J Cell Biol 127:1767–1775

Virchows Arch (2007) 450:665–670
DOI 10.1007/s00428-007-0418-3

ORIGINAL ARTICLE

Acute interstitial nephritis of HIV-positive patients under atazanavir and tenofovir therapy in a retrospective analysis of kidney biopsies

Simone Schmid · Milos Opravil · Michael Moddel · Milo Huber · Rahel Pfammatter · Gerald Keusch · Patrice Ambuhl · Rudolf P. Wuthrich · Holger Moch · Zsuzsanna Varga

Received: 12 January 2007 / Revised: 22 March 2007 / Accepted: 4 April 2007 / Published online: 27 April 2007
© Springer-Verlag 2007

Abstract We performed a retrospective analysis on kidney biopsies of 30 human immunodeficiency virus (HIV)-positive patients. Twenty-two of them received highly active antiretroviral therapy (HAART). Tenofovir containing HAART together with atazanavir, a new protease inhibitor, was administered to three patients. All of them developed acute renal failure. The kidney biopsies of these patients showed an acute interstitial nephritis or a chronic interstitial nephritis with an acute component. Withdrawal of atazanavir and tenofovir resulted in recovery of renal function in all three patients. Acute interstitial nephritis was observed only in 1 of 19 patients without atazanavir or tenofovir treatment. We conclude that acute interstitial nephritis and consecutive acute renal failure is a relevant side effect of atazanavir and tenofovir therapy in HIV-positive patients.

S. Schmid (✉) · H. Moch · Z. Varga
Department of Pathology, Institute of Surgical Pathology,
University Hospital Zurich,
Schmelzbergstrasse 12,
CH-8091 Zurich, Switzerland
e-mail: simone.schmid@usz.ch

M. Opravil · M. Huber
Department of Internal Medicine, Division of Infectious Diseases,
University Hospital Zurich,
Zurich, Switzerland

M. Moddel · R. Pfammatter · G. Keusch
Department of Nephrology, City Hospital Waid,
Zurich, Switzerland

P. Ambuhl · R. P. Wuthrich
Clinic of Nephrology, University Hospital Zurich,
Zurich, Switzerland

Keywords HIV · Interstitial nephritis · Kidney biopsy · Atazanavir

Introduction

Renal disease has become increasingly prevalent in human immunodeficiency virus (HIV)-positive patients [2, 3, 25]. This can be explained by prolonged survival due to improved treatment, resulting in increased long-term complications from the underlying disease [20, 24]. Kidney disease can be caused directly through HIV, opportunistic infections, or drug-related effects [20]. Acute renal failure in HIV infection overall is rare but may be caused by the toxic effects of antiretroviral therapy or nephrotoxic antimicrobial substances used in the treatment of opportunistic infections [2, 24]. Chronic renal disease can be caused by multiple pathophysiological mechanisms, leading to HIV-associated nephropathy (NP), a form of collapsing focal glomerulosclerosis, thrombotic microangiopathy, and various forms of immune complex glomerulonephritis (GN) [20].

HIV-infected patients frequently develop resistance patterns of their virus. Therefore, various new antiretroviral agents were introduced in recent years. Although these medications are effective, they may have unknown side-effect profiles that are discovered only during post-marketing surveillance. Acute renal failure induced by antiretroviral therapy has been described for zidovudine, delavirdine (rhabdomyolysis with myoglobinuria), tenofovir, ritonavir (direct tubular toxicity), and indinavir (crystal NP, acute interstitial nephritis) [20, 23, 24]. Atazanavir is a new protease inhibitor that shows a high specificity for HIV-1 protease. This protease inhibitor was released in

2004 [1, 20]. So far, two cases of acute interstitial nephritis under atazanavir therapy have been published in the literature [1, 17]. Consequently, we investigated the frequency of kidney pathology, especially the occurrence of acute interstitial nephritis in kidney biopsies of 30 HIV-positive patients, with special emphasis on atazanavir therapy.

Materials and methods

Patients

The reports of all kidney biopsies in the archives of the Institute of Surgical Pathology, University Hospital Zurich, between 1990 and 2006 were screened for HIV-infected patients (see also "Discussion"). The information on HIV infection came from the clinicians. There were kidney biopsies of 30 HIV-positive patients, 15 of which were performed because of renal function impairment (Table 1). Histological slides and ultrastructural findings were reevaluated in each patient (S.S, Z.V). There were 21 male and 9 female patients with an age of 23 to 63 years (median 35 years). Three patients were of African origin. Twenty-two patients received highly active antiretroviral therapy (HAART). Four patients received tenofovir-containing HAART, three of them together with atazanavir. Three other patients received indinavir-containing HAART.

Clinical data are summarized in Tables 1, 3, and 4.

Table 1 Summary of clinical data

	Values
Age	23–63
Gender	
Male/female	21/9
Antiviral therapy	22/30
Atazanavir	3
Tenofovir	4
Ritonavir	8
Lopinavir	6
Lamivudine	11
Emtricitabine	1
Didanosine	3
Zidovudine	7
Efavirenz	2
Abacavir	4
Indinavir	3
Nelfinavir	2
Stavudine	2
Foscarnet	1
Clinical symptoms	
Proteinuria	21
Hematuria	13
Renal insufficiency	15
Acute renal failure	5
Nephrotic syndrome	3

Histology and light microscopy

Tissue specimens had been routinely fixed in 4% formaldehyde and embedded in paraffin. Sections were cut (2 μm thick) and attached to polylysine-coated glass slides. Routine hematoxylin and eosin stains were performed as well as special staining procedures: periodic acid-Schiff (PAS), acid fuchsin-Orange G (SFOG), Elastin–van Gieson (EVG), and silver on all slides. Renal diseases were diagnosed according to criteria by textbooks [4, 6, 13, 15, 22]. The diagnosis of acute interstitial nephritis required interstitial edema, increased lymphocytes, and tubulitis. Eosinophilic granulocytes were present in two of three cases.

Immunofluorescence/immunohistochemistry

In all cases, stains for IgA (1:30 dilution, Dako, Glostrup, Denmark), IgG (1:25 dilution, Dako), IgM (1:40 dilution, Dako), and C3 (1:80 dilution, Dako) and, in some cases, also for C1q (1:20 dilution, Dako), kappa (1:20 dilution, Dako), and lambda (1:30 dilution, Dako) were performed on frozen sections by using the standardized Ventana Benchmark system (Ventana Medical Systems, Tucson, AZ). The reaction products were visualized with the iVIEW DAB detection kit on the Ventana Benchmark system according to the manufacturer's recommendations. If no fresh tissue was available, immunohistochemical reactions for IgA, IgG, IgM, and C3 were carried out on paraffin sections via the same procedure.

Following markers were tested immunohistochemically on paraffin sections on the cases with acute interstitial nephritis: T cell and B cell markers: CD4 (1:10 dilution, Novocastra, Newcastle, UK), CD8 (1:100 dilution, Dako), CD20 (1:400 dilution, Dako); Granzyme B (1:25 dilution, Dako), Fas (1:20 dilution, Novocastra), TIA-1 (1:400 dilution, Immunotech S.A., Marseille, France), FoxP3 (1:50 dilution, Abcam, Cambridge, UK).

Electron microscopy

Specimens were processed according to standard procedures as follows: The kidney biopsy was fixed in phosphate-buffered 2.5% glutaraldehyde and 2% osmium tetroxide, dehydrated in alcohol and propylene oxide, and embedded in Epon. Ultrathin sections were cut, contrasted

with uranyl acetate and lead citrate, and examined by transmission electron microscope.

Results

A variety of histopathological lesions were diagnosed in the 30 kidney biopsies (Table 2).

Immune complex GN was the most common histological finding, identified in 13 patients: 4 membranous GN, 3 membranoproliferative GN (1 type 1 and 2 type 3), 2 IgA NP, 1 postinfectious GN, 1 immunotactoid GN, 1 anti-GBM-GN, 1 immune complex GN not otherwise specified. Two of three patients with membranoproliferative GN were coinfected with hepatitis C virus, and one had visceral leishmaniosis.

Interstitial nephritis was diagnosed in six patients. Five patients were treated with antiretroviral therapy, the combination of atazanavir and tenofovir was taken by three of them. These latter three patients all showed acute interstitial nephritis (Fig. 1), two of them also signs of chronicity (interstitial fibrosis and tubular atrophy). Withdrawal of atazanavir and tenofovir resulted in recovery of renal function in all three patients.

Only in one of these three patients, there was a focal acute tubular necrosis as a minor component, which is the typical described manifestation of tenofovir on the kidney. One additional patient, who was administered foscarnet without anti-HIV therapy, also exhibited acute interstitial nephritis. Chronic interstitial nephritis was observed in two patients (one patient had received no antiretroviral therapy, the other patient had been treated with zidovudine, lamivudine, indinavir). The majority of the infiltrating interstitial lymphocytes were CD8 positive T cells, to lesser extent CD4 positive T cells were also present. There were a few CD20 positive B cells mixed within the T cell population. Lymphocytes in all cases showed focal positivity for Granzyme B, TIA-1, and FoxP3. Stains for Fas were not conclusive.

Table 2 Summary of renal changes

Diagnosis	Number of patients (*n*)
Immune complex glomerulonephritis	13
Interstitial nephritis	6
Acute tubular necrosis	5
Thrombotic microangiopathy	4
Focal segmental glomerulosclerosis	5
Vascular changes	2
Pyelonephritis	1
HIV-associated nephropathy	2
Indinavir crystal nephropathy	1
Amyloidosis	1

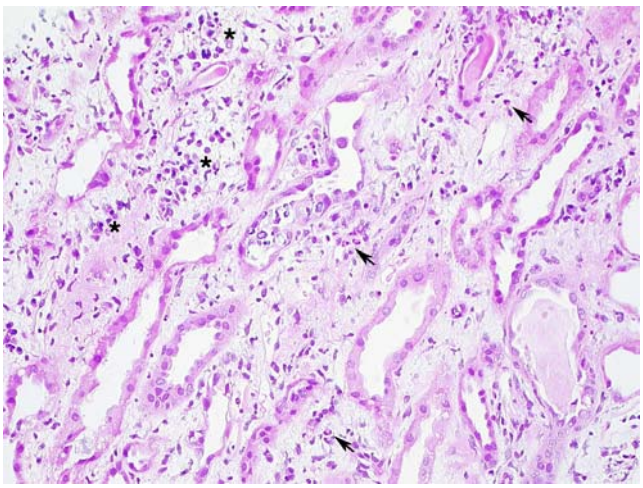

Fig. 1 Acute interstitial nephritis. The renal tubuli are separated through interstitial edema and increased inflammatory cells, as lymphocytes and plasma cells (*asterisk*) as well as eosinophilic granulocytes (*arrows*). HE, ×200

Details of patients' medication with acute interstitial nephritis are summarized in Tables 3 and 4.

Acute tubular necrosis was seen in five patients. Only one patient showed acute tubular necrosis without other findings during treatment with tenofovir, didanosine, lopinavir, ritonavir, esomeprazole, paracetamol. This patient had additionally received a contrast medium 1 month earlier. Acute tubular necrosis was observed as an epiphenomenon in the other four patients accompanying IgA NP, membranous GN, or interstitial nephritis.

Focal segmental glomerulosclerosis (FSGS) was observed in five patients. Two of these patients had a collapsing variant of FSGS (classical HIV-associated NP), both patients were of African origin.

Thrombotic microangiopathy was seen in four patients. Two biopsies with mainly vascular changes included one diabetic NP and one hypertensive NP. Renal changes caused by opportunistic infections were not observed in any of the cases in our series.

Tubuloreticular aggregates, which can be found in glomerular endothelium cells of HIV-positive patients and patients with systemic lupus, were detected by ultrastructural examination in 13 patients. They were less frequent in patients treated with HAART (30%) than in patients without antiretroviral therapy (75%).

Discussion

In this study, we identified three patients who presented with acute renal failure and acute interstitial nephritis in the

Table 3 Patients with acute renal failure and acute interstitial nephritis

Patients	Diagnosis	Drugs
51-year-old man	Acute interstitial nephritis	Atazanavir, tenofovir, ritonavir, lamivudine (all since 3 months); amoxicillin/clavulanic acid, oxazepane, methadone, esomeprazole
44-year-old woman	Chronic interstitial nephritis with acute component	Atazanavir, tenofovir, ritonavir, emtricitabine (all since 6 weeks)
63-year-old man	Chronic interstitial nephritis with acute component and focal tubular necrosis	Atazanavir (since 4 months), lopinavir/ritonavir (since 4.5 years), tenofovir (since 17 months), lamivudine (since 4 years), didanosine (since 4 months), acidum salicylicum, clopidogrelum, calcium acetate, spironolactone, metoprololi succinas, epoetinum beta, insuline, atorvastatine, rosiglitazone
31-year-old man	Acute to subacute interstitial nephritis with focal acute tubular necrosis	Foscarnet, aluminii oxidum hydricum/magnesii hydroxidum, ranitidine, calcium acetate, sucralfate

biopsy while receiving atazanavir and tenofovir containing HAART. These were the only three patients who presented with acute interstitial nephritis while receiving an antiretroviral therapy.

Improved survival of patients with HIV infection was reached with antiretroviral therapy, but may result in side effects of medication, especially in HAART-associated complications [20, 24]. Since the introduction of HAART, a wide range of renal side effects and adverse drug reactions have been recognized, varying from proteinuria to acute renal failure [20, 23, 24]. Not much data are available on side effects and kidney pathology arising under atazanavir therapy [20]. Only two patients with acute interstitial nephritis have been reported in the literature so far, one of them is a patient in our study [1, 17]. According to our knowledge, no systematic clinicopathological case series has analyzed the incidence of acute interstitial nephritis under atazanavir therapy up to now.

In our series, the three cases of acute interstitial nephritis during HAART occurred during concomitant therapy with atazanavir and tenofovir, and the kidney function normalized after both atazanavir and tenofovir were stopped. Based on treatment history, we cannot attribute this phenomenon to one of the drugs alone. In all three patients, the acute interstitial nephritis occurred between 6 and 16 weeks after starting ritonavir-boosted atazanavir. Two of these patients had initiated tenofovir together with atazanavir, while the third patient had been receiving tenofovir already for 17 months without previous increase in serum creatinine. This time course, thus, favors atazanavir to be the causative agent, which is also supported by the histological picture of interstitial nephritis without tubular

Table 4 Clinical data and time course of three patients with acute interstitial nephritis under atazanavir and tenofovir

	51-year-old man	44-year-old woman	63-year-old man
CDC stage	C2	C3	A3
Actual CD4 (count/μl)	269	160	415
Duration anti-HIV therapy	13 months	6 weeks	9.5 years
Duration atazanavir	3 months	6 weeks	4 months
Duration tenofovir	3 months	6 weeks	17 months
Other illnesses	Alcohol abuse, emphysema	i.v. drug use	Diabetes mellitus, coronary heart disease
Serum creatinine before start of atazanavir (μmol/l)	Normal	68	96
Peak serum creatinine (μmol/l)	913	302	622
Calculated GFR (ml/min, Cockcroft)	8	14	11
Urine protein (g/l)	0.75	0.5	1.0
Other abnormal urine results	Erythrocytes ↑	Leucocytes ↑, erythrocytes (↑)	Glucose ↑
Urine eosinouria	nd	nd	nd
Blood eosinophils (/μl)	200	50	240
Subsequent HAART with normalization of serum creatinine	Nevirapine, abacavir, lamivudine	Lopinavir/ritonavir, zidovudine, lamivudine	Lamivudine (monotherapy)

Histology and complete list of medication is given in Table 3
nd Not done

necrosis. Although there are several reports of renal insufficiency associated with tenofovir, the overall occurrence is rare, and only few of these patients had kidney biopsies [14, 19, 21]. The typical picture of tenofovir NP was extensive acute tubular necrosis [14, 19, 20]. There are no published reports of acute interstitial nephritis due to tenofovir; however, the European Medicines Agency recently included acute interstitial nephritis as one of the possible adverse reactions to tenofovir [5].

We cannot exclude a potential additive effect of atazanavir and tenofovir on the development of NP. In addition, atazanavir and tenofovir given together display significant interactions, with lowering of atazanavir and increasing of tenofovir plasma levels [18]. Ritonavir also increases the plasma concentrations of tenofovir. Interestingly, the combination of tenofovir with protease inhibitors seems to impair the kidney function at a higher magnitude than tenofovir with non-nucleoside reverse transcriptase [8, 9].

In the Zurich site of the Swiss HIV Cohort Study, which covers the majority of patients whose kidney biopsies would be sent to our hospital, 670 patients have received atazanavir, and 1,230 received tenofovir since their first use in 2000. Because not all treated patients in our area participate in the Swiss HIV Cohort Study, we estimate the risk of acute interstitial nephritis to be less than 0.57% (3 of 524 patients) among those who received both atazanavir and tenofovir within the framework of the Cohort Study in the last 6 years.

Atazanavir was registered in 2004. It is known to bear a favorable side-effect profile with significantly fewer lipid changes as compared to other protease inhibitors [7, 12, 16, 20]. The underlying mechanism of acute interstitial nephritis caused by atazanavir is not clear. Brewster and Perazella [1] speculate on a hypersensitivity reaction as a possible explanation for this phenomenon. The presence of eosinophilic granulocytes in two of our three cases would support this theory. We demonstrated a prevailing subset of CD8 positive T cells and some CD4 positive T cells in the interstitial lymphocytes, which supports a potential role of cell mediated mechanisms in the pathogenesis of tubulointerstitial nephritis in our patients [13]. A granulomatous reaction, usually occurring in delayed type hypersensitivity reactions caused by CD4 positive lymphocytes, could not be detected in our series. A cytotoxic T cell injury, mediated by CD4 and CD8 positive T cells, does not require prior sensitization, which is therefore a potential underlying mechanism of the tubulointerstitial injury [13]. The presence of activated cytotoxic T cells in our patients may point to this pathomechanism.

Acute renal failure as a side effect of antiretroviral therapy has been described in the literature [20, 23, 24]. Rhabdomyolysis with myoglobinuria was reported under zidovudine and delavirdine therapy [20, 23, 24]. Indinavir-induced crystal NP and acute tubular damage due to tenofovir and ritonavir are well-known side effects of drugs used for HIV treatment [20, 23, 24]. Tenofovir was administered together with atazanavir in all three patients; nevertheless, an extensive acute tubular necrosis, as a known side effect of tenofovir therapy, did not occur; we could demonstrate only a focal acute tubular necrosis in one of these patients.

Tubulointerstitial injuries, as inflammation, fibrosis, or tubular atrophy, are common features in interstitial nephropathies. If the underlying tubular or interstitial damage cannot be eliminated, these changes can give rise to chronic interstitial nephritis [13]. Furthermore, acute and chronic changes in the same tubulointerstitial compartment can coexist if etiologic factors become repeatedly manifest [13].

The frequency of interstitial nephritis in HIV infection varies in the literature. Diversity in its occurrence is mainly due to patient selection after and before antiretroviral therapies [10, 22]. In a recent study of Han et al. [11], 615 HIV-positive patients, all of them without antiretroviral therapy, were screened for proteinuria. Thirty patients were selected and underwent renal biopsy. Interstitial nephritis was only seen in 3 of 30 patients (10%). In an earlier autopsy study, Hailemariam et al. [10] determined the percentage of interstitial nephritis in Swiss HIV-positive patients, not treated with HAART, and reported a low prevalence with 14 of 239 patients (5.9%). However, of these 239 patients, 64% did not show clinical signs of NP before death. Therefore, the prevalence of interstitial nephritis might be higher in the group with clinical signs of NP.

Our study includes a time span after the introduction of HAART therapy. This might explain the higher prevalence of interstitial nephritis as compared to Han et al. and Hailemariam et al. [10].

The real frequency of interstitial nephritis arising under atazanavir and tenofovir therapy is, however, unclear. One reason is the patient selection. Not all patients receiving atazanavir and tenofovir will undergo kidney biopsy during the disease course. Subclinical or clinical acute interstitial nephritis, therefore, cannot be diagnosed and could be well missed in a subset of patients receiving this medication. Prospective studies with clearly defined patient collectives and protocol kidney biopsies will be necessary to address the incidence of acute interstitial nephritis under atazanavir and tenofovir therapy.

Interestingly, our study confirms that HIV-associated NP, a collapsing variant and secondary form of FSGS, is predominantly a disease of black patients, because we have observed this NP only in the black patients of our group. A variety of other glomerular diseases have been described in HIV-infected patients, as thrombotic microangiopathy and various forms of immune complex GN. According to the

literature [3, 4, 22], one of the most common immune complex-mediated glomerular lesion is membranoproliferative GN, particularly in HIV-infected patients coinfected with hepatitis C virus. These patients develop membranoproliferative GN type 1 or type 3 (with mixed membranous features). IgA NP, membranous GN, lupus-like GN, and immunotactoid GN are other immune complex-mediated glomerular lesions found in HIV-positive patients. The glomerular changes seen in our series correlate well with these data in the literature. Membranoproliferative GN, membranous GN, and IgA NP were the most commonly diagnosed immune complex-mediated glomerular diseases. In addition, in our study, membranoproliferative GN was particularly observed in HIV-infected patients coinfected with hepatitis C virus. It consisted of type 1 and type 3 membranoproliferative GN. Besides immune complex GN, thrombotic microangiopathy was a frequent lesion.

In summary, our findings show that acute interstitial nephritis can occur under atazanavir and tenofovir therapy. This side effect of antiretroviral medication should be considered in treatment planning for HIV-positive patients.

Acknowledgments The technical assistance of Mrs. Juliane Bigott and Mrs. Doris Guntersweiler is highly appreciated. Mr. N. Wey helped in the illustration. The study complies with the current ethical laws of the involved institutions.

References

1. Brewster UC, Perazella MA (2004) Acute interstitial nephritis associated with atazanavir, a new protease inhibitor. Am J Kidney Dis 44:e81–e84
2. Cho ME, Kopp JB (2004) HIV and the kidney: a status report after 20 years. Curr HIV/AIDS Rep 1:109–115
3. D'Agati V, Appel GB (1998) Renal pathology of human immunodeficiency virus infection. Semin Nephrol 18:406–421
4. D'Agati V, Jennette J, Silva F (2005) Non-neoplastic kidney diseases. ARP Press, Silver Spring, MD
5. European Medicines Agency (2006) http://www.emea.eu.int/humandocs/PDFs/EPAR/viread/351001en8b.pdf; accessed on 8 Mar 2007
6. Fogo A, Kashgarian M (2005) Diagnostic atlas of renal pathology, 1st edn. Elsevier, Saunders
7. Friedland G, Andrews L, Schreibman T, Agarwala S, Daley L, Child M, Shi J, Wang Y, O'Mara E (2005) Lack of an effect of atazanavir on steady-state pharmacokinetics of methadone in patients chronically treated for opiate addiction. Aids 19:1635–1641
8. Fux C, Simcock M, Wolbers M, Bucher H, Cavassini M, Opravil M, Vernazza P, Hirschel B, Bernasconi E, Furrer H, Swiss HIV Cohort Study S (2007) Tenofovir treatment is associated with a decrease in calculated glomerular filtration rates in a large observational cohort. In: 14th Conference on retroviruses and opportunistic infections, Los Angeles, USA, 25–28 February
9. Goicoechea M, Liu S, Best B, Sun S, Jain S, Kemper C, Witt M, Diamond C, Haubrich R, Louie S, California Collaborative Treatment Group CT (2007) Increased renal impairment in patients receiving TDF+PI vs TDF+NNRTI. In: 14th Conference on retroviruses and opportunistic infections, Los Angeles, USA, 25–28 February
10. Hailemariam S, Walder M, Burger HR, Cathomas G, Mihatsch M, Binswanger U, Ambuhl PM (2001) Renal pathology and premortem clinical presentation of Caucasian patients with AIDS: an autopsy study from the era prior to antiretroviral therapy. Swiss Med Wkly 131:412–417
11. Han TM, Naicker S, Ramdial PK, Assounga AG (2006) A cross-sectional study of HIV-seropositive patients with varying degrees of proteinuria in South Africa. Kidney Int 69:2243–2250
12. Izzedine H, Launay-Vacher V, Peytavin G, Valantin MA, Deray G (2005) Atazanavir: a novel inhibitor of HIV-protease in haemodialysis. Nephrol Dial Transplant 20:852–853
13. Jennette JC, Olson JL, Schwartz M, Silva F (2007) Heptinstall's pathology of the kidney, 6th edn. Lippincott Williams & Wilkins
14. Karras A, Lafaurie M, Furco A, Bourgarit A, Droz D, Sereni D, Legendre C, Martinez F, Molina JM (2003) Tenofovir-related nephrotoxicity in human immunodeficiency virus-infected patients: three cases of renal failure, Fanconi syndrome, and nephrogenic diabetes insipidus. Clin Infect Dis 36:1070–1073
15. Kern W, Laszik Z, Nadasdy T, Silva F, Bane B, Pitha J (1999) Atlas of renal pathology. Saunders, Philadelphia
16. Kim RJ, Wilson CG, Wabitsch M, Lazar MA, Steppan CM (2006) HIV protease inhibitor-specific alterations in human adipocyte differentiation and metabolism. Obesity (Silver Spring) 14:994–1002
17. Moddel M, Pfammatter R, Varga Z, Keusch G (2006) Acute tubulointerstitial nephritis in HIV infection. Schweiz Rundsch Med PRAXIS 95:949–951
18. Panel on Antiretroviral Guidelines for Adult and Adolescents (2006) Guidelines for the use of antiretroviral agents in HIV-infected adults and adolescents. Department of Health and Human Services, October 10, 2006. Available at http://www.aidsinfo.nih.gov/ContentFiles/AdultandAdolescentsGL.pdf. Accessed 8 Mar 2007, pp 1–113
19. Peyriere H, Reynes J, Rouanet I, Daniel N, de Boever CM, Mauboussin JM, Leray H, Moachon L, Vincent D, Salmon-Ceron D (2004) Renal tubular dysfunction associated with tenofovir therapy: report of 7 cases. J Acquir Immune Defic Syndr 35:269–273
20. Roling J, Schmid H, Fischereder M, Draenert R, Goebel FD (2006) HIV-associated renal diseases and highly active antiretroviral therapy-induced nephropathy. Clin Infect Dis 42:1488–1495
21. Scott JD, Wolfe PR, Bolan RK, Guyer B (2006) Serious renal impairment occurs rarely with use of tenofovir DF. HIV Clin Trials 7:55–58
22. Striker G, Striker L, D'Agati V (1997) The renal biopsy, 3rd edn. Saunders
23. Szeto CC, Chow KM (2005) Nephrotoxicity related to new therapeutic compounds. Ren Fail 27:329–333
24. Valle R, Haragsim L (2006) Nephrotoxicity as a complication of antiretroviral therapy. Adv Chronic Kidney Dis 13:314–319
25. Wyatt CM, Klotman PE (2006) Antiretroviral therapy and the kidney: balancing benefit and risk in patients with HIV infection. Expert Opin Drug Saf 5:275–287

Virchows Arch (2007) 450:671–681
DOI 10.1007/s00428-007-0417-4

ORIGINAL ARTICLE

Immunohistochemical study on caveolin-1α in regenerating process of tubular cells in gentamicin-induced acute tubular injury in rats

Yoshihide Fujigaki · Masanori Sakakima · Yuan Sun · Tetsuo Goto · Naro Ohashi · Hirotaka Fukasawa · Takayuki Tsuji · Tatsuo Yamamoto · Akira Hishida

Received: 2 August 2006 / Revised: 17 March 2007 / Accepted: 4 April 2007 / Published online: 27 April 2007
© Springer-Verlag 2007

Abstract Caveolin-1, a principal component of caveolae, modulates growth signaling, endocytosis, and intracellular transport. We examined the expression of caveolin-1α and its relation to cell cycle and caveolin-interacting growth factor receptors in regenerating proximal tubules (PTs) after gentamicin-induced acute renal failure in rats. Caveolin-1α appeared in regenerating PTs as early as day 4 after last gentamicin, peaked at days 6 to 8, and showed cytoplasmic pattern after day 8. Immunoelectron microscopy revealed caveolin-1α-positive caveolae on the cell membrane and in cytoplasms in regenerating PTs at days 4 to 8 and caveolin-positivity confined to cytoplasms after day 10. The number of PT cells with proliferation markers peaked at day 6 and decreased afterwards as expression of cyclin-dependent kinase inhibitors increased. Platelet-derived growth factor receptor-β (PDGFR-β) and epidermal growth factor receptor (EGFR) were colocalized with caveolin-1α in proliferating PTs as early as day 4. Phosphorylated EGFR increased at day 8 and afterwards when caveolins dissociated from EGFR or decreased. In case of PDGFR-β, phosphorylation seemed to be associated with the increase and association of caveolins to the receptors. Our results suggest that transient expression of caveolin-1α in early regenerating PTs might contribute to the regenerating process of PTs through modulating growth factor receptors.

Y. Fujigaki (✉) · M. Sakakima · Y. Sun · T. Goto · N. Ohashi · H. Fukasawa · T. Tsuji · T. Yamamoto · A. Hishida
First Department of Medicine,
Hamamatsu University School of Medicine,
1-20-1 Handayama,
431-3192 Hamamatsu, Japan
e-mail: yf0516@hama-med.ac.jp

Keywords Acute renal failure · Caveolae · Caveolin · Gentamicin · Proximal tubule · Regeneration · Platelet-derived growth factor · Epidermal growth factor

Introduction

Caveolae are described as 50- to 100-nm flask-shaped invaginations within the plasma membrane and are thought to play a role in important physiological functions such as cell surface signaling, endocytosis, and intracellular cholesterol transport [20]. Caveolin-1, caveolin-2, and caveolin-3, a family of ~22 kD integral membrane proteins, are the main components of caveolae [20]. Caveolin-3 is expressed exclusively in myocytes, whereas caveolin-1 and caveolin-2 are often coexpressed and are found in many tissue types [20]. Caveolins interact with multiple caveolae-associated molecules [20], such as hormones, growth factor receptors including platelet-derived growth factor (PDGF) [8], and epidermal growth factor (EGF) [14], and signaling molecules, which are involved in cell growth and proliferation, suggesting that caveolae may function as unique cell surface signal transduction domains. It is also known that the signal transducing proteins are rapidly recruited into caveolae upon PDGF [8] and EGF [14] stimulations and that caveolin-1 and caveolin-3 but not caveolin-2 directly bind to PDGF receptor-β (PDGFR-β) and EGF receptor (EGFR), inhibiting their autophosphorylation in vitro as kinase inhibitors [2, 23].

Under normal condition, terminally differentiated, senescent cells such as adipocytes, endothelial cells, and fibroblasts [20] contain high caveolin-1 levels and therefore exhibit a marked insensitivity to growth factor-mediated stimulation. Renal proximal tubules (PTs) are highly

differentiated but do not exhibit immunoreactive caveolin-1 [1]. Zager et al. [24] and Mahmoudi et al. [10] have reported marked increases in caveolin-1 in rat PT cells during the induction and maintenance phases of ischemia/reperfusion and myoglobinuric models of acute renal failure (ARF), suggesting that caveolin-1 expression may mediate PT cell death or survival of injured PT cells. However, it is not clear whether caveolins participate in regenerating PT cells after ARF. During cellular recovery after ARF, various growth factors/cytokines including EGF and PDGF [15, 16] have been reported to contribute to the tubular regeneration. As receptor tyrosine kinases, EGFR and PDGFR are caveolin-interacting molecules [2, 8, 14, 23]; caveolin might participate in the regenerating process of PT cells after ARF.

In the present study, we used a model of gentamicin-induced ARF in rats. This model is a well-established toxic ARF model known to induce PT damage followed by recovery mainly in the renal cortex [5]. We determined the expression and kinetics of caveolin-1α and defined the spatial and temporal correlations between caveolin-1α expression, state of cell cycle, and caveolin-interacting signaling molecules (PDGFR-β and EGFR) in regenerating PT cells after induction of ARF.

Materials and methods

Induction of gentamicin-induced acute tubular injury

A total of 42 male Wistar rats (200–250 g, SLC, Shizuoka, Japan) were used in the present study. Thirty-five rats were injected subcutaneously with 400 mg/kg body weight/day of gentamicin sulfate solution (Sigma-Aldrich, St. Louis, MO, USA) for 2 days in divided doses (every 8 h). We previously reported [5] that subcutaneous injection of gentamicin at this dose in rats increased serum creatinine levels and induced proximal tubular damage only in the cortex, which reached peak levels at day 6 after the end of gentamicin (day 0 falls at 8 h after the last gentamicin). On the other hand, Ki67-positive proliferating PTs were found as early as day 4 and peaked in number at day 6. Regenerating PTs almost covered the denuded tubular basement membrane by day 10 [5]. Therefore, in the present study, rats were killed at days 4, 6, 8, 10, and 12 during the repair phase after PT injury. Rats at each time point and normal rats as controls were anesthetized with intraperitoneal pentobarbital sodium (30 mg/kg), then both kidneys were removed after flushing phosphate-buffered saline (PBS) for immunohistochemistry, immunofluorescence, conventional electron microscopy, immunoelectron microscopy, and Western blot analysis.

The experimental protocol was approved by the Ethics Review Committee for Animal Experimentation of Hamamatsu University School of Medicine.

Immunohistochemistry

The kidneys were bisected through the longitudinal axis, fixed with 4% paraformaldehyde, and embedded in paraffin. Three-micrometer-thick sections were deparaffinized, and endogenous peroxidase was blocked by treatment with 3% H_2O_2 for 30 min. The sections were then incubated with the primary antibody listed in Table 1 and reacted with

Table 1 Antibodies used to detect specific antigens

Primary antibody (Ab)	Supplier
Rabbit polyclonal Ab against caveolin-1α (N-20, sc-894), epitope mapping at the N terminus of human origin	Santa Cruz Biotechnology, Santa Cruz, CA, USA
Rabbit polyclonal Ab against caveolin-2 (H-96, sc-7942), epitope corresponding to amino acids 54-149 of caveolin-2 of human origin	Santa Cruz
Rabbit polyclonal Ab against cyclin D1 (H295, sc-753)	Santa Cruz
Rabbit polyclonal Ab against p53 (FL-393, sc-6243)	Santa Cruz
Rabbit polyclonal Ab against p27 (M-197, sc-776)	Santa Cruz
Mouse monoclonal Ab against p21 (F-5, sc-6246)	Santa Cruz
Mouse monoclonal Ab against Ki67	Novocastra Laboratories, Newcastle upon Tyne, UK
Goat polyclonal Ab against EGFR (1005, sc-03G)	Santa Cruz
Rabbit polyclonal Ab against EGFR (membrane 2232)	Cell Signaling Technology, Beverly, MA, USA
Goat polyclonal AB against p-EGFR (phospho-specific Tyr 1173, sc-12351)	Santa Cruz
Goat polyclonal Ab against PDGFR-β (M-20, sc-1627)	Santa Cruz
Goat polyclonal Ab against p-PDGFR-β (Tyr857, sc-12907)	Santa Cruz
Goat polyclonal Ab against megalin (p-20, sc-16478)	Santa Cruz

PDGFR Platelet-derived growth factor receptor, *p-PDGFR* phosphorylated-PDGFR, *EGFR* epidermal growth factor receptor, *p-EGFR* phosphorylated-EGFR

the corresponding biotinylated secondary antibody (donkey polyclonal antibody against rabbit IgG, goat IgG, or mouse IgG, Chemicon International, Temecula, CA, USA) for 30 min at room temperature. Then, avidin-conjugated peroxidase (Nichirei, Tokyo, Japan) was added for 30 min. The reaction products were visualized by diaminobenzidine.

To examine the relationship between expression of caveolin-1α and state of cell cycle in PT cells, double-immunostaining only for caveolin-1α and cyclin D1 or caveolin-1α and Ki67 was performed using the method by Lan et al. [7]. After staining the sections with cyclin D1 or Ki67 as above, they were treated by microwave oven-heating for 2×5 min in 0.01 M sodium citrate, pH 6.0, at 800 W, then incubated with caveolin-1α antibody and with biotinylated secondary antibody. Then, Vectastain ABC-AP reagent (Vector Laboratories, Burlingame, CA, USA) was added, and the Vector Red alkaline Phosphatase Substrate Kit I (Vector Laboratories) was used as chromogen.

For control sections, the first antibodies were omitted or replaced by normal mouse or rabbit IgG. Signals in both control and experimental sections were negative or negligible.

Immunofluorescence studies

Portions of renal cortex were snap frozen in cold *N*-hexane and stored at −70°C for immunofluorescence studies. Immunofluorescence studies were performed on 4-μm-thick cryostat sections fixed in cold acetone. Sections were stained with rabbit polyclonal anti-caveolin-1α (Santa Cruz) followed by Alexa Fluor 488^{R} donkey anti-rabbit IgG (Molecular Probes Eugene, OR, USA) for 30 min. After staining the sections for caveolin-1α, they were incubated with polyclonal goat anti-EGFR or goat anti-PDGFR and with Alexa Fluor 546^{R} donkey anti-goat IgG (Molecular Probes) for 30 min at room temperature. All sections were observed under immunofluorescent microscopy.

Conventional electron microscopy

Small portions of renal tissues were fixed in 2% glutaraldehyde in 0.1 M phosphate buffer (pH 7.4) at 4°C for 2 h, postfixed in 1% OsO_4 resolved in the same buffer for 1 h, and then embedded in Epon. Ultra-thin sections were counterstained with uranyl acetate and lead citrate, then examined under an electron microscope (JEM-1220, JEOL, Japan).

Immunoelectron microscopy

Renal tissues were immersed in 4% paraformaldehyde for 9 h, cryoprotected in graded sucrose solution, and then snap frozen in cooled *N*-hexane. Eight-micrometer cryostat sections were incubated with caveolin-1α antibody. After the sections had been fixed in 2% glutaraldehyde for 10 min, the reaction products were visualized by diaminobenzidine, then the sections were postfixed in 1% OsO_4 for 2 h. Epon 812-embedded ultrathin sections were stained with lead citrate and examined with a JEM-1220 electron microscope.

Western blot analysis of caveolin-1α

Immunoblotting was repeated at least three times with samples from a minimum of three animals for each time point. Protein extracts were prepared from cold Triton X-100 insoluble extracts (detergent resistant membranes) of isolated renal cortical tissue using the method of Mendez et al. [13]. Equal amount of extracted protein (7.5 μg) were subjected to electrophoresis on 10% sodium dodecyl sulfate-polyacrylamide gel electrophoresis (SDS-PAGE) gels, then transferred onto polyvinylidene fluoride microporous membranes. The membranes were incubated overnight in 5% skim milk in Tris-buffered saline with Tween (TBS-T) buffer (20 mM Tris–HCl, pH 7.6; 150 mM NaCl; and 0.1% Tween-20) at room temperature for 1 h. Immunoblotting (caveolin-1α or β-actin) was then performed as described previously [25].

Semiquantitative analysis of immunohistochemically stained sections

The numbers of cyclin-D1-, Ki67-, p21-, p27- and p53-positive PT in the cortex in single immunostaining sections were counted at ×400 magnification.

Discrimination between proximal and distal tubules, even in conditions of regeneration, was performed by adapting the following criteria [18]: (a) PTs were characterized by the absence of clearly recognizable intercellular delineations and eventually by the presence of a brush border; (b) distal tubules were identified on the basis of clearly recognizable intercellular delineations and by the presence of stripes, originating from the basal cell surface and extending towards the cell apex. The number of immunoreactive cells in each rat represented the average number of 40 fields examined and the mean numbers before and at days 4, 6, 8, 10, and 12 after gentamicin injection were displayed in histograms.

Statistical analysis

Data are expressed as mean±SD. Differences between data sets were examined for statistical significance using one-way analysis of variance followed by Fisher's *t* test. A p value of <0.05 was accepted as statistically significant.

Results

Cell-cycle-related molecules in regenerating PTs

Cyclin-D1 (G1 phase marker)-positive and Ki67 (S phase marker)-positive proliferating PTs were found as early as day 4, and both peaked in number at day 6, then decreased (Fig. 1a–d,k,l). Cyclin-dependent kinase inhibitors p21 and p27 were found in PTs, peaked in number at days 10 and 8–10, respectively (Fig. 1e–h,m,n). p53 was also increased in PTs and peaked in number at day 8 (Fig. 1i,j,o).

Redifferentiation of regenerating PTs

Megalin, as a differentiated phenotype of PT, was found in the brush-border of PT in the normal kidney and reappeared in the reappeared brush-border of some regenerating PTs after day 8 and in almost all PTs by day 12 (Fig. 2 and Table 2).

Immunohistochemistry of caveolin-1α and caveolin-2 and relation between caveolin-1α and cell cycle in regenerating PTs

As reported by other investigators [1, 24], immunoreactive caveolin-1 was detected in glomerular/vascular or distal tubule structures but not in PT cells in the cortex of normal rat kidneys (Fig. 3a,f). Peritubular capillary endothelial cells showed a faint staining of caveolin-1α in normal rat kidneys, and such staining did not change after ARF (Fig. 3f,g). Caveolin-1α was found in injured PTs and exfoliated PTs after induction of ARF in the cortex (Fig. 3b, c,g). The regenerating PTs showed a weak expression of caveolin-1α as early as day 4 (Fig. 3b) and strong expression at days 6 to 8 (Fig. 3c,d,g) as membrane/cytoplasmic pattern (Table 2). Caveolin-1α staining began to be confined in the cytoplasm exhibiting a coarse granular pattern and with reduced intensity after day 8 (Fig. 3d,e). Double immunohistochemical staining for caveolin-1α and cyclin D1 revealed that cyclin-D1-positive (G1 phase marker) PT cells were also positively stained for caveolin-1α (Fig. 3h), indicating that early regenerating PT cells expressed caveolin-1. Double immunohistochemistry of caveolin-1α and Ki67 (S phase marker) revealed that caveolin-1α showed a tendency for weak intensity and granular staining in the cytoplasm of Ki67-negative PT cells after day 8 compared to that in Ki67-positive PT cells (Fig. 3i).

Immunoreactive caveolin-2 showed a distribution pattern similar to that of caveolin-1α in the normal kidneys (Fig. 3a,j). After induction of acute tubular injury, the regenerating PTs showed moderate caveolin-2 expression at day 4 (Fig. 3k) and strong expression at day 6 (Fig. 3l; Table 2). Caveolin-2 staining rapidly decreased on day 8 (Fig. 3m) and became almost negative without coarse granular pattern in the cytoplasm (Fig. 3n; Table 2).

Ultrastructural findings of caveolae and caveolin-1α–positive structures in regenerating PTs

Conventional electron microscopy revealed almost no caveolae formation in normal PT cells (not shown). However, flask-like structures of about 100 nm diameter could be focally found, some of which were open to the apical or basal fronts of the regenerating PT cells at days 4 to 6, suggesting caveolae formation (Fig. 4a). Possible caveolae-derived vesicles including interconnected structures could also be found in cytoplasm in the regenerating PT cells at days 4 to 8 (Fig. 4b), but apparent caveolae-derived structures could not be identified after day 10. Immunoelectron microscopy supported the conventional electron microscopic findings. There was almost no caveolin-1-positive structures in the normal PT (Fig. 4c); however, caveolin-1α-positive flask-like structures with or without opening to the free or basal fronts of cells or apparently free in the cytoplasm could be found at days 4 to 6 (Fig. 4d,e). The majority of the caveolin-1α-positive structures were part of large clusters of interconnected structures, grape-like structures, or with unusual shapes, accumulated at the cell periphery and in the cytoplasm (Fig. 4d,e). With time, the caveolin-1α-positive structures at the cell periphery were decreased in density and were not found in the regenerated brush-border at day 8 (Fig. 4f). After day 10, most caveolin-1 positivity was limited to certain intracellular compartments including mitochondria (Fig. 4g).

Western blot analysis of caveolin-1α

Western blot analysis of Triton X-100 insoluble fraction showed marked increase in caveolin-1α levels in the renal cortex after induction of ARF and peaked at day 6 (Fig. 5).

Expression of PDGFR-β and EGFR and their phosphorylated forms in regenerating PTs

Immunoreactive PDGFR-β was negative in normal PTs but was found in the regenerating PTs as early as day 4 and peaked at days 6 to 8, then decreased rapidly (Fig. 6a–e and Table 2). p-PDGFR-β was found as early as day 4, peaked and concentrated at the apical membrane at day 6, then almost disappeared by day 10 (Fig. 6f–j and Table 2).

Immunoreactive EGFR was constitutively positive in the brush-border in normal PTs (Fig. 6k). It was also positive in the regenerating PTs as early as day 4, and peaked at days 6 to 8 (Fig. 6l-n). It increasingly reappeared in the brush-

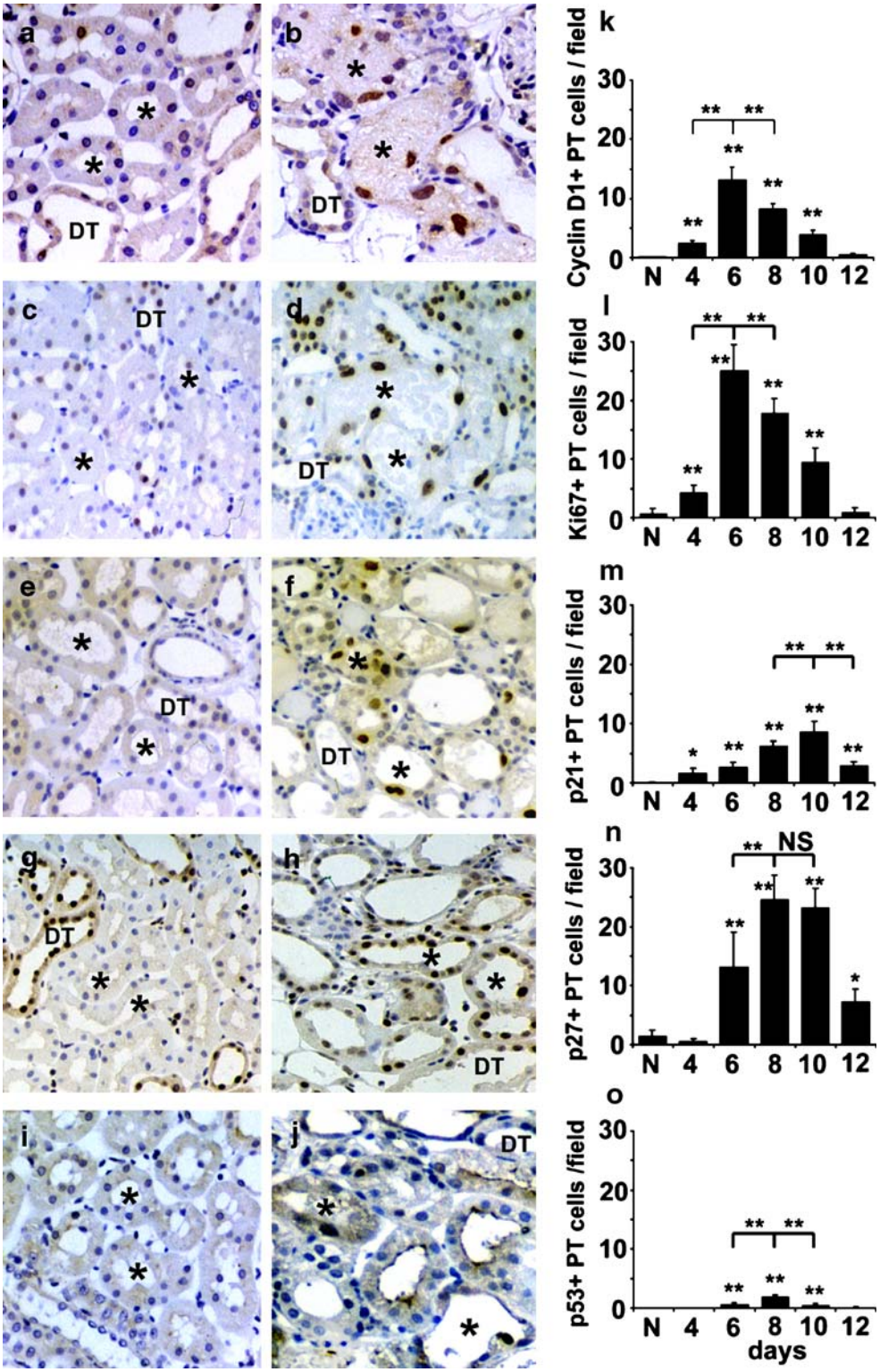

Fig. 1 **a**–**j** Immunohistochemistry of cell-cycle-related molecules (cyclin D1, Ki67, p21, p27, and p53) in PT cells before (*left column*) and at days 6 (**b**, **d**), 8 (**h**, **j**), and 10 (**f**) after (*middle column*) induction of acute tubular injury. *Asterisks* PTs; *DT* distal tubules; *brown nuclei* indicate positive immunoreaction. **k**–**o** The number of cyclin D1+, Ki67+, p21+, p27+, or p53+ PT cells per field before (**n**) and days after induction of acute tubular injury (*right column*). Data are expressed as mean±SD of five rats. *$p<0.05$, **$p<0.01$ vs normal control. *NS* Not significant

border after day 8 (Fig. 6n,o). Two different antibodies against EGFR used in this study provided similar results. p-EGFR was constitutively positive in the brush-border in normal PTs (Fig. 6p). p-EGFR was almost negative at day 4 but was found weakly at day 6 and increasingly reappeared in the brush-border after day 8 (Fig. 6q–t and Table 2).

Relationship between caveolin-1α and PDGFR-β or EGFR in regenerating PTs

Caveolin-1α colocalized with PDGFR-β partially on the cell membrane at days 4 to 8 and in the cytoplasm of the regenerating PTs at day 8 (Fig. 7a–c). Caveolin-1α was also

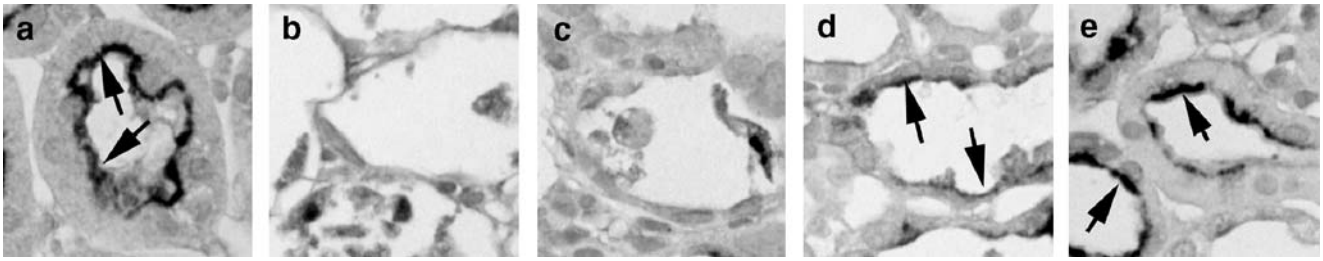

Fig. 2 Immunohistochemistry of megalin in PT cells in normal (**a**) and during repair phase of acute tubular injury at days 4 (**b**), 6 (**c**), 8 (**d**), and 10 (**e**). *Arrows* indicate positive immunoreaction

colocalized with EGFR partially on the cell membrane and in the cytoplasm of regenerating PTs at days 4 to 8 (Fig. 7d–f). After day 10, most EGFR was found on the apical surface of PT (corresponding to the brush-border) without caveolin-1α colocalization (Fig. 7g–i). EGFR transiently localized in the nuclei at days 4 to 6 (Fig. 7h).

Discussion

In the present study, induction of acute tubular injury by gentamicin resulted in appearance of caveolin-1α expression in cyclin-D1-positive PT cells at day 4. As we previously found almost no proliferating PT cells at day 2 after ARF in this model [5], cyclin-D1-positive PT cells at day 4 were early regenerating PT cells in this study. Caveolin-1α expression peaked at day 6, as shown by immunohistochemistry, at the time of peak PT proliferation, judged by the number of Ki67-positive PT cells. Western blotting also showed increased caveolin-1α levels in the cortex as early as day 4, peaking at day 6. However, the strong increasing of caveolin-1α at day 4 displayed by Western blot did not seem to correlate well with the results of corresponding immunostains in PT cells. As there were many caveolin-1α-positive injured PT cells within the tubular lumen at day 4 (Fig. 3b), it is possible that the results of the Western blot may reflect caveolin-1α protein not simply in regenerating PT cells but also in injured PT cells and other cell types. Coarse granular cytoplasmic staining of caveolin-1α was found in the late regenerating PT cells after day 8 and tended to become weaker in Ki67-negative PT cells. Some PT cells were redifferentiated after day 8, judged by megalin-positivity. Conventional electron microscopy and immunoelectron microscopy revealed the presence of caveolin-1α-positive flask-like structures, representing caveolae [20], on the plasma cell membranes of early regenerating PT cells and caveolin-1α-positive structures were increasingly internalized with time in the cytoplasm as grape-like vesicles. Caveolin-1α-positive vesicles were almost confined in various intracellular compartments in the late regenerating PT cells after day 10. The findings showed that the early proliferating, regenerating PT cells transiently expressed caveolae/caveolin-1α on the plasma membrane, and the subsequent internalization of

Table 2 Summary of staining for caveolin-1α, caveolin-2, EGFR, p-EGFR, PDGFR-β, p-PDGFR-β, and megalin in proximal tubular cells in the renal cortex of control (N=5) and gentamicin-injected rats (N=5)

Protein	Pattern	Control	Days after gentamicin injection				
			4	6	8	10	12
Caveolin-1α	M/C	−/−	+	++ to +++[a]	++ to +++[b]	+ to ++[b]	−/±[b]
Caveolin-2	M/C	−/−	++	+++	−/± to +[a]	−/±	−/±
PDGFR-β	M/C	−	+ to ++	++ to +++[a]	++ to +++[a]	−/± to +	−/±
p-PDGFR-β	M	−	− to ±	+ to ++	± to +	− to ±	−
EGFR	B	+++	ND	ND	− to +	+ to ++	+++
	M/C	−	+ to ++	++ to +++[a]	++ to +++[a]	± to +	− to ±
p-EGFR	B	+	ND	ND	+	+ to ++	++
	M/C	±	−	± to +	+	− to ±	−
Megalin	B	+++	ND	ND	− to +	+ to ++	+++

Staining intensity: −, negative; ±, trace; +, weak; ++, moderate; +++, strong. Staining intensity was graded by comparison with maximal staining in normal control and/or regenerating PT cells. The staining intensity of phosphorylated forms was evaluated by comparison with that of non-phosphorylated forms.

M Membrane pattern, *C* cytoplasmic pattern, *B* brush-border, *ND* brush-border was not detectable. See Table 1 for other abbreviations.

[a] Fine granular pattern

[b] Coarse granular pattern

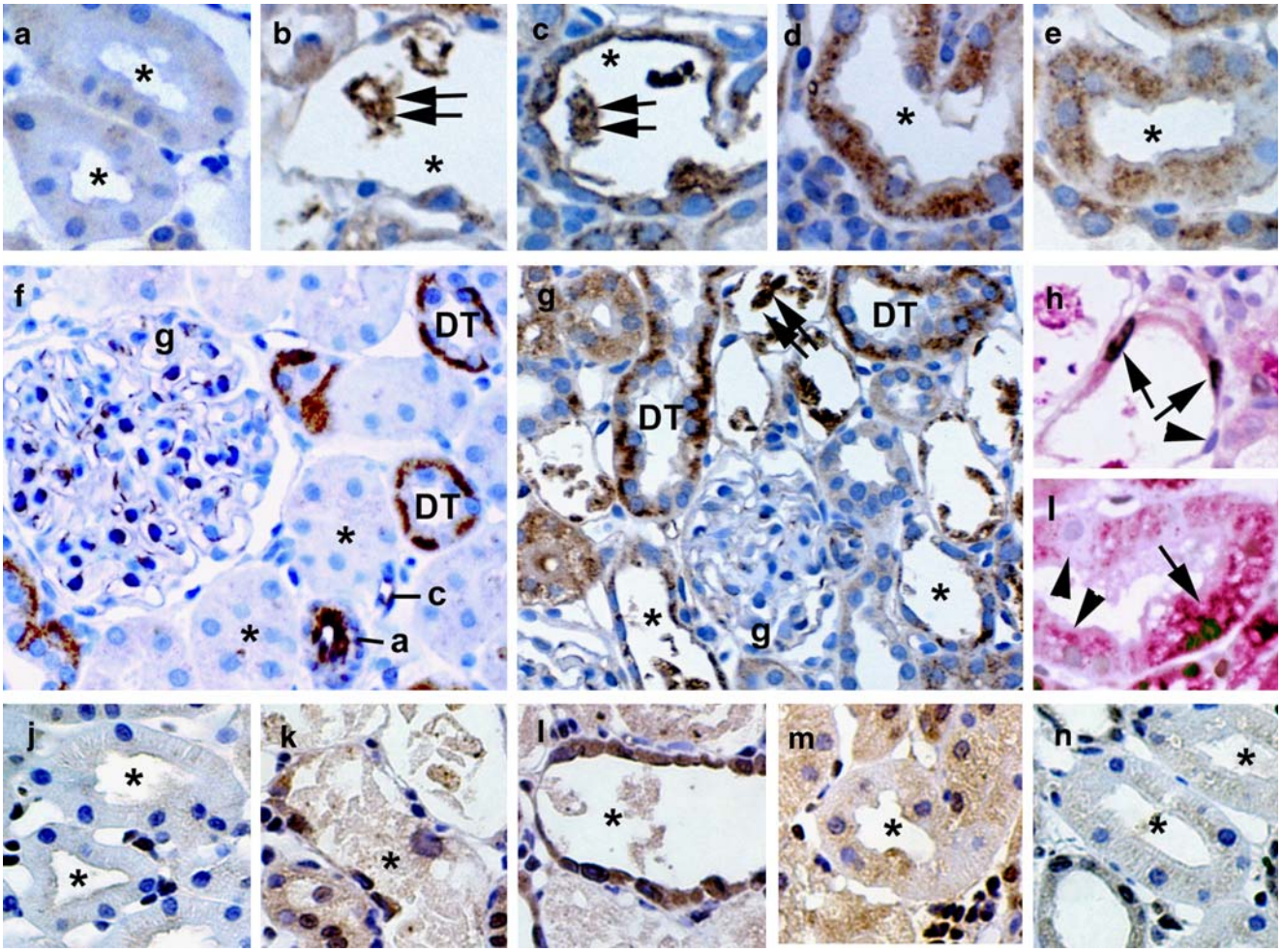

Fig. 3 **a**–**g** Immunohistochemistry of caveolin-1α in PT cells in normal (**a**, **f**) and at days 4 (**b**), 6 (**c**, **g**), 8 (**d**), and 10 (**e**) after last gentamicin injection. *Brown color* indicates positive immunoreaction. *Asterisks* PT cells; *DT* distal tubular cells; *g* glomerulus; *a* small artery; *c* peritubular capillary. *Double arrows* indicate injured PT cells with positive caveolin-1α. **h**, **i** Double immunohistochemistry of caveolin-1α (*pink color*) and cyclin D1 (*brown nuclei*) at day 4 (**h**), or caveolin-1α (*pink color*) and Ki67 (*brown nuclei*) at day 8 (**i**). *Arrows* indicate positive immunoreactive nuclei and *arrowheads* indicate negative immunoreactive nuclei. **j**–**n** Immunohistochemistry of caveolin-2 in PT cells in normal (**j**) and at days 4 (**k**), 6 (**l**), 8 (**m**), and 10 (**n**) after induction of acute tubular injury. *Brown color* indicates positive immunoreaction. *Asterisks* PT cells

the caveolin-1α was suggested in the regenerating process of PT cells.

Caveolin-1 expression was demonstrated to arrest NIH 3T3 cells in the G0/G1 phase of the cell cycle through a p53/p21-dependent pathway [4]. During the process of reduction in PT proliferation in this model, p53 and p21 expression levels were significantly increased, and the p53- and p21-expressing cells reached peak numbers among regenerating PT cells at days 8 and 10, respectively. Furthermore, the expression level of p27 increased, and the p27-positive cells reached peak numbers from days 8 to 10. The number of p27-positive PT cells was higher than that of p21-positive PT cells. These results suggest that it is unlikely that caveolin-1α expression in the regenerating PT cells mainly contributed to the induction of PT cells to exit the S-phase of the cell cycle through a p53/p21-dependent pathway in this model.

It was reported that formation of caveolae is polarized in basolateral distribution in wild-type MDCK II and caveolin-1 transfected Caco-2 cells [21]. Moreover, in nontransformed NIH 3T3 cells, as cells become confluent, caveolin-1 was found to be concentrated at the areas of cell–cell contact, suggesting the ability of caveolin-1 to regulate contact inhibition and growth arrest in nontransformed cells [22]. However, in our model, caveolae were distributed focally both on the basal and free (apical) plasma membranes of early regenerating PT cells but disappeared from the plasma membrane, suggesting that caveolin-1α does not seem to play a role in regulation of contact inhibition in our model.

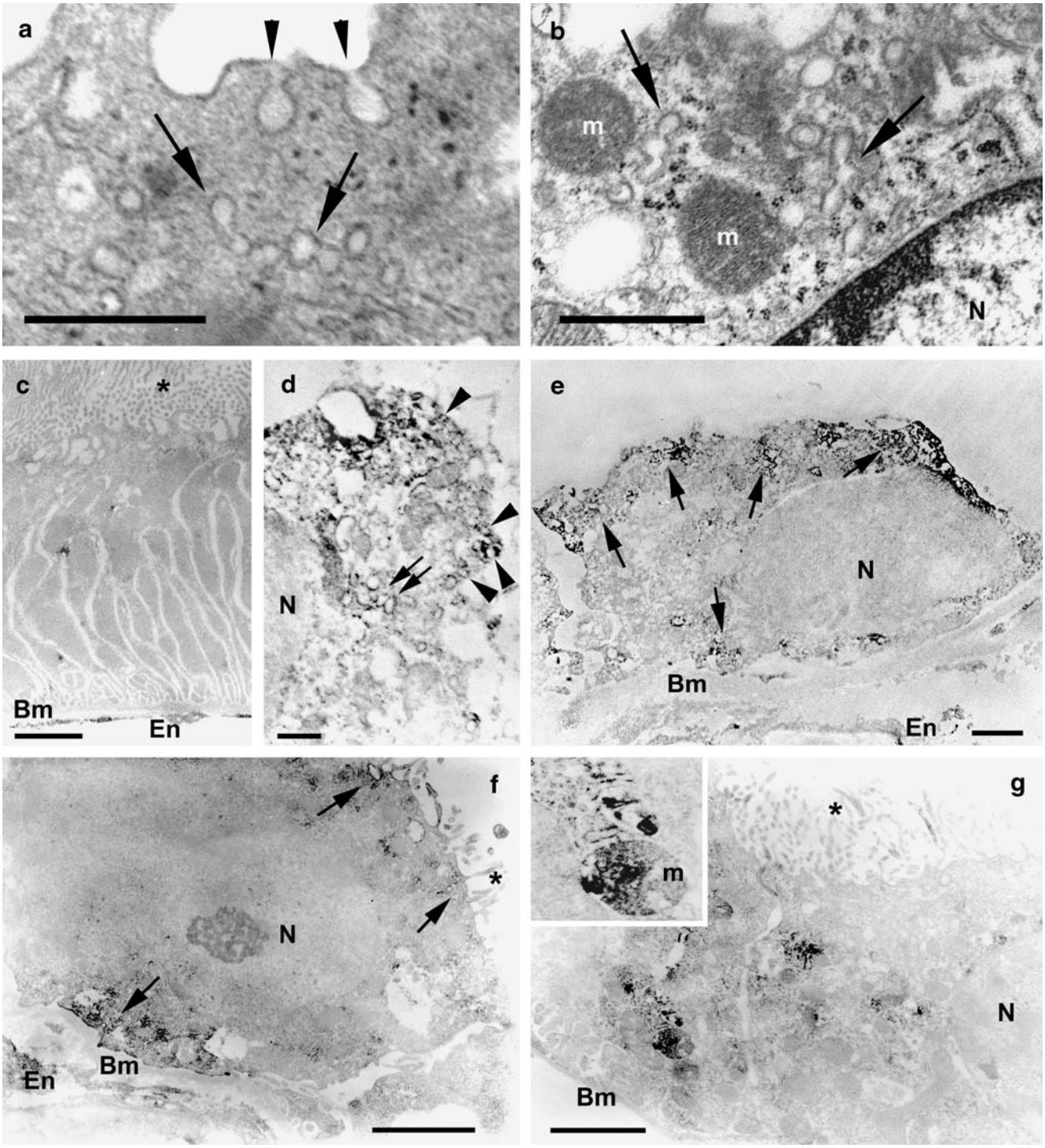

Fig. 4 Conventional electron micrographs of PT cells days 4 (**a**) and 8 (**b**) after induction of acute tubular injury. *Arrowheads* Caveolae; *arrows* possible caveolae-derived vesicles. Immunoelectron microscopic findings of immunoreactive caveolin-1α (*black color*) in PT cells in normal (**c**) and days 4 (**d**), 6 (**e**), 8 (**f**), and 10 (**g**) after induction of acute tubular injury. *Arrowheads* Caveolin-1α-positive caveolae; *double arrows* caveolin-1α-positive vesicles or interior compartments in cytoplasm; *arrows* caveolin-1α-positive caveolae or clusters of interconnected structures, grape-like structures or with unusual shapes; *asterisks* brush-border; *inset* caveolin-1α-positive interior compartment. *N* Nucleus; *m* mitochondria; *Bm* tubular basement membranes; *En* endothelial cells. **a**, **b**, **d** Bars=0.5 μm; **c**, **e**–**g** Bars=5.0 μm

In the process of caveolin-1 recycling, caveolin-1 normally moves with caveolae-derived vesicles to various intracellular compartments, such as endoplasmic reticulum and Golgi apparatus, and then recycles back to the cell surface [9]. In addition, it is suggested that caveolin-1 can enter the cytoplasm as a soluble protein embedded in lipid

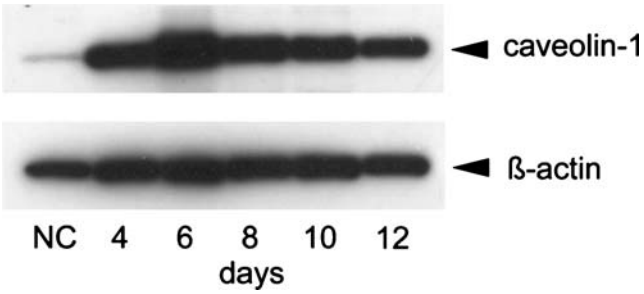

Fig. 5 Western blots of protein from the detergent-resistant membrane fraction of the renal cortex before (*NC*) and during the repair phase after acute tubular injury incubated with antibodies for caveolin-1α and β-actin

particles. Soluble caveolin-1 may translocate to the endoplasmic reticulum, remain in the cytosol, or to mitochondria [9]. Thus, it is possible that caveolin-1α-positive vesicles could be found in endomembranes and mitochondria in the present model. However, loss of caveolae on the plasma membrane of the redifferentiated PT cells may rather suggest that caveolin-1α-positive vesicles formed in Golgi apparatus were not sorted into the plasma membrane in the process of reduction in caveolin-1α synthesis, although the messenger RNA level of caveolin-1α was not examined.

Caveolin-1 and caveolin-2 are often coexpressed and are found in many tissue types because caveolin-2 seems to interact with caveolin-1, forming hetero-oligomers [20] that determine the localization of these proteins within the cell [19]. In the present study, caveolin-1α and caveolin-2 were coexpressed in proliferating PT cells; however, unlike caveolin-1α, caveolin-2 was not found in significant amounts in the cytoplasm of redifferentiating PT cells. This might reflect the dependence of caveolin-2 on caveolin-1 for plasma membrane localization [19].

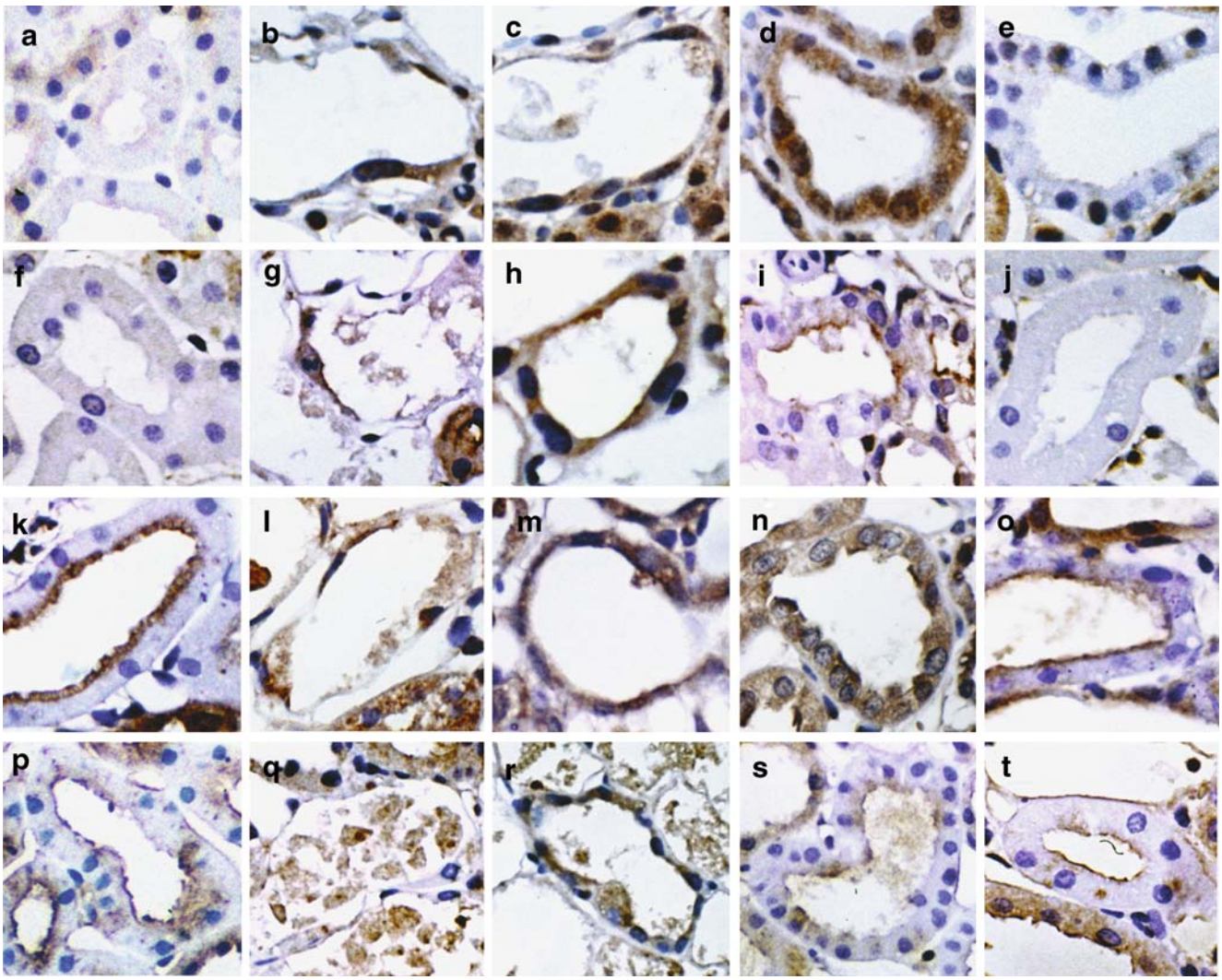

Fig. 6 Immunohistochemistry of PDGFR-β (**a**–**e**), p-PDGFR-β (**f**–**j**), EGFR (**k**–**o**), and p-EGFR (**p**–**t**) in PT cells in normal (**a**, **f**, **k**, **p**) and during repair phase of acute tubular injury at day 4 (**b**, **g**, **l**, **q**), 6 (**c**, **h**, **m**, **r**), 8 (**d**, **i**, **n**, **s**), and 10 (**e**, **j**, **o**, **t**). *Brown color* indicates positive immunoreaction

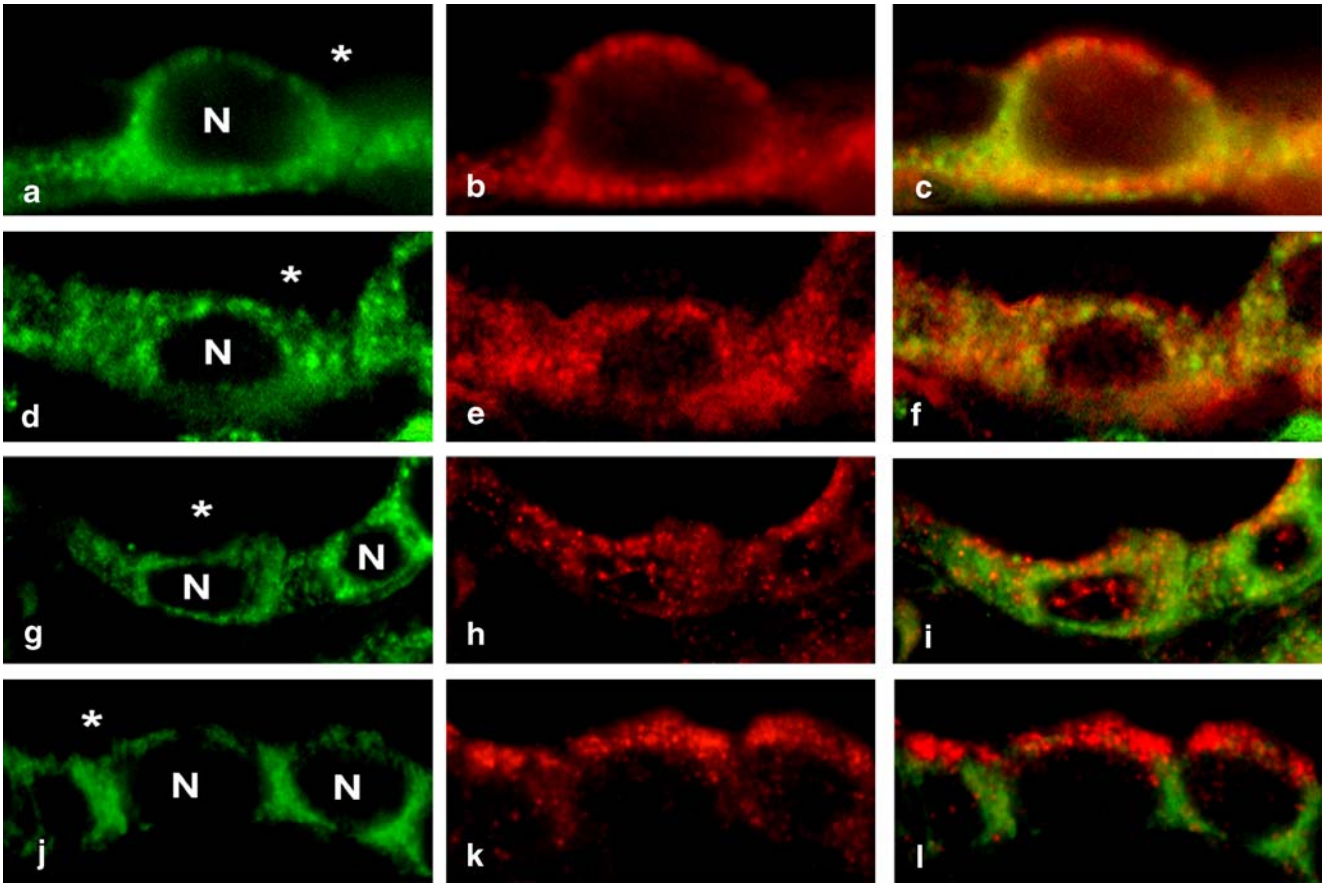

Fig. 7 Double fluorescence staining for caveolin-1α and PDGFR-β at 6 days (**a**–**c**) and 8 days (**d**–**f**) after last gentamicin injection, and for caveolin-1 and EGFR at 6 days (**g**–**i**) and 10 days (**j**–**l**) after last gentamicin injection. Caveolin-1α expression (*green*) (**a**, **d**, **g**, **j**) and PDGFR-β expression (*red*) (**b**, **e**) or EGFR (*red*) (**h**, **k**) were observed in regenerating PT cells. Superimposition of caveolin-1α and PDGFR-β images and caveolin-1α and EGFR produced by immunofluorescence staining showed yellow fluorescence on the membrane (**c**, **i**) and in the cytoplasm (**c**, **f**, **i**), indicating colocalization of caveolin-1α and PDGFR-β (**c**, **f**) or EGFR (**i**). *Asterisks* Tubular lumen; *N* nuclei

During cellular recovery after acute tubular injury, various growth factors/cytokines have been reported to contribute to tubular regeneration [6, 16]. Given the roles of caveolins in modulating/integrating signal transduction in diverse cell types [20], we speculated that transient expression of caveolins on the plasma membrane might play roles on regenerating process of the PT cells by regulating signal transduction of growth factors. PDGF-b and EGF are known as renotropic growth factors [15, 16], and their receptors, receptor tyrosine kinases (PDGFR [8, 23] and EGFR [2, 14]) are caveolae-localized and caveolin-interacting molecules. In the present study, both EGFR and PDGFR-β were found in the early regenerating PT cells (Table 2). Phosphorylated EGFR increased at day 8 and afterwards (Table 2) when caveolins dissociated from EGFR (Fig. 7l) or decreased (Table 2). This consists with the traditional hypothesis that caveolins inhibit activation of various cell surface receptors as seen in the mesangial cells [3]. In case of PDGFR-β, phosphorylation seemed to be associated with the increase and association of caveolins to the receptors in the regenerating PT cells from the very early phase of proliferation (Table 2). Caveolin-1 was demonstrated to inhibit the autophosphorylation of PDGFR and EGFR in a dose-dependent manner in vitro [2, 23]. It was reported that only in the presence of ligands, EGFR and PDGFR transiently associate with caveolae and that ligand-induced stimulation of EGFR or PDGFR can cause heterologous desensitization of other receptors by sequestration in caveolin-containing membranes or caveolae [3, 12]. Thus, it might be possible that EGFR and PDGFR are differentially phosphorylated in this model because concentration and/or kinetics of ligands for EGFR and PDGFR should be differently regulated in vivo. However, only immunohistochemical methods in this study limit drawing any functional roles of caveolins.

Several reports indicate that clathrin-independent uptake of various endogenous plasma molecules, including signaling receptors to a distinct class of caveolin-1-containing endosome, termed a caveosome, allows different types of endocytic mechanisms to have different functional consequences for the cell [17]. Together with the immunoelectron microscopic findings that caveolin-1α was translocated

from the plasma cell surface to intracellular compartments of regenerating PT cells, the immunohistochemistry of caveolin-1α, EGFR, and PDGFR indicates the possibility that caveolins may play a role in endocytosis of these cell surface receptors, or that caveolins may play as an intracellular transporter of cell surface receptors in this model. We also found that EGFR localized in the nuclei. Although transient nuclear localization of EGFR has been reported in regenerating rat liver [11], it cannot be excluded that it is just an artifact.

In conclusion, caveolin-1α expression and caveolae formation appeared on the plasma cell membrane exclusively in the early proliferating phase of regenerating PT cells in association with caveolin-interacting receptors for renotropic growth factors, then caveolin-1α might associate with endocytosis or intracellular transport of these cell surface receptors, suggesting that caveolin-1α may play a role in the regenerating process of PT cells after ARF. As caveolin has multifunctional roles, further studies such as inhibition of caveolin-1α expression are necessary to elucidate the physiological significance of transient caveolin-1α expression in regenerating PT cells in this model.

Acknowledgement We thank Ms. Etsuko Hakamata for the excellent technical assistance. This work was presented in part at the XLIIth Congress of the ERA-EDTA in Istanbul, Turkey, 2005.

References

1. Breton S, Lisanti MP, Tyszkowski R, McLaughlin M, Brown D (1998) Basolateral distribution of caveolin-1 in the kidney. Absence from H+-atpase-coated endocytic vesicles in intercalated cells. J Histochem Cytochem 46:205–214
2. Couet J, Sargiacomo M, Lisanti MP (1997) Interaction of a receptor tyrosine kinase, EGF-R, with caveolins. Caveolin binding negatively regulates tyrosine and serine/threonine kinase activities. J Biol Chem 272:30429–30438
3. Fujita Y, Maruyama S, Kogo H, Matsuo S, Fujimoto T (2004) Caveolin-1 in mesangial cells suppresses MAP kinase activation and cell proliferation induced by bFGF and PDGF. Kidney Int 66:1794–1804
4. Galbiati F, Volonte D, Liu J, Capozza F, Frank PG, Zhu L, Pestell RG, Lisanti MP (2001) Caveolin-1 expression negatively regulates cell cycle progression by inducing G0/G1 arrest via p53/p21WAF1/Cip1-dependent mechanism. Mol Biol Cell 12:2229–2244
5. Goto T, Fujigaki Y, Sun DF, Yamamoto T, Hishida A (2004) Plasma protein extravasation and vascular endothelial growth factor expression with endothelial nitric oxide synthase induction in gentamicin-induced acute renal failure in rats. Virchows Arch 444:362–374
6. Harris RC (1997) Growth factors and cytokines in acute renal failure. Adv Renal Replace Ther 4:43–53
7. Lan HY, Mu W, Nikolic-Paterson DJ, Atkins RC (1995) A novel, simple, reliable, and sensitive method for multiple immunoenzyme staining: use of microwave oven heating to block antibody crossreactivity and retrieve antigens. J Histochem Cytochem 43:97–102
8. Liu P, Ying Y, Anderson RG (1997) Platelet-derived growth factor activates mitogen-activated protein kinase in isolated caveolae. Proc Natl Acad Sci USA 94:13666–13670
9. Liu P, Rudick M, Anderson RG (2002) Multiple functions of caveolin-1. J Biol Chem 277:41295–41298
10. Mahmoudi M, Willgoss D, Cuttle L, Yang T, Pat B, Winterford C, Endre Z, Johnson DW, Gobe GC (2003) In vivo and in vitro models demonstrate a role for caveolin-1 in the pathogenesis of ischaemic acute renal failure. J Pathol 200:396–405
11. Marti U, Hug M (1995) Acinar and cellular distribution and mRNA expression of the epidermal growth factor receptor are changed during liver regeneration. J Hepatol 23:318–327
12. Matveev SV, Smart EJ (2002) Heterologous desensitization of EGF receptors and PDGF receptors by sequestration in caveolae. Am J Physiol Cell Physiol 282:C935–C946
13. Mendez AJ, Lin G, wade DP, Lawn RM, Oram JF (2001) Membrane lipid domains distinct from cholesterol/sphingomyelin rich rafts are involved in the ABCA-1-mediated lipid secretory pathway. J Biol Chem 276:3158–3166
14. Mineo C, James GL, Smart EJ, Anderson RG (1996) Localization of epidermal growth factor-stimulated Ras/Raf-1 interaction to caveolae membrane. J Biol Chem 271:11930–11935
15. Morin NJ, Laurent G, Nonclercq D, Toubeau G, Heuson-Stiennon JA, Bergeron MG, Beauchamp D (1992) Epidermal growth factor accelerates renal tissue repair in a model of gentamicin nephrotoxicity in rats. Am J Physiol 263:F806–F811
16. Nakagawa T, Sasahara M, Haneda M, Kataoka H, Nakagawa H, Yagi M, Kikkawa R, Hazama F (1999) Role of PDGF B-chain and PDGF receptors in rat tubular regeneration after acute injury. Am J Pathol 155:1689–1699
17. Nichols B (2003) Caveosomes and endocytosis of lipid rafts. J Cell Sci 116:4707–4714
18. Nouwen EJ, Verstrepen WA, Buyssens N, Zhu MQ, De Broe ME (1994) Hyperplasia, hypertrophy, and phenotypic alterations in the distal nephron after acute proximal tubular injury in the rat. Lab Invest 70:479–493
19. Parolini I, Sargiacomo M, Galbiati F, Rizzo G, Grignani F, Engelman JA, Okamoto T, Ikezu T, Scherer PE, Mora R, Rodriguez-Boulan E, Peschle C, Lisanti MP. (1999) Expression of caveolin-1 is required for the transport of caveolin-2 to the plasma membrane. Retention of caveolin-2 at the level of the Golgi complex. J Biol Chem 274:25718–25725
20. Razani B, Woodman SE, Lisanti MP (2002) Caveolae: from cell biology to animal physiology. Pharmacol Rev 54:431–467
21. Vogel U, Sandvig K, van Deurs B (1998) Expression of caveolin-1 and polarized formation of invaginated caveolae in Caco-2 and MDCK II cells. J Cell Sci 111:825–832
22. Volonte D, Galbiati F, Lisanti MP (1999) Visualization of caveolin-1, a caveolar marker protein, in living cells using green fluorescent protein (GFP) chimeras. The subcellular distribution of caveolin-1 is modulated by cell-cell contact. FEBS Lett 445:431–439
23. Yamamoto M, Toya Y, Jensen RA, Ishikawa Y (1999) Caveolin is an inhibitor of platelet-derived growth factor receptor signaling. Exp Cell Res 247:380–388
24. Zager RA, Johnson A, Hanson S, dela Rosa V (2002) Altered cholesterol localization and caveolin expression during the evolution of acute renal failure. Kidney Int 61:1674–1683
25. Zhou H, Kato A, Yasuda H, Miyaji T, Fujigaki Y, Yamamoto T, Yonemura K, Hishida A (2004) The induction of cell cycle regulatory and DNA repair proteins in cisplatin-induced acute renal failure. Toxicol Appl Pharmacol 200:111–120

Virchows Arch (2007) 450:683–690
DOI 10.1007/s00428-007-0410-y

ORIGINAL ARTICLE

A novel method to investigate pemphigus-induced keratinocyte dysmorphisms through living cell immunofluorescence microscopy

Nicola Cirillo · Felice Femiano · Antonio Dell'Ermo · Pietro Arnese · Fernando Gombos · Alessandro Lanza

Received: 14 December 2006 / Revised: 15 February 2007 / Accepted: 21 March 2007 / Published online: 21 April 2007
© Springer-Verlag 2007

Abstract Pemphigus vulgaris (PV) blistering occurs as a result of the disruption of intercellular contacts among keratinocytes, or acantholysis. The hallmark of PV acantholysis in vitro is considered to be the retraction of keratin intermediate filaments (KIF) onto the nucleus, which parallels with loss of cell–cell adhesion and rounding up of keratinocytes. However, the fine morphological changes of keratinocytes as well as the fate of cell adhesion structures cannot be appreciated on immunofluorescence by the simple cytokeratin staining. In this paper, we show that acantholytic dysmorphisms are sharply investigated by using PV IgG as a primary antibody on metabolically quiescent living cells. Indeed, PV IgG recognise a wide spectrum of molecules and enabled us to monitor the main changes occurring in acantholytic keratinocytes, including cell shrinkage with the appearance of prickle-like processes, detachment of keratinocytes from one another and collapse of cytoskeleton-bound proteins along nuclear periphery. This method has wider applications as it could be useful for staining cell periphery of keratinocytes and changes in cell shape. Furthermore, images displayed clear and sharp contours because living cell microscopy allows to avoid antigen distortion due to cell manipulation, which usually precedes the immunolabelling.

Keywords Immunofluorescence · Pemphigus · Keratinocytes · Adhesion molecules · Auto-immunity · Cell culture

N. Cirillo · P. Arnese · F. Gombos · A. Lanza
Regional Center on Craniofacial Malformations–MRI,
First School of Medicine and Surgery, II University of Naples,
80138 Naples, Italy

N. Cirillo (✉) · F. Femiano · A. Dell'Ermo · F. Gombos · A. Lanza
Department of Odontostomatology, II University of Naples,
Via Luigi de Crecchio, 7,
80138 Naples, Italy
e-mail: cirillo.sun@libero.it

N. Cirillo
Department of Experimental Medicine,
First School of Medicine and Surgery,
II University of Naples,
80138 Naples, Italy

Introduction

Pemphigus vulgaris (PV) is a chronic autoimmune disease targeting skin and mucous membranes. It is characterised by intraepithelial aphlegmasic flaccid blisters and erosions [25]. Lesions usually appear first in the mouth and, in about one half of the patients, they involve the skin, particularly the trunk later. Intraepithelial cleft develops as a consequence of the loss of cell–cell adhesion among keratinocytes, or acantholysis [5]. When acantholytic, the epithelial cells become rounded, with the cytoplasm contracted round the nucleus, and often form small groups within a vesicle. Immunofluorescence studies revealed that PV serum autoantibodies bind antigens located within the intercellular substance of keratinocytes [31, 39] and they usually correlate with the extent and the activity of the disease [20].

The main epidermal antigen recognised by PV IgG has been identified as the 130-kDa desmoglein 3 (Dsg3), a desmosomal glycoprotein belonging to the cadherin family of calcium-dependent cell adhesion molecules [1]. Indeed, mucosal PV associates with the presence of circulating IgG against Dsg3. However, skin involvement and disease progression correlate with the appearance of IgG against Dsg1, a cell adhesion protein strictly related to Dsg3 [13].

Dsg1/3 extracellular domains are critically involved in maintaining inter-cellular contacts mediated by desmo-

somes [17]. By anchoring the intermediate filament cytoskeleton to sites of cell–cell adhesion, desmosomes form a highly resilient supracellular network, which is required for tissue integrity [15, 18, 19, 32]. Although the binding of Dsg3 to keratin intermediate filaments (KIF) is mediated by a number of structural and adapter proteins that work intracellularly (including plakoglobin and the plakin family proteins, e.g. desmoplakin I/II, plakophilins, envoplakin and periplakin) [21, 23], the stability of desmosome is largely dependent by the structural and functional integrity of the desmoglein extracellular domain [2, 8, 33]. As this intercellular fraction of Dsg3 hold the main epitopes recognised by PV IgG, acantholysis could be due to the simple perturbation of Dsg3 adhesion function through steric hindrance [16, 35]. After pemphigus IgG binding to their desmosomal targets, cell surface Dsg1/3—prevalently the unassembled clusters—are thought to be partially internalised [9]. Finally, loss of cell–cell adhesion in PV is likely to take place when keratinocytes become unable in maintaining steady-state levels of Dsg3. Alternatively, proteinases such as matrix metalloproteinase (MMP)-9 may specifically digest Dsg3 extracellular domain [10, 12]. In any case, when Dsg3 function is impaired, keratin filament are thought to collapse onto nucleus and determine keratinocytes to round up. Indeed, KIF retraction is considered the hallmark of PV acantholysis in vitro [6].

However, as emerged from our personal experience, staining of cytokeratins on formalin-fixed cells has revealed unexpected difficulties and sometimes disappointing results. To eliminate experienced shortcomings in documenting the effect of PV serum by IF microscopy, here we propose a novel and useful method to stain acantholytic cells on keratinocyte monolayers.

Materials and methods

Patients and sera, and antibodies

Sera of patients with active PV (n=4, named PV1-4), and from three volunteers without any skin disease (n=3, controls) have been used for the experiments. Diagnosis was established on the basis of results of both clinical and histological examinations, following criteria detailed elsewhere [26]. The presence of autoantibodies was determined by both indirect immunofluorescence using monkey oesophagus as substrate and western blot analysis against Dsg3 and Dsg1. All sera were stored at −80°C.

For our experiments, we used the 5H10 mouse monoclonal antibody against the extracellular domain of Dsg3, H-290 rabbit antibodies against C-terminal residues 760–1046 of Dsg1, anti-pancytokeratin rabbit IgG, HRP-conjugated anti-rabbit and anti-mouse antibodies (Santa Cruz Biotechnology, Santa Cruz, CA), and flourescein isothiocyanate (FITC)-conjugated anti-human and anti-rabbit IgG antibodies (Dako Denmark A/S).

Results were representative of at least two independent experiment conducted by probing all sera.

Culture conditions

HaCaT cells, a human immortalised keratinocyte cell line capable of forming normally differentiated epidermis [4], were cultured as reported previously [10]. Cells from T-75 flasks were plated on 35-mm Petri dishes and grown to semi-confluence in complete KAD medium in an atmosphere humidified with 5% CO_2. KAD medium, consisting of a mixture (1:1) of keratinocyte growth medium (KGM) supplemented with growth factors and DMEM plus 10% FBS, was supplemented with penicillin (50 U/ml), streptomycin (50 μg/ml) and fungizone (2.5 μg/ml). When treating cells with human sera, FBS-free KAD was used [11].

Western blot analysis and immunoprecipitation

Proteins subjected to immunoprecipitation were extracted by using the IP buffer (50-mM Tris–HCl, pH 7.5, 150 mM NaCl, 0.5% Nonidet P-40, 1 mM DTT, 1 mM PMSF) and separated by 8% sodium dodecyl sulphate (SDS)-polyacrylamide gel electrophoresis (PAGE). The immunoreactivity of PV IgG against Dsg1 and Dsg3 was essayed by combined immunoprecipitation-western blotting, following the procedures reported by Cirillo et al. [11].

In vitro model of PV using cultured keratinocytes

We have exposed cultured cells to PV patients' sera as proposed originally by Swanson and Dahl on skin organ cultures [34], adapting the standard protocols to keratinocyte monolayers [9]. For reproducing the in vitro model of PV on cell cultures, keratinocytes were incubated with either threefold concentrated or unconcentrated sera from PV patients and controls for different time periods, as specified in the results section. Specific changes in cytoskeleton organisation, such as retraction of keratin filaments from cell borders onto nucleus, and detachment of keratinocytes from one another evaluated by staining of desmosomal components recognised by PV IgG, both have been investigated and compared.

Living cell immunofluorescence (LCIF) microscopy

Cells were grown on glass coverslips and incubated in the presence or absence of normal or PV sera. After washing with phosphate-buffered saline (PBS), cells were perme-

abilised with 0.1% Triton X-100 for 5 min on ice and then washed three times in PBS containing 2% bovine serum albumin (BSA) to block non-specific sites. Samples were incubated with the appropriate primary antibody (i.e. anti-pancytokeratin or PV IgG diluted 1:10 in 3% BSA/PBS) for 1 h on ice, washed in BSA/PBS, and fixed in cold 100% methanol for 5 min or 4% paraformaldehyde for 10 min. Finally, cells were exposed to specie-specific antibodies (1:100) conjugated to FITC (Dako Denmark A/S). In some experiments, cells were directly incubated with anti-human IgG to investigate deposits of PV autoantibodies. Nuclei were stained with Hoechst 33342 (5 μg/ml) on formaldehyde-fixed cells [27]. Note that all steps were performed keeping keratinocytes on ice to block cellular metabolism.

The specimens were examined with a Zeiss Axiophot microscope (Calr Zeiss, Thornwood, NY) at ×400 magnification, and fluorescence images were acquired with an Evolution VF fast digital camera (MediaCybernetics, Wokingham Berkshire, UK). Note that samples were processed simultaneously, and photographic procedures held constant to obtain semi-quantitative results.

Results

Characterisation of sera

Sera from four patients with PV were characterised on the basis of immunofluorescence on monkey oesophagus and western blotting analyses (Table 1). Consistent with the well-known correspondence between clinical phenotype and autoantibody profile, serum IgG from patients with mucosal PV bound desmoglein 3, whereas those from PV patients having cutaneous involvement reacted with Dsg1 in addition to Dsg3 (Table 1). For our experiments, we used sera from two patients with PV mucosal dominant type (PV1, PV4), two with the mucocutaneous type of PV (PV2, PV3), and three healthy donors. All PV sera tested were found to describe similar immunostaining on keratinocytes irrespective of whether they were taken from patients with mucosal dominant rather than mucocutaneous types of PV (Fig. 1a–c). Neither immunofluorescence titres of circulating anti-ICS IgG seemed to affect the staining (compare Table 1 with Fig. 1b and c), as appreciated by the evaluation of fluorescence semi-quantitative results (not shown). Furthermore, the catalogue of potential self-antigens immunoprecipitated by PV IgG included a number of molecules with different relative molecular masses (Fig. 1d).

Table 1 Clinical and laboratoristic profile of PV sera

	Clinical phenotype	Anti-Dsg3 IgG	Anti-Dsg1 IgG	Anti-ICS titres
PV1	Mucosal dominant	+	−	1:80
PV2	Mucocutaneous	+	+	1:160
PV3	Mucocutaneous	+	+	1:160
PV4	Mucosal dominant	+	−	1:320

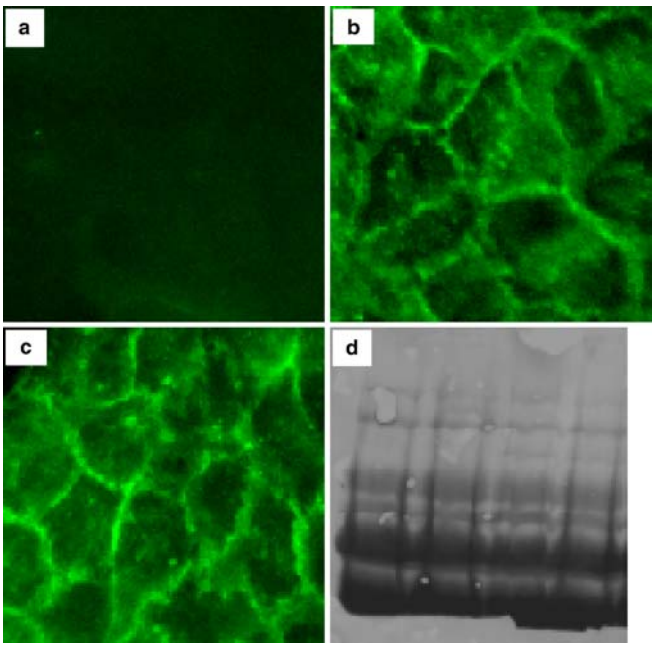

Fig. 1 IgG from PV, but not normal sera, recognize antigen located within the intercellular substance of keratinocytes (**a**–**c**). Immunofluorescence studies show as the anti-desmoglein autoantibody profile of PV sera does not affect the ability of PV IgG to "decorate" cell periphery. Indeed, photograph in **b** was obtained by using sera carrying anti-Dsg3 but not anti-Dsg1 antibodies (PV1), whereas that in **c** shows keratinocyte staining which results by using sera found positive to both antibodies (PV2). However, the spectrum of molecules recognized by PV IgG is likely to be not restricted to desmogleins, as shown by SDS-PAGE of the immunocomplexes (**d**). Immunofluorescence results were confirmed by using PV3 and PV4 sera. Note that samples were processed simultaneously and photographic procedures held constant to obtain semiquantitative results

PV serum induces specific changes in KIF arrangement

We first reproduced what is considered the classic in vitro model of PV. In HaCaT cells, KIF labelling FITC-fluorescence was predominant along cell periphery as diffuse green spots on the entire cortical cytoplasm (Fig. 2a). Keratinocytes were treated with 50% (v/v) normal or PV sera for 72 h, a time period within morphologic changes become usually visible [9]. Indeed, keratinocytes exposed to PV serum (n=4) displayed KIF retraction and rounding up within 48 h, whereas untreated cells (n=3) or those incubated with normal sera (n=3) did not exhibit changes in cytokeratin staining (Fig. 2). However, cytokeratin labelling was slightly blurred in the majority of control

samples (Fig. 2a and b) as well as in some PV treated cells (n=2, not shown). Furthermore, as in keratinocytes exposed to PV serum the intracellular network formed by keratins collapsed onto nucleus, cellular borders and/or residual contacts among acantholytic cells appeared hardly detectable (Fig. 2c and d). Our data suggest that PV sera can specifically induce keratin cytoskeleton reorganisation and cell–cell detachment. Although keratin staining is effective in highlighting this phenomenon, however, photograms are not always of reproducible quality and do not allow to label intercellular contact areas.

Cell–cell detachment and KIF collapse can be revealed by PV IgG staining

To investigate the effects of PV serum on cell morphology by using PV IgG as a primary antibody, we determined optimal conditions in pilot assays and then we carried out extensive experiments by diluting PV IgG 1:10, as reported in Materials and methods. Keratinocytes were treated with 30% (v/v) PV or normal sera for 72 h and then morphology was investigated through living cell immunofluorescence microscopy. Dramatic changes in cell shape were observed in keratinocytes exposed to PV but not normal sera (Fig. 3). These dysmorphisms paralleled with profound redistribution of PV IgG, which appeared to be markedly internalised. Nevertheless, cell borders were still clearly distinguishable. Interestingly, IgG staining also localised onto nuclear periphery as a slight green fluorescence of oval shape (Fig. 3, arrows), resembling KIF arrangement during acantholysis. This finding may be explained by the fact that Dsg3 undergoing internalisation remains partially bound to keratin cytoskeleton. Thus, staining of acantholytic keratinocytes with PV IgG by living cell immunofluorescence microscopy appeared to fulfil all the well-established hallmarks of pemphigus, that is cell–cell detachment, rounding up and collapse of cytoskeleton-associated proteins onto nucleus.

Time-course of PV-induced acantholytic dysmorphisms on keratinocytes

To study the morphological changes of keratinocytes accompanying the progressive loss of cell–cell adhesion, we used threefold concentrated 30% PV sera, which are known to induce acantholysis within 24 h (Cirillo et al., unpublished). Cell morphology was assessed through LCIF by using PV IgG as a primary antibody. Signs of cell shrinkage were appreciable within 6 h after treatment (Fig. 4). Punctuate clusters of FITC-fluorescence on cell surface, referred to as contact areas among keratinocytes, appeared as elongated processes, which brought together shrinking cells (Fig. 4b). Cell dysmorphisms became obvious 12 h after treatment, and cell–cell adhesion structures immunostained by PV IgG assumed a prickle-like appearance (Fig. 4c). After 24 h, keratinocytes were completely detached from one another (Fig. 4d). Some cellular processes extending from keratinocyte surface were

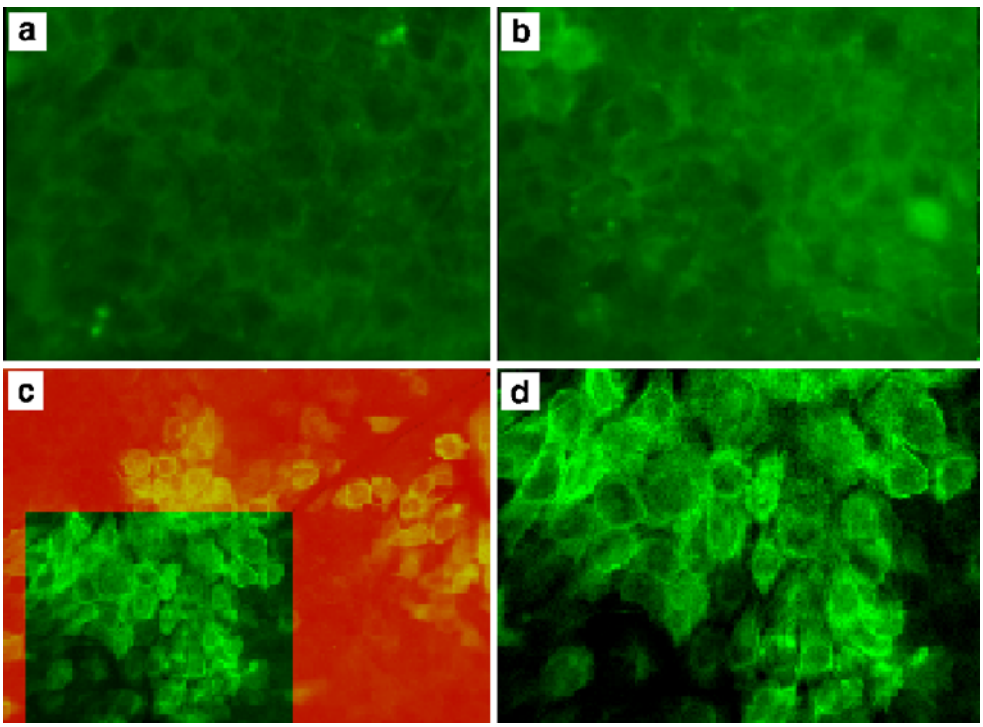

Fig. 2 Cytokeratin staining of HaCaT cells cultured for 48 h in normal conditions (**a**) or exposed to normal (**b**) or PV sera (**c**), reveals that PV serum induce specific changes of keratin cytoskeleton. As shown in the higher magnification photograph (**d**), the cells round up, keratins detach from membrane and collapse onto the nuclei

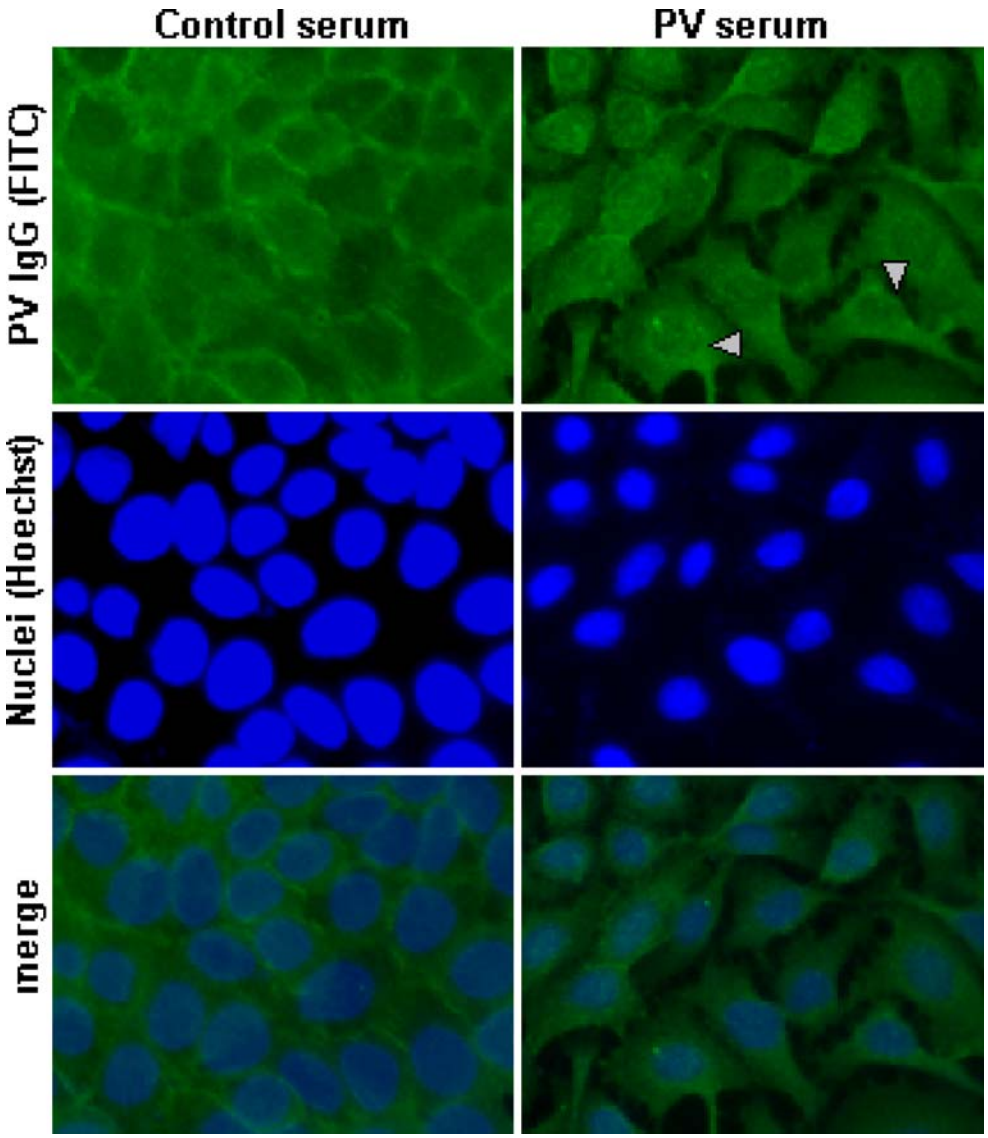

Fig. 3 Cell–cell detachment occurring after a 72-h exposition to PV, but not control sera. As shown by immunofluorescence microscopy, the use of PV IgG as a primary antibody on living but metabolically quiescent cells allow an optimal resolution of cell contours, adhesion areas, and nuclear periphery

still recognisable; however, no signs of punctuate clusters were detectable. Furthermore, perinuclear localisation of PV IgG was revealed as a sharp FITC fluorescence along nuclear periphery (Fig. 4e), resembling those induced by keratin cytoskeleton collapse in acantholytic cells. Time-course experiments were also performed with control sera, but no morphological changes were revealed on immunofluorescence (not shown). Overall, these morphological analyses showed that immunolabelling with PV IgG represents an excellent method to follow acantholytic changes on keratinocytes.

Discussion

In the present study, we have shown that immunostaining of acantholytic keratinocytes with PV IgG is effective in following the cell fate in response to PV serum. Cell shrinkage, appearance of prickle-like processes and subsequent disruption of cell–cell contact areas, detachment of keratinocytes from one another, and collapse of cytoskeleton-bound proteins around nuclear periphery, all these acantholysis-associated phenomena were well detectable by living cell immunofluorescence microscopy using PV IgG as a primary antibody.

Although the main alteration of keratinocytes subjected to PV autoimmunity in vitro was represented by cell–cell detachment and rounding up, retraction of KIF from the cortical cytoplasm onto the nucleus has been considered as the hallmark of PV-induced acantholysis. However, cell contact areas as well as keratinocyte contours are not well investigable through cytokeratin labelling, principally because KIF lose their connections with the transmembrane adhesion proteins during acantholysis. On the contrary,

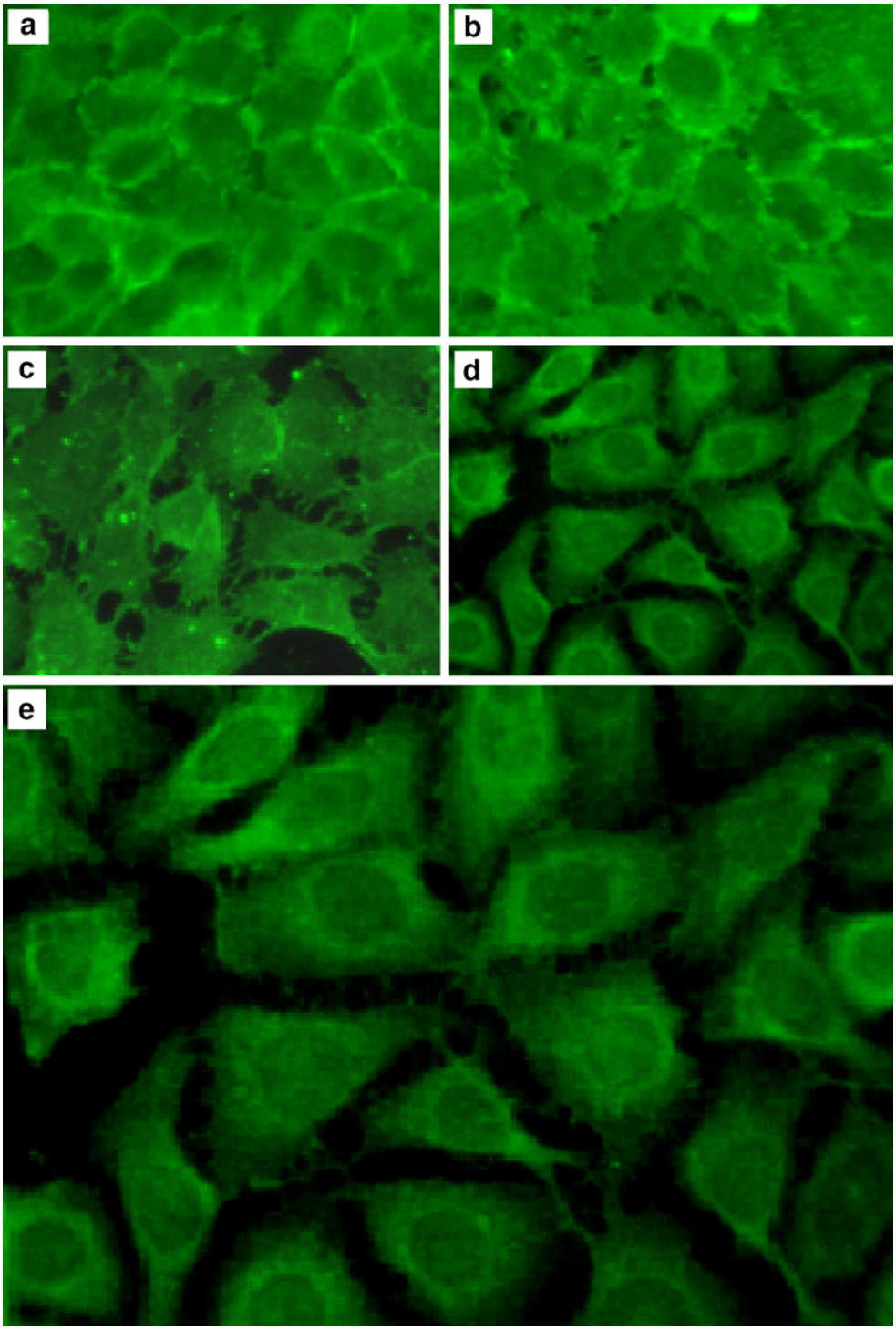

Fig. 4 Phenomenology of cell–cell detachment as revealed by living cell immunofluorescence microscopy. To emphasize the phenomena accompanying keratinocyte adhesion loss, cells were treated with threefold concentrated PV sera for 24 h. First changes in cell shape became evident within 6 h after treatment (**b**). Cell shrinkage and formation of prickle-like processes appeared within 12 h (**c**), whereas 24 h after incubation with PV serum cells were clearly detached from one another (**d**). At higher magnification, typical morphological changes of acantholytic cells were detectable (**e**), see text for details. Figures were representative of at least two independent experiments conducted by probing all sera

deposits of PV IgG along cell surface as well as within the cytoplasm (resulting from PV IgG internalisation along with PV antigens) made us able to stain both keratinocyte borders and residual cell–cell contact areas. Furthermore, as internalised desmogleins remain partially bound to keratin cytoskeleton during acantholysis, we were able to observe the collapse of presumptive KIF-associated desmogleins onto nucleus. We cannot predict whether these changes occur also in vivo, nor we actually know whether LCIF is applicable on fresh skin biopsy. However, the hallmark of PV acantholysis in vivo is well established, being represented by a gross phenomenon such as skin blistering, whose histological expression is epidermal splitting. Instead, the in vitro model of PV on cultured keratinocytes is

still debated and it is reproduced in different manner according to each author's experience.

Under a methodological point of view, by incubating the primary antibody on living—although metabolically quiescent—cells, we reduced the potential distortion of the three-dimensional folding that cadherins are likely to undergo during fixation processes. Despite living keratinocytes were incubated with non-ionic detergents to allow the penetration of PV IgG within the cell, no relevant alterations in morphology were seen in controls, suggesting that the permeabilisation procedures in such quiescent cells do not remarkably affect their shape. However, when the staining of intracellular antigens is not required, permeabilisation could be avoided to rule out the potential risk of causing alteration of cell shape. By and large, this method could be widely applied to detect keratinocyte shape and its changes. Furthermore, when studying PV acantholysis, the cells could be fixed and then directly incubated with the secondary antibody, as PV IgG are already bound to their antigen(s). It is worth of note that neither the anti-desmoglein antibody profile nor the anti-ICS titres did apparently affect the staining intensity, perhaps reflecting the saturation of binding sites for the FITC-conjugated secondary antibody due to the high serum concentration of PV IgG. Thus, neither a cut-off value of anti-ICS titres nor the precise immunoreactivity of such autoantibodies seems to be required to ensure a good staining of keratinocytes. This finding make LCIF an approachable research tool to ameliorate the study of PV pathophysiology and, more in general, to study the morphological changes in keratinocyte shape occurring in a lot of skin diseases or during biological phenomena such as apoptosis.

Keratinocyte outline and cell–cell contacts during acantholysis have been stained with antibodies against a number of cell adhesion proteins, including plakoglobin [6, 38], desmoplakins [3, 7], Dsg1 [24], Dsg3 [36] and E-cadherin [37]. These proteins share a distribution usable for studying cell periphery and changes in cell shape because they are found prevalently within cell adhesion structures such as desmosomes and adherens junctions. IgG against PV antigens recognise mainly Dsg3 and Dsg1, although the spectrum of PV autoantigens is thought to encompass molecules other than desmogleins, such as acetylcholine receptors [29, 30]. Furthermore, some putative non-desmoglein PV antigens include desmocollins [14], plakoglobin [22] and desmoplakin [28]. Hence, immunostaining with PV IgG does not simply overlap that of Dsg3. Rather, it encompass a number of proteins expressed on keratinocyte surface, thus allowing a sharp and exact reproduction of cell periphery. For these reasons, we found it useful in all cases where following changes in cell shape is required.

In summary, here we showed as living cell immunofluorescence microscopy using PV IgG as a primary antibody can be useful to stain acantholytic dysmorphisms induced by PV sera on keratinocytes. In general, this method allows a sharp labelling of cell periphery and is recommended whenever keratinocyte shape and its changes need to be investigated.

References

1. Amagai M, Klaus-Kovtun V, Stanley JR (1991) Autoantibodies against a novel epithelial cadherin in pemphigus vulgaris, a disease of cell adhesion. Cell 67:869–877
2. Amagai M (1995) Adhesion molecules. I. keratinocyte–keratinocyte interactions, cadherins and pemphigus. J Invest Dermatol 104:146–152
3. Aoyama Y, Kitajima Y (1999) Pemphigus vulgaris-IgG causes a rapid depletion of desmoglein 3 (Dsg3) from the Triton-X soluble pools, leading to the formation of Dsg3-depleted desmosomes in a human squamous carcinoma cell line, DJM-1 cells. J Invest Dermatol 112:67–71
4. Boukamp P, Petrussevska RT, Breitkreutz D, Hornung J, Markham A, Fusenig NE (1988) Normal keratinization in a spontaneously immortalized human keratinocyte cell line. J Cell Biol 106:761–771
5. Bystryn JC, Rudolph JL (2005) Pemphigus. Lancet 366:61–73
6. Caldelari R, De Bruin A, Baumann D, Suter MM, Bierkamp C, Balmer V, Muller E (2001) A central role for the armadillo protein plakoglobin in the autoimmune disease pemphigus vulgaris. J Cell Biol 153:823–834
7. Calkins CC, Setzer SV, Jennings JM, Summers S, Tsunoda K, Amagai M, Kowalczyk AP (2006) Desmoglein endocytosis and desmosome disassembly are coordinated responses to pemphigus autoantibodies. J Biol Chem 281:7623–7634
8. Chitaev NA, Troyanovsky SM (1997) Direct Ca2+-dependent heterophilic interaction between desmosomal cadherins, desmoglein and desmocollin, contributes to cell–cell adhesion. J Cell Biol 138:193–201
9. Cirillo N, Femiano F, Gombos F, Lanza A (2006) Serum from pemphigus vulgaris reduces desmoglein 3 half-life and perturbs its de novo assembly to desmosomal sites in cultured keratinocytes. FEBS Lett 580:3276–3281
10. Cirillo N, Femiano F, Gombos F, Lanza A (2006) Metalloproteinase 9 is the outer executioner of desmoglein 3 in apoptotic keratinocytes. Oral Dis DOI 10.1111/j.1601-0825.2006.01287.x
11. Cirillo N, Gombos F, Lanza A (2007) Changes in desmoglein 1 expression and subcellular localization in cultured keratinocytes subjected to anti-desmoglein 1 pemphigus autoimmunity. J Cell Physiol 210:411–416
12. Cirillo N, Lanza M, Rossiello L, Gombos F, Lanza A (2007) Defining the involvement of proteinases in pemphigus vulgaris: evidence of matrix metalloproteinase-9 overexpression in experimental models of disease. J Cell Physiol DOI 10.1002/jcp.20997
13. Ding X, Diaz LA, Fairley JA, Giudice GJ, Liu Z (1999) The anti-desmoglein 1 autoantibodies in pemphigus vulgaris sera are pathogenic. J Invest Dermatol 112:739–743
14. Dmochowski M, Hashimoto T, Garrod DR, Nishikawa T (1993) Desmocollins I and II are recognized by certain sera from patients with various types of pemphigus particularly Brazilian pemphigus foliaceus. J Invest Dermatol 100:380–384
15. Elias PM, Matsuyoshi N, Wu H, Lin C, Wang ZH, Brown BE, Stanley JR (2001) Desmoglein isoform distribution affects stratum corneum structure and function. J Cell Biol 153:243–250
16. Futei Y, Amagai M, Sekiguchi M, Nishifuji K, Fujii Y, Nishikawa T (2000) Use of domain-swapped molecules for conformational epitope mapping of desmoglein 3 in pemphigus vulgaris. J Invest Dermatol 115:829–834

17. Garrod DR, Merritt AJ, Nie Z (2002) Desmosomal cadherins. Curr Opin Cell Biol 14:537–545
18. Getsios S, Huen AC, Green KJ (2004) Working out the strength and flexibility of desmosomes. Nat Rev Mol Cell Biol 5: 271–281
19. Green KJ, Gaudry CA (2000) Are desmosomes more than tethers for intermediate filaments? Nat Rev Mol Cell Biol 1:208–216
20. Harman KE, Seed PT, Gratian MJ, Bhogal BS, Challacombe SJ, Black MM (2001) The severity of cutaneous and oral pemphigus is related to desmoglein 1 and 3 antibody levels. Br J Dermatol 144:775–780
21. Hatzfeld M, Haffner C, Schulze K, Vinzens U (2000) The function of plakophilin 1 in desmosome assembly and actin filament organization. J Cell Biol 149:209–212
22. Korman NJ, Eyre RW, Klaus-Kovtun V, Stanley JR (1989) Demonstration of an adhering-junction molecule (plakoglobin) in the autoantigens of pemphigus foliaceus and pemphigus vulgaris. N Engl J Med 321:631–635
23. Kowalczyk AP, Bornslaeger EA, Norvell SM, Palka HL, Green KJ (1999) Desmosomes: intercellular adhesive junctions specialized for attachment of intermediate filaments. Int Rev Cytol 185:237–301
24. Kowalewski C, Mackiewicz W, Schmitt D, Jablonska S, Haftek M (2001) Cell–cell junctions in acantholytic diseases. Arch Dermatol Res 293:1–11
25. Lanza A, Cirillo N, Femiano F, Gombos F (2006) How does acantholysis occur in pemphigus vulgaris: a critical review. J Cutan Pathol 33:401–412
26. Lanza A, Femiano F, De Rosa A, Cammarota M, Lanza M, Cirillo N (2006) The N-terminal fraction of desmoglein 3 encompassing its immunodominant domain is present in human serum: implications for pemphigus vulgaris autoimmunity. Int J Immunopathol Pharmacol 19:399–407
27. Lanza A, Cirillo N (2007) Caspase-dependent cleavage of desmoglein 1 depends on the apoptotic stimulus. Br J Dermatol 156:400–402
28. Mimouni D, Foedinger D, Kouba DJ, Orlow SJ, Rappersberger K, Sciubba JJ (2004) Mucosal dominant pemphigus vulgaris with anti-desmoplakin autoantibodies. J Am Acad Dermatol 51:62–67
29. Nguyen VT, Ndoye A, Grando SA (2000) Pemphigus vulgaris antibody identifies pemphaxin, a novel keratinocyte annexin-like molecule binding acetylcholine. J Biol Chem 275:29466–29476
30. Nguyen VT, Ndoye A, Grando SA (2000) Novel human alpha9 acetylcholine receptor regulating keratinocyte adhesion is targeted by pemphigus vulgaris autoimmunity. Am J Pathol 157: 1377–1391
31. Patel HP, Diaz LA, Anhalt GJ, Labib RS, Takahashi Y (1984) Demonstration of pemphigus antibodies on the cell surface of murine epidermal cell monolayers and their internalization. J Invest Dermatol 83:409–415
32. Smith EA, Fuchs E (1998) Defining the interactions between intermediate filaments and desmosome. J Cell Biol 141: 1229–1241
33. Syed SH, Trinnaman B, Martin S, Major S, Hutchinson J, Magee AI (2002) Molecular interactions between desmosomal cadherins. Biochem J 362:317–327
34. Swanson DL, Dahl MV (1983) Methylprednisolone inhibits pemphigus acantholysis in skin cultures. J Invest Dermatol 81:258–260
35. Tsunoda K, Ota T, Aoki M, Yamada T, Nagai T, Nakagawa T, Koyasu S, Nishikawa T, Amagai M (2003) Induction of pemphigus phenotype by a mouse monoclonal antibody against the amino-terminal adhesive interface of desmoglein 3. J Immunol 170:2170–2178
36. Waschke J, Bruggeman P, Baumgartner W, Zillikens D, Drenckhahn D (2005) Pemphigus foliaceus IgG causes dissociation of desmoglein 1-containing junctions without blocking desmoglein 1 trans-interaction. J Clin Invest 115:3157–3165
37. Waschke J, Spindler V, Bruggeman P, Zillikens D, Schmidt G, Drenckhahn D (2006) Inhibition of Rho A activity causes pemphigus skin blistering. J Cell Biol 175:721–727
38. Williamson L, Raess NA, Caldelari R, Zakher A, de Bruin A, Posthaus H, Bolli R, Hunziker T, Suter MM, Muller EJ (2006) Pemphigus vulgaris identifies plakoglobin as key suppressor of c-Myc in the skin. EMBO J 25:3298–3309
39. Wolff K, Schreiner E (1971) Ultrastructural localization of pemphigus autoantibodies within the epidermis. Nature 229: 59–61

Virchows Arch (2007) 450:691–697
DOI 10.1007/s00428-007-0411-x

ORIGINAL ARTICLE

Expression of estrogen and progesterone receptors and inhibin-α in hepatobiliary cystadenoma: an immunohistochemical study

Hala M. Abdul-Al · Hala R. Makhlouf · Zachary D. Goodman

Received: 27 December 2006 / Revised: 26 March 2007 / Accepted: 26 March 2007 / Published online: 25 April 2007
© Springer-Verlag 2007

Abstract To further characterize the immunohistochemical features of hepatobiliary cystadenoma with mesenchymal stroma, a battery of stains was performed on nine typical cases. All nine tumors had been resected from female patients who ranged in age from 30 to 59 years. Freshly cut sections were stained with antibodies to estrogen receptor (ER), progesterone receptor (PR), α-smooth muscle actin (SMA), inhibin-α, and cytokeratins (CK) 7, 8, 18, and 19. Nuclear staining of the mesenchymal stromal cells for ER and PR was present in all and seven out of nine cases, respectively. A strong cytoplasmic staining of the mesenchymal stromal cells for SMA was seen in all cases. A patchy pale cytoplasmic staining of the tumor epithelium for ER and PR was seen in five out of nine and four out of nine cases, respectively. Immunoreactivity of luteinized stromal cell for inhibin-α was documented in three out of nine cases. All tumors (nine out of nine) demonstrated strong cytoplasmic positivity of the epithelial lining of the cysts to CK7, CK8, CK18, and CK19, typical of biliary-type epithelium. The expression of ER, PR, and inhibin-α in the ovarian-like stroma supports the likely hormonal dependence of this tumor and probably explains its almost exclusive occurrence in women.

The opinions or assertions contained herein are the private views of the authors and are not to be construed as official or as representing the views of the Department of the Army or the Department of Defense.

H. M. Abdul-Al (✉) · H. R. Makhlouf · Z. D. Goodman
Division of Hepatic Pathology, Department of Hepatic and Gastrointestinal Pathology,
Armed Forces Institute of Pathology,
Washington, DC 20306-6000, USA
e-mail: abdulalh@afip.osd.mil

H. M. Abdul-Al · H. R. Makhlouf · Z. D. Goodman
Veterans Administration Special Reference Laboratory for Pathology,
Armed Forces Institute of Pathology,
Washington, DC 20306-6000, USA

Keywords Cystadenoma · Liver · Immunohistochemistry · Estrogen receptors · Progesterone receptors · Cytokeratins · Inhibin · Smooth muscle actin · Histogenesis

Background

Hepatobiliary cystadenomas are rare neoplasms of the liver and biliary tree with the potential for malignant transformation [1, 5, 13, 26]. A subset of these tumors is characterized by a spindle-cell mesenchymal stroma, reminiscent of ovary and occurring exclusively in female subjects [26]. Such tumors have become known as hepatobiliary cystadenoma with mesenchymal stroma. Morphologically, these are similar to mucinous cystic neoplasms that occur in the pancreas, ovary, and the retroperitoneum. This stroma, therefore, is the entity-defining feature of these neoplasms.

The largest series of this rare tumor to date is that of Devaney et al. [5], who reported 52 hepatobiliary cystadenomas and 18 hepatobiliary cystadenocarcinomas. As hepatobiliary mucinous cystic neoplasms with mesenchymal stroma occurred only in women, this led them to suggest a sex-specific factor in the pathogenesis of the tumors. Recently, there have been reports of expression of estrogen receptors (ER) and progesterone receptors (PR) in the stromal cells in formalin-fixed tissue from several cases of hepatobiliary cystadenomas [4, 6, 20, 23], and both ER and PR as well as luteinized inhibin-α positive stromal cells have been demonstrated in the closely related mucinous cystic tumors of the pancreas [10, 28], further supporting the hypothesis that these are hormonally dependant.

The aim of this study was to investigate the immunoreactivity of formalin-fixed tissue from hepatobiliary cystadenomas with antibodies to estrogen and PR using

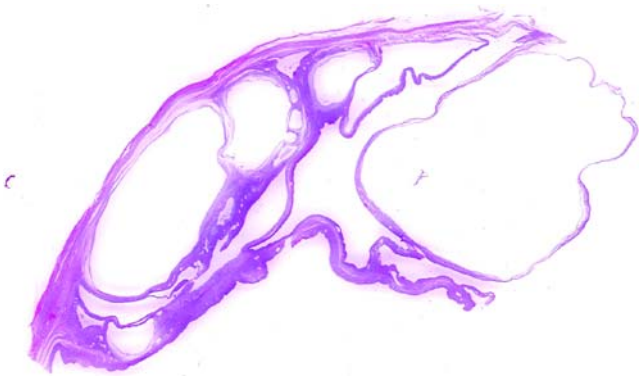

Fig. 1 At low magnification, cystadenomas are multilocular with areas of dense mesenchymal-like stroma (H&E)

conventional immunohistochemical methods for their detection in breast cancer tissue and with antibodies to inhibin-α, a marker of sex cord stromal tumors, as well as with antibodies to cytokeratins (CK) that occur in the biliary tract. To better characterize the heterogenic mix of the cells in the mesenchymal stroma, we investigated its immunoreactivity to anti-α-smooth muscle actin (SMA).

Materials and methods

Nine cases of hepatobiliary cystadenoma with adequate blocks for additional sections were selected from the files of the Armed Forces Institute of Pathology. As it has been shown that the detection of estrogen and PR can be impaired by storage of unstained paraffin slides [3, 11, 16], all immunostains were carried out on freshly cut sections. Antibodies employed included anti-ER (prediluted, Ventana, CA, USA catalogue # 760-2596), anti-PR (prediluted, Ventana, catalogue # 760-2547), anti-α-SMA (dilution 1:600, Sigma, Clone SMA, 1A4), anti-CK7 (dilution 1:400, Dako, CA, USA clone OV-TL 12/30, code # M7018), anti-CK8 (dilution 1:400, Dako, clone K8.8), anti-CK18 (dilution 1:100, Dako, clone DC-10), and anti-CK19 (dilution 1:200, Dako, clone RCK108). After deparaffinization and rehydration, sections were developed using a modified avidin–biotin–peroxidase complex technique [8]. For inhibin-α antibody (dilution 1:80, Serotec, Oxford, England, clone R1), microwave heating antigen retrieval in a sodium citrate pH 6.0 was performed before staining [19, 24]. Biotin blocking was performed with the Dako biotin-blocking system as an additional step in the staining for estrogen and PR and inhibin-α antibodies. Cases that were positive for inhibin-α were also stained for α-fetoprotein, human chorionic gonadotropin (HCG), and

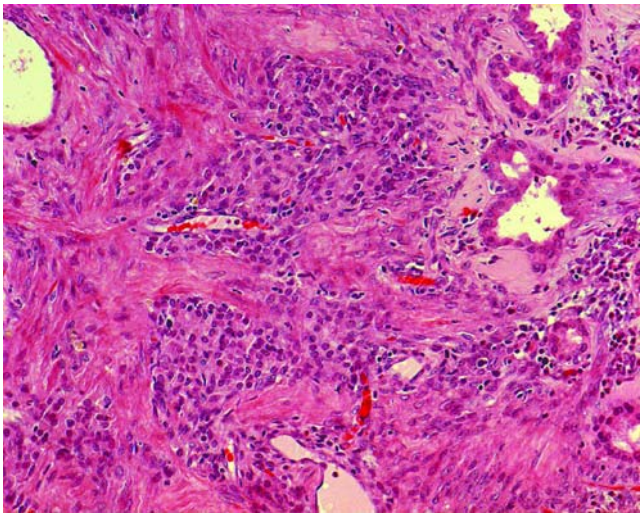

Fig. 3 Nests of luteinized cells can be found after carefully searching the dense mesenchymal-like stroma (H&E)

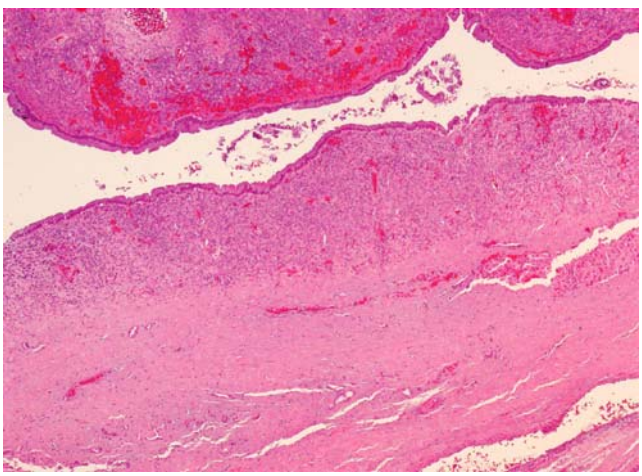

Fig. 2 Each locule is lined by a single layer of tall columnar epithelium resting on a basement membrane. The stroma is dense and cellular and is in turn surrounded by a densely hyalinized pseudocapsule (H&E)

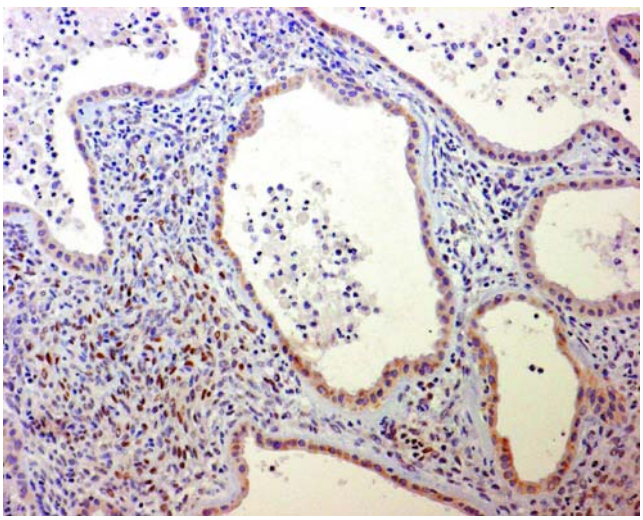

Fig. 4 Pale cytoplasmic staining of the epithelial lining of cystadenomas and nuclear staining of the mesenchymal-like stroma (immunostain for ER, the same result was obtained with immunostain for PR)

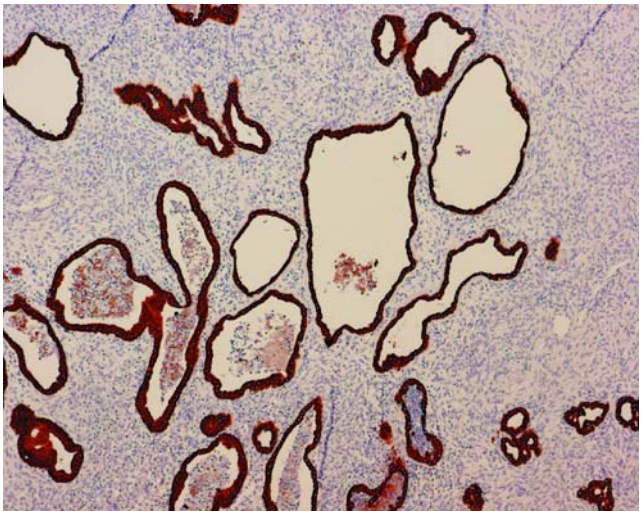

Fig. 5 Strong diffuse cytoplasmic staining of the epithelial lining of cystadenomas by CK7, the same result was seen with CK8, CK18, and CK19 (immunostain for CK7)

polyclonal carcinoembryonic antigen immunostains, all applied through the conventional methods.

In each case, the distribution of the staining was noted, and the intensity of the staining for each antibody was qualitatively graded according to the percentage of positively stained cells as 1+ staining (<25% of cells), 2+ (25–50%), and 3+ (>50%).

Results

Clinical findings

All nine tumors occurred in women whose ages ranged from 30 to 59 years (mean 42.4). There was no information about the use of contraceptive hormones in any of the cases. One patient was asymptomatic, two patients had no clinical information available, and six patients presented with upper abdominal discomfort. Five out of the six had a mass in the epigastrium, one patient had a history of previous cyst drainage, and one patient presented with acute abdomen.

The most frequently utilized imaging methods at diagnosis of the tumor were ultrasound, computed tomography scan, and angiography, usually in combination. The site of the tumor was not specified in two cases. The others were located within the liver, four in the left lobe, two in the right lobe, and one in both lobes.

Pathologic findings

Gross features

All cystadenomas were cystic, with six out of nine multilocular. The size of the cyst varied from 4–22 cm in greatest dimension. The fluid content of the cyst was clear and gelatinous in three cases, greenish and viscid in one case, thick and blood stained in one case, and forming pockets of pus in one case.

Microscopic features

All cystadenomas showed multiple locules (Fig. 1), usually lined by a single layer of cuboidal to tall columnar cells resting on a basement membrane (Fig. 2). In two cases, the epithelium showed patchy stratification, and the lumina of the cysts were filled with inflammatory cells and debris. The epithelial cells showed no atypia and had a clear or vacuolated faintly staining eosinophilic cytoplasm and uniform, small, rounded to oval nuclei. The chromatin granules were fine, the nucleoli were inconspicuous, and no mitotic figures were seen. The stroma of the tumor underlying the epithelial component varied; in eight cases

Table 1 Immunohistochemical reactivity of hepatobiliary cystadenoma to estrogen and progesterone receptors and inhibin antibodies (n=9)

Case number	Stroma	ER			PR			Inhibin-α
		Epithelium	Stroma	Adjacent hepatocytes	Epithelium	Stroma	Adjacent hepatocytes	
1	MS	1+, cyt	3+, N	3+, N	None	2+, N	None	Positive stroma
2	MS	1+, cyt	1+, N	1+, cyt	1+, cyt	None	None	None
3	MS	None	1+, N	None	None	None	None	None
4	MS	1+, cyt	2+, N	Not present in section	None	2+, N	Not present in section	Positive stroma, very patchy
5	MS	None	2+, N	Not present in section	1+, cyt	1+, N	Not present in section	None
6	MS	None	2+, N	Not present in section	None	1+, N	Not present in section	None
7	MS	2+, cyt	2+, N	None	1+, cyt	2+, N	None	None
8	Focal MS	None	2+, N	None	None	1+, N	None	None
9	MS	2+, cyt	1+, N	Not present in section	2+, cyt	2+, N	Not present in section	Positive stroma

ER Estrogen receptors, *PR* progesterone receptors, *MS* mesenchymal stroma, *cyt* cytoplasmic, *N* nuclear, *none* negative staining, *1+* less than 25% of cells are staining, *2+* 25–50% of cells are stained, *3+* more than 50% of cells are stained

Table 2 Immunohistochemical features of hepatobiliary cystadenoma (n=9)

Location of positive staining within the tumor	ER	PR	SMA	Inhibin-α	CK7	CK19	CK8	CK18
Epithelium	5/9	4/9	0/9	0/9	9/9	9/9	9/9	9/9
Stroma	9/9	7/9	9/9	3/9	0/9	0/9	0/9	0/9

ER Estrogen receptors, *PR* progesterone receptors, *SMA* anti-α-smooth muscle actin

(eight out of nine), the stroma adjacent to the epithelium consisted of a band of closely packed spindle cells, an appearance reminiscent of ovarian stroma. The stroma was only focally present in one case. Mitotic activity was not seen in the stromal component of any of the tumors. The densely cellular layer was often supported, in turn, by a densely hyalinized layer forming a pseudocapsule separating the cystadenoma from the adjacent liver tissue (Fig. 2). Small nests of luteinized stromal cells were inconspicuously seen in three cases (Fig. 3). In some lesions, nonspecific reactive changes were found in the cyst wall. These reactive changes included focal aggregation of foamy histiocytes, lipofuscin-laden macrophages, cholesterol crystal clefts, hemosiderin deposits, and focal minute areas of calcification. The liver surrounding the cystadenomas showed varying degrees of compression atrophy.

Immunohistochemistry

The epithelial lining of the cystadenomas showed variably positive, mostly pale, patchy to diffuse, occasionally granular cytoplasmic staining with antibody to ER and PR in the five out of nine and four out of nine cases, respectively (Fig. 4). However, the epithelium showed strong and diffuse cytoplasmic staining with antibodies to CK7, CK19, CK8, and CK18 (Fig. 5), but it was negative for inhibin-α (Tables 1 and 2).

The spindle cells in the stroma showed variably strong, patchy to diffuse positive nuclear staining with antibodies to estrogen and PR in all and seven of nine cases, respectively (Fig. 6). The spindled cells in the stroma showed strong diffuse cytoplasmic staining with SMA in all cases (Fig. 7). Stromal cells were negative for antibodies to CK7, CK19, CK8, and CK18 in all cases. Small nests of luteinized stromal cells exhibited strong positive membranous and cytoplasmic staining for inhibin-α in three of the nine cases (Fig. 8). These cells did not stain for HCG, although they appeared luteinized, and they were negative for α-fetoprotein and polyclonal carcinoembryonic antigen and so could not be entrapped hepatocytes.

The hepatocytes adjacent to the cystadenoma demonstrated nuclear staining for ER antibodies in one case (Fig. 9). A pale cytoplasmic staining was seen for ER antibody in another case. In five cases with adjacent normal liver, the biliary epithelium of occasional bile ductules, not the acinar ducts, showed very weak and focal cytoplasmic staining for both estrogen and PR antibodies. However, the staining was always weaker than that of the tumor epithelium. Strong cytoplasmic staining of the bile ducts for CK7 and CK19 was seen in all cases (Fig. 10). Diffuse strong membranous and cytoplasmic staining for CK8 and CK18 was seen in hepatocytes in all cases (Fig. 11). No staining of hepatocytes was detected for inhibin-α.

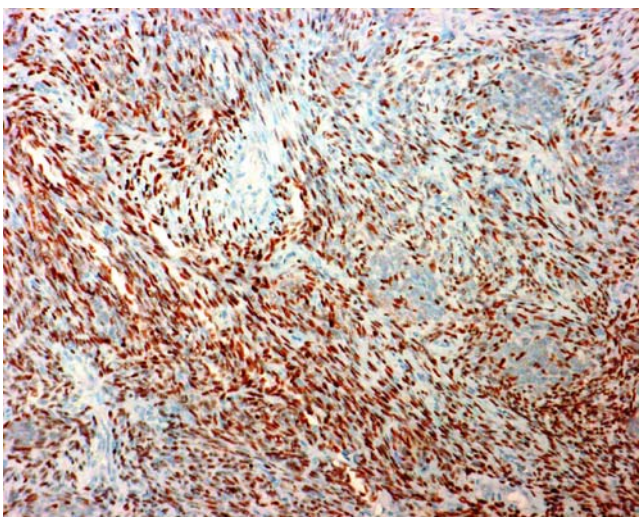

Fig. 6 Expression of ER as 3+ nuclear staining of the mesenchymal-like stroma (immunostain for ER)

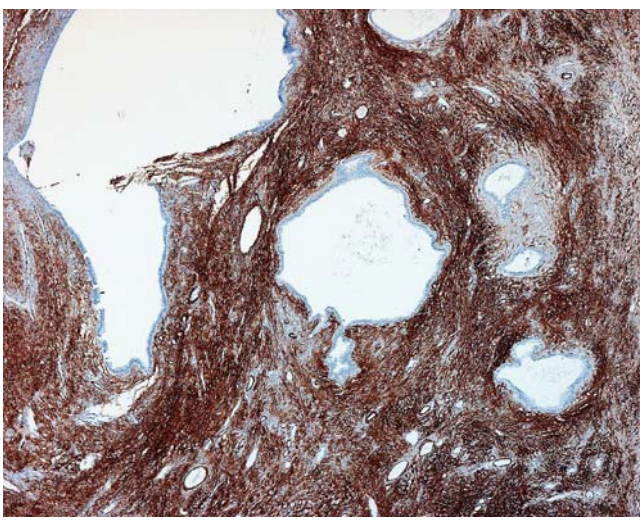

Fig. 7 Strong cytoplasmic staining of the stromal cells by smooth muscle actin

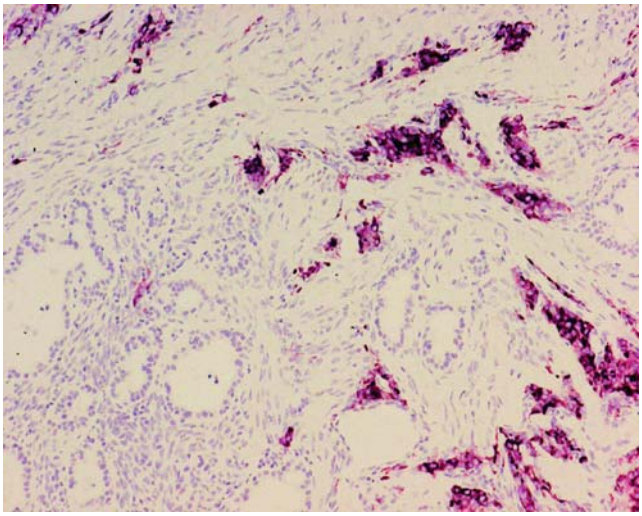

Fig. 8 The nests show dense membranous and cytoplasmic staining for inhibin-α (inhibin-α immunostain)

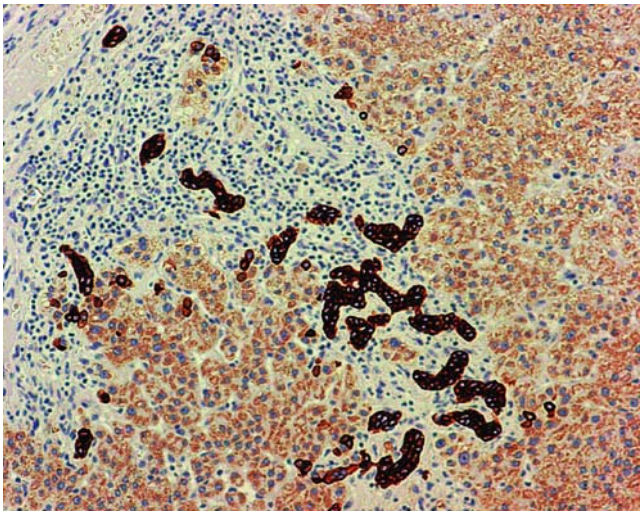

Fig. 10 Strong cytoplasmic staining of the bile ductular epithelium by CK7 served as positive internal control (immunostain for CK7)

Discussion

Hepatobiliary cystadenoma is a rare tumor; the histogenesis of which remains uncertain. The two principal theories are that they derive from ectopic intrahepatic ovary or from ectopic intrahepatic embryonic gallbladder rests [25]. Available evidence suggests that they are hormonally responsive and their occurrence almost exclusively in women seems to favor the former.

Few cases of cystadenomas with mesenchymal stroma with results of immunostaining for ER and PR staining have been reported in the literature [6, 20, 23]. Scott et al. [23] demonstrated ER immunostaining of stroma in one of three hepatobiliary cystadenomas. Grayson et al. [6] showed unequivocal immunostaining for PR in mesenchymal cells, which were negative for ER in a single case report. Pedram-Canihac et al. [20] reported the immunostaining of stromal mesenchymal cells in three of five cases and PR in all five cases. Recently, Daniels et al. [4] reported 12 cases of biliary cystadenoma with mesenchymal stroma that showed stromal ER and PR positivity in 70 and 60% of cases, respectively. In all the four reports, the positive immunoreactivity was in the form of nuclear staining. Our results are in accordance with theirs with a higher percentage (100%) positive for ER, possibly due to our use of freshly cut sections, and slightly lower (65%) for PR. The findings support the theory of a possible hormonal dependence of this tumor. The current series is, to our knowledge, the first to describe epithelial staining for ER and PR in hepatobiliary cystadenoma. We believe that the staining was not artifactual because it persisted even after we repeated the staining procedure using endogenous biotin blocking and it

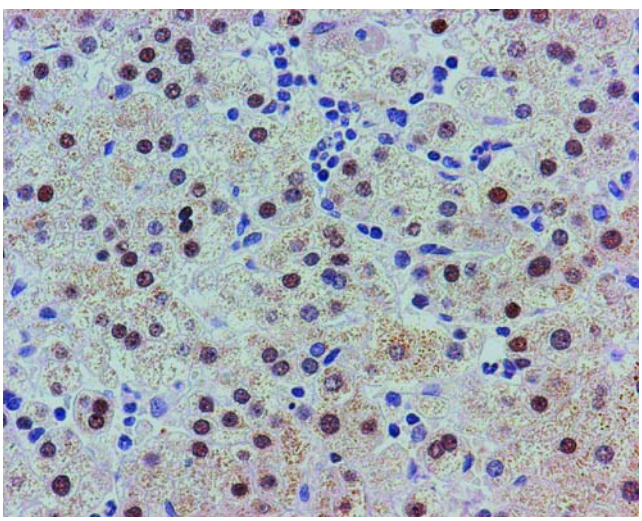

Fig. 9 Expression of ER as 3+ nuclear staining of hepatocytes documented in one case (immunostain for ER)

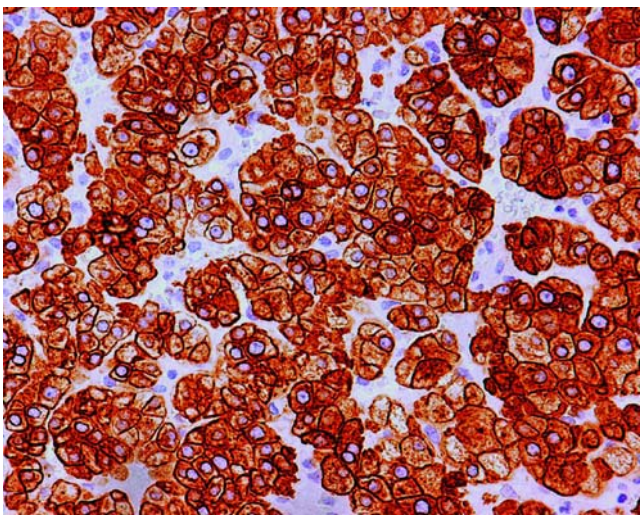

Fig. 11 Strong membranous and cytoplasmic staining of hepatocytes for CK8, which also served as positive internal control. The same result was obtained with CK18

was usually stronger than that of the very focal and weak staining of adjacent bile ductules. However, the significance of the epithelial staining is unclear. ER is a protein that has nuclear localization in human and nonhuman primate female reproductive organs [7]. Experimental evidence has documented the liver as a target organ for sex hormones [12, 21]. The liver is an estrogen-sensitive organ, and such sensitivity necessitates the presence of hepatic ER. This could explain the positive staining sometimes detected in the adjacent hepatocytes. Daniels et al. [4] reported the same finding in 43% of their cases. Recently, Moon et al. [17] reported that cytoplasmic and nuclear immunoreactivity for ER was present in hepatocellular carcinoma specimens in 46 and 12% respectively.

SMA is a monoclonal antibody that stains actin present in smooth muscle cells as well in myofibroblasts and myoepithelium. Our finding of strong immunoreactivity of the stromal cells in all tumors is in accordance with the findings of Subramony et al. [25], who reported that the stroma in five cases of hepatobiliary cystadenoma shared the expression of SMA with the subepithelial spindled cells of six cases of fetal gall bladder.

Inhibin is a polypeptide hormone secreted by granulosa cells of the ovary and Sertoli cells of the testis. In the fully processed form, its molecule consists of two distinct chains (α and β) linked by disulfide bridges. Inhibin-A consists of an α-subunit and an β-A subunit. The inhibin-α subunit is expressed in a wide range of human tissues outside the reproductive axis (e.g., prostate, brain, adrenal). Immunohistochemical staining for inhibin-α can be used as a differential marker for placental and gestational trophoblastic lesions, sex cord stromal tumors (granulosa cell tumors, luteinized thecomas, and Leydig cell tumors) [2, 15, 22]. Although it seems that inhibin-α is not specific for a particular tissue, it is a very sensitive stain. Recently, Izumo et al. [10] reported luteinization and inhibin-α immunoreactivity in the ovarian stroma of the mucinous cystic tumors of the ovary in nine out of ten cases and in the ovarian-like stroma in a similar proportion (29 of 34 cases) of mucinous cystic tumors of the pancreas. Similar findings were reported by Yeh et al. [28] in seven mucinous cystic neoplasms of the pancreas, of which, four were benign, two borderline and one malignant. In the present study, we found inhibin-α positive luteinized stromal cells in three cases of hepatobiliary cystadenoma, which, to our knowledge, is the first report of such cells in this liver tumor. The luteinized cells are inconspicuous on hematoxylin and eosin (H&E), but all were easily spotted by immunohistochemistry. This observation may further support its similarity to the true ovarian stromal tissue and may suggest a role of complex hormonal interaction in the pathogenesis of the tumor. Whether being a hormonal sensitive tissue can be a potential for hormonal manipulation in clinical management especially to prevent recurrences or in large tumors or in tumors occurring in inoperable patients is beyond the scope of this study. However, it may be worth mentioning that the first line of treatment is complete surgical resection for the relief of symptoms and malignant potential [9, 27]. Any procedure other than complete resection has been associated with treatment failure [14, 18].

Devany et al. [5] found positive staining with pancytokeratin antibodies in the epithelium of all 20 cystadenomas studied with immunohistochemistry. We extended this by staining for the four types of CK (7, 8, 18, 19) that can be found in normal bile ducts and found strong and uniform immunoreactivity to all four antibodies, consistent with origin from biliary epithelium.

In summary, hepatobiliary cystadenoma with mesenchymal stroma has a CK profile that supports an origin from the biliary tract, while the finding of ER, PR, and inhibin-α positivity in the ovarian-type stroma supports its hormonal dependence and explains its exclusive occurrence in women.

References

1. Akwari OE, Tucker A, Seigler HF, Itani KMF (1990) Hepatobiliary cystadenoma with mesenchymal stroma. Ann Surg 211:18–27
2. Arora DS, Cooke IE, Ganesan TS, Ramsdale J, Manek S, Charnock FM, Groome NP, Wells M (1997) Immunohistochemical expression of inhibin/activin subunits in epithelial and granulosa cell tumors of the ovary. J Pathol 181:413–418
3. Bertheau P, Cazals-Hatem D, Meignin V, de Roquancourt A, Verola O, Lesourd A, Sene C, Brocheriou C, Janin A (1998) Variability of immunohistochemical reactivity on stored paraffin slides. J Clin Pathol 51:370–374
4. Daniels J, Coad J, Payne W, Kosari K, Sielaff T (2006) Biliary cystadenomas: hormone receptor expression and clinical management. Dig Dis Sci 51:623–628
5. Devaney K, Goodman ZD, Ishak KG (1994) Hepatobiliary cystadenoma and cystadenocarcinoma. A light microscopic and immunohistochemical study of 70 patients. Am J Surg Pathol 18:1078–1091
6. Grayson W, Teare J, Myburgh JA, Paterson AC (1996) Immunohistochemical demonstration of progesterone receptor in hepatobiliary cystadenoma with mesenchymal stroma. Histopathology 29:461–463
7. Greene GL, Sobel NB, King WJ, Jensen EV (1984) Immunohistochemical study of estrogen receptor. J Steroid Biochem 20:51–56
8. Hsu SM, Raine L, Fanger H (1981) Use of avidin–biotin–peroxidase complex (ABC) in immunoperoxidase techniques: a comparison between ABC and unlabelled antibody procedures. J Histochem Cytochem 29:577–580
9. Ishak KG, Willis GW, Cummins SD, Bullock AA (1977) Biliary cystadenoma and cystadenocarcinoma. Report of 14 cases and review of the literature. Cancer 38:322–328
10. Izumo A, Yamaguchi K, Eguchi T, Nishiyama K, Yamamoto H, Yonemasu H, Yao T, Tanaka M, Tsuneyoshi M (2003) Mucinous cystic tumor of the pancreas: immunohistochemical assessment of "ovarian-type stroma". Oncol Rep 10:515–525
11. Jacobs TW, Prioleau JE, Stillman IE, Schnitt SJ (1996) Loss of tumor marker-immunostaining intensity on stored paraffin slides of breast cancer. J Natl Cancer Inst 88:1054–1059

12. King WJ, Greene GL (1984) Monoclonalantibodies localize estrogen receptor in the nuclei of target cells. Nature 307: 745–747
13. Korobkin M, Stephens DH, Lee JK, Stanley RJ, Fishman EK, Francis IR, Alpem MB, Rynties M (1989) Biliary cystadenoma and cystadenocarcinoma: CT scan and sonographic findings. AJR Am J Roentgenol 153:507–511
14. Litwin D, Taylor B, Greig P, Langer B (1987) Nonparasitic cysts of the liver the case for conservative surgical management. Ann Surg 205:45–48
15. McCluggage WG (2001) Value of inhibin staining in gynecological pathology. Int J Gynecol Pathol 20:79–85
16. Mirlacher M, Kasper M, Storz M, Knecht Y, Durmuller U, Simon R, Mihatsch MJ, Sauter G (2004) Influence of slide aging on results of translational research studies using immunohistochemistry. Mod Pathol 17:1414–1420
17. Moon WS, Chang K, Tarnawski AS (2004) Overexpression of metastatic tumor antigen 1 in hepatocellular carcinoma: relationship to vascular invasion and estrogen receptor-α. Hum Pathol 35:424–429
18. Moorthy K, Houghton P, Houghton PW (2001) The management of simple hepatic cysts: sclerotherapy or laparoscopic fenestration. Ann R Coll Surg Engl 83:409–414
19. Oxford Brooks University (2001) Oxford Brooks University Inhibin Web Page. Available at: http://www.brooks.ac.uk/schools/bms/research/peptides/index.html
20. Pedram-Canihac M, Le Bail B, Rivel J, Blanc JF, Saric J, Bioulac-Sage P (2000) Hepatobiliary cystadenoma with mesenchymal stroma: a hormonal dependant tumor. Report of five cases with immunohistochemical study of hormone receptors. Ann Pathol 20:14–18
21. Press MF, Greene GL (1984) An immunohistochemical method for demonstrating estrogen receptor in human uterus using monoclonal antibodies to human estrophilin. Lab Invest 50:480–486
22. Renshaw AA, Granter SR (1998) A comparison of A 103 and inhibin reactivity in adrenal cortical tumors: distinction from hepatocellular carcinoma and renal tumors. Mod Pathol 11:1160–1164
23. Scott FR, More L, Dhillon AP (1995) Hepatobiliary cystadenoma with mesenchymal stroma: expression of estrogen receptors in formalin-fixed tissue. Histopathology 26:555–558
24. Serotec (2001) Serotec distributor information. Available at: http://www.serotec.co.uk/inhibin.html
25. Subramony C, Herrera GA, Elba EA, Turbat-Herrera EA (1993) Hepatobiliary cystadenoma. A study of five cases with reference to histogenesis. Arch Pathol Lab Med 117:1036–1042
26. Wheeler DA, Edmondson HA (1985) Cystadenoma with mesenchymal stroma (CMS) in the liver and bile ducts. A clinicopathologic study of 17 cases, 4 with malignant change. Cancer 56:1434–1445
27. Woods G (1981) Biliary cystadenocarcinoma case report of hepatic malignancy originating in benign cystadenoma. Cancer 47:2936–2940
28. Yeh MM, Tang LH, Wang S, Robert ME, Zheng W, Jain D (2004) Inhibin expression in ovarian-type stroma in mucinous cystic neoplasms of the pancreas. Appl Immunohistochem Mol Morphol 12:148–52

Virchows Arch (2007) 450:699–711
DOI 10.1007/s00428-007-0412-9

ORIGINAL ARTICLE

Global gene expression profiling of formalin-fixed paraffin-embedded tumor samples: a comparison to snap-frozen material using oligonucleotide microarrays

Matthias Frank · Claudia Döring · Dirk Metzler · Susan Eckerle · Martin-Leo Hansmann

Received: 13 December 2006 / Revised: 21 March 2007 / Accepted: 24 March 2007 / Published online: 4 May 2007
© Springer-Verlag 2007

Abstract Oligonucleotide microarrays are widely used to investigate gene expression in a large-scale approach. A major limitation is the dependency on frozen material to obtain high-quality ribonucleic acid because most clinical specimens are formalin-fixed and paraffin-embedded (FFPE). The ability to analyze these samples using microarrays would enlarge the investigable sample stocks manifold. We conducted a comparison of snap-frozen and FFPE tissues investigating two malignomas. Gene expression profiles were obtained from both materials of the tumors. Independently processed triplicates of snap-frozen and FFPE specimen, respectively, were two-round-amplified and hybridized on Affymetrix GeneChips® (Palo Alto, CA, USA). Differentially expressed genes were identified in both FFPE and frozen material. All replicates had a correlation coefficient (R) of greater than 0.95 after normalization. Only direct comparison of FFPE to frozen replicates resulted in a mean R of 0.86, rendering a "mixed" investigation unfeasible. More than 50% (419 genes) of the more than fivefold differentially expressed genes (800 in FFPE, 685 in frozen material) were detected concomitantly regardless of the material used, which is similar to other comparisons of different gene expression analysis platforms. Thus, global gene expression analyses using solely FFPE material seem to be feasible with nearly comparable results to frozen tissue studies.

M. Frank (✉) · C. Döring · S. Eckerle · M.-L. Hansmann
Senckenbergisches Institut für Pathologie, Klinikum der Johann Wolfgang Goethe-Universität Frankfurt,
Theodor-Stern-Kai 7,
60590 Frankfurt am Main, Germany
e-mail: Matthias.Frank@em.uni-frankfurt.de

D. Metzler
Institut für Informatik, Fachbereich Informatik und Mathematik,
Johann Wolfgang Goethe-Universität Frankfurt,
Frankfurt am Main, Germany

Keywords Comparison · Formalin-fixed and paraffin-embedded material (FFPE) · Gene expression profiling · Oligonucleotide microarrays · Two-round amplification

Introduction

Oligonucleotide microarray investigations of gene expression are an important source of new insights into pathogenesis and mechanisms of disease because they allow for gene expression measurements of many thousand genes within one experiment. Thus, they have been used to find new markers or classifications of disease entities based on gene expression patterns or to conduct prognosis or treatment response studies [2, 11, 15, 18, 19, 25, 28].

So far, the gene expression investigation of formalin-fixed and paraffin-embedded (FFPE) materials, which represent the by-far greatest stock of archived disease entities, was limited mainly to investigations of a small number of genes at a given time using methods like quantitative real-time reverse transcription polymerase chain reactions (qRT-PCRs) [3, 5, 13, 17, 24, 26, 28].

The main reason for this restriction is the chemically altered and degraded state of the ribonucleic acid (RNA) within FFPE material because microarray analyses depend on good-quality RNA, which usually can only be derived from frozen material. This study compared the gene expression of frozen-material-derived two-round amplified total RNA to data generated with a similar two-round amplified complementary RNA (cRNA) obtained from FFPE material using reagents that were developed to, at least in part, reverse the alterations of the FFPE RNA (http://www.arctur.com/research_portal/

products/paradise_addl_info.htm). The yielded labeled cRNA was hybridized to oligonucleotide microarrays that were designed for more degraded starting material.

Materials and methods

Tissue specimens

Tumor samples were drawn from the files of the Senckenberg department of Pathology, University of Frankfurt. All specimens had been taken for diagnostic purpose. Representative samples of tumor tissues were cut, brought into liquid nitrogen, and stored at −80°C and/or in liquid nitrogen storage tanks. FFPE samples had been fixed in 4% buffered formalin (pH 6.8–7.2), processed, and embedded in paraffin. The tissue was used in accordance with national ethical principles.

RNA isolation, quality control, amplification, and labeling of snap-frozen tissue samples

For RNA-quality control, five 10-μm sections of the snap-frozen tissue were cut. The tissue was homogenized using Qiashredder spin columns (Qiagen, Hilden, Germany). Total RNA was extracted using the RNeasy Mini Kit (Qiagen) according to manufacturers' instructions following the animal cell spin protocol. One microliter of the RNA was analyzed on the Bioanalyzer 2100 (Agilent, Palo Alto, CA, USA) using a RNA 6000 Nano LabChip according to the manufacturers' instructions.

For the dissection of an area of approximately 0.3 cm^2 of tumor tissue, 7-μm thick sections of frozen tissue were cut and stained with H&E essentially as described previously [22]. The tissue was dissected with a scalpel and transferred into a 0.5-ml tube. Total RNA was extracted using the Purescript® RNA Purification Kit (Gentra Systems, Minneapolis, MN, USA) according to the manufacturers' protocol for 10^5 to 10^6 cells with minor modifications. Amplification of the RNA was performed with the RiboAmp Kit (Arcturus Bioscience, Mountain View, CA, USA). Approximately 20 ng of the total RNA was amplified one-and-a-half rounds, as recommended by the manufacturer. From the yielded double stranded complementary deoxyribonucleic acid (cDNA), biotin-labeled cRNA was generated using the IVT-Labeling Kit (Affymetrix) according to manufacturers' instructions. Column-based cleanup of the biotin-labeled cRNA was done using the sample cleanup kit (Affymetrix) as recommended by the manufacturer.

RNA isolation, quality control, amplification and labeling of FFPE-tissue samples

For extraction and amplification of RNA from FFPE samples, the Paradise™ Reagent System (Arcturus) was used as recommended by the manufacturer. Briefly, 7-μm sections were deparaffinized, rehydrated, and stained using included reagents. Approximately 0.3 cm^2 of tumor tissue was dissected with a scalpel and transferred into a 0.5-ml tube. Proteinase K digestion was done overnight at 50°C. Total RNA was isolated using provided columns. An on-column-DNase-digestion was performed. The yielded total RNA was quantified on the Bioanalyzer 2100 (Agilent) using RNA 6000 Pico LabChips as recommended by the manufacturer. RNA quality from FFPE samples was assessed with a SYBR® green qRT-PCR assay for detection of the expression of beta-actin mRNA as described in the Paradise® Reagent System User Guide version B (Arcturus). The amplification was carried out on the ABI PRISM 7900HT RT-PCR system (Applied Biosystems, Foster City, CA, USA) applying the protocol recommended. Briefly, single-stranded cDNA was generated using the reagents for oligo-dT priming of the Paradise kit (Arcturus) as recommended. Two amplicons of beta-actin mRNA were amplified using the primer pairs (MWG-Biotech, Ebersberg, Gemany) as specified in the user guide.

For the generation of labeled cRNA approximately 20 ng of total RNA were transcribed into double-stranded cDNA and purified using the provided Columns. Antisense RNA (aRNA) was generated by a T7 polymerase-based IVT and also purified. Double-stranded cDNA was generated and purified for a second round of amplification according to the manufacturers' instructions. Biotin-labeled cRNA was then generated in another T7-based IVT reaction using the IVT-Labeling Kit (Affymetrix) as recommended. Column-based cleanup of the yielded biotin-labeled cRNA was done using the sample cleanup kit (Affymetrix) according to the manufacturers' instructions. The generated cRNAs of both materials were also tested on the Bioanalyzer 2100 (Agilent) RNA 6000 Nano LabChips as recommended by the manufacturer.

Oligonucleotide microarray assays

Human X3P GeneChips® (Affymetrix) were used for the FFPE and frozen-material-derived cRNA, and in addition, HG-U133 Plus 2.0 GeneChips® (Affymetrix) were used for the frozen material as well. Hybridization, washing, and staining procedures were conducted as recommended by the manufacturer using the Wash protocol EukGE-WS2v5 on a GeneChip Fluidics Station 400 (Affymetrix). Data acquisition was performed using a GeneChip Scanner 3000 (Affymetrix).

Data analysis

Data analysis for evaluation of the technical performance of the arrays was done using the GeneChip Operating Software (Affymetrix). Default statistical algorithm parameters were applied and the signal intensity was scaled to a target value of 2,000 for the 100 control transcripts, as provided by Affymetrix in the Human Genome U133 2.0 Array Normalization Controls mask file (http://www.affymetrix.com/Auth/support/downloads/mask_files/hgu133_plus_2norm.zip).

Probe intensity normalization for further analysis was conducted using the variance stabilization method as described by Huber et al. [8] using "Bioconductor" (http://www.bioconductor.org) and "R" software (http://www.r-project.org). Gene expression levels were estimated by fitting the additive model described by Irizarry et al. [9] employing a median polish routine. The quality of hybridizations was assessed by visual inspection of the residuals of the model. Unsupervised hierarchical clustering was performed for the 1,000 genes with the greatest variance across all assays using the Manhattan distance and the average linkage method. Two lists of differentially expressed genes between the two investigated tumor entities were built by using the unpaired *t* statistics (variance equal = TRUE) for the frozen and the FFPE materials, respectively. The false discovery rates (FDRs) of these lists were estimated with the method of Benjamini and Hochberg [7]. Two new lists were generated from the complete lists containing only those genes that were differentially expressed fivefold or more (and also threefold or more, respctively) and had *t* test–*p* value and Benjamini–Hochberg FDR equal to or below 0.01. A similar threefold-change list was also created for the HGU133 Plus 2.0 data and matched to the X3P data using the RefSeq Transcript IDs.

The X3P-fivefold change lists of FFPE and frozen material were compared to each other, and a hierarchical clustering analog to the former was conducted using only those genes from the 1,000 highest variant genes list, which could also be found in both of the fivefold change lists. To analyze the "falsely" classifying genes of the FFPE material data, a list was generated containing the genes, which seemed to differentiate FFPE from frozen tissue instead of diffuse large B-cell lymphoma (DLCL) from follicular thyroid carcinoma (FTC) with a fold change of more than threefold (and fivefold, respectively) in the FFPE and less than twofold in the frozen-chip data with a two-sided *t* test *p* value of less than 0.01 and compared against the corresponding list generated for the frozen material data.

Results

Three independently processed replicates of FFPE and frozen material of one case of FTC and one case of diffuse large B-cell lymphoma, respectively, were investigated (Fig. 1). Two completely different tumor entities of two different tissue types (thyroid and lymph node, respectively) were chosen to ensure a great number of differentially expressed genes.

RNA quality

Global gene expression experiments depend on adequate preservation of the applied total RNA. RNA quality from frozen material was assessed by the Agilent Bioanalyzer. The software calculates an RNA integrity number (RIN)

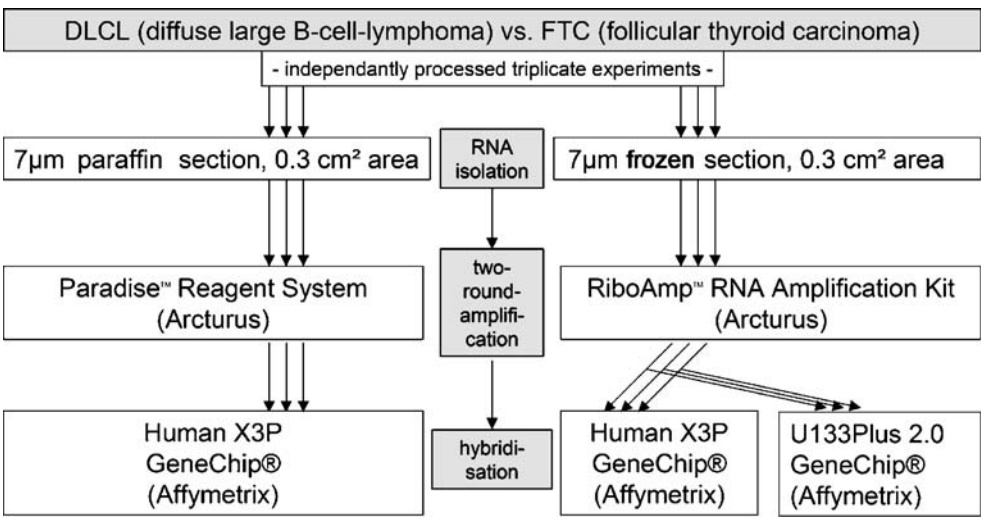

Fig. 1 Experiment design. Three independently processed replicates of FFPE and frozen material derived total RNA of one case of FTC and one case of diffuse large B-cell lymphoma, respectively, were investigated using two-round amplification protocols to generate biotin-labeled cRNA, which was hybridized on Affymetrix oligonucleotide microarrays

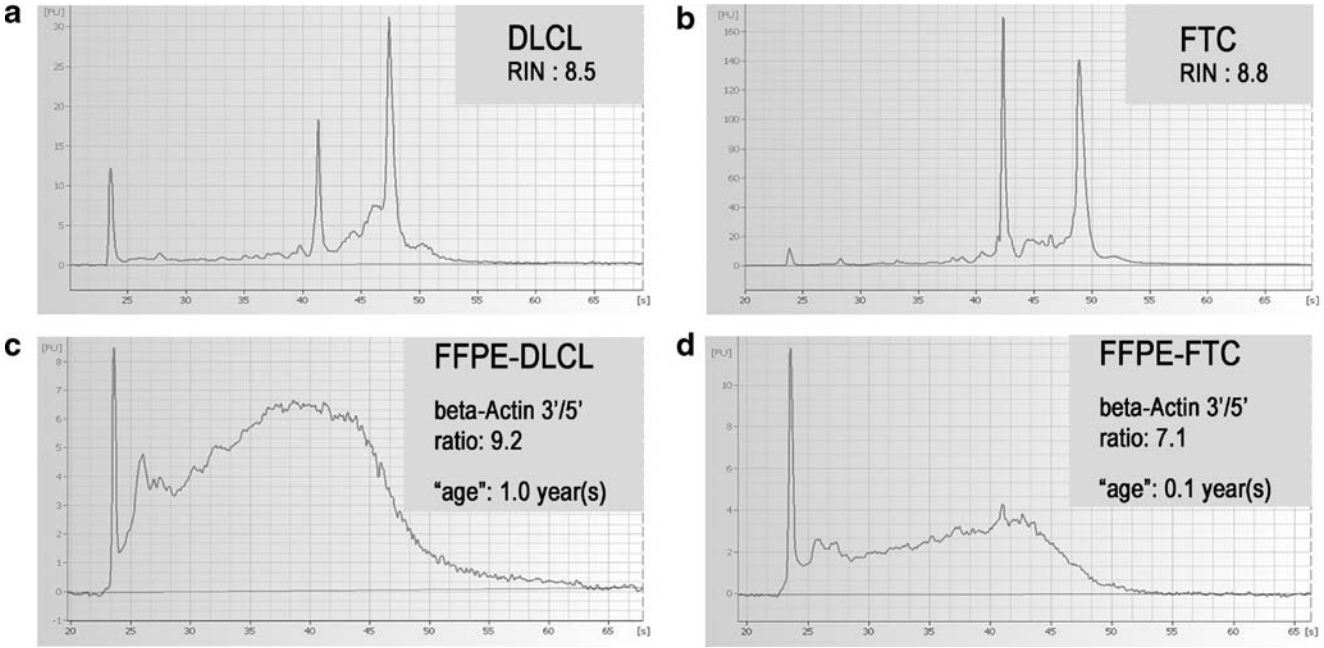

Fig. 2 Quality of the used RNA. The gelelectropherograms show the fluorescence signal intensity resembling the RNA concentration at a given point on the *vertical axis* and a timescale(s) resembling RNA fragment size on the *horizontal axis*. The *area under the curve* resembles the total RNA concentration. **a** DLCL total RNA from frozen material. **b** FTC total RNA from frozen material. **c** DLCL total RNA from FFPE material. **d** FTC total RNA from FFPE material

[21] that ranges from 1 (completely degraded sample) to 10 (no measurable degradation). The frozen samples included in this study had a RIN higher than 8.5 (Fig. 2a,b).

The extent of degradation of the FFPE samples was estimated by conducting a qRT-PCR assay for beta-actin mRNA, yielding a quantity for each primer pair 1 = [RNA]1650 and primer pair 2 = [RNA]1355. Primer pair 1 defines an amplicon close to the 3′ end of the beta-actin mRNA and primer pair 2 defines an amplicon approximately 300 base pairs closer to the 5′ end. The ratio of these quantities ([RNA]1650/[RNA]1355) resembles the degree of fragmentation of the investigated FFPE RNA (http://www.arctur.com/research_portal/images/pdf/aacrposter_gene_expression_lding.pdf). For the used samples, this ratio was below 10 and the processed RNA showed a sufficient performance on the GeneChips (Fig. 2c,d). Of the ten tested FFPE-RNA samples (five lymphomas and five thyroid samples; Fig. 2c,d and Fig. 3a,b) eight were approximately 1 year old or younger. Three of these had a beta-actin PCR ratio above 10. One DLCL sample was 3.5 years old and one was 4.9 years old. Both had ratios far above 10 (24.6 and 32.6, respectively). The generated biotin-labeled cRNAs of both materials showed similar shapes on the gelelectropherograms, resembling similar fragment-length distributions, although the mean fragment length of the FFPE cRNA was somewhat shorter than that of the frozen cRNA (Fig. 3b).

Technical performance and reproducibility of the oligonucleotide microarray data

The Human X3P GeneChip was used for cRNA of both materials and the HG-U133 Plus 2.0 GeneChip for another aliquot of the same cRNA of the frozen material only. The HG-U133 Plus 2.0-array contains more than 47,000 transcripts. The X3P array has identical target sequences as the HG-U133 Plus 2.0-array, but the probe sequences are located closer to the 3′ end, where possible (http://www.affymetrix.com/support/technical/datasheets/made_datasheet.pdf).

The technical performance of the arrays was evaluated by assessing the scale factor as a value for the average signal intensity of the 100 control transcripts; the percentage of present calls, which resembles the number of detected transcripts; and the correlation of the replicates to determine the technical consistency and reproducibility of the results (Table 1). The scale factors were between 1.9 and 5.6 for all X3P arrays, which means a less than threefold difference in the mean signal intensity without normalization. Within the replicates, this difference averaged to 1.7 (±0.4). The percent present calls exceeded 20% for all but one frozen X3P array, which had a detection rate of 19.7% (19.7–29.2%). The average percent present call was 26.2% (±2.0%) for all FFPE arrays and 22.4% (±2.3%) for all frozen material arrays (Table 1).

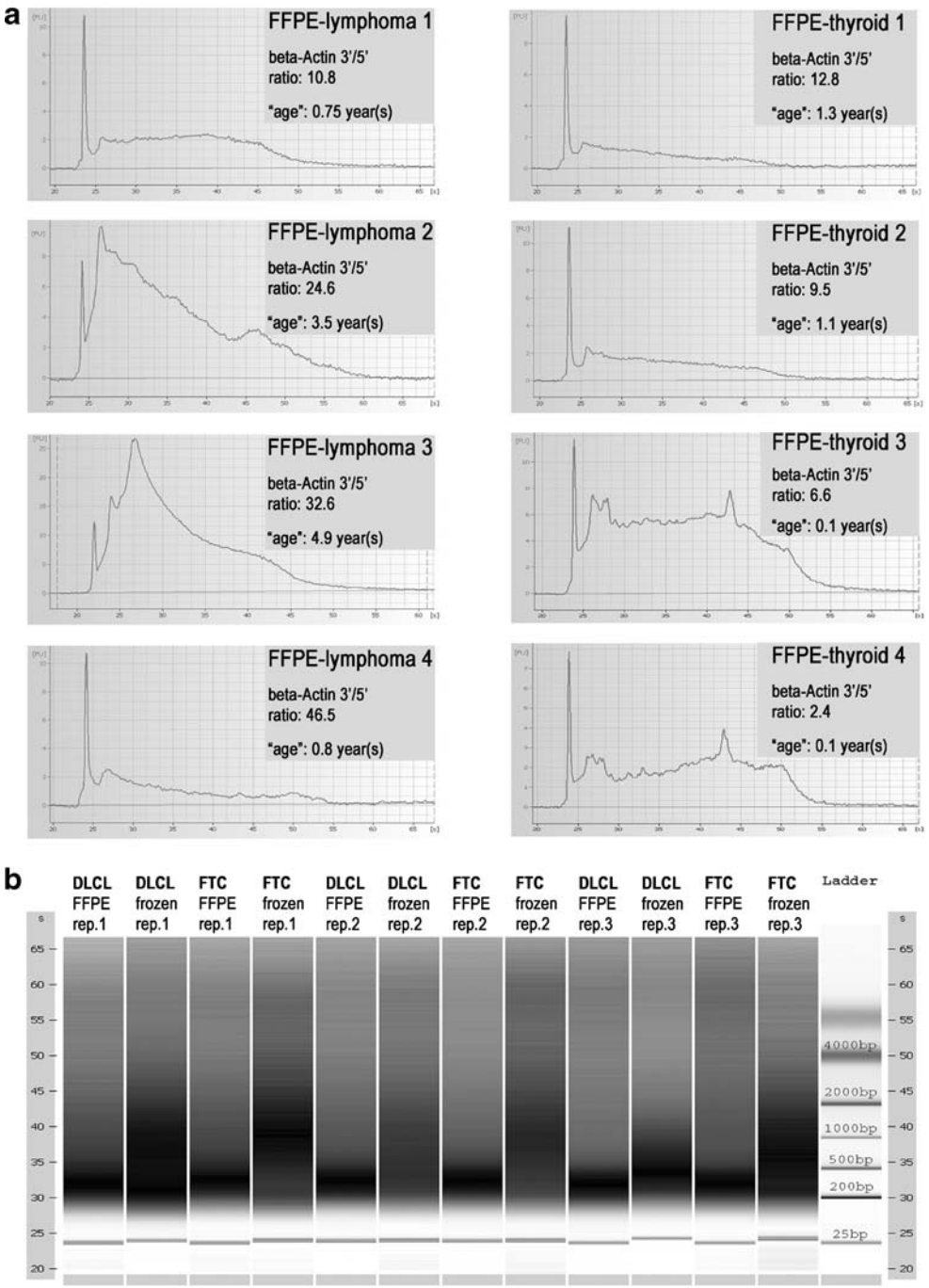

Fig. 3 Quality of the FFPE RNA of the tested samples. **a** Total RNA from FFPE material of the other investigated samples. **b** Gel-like image of biotin-labeled cRNAs of all FFPE and frozen replicates. Frozen samples show a fragment length distribution maximum in the area of 500 to 1,000 base pairs, while the FFPE samples show a fragment length distribution maximum in the area of 200 to 500 base pairs

The average percentage of detected genes of all frozen samples was 5.0% higher on the Human X3P than on the HG-U133 Plus 2 GeneChips. The mean signal intensity showed an increase of approximately 15% on the X3P arrays. The box plots of all X3P arrays before and after normalization show a homogenous signal distribution already before normalization (Fig. 4a,b).

The correlation coefficient *R* (Pearson correlation) over all measured genes was above 0.95 in comparisons of all replicates after the variance stabilization normalization (Fig. 5, Table 2), indicating a sufficient technical reproducibility for both materials on the X3P chips. However, direct comparison of the signal intensities of frozen to FFPE replicates yielded a mean correlation coefficient of 0.86, while the mean correlation coefficients of all FFPE replicates, as well as all frozen-replicates (X3P and HGU133 Plus 2.0 GeneChips®), were 0.97 each (Tables 2 and 3). This indicates that the bias introduced by the different starting materials (and processing protocols) is too high for a direct comparison of these materials.

Table 1 Technical quality metrics (excerpt) of the GeneChips®, as provided within the report files of the GeneChip Operating Software (Affymetrix)

	Array type	Scale factor	Background	Percent present calls
FFPE_DLCL1	U133_X3P	2.211	70.12	29.22
FFPE_DLCL2	U133_X3P	4.383	54.38	25.81
FFPE_DLCL3	U133_X3P	4.377	60.2	24.83
FFPE_FTC1	U133_X3P	1.897	87.31	28.22
FFPE_FTC2	U133_X3P	3.916	55.02	25.15
FFPE_FTC3	U133_X3P	4.182	60.13	24.18
Frozen_DLCL1	U133_X3P	5.076	57.4	20.22
Frozen_DLCL2	U133_X3P	4.085	61.44	19.7
Frozen_DLCL3	U133_X3P	2.608	55.09	23.98
Frozen_FTC1	U133_X3P	5.603	59.7	21.43
Frozen_FTC2	U133_X3P	5.491	54.95	23.37
Frozen_FTC3	U133_X3P	4.254	46.25	25.53
Frozen_DLCL1	HG-U133_P2	4.695	56.6	17.32
Frozen_DLCL2	HG-U133_P2	4.42	63.81	16.11
Frozen_DLCL3	HG-U133_P2	3.136	68.9	18.55
Frozen_FTC1	HG-U133_P2	5.508	62.73	17.64
Frozen_FTC2	HG-U133_P2	7.305	57.63	17.24
Frozen_FTC3	HG-U133_P2	5.774	62.46	17.6

Comparison of gene-expression changes

The data of the 1,000 genes with the highest variance across all X3P arrays were subjected to an unsupervised hierarchical clustering to test the extent of bias introduced by formalin-fixation and paraffin-embedding; that is, to see whether the biological relatedness of the disease entities was preserved or whether the type of starting material determined most of the features of the measured gene expression patterns. The latter was not the case because the first branch of the hierarchical tree separated the biologically distinct entities FTC and DLCL (Fig. 6a). The second branch then divided frozen and FFPE replicates from each other. The closest relation to each other was found amongst the replicates. Thus, the gene expression data filtered only for the most variant genes that already reflected the biology of the samples. However, a significant number of these arbitrarily selected genes seemed to be influenced more by the type of starting material than its biology (Fig. 6a). So two further lists were generated, which contained all genes that were differentially expressed fivefold or more (two sample *t* test *p* value and FDR <0.01) between the tumor entities for each starting material. These lists resulted in 800 statistically significant fivefold or more differentially expressed genes for the FFPE samples and 685 genes for the frozen samples (Fig. 7a). Four hundred nineteen genes (238 more than fivefold higher expressed genes in DLCL and 181 in FTC) of the 800 genes in FFPE and 685 genes in frozen material, respectively, were detected in both lists concomitantly (52.4 and 61.2%, respectively).

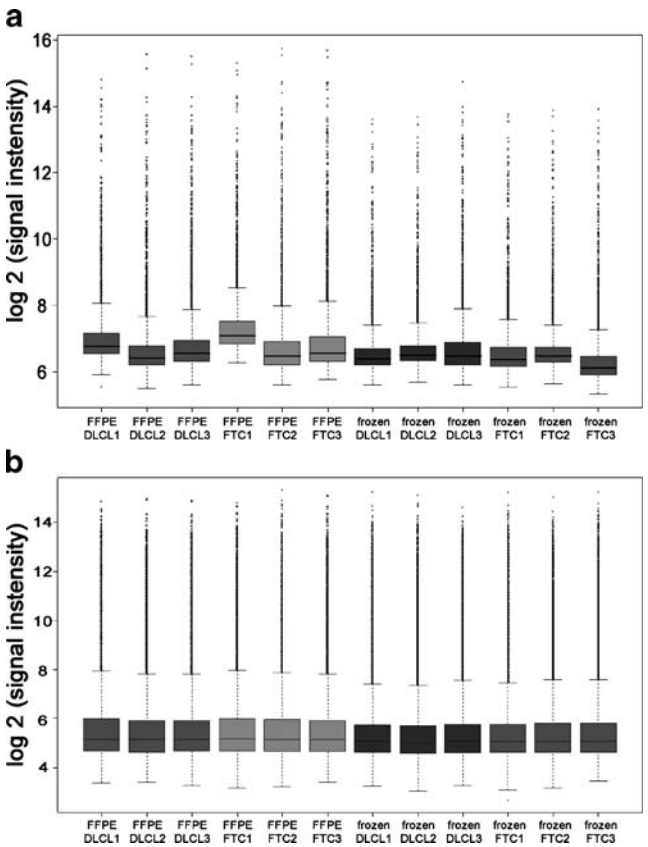

Fig. 4 Box plots of all Human X3P arrays (frozen and FFPE) before (**a**) and after (**b**) normalization

The threefold change lists resulted in 1,360 statistically significant differentially expressed genes for the FFPE samples and 1,333 genes for the frozen samples, of which 1,052 had a unique RefSeq Transcript ID. Seven hundred thirty three genes (397 more than threefold higher expressed genes in DLCL and 336 in FTC) of the FFPE and frozen material lists, respectively, were detected in both threefold change lists concomitantly, which was still 53.9

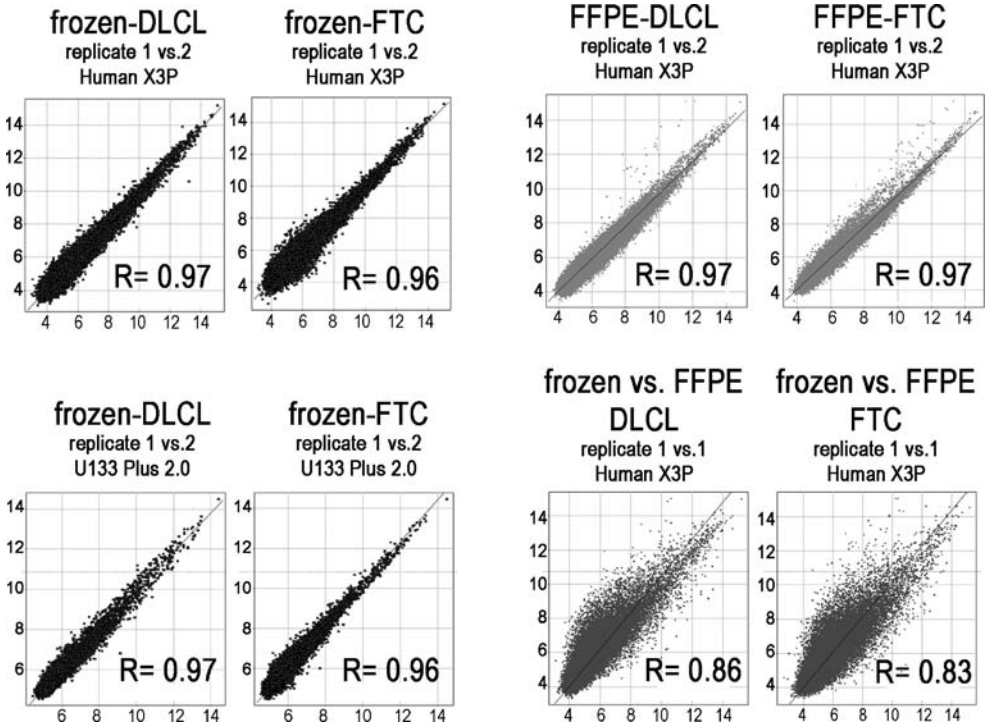

Fig. 5 Scatter plots and Pearson correlation coefficients (*R*) of the signal intensities of representative replicate experiments. The signal intensities of one replicate are shown on the *vertical axis* and the corresponding signal intensities of the other replicate on the *horizontal axis*

and 55.0%, respectively. The threefold change list of Plus 2.0-chip-data resulted in 422 statistically significant differentially expressed genes, of which 327 had a unique RefSeq Transcript ID. Two hundred forty five genes were detected in both RefSeq-matched threefold change lists of the frozen material concomitantly, which was 74.9 and 23.3%, respectively.

Three hundred fifty seven genes (85.2%) from the 419 more than fivefold common genes list were also found among the 1,000 most variant genes (Fig. 7b). A supervised hierarchical clustering was conducted, and a heat map (Fig. 6b) was generated using those 357 genes. By this, only the statistically significant more than fivefold differentially expressed genes (*t* test *p* value and Benjamini–Hochberg FDR <0.01) from the 1,000 highest variant genes were selected. As a consequence of this filtering to stringent criteria, a significant reduction of the seemingly material-dependent and, thus, falsely classifying genes in comparison to the first heat map could be seen (Fig. 6a,b). Thus, a gene list containing an essence of the most meaningful genes independent of starting material was obtained, leaving still more than one third of the 1,000 highest variant genes. Those 62 genes of the 419 concomitantly more than fivefold differentially expressed genes, which were not among the 1,000 highest variant genes, all had relatively low fold changes (6.45/6.09 in average for frozen

Table 2 Correlation matrix showing the global correlation coefficients of all X3P-GeneChip® replicates over all normalized measured genes

	FFPE_ DLCL1	FFPE_ DLCL2	FFPE_ DLCL3	FFPE_ FTC1	FFPE_ FTC2	FFPE_ FTC3	Frozen_ DLCL1	Frozen_ DLCL2	Frozen_ DLCL3	Frozen_ FTC1	Frozen_ FTC2	Frozen_ FTC3
FFPE_DLCL1	1	0.97	0.97	0.87	0.88	0.87	0.86	0.85	0.85	0.8	0.8	0.8
FFPE_DLCL2	0.97	1	0.98	0.85	0.88	0.88	0.89	0.88	0.89	0.83	0.83	0.82
FFPE_DLCL3	0.97	0.98	1	0.85	0.88	0.88	0.9	0.89	0.89	0.84	0.83	0.82
FFPE_FTC1	0.87	0.85	0.85	1	0.97	0.97	0.73	0.73	0.73	0.83	0.84	0.83
FFPE_FTC2	0.88	0.88	0.88	0.97	1	0.98	0.77	0.76	0.77	0.86	0.86	0.85
FFPE_FTC3	0.87	0.88	0.88	0.97	0.98	1	0.78	0.78	0.78	0.87	0.87	0.86
Frozen_DLCL1	0.86	0.89	0.9	0.73	0.77	0.78	1	0.97	0.97	0.88	0.88	0.88
Frozen_DLCL2	0.85	0.88	0.87	0.73	0.76	0.78	0.97	1	0.97	0.88	0.88	0.88
Frozen_DLCL3	0.85	0.89	0.89	0.73	0.77	0.78	0.97	0.97	1	0.9	0.88	0.89
Frozen_FTC1	0.8	0.83	0.84	0.83	0.86	0.87	0.89	0.88	0.9	1	0.96	0.97
Frozen_FTC2	0.8	0.83	0.83	0.84	0.86	0.87	0.88	0.88	0.88	0.96	1	0.96
Frozen_FTC3	0.8	0.82	0.82	0.83	0.85	0.86	0.88	0.88	0.89	0.97	0.96	1

Table 3 Correlation matrix showing the global correlation coefficients of all HGU133 Plus 2.0-GeneChip® replicates over all normalized measured genes

	Frozen_DLCL1	Frozen_DLCL2	Frozen_DLCL3	Frozen_FTC1	Frozen_FTC2	Frozen_FTC3
Frozen_DLCL1	1	0.97	0.97	0.86	0.87	0.87
Frozen_DLCL2	0.97	1	0.97	0.85	0.86	0.87
Frozen_DLCL3	0.97	0.97	1	0.86	0.87	0.88
Frozen_FTC1	0.86	0.85	0.86	1	0.96	0.96
Frozen_FTC2	0.87	0.86	0.87	0.96	1	0.97
Frozen_FTC3	0.87	0.87	0.88	0.96	0.97	1

and FFPE, respectively, against 17.61/20.59 in average for frozen and FFPE, respectively, within the whole 419 genes list) and, thus, a relatively low variance across all arrays.

In microarray experiments, fold changes can vary a lot, especially if compared to, for example, q-RT-PCR results or cDNA-array data [27, 29]. Taking this into account, there were 122 of the 381 genes of the FFPE fivefold change list, which were not within the frozen–fivefold change list but were also significant differentially expressed in frozen material at least twofold or more. Additionally, vice versa, there were 122 of the 266 genes of the frozen–fivefold change list, which were not within the FFPE fivefold change list but were also significant differentially expressed in FFPE material at least twofold or more (Fig. 7c). This resulted in then 58.8/67.2% of the genes of the two fivefold change lists to be commonly detected as significantly "regulated" (at least twofold) for FFPE and frozen material, respectively. This is a percentage of codetection, which is in the range similar to other comparisons of different platforms for gene expression analysis using frozen materials only [6]. By choosing two tumor entities like FTC and DLCL, a large number of differentially expressed genes could be expected, with specific known markers for each entity or cell type. Some of the markers known could indeed be found among the highest fold-change values in the generated lists, for example, thyroglobulin (330-/514-fold "up-regulated" in FFPE/frozen FTC), thyroid peroxidase (228-/243-fold "up-regulated" in FFPE/frozen FTC), or thyroid transcription factor 1 (also known as TTF1; 66-/83-fold "up-regulated" in FFPE/frozen FTC) on one side and BCL2-related protein A1 (64-/75-fold "up-regulated" in FFPE-/frozen-DLCL); POU domain, class 2, associating factor 1 (also known as BOB1; 55-/69-fold "up-regulated" in FFPE-/frozen-DLCL); or CD22 antigen (CD22; 52-/30-fold "up-regulated" in FFPE-/frozen-DLCL). Other known markers and the associated gene expression values are listed in Table 4.

The "falsely" classifying genes list with a fold change of at least threefold for the FFPE material data containing the genes, which seemed to differentiate FFPE from frozen tissue, consisted of 49 probe sets resembling 38 annotated genes, while the similar list for the frozen material data consisted of only eight probe sets resembling eight annotated genes. In addition, a fold change of at least five "falsely" classifying genes for the FFPE material data and none for the frozen material data remained.

Discussion

FFPE-RNA Quality

Because the quality of the RNA is crucial, even for a microarray approach that takes into account some extent of degradation, the quality test is an important step for choosing suitable samples. Here, eight of the ten tested FFPE-RNA samples were approximately 1 year old or younger, and only three of these had a beta-actin PCR-ratio above 10, but both of the older samples tested did so. Thus, it seems that the quality of the FFPE RNA correlates with the sample storage time. Additionally, because all of the tested thyroid samples were approximately 1 year old or younger, the fact that four of them but only one of the lymphoma samples yielded a ratio less than 10 might also be attributed to age more likely than kind of tissue or other factors like those mentioned below. Yet, more samples need to be analyzed to strengthen this assumption and we did not test other kinds of tissues so far. However, there are also data showing satisfying results with samples older than 10 years (http://www.arctur.com/research_portal/images/pdf/aacrposter_gene_expression_lding.pdf). On the other hand, a degradation state increasing over time was also reported [4, 16].

The cutoff of the beta-actin PCR-ratio of 10 was somewhat arbitrarily chosen and remains to be further evaluated. The used samples had a ratio relatively close to 10 and still gave satisfying results on the GeneChips®.

Of this limited data set, about 50% of the tested samples appeared to be suitable for large-scale gene expression studies using oligonucleotide microarrays. It might also be expedient to use samples with similar beta-actin PCR ratios for a given experiment, which would reduce the usable fraction of a given stock of FFPE samples furthermore.

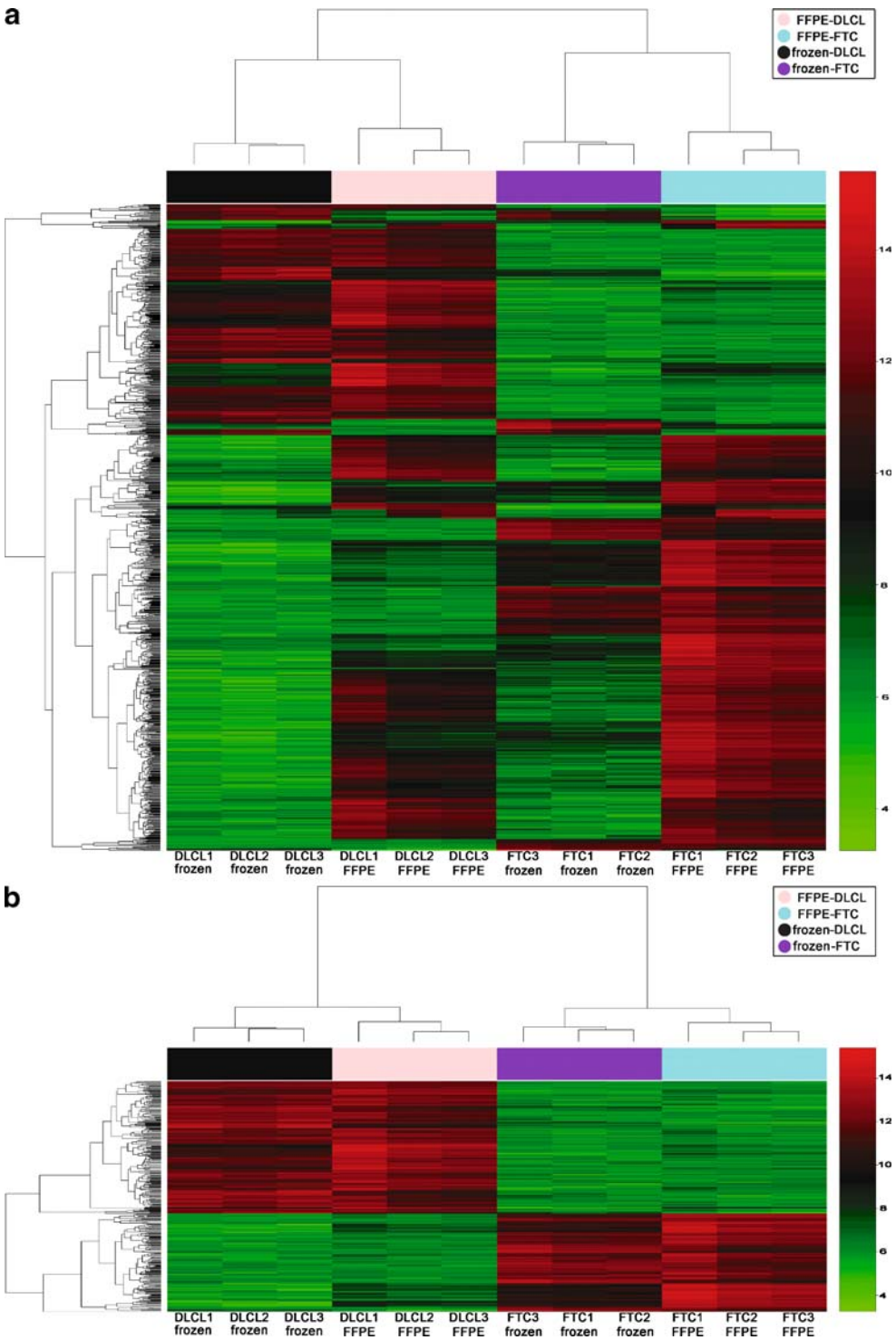

Fig. 6 Heat maps of hierarchical clustering. Replicates are displayed on the *vertical axis*, genes on the *horizontal axis*. Log2-transformed signal intensities are depicted in color code (*bar* at the right). Relationships are resembled by the *tree lines* at the top of the heat maps (*short line*, close relation; *long line*, distant relation). **a** Unsupervised hierarchical clustering of the 1,000 genes with the highest variance of the signal intensities across all 12 Human X3P GeneChips®. **b** Supervised hierarchical clustering of the remaining 357 of the 1,000 genes with the highest variance of the signal intensity across all 12 Human X3P GeneChips® after filtering of all genes, which could not be found in both fivefold change lists

The condition of the FFPE RNA might be influenced by factors like differences in age, possible discrepancies in specimen size, time before fixation, different procedures and reagents for fixation and paraffin embedding, or origin of the sample [1, 14]. Whether or not the influence of all these factors can be estimated adequately by the applied RNA quality tests also remains a topic for further investigations.

Technical performance and reproducibility of the oligonucleotide microarray data

In comparison to typical detection rates and signal intensities derived from one-round amplified "standard" protocol cRNA, the values achieved with the used two-round protocols were slightly lower, which results in at least some loss of sensitivity (expressed, for example, in

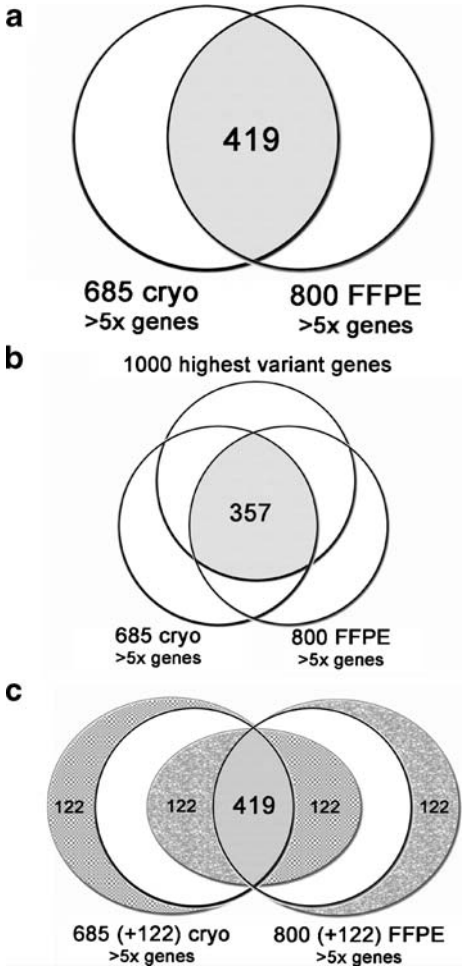

Fig. 7 Venn diagrams of the frozen and FFPE-gene lists of the differentially expressed genes. **a** Common genes within the two lists of the more than fivefold regulated genes in frozen and FFPE material, respectively, with two sample *t* test *p* value and FDR <0.01. **b** Common genes within the two lists of the more than fivefold regulated genes and the 1,000 highest variant genes across all arrays. **c** Common genes within the two lists of the more than fivefold regulated genes and the added less than fivefold, but more than twofold, regulated genes with two sample *t* test *p* value and FDR <0.01 in one and more than fivefold regulated genes in the other list, respectively

less percent present calls) [10], but as can be derived from parameters for reproducibility like the correlation of the replicates, an at least acceptable specificity can be maintained for both materials.

The lower detection rates and average signal intensities of the frozen material arrays in this experiment, even on the X3P-GeneChips®, might be attributed to the slightly different protocol for RNA-isolation and amplification used. Both were in a range experienced with other samples processed with the same protocol (unpublished data). As well, the lower detection rates and loss of differentially expressed genes of the frozen material arrays on the HGU133 Plus 2.0 chips compared to the X3P chips might be attributed to shorter cRNA fragments and, thus, also a higher "fragmentation state" due to the two-round amplification. The RiboAmp Kit was used for the frozen material because of its similarity to the Paradise Kit.

Comparison of gene-expression changes

Gene expression studies using FFPE material and qRT-PCR approaches have been conducted successfully by many authors [3, 13, 24, 26, 28], and thus, the general possibility to investigate the mRNA expression of this material has already been proved. As can be derived from the unsupervised clustering results and the comparisons of gene expression "changes" of this experiment, there is a great extent of concordance between the two materials suggesting the feasibility of also large-scale gene expression profiling of FFPE material. However, a number of genes remained in the unsupervised clustering heat map, which seemed to separate FFPE from frozen material rather than the biologically different samples. If not reduced by proper analysis and filtering strategies, this would affect the expressiveness of data from FFPE material and introduce a further bias. This emphasizes the importance to evaluate possible targets of interest with an independent method. The disadvantages of a bigger effort, higher technical variance, and loss of detectable genes as compared to standard protocol microarray experiments, on the other hand, allow for large-scale gene expression investigation of samples from a many-times-larger pool, which otherwise could not be analyzed in that extent at all.

The "falsely" classifying genes list of the FFPE material data was with 38 genes larger than the corresponding list for

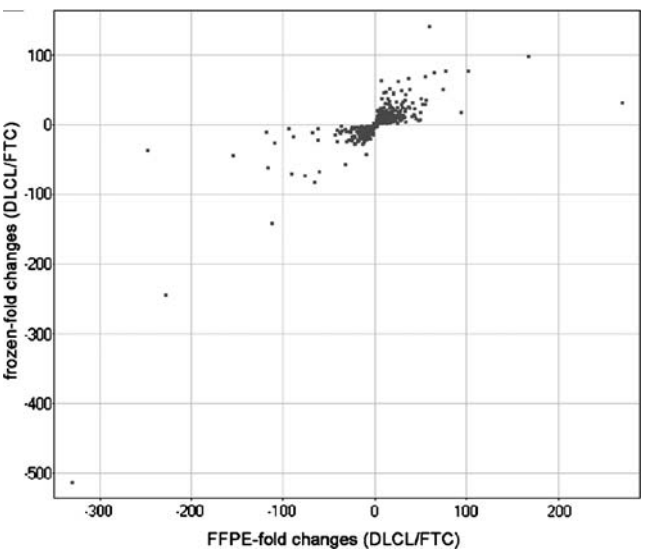

Fig. 8 Scatter plot of the fold change values of the 419 fivefold or more differentially expressed genes. Fold change values of the frozen samples are shown on the *vertical axis* and fold change values of the FFPE samples on the *horizontal axis*

Table 4 Fold change values of known lymphoma/B-cell and FTC/thyroid markers

Marker for	Probe set ID (Affymetrix annotation)	Gene title (Affymetrix annotation)	Gene symbol	Fold change I[a] FFPE	*t* test *p* value FFPE	Fold change I[a] frozen	*t* test *p* value frozen
DLCL/ B cells	Hs.170121.1. A3_3p_at	Protein tyrosine phosphatase, receptor type, C	PTPRC	12.7	0.002386594	4.4	3.19832E-05
	g10835052_3p_s_at	CD19 antigen	CD19	3.5	0.000658192	1.9	0.004354094
	g12803920_3p_a_at	Membrane-spanning 4-domains, subfamily A, member 1	MS4A1	3.0	0.000546848	6.2	0.000421706
	g4502650_3p_at	CD22 antigen	CD22	52.0	6.31095E-06	30.0	8.20712E-05
	g4502684_3p_a_at	CD79A antigen (immunoglobulin-associated alpha)	CD79A	12.8	0.000269145	11.8	0.000803207
	g4507588_3p_at	Tumor necrosis factor receptor superfamily, member 8	TNFRSF8	2.0	0.01860349	3.4	0.002568064
	g4502382_3p_at	B-cell CLL/lymphoma 6 (zinc finger protein 51)	BCL6	6.5	0.000758716	3.0	3.27055E-05
FTC/ thyroid	g6631113_3p_at	Thyroglobulin	TG	−329.5	3.06173E-06	−513.5	1.89341E-06
	Hs.296746.0. S1_3p_at	Thyroglobulin	TG	−108.9	2.32849E-06	−26.2	5.79053E-06
	g13623242_3p_s_at	Thyroid transcription factor 1	TITF1	−65.6	4.53104E-05	−83.3	1.22643E-06
	g2627170_3p_s_at	Thyroid transcription factor 1	TITF1	−1.1	0.592529204	−1.2	0.023979725
	g12803726_3p_at	Keratin 7	KRT7	−18.3	1.31398E-05	−22.3	2.60552E-05
	g4504916_3p_at	Keratin 19	KRT19	−1.4	0.024761082	−6.2	1.26314E-05
	g340184_3p_a_at	Cadherin 1, type 1, E-cadherin (epithelial)	CDH1	−1.1	0.072001421	1.1	0.302747846
	g4757959_3p_a_at	Cadherin 1, type 1, E-cadherin (epithelial)	CDH1	−10.4	6.18622E-05	−20.5	5.48167E-05
	g11493474_RC_3p_at	Catenin (cadherin-associated protein), beta 1, 88kDa	CTNNB1	1.1	0.403716061	−1.2	0.025434288
	g4503130_3p_at	Catenin (cadherin-associated protein), beta 1, 88kDa	CTNNB1	−1.8	0.002757311	−3.2	5.60018E-06
	208712_3p_at	Cyclin D1 (PRAD1: parathyroid adenomatosis 1)	CCND1	−4.3	0.000469035	−3.8	0.000399604
	g179364_3p_at	Cyclin D1 (PRAD1: parathyroid adenomatosis 1)	CCND1	−3.0	0.00433312	−1.9	0.004705116
	g12805034_3p_at	Cyclin-dependent kinase inhibitor 1B (p27, Kip1)	CDKN1B	−1.5	0.127097947	−1.9	0.037430005

TG thyroglobulin, *TITF1* thyroid transcription factor 1

[a] Positive values = higher expression in DLCL, negative values = higher expression in FTC, with corresponding two sample *t* test *p* values

the frozen material data with only eight genes, indicating a slightly higher bias for the FFPE data. Nevertheless, both lists consisted of only a few "outlier" genes in relation to the other data lists. In addition, with a fold change of at least five, as chosen for most of the other lists, only eight "falsely" classifying genes for the FFPE material data and none for the frozen material data remained.

Because not one of the more than fivefold regulated genes is classified as up-regulated within one and down-regulated within the other material list, the specificity of the method appears to be high (Fig. 8), although there is some variance in the fold change values themselves. This is a phenomenon that also occurs when different gene expression measurement approaches are used [6, 20, 27].

As a result, it is, similar to data of different gene expression platforms, not possible to compare the chip data of global gene expression measurements using oligonucleotide microarrays of FFPE samples and frozen samples within one experiment directly. However, derived from the results shown, it appears to be feasible to apply the same strategies of large-scale gene expression analysis as for frozen material samples, like screening for interesting marker genes or generating gene expression signatures for specific entities, also to FFPE material

samples (http://www.arctur.com/research_portal/products/paradise_addl_info.htm) [12, 23].

Acknowledgements This work was supported by the Deutsche Krebshilfe (70-3173-Tr3) and Affymetrix, who provided their GeneChips, and by Dr. Wieland Keilholz. The authors thank Ralf Lieberz for technical assistance, Dr. Birgit Anderegg (formerly of Arcturus) for support on the Paradise Reaction System, and Dr. Klaus Willenbrock for critical reading of the manuscript. The experiments were conducted and the tissues were used and processed in accordance with national ethical principles and comply with the current laws in Germany.

References

1. Abrahamsen HN, Steiniche T, Nexo E, Hamilton-Dutoit SJ, Sorensen BS (2003) Towards quantitative mRNA analysis in paraffin-embedded tissues using real-time reverse transcriptase-polymerase chain reaction: a methodological study on lymph nodes from melanoma patients. J Mol Diagn 5:34–41
2. Alizadeh AA, Eisen MB, Davis RE, Ma C, Lossos IS, Rosenwald A, Boldrick JC, Sabet H, Tran T, Yu X, Powell JI, Yang L, Marti GE, Moore T, Hudson J Jr, Lu L, Lewis DB, Tibshirani R, Sherlock G, Chan WC, Greiner TC, Weisenburger DD, Armitage JO, Warnke R, Levy R, Wilson W, Grever MR, Byrd JC, Botstein D, Brown PO, Staudt LM (2000) Distinct types of diffuse large B-cell lymphoma identified by gene expression profiling. Nature 403:503–511
3. Antonov J, Goldstein DR, Oberli A, Baltzer A, Pirotta M, Fleischmann A, Altermatt HJ, Jaggi R (2005) Reliable gene expression measurements from degraded RNA by quantitative real-time PCR depend on short amplicons and a proper normalization. Lab Invest 85:1040–1050
4. Cronin M, Pho M, Dutta D, Stephans JC, Shak S, Kiefer MC, Esteban JM, Baker JB (2004) Measurement of gene expression in archival paraffin-embedded tissues: development and performance of a 92-gene reverse transcriptase-polymerase chain reaction assay. Am J Pathol 164:35–42
5. Godfrey TE, Kim SH, Chavira M, Ruff DW, Warren RS, Gray JW, Jensen RH (2000) Quantitative mRNA expression analysis from formalin-fixed, paraffin-embedded tissues using 5′ nuclease quantitative reverse transcription-polymerase chain reaction. J Mol Diagn 2:84–91
6. Hardiman G (2004) Microarray platforms—comparisons and contrasts. Pharmacogenomics 5:487–502
7. Hochberg Y, Benjamini Y (1990) More powerful procedures for multiple significance testing. Stat Med 9:811–818
8. Huber W, von Heydebreck A, Sultmann H, Poustka A, Vingron M (2002) Variance stabilization applied to microarray data calibration and to the quantification of differential expression. Bioinformatics 18(Suppl 1):96–104
9. Irizarry RA, Hobbs B, Collin F, Beazer-Barclay YD, Antonellis KJ, Scherf U, Speed TP (2003) Exploration, normalization, and summaries of high density oligonucleotide array probe level data. Biostatistics 4:249–264
10. Kenzelmann M, Klaren R, Hergenhahn M, Bonrouhi M, Grone HJ, Schmid W, Schutz G (2004) High-accuracy amplification of nanogram total RNA amounts for gene profiling. Genomics 83:550–558
11. Kuppers R, Klein U, Schwering I, Distler V, Brauninger A, Cattoretti G, Tu Y, Stolovitzky GA, Califano A, Hansmann ML, Dalla-Favera R (2003) Identification of Hodgkin and Reed–Sternberg cell-specific genes by gene expression profiling. J Clin Invest 111:529–537
12. Ma XJ, Patel R, Wang X, Salunga R, Murage J, Desai R, Tuggle JT, Wang W, Chu S, Stecker K, Raja R, Robin H, Moore M, Baunoch D, Sgroi D, Erlander M (2006) Molecular classification of human cancers using a 92-gene real-time quantitative polymerase chain reaction assay. Arch Pathol Lab Med 130:465–473
13. Ma XJ, Wang Z, Ryan PD, Isakoff SJ, Barmettler A, Fuller A, Muir B, Mohapatra G, Salunga R, Tuggle JT, Tran Y, Tran D, Tassin A, Amon P, Wang W, Wang W, Enright E, Stecker K, Estepa-Sabal E, Smith B, Younger J, Balis U, Michaelson J, Bhan A, Habin K, Baer TM, Brugge J, Haber DA, Erlander MG, Sgroi DC (2004) A two-gene expression ratio predicts clinical outcome in breast cancer patients treated with tamoxifen. Cancer Cell 5:607–616
14. Masuda N, Ohnishi T, Kawamoto S, Monden M, Okubo K (1999) Analysis of chemical modification of RNA from formalin-fixed samples and optimization of molecular biology applications for such samples. Nucleic Acids Res 27:4436–4443
15. Monti S, Savage KJ, Kutok JL, Feuerhake F, Kurtin P, Mihm M, Wu B, Pasqualucci L, Neuberg D, Aguiar RC, Dal Cin P, Ladd C, Pinkus GS, Salles G, Harris NL, Dalla-Favera R, Habermann TM, Aster JC, Golub TR, Shipp MA (2005) Molecular profiling of diffuse large B-cell lymphoma identifies robust subtypes including one characterized by host inflammatory response. Blood 105:1851–1861
16. Paik S, Kim CY, Song YK, Kim WS (2005) Technology insight: application of molecular techniques to formalin-fixed paraffin-embedded tissues from breast cancer. Nat Clin Pract Oncol 2:246–254
17. Reichmuth C, Markus MA, Hillemanns M, Atkinson MJ, Unni KK, Saretzki G, Hofler H (1996) The diagnostic potential of the chromosome translocation t(2;13) in rhabdomyosarcoma: a PCR study of fresh-frozen and paraffin-embedded tumour samples. J Pathol 180:50–57
18. Robison JE, Perreard L, Bernard PS (2004) State of the science: molecular classifications of breast cancer for clinical diagnostics. Clin Biochem 37:572–578
19. Rosenwald A, Wright G, Chan WC, Connors JM, Campo E, Fisher RI, Gascoyne RD, Muller-Hermelink HK, Smeland EB, Giltnane JM, Hurt EM, Zhao H, Averett L, Yang L, Wilson WH, Jaffe ES, Simon R, Klausner RD, Powell J, Duffey PL, Longo DL, Greiner TC, Weisenburger DD, Sanger WG, Dave BJ, Lynch JC, Vose J, Armitage JO, Montserrat E, Lopez-Guillermo A, Grogan TM, Miller TP, LeBlanc M, Ott G, Kvaloy S, Delabie J, Holte H, Krajci P, Stokke T, Staudt LM (2002) The use of molecular profiling to predict survival after chemotherapy for diffuse large-B-cell lymphoma. N Engl J Med 346:1937–1947
20. Schlingemann J, Habtemichael N, Ittrich C, Toedt G, Kramer H, Hambek M, Knecht R, Lichter P, Stauber R, Hahn M (2005) Patient-based cross-platform comparison of oligonucleotide microarray expression profiles. Lab Invest 85:1024–1039
21. Schroeder A, Mueller O, Stocker S, Salowsky R, Leiber M, Gassmann M, Lightfoot S, Menzel W, Granzow M, Ragg T (2006) The RIN: an RNA integrity number for assigning integrity values to RNA measurements. BMC Mol Biol 7:3
22. Schwering I, Brauninger A, Distler V, Jesdinsky J, Diehl V, Hansmann ML, Rajewsky K, Kuppers R (2003) Profiling of Hodgkin's lymphoma cell line L1236 and germinal center B cells: identification of Hodgkin's lymphoma-specific genes. Mol Med 9:85–95
23. Scicchitano MS, Dalmas DA, Bertiaux MA, Anderson SM, Turner LR, Thomas RA, Mirable R, Boyce RW (2006) Preliminary comparison of quantity, quality, and microarray performance of RNA extracted from formalin-fixed paraffin-embedded and unfixed frozen tissue samples. J Histochem Cytochem 54 (11):1229–1237

24. Sheils OM, Sweeney EC (1999) TSH receptor status of thyroid neoplasms—TaqMan RT-PCR analysis of archival material. J Pathol 188:87–92
25. Shipp MA, Ross KN, Tamayo P, Weng AP, Kutok JL, Aguiar RC, Gaasenbeek M, Angelo M, Reich M, Pinkus GS, Ray TS, Koval MA, Last KW, Norton A, Lister TA, Mesirov J, Neuberg DS, Lander ES, Aster JC, Golub TR (2002) Diffuse large B-cell lymphoma outcome prediction by gene-expression profiling and supervised machine learning. Nat Med 8:68–74
26. Specht K, Richter T, Muller U, Walch A, Werner M, Hofler H (2001) Quantitative gene expression analysis in microdissected archival formalin-fixed and paraffin-embedded tumor tissue. Am J Pathol 158:419–429
27. Tan PK, Downey TJ, Spitznagel EL Jr, Xu P, Fu D, Dimitrov DS, Lempicki RA, Raaka BM, Cam MC (2003) Evaluation of gene expression measurements from commercial microarray platforms. Nucleic Acids Res 31:5676–5684
28. Tothill RW, Kowalczyk A, Rischin D, Bousioutas A, Haviv I, van Laar RK, Waring PM, Zalcberg J, Ward R, Biankin AV, Sutherland RL, Henshall SM, Fong K, Pollack JR, Bowtell DD, Holloway AJ (2005) An expression-based site of origin diagnostic method designed for clinical application to cancer of unknown origin. Cancer Res 65:4031–4040
29. Yuen T, Wurmbach E, Pfeffer RL, Ebersole BJ, Sealfon SC (2002) Accuracy and calibration of commercial oligonucleotide and custom cDNA microarrays. Nucleic Acids Res 30:e48

Virchows Arch (2007) 450:713–717
DOI 10.1007/s00428-007-0415-6

CASE REPORT

Pathology of the large intestine in patients with vascular type Ehlers-Danlos syndrome

Hendrik Bläker · Benjamin Funke · Ingrid Hausser · Thilo Hackert · Peter Schirmacher · Frank Autschbach

Received: 14 January 2007 / Revised: 30 March 2007 / Accepted: 2 April 2007 / Published online: 9 May 2007
© Springer-Verlag 2007

Abstract The vascular type of Ehlers-Danlos syndrome (type IV) is an infrequent disease caused by heterozygous germline mutations in the procollagen 3A gene (COL3A1). Clinical signs include characteristic facial features, easy bruising, and a translucent skin. These signs are less obvious than the hyperflexibility of skin and joints seen in other types of Ehlers-Danlos syndrome. Therefore, diagnosis of Ehlers-Danlos syndrome type IV is usually not considered until complications have occurred. Complications include spontaneous ruptures of vessels and hollow organs, particularly the colon. We, herein, report pathologic findings in colon specimens from related Ehlers-Danlos syndrome type IV patients. Thorough examination revealed abnormalities of the large bowel architecture including abrupt changes in the caliber of the lamina muscularis, secondary diverticula formation, and strongly reduced expression of abnormal collagen 3. These findings are not seen in other diseases of the colon and should prompt the pathologist to include Ehlers-Danlos syndrome type IV in the differential diagnosis of spontaneous bowel perforation in younger patients.

H. Bläker (✉) · B. Funke · P. Schirmacher · F. Autschbach
Institute of Pathology, University of Heidelberg,
INF 220,
69120 Heidelberg, Germany
e-mail: hendrik_blaeker@med.uni-heidelberg.de

I. Hausser
Department of Dermatology, University of Heidelberg,
Voß Str. 11,
69115 Heidelberg, Germany

T. Hackert
Department of Surgery, University of Heidelberg,
INF 110,
69120 Heidelberg, Germany

Keywords Ehlers-Danlos syndrome type IV · Vascular type · COL3A1 · Large bowel perforation

Introduction

Ehlers-Danlos syndrome comprises a group of hereditary connective tissue disorders with different genetic backgrounds and heterogenous clinical features. The Villefranche classification distinguishes six types of Ehlers-Danlos syndrome [2, 15]. Common to all of these types is an underlying defect in either collagen production or processing. The vascular type of Ehlers-Danlos syndrome (type IV) is caused by heterozygous germline mutations in the type 3 procollagen gene (COL3A1) [19, 22, 23]. Patients with Ehlers-Danlos syndrome type IV clinically present with translucent skin and transparent veins; they show easy bruising and have characteristic facial features [18]. These signs are overall less apparent than the hyperflexibility of skin and joints seen in other types of Ehlers-Danlos syndrome. Therefore, diagnosis of Ehlers-Danlos syndrome type IV is usually not considered until complications have occurred. Most relevant complications are ruptures of arteries and perforations of hollow organs [8, 17, 18]. These complications relate to a reduced strength of the vascular and hollow organ soft tissue. Diagnosis of Ehlers-Danlos syndrome type IV is confirmed by fibroblast culture demonstrating reduced levels of collagen 3A [21] or by identifying germline missense or nonsense mutations in the COL3A1 gene.

Ehlers-Danlos syndrome type IV is rare; its true population frequency is unknown. Spontaneous bowel perforation may be the first presentation of the disease. It may be clinically and pathologically misinterpreted as diverticular perforation, as diverticula occur secondary to

the reduced resistance of the submucosal soft tissue [3, 21]. Only few reports on structural abnormalities in perforated colons of Ehlers-Danlos syndrome type IV are available [3, 5]. In this study, we present histopathological, immunohistochemical, and ultrastructural findings of resected colon specimens from related patients with Ehlers-Danlos syndrome type IV. We found primary and secondary architectural abnormalities usually not seen in other diseases of the colon. These pathologic findings should prompt the pathologist to consider Ehlers-Danlos syndrome type IV in cases of spontaneous bowel perforation in younger patients.

Fig. 1 Macroscopic appearance of the resected colon. The lamina muscularis propria shows abrupt changes in thickness; in some areas it is almost missing (*large arrows*). Secondary diverticle formation into the lamina muscularis propria is seen (*small arrows*)

Clinical histories

Patient 1 A 42-year-old female patient was referred to a local hospital with abdominal pain. A perforation of the sigmoid colon was identified, and the sigma was removed. Postoperatively, the patient again developed an acute abdomen, and she was referred to our university hospital. Relaparotomy was performed, and an insufficiency of anastomosis was seen. During surgery, the patient developed diffuse bleeding in the capsule of the liver and died a few days later from multiorgan failure. Her personal history was remarkable for a pneumothorax.

The patient's sister died at age 35 from aneurysma bleeding. A cavernous sinus fistula had raised suspicion of Ehlers-Danlos syndrome type IV, and DNA analysis revealed a missense mutation in exon 8 of the COL3A1 (G721A). The same mutation was identified in the 42-year-old patient presented in this study. The mutation is located in the α-helix of procollagen 3a; mutations in this area are frequently found in patients with Ehlers-Danlos syndrome type IV [11, 18, 24].

Patient 2 One month after his mother (patient 1) died, her 21-year-old son presented with acute abdomen. He was diagnosed with spontaneous perforation of the sigmoid colon. The sigma was removed, given the diagnosis of Ehlers-Danlos syndrome type IV; a total colectomy was performed 2 weeks later. The postoperative course was uneventful, and the patient is alive. His personal history is remarkable for a pneumothorax.

Materials and methods

Tissue specimen

Formalin-fixed colon specimens from the 42-year-old female patient and her 21-year-old son were investigated.

Immunohistochemistry

Immunohistochemistry was performed using a monoclonal antibody against human collagen 3 (MU167-UC, Biogenex, CA, USA) at a dilution of 1:100 and an antibody against smooth muscle actin (undiluted; HHF 35, Enzo Life Sciences, NY, USA). Slides were pretreated by microwave boiling in 6-mM citrate buffer. Antibody

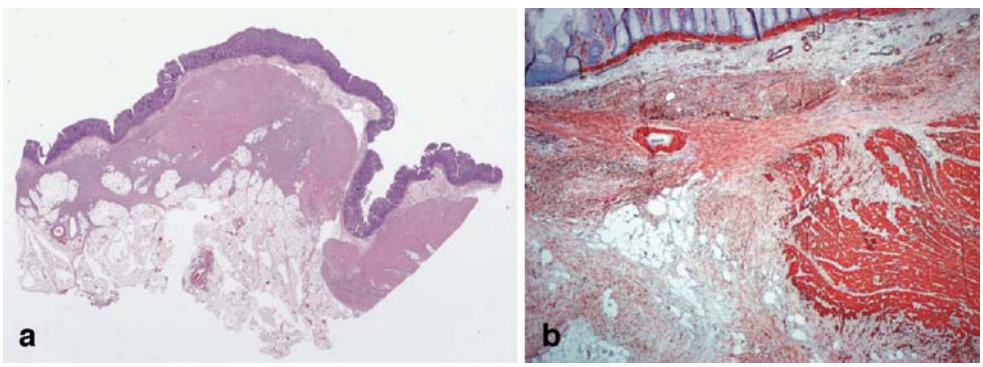

Fig. 2 The architecture of the bowel wall is strongly altered with areas showing a complete lack of the lamina muscularis propria (**a** whole mount view; **b** immunohistochemistry for smooth muscle actin)

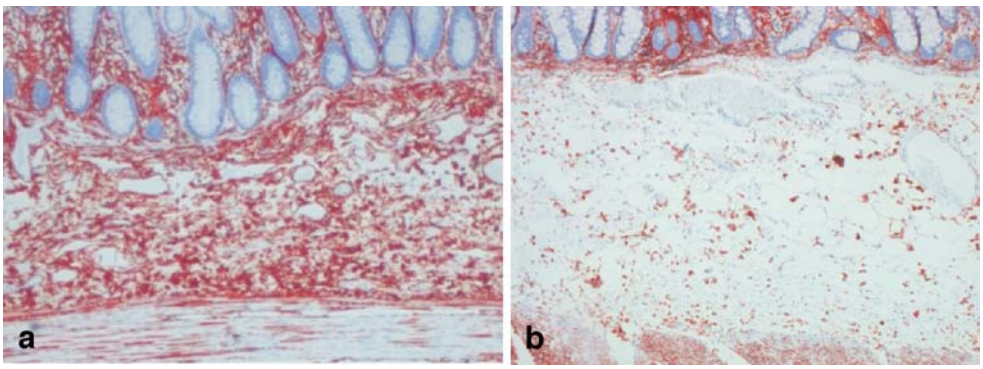

Fig. 3 Immunohistochemistry for collagen 3. In comparison to a control (**a**), strongly reduced expression of collagen 3, particularly in the submucosa, can be seen in Ehlers-Danlos syndrome type IV (**b**)

incubation was performed for 25 min at room temperature. For visualization, the streptavidin-biotin-peroxidase system (Dako, Hamburg, Germany) with 3-amino, 9 ethyl-carbazole as chromogen was applied in an automated staining system (Techmate Horizon, Dako, Hamburg, Germany). To evaluate the significance of collagen 3 staining pattern in the colonic tissue of the presented cases, control tissues from patients without Ehlers-Danlos syndrome and sigmoid resection for diverticulosis or carcinoma were investigated.

Electron microscopy

Paraffin-embedded tissue was deparaffinized, fixed in 3% glutaraldehyde, dehydrated with ethanol, and epon-embedded. Semi-thin sections were stained with 1% toluidin blue and examined using light microscopy to find appropriate areas (submucosa/lamina muscularis propria) for ultramicrotomy. Ultra-thin sections were contrasted with lead and uranyl actetate and examined under an electron microscope (Zeiss 902, Carl Zeiss, Jena, Germany).

Results

Pathology

Resected colon specimens from the mother (patient 1) and her son (patient 2) showed almost identical abnormalities. Macroscopic inspection revealed abrupt changes in the thickness of the lamina muscularis propria (Fig. 1). In some areas, the lamina muscularis propria was extremely thin, in others almost missing. In these areas, diverticula protruded into the pericolonic fat (Fig. 1, arrows). In both specimens, a perforation was seen occurring at segments in which the muscularis propria was replaced by dense gray-whitish tissue suggestive of local scarring. Tissue preparation for histologic examination was made difficult by an extreme fragility of the colonic wall. Tearing of mucosal and submucosal layers was observed after minimal manual manipulation.

Results of a histological analysis confirmed abrupt changes in the caliber of the lamina muscularis propria (Fig. 2a). Defects with missing muscular layer were replaced by abundant fibroblasts surrounding islets of fat (Fig. 2b). The submucosa was flattened, and focally dense fibrous tissue was seen. Compared to control tissues from patients without Ehlers-Danlos syndrome which showed intense staining for collagen 3 in the submucosa and the lamina muscularis propria (Fig. 3a), a decrease in collagen 3 staining was noted in the patients with Ehlers-Danlos syndrome IV (Fig. 3b). The extent was variable in different sections. While in the most normal appearing areas a decrease in collagen 3 was mainly found in the submucosa, some areas showed almost a complete lack of reactivity throughout all layers of the colonic wall (Fig. 3b). The finding was more intense in the colon of the son than in that of his mother.

Electron microscopy showed distorted and regular collagen fibrils in a ratio of approximately 2:1 (Fig. 4).

Discussion

Collagen is the main extracellular component of the human body comprising approximately 30% of total body protein. Collagen 3 is the dominant collagen component of vessels

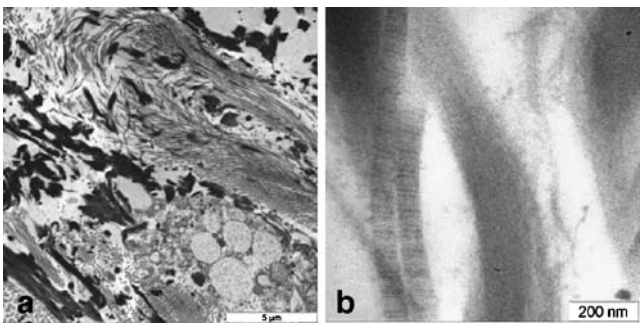

Fig. 4 Electron microscopy of the submucosal soft tissue showing distorted collagen fibrils in a ratio to normal fibrils of approximately 2:1

and hollow organs [13]. As seen by immunohistochemistry, it is highly present in the inner layers of the abdominal wall. Pro α1 (III) chains associate to form trimeric procollagen. If wild-type and mutated COL3A1 are equally transcribed and translated, only one of eight procollagen molecules are normal. This dominant negative effect of a COL3A1 mutation explains the autosomal dominant inheritance of Ehlers-Danlos syndrome type IV. Given the main presence of collagen 3 in vessels and hollow organ soft tissue, it is plausible that defects in collagen 3 production result in vascular and hollow organ complications. Vessel ruptures are the most commonly reported complications in Ehlers-Danlos syndrome type IV [1, 4, 6, 7, 10, 18]. They are often lethal, as the aorta or other large arteries are affected by the rupture. Over the past decade, our autopsy files include three young patients diagnosed postmortem with Ehlers-Danlos syndrome type IV. All of them died from arterial ruptures.

Ruptures of large vessels in young patients normally prompt the pathologist and the clinician to consider a soft tissue disorder, including Ehlers-Danlos, Marfan, and the recently described Loeys-Dietz syndrome [16]. The complication of spontaneous hollow organ perforation in Ehlers-Danlos syndrome type IV is less well known. Being unaware of family history and genetics and confronted with the pathology of the herein presented colon specimen, we considered an inborn structural disorder. Diagnosis of desmosis coli, a disease associated with idiopathic megacolon on the background of a tendinous fiber net disturbance [9, 12] and of secondary structural abnormalities as seen in autoimmune disease, was dismissed in view of the definite primary structural alterations. The abrupt changes in thickness of the lamina propria and the absence of apparent vascular abnormalities lead us to consider a visceral myopathy. Yet, colonic perforation is unusual in this condition, and by evaluation of the family history, which included vascular complications and a COL3A1 mutation, diagnosis of Ehlers-Danlos syndrome was achieved.

Collagen 3 is a main component of fetal soft tissue [20]. During fetal maturation, it is replaced by other collagens, mainly by collagen 1. If collagen 3 plays a role in primary structural building of fetal organs, a defect in collagen 3 production may have a consequence on the architecture not only of structures that contain collagen 3 in adulthood. Interestingly, organ malformations have been described more frequently than expected in Ehlers-Danlos syndrome type IV [14, 18]. The primary structural abnormalities in the colons of the herein presented patients fulfill the criterion of a subtle organ malformation.

In contrast to other types of Ehlers-Danlos syndrome, the vascular type is associated with reduced life expectancy [10, 18]. The complications are frequently life threatening. Colonic perforation may be managed surgically by resection, but the follow-up is usually complicated by repeated insufficiency of anastomosis. Complete colonic resection has therefore been recommended [8].

The benefit of diagnosing Ehlers-Danlos syndrome type IV in patients that already encountered complications is disputable. There is no specific therapy that has been shown to delay or prevent further complications. However, knowledge of the disease can influence surgical procedures and reproductive counseling. Relatives can be tested genetically and plan their life depending on whether they are affected or not.

Spontaneous colonic perforation in young patients should prompt the pathologists and the clinician to consider Ehlers-Danlos syndrome type IV. Thorough macroscopic and histologic examination of resected colon specimens as well as information of family background is needed to diagnose this disease.

References

1. Anderson DW, Thakker-Varia S, Tromp G, Kuivaniemi H, Stolle CA (1997) A glycine (415)-to-serine substitution results in impaired secretion and decreased thermal stability of type III procollagen in a patient with Ehlers-Danlos syndrome type IV. Hum Mutat 9:62–63
2. Beighton P, De Paepe A, Steinmann B, Tsipouras P, Wenstrup RJ (1998) Ehlers-Danlos syndromes: revised nosology, Villefranche, 1997. Am J Med Genet 77:31–37
3. Collins MH, Schwarze U, Carpentieri DF, Kaplan P, Nathanson K, Meyer JS, Byers PH (1999) Multiple vascular and bowel ruptures in an adolescent male with sporadic Ehlers-Danlos syndrome type IV. Pediatr Dev Pathol 2:86–93
4. Cikrit DF, Glover JR, Dalsing MC, Silver D (2002) The Ehlers-Danlos specter revisited. Vasc Endovascular Surg 36:213–217
5. Demirogullari B, Karabulut R, Demirtola A, Karabulut B, Gol IH, Aybay C, Symoens S, Sonmez K, Basaklar AC, Kale N (2006) A novel mutation in the vascular Ehlers-Danlos syndrome: a case presenting with colonic perforations. J Pediatr Surg 41:27–30
6. De Paepe A, Malfait F (2004) Bleeding and bruising in patients with Ehlers-Danlos syndrome and other collagen vascular disorders. Br J Haematol 127:491–500
7. Forlodou P, de Kersaint-Gilly A, Pizzanelli J, Viarouge MP, Auffray-Calvier E (1996) Ehlers-Danlos syndrome with a spontaneous caroticocavernous fistula occluded by detachable balloon: case report and review of literature. Neuroradiology 38:595–597
8. Freeman RK, Swegle J, Sise MJ (1996) The surgical complications of Ehlers-Danlos syndrome. Am Surg 62:869–873
9. Gassler N, Helmke B, Sido B, Otto HF, Autschbach F (2001) Desmosis coli in adults. Differential diagnosis in chronic constipation. Pathologe 22:214–217
10. Germain DP, Herrera-Guzman Y (2004) Vascular Ehlers-Danlos syndrome. Ann Genet 47:1–9
11. Giunta C, Steinmann B (2000) Characterization of 11 new mutations in COL3A1 of individuals with Ehlers-Danlos syndrome type IV: preliminary comparison of RNase cleavage, EMC and DHPLC assays. Hum Mutat 16:176–177
12. Hubner U, Meier-Ruge W, Halsband H (2002) Four cases of desmosis coli: severe chronic constipation, massive dilatation of

the colon, and hypoperistalsis due to of changes in the colonic connective-tissue net. Pediatr Surg Int 18:198–203
13. Kadler KE, Holmes DF, Trotter JA, Chapman JA (1996) Collagen fibril formation. Biochem J 316:1–11
14. Kahn T, Reiser M, Gmeinwieser J, Heuck A (1988) The Ehlers-Danlos syndrome, type IV, with an unusual combination of organ malformations. Cardiovasc Intervent Radiol 11:288–291
15. Kuivaniemi H, Tromp G, Prockop DJ (1997) Mutations in fibrillar collagens (types I, II, III, and XI), fibril-associated collagen (type IX), and network-forming collagen (type X) cause a spectrum of diseases of bone, cartilage, and blood vessels. Hum Mutat 9:300–315
16. Loeys BL, Schwarze U, Holm T, Callewaert BL, Thomas GH, Pannu H, De Backer JF, Oswald GL, Symoens S, Manouvrier S, Roberts AE, Faravelli F, Greco MA, Pyeritz RE, Milewicz DM, Coucke PJ, Cameron DE, Braverman AC, Byers PH, De Paepe AM, Dietz HC (2006) Aneurysm syndromes caused by mutations in the TGF-beta receptor. N Engl J Med 355:788–798
17. Oderich GS, Panneton JM, Bower TC, Lindor NM, Cherry KJ, Noel AA, Kalra M, Sullivan T, Gloviczki P (2005) The spectrum, management and clinical outcome of Ehlers-Danlos syndrome type IV: a 30-year experience. J Vasc Surg 42:98–106
18. Pepin M, Schwarze U, Superti-Furga A, Byers PH (2000) Clinical and genetic features of Ehlers-Danlos syndrome type IV, the vascular type. N Engl J Med 342:673–680
19. Pope FM, Martin G, Lichtenstein J, Penttinen R, Gerson B, Rowe D, McKusick V (1975) Patients with Ehlers-Danlos syndrome type IV lack type III collagen. Proc Natl Acad Sci 72:1314–1316
20. Schiebler TH, Peiper U, Schneider F (eds) (1986) Histologie, 2nd edn. Springer, Berlin
21. Steinmann B, Superti-Furga A, Joller-Jemelka HI, Cetta G, Byers PH (1989) Ehlers-Danlos syndrome type IV—a subset of patients distinguished by low serum levels of the amino-terminal propeptide of type III procollagen. Am J Med Genet 34:68–71
22. Superti-Furga A, Steinmann B (1988) Impaired secretion of type III procollagen in Ehlers-Danlos syndrome type IV fibroblasts: correction of the defect by incubation at reduced temperature and demonstration of subtle alterations in the triple-helical region of the molecule. Biochem Biophys Res Commun 150:140–147
23. Superti-Furga A, Gugler E, Gitzelmann R, Steinmann B (1988) Ehlers-Danlos syndrome type IV: a multi-exon deletion in one of the two COL3A1 alleles affecting structure, stability, and processing of type III procollagen. J Biol Chem 263:6226–6232
24. Watanabe A, Kawabata Y, Okada O, Tanabe N, Kimura H, Hatamochi A, Shinkai H, Sakai N, Shimada T, Hiroshima K, Kuriyama T (2002) Ehlers-Danlos syndrome type IV with few extrathoracic findings: a newly recognized point mutation in the COL3A1 gene. Eur Respir J 19:195–198

The tumor was completely resected via a partial pancreaticoduodenectomy (classical Whipple procedure). Histopathologically, the resected tumor was staged pT3 pN0. The postoperative course was uneventful, and the patient was discharged from the hospital without adjuvant treatment. After an asymptomatic period of 1 year, routine follow-up CT scan detected three new masses located in segment 5 of the liver (1.2 and 3.5 cm in largest diameter; Fig. 1) and in the right lower lobe of the lung (1.1 cm). After an explorative laparotomy and confirmation of metastases of the primary pancreatic tumor by frozen section, the masses were resected performing an extended right hemihepatectomy and a wedge resection of the right lower lobe of the lung. After another disease-free period of 2 years, further routine follow-up revealed a 5-cm abdominal mass. Again, the patient underwent an explorative laparotomy, now showing a mass adhering to the right colon flexure and the small bowel. A complete surgical resection of the tumor was achieved by performing a right hemicolectomy and segmental resection of the ileum. After another disease-free interval of 2 years, the patient presented with weight loss and abdominal discomfort. A CT scan of the abdomen revealed diffuse liver metastases and local recurrence in the right abdomen with infiltration of the right renal vein. Currently, 4 years after the initial diagnosis, the patient is still alive, although with disease.

Materials and methods

Histology and immunohistochemistry

For histological examination, sections obtained from formalin-fixed, paraffin-embedded tumor tissue were stained with hematoxylin and eosin (H and E) and periodic acid-Schiff (PAS). Immunohistochemical analyses were carried out with primary antibodies directed against pancytokeratins (KL-1; 1:20; Immunotech), cytokeratins 5/6 (1:25; Dako, Carpenteria, CA), cytokeratin 7 (1:50; Dako), cytokeratin 8 (1:100; Dako), cytokeratin 18 (1:10; Dako), cytokeratin 19 (1:50; Dako), cytokeratin 20 (1:20; Dako), p53 (1:100; Dako), DPC/SMAD4 (1:50; Santa Cruz Biotechnology, Santa Cruz, CA), β-catenin (1:200; BD Transduction Laboratories, Lexington, KY), epidermal growth factor receptor (EGFR; 1:50; Zymed Laboratories, Invitrogen, Carlsbad, CA), estrogen receptor (1:50; Dako), progesterone receptor (1:50; Dako), synaptophysin (1:2; BioGenex, San Ramon, CA), chromogranin A (1:2; Histoprime), neuron specific enolase (1:5; Histoprime), vimentin (1:1,000; Dako), actin (1:2; Enzo Diagnostics), desmin (1:2; Linaris), HMB-45 (undiluted, Enzo Diagnostics), LCA (1:5; Immunotech, Beckman Coulter, Fullerton, CA), melan A (1:25; Dako), alpha-1-fetoprotein (1:100; Dako), OCH1E5 (1:50; Dako), CD56 (1:50; Novocastra Laboratories, Newcastle upon Tyne, UK), S100 protein (1:300; Dako), MUC-1 (1:100; Novocastra, Newcastle, UK), CD99 (1:20; WAK-Chemie), trypsin (1:500; Ventrex Laboratories, Portland, OR), alpha-amylase (1:150; Gene Tex, San Antonio, TX), and WT1 (1:50; Dako), using the avidin–biotin–complex method. If necessary, antigen retrieval was achieved by microwave pretreatment in citrate buffer (p53, Smad4, β-catenin, estrogen and progesterone receptors, cytokeratin 20, OCH1E5) or in ethylenediaminetetraacetic acid (EDTA) buffer (cytokeratin 5/6) or by pronase digestion (EGFR, S100) of the slides.

Fig. 1 Helical CT scan of the abdomen showing a metastasis in segment 5 of the liver. The tumor displayed in this figure was resected performing a right hemihepatectomy

Molecular analyses

For mutation analyses of exon 1 of *K-ras* and exon 3 of *β-catenin*, genomic DNA was extracted and amplified by polymerase chain reaction (PCR), using standard protocols. The following primers were used: *K-ras* 1F: 5′-GTG TGA CAT GTT CTA ATA TAG TCA-3′; *K-ras* 1R: 5′-GAA TGG TCC TGC ACC AGT AA-3′;*β-cat* 3 F: 5′-GGA GTT GGA CAT GGC CAT GG-3′; *β-cat* 3R: 5′-CCT GTT CCC ACT CAT ACA GG-3′. After purification, the PCR products were bidirectionally sequenced on an ABIPrism 377 DNA sequencer (Applied Biosystems, Foster City, CA, USA), using the BigDye Termination kit (Applied Biosystems).

For analysis of the SYT-SSX1/2 fusion transcript, total RNA was extracted using standard protocols. Reverse transcriptase PCR was performed using the following primers: FP (SYT) 5′-CCAGCGAGGCCTTATGGATA-3′ and RP (SSX): 5′-TTTGTGGGCCAGATGCTTC-3′.

DNA microarrays

In total, 3,872 human complementary DNAs (cDNAs) representing genes that are of relevance to pancreatic cancer were selected [7, 14]. Amino-modified PCR products were arrayed onto slides with an epoxy surface (Epoxy Slides,

Quantifoil Micro Tools, Jena, Germany) with a Micro-Arrayer from Engineering Services (Virtek's arrayer system, BioRad, Munich, Germany).

Transcriptional profiling

Total RNA was extracted with guanidine isothiocyanate from snap-frozen pancreatic tissues, including ten normal pancreas samples and five pancreatic ductal adenocarcinomas. Fluorescence-labeled cDNA samples were prepared from 10-μg total RNA and incorporation of Cy3-or Cy5-labeled dCTP during first-strand synthesis. The labeling reaction was performed at least three times in total. To prevent bias caused by preferential label incorporation into particular sequences, the dyes were swapped between hybridizations. Hybridization was done under glass coverslips at 62°C overnight. After washing in 0.1× sodium saline citrate, fluorescence signals were detected on a confocal ScanArray 5000 scanner (Packard BioChip Technologies, Billerica, MA). Quantification of the signal intensities was performed with the GenePix Pro 4.1 software (Axon Instruments, Union City, CA).

Data analysis

Data quality assessment, normalization, and correspondence cluster analysis were performed with the analysis and data warehouse software package M-CHiPS (Multi-Conditional Hybridization Intensity Processing System), in which more than 7,800 hybridization experiments are currently stored (http://www.mchips.org) [12, 13]. Normalization was performed as described in detail by Beissbart et al. [4]. For further analysis, only genes that exhibited significant changes between at least one sample and the control material of the normal pancreas were selected. Data analysis and also the compilation of experimental and sample-specific annotations met the criteria for MIAME2 compliance [8]. Correspondence analysis [12] is an explorative computational method for the study of associations between variables, such as genes and hybridizations, in a multidimensional space. It simultaneously displays data for two or more variables in a low-dimensional projection, thus revealing associations between them. The closer the positional location in the blot, the higher is the degree of correspondence, enabling better data interpretation.

Results

Pathomorphological, immunohistochemical, and molecular findings

At gross examination, the primary pancreatic tumor, measuring 5 cm in largest diameter, displayed a well-circumscribed, firm, homogeneously white to yellowish cut surface without cystic changes. Microscopically, the tumor consisted of round to oval cells with large nuclei and eosinophilic or clear cytoplasm (Fig. 2), the latter being found in approximately 70 to 80% of the cells. The tumor cells were predominantly arranged in solid sheets, intermingled with abundant fibrovascular stalks. Focally, the tumor both displayed trabecular and acinar-like growth patterns. PAS staining did not reveal any cytoplasmatic granules.

Microscopically, the tumor had poorly defined margins and infiltrated the peri-pancreatic fatty tissue and the duodenal wall. Invasion of blood vessels was not seen. There were no regional lymph node metastases.

Immunohistochemically, the tumor cells displayed strong and diffuse staining reactions for pancytokeratin (KL1), cytokeratin 18, β-catenin (membrane bound), and EGFR (in 80% of the tumor cells). Staining for DPC4/SMAD4 was positive but rather weak in comparison with non-neoplastic tissue, the latter displaying strong and diffuse positivity. Focal positive staining reactions were observed for cytokeratin 7, cytokeratin 8, S100, MUC-1, and vimentin, whereas no staining was detected for cytokeratins 5/6, 19, and 20, trypsin, alpha-amylase, actin, desmin, progesterone receptor, estrogen receptor, lymphocytic common antigen, melan A, HMB-45, alpha-1-fetoprotein, CD99, OCH1E5, WT1, and the neuroendocrine markers synaptophysin, chromogranin A, CD56, and neuron-specific enolase. There was no nuclear accumulation of p53 (Table 1).

Molecular analyses revealed wild-type copies of exon 1 of *K-ras* and of exon 3 of *β-catenin*. A SYT-SSX1/2 fusion transcript was not detected.

The resected metastases (liver, lung, and abdominal cavity) showed comparable gross, microscopic, and immunohistochemical characteristics as the primary pancreatic tumor. The resection specimen of the primary tumor as well as the resection specimens of the metastases displayed resection margins free of tumor.

Based on these findings, the working diagnosis of a well-differentiated clear cell carcinoma with unusual expression of vimentin, S100, and MUC-1 was established.

Microarray analysis

Gene expression profiles were generated using high-density DNA microarrays with 3,872 human genes that had been identified to be tumor-associated [7]. The samples obtained from pancreatic ductal adenocarcinomas and normal pancreatic tissues, labeled with either Cy3 or Cy5, were analyzed in competitive hybridizations.

After scanning and quantification of the spot intensities, data were normalized and filtered. In total, 168 PCR fragments contained sequences that were significantly

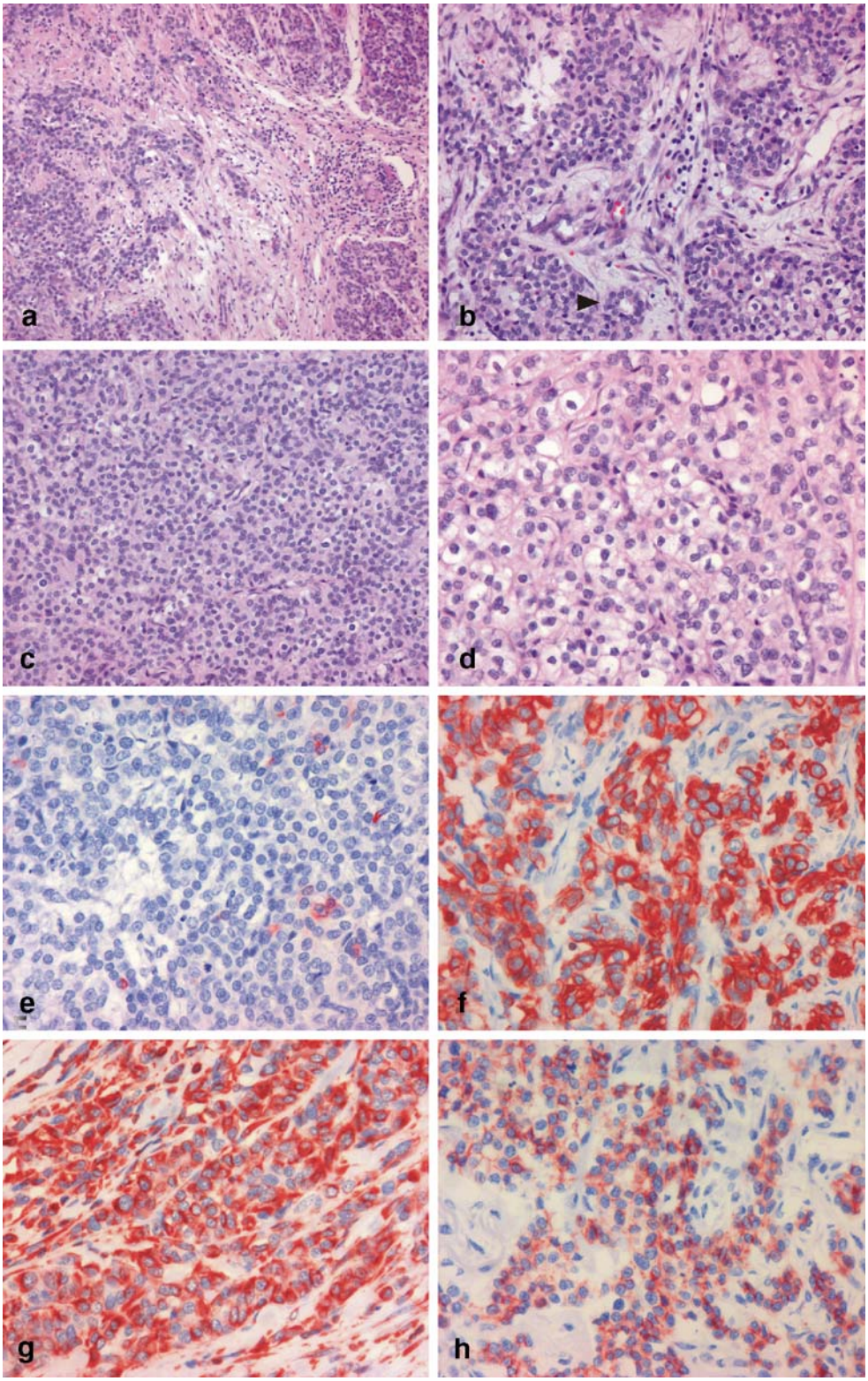

Fig. 2 Histomorphological and immunohistochemical findings. Microscopically, the tumor displayed round to oval cells (**a**–**c**; H and E) that frequently displayed clear cytoplasm (**d**). The tumor cells were predominantly arranged in solid sheets, intermingled by fibrovascular stalks (**b**). Focally, acinar-like formations were seen (**b**, *arrowhead*). The tumor borders were microscopically ill defined (**a**). Immunohistochemically, the tumor cells showed focal positivity for cytokeratin 7 (*staining red*; **e**), diffuse positivity for cytokeratin 18 (**f**), membranous positivity for β-catenin (**g**), and diffuse positivity for vimentin (**h**). Original magnifications: ×32 (**a**), ×64 (**b** and **c**), ×102 (**d**–**h**)

differentially transcribed in at least one of the samples analyzed. The results were subjected to correspondence cluster analysis [4], which is an explorative computational method for the investigation of associations between variables, such as genes and hybridizations, in a multidimensional space. It simultaneously displays data for two (or more) variables in a low-dimensional projection, thus revealing associations between them.

In Fig. 3, not only the differentially transcribed genes (gray dots) but also the results of clustering of the

Table 1 Tested immunohistochemical markers

Immunohistochemical marker	Result
Actin	−
Alpha-amylase	−
Alpha-1-fetoprotein	−
β-catenin	+[a]
CD56	−
CD99	−
CEA	−
Chromogranin A	−
CK5/6	−
CK7	+[b]
CK8	+[b]
CK18	+
CK19	−
CK20	−
c-Kit	−
Desmin	−
EGFR	+[a]
Estrogen receptor	−
HMB-45	−
Lymphocytic common antigen	−
Melan A	−
MUC-1	+[b]
Neuron-specific enolase	−
OCH1E5	−
Pancytokeratin (KL1)	+
Progesterone receptor	−
p53	−
Synaptophysin	−
S-100	+[b]
Trypsin	−
Vimentin	+[b]
WT1	−

(*Plus sign*) positive staining, (*minus sign*) no staining
[a] Membrane positivity
[b] Focal positivity

individual hybridizations—and, thus, the individual tissue samples (colored squares)—are shown. Co-localization of genes and individual experiments are indicative of a strong association between them.

As is apparent from Fig. 3, the transcript profiles permitted an accurate classification of normal pancreatic tissue (cluster I, red circle) and pancreatic ductal adenocarcinoma (cluster II, blue squares). Profiling the RNA of the patient's tumors described here produced a novel distinct blot position (cluster III, green squares; cluster IV, turquoise squares; cluster V, pink squares). Cluster III represents the patient's primary pancreatic tumor, cluster IV the liver metastasis, and cluster V the abdominal metastasis. All repetitions of the analysis produced the same result, actually forming a cluster of their own in the correspondence analysis. Distances to the other tumor cluster demonstrated that the samples exhibited a significantly different transcriptional profile. The distribution of clusters II–V is highlighted by circles.

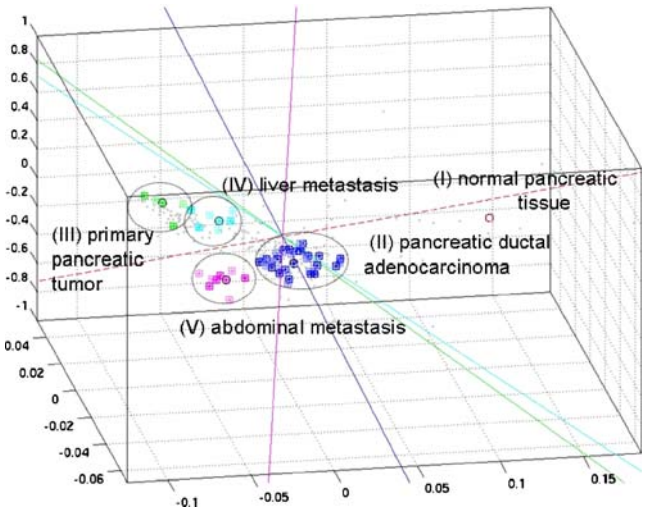

Fig. 3 Cluster analysis. Correspondence cluster analysis of transcript profiles made from normal pancreatic tissue (cluster I, *red circle*), pancreatic ductal adenocarcinomas (cluster II, *blue squares*), and tumors described here (clusters III–V). In the resulting bi-plot, each hybridization of an individual sample is depicted as a *colored square*. Genes that exhibited significantly differential transcription levels are shown as *gray dots*. The closer the co-localization of two spots (both genes and tumors), the higher is the degree of association between them. As a control, normal pancreatic tissue was used (cluster I, *red circle*). As all other experiments were compared to this control, only the center of gravity of all normal tissue samples is shown rather than individual experiments. Cluster II (*blue squares*) is made of pancreatic ductal adenocarcinomas. Cluster III represents the patient's primary pancreatic tumor (*green squares*), cluster IV the liver metastasis (*turquoise squares*), and cluster V the abdominal metastasis (*pink squares*). The distribution of clusters II–V is highlighted by *circles*

Additional immunohistochemical analysis

For verification of the microarray analysis, additional immunohistochemical analysis was carried out for two genes (fibronectin and vitronectin). Transcriptional microarray analysis showed a strong difference in fibronectin expression between the tumor and normal pancreatic tissue. Therefore, we performed immunohistochemical stainings against fibronectin and vitronectin to confirm the results of the microarray analysis. The patient's pancreatic tumors showed a massive increase in the expression of both fibronectin and vitronectin when compared with normal pancreatic tissue. The differences in fibronectin expression of the patient's primary pancreatic tumor in comparison to normal pancreatic tissue are displayed in Fig. 4.

Discussion

We report the clinicopathological, immunohistochemical, and molecular findings of a malignant pancreatic tumor that could

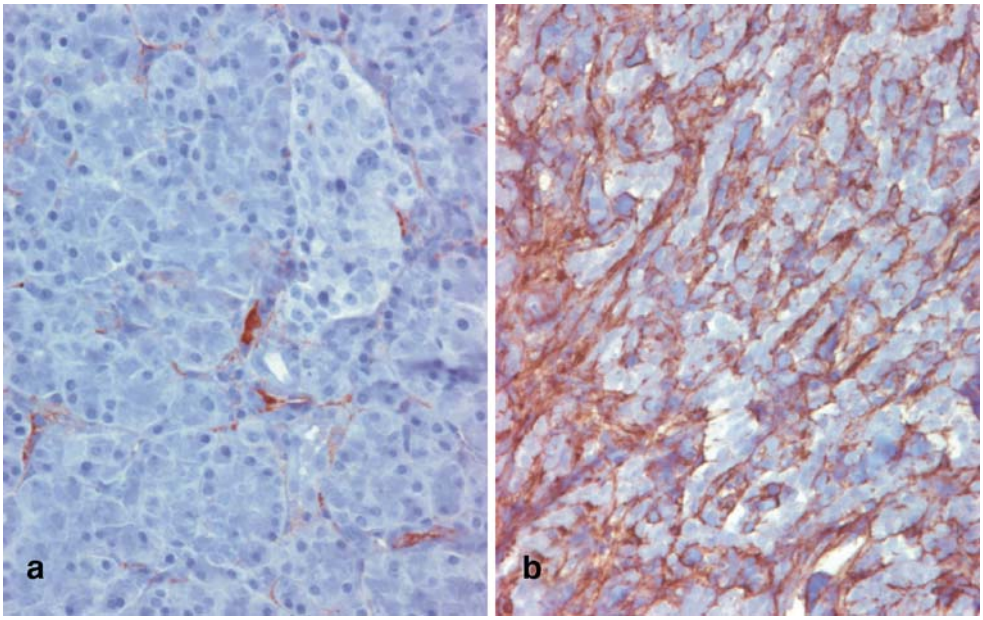

Fig. 4 Verification of gene transcription data by immunohistochemistry: Normal pancreas showed rather weak and focal expression of fibronectin (**a**; *brownish staining*), whereas strong expression was seen in the patient's primary pancreatic tumor (**b**). Original magnification: ×102

not be assigned to any known pancreatic tumor entity [16, 33]. The predominantly solid growth pattern and clear cell features displayed by this tumor are frequent findings in endocrine pancreatic neoplasms. Nevertheless, the present tumor lacked the expression of neuroendocrine markers and, therefore, did not qualify for this diagnosis [10].

Some endocrine neoplasms of the pancreas display a morphologic overlap with acinar cell carcinoma [28]. This might be due to a common cell of origin, which to date has not been identified [28]. Focal acinar-like differentiation and the strong immunohistochemical expression of cytokeratin 18 suggested the diagnosis of an acinar cell carcinoma [2, 18, 19]. However, this diagnosis was rejected because the tumor did not show any expression of the pancreatic enzymes trypsin and amylase.

Due to the relatively young age and female gender of the patient, a solid pseudopapillary neoplasm had to be considered for differential diagnosis [1]. Recently, a clear cell variant of this tumor entity has been described [3]. Although solid pseudopapillary neoplasms usually present a benign clinical course, a few cases of an aggressive variant have been reported [35, 36]. However, the lack of any cystic or pseudopapillary histomorphological features, and the immunohistochemical profile of the tumor, in particular the lack of expression of neuron-specific enolase and the membrane-bound expression of β-catenin, were not in accordance with the diagnosis of solid pseudopapillary neoplasms. Furthermore, the present tumor displayed a wild-type genotype of β-catenin, whereas solid pseudopapillary neoplasms characteristically display point mutations in exon 3 of this gene [1, 21].

Ductal adenocarcinoma is by far the most common primary tumor of the pancreas. As a variant, few cases of a clear cell ductal adenocarcinoma have been described [23, 29]. As in the present case, some of these tumors were found to display solid arrangements of clear cell tumor cells. *K-ras* mutation analyses were obtained in two of these cases, both revealing point mutations in codon 12, a finding that could not be reproduced for the present case. Other frequent alterations include p53 mutations (up to 70%) and DPC4/SMAD4 mutations (approximately 50%) [38], leading to abnormal protein expression. p53 mutations can result in nuclear accumulation of p53 [32]. The DPC4/SMAD4 tumor-suppressor gene can be inactivated either by intragenic mutation in one allele coupled with loss of the other allele (loss of heterozygosity) or deletion of both alleles (homozygous deletion) [20]. In our case, however, there was no evidence for a mutation in the p53 gene or loss of DPC4/SMAD4 expression. Immunohistochemical labeling showed diffuse DPC4/SMAD4 expression but no nuclear accumulation of p53. Because there is a good correlation between immunohistochemical labeling and genetic analysis [28], alterations in the p53 gene and DPC4/SMAD4 gene were deemed very unlikely. Although the present tumor displayed some features of pancreatic ductal adenocarcinoma such as expression of EGFR [22], the immunohistochemical staining pattern for cytokeratins (only scarce positivity for cytokeratins 7 and 8 and negativity for cytokeratin 19) did not match the diagnosis of ductal adenocarcinoma [38]. Furthermore, transcriptional profiling revealed strong evidence for a tumor that significantly differed from ductal adenocarcinoma.

The tumor's clear cell morphology and immunohistochemical positivity for cytokeratin, vimentin, and S100 suggested the possibility of a myoepithelial carcinoma (malignant myoepithelioma). This tumor represents approximately 1% of salivary gland tumors, most frequently affecting the parotid gland [26, 31], and is rarely found to

arise from submucosal bronchial glands [25]. For the present case, the diagnosis of myoepithelial carcinoma became unlikely because it lacked expression of actin, which is seen in up to 80% of myoepithelial carcinomas [26, 31], and because it lacked the expression of the myoepithelial marker cytokeratin 5/6.

On rare occasions, the pancreas gives rise to mesenchymal tumors [5, 24]. Due to the clear cell morphology and the strong expression of vimentin, the differential diagnosis of a synovial sarcoma was taken into account. However, lack of expression of the immunohistochemical marker CD99 and of the SYT/SSX172 fusion transcript made the diagnosis improbable.

Finally, the possibility of a metastasis to the pancreas was taken into account. Metastases in the pancreas have been described for various tumors, including renal cell carcinoma, breast carcinoma, colon carcinoma, malignant melanoma, and sarcoma [37]. Although metastases in the pancreas usually occur as part of disseminated disease, large autopsy series have described the prevalence of solitary pancreatic metastasis to be as high as 6 to 11% [9, 17, 27, 30, 34, 39]. However, clinical investigation failed to detect any extra-pancreatic primary tumor in our patient. In some cases, lack of detection of a primary tumor may be due to spontaneous tumor regression. This phenomenon has been described for malignant melanoma, including few cases of occult primary tumors and solitary pancreatic metastases [6]. However, malignant melanoma was excluded by immunohistochemical analyses.

In summary, the case described in this report represents a primary pancreatic tumor with histomorphological, immunohistochemical, and molecular features that cannot be assigned to any known pancreatic or extra-pancreatic tumor entity. We propose that this tumor be called solid type clear cell carcinoma of the pancreas.

References

1. Abraham SC, Klimstra DS, Wilentz RE, Yeo CJ, Conlon K, Brennan M, Cameron JL, Wu TT, Hruban RH (2002) Solid pseudopapillary tumors of the pancreas are genetically distinct from pancreatic ductal adenocarcinomas and almost always harbor beta-catenin mutations. Am J Pathol 160:1361–1369
2. Abraham SC, Wu TT, Hruban RH, Lee JH, Yeo CJ, Conlon K, Brennan M, Cameron JL, Klimstra DS (2002) Genetic and immunohistochemical analysis of pancreatic acinar cell carcinoma: frequent allelic loss on chromosome 11p and alterations in the APC/beta-catenin pathway. Am J Pathol 160:953–962
3. Albores-Saavedra J, Simpson K, Bilello SJ (2006) The clear cell variant of solid pseudopapillary tumor of the pancreas: a previously unrecognized pancreatic neoplasm. Am J Surg Pathol 30:1237–1242
4. Beissbarth T, Fellenberg K, Brors B, Arribas-Prat R, Boer J, Hauser NC, Scheideler M, Hoheisel JD, Schutz G, Poustka A, Vingron M (2000) Processing and quality control of DNA array hybridization data. Bioinformatics 16:1014–1022
5. Bergmann F, Hackert T, Mechtersheimer G, Penzel R, Bläker H, Berger I, Esposito I, Büchler MW, Otto HF (2004) Differential diagnosis of non-epithelial tumors of the pancreas: malignant non-epithelial pancreatic tumor with focal pigmentation. Virchows Arch 444:190–193
6. Bianca A, Carboni N, Di Carlo V, Falleni M, Ferrero S, Liverani C, Staudacher C, Turra G, Vergani D, Zerbi A (1992) Pancreatic malignant melanoma with occult primary lesion. A case report. Pathologica 84(1092):531–537
7. Brandt R, Grützmann R, Bauer A, Jesnowski R, Ringel J, Löhr M, Pilarsky C, Hoheisel JD (2004) DNA microarray analysis of pancreatic malignancies. Pancreatology 4:587–597
8. Brazma A, Hingamp P, Quackenbush J, Sherlock G, Spellman P, Stoeckert C, Aach J, Ansorge W, Ball CA, Causton HC, Gaasterland T, Glenisson P, Holstege FC, Kim IF, Markowitz V, Matese JC, Parkinson H, Robinson A, Sarkans U, Schulze-Kremer S, Stewart J, Taylor R, Vilo J, Vingron M (2001) Minimum information about a microarray experiment (MIAME)—toward standards for microarray data. Nat Genet 29:365–371
9. Cubilla A, Fitzgerald P (1984) Tumors of the exocrine pancreas. Atlas of tumor pathology. Armed Forces Institute of Pathology, Washington, DC
10. Eriksson B, Oberg K (2000) Neuroendocrine tumors of the pancreas. Br J Surg 87:129–131
11. Esposito I, Bauer A, Hoheisel JD, Kleeff J, Friess H, Bergmann F, Rieker RJ, Otto HF, Klöppel G, Penzel R (2004) Microcystic tubulopapillary carcinoma of the pancreas: a new tumor entity? Virchows Arch 444:447–453
12. Fellenberg K, Hauser NC, Brors B, Neutzner A, Hoheisel JD, Vingron M (2001) Correspondence analysis applied to microarray data. Proc Natl Acad Sci USA 98:10781–10786
13. Fellenberg K, Hauser NC, Brors B, Hoheisel JD, Vingron M (2002) Microarray data warehouse allowing for inclusion of experiment annotations in statistical analysis. Bioinformatics 18:423–433
14. Friess H, Ding J, Kleeff J, Fenkell L, Rosinski JA, Guweidhi A, Reidhaar-Olson JF, Korc M, Hammer J, Büchler MW (2003) Microarray-based identification of differentially expressed growth- and metastasis-associated genes in pancreatic cancer. Cell Mol Life Sci 60:1180–1199
15. Grützmann R, Foerder M, Alldinger I, Staub E, Brummendorf T, Ropcke S, Li X, Kristiansen G, Jesnowski R, Sipos B, Löhr M, Lüttges J, Ockert D, Klöppel G, Saeger HD, Pilarsky C (2003) Gene expression profiles of microdissected pancreatic ductal adenocarcinoma. Virchows Arch 443:508–517
16. Hamilton SR, Aaltonen LA (eds) (2000) World health organization classification of tumours. Pathology and genetics of tumors of the digestive system. IARC, Lyon
17. Hiotis SP, Klimstra DS, Conlon KC, Brennan MF (2002) Results after pancreatic resection for metastatic lesions. Ann Surg Oncol 9:675–679
18. Holen KD, Klimstra DS, Hummer A, Gonen M, Conlon K, Brennan M, Saltz LB (2002) Clinical characteristics and outcomes from an institutional series of acinar cell carcinoma of the pancreas and related tumors. J Clin Oncol 20:4673–4678
19. Hoorens A, Lemoine NR, McLellan E, Morohoshi T, Kamisawa T, Heitz PU, Stamm B, Ruschoff J, Wiedenmann B, Kloppel G (1993) Pancreatic acinar cell carcinoma. An analysis of cell lineage markers, p53 expression, and K-ras mutation. Am J Pathol 143:685–698
20. Hruban RH, Offerhaus GJA, Kern SE, Goggins M, Wilentz RE, Yeo CI (1998) Tumor-suppressor genes in pancreatic cancer. J Hepato Biliary Pancreatic Surgery 5:383–391
21. Kosmahl M, Seada LS, Janig U, Harms D, Klöppel G (2000) Solid-pseudopapillary tumor of the pancreas: its origin revisited. Virchows Arch 436:473–480
22. Lemoine NR, Hughes CM, Barton CM, Poulsom R, Jeffery RE, Klöppel G, Hall PA, Gullick WJ (1992) The epidermal growth factor receptor in human pancreatic cancer. J Pathol 166:7–12

23. Lüttges J, Vogel I, Menke M, Henne-Bruns D, Kremer B, Klöppel G (1998) Clear cell carcinoma of the pancreas: an adenocarcinoma with ductal phenotype. Histopathology 32:444–448
24. Lüttges J, Mentzel T, Hubner G, Klöppel G (1999) Solitary fibrous tumour of the pancreas: a new member of the small group of mesenchymal pancreatic tumours. Virchows Arch 435:37–42
25. Miura K, Harada H, Aiba S, Tsutsui Y (2000) Myoepithelial carcinoma of the lung arising from bronchial submucosa. Am J Surg Pathol 24:1300–1304
26. Nagao T, Sugano I, Ishida Y, Tajima Y, Matsuzaki O, Konno A, Kondo Y, Nagao K (1998) Salivary gland malignant myoepithelioma. A clinicopathologic and immunohistochemical study of ten cases. Cancer 83:1292–1299
27. Nakamura E, Shimizu M, Itoh T, Manabe T (2001) Secondary tumors of the pancreas: clinicopathological study of 103 autopsy cases of Japanese patients. Pathol Int 51:686–690
28. Ohike N, Kosmahl M, Klöppel G (2004) Mixed acinar–endocrine carcinoma of the pancreas. A clinicopathological study and comparison with acinar-cell carcinoma. Virchows Arch 445:231–235
29. Ray S, Lu Z, Rajendiran S (2004) Clear cell ductal adenocarcinoma of pancreas: a case report and review of the literature. Arch Pathol Lab Med 128:693–696
30. Robbins EG II, Franceschi D, Barkin JS (1996) Solitary metastatic tumors to the pancreas: a case report and review of the literature. Am J Gastroenterol 91:2414–2417
31. Savera AT, Sloman A, Huvos AG, Klimstra DS (2000) Myoepithelial carcinoma of the salivary glands: a clinicopathologic study of 25 patients. Am J Surg Pathol 24:761–774
32. Scarpa A, Capelli P, Mukai K, Zamboni G, Oda T, Iacono C, Hirohashi S (1993) Pancreatic adenocarcinomas frequently show p53 gene mutations. Am J Pathol 142:1534–1543
33. Solcia E, Capella C, Klöppel G (1997) Tumors of the pancreas. Atlas of tumor pathology. Armed Forces Institute of Pathology, Washington, DC
34. Stamm BH (1984) Incidence and diagnostic significance of minor pathologic changes in the adult pancreas at autopsy: a systematic study of 112 autopsies in patients without known pancreatic disease. Hum Pathol 15:677–683
35. Takahashi Y, Hiraoka N, Onozato K, Shibata T, Kosuge T, Nimura Y, Kanai Y, Hirohashi S (2006) Solid-pseudopapillary neoplasms of the pancreas in men and women: do they differ? Virchows Arch 448:561–569
36. Tang LH, Aydin H, Brennan MF, Klimstra DS (2005) Clinically aggressive solid pseudopapillary tumors of the pancreas: a report of two cases with components of undifferentiated carcinoma and a comparative clinicopathologic analysis of 34 conventional cases. Am J Surg Pathol 29:512–519
37. Thompson LD, Heffess CS (2000) Renal cell carcinoma to the pancreas in surgical pathology material. Cancer 89:1076–1088
38. Wilentz RE, Su GH, Dai JL, Sparks AB, Argani P, Sohn TA, Yeo CJ, Kern SE, Hruban RH (2000) Immunohistochemical labeling for dpc4 mirrors genetic status in pancreatic adenocarcinomas: a new marker of DPC4 inactivation. Am J Pathol 156:37–43
39. Z'Graggen K, Fernandez-del Castillo C, Rattner DW, Sigala H, Warshaw AL (1998) Metastases to the pancreas and their surgical extirpation. Arch Surg 133:413–417

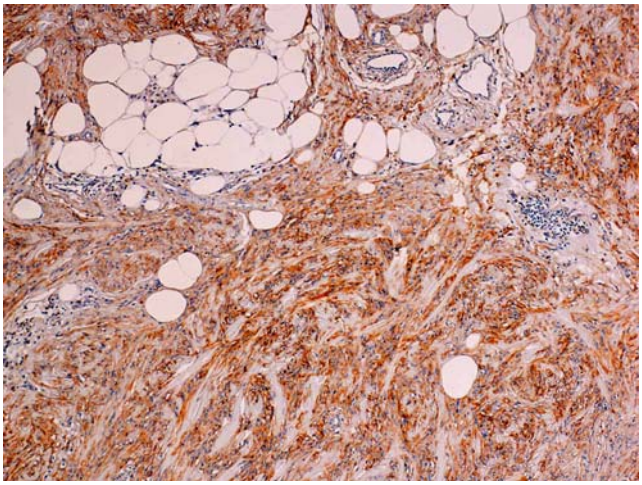

Fig. 1 Mammary myofibroblastoma with fatty component. Neoplastic spindle cells are diffusely and strongly stained with CD10. Typical thick collagen bands are interspersed among cells

This is an interesting and novel finding as we first show that CD10 is a reliable marker of SCL in addition to CD34.

The common expression of CD10 by MFB and SCL is an additional evidence of their close histogenetic relationships. Although we admit that some clinical, morphological and immunohistochemical differences between these two tumours do exist—the most important of which is the expression of myogenic markers (desmin and/or α-smooth muscle actin) in MFB—we think that MFB and SCL, apart from their original site (mammary or soft tissue), arise from a common vimentin+/CD34+/CD10+ mesenchymal stem cell, as previously suggested by one of us (MG) [3, 4]. This speculation is supported by the evidence that MFB may contain a variable amount of fatty component, whilst some SCLs (<2%) may have many desmin+ spindle cells [5]. This could be explained only if we admit that precursor cell has the plasticity to differentiate along three cellular lines: fibroblastic, lipomatous and myofibroblastic lines. According to this point of view, if the precursor is differentiating along a fibroblastic and lipomatous lines, it gives origin to a SCL; whilst if the fibro-myofibroblastic line predominate (or it is solely represented), the result will be a MFB. If future molecular studies will support this hypothesis, MFB and SCL should not be considered as two separate entities rather merely different phenotypes of the same disease.

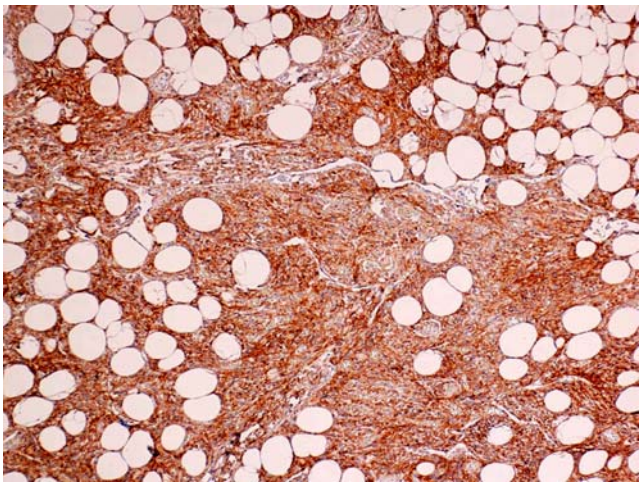

Fig. 2 Soft tissue spindle cell lipoma. Spindle cells are diffusely and strongly positive to CD10

References

1. Maggiani F, Debiec-Rychter M, Verbeeck G, Sciot R (2006) Extramammary myofibroblastoma is genetically related to spindle cell lipoma. Virchows Arch 449:244–247
2. Magro G, Michal M, Vasquez E, Bisceglia M (2000) Lipomatous myofibroblastoma: a potential diagnostic pitfall in the spectrum of the spindle cell lesions of the breast. Virchows Arch 437:540–544
3. Magro G, Michal M, Bisceglia M (2001) Benign spindle cell tumors of the mammary stroma: diagnostic criteria, classification, and histogenesis. Pathol Res Pract 197:453–466
4. Magro G, Bisceglia M, Michal M (2002) Spindle cell lipoma-like tumor, solitary fibrous tumor and myofibroblastoma of the breast: a clinico-pathological analysis of 13 cases in favor of a unifying histogenetic concept. Virchows Arch 440:249–260
5. McMenamin M, Fletcher CD (2001) Mammary-type myofibroblastoma of soft tissue: a tumor closely related to spindle cell lipoma. Am J Surg Pathol 25:1022–1029
6. Pauwels P, Sciot R, Croiset F, Rutten H, Van den Berghe H, Dal Cin P (2000) Myofibroblastoma of the breast: genetic link with spindle cell lipoma. J Pathol 191:282–285
7. Zamecnik M, Kinkor Z, Chlumska A (2006) CD10+ stromal cells in fibroadenoma and phylloides tumors of the breast. Virchows Arch 448:871–872

Virchows Arch (2007) 450:729–730
DOI 10.1007/s00428-007-0436-1

ANNOUNCEMENTS

Announcements

© Springer-Verlag 2007

24–27 July, 2007
Practical Pulmonary Pathology
London, UK

This course is designed to provide histopathology and cytopathology trainees and consultants with an opportunity to study diagnostic lung pathology in a comprehensive manner. It comprises lectures and practical microscopy sessions, the latter making up roughly half the time and consisting of individual study of a unique collection of cases.

For further information and application forms please contact:
Professor B Corrin,
Brompton Hospital,
London SW3 6NP, UK
Fax +44 20 7351 8293
E-mail: b.corrin@ic.ac.uk

27–31 August 2007 (Part I+II), 29–31 October 2007 (Part III)
Postgraduate Course Lung, Pleural & Mediastinal Diseases,
Department of Pathology,
Medical University, Graz, Austria

Course Director: Helmut Popper, MD (Graz)

Course Objectives:
This three-part course (common and rare lung and pleural, and mediastinal diseases) is designed for trainees as well as for experienced colleagues. Lectures as well as microscopy sessions alternate for each part. Clinical lectures and case studies are also included in selected lung diseases. Each part can be booked separately.

Course fee:
Part I (Common diseases) Aug 27–29, 2007€ 240,00
Part II (Mediastinal diseases) Aug 30–31, 2007€ 240,00
Part III (Rare diseases) Oct 29–31, 2007€ 240,00
Whole 8-day course (Part I + II + III) € 600,00
Two parts (Part I + II or Part I + III or Part II + III) € 450,00

For more information and registration please contact:
Edith Kleinferchner
Department of Pathology, Medical University Graz
Auenbruggerplatz 25
8036 Graz, Austria
Fax: 0043 (0)316 385-3432
e-mail:edith.kleinferchner@meduni-graz.at
http://pathologie.meduni-graz.at/Pathologie/veranstaltungen.htm

September 28th – October 1st, 2007
10th International Pituitary Pathology Meeting
Stresa, Italy

A four day long meeting designed for pathologists, endocrinologists, neurosurgeons interested in pituitary pathology. The course will provide comprehensive coverage of pathogenic and hispathologocal features of pituitary adenomas and an overview on lesions of the parasellar region.

Meeting Organizers: Carlo Capella, Luigi Bartalena, Giustino Tomei.

For further information please contact:
Prof. Carlo Capella
Dept. of Pathology
Ospedale di Circolo
Viale Borri, 57
1-21100 Varese, Italy
Tel: +39 0332 270601
Fax: +39 0332 270600
e-mail: carlo.capella@ospedale.varese.it

8 December 2007
International Board Certification in Dermatopathology
Frankfurt/Main, Germany

The European Union of Medical Specialists (Union Européenne des Médecins Spécialistes=UEMS)/Section of Dermato-Venereology and Section of Pathology will

organize under the auspices of the International Committee for Dermatopathology the **5th International Board Certifying Examination in Dermatopathology (Diploma in Dermatopathology).**

For further information and application forms, please contact:

Lorenzo Cerroni, M.D.
Department of Dermatology
Medical University of Graz
Auenbruggerplatz 8
A-8036 Graz/Austria
Ph.: +43-316-3852423
Fax: +43-316-3852466
e-mail:lorenzo.cerroni@meduni-graz.at
http://www.icdermpath.org